Universidad de Sevilla

Escuela Técnica Superior de Ingeniería

PhD Thesis

Three-Time-Scale Nonlinear Control of an Autonomous Helicopter on a Platform

Sergio Esteban Roncero

Sevilla

2011

This page intentionally left blank

Universidad de Sevilla

Escuela Técnica Superior de Ingeniería

PhD Thesis

Three-Time-Scale Nonlinear Control of an Autonomous Helicopter on a Platform

PhD. Thesis submitted to the Depto. de Ingeniería de Sistemas y Automática,
Escuela Técnica Superior de Ingeniería,
in partial fulfillment of the requisites for a degree of
Doctor of Philosophy in
Automation, Robotics and Telematic Engineering
at the
Universidad de Sevilla

By

Sergio Esteban Roncero

Sevilla, July, 2011

This page intentionally left blank

Universidad de Sevilla

Escuela Técnica Superior de Ingeniería

PhD Thesis

Three-Time-Scale Nonlinear Control of an Autonomous Helicopter on a Platform

Author: Sergio Esteban Roncero

Thesis Supervisors: Prof. Javier Aracil Santonja, Dr.

Prof. Francisco Gordillo Álvarez, Dr.

Abstract

A three-time scale singular perturbation control is applied to an autonomous helicopter model on a platform to regulate its vertical position. Two singularly perturbation time-scale analysis approaches are presented, the *Top-Down* (TD), and the *Bottom-Up* (BU), which permit to analyze multi-time scale systems. These methodologies are based in a sequential application of the general two-time-scale singular perturbation formulation, allowing to decouple the helicopter three-time-scale problem into two simpler two-time-scale models.

The TD and BU methodologies provide a step-by-step procedure that allows to design the proper control laws that allows to achieve the desired helicopter's altitude by either actuating on both the collective pitch angle and the angular velocity of the blades. In addition, the same methodology, provides a tool to select an appropriate composite Lyapunov function for the complete singularly perturbed system, and to demonstrate the asymptotic stability for the resulting closed-loop nonlinear singularly perturbed system for sufficiently small singular perturbation parameters using Lyapunov stability methods, and everything in an all-in-one step-by-step methodology.

The equivalency between both the TD and BU methodologies, permits the designer to choose which *direction* is to be used, depending on the structure of the system to be studied, and in special cases, determine which combination of both methodologies is the most appropriate according to the natural flow of the variables.

The validity of the methodology has been proved by obtaining the stability upper bound limits for the three-time-scale boundary layers, ε_1 and ε_2, and ensuring that the selected parasitic constants for the proposed control law satisfy $\varepsilon_1 \leq \varepsilon_1^*$ and $\varepsilon_2 \leq \varepsilon_2^*$ for both the helicopter and the simplified model here employed. The stability results have also presented a closed form solution for the proper selection of the *stability parameters* such that fulfill the required growth requirements among different singularly perturbed subsystem, providing asymptotic stability for the helicopter Σ_{SFU} full system with prescribed upper bounds on the parasitic parameters.

The TD and BU time scale analysis is also extended to the more general N^{th}-time-scale analysis using a 4^{th}-time-scale general example. The sequential strategy of decomposing the 4^{th}-time-scale system, into simpler two-time-scale subsystems provides valuable tools for both the analysis of time-scale singularly perturbed systems, and the stability properties of any general singularly perturbed N^{th}-time-scale system.

This page intentionally left blank

Acknowledgments

The work conducted in this PhD Thesis has been possible thanks to the support under MCyT-FEDER grants DPI2003-00429, DPI2006-07338 and MICINN-FEDER grant DPI2009-09961. Without the help of the sponsors this research would have not been able to be conducted and, because of this, I gratefully thank for the opportunity given by them.

The work conducted in this thesis would neither be possible without the feedback from many people that have helped me throughout these years to incorporate new tools that have allowed me to reach to this point, provide different points of view for both old and new concepts, and raise questions that, at one point or another, have light up the ideas that have translated to the work captured in this pages.

I would like to thank Dr. Javier Aracil and Dr. Francisco Gordillo for their guidance and support throughout all these years and for giving me the opportunity to add a stone to my academic training under their wings. Their knowledge, patience, points of view, transmitted to me over the past years, have made of me a better researcher, and I will always be in debt with them.

I would like also to thank Dr. Damián Rivas for believing in me to form part of his vision of future, which has made easier to be able to conduct this research with the security that provides to form part of the Departamento de Ingeniería Aeroespacial y Mecánica de Fluidos. It has been a slow journey, that has finally reached to an end. In general I would like to thank the entire *Grupo de Ingeniería Aeroespacial* (*GIA*), which have made possible for me to have full time dedication to complete this thesis.

I would also like to thanks both professor Dr. Oscar López and Alfonso Valenzuela for their invaluable help understanding concepts on helicopter theory, and helping with the development of plausible helicopter models. An special gratitude to professor Dr. Oscar López, for the much missed transcendental and philosophical conversations, that have helped me so many times to continue walking forward despite the encountered setbacks. I would like also to thank to professor Dr. Rafael Vázquez for helping with the mathematical aspects of the thesis discovering me the realm of inequalities, and making so easy the mathematics that for the rest of us seem so difficult.

Thanks to Dr. S. N. Balakrishnan, for still being there making sure I continue in the right path, and continuing looking over my shoulder both personally and academically. Thankfully, despite the distance and the years, his teachings, both academically and in life, are still guiding my steps.

I would like to express special thanks and gratitude to my parents Jerónimo and María, my sisters Ruth and Judith, family and friends on both sides of the *pond* for their continuous support and encouragement in pursuit of my goals throughout the years and the distance, to those still among us, and to those that are still looking after me from above, and in special, to my better half Sara, for supporting me, with her patience, and understanding during the most difficult part of this journey, which is only the beginning of a new and more exciting one.

Thanks to everyone.

Sergio Esteban Roncero

This page intentionally left blank

Contents

This page intentionally left blank

List of Figures

List of Tables

This page intentionally left blank

Mathematic Notation

Notation

a	italic lower case letters denote scalars
$\boldsymbol{a}$	boldface italic lower case letters denote vectors
$\mathbf{a}$	denote additional vectors of variables that use lower case letters to avoid confusion
$\boldsymbol{A}$	boldface upper case letters denote matrices
$\mathbf{A}$	denote vectors of variables that use upper case letters

Symbols

$\boldsymbol{x}$	vector with nth order, where x_i, $i = 1 \ldots n$ $\boldsymbol{z}\forall\mathcal{R}^n$
$\boldsymbol{x}^T$	transpose vector of $\boldsymbol{x}$
$\dot{x}$	time-derivative of x
x^*	desired value of x
$\tilde{x}$	error vector of the variable x, $\tilde{x} = x - x^*$
$\bar{x}$	equilibrium of x
x_{MIN}	minimum state value
x_{MAX}	maximum state value

Model Notation

A	main rotor disk area
A_b	blade area
A_e	main rotor effective disk area
B	tip-loss factor
c	tip chord of the main blade
c_o	root chord of the main blade
C_l	local blade lift coefficient
C_{l_α}	2-D lift-curve-slope
C_d	local blade drag coefficient
C_{D_f}	drag of the fuselage
C_{D_0}	profile drag of the blade
C_P	main rotor power coefficient
C_Q	main rotor torque coefficient
C_T	main rotor thrust coefficient
$\mathrm{dC_{P_i}}$	increment profile power coefficient per unit span
$\mathrm{dC_T}$	increment thrust coefficient per unit span

dD	increment drag per unit span
dL	increment lift per unit span
dm	helicopter mass element
dP	increment power per unit span
dQ	increment torque per unit span
dr	increment of radius per span
$d\mathbf{S}$	increment of the unit normal area vector of the control volume
dT	increment thrust per unit span
dv	helicopter volume element
dy	increment of unit span
f^{blade}	equivalent flat plate area of the blade
f_x^{fus}	equivalent flat plate area of the fuselage in the x-axis
f_y^{fus}	equivalent flat plate area of the fuselage in the y-axis
f_z^{fus}	equivalent flat plate area of the fuselage in the z-axis
$\mathbf{F}$	helicopter's combined aerodynamic and thrust external forces per unit area
$F_{damping}$	ground effect
F_{drag}	normalized constant helicopter drag
$\mathbf{F}_f$	fuselage combined aerodynamic and thrust external forces per unit area
$\mathbf{F}_{fn}$	vertical fin combined aerodynamic and thrust external forces per unit area
$\mathbf{F}_R$	main rotor combined aerodynamic and thrust external forces per unit area
$\mathbf{F}_{tp}$	tail plane combined aerodynamic and thrust external forces per unit area
$\mathbf{F}_{TR}$	tail rotor combined aerodynamic and thrust external forces per unit area
F_x, F_y, F_z	external forces applied to the helicopter on the X, Y, and Z axis
$\mathbf{g}$	acceleration of gravity
G_{eff}	ground effect model
$\mathbf{h}$	total angular momentum of spinning rotors
h	vertical component of the helicopter position on the surface of the Earth
$\dot{h}$	vertical component of the helicopter velocity on the surface of the Earth
$\boldsymbol{I_{ts}}$	inertia tensor of the helicopter
I_r	main rotor inertia
I_{xx}, I_{yy}, I_{zz}	Moment of inertia about the principal axis X, Y, Z
$I_{\beta_{es}}$	engine shaft blade inertia
$I_{\beta_{mr}}$	main rotor blade inertia
$I_{\beta_{tr}}$	tail rotor blade inertia
l_f	arm from the helicopter center of mass to the fuselage
l_{fn}	arm from the helicopter center of mass to the vertical fin
l_R	arm from the helicopter center of mass to the main rotor
l_{tp}	arm from the helicopter center of mass to the tail plane
l_{TR}	arm from the helicopter center of mass to the tail rotor
L	roll moment
m	total helicopter mass
$\dot{m}$	air mass flow rate
M	pitch moment
$\mathbf{M}$	helicopter's combined aerodynamic and thrust external moments
$\mathbf{M}_f$	fuselage combined aerodynamic and thrust external moments
$\mathbf{M}_{fn}$	vertical fin combined aerodynamic and thrust external moments
$\mathbf{M}_R$	main rotor combined aerodynamic and thrust external moments

$\mathbf{M}_{tp}$	tail plane combined aerodynamic and thrust external moments
$\mathbf{M}_{TR}$	tail rotor combined aerodynamic and thrust external moments
M_x, M_y, M_z	external moments applied to the helicopter on the X, Y, and Z axis
n_{tr}	tail rotor gear ratio
n_{es}	engine gear ratio
N	yaw moment
N_b	number of blades
p	perturbed roll rate flight condition
P	roll rate
P_{CM}	helicopter's center of mass
p_N	North component of the helicopter position on the surface of the Earth
p_E	East component of the helicopter velocity on the surface of the Earth
$\dot{p}_E$	East component of the helicopter velocity on the surface of the Earth
$\dot{p}_N$	North component of the helicopter position on the surface of the Earth
q	perturbed pitch rate flight condition
Q	pitch rate
r	perturbed yaw rate flight condition
r_0	radius of the helicopter blade root cut-out
$\mathbf{r}$	vector that connects the origin $X^{'}Y^{'}Z^{'}$ with each mass element of the helicopter
R	yaw rate
R_b	rotor radius
R_e	effective rotor radius
S_{blade}	blade area
S_{fus}	maximum fuselage cross area in the $x-y$
T	helicopter thrust
T_{loss}	loss in thrust as the helicopter moves through the air
u	perturbed forward velocity flight condition
u_{th}	input to the throttle servo
u_{θ_c}	collective servomechanism input
U	forward velocity
U_P	out-of-plane local flow velocity component
U_T	in-plane local flow velocity component
v	perturbed side-slip velocity flight condition
v_h	induced inflow velocity at the rotor disk for hover flight
v_i	main rotor induced velocity
V	side-slip velocity
V_c	helicopter climb velocity
V_{tip}	blade tip speed in hoovering flight
V_∞	free stream velocity
$\mathbf{V}_P$	velocity vector of the helicopter center of mass
w	main rotor far downstream velocity
w	perturbed downward velocity flight condition
W	downward velocity
X, Y, Z	helicopter body fixed system
$X^{'}Y^{'}Z^{'}$	Earth-fixed system
α	effective angle of attack
θ	perturbed pitch attitude angle flight condition

θ_0	pitch that the blade would have if it extended into the center of rotation
$\theta_{0.75}$	reference blade-pitch angle at 3/4-radius of the blade
θ_{1_c}	lateral cyclic control signal
θ_{1_s}	longitudinal cyclic control signal
θ_c	collective pitch angle of the main rotor blades
θ_t	pitch at the blade tip
θ_{tr}	collective pitch angle of the tail rotor
θ_{tw}	negative angle of twist between the center of rotation and the tip
Θ	pitch attitude angle of the helicopter
λ_h	induced inflow ratio in hover
λ_i	inflow ratio
ρ_H	local mass density of the helicopter
σ	main rotor solidity ration
τ_r	blade taper ratio
ϕ	perturbed roll angle flight condition
ϕ_i	relative inflow angle, or induced angle of attack, at the blade element
Φ	roll angle of the helicopter
ψ	perturbed yaw angle flight condition
Ψ	yaw angle of the helicopter
ξ	height of the helicopter mounted in the platform above the ground
$\boldsymbol{\omega}$	helicopter angular velocity
ω, Ω	rotational speed of the rotor blades

Helicopter Model Notation

a_*	helicopter normalized physical coefficients
c_*	helicopter singular perturbation normalized physical coefficients
f	helicopter angular velocity dynamics function
$\boldsymbol{g}$	helicopter vertical position dynamics vector function
g_z	acceleration of gravity in the z-axis
$\boldsymbol{h}$	helicopter collective pitch dynamics vector function
K_*	helicopter estimated physical coefficients
x	helicopter angular velocity of the blades
$\boldsymbol{y}$	helicopter vertical position vector
y_1	helicopter vertical position
y_2	helicopter vertical velocity
$\boldsymbol{z}$	helicopter collective pitch vector
z_1	helicopter collective pitch angle
z_2	helicopter collective pitch rate

Singular Perturbation Analysis Notation

f	slow dynamics function
g	fast dynamics function
$\hat{g}$	fast dynamics normalized function $\hat{g} \triangleq \varepsilon_1 g$
$\mathrm{g}(x)$	quasi-steady-state equilibrium for the fast subsystem, Σ_F
h	ultra-fast dynamics function

$\hat{h}$	ultra-fast dynamics normalized function $\hat{h} \triangleq \varepsilon_1\varepsilon_2 h$
$\mathrm{h}(x, y)$	quasi-steady-state equilibrium for the ultra-fast subsystem, Σ_U
$\mathrm{h}(x, \mathrm{g}(x))$	quasi-steady-state equilibrium for the combined fast and ultra-fast subsystem, Σ_{FU}
Q_s	*stability parameter* for slow movement of the simplified example
Q_S	*stability parameter* for the slow movement of the model of the helicopter model
Q_f	*stability parameter* for the fast movement of the simplified example
$\boldsymbol{Q_F}$	*stability parameter* matrix for the fast movement of the helicopter model
q_{f_1},q_{f_2}	*stability parameters* for the fast movement of the helicopter model
Q_u	*stability parameter* for the ultra-fast movement of the simplified example
$\boldsymbol{Q_U}$	*stability parameter* matrix for the ultra-fast movement of the helicopter model
q_{u_1},q_{u_2}	*stability parameters* for the ultra-fast movement of the helicopter model
V_f	Lyapunov function candidate for the fast movement of the simplified example
V_F	Lyapunov function candidate for the fast movement of the helicopter model
V_s	Lyapunov function candidate for the slow movement of the simplified example
V_S	Lyapunov function candidate for the slow movement of the helicopter model
V_u	Lyapunov function candidate for the ultra-fast movement of the simplified example
V_U	Lyapunov function candidate for the ultra-fast movement of the helicopter model
x	slow state variable
y	fast state variable
$\tilde{y}$	fast error dynamics, $\tilde{y} \triangleq y - y^*$
$\hat{y}$	quasi-steady-state fast error dynamics, $\hat{y} \triangleq \tilde{y} - \tilde{\mathrm{g}}(\tilde{x})$
z	ultra-fast state variable
$\tilde{z}$	ultra-fast error dynamics, $\tilde{z} \triangleq z - z^*$
$\hat{z}$	quasi-steady-state ultra-fast error dynamics, $\hat{z} \triangleq \tilde{z} - \tilde{\mathrm{h}}(\tilde{x}, \tilde{y})$
ε	singular perturbation parameter
ε_1	singular perturbation parameter for the fast time scale
ε_2	singular perturbation parameter for the ultra-fast time scale
Σ_S	slow movement of the Σ_{SFU} system
	reduced order (slow) movement of the Σ_{SF}-subsystem
	reduced order (slow) movement of the Σ_{FU}-subsystem
Σ_F	fast movement of the Σ_{SFU} system
	boundary layer (fast) movement of the Σ_{SF}-subsystem
	reduced order (slow) movement of the Σ_{FU}-subsystem
Σ_U	ultra-fast movement of the Σ_{SFU} system
	boundary layer (fast) movement movement of the Σ_{SF}-subsystem
	boundary layer (fast) movement movement of the Σ_{FU}-subsystem
τ_1	stretched time scale for the fast time-scale
τ_2	stretched time scale for the ultra-fast time-scale
$\phi_*(\cdot)$	boundary layer comparison function
$\psi_*(\cdot)$	reduced order comparison function

Controller Notation

$\tilde{b}_x$	desired slow dynamics time response (simplified example and helicopter model)
$\tilde{b}_y$	desired fast dynamics time response for the simplified example
$\tilde{b}_{y_1}$	desired helicopter's vertical position time response
$\tilde{b}_{y_2}$	desired helicopter's vertical velocity time response

$\tilde{b}_z$	desired ultra-fast dynamics time response for the simplified example
$\tilde{b}_{z_1}$	desired helicopter's collective pitch angle time response
$\tilde{b}_{z_2}$	desired helicopter's collective pitch rate time response
$\omega_{n_{y^*}}$	desired helicopter's vertical displacement dynamics natural frequency
$\omega_{n_{z^*}}$	desired helicopter's collective pitch dynamics natural frequency
ζ_{y^*}	desired helicopter's vertical displacement dynamics damping ratio
ζ_{z^*}	desired helicopter's collective pitch dynamics damping ratio

Acronyms

Notation	
ACNN	Adaptive Critic Neural Network
AFLS	Adaptive Fuzzy Logic System
ANN	Action Neural Network
BET	Blade Element Theory
BEMT	Blade Element Theory and Momentum Theory
BU	*Bottom-Up* time scale analysis
CNN	Critic Neural Network
$\mathcal{CF}$-*TD*	*Composite Feedback Top-Down* control strategy
DOF	Degrees Of Freedom
EKF	Extended Kalman Filter
EM	Energy Management
FLC	Fuzzy Logic Control
FSPT	Forced Singular Perturbations
GA	Genetic Algorithms
GCNL	Grupo de Control Nolineal
HJB	Hamilton-Jacobi-Bellman
IDC	Inverse Dynamics Control (IDC)
ISS	Input-to-State Stable
LQR	Linear Quadratic Regulator
MMOs	Mixed-Mode Oscillations
MT	Momentum Theory
NGPC	Neural Generalized Predictive Control
NN	Neural Networks
ODEs	Ordinary Differentia Equations
PD	Proportional plus Derivative control action
PI	Proportional plus Integral control action
PID	Proportional plus Integral plus Derivative control action
PWM	Pulse With Modulation
R/C	Radio Control
RLIDC	Repetitive Learning Inverse Dynamics Control
RLFLC	Repetitive Learning Fuzzy Logic Control
RPM	Revolution Per Minute
SDRE	State Dependent Riccati Equation
SP	Singular Perturbations
SPATS	Singular Perturbations and Time Scales

TD	*Top-Down* time scale analysis
SDRE	State Dependent Riccati Equation
TSS	Timescale Separation
VTOL	Vertical Take-Off and Landing
UAV	Unmanned Aerial Vehicle

Chapter 1

Introduction

1.1 Motivation

Control of rotary wing aircrafts represents a very challenging task due to the nonlinearities and inherent instabilities present in such systems. The versatility of rotorcrafts allows them to perform almost any task that no conventional aircraft can do, but this ability is ultimately associated to the control of its stability characteristics, which are generally obtained via automatic control design (Curtiss Jr., 2003). These stability and control properties come at the price of requiring complex control designs in order to deal with these highly nonlinear aerospace systems.

Historically, classical linear control techniques have been sufficient to obtain reasonable control responses of these type aerospace systems (Curtiss Jr., 2003). The evolution of the aerospace industry, and the consequent improvement of technologies, have increased the performance requirements of all systems in general, which has called for better control designs that can deal with more complex systems, making linear control techniques insufficient to cope with these performance requirements. Specifically, in the area of aerospace systems, a wide range of different nonlinear control techniques have been studied to deal with the nonlinear dynamics of such systems, from singular perturbation (Kokotović et al., 1999), feedback linearization (Brockett, 1978; Meyer et al., 1984; Hunt et al., 1983), dynamic inversion (Buffington et al., 1993; Bugajski et al., 1990; Reiner et al., 1995; Snell et al., 1992), sliding mode control (Sira-Ramírez et al., 1994), or backstepping control methods (Khalil, 1996; Lee and Kim, 2001), to name a few. Neural Networks (NN) are also included within the realm of nonlinear control techniques, and seem to provide improved robustness properties under system uncertainties.

Focusing in the system being treated in this thesis, in the past, helicopter control has been solved using mechanical stabilizers, which has been demonstrated to be sufficient to perform simple stabilization control tasks. Some of those mechanical systems are still in use in the majority of small helicopters, but have been proved to be insufficient to cope with the more demanding and agile maneuvers that are expected in the always expanding roles and missions of helicopters. Complex maneuvers such aerial refueling, landing on small ships, decelerating approaches in poor weather conditions, to name few, would be difficult, if not impossible to perform without the aid of stabilization and control augmentation, and the use of high-gain, full authority systems (Tischler, 1987; Tischler, 1989). As the helicopter performance requirements increased, it was necessary to introduce electronic stabilization, digital systems or high-gain controls (Curtiss Jr., 2003) in order to generate adequate control responses, which in return require the obtention of more detailed and sophisticated dynamic mathematical models.

These same requirements of more detailed models represent a basic problem in control design, which is to determine the mathematical modeling complexity required to adequately describe a physical system. The modeling of many systems calls for high-order dynamic equations, which for the case of rotorcraft systems, represents a unique challenge due to the involved rotatory parts. Generally, the presence of parasitic parameters, such as small time constants, is often the source of an increased order and stiffness of these systems (Naidu and Calise, 2001). The stiffness, attributed to the simultaneous occurrence of slow and fast phenomena, gives rise to time scales, and the suppression of the small parasitic variables results in degenerated, reduced order systems, that can be stabilized separately, thus simplifying the burden of control design of high-order systems. The use of singular perturbation methods to simplify the control burden parts from the assumption that the associated subsystem are each asymptotically stable, but such assumption needs additional conditions that will guarantee the asymptotical stability of the original nonlinear singular perturbed system for sufficient small singular perturbation parasitic constants, which will have bounded in order to guarantee the stability properties among the different time-scale subsystems.

This time-scale separation phenomena is quite common in aerospace systems, thus being usual the use of singular perturbation methodologies to both provide control and analyze the analyze the stability properties of such systems. Naidu and Calise (Naidu and Calise, 2001) give an extended survey of the use of singular perturbed and time-scale control methods for aerospace systems which serves as the basis for the literature review of singular perturbation and time-scale control methods in aerospace systems that is conducted in section 1.3.2.

As will be described in later sections,several works have been conducted towards demonstrating the asymptotic stability properties of singularly perturbed systems (Saberi and Khalil, 1984; Saberi and Khalil, 1985; Khalil, 1987), and all of them show a high degree of complexity required to demonstrate the stability properties of the different time-scale subsystems. Some of them approach the multi-parameter asymptotic stability analysis (Abed, 1985c; Abed, 1986; Desoer and Shahruz, 1986; Kokotović et al., 1987) using similar composite stability methods of large scale dynamical systems (Michel and Miller, 1977; Araki, 1978) based in Lyapunov stability methods, which will also be employed in this thesis, but without some of the restrictions encountered in the literature. For instance Araki (Araki, 1978) presents a composite method for analyzing the stability of large-scale systems focusing on the quadratic-order theorems using M-matrices, where the large-scale system is decomposed into smaller subsystems, and proceed to make a two-step analysis, in which the resulting subsystems are first analyzed, and secondly the obtained results are combined to reduce the property of the whole system, by using Lyapunov stability theories, with the restriction that the presented theorems, although elegant and easy to apply, suffer from the drawback that they can assure stability only for the systems with weak interconnections. The asymptotic stability procedure here presented do not depend on the nature of the interconnection properties among the reduced subsystems, and asymptotic stability properties are not inferred from the asymptotic stability of the different reduced systems, but demonstrating the asymptotic stability of the full singularly perturbed system by itself following the proposed step-by-step time-scale methodology.

The work presented in this thesis approaches the problem of multi-parameter asymptotic stability analysis by extending the procedures defined by Kokotović (Kokotović et al., 1999) for the two-time-scale singular perturbation problems, to the three-time-scale singular perturbation problem of an autonomous helicopter on a platform, although the methodology here presented can be extended to any general nonlinear singular perturbed dynamical system, as it is demonstrated in the results presented in Appendix C, where the asymptotic stability analysis is also demonstrated for more general three-time-scale model. The main contribution of the thesis is that the proposed *Top-Down* and *Bottom-Up* methodology allows to determine, in a all-in-one simple step-by-step process, the control laws that guarantee desired closed loop dynamics, provides also a methodology that constructs a composite Lyapunov function for the general resulting closed-loop singularly perturbed system, which is also use to demonstrate the asymptotic stability properties of the origin. These properties are also extended to semiglobal stability, by the definition in (Kokotović, 1992; Sussmann and Kokotović, 1991; Braslavsky and Miidleton, 1996), by providing upper bounds on the parasitic singularly perturbed parameters for the entire range of admissible state values, thus extending the domain of attraction to that same rage of admissible states.

The original motivation to this thesis comes from the work conducted by Sira-Ramirez (Sira-Ramírez et al., 1994) that used a dynamical multivariable discontinuous sliding mode control strategy for the stabilization of a nonlinear helicopter model in vertical flight which includes the dynamics of the collective pitch actuators, and the work conducted by the authors over the past years towards deriving a suitable control law, and the asymptotical stability analysis that demonstrates the validity of the proposed control laws (Esteban et al., 2005a; Esteban et al., 2008a; Esteban et al., 2008b). The use of singular perturbation methods to simplify the control system structure of helicopter models has been considered in the past as seen in (Heiges et al., 1992; Njaka et al., 1994; Prasad and Lipp, 1993; Hamidi and Ohta, 1995; Avanzini and de Matteis, 2001; López-Martínez et al., 2007), to name few, but to the knowledge of the author, the work conducted here, along with that conducted by Bertrand, Hamel and Piet-Lahanier (Bertrand et al., 2008), that presented a stability analysis of a hierarchical controller for an unmanned Aerial Vehicle, are the only investigations that theoretically address stability issues for *VTOL UAVs* using singular perturbations theory, which is necessary to guarantee the bounds of the selected parasitic constants. Is that necessity to demonstrate the asymptotic stability properties of the selected helicopter model using singular perturbation formulation (Esteban et al., 2005a), that presents the principal motivation for the work here conducted.

Due to the nature of the selected helicopter model, which represents a three-time-scale model, highly coupled system structure, as seen in Figure 2.30, and the complexity involved in applying the existing multiparameter stability analysis tools for singularly perturbed multiparameter systems, which although extensive and quite documented (Saberi and Khalil, 1984; Saberi and Khalil, 1985; Khalil, 1987; Abed, 1985c; Abed, 1986; Kokotović et al., 1987), are mainly theoretic formulations, with a high degree of complexity involved in the demonstrations that provide stability properties of the different time-scale subsystems, it was clear that a simpler and easier strategy was to be sought. In addition to the complex demonstrations, the available methods required the existence of appropriate Lyapunov function candidates for each of the time-scale subsystem, which are extremely difficult to derive since they are obtained at the same time that the fulfillment of the growth requirements among the time-scale subsystems, that is, depending on the complexity of the system being analyzed, and the growth requirement that must satisfy, thus making the selection of the Lyapunov function dependent of the selection of the comparison functions that demonstrate the stability and interconnection properties among the time-scale subsystems, that is the more complex the demonstrations, the more complex the Lyapunov functions need to be, and thus more difficult to derive as seen in the example provided in (Kokotović et al., 1986; Kokotović et al., 1987).

This motivated the author to pursue an analysis strategy that helped to analyze the asymptotic stability analysis of multiple time-scale systems in a straight step-by-step procedure, that do not relay on obtaining complex Lyapunov functions, since the Lyapunov structure is fixed a priori, and based on the natural desired closed loop response of each resulting subsystem, as selected during the control design that used the same philosophy, therefore making simpler to tackle the fulfillment of the growth requirements among the different time-scale subsystems that guarantee the asymptotic stability of the full singularly perturbed system, that is providing bounds on the singularly parasitic constants that guarantee the stability among the tim-scale subsystems. This methodology is not only limited to the three-times-scale problem here treated, both for the helicopter model and the more general example, but to any N^{th}-time-scale singularly perturbed system as it will shown in later chapters.

This thesis is structured as follows: Chapter 1 provides a brief introduction to the motivation, and a review of the literature for nonlinear control and in special to singular perturbation control in aerospace systems; Chapter 2 provides a general description to helicopter dynamics, including the derivation of the selected helicopter model; Chapter 3 describes the extension conducted from the general two-time-scale singular perturbation formulation to a general multi-time-scale system by introducing the proposed *Top-Down* and *Bottom-Up* Time-Scale Analysis; the proposed time-scale control strategy is developed in chapter 4, which includes sensitivity analysis simulation results for the proposed control laws; the stability analysis for the general case is conducted in chapter 5. Chapter 6 applies the derived stability analysis to the model here studied; the considerations of unmodeled dynamics to the proposed control laws is studied in Chapter 7; the conclusions are summarized in chapter 8, and the recommended lines for the future work in chapter 9.

For conciseness of the thesis, a series of Appendices are presented in which relevant material for the thesis is presented: the proposed test bench helicopter axial flight models are presented in Appendix A; Appendix B presents the control strategy selected for the simplified example, while Appendix C presents the asymptotic stability analysis for the simplified model, and finally some results for the asymptotic stability analysis for the helicopter model are presented in Appendix D. The work presented in this Appendixes, in special the work presented in Appendices B and C, have been very valuable to provide the necessary generality to the methodology here presented, which can be applied to a wide range of singularly perturbed systems.

1.2 Nonlinear Control in Aerospace Systems

This section provides a background to some of the different control theory approaches that are available for nonlinear problems, from classical control methods to non-classical methods. This section does not pretend to be a compilation of all existing control techniques that are applied to the aerospace systems, but rather being a compilation of some of the techniques that the author has been exposed over the past years.

1.2.1 Classical Control

Many approaches have been used over the years to solve the problem of automated control. Classic control techniques try to obtain feedback control laws by conducting comprehensive analysis of the system model. Some of these classic control techniques include design via root locus techniques, frequency response techniques and state space techniques to name a few. Nise gives a detailed definition of all the classical controllers described above in his reference book *Control Systems Engineering* (Nise, 1995). The author will try to recap some of the definitions contained in (Nise, 1995) in the next paragraphs.

In the design via root locus, the designer is able to choose the proper loop gain to meet a transient response specification by graphically analyzing both the transient and the stability information provided by the root locus. Since the transient response is dictated by the poles at a point in the root locus, this technique is limited to the transient responses and the steady-state error represented by points along where the root locus are available. In order to improve these limitations, cascade compensators are introduced in the form of ideal integral, or proportional-integral (PI) controller, ideal derivative or proportional derivative (PD) controller, proportional-plus-integral-plus-derivative (PID) controller, lag compensators, lead compensators, lag-lead compensators and feedback compensation.

Steady-state design compensators are implemented via PI controllers or lag compensators. PI controllers add a pole at the origin, thereby increasing the system type. Lag compensators, usually implemented with passive networks, do not place the pole at the origin but near it. Both methods add a zero very close to the pole in order not to affect the transient response.

The transient response design compensators are implemented through PD controllers or lead compensators. PD controllers add a zero to compensate the transient response, while lead compensators add a pole along with the zero. Lead compensators are usually passive networks. We can correct both transient response and steady-state error with a PID or lag-lead compensator. Both of these are simply combinations of the previously described compensators.

Feedback compensation can also be used to improve the transient response, where the compensator is placed in the feedback path. The feedback gain is used to change the compensator zero or the system's open-loop poles, giving the designer a wide choice of various root loci. The system gain is then varied to move along the selected root locus to the design point. An advantage of feedback compensation is the ability to design a fast response into a subsystem independently of the system's total response. Other classical approach is the design via frequency response. This approach follows the same lines of root locus via gain adjustment with the difference that the tools used do not require a computer. Instead Bode plots and Nyquist diagrams are used along side each other to provide stability and transient information about the system that is used to design a desirable controller (Nise, 1995). Nyquist criterion is used to determine if a system is stable by looking at the magnitude of the frequency response. Increasing the phase margin reduces the percent of overshoot of the response, decreasing the bandwidth increases the speed of the response, and the steady-state error is improved by increasing the low-frequency magnitude responses.

Another classical method is the state-space design, in which the desired system's pole locations are specified and then a controller consisting of state-variable feedback gains is designed to meet these requirements. Controller design consists of feeding back the state variables to the input of the system through specified gains that were found by matching the coefficients of the system's characteristic polynomial with the coefficients of the desired characteristic polynomial. If the state variables are not available, an observer is designed to emulate the plant and provide estimated state variables that will be used to obtain the gains.

Today systems operate in wider regimes than those in which they were originally designed and therefore the controllers need to be much more robust to be able to operate beyond the design envelope. Classic control techniques lack the robustness that is necessary to approach the extreme situations that define problems like the helicopter's altitude regulation problem that has motivated this study. The classic linear control techniques that were once sufficient to obtain reasonable control responses, fall short of today's industry requirements, in special when regulating the highly nonlinear and rotating mechanisms involved in helicopters. Following sections describe some of the nonlinear tools employed to solve aerospace control problems.

1.2.2 Nonlinear Control Methods in Aerospace

This section describes some of tools used in nonlinear control. Khalil (Khalil, 2002) lists in his *Nonlinear Systems* textbook various common tools used for nonlinear design, such as linearization, integral control, gain scheduling, feedback linearization, sliding mode control, Lyapunov redesign, backstepping, passivity-based control, and high gain observers. A brief description of each one of the methods without getting into the details of the formulation is provided by (Khalil, 2002) and summarized below.

In the design via linearization, the controller is guaranteed to work over the neighborhood of the single operating point that was used for the linearization. This limitation is extended to a wider range of operating points with the gain scheduling method, by parameterizing several operating points by one or more variables. The system is then linearized at the chosen points, and linear feedback controllers are designed and implemented at each point. This creates a series of linear controllers that are activated by monitoring the scheduling variables and hence being able to operate at different points of the envelope. This is one of the most commonly used design tools in the aviation industry today, due to the simplicity of the design and its capability to work at different operating points.

The integral control approach ensures asymptotic regulation under all parameters that do not destroy the stability of the closed-loop. The integral action is introduced by integrating the regulation error between the measured and desired states. By regulating the integrated error to be zero at equilibrium, the feedback controller creates an asymptotically stable equilibrium point.

Feedback linearization is one of the most widely used methods when trying to control nonlinear systems by taking a different perspective to linearization of the systems. The idea behind the feedback linearization problem consists in the stabilization of the nonlinear state equation into a controllable linear state equation by introducing terms in the controller to reduce or cancel the nonlinearities. Feedback linearization can be divided in full-state linearization, where the state equation is completely linearized, and input-output linearization, where the input-output map is linearized, and the state equation may be only partially linearized.

In the sliding mode control approach, trajectories are forced to reach a sliding manifold in finite time and to stay on the manifold for all future time. Motion on the manifold is independent of matching uncertainties. By using a lower order model, the sliding manifold is designed to achieve the control objective. The Lyapunov redesign uses a Lyapunov-like function of a nominal system to design an additional control component that makes the design robust to large matched uncertainties. Both the sliding mode control and the Lyapunov redesign produce discontinuous controllers, which could suffer from chattering in the presence of delays or unmodeled high-frequency dynamics.

Backstepping is a recursive procedure that interlaces the choice of Lyapunov function with the design feedback control. It breaks a design problem for the full system into a sequence of design problems for low order subsystems, using this extra flexibility between the lower order and scalar subsystems to solve stabilization, tracking and robust control problems under less restrictive conditions. Passivity based controllers exploit passivity of the open-loop system in the design of feedback control by damping injection. High-gain observers consider the fact that state feedback might not be available in many practical problems and extends previous control techniques to output feedback.

These are some of the most important nonlinear methods that are available in the academic literature, but many other methods have emerged through the years by merging the best parts and pieces of the above methods described with the power of Neural Networks (NN) (Balakrishnan and Biega, 1996; Jagannathan and Lewis, 1996; Kim and Calise, 1997; Prasad et al., 1999; Soloway and Haley, 2001), fuzzy logic (Hartana and Sasiadek, 2002), Genetic Algorithms (GA) (Holland, 1975; Rechenberg, 1973), State Dependent Riccati Equation methods ($SDRE$) (Cloutier et al., 1996a; Cloutier et al., 1996b), or $\theta - D$ methodologies (Xin and S.N., 2008; Xin et al., 2004), which all yielding very powerful methods that are able to solve some of the more complex nonlinear problems. A brief description of some of these methods is presented bellow.

Neural Networks have gained a lot of attention in the field of control over the last twenty years. Optimal control formulations often lead to two point boundary value problems (Bryson and Ho, 1975). For this reason, except for a very special class of problems, like Linear Quadratic Regulator roblems (LQR), it is quite difficult to solve for the controller in state feedback form. Moreover for nonlinear problems, the solution depends on the initial conditions. In real-life problems, however, it is difficult to predict the initial conditions a priori. Hence, it is necessary to obtain control functions that apply to an entire range of initial conditions to retain the feedback nature of the solution. The method of dynamic programming handles this problem by producing a family of optimal paths, or what is known as the field of extremals (Bryson and Ho, 1975). One great drawback of the dynamic programming approach, however, is that it requires a prohibitive amount of computation and storage in producing this entire field of extremals (Bryson and Ho, 1975). *NN* provides a solution to the problem of covering the entire field of extremals. This section intends to introduce some of the work done in the area of *NN* towards solving the highly demanded nonlinear control problems.

NN have been used extensively in the control of lumped parameter systems, which includes control of nonlinear plants. Various studies have realized neural network assisted controllers based on feedback linearization, dynamic inversion, reinforcement learning etc., in many fields like robotics, flight vehicles, chemical processes, motors, automobiles etc. A survey paper (Hunt et al., 1983) is cited for reference.

One of the most successful *NN* approaches is Adaptive Critic Neural Network ($ACNN$) method presented in Balakrishnan and Biega (Balakrishnan and Biega, 1996) and Balakrishnan and Saini (Saini et al., 1997). Balakrishnan and Viega focus on the use of the Adaptive Critic Neural Networks ($ACNN$) architecture to obtain an optimal neurocontroller based in the dual network architecture formed by an action neural network (ANN) and a critic neural network (CNN). The ANN maps the states of a system to the control, while the second network, the *CNN*, captures the mapping between the states of a dynamical system and the co-states that arise in an optimal control problem. The equations that satisfy the optimality of the problem are solved with the help of *NN*. This makes it possible to synthesize the closed loop controllers for this complex process. It also allows the philosophy of dynamic programming to be carried out without the need for near impossible computation and storage requirements. Another advantage of this neural network approach include the fact that no a priori assumptions about the form of the feedback control are needed; i.e., one need not assume the control expressed in any particular form. The consequence of this off-line computational method is that the resulting control is available to be used as on-line state-feedback control for an entire envelope of initial conditions.

Balakrishnan and Saini (Saini et al., 1997) use the $ACNN$ architecture to design a controller for auto landing an aircraft. Balakrishnan and Han (Balakrishnan and Han, 2002) extend the $ACNN$ formulation to solve a terminal constraint optimal control problem using an expanded form of the $ACNN$ architecture where the optimization goal is for a trajectory in minimum time to reach a set of final state constraints. The approach taken for the terminal constrain problem is to reformulate the state and optimal control equations to change the independent variable to that of one of the former states, generating a fixed final condition with respect to the independent variable. This sets a hard constraint on the Hamiltonian equations so that the final conditions are met exactly through the one-dimensional state equation, which is no longer invariant to the independent variable. This implies that a series of $ACNN$ pairs are used in sequence along the trajectory to account for the variance. This methodology has been applied to a wide range of aerospace problems, from aircraft optimal control, helicopter control, or high-angle of attack fighter maneuvers (Balakrishnan and Biega, 1996; Huang and Balakrishnan, 2005; Balakrishnan and Esteban, 2001). The author conducted his Master Thesis in Aerospace Engineering in this last topic, controllers for high angle of attack fighter airplanes (Esteban-Roncero, 2002) using $ACNN$ under the supervision of Professor S.N. Balakrishnan.

Other *NN* methodology by Plummer (Plumer, 1996) touches a family of terminal control problems in which he extends one of the most popular training algorithms for feed forward *NN*, backpropagation-through-time, to address the limitation that the feedforward *NN* algorithms have when dealing with the family of problems in which the cost function includes the elapsed trajectory-time. He approaches these limitations by reforming the controller design as a constraint optimization problem defined over the entire field of extremals for which the set of trajectory-times is incorporated into the cost which correspond to standard backpropagation-through-time with the addiction of certain transversality conditions. The new gradient algorithm based on these conditions, called time-optimal backpropagation-through-time, is tested on two benchmark minimum-time control problems.

Jagannathan and Lewis (Jagannathan and Lewis, 1996) introduced a family of novel multilayer discrete-time neural-net controllers for the control of a class of multi-input multi-output dynamical systems. The neural net controller includes modified delta rule weight tuning and exhibits an on-line learning instead of an off-line, so that control is immediate with no explicit learning phase needed. The structure of the neural network controller is derived using a filtered error/passivity approach in which the linearity in the parameters is not required and certainty equivalence is not used, hence overcoming several limitations of standard adaptive control. The stability analysis of the neurocontroller is done using the Lyapunov's direct method to guarantee the performance and the stability of the weight tuning algorithms of the neural nets. They make use of the passivity based controller properties described above despite the original system having not passivity properties, by using the neurocontroller to make the closed-loop system passive. This allows that the additional unknown bounded disturbances do not destroy the stability and tracking performance of the system.

Calise and Kim (Kim and Calise, 1997) demonstrated the power of the neural network within the realm of nonlinear control systems, with specific focus on aircraft control. The strength of their design lays in the implementation of feedback linearization along with *NN* as an alternative to gain scheduling, which simplifies the problem of designing complex flight control system for high-performance fighter aircrafts. Their design consists of a command and stability augmentation control system based on the feedback linearization, that uses an off-line trained network to invert the nonlinearities, while an online trained neural network is used to compensate for imperfections in the inversion and changes to the original dynamics and/or failures in the controls surfaces. A stable weight adjustment rule for the weights of the on-line neural network is also presented using a Lyapunov-like function.

Calise's effort to demonstrate the power of merging nonlinear control theory with the *NN* ability to model nonlinearities has yielded an extensive series of papers for a wide range of problems, the aerospace realm being the one with the most contributions. From helicopters to reusable launch vehicles, Calise and many more other authors have dedicated an incredible amount of work and resources to design neurocontrollers that would be able to approach the reconfigurable control problem in an innovative and efficient approach. Some of these novel works are introduced below.

In Calise (Prasad et al., 1999) shows, in an actual flight system of an unmanned helicopter, the potential benefits of neural network direct adaptive control by designing an outer loop trajectory-tracking controller. Calise, Johnson and Rysdyk (Johnson et al.,), use the X-33 Reusable Launch Vehicle technology demonstrator model to demonstrate a version of Calise's neurocontroller. The specific adaptive control method, called Pseudo-Control Hedging, is based in the concept of modifying a reference model to prevent an adaptation law from adapting to saturation of the vehicle input characteristic such as actuator position limits, actuator position rate limits and linear input dynamics. The same methodology is applied by Calise and Johnson (Calise and Johnson, 2001) to a type of failures that led to a reduction in total control authority of the X-33 model. They accomplish this by preventing the outer loop dynamics to adapt to the inner-loop dynamics while operating at the control limits. Calise, Lee, and Sharma

(Calise et al., 1998; Calise et al., 2000) show the approach taken to the *RFC* problem using a model of a tailless fighter aircraft configured with multiple and redundant control actuation devices, which is later tested in both a piloted simulation and in flight test on the X-36 aircraft.

A different *NN* approach is presented by Haley and Soloway (Soloway and Haley, 2001) in which they propose a Neural Generalized Predictive Control (*NGPC*) algorithm capable of real-time control law reconfiguration, model adaptation, and the ability to identify failures in control effectiveness by using an innovative user define cost function that can be associated to either the aircraft outputs or to the control inputs. The *NGPC* algorithm operates in two modes, prediction mode, in which uses the aircraft model to predict the aircraft's response, and control mode in which the control input that minimized the user specified function is passed to the aircraft as actuator position commands which then produce the desired aircraft response. When failure simulations are introduced, such as frozen elevator, the NGPC algorithm learns the changed dynamics and reconfigures to use alternative controllers, like symmetric ailerons to stabilize the aircraft.

Bull, Kaneshige, and Totah (Kaneshige et al., 2000) introduce an innovative generic neural flight control and autopilots system to provide adaptive flight control, without requiring extensive gain-scheduling or explicit system identification. The autopilot system is applied to a wide range of vehicle systems and is formed by a generic autopilot, a neural flight controller and a mode control panel, and a flight director. The generic guidance system performs automatic gain-scheduling using frequency separation, based upon the neural flight control system's specified reference model. The neural flight control architecture is based on the augmented model inversion controller developed by Calise and Rysdyk (Calise and Rysdyk, 1998), which is a direct adaptive tracking controller that integrates feedback linearization theory with both pre-trained and on-line learning *NN*. Pre-trained *NN* provide estimates of the aerodynamics stability and control characteristics required for model inversion. The on-line learning *NN* are used to generate command augmentation signals to compensate for the errors in the estimates and from the model inversion. The online learning *NN* also provide additional potential for adapting to changes in aircraft dynamics due to damage or failure. The mode control panel is the pilots' interface with the generic autopilot, and the flight directors, provide guidance commands to the pilot through the graphical display of pitch and bank errors.

Reference (Idan et al., 2002) describes an intelligent fault tolerant flight control system that blends aerodynamic and propulsion actuation for safe flight operation in the presence of actuators failures. Fault tolerance is obtained by a nonlinear adaptive control strategy based on on-line learning *NN* and actuator relocation scheme. The adaptive control block incorporates a recently developed technique for adaptation in the presence of actuator saturation, rate limits and failure. The proposed integrated aerodynamic/propulsion flight control system is evaluated in a nonlinear flight simulation.

Kim and Lee (Lee and Kim, 2001) propose a nonlinear flight control system using back-stepping and a *NN* controller that is tested in a non-linear six-degree-of-freedom simulation for an F-16 aircraft. The back-stepping controller is used to stabilize all state variables simultaneously without separating the fast dynamics from the slow dynamics, while the adaptive *NN* controller is used to compensate for the effect of the aerodynamic modeling errors, by assuming that the aerodynamic coefficients include uncertainty. The Lyapunov stability theorem is used to demonstrate that the tracking errors and weights of *NN* exponentially converge to a compact set under mild assumptions on the aerodynamic uncertainties and nonlinearities.

Ferrari and Stengel (Ferrari and Stengel, 2002) take the approach of designing a nonlinear control system that takes advantage of priori knowledge and experience gained from linear controllers, while capitalizing in the broader capabilities of adaptive, nonlinear control theory and computational *NN*. The importance of this novel approach lies in the fact that the gradients of the nonlinear control law represents the gain matrices of the equivalent locally linearized controllers by using a set of hypersurfaces expressed as NN that represent satisfactory linear controllers designed over the plant's operating range.

Other areas like fuzzy logic, originally introduced by Zadeh (Zadeh, 1965) in 1965, have demonstrated innovative approaches combining information classification concepts in binary patterns, so that decisions can be made using the reasoning associated to the complex human behavior, allowing high levels of autonomy and adaptability, and being applied in a wide range of applications (Boverie et al., 1997). Hartana and Sasiadek (Hartana and Sasiadek, 2002) present a sensor fusion for dead-reckoning mobile robot navigation. Odometry and sonar measurement signals are fused together using extended Kalman filter (EKF) and Adaptive Fuzzy Logic System ($AFLS$). Two different methods are used to adapt EKF, the first uses two exponential data weighting functions to estimate the process and white noise covariance, while the second method only uses the white noise covariance. The paper shows that the fused signal of odometry and sonar measurements along with the EKF and the $AFLS$ is more accurate than any of the original signals considered separately, and the enhanced, more accurate signal, is used to successfully guide and navigate the robot.

Green and Sasiadek (Green and Sasiadek, 2002) show the comparison results for tracking of a square trajectory by a two-link flexible robot manipulator, using as comparison an inverse dynamics control (IDC) and fuzzy logic control (FLC). A repetitive control technique is used to train a robot on the premise that it must execute periodic motions so that its performance improves after each iteration. The results show that while the repetitive learning inverse dynamics control ($RLIDC$) achieves no improvement in tracking, repetitive learning fuzzy logic control ($RLFLC$) achieves greater precision where cyclic tracking enables the fuzzy inference system to self-adapt and further reduce tracking errors.

Another point of view that uses natural selection of the species, are the Genetic Algorithms (GA), and the Evolutionary Strategies, that were originally introduced by Holland in 1975 (Holland, 1975) and by Rechenberg in 1973 (Rechenberg, 1973). Genetic algorithms take advantage of evolution and mutation in order to solve technical optimization problems.

Optimal control techniques have been also used in the realm of aerospace system, but one of the main problems encountered is that the optimal feedback control depends on the solution to the Hamilton-Jacobi-Bellman (HJB) equation (Bryson and Ho, 1975). The HJB equation is extremely difficult to solve in general, rendering optimal control techniques of limited use for nonlinear systems. Multiple suboptimal control techniques for nonlinear control problems have been investigated in the past decades. A widely used technique solves the nonlinear regulator problem in the State Dependent Riccati Equation ($SDRE$) (Cloutier et al., 1996a; Cloutier et al., 1996b) method. This method turns the nonlinear equations of motion into a linear-like structure, and therefore permitting the designer to use linear optimal control method like LQR and H_∞ design techniques in order to synthesis the associated control laws. This methodology requires extensive online computation since it is necessary to solve the associated algebraic Riccati equation at each sample time, which makes it difficult to implement in a real system. Some alternative methodologies use Taylor series expansions based methods to solve the associated Riccati equation, thus simplifying the online computational cost, but these techniques have problems related with the initial required control efforts when the initial states are also large. An extended survey on SDRE based techniques is presented in (Çimen, 2008).

An alternative control methodology to the Taylor series expansion based methodologies is the $\theta - D$ approximation which was originally derived by Balakrishnan and Xin (Xin and Balakrishnan, 2002), and extended to several aerospace systems (Xin and S.N., 2008; Xin et al., 2004). This control approach obtains a closed-form solution based on approximations to the HJB equation and solves the large-control-for-large-initial-states problem that occurs in some Taylor series expansion based models. In this article, the singular perturbation methods are compared with a nonlinear controller synthesis ($\theta - D$ approximation) technique based on the approximate solution to the Hamilton-Jacobi-Bellman equation. The author has also conducted some work with the $\theta - D$ methodology (Esteban et al., 2008b) using the same helicopter problem here studied, by comparing the singular perturbation methodologies presented in this thesis with the results obtained with the $\theta - D$ methodology, and comparable results were obtained although further work will be conducted in the future

On the realm of helicopter control, many different nonlinear techniques have been employed trying to cope with the challenging task of regulating the inherent instabilities present in such systems, although some of these nonlinear control techniques have been already described in the review conducted above. Pallet and Ahmad (Pallett and Ahmad, 1993) use an online two-layer adaptive neural networks to control a miniature helicopter during hover. The on-line control learns and adapt to changes in the plant on-line. Sira-Ramirez et al. (Sira-Ramírez et al., 1994) use a dynamical multivariable discontinuous feedback control strategy of the sliding mode to regulate the altitude of a nonlinear helicopter model in vertical flight. The proposed control strategy retaining the basic robustness features associated with sliding mode control policies, and in addition results non-chattering input trajectories and controlled state variable responses. Balakrishnan and Huang (Huang and Balakrishnan, 2005) use the adaptive critic method $ACNN$ previously defined, in a helicopter platform equivalent to the one used in this thesis.

Kaloust *et al.* (Kaloust et al., 2002) presents a robust control scheme for application to helicopters in vertical flight mode to guarantee altitude stabilization. A nonlinear helicopter model similar to the use in this thesis is used to derive the proposed control in which Lyapunov's direct method is used to establish the overall system stability. Tee *et al.* (Tee et al., 2008) propose a robust adaptive neural network (*NN*) control for helicopters in vertical flight, similar to the one used in this thesis, with dynamics in single-input-single-output (*SISO*) nonlinear nonaffine form. Based on the use of the implicit function theorem and the mean value theorem, they propose a constructive approach for adaptive *NN* control design with guaranteed stability. They consider both full-state and output feedback cases, in which it is shown that the output tracking error converge to a small neighborhood of the origin, while the remaining closed-loop signals remain bounded. Recall that these five helicopter control strategies, (Pallett and Ahmad, 1993; Sira-Ramírez et al., 1994; Huang and Balakrishnan, 2005; Kaloust et al., 2002; Tee et al., 2008), use a nonlinear helicopter model in vertical flight equivalent to one used in this thesis, and all of them propose diverse solutions for the control strategy employed to regulat the vertical position of the helicopter model mounted on a stand.

Frazzoli *et al.* (Frazzoli et al., 2000) present a tracking controller for an underactuated small helicopterdynamics, based on a backstepping procedure. The control design provides asymptotic tracking for an approximate model of small helicopters, and bounded tracking when more complete models are considered. The control strategies are simulated in both point stabilization and aggressive maneuver tracking. Shim *et al.* (Shim et al., 1998) compare three different control methodologies for helicopter autopilot design: linear robust multivariable control, fuzzy logic control with evolutionary tuning, and nonlinear tracking control. The control design is based on nonlinear dynamic model with a simplified thrust-torque generation model which is valid for hovering and low velocity flight.

Koo and Sastry (Koo and Sastry, 2002) present an output tracking controllers based on exact and approximate input-output linearization of a rigid body helicopter based on the Newton-Euler equations. By neglecting the couplings between moments and forces, they show that the approximated system with dynamic decoupling is full state linearizable by choosing positions and heading as outputs, and bounded tracking is achieved by applying the approximate control.

Walker *et al.* (Walker et al., 1999), and Walker (Walker, 2003), describe the design and testing of longitudinal and lateral controllers for the Bell 205 helicopter. The controllers are designed using H_∞ optimization in conjunction with low order linearizations taken from a non-linear flight mechanic model.

Flight test results are also included in which decoupled responses were obtained, and desired handling qualities achieved, and the bandwidths achieved in flight were close to those predicted by the linear analysis.

Kim and Shim (Kim and Shim, 2003) present a hierarchical flight control system for unmanned aerial vehicles, where the proposed system executes high-level mission objectives by progressively substantiating them into machine-level commands. The acquired information from various sensors is propagated back to the higher layers for reactive decision making. These control strategies have been successfully implemented on a number of small helicopters.

Isidori *et al.* (Isidori et al., 2003) consider the problem of controlling the vertical motion of a nonlinear model of a helicopter, while stabilizing the lateral and horizontal position and maintaining a constant attitude. The controller is tested under a situation in which is required to synchronize the vehicle motion with that of an oscillating platform, such as the deck of a ship in high seas. This is achieved by providing a reference to be tracked of sinusoidal nature, and assuming that the tracking reference is not to be available to the controller. Simulation results show the effectiveness of the method and its ability to cope with uncertainties on the plant and actuator model.

Dzul *et al.* (Dzul et al., 2004) design and implement a controller of a Lagrangian based small-scale helicopter which is mounted on a vertical platform. The control is obtained by classical pole-placement techniques for the yaw dynamics and adaptive pole-placement for the altitude dynamics. Mahony and Hamel (Mahony and Hamel, 2004) approach the control of an idealized model of a scale model autonomous helicopter, by first obtaining an a priori bound on the tracking performance, for an arbitrary trajectory. The control strategy uses backstepping techniques using an approximate model in which the small body forces that cannot be directly incorporated into the control design are neglected. The closed-loop performance of the full system, including the small body forces, is analyzed with a derived Lyapunov function, which provides a priori bounds on initial error and the trajectory parameters that guarantees acceptable tracking performance of the system.

Marconi and Naldi (Marconi and Naldi, 2007) consider the problem of controlling the vertical, lateral, longitudinal and yaw attitude motion of a helicopter along desired arbitrary trajectories with only restrictions on the time derivatives imposed by the functional controllability of the system. The nonlinear control strategy presented use a combination of feedforward control actions and high-gain and nested saturation feedback laws, which succeeds in enforcing the desired trajectories robustly with respect to uncertainties characterizing the physical and aerodynamical parameters of the helicopter.

1.3 Singular Perturbation Literature Review

1.3.1 Singular Perturbation in General

As described by Naidu and Calise (Naidu and Calise, 2001) one of the most important problems found in the theory of systems and control is the mathematical modeling of a physical system. The realistic representation of many systems calls for high-order dynamic equations. The presence of some parasitic parameters, such as small time constants, masses, resistances, inductances, capacitances, moments of inertia, Reynolds number, etc, is often the source for the increased order and stiffness of these systems. The presence of these small *parasitic* parameters appear multiplying time derivatives or, in more disguised form, due to the presence of large feedback gains and weak coupling.

The principal purpose of the singular perturbation approach is to provide an analysis and design tool that alleviates the high dimensionality and ill-conditioning resulting from the interaction of slow and fast dynamic modes. Is this simultaneous occurrence of slow and fast phenomena, produces both the stiffness in the dynamical systems, and gives rise to time scales. The systems in which the suppression of a small parameter is responsible for the degeneration (or reduction) of dimension (or order) of the system are labeled as singularly perturbed systems, which are a special representation of the general class of time scale systems. The curse of dimensionality coupled with stiffness poses formidable computational complexities for the analysis and design of multiple time scale systems. This time-scale approach is asymptotic, that is, exact in the limit as the ratio ε of the speeds of the slow versus the fast dynamics tends to zero. When ε is small, approximations are obtained from reduced-order models in separate time scales (Saksena et al., 1984), and this separation of time scales helps to reduce the order of complexity of the systems being controlled.

In the realm of control, two difficult task must be accomplished by a control engineer in order to guarantee the design of a proper control strategy that will regulate the system being studied. The first problem deals with the modeling of the system to be controlled. Modeling of systems having in mind that these systems are pursued to be controlled, have the peculiarity that the model should not be more detailed than required by the specific control task, while at the same time, the extent of necessary detail is not known before the control task is accomplished. Some of the common control tasks are optimal regulation, tracking and guidance, which are generally accomplished in the presence of unknown disturbances, parameter variations and other uncertainties, therefore, the control system must possess a sufficient degree of insensitivity and robustness (Kokotović, 1984). Singular perturbation techniques tackles this problem by legitimizing the long time used ad hoc simplifications of dynamic models among the control engineers by allowing to neglect the parasitic parameters which, in return, increase the dynamic order of the model, but at the same time, the proposed time-scale analysis tool must help to improve the oversimplified design by dividing the analysis in two steps. The first step provides a simplified design which captures the dominant phenomena, while the disregarded phenomena, if important, is to be treated in the second step.

The known asymptotic expansions into reduced (*outer*) and boundary layer (*inner*) series, becomes the main characteristic of singular perturbation techniques. In general, most control systems are dynamic, and the decomposition into stages is dictated by a separation of time scales, where the reduced model represents the slowest phenomena which in most applications are dominant, and Boundary layer models evolve in faster time scales and represent deviations from the predicted slow behavior. The goal of the second, third, and later design stages is to make the boundary layers and sublayers asymptotically stable, so that the deviations rapidly decay. The separation of time scales also eliminates stiffness difficulties and prepares for a more efficient hardware and software implementation of the controller (Kokotović, 1984).

Singular perturbation theory represents a traditional tool of fluid dynamics and nonlinear mechanics, which embraces a wide variety of dynamic phenomena possessing slow and fast modes. Singular Perturbations in Mathematics and Fluid Dynamics Singular perturbations has its birth in the boundary layer theory in fluid dynamics due to Prandtl (Prandtl, 1904). In a paper, given at the Third International Congress of Mathematicians in Heidelberg in 1904, he pointed out that, for high Reynolds numbers, the velocity in incompressible viscous flow past an object changes very rapidly from zero at the boundary to the value as given by the solution of the Navier-Stokes equation. This change takes place in a region near the wall, which is called the boundary layer, the thickness of which is proportional to the inverse of the square root of the Reynolds number. Boundary-layer theory was further developed into an important topic in fluid dynamics (van Dyke, 1975; Kaplun et al., 1967). The term singular perturbations was first introduced by Friedrichs and Wasow in the 1940s (Friedrichs and Wasow,). In Russia, mainly at Moscow State University, research activity on singular perturbations for ordinary differential equations, originated and developed by Tikhonov in the 1950s (Tikhonov, 1952) and his students, especially Vasil'eva (Vasil'eva, 1963), continues to be vigorously pursued even today (Vasil'eva et al., 1995). An excellent survey of the historical development of singular perturbations is found in a book by O'Malley (O'Malley Jr, 1991). Other historical surveys concerning the research activity in singular perturbation theory at Moscow State University and elsewhere can are found (Vasil'Eva, 1976; Vasil'Eva, 1994).

Singular perturbation and time-scale methods have been applied to a wide range scientific branches, from aerospace systems, to electrical systems and electronics, structures and mechanics, robotics, chemical reactors, soil mechanics, celestial mechanics, quantum mechanics, thermodynamics, thermoelasticity, elasticity, lubrication, vibrations, renewal processes, agricultural engineering, ecology, biology, and the list could continue, where (Naidu, 2002) can be consulted for a detailed survey on the use of singular perturbations and time scales. Among all these areas, it is quite interesting the use of singular perturbations in the realm of biology modeling, in special the research conducted to analyze the predator-prey theory by Deng *et al.* (Deng, 2001) where considerations are given to a basic food chain model satisfying the trophic time diversification hypothesis which translates the model into a singularly perturbed system of three time scales that it is used to provide rigorous but dynamical explanations as to why basic food chain dynamics can be chaotic. Later works of the same authors (Deng and Hines, 2002), provide that assuming that the reproduction rate ratio of the predator over the prey is sufficiently small thus resulting in a basic tri-trophic food chain model. The use of singular perturbation time-scale analysis permit to study the different interactions among the well established predator pray models, in which the top-predator is considered the slowest of the three time-scales, the predator model is faster than the top-predator, and slower than the prey, which represents the fastest of the three-time-scale models, and where the reproduction ratio rates are considered as the parasitic constants that define the time-scales. The use of such singularly perturbed models allows them to demonstrate that a singular Shilnikov's saddle-focus homoclinic orbit can exist as the reproduction rate ratio ε of the top-predator over the predator is greater than a modest value. In a sequel of his work, Deng and Hines, the singular perturbation and time-scale analysis allows them to investigate a new chaos generating mechanism in a basic food chain model and determine the ecological parameter ranges in which this type of chaos occurs, which otherwise, without the existence of these three-time-scale singularly perturbed methods, will be extremely difficult to analyze (Deng and Hines, 2003).

In the realm of biology is also interesting the study by Krupa *et al* (Krupa et al., 2008) of mixed-mode dynamics that represent a complex type of dynamical behavior that has been observed both, numerically, and experimentally, in numerous prototypical systems in the natural sciences. They use the compartmental Wilson-Callaway model for the dopaminergic neuron as an example of a system that exhibits a wide variety of mixed-mode patterns upon variation of a control parameter. By using singular perturbation and time-scales, the problem can be analyzed from a geometrical point of view, which permits to observe that the mixed-mode dynamics is caused by a slowly varying canard structure. Similarly, Krupa *et al* (Jalics et al., 2010) present a mathematical study of some aspects of mixed-mode oscillation (*MMOs*) dynamics in a three time scale system of ODEs as well as analyze related features of a biophysical model of a neuron from the entorhinal cortex, which, thanks to the use of singular perturbation, allows them to reduce the dimensionality of the neuronal model from six to three dimensions which permits them to investigate a regime in which *MMOs* are generated, which motivates the three-time-scale model system used.

The assimilation of singular perturbation techniques in control theory is more recent that in the field of fluid dynamics, and is rapidly developing, as seen by the large amount of surveys conducted, where for completeness only few of them are here referenced (Kokotović et al., 1976; Saksena et al., 1984; Kokotović, 1984; Kokotović, 1985; Naidu, 2002). Singular perturbation techniques have been widely used in many control problem areas, from open loop optimal control (Kelley, 1973; Cliff et al., 1992), to closed-loop optimal control which has provided some very elegant results for linear systems leading to a matrix Riccati differential or algebraic equations (Moerder and Calise, 1984; Moerder and Calise, 1985b; Moerder and Calise, 1985a), to high-gain feedback problems, observers, stochastic systems, H_∞, adaptive control, or sliding-mode control, to name few. Singular perturbation and time-scale analysis can be therefore viewed more like an analysis and design tool that alleviates the high dimensionality and ill-conditioning resulting from the interaction of slow and fast dynamic modes, therefore allowing to reduce the dynamic order of the studied models, thus permitting the use of control strategies that otherwise would difficult, if not impossible, to implement. Some of the control strategies used with singularly perturbation and time-scale analysis are described bellow.

Saberi and Khalil propose a composite control designed for stabilization and regulation of a class of nonlinear singularly perturbed systems by establishing well-posedness of the full regulator problem, providing explicit upper and lower bounds on a cost function, and upper bounds on the perturbation parameter ε are also provided (Saberi and Khalil, 1985; Saberi and Khalil, 1984). Khorasani and Pai addresses feedback linearization of full order nonlinear system via that of reduced-order systems, and show improvements for estimating the upper bound of the perturbation parameter and the region of attraction while studying the asymptotic stability properties of multiparameter singularly perturbed systems by introducing high order corrections on the in the model (Khorasani and Pai, 1984; Khorasani and Pai, 1985)

Oh and Khalil (Oh and Khalil, 1997) stabilize a class of nonlinear systems using singular perturbation by using a globally bounded output-feedback variable structure controller with a high gain observer for a feedback-linearizable minimum-phase nonlinear system in the presence of unknown disturbance. The high-gain observer is used to estimate derivatives of the tracking error while rejecting the effect of the disturbances. The results is the design of a globally bounded output-feedback variable structure controller that ensures tracking of the reference signal in the presence of unknown time-varying disturbances and modeling errors.

Chen (Chen, 2002) proposes a globally exponentially stabilizing composite feedback control for a general class of nonlinear singularly perturbed systems, where the chosen design manifold becomes an exact integral manifold and the trajectories of the closed-loop systems, starting from any initial states, are steered along the integral manifold to the origin for all sufficiently small singular perturbation parameters ε. Two appropriate Lyapunov functions are chosen, one for the reduced-order system, and the other for boundary layer system and then forming a composite Lyapunov function to investigate the stability for the full-order nonlinear system.

Abed has conducted an extensive amount of work related to demonstrate the stability properties of multiparameter systems (Abed, 1985a; Abed, 1985d; Abed, 1985e; Abed, 1985b; Abed and Silva-Madriz, 1988; Abed, 1986). In (Abed, 1985b) presents time-scale separation and stability of linear time-varying and time-invariant multiparameter singular perturbation problems, in which derives upper bounds on the small *parasitic* parameters ensuring the existence of an invertible, bounded transformation exactly separating fast and slow dynamics. The study of the time-varying case it is required the two-time-scale methodology introduced by (Khalil and Kokotović, 1979b), which yields that the mutual ratios of the small parameters are bounded by known positive constants. Abed also derives the parameter bounds ensuring that the system in question is uniformly asymptotically stable, which permit to facilitate the derivation of these latter bounds. The concept of *strong D-stability* is also introduced and shown to greatly simplify the stability analysis of time-invariant multiparameter problems. The concept is extended in (Abed, 1986) where Abed defines that a system F is said to be *D-stable* if the eigenvalues of DF have negative real parts for any diagonal matrix D with positive diagonal elements. Abed also defines that a matrix is *strongly D-stable* if it is *D-stable* and if every sufficiently small perturbation of the matrix is also *D-stable*. The concept proves a stability theorem for time-invariant multiparameter singular perturbation problems applied to two time scale as well as multiple time scale systems, regardless of the relative magnitudes of the singular perturbation parameters, assuming strong block *D-stability* of an associated boundary layer system. He also shows that for linear time-invariant systems the bounded mutual ratios assumption can be lifted, and typically less conservative parameter estimates are obtained (Abed, 1985e).

Robustness analysis has been extensively studied to cope with the uncertainty of parameters, where for instance, in (Khorasani, 1989), robustness is studied for a feedback stabilization of a nonlinear system subject to two sources of uncertainties, uncertainty of parameters and unmodeled high frequency dynamics, while in (Shi et al., 1998) presents the results for robust stability and robust disturbance attenuation with norm-bounded parameter uncertainties in both state and output relations. Ioannou (Ioannou and Tsakalis, 2002) proposes a new direct adaptive control algorithm which is robust with respect to additive and multiplicative plant unmodeled dynamics. The algorithm is designed based on the reduced order plant, which is assumed to be minimum phase and of known order and relative degree, but is analyzed with respect to the overall plant which, due to the unmodeled dynamics, may be non minimum phase and of unknown order and relative degree.

More recent robustness results using singular perturbation techniques can be seen in (Christofides, 2000), where Christofides *et al.* consider nonlinear singularly perturbed systems with time-varying uncertain variables, for which the fast subsystem is asymptotically stable and the slow subsystem is input/output linearizable and possesses input-to-state stable (*ISS*) inverse dynamics. They propose a robust output feedback controller that ensures boundedness of the state and enforces robust asymptotic output tracking with attenuation of the effect of the uncertain variables on the output of the closed-loop system. Chakrabortty *et al.* (Chakrabortty and Arcak, 2007; Chakrabortty and Arcak, 2008; Chakrabortty and Arcak, 2009) propose also a robust redesign technique which recovers the trajectories of a nominal control design in the presence of additive input uncertainties by using a high-gain filter and employing the fast variables arising from this filter in the feedback control law to cancel the effect of the uncertainties in the plant. Singular perturbation and time-scale analysis is used to prove that the trajectories of the redesigned system approach those of the nominal system when the filter gain is increased.

The high-gain feedback is a source for singular perturbation behavior of any physical system. In (Saberi, 1987), a stabilizing high-gain dynamic output feedback controller with almost-disturbance-decoupling property is designed for a class of square-invertible and minimum phase systems. See reference (Dragan and Halanay, 1987) for stabilizing a linear system by using high-gain feedback using procedures similar to the stabilization of singularly perturbed systems. See (Alvarez-Gallegos and Silva-Navarro, 1997; Heck, 1991; Ahmed et al., 2005) for addressing robust asymptotic stability of a class of nonlinear singularly perturbed systems using sliding-mode control techniques.

The use of singular perturbation and time-scale analysis although is generally applied to two-time-scale models, it is not limited to these systems, and many more works in the literature are oriented towards large scale or multiparameter singularly perturbed systems. Khalil and Kokotović (Khalil and Kokotović, 1979a) extended the singularly perturbed theory to systems with several small parameters which can change the system order, and discussed the difficulties that arise when testing the boundary layer stability in multiparameter linear problems, and test their theories to linear quadratic optimal control and Nash game problems. Winkelman *et al.* (Winkelman et al., 1980), present a time-scale separation procedure which is applied to a three machine interconnected power system modeled with flux linkage and voltage regulator dynamics, that provided reduced models which yielded good eigenvalue and time response approximations of the original system.

Kotovic (Kokotović, 1981) extended the singular perturbation and time-scales philosophy to the analysis of large-scale systems, in which historically it was assumed that the model studied had some known diagonal dominance properties which permitted eliminate the burden of properly modeling these large-scale systems. These assumptions are only acceptable for small size systems, loosing too much of the information that appears in the large-scale systems, therefore proposing the use of the standard singular perturbation theory, such that instead of assuming the existence of N *diagonally dominant blocks*, it is possible to justify one strongly coupled slow core and N weakly coupled fast subsystems.

Khalil (Khalil, 1981) extends the study of the stability of nonlinear, multiparameter, singularly perturbed systems, recalling that the stability properties of reduced-order and boundary-layer systems can be used to obtain a Lyapunov function for the singularly perturbed system and an estimate of its domain of attraction by deriving sufficient conditions that guarantee the asymptotic stability of a class of nonlinear singularly perturbed systems with several perturbation parameters of the same order, and provide estimates of the region of attraction and bounds on the small parameters.

Ladde and Šiljak (Ladde and Siljak, 1983) propose a scheme for order-decomposition and hierarchial aggregation of small parameters according to their order, for multiparameter singular perturbation of linear systems, when dealing with singular perturbation models in which, due to the fact that there are more than one small parasitic parameter representing physical constants, becomes necessary the use of multiple time-scales assumptions.

Abed (Abed, 1985c) derives the recursive formulae which yield asymptotic expansions for the eigenvalues of multiparameter singular perturbation problems, where the formulae follow readily from an exact expression for the eigenvalues which involves an implicit matrix function. The resulting implicit function satisfies an algebraic matrix Riccati equation reminiscent of a similar equation of the single parameter theory, and also demonstrate the *block D-stability* criterion concept for asymptotic stability (Khalil and Kokotović, 1979b) for multiparameter singularly perturbed systems.

Wang *et al.* (Wang et al., 1994) propose a series of perturbation techniques for the decomposition of near-optimal regulators for linear systems with multiparameter and multi-time scale singular perturbations. These near-optimal regulators have no knowledge of the perturbation parameters, which reduces the computation in regulator synthesis. For the case of multiparameter singular perturbations, the near optimal control is a cascade connection of separately designed slow and fast subregulators, while for the case of multitime scale singular perturbations, the near-optimal control is hierarchically composed of $N + 1$ subregulators, in which a parallel algorithm is provided for designing the different subregulators separately.

Pan and Başar (Pan and Başar, 1995) obtain the necessary and sufficient conditions for the existence of *approximate* saddle-point solutions in linear-quadratic zero-sum differential games when the state dynamics are defined on three time scales. They shown that under perfect state measurements, the original game can be decomposed into three subgames, denoted as slow, fast and fastest. The composite saddle-point solution of the resulting three subgames make up the approximate saddle-point solution of the original game. The conditions are obtained for the minimizing and maximizing player goals, and for both the finite and infinite-horizon cases, providing direct applications in the H^{∞}-optimal control of three-time scale singularly perturbed linear systems under perfect state measurements.

Mukaidani *et al.* (Mukaidani et al., 2003) consider the linear quadratic optimal control problem for multiparameter singularly perturbed systems in which N lower-level fast subsystems are interconnected through a higher-level slow subsystem, and develop a new method to design a near-optimal controller which does not depend on the unknown small parameters. They show that the resulting controller achieves an $O \parallel \mu \parallel^2$ approximation to the optimal cost of the original optimal control problem.

Grammel (Grammel, 2004) presents an order reduction procedure for nonlinear control systems with multiple time scales. A limit system for the slowest motion describing the situation that all singular perturbation parameters vanish is constructed using a refined two-scale averaging method in a way that allows a re-iteration. It is shown that for the case in which the control range vanishes, the results reduce to the well-known Tychonoff theorem on order reduction for singularly perturbed *ODEs*.

1.3.2 Singular Perturbation in Aerospace Systems

Trying to conduct n review of the literature of singular perturbation methods applied to aerospace systems becomes a challenging task due to the extensive work conducted, that can be traced back to the early works of Prandtl (Prandtl, 1904) the early 20^{th} century, to the work conducted by the author (Esteban et al., 2005a; Esteban et al., 2008a; Esteban et al., 2008b) and by Bertrand, Hamel and Piet-Lahanier (Bertrand et al., 2008), related to the theoretically addressing of stability issues for *VTOL UAVs* using singular perturbations theory. Trying to compile a complete review would be an impossible task, that would not match the great literature reviews that have been already conducted, in special the one by Naidu and Calise (Naidu and Calise, 2001), which provides an extended and excellent survey on the use of singular perturbed and time-scale control methods for aerospace systems. This section, rather than trying to create new literature reviews of the methods employed in this thesis, is based on the excellent existing reviews (Naidu and Calise, 2001; Naidu, 2002) and tries only to summarized them, making special emphasis on those works that have specially influenced, and helped, the author throughout the work conducted in these past years, and furthermore, have raised enough interest and suggested many ideas that have not been covered in this thesis, for obvious time and space limitations, but that will surely be tackled in future works of the author.

The application of singular perturbation to aerospace systems was first applied to solve complex flight optimization problems in the late 1960s. An excellent account of the "historical development of techniques for flight path optimization of high performance aircraft" is found in the *NASA* report by Mehra *et al.* (Mehra et al., 1979) in the late 1970s, that provides an extensive account of the "historical development of techniques for flight path optimization of high performance aircraft". The report starts with the introduction of the work conducted by Kaiser (Kaiser, 1944) on the vertical-plane minimum-time problem and reviews other works conducted by Miele (Miele, 1950), and Kelley (Kelley, 1959). In the horizontal-plane, minimum-time problem, the report reviews the works of Connor (Connor, 1967) which extends the existing closed-form solution of the optimal straight-line trajectories within the atmosphere to the case of a lateral maneuver at constant height, and Bryson and Lele (Bryson Jr and Lele, 1969) that present the thrust, bank angle, and angle-of-attack control laws for an aircraft to turn through a desired heading angle using minimum fuel, while staying at constant altitude, and starting and ending with specified velocities. In the three-dimensional, minimum-time problem, important contributions were made by Kelley and Edelbaum (Kelly and Edelbaum, 1986), Hedrick (Hedrick and Bryson, 1971) and Bryson (Bryson, 1971), in which solve supersonic airplane minimum time turns at constant altitude, determining thrust, bank angle and angle of attack programs with optimal control theory. Kelley and Lefton *et al.* (Kelley and Lefton, 1972) present a family of variable-altitude turns obtained by numerical integration in the reduced-order approximation for a hypothetical supersonic aircraft, including the effects of constraints on altitude, dynamic pressure, Mach number, lift coefficient, and normal load factor.

As described by Naidu and Calise (Naidu and Calise, 2001), singular perturbation analysis in flight mechanics is intimately connected with the concept of energy-state approximation, first introduced by Kaiser (Kaiser, 1944), to deal with the vertical-plane minimum-time problem. Kaiser introduced the notion of resultant height, which is today called energy height or specific energy, as the sum of an aircraft's potential and kinetic energy per unit weight. An excellent account of the connection of Kaiser's (Kaiser, 1944) early work and that of singular perturbation analysis of aircraft energy climbs can be found in the revisited article by Merritt *et al.* (Merritt et al., 1985), where minimum-time and distance-climb trajectories are compared with the original results for both the minimum-time calculations and the distance climbs.

It can be seen by the extensive literature, that the use of energy-state approximation in both two- and three-dimensional optimal trajectory analysis was extensively used until the late 1960s as it can be seen in the works of Rutowski (Rutowski, 1954), and later by Bryson *et al.* (Bryson, 1968), in which energy state approximation for supersonic aircraft performance optimization with extension to maximum range problems, and Hedrick and Bryson (Hedrick and Bryson Jr, 1972) which apply energy-state approximation to minimum-time three-dimensional turns for a particular aircraft capable of speeds up to Mach number two for a series of maneuvers where the change in heading-angle and/or final energy are specified.

The specific investigation on the application of the theory of singular perturbation and time-scales to aerospace systems began in the early 1970s with Kelley (Kelley, 1970b) which considers the use of singular perturbations to obtain simplest variational problems that can be solve approximately in terms of a reduced-order solution plus boundary layers at each end, therefore proposing this as an alternative to asymptotical expansions used to obtain approximate solution of optimal trajectory and control problems. Mehra *et al.* (Mehra et al., 1979) indicated in his study of the application of singular perturbation theory to develop a hierarchical real-time algorithm for optimal three-dimensional aircraft maneuvers that Kelley and his associates (Kelley, 1970b; Kelley, 1973; Kelly and Edelbaum, 1986) in the early 1970s, were the first to apply the theory of singular perturbations to aircraft trajectory optimization problems (Naidu and Calise, 2001). Kelley (Kelley, 1973) also extended the energy type of approximation to aircraft flight in terms of singular perturbation theory to three-dimensional maneuvers by first studying differential equations arising in optimal control of fairly general form but low order, and then extend the results to the attitude dynamics for optimal flight of a rocket in vacuum. Finally, optimal aircraft flight in various reduced-order approximations is investigated thus demonstrating that the use of reduced-order approximation facilitates numerical computations by reducing the number of multiplier initial values that must be determined simultaneously and by improving the conditioning of the differential equations.

Kelley was the first to suggest the use of an artificial small parameter to provide a singular perturbation structure. This analysis was later called forced singular perturbation analysis by Shinar and Farber (Shinar and Farber, 1984), where they analyzed the time-optimal pursuit-evasion game in the horizontal plane between two airplanes by applying the technique of forced singular perturbations ($FSPT$). They show that by assuming multiple time scale separation, a zeroth-order closed-form solution is obtained, which permits the use of realistic aerodynamic and propulsion data, which otherwise, without the time-scale separation, would be extremely difficult to include. Kelley (Kelley, 1971a) also uses multiple time-scales to conduct flight path optimization, discussing decoupling of high order three dimensional aircraft flight problem into several low order problems.

Ashley (Ashley, 1967) first suggested the use of multiple time scales in vehicle dynamic analysis by proposing multiple scaling as a systematic means for determining when motions occurring with distinctly different characteristic times can be decoupled during the analytical study of flight vehicle performance and dynamic behavior (Naidu and Calise, 2001). Ashley presented the basis for separating the problems of performance and dynamic response by identifying slowly varying control inputs and high lift-to-drag ratio, which results in temporarily omission of damping terms, thus defining a simple parameter whose smallness permits the short-period and phugoid modes to be separated, thus yielding approximate solutions for the frequency and decay rate of the short period.

In (Kelly and Edelbaum, 1986) three-dimensional maneuvers, both energy climbs and energy turns are addressed via singular perturbation by Kelly, and later theoretical works addressed problems for a two-state system (Kelley, 1970b) and horizontal plane control (Kelley, 1970a) of a rocket vehicle flight optimization using a model that includes rigid body degrees of freedom in boundary layer approximation to attitude transients. Other problems considered by Kelley were energy state models with turns (Kelley, 1971b) which considered flight path optimization with multiple time scales by discussing decoupling of high order three dimensional aircraft flight problem into several low order problems. Kelley (Kelley, 1973) also derives an alternate third-order model featuring instantaneously variable speed by means of time-scale separation, which provides an alternative to more complex particle-dynamics model that comprise three velocity and three position components.

Ardema (Ardema, 1976) applied the method of matched asymptotic expansions (MAE) to obtain an approximate solution to the vertical plane minimum time-to-climb problem, by obtaining outer, boundary-layer, and composite solutions for zeroth and first orders, although the zeroth-order solution proves to be a poor approximation, but the first-order solution gives a good approximation for both the trajectory and the minimum time-to-climb, which in addition shows that the computational cost of the singular perturbation solution is considerably less than that of a steepest descent solution

Breakwell (Breakwell, 1977) identified the vertical plane minimum-time problem where the dependence of drag (D) on lift (L) is suppressed by calculating the induced drag corresponding to the assumption that the lift is equal to the weight (W), that is $L = W$, therefore allowing to obtain the minimum-time climb path, which obtained by using either using the energy state analysis or by Green's Theorem, leads to discontinuities in the flight-path angle (γ). By considering the vertical plane minimum-time problem where D is much less than L, thus defining a natural singular perturbation parameter as of D/L dependent on Mach number, and demonstrating that the discontinuities in γ can be replaced by transitional boundary layers on time scales of the same order the value of the perturbation parameter D/L at the moment of the γ discontinuities. An extension of this work (Breakwell, 1978) show that the transitions satisfy, on an appropriate time scale, the identical fourth order system, not only when mass loss is taken into account in a minimum-time climb but also if the problem is changed, for example, to the maximum-altitude climb for given mass expenditure, and time being free.

All the works conducted until this point applied the theory of singular perturbation and time scales for aerospace systems to obtain open-loop optimal controls (Naidu and Calise, 2001). Calise, in a series of papers, focused on complete time scale separation and obtained closed-loop (feedback) controls. In particular, Calise (Calise, 1977b; Calise, 1978) developed a singular perturbation approach to extend existing energy management (EM) methods by outlining a procedure for modeling altitude and flight path angle dynamics which were previously ignored in EM solutions of the vertical plane minimum-time problem. Calise show that feedback solutions can be obtained, even for EM problem formulations which currently result in a two-point boundary value problem. The proposed methodology is general and applicable to solving a wide class of optimal control problems, which solves the *matching* problem that exists when applying singular perturbation theory to nonlinear problems, resulting in asymptotically stable boundary layer solutions as natural results of the presented approach.

Mehra *et al.* (Mehra et al., 1979) provide an excellent study devoted entirely to the application of singular perturbation theory to a variety of aerospace problems with special emphasis on real-time computation of nonlinear feedback controls for optimal three-dimensional minimum time long range intercept problem for an F-4 aircraft model given by six state, three control variable, and assuming a point mass model. Nonlinear feedback laws are presented for computing the optimal control variables, throttle, bank angle, and angle-of-attack, as a function of target and pursuer aircraft states and desired terminal conditions. These advances created a continuous and steady interest in this area of the application of singular perturbation and time scales to aerospace problems (Naidu and Calise, 2001).

Among others are Ardema (Ardema, 1983), which assesses the applicability and usefulness of several classical and other methods for solving the two-point boundary-value problem which arises in nonlinear singularly perturbed optimal control by analyzing and comparing the computational requirements associated with the studied algorithms (Picard, Newton and averaging types). Ardema and Rajan (Ardema and Rajan, 1985a), in which proposed two methods for time-scale separation analysis of dynamic systems, thus closing the existent gap of a nonexistent systematic application of singular perturbation methods for casting complex (high-order, highly coupled, highly nonlinear) aircraft trajectory optimization problems in a singular perturbation. The proposed methods are based on the concept of state variable speed and require knowledge only of the dynamical equations and bounds on state and control variables.

Kelley *et al.*(Kelley et al., 1986), review the minimum-time climbs in the energy approximation giving further consideration to the choice of variables, presenting a pair of variables which seems to offer an attractive replacement for altitude and air-speed in singular-perturbation procedures. Naidu and Price (Naidu and Price, 1988) present the results of applying the Singular Perturbations and Time Scales (*SPATS*) methodology to the control of digital flight systems. A block diagonalization method is described to decouple a full order, two time (slow and fast) scale, discrete control system into reduced order slow and fast subsystems.

Naidu and Price present a composite, closed-loop, suboptimal control from the sum of the slow and fast optimal feedback controls, and show that numerical results obtained for an aircraft model showed very close agreement between the exact (optimal) solution and the composite (suboptimal) solution which is computationally simpler and implies a considerable reduction in the overall computational requirements for obtaining the closed-loop, optimal control laws of digital flight systems.

In the area of flight mechanics, in order to provide appropriate performance analysis and develop precise guidance and control strategies, it is necessary the use of complex nonlinear equations, which are further complicated by the presence of aerodynamic and propulsive forces that are dependent on flight conditions in the form of stability derivatives which are often given in the form of tabular data. This resulted from the very beginning of the studies of aircraft performance analysis and design, in the use of simplified analysis models based on quasi-steady approximations. In a natural manner, the necessity of using these simplified examples translated into an increasing interest in singular perturbation methods in flight dynamics, which permitted an approximate analysis of an otherwise complicated optimization problem (Naidu and Calise, 2001).

The use of these simplified models and approximations provided an invaluable tool at the time they were originally introduced, when the use of high-speed digital computation and powerful numerical optimization algorithms based on either the calculus of variations or nonlinear programming were not available to solve optimal control problems in flight mechanics (Ashley, 1967; Kelley, 1971a; Kelley, 1970b; Kelley, 1973; Kelly and Edelbaum, 1986; Shinar and Farber, 1984). Despite the increase of computational power of today's computers, the development of simplified models, order reduction, and perturbation methods of analysis continue to play an important role since these methods lead to the development of near-optimal, closed-loop solutions, which in addition provide an insight view into the physics of the problem which is much harder to identify when analyzing the complete problem (Naidu and Calise, 2001).

Singular perturbation and time-scale analysis provide a mathematical realization of the inherent and intuitive analysis approach to simplified models obtained via order reduction, and probably, what it is most important the theory of singular perturbation and time scales provides a mechanism for correcting the solutions for the neglected dynamics that is essential to the development of guidance and control strategies for many aerospace systems such the slow phugoid mode and a fast short-period mode, which are well-know time-scale characteristics of the longitudinal motion of an airplane to any aerospace engineer (Naidu and Calise, 2001). This translates to the fact that singular perturbation and time scale analysis has been applied in almost all possible branches in aerospace control design, ranging from atmospheric flight control problems, pursuit-evasion and target interception problems, digital flight control systems, atmospheric reentry, satellite and interplanetary trajectories, missiles, launch vehicles and hypersonic flight, or orbital transfer to name few of the areas (Naidu and Calise, 2001).

In the area of atmospheric flight, Chen and Khalil (Chen and Khalil, 1990) use singular perturbation and time-scale analysis to obtain lower-order slow (phugoid) and fast (short-period) models. The accuracy of these models in approximating eigenvalues is demonstrated using typical numerical data for stable as well as unstable airplanes, and the slow and fast models are employed in a sequential design procedure to design a two-time-scale compensator for an unstable transport airplane (F-8 aircraft) by using a fast compensator first using the fast model; then a slow compensator is designed using a modified slow model. Menon *et al.* (Menon et al., 1987) design flight test trajectory control systems that enable the pilot to follow complex trajectories for valuating an aircraft within its known flight envelope and to explore the boundaries of its capabilities by using singular perturbation theory and the theory of prelinearizing transformations.

Ridgely and Banda (Ridgely et al., 1984) present a control system design that produces the tracking of command inputs and the decoupling of outputs of high-gain multivariable control systems applied to fighter/military aircraft (an experimental vertical/standard takeoff and landing aircraft) performing a number of maneuvers. Vian and Moore (Vian and Moore, 1989) present an interesting application of the singular perturbation method in time-controlled optimal flight trajectory involving a military aircraft that include the effects of risk from a threat environment by considering the horizontal plane aircraft motion using lateral equations, with the slow variables identified as the downrange position and aircraft mass, whereas cross-track position, energy height, and heading angle are identified as fast variables. Lateral and vertical algorithms are developed with the intent of near real-time application. A constant altitude, lateral flight-trajectory generation method is developed that optimizes with respect to time, fuel, final position, and risk exposure by using singular perturbation methods that obtain reduced-order airplane models that allow static rather than dynamic optimization. Pontryagin's Minimum Principle is used with a Fibonacci search method to minimize the cost functional.

Cliff *et al.* (Cliff et al., 1982) uses a simple singularly perturbed energy approximation point-mass three-dimensional aircraft model that incorporate thrust-vector control in aircraft optimization where for certain boundary conditions there are two families of extremal solutions giving rise to a Darbout locus. For aircraft with static thrust in excess of weight, a spectacular improvement in maneuverability is realized at energies low enough to permit hover, which in energy approximation, this amounts to instantaneous turn capability. Reiner *et al.* (Reiner et al., 1996) presents a robust linear controller with nonlinear feedback linearization to design robust dynamic inversion controllers. This methodology is applied to an angle-of-attack command system for longitudinal control of a high performance aircraft(model of the *NASA* high-angle-of-attack research vehicle) using feedback linearization coupled with structured singular value μ synthesis. Nonlinear simulations demonstrate that the controller satisfies handling quality requirements, provides good tracking of pilot inputs, and exhibits excellent robustness over a wide range of angles-of-attack and Mach numbers.

Ardema and Yang (Ardema and Yang, 1988) consider interior transition layers in vertical-plane climb path optimization. They treat the interior layer associated with the transonic energy state discontinuity as two boundary layers, one in forward time and the other in backward time. The initial states of the two boundary layers are matched to give continuous composite solutions at the point of reduced solution discontinuity. They show that the transition maneuver is relatively tolerant in terms of deviations from reduced solution values of load factor and flight path angle.

Avanzini *et al.* (Avanzini et al., 1999) present a method for the inverse simulation that is based on the idea of timescale separation (*TSS*). The proposed control strategy is based in the integration method, which has been extensively applied in the inverse simulation of aircraft motion where control inputs are determined once a maneuver or flight task is assigned, and where the concept of timescale separation is merged into an integration technique and a constrained optimization method, which solves some of the problems of accuracy and stability in the numerical algorithm that introduce the presence of multiple timescales and right half-plane transmission zeros in aircraft dynamics. The application of singular perturbation theory results in two subscale problems that are solved separately for the slow and fast timescales and a numerical algorithm is devised that presents significant advantages in terms of numerical efficiency and robustness, and that also deal with control saturation. Simulation results show that has improved performances of the proposed control strategy in comparison with an integration method that is based on the local optimization concept.

Many trajectory optimization problems, however, have discontinuous reduced-order solutions. Typical situations are the vertical-plane optimal climb problem when posed so that energy E is the single slow variable (Ardema, 1976; Ardema, 1977) and altitude h and velocity V are modeled as slow variables (Breakwell, 1977). For supersonic aircraft, the outer solution, that is, the energy climb path, is typically discontinuous in the transonic region (Rajan and Ardema, ; Weston et al., 1983). These discontinuities, which occur at interior points, give rise to instantaneous jumps called interior transition layers and have the nature of boundary (initial and final) layers.

In the area of optimal control control navigation and guidance (Ardema, 1980) presented a third-order, nonlinear, singularly perturbed optimal control problem defined by assumptions that define the full problem as a singular one, while the reduced problem becomes nonsingular. The separation scales resulted in the separation between the singular arc of the full problem and the optimal control law for the reduced problem which become hypersurfaces in state space. The boundary solutions are constructed such that are stable and reach the outer solution in a finite time, and a uniformly valid composite solution is then formed from the reduced and boundary-layer solutions and applied to obtain an approximate solution of a simplified version of the aircraft minimum time-to-climb problem. Calise (Calise, 1976) approached the solution of variational problems by singular perturbation methods, by provided the necessary tools to treat the singularities arising in problems where the control appears linearly and/or in state-constrained control problems, and also allowing to derive approximate feedback solutions for problem formulations if not treated with singular perturbation methods resulted in a nonlinear two-point boundary value problems that are applied to a three-dimensional minimum time turns for an F-106 and an F-4E aircraft. Calise (Calise, 1979; Calise, 1977a) also approaches the navigational guidance problem using singular perturbation methods to obtain optimal aerodynamic and thrust control laws. In (Calise, 1979) the use the application of singular perturbation methods to optimal thrust magnitude control and optimal lift control is applied to missiles restricted to the horizontal plane dynamics. The multiple time scaling procedure employed avoided the problems of selecting unknown adjoints to suppress unstable modes in the boundary layer when using asymptotic methods, and therefore permitting to reduce the two-point boundary value problems to a series of pointwise function extremizations, thus resulting in an analytic and algebraic optimal control solution

On the realm of helicopter singular perturbation control control, although the use of singular perturbation theory has been employed to simplify the control system structure (Heiges et al., 1992; Njaka et al., 1994; Prasad and Lipp, 1993; Hamidi and Ohta, 1995; Avanzini and de Matteis, 2001;

López-Martínez et al., 2007), to the knowledge of the author, the work conducted in this thesis, along with the articles presented by the author and his thesis co-directors in (Esteban et al., 2005b; Esteban et al., 2005b; Esteban et al., 2007; Esteban et al., 2008a), along with the work of Bertrand, Hamel and Piet-Lahanier (Bertrand et al., 2008), that presented a stability analysis of a hierarchical controller for an unmanned Aerial Vehicle, are the only works that theoretically addresses stability issues for *VTOL UAVs* using singular perturbation theory.

Heiges *et al.* (Heiges et al., 1992) use forced singular perturbation theory to reduced the order of a *6-DOF* helicopter model, thus reducing the twelfth-order nonlinear system of equations by separating the position (slow) and attitude (fast) dynamics, which leads to simpler transformations that are used to design a full-authority controller separately for each of the reduced order systems. The control strategy is developed analytically on the basis of nonlinear transformation theory. They provide details of the inverse transformation and the solution of the inverse kinematics problem, along with the description of the transformed linear feedback controller. The control strategy is simulated using the *NASA AMES* TMAN program (Lewis and Aiken, 1985) to simulate one-on-one Helicopter Air Combat at NOE (Nap-of-the-Earth).

Njaka *et al.* (Njaka et al., 1994) proposed singular perturbation theory as an alternative to common helicopter flight control strategies that rely heavily on plant models which have been linearized about various operating set points, and that translate into the use of linear controllers that are designed and scheduled to cover the operational flight envelope. Simplification of the control design process are conducted by dividing the rotorcraft dynamics into multiple time scales using the singular perturbation theory that results in a two-time-scale controller in which the fast dynamics of the rotational state components appear decoupled from the slower state components associated with translational dynamics. The controllers for the two resulting reduced-order dynamic systems are then designed separately, with commanded attitude output from the slow-time-scale system providing the necessary coupling between the controllers. The use of the fast-time-scale control law provides rotorcraft attitude stability augmentation while imparting the desired handling qualities, which alleviates the pilot's work load.

Prasad and Lipp (Prasad and Lipp, 1993) proposed a helicopter full authority flight controller using an approximate inversion of the nonlinear model of the vehicle, which is derived by recognizing the natural time scale separation between position and attitude dynamics of the helicopter. This translates into that the helicopter's attitudes are treated as pseudo-command variables. The controller is simplified by assuming approximations to the body axes forces, neglecting first the cyclic and pedal control force terms, and in a second approximation neglecting the body x- and y-axis force components in the controller calculations. Simulations are conducted to evaluate the control strategies in a nonlinear simulation model of the Apache helicopter, and tested using typical command maneuvers.

Hamidi and Ohta (Hamidi and Ohta, 1995) used singular perturbation theory to simplify the control system structure, which is based in nonlinear transformation theory to represent nonlinearities in the model of the system, yielding a new algorithm for the inverse nonlinear transformation of the control terms. They investigate the unmodeled system errors with nonlinear inverse dynamics theory, and show, via simulations, that the control system could track commanded values under the presence of modeling errors and disturbances.

Avanzini and de Matteis (Avanzini and de Matteis, 2001) developed and evaluated a fast and reliable multiple-timescale algorithm for the inverse simulation of rotorcraft maneuvering tasks. Avanzini used his own previous work (Avanzini et al., 1999) based on a two-timescale approach to the solution of inverse problems of aircraft motion represents the background for devising a technique that accounts for specific issues of rotorcraft dynamics such as the large effects of the fast, primary moment generating controls on the slow dynamics associated to the vehicle trajectory and the system being frequently non minimum phase. The inverse simulations provide accurate solutions of the fast and slow reduced-order systems due to the fact that the quasi-steady-state values of the fast controls are considered in the slow timescale. They identify non observable motions that are ruled out by the multiple timescale approach, and via simulations show that the expected computer time reduction is realized, that the well-known difficulties of inverse methods for finding feasible solutions at convergence are practically eliminated, and, finally, that steady-state flight conditions are accurately recovered at the end of the prescribed maneuvers.

López *et al.* (López-Martínez et al., 2007) presented the problem of a nonlinear L_2-disturbance rejection design for a laboratory twin-rotor system, in which control is only achieved via rotor speed, since the collective pitch angle is fixed for both rotors. The control strategy is derived considering a reduced order model of the rotors obtained by application time-scale separation, which also includes integral terms on the tracking error to deal with persistent disturbances. An explicit suboptimal solution to the associated partial differential ($HJBI$) equation is applied, which yields global asymptotical stability for the reduced system, where the control is of the form of a partial feedback linearization with an external nonlinear PID, which is tested in a experimental laboratory twin rotor.

Bertrand *et al.* (Bertrand et al., 2008) presented the stability analysis of a hierarchical controller of a two-time-scale $VTOL$ UAV using singular perturbation theory. Control laws are derived using time-scale separation between the translational dynamics and the orientation dynamics of a six degrees of freedom $VTOL$ UAV model to regulate both position and attitude control. They assume that the linear velocity is not measured, and thus a partial state feedback control law is proposed, based on the introduction of virtual states in the translational dynamics of the system. They also identify that although reduced-order subsystems can be considered for control design, the stability must be analyzed by considering the complete closed loop system, which in the realm of $VTOL$ aircraft systems, to the knowledge of the author, has only been addressed by Bertrand *et al.* (Bertrand et al., 2008) and the work conducted by Esteban *et al.* (Esteban et al., 2005b; Esteban et al., 2005b; Esteban et al., 2007; Esteban et al., 2008a).

This concludes the review of the literature section, which only intended to touch the surface of general control strategies in aerospace systems, specially in helicopter, and how singular perturbations and time-scale methods have been applied to both general aerospace systems and helicopter. Extensive reviews on the singular perturbation and time-scale methods in aerospace systems can be found in (Naidu and Calise, 2001), and literature reviews in singular perturbation and time-scales in general can be found in (Kokotović et al., 1976; Vasil'Eva, 1976; Saksena et al., 1984; Kokotović, 1984; Kokotović, 1985; O'Malley Jr, 1991; Vasil'Eva, 1994; Naidu, 2002).

This page intentionally left blank

Chapter 2

Helicopter Dynamics

2.1 Introduction to the Helicopter System

The principle objective of this chapter is to provide an insight view that helps to understand the dynamics of the problem here investigated, rather than treating the problem as just a plant. From a control designer perspective, having a priori knowledge of the physics of the plant is not a requirement, but it helps to ensure that the chosen control strategy is pushing in the same direction as the natural behavior of the system being analyzed. Furthermore, the aerospace background of the author has provided an additional edge in determining the natural times-scales appearing in the helicopter, which, as it will be seen in section 3.5, although the mathematics does generally provide criteria to determine the existence and the determination of time-scales, the physics of the problem, and knowledge of the natural behavior of the system, makes time-scale identification and selection of appropriate singularly perturbed parameters that determine the different boundary layers a much simpler task.

This chapter also derives the necessary tools to obtain the dynamics of the helicopter model here studied, making special emphasis on the modelization of the thrust force that drives the helicopter in axial flight. Some of the proposed models will reproduce with higher fidelity the helicopter dynamics in axial flight by using discontinuous functions, but, due to restrictions on the proposed control strategy, and the stability methodology, both the system being studied, and the selected control, being required to be continuously differentiable at every point, only one of the proposed models will be selected. The selected model represents a degeneration of the axial flight, which is the condition of hovering flight, but it will be demonstrated that will be a valid approximation model due to the characteristic maneuvers of the helicopter being studied. The rest of the models, which include the more precise and discontinuous models, will be used as test bench models to test both validity of the proposed control strategy, and robustness under unmodeled dynamics.

Many definitions of what is a helicopter can be found on the literature, being one of these the definitions the one that appears in (McLean, 1990) "helicopters are a type of aircraft known as rotorcraft, for they produce the lift needed to sustain flight by means of a rotating wing, the rotor". A more technical definition is provided by The International Civil Aviation Organization ($ICAO$) which defines the helicopter as a "heavier-than-air aircraft supported in flight chiefly by the reactions of the air on one or more power-driven rotors on substantially vertical axes" (The International Civil Aviation Organization, 2009), or a more general definition such the one that states that the helicopter is a type of rotorcraft in which the necessary forces to maintain flight, lift and thrust, are supplied by one or more engine driven rotors. All these definitions focus on the unique feature that helicopters have the possibility of directing the thrust vector in any selected direction. Is this unique feature that permits the helicopter to take off and land vertically, to hover, and to fly forwards, backwards and laterally, which makes them much more versatile than the fixed-wing aircraft. But this flexibility comes at the price of the complexity of the dynamics that govern such systems.

The model definition will be done by first giving an introduction to all the systems that compose the helicopter and a basic introduction of how they work in section 2.2. This can be extended to any single rotor helicopter, from an Radio-Control (R/C) helicopter, to a multi-purpose military helicopter; section 2.3 provides an introduction to the helicopter dynamics and the reference coordinate system employed, while section 2.4 introduces the non-linear six-degrees-of-freedom (*6-DOF*) models, and the simplified helicopter models that are historically used to study in more detail the decoupled longitudinal, lateral-directional, and axial flight dynamics. Section 2.5 describes the perturbed state equation that leads to the axial flight model that will be derived in detail in section 2.6 with the definition of the proposed thrust/lift models for a rotor, the proposed closed-form solutions for the thrust coefficient model C_T are presented in 2.7, and finally the derivation of the proposed helicopter model is given in section 2.8, while the derivations of the alternative and more precise models are sent to Appendix A for completeness of the thesis since the derivations might become cumbersome for the reader. It is also advised to the reader that for easiness of the reading process, if only interested in the selected model that is studied in this thesis, and not with the mathematical derivation process, proceed to section 2.8.

2.2 Helicopter Systems

Although there are many types of helicopters depending on number and configuration of the rotors, from single rotor, to tandem, intermeshing, transverse or coaxial helicopters, this thesis focuses only on the single main rotor type. Figure 2.1 describes the types of helicopter regarding the type of rotors, where the one that is the focus of this document is the center one, the single main rotor. A single main rotor helicopter, and in general most helicopters, are formed primarily by a main rotor, tail rotor, fuselage, engine, fuel tank, transmission, mast, tail rotor drive shaft, tail fin, horizontal fin, and landing skid. Figure 2.2 in a more simple way, and Figure 2.3 with a little more detail show the schematic representation of the major components of a helicopter, which are described in more detail bellow (Federal Aviation Administration, 2000).

The principal element that makes helicopters such a versatile aircraft is the rotor system. The rotor system is the rotating part of a helicopter which generates main component of lift. A rotor system may be mounted horizontally as main rotors are, providing lift vertically, or it may be mounted vertically, such as a tail rotor, to provide lift horizontally as thrust to counteract torque effect. A helicopter main rotor, is a type of fan that is used to generate both the aerodynamic lift force that supports the weight of the helicopter, and the thrust force which counteracts the aerodynamic drag in forward flight. Each main rotor is mounted on a vertical mast over the top of the helicopter, as opposed to a helicopter tail rotor, which is connected through a combination of drive shaft(s) and gearboxes along the tail boom. A helicopter's rotor is generally made up of two or more rotor blades. The amount of lift generated by the rotor can be varied by either the blade pitch or the angular velocity of the main rotor, which is ultimately connected with the engine's *RPM*. The blade pitch is typically controlled by a swash plate connected to the helicopter flight controls.

The swash plate is a device that translates input via the helicopter flight controls into motion of the main rotor blades, which effectively modify the forces and moments acting on the helicopter. Because the main rotor blades are spinning, the swash plate is used to transmit three of the pilot's commands from the non-rotating fuselage to the rotating rotor hub and main blades. These three commands can be seen in Figure 2.4 denoted with the black link for the collective pitch, the yellow for the longitudinal cyclic, and the pair pink and blue for the lateral cyclic. The following section describes in more detail each of the control actions. The swash plate consists of two main parts: a stationary swash plate and a rotating swash plate, which can be better observed in a typical swash plate of a R/C helicopter in Figure 2.5, where the blue component, denoted with the number 1, represents the non-rotating outer ring or swash plate, while the turning inner ring is denoted in silver, denoted with the number 2. The stationary (outer) swash plate is mounted on the main rotor mast and is connected to the cyclic and collective controls by a series of pushrods. The swash plate is able to tilt in all directions and move vertically. The rotating (inner) swash plate is mounted to the stationary swash plate by means of a bearing and is allowed to rotate with the main rotor mast. An anti-rotation link prevents the inner swash from rotating independently of the blades, which would apply torque to the actuators. The outer swash typically has an anti-rotation slider as well to prevent it from rotating. Both swash plates tilt up and down as one unit. The rotating swash plate is connected to the pitch horns by the pitch links, which are denoted in silver and with the number 6, as seen in Figure 2.5. The outer non-rotating swash plate receives the pilot commands through the control links as it can seen in Figure 2.4 with the black, yellow, and the pair pink and blue control links.

The mast is a cylindrical metal shaft which extends upwards from and is driven by the transmission. At the top of the mast is the attachment point for the rotor blades, also called the hub. The rotor blades are then attached to the hub by a number of different methods. Main rotor systems are classified according to how the main rotor blades are attached and move relative to the main rotor hub. There are three basic classifications: rigid, semirigid, or fully articulated, although some modern rotor systems use an engineered combination of these types.

The tail rotor, or anti-torque rotor, is a smaller rotor mounted so that it rotates vertically or near-vertically at the end of the tail of a traditional single-rotor helicopter. The tail rotor's position and distance from the center of gravity allow it to develop thrust in the same direction as the main rotor's rotation which in results serves as to counter the torque effect created by the main rotor as seen in Figure 2.6. Tail rotors are simpler than main rotors since they require only collective changes in pitch to vary the amount of thrust. The pitch of the tail rotor blades provides also directional control by allowing the pilot to rotate the helicopter around its vertical axis.

The tail rotor drive system consists of a shaft powered from the main transmission and a gearbox mounted at the end of the tail boom. The drive shaft may consist of one long shaft or a series of shorter shafts connected at both ends with flexible couplings, that allow the drive shaft to flex with the tail boom. The gearbox at the end of the tailboom provides an angled drive for the tail rotor, and may also include gearing to adjust the output to the optimum rotational speed for the tail rotor. Figure 2.7 shows a conventional helicopter rotor drive system. For more details see references (Prouty, 1986; Leishman, 2006; López and Valenzuela, 2010; Cuerva et al., 2009).

2.2.1 Helicopter Flight Controls

A helicopter pilot manipulates the helicopter flight controls in order to achieve controlled aerodynamic flight (Gablehouse, 1967; Gablehouse, 1969). The changes made to the flight controls are transmitted mechanically to the rotor, producing aerodynamic effects on the helicopter's rotor blades which allow the helicopter to be controlled. For tilting forward and back (pitch), or tilting sideways (roll), the angle of attack of the main rotor blades is altered cyclically during rotation, creating different amounts of lift at different points in the cycle. For increasing or decreasing the overall lift, the angle of attack for all the blades is collectively altered by equal amounts at the same time resulting in ascents, descents, acceleration and deceleration.

A helicopter has four flight control inputs. These are the cyclic, the collective, the tail rotor collective, and the throttle. The first control input is called the cyclic because it changes the pitch of the rotor blades cyclically. Cyclic controls are used to change a helicopter's roll and pitch. Push rods or hydraulic actuators tilt the outer swash in response to the pilot's commands. The swash plate, depending in the mode in which the links are connected, moves in the intuitively expected direction, tilting forwards to tilt the rotor "disc" forwards, for instance, but "pitch links" on the blades transmit the pitch information ahead of the blade's actual position, giving the blades time to "fly up" or "fly down" to reach the desired position which creates a difference of lift around the blades, and the helicopter will tilt towards the side with lower lift (Federal Aviation Administration, 2000).

This results in that the pitch angle of the rotor blades changes depending upon their position as they rotate around the hub so that all blades will change their angle the same amount at the same point in the cycle. The change in cyclic pitch has the effect of changing the angle of attack and thus the lift generated by a single blade as it moves around the rotor disk. This in turn causes the blades to fly up or down in sequence, depending on the changes in lift affecting each individual blade (Federal Aviation Administration, 2000).

The net result is that, for conventional swash place combinations as the one treated in this thesis, when tilting the rotor disk in a particular direction, the main rotor forces tilt also in that direction. If the pilot pushes the cyclic forward, the rotor disk tilts forward, and the rotor produces a thrust vector in the forward direction as seen in Figure 2.8 while if the pilot pushes the cyclic rearward, the rotor disk tilts rearward, and the rotor produces a thrust vector in the rearward direction as seen in Figure 2.9. If the pilot pushes the cyclic to the right, the rotor disk tilts to the right and produces thrust in that direction, causing the helicopter to move sideways and roll in a hover, or to roll into a right turn during forward flight as seen in Figure 2.10, much as in a conventional aircraft (Federal Aviation Administration, 2000).

On any rotor system there is a delay between the point in rotation where a change in pitch is introduced by the flight controls and the point where the desired change is manifest in the rotor blade's flight. While often discussed as gyroscopic precession (Department of the Army, 2007), this phase lag varies with the geometry of the rotor system it can be defined as the time it takes for the blade to change its flapped position after a change in lift. The lag is an example of a dynamic system in resonance but is never more than ninety degrees.

The collective pitch control, or collective, changes the pitch angle of all the main rotor blades collectively (i.e. all at the same time) and independently of their position. Therefore, if a collective input is made, all the blades change equally, and the result is the helicopter increasing or decreasing in altitude due to a change in vertical velocity if in hover, as seen in Figure 2.11 (Federal Aviation Administration, 2000), and an additional increase in forward speed if the helicopter was moving forward.

To control the collective pitch of the main rotor blades, the entire swash plate must be moved up or down along its axis without changing the orientation of the cyclic controls. Conventionally, the entire swash plate is moved along the main shaft by a separate actuator. However, some newer model helicopters remove this mechanically complex separation of functionalities by using three interdependent actuators that can each move the entire swash plate, as seen by the three control links in Figure 2.4, number 3. When the three control links are moved uniformly up or down, they actuate as collective pitch, and when they move with a prescribed combination of the control links provide the cyclic longitudinal and lateral motions. This is called cyclic/collective pitch mixing (Federal Aviation Administration, 2000).

The collective tail rotor provide control in the direction in which the nose of the aircraft is pointed. The application of the collective tail rotor changes the pitch of the tail rotor blades, which increases or reduces the thrust produced by the tail rotor, thus causing the nose to yaw in the opposite direction in which the thrust is increased. Helicopter rotors are designed to operate at a specific *RPM*, which is actually proportional to the main rotor *RPM*, implying that a change in the main rotor angular velocity translates in a change in the thrust produced by the tail rotor, that is a yawing moment that needs to be compensated. And finally, the throttle controls the power produced by the engine, which is connected to the rotor by a transmission. The purpose of the throttle is to maintain enough engine power to keep the rotor *RPM* within allowable limits in order to keep the rotor producing enough lift for flight (Federal Aviation Administration, 2000).

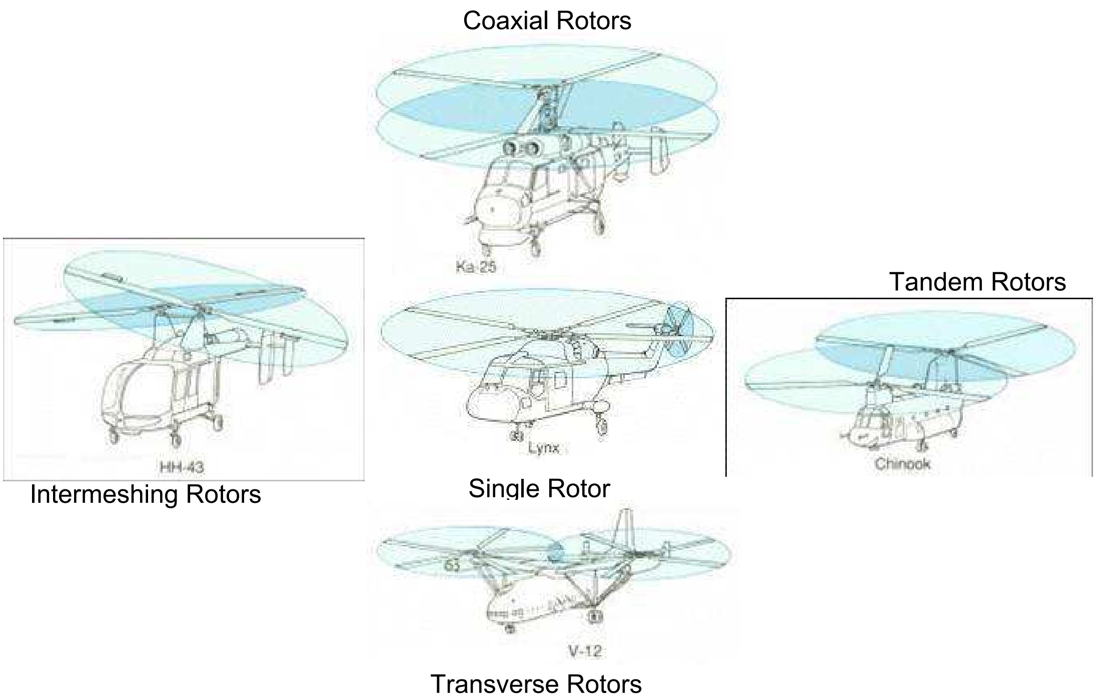

Figure 2.1: Types of helicopters according to the Type of Rotor

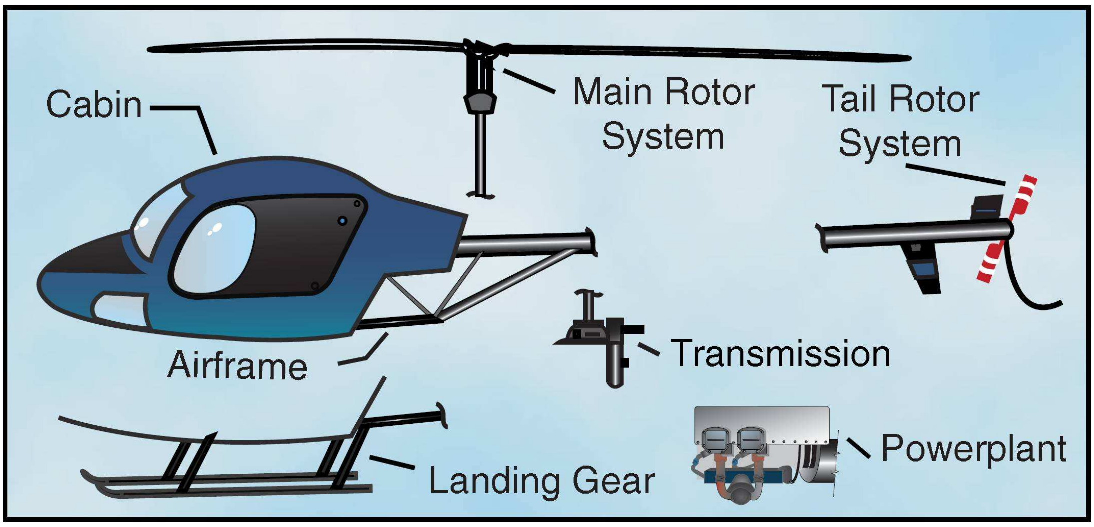

Figure 2.2: Major helicopter components (Federal Aviation Administration, 2000).

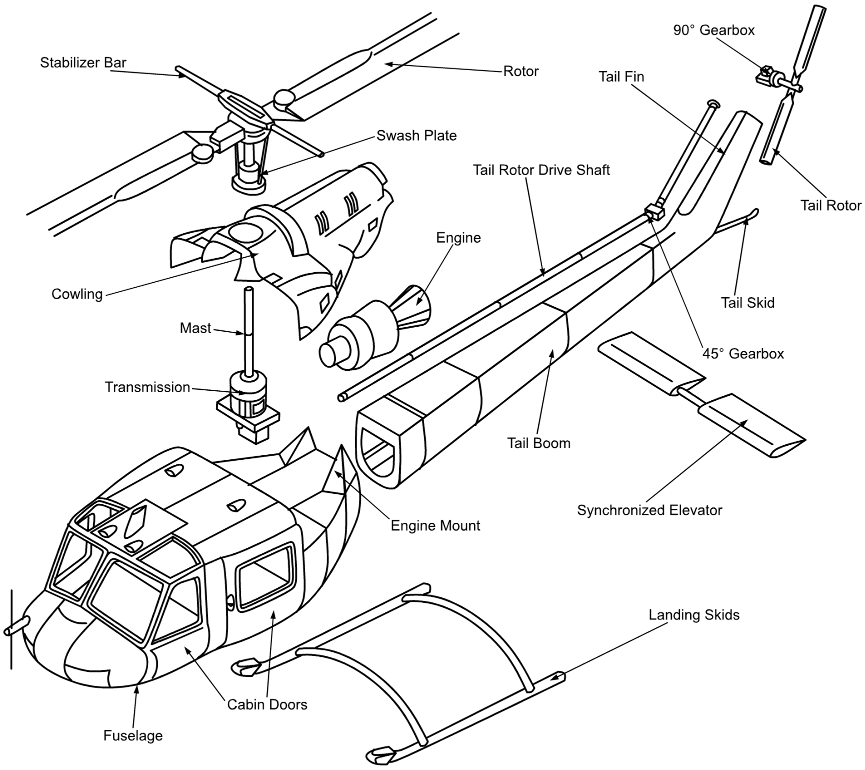

Figure 2.3: Schematic representation of the major components of a helicopter ((Zephyris), 2005)

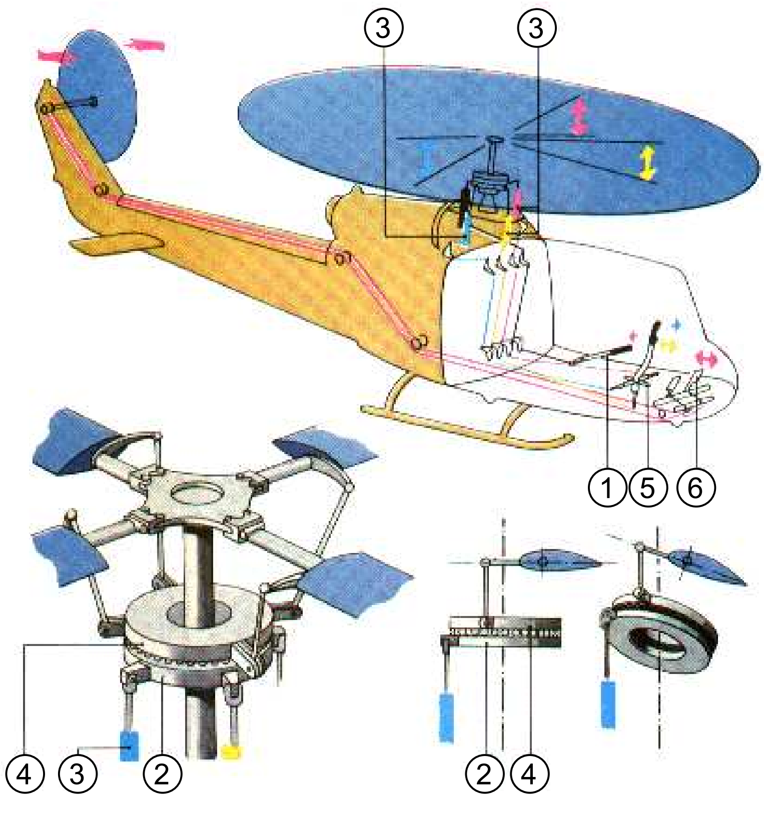

Figure 2.4: Flight controls on a helicopter

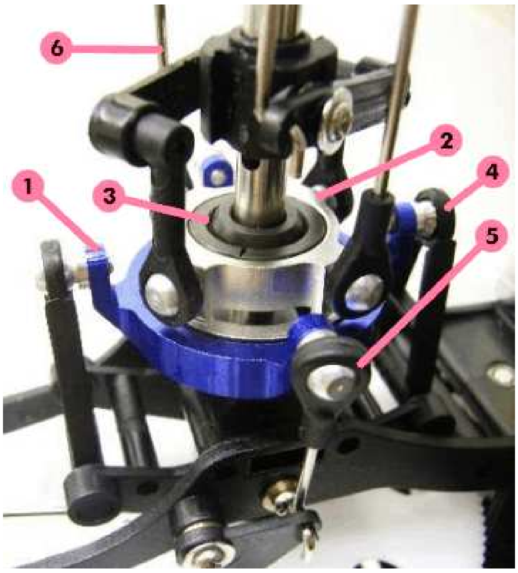

1. Non-rotating outer ring (blue)
2. Turning inner ring (silver)
3. Ball joint
4. Control (pitch) preventing turning of outer ring
5. Control (roll)
6. Linkages (silver) to the rotor blade
7. Linkages (black) that make the inner ring turn

Figure 2.5: Swashplate on a radio-controlled helicopter (Gruss Guido Büscher, RC-Discount, 2006)

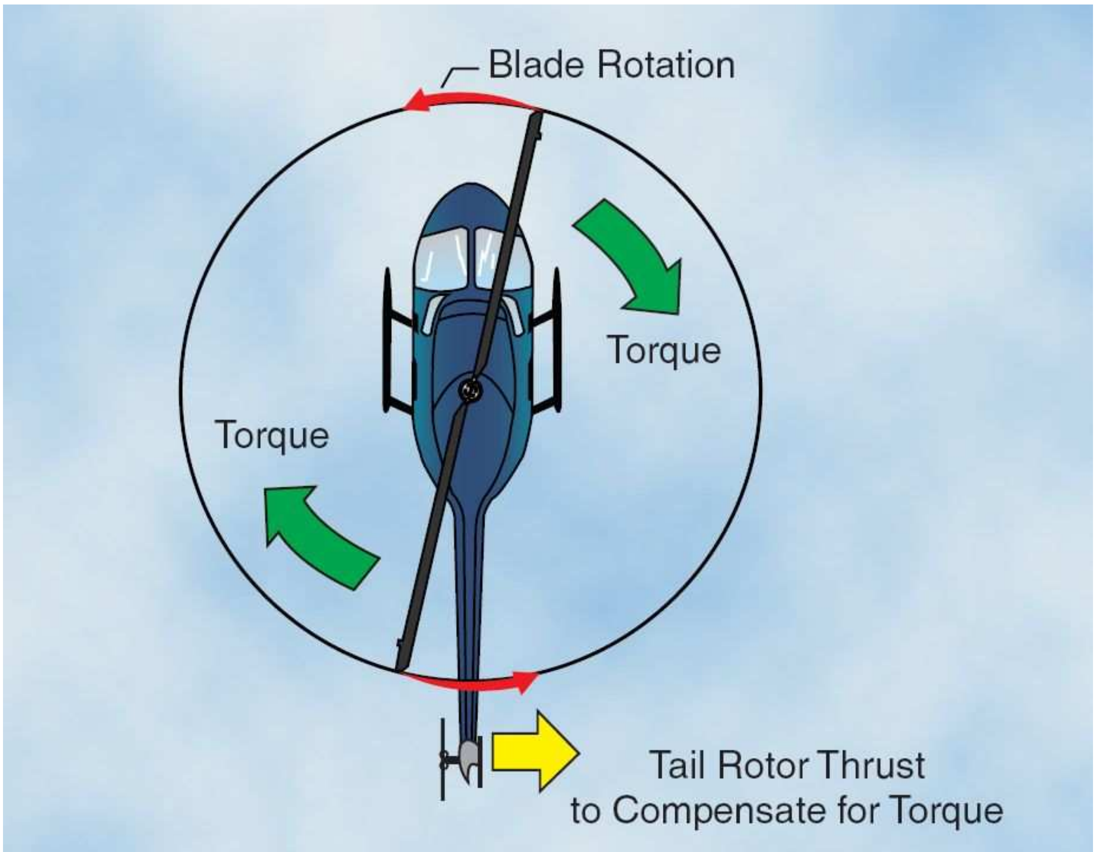

Figure 2.6: Description of helicopter torque effect (US DoT - FAA, 2006b) (Federal Aviation Administration, 2000).

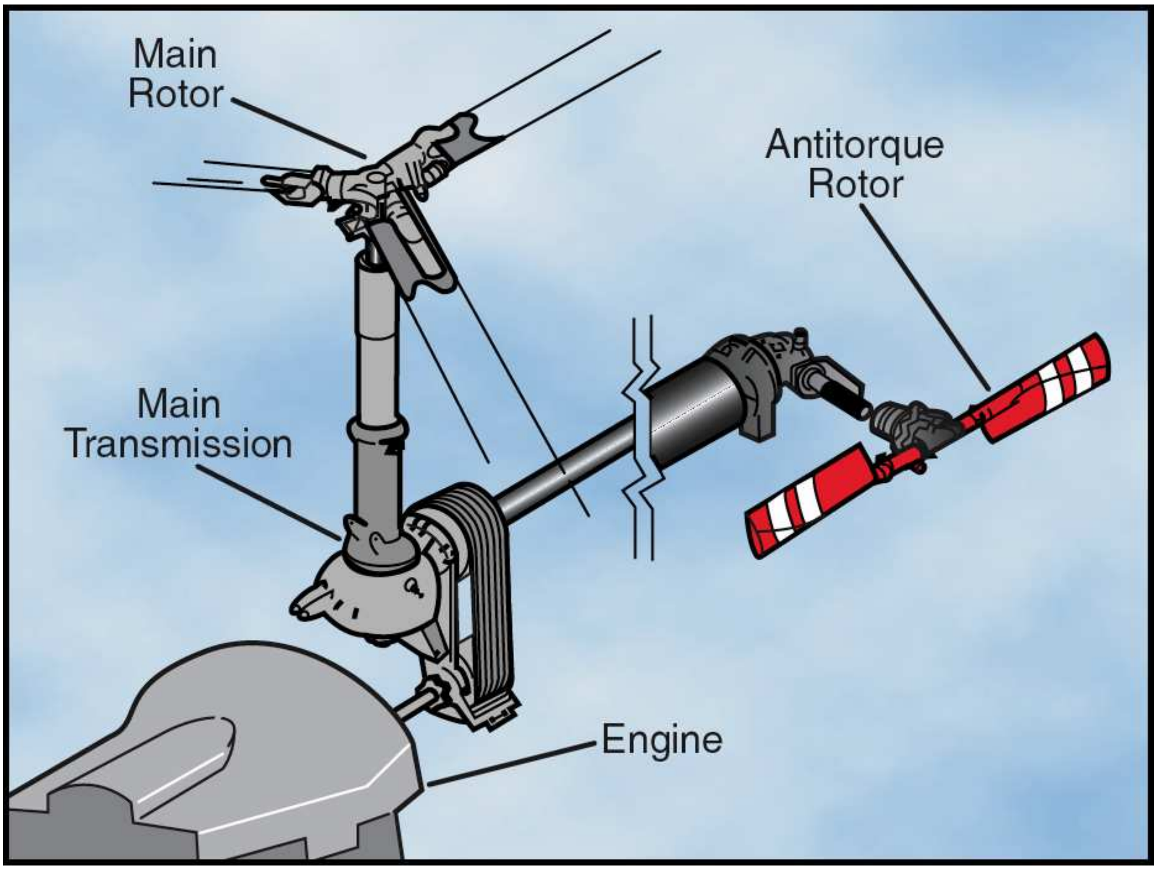

Figure 2.7: Helicopter rotor drive system (US DoT - FAA, 2006a) (Federal Aviation Administration, 2000).

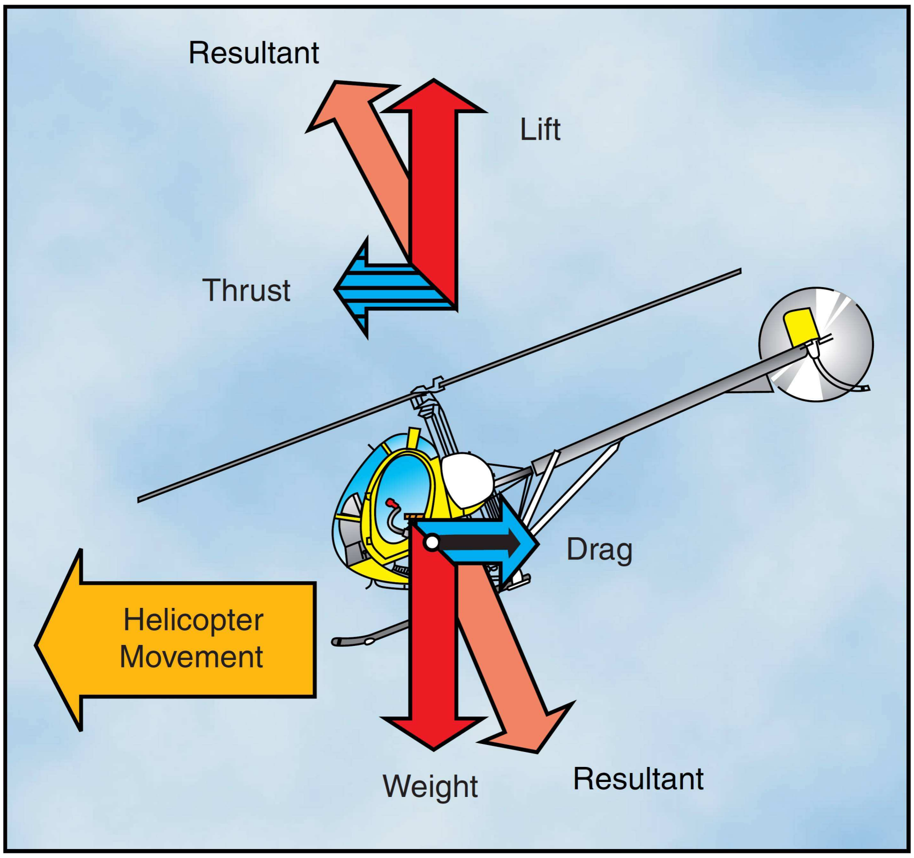

Figure 2.8: Helicopter forward flight (Federal Aviation Administration, 2000).

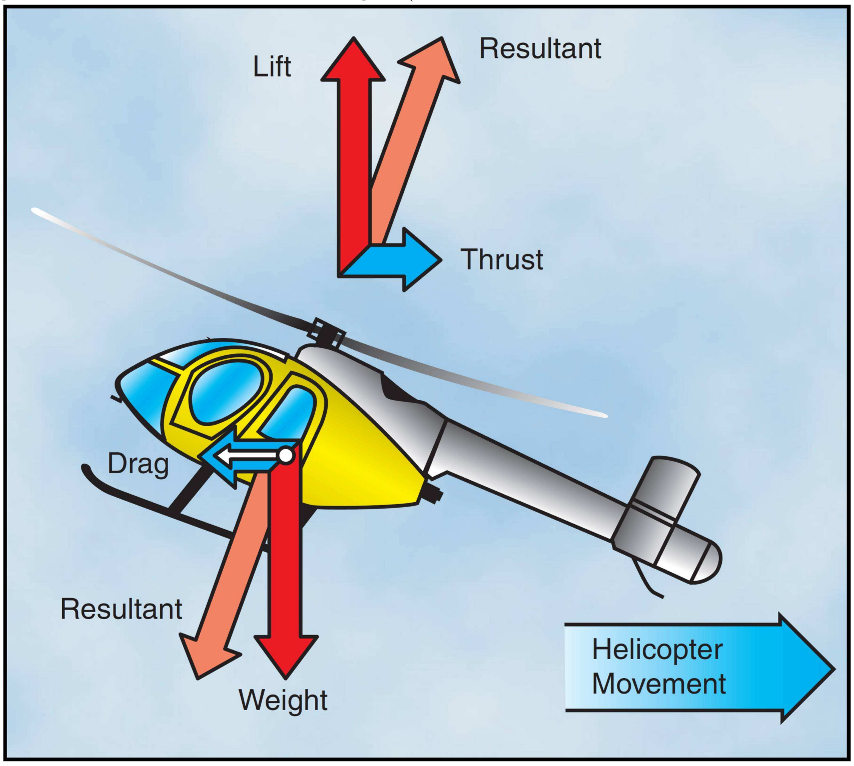

Figure 2.9: Helicopter Rearward Flight (Federal Aviation Administration, 2000).

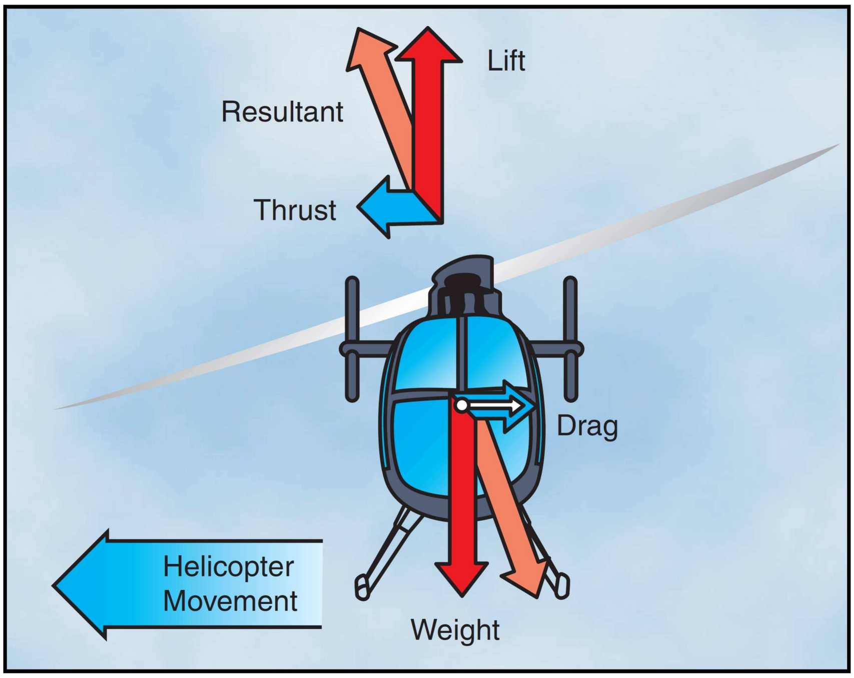

Figure 2.10: Helicopter sideward flight (Federal Aviation Administration, 2000).

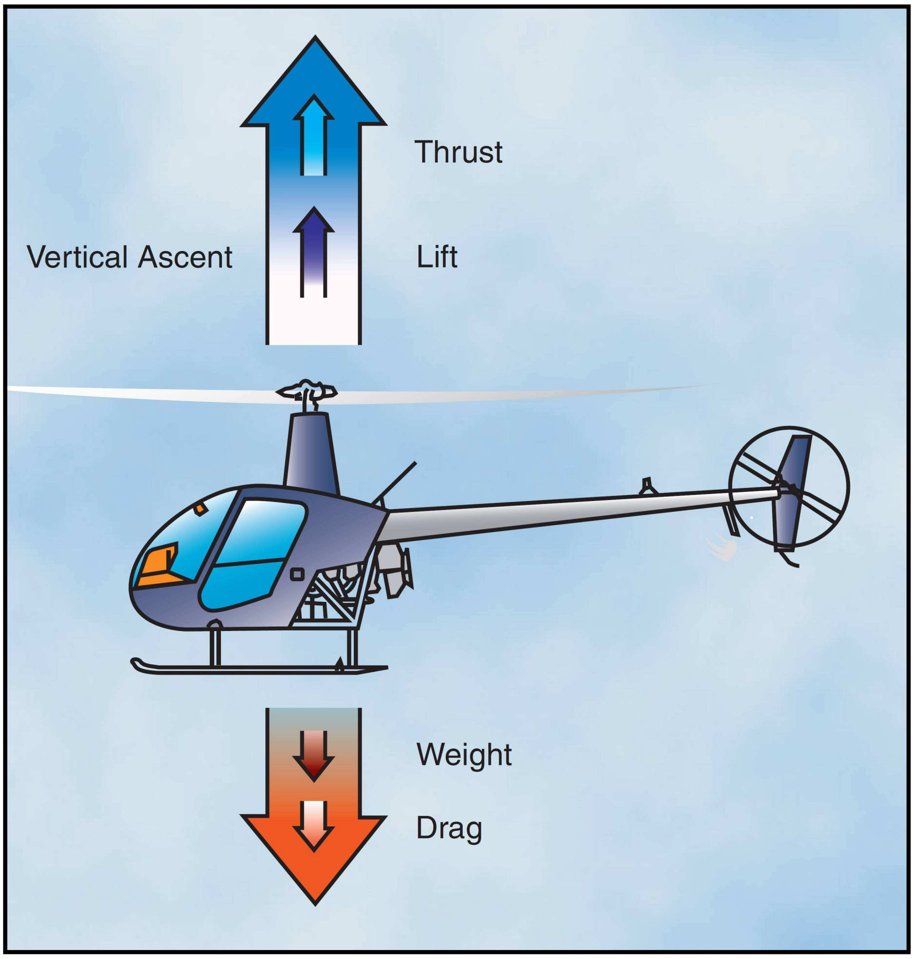

Figure 2.11: Helicopter axial flight (Federal Aviation Administration, 2000).

2.3 Helicopter Dynamics

The relative movement of some of the helicopter components such the main or the tail rotor, or the moving parts of its engines, can be taken into account in the equations of motion in many different ways, such as external forces, inertial actions associated to the change in momentum, or angular momentum due to the relative motion of these components. The acting external forces can be divided into aerodynamic, propulsive and gravitational forces, and the estimation of these forces represents one of the most challenging tasks when dealing with helicopter modeling.

The stabilization of a helicopter requires that the sum of the external forces acting on the system to be identically zero, where, in these conditions, the movement of the center of mass with respect to a selected inertial reference system is uniform and rectilinear, and the position of the space axes with respect to the inertial reference system does not change with time (López Ruiz, 1993). In order to better understand the problem of helicopter stabilization, it is necessary to define the dynamics of the helicopter with respect to a inertial reference coordinate system, where the dynamics of the helicopter, and in general of any aerospace system is decomposed in two parts:

- The movement of its center of mass, which is considered fixed in the helicopter, although the fuel consumption or the shift of onboard masses might induce slight center of mass variations with respect to its reference system
- The movement of the rigid solid or the characteristic three-axes-system with respect to a parallel inertial reference system.

The two dynamics decomposition refer to distinct problems, where the first one represents the dynamics associated to a point-mass (the center of mass) which is subject to external forces, while the second type of dynamics represents the dynamics of a rigid solid with a fixed point subject to the external forces which, at the same time produce a moment with respect to the fixed point. Both problems are quite similar since the aerodynamic forces acting on the helicopter depend both on the rotational and translational velocities of the elements that generate those external forces, i.e. the main and tail rotor. In addition, the forces acting on the helicopter can also be modified by acting on the geometry itself through the rotor actuators, although both dynamic problems are studied separately. Following sections describe the reference coordinate system that will help in the task of defining the appropriate dynamic model.

2.3.1 Reference Coordinate Systems

In order to better understand the model that will be used in the formulation for the nonlinear singular perturbation helicopter model, which is introduced in section 2.8, it is necessary to define the equations that govern the motion of a rigid helicopter. Several references (Padfield, 2007; Prouty, 1986; Cooke et al., 2002; López Ruiz, 1993; Cuerva et al., 2009) will be used throughout the reminder of this section, to define the helicopter's equations of motion, and the reference system where these equations are valid. Figure 2.12 shows the two systems used to define the equations that govern the motion of a rigid airplane, the Earth-fixed system and the airplane body-fixed system. The Earth-fixed system is denoted by $X^{'}Y^{'}Z^{'}$, which will be considered the inertial reference frame in which the Newton's laws of motion are valid. This model reference neglects rotational velocity of the Earth. The helicopter body fixed system is defined by XYZ.

The XYZ helicopter body fixed system is fixed relative to the helicopter, where the positive X axis is along the fuselage, the positive Y axis is along the starboard (right) side of the fuselage, and the positive Z axis is directed downward, perpendicular to the XY plane as shown by the directions of the arrows in Figure 2.12. The origin is located at the geometric center of gravity. The translational motion of the helicopter is given by the components of the velocity: forward velocity (U), side-slip velocity (V), and downward velocity (W) which are directed along the X, Y, and Z directions, respectively. The free stream velocity, V_∞, represents the vector sum resultant of the velocity components, U, V, and W. The rotational motion is given by the angular velocity components: roll rate (P), pitch rate (Q), and yaw rate (R), about the X,Y, and Z axes respectively. These rotational velocities are due to the moments about the helicopter body-fixed system: roll moment (L), pitch moment (M), and yaw moment (N) about the X,Y, and Z axes, respectively.

The helicopter is assumed to consist of continuum mass elements, dm, as seen in Figure 2.12, that are kept track by a series of vectors, $\mathbf{r}$, which connect the origin $X^{'}Y^{'}Z^{'}$ with each mass element. Each mass element is subject to the acceleration of gravity, $\mathbf{g}$, which is assumed to be oriented along the positive Z'-axis of the Earth-fixed coordinate system, thus assuming that the Earth is flat. This creates a gravitational force acting in each element mass equal to $\rho_H \mathbf{g}\mathrm{dv} = \mathbf{g}\mathrm{dm}$, where ρ_H represents the local mass density of the helicopter and dv is a helicopter volume element. The elements that are located in the surface of the helicopter are also subject to combined aerodynamic and thrust forces per unit area denoted by $\mathbf{F}$. These aerodynamic and thrust-combined forces will be expanded in the next section.

The orientation of the aircraft relative to the Earth-fixed coordinate system $X^{'}Y^{'}Z^{'}$, is obtained by introducing three sequential rotations over the Euler angles: heading angle (Ψ), the pitch attitude angle (Θ), and the bank o roll angle (Φ). In order to keep track of the three sequential rotations, the Earth-fixed coordinate system $X^{'}Y^{'}Z^{'}$ is redefined with $X_1Y_1Z_1$. The first rotation is produced by rotating the coordinate system $X_1Y_1Z_1$ over an angle Ψ so that the helicopter is taken to its heading angle after which the coordinate system is re-labeled $X_2Y_2Z_2$. Figure 2.13 shows the first rotation. The change of coordinates between the Earth-fixed coordinate system $X_1Y_1Z_1$ and the new coordinate system $X_2Y_2Z_2$ is given by the transformation matrix

$$\left\{\begin{array}{c} X_2 \\ Y_2 \\ Z_2 \end{array}\right\} = \left[\begin{array}{ccc} \cos\Psi & \sin\Psi & 0 \\ -\sin\Psi & \cos\Psi & 0 \\ 0 & 0 & 1 \end{array}\right]\left\{\begin{array}{c} X_1 \\ Y_1 \\ Z_1 \end{array}\right\}. \tag{2.1}$$

The second rotation is produced by rotating the coordinate system $X_2Y_2Z_2$ over a pitch attitude angle Θ after which the coordinate system is re-labeled $X_3Y_3Z_3$. Figure 2.14 shows the second rotation, where the change of coordinates between the coordinate system $X_2Y_2Z_2$ and the coordinate system $X_3Y_3Z_3$ is given by the transformation matrix given by

$$\left\{\begin{array}{c} X_3 \\ Y_3 \\ Z_3 \end{array}\right\} = \left[\begin{array}{ccc} \cos\Theta & 0 & -\sin\Theta \\ 0 & 1 & 0 \\ \sin\Theta & 0 & \cos\Theta \end{array}\right]\left\{\begin{array}{c} X_2 \\ Y_2 \\ Z_2 \end{array}\right\}, \tag{2.2}$$

and a third, and final, rotation is conducted about a roll angle Φ to reach the body-fixed coordinate system XYZ. Figure 2.15 shows the final rotation, where the change of coordinates between the coordinate system $X_3Y_3Z_3$ and the body-fixed coordinate system XYZ is given by the transformation matrix given by

$$\left\{\begin{array}{c} X \\ Y \\ Z \end{array}\right\} = \left[\begin{array}{ccc} 1 & 0 & 0 \\ 0 & \cos\Psi & \sin\Psi \\ 0 & -\sin\Psi & \cos\Psi \end{array}\right]\left\{\begin{array}{c} X_3 \\ Y_3 \\ Z_3 \end{array}\right\}. \tag{2.3}$$

Figure 2.16 shows the three sequential rotations from the point of view of an observer far away from the reference coordinate systems. With this in mind, the relation between the Earth fixed coordinate system and the helicopter body fixed system can be defined as

$$
\begin{aligned}
X &= X^{'}\cos\Theta\cos\Psi + Y_T\cos\Theta\sin\Psi - Z^{'}\sin\Theta, && (2.4)\\
Y &= X^{'}(\sin\Phi\sin\Theta\cos\Psi - \cos\Phi\sin\Psi) + \\
&\quad Y^{'}(\sin\Phi\sin\Theta\sin\Psi + \cos\Phi\cos\Psi) + Z^{'}\sin\Phi\cos\Theta, && (2.5)\\
Z &= X^{'}(\cos\Phi\sin\Theta\cos\Psi + \sin\Phi\sin\Psi) + \\
&\quad Y^{'}(\cos\Phi\sin\Theta\sin\Psi - \sin\Phi\cos\Psi) + Z^{'}\cos\Phi\cos\Theta, && (2.6)
\end{aligned}
$$

where, equations (2.4), (2.5) and (2.6) describe the three rotations that generate the body-fixed axis kinematic equations given by

$$
\begin{aligned}
\dot{\Phi} &= P + (Q\sin\Phi + R\cos\Phi)\tan\Theta, && (2.7)\\
\dot{\Theta} &= Q\cos\Phi - R\sin\Phi, && (2.8)\\
\dot{\Psi} &= \frac{Q\sin\Phi + R\cos\Phi}{\cos\Theta}, && (2.9)
\end{aligned}
$$

which can also be expressed as

$$
\begin{aligned}
P &= \dot{\Phi} - \dot{\Psi}\sin\Theta, && (2.10)\\
Q &= \dot{\Theta}\cos\Phi + \dot{\Psi}\cos\Theta\sin\Phi, && (2.11)\\
R &= \dot{\Psi}\cos\Theta\cos\Phi - \dot{\Theta}\sin\Phi. && (2.12)
\end{aligned}
$$

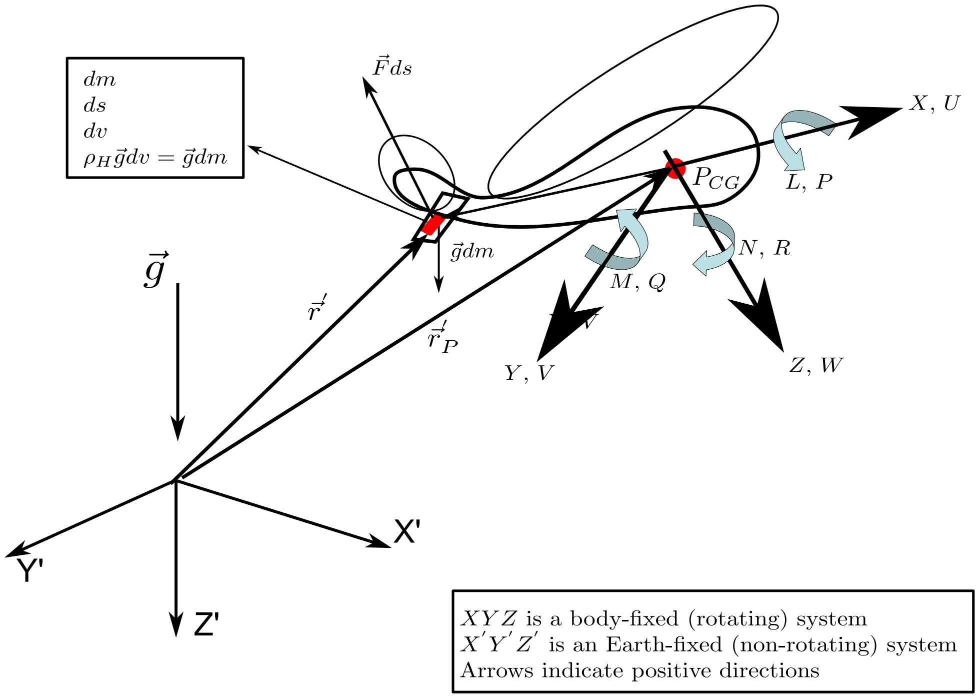

Figure 2.12: Earth-fixed and body-fixed coordinate systems.

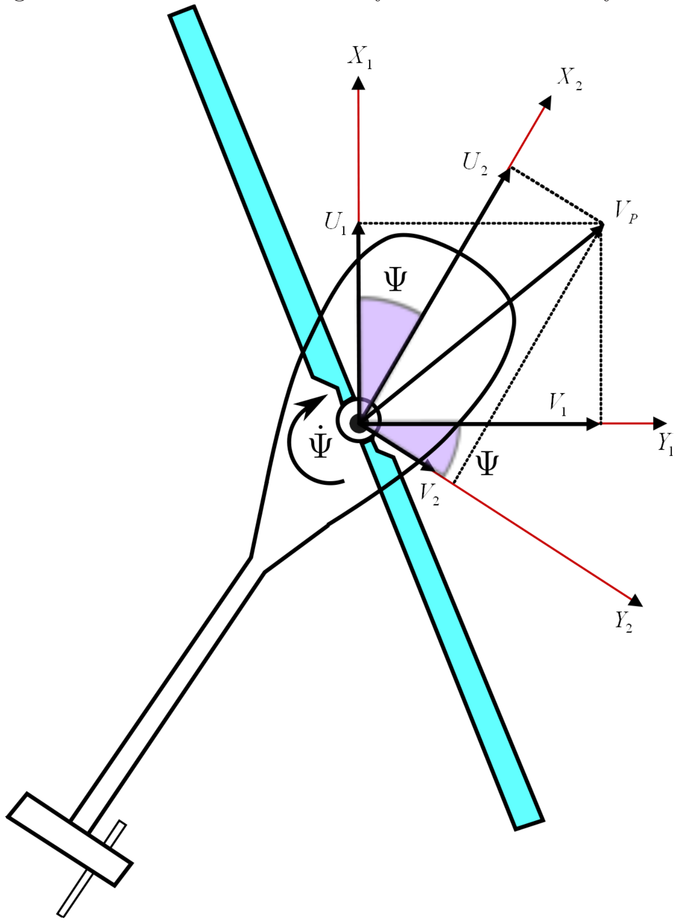

Figure 2.13: Rotation over a heading angle of Ψ about Z_1.

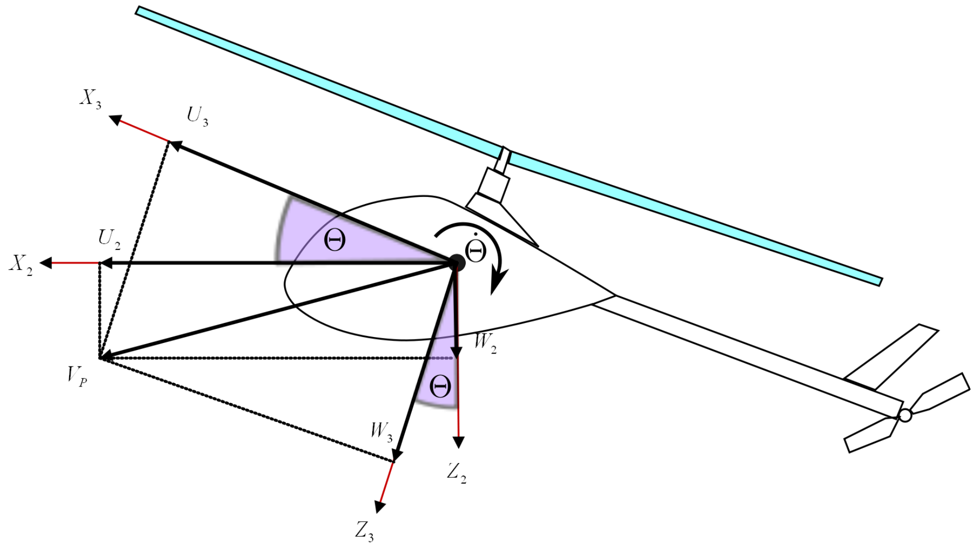

Figure 2.14: Rotation over a pitch angle of Θ about Y_2.

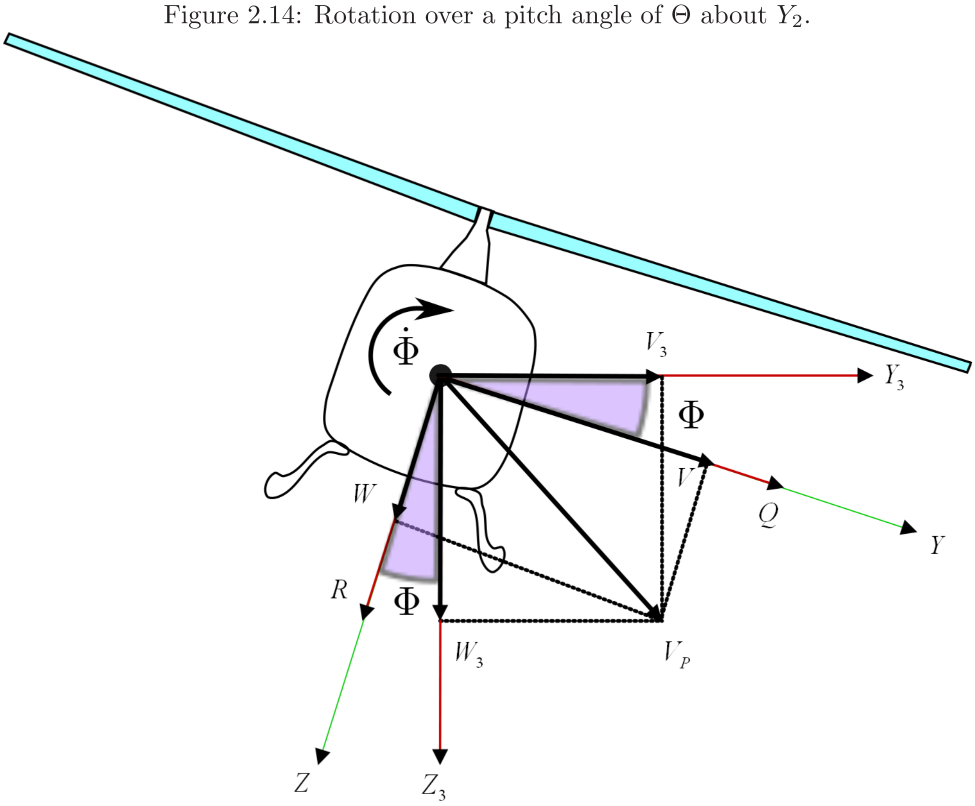

Figure 2.15: Rotation over a roll angle of Φ about X_3.

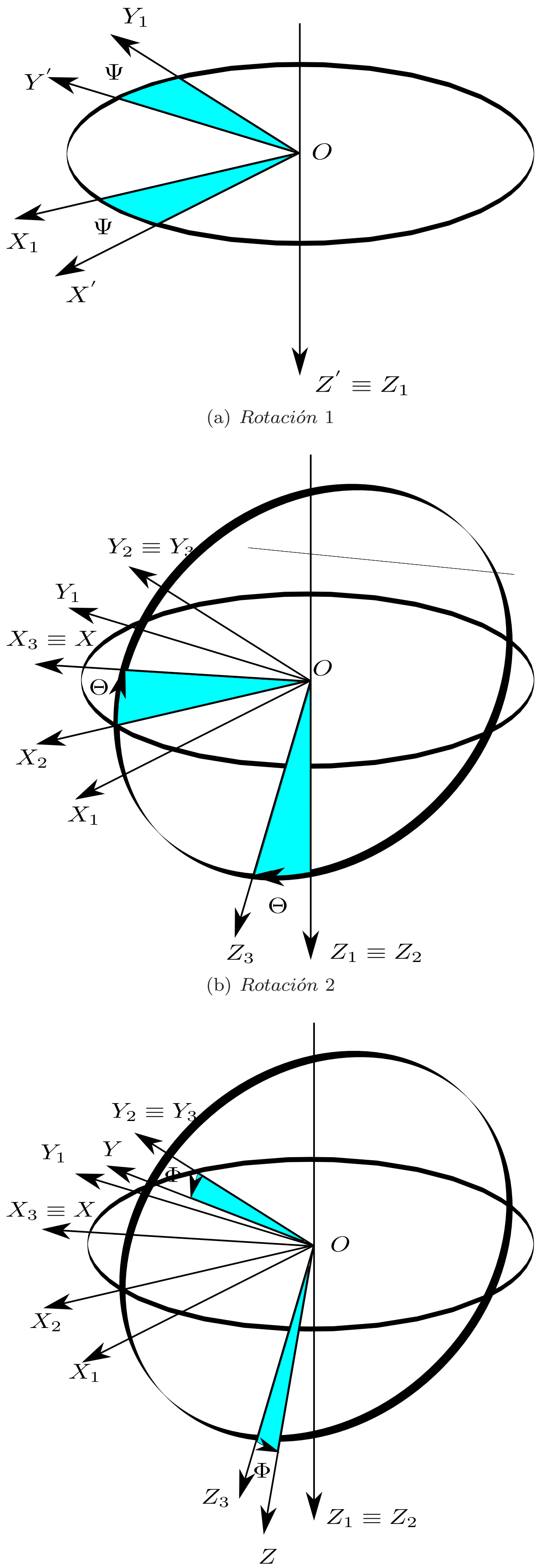

(a) *Rotación* 1

(b) *Rotación* 2

(c) *Rotación* 3

Figure 2.16: Relation between the Earth-fixed system and the helicopter(López Ruiz, 1993).

2.4 Non-linear Six-Degrees-of-Freedom Model

This section describes the non-linear six-degrees-of-freedom ($6-DOF$) equations for the helicopter model by employing the general aircraft formulation (Roskam, 2001). By applying the Newton's second law to Figure 2.12, such as the linear and angular momentum are equal to the externally applied forces and moments respectively, the results are the creation of the vector-integral form of the equations of motion for the linear momentum which given by

$$\frac{\mathrm{d}}{\mathrm{dt}}\int_v \rho_H \frac{d\mathbf{r}^{'}}{\mathrm{dt}}\mathrm{dv} \quad = \quad \int_v \rho_H \mathbf{g}\mathrm{dv} + \int_S \mathbf{F}\mathrm{ds}, \tag{2.13}$$

where the left-hand side of Eq. (2.13) represents the linear momentum, and the right-hand side represents the applied forces. The angular momentum given by

$$\frac{\mathrm{d}}{\mathrm{dt}}\int_v \mathbf{r}\times\rho_H \frac{d\mathbf{r}}{\mathrm{dt}}\mathrm{dv} \quad = \quad \int_v \mathbf{r}\times\rho_H \mathbf{g}\mathrm{dv} + \int_S \mathbf{r}\times\mathbf{F}\mathrm{ds}, \tag{2.14}$$

where the left-hand side of Eq. (2.14) represents the angular momentum, and the right-hand side represents the applied moments. The integrals $\int_v$ and $\int_s$ represent volume and surface integrals for the entire helicopter. The total mass of the helicopter is then given by the expression

$$m = \int_v \rho_H \mathrm{dv}, \tag{2.15}$$

where it is assumed that the total mass of the helicopter remains constant with time

$$\frac{\mathrm{dm}}{\mathrm{dt}} = 0. \tag{2.16}$$

This last assumption is justified as long as the mass change is sufficiently small over a period of $30-60$ seconds, which is the typical time period over which the aircraft responses are evaluated (Roskam, 2001). It is also assumed that the mass distribution is also constant with time, that is, the center of gravity stays in the same place during the same interval of time, $30-60$ seconds.

Recall from Figure 2.12 that all the helicopter mass elements are tracked with the help of vector $\mathbf{r}^{'}$, but it is most convenient to use the vectors $\mathbf{r}$ and $\mathbf{r}^{'}_P$, being the relation between the three vector given by the expression

$$\mathbf{r}^{'} = \mathbf{r}^{'}_P + \mathbf{r}. \tag{2.17}$$

Recall also that as observed in Figure 2.12, P_{CM} is assumed to be the center of mass of the helicopter, therefore the body-fixed coordinate system XYZ has its origin at P_{CM}. If P_{CM} is the center of mass, then the following relation must be satisfied

$$\int_v \mathbf{r}\rho_H \mathrm{dv} = 0, \tag{2.18}$$

therefore resulting in

$$\mathbf{r}^{'}_P = \frac{1}{m}\int_v \rho_H \mathbf{r}^{'}\mathrm{dv}, \tag{2.19}$$

thus rewriting the left-hand side of the linear momentum, Eq (2.13), as

$$\frac{\mathrm{d}}{\mathrm{dt}}\frac{\mathrm{d}}{\mathrm{dt}}\int_v \rho_H \left(\mathbf{r}^{'}_P + \mathbf{r}^{'}\right)\mathrm{dv} = \frac{\mathrm{d}}{\mathrm{dt}}\frac{\mathrm{d}}{\mathrm{dt}} m\mathbf{r}^{'}_P = m\frac{d\mathbf{V}_P}{\mathrm{dt}}, \tag{2.20}$$

where $\mathbf{V}_P$ represents the velocity vector of the helicopter center of mass and given by

$$\mathbf{V}_P = \frac{d\mathbf{r}^{'}_P}{\mathrm{dt}}. \tag{2.21}$$

The right-hand side of the linear momentum Eq. (2.13) can be rewritten as

$$\int_v \rho_H \mathbf{g} \mathrm{dv} + \int_s \mathbf{F} \mathrm{ds} = m\mathbf{g} + \mathbf{F}, \tag{2.22}$$

where $\mathbf{F}$ represent the vector form of the external forces acting on the helicopter, which can be written as the sum of the contributions from the different aircraft components such as

$$\mathbf{F} = \mathbf{F}_R + \mathbf{F}_{TR} + \mathbf{F}_f + \mathbf{F}_{tp} + \mathbf{F}_{fn}, \tag{2.23}$$

where the subscripts refer to the different elements of the helicopter, R for the rotor, TR for the tail rotor, f for the fuselage, tp for the horizontal plane, and fn for the vertical fin (Padfield, 2007). Using Eqns. (2.20) and (2.22) into the linear momentum Eq. (2.13) results in

$$m\frac{d\mathbf{V}_P}{\mathrm{dt}} = m\mathbf{g} + \mathbf{F}, \tag{2.24}$$

where Eq. (2.24) implies that the time rate of change of linear momentum, $m\mathbf{V}_P$, is equal to the sum of the externally applied forces in the helicopter. In a similar manner as for the linear momentum, the angular momentum can be rewritten by substituting Eq. (2.17) into Eq. (2.14), and accounting for Eqns. (2.18) and (2.14) leading to

$$\frac{\mathrm{d}}{\mathrm{dt}} \int_v \mathbf{r} \times \rho_H \frac{d\mathbf{r}}{\mathrm{dt}} \mathrm{dv} \quad = \quad \int_s \mathbf{r} \times \mathbf{F} \mathrm{ds} = \mathbf{M}, \tag{2.25}$$

where $\mathbf{M}$ represent the external moments vector acting on the helicopter, which can be written as the sum of the contributions from the different aircraft components such as

$$\mathbf{M} \quad = \quad \mathbf{M}_R + \mathbf{M}_{TR} + \mathbf{M}_f + \mathbf{M}_{tp} + \mathbf{M}_{fn}, \tag{2.26}$$

and l_R, l_{TR}, l_f, l_{tp}, and l_{fn} represent the arms from the helicopter center of mass to the point where the forces of the different elements, $\mathbf{F}_R$, $\mathbf{F}_{TR}$, $\mathbf{F}_f$, $\mathbf{F}_{tp}$, and $\mathbf{F}_{fn}$, are applied. Equation (2.25) implies that the time rate of change of angular momentum, $\int_v \mathbf{r} \times \rho_H \frac{d\mathbf{r}}{\mathrm{dt}} \mathrm{dv}$, is equal to the sum of the externally applied moments in the helicopter. It is important to note that the estimation of the external forces and moments acting on a helicopter, and in general in any aircraft, is one of the most challenging issues since if they are not modeled correctly, it is quite difficult, if not impossible, to precisely predict the performance characteristics, and therefore making almost impossible to design proper control laws.

The approach of decoupling the different constitutive elements of a helicopter and obtain the forces, Eq. (2.23), and moments, Eq. (2.25), of each of the different helicopter components separately, and sum them all together in the right hand side of the linear and angular momentum, Eqns. (2.24) and (2.25), respectively, is a very extended practice on the world of helicopter modeling and simulation (Padfield, 2007; Theodore, 2000; Gavrilets et al., 2002b; Gavrilets et al., 2001). This can be better seen in Figure 2.17.

The definition of the angular momentum implies that the volume integral in the left-hand side of Eq. (2.25) is a time dependent function, which it is really difficult to work with, therefore, and to eliminate the time-dependance, a switch of coordinate system is introduced, such that the linear momentum and angular momentum equations, Eqns. (2.24) and (2.25), respectively, are rewritten with respect to the body-fixed coordinate system, that is XYZ, instead of $X^{'}Y^{'}Z^{'}$. This translates in that the volume integral is not longer time-dependent. This raises a new problem, and it is the fact that the coordinate system XYZ is a rotating (non-inertial) coordinate system, where the Newton's Laws do not apply as they were used earlier. This can be ssolved by using a vector transformation relationship given by

$$\frac{\mathrm{d}\mathbf{A}}{\mathrm{dt}} = \frac{\mathrm{d}\mathbf{A}}{\mathrm{dt}} + \boldsymbol{\omega} \times \mathbf{A} = \dot{\mathbf{A}} + \boldsymbol{\omega} \times \mathbf{A}, \tag{2.27}$$

where $\mathbf{A}$ represents any vector which is to be transformed, therefore $\frac{d\mathbf{A}}{\mathrm{dt}}$ represents the fixed coordinate system $X^{'}Y^{'}Z^{'}$, and $\frac{\mathrm{d}\mathbf{A}}{\mathrm{dt}} + \boldsymbol{\omega} \times \mathbf{A}$ the rotating coordinate system XYZ. With this in mind, the transformation formula, Eq. (2.27), is applied to the left-hand side of both (2.24) and (2.25), where for the linear momentum is given by

$$m\frac{\mathrm{d}\mathbf{V}_P}{\mathrm{dt}} = m\left(\frac{\mathrm{d}\mathbf{V}_P}{\mathrm{dt}} + \boldsymbol{\omega} \times \mathbf{V}_P\right), \tag{2.28}$$

therefore rewriting Eq. (2.13) as

$$m\left(\frac{\mathrm{d}\mathbf{V}_P}{\mathrm{dt}} + \boldsymbol{\omega} \times \mathbf{V}_P\right) = m\mathbf{g} + \mathbf{F}, \tag{2.29}$$

while for the angular momentum is given by

$$\begin{aligned}\frac{\mathrm{d}}{\mathrm{dt}}\int_v \mathbf{r} \times \rho_H \frac{d\mathbf{r}}{\mathrm{dt}}\mathrm{dv} &= \int_v \mathbf{r} \times \frac{\mathrm{d}}{\mathrm{dt}}\frac{d\mathbf{r}}{\mathrm{dt}}\rho_H \mathrm{dv} = \int_v \mathbf{r} \times \frac{\mathrm{d}}{\mathrm{dt}}\left(\dot{\mathbf{r}} + \boldsymbol{\omega} \times \mathbf{r}\right)\rho_H \mathrm{dv} \\ &= \int_v \mathbf{r} \times \left(\ddot{\mathbf{r}} + \dot{\boldsymbol{\omega}} \times \mathbf{r} + 2\boldsymbol{\omega} \times \mathbf{r} + \boldsymbol{\omega} \times (\boldsymbol{\omega} \times \mathbf{r})\right)\rho_H \mathrm{dv}. \end{aligned} \tag{2.30}$$

The angular momentum, Eq. (2.30), can be simplified by assuming that all the mass elements stay together, and that there are no spinning rotors in the aircraft, therefore it is easily recognized that $\dot{\mathbf{r}} = \ddot{\mathbf{r}} = 0$ and therefore permitting to rewrite Eq. (2.30) as

$$\int_v \mathbf{r} \times \left(\dot{\boldsymbol{\omega}} \times \mathbf{r} + \boldsymbol{\omega} \times (\boldsymbol{\omega} \times \mathbf{r})\right)\rho_H \mathrm{dv} = \mathbf{M}. \tag{2.31}$$

Since vector $\dot{\boldsymbol{\omega}}$ is a property of system XYZ, that is, the angular acceleration of the axis system XYZ relative to axis $X^{'}Y^{'}Z^{'}$ is equal to the angular acceleration of the aircraft relative to the earth, it can be taken outside the volume integral, which makes the volume integral time-independent. For the case in which the existence of spinning rotors cannot be neglected, the gyroscopic moments due to spinning rotors can be taken into account by a simple addition to the angular momentum equation (2.25) given by

$$\frac{\mathrm{d}}{\mathrm{dt}}\int_v \mathbf{r} \times \frac{d\mathbf{r}}{\mathrm{dt}}\rho_H \mathrm{dv} + \frac{d\mathbf{h}}{\mathrm{dt}} = \int_s \mathbf{r} \times \mathbf{F}\mathrm{ds} = \mathbf{M}, \tag{2.32}$$

where $\mathbf{h}$ is the total angular momentum of spinning rotors given by

$$\mathbf{h} = \Sigma_{i=1}^{i=n}\mathbf{h}_i, \tag{2.33}$$

where the rotor is assumed to have a moment of inertia I_{R_i} about its spinning axis, and it is also assumed that the rotor spins with angular velocity $\boldsymbol{\omega}_{R_i}$, therefore permitting to rewrite Eq. (2.33) as

$$\mathbf{h} = \Sigma_{i=1}^{i=n} I_{R_i}\boldsymbol{\omega}_{R_i}, \tag{2.34}$$

or in its component for

$$\mathbf{h} = ih_x + jh_y + kh_z, \tag{2.35}$$

where i, j and k are unit vectors along the X, Y and Z axes respectively. The total angular momentum due to the spinning rotors is generally neglected since the mass of the blades represents typically less than 5 % of the total mass of the helicopter, thus neglecting the mass shift and its effects of the flapping and lagging motion of the rotor (Padfield, 2007). In addition, the rotor is assumed to be a fixed force and moment generating device (Cooke et al., 2002), and furthermore, since the changes in the inertia tensor with time are small when compared with the perturbing forces and moments, it is customary and acceptable to simply drop the terms involving time derivatives of the mass properties (Dreier, 2007). Therefore, the volume integral in the angular momentum Eq. (2.31) is conducted solely over the fuselage of the helicopter, which is treated like a rigid body, in which the structural distortions are neglected (Cooke et al., 2002). This reduces Eq. (2.32) to Eq. (2.31), which can now be rewritten in state space form as

$$m\left(\frac{\mathrm{d}\mathbf{V}_P}{\mathrm{dt}} + \boldsymbol{\omega} \times \mathbf{V}_P\right) = m\mathbf{g} + \mathbf{F}, \tag{2.36}$$

and where the angular momentum is given by

$$\boldsymbol{I}_{ts}\frac{\mathrm{d}\boldsymbol{\omega}}{\mathrm{dt}} + \boldsymbol{\omega} \times \mathbf{I}\boldsymbol{\omega} = \mathbf{M}, \tag{2.37}$$

where $\mathbf{F}$ and $\mathbf{M}$ have been previously defined in Eqns. (2.23) and (2.27), respectively, and as seen previously, $\mathbf{V}_P$ is the velocity of the helicopter center of mass and given in vector form by

$$\mathbf{V}_P = \begin{bmatrix} U & V & W \end{bmatrix}^T, \tag{2.38}$$

with U, V and W being the velocity components of $\mathbf{V}_P$ along X, Y, and Z components respectively of the body-fixed coordinate system XYZ. The angular rotation vector of the helicopter $\boldsymbol{\omega}$ is given by

$$\boldsymbol{\omega} = \begin{bmatrix} P & Q & R \end{bmatrix}^T, \tag{2.39}$$

with P, Q and R being the helicopter angular velocity components of $\boldsymbol{\omega}$ along X, Y, and Z components, respectively. The inertia tensor of the helicopter is given by

$$\boldsymbol{I}_{ts} = \begin{bmatrix} I_{xx} & 0 & -I_{xz} \\ 0 & I_{yy} & 0 \\ -I_{xz} & 0 & I_{zz} \end{bmatrix}, \tag{2.40}$$

where it is considered that the moments of inertia $I_{xy} = I_{yz} = 0$. Finally, $\mathbf{g}$ is the gravitation vector and given in vector form by

$$\mathbf{g} = g\begin{bmatrix} -\sin\Theta & \cos\Theta\sin\Theta & \cos\Theta\cos\Phi \end{bmatrix}^T. \tag{2.41}$$

Recalling the operations between vectors and tensors, where

$$\boldsymbol{I}_{ts}\boldsymbol{\omega} = \begin{bmatrix} I_{xx} & 0 & -I_{xz} \\ 0 & I_{yy} & 0 \\ -I_{xz} & 0 & I_{zz} \end{bmatrix}\begin{Bmatrix} P \\ Q \\ R \end{Bmatrix} = \begin{Bmatrix} I_{xz}P - I_{xz}R \\ I_{yy}Q \\ -I_{xz}P + I_{zz}R \end{Bmatrix}, \tag{2.42}$$

and

$$\boldsymbol{\omega}\times = \begin{bmatrix} 0 & -R & Q \\ R & 0 & -P \\ -Q & P & 0 \end{bmatrix}, \tag{2.43}$$

therefore substituting Eqns. (2.38–2.41), and using Eq. (2.43) and (2.42) into Eqns. (2.36) and (2.37), results in the helicopter dynamic equations in state space form

$$\mathbf{F} = m\begin{pmatrix} \dot{U} + WQ - VR \\ \dot{V} + UR - WP \\ \dot{W} + Vp - UQ \end{pmatrix} - mg\begin{pmatrix} -\sin\Theta \\ \cos\Theta\sin\Phi \\ \cos\Theta\cos\Phi \end{pmatrix}, \tag{2.44}$$

$$\mathbf{M} = \begin{pmatrix} I_{xx}\dot{P} - I_{xz}\dot{R} + (I_{zz} - I_{yy})\,RQ - I_{xz}PQ \\ I_{yy}\dot{Q} + (I_{xx} - I_{zz})\,PR + I_{xz}\left(P^2 - R^2\right) \\ I_{zz}\dot{R} - I_{xz}\dot{P} + (I_{yy} - I_{xx})\,PQ + I_{xz}QR \end{pmatrix}, \tag{2.45}$$

where Eq. (2.44) represents the force equations, and where Eq. (2.45) represents the moment equations with

$$\mathbf{F} = \begin{pmatrix} F_x & F_y & F_z \end{pmatrix}, \tag{2.46}$$

$$\mathbf{M} = \begin{pmatrix} M_x & M_y & M_z \end{pmatrix}, \tag{2.47}$$

where F_x, F_y, and F_z being the external forces applied to the helicopter on the X, Y, and Z axis, respectively. Recalling Eq. (2.23), the forces can be expressed as

$$\begin{aligned} F_x &= F_{x_R} + F_{x_{TR}} + F_{x_f} + F_{x_{tp}} + F_{x_{fn}}, && (2.48)\\ F_y &= F_{y_R} + F_{y_{TR}} + F_{y_f} + F_{y_{tp}} + F_{y_{fn}}, && (2.49)\\ F_z &= F_{z_R} + F_{z_{TR}} + F_{z_f} + F_{z_{tp}} + F_{z_{fn}}, && (2.50) \end{aligned}$$

where again, the subscripts stand for: rotor, R, tail rotor, TR, fuselage, f, horizontal plane tp, and vertical fin, fn, and where M_x, M_y, and M_z represent the external moments being applied to the helicopter on the X, Y, and Z axis respectively, and expanded as

$$\begin{aligned} M_x &= M_{x_R} + M_{x_{TR}} + M_{x_f} + M_{x_{tp}} + M_{x_{fn}}, && (2.51)\\ M_y &= M_{y_R} + M_{y_{TR}} + M_{y_f} + M_{y_{tp}} + M_{y_{fn}}, && (2.52)\\ M_z &= M_{z_R} + M_{z_{TR}} + M_{z_f} + M_{z_{tp}} + M_{z_{fn}}. && (2.53) \end{aligned}$$

With this in mind, Eq. (2.44) is rewritten as

$$\begin{aligned} \dot{U} &= VR - WQ - g\sin\Theta + \frac{F_x}{m}, && (2.54)\\ \dot{V} &= WP - UR + g\sin\Phi\cos\Theta + \frac{F_y}{m}, && (2.55)\\ \dot{W} &= UQ - VP + g\cos\Phi\cos\Theta + \frac{F_z}{m}, && (2.56) \end{aligned}$$

and Eq. (2.45) is rewritten as

$$\begin{aligned} I_{xx}\dot{P} &= (I_{yy} - I_{zz})\,RQ + I_{xz}\left(\dot{R} + PQ\right) + M_x, && (2.57)\\ I_{yy}\dot{Q} &= (I_{zz} - I_{xx})\,RP + I_{xz}\left(R^2 - P^2\right) + M_y, && (2.58)\\ I_{zz}\dot{R} &= (I_{xx} - I_{yy})\,PQ + I_{xz}\left(\dot{P} - QR\right) + M_z. && (2.59) \end{aligned}$$

The force and the moments equations, Eqns. (2.54–2.56) and (2.57–2.59), respectively, are complemented with the kinematic equations, Eqns. (2.7-2.9), that connect the components of the angular rotation vector, $\boldsymbol{\omega}$, with the aircraft's bank velocity, Φ, the pitch attitude velocity, Θ, and the heading velocity, Ψ. This results in the nine differential equations that permit to determine the evolution with respect to time of the state vector $\mathcal{X}$ given by

$$\boldsymbol{\mathcal{X}} = \left[\begin{array}{ccccccccc} U & V & W & P & Q & R & \Phi & \Theta & \Phi \end{array}\right]^T. \qquad (2.60)$$

Generally, vectors $\mathbf{F}$ and $\mathbf{M}$, Eqns. (2.46) and (2.47) are complex functions of the state variables and the control signals such

$$\mathbf{F} = \mathbf{F}\left(U, V, W, P, Q, R, \dot{U}, \dot{V}, \dot{W}, \dot{P}, \dot{Q}, \dot{R}, \theta_c, \theta_{1_s}, \theta_{1_c}, \theta_{tr}, \dot{\theta}_c, \dot{\theta}_{1_s}, \dot{\theta}_{1_c}, \dot{\theta}_{tr}\right), \qquad (2.61)$$

$$\mathbf{M} = \mathbf{M}\left(U, V, W, P, Q, R, \dot{U}, \dot{V}, \dot{W}, \dot{P}, \dot{Q}, \dot{R}, \theta_c, \theta_{1_s}, \theta_{1_c}, \theta_{tr}, \dot{\theta}_c, \dot{\theta}_{1_s}, \dot{\theta}_{1_c}, \dot{\theta}_{tr}\right), \qquad (2.62)$$

with θ_c being the collective pitch angle signal for the main rotor, θ_{1_s} is the longitudinal cyclic control signal, θ_{1_c} is the lateral cyclic control signal, and θ_{tr} is the collective pitch angle of the tail rotor. The nine differential equations are therefore given by

$$\begin{aligned} \dot{U} &= VR - WQ - g\sin\Theta + \frac{F_x}{m}, && (2.63)\\ \dot{V} &= WP - UR + g\sin\Phi\cos\Theta + \frac{F_y}{m}, && (2.64)\\ \dot{W} &= UQ - VP + g\cos\Phi\cos\Theta + \frac{F_z}{m}, && (2.65) \end{aligned}$$

$$I_{xx}\dot{P} = (I_{yy} - I_{zz})\,RQ + I_{xz}\left(\dot{R} + PQ\right) + M_x, \tag{2.66}$$

$$I_{yy}\dot{Q} = (I_{zz} - I_{xx})\,RP + I_{xz}\left(R^2 - P^2\right) + M_y, \tag{2.67}$$

$$I_{zz}\dot{R} = (I_{xx} - I_{yy})\,PQ + I_{xz}\left(\dot{P} - QR\right) + M_z, \tag{2.68}$$

$$P = \dot{\Phi} - \dot{\Psi}\sin\Theta, \tag{2.69}$$

$$Q = \dot{\Theta}\cos\Phi + \dot{\Psi}\cos\Theta\sin\Phi, \tag{2.70}$$

$$R = \dot{\Psi}\cos\Theta\cos\Phi - \dot{\Theta}\sin\Phi. \tag{2.71}$$

The navigation equations that determine the location of the aircraft at any given time are given by (Lewis and Stevens, 2003)

$$\begin{aligned} \dot{p_N} &= U\cos\Theta\cos\Psi + V(-\cos\Phi\sin\Psi + \sin\Phi\sin\Theta\cos\Psi) + \\ &\quad W(\sin\Phi sin\Psi + \cos\Phi\sin\Theta\cos\Psi), \end{aligned} \tag{2.72}$$

$$\begin{aligned} \dot{p_E} &= U\cos\Theta\sin\Psi + V(\cos\Phi\cos\Psi + \sin\Phi\sin\Theta\sin\Psi) + \\ &\quad W(-\sin\Phi\cos\Psi + \cos\Phi\sin\Theta\sin\Psi), \end{aligned} \tag{2.73}$$

$$\dot{h} = U\sin\Theta - V\sin\Phi\cos\Theta - W\cos\Phi\cos\Theta, \tag{2.74}$$

where $\dot{p_N}$, $\dot{p_E}$ and $\dot{h}$ are, respectively, the north, east, and vertical components of the helicopter velocity in the local level geographic frame on the surface of the Earth. This concludes the nonlinear $6 - DOF$ model, and the following section presents the perturbed state equations of motion that will lead to the axial flight model that will be used in this thesis.

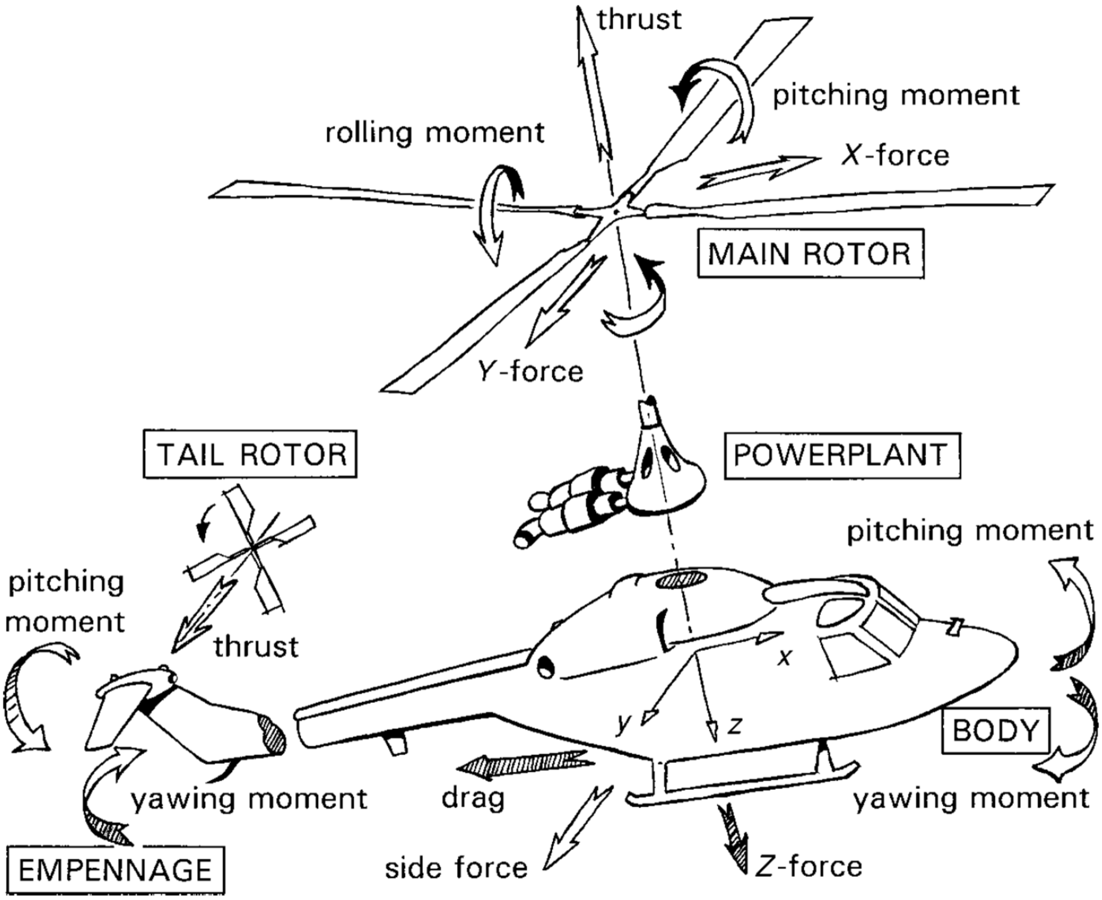

Figure 2.17: Modeling Components of a Helicopter (Padfield, 2007).

2.5 Perturbed State Equations of Motion

In order to simplify the highly nonlinear equations of motion defined in Eqns. (2.63–2.71), two special flight conditions, are considered in more detail:

- Steady state flight condition.
- Perturbed state flight condition.

Only the second flight condition will be discussed in this thesis, yielding the equations that form the basis for the helicopter model that will be used in this study. The perturbation state equations decouples the highly non-linear $6-DOF$ problem into the longitudinal and the lateral-directional problems, while the work conducted in this thesis will focus on a special case of the first problem, the axial flight condition, which is further discussed in section 2.8. Prior to start with the decoupling let recall Roskam's definition (Roskam, 2001) of perturbed state flight given as

A perturbed state flight condition is defined as one for which ALL motion variables are defined relative to a known steady state flight condition.

For that case, the substitutions are applied to all motion variables, forces and moments in the original Eqns. of motion (2.63)-(2.71). For example, the forward velocity state, U, uses the substitution $U = U_1 + u$, where the subscript in U_1 defines a perturbed motion about a general trim condition, and the lower case variable, u, defines the perturbed state flight condition, where a trim condition is considered state that provides moment equilibrium at a given flight regime. Similar substitutions are conducted for the rest of the states as seen bellow

$$U = U_1 + u, \quad V = V_1 + v, \quad W = W_1 + w \ , \tag{2.75}$$

$$P = P_1 + p, \quad Q = Q_1 + q, \quad R = R_1 + r \ , \tag{2.76}$$

$$\Phi = \Phi_1 + \phi, \quad \Theta = \Theta_1 + \theta, \quad \Psi = \Psi_1 + \psi \ , \tag{2.77}$$

and the same is done with the forces and moments resulting in

$$F_x = F_{x_1} + f_x, \quad F_y = F_{y_1} + f_y, \quad F_z = F_{z_1} + f_z \ , \tag{2.78}$$

$$M_x = M_{x_1} + m_x, \quad M_y = M_{y_1} + m_y, \quad M_z = M_{z_1} + m_z \ . \tag{2.79}$$

Using Eqns. (2.75–2.77) and (2.78–2.79) into the non-linear equations of motion (2.63–2.71) results in the perturbation equations of motion defined as

$$\begin{aligned}
\dot{u} &= (V_1+v)(R_1+r) - (W_1+w)(Q_1+q) - g\sin(\Theta_1+\theta) + \frac{F_x}{m} + \frac{f_x}{m}, && (2.80)\\
\dot{v} &= -(U_1+u)(R_1+r) + (W_1+w)(P_1+p) + g\sin(\Phi_1+\phi)\cos(\Theta_1+\theta) \\
&+ \frac{F_y}{m} + \frac{f_y}{m}, && (2.81)\\
\dot{w} &= (U_1+u)(Q_1+q) - (V_1+v)(P_1+p) + g\cos(\Phi_1+\phi)\cos(\Theta_1+\theta) \\
&+ \frac{F_z}{m} + \frac{f_z}{m}, && (2.82)\\
I_{xx}\dot{p} &= I_{xz}\dot{r} + I_{xz}(P_1+p)(Q_1+q) - (I_{zz}-I_{yy})(R_1+r)(Q_1+q) + M_x + m_x, && (2.83)\\
I_{yy}\dot{q} &= -(I_{xx}-I_{zz})(P_1+p)(R_1+r) - I_{xz}\left[(P_1+p)^2 - (R_1+r)^2\right] + M_y + m_y, && (2.84)\\
I_{zz}\dot{r} &= I_{xz}\dot{p} - (I_{yy}-I_{xx})(P_1+p)(Q_1+q) - I_{xz}(Q_1+q)(R_1+r) + M_z + m_z, && (2.85)\\
P_1+p &= (\dot{\Phi}_1+\dot{\phi}) - (\dot{\Psi}_1+\dot{\psi})\sin(\Theta_1+\theta), && (2.86)\\
Q_1+q &= (\dot{\Theta}_1+\dot{\theta})\cos(\Phi_1+\phi) + (\dot{\Psi}_1+\dot{\psi})\cos(\Theta_1+\theta)\sin(\Phi_1+\phi), && (2.87)\\
R_1+r &= (\dot{\Psi}_1+\dot{\psi})\cos(\Theta_1+\theta)\cos(\Phi_1+\phi) - (\dot{\Theta}_1+\dot{\theta})\sin(\Phi_1+\phi), && (2.88)
\end{aligned}$$

where f_x, f_y, and f_z represent the external perturbed forces being applied to the helicopter on the X, Y, and Z axis respectively, where

$$\begin{aligned}
f_x &= f_{x_R} + f_{x_{TR}} + f_{x_f} + f_{x_{tp}} + f_{x_{fn}}, && (2.89)\\
f_y &= f_{y_R} + f_{y_{TR}} + f_{y_f} + f_{y_{tp}} + f_{y_{fn}}, && (2.90)\\
f_z &= f_{z_R} + f_{z_{TR}} + f_{z_f} + f_{z_{tp}} + f_{z_{fn}}, && (2.91)
\end{aligned}$$

and where l_x, m_y, and m_z represent the external perturbed moments being applied to the helicopter on the X, Y, and Z axis respectively, where

$$\begin{aligned}
m_x &= m_{x_R} + m_{x_{TR}} + m_{x_f} + m_{x_{tp}} + m_{x_{fn}}, && (2.92)\\
m_y &= m_{y_R} + m_{y_{TR}} + m_{y_f} + m_{y_{tp}} + m_{y_{fn}}, && (2.93)\\
m_z &= m_{z_R} + m_{z_{TR}} + m_{z_f} + m_{z_{tp}} + m_{z_{fn}}, && (2.94)
\end{aligned}$$

although for simplicity, the force and moment equations will be kept in their non-expanded form. After some trigonometric manipulations and approximations, which include some restrictions to the allowable magnitude of the motion perturbations, see reference (Roskam, 2001) for further details, Eqns. (2.80–2.88) are simplified by eliminating the small perturbations and neglecting the nonlinear terms compared with the linear terms, thus reducing to

$$\begin{aligned}
\dot{u} &= V_1 r + R_1 v - W_1 q - Q_1 w - g\theta\cos\Theta_1 + \frac{f_x}{m}, && (2.95)\\
\dot{v} &= -U_1 r - R_1 u + W_1 p + P_1 w - g\theta\sin\Phi_1\sin\Theta_1 + g\phi\cos\Phi_1\cos\Theta_1 + \frac{f_y}{m}, && (2.96)\\
\dot{w} &= U_1 q + Q_1 u - V_1 p - P_1 v - g\theta\cos\Phi_1\sin\Theta_1 - g\phi\sin\Phi_1 cos\Theta_1 + \frac{f_z}{m}, && (2.97)\\
I_{xx}\dot{p} &= I_{xz}\dot{r} + I_{xz}(P_1 q + Q_1 p) - (I_{zz} - I_{yy})(R_1 q + Q_1 r) + m_x, && (2.98)\\
I_{yy}\dot{q} &= -(I_{xx} - I_{zz})(P_1 r + R_1 p) - I_{xz}(2P_1 p - 2R_1 r) + m_y, && (2.99)\\
I_{zz}\dot{r} &= I_{xz}\dot{p} - (I_{yy} - I_{xx})(P_1 q + Q_1 p) - I_{xz}(Q_1 r + R_1 q) + m_z, && (2.100)\\
p &= \dot{\phi} - \dot{\Psi}_1\theta\cos\Theta_1 - \dot{\psi}\sin\Theta_1, && (2.101)\\
q &= -\dot{\Theta}_1\phi\sin\Phi_1 + \dot{\theta}\cos\Phi_1 + \dot{\Psi}_1\phi\cos\Theta_1\cos\Phi_1 - \dot{\Psi}_1\theta\sin\Theta_1\sin\Phi_1\\
&+ \dot{\psi}\cos\Theta_1\sin\Phi_1, && (2.102)\\
r &= -\dot{\Psi}_1\phi\cos\Theta_1\sin\Phi_1 - \dot{\Psi}_1\theta\sin\Theta_1\cos\Phi_1 + \dot{\psi}\cos\Theta_1\cos\Phi_1 - \dot{\Theta}_1\phi\cos\Phi_1\\
&- \dot{\theta}\sin\Phi_1, && (2.103)
\end{aligned}$$

which form the nine perturbed equations of motion relative to a very general steady state in which all motion variables are allowed to have non-zero steady state values. It can be shown that the aircraft kinematic Eqns. (2.101–2.103) can be rewritten as

$$\begin{aligned}
\dot{\phi} &= p + \left(q\sin\Phi_1 + r\cos\Phi_1 + \phi\dot{\Theta}_1\right)\tan\Theta_1 + \theta\dot{\Psi}_1\sec\Theta_1, && (2.104)\\
\dot{\theta} &= q\cos\Phi_1 - r\sin\Phi_1 - \phi\cos\Theta_1\dot{\Psi}_1, && (2.105)\\
\dot{\psi} &= \left(q\sin\Phi_1 + r\cos\Phi_1 + \phi\Theta_1 + \theta\sin\Theta_1\dot{\Psi}_1\right)\sec\Theta_1. && (2.106)
\end{aligned}$$

With the nine perturbed equations of motion, Eqns. (2.95–2.100) and (2.104–2.106), the next step towards the definition of the axial flight model shifts towards the linearization of the force and moments. Recall from reference (Padfield, 2007) that:

> *A fundamental assumption of linearization is that the external forces F_x, F_y and F_z and moments M_x, M_y and M_z can be represented as analytic functions of the disturbed motion variables and their derivatives. Taylor's theorem for analytic functions then implies that if the force and moment functions (i.e., the aerodynamic loadings) and all its derivatives are known at any one point (the trim*

condition), then the behavior of that function anywhere in its analytic range can be estimated from an expansion of the function in a series about the known point. The requirement that the aerodynamic and dynamic loads be analytic functions of the motion and control variables is generally valid, but features such as hysteresis and sharp discontinuities are examples of non-analytic behaviour where the process will break down. Linearization amounts to neglecting all except the linear terms in the expansion. The validity of linearization depends on the behaviour of the forces at small amplitude, i.e., as the motion and control disturbances become very small, the dominant effect should be a linear one.

With this in mind, the perturbed forces can then be written in the approximate form by recalling the forces and moments dependencies, as seen in Eqns. (2.61) and (2.62), resulting in

$$f_x = f_{x_1} + \frac{\partial f_x}{\partial u}u + \frac{\partial f_x}{\partial v}v + \frac{\partial f_x}{\partial w}w + \cdots + \frac{\partial f_x}{\partial \theta_c}\theta_c + \ldots etc, \tag{2.107}$$

$$f_y = f_{y_1} + \frac{\partial f_y}{\partial u}u + \frac{\partial f_y}{\partial v}v + \frac{\partial f_y}{\partial w}w + \cdots + \frac{\partial f_y}{\partial \theta_c}\theta_c + \ldots etc, \tag{2.108}$$

$$f_z = f_{z_1} + \frac{\partial f_z}{\partial u}u + \frac{\partial f_z}{\partial v}v + \frac{\partial f_z}{\partial w}w + \cdots + \frac{\partial f_z}{\partial \theta_c}\theta_c + \ldots etc, \tag{2.109}$$

and the same can be applied to the perturbed moments, which are given by

$$m_x = m_{x_1} + \frac{\partial m_x}{\partial u}u + \frac{\partial m_x}{\partial v}v + \frac{\partial m_x}{\partial w}w + \cdots + \frac{\partial m_x}{\partial \theta_c}\theta_c + \ldots etc, \tag{2.110}$$

$$m_y = m_{y_1} + \frac{\partial m_y}{\partial u}u + \frac{\partial m_y}{\partial v}v + \frac{\partial m_y}{\partial w}w + \cdots + \frac{\partial m_y}{\partial \theta_c}\theta_c + \ldots etc, \tag{2.111}$$

$$m_z = m_{z_1} + \frac{\partial m_z}{\partial u}u + \frac{\partial m_z}{\partial v}v + \frac{\partial m_z}{\partial w}w + \cdots + \frac{\partial m_z}{\partial \theta_c}\theta_c + \ldots etc. \tag{2.112}$$

The linear approximation will therefore contain terms in the rates of change of motion and control variables with time (i.e. $\dot{u}, \dot{v}, \ldots, \dot{\theta}_c, \ldots, etc.$), but initially they will be neglected. The partial nature of the derivatives indicates that they are obtained with all the other degrees-of-freedom held fixed, which is simply another manifestation of the linear assumption (Padfield, 2007). For simplification, the derivatives are written in the form, where the derivatives for the force in the X axis are given by

$$\frac{\partial f_x}{\partial u} = X_u,\ \frac{\partial f_x}{\partial v} = X_v,\ \frac{\partial f_x}{\partial w} = X_w, \tag{2.113}$$

$$\frac{\partial f_x}{\partial p} = X_p,\ \frac{\partial f_x}{\partial q} = X_q,\ \frac{\partial f_x}{\partial r} = X_r, \tag{2.114}$$

$$\frac{\partial f_x}{\partial \theta_c} = X_{\theta_c},\ \frac{\partial f_x}{\partial \theta_{1_s}} = X_{\theta_{1_s}},\ \frac{\partial f_x}{\partial \theta_{1_c}} = X_{\theta_{1_s}},\ \frac{\partial f_x}{\partial \theta_{TR}} = X_{\theta_{TR}}, \tag{2.115}$$

and the force derivatives in the Y axis are given by

$$\frac{\partial f_y}{\partial u} = Y_u,\ \frac{\partial f_y}{\partial v} = Y_v,\ \frac{\partial f_y}{\partial w} = Y_w, \tag{2.116}$$

$$\frac{\partial f_y}{\partial p} = Y_p,\ \frac{\partial f_y}{\partial q} = Y_q,\ \frac{\partial f_y}{\partial r} = Y_r, \tag{2.117}$$

$$\frac{\partial f_y}{\partial \theta_c} = Y_{\theta_c},\ \frac{\partial f_y}{\partial \theta_{1_s}} = Y_{\theta_{1_s}},\ \frac{\partial f_y}{\partial \theta_{1_c}} = Y_{\theta_{1_s}},\ \frac{\partial f_y}{\partial \theta_{TR}} = Y_{\theta_{TR}}, \tag{2.118}$$

and the force derivatives in the Z axis are given by

$$\frac{\partial f_z}{\partial u} = Z_u,\ \frac{\partial f_z}{\partial v} = Z_v,\ \frac{\partial f_z}{\partial w} = Z_w, \tag{2.119}$$

$$\frac{\partial f_z}{\partial p} = Z_p,\ \frac{\partial f_z}{\partial q} = Z_q,\ \frac{\partial f_z}{\partial r} = Z_r, \tag{2.120}$$

$$\frac{\partial f_z}{\partial \theta_c} = Z_{\theta_c},\ \frac{\partial f_z}{\partial \theta_{1_s}} = Z_{\theta_{1_s}},\ \frac{\partial f_z}{\partial \theta_{1_c}} = Z_{\theta_{1_s}},\ \frac{\partial f_z}{\partial \theta_{TR}} = Z_{\theta_{TR}}. \tag{2.121}$$

Similarly, with the perturbed moment derivatives in the X axis being written as

$$\frac{\partial m_x}{\partial u} = L_u,\ \frac{\partial m_x}{\partial v} = L_v,\ \frac{\partial m_x}{\partial w} = L_w, \tag{2.122}$$

$$\frac{\partial m_x}{\partial p} = L_p,\ \frac{\partial m_x}{\partial q} = L_q,\ \frac{\partial m_x}{\partial r} = L_r, \tag{2.123}$$

$$\frac{\partial m_x}{\partial \theta_c} = L_{\theta_c},\ \frac{\partial m_x}{\partial \theta_{1_s}} = L_{\theta_{1_s}},\ \frac{\partial m_x}{\partial \theta_{1_c}} = L_{\theta_{1_s}},\ \frac{\partial m_x}{\partial \theta_{TR}} = L_{\theta_{TR}}, \tag{2.124}$$

and the force derivatives in the Y axis are given by

$$\frac{\partial m_y}{\partial u} = M_u,\ \frac{\partial m_y}{\partial v} = M_v,\ \frac{\partial m_y}{\partial w} = M_w, \tag{2.125}$$

$$\frac{\partial m_y}{\partial p} = M_p,\ \frac{\partial m_y}{\partial q} = M_q,\ \frac{\partial m_y}{\partial r} = M_r, \tag{2.126}$$

$$\frac{\partial m_y}{\partial \theta_c} = M_{\theta_c},\ \frac{\partial m_y}{\partial \theta_{1_s}} = M_{\theta_{1_s}},\ \frac{\partial m_y}{\partial \theta_{1_c}} = M_{\theta_{1_s}},\ \frac{\partial m_y}{\partial \theta_{TR}} = M_{\theta_{TR}}. \tag{2.127}$$

Finally the force derivatives in the Z axis are given by

$$\frac{\partial m_z}{\partial u} = N_u,\ \frac{\partial m_z}{\partial v} = N_v,\ \frac{\partial m_z}{\partial w} = N_w, \tag{2.128}$$

$$\frac{\partial m_z}{\partial p} = N_p,\ \frac{\partial m_z}{\partial q} = N_q,\ \frac{\partial m_z}{\partial r} = N_r, \tag{2.129}$$

$$\frac{\partial m_z}{\partial \theta_c} = N_{\theta_c},\ \frac{\partial m_z}{\partial \theta_{1_s}} = N_{\theta_{1_s}},\ \frac{\partial m_z}{\partial \theta_{1_c}} = N_{\theta_{1_s}},\ \frac{\partial m_z}{\partial \theta_{TR}} = N_{\theta_{TR}}. \tag{2.130}$$

Therefore, with the use of the force and moment stability derivatives, the linearized equations of motion for the full six degrees of freedom, Eqns. (2.95–2.100), and (2.104–2.106), describing perturbed motion about a general trim condition can be written as (Padfield, 2007)

$$\dot{\hat{\boldsymbol{\mathcal{X}}}} = \boldsymbol{\mathcal{A}}\hat{\boldsymbol{\mathcal{X}}} + \boldsymbol{\mathcal{B}}\boldsymbol{\mathcal{U}}(t), \tag{2.131}$$

where $\boldsymbol{\mathcal{A}}$ and $\boldsymbol{\mathcal{B}}$ are the so called system and control matrices which are formed by the partial derivatives of the non-linear $6-DOF$, Eqns. (2.63–2.71), with $\hat{\boldsymbol{\mathcal{X}}}$ being just the state vector $\boldsymbol{\mathcal{X}}$, Eq. (2.60), reorganized such that the perturbed longitudinal dynamic variables and the lateral directional variables are grouped as

$$\hat{\boldsymbol{\mathcal{X}}} = \begin{bmatrix} \hat{\boldsymbol{\mathcal{X}}}_{long} & \hat{\boldsymbol{\mathcal{X}}}_{lat} \end{bmatrix}^T = \begin{bmatrix} u & w & q & \theta & v & p & \phi & r & \psi \end{bmatrix}^T, \tag{2.132}$$

with

$$\hat{\boldsymbol{\mathcal{X}}}_{long} = \begin{bmatrix} u & w & q & \theta \end{bmatrix}^T, \tag{2.133}$$

$$\hat{\boldsymbol{\mathcal{X}}}_{lat} = \begin{bmatrix} v & p & \phi & r & \psi \end{bmatrix}^T, \tag{2.134}$$

resulting in

$$\boldsymbol{\mathcal{A}} = \left(\frac{\partial \boldsymbol{\mathcal{F}}}{\partial \hat{\boldsymbol{\mathcal{X}}}}\right)_{\hat{\boldsymbol{\mathcal{X}}}=\hat{\boldsymbol{\mathcal{X}}}_1}, \tag{2.135}$$

and

$$\boldsymbol{\mathcal{B}} = \left(\frac{\partial \boldsymbol{\mathcal{F}}}{\partial \boldsymbol{\mathcal{U}}}\right)_{\hat{\boldsymbol{\mathcal{X}}}=\hat{\boldsymbol{\mathcal{X}}}_1}, \tag{2.136}$$

with $\boldsymbol{\mathcal{F}}$ being the vector function that includes the complete $6-DOF$ model, Eqns. (2.63–2.71), and where $\boldsymbol{\mathcal{U}}$ being the control vector and given by

$$\boldsymbol{\mathcal{U}} = \begin{bmatrix} \boldsymbol{\mathcal{U}}_{long} & \boldsymbol{\mathcal{U}}_{lat} \end{bmatrix}^T, \tag{2.137}$$

with the longitudinal and lateral-directional control signals given by

$$\boldsymbol{\mathcal{U}_{long}} = [\theta_c, \theta_{1_s}]^T, \tag{2.138}$$

$$\boldsymbol{\mathcal{U}_{lat}} = [\theta_{1_c}, \theta_{tr}]^T. \tag{2.139}$$

In order to simplify the stability and control analysis of any aircraft in general, the perturbed equations of motion are generally decoupled into longitudinal and lateral-directional modes, therefore lets make the distinction between pure longitudinal, pure lateral-directional, and coupled longitudinal and lateral directional stability derivatives by reorganizing the system and control matrices, $\boldsymbol{\mathcal{A}}$ and $\boldsymbol{\mathcal{B}}$ such

$$\boldsymbol{\mathcal{A}} = \begin{pmatrix} \boldsymbol{\mathcal{A}_{long}} & \boldsymbol{\mathcal{A}_{long-lat}} \\ \boldsymbol{\mathcal{A}_{lat-long}} & \boldsymbol{\mathcal{A}_{lat}} \end{pmatrix}, \tag{2.140}$$

where $\boldsymbol{\mathcal{A}_{long}}$ is a 4×4 matrix that represents the pure longitudinal dynamics of the helicopter, and where $\boldsymbol{\mathcal{A}_{lat}}$ is a 5×5 matrix that represents the pure lateral dynamics of the helicopter, $\boldsymbol{\mathcal{A}_{long-lat}}$ is a 4×5 matrix that defines the lateral-directional coupling of the longitudinal equations of motion, and $\boldsymbol{\mathcal{A}_{lat-long}}$ is a 5×4 matrix that defines the longitudinal coupling of the lateral-directional equations of motion. A similar reorganization is conducted for the control matrix yielding

$$\boldsymbol{\mathcal{B}} = \begin{pmatrix} \boldsymbol{\mathcal{B}_{long}} & \boldsymbol{\mathcal{B}_{long-lat}} \\ \boldsymbol{\mathcal{B}_{lat-long}} & \boldsymbol{\mathcal{B}_{lat}} \end{pmatrix}, \tag{2.141}$$

where similarly, $\boldsymbol{\mathcal{B}_{long}}$ is a 4×2 matrix that represents the control signals for the pure longitudinal dynamics, that is the collective pitch angle of the main rotor θ_c, and the longitudinal cyclic θ_{1_s}, while $\boldsymbol{\mathcal{B}_{lat}}$ is a 5×2 matrix that represents the control signals for the pure lateral-directional dynamics, that is the lateral cyclic θ_{1_c}, and the tail rotor collective pitch θ_{TR}. In its expanded form, Eq. (2.140) can be defined as (Leishman, 2006)

$$\boldsymbol{\mathcal{A}_{long}} = \begin{pmatrix} X_u & X_w - Q_1 & X_q - W_1 & -g\cos\Theta_1 \\ Z_u + Q_1 & Z_w & Z_q + U_1 & -g\cos\Phi_1\sin\Theta_1 \\ M_u & M_w & M_q & 0 \\ 0 & 0 & \cos\Theta_1 & 0 \end{pmatrix}, \tag{2.142}$$

and

$$\boldsymbol{\mathcal{A}_{long-lat}} = \begin{pmatrix} X_v + R_1 & X_p & 0 & X_r + V_1 & 0 \\ Z_p - P_1 & Z_p - V_1 & -g\sin\Phi_1\cos\Theta_1 & Z_r & 0 \\ M_v & \boldsymbol{\mathcal{A}_{long-lat_1}} & 0 & \boldsymbol{\mathcal{A}_{long-lat_2}} & 0 \\ 0 & 0 & -\dot{\Psi}_1\cos\Theta_1 & -\sin\Phi_1 & 0 \end{pmatrix}. \tag{2.143}$$

For simplicity the constants are defined as

$$\boldsymbol{\mathcal{A}_{long-lat_1}} = M_p - 2P_1\frac{I_{xz}}{I_{yy}} - R_1\frac{I_{xx} - I_{zz}}{I_{yy}}, \tag{2.144}$$

$$\boldsymbol{\mathcal{A}_{long-lat_2}} = M_r + 2R_1\frac{I_{xz}}{I_{yy}} + P_1\frac{I_{xx} - I_{zz}}{I_{yy}}, \tag{2.145}$$

and

$$\boldsymbol{\mathcal{A}_{lat-long}} = \begin{pmatrix} Y_u - R_1 & Y_w + P_1 & Y_q & -g\sin\Phi_1\sin\Theta_1 \\ L'_u - P_1 & L'_w & L'_q + k_1P_1 - k_2R_1 & 0 \\ 0 & 0 & \sin\Phi_1\tan\Theta_1 & \dot{\Psi}_1\sec\Theta_1 \\ N'_u & N'_w & N'_q - k_1R_1 - k3P_1 & 0 \\ 0 & 0 & \sin\Phi_1\sec\Theta_1 & \dot{\Psi}_1\tan\Theta_1 \end{pmatrix}, \tag{2.146}$$

and

$$\boldsymbol{\mathcal{A}_{lat}} = \begin{pmatrix} Y_v & Y_p - W_1 & g\cos\Phi_1\cos\Theta_1 & Y_r - U_1 & 0 \\ L_v^{'} & L_p^{'} + k_1 Q_1 & 0 & L_r^{'} - k_2 Q_1 & 0 \\ 0 & 1 & \dot{\Theta}_1 \tan\Theta_1 & \cos\Phi_1 \tan\Theta_1 & 0 \\ N_v^{'} & N_p^{'} - k_3 Q_1 & 0 & N_r^{'} - k_1 Q_1 & 0 \\ 0 & 0 & \dot{\Theta}_1 \sec\Theta_1 & \cos\Phi_1 \sec\Theta_1 & 0 \end{pmatrix}. \quad (2.147)$$

Recall that the X, Y and Z derivatives are written in a semi-normalized form with respect to the mass of the aircraft, m, i.e.

$$X_* = \frac{X_*}{m}, \quad (2.148)$$

$$Y_* = \frac{Y_*}{m}, \quad (2.149)$$

$$Z_* = \frac{Z_*}{m}, \quad (2.150)$$

and where also the longitudinal moment derivatives are normalized with the moment of inertias such

$$M_* = \frac{M_*}{I_{yy}}, \quad (2.151)$$

and the lateral-directional moment derivatives are normalized with respect to the moment inertias resulting in

$$L_*^{'} = \frac{I_{zz}}{I_{xx}I_{zz} - I_{xz}^2} L_* + \frac{I_{xz}}{I_{xx}I_{zz} - I_{xz}^2} N_*, \quad (2.152)$$

$$N_*^{'} = \frac{I_{xz}}{I_{xx}I_{zz} - I_{xz}^2} L_* + \frac{I_{xx}}{I_{xx}I_{zz} - I_{xz}^2} N_*, \quad (2.153)$$

where I_{xx} and I_{zz} are the roll and yaw moments of inertia, and I_{xz} is the roll/yaw product of inertia. The k_* constants in Eqns. (2.146–2.147) are given by the expressions

$$k_1 = \frac{I_{xz}(I_{zz} + I_{xx} - I_{yy})}{I_{xx}I_{zz} - I_{xz}^2}, \quad (2.154)$$

$$k_2 = \frac{I_{zz}(I_{zz} - I_{yy}) + I_{xz}^2}{I_{xx}I_{zz} - I_{xz}^2}, \quad (2.155)$$

$$k_4 = \frac{I_{xx}(I_{yy} - I_{xx}) - I_{xz}^2}{I_{xx}I_{zz} - I_{xz}^2}. \quad (2.156)$$

In their expanded form, (2.141) is defined as

$$\boldsymbol{\mathcal{B}_{long}} = \begin{pmatrix} X_{\theta_c} & X_{\theta_{1_s}} \\ Z_{\theta_c} & Z_{\theta_{1_s}} \\ M_{\theta_c} & M_{\theta_{1_s}} \\ 0 & 0 \end{pmatrix}, \quad (2.157)$$

$$\boldsymbol{\mathcal{B}_{long-lat}} = \begin{pmatrix} X_{\theta_{1_c}} & X_{\theta_{tr}} \\ Z_{\theta_{1_c}} & Z_{\theta_{tr}} \\ M_{\theta_{1_c}} & M_{\theta_{tr}} \\ 0 & 0 \end{pmatrix}, \quad (2.158)$$

$$\boldsymbol{\mathcal{B}_{lat-long}} = \begin{pmatrix} Y_{\theta_c} & Y_{\theta_{1_s}} \\ L_{\theta_c}^{'} & L_{\theta_{1_s}}^{'} \\ 0 & 0 \\ N_{\theta_c}^{'} & N_{\theta_{1-s}}^{'} \\ 0 & 0 \end{pmatrix}, \quad (2.159)$$

$$\boldsymbol{\mathcal{B}_{lat}} = \begin{pmatrix} Y_{\theta_{1_c}} & X_{\theta_{tr}} \\ L'_{\theta_{1_c}} & L'_{\theta_{tr}} \\ 0 & 0 \\ N'_{\theta_{1_c}} & N'_{\theta_{tr}} \\ 0 & 0 \end{pmatrix}. \tag{2.160}$$

Recall that in addition to the linearized aerodynamic forces and moments, the state and control matrices, Eqns. (2.140) and (2.141) respectively, also contains perturbation inertial, gravitational and kinematic effects linearized about the trim conditions defined by

$$\Phi_1,\ \Theta_1,\ \Psi_1,\ U_1,\ V_1,\ W_1,\ P_1,\ Q_1,\ R_1. \tag{2.161}$$

The coefficients in the different state and control matrices represents the slope of the forces and moments at the trim point reflecting the strict definition of the stability and control derivatives.

2.5.1 Longitudinal Linearized Model

In order to simplify the stability and control analysis problems for aircrafts, it is customary, as seen in the literature (Etkin and Reid, ; Roskam, 2001; Padfield, 2007), to decouple the perturbed equations of motion into its longitudinal and lateral-directional modes, where the first one is given by

$$\boldsymbol{\hat{\dot{\mathcal{X}}}_{long}} = \boldsymbol{\mathcal{A}_{long}} \boldsymbol{\hat{\mathcal{X}}_{long}} + \boldsymbol{\mathcal{B}_{long}} \boldsymbol{\mathcal{U}_{long}}(t), \tag{2.162}$$

with $\boldsymbol{\hat{X}_{long}}$, $\boldsymbol{\mathcal{A}_{long}}$, $\boldsymbol{\mathcal{B}_{long}}$, and $\boldsymbol{\mathcal{U}_{long}}$ being defined by Eqns. (2.133), (2.142), (2.157), and (2.138) respectively. Only the longitudinal model will be developed in this section, since the work described here only looks at a degenerated case of the longitudinal dynamics. This longitudinal linearized approximate model permits a small amplitude stability analysis of the helicopter motion, which recalling the linear system theory (Chen, 1998) implies that the helicopter motion can be described as a linear combination of the natural modes, each having its own unique frequency damping and distribution of the response variables (Leishman, 2006).

Without getting in detail into the linear system theory, the analysis of the dynamic response of the longitudinal state-space model can be conducted via modal or eigenvector analysis, which shows that by analyzing the characteristic equation of the longitudinal linearized model for helicopters, (2.162), it can be differentiated three modes. The characteristic equation ($\boldsymbol{CE}$), when solved, will show the nature of the controls fixed response of the helicopter to a disturbance (Cooke et al., 2002), which is given by

$$\det(s\boldsymbol{I} - \boldsymbol{\mathcal{A}_{long}}) = 0, \tag{2.163}$$

where $\boldsymbol{I}$ is a 4×4 identity matrix, and where expanding (2.163) results in

$$\boldsymbol{CE} = \left| \begin{pmatrix} s & 0 & 0 & 0 \\ 0 & s & 0 & 0 \\ 0 & 0 & s & 0 \\ 0 & 0 & 0 & s \end{pmatrix} - \begin{pmatrix} X_u & X_w - Q_1 & X_q - W_1 & -g\cos\Theta_1 \\ Z_u + Q_1 & Z_w & Z_q + U_1 & -g\cos\Phi_1 \sin\Theta_1 \\ M_u & M_w & M_q & 0 \\ 0 & 0 & \cos\Theta_1 & 0 \end{pmatrix} \right| = 0, \tag{2.164}$$

this results in

$$\boldsymbol{CE} = \begin{vmatrix} s - X_u & -X_w - Q_1 & -(X_q - W_1) & g\cos\Theta_1 \\ -(Z_u + Q_1) & s - Z_w & -(Z_q + U_1) & g\cos\Phi_1 \sin\Theta_1 \\ -M_u & -M_w & s - M_q & 0 \\ 0 & 0 & -\cos\Theta_1 & s \end{vmatrix} = 0, \tag{2.165}$$

where the determinant of Eq. (2.165) is of the form $As^4 + Bs^3 + Cs^2 + Ds + E = 0$. The coefficients in the polynomial can be expressed in terms of aerodynamics derivatives, see (Bramwell et al., 2001) for mode details. For helicopters, in most cases, the equation can be factorized into

$$(T_1 s + 1)(T_2 s + 1)\left(s^2 + 2\zeta\omega_n s + \omega_n^2\right) = 0, \tag{2.166}$$

which represent the three helicopter modes in longitudinal flight. These there modes can be summarized as (Cooke et al., 2002):

1. *Vertical Velocity Mode*: The vertical velocity mode, which is described by the first factorization $(T_1 s + 1) = 0$, is a stable, heavily damped subsidence in the vertical velocity. The motion is decoupled from the speed and pitch and has a time constant of the order of 1 to 2 seconds.
2. *Forward Speed Mode*: The forward speed mode, which is described by the second factorization $(T_2 s + 1) = 0$, is a stable heavily damped subsidence in speed. The motion is coupled with pitch attitude and pitch rate. It has a short time constant of the order of 0.5 seconds.
3. *Pitching Oscillation*: The stability of the pitching oscillation is both speed and flight condition dependent. In the climb or at high speed the oscillation can be unstable, possibly generating to an exponential divergence at high speed. The oscillation couples with the forwards speed mode and is mainly due to the rotor flapping caused by speed changes.

With this in mind, and in order to justify the proposed model in vertical flight, and recalling that only the first of the modes, the vertical velocity mode, is the mode of interest for this thesis, the following section focuses only on this mode.

2.5.2 Simplified Vertical Displacement Model

As shown above, the vertical velocity mode is decoupled from the speed and pitch modes. In order to obtain an axial flight model, the original longitudinal simplified model has to be studied for the hover flight condition, in which $U_1 = W_1 = Q_1 = \Theta_1 = \Psi_1 = 0$ and also can be assumed that some derivatives are approximately zero (López Ruiz, 1993; Cooke et al., 2002), that is $X_w = X_{\theta_c} = Z_u = Z_q = Z_{\theta_{1_s}} = M_w = M_{\theta_c} = 0$, therefore reducing Eq. (2.162) to

$$\hat{\boldsymbol{\mathcal{X}}}_{\boldsymbol{long}} = \boldsymbol{\mathcal{A}}_{\boldsymbol{long}_H} \hat{\boldsymbol{\mathcal{X}}}_{\boldsymbol{long}} + \boldsymbol{\mathcal{B}}_{\boldsymbol{long}_H} \boldsymbol{\mathcal{U}}_{\boldsymbol{long}}(t), \tag{2.167}$$

with the hovering state and control matrices being given by

$$\boldsymbol{\mathcal{A}}_{\boldsymbol{long}_H} = \begin{pmatrix} X_u & 0 & X_q & -g \\ 0 & Z_w & 0 & 0 \\ M_u & 0 & M_q & 0 \\ 0 & 0 & 1 & 0 \end{pmatrix}, \tag{2.168}$$

$$\boldsymbol{\mathcal{B}}_{\boldsymbol{long}_H} = \begin{pmatrix} 0 & X_{\theta_{1_s}} \\ Z_{\theta_c} & 0 \\ M_{\theta_c} & M_{\theta_{1_s}} \\ 0 & 0 \end{pmatrix}. \tag{2.169}$$

This permits to separate the longitudinal dynamics in hover into the axial displacement and the combined forward speed and pitch attitude movement of the helicopter (López Ruiz, 1993) resulting in

$$\dot{u} = X_u u + X_q q - g\theta + X_{\theta_{1_s}} \theta_{1_s}, \tag{2.170}$$

$$\dot{w} = Z_w w + Z_{\theta_c} \theta_c, \tag{2.171}$$

$$\dot{q} = M_u u + M_q q - g\theta + M_{\theta_c} \theta_c + M_{\theta_{1_s}} \theta_{1_s}, \tag{2.172}$$

$$\dot{\theta} \quad = \quad q. \tag{2.173}$$

Focusing on Eq. (2.171), it can be seen that the analysis of the vertical velocity mode, yields that it has a real root given by $s - Z_w = 0$, so that its eigenvalue is given by $s = Z_w$. This presents a heavily damped subsidence, which translates to the fact that if a helicopter is disturbed, by a vertical gust for example, the subsequent heave (vertical) motion is quickly damped out (Cooke et al., 2002). As seen in (2.171), this motion is a pure convergence with no oscillation and confirms that the vertical motion is completely decoupled from the pitching and the forward motions as seen in Eq. (2.171).

The performance of a helicopter in axial flight near the hover condition can be predicted by analyzing (2.171), where Z_w is the vertical force due to vertical speed, and Z_{θ_c} is the vertical force due to the collective control signal θ_c. Therefore, in order to have a feasible model that can approximately predict the performance of a helicopter in axial flight, and considering the resulting simplified axial dynamics (2.171), is it necessary to derive a model that can accurately predict both vertical forces derivatives, Z_w and Z_{θ_c}, along with some other significate contributions in vertical flight that are not considered in this simplified vertical motion model. In order to do so, the following sections approach the problem by defining nonlinear models that can both, predict in a precisely manner the performance characteristics of a helicopter rotor in axial flight.

This implies that the selected model has to be able to collect the most significate nonlinear dynamics of the problem, but also be simply enough that can be tackled down from a control perspective. Section 2.6 will define such models, and section 2.8 will define the proposed model definition for a miniature helicopter in axial flight which is the main focus of this thesis. The proposed mathematical model will include the nonlinear vertical motion of the helicopter, the nonlinear dynamics of the collective pitch actuators, but also a nonlinear model for the combustion engine which permits the rotational velocity of the blades. The use of collective pitch dynamics will increases considerably the complexity of the model, but will also depict a more realistic system, with views of being able to implement in the future the control and stability analysis results here obtained in the *GCNL* real autonomous platform with a higher rate of success.

2.6 Helicopter Aerodynamics in Axial Flight

This section is dedicated to define the basis of the theory that will be employed to determine the dynamic equations of a helicopter in axial flight. The correct understanding of the vertical flight of helicopters requires an in depth analysis and study of the two main theories that explain rotor performance: momentum theory (MT) and blade element theory (BE). A dynamic model of the thrust coefficient of the main rotor for a helicopter in hover or axial flight can be obtained through a combination of these two theories. The momentum theory provides a direct explanation of how vertical flight is obtained through a global analysis, but it is unable to provide alone the required tools to predict the performance of rotors. On the other side, blade element theory provides this required in depth look into the physics that permits to predict the rotor performance, but unfortunately at the cost of added complexity. This in-depth analysis is out of the scope of this thesis, and the author encourages the reader to solve any doubts with some of the references employed in this section (Payne, 1959; Johnson, 1994; Layton, 1984; Prouty, 1986; Leishman, 2006; Padfield, 2007; Cuerva et al., 2009).

In this section, the author tries to resume the most important parts of the two theories that lead to the axial flight model that is employed in the thesis by using the available literature (Johnson, 1994; Prouty, 1986; Leishman, 2006). Although several axial flight models are employed in certain parts of this thesis, this section focuses on describing solely the axial flight model that will be selected, which is based on the momentum theory with the assumption of the existence of uniform inflow and hover flight condition, where for completeness this model will be referred as MT_H model from now on. The MT_H model is based on the proposed model selected by Pallet and Ahmad, which presented in several technical reports written at the University of Purdue (Pallet et al., 1991; Pallet and Ahmad, 1991), although with some modifications regarding some of the aerodynamic parameters that were not completely defined in the original work. The resulting model describes the vertical motion of an autonomous helicopter mounted on a stand, along with the dynamics of the rotational speed of the blades, and the dynamics of the collective pitch actuators.

Although the selected model implies a series of hypothesis, such that the inflow ratio along the blades is constant and equal to that of a hovering helicopter, it can be demonstrated (Johnson, 1994) that for small enough axial velocities the simplification is valid and permits to have quite precise predictions of the rotor performance. This thrust model is based in the sum of the blade element (BE) and the moment theory (MT) at the hover flight condition and assuming uniform inflow along the blade. The author contribution to the original model, in addition to the definition of some of the coefficients by relating them to the aerodynamic parameters of the MT_H model, includes also the use of a more realistic thrust coefficient models that are easily implemented in the MT_H model which considers axial flight and non-uniform inflow along the blades. The use of these more realistic, and therefore much more complex models, will permit to test the validity of the hypothesis that the selection of simplified models around the hovering condition is still valid for small vertical axial velocities, as it will be shown in the simulations. The use of these models, which are described in detail in Appendix A, is limited to test the robustness of the control laws that will be derived in this thesis by considering that these more accurate and complex models can be used to account for unmodeled dynamics not being accounted for in the original model.

Although these models, described in detail in Appendix A, are widely used in the literature, and are known to describe in higher detail, and with much more fidelity, the axial flight forces generated by a rotor in axial flight, due to the discontinuities of these models, as previously described, are not implementable models for the proposed control and analysis strategies which require continuously differentiable models, thus will serve as test bench models where to test the robustness of the proposed control laws. Prior to define the MT_H model, the basis for both the BE and MT are presented so that they provide an insight view of the mathematics of the problem.

2.6.1 Momentum Theory Analysis

Momentum theory applies the basic conservation laws of fluid mechanics (conservation of mass, momentum, and energy) to the rotor and flow as a whole to estimate the rotor performance. It is a global analysis, relating the overall flow velocities and the total rotor thrust and power (Johnson, 1994). The rotor disk supports a thrust created by the action of the air on the blades. By Newton's law there must be an equal and opposite reaction of the rotor on the air. As a result, the air in the rotor wake acquires a velocity increment directed opposite to the thrust direction. It follows that there is kinetic energy in the wake flow field which must be supplied by the rotor. In order to simplify the analysis let consider the control volume defined in Figure 2.18.

To simplify the dynamics of the rotor in the momentum theory, the rotor is modeled as an actuator disk, which is a circular surface of zero thickness that can support a pressure difference, while accelerating the air through the disk, and with the loading assumed to be steady, although it can vary over the surface of the disk. The actuator disk may also support a torque, which imparts angular momentum to the fluid as it passes through the disk. The actuator disk model is only an approximation to the actual rotor that provides a simplification by assuming that the distribution of the rotor blade loading over a disk is equivalent to considering an infinite number of blades, in which pressure and velocity can be measured along the control volume. Let also be assumed that the flow through the rotor is one-dimensional, quasi-steady, incompressible and inviscid (Leishman, 2006). To help understand the momentum theory, let define four relevant positions in the vicinity of the rotor model being:

- Station 0: in a position far upstream,
- Station 1: in a position right before the rotor blades,
- Station 2: in a position right after rotor blades,
- Station ∞: in a position far downstream.

The location of the stations can be seen in Figure 2.18, and where the velocity of the mass of air at station 0 is given by $v_0 = 0$, the velocities of the mass of air at station 1 and station 2 are the same, and are given by v_i, which represents the induced velocity, or the velocity imparted to the mass of air contained in the control volume at the rotor disk, and the velocity of the mass of air at station 2 is given by given by w. Following sections describe the momentum theory on two important helicopter flight conditions: the hover and the axial flight. The first one, the hover condition, it is associated with a equilibrium condition of the dynamic model employed in this thesis. The second flight condition, the axial flight, represents the means by which the helicopter moves from one equilibrium point to another. These two flight conditions are the basis for the control strategy adopted in this thesis of moving from equilibrium to equilibrium in order to regulate the desired altitude of a helicopter. The controller must be able to change its altitude from any prescribed initial altitude to any selected final altitude, always taking into account that at the initial altitude the helicopter is already in equilibrium flight, that is, maintaining the hover condition at that initial altitude, and that both, the initial and final altitudes are limited by the physics of the problem, that is, the helicopter is restricted by the stand.

2.6.1.1 Momentum Theory Analysis in Hovering Flight

Let first consider the hover problem, where the control volume surrounding the rotor and its wake has surface area S, as seen in Figure 2.18. Let $\mathrm{d}\mathbf{S}$ be the unit normal area vector which by convention always points out of the control volume across the surface S. The general equation governing the conservation of fluid mass applied to this finite control volume can be written as

$$\int_S \rho \mathbf{V} \cdot \mathrm{d}\mathbf{S} = 0, \tag{2.174}$$

where $\mathbf{V}$ is the local velocity and ρ is a scalar function of the density of the fluid. This equation states that the mass flow into the control volume must equal the mass flow of the control volume. Similarly, the equation governing the conservation of fluid momentum can be written as

$$\mathbf{F} = \int \rho \mathbf{V}\mathbf{V} \mathrm{d}\mathbf{S}. \tag{2.175}$$

For unconstrained flow, the net pressure force on the fluid inside the control volume is zero, therefore the net force on the fluid, $\mathbf{F}$, is simply equal to the rate of change with time of the fluid momentum across the control surface, S. Although Eq. (2.175) is a vector equation, it is simplified with the assumption of quasi-dimensional flow. Because the force of the fluid is supplied by the rotor, by Newton's third law the fluid must exert an equal and opposite force on the rotor, which is the rotor thrust T. Finally the conservation laws of aerodynamics are completed with the equation governing the conservation of energy in the flow given by

$$W = \int_S \frac{1}{2} (\rho \mathbf{V} \cdot \mathrm{d}\mathbf{S}) \, |\mathbf{V}|^2, \tag{2.176}$$

which states simply that the work done on the fluid by the rotor is a scalar function that can be identified as a gain in kinetic energy of the fluid in the rotor slipstream per unit time. These general equations of mass, momentum, and energy conservation are applied to the specific problem of a hovering rotor following the standardized procedures (Glauert, 1935; Johnson, 1994; Leishman, 2006). Following the assumption that the flow is quasi-steady and by the principle of conservation of mass, Eq. (2.174), the mass flow rate, $\dot{m}$, must be contained within the boundaries of the rotor wake, therefore resulting in the flow rate which is given by

$$\dot{m} = \int_{\infty} \rho \mathbf{V} \cdot \mathrm{d}\mathbf{S} = \int_{2} \rho \mathbf{V} \cdot \mathrm{d}\mathbf{S}, \tag{2.177}$$

which implies that the mass flow rate at station 2, see Figure 2.18, must be the same that the mass flow rate at station ∞. The mass flow rate model can be simplified by rewriting Eq. (2.177) can be rewritten for one-dimension $(1-D)$ incompressible flow as

$$\dot{m} = \rho A_{\infty} w = \rho A v_i. \tag{2.178}$$

The conservation of fluid momentum, Eq. (2.175), gives the relationship between the rotor thrust, T, and the net time rate-of-change of fluid momentum out of the control volume, obeying Newton's second law. Therefore resulting in that the rotor thrust is equal and opposite to the force on the fluid, which is given by

$$-\mathbf{F} = T = \int_{\infty} \rho \left(\mathbf{V} \cdot \mathrm{d}\mathbf{S}\right) \mathbf{V} - \int_{0} \rho \left(\mathbf{V} \cdot \mathrm{d}\mathbf{S}\right) \mathbf{V}. \tag{2.179}$$

Because in hovering flight the velocity far upstream of the rotor, station 0 in Figure 2.18, is quiescent, the second term on the right-hand side of Eq. (2.179) is zero, therefore, for the hover problem, the rotor thrust reduces to

$$T = \int_{\infty} \rho \left(\mathbf{V} \cdot \mathrm{d}\mathbf{S}\right) \mathbf{V} = \dot{m} w. \tag{2.180}$$

From the principle of conservation of energy, the work done on the rotor is equal to the gain in energy of the fluid per unit time, where the work done per unit time, or power consumed by the rotor is, Tv_i, therefore having that

$$T v_i = \int_{\infty} \frac{1}{2} \rho \left(\mathbf{V} \cdot \mathrm{d}\mathbf{S}\right) \mathbf{V}^2 \rho - \int_{0} \frac{1}{2} \rho \left(\mathbf{V} \cdot \mathrm{d}\mathbf{S}\right) \mathbf{V}^2 \rho, \tag{2.181}$$

where in hover, the second term in (2.181) is zero reducing to

$$T v_i = \int_{\infty} \frac{1}{2} \rho \left(\mathbf{V} \cdot \mathrm{d}\mathbf{S}\right) \mathbf{V}^2 \rho = \frac{1}{2} \dot{m} w^2. \tag{2.182}$$

Using Eqns. (2.180) and (2.182) it can be easily seen that

$$v_i = \frac{1}{2} w, \tag{2.183}$$

therefore obtaining a direct relationship between the induced velocities at the rotor and far downstream of the rotor

$$w = 2 v_i. \tag{2.184}$$

It is also important to define the induced velocity at the rotor disk. As seen previously in Eq. (2.180), the momentum theory is used to relate the rotor thrust to the induced velocity a the rotor disk by using the relations previously derived resulting in

$$T = \dot{m} w = \dot{m}(2 v_i) = 2(\rho A v_i) v_i = 2 \rho A v_i^2, \tag{2.185}$$

which can be rearranged and solved for the induced velocity at the plane of the rotor disk by the expression

$$v_h \equiv v_i = \sqrt{\frac{T}{2\rho A}}, \tag{2.186}$$

where note that the induced inflow velocity at the rotor disk, v_i, can be written as

$$v_h \equiv v_i = \lambda_h \Omega R, \tag{2.187}$$

where the nondimensional quantity λ_h is called the induced inflow ration in hover and is defined by

$$\lambda_h = \frac{v_i}{\Omega R}, \tag{2.188}$$

where Ω represents the angular rotational speed of the rotor, and R is the rotor radius, and the product ΩR is just the blade tip speed V_{tip}. The inflow ratio is a very important parameter which is preferable used when comparing results from different rotors because it is a nondimensional quantity. For rotating-wing aircraft (i.e. helicopters), it is convention to nondimensionalize all velocities with the blade tip speed (i.e. by $V_{tip} = \Omega R$) (Leishman, 2006). In helicopter analysis it is also customary to define formally the rotor thrust coefficient as

$$C_T = \frac{T}{\rho A V_{tip}^2} = \frac{T}{\rho A \Omega^2 R^2}, \tag{2.189}$$

where the reference area is the rotor disk area, A, and the reference speed is the blade tip speed, ΩR. The inflow ratio (λ_i) is related to the thrust coefficient in hover by using the expression

$$\lambda_h \equiv \lambda_i = \frac{v_i}{\Omega R} = \frac{1}{\Omega R}\sqrt{\frac{T}{2\rho A}} = \sqrt{\frac{T}{2\rho A\left(\Omega R\right)^2}} = \sqrt{\frac{C_T}{2}}, \tag{2.190}$$

where Eq. (2.190) is the result of the assumption that the flow is a one-dimensional flow, which implies that this value of inflow is assumed to be distributed uniformly over the disk. This relation is quite important and it is used in following sections as a reference when describing the momentum theory for the axial flight both the ascend and descend regimes.

2.6.1.2 Induced Tip Loss

Prior to describe the blade element theory, it is important to first introduce a physical real effect that can be easily implemented in both the momentum theory, and as it will be demonstrated later, also in the blade element theory, and in the subsequent proposed closed-form solutions for the thrust coefficient models. The formation of a trailed vortex at the tip of each blade produces a high local inflow over the tip region and effectively reduces the lifting capability there, this results in that the lifting-line theory is not strictly valid near wing tips. When the chord at the tip is finite, blade element theory gives a nonzero lift all the way out to the end of the blade. In reality, the blade loading drops to zero at the tip and at the root, or hub of the blade because of three-dimensional flow effects. This translates into that, unless these effects are accounted for in the modeling of the thrust forces, will result in an overestimated overall thrust coefficient that will make the R/C helicopter to behave different that expected. These tip-losses can be better seen in Figure (2.19).

The dynamic pressure loading for a rotary wing, which is proportional to r^2, is concentrated at the tip and drops off even faster than that for fixed wings. The loss of lift at the tip is an important factor in calculating the rotor performance. If this loss is neglected, the rotor thrust for a given power or collective will be significantly overestimated. A rigorous treatment of the tip loading would require a lifting surface analysis. One way to take this effect into account is to integrate the incremental lift from some r_0 to BR

where r_0 is radius of the root cut-out, and BR is the effective outer radius, $R_e < R$. These values are chosen such that the area under the theoretical curve out to BR is the same as the area under the actual lift curve out to R. this resulting in that the tip loss corresponds to a reduction in the rotor disk area by a factor B^2, that is

$$A_e = \pi R_e^2 = \pi(BR)^2 = B^2(\pi R^2) = B^2 A. \tag{2.191}$$

Recalling that r_0 is defined as the nondimensional radius of the cut-out, then the effective area of the hovering rotor for momentum theory purposes becomes

$$A_e = \pi B^2 R^2 - \pi r_0^2 R^2, \tag{2.192}$$

which can be written in terms of an area ratio as

$$\frac{A_e}{A} = \frac{\pi B^2 R^2 - \pi r_0^2 R^2}{\pi R^2} = B^2 - r_0^2. \tag{2.193}$$

Both, the root cutout, and the tip loss effects, can be included into an empirical equation for B that was first derived by Prandtl and Betz (Betz, 1919) which gives good correlation to numerical method determinations (Glauert, 1935; Johnson, 1994; Prouty, 1986; Leishman, 2006). Prandtl showed that when accounting for the tip loss, the effective blade radius, R_e is given by

$$\frac{R_e}{R} \approx 1 - \left(\frac{1.386}{N_b}\right)\frac{\lambda_i}{\sqrt{1+\lambda_i^2}}, \tag{2.194}$$

where N_b being the number of blades. For helicopter rotors λ_i is typically less than 0.07 (Leishman, 2006), therefore λ_i^2 is small and Eq. (2.194) can be simplified into

$$\frac{R_e}{R} \approx 1 - \left(\frac{1.386}{N_b}\right)\lambda_i, \tag{2.195}$$

therefore resulting in a more general tip-loss equation given by

$$B = 1 - \frac{1.386\lambda_i}{N_b}. \tag{2.196}$$

Recall that the inflow ratio is given by

$$\lambda_i = \frac{V_c + v_i}{\Omega R}, \tag{2.197}$$

where V_c is the climb velocity, and that for the hovering flight condition with the assumption of uniform inflow, it has already been demonstrated in Eq. (2.190) that the inflow ratio can be assumed to be given by

$$\lambda_i = \sqrt{\frac{C_T}{2}}, \tag{2.198}$$

therefore the tip-loss factor can be approximated by

$$\frac{R_e}{R} = B = 1 - \left(\frac{1.386}{N_b}\right)\frac{\sqrt{C_T}}{N_b} \approx 1 - \frac{\sqrt{C_T}}{N_b}. \tag{2.199}$$

Values for helicopter rotors are found to range from about 0.95 to 0.98, depending on the number of blades (Leishman, 2006). Other empirical tip-loss factors are derived in the literature (Gessow and Myers, 1985) based on blade geometry alone where

$$B = 1 - \frac{c}{R}, \tag{2.200}$$

where c is the tip chord, but this result is limited to rectangular blade tips. Another alternative method

(Sissingh, 1939; Sissingh, 1941) provides an expression for the tip-loss factor given by

$$B = 1 - \frac{c_0(1 + 0.7\tau_r)}{1.5R}, \tag{2.201}$$

where c_0 is the root chord of the main blade, and τ_r is the blade taper ratio. The tip-loss factor will be used in the different proposed closed-form solutions for the thrust coefficient models described in Appendix A.3. The following section describes the blade element theory which provides the needed physical insight to understand how the collective, θ_c, and the rotational speed, Ω, affect the developed thrust.

2.6.2 Blade Element Theory

In order to obtain a mathematical model of how a helicopter in vertical flight generates thrust, it is necessary investigate the blade element theory (BET) (Johnson, 1994; Prouty, 1986; Padfield, 2007; Leishman, 2006; Cuerva et al., 2009; López and Valenzuela, 2010). This theory will provide a closer look of how the thrust force is generated. Blade element theory calculates the forces on the blade due to its motion through the air, and hence the forces and the performance of the entire rotor. Basically, blade element theory is a lifting-line theory applied to the rotating wing. It is assumed that each blade section acts as a two-dimensional airfoil to produce aerodynamic forces, with the influence of the wake and the rest of the rotor contained entirely in an induced angle of attack at the section. Basically the thrust at the blade element is the same as the lift at a wing section. Several works (Anderson Jr., 1989; Anderson Jr., 1991; Bertin and Smith, 2002) can be referenced for further explanations on the lifting line theory, since discussing such theory is out of the scope of this thesis.

Blade element theory is the foundation of almost all analysis of helicopter aerodynamics because it deals with the detailed flow and loading of the blade, and hence relates the rotor performance and other characteristics to the detailed design parameters. In contrast, momentum theory, or any actuator disk analysis, is a global analysis, which provides useful results but cannot alone be used to design the rotor. Again, similarly as in the momentum theory analysis, the blade element theory analysis here conducted follows closely the work done in the literature (Payne, 1959; Bramwell et al., 2001; Johnson, 1994; Prouty, 1986) which is greatly compiled and developed by Leishman (Leishman, 2006) and serves as the main basis for all derivations conducted in this chapter.

Prior to start with the BET analysis, it is important to define the incident velocities and the aerodynamics environment at a typical blade element as given in Figure 2.20, where it can be seen that the resultant local flow velocity at any blade element at a radial distance y from the rotational axis has an out-of-plane component $U_P = V_c + v_i$ normal to the rotor as a result of climb and induced inflow, an in-plane component $U_T = \Omega y$ parallel to the rotor because of the blade rotation relative to the disk plane, and also a radial component U_R. This last component is generally assumed negligible, thus the resultant velocity at the blade element is given by

$$U = \sqrt{U_T^2 + U_P^2}, \tag{2.202}$$

where the relative inflow angle, or also called induced angle of attack, at the blade element is given by

$$\phi_i = \tan^{-1}\left(\frac{U_P}{U_T}\right), \tag{2.203}$$

which for small angles reduces to

$$\phi_i = \tan^{-1}\left(\frac{U_P}{U_T}\right) \approx \frac{U_P}{U_T}. \tag{2.204}$$

If the blade pitch angle at the blade element is θ_c, the aerodynamic or effective angle of attack is given by

$$\alpha = \theta_c - \phi_i = \theta_c - \frac{U_P}{U_T}, \tag{2.205}$$

therefore the resultant increment lift dL and drag dD per unit span on this blade element are given by

$$\begin{aligned} \mathrm{dL} &= \frac{1}{2}\rho U^2 c C_l \mathrm{dy}, & (2.206)\\ \mathrm{dD} &= \frac{1}{2}\rho U^2 c C_d \mathrm{dy}, & (2.207) \end{aligned}$$

where C_l and C_d are the lift and drag coefficients, respectively. The lift (dL) and drag (dD) act perpendicular and parallel to the resultant flow velocity, respectively, and where c is the local bade chord. The forces can be resolved perpendicular and parallel to the rotor disk plane by using the diagram in Figure 2.20, resulting in

$$\begin{aligned} \mathrm{dF_z} &= \mathrm{dL}\cos\phi_i - \mathrm{dD}\sin\phi_i, & (2.208)\\ \mathrm{dF_x} &= \mathrm{dL}\sin\phi_i + \mathrm{dD}\cos\phi_i, & (2.209) \end{aligned}$$

thus the contribution to the thrust, torque and power at the rotor are given by

$$\begin{aligned} \mathrm{dT} &= N_b \mathrm{dF_z}, & (2.210)\\ \mathrm{dQ} &= N_b \mathrm{dF_x} y, & (2.211)\\ \mathrm{dP} &= N_b \mathrm{dF_x} \Omega y, & (2.212) \end{aligned}$$

where N_b is the number of blades that form the rotor. Substituting Eqns. (2.208–2.209) into Eqns. (2.210-2.212) results in

$$\begin{aligned} \mathrm{dT} &= N_b \left(\mathrm{dL}\cos\phi_i - \mathrm{dD}\sin\phi_i\right), & (2.213)\\ \mathrm{dQ} &= N_b \left(\mathrm{dL}\sin\phi_i + \mathrm{dD}\cos\phi_i\right) y, & (2.214)\\ \mathrm{dP} &= N_b \left(\mathrm{dL}\sin\phi_i + \mathrm{dD}\cos\phi_i\right) \Omega y. & (2.215) \end{aligned}$$

A series of assumptions for helicopter rotors can be made (Leishman, 2006) to simplify the analysis, such that the out of plane velocity U_P is much smaller than the in-plane velocity U_T, and this allowing to rewrite Eq. (2.202) as

$$U = \sqrt{U_T^2 + U_P^2} \approx U_T, \tag{2.216}$$

which is a valid approximation except near the blade root, where the aerodynamics forces are small anyway due to the low local velocity. The induced angle ϕ_i is small so that it can be rewritten as

$$\phi_i = \tan^{-1}\left(\frac{U_P}{U_T}\right) \approx \frac{U_P}{U_T}, \tag{2.217}$$

and also using the following trigonometric approximations

$$\begin{aligned} \sin\phi_i &\approx \phi_i, & (2.218)\\ \cos\phi_i &\approx 1. & (2.219) \end{aligned}$$

Finally, since the drag for aerodynamic surfaces is at least one order of magnitude less than the lift, it can be assumed that

$$\mathrm{dD}\sin\phi_i \ll \mathrm{dL}\cos\phi_i \approx 0. \tag{2.220}$$

Using Eqns. (2.216–2.220) into Eqns. (2.213–2.215) results in

$$\begin{aligned} \mathrm{dT} &= N_b \mathrm{dL}, & (2.221)\\ \mathrm{dQ} &= N_b \left(\phi_i \mathrm{dL} + \mathrm{dD}\right) y, & (2.222)\\ \mathrm{dP} &= N_b \Omega \left(\phi_i \mathrm{dL} + \mathrm{dD}\right) y. & (2.223) \end{aligned}$$

Let introduce the nondimensional quantities by dividing lengths by R and velocities by ΩR thus resulting in

$$\begin{aligned} r &= \frac{y}{R}, & (2.224)\\ \frac{U}{\Omega R} &= \frac{\Omega y}{\Omega R} = \frac{y}{R} = r, & (2.225) \end{aligned}$$

and also rewriting Eqns. (2.221–2.223)

$$\mathrm{dC_T} = \frac{\mathrm{dT}}{\rho A \left(\Omega R\right)^2}, \qquad (2.226)$$

$$\mathrm{dC_Q} = \frac{\mathrm{dQ}}{\rho A \left(\Omega R\right)^2 R}, \qquad (2.227)$$

$$\mathrm{dC_P} = \frac{\mathrm{dP}}{\rho A \left(\Omega R\right)^3}. \qquad (2.228)$$

The inflow ratio can therefore be written as

$$\lambda = \frac{V_c + v_i}{\Omega R} = \frac{V_c + v_i}{\Omega y}\left(\frac{\Omega y}{\Omega R}\right) = \frac{U_P}{U_T}\left(\frac{y}{R}\right) = \phi_i r, \qquad (2.229)$$

therefore the increment in thrust coefficient is given by

$$\begin{aligned} \mathrm{dC_T} &= \frac{N_b \mathrm{dL}}{\rho A \left(\Omega R\right)^2}\\ &= \frac{1}{2}\left(\frac{N_b c}{\pi R}\right) C_l \left(\frac{y}{R}\right)^2 d\left(\frac{y}{R}\right)\\ &= \frac{1}{2}\left(\frac{N_b c}{\pi R}\right) C_l r^2 \mathrm{dr}. & (2.230) \end{aligned}$$

Let also recall that for a rectangular blade (c = constant) the ratio of the rotor area to the rotor disk area is known as solidity ratio and is given by

$$\sigma = \frac{\text{Blade area}}{\text{Disk area}} = \frac{A_b}{A} = \frac{N_b c R}{\pi R^2} = \frac{N_b c}{\pi R}, \qquad (2.231)$$

therefore the rotor thrust coefficient in Eq. (2.230) is reduced to

$$\mathrm{dC_T} = \frac{1}{2}\sigma C_l r^2 \mathrm{dr}. \qquad (2.232)$$

Equation (2.232) is one of the most fundamental equations for rotating-wing analysis by means of the BET. Similarly, it can be shown that the rotor-torque coefficient increment is given by

$$\begin{aligned} \mathrm{dC_Q} \equiv \mathrm{dC_P} &= \frac{\mathrm{dQ}}{\rho A \left(\Omega R\right)^2 R} = \frac{N_b \left(\phi_i \mathrm{dL} + \mathrm{dD}\right) y}{\rho \left(\pi R^2\right) \left(\Omega R\right)^2 R} = \frac{1}{2}\left(\frac{N_b c}{\pi R}\right) \left(\phi_i C_l + C_d\right) r^3 \mathrm{dr}\\ &= \frac{1}{2}\sigma \left(\phi_i C_l + C_d\right) r^3 \mathrm{dr}, & (2.233) \end{aligned}$$

which represents the sum of an induced part and a profile part. To find the total C_T and C_Q, the incremental thrust, Eq. (2.232), and the incremental power, Eq. (2.233), must be integrated along the blade from the root to the tip. For a rectangular blade the thrust coefficient is given by

$$C_T = \frac{1}{2}\sigma \int_0^1 C_l r^2 \mathrm{dr}, \qquad (2.234)$$

where the limits of integration are $r = 0$ at the root to $r = 1$ at the tip. For the corresponding torque or power coefficient

$$C_Q \equiv C_P = \frac{1}{2}\sigma \int_0^1 (\phi_i C_l + C_d)\, r^3 \mathrm{dr} = \frac{1}{2}\sigma \int_0^1 \left(\lambda C_l r^2 + C_d r^3\right) \mathrm{dr}, \tag{2.235}$$

To evaluate C_T it is necessary to predict the span-wise variation in the inflow ratio, λ, as well as the sectional aerodynamic force coefficients, C_T and C_D. Assuming 2-D aerodynamics, then $C_l = C_l(\alpha, R_e, M)$ and $C_d = C_d(\alpha, R_e, M)$, where R_e and M are the local Reynolds number and Mach number, respectively, and $\alpha = \alpha(V_c, \theta_c, v_i)$ and $v_i = v_i(r)$. Because these effects cannot, in general, be expressed as simply analytic results, it is necessary to numerically solve the integrals for C_T. However, with certain assumptions and approximations, it is possible to find closed-form analytical solutions.

These solutions are very useful because they serve to illustrate the fundamental form of the results in terms of the operational and geometric parameters of the rotor, and also provide exact check cases for the numerical solutions to the blade element theory (Leishman, 2006). With this in mind, in order to obtain a closed form solution of C_T (2.234) it is necessary to define the form of the local lift coefficient C_l. Based on steady linearized aerodynamics, the local blade lift coefficient can be written as

$$C_l = C_{l_\alpha}(\alpha - \alpha_0) = C_{l_\alpha}(\theta_c - \alpha_0 - \phi_i), \tag{2.236}$$

where C_{l_α} is the 2-D lift-curve-slope of the airfoil section comprising the rotor and α_0 is the corresponding zero-lift angle. For an incompressible flow, C_{l_α} would have a value close to the thin-airfoil result of 2π per radian (Leishman, 2006). Although C_{l_α}, will take a different values at each blade station because it is a function of local incident Mach number and Reynolds number, an average value for the rotor can be assumed without by selecting $C_{l_\alpha} = 5.73$ per radian, which will be the value used throughout the remainder of the thesis. Also it will be assumed that α_0 can be combined into collective pitch angle θ_c, reducing Eq. (2.236) to

$$C_l = C_{l_\alpha}(\theta_c - \alpha_0 - \phi_i) = C_{l_\alpha}(\theta_c - \phi_i). \tag{2.237}$$

Therefore, due to the assumption that C_{l_α} does not depend on r, it can be taken outside of the integral sign, allowing to rewrite (2.234) as

$$C_T = \frac{1}{2}\sigma \int_0^1 C_l r^2 \mathrm{dr} = \frac{1}{2}\sigma \int_0^1 C_{l_\alpha}(\theta_c - \phi_i) r^2 \mathrm{dr} = \frac{1}{2}\sigma C_{l_\alpha} \int_0^1 (\theta_c - \phi_i) r^2 \mathrm{dr}, \tag{2.238}$$

which can be rewritten by recalling the definition of the inflow angle $\phi_i = \lambda / r$ resulting in

$$C_T = \frac{1}{2}\sigma C_{l_\alpha} \int_0^1 (\theta_c r^2 - \lambda r) \mathrm{dr}. \tag{2.239}$$

Similarly to the thrust approximation, torque-power approximations can be obtained by recognizing that Eq. (2.233) can be rewritten by using also the definition of the inflow angle resulting in

$$\begin{aligned} \mathrm{dC_Q} \equiv \mathrm{dC_P} &= \frac{\sigma}{2}\phi_i C_l r^3 \mathrm{dr} + \frac{\sigma}{2} + C_d r^3 \mathrm{dr} \\ &= \frac{\sigma}{2} C_l \lambda r^2 \mathrm{dr} + \frac{\sigma}{2} + C_d r^3 \mathrm{dr} \\ &= dC_{P_i} + dC_{P_0}, \end{aligned} \tag{2.240}$$

where dC_{P_i} is the induced power and dC_{P_0} is the profile power. Recalling from the definition of the incremental thrust Eq. (2.232), the induced power can be written as

$$dC_{P_i} = \lambda dC_T, \tag{2.241}$$

which can be used to rewrite Eq. (2.240) as

$$dC_P = \lambda dC_T + dC_{P_0}, \tag{2.242}$$

and the total power coefficient is given

$$C_P = \int_{r=0}^{r=1} \lambda dC_T + \int_0^1 \frac{\sigma}{2} C_d r^3 \mathrm{dr}. \tag{2.243}$$

By assuming uniform inflow and $C_d = C_{d_0} = constant$, then after integration it is obtained

$$C_P = \lambda C_T + \frac{\sigma}{8} C_{d_0}, \tag{2.244}$$

which can be simplified by assuming hover condition and uniform inflow, Eq. (2.190) resulting in

$$C_P \equiv C_Q = \frac{C_T^{3/2}}{\sqrt{2}} + \frac{\sigma}{8} C_{d_0}, \tag{2.245}$$

where the first term reduces to the simple momentum theory, while the second term in Eq. (2.245) is the extra power predicted by the BET that is required to overcome profile drag of the rotor blades. This concludes the BET analysis, which results in an integral form, Eq. (2.239) that can be used to obtain the thrust coefficient, $C_T(\lambda)$, which depends on the model used to obtain λ. The following section provides the proposed closed-form solution for the selected thrust coefficient.

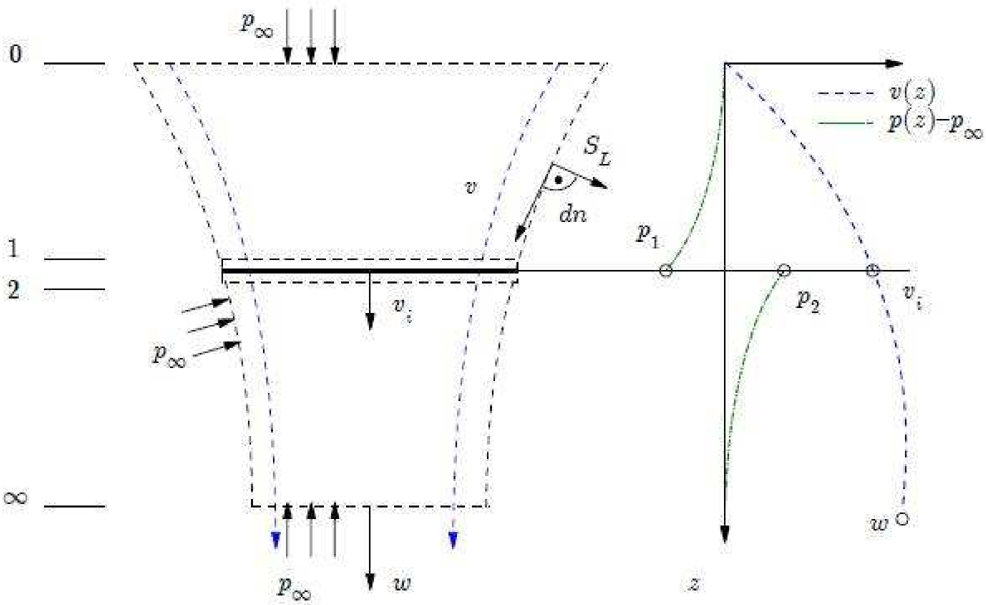

Figure 2.18: Induced velocities in the vicinity of hovering rotor (Leishman, 2006; Cuerva et al., 2009).

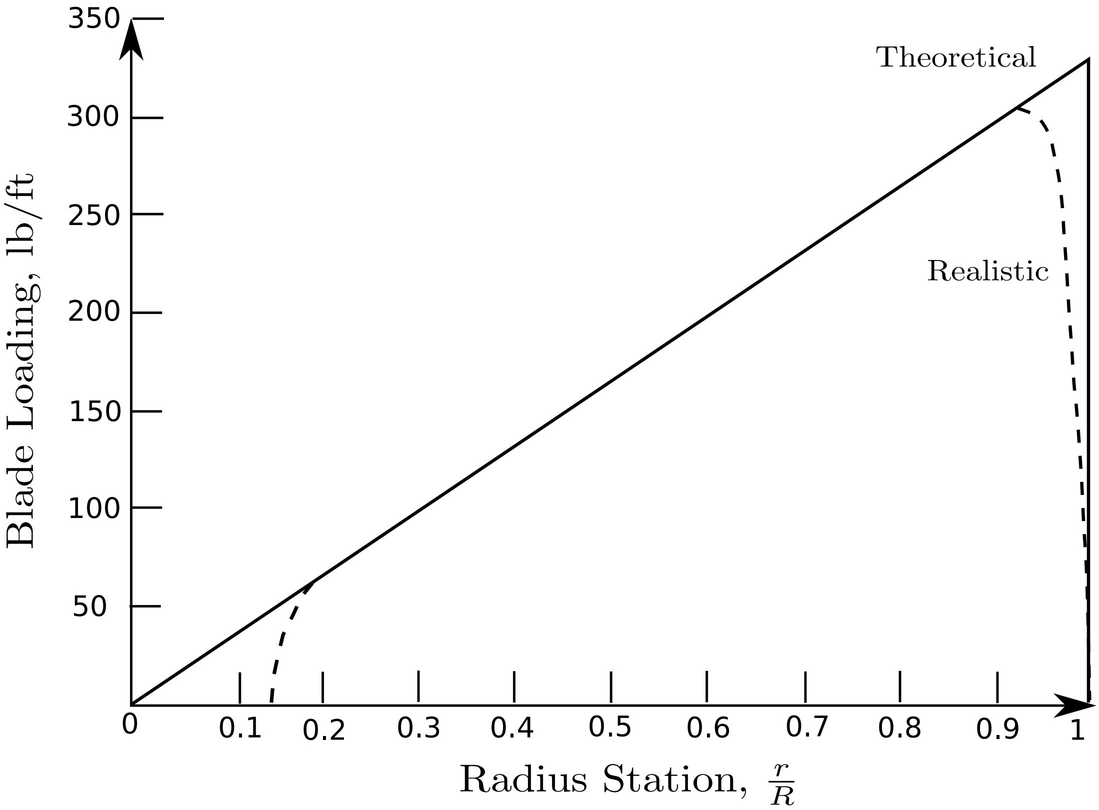

Figure 2.19: Theoretical and realistic lift distribution (Prouty, 1986).

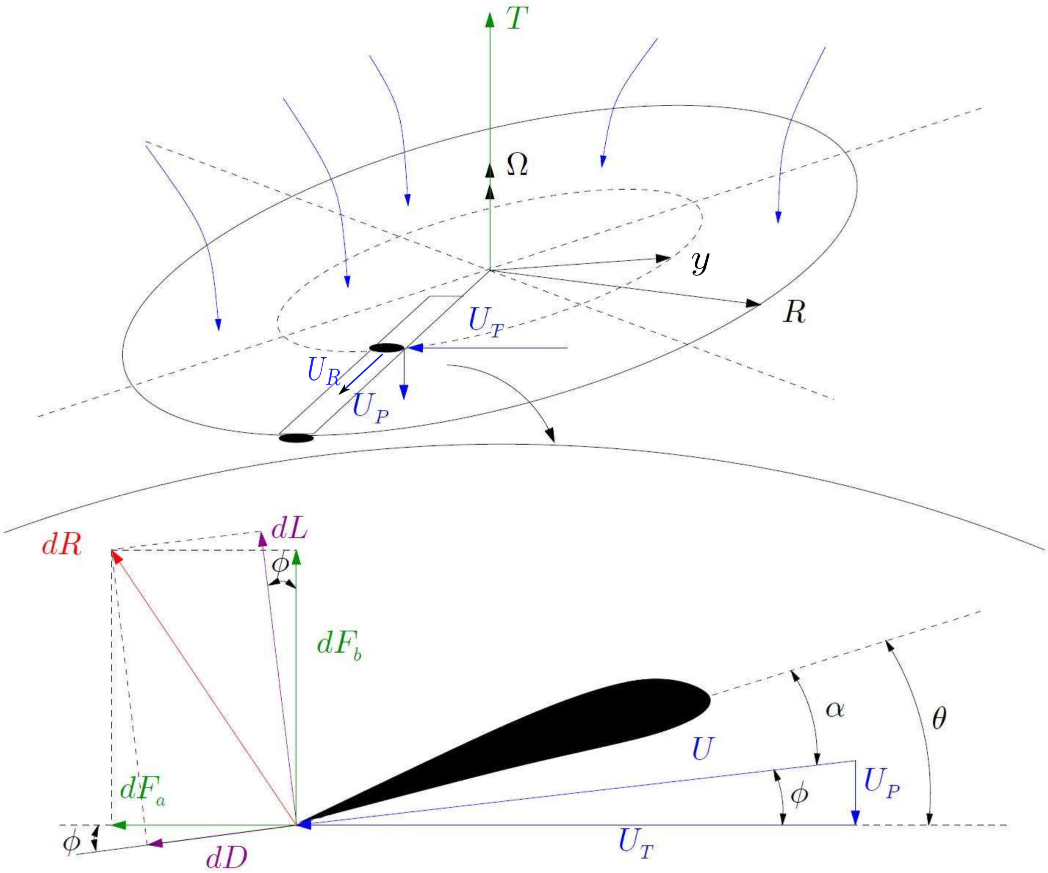

Figure 2.20: Incident velocities and aerodynamic environment at a typical blade element (Leishman, 2006; Cuerva et al., 2009).

2.7 Proposed Closed-Form Solutions for the Thrust Coefficient Model

The previous sections have described separately both the momentum theory (MT) and the blade element theory (BET). The momentum theory provided some good insight into how the helicopter hovers by providing definitions for the inflow ratio depending on the flight condition, while blade element theory provide physical explanations at how the collective pitch and rotational speed affect the developed thrust, but lack to provide closed-form solutions since the integral form, Eq. (2.239), depends on the inflow angle. Therefore it is necessary to combine both theories in order to obtain closed-form solutions of the thrust coefficient which can be used in the proposed axial flight dynamic model for this thesis.

Four closed-form solutions will be proposed for the thrust coefficient C_T which depends on the flight condition that it is assumed, the type of blade, and the assumed flow distribution along the blade of the rotor. These models, all of them available in the literature (Leishman, 2006), will be denoted, following the standard literature nomenclature, and are given by:

- Moment theory for uniform inflow in hover flight condition MT_H
- Moment theory for uniform inflow in axial flight condition MT_C
- Combined blade element theory and momentum theory ($BEMT$)
- Combined blade element theory and momentum theory with Prandtl's Tip-Loss Model ($BEMT_{TL}$)

The first proposed model, the MT_H model, will be the selected model to implement the helicopter dynamics presented in this thesis, and although the model implies a series of hypothesis, it can be demonstrated (Johnson, 1994; Leishman, 2006) that for maneuvers in which the climb and descent velocities are low enough, the MT_H is a really good approximation without any loss of generality, as it will be demonstrated in the simulations. Also, and most important, the first model is the only closed-form continuous model of the four proposed models, therefore, becoming a good candidate, if not the only candidate, that can be used for a control strategy of the continuous type.

Although there are much more precise, and also much more complex thrust coefficient models in the literature (Cuerva et al., 2006a; Cuerva et al., 2006b; Theodore, 2000), the author has chosen the MT_C, $BEMT$ and the $BEMT_{TL}$ models as significate models that are both, much more complex than the selected thrust model MT_H, but are also easily implemented in the simulation platform defined by the author. These "alternative" models will serve as great test-bench problems where to test the robustness of the proposed control strategies under model uncertainties, and for conciseness of the thesis will be described Appendix A, and only a resumed version of the MT_C, $BEMT$, and $BEMT_{TL}$ models will be presented in this section.

2.7.1 Proposed Closed-Form Solution for the Thrust Coefficient Model - The Moment Theory For Uniform Inflow in Hover Flight Condition MT_H

In order to obtain a closed-form blade element and moment theory model for uniform inflow let recall the integral form of the thrust coefficient obtained in the BET analysis, Eq. (2.239). The closed-form solution is obtained by solving the integral along the entire blade, from root to tip, but prior to do so, it is important to introduce the blade-twist concept. For structural purposes, it is desirable to have blades that produce equal amount of thrust along the entire blade, but recalling that the amount of lift of a blade element at a given rotational speed increases with the square of the radius, this implies that the amount of lift generated for a given pitch angle is much greater at the tip, than at the root of the blade, and in return, the structural rigidity of the blade at the tip must be much greater than that at the root of the blade. In order to avoid such construction complexity, most common blades are twisted such that the pitch at the tip is less than the pitch at the rotor. Ideally, it is desired that the twist of the blade be given by the expression

$$\theta_c = \frac{\theta_t}{r}, \tag{2.246}$$

where θ_t is the pitch at the blade tip. This distribution is known as the ideal twist (Johnson, 1994; Prouty, 1986; Leishman, 2006). Due to the complexity associated to the construction of the blades with ideal twist, generally the blades present a linear twist which is defined as

$$\theta_c = \theta_0 + r\theta_{tw}, \tag{2.247}$$

where θ_0 is the pitch that the blade would have if it extended into the center of rotation, and θ_{tw} is the negative angle of twist or washout between the center of rotation and the tip. This negative angle makes possible that the pitch angle of the blade, as it moves toward the tip of the blade, is effectively reduced, which in return, also implies that the amount of lift generated is also reduced from the root to the tip.

Although the ideal twist produces better performance than any other type of twist, the margin between both blades is relatively small, and the simplicity in the manufacturing of the linear twist blades, results in that most helicopters use blades with linear twist. It is important to note that for small radio control (R/C) helicopters, it it easier to construct blades that are rigid enough that there is no need to use twist. With this in mind, and considering first the case in which the blade is untwisted, that is $\theta = \theta_0 =$ constant, recall that, for uniform inflow ratio, which is assumed in simple momentum theory, $\lambda =$ constant, and therefore not dependant on the location of the blade, the thrust coefficient, Eq. (2.239), can be rewritten as

$$\begin{aligned} C_T &= \frac{1}{2}\sigma C_{l_\alpha} \int_0^1 (\theta_c r^2 - \lambda r)\mathrm{d}r = \frac{1}{2}\sigma C_{l_\alpha} \left[\frac{\theta_0 r^3}{3} - \frac{\lambda r^2}{2}\right]_0^1 \\ &= \frac{1}{2}\sigma C_{l_\alpha} \left[\frac{\theta_0}{3} - \frac{\lambda}{2}\right]. \end{aligned} \tag{2.248}$$

To find the direct relationship between C_T and the blade pitch, we can use the relationship between C_T and λ introduced in the momentum theory section for hover flight, Eq. (2.190), therefore reducing Eq. (2.239) such

$$C_T = \frac{1}{2}\sigma C_{l_\alpha} \left[\frac{\theta_0}{3} - \frac{1}{2}\sqrt{\frac{C_T}{2}}\right]. \tag{2.249}$$

Equation (2.249) can be solved to find C_T for a given value of θ_0. Alternatively, Eq. (2.239) can be solved directly for the pitch angle, θ_0, in terms of an assumed thrust resulting in

$$\theta_0 = \frac{6C_T}{\sigma C_{l_\alpha}} + \frac{3}{2}\sqrt{\frac{C_T}{2}}, \tag{2.250}$$

where the first term in Eq. (2.250) is the blade pitch required to produce thrust, and the second term is the additional pitch required to compensate for the inflow resulting from that thrust (Johnson, 1994; Leishman, 2006). It can be shown that by either solving Eq. (2.249) or (2.250), an expression of C_T as a function of θ_c can be obtained resulting in (Pallet and Ahmad, 1991)

$$C_T = \left[\frac{\sigma C_{l_\alpha}}{12}\left(-\frac{3}{2\sqrt{2}} + \sqrt{\frac{9}{8} + \frac{24\theta_c}{\sigma C_{l_\alpha}}}\right)\right]^2. \tag{2.251}$$

Recalling the previously defined thrust coefficient and solidity ration in Eqns. (2.189) and (2.231), respectively, then the thrust force for a given rectangular blade can be rewritten as

$$T = \rho N_b c(\Omega R)^2 R \frac{C_T}{\sigma}, \tag{2.252}$$

and substituting Eq. (2.251) into Eq. (2.252) results in a relation to obtain the thrust force as a function of the angular rotational speed of the blades and its pitch angle given by

$$T = \rho N_b c(\Omega R)^2 R \frac{\sigma C_{l_\alpha}^2}{144} \left(-\frac{3}{2\sqrt{2}} + \sqrt{\frac{9}{8} + \frac{24\theta_c}{\sigma C_{l_\alpha}}} \right)^2. \tag{2.253}$$

Since the blade of A R/C helicopter is untwisted, and the control signal associated to the collective pitch angle has been defined as θ_c, yielding

$$T = \rho N_b c(\Omega R)^2 R \frac{\sigma C_{l_\alpha}^2}{144} \left(-\frac{3}{2\sqrt{2}} + \sqrt{\frac{9}{8} + \frac{24\theta_c}{\sigma C_{l_\alpha}}} \right)^2. \tag{2.254}$$

It can be shown from experimental results (Leishman, 2006) that the agreement between Eq. (2.249) for a given rotor, and the measurements for the same rotor is found to be good, although there is a slight overprediction of the thrust because the nonuniformity of the inflow and nonideal effects, such as tip-loss which have not been taken into account. Considering now the case for linearly twisted blades, that is $\theta_c(r) = \theta_0 + r\theta_{tw}$, where θ_{tw}, as seen previously, is the blade twist rate per radius of the rotor (i.e., in degrees per rotor radius or the equivalent in degrees per unit length of blade). Using this variation in $\theta_c(r)$, in Eq. (2.239) gives

$$\begin{aligned}
C_T &= \frac{1}{2}\sigma C_{l_\alpha} \int_0^1 (\theta_c r^2 - \lambda r)\mathrm{d}r \\
&= \frac{1}{2}\sigma C_{l_\alpha} \int_0^1 \left[(\theta_0 + r\theta_{tw})\, r^2 - \lambda r\right] \mathrm{d}r \\
&= \frac{1}{2}\sigma C_{l_\alpha} \left[\frac{\theta_0 r^3}{3} + \frac{\theta_{tw} r^4}{4} - \frac{\lambda r^2}{2}\right]_0^1 \\
&= \frac{1}{2}\sigma C_{l_\alpha} \left[\frac{\theta_0}{3} + \frac{\theta_{tw}}{4} - \frac{\lambda}{2}\right].
\end{aligned} \tag{2.255}$$

If the reference blade-pitch angle (or collective pitch) is taken at 3/4-radius (also referred as $\theta_{0.75}$), then $\theta_c(r) = \theta_{0.75} + (r - 0.75)\theta_{tw}$ and Eq. (2.255) can be rewritten as

$$\begin{aligned}
C_T &= \frac{1}{2}\sigma C_{l_\alpha} \int_0^1 (\theta_c r^2 - \lambda r)\mathrm{d}r \\
&= \frac{1}{2}\sigma C_{l_\alpha} \int_0^1 \left[\left[\theta_{0.75} + (r - 0.75)\theta_{tw}\right] r^2 - \lambda r\right] \mathrm{d}r \\
&= \frac{1}{2}\sigma C_{l_\alpha} \int_0^1 \left(\theta_{0.75} r^2 + \theta_{tw} r^3 - 0.75\theta_{tw} r^2 - \lambda r\right) \mathrm{d}r \\
&= \frac{1}{2}\sigma C_{l_\alpha} \left[\frac{\theta_{0.75}}{3} + \frac{\theta_{tw}}{4} - \frac{\theta_{tw} r^4}{4} - \frac{\lambda}{2}\right] \\
&= \frac{1}{2}\sigma C_{l_\alpha} \left[\frac{\theta_{0.75}}{3} - \frac{\lambda}{2}\right],
\end{aligned} \tag{2.256}$$

which shows that it is equivalent with Eq. (7.2), therefore showing an interesting result, namely that a blade with linear twist has the same thrust coefficient as one of constant pitch when θ_c is set to the pitch the twisted blade defined at the 3/4-radius (Gessow and Myers, 1985; Johnson, 1994; Leishman, 2006). In a similar manner as for the untwisted analysis, an expression of C_T as a function of θ_c can be obtained

resulting in

$$C_T = \left[\frac{\sigma C_{l_\alpha}}{12}\left(-\frac{3}{2\sqrt{2}} + \sqrt{\frac{9}{8} + \frac{24\theta_{0.75}}{\sigma C_{l_\alpha}}}\right)\right]^2, \tag{2.257}$$

and similarly, the thrust force is given by

$$T = \rho N_b c(\Omega R)^2 R \frac{\sigma C_{l_\alpha}^2}{144}\left(-\frac{3}{2\sqrt{2}} + \sqrt{\frac{9}{8} + \frac{24\theta_{75}}{\sigma C_{l_\alpha}}}\right)^2. \tag{2.258}$$

2.7.2 Proposed Thrust Coefficient Model

This section presents the different proposed thrust coefficient models, the MT_C, the $BEMT$ and the $BEMT_{TL}$ models that will be used as bench models to test the robustness of the proposed control strategies under unmodelled dynamics since they provide more accurate C_T modes than the selected MT_H. These three models are described in detail in the Appendix section A.3.

For the first model, the MT_C, the thrust coefficient for the three flight axial conditions are given by

$$C_{T_{MT_C}} = -\frac{\rho A \sigma C_{L_\alpha} R\Omega\left(-3\sigma C_{L_\alpha} R\Omega + \mathcal{T}_1 - 32R\theta_c\Omega + 24V_c\right)}{192\rho A\Omega^2 R^2}, \tag{2.259}$$

$$C_{T_{MT_D}} = \frac{T_{MT_D}}{\rho A\Omega^2 R^2}, \tag{2.260}$$

$$C_{T_{MT_{WM}}} = -\frac{\rho A \sigma C_{L_\alpha} R\Omega\left(3\sigma C_{L_\alpha} R\Omega - \mathcal{T}_2 - 32R\theta_c\Omega + 24V_c\right)}{192\rho A\Omega^2 R^2}, \tag{2.261}$$

where $\mathcal{T}_1$ and $\mathcal{T}_2$ are described in Eqns. (A.45) and (A.49), respectively, and where

$$V_c/v_h \geq 0 \;\rightarrow\; C_{T_{MT_C}}, \tag{2.262}$$

$$-2 \leq V_c/v_h \leq 0 \;\rightarrow\; C_{T_{MT_D}}, \tag{2.263}$$

$$-2 \geq V_c/v_h \;\rightarrow\; C_{T_{MT_{WM}}}. \tag{2.264}$$

For the second model, the $BEMT$, the thrust coefficient in axial ascent is given by integrating along the entire blade of the integral dC_T given by

$$\mathrm{dC_T} = \frac{\sigma C_{l_\alpha}}{2}\left(\theta_c r^2 - \lambda r\right)\mathrm{dr}, \tag{2.265}$$

with the inflow ratio given by

$$\lambda(r,\lambda_c) = \sqrt{\left(\frac{\sigma C_{l_\alpha}}{16} - \frac{\lambda_c}{2}\right)^2 + \frac{\sigma C_{l_\alpha}}{8}\theta_c r} - \left(\frac{\sigma C_{l_\alpha}}{16} - \frac{\lambda_c}{2}\right), \tag{2.266}$$

and where for the particular case in which the hover flight condition is considered, thus $\lambda_c = 0$, Eq. (2.266) simplifies to

$$\lambda(r) \equiv \lambda_i(r) = \frac{\sigma C_{l_\alpha}}{16}\left(\sqrt{1 + \frac{32}{\sigma C_{l_\alpha}}\theta_c r} - 1\right), \tag{2.267}$$

while for the axial descent is given by

$$C_{T_{MT_D}} = \frac{T_{MT_D}}{\rho A\Omega^2 R^2}, \tag{2.268}$$

$$C_{T_{MT_{WM}}} = -\frac{\rho A \sigma C_{L_\alpha} R\Omega\left(3\sigma C_{L_\alpha} R\Omega - \mathcal{T}_2 - 32R\theta_c\Omega + 24V_c\right)}{192\rho A\Omega^2 R^2}, \tag{2.269}$$

where

$$-2 \leq V_c/v_h \leq 0 \quad \rightarrow \quad C_{T_{MT_D}}, \tag{2.270}$$

$$-2 \geq V_c/v_h \quad \rightarrow \quad C_{T_{MT_{WM}}}. \tag{2.271}$$

And finally, for the fourth model, the $BEMT_{TL}$, the thrust coefficient is also given by integrating along the entire blade of the integral dC_T given as

$$\mathrm{dC_T} = \frac{\sigma C_{l_\alpha}}{2}\left(\theta_c r^2 - \lambda r\right)\mathrm{dr} \tag{2.272}$$

with the inflow ratio given by

$$\lambda(r) = \sqrt{\left(\frac{\sigma C_{l_\alpha}}{16F(r,\lambda(r))} - \frac{\lambda_c}{2}\right)^2 + \frac{\sigma C_{l_\alpha}}{8F(r,\lambda(r))}\theta_c r} - \left(\frac{\sigma C_{l_\alpha}}{16F(r,\lambda(r))} - \frac{\lambda_c}{2}\right), \tag{2.273}$$

and where for the particular case in which the hover flight condition is considered, thus $\lambda_c = 0$, Eq. (2.273) simplifies to

$$\lambda(r) \equiv \lambda_i(r) = \frac{\sigma C_{l_\alpha}}{16F(r,\lambda(r))}\left(\sqrt{1 + \frac{32F(r,\lambda(r))}{\sigma C_{l_\alpha}}\theta_c r} - 1\right), \tag{2.274}$$

while again, for the axial descent is given by

$$C_{T_{MT_D}} = \frac{T_{MT_D}}{\rho A \Omega^2 R^2}, \tag{2.275}$$

$$C_{T_{MT_{WM}}} = -\frac{\rho A \sigma C_{L_\alpha} R\Omega\left(3\sigma C_{L_\alpha} R\Omega - \mathcal{T}_2 - 32R\theta_c\Omega + 24V_c\right)}{192\rho A \Omega^2 R^2}, \tag{2.276}$$

where

$$-2 \leq V_c/v_h \leq 0 \quad \rightarrow \quad C_{T_{MT_D}}, \tag{2.277}$$

$$-2 \geq V_c/v_h \quad \rightarrow \quad C_{T_{MT_{WM}}}. \tag{2.278}$$

Recall that both MT_H and MT_C produce close-form solutions for the thrust coefficient C_T, Eq. (2.248), which are both explicit functions of the collective pitch angle θ_c and the inflow angle. Recall also that while for the MT_H model, the hover flight condition, the inflow angle is a function of C_T, resulting in a continuous closed-form solution for the thrust coefficient. The proposed MT_C model presents nonlinearities depending on the nature of the climb flight region, and therefore being unfeasible to integrate into a set of continuous differential equations if the goal is to design continuous and differentiable control laws.

On the other side, for both blade element theory models, $BEMT$ and $BEMT_{TL}$, it is required numerical integration at each instant in order to obtain the thrust coefficient, therefore making impossible to obtain a closed-form solution to which be able to design a proper control law to regulate the amount of thrust generated, but they will serve as a great bench-mark problems where to test the validity of the selected model, and to test the robustness of the proposed control laws under model uncertainties.

With this in mind, this makes MT_H the only implementable thrust coefficient model C_T, and will be the model employed for the helicopter dynamics proposed in section 2.8, which, once integrated into the proposed dynamics for axial flight, it will be tested against the rest of models, and it will be shown, via simulations, that the MT_H model, although much more simpler, it reproduces the dynamics of the more detailed and complex models (MT_C, $BEMT$ and $BEMT_{TL}$) without loss of generality for the low vertical speeds at which the R/C helicopter is to be operated, thus corroborating the validity of its selection (Johnson, 1994; Leishman, 2006).

Nevertheless, the validity of the MT_H model is subject to the series of hypothesis that have been exposed throughout the previous derivations, and are exposed in the following sections to justify that the selected model can be implemented in the R/C helicopter model that will be derived in detail in A.4. These hypothesis are standard and well established hypothesis, which are necessary in order to be able to obtain reduced empirical models that are able to model, to a certain degree, the highly complex and non linear behavior of rotating blades (Leishman, 2006).

As it will be described in section 2.8, the dynamics of the helicopter in axial flight will consist in three distinct dynamics, the axial flight dynamics, that is, the dynamics that define the axial displacement and velocity of the helicopter, the combustion engine and rotational velocity dynamics, which define the rotational angular velocity of the blades, and the collective pitch dynamics, which describe the collective pitch angle of the blades. All three dynamics are somehow affected, in one way or another, by the above mentioned hypothesis.

The author believes that it is important to note that the solution adopted, although is not the only possible solution, and maybe not the optimal solution, it is a feasible solution that has been adopted previously in (Pallett and Ahmad, 1993; Sira-Ramírez et al., 1994; Huang and Balakrishnan, 2005; Kaloust et al., 2002; Tee et al., 2008) with great success. The proposed methodology employed to model the dynamics of the helicopter in axial flight, and the methodology proposed to determine the required parameters being involved in the different dynamic models, both presented in (Pallet et al., 1991; Pallet and Ahmad, 1991), follow a logic process that is consistent with the blade element and momentum theory previously presented, making this a feasible methodology, and, what it is probably more important, a suitable methodology for both the actual goals, and the near future goals of this thesis.

The first one, the actual goal, is having a helicopter model where to test the proposed control laws, and the second, the near future goals, is to have a step-by-step process that can be used to identify the parameters that are used in the presented model since ultimately it is desired to be able to validate the results here presented in a real R/C helicopter platform, and a theoretical model is only good if it serves the purposes for which it was created, and in this case it was selected having in mind that had to be implemented. With this in mind, it is expected that when trying to implement the obtained control laws into the real R/C helicopter, some of the proposed identification methods (Pallet and Ahmad, 1991) will need to be revised and/or improved, as it has been already done with some of the aerodynamic parameters, to account for some lost dynamics, but this is out of the scope of this thesis, and throughout the remainder will be assumed that the proposed methods are the proper ones.

2.8 Proposed Model Definition for a Miniature Helicopter in Axial flight

This section proposes a model for a miniature helicopter, which will be used throughout the remainder of this thesis, and it is based on the technical reports that were written at the University of Purdue (Pallet et al., 1991; Pallet and Ahmad, 1991), that describe the vertical motion of an autonomous helicopter mounted on a stand as seen in Figure 2.23. This model is used to derive the control laws that will be implemented in the future in a similar platform to (Pallet and Ahmad, 1991), which can be seen in Figures 2.24 and 2.25.

The model is based in the MT_H model previously derived in section 2.6, which includes the helicopter dynamics in the axial flight condition, and also includes some of the losses that were introduced in the hypothesis presented in section A.4, and that were not accounted for in the proposed MT_H model. It is important to note that although miniature helicopters are functionally similar to their full-scale counterparts, there are a few differences (mainly in rotor construction) which require modification to the normal thrust equations used to model full-scale helicopters. For example, as noted in the hypothesis

A.4.8, the model helicopter has straight rotor blades instead of linearly twisted blades as is the case for real helicopters. Another significant difference between a miniature *RC* helicopter and full-scale helicopter is that, generally, *RC* helicopters compensate for the lack of a flapping and lead-lag hinges (Layton, 1984; Prouty, 1986) by using a teetering hinge which produces the same effect.

The teeter system works around a central hinge. The position of the blades is due to the balance between centrifugal force which is trying to hold the blades "straight out", versus lift which is trying to make them fold straight up. The balance of the forces will cause the blades to fly at some angle. If one blade starts to develop more lift, while the other blade starts to develop less lift, one blade will want to climb while the other will want to descend. The result will be that the rotor head will teeter, allowing one blade to go up while the other goes down. Figure 2.21 shows the main rotor of a Bell 206 where it can be distinguished the teeter hinge, and Figure 2.22 shows the teetering movement on a Robinson 22. The use of a teetering rotor will not be a concern for modeling the hovering of the *RC* helicopter and will not introduce any changes.

The helicopter model here presented, although constrained to vertical flight with the selected thrust coefficient model, the MT_H model, it also includes the nonlinear dynamics of the collective pitch actuators, which increases considerably the complexity of the model, but also depicts a more realistic model. The helicopter dynamics in vertical flight will be initially separated into three equations: vertical position of the helicopter, collective pitch of the blades, and rotational velocity of the main rotor. The following sections describe in more detail each of the governing equations, with each of the parameters of the equations being described and justified using the proposed methods in (Pallet and Ahmad, 1991). After the models have been defined, methods to determine the unknown constants of the proposed models will be presented also derived from (Pallet and Ahmad, 1991).

2.8.1 Proposed Model for the Vertical Displacement Equations

Recalling the resulting simplified vertical displacement dynamics, Eq. (2.171), the vertical force that provides the axial displacement can be modeled by considering the differential set of equations that describes the vertical motion of a model miniature helicopter given by:

$$\ddot{\xi} = \frac{T}{m}(1 + G_{eff}) - g_z - F_{damping} - T_{loss} - F_{drag}, \tag{2.279}$$

where Ω ($radians$) is the rotational speed of the rotor blades, ξ ($meters$) is the height of the helicopter above the ground, g_z (m/s^2) is the gravitational acceleration, and G_{eff} models the ground effect, but during the remainder of this thesis it will be considered negligible ($G_{eff} = 0$), since at it can be seen in Figure 2.24, the constructed setup for the flying helicopter stand is elevated more than one rotor diameter, which as previously discussed, is the distance required so that the ground effect does not have any significate influence the helicopter's performance. In Eq. (2.279), T is the thrust force defined in Eq. (7.2) which for completeness is written as:

$$T = \rho N_b c(\Omega R)^2 R \frac{C_T}{\sigma}, \tag{2.280}$$

where C_T is the thrust coefficient of the helicopter model, which was defined by the MT_H derived model, Eq. (7.1), and for completeness of the section rewritten again as:

$$C_T = \left[\frac{\sigma C_{l_\alpha}}{12}\left(-\frac{3}{2\sqrt{2}} + \sqrt{\frac{9}{8} + \frac{24\theta_c}{\sigma C_{l_\alpha}}}\right)\right]^2, \tag{2.281}$$

where recall that σ is the solidity ratio, C_{l_α} is the blade lift slope, and θ_c is the collective pitch angle of the rotor blades. For simplification purposes in the parameter determination process, the thrust coefficient can also be expressed as:

$$C_T = \left(-K_{C1} + \sqrt{K_{C1}^2 + K_{C2}\theta_c}\right)^2, \tag{2.282}$$

where:

$$K_{C1} = \frac{\sigma C_{l_\alpha}}{8\sqrt{2}}, \tag{2.283}$$

$$K_{C2} = \frac{2\sigma C_{l_\alpha}}{12}. \tag{2.284}$$

With this in mind Eq. (2.279) can be expanded as:

$$\ddot{\xi} = \rho N_b c(\Omega R)^2 R \frac{\sigma C_{l_\alpha}^2}{144m}\left(-\frac{3}{2\sqrt{2}} + \sqrt{\frac{9}{8} + \frac{24\theta_c}{\sigma C_{l_\alpha}}}\right)^2 m(1+G_{eff}) - g_z - F_{damping} - T_{loss} - F_{drag}. \tag{2.285}$$

The first term on the right-hand side of (2.290), can be rewritten as $K_1 C_T(1+G_{eff})$ with

$$K_1 = \frac{\rho N_b c R^3}{\sigma m}. \tag{2.286}$$

This term represents the main thrust/lift term which is based on the MT_H model previously derived. The second term, g_z, is the acceleration due to gravity acting on the helicopter. The third term in (2.290), $F_{damping}$, represents the damping in the flight test stand especially due to the piston mounted to offset the weight of the helicopter and the structure itself, and can be defined as $K_2\dot{\xi}$. The fourth term, T_{loss}, represents the resistance to motion of the helicopter as seen in section A.4.5, where this term represents the parasitic drag that will result in losses to the generated thrust, when moving the helicopter through the air. Recalling that the loss in thrust that will be appreciated as the helicopter moves through the air, the T_{loss} was defined as of the form:

$$T_{loss} = \frac{1}{2m}\rho V_c^2 f_z^{fus}, \tag{2.287}$$

where f_z^{fus} is the equivalent flat plate area of the fuselage in the z-axis direction, also defined as $f_z^{fus} = S_{fus}C_{D_f}$, with S_{fus} being the maximum fuselage cross area in the x-y plane, and C_{D_f} the drag of the fuselage, and V_c is the climb velocity of the helicopter, where $\dot{\xi} \equiv V_c$. Equation 2.288 can be defined as:

$$T_{loss} = K_3 V_c^2, \tag{2.288}$$

with K_3 of the form:

$$K_3 = \frac{1}{2m}\rho f_z^{fus}, \tag{2.289}$$

where although f_z^{fus} can be initially estimated using simple equivalent skin friction methods used for aircraft design (Raymer, 2006; Roskam and Lan, 1997), methods trends for helicopter (Cheeseman and Bennett, 1957; Yeo et al., 2004; Leishman, 2006), or even due to the limitation of these last, use estimations for similar RC helicopters (Gavrilets, 2003) which has been extensively used in the literature (Gavrilets et al., 2002a; Ng et al., 2006; Budiyono et al., 2008; Garratt, 2007), and resembles the helicopter model here selected as it will be seen in section 2.8.4.1. The obtention of the proper equivalent flat plate area is out of the scope of this thesis, and will be assumed that it is obtained via experimentation. The values employed in this thesis for K_3 will be the ones described in (Pallet et al., 1991; Pallet and Ahmad, 1991), ans as it will be seen in section 2.8.4.1, don't differ from the predicted values existing in the literature.

Finally, the last term, F_{drag} is the normalized constant drag, $F_{drag} = D_{const}/m$. The constant drag, which will be represented by parameter K_4, is due mainly to the fact that the area taken up by the helicopter body itself will reduce the amount of lift force that can be produced from the blades. The helicopter body takes up area through which the blades would push air through if the helicopter body was not present. This drag loss should be small, since the majority of the thrust is produced in the middle of the blade instead of at the root or the tip of the blade. With all this in mind, the original vertical position equation (2.290) can be written as:

$$\ddot{\xi} = K_1 C_T (1 + G_{eff}) \Omega^2 - g_z - K_2 \dot{\xi} - K_3 \dot{\xi}^2 - K_4, \tag{2.290}$$

which can be reduced if it is assumed that the helicopter is at an altitude in which ground effects are negligible, as seen in Figures 2.24 and 2.25, thus reducing Eq. (2.290) to:

$$\ddot{\xi} = K_1 C_T \Omega^2 - g_z - K_2 \dot{\xi} - K_3 \dot{\xi}^2 - K_4. \tag{2.291}$$

The model proposed in (Pallet et al., 1991; Pallet and Ahmad, 1991) does not provide a detailed description of each of the presented constants, and it leaves their estimation to the experiments. This section has provided mathematical expression for K_1 and K_3, Eqns. (2.286) and (2.289) that will help in the modelization process, and in future improvements of the existing theoretical $2 - D$ models.

2.8.2 Proposed Model for the Combustion Engine and Rotational Velocity

The dynamics of the angular velocity of the blades can be modeled as:

$$\dot{\Omega} = -K_5 \Omega - K_6 \Omega^2 - K_7 \Omega^2 \sin\theta_c + f(u_{th}), \tag{2.292}$$

with:

$$f(u_{th}) = (K_8 u_{th} + K_9), \tag{2.293}$$

where $f(u_{th})$ is the input to the throttle servo, u_{th}. It is assumed that the time delay is negligible (Pallet et al., 1991; Pallet and Ahmad, 1991), and therefore not modeled thus resulting in:

$$\dot{\Omega} = -K_5 \Omega - K_6 \Omega^2 - K_7 \Omega^2 \sin\theta_c + K_8 u_{th} + K_9. \tag{2.294}$$

Note that all of the five unknown constants have been divided by the rotor's effective inertia, I_r. which includes the inertia of the motor reflected through the gears. The first term on the right-hand side of Eq. (2.292), $K_5\Omega$, is a damping term that opposes the motion of the rotor blades due to the friction within the rotor gears and the gasoline engine that produces an opposing torque that will tend to slow the rotational speed. The second term in Eq. (2.292), $K_6\Omega^2$, are considered in (Pallet et al., 1991; Pallet and Ahmad, 1991) as a drag term that is constant with respect to the collective pitch. This drag can be thought as the drag on the blade when the collective pitch angle is zero, that is $\theta_c = 0$. Pallet *et al.* (Pallet et al., 1991; Pallet and Ahmad, 1991) does not provide a mathematical expression for K_6, and again leaves its calculation to the experimentation. A mathematical model can be proposed by considering BET theory presented previously in section 2.6.2, thus it can be assumed that K_6 is of the form:

$$K_6 = \frac{N_b}{I_r} f_{Q_{profile}}, \tag{2.295}$$

where N_b is the number of blades, and $f_{Q_{profile}}$ is a function of the profile torque, which in addition it can be assumed to be a function of the equivalent flat plate area, f^{blade}, of the blade, which can be defined as $f^{blade} = S_{blade} C_{D_0}$, with S_{blade} being the blade area, and C_{D_0} the profile drag of the blade. Similarly, the third term in Eq. (2.292), $K_7\Omega^2 \sin\theta_c$, is considered in (Pallet et al., 1991; Pallet and Ahmad, 1991) as an air drag loss for the rotational speed of the blades, which is proportional to the drag area of the blades. This air drag loss will oppose the rotation of the blades, and it varies as the effective area of the blades cutting through the air. It is assumed that the induced drag term, the third term in Eq. (2.292), is approximated by observing the projected blade surface area perpendicular to the rotation of the blades, as seen in Figure 2.26, it can be seen that the effective drag area of the main rotor blades can be defined as:

$$A_{F_e} = N_b R c \sin\theta_c = N_b A \sin\theta_c, \tag{2.296}$$

with R being the radius of the blade, and c the chord, and A the area blade if it is assumed that the blade is not tapered in planform, i.e. rectangular blade, that is $A = Rc$, therefore it can be assume that K_7 is of the form:

$$K_7 = \frac{N_b A}{I_r} f_{Q_{induced}}, \tag{2.297}$$

where $f_{Q_{induced}}$ is a function of the induced torque. A better modelization of these two terms can be obtained by recalling the MT and BET presented in Chapter 2.6, and recognizing that they represent the induced torque and the profile torque losses of the main rotor, or what it is the same the extra power required to overcome the induced drag and the profile drag of the rotor blades. By considering BET the second and third term in Eq. (2.292) can be replaced resulting in:

$$\dot{\Omega} = -K_5 \Omega - \frac{Q}{I_r} + f(u_{th}, T_d), \tag{2.298}$$

with Q being the sum of the profile and induced rotor torque, and defined by BET as:

$$Q = \frac{1}{2}\rho N_b (\Omega R)^2 \Omega R A C_Q = \frac{1}{2}\rho N_b (\Omega R)^2 \Omega R A (C_{Q_i} + C_{Q_0}), \tag{2.299}$$

where C_Q is formed by the induced torque coefficient, C_{Q_i}, and the profile torque coefficient, C_{Q_0}, which can be approximated for uniform inflow and constant profile drag by using Eq. (2.245) resulting in:

$$\begin{aligned} Q &= \frac{1}{2}\rho N_b (\Omega R)^2 \Omega R A \left(\frac{C_T^{3/2}}{\sqrt{2}} + \frac{\sigma}{8} C_{d_0} \right) \\ &= \frac{1}{2}\rho N_b (\Omega R)^2 \Omega R A \frac{C_T^{3/2}}{\sqrt{2}} + \frac{1}{2}\rho N_b (\Omega R)^2 \Omega R A \frac{\sigma}{8} C_{d_0}, \end{aligned} \tag{2.300}$$

where the main rotor inertia, I_r is a difficult parameter to determine. Gavrilets (Gavrilets, 2003; Gavrilets et al., 2001) has proposed a highly nonlinear complete 6-DOF helicopter model that has been extensively used in the literature due to the available complete model and the values of all parameters. The success of such model relays in that the helicopter modeled is a X-Cell 60 RC helicopter, with a hingeless main rotor equipped with a Bell-Hiller stabilizer bar (Bramwell et al., 2001), which provides lagged rate feedback and augments the servo torque with aerodynamic moment to change the cyclic pitch of the blades, of approximately 11 lbs (4,98 kg), which has been a commonly available UAV platform, and used by many university and research institutions. This model is equivalent in size to the R/C model helicopter used in (Pallet et al., 1991; Pallet and Ahmad, 1991), and used throughout this thesis, an X-Cell 50, which is equivalent in size and with the only difference affecting the engine plant. For that reason, the geometrical parameter estimations presented in (Gavrilets, 2003) provide valuable data that can be used in the more precise modelization presented in this section. With this in mind, and due to the difficulty associated in determining the main rotor inertia, the process presented by Gavrilets (Gavrilets, 2003) is used where:

$$I_r = 2I_{\beta_{mr}} + I_{es} n_{es}^2 + 2I_{\beta_{tr}} n_{tr}^2, \tag{2.301}$$

where $I_{\beta_{mr}}$ and $I_{\beta_{tr}}$ represent the main rotor and the tail rotor blade inertias, respectively, I_{es} is the inertia of the engine shaft and all components rotating at the engine speed, n_{tr} is the tail rotor gear ratio, and n_{es} is the engine gear ratio. As defined in (Gavrilets, 2003), the most important contribution comes from the main rotor blades. The tail rotor inertia, after scaling with the gear ratio squared, amounts to 5% percent of the main rotor inertia. The rotating inertia referenced to the engine speed is harder to estimate, but an upper bound can be found by estimating the total mass of rotating components for the X-Cell 0.2 kg, and its effective radius of inertia, 0.04 m. They arrive to an estimate for I_{rot} equal to 2.5 inertias of the main rotor blade, where from (Gavrilets, 2003), for the X-Cell 60, $I_{\beta_{mr}} = 0.038kgm^2$, this resulting in $I_r = 0.095kgm^2$.

The final term $f(u_{th})$ is due to the throttle servo input. The exact dependance of the throttle input to the rotational speed of the blades and the engine is quite difficult to predict precisely since the dynamics of the engine's thermal process are not well understood in terms of linear or nonlinear models which could be simply derived. However, an approximate model is selected (Pallet and Ahmad, 1991) by observing that the angular acceleration near the typical hovering rotation velocities is affected by the throttle input in a linear manner, and defined by Eq. (2.293).

Despite the differences between the theoretical models presented by Pallet *et al.* (Pallet et al., 1991; Pallet and Ahmad, 1991), Eq. (2.292), and the proposed alternative angular velocity model here presented, which is based in the BET, Eq. (2.298), the first model will be the one selected throughout the remainder of this thesis, since it has been widely used in the literature as a test bench problem (Pallett and Ahmad, 1993; Sira-Ramírez et al., 1994; Huang and Balakrishnan, 2005; Kaloust et al., 2002; Tee et al., 2008).

The alternative, and more precise angular velocity model will be used in future related works as a test bench model to test the robustness for the selected engine-throttle control strategy, although in the work conducted in this thesis, the robustness to unmodeled dynamics will only be studied on the thrust coefficient modelization.

The parameter estimation process developed in section 2.8.4.1 will define a process that allows to determine the proposed throttle input models and also the rest of the parameters in Eq. (2.292) based in (Pallet and Ahmad, 1991). It is important to note that many other external factors can affect the engine performance, and that the proposed model does not take into account, like the air condition, the fuel or lubrication employed which can modify engine performance, to name few.

The above mentioned will result in that the helicopter's performance will change from day to day, and even from experiment to experiment. With this in mind, the parameter estimation experiments will be used to obtain a set of nominal values about which the engine is expected to be operated. It is therefore recommended to try to replicate the external conditions of the experiments, both during the identification experiments, and through the testing process, to ensure the validity of the proposed model.

2.8.3 Proposed Model for the Collective Pitch Dynamics

The dynamics of the collective pitch angle can be defined as:

$$\ddot{\theta}_c = K_{10} f(u_{\theta_c}, \theta_c) - K_{11}\dot{\theta}_c - K_{12}\Omega^2 \sin\theta_c, \tag{2.302}$$

where $f(u_{\theta_c}, \theta_c)$ in a function that defines the collective servomechanism input, u_{θ_c} and is given by:

$$f(u_{\theta_c}, \theta_c) = A_{\theta_{c_1}} u_{\theta_c} + A_{\theta_{c_2}} - \theta_c, \tag{2.303}$$

therefore resulting in:

$$\ddot{\theta}_c = K_{10}\left(A_{\theta_{c_1}} u_{\theta_c} + A_{\theta_{c_2}} - \theta_c\right) - K_{11}\dot{\theta}_c - K_{12}\Omega^2 \sin\theta_c. \tag{2.304}$$

The first term in Eq. (2.302), $K_{10}f(u_{\theta_c}, \theta_c)$, represents the force input produced by the collective pitch servo actuating the collective pitch mechanism to the desired position. The second term in Eq. (2.302), $K_{11}\dot{\theta}_c$, is a damping term due to the linkages and the built in servo gear ratio, which generally can be demonstrated that this type of servomechanisms will have naturally some damping (Pallet and Ahmad, 1991).

The third term in Eq. (2.302), $K_{12}\Omega^2 \sin\theta_c$, represents the drag/resistence to motion due to the blade striking the air. Since the *RC* helicopter will always be operating with a positive collective pitch, the blade will naturally tend to move towards a position of least resistance. Note, that all of the three unknown constants include a divide by the inertia of the blades and mechanical linkages about the collective pitch axis, I_a, and also due to the difficulty on its difficult calculation, its value will be left for the identification experiments, and for the model employed in this thesis, the estimates presented in (Pallet and Ahmad, 1991) will be used.

2.8.4 Proposed Methods for Parameter Determination and Model Verification

This section describes the proposed methods for parameter determination and model verification which are based on the works of (Pallet et al., 1991; Pallet and Ahmad, 1991) and described the parameter determination process for the three proposed dynamics, the axial flight dynamics, the engine actuation and the rotational velocity of the blades, and the collective pitch actuators dynamics. The determination of the parameters for each of the three dynamics is described bellow.

2.8.4.1 Parameter Determination For Axial Flight Dynamics

The proposed methodology to determine the different parameters for the axial flight dynamics (2.305), that is K_1, K_2, K_3, and K_4, can be divided in two parts (Pallet and Ahmad, 1991). In a first part, the main objective is to determine empirically the coefficients that do not depend on the axial velocity, $\dot{\xi}$, and this can be done by conducting several experiments is which the *RC* helicopter if flown at the hover flight condition, this resulting in that the terms involving the axial velocity cancel out, since at hover $\dot{\xi} = 0$ therefore reducing (2.305) to:

$$\ddot{\xi} \quad = \quad K_1 C_T \Omega^2 - g_z - K_4. \tag{2.305}$$

This flight condition reduces the axial flight dynamics to a equation with the thrust/lift term, the gravitational force, and the constant drag term. Although K_1 has been defined in (2.286), it is necessary to determine its value through experiments to account for possible losses. This is done by conducting several experiments in which known amounts of weight are added to the helicopter for a given fixed rotational speed, Ω_1, and a fixed collective pitch angle, θ_c, until the helicopter is able to hover at a fixed position.

Once the helicopter is able to sustain that hover flight condition, and assuming that the thrust coefficient model, MT_H is an accurate model, the weight is recorded, W_1, and a new experiment is conducted, for different fixed rotational speed, Ω_2, the same fixed collective pitch angle, θ_c, and in a similar manner, different weights are added until the helicopter is able to hover at a fixed altitude, which will again be associated to a new weight, W_2. For the different loading test the constant drag term, K_4 will be constant, and the value of both K_1 and K_4 can be determined empirically. The process could be defined like:

$$W_1 \quad = \quad K_1 C_{T_1} \Omega_1^2 - \hat{K}_4, \tag{2.306}$$

$$W_2 = K_1 C_{T_1} \Omega_2^2 - \hat{K}_4, \tag{2.307}$$

where $\hat{K}_4 = g_z + K_4$. Let solve K_1 in Eq. (2.306) as a function of constant drag term, $\hat{K}_4$ resulting in:

$$K_1 = \frac{W_1 + \hat{K}_4}{C_{T_1}\Omega_1^2}, \tag{2.308}$$

and substitute Eq. (2.308) into Eq. (2.307) resulting in:

$$\begin{aligned} W_2 &= \frac{W_1 + \hat{K}_4}{C_{T_1}\Omega_1^2} C_{T_1}\Omega_2^2 - \hat{K}_4 \\ &= (W_1 + \hat{K}_4)\frac{\Omega_2^2}{\Omega_1^2} - \hat{K}_4, \end{aligned} \tag{2.309}$$

which can be solved for $\hat{K}_4$ resulting in:

$$\hat{K}_4 = \frac{W_2 - W_1 \frac{\Omega_2^2}{\Omega_1^2}}{\frac{\Omega_2^2}{\Omega_1^2} - 1}, \tag{2.310}$$

thus recalling $\hat{K}_4 = g_z + K_4$ results in:

$$\begin{aligned} K_4 &= \hat{K}_4 - g_z \\ &= \frac{W_2 - W_1 \frac{\Omega_2^2}{\Omega_1^2}}{\frac{\Omega_2^2}{\Omega_1^2} - 1} - g_z, \end{aligned} \tag{2.311}$$

and substituting Eq. (2.311) back into Eq. (2.306) results in:

$$W_1 = K_1 C_{T_1}\Omega_1^2 - \frac{W_2 - W_1 \frac{\Omega_2^2}{\Omega_1^2}}{\frac{\Omega_2^2}{\Omega_1^2} - 1}, \tag{2.312}$$

which can be solved for K_1 resulting in:

$$K_1 = \frac{1}{C_{T_1}\Omega_1^2}\left(W_1 - \frac{W_2 - W_1 \frac{\Omega_2^2}{\Omega_1^2}}{\frac{\Omega_2^2}{\Omega_1^2} - 1} + g_z \right), \tag{2.313}$$

thus resulting in an empirical equation for both K_1 and K_4. It is convenient to run the experiment several times to reduce the error associated to bias measurements. The second part of the identification process deals with the constants that depend on the axial velocity, $\dot{\xi}$, that is K_2 and K_3.

Once determined K_1 and K_4, the determination of the parameters shifts towards step responses in throttle and collective pitch, (u_{θ_c}, θ_c) which will result in vertical motion of the helicopter. From this data it is able to determine the damping constant, K_2 , and the parasitic drag constant, K_3, by fitting the step response data curves.

2.8.4.2 Parameter Determination for Rotational Speed Dynamics

The proposed methodology to determine the different parameters in (2.294), that is K_5, K_6, K_7, K_8, and K_9, uses also a series of experiments described bellow (Pallet and Ahmad, 1991). The rotational speed equation constants may turn out to be the most difficult to determine as a result of the variations in plant output from day to day as mentioned above.

First, and in a similar manner as for the vertical velocity equation, the identification process can be simplified by canceling terms by taking use of the available control signals, that is, let cancel the collective pitch angle terms by selecting $\theta_c = 0$, and by running the helicopter at a constant rotational velocity.

This will results in an equation with K_5, K_6, K_8 and K_9 terms resulting in:

$$0 = -K_5\Omega - K_6\Omega^2 + K_8 u_{th} + K_9, \tag{2.314}$$

which can be rewritten to obtain an expression for the throttle input servo u_{th} resulting in:

$$u_{th} = \bar{K}_5\Omega + \bar{K}_6\Omega^2 - \bar{K}_9, \tag{2.315}$$

with:

$$\bar{K}_5 = \frac{K_5}{K_8}, \tag{2.316}$$

$$\bar{K}_6 = \frac{K_6}{K_8}, \tag{2.317}$$

$$\bar{K}_9 = \frac{K_9}{K_8}. \tag{2.318}$$

The determination process for the constants $\bar{K}_5$, $\bar{K}_6$, $\bar{K}_9$ is conducted by selecting steady state pairs of measured rotational angular speeds, Ω, and input to the throttle servo, u_{th}, for the given range of rotational speed during the hover flight condition, resulting in a set of linear equations:

$$u_{th_i} = \bar{K}_5\Omega_1 + \bar{K}_6\Omega_1^2 - \bar{K}_9, \tag{2.319}$$

$$u_{th_2} = \bar{K}_5\Omega_2 + \bar{K}_6\Omega_2^2 - \bar{K}_9, \tag{2.320}$$

$$u_{th_3} = \bar{K}_5\Omega_3 + \bar{K}_6\Omega_3^2 - \bar{K}_9, \tag{2.321}$$

$$\vdots$$

$$u_{th_n} = \bar{K}_5\Omega_n + \bar{K}_6\Omega_n^2 - \bar{K}_9. \tag{2.322}$$

The steady state pairs obtained in the experiments , that is $(\Omega_i u_{th_i})_{i=1,n}$, can be used to solve for the constants $\bar{K}_5$, $\bar{K}_6$, $\bar{K}_9$ by rewriting the linear equations (2.319–2.322) as:

$$\begin{bmatrix} \Omega_1^2 & \Omega_1 & -1 \\ \Omega_2^2 & \Omega_2 & -1 \\ \vdots & \vdots & \vdots \\ \Omega_n^2 & \Omega_n & -1 \end{bmatrix} \begin{bmatrix} \bar{K}_5 \\ \bar{K}_6 \\ \bar{K}_9 \end{bmatrix} = \begin{bmatrix} u_{th_1} \\ u_{th_2} \\ \vdots \\ u_{th_n} \end{bmatrix}, \tag{2.323}$$

where Eq. (2.323) can be expressed in a more simple manner as $\boldsymbol{A}_\Omega \boldsymbol{x}_K = \boldsymbol{B}_{u_{th}}$ with:

$$\boldsymbol{A}_\Omega = \begin{bmatrix} \Omega_1^2 & \Omega_1 & -1 \\ \Omega_2^2 & \Omega_2 & -1 \\ \vdots & \vdots & \vdots \\ \Omega_n^2 & \Omega_n & -1 \end{bmatrix}, \tag{2.324}$$

$$\boldsymbol{x}_K = \begin{bmatrix} \bar{K}_5 \\ \bar{K}_6 \\ \bar{K}_9 \end{bmatrix}, \tag{2.325}$$

$$\boldsymbol{B}_{u_{th}} = \begin{bmatrix} u_{th_1} \\ u_{th_2} \\ \vdots \\ u_{th_n} \end{bmatrix}, \tag{2.326}$$

therefore, Eq. (2.323) can be solved for $\bar{K}_5$, $\bar{K}_6$, and $\bar{K}_9$ by using a Moore-Penrose left pseudo-inverse method to obtain the least square error fit as:

$$\boldsymbol{x}_K = \begin{bmatrix} \hat{K}_5 \\ \hat{K}_6 \\ \hat{K}_9 \end{bmatrix} = \left(\boldsymbol{A}_\Omega^T \boldsymbol{A}_\Omega\right)^{-1} \boldsymbol{B}_{u_{th}}, \tag{2.327}$$

where $\hat{K}_5$, $\hat{K}_6$, and $\hat{K}_9$ represents the obtained results of the constants using the Moore-Penrose left pseudo-inverse method. Also recall that in order to determine K_5, K_6 and K_9 it is necessary to determine also K_8. This can be done by recalling Eq. (2.315) and using the values obtained in (2.327) into the proposed rotational velocity assuming that the collective pitch angle is zero resulting in:

$$\begin{aligned} \dot{\Omega} &= -K_5\Omega - K_6\Omega^2 - K_7\Omega^2 \sin\theta_c + K_8 u_{th} + K_9 \\ &= K_8\left(-\hat{K}_5\Omega - \hat{K}_6\Omega^2 + u_{th} - \hat{K}_9\right), \end{aligned} \tag{2.328}$$

where K_8 can be obtained by looking into the step response data obtained using throttle step responses with zero pitch angle, $\theta_c = 0$, and conducting a parameter adjustment on K_8 until the simulated step responses match the data from actual flight data. The determination of the term associated to the air drag loss for the rotational speed of the blades, K_7, is conducted by running a series of steady-state experiments for pairs of pitch angles, θ_{c_i}, and throttle settings, u_{th_i} for hovering flight conditions. From the different experiment flight data, and using the results obtained for the degenerated rotational speed of the blades Eq. (2.328), a fit analysis can be conducted to obtain the K_7 that best fits the flight results. With K_8 obtained, constants K_5, K_6 and K_9 can be determined using Eqns. (2.316–2.318).

2.8.4.3 Parameter Determination for Collective Pitch Dynamics

In order to determine the unknown constants, K_{10}, K_{11}, and K_{12} a potentiometer needs to be mounted on the collective pitch servo to measure the exact magnitude of the pitch as seen in Figure 2.28. Figure 2.28 reproduces the installation of the potentiometer in the collective pitch angle for the selected solution in the *ESI RC* helicopter (Navarro-Collado, 2010).

Ideally, it would be desirable to mount the potentiometer directly to the blades but given the physical limitations, it can only be measured the servo position. This set up has the limitations that possible flexing in the drive links from the servo to the blades will not be taken into account, but if the links are rigid enough, this flexing can be negligible which is the case in all the *RC* helicopter main rotor heads. Effects of backlash will also be ignored. The first term in (2.304) is determined by comparing the collective servomechanism input, u_{θ_c}, to the measured pitch, θ_c as measured by the collective pitch with the helicopter at rest, which reduces (2.304) to:

$$K_{10} f(u_{\theta_c}, \theta_c) = 0, \tag{2.329}$$

This allows to determine the structure of the $f(u_{\theta_c}, \theta_c)$ which is obtained after comparing the servo inputs to the measured collective pitch angles. After experimentation (Pallet et al., 1991; Pallet and Ahmad, 1991) it is observed that the resulting collective pitch seems to behave in a linear fashion with respect to the collective pitch servo input u_{θ_c}, therefore it is selected to determine the structure of $f(u_{\theta_c}, \theta_c)$ by using a least squares fit for a model of the form:

$$f(u_{\theta_c}, \theta_c) = A_{\theta_{c_1}} u_{\theta_c} + A_{\theta_{c_2}} - \theta_c, \tag{2.330}$$

which can be determine employing a methodology similar to the one conducted for the rest of unknown parameters by conducting a series of experiments in which a series of state pairs of collective pitch angles, θ_{c_i}, and servo control inputs, $u_{\theta_{c_i}}$ are obtained to try to model the actuator dynamics. The sets of pairs can be written in the form:

$$\begin{bmatrix} u_{\theta_{c_1}} & 1 \\ u_{\theta_{c_2}} & 1 \\ \vdots & \vdots \\ u_{\theta_{c_n}} & 1 \end{bmatrix} \begin{bmatrix} A_{\theta_{c_1}} \\ A_{\theta_{c_2}} \end{bmatrix} = \begin{bmatrix} \theta_{c_1} \\ \theta_{c_2} \\ \vdots \\ \theta_{c_n} \end{bmatrix}, \tag{2.331}$$

Equation (2.331) can be solved for $A_{\theta_{c_1}}$ and $A_{\theta_{c_2}}$ by using a Moore-Penrose left pseudoinverse and therefore identifying the original model, Eq. (2.304), as:

$$\begin{aligned} \ddot{\theta}_c &= K_{10} f(u_{\theta_c}, \theta_c) - K_{11}\dot{\theta}_c - K_{12}\omega^2 \sin\theta_c \\ &= K_{10}\left(A_{\theta_{c_1}} u_{\theta_c} + A_{\theta_{c_2}} - \theta_c\right) - K_{11}\dot{\theta}_c - K_{12}\omega^2 \sin\theta_c. \end{aligned} \tag{2.332}$$

Once defined the collective pitch actuator dynamics, let proceed to determine constants K_{10} and K_{11} which is done by considering the helicopter at rest. In this situation the angular velocity of the blades is zero, $\Omega = 0$, therefore reducing Eq. (2.332) to:

$$0 = K_{10}\left(A_{\theta_{c_1}} u_{\theta_c} + A_{\theta_{c_2}} - \theta_c\right) - K_{11}\dot{\theta}_c, \tag{2.333}$$

where both K_{10} and K_{11} can be obtained by looking into the step response data obtained using collective step responses for zero angular velocity, $\Omega = 0$, and conducting a parameter adjustment on K_{10} and K_{11} that provide the best fit to the curves. The last term to be accounted for is the collective pitch angle behavior while the blades are in motion, that is the third term in Eq. (2.302), K_{12}. This term relates the rotational speed of the rotor with the pitch position of the blades. Experiments are conducted with the same pair of conditions used to determine the actuator dynamics, Eq. (2.330), but with varying rotational angular velocity of the blades, Ω, and therefore adjusting the coefficient K_{12} until matches the actual results obtained with $\Omega = 0$. It is expected that K_{12} will be small since due to the nature of *RC* servomotors, the internal position control loop of the servo subsystems keeps the collective pitch at a constant position even in the presence of resistance up to the torque at which they are rated (Wikipedia, the free encyclopedia, 2010b; Wikipedia, the free encyclopedia, 2010a).

Although in (Pallet et al., 1991; Pallet and Ahmad, 1991) the term including K_{12} is neglected from experimental results and for simplicity, in the two control papers that originally motivated the work presented in this thesis (Huang and Balakrishnan, 2005; Sira-Ramírez et al., 1994), the different control strategies used in both works leave the K_{12} term and therefore for control purposes, since the existence of this term increases the degree of complexity of the model. It is left for future work the adjusted of the presented model with the real *RC* helicopter, since this is out of the scope of this thesis.

The servo motors that will be used in the *RC* helicopter are standardized *RC* servos as seen in Figure (2.29) where it can be seen that the servo consist of an output spline where the arm that converts the angular motion to linear motion is attached, the drive gears that allows to convert the produced rotational speed of the motor to the desired rotational speed and torque, the motor, the potentiometer that allows to determine the actual position of the servo, and a electric motor which by using the read from the potentiometer, ensures that the servo is at the commanded position.

RC servos are composed of an electric motor mechanically linked to a potentiometer (Wikipedia, the free encyclopedia, 2010b; Wikipedia, the free encyclopedia, 2010a). Pulse-width modulation (PWM) signals which are sent to the servo, and are translated into position commands by the electronics inside the servo. When the servo is commanded to rotate, the motor is powered until the potentiometer reaches the value corresponding to the commanded position. The servo is usually controlled by three wires: ground, power, and control. The servo will move based on the pulses sent over the control wire, which set the angle of the actuator arm. The servo expects a pulse every 20 ms in order to gain correct information about the angle. The width of the servo pulse dictates the range of the servo's angular motion. A servo pulse of 1.5 ms width will typically set the servo to its "neutral" position or 45°, a pulse of 1.25 ms could set it to 0° and a pulse of 1.75 ms to 90°.

The physical limits and timings of the servo hardware varies between brands and models, but a general servo's angular motion will travel somewhere in the range of $90° - -120°$ and the neutral position is almost always at 1.5 ms. This is the "standard pulse servo mode" used by all hobby analog servos. When these servos are commanded to move they will move to the position and hold that position. If an external force pushes against the servo while the servo is holding a position, the servo will resist from moving out of that position. The maximum amount of force the servo can exert is the torque rating of the servo. Servos will not hold their position forever though; the position pulse must be repeated to instruct the servo to stay in position.

A hobby digital servo is controlled by the same "standard pulse servo mode" pulses as an analog servo (of Robots, 2008). Some hobby digital servos can be set to another mode that allows a robot controller to read back the actual position of the servo shaft. Some hobby digital servos can optionally be set to another mode and "programmed", so it has the desired PID controller characteristics when it is later driven by a standard pulse servo receiver (Hitec, 2007). The way in which servos work is out of the scope of this thesis, so for further detail refer to (Wikipedia, the free encyclopedia, 2010b; Wikipedia, the free encyclopedia, 2010a; of Robots, 2008).

2.8.5 Final Helicopter Model

The proposed helicopter model is defined by identifying that Eqns. (2.305), (2.294), and (2.332) can be written into a set of first order nonlinear equations of motion by defining the state space vector as:

$$\boldsymbol{\chi} \triangleq \begin{bmatrix} x \\ \boldsymbol{y} \\ \boldsymbol{z} \end{bmatrix}, \tag{2.334}$$

where x represents angular velocity of the blades, that is $x \triangleq \Omega$, $\boldsymbol{y}$ represent the state vector for the vertical motion of the helicopter, that is $y_1 \triangleq \xi$, and is given by:

$$\boldsymbol{y} \triangleq \begin{bmatrix} y_1 \\ y_2 \end{bmatrix} \triangleq \begin{bmatrix} \xi \\ \dot{\xi} \end{bmatrix}, \tag{2.335}$$

and $\boldsymbol{z}$ represents the state vector for the collective pitch angle dynamics, that is $z_1 \triangleq \theta_c$ and is given by:

$$\boldsymbol{z} \triangleq \begin{bmatrix} z_1 \\ z_2 \end{bmatrix} \triangleq \begin{bmatrix} \theta_c \\ \dot{\theta}_c \end{bmatrix}. \tag{2.336}$$

The control vector is given by:

$$\boldsymbol{u} \triangleq \begin{bmatrix} u_1 \\ u_2 \end{bmatrix} = \begin{bmatrix} K_8 u_{th} \\ A_{\theta_{c_1}} K_{10} u_{\theta_c} \end{bmatrix}, \tag{2.337}$$

with u_1 being the normalized input to throttle servo signal (u_{th}), and u_2 being the normalized input to collective pitch servo signals (u_{θ_c}). This results in the nonlinear equations of the form:

$$\begin{aligned} \dot{x} &= f(x, \boldsymbol{y}, \boldsymbol{z}, u_1), \\ \dot{\boldsymbol{y}} &= \boldsymbol{g}(x, \boldsymbol{y}, \boldsymbol{z}), \\ \dot{\boldsymbol{z}} &= \boldsymbol{h}(x, \boldsymbol{y}, \boldsymbol{z}, u_2), \end{aligned} \tag{2.338}$$

resulting in

$$\dot{x} = a_8 x + a_{10} x^2 \sin z_1 + a_9 x^2 + a_{11} + u_1, \tag{2.339}$$

$$\dot{y}_1 = y_2, \tag{2.340}$$

$$\dot{y}_2 = x^2(a_1 + a_2 z_1 - \sqrt{a_3 + a_4 z_1}) + a_5 y_2 + a_6 y_2^2 + a_7, \tag{2.341}$$

$$\dot{z}_1 = z_2, \tag{2.342}$$

$$\dot{z}_2 = a_{13} z_1 + a_{14} x^2 \sin z_1 + a_{15} z_2 + a_{12} + u_2, \tag{2.343}$$

where the constants are given by in table 2.1. Recall that $\boldsymbol{g}(x, \boldsymbol{y}, \boldsymbol{z})$ denotes the vector function that describe the vertical displacement dynamics of the helicopter given by

$$\dot{\boldsymbol{y}} = \begin{bmatrix} \dot{y}_1 \\ \dot{y}_2 \end{bmatrix} = \boldsymbol{g}(x, \boldsymbol{y}, \boldsymbol{z}) = \begin{bmatrix} g_1(x, \boldsymbol{y}, \boldsymbol{z}) \\ g_2(x, \boldsymbol{y}, \boldsymbol{z}) \end{bmatrix}, \tag{2.344}$$

$$\tag{2.345}$$

with g_1 and g_2 given by Eqns. (2.340) and (2.341), respectively, and $\boldsymbol{h}(x, \boldsymbol{y}, \boldsymbol{z})$ denotes the vector function that describes the collective pitch dynamics of the helicopter given by

$$\dot{\boldsymbol{z}} = \begin{bmatrix} \dot{z}_1 \\ \dot{z}_2 \end{bmatrix} = \boldsymbol{h}(x, \boldsymbol{y}, \boldsymbol{z}, u_2) = \begin{bmatrix} h_1(x, \boldsymbol{y}, \boldsymbol{z}) \\ h_2(x, \boldsymbol{y}, \boldsymbol{z}, u_2) \end{bmatrix}, \tag{2.346}$$

$$\tag{2.347}$$

with h_1 and h_2 given by Eqns. (2.342) and (2.343), respectively. Figure 2.30 depicts a simplified block diagram that helps to understand the high degree of coupling and the dependence between the three subsystems in which are organized the five differential equations of time (2.339–2.343). These subsystems correspond to the vertical position and velocity of the helicopter $\boldsymbol{y}$, the main rotor angular velocity x, and the collective pitch dynamics $\boldsymbol{z}$.

This concludes the definition of the model that will be used through the remainder of this thesis. The following subsections are dedicated to an in depth analysis of the equilibrium equations, the definition of the available ranges of the states variables, which will be used to determine the semi-global stability properties in future sections, and a performance analysis of the selected model against the more complex thrust models previously presented to justify the validity of the proposed model which is presented in Appendix A. The constants in table 2.1 used throughout the remainder of this thesis are defined in table 2.2 which are slightly different from the original techreport (Pallet and Ahmad, 1991). See A.5 for further details on the derivation of the coefficients.

$a_1 = K_1 \frac{\sigma^2 C_{L_\alpha}^2}{64}$	$a_2 = K_1 \frac{\sigma C_{L_\alpha}}{6}$	$a_3 = 3(2K_1)^2 \left(\frac{\sigma C_{L_\alpha}}{4}\right)^4$	$a_4 = 2K_1^2 \frac{(\sigma C_{L_\alpha})^3}{4}$	$a_5 = -K_2$
$a_6 = -K_2$	$a_7 = -g_z - K_4$	$a_8 = -K_5$	$a_9 = -K_6$	$a_{10} = -K_6$
$a_{11} = K_9$	$a_{12} = A_{\theta_{c_2}} K_{10}$	$a_{13} = -K_{10}$	$a_{14} = -K_{12}$	$a_{15} = -K_{11}$

Table 2.1: Relation between the helicopter estimated physical coefficients K_* and the helicopter normalized physical coefficients a_* - Eqns. (2.339–2.343).

$a_1 = 5.19791 \times 10^{-4}$	$a_2 = 1.51992 \times 10^{-2}$	$a_3 = 2.70183 \times 10^{-7}$	$a_4 = 1.58009 \times 10^{-5}$
$a_5 = -0.1$	$a_6 = -0.1$	$a_7 = -17.67$	$a_8 = -0.7$
$a_9 = -0.0028$	$a_{10} = -0.0028$	$a_{11} = -13.92$	$a_{12} = 434.88$
$a_{13} = -800$	$a_{14} = -0.1$	$a_{15} = -65$	

Table 2.2: Values of the normalized physical coefficients a_*.

2.8.5.1 Equilibrium Points Analysis for the Helicopter Model

In order to better understand the behavior of the helicopter system, an analysis of its equilibrium points is conducted. The equilibrium points are obtained by setting all the derivatives of the system Eqns. (2.339–2.343) to zero, thus yielding the equilibrium equations:

$$\dot{x} = 0 = a_8\bar{x} + a_{10}\bar{x}^2 \sin \bar{z}_1 + a_9\bar{x}^2 + a_{11} + \bar{u}_1, \tag{2.348}$$

$$\dot{y}_1 = 0 = \bar{y}_2, \tag{2.349}$$

$$\dot{y}_2 = 0 = \bar{x}^2(a_1 + a_2\bar{z}_1 - \sqrt{a_3 + a_4\bar{z}_1}) + a_5\bar{y}_2 + a_6\bar{y}_2^2 + a_7, \tag{2.350}$$

$$\dot{z}_1 = 0 = \bar{z}_2, \tag{2.351}$$

$$\dot{z}_2 = 0 = a_{13}\bar{z}_1 + a_{14}\bar{x}^2 \sin \bar{z}_1 + a_{15}\bar{z}_2 + a_{12} + \bar{u}_2, \tag{2.352}$$

where the symbol $\bar{\square}$ denotes that the variable is at an equilibrium condition. As seen by the equilibrium equations, the system is formed by five state variables, and two control signals. It can be seen that the altitude variable y_1 does not appear in any of the equilibrium equations, which implies that any of the equilibrium points of the helicopter system can be attained at any altitude, always taking into consideration the physical limitations of the problem. This implies that there exists an infinitely number of equilibrium points, and one of the variables needs to be fixed in order to determine a single equilibrium point. This also implies that the system is an underactuated one, which will increase the degree of complexity involved in trying to regulate the helicopter vertical motion, in special considering that the vertical displacement dynamics have no direct control action, and in order to effect in both the vertical position and velocity of the helicopter will be required to provide the proper control signals to both the angular velocity and the collective pitch angle of the blade. This will provide an excellent nonlinear frame where to test the validity of the proposed control strategies.

Equations (2.349) and (2.351) yield the solutions for the equilibrium vertical velocity of the helicopter ($\bar{y}_2 = 0$), and the equilibrium collective pitch rate of the blades ($\bar{z}_2 = 0$). Equation (2.350) defines the equilibrium space of configuration by selecting a desired value for either $\bar{x}$ or $\bar{z}_1$, such that an expression can be determined as a function of the selected desired variable, defined from now on as x^* or z_1^* respectively. Equations (2.348) and (2.352), define the control signals required to achieve the selected equilibrium points. This implies that in order to determine the equilibrium points, it will be first necessary to select between x or z_1 as the desired initial value, which will in return provide a relation to determine the equilibrium for the other variable. If the collective pitch angle is selected as the desired fixed variable z_1^*, the expressions that determine the rest of the variables at the equilibrium points are given by:

$$\bar{x}(z_1^*) = \pm\sqrt{-\frac{a_7}{a_1 + a_2 z_1^* - \sqrt{a_3 + a_4 z_1^*}}}, \tag{2.353}$$

$$\bar{u}_1(z_1^*) = -a_8\bar{x} - a_{10}\bar{x}^2 \sin z_1^* - a_9\bar{x}^2 - a_{11}, \tag{2.354}$$

$$\bar{u}_2(z_1^*) = -a_{13}z_1^* - a_{14}\bar{x}^2 \sin \bar{z}_1 - a_{12}. \tag{2.355}$$

On the other side, if the angular velocity of the blades is selected as the desired variable x^*, the expressions become:

$$\bar{z}_1(x^*) = \frac{a_4 x^* \pm \sqrt{C_a {x^*}^2 + C_b}}{2a_2^2 x^*} + C_c + \frac{C_d}{{x^*}^2}, \tag{2.356}$$

$$\bar{u}_1(x^*) = -a_8 x^* - {x^*}^2(a_{10}\sin \bar{z}_1 + a_9) - a_{11} \tag{2.357}$$

$$\bar{u}_2(x^*) = -a_{13}\bar{z}_1 - a_{14}{x^*}^2 \sin \bar{z}_1 - a_{12}, \tag{2.358}$$

being the constants defined by:

$$C_a = a_4^2 - 4a_2a_1a_4 + 4a_2^2a_3, \tag{2.359}$$
$$C_b = -4a_2a_7a_4, \tag{2.360}$$
$$C_c = -\frac{a_1}{a_2}, \tag{2.361}$$
$$C_d = -\frac{a_7}{a_2}. \tag{2.362}$$

It can be observed that Eq. (2.353) has two solutions for the equilibrium rotational speed of the blades $\bar{x}$, but constrained by the physical nature of the problem, that is, the clockwise rotation of the blades, only the positive solution is considered. It is observed that Eq. (2.356) has also two solutions for the equilibrium collective pitch angle of the blades $\bar{z}_1$, but it can be demonstrated substituting both solutions in the original equilibrium Eqns. (2.348)–(2.352), that the solution corresponding to the minus sign in front of the square root is a spurious solution introduced in the previous computations, therefore only the positive solution is considered in the sequel.

From the physics of axial helicopter flight, is is customary, for both RC and full size helicopters, to maintain the engine's RPM constant, and use collective pitch angle to provide the differential thrust required to regulate the helicopter's vertical position, since the collective pitch angle effect in the amount of vertical force is much faster than the effect that has the angular velocity of the blades on the generation of thrust. This translates that Eq. (2.356) will be used instead of Eq. (2.353).

Taking into consideration the physical restrictions of the proposed model, it is necessary to define the range of the reachable states, and also their reachable desired final conditions (y_1^*, y_2^*, x^*, z_1^* and z_2^*). These reachable states and equilibrium points are defined by the physical limits of the state variables. The altitude limits are defined by the limitations of the platform in which the helicopter is mounted, $0 < y_1 < 2\ m.$; the vertical velocity limitations for the descent phase are defined by the velocity at which the effects of vertical velocity cannot be neglected, which can be approximated by the induced velocity of the helicopter at the rotor disk in the hover flight condition (Leishman, 2006), that is $-v_i < y_2$, and where v_i ($meter/second$) represents the induced velocity at the rotor disk, and is defined as seen previously by:

$$v_i = \frac{T}{2\rho A},$$

where T ($Newton$) is the necessary thrust force to maintain the hover flight condition, and given by $T = mg_z$, where m ($kg.$) is the mass of the helicopter, ρ (kg/m^3) is the air density, and A (m^2) is the rotor disk area, that is $A = \pi R^2$, with R ($meter$), being the radius of the helicopter blade. For the helicopter case discussed through the thesis it is assumed that $m = 3.1488$ kg, $\rho = 1.225\ kg/m^3$, and $R = 0.7025\ m$. Refer to A.5 for further details. The maximum ascend velocity is fixed as $2v_i$ thus yielding the limits for the vertical velocity as $-2.8505 < y_2 < 5.7010$ m/s; the limits on the angular speed of the motor comes defined by the physical limitations of the rotorcraft engine, $x_{max} = 180$ rads/s, (approximately 1718 RPM's), while the lower boun is fixed by assuming that the idle speed of the engine is set at $x_{min} = 74.25$ rads/s; the limits on the angular velocity of the pitch is modeled after the specifications of a high speed servo, Futaba S9250 Servo Digital Heli, which has a speed of 9.51 $rads/s$ (Futaba®, 2006). For the range of collective pitch angles, a maximum collective pitch angle of $z_{1_{max}} = 0.35$ rads $\approx 20.05°$ is considered; the minimum collective pitch angle can be determined analyzing the selected modelization of the thrust coefficient, as seen in Eq. (2.282), where it can be observed that due to the nature of the square root in the thrust coefficient equation, only collective pitch angles greater than $z_1 > -K_{C_1}^2/K_{C_1} = -a_3/a_4$ will be defined. Analysis of $\bar{x}(z_1^*)$ and $\bar{z}_1(x^*)$, Eqs. (2.353) and (2.356) respectively, show that there is a region within the considered collective pitch angle range that it is not defined as an attainable desired final condition, thus defining two distinctive regions of reachable collective pitch angles:

$$z_{1_{lim_1}} > z_1^* > -\frac{a_3}{a_4} \text{ , and } z_{1_{max}} > z_1^* > z_{1_{lim_2}}, \tag{2.363}$$

being $z_{1_{lim_1}}$ and $z_{1_{lim_2}}$ the roots of the denominator of Eq. (2.353) given as:

$$\begin{aligned} z_{1_{lim_1}} &= \frac{a_4 - 2a_1a_2 - \sqrt{a_4^2 - 4a_4a_1a_2 + 4a_2^2a_3}}{2a_2^2}, \\ z_{1_{lim_2}} &= \frac{a_4 - 2a_1a_2 + \sqrt{a_4^2 - 4a_4a_1a_2 + 4a_2^2a_3}}{2a_2^2}, \end{aligned} \tag{2.364}$$

for the constants defined in this problem, the collective pitch angle equilibrium points are given by -0.3992×10^{-3} rads $> z_1^* > -0.1727 \times 10^{-1}$ rads and 0.25 rads $> z_1^* > 0.4138 \times 10^{-3}$ rads. Analyzing in detail the relation between the equilibrium states and the range of the desired states, it is concluded that, despite that the entire range of desired final conditions generate defined equilibrium points, it is not feasible to consider desired collective pitch angle values smaller than $z_1 < 4.87°$, which as it can be seen in Figure 2.31, in order to provide the thrust force required to maintain an equilibrium position, that is generating the same amount of thrust for a given weight, it requires angular velocities $x > 180$ radians, which is not possible due to the limitations on the engines's *RPM*.

For safety purposes and to avoid ranges of angle of attack in which the airfoil might be operating in a near stall region, the maximum value of the collective pitch angle is restricted to $14° > z_1$ therefore resulting that the range of desired collective pitch angles is limited to $14° > z_1^* > 4.87°$. Refer to (Esteban et al., 2005a) for more details. Figure 2.31 represents the relation of $\bar{x}(z_1^*)$, $\bar{z}_1(x^*)$, Eqns. (2.353) and (2.356) respectively, for the ranges of considered desired collective pitch angle and angular velocity of the blades.

2.8.5.2 Error Dynamics and Range of Variables for the Helicopter Model

As it is shown later, one of the requirements for the analysis of the asymptotic stability of a singular perturbed system is the necessity to ensure that the closed loop system has an isolated equilibrium at the origin. To satisfy this requirement we introduce a change of variables that define the new system in terms of its error dynamics as:

$$\tilde{\boldsymbol{\chi}} = \boldsymbol{\chi} - \boldsymbol{\chi}^*, \tag{2.365}$$

where $\boldsymbol{\chi}$ is defined in Eq. (2.334), and $\boldsymbol{\chi}^*$ represents the desired values of the state vector defined in the previous section. This translates into:

$$\tilde{x} = x - x^*, \tag{2.366}$$

$$\tilde{\boldsymbol{y}} = \boldsymbol{y} - \boldsymbol{y}^* = \begin{bmatrix} \tilde{y}_1 \\ \tilde{y}_2 \end{bmatrix} = \begin{bmatrix} y_1 - y_1^* \\ y_2 - y_2^* \end{bmatrix}, \tag{2.367}$$

$$\tilde{\boldsymbol{z}} = \boldsymbol{z} - \boldsymbol{z}^* = \begin{bmatrix} z_1 \\ z_2 \end{bmatrix} = \begin{bmatrix} z_1 - z_1^* \\ z_2 - z_2^* \end{bmatrix}, \tag{2.368}$$

where constants x^*, y_1^*, y_2^*, z_1^*, z_2^* represent the desired values of the states variables, and as discussed previously in the equilibrium analysis section, in order to have the helicopter at a given equilibrium position, that is, maintaining a stationery hover position, it is required that the vertical speed of the helicopter, y_2^*, and the pitch angular velocity of the blades to be $y_2^* = z_2^* = 0$, and z_1^* can be obtained as a function of the selected angular velocity of the blades, x^*, by using Eq. (2.356), resulting in $z_1^* = z_1^*(x^*, y_2^*)$. The limits of all the state variables are defined in Table 2.3. Using (2.366–2.368) into

(2.339–2.343) results in the error dynamics of the problem given by:

$$
\begin{aligned}
\dot{\tilde{x}} &= a_8(\tilde{x}+x^*) + a_{10}(\tilde{x}+x^*)^2 \sin(\tilde{z}_1 + z_1^*) \\
&+ a_9(\tilde{x}+x^*)^2 + a_{11} + \tilde{u}_1 + \bar{u}_1, \\
\dot{\tilde{y}}_1 &= \tilde{y}_2, \\
\dot{\tilde{y}}_2 &= (\tilde{x}+x^*)^2 \left(a_1 + a_2(\tilde{z}_1+z_1^*) - \sqrt{a_3 + a_4(\tilde{z}_1+z_1^*)} \right) \\
&+ a_5\tilde{y}_2 + a_6\tilde{y}_2^2 + a_7 \\
\dot{\tilde{z}}_1 &= \tilde{z}_2, \\
\dot{\tilde{z}}_2 &= a_{13}(\tilde{z}_1+z_1^*) + a_{14}(\tilde{x}+x^*)^2 \sin(\tilde{z}_1+z_1^*) + a_{15}\tilde{z}_2 + a_{12} + \tilde{u}_2 + \bar{u}_2,
\end{aligned}
\tag{2.369}
$$

where:

$$
\tilde{\boldsymbol{u}} \triangleq \begin{bmatrix} \tilde{u}_1 \\ \tilde{u}_2 \end{bmatrix} = \boldsymbol{u} - \bar{\boldsymbol{u}} \triangleq \begin{bmatrix} u_1 - \bar{u}_1 \\ u_2 - \bar{u}_2 \end{bmatrix}, \tag{2.370}
$$

where $\bar{u}_1$ and $\bar{u}_2$ are given by Eqns. (2.354) and (2.355) or Eqns. (2.357) and (2.358) respectively, but as mentioned in the previous section, due to the physics of flight selected, and, as it is shown later, due to the time-scale selection, only Eqns. (2.357) and (2.358) are used. This resulting in the limits of the real variables defined by:

$$
\boldsymbol{\chi_{MIN}} \leq \boldsymbol{\chi} \leq \boldsymbol{\chi_{MAX}}. \tag{2.371}
$$

From analysis of the maximum allowable state variables and desired final states it can therefore be defined the ranges of the error-dynamics given by:

$$
\tilde{\boldsymbol{\chi}}_{\boldsymbol{MIN}} \leq \tilde{\boldsymbol{\chi}} \leq \tilde{\boldsymbol{\chi}}_{\boldsymbol{MAX}}, \tag{2.372}
$$

with the minimum values of the error dynamic variables being given by:

$$
\tilde{\boldsymbol{\chi}}_{\boldsymbol{MIN}} = \boldsymbol{\chi_{MIN}} - \boldsymbol{\chi_{MAX}}, \tag{2.373}
$$

and the maximum values of the error dynamic variables being given by

$$
\tilde{\boldsymbol{\chi}}_{\boldsymbol{MAX}} = \boldsymbol{\chi_{MAX}} - \boldsymbol{\chi_{MIN}}. \tag{2.374}
$$

Table 2.3 resumes the limits for the helicopter variables, for the actual values, the desired and the error dynamics. Note that for safety purposes, the desired values for the angular velocity of the blades and the collective pitch angle, are limited an additional 10% on both the minimum and maximum allowable desired values. Similarly, the desired values on the altitude are limited 10 cm. on both the minimum and maximum possible altitudes.

States	$\boldsymbol{\chi_{MIN}}$	$\boldsymbol{\chi_{MAX}}$	$\boldsymbol{\chi^*_{MIN}}$	$\boldsymbol{\chi^*_{MAX}}$	$\tilde{\boldsymbol{\chi}}_{\boldsymbol{MIN}}$	$\tilde{\boldsymbol{\chi}}_{\boldsymbol{MAX}}$
x [rad/s]	74.25	180	81.675	162	87.75	98.325
y_1 [m]	0	2	0.1	1.9	−1.9	1.9
y_2 [m/s]	−2.8505	5.7009	0	0	−2.8505	5.7009
z_1 [rad]	0.0175	0.2443	0.0935	0.2199	−0.2025	0.1508
x_5 [rad/s]	−9.52	9.52	0	0	−9.52	9.52

Table 2.3: Error-Dynamic Limits for the Helicopter Variables.

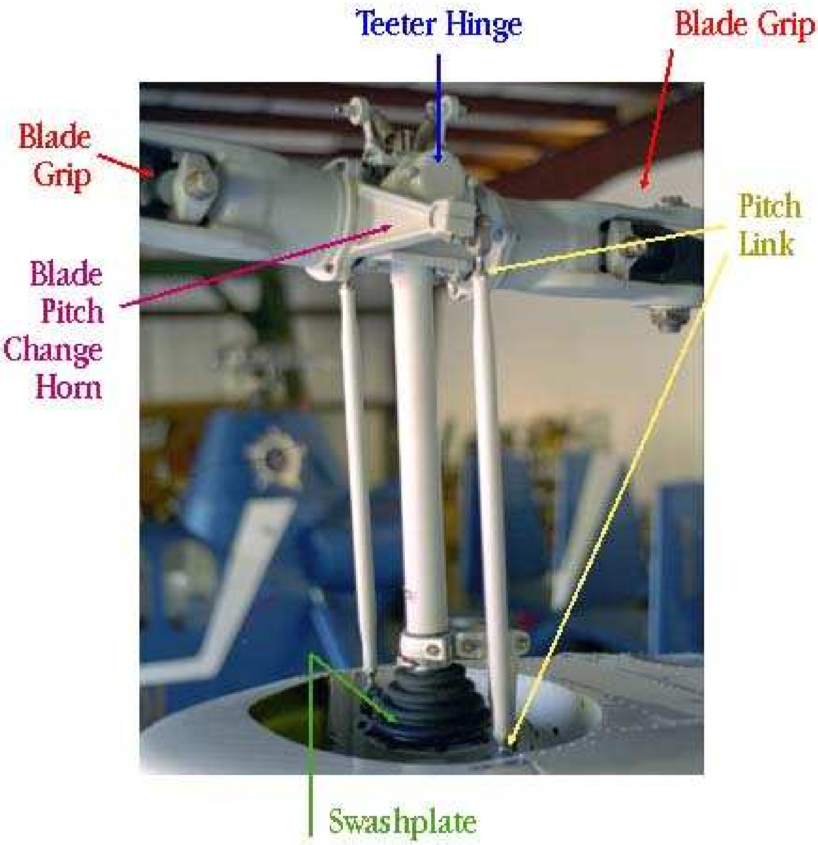

Figure 2.21: Teeter mechanism in Bell 206 rotor head

Figure 2.22: Teeter movement in a Robinson 22

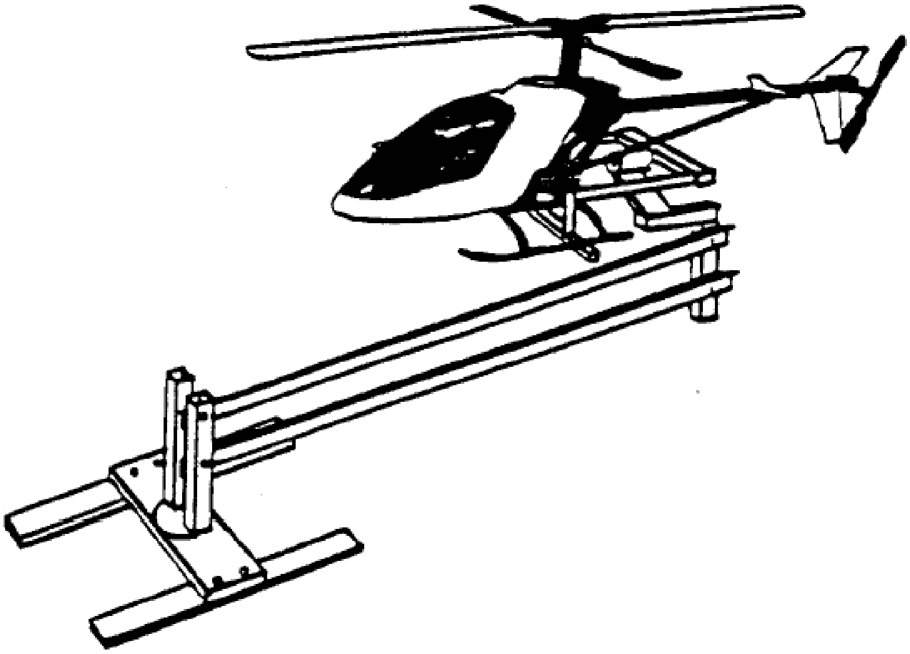

Figure 2.23: Helicopter stand (Pallet et al., 1991; Pallet and Ahmad, 1991)

Figure 2.24: *Grupo de Control Nolineal* autonomous helicopter platform

Figure 2.25: *Grupo de Control Nolineal* autonomous helicopter platform

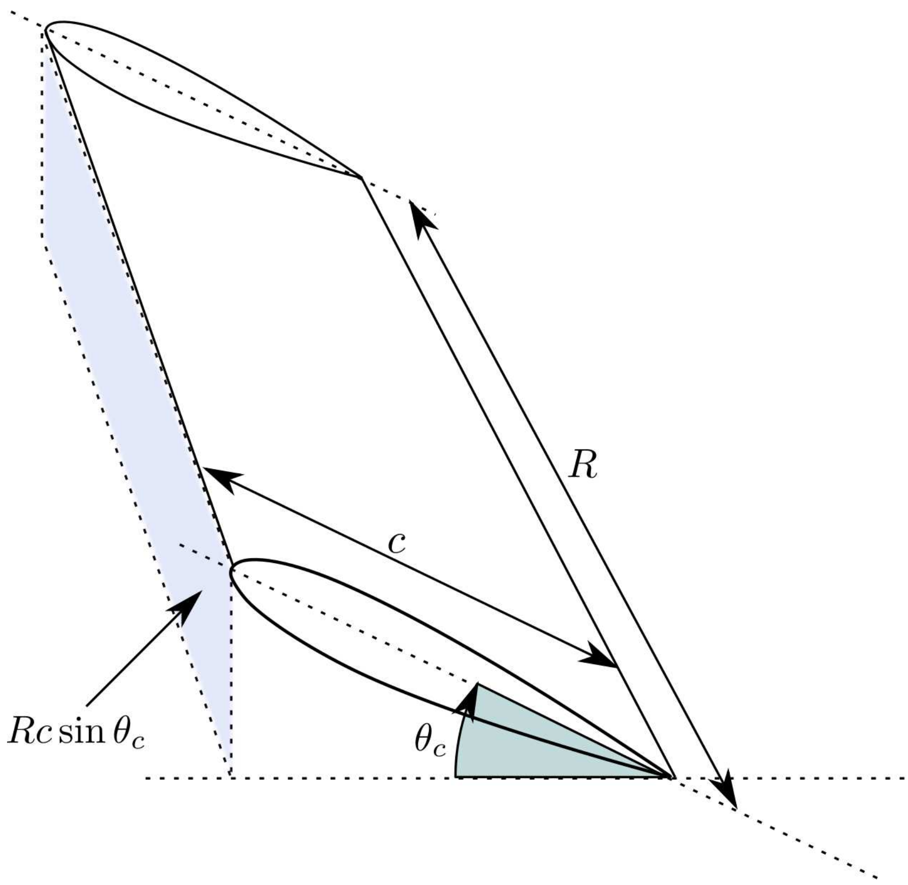

Figure 2.26: Effective drag area of the rotor blades (Pallet and Ahmad, 1991)

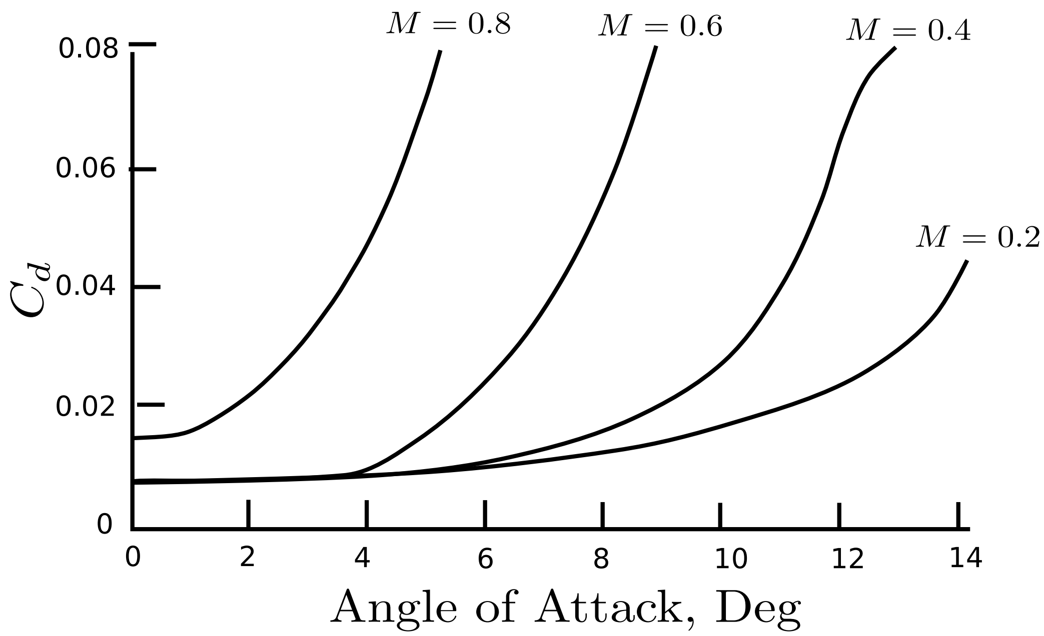

Figure 2.27: Aerodynamic characteristics for a NACA 0012 airfoil (Prouty, 1986).

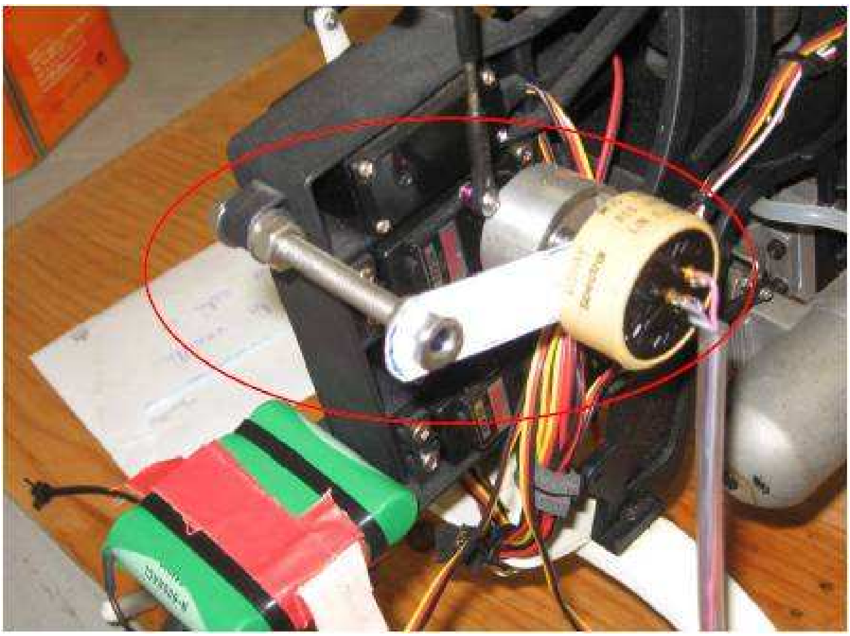

Figure 2.28: Potentiometer installed in the helicopter collective pitch servo for the *Grupo de Control Nolineal RC* helicopter (Navarro-Collado, 2010)

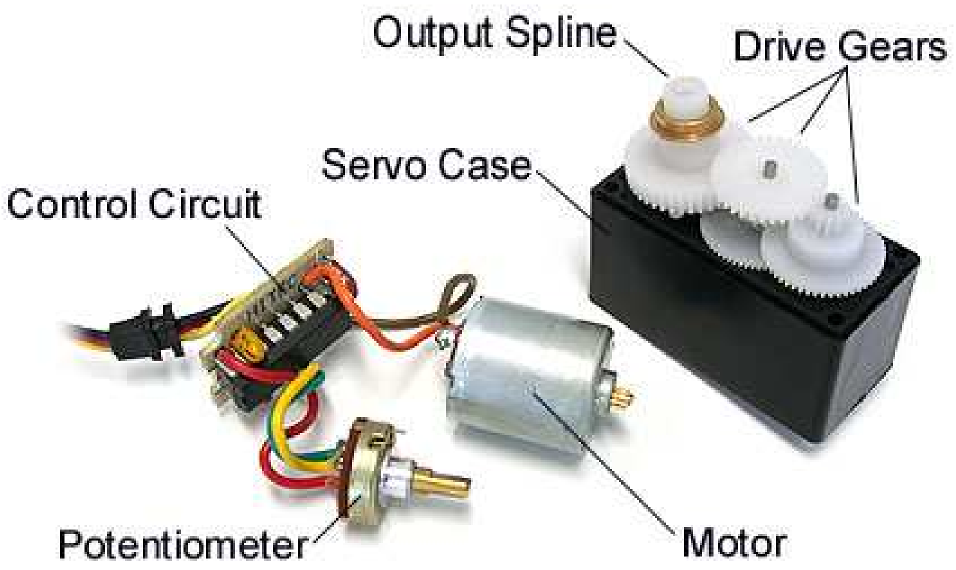

Figure 2.29: Standard servo breakdown (ServoCity, 2008).

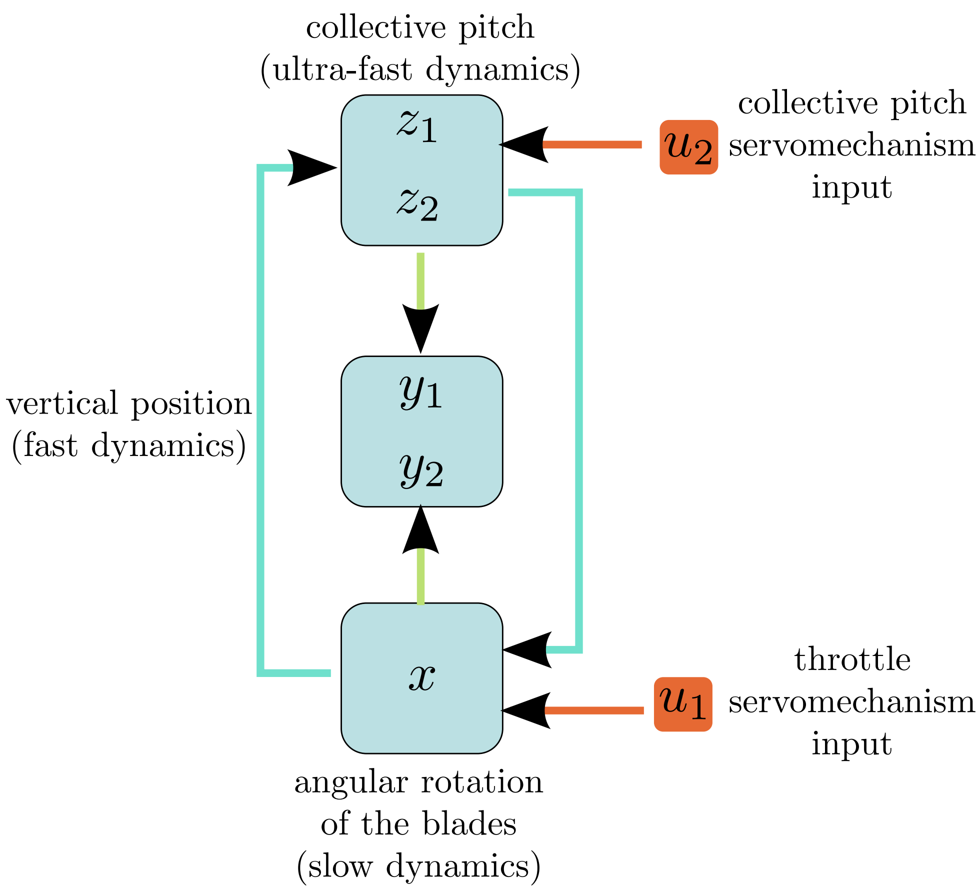

Figure 2.30: Block diagram of the helicopter dynamics.

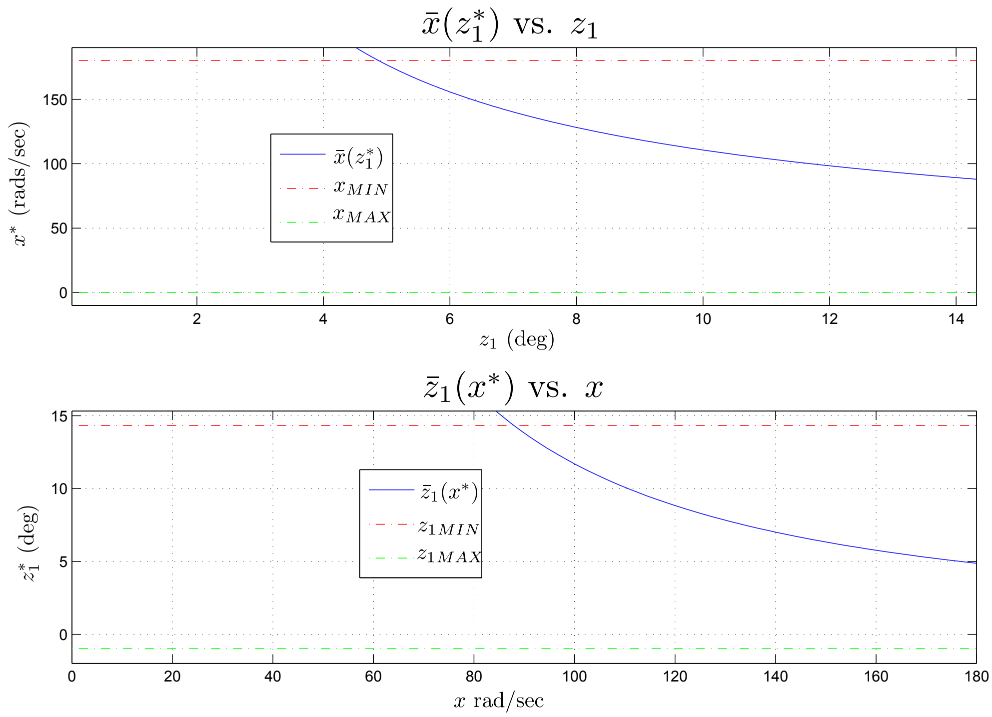

Figure 2.31: Relation between $\bar{x}(z_1^*)$ y $\bar{z}_1(x^*)$.

2.9 Conclusions

A model for a miniature helicopter in axial flight mounted on a platform has been presented. The model will be used throughout the remainder of the thesis to design the proper control laws that regulate the vertical position of the helicopter, and to demonstrate the asymptotic stability properties of the resulting autonomous system. The model is based in the MT_H model previously derived in section 2.6, which includes the helicopter dynamics in the axial flight condition, and also includes some of the losses presented in section A.4, and that were not accounted for in the original proposed MT_H model. The presented model

The helicopter model, although mainly focuses on the nonlinear vertical displacement, which is based on the selected thrust model, the MT_H model, it also includes the nonlinear dynamics of the collective pitch actuators, which increases considerably the degree of complexity of the model, but also depicts a more realistic model, and also includes the nonlinear dynamics of the rotational velocity of the main rotor. Although the model is based on an existing model that has been quite used in the literature (Pallett and Ahmad, 1993; Sira-Ramírez et al., 1994; Huang and Balakrishnan, 2005; Kaloust et al., 2002; Tee et al., 2008), the author has proposed some changes, mainly in the definition of some of the variables in vertical displacement and angular velocity of the blades dynamics, taking into account the derived BE and MT derivations conducted in section 2.6 and Appendix A.

The author has also proposed three alternative thrust coefficient models, MT_c, $BEMT$, and $BEMT_{TL}$, described in detail in Appendix A, that will serve as test bench to test the validity of the selected model for axial flight, and to test the robustness of the proposed control strategy under unmodeled dynamics.

This chapter also introduces the range of reachable values for the states, the desired values and the error dynamics according to the real physic limitations of the model here presented. The definition of the ranges of the reachable values will be of great importance when conducting the stability analysis for the resulting closed-loop system, and will provide the tools to infer semi-global stability by extending the asymptotic stability properties of the selected control strategy not only to the origin, but extending the domain of attraction to the entire domain of reachable states.

Chapter 3

Singular Perturbation Analysis: *Top-Down* and *Bottom-Up* Approaches

3.1 Introduction

This chapter focuses on the time-scale analysis of singularly perturbed systems. Singular perturbation analysis of complex nonlinear systems provide a valuable tool that simplifies the burden of both, designing appropriate control laws, and guaranteing the asymptotic stability of the original nonlinear system. As noted in the introduction, section 1.3, singular perturbation techniques permit to deal with the complexity and nonlinearities present in many aerospace systems, and of many systems in general, by identifying the existence of times-scale behaviors among the different dynamics that are used to model the systems. This time-scale separation permits to describe the different aspects of the dynamic phenomena of each of the different time-scale subsystems with respect to each of the defined time-scales and, therefore, allowing to express the full problem as a composite description of the complex dynamics of each of the subsystems. This time-scale decomposition permits to easily understand the behavior of each of the resulting subsystems when being analyzed with respect to their new time-scales, something that would be quite difficult when trying to accomplish for the full system.

A priori, this can be thought as a process to decouple complex dynamics into lower order dynamics, and then apply the respective controls, where the power and the success of singular perturbation and time-scales philosophy lies on the use of approximate theory and, in particular, on the concept of asymptotic analysis that needs to be conducted to guarantee that the resulting time-scale subsystems satisfy the so called boundary layer requirements among the different resulting time-scales (Ramnath, 2010).

The time-scale analysis that will be here presented is based in a extension from the general two-time-scale singular perturbation formulation, to a three-time-scale singularly perturbed system, and as it will be shown also extended to a more general N^{th}-time-scale singular perturbation formulation. These methodologies will be employed throughout the reminder of this thesis, and applied to both a general three-time-scale model and a three-time-scale helicopter model. The use of a more general three-time-scale example will serve to extend the formulation described in this thesis to any N^{th}-time-scale singularly perturbed system in general.

The methodologies presented in this thesis provide an approach in which, for a specific class of singularly perturbed nonlinear systems, a step-by-step procedure can be used, such that allows to design the proper control laws that guarantee a desired degree of stability, select an appropriate composite Lyapunov function for the complete singularly perturbed system, and demonstrate the asymptotic stability for the resulting closed-loop nonlinear singularly perturbed system for sufficiently small singular perturbation parameters, and everything in an all-in-one step-by-step process.

These step-by-step methodologies will be denoted as *Top-Down* (*TD*) and *Bottom-Up* (*BU*) methodologies, and receive their names from the direction in which the singular perturbation parameters are considered, which in return result in different time-scales subsystem. For example, for a three-time scale singularly perturbed system, see Figure 3.1, the *Top-Down* methodology analyzes the time-scales in a descending manner, considering first the top singularly perturbed parameter, ε_1, resulting in a simplified two-time-scale problem formed by a one-dimension subsystem, and a two-dimension subsystem, denoted both by the red dashed boxes; in a second instance, and following the descending direction, the bottom singularly perturbed parameter is applied, ε_2, such that simplifies the second-order subsystem into another two-time-scale problem formed this time by two one-dimension subsystems, denoted both by the blue dashed-dotted boxes. A similar methodology is applied in the *Bottom-Up* methodology, but in an ascending manner as seen in Figure 3.2. This ascending or descending philosophy will be discussed in more detail in future sections.

The strategy analysis of the *TD* or *BU* methodologies here presented, consists on treating the different N^{th}-time-scales as $N-1$ distinct two-time-scale singular perturbed problems, using sequential analysis, and using the standard two-time-scale analysis (Kokotović et al., 1986) for each of the $N-1$ resulting two-time-scale subproblems. This singularly perturbed strategy becomes the main pillar of the methodology employed in this thesis and, as will be demonstrated in the following chapters, unifies in one simple process, the ability to solve the main problems treated on this thesis

1. Define a control design strategy that permits to select the desired degree of stability of each of the time-scale subsystems.
2. Define a methodology that permits to demonstrate the asymptotic stability properties of the resulting closed loop full system, by selecting the Lyapunov functions for each of the singularly perturbed subsystems, and construct the associated composite Lyapunov function for the full system.

The *TD* and *BU* methodologies simplify the burden of satisfying the requirements that guarantee the stability between the different time-scale subsystems by defining natural Lyapunov functions based on the desired dynamics for each of the time-scale subsystems resulting from applying the sequential *TD* and *BU* methodologies, and using these functions to demonstrate the requirements, rather than trying to obtain Lyapunov functions that satisfy the requirements for each of the subsystems, which proves to be a complex and difficult task, in special when the dynamics of the systems present a high degree of complexity (Kokotović et al., 1986; Kokotović et al., 1987; Kokotović et al., 1987).

The *TD* and the *BU* methodologies here proposed are introduced by first describing the general two-time-scale singular perturbation formulation in which are based, described in section 3.2; the extension to a three-time-scale formulation is derived in section 3.3, along with the methodology employed for the proper time-scale selection; section 3.4 describes in detail both the *TD* and the *BU* time-scale analysis, and section 3.5 introduces an intuitive description of the three-time-scale decomposition that will help to understand the time-scale evolution of a general three.time-scale system.

The *TD* and the *BU* methodologies are presented as two different, but equivalent approaches that help to analyze the three-time-scale singularly perturbed systems here studied. The selection of the *TD*, or the *BU* methodologies, will be taken by the designer, since depending on the structure of the system being analyzed, it might be more desirable to select one or another methodology, as it will be shown in later sections. The results obtained in this chapter will lead to the derivation of the proposed control strategy, which will be described in detail in chapter 4, and an extension of the standard two-time scale methodology to demonstrate the asymptotic stability of the three-time-scale autonomous systems obtained also using this same methodology, which will be also described in more detail in chapter 5.

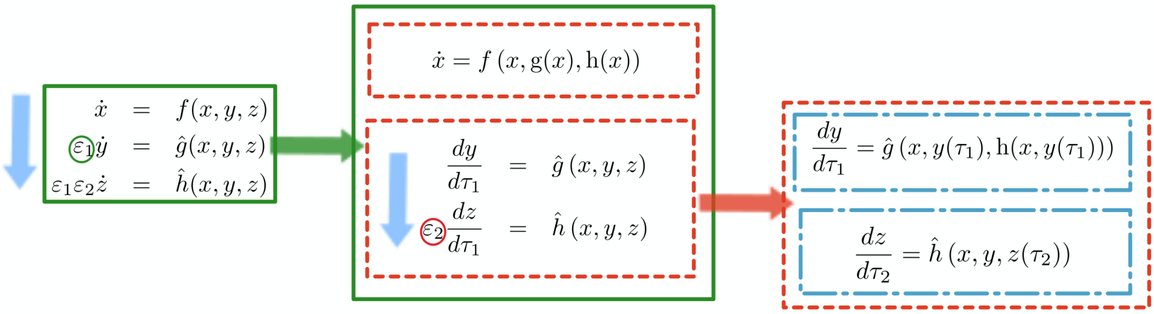

Figure 3.1: *Top-Down* methodology

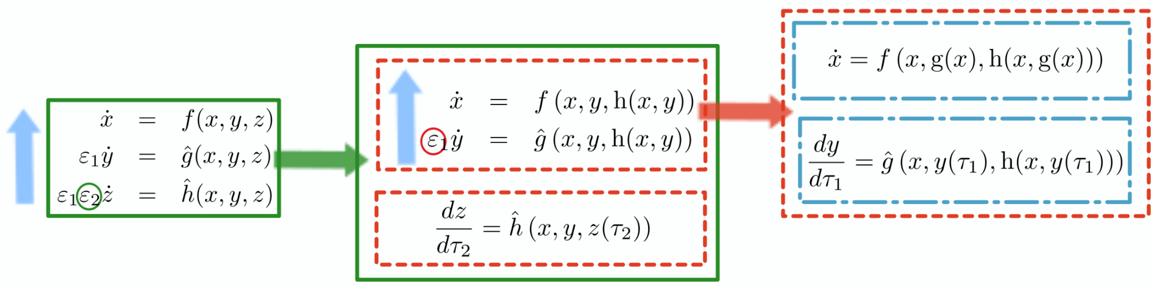

Figure 3.2: *Bottom-Up* methodology

3.2 General Two-Time Scale Singular Perturbation Formulation

The general two-time scale singular perturbation model formulation, that represents the basis for the N^{th}-time-scale and singular perturbation formulation here presented, has been extensively studied in the literature (Tikhonov, 1952; Tikhonov, 1948; Levinson, 1950; Vasil'eva, 1963; O'Malley Jr, 1971), to name few, and was also one of the first to be used in control and systems theory (Kokotović et al., 1986). The general two-time-scale singularly perturbed model, that it is the basis for the strategy conducted in this thesis, is in the explicit state-variable form in which the derivatives of some of the states are multiplied by a small positive scalar, ε, that is

$$\dot{x} = f(x, z, \varepsilon, t), \; x(t_0) = x^0, \; x \in \mathcal{R}^n, \tag{3.1}$$

$$\varepsilon\dot{z} = h(x, z, \varepsilon, t), \; z(t_0) = z^0, \; z \in \mathcal{R}^m, \tag{3.2}$$

where a dot denotes a derivative with respect to time t, and f and h are functions that are assumed to be sufficiently many times continuously differentiable functions of their arguments x, z, ε, t. Let also $B_x \subset \mathcal{R}^m$ and $B_z \subset \mathcal{R}^n$ denote closed sets. The scalar ε represents all the small parameters to be neglected. In control and systems theory, the model defined by Eqns. (3.1–3.2) is a step towards *reduced order modeling*, a common engineering task (Kokotović et al., 1986). The order reduction is converted into a parameter perturbation, called *singular*. When setting the *singular* parameter $\varepsilon = 0$, the dimension of the state space of Eqns. (3.1–3.2) reduces from $n + m$ to n because the differential equation (3.2) degenerates into the algebraic or transcendental equation given by

$$0 = g(\bar{x}, \bar{z}, 0, t), \tag{3.3}$$

where the bar denotes that the variables belong to a system with $\varepsilon = 0$. Equation (3.3) can also be defined as the quasi-steady-state equilibrium of the fast-subsystem. The new model is considered in standard form if and only if, in a domain of interest, Eq. (3.3) has $k \geq 1$ distinct and unique real roots such

$$\bar{z} = \bar{\mathrm{h}}(\bar{x}, t), \; i = 1, 2, ..., k, \tag{3.4}$$

where $\bar{\mathrm{h}}(\bar{x}, t)$ represents the quasi-steady-state equilibrium of the fast-subsystem. This assumption assures that a well defined n-dimensional reduced model will correspond to each root of Eq. (3.4). To obtain the i^{th} reduced model, Eq. (3.4) is substituted into Eq. (3.1) resulting in

$$\dot{\bar{x}} = f(\bar{x}, \bar{z}, 0, t), \; \bar{x}(t_0) = x^0, \tag{3.5}$$

which keeps the same initial conditions for the state variable $\bar{x}(t)$ as for $x(t)$. This model is called a *quasi-steady-state model* (Kokotović et al., 1987; Kokotović et al., 1986) because z, whose velocity $\dot{z} = g/\varepsilon$ can be large when ε is small, may rapidly converge to a root of Eq. (3.3), which is the quasi-steady-state form of Eq. (3.2). The slow response is approximated by the reduced model defined in Eq. (3.5), while the discrepancy between the response of the reduced model, Eq. (3.5), and that of the full model, Eqns. (3.1) and (3.2), is the fast transient. These relations between both the reduced model, Eq. (3.5), and the quasi-steady-state equilibrium of the fast subsystem, Eq. (3.4) represents the basis for powerful tools that singular perturbation provides to the analysis of systems. For simplicity, in future derivations the dependance of the functions in ε and t will be omitted. Additionally, to reduce the complexity of the nomenclature the bar denoting that the variables belong to a system with $\varepsilon = 0$ will be also omitted, which will be easily identified through the context.

Singular perturbation techniques simplify considerably the complexity of coupled dynamics such those present in aerospace systems (Naidu and Calise, 2001; Naidu, 2002) and, as described in the introduction, singular perturbation techniques are used in this thesis as a methodology that permits to perform a complete analysis of nonlinear systems, by providing control law strategies for the singularly perturbed systems, and also demonstrate the asymptotic stability properties of the resulting closed-loop system. This approach permits to create nonlinear control laws that can be derived directly from the original nonlinear systems without the need of making unreasonable simplifications, being only required to guarantee the interconnection properties between the different time-scale subsystems. Following sections will extend these tools to more general time-scale systems.

3.3 Extension to the Multi-Time Scale Singular Perturbation Model Formulation

For simplicity, rather than dealing with a general N^{th}-time-scale singularly perturbed system, the analysis conducted in this chapter will be simplified to a three-time-scale model, which will aid through the remainder of this chapter to visualize the different time-scale strategies. With this in mind, this section provides the extension conducted from the general two-time-scale singular perturbation formulation, to the three-time-scale singular perturbation formulation which will be employed throughout the reminder of this thesis. This extension was originally motivated by the type of problems being dealt in this thesis, singularly perturbed three time-scale problems.

The extension from two to three time-scale analysis is conducted by first introducing the basis for the time-scale selection employed in this thesis, both related to a simplified example, and later to the more complex three-time-scale helicopter model previously presented in section 2.8. The simplified model will help the reader to understand the proposed singular perturbation methods that will be later used on the more complex helicopter model.

3.3.1 Simplified Three-Time-Scale Model

As stated previously, a simplified three-time-scale model is proposed in this section in order to simplify the burden of understanding the proposed time-scale analysis methodology. The use of the simplified model throughout the thesis can be used by the reader as an alternative to understand the proposed solutions to the three-time-scale problems here presented. This simplification can be taken up to the extreme point by the reader so that the proposed strategies for the control design, the Lyapunov function selections and the asymptotic stability analysis for the helicopter model can be initially omitted by the reader, since they only represent the application of the same methodologies to a much more complex model, allowing the reader to focus on the simplified model, and only deal with the helicopter problem once the methodologies have been fully understood.

For completeness of the thesis, all the derivations regarding the proposed *TD* control strategies, and the stability analysis for the simplified example are moved to appendixes B and C respectively. It is advised to the reader, that if, while reading the respective control strategy, and asymptotic stability analysis for the helicopter model, chapters 4 and 6, respectively, the complexity associated to the problem makes the understanding troublesome, start with the respective strategies for the simplified example in Appendixes B and C, and only proceed with the helicopter derivations if wants to get further into the details.

The selected simplified model has been defined possessing many similarities with the helicopter model that is the main focus of this thesis, i.e. the simplified model possesses three distinct variables, x, y, and z, which can be defined as three distinct time-scales, and has the same control authority as the helicopter model, that is, the control signal is only present on two of the dynamics, becoming an underactuated system, in which the objective is to regulate the dynamics that does not have any control signal, this becoming a distinctive challenge when trying to regulate the underactuated variable. Similarly as in Eq. (2.338), the selected model is of the form

$$\dot{x} = f(x, y, z, u_1) = -\rho_1 \left(x + x^2 z + 1\right) + u_1, \tag{3.6}$$

$$\dot{y} = g(x, y, z) = -\rho_2 \left(y + xz + 1\right), \tag{3.7}$$

$$\dot{z} = h(x, y, z, u_2) = -\rho_3 \left(z + x^2 + y\right) + u_2, \tag{3.8}$$

where $\rho_1 = 0.001$, $\rho_2 = 0.1$ and $\rho_3 = 100$, which will be referred as parasitic constants. It will be seen in later chapters that this model simplifies considerably the understanding of the time-scale dependance between each of the different dynamics by observing the magnitude of the associated parasitic constants of each of the three systems (ρ_1, ρ_2, ρ_3).

3.3.1.1 Error Dynamics Formulation for the Simplified Model

Similarly as conducted for the helicopter model in section 2.8.5.2, the simplified example state variables are expressed in their error dynamics form by defining

$$\tilde{x} = x - x^*, \tag{3.9}$$

$$\tilde{y} = y - y^*, \tag{3.10}$$

$$\tilde{z} = z - z^*, \tag{3.11}$$

where x^*, y^*, and z^* represent the desired values of the states variables, and

$$\tilde{u}_1 = u_1 - \bar{u}_1, \tag{3.12}$$

$$\tilde{u}_2 = u_2 - \bar{u}_2, \tag{3.13}$$

with $\bar{u}_1$ and $\bar{u}_2$ represent the steady-state control signals, thus becoming the error-dynamics of the simplified model, Eqns. (3.6–3.8), defined by

$$\dot{\tilde{x}} = -\rho_1 \Big((\tilde{x} + x^*) + (\tilde{x} + x^*)^2 (\tilde{z} + z^*) + 1 \Big) + \tilde{u}_1 + \bar{u}_1, \tag{3.14}$$

$$\dot{\tilde{y}} = -\rho_2 \left((\tilde{y} + y^*) + (\tilde{x} + x^*)(\tilde{z} + z^*) + 1 \right), \tag{3.15}$$

$$\dot{\tilde{z}} = -\rho_3 \Big((\tilde{z} + z^*) + (\tilde{x} + x^*)^2 + (\tilde{y} + y^*) \Big) + \tilde{u}_2 + \bar{u}_2. \tag{3.16}$$

3.3.1.2 Range of Variables for the Simplified Model

In order to define the admissible range of the proposed error-dynamics variables, it is necessary to determine first the maximum range for both, the state variables, and the desired final states. For the problem here studied, the state variables are bounded and given from the physics of the problem, although for the proposed simplified model, since it has no physical significance, the definition of the ranges are determined from simulations, and imposed by the author, therefore, different ranges could be employed which in return, and due to the dependance of the stability analysis on the physics of the problem, could vary the obtained results. For the problem here discussed, and throughout the remainder of this thesis, the range limits for the states variable for the simplified example, and its associated desired values, are defined in Table 3.1 where, similarly as in the helicopter model, the vector that represents the variables is defined as

$$\boldsymbol{\chi} = \begin{bmatrix} x \\ y \\ z \end{bmatrix}, \tag{3.17}$$

therefore being the limits of the ranges defined as

$$\chi_{MIN} \leq \chi \leq \chi_{MAX}, \tag{3.18}$$

where the range of the error-dynamics is defined by

$$\tilde{\chi}_{MIN} \leq \tilde{\chi} \leq \tilde{\chi}_{MAX}, \tag{3.19}$$

with

$$\tilde{\chi}_{MIN} = \chi_{MIN} - \chi_{MAX}, \tag{3.20}$$

$$\tilde{\chi}_{MAX} = \chi_{MAX} - \chi_{MIN}, \tag{3.21}$$

where the selected limits for the simplified example can be seen in Table 3.1.

States (χ)	χ_{MIN}	χ_{MAX}	χ^*_{MIN}	χ^*_{MAX}	$\tilde{\chi}_{MIN}$	$\tilde{\chi}_{MAX}$
x	50	140	60	135	-90	90
y	0	3	0.1	2.9	-3	3
z	-1	1	-1	$+1$	-2	$+2$

Table 3.1: Error-Dynamic Limits for the Simplified Model Variables.

3.3.2 Time-Scale Selection

This section describes one of the most challenging issues when dealing with singularly perturbed systems: identifying the presence of time-scales, and once identified, select the appropriate magnitude of the small parameters that guarantee the asymptotic properties of the different boundary layers. The appropriate selection of time scales is an important aspect of the singular perturbation and time-scales theory (Ardema and Rajan, 1985a; Ardema and Rajan, 1985b; Calise et al., 1994; Mehra et al., 1979; Naidu and Calise, 2001), and, as described in section 1.3.2, can be categorized into three approaches:

- direct identification of small parameters such small time constants, moments of inertia, high Reynolds numbers, and so on.
- transformation of state equations.
- linearization of the state equations.

The first of the three approaches is the one employed to determine the different time scales in this thesis. The challenge comes in identifying those time-scales. Naidu and Calise (Naidu and Calise, 2001) define singular perturbation time-scale characteristics for aerospace systems, and for any system in general, as often associated with small parameter multiplying the highest derivative of the differential equation, or multiplying some of the state equations describing a physical system. They also state that often occurs that the parasitic constant does not appear in the desired form, or the small parameter may not be identifiable at all, and only the physical insight, and past experiences of the behavior of the systems in question, might give clues of how to identify the small parameters. In this thesis, the later proposed method, experience of the behavior of the systems, is the principal methodology employed to identify the parasitic constants, but in addition, mathematical reasoning is also employed during the time-scale identification process. In order to identify the type of systems that will be dealt in this thesis, let first define the general three-time-scale model description used throughout this thesis is given by

$$\dot{x} = f(x, y, z), \tag{3.22}$$

$$\dot{y} = g(x, y, z), \tag{3.23}$$

$$\dot{z} = h(x, y, z), \tag{3.24}$$

where x, y, and z are the state variables. The general three-time-scale singular perturbed model used throughout the thesis is required to possess three different time-scales that can be written as

$$\begin{aligned} \dot{x} &= f(x, y, z), & (3.25)\\ \varepsilon_1 \dot{y} &= \hat{g}(x, y, z), & (3.26)\\ \varepsilon_1 \varepsilon_2 \dot{z} &= \hat{h}(x, y, z), & (3.27) \end{aligned}$$

being x the slow state variable, y the fast state variable, and z the ultra-fast state variable, and holding that $0 < \varepsilon_1 \varepsilon_2 << \varepsilon_1 << 1$, thus $\varepsilon_2 << 1$. Let also define the relationship between the original nonlinear dynamics and the singularly perturbed dynamics through the relationship given by

$$\begin{aligned} \hat{g}(x, y, z) &= \varepsilon_1 g(x, y, z), & (3.28)\\ \hat{h}(x, y, z) &= \varepsilon_1 \varepsilon_2 h(x, y, z). & (3.29) \end{aligned}$$

Equations (3.25–3.27) represent the singularly perturbed full system, and for simplicity will be denoted as Σ_{SFU} full system throughout the reminder of this thesis. The following sections will describe the time-scale selection process employed for the simplified and the helicopter model. For simplicity, and completeness of the thesis, the notation to denote the different time-scale subsystems it is defined as $\Sigma_{(\cdot)}$, where the subindex denotes the different subsystems, that is: Σ_S for the slow subsystem, Σ_F for the fast subsystem, and the Σ_U for the ultra-fast subsystem.

In the (slow) Σ_S-subsystem the fast and ultra-fast state variables, y and z, respectively, are assumed to evolve in their configuration spaces, given by $y = \mathrm{g}(x)$ and $z = \mathrm{h}(x, y)$, respectively, where $\mathrm{g}(x)$ represents the quasi-steady-state equilibrium of Eq. (3.26) when setting $\varepsilon_1 = 0$ that is $\hat{g}(x, y, z) = 0 \rightarrow y = \mathrm{g}(x)$, and where $\mathrm{h}(x, y)$ represents the quasi-steady-state equilibrium of Eq. (3.27) when setting $\varepsilon_2 = 0$ that is $\hat{h}(x, y, z) = 0 \rightarrow z = \mathrm{h}(x, y)$. Note that for completeness, throughout the remainder of this thesis, while the functions will be denoted with italic lower case, i.e.: g and h, the associated quasi-steady-equilibrium for the same functions will be denoted in Roman lower case g and h.

In the (fast) Σ_F-subsystem, it is assumed that the ultra-fast state variable z evolve on its configuration space, that is $z = \mathrm{h}(x, y)$, while the slow state variable x is treated like a fixed parameter, and finally, in the (ultra-fast) Σ_U-subsystem, both x and y are treated like constants. Refer to Figure (3.9) for completeness, although it will be described in detail in section 3.5.

3.3.2.1 Time-Scale Selection for the Simplified Example

The simplified three-time-scale singular perturbed model that is employed in this thesis can be rewritten in a three-time-scale structure similar to Eqns. (3.25–3.27), and defined as

$$\begin{aligned} \dot{x} &= f(x, y, z, u_1), & (3.30)\\ \varepsilon_1 \dot{y} &= \hat{g}(x, y, z), & (3.31)\\ \varepsilon_1 \varepsilon_2 \dot{z} &= \hat{h}(x, y, z, u_2), & (3.32) \end{aligned}$$

being x the slow variable, y the fast variable, and z the ultra-fast variable, and also holding that $0 < \varepsilon_1 \varepsilon_2 << \varepsilon_1 << 1$, thus $\varepsilon_2 << 1$ where

$$\begin{aligned} \hat{g}(x, y, z) &= \varepsilon_1 g(x, y, z), & (3.33)\\ \hat{h}(x, y, z, u_2) &= \varepsilon_1 \varepsilon_2 h(x, y, z, u_2). & (3.34) \end{aligned}$$

Equations (3.30–3.32) represent the singularly perturbed full system, and for simplicity, as noted previously, it will be also denoted as Σ_{SFU} full system throughout the reminder of the simplified model analysis. These equations differ from the general three-time-scale singularly perturbed Eqns. (3.25–3.27), in the inclusion of the control signals.

The time scales of the simplified model can be identified by analyzing the mathematics of the problem. Observing the nature of the coefficients multiplying the original Eqns. (3.6–3.8), ρ_1, ρ_2, ρ_3, it can be identified the existence of small and large parameters that multiply the highest derivative of the differential Eqns. (3.6–3.8), where recalling that $\rho_1 = 0.001$, $\rho_2 = 0.1$ and $\rho_3 = 100$, thus $\rho_1 \ll \rho_2 \ll \rho_3$, being obvious the choice of x as the slow variable, y as the fast variable, and z as the ultra-fast variable.

In order to express the original set of time differential Eqns. (3.6–3.8) in the proper three time-scale singular perturbation formulation, Eqns. (3.30–3.32), a series of algebraic modifications, using the identified time constants that multiply the original equations (ρ_1, ρ_2, ρ_3), are introduced re-writing the equations in the form

$$\begin{aligned} I_x\dot{x} &= I_x f(x,y,z,u_1) = \hat{f}(x,y,z,u_1), & (3.35)\\ I_y\dot{y} &= I_y g(x,y,z) = \hat{g}(x,y,z), & (3.36)\\ I_z\dot{z} &= I_z h(x,y,z,u_2) = \hat{h}(x,y,z,u_2), & (3.37)\end{aligned}$$

where I_x, I_y and I_z represent the perturbation parameters of each of three time-scales, and can be thought as inertias multiplying the time-derivatives, and are given by

$$\begin{aligned} I_x &= \frac{1}{\rho_1}, & (3.38)\\ I_y &= \frac{1}{\rho_2}, & (3.39)\\ I_z &= \frac{1}{\rho_3}. & (3.40)\end{aligned}$$

It can be seen that $I_x >> I_y >> I_z$, therefore in order to express Eqns. (3.35–3.37) in the correct multi-time singular perturbation formulation, Eqns. (3.30–3.32), all the perturbation parameters are normalized with respect to the slowest coefficient, that is, I_x, yielding the parasitic constants selected for this problem as

$$\begin{aligned} \varepsilon_1 &= \frac{I_y}{I_x} = \frac{\rho_1}{\rho_2} = 0.01, & (3.41)\\ \varepsilon_2 &= \frac{I_z}{I_y} = \frac{\rho_2}{\rho_3} = 0.001, & (3.42)\\ \varepsilon_1\varepsilon_2 &= \frac{I_z}{I_x} = \frac{\rho_1}{\rho_3} = 0.00001, & (3.43)\end{aligned}$$

satisfying that $0 < \varepsilon_2 << \varepsilon_1 << 1$, and that $0 < \varepsilon_1\varepsilon_2 << \varepsilon_1 << 1$, thus $\varepsilon_2 << 1$, and therefore, allowing to rewrite the three-time-scale Σ_{SFU} simplified model as

$$\begin{aligned} \dot{x} &= -\rho_1\left(x + x^2 z + 1\right) + u_1, & (3.44)\\ \varepsilon_1\dot{y} &= -\eta_1\left(y + xz + 1\right), & (3.45)\\ \varepsilon_1\varepsilon_2\dot{z} &= -\eta_2\left(z + x^2 + y\right) + \eta_3 u_2, & (3.46)\end{aligned}$$

where

$$\begin{aligned} \eta_1 &= \varepsilon_1\rho_2, & (3.47)\\ \eta_2 &= \varepsilon_1\varepsilon_2\rho_3, & (3.48)\\ \eta_3 &= \varepsilon_1\varepsilon_2. & (3.49)\end{aligned}$$

3.3.2.2 Time-Scale Selection for the Helicopter Model

The three-time-scale singular perturbed helicopter model that will be employed in this thesis also possess the same structure as Eqns. (3.30–3.32). Both the simplified, and the helicopter model, will use the same nomenclature to refer to each of the subsystems being analyzed, and this will be the common trend throughout the remainder of this thesis, since the context will be sufficient condition to identify if the nomenclature is referring to the simplified or the helicopter model. The author believes that by maintaining the same nomenclature, it is going to be easier for the reader to benefit from the simplified example when trying to understand how the proposed singular perturbed methodologies apply to the more complex helicopter model, otherwise, the use of different nomenclature will confuse and distract the reader from understanding the proposed methodologies.

As previously described, the time scales can be identify by analyzing the mathematics of the problem, and observing the existence of small and large parameters that multiply the highest derivative of the differential equations. The identification of the three-time-scales for the helicopter model is obtained conducted from initial inspection of the helicopter dynamics, Eqns. (2.339–2.343), and recalling the helicopter modeling process described in section 2.8, it can be deduced that a three-time-scale model is more suitable than a two-time-scale one. From a physical point of view it is clear that z_1 and z_2 are much faster than the rest, since they represent the collective pitch and its actuator dynamics, which are generally treated as a control input, and here are treated as state variables. The vertical motion of the helicopter, variables y_1 and y_2, are much faster than the angular velocity of the blades, x, and as is shown in later sections, through the design of appropriate control laws, we can modify both the vertical maneuverability of the helicopter and its engine behavior to adequate their reactions to the desired transient responses.

After identifying the time scales from a physical perspective, it is necessary to identify them from a mathematical point of view. Analyzing the mathematics of the problem it can be identified the existence of small and large parameters that multiply the highest derivative of the differential equations such that the higher order dynamics of the angular speed of the blades in Eq. (2.339), terms in x^2, are multiplied by $a_9 = a_{10} = -0.0028$; the higher order dynamics of the vertical motion of the helicopter in (2.340), terms in y_2 and y_2^2, are multiplied by $a_5 = a_6 = -0.1$; and the higher order dynamics of the collective pitch angle in (2.343), z_1 and z_2, are multiplied by $a_{13} = -800$ and $a_{15} = -65$ respectively. The mathematical characteristics of the system corroborate the three time-scale selection based on the physical point of view, and by observing that the parameters that multiply the highest derivatives of the differential equations. Therefore, let proceed to select x as the slow variable, $\boldsymbol{y} \triangleq [y_1\ y_2]^T$ as the fast state vector, and $\boldsymbol{z} \triangleq [z_1\ z_2]^T$ as the ultra-fast state vector.

In order to express the original set of differential Eqns. (2.339–2.343) in the standard three time-scale singular perturbation formulation, Eqns. (3.30–3.32), and similarly as in the simplified example, a series of algebraic modifications using the identified large and small parameters that multiply the original equations are introduced, re-writing the equations similarly as in Eqns. (3.35–3.37), where the perturbation parameters of each of three time-scales, I_x, I_y and I_z, are given by

$$I_x = \frac{1}{a_9}, \tag{3.50}$$

$$I_y = \frac{1}{a_5}, \tag{3.51}$$

$$I_z = \frac{1}{a_{13}}. \tag{3.52}$$

It can also be seen that $I_x >> I_y >> I_z$, therefore in order to express the equations of the three time-scales in the correct multi-time singular perturbation formulation, all the perturbation parameters are normalized with respect to the slowest coefficient, that is I_x, yielding the parasitic constants selected for this problem given by

$$\varepsilon_1 = \frac{I_y}{I_x} = \frac{a_9}{a_5} = 2.8 \times 10^{-2}, \tag{3.53}$$

$$\varepsilon_2 = \frac{I_z}{I_y} = \frac{a_5}{a_{13}} = 1.25 \times 10^{-4}, \tag{3.54}$$

$$\varepsilon_1\varepsilon_2 = \frac{I_z}{I_x} = \frac{a_9}{a_{13}} = 3.5 \times 10^{-6}, \tag{3.55}$$

satisfying that $0 < \varepsilon_2 << \varepsilon_1 << 1$, and that $0 < \varepsilon_1\varepsilon_2 << \varepsilon_1 << 1$, thus $\varepsilon_2 << 1$, thus rewriting Eqns. (2.339–2.343) as

$$\dot{x} = a_8 x + a_{10}x^2 \sin z_1 + a_9 x^2 + a_{11} + u_1, \tag{3.56}$$

$$\varepsilon_1 \dot{y}_1 = c_1 y_2 \tag{3.57}$$

$$\varepsilon_1 \dot{y}_2 = x^2(c_2 + c_3 z_1 - \sqrt{c_4 + c_5 z_1}) + a_9 y_2 + a_9 y_2^2 + c_6, \tag{3.58}$$

$$\varepsilon_1\varepsilon_2 \dot{z}_1 = c_7 z_2 \tag{3.59}$$

$$\varepsilon_1\varepsilon_2 \dot{z}_2 = a_9 z_1 + c_8 x^2 \sin z_1 + c_9 z_2 + c_{10} + c_{11} u_2, \tag{3.60}$$

being the helicopter singular perturbation normalized physical coefficients defined as

$$\begin{aligned}
c_1 &= \frac{a_9}{a_5} = 0.028,\ c_2 = \frac{a_1 a_9}{a_5} = c_1 a_1 = 1.2229 \times 10^{-5} \\
c_3 &= \frac{a_2 a_9}{a_5} = c_1 a_2 = 3.9011 \times 10^{-4},\ c_4 = \left(\frac{a_9}{a_5}\right)^2 = c_1^2 a_3 = 1.4956 \times 10^{-10} \\
c_5 &= \left(\frac{a_9}{a_4}\right)^2 a_5 = c_1^2 a_4 = 9.5418 \times 10^{-9},\ c_6 = \frac{a_7 a_9}{a_5} = c_1 a_7 = -4.9476 \times 10^{-1} \\
c_7 &= c_{11} = \frac{a_9}{a_{13}} = 3.500 \times 10^{-6},\ c_8 = \frac{a_9 a_{14}}{a_{13}} = c_7 a_{14} = -3.500 \times 10^{-7} \\
c_9 &= \frac{a_9 a_{15}}{a_{13}} = c_7 a_{15} = -2.2750 \times 10^{-4},\ c_{10} = \frac{a_9 a_{12}}{a_{13}} = c_7 a_{12} = 1.52208 \times 10^{-3}.
\end{aligned}$$

3.4 *Top-Down* and *Bottom-Up* Time-Scale Analysis

The strategy presented in this thesis for the analysis of three-time-scale singular perturbed problems consists on treating the three different time-scales as two distinct two-time-scale singular perturbed problems using the standard two-time-scale analysis (Kokotović et al., 1986) for each of the two obtained subproblems as seen in Figures 3.1 and 3.2. Each one of the two resulting two-time-scale singularly perturbed sub-problems is considerably simplified, and thus permitting to easily obtain the appropriate control laws that stabilize each of the resulting subsystems, or in the case in which the proposed methodology is employed to analyze the stability properties, it will ease the complexity associated to guarantee the interconnection properties among the different time-scale subsystems. Each one of the two-time-scale singularly perturbed sub-problems consists of a slow and a fast subsystem, and by the selection of the appropriate control laws, it is ensured that the associated subsystems are each asymptotically stable.

The importance of the proposed *Top-Down* (*TD*) and *Bottom-Up* (*BU*) time-scale analysis presented in this section will be understood realizing that the problems addressed in this thesis, the control design strategy, the obtention of the associated Lyapunov functions, and the demonstration of the asymptotic stability properties of the closed-loop system, are all based on the *TD*, the *BU*, or a combination of both methodologies. This section tries to describe in detail the generic methodology that will serve throughout the rest of this thesis as a basis for selecting the proper control laws, and guaranteeing that the resulting closed-loop systems are asymptotically stable. The strategy employed can be conducted by either selecting the *TD* approach, or the *BU* approach, depending in the direction in which the time-scales are applied, being both approaches equivalent for the analysis of the time-scale properties. This results in that either strategy can be selected depending in the direction in which the time-scales are desired to be applied, that is, according to the complexity of the nonlinear systems being treated, it might be desirable to use either direction.

The strategy of treating the three different time-scales as two distinct two-time-scale singular perturbed problems using the standard two-time-scale analysis for each of the two sub-problems is based on sequentially considering the different time scales appearing on the original three-time-scale system, Eqns. (3.25–3.27), that is, selecting the time scales associated to the small parasitic constants ε_1 and ε_2. For the general three-time-scale problems here described, the use of either the *TD* or the *BU* methodologies produce equivalent results, although for conciseness and completeness, the *BU* methodology will be selected as the principal analysis methodology, although, as it will be seen in chapter 4, the selected control strategy will use the *TD* methodology. Following sections described in much more detail both the *TD* and *BU* time-scale analysis.

3.4.1 *Top-Down* Time-Scale Analysis

The first presented methodology, denoted as *Top-Down* (*TD*), deals with the subsystems that result when considering first the time-scale defined by the *Top* condition, that is, applying the stretched time scale given by $\tau_1 = t/\varepsilon_1$, to the original Σ_{SFU} system, Eqns. (3.25–3.27). This results in a two-time-scale subproblem where the reduced (slow) subsystem is defined by

$$\dot{x} = f(x, \mathrm{g}(x), \mathrm{h}(x, \mathrm{g}(x))), \tag{3.61}$$

and where the boundary layer (fast) subsystem for the *TD* subproblem is defined by

$$\frac{dy}{d\tau_1} = \hat{g}(x, y(\tau_1), z(\tau_1)), \tag{3.62}$$

$$\varepsilon_2 \frac{dz}{d\tau_1} = \hat{h}(x, y(\tau_1), z(\tau_1)), \tag{3.63}$$

where $\tau_1 = t/\varepsilon_1$, and where the expressions $\mathrm{g}(x)$ and $\mathrm{h}(x, \mathrm{g}(x))$ in Eq. (3.61) represent the quasi-steady-state equilibria of the boundary layer, Eqns. (3.62–3.63), when $\varepsilon_1 = 0$, that is

$$0 = \hat{h}(x, y, z) \to z = \mathrm{h}(x, y) = \mathrm{h}(x, \mathrm{g}(x)), \tag{3.64}$$

$$0 = \hat{g}(x, y, \mathrm{h}(x, y)) \to y = \mathrm{g}(x), \tag{3.65}$$

where both $\mathrm{g}(x)$ and $\mathrm{h}(x, y)$ evolve on their own configuration spaces. The reduced order (slow) subsystem, Eq. (3.61), resulting from the *Top*-condition analysis will be denoted as Σ_S-subsystem, while the boundary layer (fast) subsystem resulting from the same *Top*-condition analysis, Eqns. (3.62-3.63), will be referred as Σ_{FU}-subsystem for simplicity. Recall that in the space of configuration of the boundary layer Σ_{FU}-subsystem, Eqns. (3.62-3.63), x is treated like a fix parameter. Figure 3.3 depicts the *Top*-sequence of the *Top-Down* methodology.

The second sequence of the *TD* time-scale analysis, the *Down* sequence, permits to analyze the behavior of the boundary layer Σ_{FU}-subsystem, Eqns. (3.62-3.63). It can be identified that the resulting Σ_{SF}-subsystem can be treated again like a two-time-scale singular perturbation problem by analyzing the subsystem that results when applying the stretched time scale given by $\tau_2 = \tau_1/\varepsilon_2 = t/\varepsilon_1\varepsilon_2$. This results in a new reduced (slow) subsystem, denoted as Σ_F-subsystem for simplicity, and defined by

$$\frac{dy}{d\tau_1} = \hat{g}(x, y(\tau_1), \mathrm{h}(x, y(\tau_1))), \tag{3.66}$$

and where the new boundary layer (fast) subsystem is given by

$$\frac{dz}{d\tau_2} = \hat{h}(x, y, z(\tau_2)). \tag{3.67}$$

The boundary layer, Eq. (3.67), will be denoted as Σ_U-subsystem for simplicity. The function $\mathrm{h}(x, y(\tau_1))$ in the reduced order Σ_F-subsystem, Eq. (3.66), represents the quasi-steady-state of the boundary layer Σ_U-subsystem, Eq. (3.67), when setting $\varepsilon_2 = 0$, that is

$$0 = \hat{h}(x, y, z) \rightarrow z = \mathrm{h}(x, y), \tag{3.68}$$

where x and y are treated like fix parameters. This concludes the *Top-Down* methodology (*TD*). The following section describes the *Bottom-Up* methodology, which in a similar manner to the *TD* methodology, analyzes the three time-scale system by decomposing it into two distinct two-time-scale singular perturbed problems. Figure 3.5 depicts the complete *Top-Down* time-scale analysis.

3.4.2 *Bottom-Up* Time-Scale Analysis

The *Bottom-Up* methodology (*BU*), uses a philosophy similar to *TD* methodology presented in the previous section, but the analysis is conducted considering the time-scale defined by first the *Bottom* condition, that is, applying the stretched time scale given by $\tau_2 = t/\varepsilon_2$, and secondly the *Up* condition, that is the stretched time scale $\tau_1 = t/\varepsilon_1$. Applying first the *Bottom* stretched time-scale condition to the Σ_{SFU} full system yields the new reduced (slow) subsystem defined by

$$\dot{x} = f(x, y, \mathrm{h}(x, y)), \tag{3.69}$$

$$\varepsilon_1 \dot{y} = \hat{g}(x, y, \mathrm{h}(x, y)), \tag{3.70}$$

and denoted as Σ_{SF}-subsystem, and where the new boundary layer (fast) subsystem is given by

$$\frac{dz}{d\tau_2} = \hat{h}(x, y, z(\tau_2)), \tag{3.71}$$

and denoted also as Σ_U-subsystem. The function $\mathrm{h}(x, y)$ in the reduced order Σ_{SF}-subsystem, Eqns. (3.69–3.70), represents the quasi-steady-state of the boundary layer, Eq. (3.71) when $\varepsilon_2 = 0$, that is

$$0 = \hat{h}(x, y, z) \rightarrow z = \mathrm{h}(x, y), \tag{3.72}$$

where $\mathrm{h}(x, y)$ evolves on its own configuration space. Recall that Eq. (3.67) in the *TD* time-scale analysis, and Eq. (3.71) in the *BU* are equivalent and both denoted as Σ_U-subsystem. Figure 3.4 depicts the *Bottom*-sequence of the *BU* methodology. Let also recall that, in the boundary layer Σ_U-subsystem, the variables x and y are treated like fixed parameters. The analysis of the *BU* methodology is continued by identifying that the reduced order Σ_{SF}-subsystem, Eqns. (3.69-3.70), can be treated again like a two-time-scale singular perturbed problem, by dealing with the subsystem that results when applying the *Up* condition, that is, applying the stretched time scale given by $\tau_1 = t/\varepsilon_1$, where the new reduced (slow) subsystem, denoted as Σ_S-subsystem for simplicity, is now defined by

$$\dot{x} = f(x, \mathrm{g}(x), \mathrm{h}(x, y)), \tag{3.73}$$

and the new boundary layer is defined by

$$\frac{dy}{d\tau_1} = \hat{g}(x, y(\tau_1), \mathrm{h}(x, y(\tau_1))), \tag{3.74}$$

where $\mathrm{g}(x)$ represents the quasi-steady-state of the boundary layer, Eq. (3.74), when $\varepsilon_1 = 0$, that is

$$0 = \hat{g}(x, y, z) = \hat{g}(x, y, \mathrm{h}(x, y)) \rightarrow y = \mathrm{g}(x), \tag{3.75}$$

where g(x) and h(x, y) evolve on their own configuration spaces. Figure 3.6 depicts the complete analysis of the *Top-Down* subproblem.

3.4.3 *Top-Down* and *Bottom-Up* Interconnection Properties

It is important to clarify the interconnection properties between the *TD* and *BU* time-scale analysis are of great importance to help understanding the equivalencies between both strategies. These interconnection properties guarantee that the presented strategy for treating the three different time-scales as two distinct two-time-scale singular perturbed problems, result in that the two-different two-time-scale resulting problems are both complementary.

The resulting Σ_S, Σ_F, and Σ_U subsystems obtained in the *TD* methodology, Eqns. (3.61), (3.66), and (3.67), respectively, are equivalent to the ones obtained in the *BU* methodology, Eqns. (3.73), (3.74), and (3.71), respectively. For simplicity, throughout the remainder of this thesis, in the boundary-layer Σ_F-subsystem, Eq. (3.74), state variable $y(\tau_1)$ will be denoted as y, and in the boundary-layer Σ_U-subsystem, Eq. (3.71), the state variable $z(\tau_2)$ will be denoted as z

These complementary interconnection properties can be better identified when considering the similarities between both the *TD* two-time-scale sequential decomposition seen in Fig. 3.5, and the *BU* two-time-scale sequential decomposition seen in Fig. 3.6. These similarities can be resumed as:

- The reduced order Σ_S-subsystem of the *TD* analysis is also the slow movement of the Σ_{SF}-subsystem obtained in the *BU* analysis, Eqns. (3.61) and (3.73) respectively.
- The Σ_F-subsystem is the slow movement of the Σ_{FU}-subsystem from the *TD* analysis and the fast movement of the Σ_{SF}-subsystem from the *BU* analysis, becoming the interconnected subsystem between both the *TD* and *BU* methodologies, Eqns. (3.66) and (3.74) respectively.
- The Σ_U-subsystem is the fast movement of the Σ_{FU}-subsystem from the *TD* analysis, and also the boundary layer for the *BU* analysis, and the ultra-fast movement of Σ_{SFU}, Eqns. (3.67) and *TD* and (3.71) respectively.

These similarities can be further understood by analyzing Figure 3.7, which depicts these interconnections among the different subsystems by merging both sequential time-scale decompositions defined in Figs. 3.5 and 3.6. It can be clearly identified the interconnected subsystems where the labels 1_A and 1_B denote the *BU* and *TD* reduced order Σ_S-subsystems, labels 2_A and 2_B denote the *BU* and *TD* Σ_F-subsystems, and finally, labels 3_A and 3_B denote the boundary layer *BU* and *TD* Σ_U-subsystems, therefore becoming both approaches complementary, and equivalent.

For three-time-scale singularly perturbed systems, one of the two methodologies is sufficient to conduct the stability analysis, the control design, and the selection the appropriate Lyapunov functions for each of the singularly perturbed subsystems. The equivalency between each of the two analysis strategies is guaranteed by the superposition principle, which despite the combination of the *TD* and *BU* methodologies, the final results will be equivalent.

For the more general N^{th}-time-scale system, the same methodologies are applicable, with the exception that, after each obtained subsystem reduction, the designer can continue with the time-scale decomposition using either the *TD* or the *BU* methodologies, depending on the system structure of the resulting reduced order and boundary layer subsystems, and what suits better in order to proceed with the time-scale decomposition.

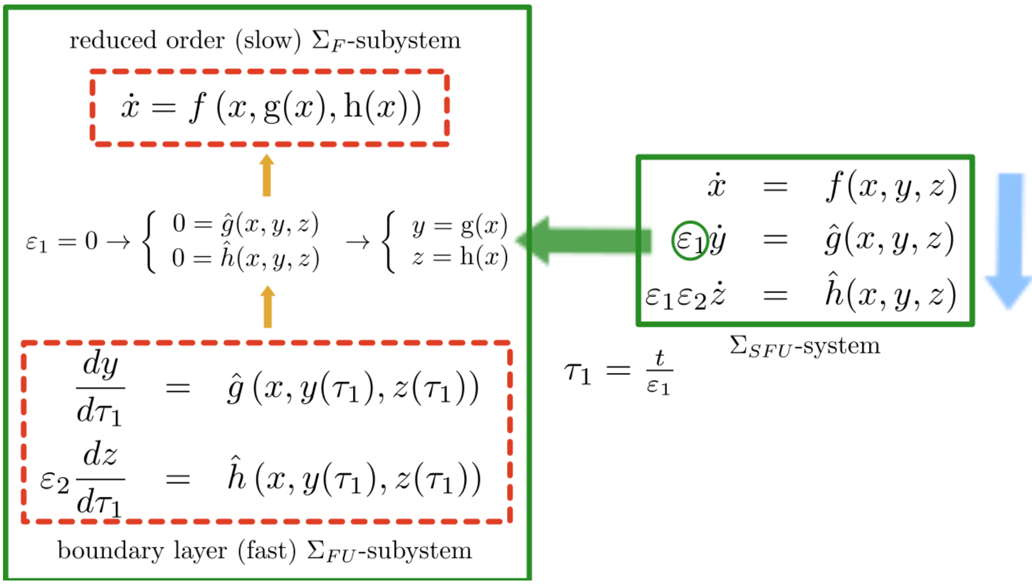

Figure 3.3: *Top*-sequence of the *Top-Down* methodology.

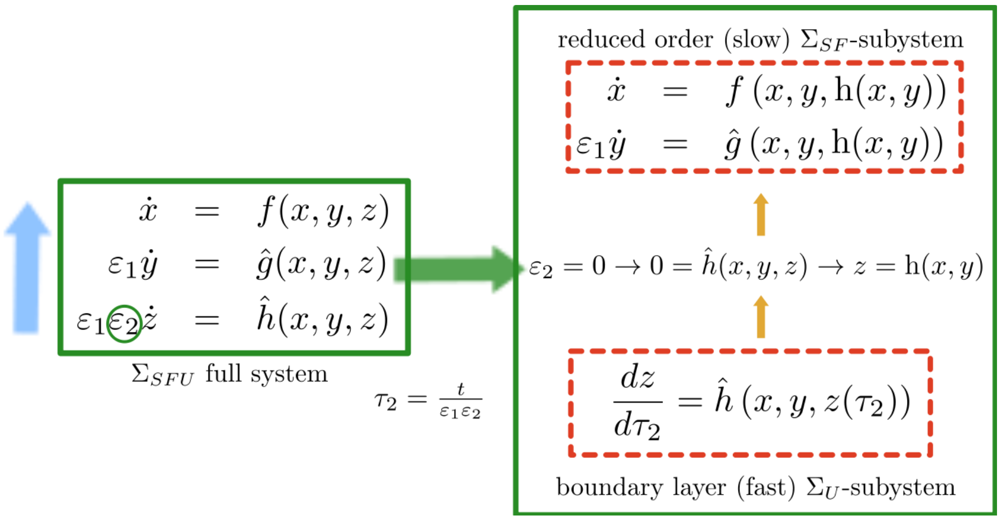

Figure 3.4: *Bottom*-sequence of the *Bottom-Up* subproblem.

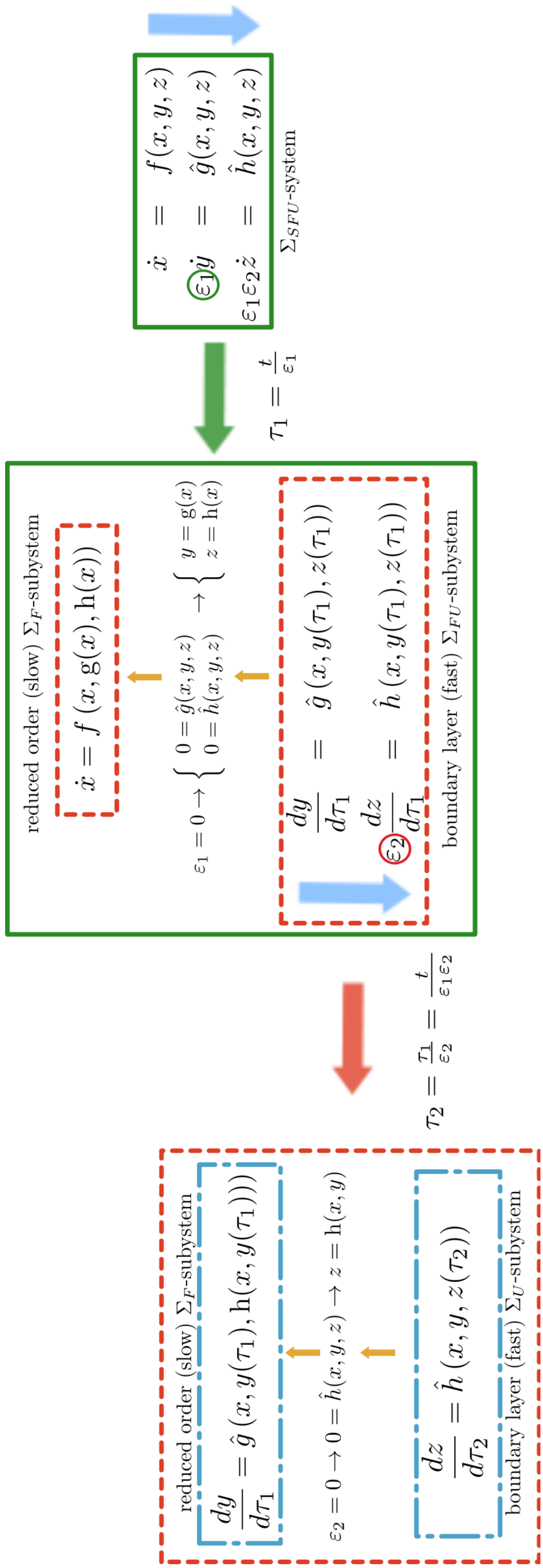

Figure 3.5: *Top-Down* Two-time-scale sequential decomposition.

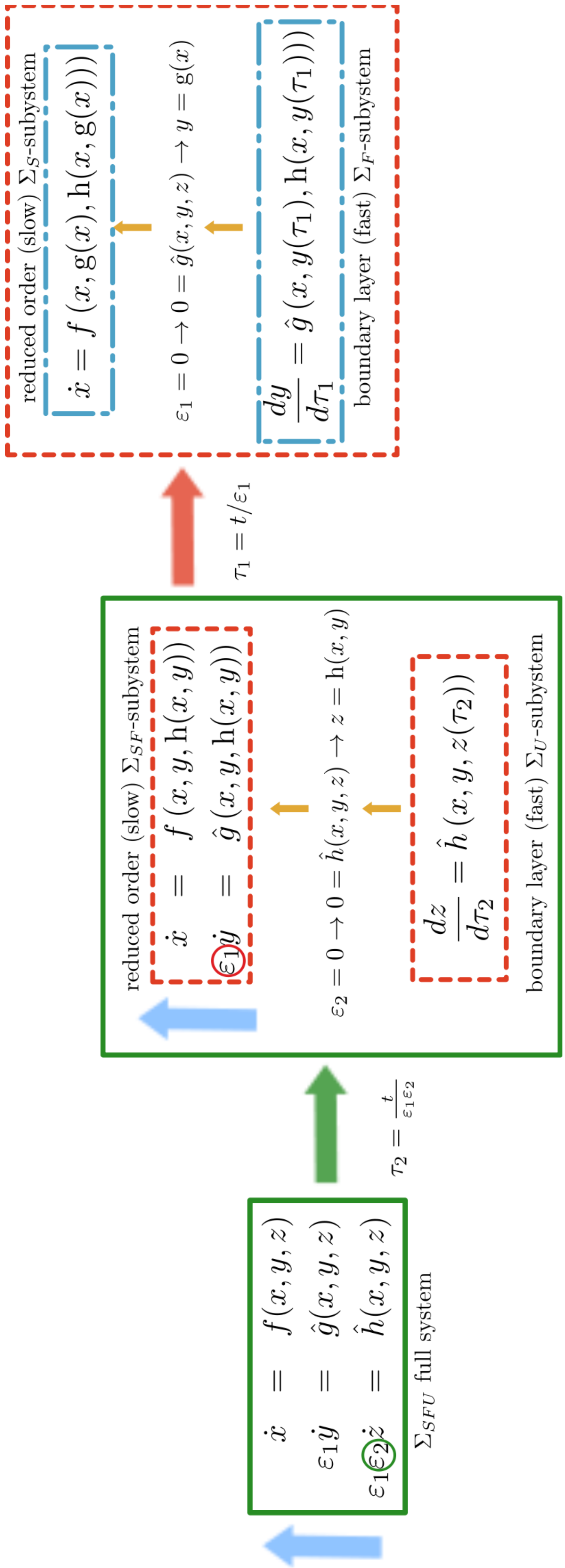

Figure 3.6: *Bottom-Up* Two-time-scale sequential decomposition.

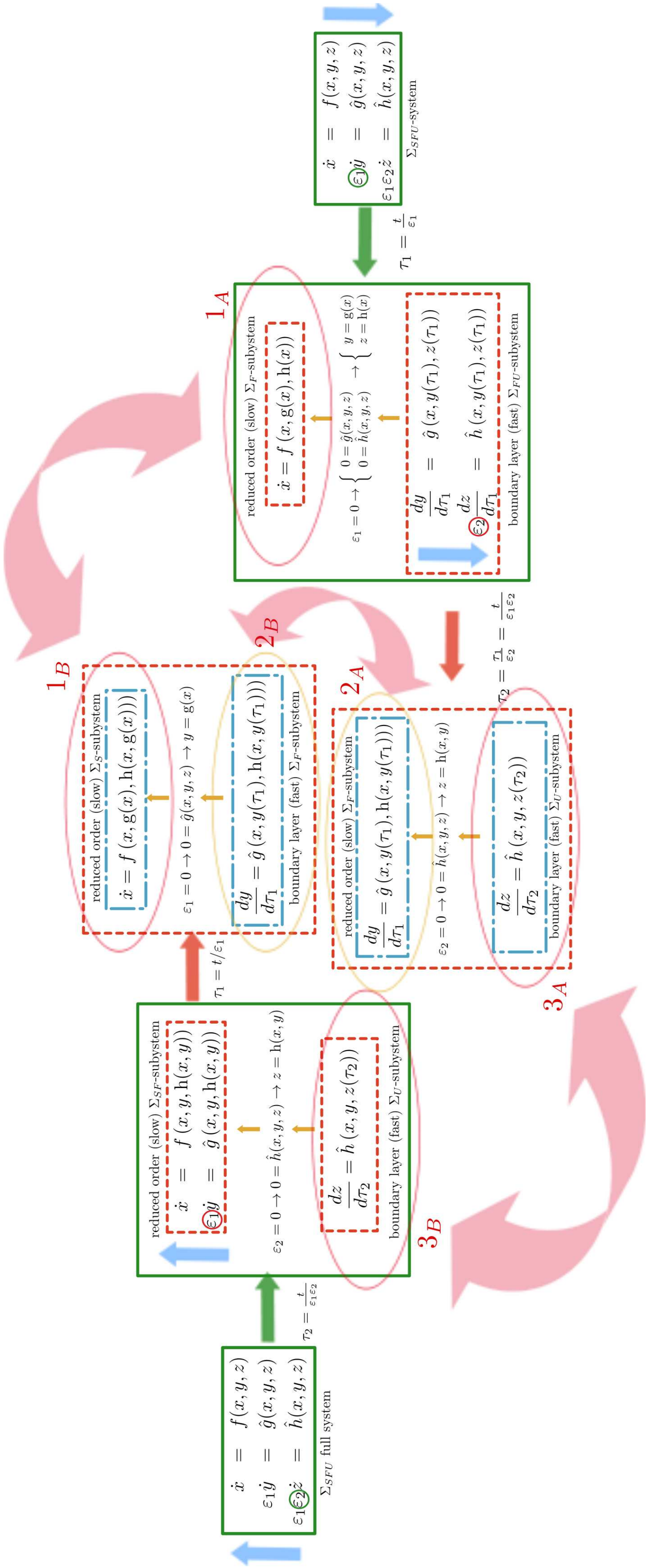

Figure 3.7: Interconnection between *Top-Down* and *Bottom-Up* methodologies.

3.5 Intuitive Description of the Three-Time-Scale Decomposition

The *TD* and *BU* methodologies previously presented can be used separately for analysis purposes, producing equivalent results, and when combined can be used to determine the appropriate control laws, and the Lyapunov function for each of the Σ_S, Σ_F, and Σ_U-subsystems as it will be shown in later chapters. The understanding of the natural evolution of a generic three-time-scale model, can be achieved by focusing only on the *BU* sequential methodology, which will help to describe how the ultra-fast, fast and slow variables of a stable system evolve through their own configuration spaces, or manifolds.

In order to better understand how a three-time-scale singularly perturbed systems behaves, it is important to first understand how a stable two-time-scale singularly perturbed system behaves. In such systems, the fastest variable of the system evolves towards its equilibrium through its fast manifold, while the slowest variable remains almost unchanged until the fastest variable reaches its configuration space. At that point, the slowest variable evolves towards its equilibrium through the slow manifold while the fast variable moves through its configuration space. This two-time-scale evolution can be easily observed in Fig. 3.8, where z represents the fast variable, while x represents the slow variable of the system.

For a three-time-scale singularly perturbed system, the evolution is a bit more complex than the two-time-scale behavior, but shows lots of resemblances, and can be described considering the *BU* time-scale analysis. In order to be able understand the evolution of a generic three-time-scale model let recall that the generic three-time-scale Σ_{SFU} model, Eqns. (3.25–3.27), can be sequentially decomposed into two different two-time-scale models. The first two-time-scale model considers the time-scale defined by $\tau_2 = t/(\varepsilon_1\varepsilon_1)$, where the reduced (slow) Σ_{SF}-subsystem was given in Eqns. (3.69–3.70), and where the boundary layer of the Σ_{SFU} system is given by the Σ_U-subsystem, Eq. (3.71). This first two-time-scale decomposition represents the *Bottom* sequence previously defined in the *BU* analysis as seen in Fig. 3.4. The reduced order Σ_{SF}-subsystem, Eqns. (3.69–3.70), can be treated again like a two-time-scale singular perturbation problem by considering the time scale defined by $\tau_1 = t/\varepsilon_1$, where the reduced Σ_S-subsystem is given by Eq. (3.73), and where the new boundary layer for the Σ_{SF}-subsystem, denoted as Σ_F-subsystem, is given by Eq. (3.74). This second time-scale decomposition represents the *Up*-sequence of the *BU*, and can be better appreciated in the right-hand-side of Figure 3.6.

In order to have a better understanding of the evolution of the different time-scales Figure 3.9 shows the complete evolution of a generic stable three-time-scale model. Figure 3.9(a) shows the evolution of the ultra-fast variable z as it moves through the configuration space of the boundary layer, Σ_U-subsystem, towards the surface that defines the quasi-steady-state equilibrium of the Σ_U-subsystem, given by $\hat{h}(x, y, z) = 0$, that is $z = \mathrm{h}(x, y)$, while x and y behave as fixed parameters.

Figure 3.9(b) shows the evolution of the fast state variable y as it moves on the configuration space of the boundary layer of the Σ_{SF}-subsystem towards the surface that defines the quasi-steady-state equilibrium of Σ_F-subsystem given by $\hat{g}(x, y, \mathrm{h}(x, y)) = 0$, that is $y = \mathrm{g}(x)$, while the slow variable x behaves as a fixed parameter, and $z = \mathrm{h}(x, y)$ evolves also on its manifold. Finally, Figure 3.9(c) shows the evolution of the slow variable x as it moves in the manifold of the Σ_S-subsystem, which is given by the intersection between the planes $\hat{g}(x, y, \mathrm{h}(x, y)) = 0$ and $\check{h}(x, y, z) = 0$.

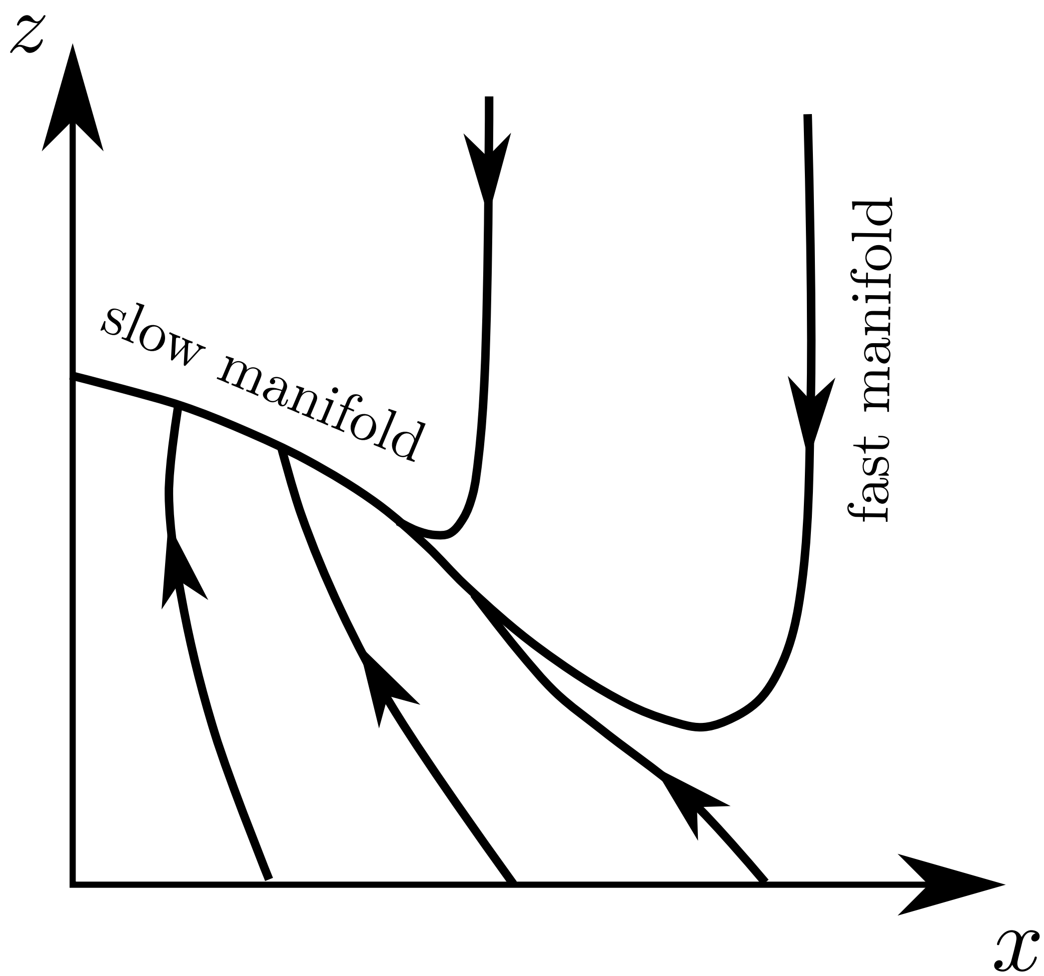

Figure 3.8: Example of slow and fast manifolds.

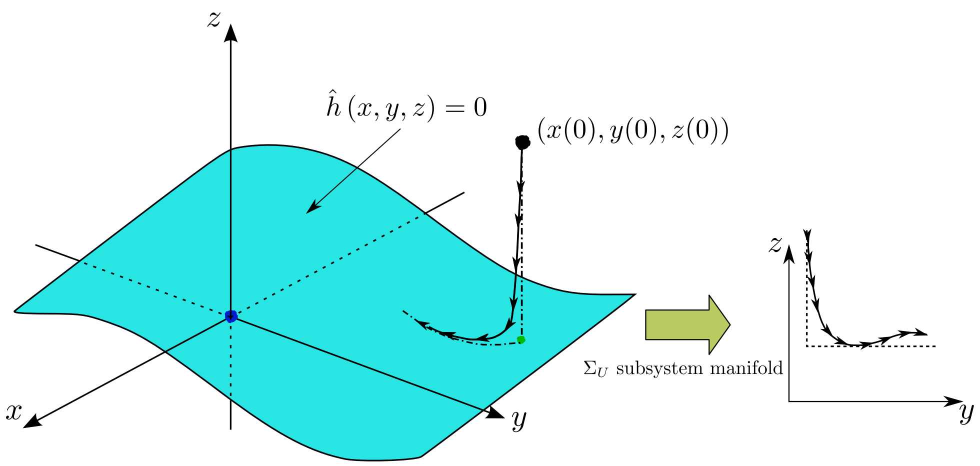

(a) Σ_U-subsystem movement

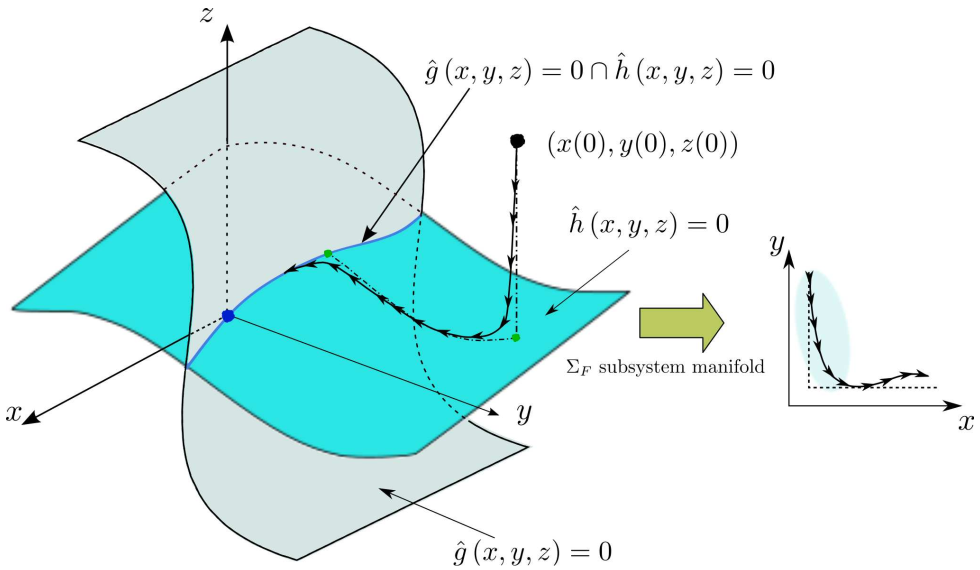

(b) Σ_F-subsystem movement

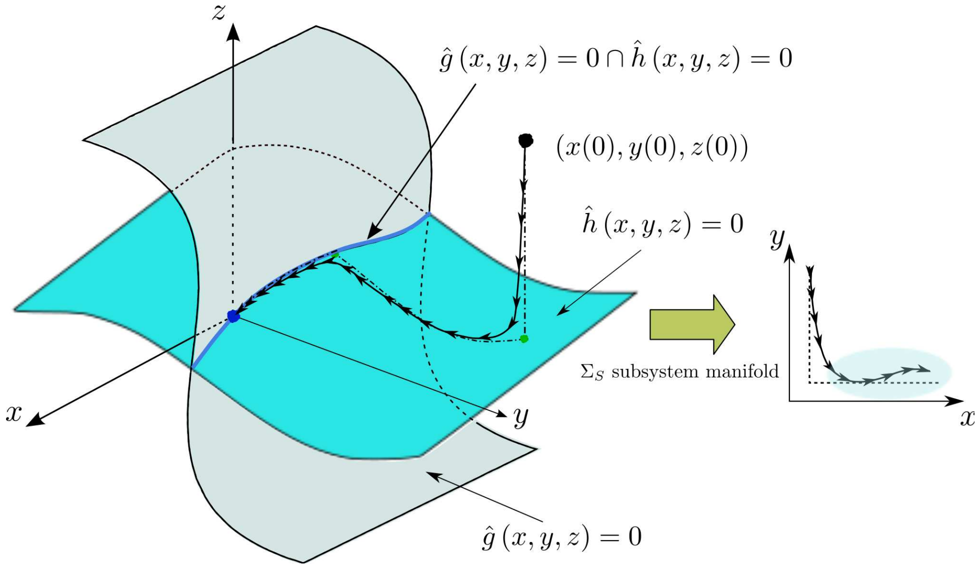

(c) Σ_S-subsystem movement

Figure 3.9: Generic three-time-scale Evolution

3.6 *Top-Down* and *Bottom-Up* Analysis Extension for N^{th}-Time-Scale System

The same presented time-scale analysis methodologies are applicable for a more general N^{th}-time-scale system, with some significate differences that provide an additional degree of freedom to the designer. For the three-time scale analysis previously described, the direction in which the singular perturbation parameters are analyzed is maintained, that is, once selected either the *TD* or the *BU* time-scale analysis, it is continued until the end of the time scale analysis, as it can be seen in Figure 3.1.

Figure 3.1 shows that the *TD* analysis is selected by first considering the *Top* singularly perturbed parameter, ε_1, and secondly considers the *Down* singularly perturbed parameter ε_2, following the descending direction as indicated by the arrow. In a similar manner, Figure 3.2 shows that for the *BU* time-scale analysis, the same philosophy is applied but with an ascending direction as indicated by the arrow.

For the general singularly perturbed N^{th}-time-scale system, the major difference, when comparing with the three-time-scale *TD* and *BU* time-scale analysis, consists in the fact that after each subsystem reduction that results when applying the selected stretched time scale, the designer can continue with the time-scale decomposition using either the *TD* or the *BU* methodologies, depending on the system structure of the resulting reduced order and boundary layer subsystems, and what suits better in order to proceed with the time-scale decomposition. This results in, assuming that the first time-scale decomposition is conducted only on the *Top* or *Bottom* singularly perturbed parameter, in 2^{N-2} possible combinations, that is, for he 4^{th}-time-scale system, will result in $2^{4-2} = 4$ possible combinations, or for a 5^{th}-time-scale system, will result in $2^{5-2} = 8$ combinations. What it is most important, the combinations are all equivalent as it will be shown for the 4^{th}-time-scale system.

In order to help understanding the extension of the *TD* and *BU* strategies here proposed for a more general N^{th}-time-scale system, the author has chosen a general 4^{th}-time-scale system, that will used throughout the remainder of the thesis when extending the obtained results to a more general N^{th}-time-scale system. The proposed 4^{th}-time-scale system, denoted as Σ_{SFU_2} for simplicity, is of the form given by

$$\begin{aligned} \dot{x} &= f(x,y,z,w) & (3.76)\\ \varepsilon_1\dot{y} &= \hat{g}(x,y,z,w) & (3.77)\\ \varepsilon_1\varepsilon_2\dot{z} &= \hat{h}(x,y,z,w) & (3.78)\\ \varepsilon_1\varepsilon_2\varepsilon_3\dot{w} &= \hat{i}(x,y,z,w). & (3.79)\end{aligned}$$

Figure 3.10 presents a schematic of the four possible solutions for the 4^{th}-time-scale analysis, and where for conciseness, only the first one will be briefly described in this section since uses the same philosophy employed for the three-time-scale analysis previously presented. The analysis for the first possible combination of Figure 3.10 starts by applying the *Top* stretched time-scale condition to the 4^{th}-time-scale original system, Eqns. (3.76–3.79), and identified as a solid green line in Figure 3.10. The application of the first stretched time-scale condition results in the reduced order Σ_S-subsystem, given by

$$\dot{x} = f\left(x, \mathrm{g}(x), \mathrm{h}(x), \mathrm{i}(x)\right), \qquad (3.80)$$

where the boundary layer (fast), denoted as $\Sigma_{U_{\tau_1}}$-subsystem for simplicity, and denoted by the short-dashed red line in Figure 3.10, is given by

$$\frac{dy}{d\tau_1} = \hat{g}\left(x, y(\tau_1), z(\tau_1), w(\tau_1)\right), \qquad (3.81)$$

$$
\begin{aligned}
\varepsilon_2 \frac{dz}{d\tau_1} &= \hat{h}\left(x, y(\tau_1), z(\tau_1), w(\tau_1)\right), && (3.82)\\
\varepsilon_2\varepsilon_3 \frac{dw}{d\tau_1} &= \hat{i}\left(x, y(\tau_1), z(\tau_1), w(\tau_1)\right), && (3.83)
\end{aligned}
$$

where $\tau_1 = t/\varepsilon_1$, and where the expressions $\mathrm{g}(x)$, $\mathrm{h}(x)$ and $\mathrm{i}(x)$ in Eq. (3.80) represent the quasi-steady-state equilibria of the boundary layer $\Sigma_{U_{\tau_1}}$-subsystem, Eqns. (3.81–3.83), when $\varepsilon_1 = 0$, that is

$$
\begin{aligned}
0 &= \hat{i}(x, y, z, w) \to w = \mathrm{i}(x, y, z) = \mathrm{i}(x, \mathrm{g}(x), \mathrm{h}(x, \mathrm{g}(x))) \equiv \mathrm{i}(x), && (3.84)\\
0 &= \hat{h}(x, y, z, \mathrm{i}(x, y, z)) \to z = \mathrm{h}(x, y) = \mathrm{h}(x, \mathrm{g}(x)) \equiv \mathrm{h}(x), && (3.85)\\
0 &= \hat{g}(x, y, \mathrm{h}(x, y), \mathrm{i}(x, y, \mathrm{h}(x))) \to y = \mathrm{g}(x), && (3.86)
\end{aligned}
$$

where $\mathrm{g}(x)$, $\mathrm{h}(x)$, and $\mathrm{i}(x)$ evolve on their own configuration spaces. Recall that in the space of configuration of the boundary layer given by the stretched time scale $\tau_1 = t/\varepsilon_1$, Eqns. (3.81–3.83), x is treated like a fixed parameter. This is the point at which the N^{th}-time-scale analysis differs from the three-time-scale analysis previously presented, by providing with the additional degree of freedom which permits to select either the *TD* or *BU* time scale analysis.

For the first of the four cases here described, the time scale analysis continues by applying the *BU* strategy to the $\Sigma_{U_{\tau_1}}$-subsystem, which implies selecting the stretched time scale given by $\tau_3 = \tau_1/(\varepsilon_2\varepsilon_3) = t/(\varepsilon_1\varepsilon_2\varepsilon_3)$. This results in a new reduced (slow) subsystem, denoted as Σ_{FU}-subsystem for simplicity and identified with the dashed-dotted blue line, and defined by

$$
\begin{aligned}
\frac{dy}{d\tau_1} &= \hat{g}\left(x, y(\tau_1), z(\tau_1), \mathrm{i}(x, y(\tau_1), z(\tau_1))\right), && (3.87)\\
\varepsilon_2 \frac{dz}{d\tau_1} &= \hat{h}\left(x, y(\tau_1), z(\tau_1), \mathrm{i}(x, y(\tau_1), z(\tau_1))\right), && (3.88)
\end{aligned}
$$

and where the new boundary layer (fast) subsystem, denoted as Σ_{U_2}-subsystem for simplicity, is given by

$$
\frac{dw}{d\tau_3} = \hat{i}\left(x, y, z, w(\tau_3)\right). \tag{3.89}
$$

The function $\mathrm{i}(x, y(\tau_1), z(\tau_1))$ in the reduced order Σ_{FU}-subsystem, Eqns. (3.87–3.88), represents the quasi-steady-state of the boundary layer Σ_{U_2}-subsystem, Eq. (3.89), when setting $\varepsilon_3 = 0$, that is

$$
0 = \hat{i}(x, y, z, w) \to w = \mathrm{i}(x, y, z), \tag{3.90}
$$

where x, y,and z are treated like fixed parameters. Finally, it can be recognized that the Σ_{FU}-subsystem can be decomposed again into another two-time-scale singularly perturbed problem by considering the last stretched time scale given by applying $\tau_2 = \tau_1/\varepsilon_2 = t/(\varepsilon_1\varepsilon_2)$. This results in a new reduced (slow) subsystem, denoted as Σ_F-subsystem for simplicity, and defined by

$$
\frac{dy}{d\tau_1} = \hat{g}\left(x, y(\tau_1), \mathrm{h}(x, y(\tau_1)), \mathrm{i}(x, y(\tau_1))\right), \tag{3.91}
$$

and where the new boundary layer (fast) subsystem is given by

$$
\frac{dz}{d\tau_2} = \hat{h}\left(x, y, z(\tau_2), \mathrm{i}(x, y, z(\tau_2))\right). \tag{3.92}
$$

The boundary layer, Eq. (3.92), will be denoted as Σ_U-subsystem for simplicity. The function $\mathrm{h}(x, y(\tau_1))$ in the reduced order Σ_F-subsystem, Eq. (3.91), represents the quasi-steady-state of the boundary layer Σ_U-subsystem, Eq. (3.92), when setting $\varepsilon_2 = 0$, that is

$$
0 = \hat{h}(x, y, z, \mathrm{i}(x, y, z)) \to z = \mathrm{h}(x, y), \tag{3.93}
$$

where x and y are treated like fixed parameters, and w it is assumed that is moving through its configuration space. Both the reduced order Σ_F-subsystem, and the boundary layer Σ_{U_1}-subsystem for the first combination, are identified with the yellow long-spaced-dashed lines. Note that the color code for the lines of the four different approaches do not imply the same reduced order subsystem, but the same order in the sequential model order reduction.

This concludes the first of the four possible combinations that appear in Figure 3.10. It can be seen by analyzing the rest of the four possible combinations appearing in Figure 3.10, that despite the combination of *TD* and *BU* strategies, all the one-dimension final reduced order subsystems obtained using any of the four possible *TD* and *BU* combinations are equivalent. This can be appreciated in Figure 3.10 when comparing the different resulting reduced order subsystem, where the Σ_S-subsystem is denoted with the circle, the Σ_F-subsystem is denoted with a star, the Σ_{U_1}-subsystem is denoted with a pentagon, and finally, the Σ_{U_2}-subsystem is denoted with a square. This demonstrates the equivalency among all four possible combinations of the*TD* and *BU* time-scale analysis.

The extension to the N^{th}-time scale can easily be identified from the analysis of the 4^{th}-time-scale example above described. The sequential strategy of decomposing the 4^{th}-time-scale system, into simpler two-time-scale subsystems provides a valuable tool that will help in analyzing any general singularly perturbed N^{th}-time-scale system, and, as it will be seen in the sequel, provide powerful tools for both selecting proper control strategies, and determining the stability properties of the resulting singularly perturbed N^{th}-time-scale system.

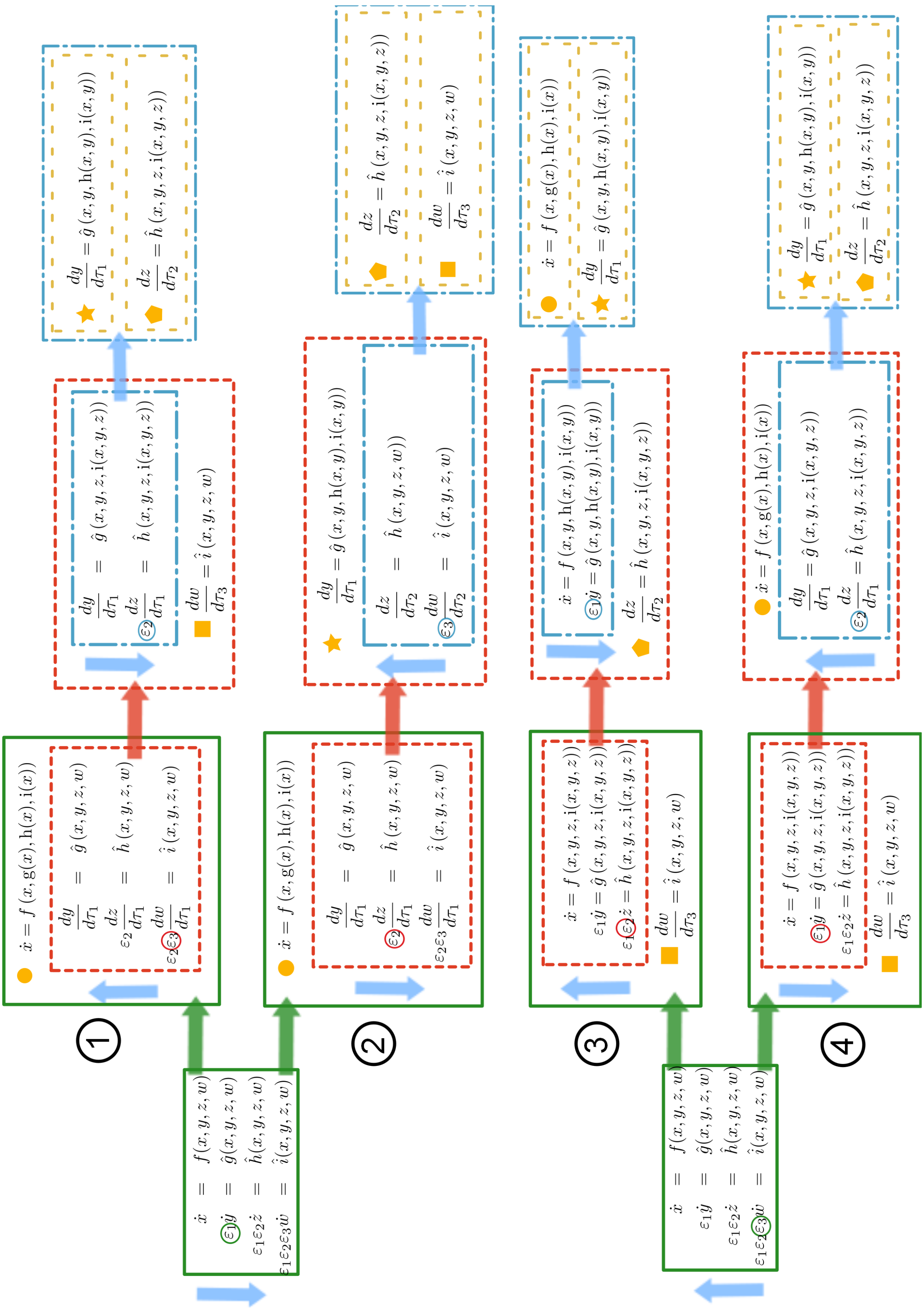

Figure 3.10: 4^{th}-time-scale *Top-Down* and *Bottom-Up* analysis strategy.

3.7 Conclusions

Two singularly perturbation time-scale analysis approaches, the *Top-Down* (TD), and the *Bottom-Up* (BU), have been presented. These methodologies are based in a sequential application of the general two-time-scale singular perturbation formulation, allowing to decouple a general N^{th}-time-scale problem into $N-1$ simpler reduced order two-time-scale models that simplify considerably the burden of designing appropriate control strategies, and demonstrate the asymptotic stability properties of the resulting closed-loop systems, as it will be shown in later chapters.

The equivalency between the use of the TD and BU time-scale strategies, permits to reduced the order of complexity of the original system, thus becoming a tool that can be employed by the designer to select the order in which the strategies are applied depending on the complexity of the original system being analyzed.

The TD and BU time scale analysis is also extended to the more general N^{th}-time scale analysis using a 4^{th}-order time-scale general example. The sequential strategy of decomposing the 4^{th}-time-scale system, into simpler two-time-scale subsystems provides a valuable tool that will help in analyzing any general singularly perturbed N^{th}-time-scale system, and provide additional tools for the time-scale analysis of singularly perturbed systems.

In conclusion, the TD and BU singularly perturbed strategy here presented becomes the main pillar of the methodology employed in this thesis and, as shown in following chapters, provides, in one simple step-by-step process, the ability to solve the main problems treated on this thesis:

1. Define a control design strategy that permits to select the desired degree of stability of each of the time-scale subsystems.

2. Define a methodology that permits to demonstrate the asymptotic stability properties of the resulting closed loop full system, by selecting the Lyapunov functions for each of the singularly perturbed subsystems, and construct the associated composite Lyapunov function for the full system.

This page intentionally left blank

Chapter 4

Control Strategy

4.1 Introduction

Generally, feedback control designs for systems resulting from the interaction of slow and fast dynamic modes, suffer from the higher dimensionality and ill-conditioning. The time-scale control strategies taken advantage of these stiffness properties by decomposing the original ill-conditioned system into two subsystems with separate time scales, the reduced order (slow) and the boundary layer (fast) (Kokotović et al., 1986). This chapter takes advantage of this strategy by introducing two singular-perturbation-based control strategies that are employed in this thesis.

Both control strategies take advantage from the methodology previously derived, the *TD* and the *BU* methodologies, in which the control laws that stabilize the full problem are obtained by sequentially applying the selected methodology. Although both methodologies are valid for the general time-scale system, for the underactuated model here used, in which the main purpose of the control strategy is to regulate the underactuated fast subsystem, Σ_F, it is necessary to employ the *TD* control strategy.

The sequential application of *TD* time-scale analysis methodology results in two distinctive degenerated two-time-scale subproblems considerably simplified, this permitting to easily obtain appropriate control laws that stabilize each of the subsystems. In addition, each one of the two-time-scale singular perturbed subproblems will consist of a slow and fast subsystems, and, by selecting the appropriate control laws, it will be ensured that the associated subsystems are asymptotically stable. The two proposed control laws that will be used to regulate the dynamics of both the simplified model, and the helicopter model, will be referred as

- *Top-Down* Control Design (*TD*).
- *Composite Feedback Top-Down* Control Design ($\mathcal{CF}$-*TD*).

For completeness of the thesis, although both control strategies have been applied to both the simplified and the helicopter three-time scale models, the control strategy for the simplified model has been moved to Appendix B as a reference tool. Again, it is advised to the reader to use the derivations for the simplified model as a reference and reinforcing tool to help understanding the proposed control strategies.

The first control strategy, the *Top-Down* (*TD*) control design, uses sequentially the different stretched-time-scales to stabilize the intermediate Σ_F-subsystem with a desired degree of stability, and once has been stabilized, and assuming the ultra-fast Σ_U-subsystem becomes inherently stable with the control signal selected to stabilize the Σ_F-subsystem, then proceeds to stabilize the slowest Σ_S-subsystem with also a desired degree of stability by using the second stretched time-scale.

The second proposed control strategy, the *Composite Feedback Top-Down* control design ($\mathcal{CF}$-*TD*), uses a similar sequential application of the *TD* control design, with the particularity that this methodology allows the user to select also a prescribed degree of desired stability for the ultra-fast subsystem, Σ_U, therefore not being necessary to assume that the closed-loop ultra-fast subsystem has inherent stable properties. Both control strategies are based in the approximations introduced by singular perturbation theory, and the stability of the resulting closed-loop systems will be studied in later chapters.

As previously noted, for simplicity, and completeness of the thesis, the author has chosen to keep the same nomenclature presented in chapter 3 for the different time-scale subsystems for both the simplified example, and the helicopter model, since the context will be significate enough to determine to which model is referring, and maintaining the same nomenclature will help in the process of using the simplified example as a reference tool.

Similarly, the different time-scale subsystems will be defined as a function of the form $\Sigma_{(\cdot)}$, where the subindex denotes the different subsystems, that is, Σ_S for the slow subsystem, Σ_F for the fast subsystem, and finally, Σ_U for ultra-fast subsystem, where $\tilde{x}$ and $\tilde{y}$ are treated like constants.

The following sections describe in further detail both control designs by first deriving them for a generic three-time-scale singularly perturbed model, and then extending the results to the helicopter model. Prior the selected control strategies employed in this chapter for a class of underactuated nonlinear systems, a brief description of what would be the natural control strategy for a general nonlinear three-time-scale singularly perturbed system is introduced.

4.2 *Top-Down* and *Bottom-Up* Control Design Strategies for General Three-Time-Scale Systems

Prior to derive the selected *TD* control strategy for the underactuated system analyzed in this thesis, this section presents a general description of both the *TD* and *BU* control strategies for a general three-time-scale system of the form

$$\dot{x} = f(x, y, z, u_1), \tag{4.1}$$
$$\varepsilon_1 \dot{y} = \hat{g}(x, y, z, u_2), \tag{4.2}$$
$$\varepsilon_1 \varepsilon_2 \dot{z} = \hat{h}(x, y, z, u_3). \tag{4.3}$$

Similarly as in the time-scale analysis, both the *TD* and *BU* control strategies will produce equivalent results as it is shown in the following sections.

4.2.1 *Top-Down* Control Design Strategy for General Three-Time-Scale Systems

The *TD* control strategies for the general three-time-scale system follows the same philosophy as the *TD* time scale analysis described in section 3.4.1, where the control strategy employed is quite simple, since each subsystem in the Σ_{SFU} system has sufficient control authority such that the control signal associated to each subsystem will be sufficient to stabilize the system to whom it belongs. The *TD* control strategy starts by first considering the time-scale defined by the *Top* condition, yielding the reduced (slow) Σ_S-subsystem defined by

$$\dot{x} = f(x, \mathrm{g}(x), \mathrm{h}(x), u_1), \tag{4.4}$$

and where the boundary layer (fast) Σ_{FU}-subsystem for the *TD* subproblem is defined by

$$\frac{\mathrm{d}y}{\mathrm{d}\tau_1} = \hat{g}(x, y, z, u_2). \tag{4.5}$$

$$\varepsilon_2 \frac{\mathrm{d}z}{\mathrm{d}\tau_1} = \hat{h}(x, y, z, u_3). \tag{4.6}$$

Recall that in the Σ_S-subsystem, g and h are the quasi-steady-state equilibria for the boundary layer Σ_{FU}-subsystem, Eqns. (4.5–4.6), when setting $\varepsilon_1 = 0$ and being solved simultaneously yielding

$$0 = \hat{g}(x, y, z, u_2) \to y = \mathrm{g}(x, u_2), \tag{4.7}$$

$$0 = \hat{h}(x, y, z, u_3) \to z = \mathrm{h}(x, u_3). \tag{4.8}$$

The reduced order Σ_S-subsystem will not be stabilized until the boundary layer Σ_{FU}-subsystem is stabilized, which is done by recognizing that can be treated again like a two-time-scale singularly perturbed system by applying the *Down* condition, that is applying the stretched time constant $\tau_2 = \varepsilon_1/\varepsilon_2 = t/(\varepsilon_1\varepsilon_2)$, which results in a new reduced (slow) subsystem, denoted as Σ_F-subsystem for simplicity, defined by

$$\frac{\mathrm{d}y}{\mathrm{d}\tau_1} = \hat{g}(x, y, \mathrm{h}(x, y), u_2), \tag{4.9}$$

and where the new boundary layer (fast) Σ_U-subsystem is defined by

$$\frac{\mathrm{d}z}{\mathrm{d}\tau_2} = \hat{h}(x, y, z, u_3), \tag{4.10}$$

The Σ_U-subsystem, Eq. (4.10), is stabilized by selecting a control signal $u_3(x, y, z)$ such that provides a desired prescribed performance given by

$$\frac{\mathrm{d}z}{\mathrm{d}\tau_2} = -\tilde{b}_z(z - z^*), \tag{4.11}$$

where $\tilde{b}_z$ represents the desired time response of the ultra-fast dynamics. Once stabilized the Σ_U-subsystem, its quasi-steady-state equilibrium is obtained by setting $\varepsilon_2 = 0$ yielding

$$0 = \hat{h}(x, y, z) \to z = \mathrm{h}(x, y), \tag{4.12}$$

with $\mathrm{h}(x, y)$ evolving on its own configuration space on the boundary layer Σ_U-subsystem, where both x and y are being treated like fixed parameters. With the Σ_U-subsystem stable, the strategy shifts towards stabilizing the Σ_F-subsystem, (4.9), which is achieved by selecting the control signal $u_2(x, y)$ such that stabilizes the Σ_F-subsystem with a desired prescribed performance given by

$$\frac{\mathrm{d}y}{\mathrm{d}\tau_1} = -\tilde{b}_y(y - y^*), \tag{4.13}$$

where $\tilde{b}_y$ represents the desired time response of the fast dynamics. Once stabilized both the Σ_F and Σ_U-subsystems, their quasi-steady-state equilibria can be obtained recalling Eqns. (4.7–4.8), resulting in

$$0 = \hat{g}(x, y, z, u_2) \to u_2(x, y) \to y = \mathrm{g}(x), \tag{4.14}$$

$$0 = \hat{h}(x, y, z, u_3) \to u_3(x, y, z) \to z = \mathrm{h}(x, y) = \mathrm{h}(x, \mathrm{g}(x)) = \mathrm{h}(x). \tag{4.15}$$

which are used to define the Σ_S-subsystem, Eq. (4.4). With the functions $\mathrm{g}(x)$ and $\mathrm{h}(x)$, Eqns. (4.14) and (4.15), respectively, evolving on their own configuration spaces, the control signal $u_1(x)$ in the resulting reduced order Σ_S-subsystem, Eq. (4.4), is selected such that stabilizes the Σ_S-subsystem with a desired degree of stability given by

$$\dot{x} = -b_x(x - x^*), \tag{4.16}$$

where $\tilde{b}_y$ represents the desired time response of the fast dynamics. This concludes the general *Top-Down* control design with all three subsystems being stabilized with a desired prescribed degree of stability. Figure 4.1 depicts the complete *TD* control design sequence for a general three-time-scale singularly perturbed problem.

4.2.2 *Bottom-Up* Control Design Strategy for General Three-Time-Scale Systems

The *BU* control strategies for the general three-time-scale system follows the same philosophy as the *BU* time scale analysis described in section 3.4.2. Similarly as for the *TD* control design, the control strategy employed is quite simple, since the control signal of each subsystem in Eqns. (4.1–4.3), is sufficient to stabilize the system to whom it belongs. This translates to that, following the natural and logical flow of the states, as seen in intuitive description of the three-time-scale decomposition, described in section 3.5, the *Bottom-Up* analysis is first applied to the general system, Eqns. (4.1–4.3), by first considering the time-scale defined by the *Bottom* condition, yielding the reduced (slow) Σ_{SF}-subsystem defined by

$$\dot{x} = f(x, y, \mathrm{h}(x, y), u_1), \tag{4.17}$$

$$\varepsilon_1 \dot{y} = \hat{g}(x, y, \mathrm{h}(x, y), u_2), \tag{4.18}$$

and where the boundary layer (fast) Σ_U-subsystem for the *BU* subproblem is defined by

$$\frac{\mathrm{d}z}{\mathrm{d}\tau_2} = \hat{h}(x, y, z, u_3). \tag{4.19}$$

The boundary layer Σ_U-subsystem, Eq. (4.19), is stabilized by selecting the control signal $u_3(x, y, z)$ such that stabilizes the Σ_U-subsystem with a desired prescribed performance as

$$\frac{\mathrm{d}z}{\mathrm{d}\tau_2} = -\tilde{b}_z(z - z^*), \tag{4.20}$$

where $\tilde{b}_z$ represents the desired time response of the ultra-fast dynamics. Once stabilized the Σ_U-subsystem, its quasi-steady-state equilibrium is obtained by setting $\varepsilon_2 = 0$ yielding

$$0 = \hat{h}(x, y, z) \to z = \mathrm{h}(x, y), \tag{4.21}$$

with $\mathrm{h}(x, y)$ evolving on its own configuration space on the boundary layer Σ_U-subsystem, where both x and y are being treated like fixed parameters. The Σ_{SF}-subsystem is completed after substituting $\mathrm{h}(x, y)$ into the Eqns. (4.17–4.18). With Σ_U-subsystem being stable, the control strategy continues by recognizing that the Σ_{SF}-subsystem can be treated again like a two-time-scale singularly perturbed system by dealing with the subsystem that results when considering the time-scale defined by the *Up* condition, that is the second stretched time scale of the *BU* control design, and given by $\tau_1 = t/\varepsilon_1$, where the new reduced (slow) Σ_S-subsystem is now defined by

$$\dot{x} = f(x, \mathrm{g}(x), \mathrm{h}(x, \mathrm{g}(x)), u_1), \tag{4.22}$$

and where the new boundary layer Σ_F-subsystem is given by

$$\frac{\mathrm{d}y}{\mathrm{d}\tau_1} = \hat{g}(x, y, \mathrm{h}(x, y), u_2). \tag{4.23}$$

The new boundary layer Σ_F-subsystem, Eq. (4.23), is first stabilized by selecting the control signal $u_2(x, y)$ such that provides a desired prescribed performance given by

$$\frac{\mathrm{d}y}{\mathrm{d}\tau_1} = -\tilde{b}_y(y - y^*), \tag{4.24}$$

where $\tilde{b}_y$ represents the desired time response of the fast dynamics. Once stabilized the Σ_F-subsystem, its quasi-steady-state equilibrium is obtained by setting $\varepsilon_1 = 0$ such

$$0 = \hat{g}(x, y, \mathrm{h}(x, y)) \to y = \mathrm{g}(x). \tag{4.25}$$

With the functions $\mathrm{g}(x)$ and $\mathrm{h}(x, y) = \mathrm{h}(x, \mathrm{g}(x)) = \mathrm{h}(x)$, Eqns. (4.25) and (4.21), respectively, the control signal $u_1(x)$ in the resulting reduced order Σ_S-subsystem, Eq. (4.22), is selected such that stabilizes the slow subsystem with a desired degree of stability given by

$$\dot{x} = -b_x(x - x^*), \tag{4.26}$$

where $\tilde{b}_x$ represents the desired time response of the slow dynamics. This concludes the general *BU* control design with all three subsystems being stabilized with a desired prescribed degree of stability. Figure 4.2 depicts the complete *BU* control design sequence for a general three-time-scale singularly perturbed problem. The following section deals with the control strategy for a non-general underactuated system, in which the control strategy is required to be more elaborated in order to solve the problem of controlling an underactuated system.

4.3 *Top-Down* Control Strategy for Underactuated Singular Perturbed Systems

Due to the nature of the dynamics of the selected helicopter problem, Eq. (2.338), in which the control signals are allocated only in two of the singularly perturbed subsystems, therefore becoming an underactuated system with a structure of the form

$$\begin{aligned} \dot{x} &= f(x, y, z, u_1), && (4.27)\\ \varepsilon_1 \dot{y} &= \hat{g}(x, y, z), && (4.28)\\ \varepsilon_1 \varepsilon_2 \dot{z} &= \hat{h}(x, y, z, u_2). && (4.29) \end{aligned}$$

in which the variable that it is desired to be regulated is the underactuated one, i.e.: it is desirable to regulate the y variable, implies that only the *TD* control strategy above presented can be employed. The selected control strategy, needs to deal with the underactuated structure defined in Eqns. (4.27–4.29), and does so by proposing a control design based in the *TD* strategies.

The *TD* control design strategy for the three-time scale singular perturbation formulation consists on treating the three-different time scales as two-distinct two-time-scale singular perturbed problems. Following the logic flow in a control process, in which the fastest variables are stabilized first, the *TD* control strategy uses a two stage process to stabilize the full Σ_{SFU} system. The first stage focusses on the *Down* sequence of the *TD* control design by applying, in a sequential manner, first the stretched time scales $\tau_1 = t/\varepsilon_1$, yielding the reduced order Σ_S-subsystem, and the boundary layer Σ_{FU}-subsystem, and secondly, applying the stretched time-scale $\tau_2 = t/\varepsilon_1\varepsilon_2$ to the Σ_{FU}-subsystem, to accomplish the stabilization of the Σ_{FU}-subsystem, with the proper u_2, and once stabilized, the second stage focuses on the *Top* sequence by using the first time-scale decomposition, along with the obtained results in the first time-scale decomposition, and proceeds to stabilize the slow Σ_S-subsystem with the proper u_1. The following subsections describe in detail both stages of the *TD* control design strategies.

4.3.1 Control Design for u_2: 1^{st} Stage of the *Top-Down* Control Design

The first stage of the *Top-Down* subproblem applies first the stretched time-scale $\tau_1 = t/\varepsilon_1$ to the original Σ_{SFU} (4.27–4.29), resulting in the reduced (slow) subsystem defined by

$$\dot{x} \;=\; f(x, \mathrm{g}(x, u_2), \mathrm{h}(x, \mathrm{g}(x), u_2), u_1), \tag{4.30}$$

and where the boundary layer (fast) Σ_{FU}-subsystem for the *TD* subproblem is defined by

$$\frac{\mathrm{d}y}{\mathrm{d}\tau_1} \;=\; \hat{g}(x, y, z), \tag{4.31}$$

$$\varepsilon_2 \frac{\mathrm{d}z}{\mathrm{d}\tau_1} \;=\; \hat{h}(x, y, z, u_2), \tag{4.32}$$

where the quasi-steady-state equilibria of the boundary layer Σ_{FU}-subsystem, Eqns. (4.31–4.32), are obtained when setting $\varepsilon_1 = 0$, and solving simultaneously resulting in

$$0 = \hat{h}(x, y, z, u_2) \quad \rightarrow \quad z = \mathrm{h}(x, y, u_2) = \mathrm{h}(x, \mathrm{g}(x), u_2), \tag{4.33}$$

$$\updownarrow$$

$$0 = \hat{g}(x, y, z) = \hat{g}(x, y, \mathrm{h}(x, y, u_2)) \quad \rightarrow \quad y = \mathrm{g}(x, u_2), \tag{4.34}$$

Note that on the boundary layer Σ_{FU}-subsystem, the variable x is treated like a fixed parameter. Note that in order to completely determine the reduced order Σ_S-subsystem, it is necessary to completely define the equilibria of the Σ_{FU} subsystem, that is, defining $\mathrm{h}(x, \mathrm{g}(x), u_2)$ and $\mathrm{g}(x, u_2)$, Eqns. (4.33–4.34), therefore being necessary to define the control signal u_2, which implies to complete the *Down*-sequence of the *TD* control strategy, and this is achieved by first stabilizing the Σ_{FU}-subsystem using singular perturbation time-scale analysis.

The stabilization of the Σ_{FU}-subsystem is accomplished by identifying that the boundary layer Σ_{FU}-subsystem, Eqns. (4.31–4.32), can be decomposed into a two-time-scale singular perturbed problem by dealing with the subsystem that results when applying the second stretched time-scale $\tau_2 = \tau_1/\varepsilon_2 = t/(\varepsilon_1\varepsilon_2)$, where the new reduced (slow) subsystem, denoted as Σ_F-subsystem for simplicity, is now defined by

$$\frac{\mathrm{d}y}{\mathrm{d}\tau_1} \;=\; \hat{g}(x, y, \mathrm{h}(x, y, u_2)), \tag{4.35}$$

and where the new boundary layer (fast) Σ_U-subsystem is defined by

$$\frac{\mathrm{d}z}{\mathrm{d}\tau_2} \;=\; \hat{h}(x, y, z, u_2), \tag{4.36}$$

and where the quasi-steady-state equilibrium of the boundary layer Σ_U-subsystema, Eq. (4.36), when setting $\varepsilon_2 = 0$, resulting in

$$0 = \hat{h}(x, y, z, u_2) \rightarrow z = \mathrm{h}(x, y, u_2). \tag{4.37}$$

Note that the control signal is embedded in the quasi-steady-state equilibrium $z = \mathrm{h}(x, y, u_2)$, Eq. (4.37), which, once substituted back into the reduced order Σ_F-subsystem, Eq. (4.35), will be chosen such that stabilizes the Σ_F-subsystem with a desired degree of stability, i.e. the control signal is selected such that guarantees to match a selected degree of performance. It is assumed that the boundary layer Σ_U-subsystem is stable after selecting the control signal that stabilizes the Σ_F-subsystem.

In the contrary, if the boundary layer Σ_U-subsystem is not stable, or does not have the desired performance, the control strategy can be modified to account for the desired stable behavior of the Σ_U boundary layer by introducing a modification in the control strategy that will be addressed in the $\mathcal{CF}$-*TD* control design developed in section 4.5.1.

The first stage of the *TD* control strategy finalizes with the selected control strategy u_2 that guarantees a desire degree of stability for the underactuated Σ_{FU}-subsystem. The control strategy for the complete Σ_{SFU} system continues with the second stage of the *TD* control strategy, in which will be addressed the stabilization of the Σ_{SF}-subsystem. Figure 4.3 depicts the complete first stage of the *TD* control design sequence.

4.3.2 Control Design for u_1: 2^{nd} Stage of the *Top-Down* Control Design

The second stage of the *Top-Down* subproblem focuses on the control design for u_1 for the stabilization of the Σ_S-subsystem. For that purpose, recall first that after selecting the control signal $u_2(x, y, z)$, the Σ_{FU}-subsystem, Eqns. (4.31–4.32), can be rewritten as

$$\frac{\mathrm{d}y}{\mathrm{d}\tau_1} = \hat{g}(x, y, z), \tag{4.38}$$

$$\varepsilon_2 \frac{\mathrm{d}z}{\mathrm{d}\tau_1} = \hat{h}(x, y, z), \tag{4.39}$$

In order to determine the equilibria that will define the Σ_S-subsystem, Eq. (4.30), the Σ_{FU}-subsystem, Eqns. (4.38–4.39), can be decomposed by applying the stretched time scale τ_2 resulting in the Σ_F-subsystem given by

$$\frac{\mathrm{d}y}{\mathrm{d}\tau_1} = \hat{g}(x, y, \mathrm{h}(x, y)), \tag{4.40}$$

and where the new boundary layer (fast) Σ_U-subsystem is defined by

$$\frac{\mathrm{d}z}{\mathrm{d}\tau_2} = \hat{h}(x, y, z), \tag{4.41}$$

with their equilibria being now completely determined resulting in

$$0 = \hat{h}(x, y, z) \to u_2(x, y) \to z = \mathrm{h}(x, y), \tag{4.42}$$

$$0 = \hat{g}(x, y, \mathrm{h}(x, y)) \to y = \mathrm{g}(x), \tag{4.43}$$

with this in mind, the reduced order (slow) Σ_S-subsystem, Eq. (4.30) reduces to

$$\dot{x} = f(x, \mathrm{g}(x), \mathrm{h}(x, \mathrm{g}(x)), u_1). \tag{4.44}$$

The control signal (u_1) is selected such that stabilizes the Σ_S-subsystem with a desired degree of stability. This concludes the *TD* control design. Figure 4.4 depicts the complete *TD* control design sequence, including both the *Top* and *Down* sequences, control design for u_2 and u_1, respectively.

4.3.3 Conclusions for the *Top-Down* Control Design

Due to the underactuated structure of the system being controlled, a sequential application of the *TD* has allowed to control the full Σ_{SFU} system, by stabilizing separately first the Σ_{FU}-subsystem, and once stable, and using the results obtained in this first stabilization, proceed with the Σ_S-subsystem, which follows the logic flow of the dynamics of a singular perturbed time scale system, as described in Figure 3.9.

The complete evolution of a generic stable three-time-scale model is described in Figure 3.9(a), where it can be seen the evolution of the ultra-fast variable z as it moves through the configuration space of the boundary layer, Σ_U-subsystem, Eq. (4.41), towards the surface that defines the quasi-steady-state equilibrium of the Σ_U-subsystem, given by the first part of the first stage of the *TD* control strategy, Eq. (4.42), while x and y behave as fixed parameters.

The end of the first stage of the *TD* control strategy is observed in Figure 3.9(b), which depicts the evolution of the fast variable y as it moves on the configuration space of the reduced order of the Σ_{FU}-subsystem, which is equivalent to the boundary layer of the Σ_{SF}-subsystem, Eqns. (4.38) and (4.39), respectively, towards the surface that defines the quasi-steady-state equilibrium of Σ_F-subsystem given by Eq. (4.40), while the slow variable x behaves as a fixed parameter, and $z = \mathrm{h}(x, y)$ evolves also on its manifold.

The second stage of the *TD* control strategy can be seen in Figure 3.9(c), which shows the evolution of the slow variable x as it moves in the manifold of the Σ_S-subsystem, which is given by the intersection between the planes $\hat{g}(x, y, \mathrm{h}(x, y)) = 0$ and $\hat{h}(x, y, z) = 0$, which results in the manifold of the Σ_S-subsystem given by Eq. (4.44). The following subsections will extend this formulation to both the three-time-scale singularly perturbed helicopter model, while the control strategies for the simplified model are moved to Appendix .

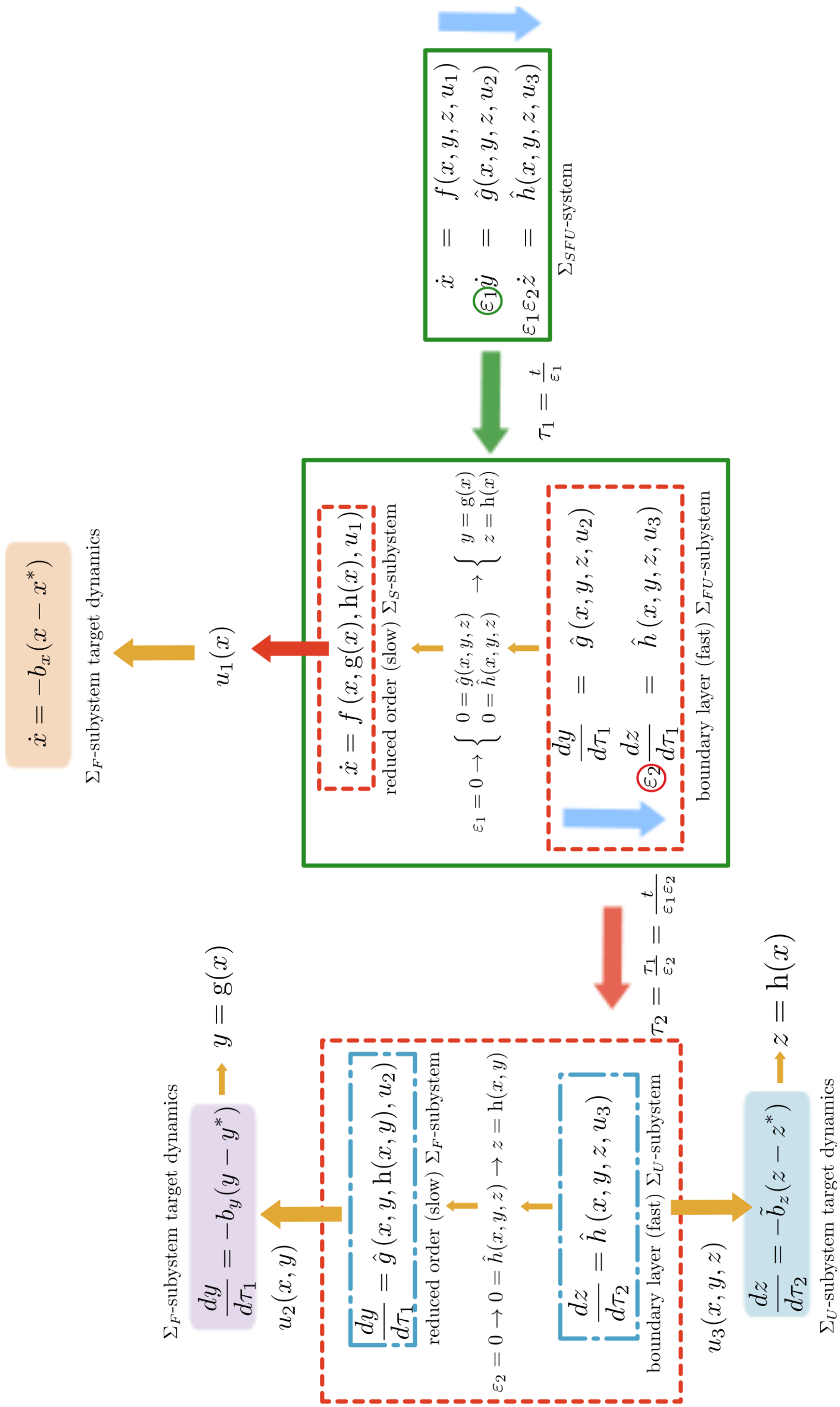

Figure 4.1: *Top-Down* control design sequence for a general three-time-scale system

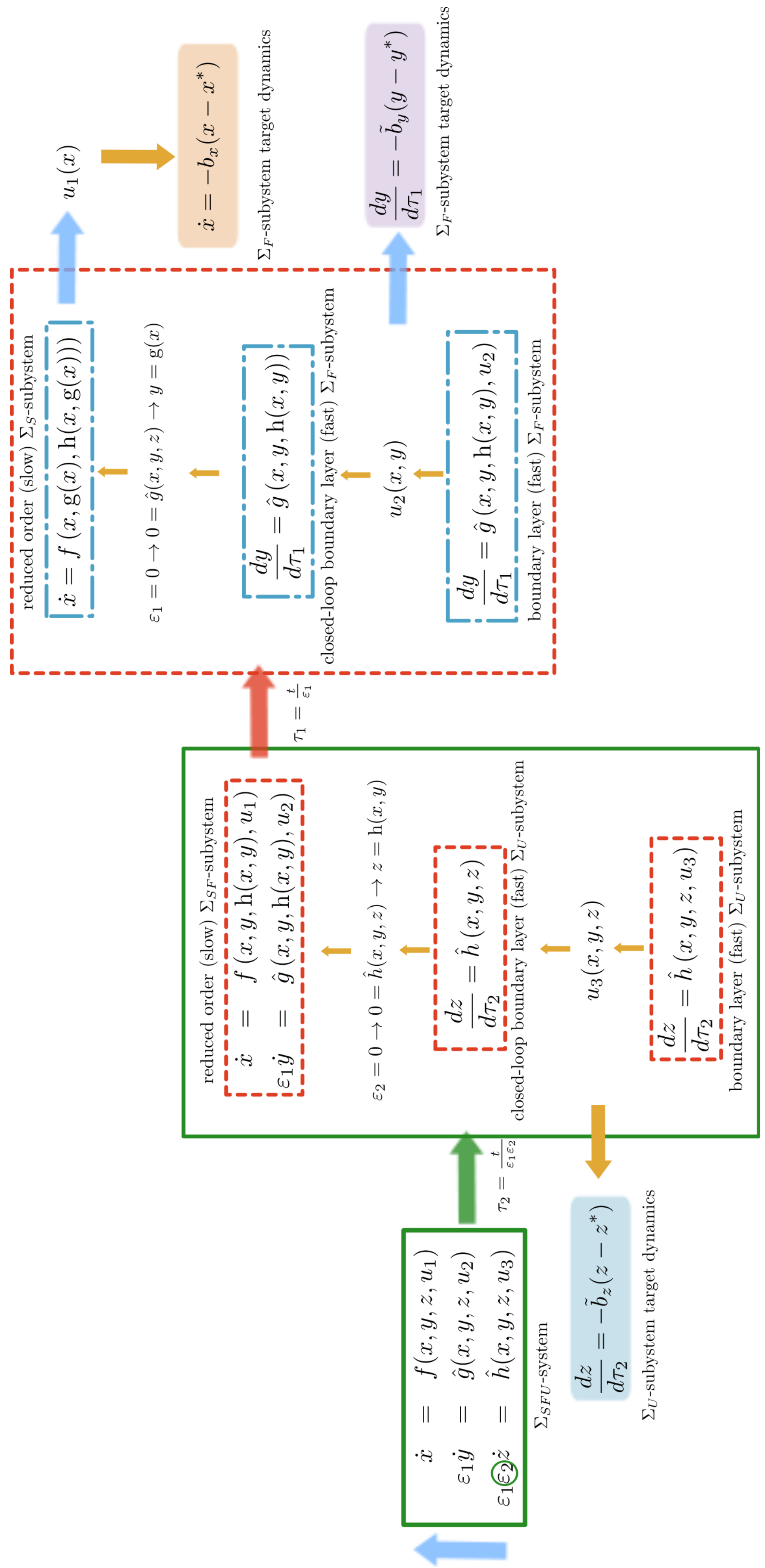

Figure 4.2: *Bottom-Up* control design sequence for a general three-time-scale system

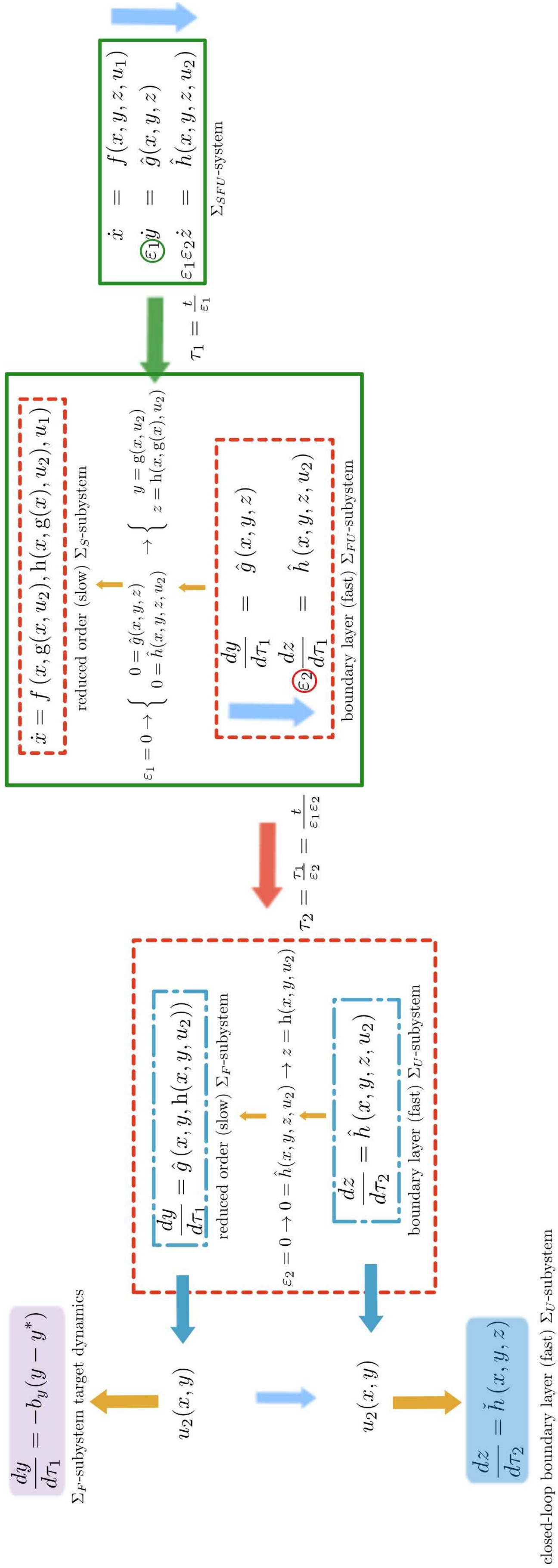

Figure 4.3: 1^{st} Stage of the *Top-Down* control design sequence.

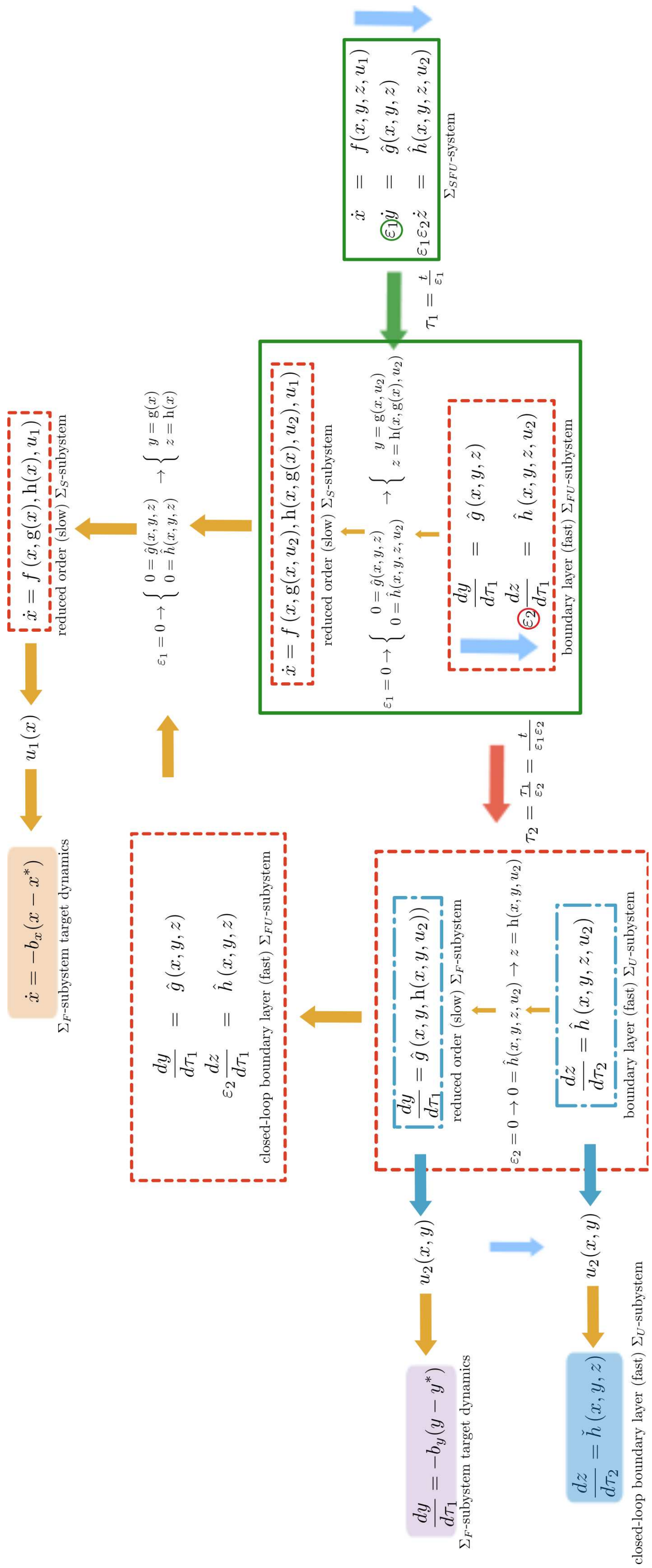

Figure 4.4: Complete *Top-Down* control design sequence.

4.4 *Top-Down* Control Design for the Helicopter Model

The control strategy for the nonlinear underactuated three-time-scale singularly perturbed helicopter model, Eqns. (3.56–3.60), with a structure equivalent to Eqns. (4.27–4.29), is the same as the one defined in section 4.3, which consists on treating the three different time scales as two-distinct two-time-scale singular perturbed problems. The *TD* control strategy is divided in two stages, being each stage dedicated to design each of the two control signals.

The first stage of the *TD* control strategy, applies sequentially the *Top* and *Down* time constant conditions, to select the control law that stabilizes the Σ_{FU}-subsystem using singular perturbation time-scale analysis to obtain the appropriate control law (u_2) that stabilizes the vertical position of the helicopter (y_1) by taking the helicopter to a desired altitude (y^*), and therefore, regulating its vertical velocity (y_2).

The second stage of the *TD* control strategy focuses on the *Top* sequence by using the first time-scale decomposition, along with the obtained results in the second time-scale decomposition, and proceeds to stabilize the angular velocity of the blades with the proper u_1. The following sections describe in detail both stages of the *TD* control formulation applied to the helicopter model.

4.4.1 Control Design for u_2: 1^{st} Stage of the *Top-Down* Control Design for the Helicopter Model

The *TD* control strategy applies the *Top* stretched-time-scale, resulting in the reduced order (slow) Σ_S-subsystem, given by

$$\dot{x} = a_8 x + a_{10} x^2 \sin \mathrm{h}_1(x, u_2) + a_9 x^2 + a_{11} + u_1, \tag{4.45}$$

with $\mathrm{h}_1(x, u_2)$ being the equilibria of the Σ_{FU}-subsystem, as it will be seen bellow, and where the resulting boundary layer (fast) Σ_{FU}-subsystem is given by

$$\frac{\mathrm{d}y_1}{\mathrm{d}\tau_1} = c_1 y_2 \tag{4.46}$$

$$\frac{\mathrm{d}y_2}{\mathrm{d}\tau_1} = x^2(c_2 + c_3 z_1 - \sqrt{c_4 + c_5 z_1}) + a_9 y_2 + a_9 y_2^2 + c_6, \tag{4.47}$$

$$\varepsilon_2 \frac{\mathrm{d}z_1}{\mathrm{d}\tau_1} = c_7 z_2 \tag{4.48}$$

$$\varepsilon_2 \frac{\mathrm{d}z_2}{\mathrm{d}\tau_1} = a_9 z_1 + c_8 x^2 \sin z_1 + c_9 z_2 + c_{10} + c_{11} u_2. \tag{4.49}$$

Recall that neither the angular velocity of the blades dynamics, Eq. (4.45), nor the collective pitch dynamics, Eqns. (4.48–4.49), depend on the helicopter vertical movement dynamics, therefore, only the quasi-steady-state equilibria of the collective pitch dynamics, $\mathbf{h}(x, \boldsymbol{y}, u_2)$, is substituted into Eq. (4.45) to obtain the reduced order Σ_S-subsystem, where $\mathrm{h}_1(x, u_2)$ represents the collective pitch angle quasi-steady-state equilibrium. Recall that the Roman boldbace quasi-steady-state equilibria denotes a vector.

Recall also that, for completeness, and simplicity, throughout the remainder of the thesis, when dealing with the helicopter model, the vector state denoting the vertical displacement dynamics will be written in italic bold font, $\boldsymbol{y} = [\begin{array}{cc} y_1 & y_2 \end{array}]^T$, and the vector state denoting the collective pitch dynamics will be written in italic bold font, $\boldsymbol{z} = [\begin{array}{cc} z_1 & z_2 \end{array}]^T$.

The control strategy employed obtains the associated control law u_2 that stabilizes the Σ_{FU}-subsystem, Eqns. (4.46–4.49), assuming that the slow variable, the angular velocity of the blades (x) is constant, and that the fast variables have reached their quasi-steady-state equilibria and evolve on it. In order to do so, the boundary layer Σ_{FU}-subsystem can be treated again like a two-time-scale singular perturbation problem by applying the *Down* stretched time-scale condition resulting in the new reduced (slow) Σ_F-subsystem given by

$$\frac{\mathrm{d}y_1}{\mathrm{d}\tau_1} = c_1 y_2 \tag{4.50}$$

$$\frac{\mathrm{d}y_2}{\mathrm{d}\tau_1} = x^2\left(c_2 + c_3 \mathrm{h}_1(x,\boldsymbol{y},u_2) - \sqrt{c_4 + c_5 \mathrm{h}_1(x,\boldsymbol{y},u_2)}\right) + a_9 y_2 + a_9 y_2^2 + c_6, \tag{4.51}$$

and with the new boundary layer Σ_U-subsystem given by

$$\frac{\mathrm{d}z_1}{\mathrm{d}\tau_2} = c_7 z_2 \tag{4.52}$$

$$\frac{\mathrm{d}z_2}{\mathrm{d}\tau_2} = a_9 z_1 + c_8 x^2 \sin z_1 + c_9 z_2 + c_{10} + c_{11} u_2, \tag{4.53}$$

where the quasi-steady-state vector equilibria of the boundary layer Σ_U-subsystem is given by

$$\mathbf{h}(x,\boldsymbol{y},u_2) = \begin{bmatrix} \mathrm{h}_1(x,\boldsymbol{y},u_2) \\ \mathrm{h}_2(x,\boldsymbol{y},u_2) \end{bmatrix}. \tag{4.54}$$

Prior to define in detail the quasi-steady-state equilibria (4.54), and therefore the control law, a feedback transform is introduced in Eq. (4.53) to guarantee that the Σ_U-subsystem is stable by selecting the function

$$v_2 = c_8 x^2 \sin z_1 + c_{10} + c_{11} u_2, \tag{4.55}$$

thus rewriting Eqns. (4.52–4.53) such

$$\frac{\mathrm{d}z_1}{\mathrm{d}\tau_2} = c_7 z_2 \tag{4.56}$$

$$\frac{\mathrm{d}z_2}{\mathrm{d}\tau_2} = a_9 z_1 + c_9 z_2 + v_2. \tag{4.57}$$

The appropriate selection on v_2, and the inherit nature of the actuator dynamics, results in a stable Σ_U-subsystem, and also faster than the rest of the time scales. This can be proven by analyzing the open-loop eigenvalues of the Σ_U-subsystem, Eqns. (4.56–4.57), given by $\lambda_1 = -0.5772 \times 10^{-4}$ and $\lambda_2 = -0.1697 \times 10^{-4}$. This ensures that the response of the Σ_U-subsystem dynamics is stable and much faster than the rest of the dynamics, but with the limitation that the current control strategy cannot provide desired transient response for the ultra-fast variables.

To tackle such limitation, the author has also proposed an alternative control law (Esteban et al., 2008b) to the one here used, based in the *Composite Feedback* control for singular perturbed systems (Kokotović et al., 1999), in which using additional feedback control strategies permit the selection of the desired target dynamics for the Σ_U-subsystem, therefore, ensuring that if the boundary layer system is unstable, or that the response is stable but not adequate, it can be made stable via control design. This alternative control strategy will be dealt with in section 4.5.1, and for the time being, it will be assumed that for the *TD* control design, the Σ_U-subsystem is inherently stable after substituting the derived control signal u_2, and with a sufficient transient response.

Once introduced the feedback transform, the quasi-steady-state equilibria of the Σ_U-subsystem, Eqns. (4.56–4.57), is obtained by setting $\varepsilon_2 = 0$, yielding

$$0 = \hat{\boldsymbol{h}}(x,\boldsymbol{y},\boldsymbol{z},v_2) \rightarrow \boldsymbol{z} = \mathbf{h}(x,\boldsymbol{y},v_2), \tag{4.58}$$

resulting in

$$\boldsymbol{z} = \mathbf{h}(x, \boldsymbol{y}, v_2) = \begin{bmatrix} \mathrm{h}_1(x, \boldsymbol{y}, v_2) \\ \mathrm{h}_2(x, \boldsymbol{y}, v_2) \end{bmatrix}, \tag{4.59}$$

with

$$\mathrm{h}_1 = z_1 = c_{13} v_2, \tag{4.60}$$

$$\mathrm{h}_2 = z_2 = 0, \tag{4.61}$$

where $\mathrm{h}_1(v_2)$ and h_2 represent the quasi-steady-state equilibria of the Σ_U-subsystem, and with $c_{13} = -\frac{1}{a_9}$. Substituting the equilibria (4.60–4.61) into Eqns. (4.50–4.51), results in the reduced order (slow) Σ_F-subsystem is given by

$$\frac{\mathrm{d}y_1}{\mathrm{d}\tau_1} = c_1 y_2 \tag{4.62}$$

$$\begin{aligned} \frac{\mathrm{d}y_2}{\mathrm{d}\tau_1} &= x^2 \left(c_2 + c_3 \mathrm{h}_1(v_2) - \sqrt{c_4 + c_5 \mathrm{h}_1(v_2)} \right) a_9 y_2 + a_9 y_2^2 + c_6 \\ &= x^2 \left(c_2 + c_3 c_{13} v_2 - \sqrt{c_4 + c_5 c_{13} v_2} \right) + a_9 y_2 + a_9 y_2^2 + c_6. \end{aligned} \tag{4.63}$$

The control law that stabilizes the fast subsystem is obtained after a series of algebraic substitutions. Let first introduce the transformation given by

$$w^2 = c_4 + c_5 \left(c_{13} v_2 \right), \tag{4.64}$$

where an expression of v_2, as a function of w, can be obtained from Eq. (4.64) such

$$v_2 = \frac{w^2 - c_4}{c_5 c_{13}}, \tag{4.65}$$

where substituting Eqns. (4.64) and (4.65) into Eq. (4.63) yields

$$\begin{aligned} \frac{\mathrm{d}y_1}{\mathrm{d}\tau_1} &= c_1 y_2 \\ \frac{\mathrm{d}y_2}{\mathrm{d}\tau_1} &= x^2 \left(c_2 + c_3 \left(\frac{w^2 - c_4}{c_5} \right) - w \right) + a_9 y_2 + a_9 y_2^2 + c_6, \end{aligned} \tag{4.66}$$

which can be simplified into

$$\begin{aligned} \frac{\mathrm{d}y_1}{\mathrm{d}\tau_1} &= c_1 y_2 \\ \frac{\mathrm{d}y_2}{\mathrm{d}\tau_1} &= x^2 \left(c_{12} w^2 - w + K_a \right) + a_9 y_2 + a_9 y_2^2 + c_6, \end{aligned} \tag{4.67}$$

being the constants given by

$$c_{12} = \frac{c_3}{c_5}, \tag{4.68}$$

$$K_a = c_2 - c_4 c_{12}. \tag{4.69}$$

After choosing

$$v = c_{12} w^2 - w + K_a, \tag{4.70}$$

Eq. (4.67) becomes

$$\frac{\mathrm{d}y_1}{\mathrm{d}\tau_1} = c_1 y_2, \tag{4.71}$$

$$\frac{\mathrm{d}y_2}{\mathrm{d}\tau_1} = x^2 v + a_9 y_2 + a_9 y_2^2 + c_6. \tag{4.72}$$

In order to select a proper control law, let choose a stable target system of the form given by

$$\frac{\mathrm{d}y_1}{\mathrm{d}\tau_1} = c_1 y_2 \tag{4.73}$$

$$\frac{\mathrm{d}y_2}{\mathrm{d}\tau_1} = -\tilde{b}_{y_1}(y_1 - y_1^*) - \tilde{b}_{y_2} y_2, \tag{4.74}$$

where y_1^* represents the desired altitude of the helicopter, and $\tilde{b}_{y_1}$, and $\tilde{b}_{y_2}$ are control design parameters that determine the desired transient response of the fast dynamics, and given by selecting the natural frequency ($\omega_{n_{y^*}}$) and the damping ratio (ζ_{y^*}) such as

$$\tilde{b}_{y_1} = \varepsilon_1 b_{y_1}, \tag{4.75}$$

$$\tilde{b}_{y_2} = \varepsilon_1 b_{y_2}, \tag{4.76}$$

with

$$b_{y_1} = \omega^2_{n_{y^*}}, \tag{4.77}$$

$$b_{y_2} = 2\omega_{n_{y^*}} \zeta_{n_{y^*}}, \tag{4.78}$$

where $\omega_{n_{y^*}}$ and $\zeta_{n_{y^*}}$ are the desired natural frequency and damping ratio for the fast-dynamics on the stretched time-scale given by $\tau_1 = t/\varepsilon_1$. The control problem can be solved if a control signal v is chosen such that the Σ_F-subsystem , Eqns. (4.71–4.72), behaves like the selected target system defined in Eqns. (4.73–4.74). The control signal v is therefore chosen to be

$$v(x, \boldsymbol{y}) = -\frac{a_9 y_2^2 + \left(a_9 + \tilde{b}_{y_2}\right) y_2 + \tilde{b}_{y_1}(y_1 - y_1^*) + c_6}{x^2}, \tag{4.79}$$

where it should be noted that this control law is not defined for zero angular velocity of the blades, $x = 0$, but this will not be a problem since the blades of the helicopter will always have an angular velocity $x > x_{MIN} > 0$. The control law u_2 can be obtained by tracking back the algebraic feedback transform substitution presented in Eq. (4.55), resulting in

$$u_2 = \frac{v_2 - c_8 x^2 \sin z_1 - c_{10}}{c_{11}}, \tag{4.80}$$

where x is treated, at the moment, as a constant, and v_2 is given by the expression defined in Eq. (4.65), and w can be obtained solving for the roots of the quadratic polynomial of Eq. (4.70), yielding

$$w = \frac{1 \pm \sqrt{1 - 4c_{12}(K_a - v(x, \boldsymbol{y}))}}{2c_{12}}. \tag{4.81}$$

It can be proven, by substituting into the equilibria Eqns. (2.349)–(2.348), that the solution corresponding to the minus sign in front of the square root is a spurious solution introduced in the previous computations. In the following, only the positive root will be considered. The control law is therefore defined as

$$\begin{aligned} u_2(x, \boldsymbol{y}, y_1^*, z_1) &= K_b\left(1 + \sqrt{1 - 4c_{12}\left(K_a - v(x, \boldsymbol{y})\right)}\right)^2 + K_c + K_d x^2 \sin z_1 \\ &= K_b\left(1 + \sqrt{s_3 v(x, \boldsymbol{y})}\right)^2 + K_c + K_d x^2 \sin z_1, \end{aligned} \tag{4.82}$$

with $v(x, \boldsymbol{y})$ being given by

$$v(x, \boldsymbol{y}) = -\frac{a_9 y_2^2 + \left(a_9 + \tilde{b}_{y_2}\right) y_2 + \tilde{b}_{y_1}(y_1 - y_1^*) + c_6}{x^2}, \tag{4.83}$$

and the coefficients of the control law being given by

$$K_a = c_2 - c_4 c_{12} = \frac{a_1 a_9}{a_5} - \frac{a_2 a_3 a_9^2}{a_5^2 a_7}, \tag{4.84}$$

$$K_b = \frac{1}{4c_5 c_{11} c_{12}^2 c_{13}} = -\frac{a_5 a_7 a_{13}}{4a_2^2 a_9}, \tag{4.85}$$

$$K_c = -\frac{c_4}{c_5 c_{11} c_{13}} - \frac{c_{10}}{c_{11}} = \frac{a3 a_9 a_{13}}{a_5 a_7} - a_{12}, \tag{4.86}$$

$$K_d = -\frac{c_8}{c_{11}} = -a_{14}, \tag{4.87}$$

$$s_3 = 4c_{12} = 4\frac{c_3}{c_5} = 4\frac{a_2 c_1}{a_4 c_1^2} = \frac{a_2 a_5}{a_4 a_9}. \tag{4.88}$$

It should be noted that due to the nature of the derived control law u_2, Eq. (4.82), it needs to be ensured that the control law is defined for all possible conditions, which is done by selecting the appropriate control design variables $\tilde{b}_{y_1}$ and $\tilde{b}_{y_2}$. It is assumed that the boundary layer is stable after selecting the control signal that stabilizes the Σ_F-subsystem.

4.4.2 Control Design for u_1: 2^{nd} Stage of the *Top-Down* Control Design for the Helicopter Model

The second stage of the *TD* subproblem focuses on the control design for u_1 for the stabilization of the Σ_S-subsystem. For that purpose, recall first that after selecting the control signal $u_2(x, \boldsymbol{y}, y_1^*, z_1)$, the Σ_{FU}-subsystem, Eqns. (4.46–4.49), can be rewritten as

$$\frac{\mathrm{d}y_1}{\mathrm{d}\tau_1} = c_1 y_2, \tag{4.89}$$

$$\frac{\mathrm{d}y_2}{\mathrm{d}\tau_1} = x^2(c_2 + c_3 z_1 - \sqrt{c_4 + c_5 z_1}) + a_9 y_2 + a_9 y_2^2 + c_6, \tag{4.90}$$

$$\varepsilon_2 \frac{\mathrm{d}z_1}{\mathrm{d}\tau_1} = c_7 z_2 \tag{4.91}$$

$$\varepsilon_2 \frac{\mathrm{d}z_2}{\mathrm{d}\tau_1} = a_9 z_1 + c_9 z_2 + J_2 \left[\left(1 + \sqrt{s_3 v(x, \boldsymbol{y})}\right)^2 - 1 \right], \tag{4.92}$$

where the constat J_2 is given by

$$J_2 = \frac{a_9}{a_{13}} K_b = -\frac{a_3 a_9}{a_4}. \tag{4.93}$$

In order to determine the equilibria that will define the Σ_S-subsystem, Eq. (4.45), the Σ_{FU}-subsystem, Eqns. (4.89–4.92), can be decomposed by applying the stretched time scale τ_2 resulting in the Σ_F-subsystem given by

$$\frac{\mathrm{d}y_1}{\mathrm{d}\tau_1} = c_1 y_2, \tag{4.94}$$

$$\frac{\mathrm{d}y_2}{\mathrm{d}\tau_1} = x^2(c_2 + c_3 \mathrm{h}_1(x, \boldsymbol{y}) - \sqrt{c_4 + c_5 \mathrm{h}_1(x, \boldsymbol{y})} + a_9 y_2 + a_9 y_2^2 + c_6, \tag{4.95}$$

and where the new boundary layer (fast) Σ_U-subsystem is defined by

$$\frac{\mathrm{d}z_1}{\mathrm{d}\tau_2} = c_7 z_2 \tag{4.96}$$

$$\frac{\mathrm{d}z_2}{\mathrm{d}\tau_2} = a_9 z_1 + c_9 z_2 + J_2 \left[\left(1 + \sqrt{s_3 v(x, \boldsymbol{y})}\right)^2 - 1 \right]. \tag{4.97}$$

The new Σ_U-subsystem quasi-steady-state equilibria is given by setting $\varepsilon_2 = 0$, resulting in

$$0 = \hat{\boldsymbol{h}}(x, \boldsymbol{y}, \boldsymbol{z}) \rightarrow \boldsymbol{z} = \mathbf{h}(\boldsymbol{x}, \boldsymbol{y}) = \begin{bmatrix} \mathrm{h}_1(x, \boldsymbol{y}) \\ \mathrm{h}_2(x, \boldsymbol{y}) \end{bmatrix}, \tag{4.98}$$

that is

$$0 = c_7 z_2 \to z_2 = \mathrm{h}_2(x, y), \tag{4.99}$$

$$0 = a_9 z_1 + c_9 z_2 + J_2 \left[\left(1 + \sqrt{s_3 v(x, \boldsymbol{y})}\right)^2 - 1 \right] \to z_1 = \mathrm{h}_1(x, \boldsymbol{y}), \tag{4.100}$$

therefore yielding

$$\mathrm{h}_1(x, \boldsymbol{y}) = z_1 = s_2 \left[\left(1 + \sqrt{s_3 v(x, \boldsymbol{y})}\right)^2 - 1 \right], \tag{4.101}$$

$$\mathrm{h}_2(x, \boldsymbol{y}) = z_2 = 0, \tag{4.102}$$

where the constant s_2 is given by

$$s_2 = -\frac{J_2}{a_9}. \tag{4.103}$$

With the quasi-steady-state equilibria of the Σ_U-subsystem, Eqns. (4.101–4.102), the reduced order Σ_F-subsystem, Eqns. (4.94–4.95) is therefore given by

$$\frac{\mathrm{d}y_1}{\mathrm{d}\tau_1} = c_1 y_2, \tag{4.104}$$

$$\begin{aligned} \frac{\mathrm{d}y_2}{\mathrm{d}\tau_1} &= x^2(c_2 + c_3 \mathrm{h}_1(x, \boldsymbol{y}) - \sqrt{c_4 + c_5 \mathrm{h}_1(x, \boldsymbol{y})} + a_9 y_2 + a_9 y_2^2 + c_6 \\ &= -\tilde{b}_{y_1}(y_1 - y_1^*) - \tilde{b}_{y_2} y_2. \end{aligned} \tag{4.105}$$

Recall that when substituting the quasi-steady-state equilibria of the Σ_U-subsystem, Eqns. (4.101–4.102) into Eqns. (4.94–4.95), they degenerate into the selected Σ_F target dynamics, Eqns. (4.73–4.74). Setting the perturbation parameter $\varepsilon_1 = 0$, reduces the dimension of the Σ_F-subsystem because the differential equations (4.104–4.105) degenerate into the equation that determine the roots of the fast manifold, defined as

$$0 = \hat{\boldsymbol{g}}(x, \boldsymbol{y}, \mathbf{h}(x, \boldsymbol{y})) \to \boldsymbol{y} = \mathbf{g}(x) = \begin{bmatrix} g_1(x) \\ g_2(x) \end{bmatrix}, \tag{4.106}$$

that is

$$0 = c_1 y_2 \to y_2 = \mathrm{g}_2(x), \tag{4.107}$$

$$0 = -\tilde{b}_{y_1}(y_1 - y_1^*) - \tilde{b}_{y_2} x_2 \to y_1 = \mathrm{g}_1(x), \tag{4.108}$$

therefore yielding the equilibria for the vertical motion of the helicopter given by

$$g_1(x) = y_1 = y^*, \tag{4.109}$$

$$g_2(x) = y_2 = 0, \tag{4.110}$$

where Eq. (4.109) represents that the equilibrium altitude position is the desired altitude, while Eq. (4.110), provides that, as expected, the equilibrium vertical position must be zero in order to achieve a vertical equilibrium point. The control law u_1 that stabilizes the slow Σ_S-subsystem is obtained by substituting the Σ_F and Σ_U-subsystem equilibria, Eqns. (4.109–4.110), and (4.101–4.102), respectively, into Eq. (4.45), yielding the reduced order Σ_S-subsystem given by

$$\dot{x} = a_8 x + a_{10} x^2 \sin \mathrm{h}_{1_{\mathrm{SS}}}(x, \mathbf{g}(x)) + a_9 x^2 + a_{11} + u_1, \tag{4.111}$$

where $\mathrm{h}_{1_{\mathrm{SS}}}(x, \mathbf{g}(x))$ represents the quasi-steady-state equilibrium of the collective pitch angle, Eq. (4.101) when substituting the quasi-steady-state equilibria for the vertical displacement dynamics, Eqns (4.109–

4.110), resulting in

$$\mathrm{h}_{1_{\mathrm{SS}}}(x, \mathbf{g}(x)) = \mathrm{h}_1(x, \boldsymbol{y})|_{\boldsymbol{y}=\mathbf{g}(x)} = s_2 \left[\left(1 + \sqrt{s_3 v_{SS}(x, \mathbf{g}(x))}\right)^2 - 1 \right], \tag{4.112}$$

with $v_{SS}(x, \mathbf{g}(x))$ is the results of substituting Eqns. (4.109) and (4.110) into Eq. (4.83), yielding

$$v_{SS}(x, \mathbf{g}(x)) = v(x, \boldsymbol{y})|_{\boldsymbol{y}=\mathbf{g}(x)} = -\frac{c_6}{x^2}. \tag{4.113}$$

The control law is selected by defining a target system of the form

$$\dot{x} = -b_x(x - x^*), \tag{4.114}$$

where b_x is a control design parameter that defines the desired transient response of the collective pitch angular velocity of the blades. The associated control law that stabilizes the Σ_S-subsystem is therefore selected as

$$\begin{aligned} u_1(x, x^*) &= -a_8 x - a_{10} x^2 \sin\left(\mathrm{h}_{1_{\mathrm{SS}}}(x, \mathbf{g}(x))\right) - a_9 x^2 - a_{11} - b_x(x - x^*) \\ &= -a_8 x - a_{10} x^2 \sin\left(\mathrm{h}_{1_{\mathrm{SS}}}(x)\right) - a_9 x^2 - a_{11} - b_x(x - x^*). \end{aligned} \tag{4.115}$$

This concludes the *TD* control design.

4.4.3 Closed-Loop of the Helicopter Model

After substituting the selected control laws, Eqns. (4.82) and (4.115), into the original nonlinear equations of the helicopter, Eqns. (2.339–2.343), the closed-loop system is given by

$$\dot{x} = a_{10} x^2 \left[\sin(z_1 - \sin \mathrm{h}_{1_{\mathrm{SS}}}(x))\right] - b_x(x - x^*) \tag{4.116}$$

$$\dot{y}_1 = y_2 \tag{4.117}$$

$$\dot{y}_2 = x^2\left(a_1 + a_2 z_1 - \sqrt{a_3 + a_4 z_1}\right) + a_5 y_2 + a_6 y_2^2 + a_7 \tag{4.118}$$

$$\dot{z}_1 = z_2 \tag{4.119}$$

$$\dot{z}_2 = a_{13} z_1 + a_{15} z_2 + K_b \left[\left(1 + \sqrt{s_3 v(x, \boldsymbol{y})}\right)^2 - 1\right], \tag{4.120}$$

The equilibria of the closed-loop system are obtained by setting all derivatives of Eqns. (4.116–4.120) to zero, thus yielding the equilibrium equations, where the equilibria of ultra-fast dynamics, Eqns. (4.119–4.120), results in the quasi-steady-state equilibria given by

$$0 = \hat{\boldsymbol{h}}(x, \boldsymbol{y}, \boldsymbol{z}) \to \boldsymbol{z} = \mathbf{h}(x, \boldsymbol{y}) = \begin{bmatrix} \mathrm{h}_1(x, \boldsymbol{y}) \\ \mathrm{h}_2(x, \boldsymbol{y}) \end{bmatrix}, \tag{4.121}$$

that is

$$0 = z_2 \to z_2 = \mathrm{h}_2(x, \boldsymbol{y}), \tag{4.122}$$

$$0 = a_{13} z_1 + a_{15} z_2 + K_b \left[\left(1 + \sqrt{s_3 v(x, \boldsymbol{y})}\right)^2 - 1\right] \to z_1 = \mathrm{h}_1(x, \boldsymbol{y}), \tag{4.123}$$

therefore yielding

$$\mathrm{h}_1(x, \boldsymbol{y}) = z_1 = -\frac{K_b}{a_{13}} \left[\left(1 + \sqrt{s_3 v(x, \boldsymbol{y})}\right)^2 - 1\right] = s_2 \left[\left(1 + \sqrt{s_3 v(x, \boldsymbol{y})}\right)^2 - 1\right], \tag{4.124}$$

$$\mathrm{h}_2(x, \boldsymbol{y}) = z_2 = 0, \tag{4.125}$$

Recall that observing the closed-loop ultra-fast dynamics, Eqns. (4.119–4.120), can be expressed as a function of a pseudo error dynamics by using the definition of the quasi-steady-state equilibrium $\mathrm{h}_1(x, \boldsymbol{y})$, Eq. (4.124), resulting in

$$\dot{z}_1 = z_2 \tag{4.126}$$

$$\begin{aligned} \dot{z}_2 &= a_{13}z_1 + a_{15}z_2 + K_b\left[\left(1+\sqrt{s_3 v(x,\boldsymbol{y})}\right)^2 - 1\right] \\ &= a_{13}\left(z_1 - \mathrm{h}_1(x,\boldsymbol{y})\right) + a_{15}z_2, \end{aligned} \tag{4.127}$$

which provides the transient response of the ultra-fast dynamics given by a second order time response of the form

$$\ddot{z}_1 = -\omega_{n_z}^2\left(z_1 - \mathrm{h}_1(x,\boldsymbol{y})\right) - 2\omega_{n_z}\zeta_z\dot{z}_1, \tag{4.128}$$

with ω_{n_z} being the natural frequency of the closed-loop ultra-fast system, and ζ_z being the damping ratio of the ultra-fast dynamics, which can be defined as

$$\omega_{n_z} = \sqrt{-a_{13}}, \tag{4.129}$$

$$\zeta_z = \frac{-a_{15}}{2\omega n_z} = \frac{-a_{15}}{2\sqrt{-a_{13}}}, \tag{4.130}$$

Substituting the equilibria of the ultra-fast subsystem, Eqns. (4.124-4.125), into the equilibrium equations of the fast dynamics, Eqns. (4.117-4.118), results in

$$0 = y_2 \tag{4.131}$$

$$\begin{aligned} 0 &= x^2\left(a_1 + a_2\mathrm{h}_1(x,\boldsymbol{y}) - \sqrt{a_3 + a_4\mathrm{h}_1(x,\boldsymbol{y})}\right) + a_5y_2 + a_6y_2^2 + a_7 \\ &= -b_{y_1}\left(y_1 - y_1^*\right) - b_{y_2}\left(y_2 - y_2^*\right), \end{aligned} \tag{4.132}$$

yielding the equilibrium of the fast dynamics

$$y_1 = y_1^*, \tag{4.133}$$

$$y_2 = y_2^* = 0. \tag{4.134}$$

The transient response of the fast dynamics is given by a second order time response of the form

$$\begin{aligned} \ddot{y}_1 &= -b_{y_1}y_1 - b_{y_2}\dot{y}_1 \\ &= -\omega_{n_{y^*}}^2 y_1 - 2\omega_{n_{y^*}}\zeta_{y^*}\dot{y}_1, \end{aligned} \tag{4.135}$$

with $\omega_{n_{y^*}}$ being the desired natural frequency of the closed-loop ultra-fast system, and ζ_{y^*} being the desired damping ratio of the ultra-fast dynamics, which can be defined as

$$\omega_{n_{y^*}} = \sqrt{b_{y_1}}, \tag{4.136}$$

$$\zeta_{y^*} = \frac{b_{y_2}}{2\omega n_{y^*}} = \frac{b_{y_2}}{2\sqrt{b_{y_1}}}, \tag{4.137}$$

and finally, substituting the equilibria of the ultra-fast subsystem, Eqns. (4.124-4.125), and the fast subsystem, Eqns. (4.133-4.134), into the equilibrium equation of the slow dynamics (4.116) results in

$$0 = a_{10}x^2\left[\sin\left(s_2\left[\left(1+\sqrt{s_3 v(x,\boldsymbol{y})}\right)^2 - 1\right]\right) - \sin \mathrm{h}_{1_{\mathrm{SS}}}(x)\right] - b_x(x - x^*) \tag{4.138}$$

$$= -b_x(x - x^*), \tag{4.139}$$

yielding the equilibrium of the slow dynamics

$$x = x^*, \tag{4.140}$$

with b_x being the transient response for the slow system. This satisfies that the resulting equilibria of the closed-loop Σ_{SFU} system are those selected in the *TD* control design. The asymptotic stability analysis of the resulting closed-loop system will be conducted in future sections. Simulations are conducted to test the proposed control laws on the helicopter model, and significate results are presented in section 4.8.

4.5 *Composite Feedback* Control Design

This section proposes an alternative singularly perturbed based control methodology to the *TD* control design proposed in section 4.3. This control strategy follows a similar philosophy as the *TD* control design, with the peculiarity that benefits from the properties of the well-known *Composite Feedback* ($\mathcal{CF}$) control for two-time-scale singularly perturbed models (Kokotović et al., 1986).

Generally, feedback control designs for systems resulting from the interaction of slow and fast dynamic modes, suffer from the higher dimensionality and ill-conditioning, while in the two-time-scale $\mathcal{CF}$ control approach, these stiffness properties are taken advantage of by decomposing the original ill-conditioned system into two subsystems in separate time scales(Kokotović et al., 1986). These properties of the feedback control design in conjunction with the properties of the two-time-scale singularly perturbed problems are joined in the $\mathcal{CF}$ control design defined in (Kokotović et al., 1986).

The general two-time-scale $\mathcal{CF}$ design proceeds to stabilize each lower-order subsystem, and then combines the obtained results yielding the composite state-feedback control for the original system. At the same time, the composite controller is required to achieve an asymptotic approximation to the closed-loop system performance that would have been obtained had a state-feedback controller been designed without the use of singular perturbation methods. The composite-feedback control design proposed in this section extends the general two-time-scale $\mathcal{CF}$ control design, to a three-time-scale control design by merging its properties with the *TD* control strategy previously proposed.

The main difference between the two proposed control strategies is that, the $\mathcal{CF}$ control design permits to stabilize the boundary layer Σ_U-subsystem if becomes unstable after substituting the control law that stabilizes the Σ_F-subsystems, which occurs at the end of the *TD* subproblem. It could also happen that the resulting closed-loop boundary layer Σ_U-subsystem does not have the desired degree of prescribed stability, therefore, would require a different control strategy in order to provide that same desired degree of stability to the Σ_U-subsystem. In any of the two possible scenarios in which the *TD* control design lacks to provide the sufficient stability properties to the Σ_U-subsystem, the $\mathcal{CF}$ control design, adapted to the three-time-scale singularly perturbed problem, will satisfy these stability requirements on the ultra-fast Σ_U-subsystem.

This section will first describe the general two-time-scale $\mathcal{CF}$ control formulation, then extend the formulation to the generic three-time-scale $\mathcal{CF}$-*TD* control design, and finally applies the resulting control strategy to the helicopter model, and again, as a reference, the application the control strategy to the simplified model is moved to the Appendix B.

4.5.1 General Two-Time-Scale *Composite Feedback* Control Formulation

The general two-time-scale $\mathcal{CF}$ control method for nonlinear autonomous systems (Kokotović et al., 1986), is defined for a model of the form

$$\dot{x} = f(x, z, u), \; x \in \mathcal{R}^n \tag{4.141}$$

$$\varepsilon\dot{z} = g(x, z, u), \; z \in \mathcal{R}^m, \tag{4.142}$$

where $u \in \mathcal{R}^r$ is a control input. Assuming that the open-loop system, Eqns. (4.141-4.142), is a standard singular perturbation system for every $u \in B_u \subset \mathcal{R}^r$, or what it is the same

$$0 = g(x, z, u), \tag{4.143}$$

has a unique root $z = h(x, u)$ in $B_x \times B_z \times B_u$. The $\mathcal{CF}$ control method seeks the control u as the sum of slow and fast controls, given by

$$u = u_s + u_f, \tag{4.144}$$

where u_s is a feedback function of x, given by

$$u_s = \Gamma_s(x), \tag{4.145}$$

and u_f is a feedback function of x and z, given by

$$u_f = \Gamma_f(x, z). \tag{4.146}$$

The fast feedback function $\Gamma_f(x, z)$ is designed to satisfy two crucial requirements. First, when the feedback control, Eq. (4.145), is applied to the singularly perturbed system, Eqns. (4.141-4.142), the closed-loop system should remain a standard singular perturbed system, given by

$$0 = g(x, z, \Gamma_s(x) + \Gamma_f(x, z)), \tag{4.147}$$

should have a unique root given by $z = \mathrm{h}(x)$ in $B_x \times B_z$. This requirement assures that the choice of Γ_f will not destroy this property of the function g in the open-loop system. The second requirement on the fast feedback function $\Gamma_f(x, z)$ is that it be "inactive" for $z = h(x, u_s)$, that is

$$\Gamma_f(x, h(x, \Gamma_s(x))) = 0. \tag{4.148}$$

The importance of the results in Eq. (4.148) can be seen from the resulting closed-loop equation, given by

$$\dot{x} = f(x, z, u_s + u_f), \tag{4.149}$$

$$\varepsilon\dot{z} = g(x, z, u_s + u_f). \tag{4.150}$$

The requirement in Eq. (4.148) guarantees that $z = h(x, \Gamma_s(x))$ is a root of

$$0 = g(x, z, \Gamma_s(x) + \Gamma_f(x, z)). \tag{4.151}$$

Recalling Eq. (4.147), it can be seen that Eq. (4.151) has a unique root $z = \mathrm{h}(x)$. With this in mind, and considering Eqns. (4.147) and (4.148), the quasi-steady-state equilibrium of the boundary layer is given by

$$\mathrm{h}(x) = \mathrm{h}(x, \Gamma_s(x)), \tag{4.152}$$

which holds as an identity. With Eqns. (4.148) and (4.152), the reduced order model of the closed-loop system, Eqns. (4.149-4.150) is given by

$$\dot{x} = f(x, \mathrm{h}(x, u_s), u_s), \tag{4.153}$$

which is independent of Γ_f and is the same reduced model obtained from the open loop system, that is, Eqns. (4.141-4.142), when u is taken as u_s. Therefore, it can be seen that the design of the slow control $u_s = \Gamma_s(x)$ can be carried out independently of the fast design Γ_f. Once $\Gamma_s(x)$ has been chosen, the boundary layer model of the closed-loop system is defined as

$$\frac{\mathrm{d}z}{\mathrm{d}\tau} = g(x, z, \Gamma_s(x) + u_f), \tag{4.154}$$

where x is treated as a fixed parameter. The requirement in Eq. (4.148) is now interpreted as a requirement on the feedback control $u_f = \Gamma_f(x, z)$ not to shift the equilibrium $z = h(x, \Gamma_s(x))$ of the boundary layer system, Eq. (4.154). The design of u_f must guarantee that $z = h(x, \Gamma_s(x))$ is an asymptotically stable equilibrium of Eq. (4.154) uniformly in x. Following sections extend this formulation to the three-time-scale model.

4.6 *Composite Feedback-Top-Down* Control Strategy for Underactuated Singular Perturbed Systems

The *Composite Feedback Top-Down* ($\mathcal{CF}$-*TD*) control formulation for the three-time-scale underactuated model presented in section 4.3, Eqns. (4.27–4.29), follows a control strategy similar to that for the *TD* control design, with the principal difference that the control signal in the ultra-fast subsystem, Eq. (4.157), is divided into a slow and a fast control component, i.e. $u_{2_c} = u_{2_s} + u_{2_f}$, therefore rewriting the model as

$$\begin{aligned} \dot{x} &= f(x, y, z, u_1), && (4.155)\\ \varepsilon_1 \dot{y} &= \hat{g}(x, y, z), && (4.156)\\ \varepsilon_1 \varepsilon_2 \dot{z} &= \hat{h}(x, y, z, u_{2_c}) = \hat{h}(x, y, z, u_{2_s} + u_{2_f}). && (4.157) \end{aligned}$$

The control strategy for the three-time scale $\mathcal{CF}$ singular perturbation formulation consists on treating the three different time scales as two distinct two-time-scale singular perturbed problems similarly as in the *TD* control design, where following the logic flow in a control process, in which the fastest variables are stabilized first, the *TD* control strategy uses a two stage process to stabilize the full Σ_{SFU} system, where following the same control logic as in the *TD* control strategy, the full Σ_{SFU} system is stabilized in a two stage process in which the fastest variables are stabilized first.

The first stage of the $\mathcal{CF}$-*TD* subproblem applies sequentially first the stretched time scale $\tau_1 = t/\varepsilon_1$ and right after the stretched time-scale $\tau_2 = t/\varepsilon_1\varepsilon_2$, thus obtaining the associated control law u_{2_c}. This control law is formed by the sum of a slow (u_{2_s}) and a fast control signal (u_{2_f}). The slow control signal u_{2_s} is used to stabilize the Σ_F-subsystem, and once stabilized, the fast control law u_{2_s} is used to stabilize the Σ_U-subsystem, or in the case that already stable, provide the desired response. The selected fast control signal has to satisfy certain conditions in order to guarantee that the properties of the singularly perturbed system remains unchanged, as it will be seen.

The second stage of the $\mathcal{CF}$-*TD*, focuses on the *Top* sequence by using the first time-scale decomposition, along with the obtained results in the first time-scale decomposition, and proceeds to stabilize the slow Σ_S-subsystem with the proper u_1. Following sections describe in detail the general $\mathcal{CF}$-*TD* control design.

4.6.1 Control Design for u_2: 1^{st} Stage of the *Composite Feedback Top-Down* Control Design

The first stage of the $\mathcal{CF}$-*TD* considers the subsystem that results when considering the time-scale defined by the *Top* condition to the original Σ_{SFU}, Eqns. (4.155–4.157), where the reduced (slow) subsystem is defined by

$$\dot{x} \quad = \quad f(x, \mathrm{g}(x, u_{2_c}), \mathrm{h}(x, \mathrm{g}(x), u_{2_c}), u_1), \tag{4.158}$$

and where the boundary layer (fast) Σ_{FU}-subsystem for the *TD* subproblem is defined by

$$\frac{\mathrm{d}y}{\mathrm{d}\tau_1} \quad = \quad \hat{g}(x, y, z), \tag{4.159}$$

$$\varepsilon_2 \frac{\mathrm{d}z}{\mathrm{d}\tau_1} \quad = \quad \hat{h}(x, y, z, u_{2_c}), \tag{4.160}$$

where $\mathrm{g}(x, u_{2_c})$ and $\mathrm{h}(x, u_{2_c})$ in the reduced order Σ_S-subsystem, Eq. (4.158), represent the quasi-steady-state equilibria of the boundary layer Σ_{FU}-subsystem, Eqns. (4.159–4.160), which are obtained when setting $\varepsilon_1 = 0$,

and solving simultaneously resulting in

$$0 = \hat{h}(x, y, z, u_{2_c}) \quad \rightarrow \quad z = \mathrm{h}(x, y, u_{2_c}) = \mathrm{h}(x, \mathrm{g}(x), u_2), \tag{4.161}$$

$$\updownarrow$$

$$0 = \hat{g}(x, y, z) = \hat{g}(x, y, \mathrm{h}(x, y, u_{2_c})) \quad \rightarrow \quad y = \mathrm{g}(x, u_2), \tag{4.162}$$

Note that on the boundary layer Σ_{FU}-subsystem, the variable x is treated like a fixed parameter. It is important to note the difference between this method and the one previously presented in section 4.3, since the *Composite Feedback* control method seeks the control signal of the Σ_U-subsystem as the sum of the slow and fast control that is

$$u_{2_c} = u_{2_s} + u_{2_f}, \tag{4.163}$$

where u_{2_s} is a feedback function of slow variables, x and y, given by

$$u_{2_s} = \Gamma_s(x, y), \tag{4.164}$$

that stabilizes with the desired degree of stability the intermediate fast Σ_F-subsystem, and u_{2_f} is a feedback function of x, y, and z, given by

$$u_{2_f} = \Gamma_f(x, y, z), \tag{4.165}$$

that stabilizes the ultra-fast Σ_U-subsystem with the desired degree of stability, thus rewriting the Σ_{FU}-subsystem as

$$\frac{\mathrm{d}y}{\mathrm{d}\tau_1} \quad = \quad \hat{g}(x, y, z), \tag{4.166}$$

$$\varepsilon_2 \frac{\mathrm{d}z}{\mathrm{d}\tau_1} \quad = \quad \hat{h}(x, y, z, \Gamma_s(x, y) + \Gamma_f(x, y, z)), \tag{4.167}$$

where x is treated like a fixed parameter, and $\tau_1 = t/\varepsilon_1$. Recall that as noted in the general two-time-scale *Composite Feedback* formulation, the fast feedback function $\Gamma_f(x, y, z)$ is designed to satisfy two crucial requirements. First, when the feedback control, Eq. (4.163), is applied to Eqns. (4.166–4.167), the closed-loop system should remain a standard singularly perturbed system. This translates to that the equilibrium of the boundary layer

$$0 = \hat{h}(x, y, z, \Gamma_s(x, y) + \Gamma_f(x, y, z)), \tag{4.168}$$

should have a unique root given by $z = \mathrm{h}(x, y)$ in $B_x \times B_y \times B_z$. This requirement assures that the choice of Γ_f will not destroy this property of the function $\hat{h}$ in the open-loop system. The second requirement on $\Gamma_f(x, y, z)$ is that it be *inactive* for $z = \mathrm{h}(x, y, u_{2_s})$, that is

$$\Gamma_f \left[x, y, \mathrm{h}(x, y, \Gamma_s(x, y))\right] = 0. \tag{4.169}$$

The control strategy continues by identifying that the Σ_{FU}-subsystem, Eqns. (4.166–4.167), can be treated again like a two-time-scale singularly perturbed system by applying the *Down* time-scale decomposition, τ_2, where the new reduced order Σ_F-subsystem is given by

$$\frac{\mathrm{d}y}{\mathrm{d}\tau_1} = \hat{g}(x, y, \mathrm{h}(x, y, u_{2_s})) \tag{4.170}$$

and the new boundary layer Σ_U-subsystem is given by

$$\frac{\mathrm{d}z}{\mathrm{d}\tau_2} = \hat{h}(x, y, z, u_{2_c}) = \hat{h}(x, y, z, u_{2_s} + u_{2_f}), \tag{4.171}$$

where x and y are treated like fix parameters. The function $\mathrm{h}(x, y, u_{2_s})$ represents the quasi-steady-state equilibrium of the boundary layer Eq. (4.171) when $\varepsilon_2 = 0$, yielding

$$0 = \hat{h}(x, y, z, u_{2_c}) \rightarrow z = \mathrm{h}(x, y, u_{2_c}) = \mathrm{h}(x, y, u_{2_s} + u_{2_f}). \tag{4.172}$$

Recall that according to Eq. (4.169), Eq. (4.173) reduces to

$$z = \mathrm{h}(x, y, u_{2_s}) = \mathrm{h}(x, y, \Gamma_s(x, y)). \tag{4.173}$$

The substitution of the quasi-steady-state equilibrium, Eq. (4.173), back into the reduced order Σ_F-subsystem, Eq. (4.171), permits to obtain the associated slow control law u_{2_s} that stabilizes the Σ_F-subsystem. Once the design of the slow control $u_{2_s} = \Gamma_s(x, y)$ has been conducted, the strategy shifts towards selecting the fast control law u_{2_f} that permits to select the desired degree of stability of the boundary layer Σ_U-subsystem which is given by after substituting the slow control, $u_{2_s} = \Gamma_s(x, y)$, back into Eq. (4.171), resulting in

$$\frac{\mathrm{d}z}{\mathrm{d}\tau_2} = \hat{h}(x, y, z, u_{2_s} + u_{2_f}), \tag{4.174}$$

where x and y are treated as fixed parameters, and with u_{2_s} defined by the previously obtained slow control law that stabilizes the Σ_F-subsystem. The fast control $u_{2_f} = \Gamma_s(x, y, z)$ needs to satisfy the requirement described in Eq. (4.169), which is now interpreted as a requirement on the feedback control $u_{2_f} = \Gamma_f(x, y, z)$ not to shift the equilibrium $z = \mathrm{h}(x, y, \Gamma_s(x, y))$, Eq. (4.173), of the boundary layer system, Eq. (4.174).

The design of u_{2_f} must also guarantee that $z = \mathrm{h}(x, y, \Gamma_s(x, y))$ is an asymptotically stable equilibrium of Eq. (4.174) uniformly in x and y. This concludes the first stage of the $\mathcal{CF}$-*TD* control design, and the results obtained are used to solve the second stage which is described in detail in the following section. Figure 4.5 depicts the first stage of the $\mathcal{CF}$-*TD* control design sequence.

4.6.2 Control Design for u_1: 2^{nd} Stage of the *Composite Feedback Top-Down* Control Design

The second stage of the$\mathcal{CF}$-*TD* subproblem focuses on the control design for u_1 for the stabilization of the Σ_S-subsystem. For that purpose, recall first that after selecting the control signal $u_2(x, y, z) = u_{2_s} + u_{2_f}$, the Σ_{FU}-subsystem, Eqns. (4.159–4.160), can be rewritten as

$$\frac{\mathrm{d}y}{\mathrm{d}\tau_1} = \hat{g}(x, y, z), \tag{4.175}$$

$$\varepsilon_2 \frac{\mathrm{d}z}{\mathrm{d}\tau_1} = \hat{h}(x, y, z), \tag{4.176}$$

Similarly as in the *TD* control design, in order to determine the equilibria that will define the Σ_S-subsystem, (4.158), the Σ_{FU}-subsystem, Eqns. (4.175–4.176), can be decomposed by applying the stretched time scale τ_2 resulting in the Σ_F-subsystem given by

$$\frac{\mathrm{d}y}{\mathrm{d}\tau_1} = \hat{g}(x, y, \mathrm{h}(x, y)), \tag{4.177}$$

and where the new boundary layer (fast) Σ_U-subsystem is defined by

$$\frac{\mathrm{d}z}{\mathrm{d}\tau_2} = \hat{h}(x, y, z), \tag{4.178}$$

with their equilibria being now completely determined resulting in

$$0 = \hat{h}(x, y, z) \rightarrow u_2(x, y) \rightarrow z = \mathrm{h}(x, y), \tag{4.179}$$

$$0 = \hat{g}(x, y, \mathrm{h}(x, y)) \rightarrow y = \mathrm{g}(x), \tag{4.180}$$

with this in mind, the reduced order (slow) Σ_S-subsystem, Eq. (4.158) reduces to

$$\dot{x} = f(x, \mathrm{g}(x), \mathrm{h}(x, \mathrm{g}(x)), u_1). \tag{4.181}$$

The control signal u_1 is selected such that stabilizes the resulting Σ_S-subsystem (4.181) to ensure that guarantees the desired degree of stability.

4.6.3 Conclusions for the $\mathcal{CF}$-*Top-Down* Control Design

This concludes the $\mathcal{CF}$-*TD* control design. Following sections will extend this formulation to the helicopter model, and in Appendix B to the simplified model. Again, and similarly as in the *TD* control design, due to the underactuated structure of the system being controlled, a sequential application of the *TD* has allowed to control the full Σ_{SFU} system, by stabilizing separately first the Σ_{FU}-subsystem, and once stable, and using the results obtained in this first stabilization, proceed with the Σ_S-subsystem, which follows the logic flow of the dynamics of a singular perturbed time scale system, as described in Figure 3.9. For better understanding of the complete $\mathcal{CF}$-*TD*, it can be refer the Figure in the *TD* control strategy Figure 4.6.

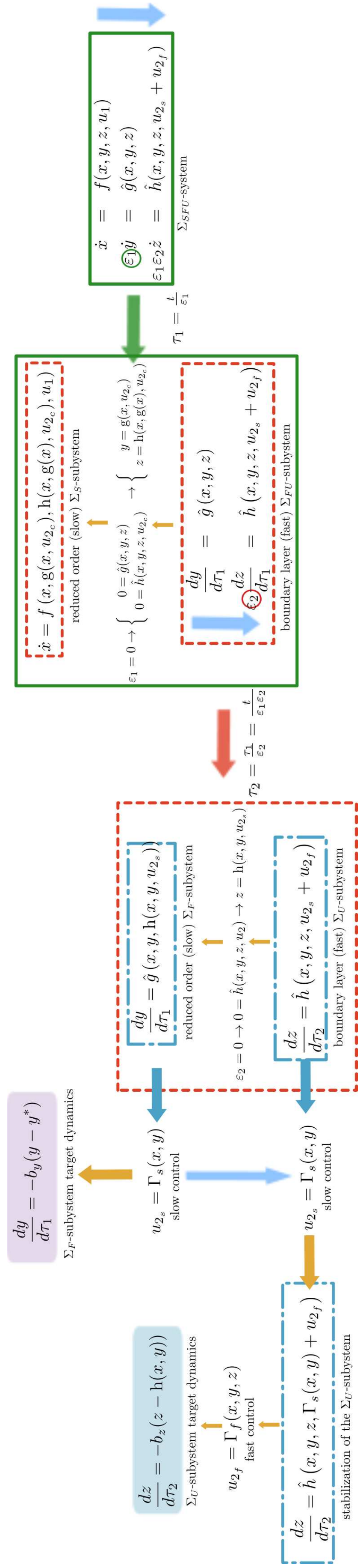

Figure 4.5: 1^{st} Stage of the *Composite Feedback-Top-Down* control design sequence.

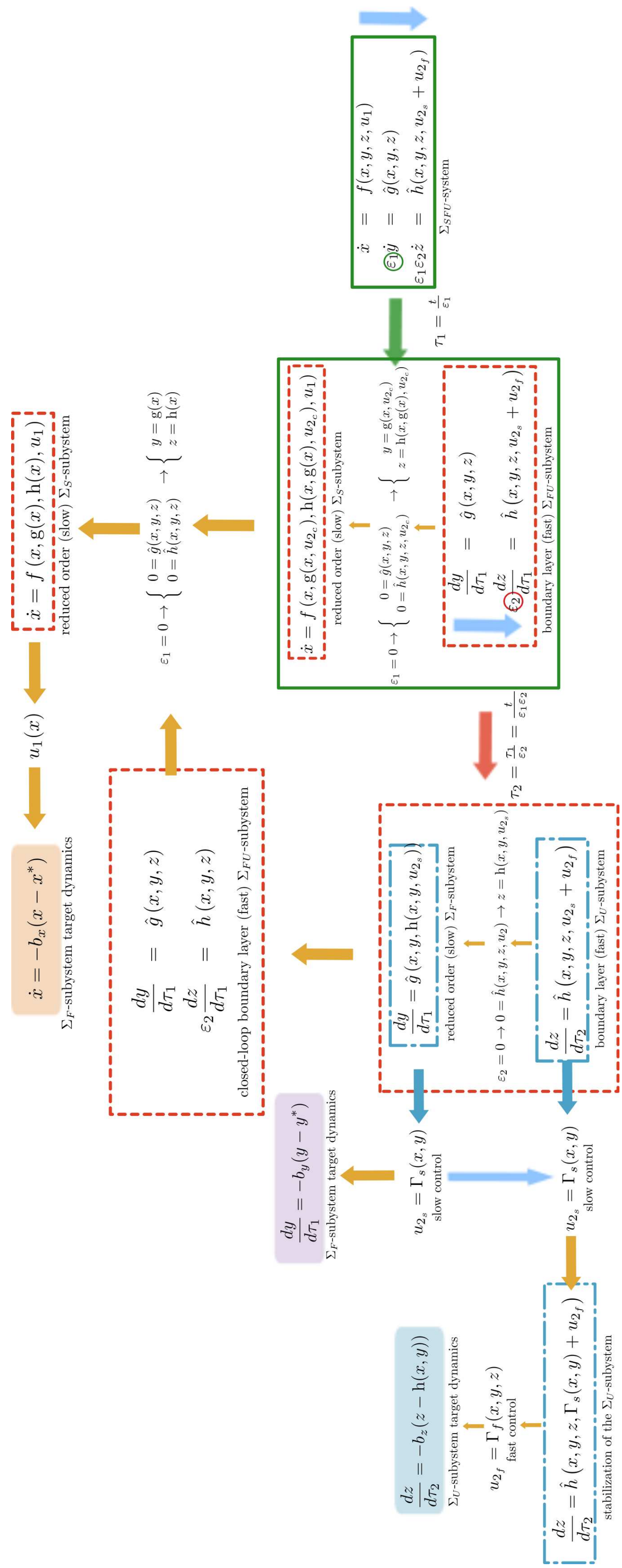

Figure 4.6: Complete *Composite Feedback-Top-Down* control design sequence.

4.7 *Composite Feedback Top-Down* Control Design for the Helicopter Model

The $\mathcal{CF}$-*TD* control strategy for the nonlinear underactuated three-time-scale singularly perturbed helicopter model, Eqns. (3.56–3.60), follows a similar strategy to the one used for the *TD* control design, with the main difference that the control signal in the ultra-fast dynamics is divided into a slow and a fast component, $u_{2_c} = u_{2_s} + u_{2_f}$, which permits to select the desired transient behavior for the Σ_U-subsystem, hence becoming the full Σ_{SFU} system defined by

$$\begin{aligned}
\dot{x} &= a_8 x + a_{10} x^2 \sin z_1 + a_9 x^2 + a_{11} + u_1, && (4.182)\\
\varepsilon_1 \dot{y}_1 &= c_1 y_2, && (4.183)\\
\varepsilon_1 \dot{y}_2 &= x^2 (c_2 + c_3 z_1 - \sqrt{c_4 + c_5 z_1}) + a_9 y_2 + a_9 y_2^2 + c_6, && (4.184)\\
\varepsilon_1 \varepsilon_2 \dot{z}_1 &= c_7 z_2, && (4.185)\\
\varepsilon_1 \varepsilon_2 \dot{z}_2 &= a_9 z_1 + c_8 x^2 \sin z_1 + c_9 z_2 + c_{10} + c_{11} \left(u_{2_s} + u_{2_f}\right). && (4.186)
\end{aligned}$$

The $\mathcal{CF}$-*TD* control strategy, similarly as the *TD* control strategy, consists on treating the three different time scales as two-distinct two-time-scale singular perturbed problems. The $\mathcal{CF}$-*TD* control strategy is also divided in two stages, being each stage dedicated to design each of the two control signals.

In the first stage, the control strategy focuses on defining a control signal, $u_{2_s} = \Gamma_s(x, \boldsymbol{y})$, that stabilizes the intermediate fast Σ_F-subsystem with the desired degree of stability, while $u_{2_f} = \Gamma_f(x, \boldsymbol{y}, \boldsymbol{z})$ is a feedback function of x, y, and z, that stabilizes the ultra-fast Σ_U-subsystem with the desired degree of stability. Once stabilized the Σ_{FU}-subsystem, the control strategy shifts towards obtaining the control signal u_1 that stabilizes the Σ_S-subsystem. The following subsections describe in detail each one of the $\mathcal{CF}$-*TD* control methods for the helicopter problem.

4.7.1 Control Design for u_2: 1^{st} Stage of the *Composite Feedback Top-Down* Control Design for the Helicopter Model

The first stage of the $\mathcal{CF}$-*TD* starts by decomposing the Σ_{SFU}, Eqns. (4.182–4.186), into a two-time-scale subsystem by applying the *Top* condition, resulting in the reduced order (slow) Σ_S-subsystem

$$\dot{x} = a_8 x + a_{10} x^2 \sin\left[\mathrm{h}_{1_c}(x, u_{2_c})\right] + a_9 x^2 + a_{11} + u_1, \tag{4.187}$$

and where the resulting boundary layer (fast) Σ_{FU}-subsystem is given by

$$\begin{aligned}
\frac{\mathrm{d}y_1}{\mathrm{d}\tau_1} &= c_1 y_2, && (4.188)\\
\frac{\mathrm{d}y_2}{\mathrm{d}\tau_1} &= x^2 (c_2 + c_3 z_1 - \sqrt{c_4 + c_5 z_1}) + a_9 y_2 + a_9 y_2^2 + c_6, && (4.189)\\
\varepsilon_2 \frac{\mathrm{d}z_1}{\mathrm{d}\tau_1} &= c_7 z_2, && (4.190)\\
\varepsilon_2 \frac{\mathrm{d}z_2}{\mathrm{d}\tau_1} &= a_9 z_1 + c_8 x^2 \sin z_1 + c_9 z_2 + c_{10} + c_{11} \left(u_{2_s} + u_{2_f}\right). && (4.191)
\end{aligned}$$

Similarly as in the *TD* control design, the proposed control strategy obtains the associated control law u_{2_c} that stabilizes the Σ_{FU}-subsystem by recognizing that Σ_{FU}-subsystem, Eqns. (4.188–4.190), can be treated again like a two-time-scale singular perturbation problem by applying the *Down* condition, but prior to proceed with the time-scale decomposition, and similarly as conducted in the *TD* control design section, a feedback transform is introduced to guarantee that the Σ_U-subsystem is stable by selecting

$$v_{2_s} = c_8 x^2 \sin z_1 + c_{10} + c_{11} u_{2_s}, \tag{4.192}$$

thus rewriting Eqns. (4.190–4.191) such

$$\varepsilon_2 \frac{\mathrm{d}z_1}{\mathrm{d}\tau_1} = c_7 z_2, \tag{4.193}$$

$$\varepsilon_2 \frac{\mathrm{d}z_2}{\mathrm{d}\tau_1} = a_9 z_1 + c_9 z_2 + v_{2_s}. \tag{4.194}$$

As demonstrated in the *TD* control design, with the appropriate selection on v_{2_s}, and taking into account the inherit nature of the actuator dynamics, the Σ_U-subsystem dynamics become stable, and faster than the rest of the time scales and with open loop eigenvalues given by $\lambda_1 = -0.5772 \times 10^{-4}$ and $\lambda_2 = -0.1697 \times 10^{-4}$.

Recall that the main difference between the $\mathcal{CF}$-*TD* control strategy presented in this section, and the *TD* control strategy previously presented in section 4.3, is the liberty of modifying the resulting transient response of the Σ_U-subsystem after obtaining the slow control signal (u_{2_s}), therefore allowing to modify both λ_1 and λ_2 to a desired transient response as it will be shown in the second part of the $\mathcal{CF}$-*TD* control design. Using a similar control strategy as the one employed in the *TD* control design in section 4.4, and recalling that the requirement on $\Gamma_f(x, \boldsymbol{y}, \boldsymbol{z})$ is that it be *inactive* for $\boldsymbol{z} = \mathbf{h}(x, u_{2_s})$, that is

$$\Gamma_f(x, \boldsymbol{y}, \mathbf{h}(x, \boldsymbol{y}, \Gamma_s(x, \boldsymbol{y}))) = 0, \tag{4.195}$$

the control law that stabilizes the vertical displacement of the helicopter is therefore defined as

$$\begin{aligned} u_{2_s} &= K_b \left(1 + \sqrt{1 - 4c_{12}(K_a - v_s(x, \boldsymbol{y}))}\right)^2 + K_c + K_d x^2 \sin z_1 \\ &= K_b \left(1 + \sqrt{s_3 v_s(x, \boldsymbol{y})}\right)^2 + K_c + K_d x^2 \sin z_1, \end{aligned} \tag{4.196}$$

with

$$v_s(x, \boldsymbol{y}) = -\frac{a_9 y_2^2 + \left(a_9 + \tilde{b}_{y_2}\right) y_2 + \tilde{b}_{y_1} (y_1 - y_1^*) + c_6}{x^2}, \tag{4.197}$$

and K_a, K_b, K_c, K_d, and s_3 being defined in Eqns. (4.84–4.88). Recall that the control law obtained in the *TD* control design, (4.82), is equivalent as the slow component control law u_{2_s}, therefore, being also equivalent the closed loop Σ_U-subsystem from the *TD* control design, and $dz/d\tau_2 = \hat{\boldsymbol{h}}(x, \boldsymbol{y}, \boldsymbol{z}, \Gamma_s(x, u_{2_c}))$, this resulting in equivalent quasi-steady-state equilibria, given by

$$\boldsymbol{z} = \mathbf{h_c}(x, \boldsymbol{y}) = \begin{bmatrix} \mathrm{h}_{1_c}(x, \boldsymbol{y}), \\ \mathrm{h}_{2_c}(x, \boldsymbol{y}), \end{bmatrix}, \tag{4.198}$$

with

$$\mathrm{h}_{1_c}(x, \boldsymbol{y}) = z_1 = s_2 \left[\left(1 + \sqrt{s_3 v_s(x, \boldsymbol{y})}\right)^2 - 1\right] \tag{4.199}$$

$$\mathrm{h}_{2_c}(x, \boldsymbol{y}) = z_2 = 0, \tag{4.200}$$

and with s_2 defined in Eq. (4.103). Once the design of the slow control $u_{2_s} = \Gamma_s(x, \boldsymbol{y})$, that stabilizes the Σ_F-subsystem has been selected, the strategy shifts towards selecting the desired degree of stability of the boundary layer Σ_U-subsystem by selecting the appropriate fast control signal $u_{2_f} = \Gamma_f(x, \boldsymbol{y}, \boldsymbol{z})$. The selection of u_{2_f} needs to be done taken into consideration that has to fulfill the requirement that assures that the choice of Γ_f will not destroy the property that the boundary layer Σ_U-subsystem will only have a unique root $z = \mathbf{h}(x, \boldsymbol{y})$ in $B_x \times B_y \times B_z$ of the function $\hat{\boldsymbol{h}}$ in the open-loop system, and that

$\Gamma_f(x, \boldsymbol{y}, \boldsymbol{z})$ it be *inactive* for $\boldsymbol{z} = \mathbf{h}(x, \boldsymbol{y}, \Gamma_s(x, \boldsymbol{y}))$, that is

$$\frac{\mathrm{d}z_1}{\mathrm{d}\tau_2} = c_7 z_2, \tag{4.201}$$

$$\begin{aligned}\frac{\mathrm{d}z_2}{\mathrm{d}\tau_2} &= a_9 z_1 + c_8 x^2 \sin z_1 + c_9 z_2 + c_{10} + c_{11}(u_{2_s} + u_{2_f}) \\ &= a_9 z_1 + c_8 x^2 \sin z_1 + c_9 z_2 + c_{10} + c_{11} u_{2_s} \\ &= a_9 z_1 + c_9 z_2 + J_2 \left[\left(1 + \sqrt{s_3 v_s(x, \boldsymbol{y})}\right)^2 - 1 \right],\end{aligned} \tag{4.202}$$

which reduces to the closed loop of the *TD* control design, and with with $\mathbf{h}(x, \boldsymbol{y}, \Gamma_s(x, \boldsymbol{y}))$ given in Eq. (4.198).

The requirement (4.195) is now interpreted as a requirement on the feedback control $u_{2_f} = \Gamma_f(x, \boldsymbol{y}, \boldsymbol{z})$ not to shift the equilibrium $\boldsymbol{z} = \mathbf{h}(x, \boldsymbol{y}, \Gamma_s(x, \boldsymbol{y}))$, Eq. (4.198), of the boundary layer system (4.201–4.202), such that the design of u_{2_f} must guarantee that $\boldsymbol{z} = \mathbf{h}(x, y, \Gamma_s(x, \boldsymbol{y}))$ is an asymptotically stable equilibrium of Eqns. (4.201–4.202) uniformly in x and $\boldsymbol{y}$. Therefore, in order to obtain the fast control law, u_{2_f}, let first substitute the control law u_{2_s}, Eq. (4.196), into the Σ_U-subsystems resulting in

$$\frac{\mathrm{d}z_1}{\mathrm{d}\tau_2} = c_7 z_2 \tag{4.203}$$

$$\begin{aligned}\frac{\mathrm{d}z_2}{\mathrm{d}\tau_2} &= a_9 z_1 + c_8 x^2 \sin z_1 + c_9 z_2 + c_{10} + c_{11}\left(u_{2_s} + u_{2_f}\right) \\ &= a_9 z_1 + c_9 z_2 + J_2 \left[\left(1 + \sqrt{s_3 v_s(x, \boldsymbol{y})}\right)^2 - 1 \right] + c_{11} u_{2_f}.\end{aligned} \tag{4.204}$$

Let select a desired target dynamics for the boundary layer of the form

$$\frac{\mathrm{d}z_1}{\mathrm{d}\tau_2} = c_7 z_2, \tag{4.205}$$

$$\frac{\mathrm{d}z_2}{\mathrm{d}\tau_2} = -\tilde{b}_{z_1}(z_1 - \mathrm{h}_{1_c}(x, \boldsymbol{y})) - \tilde{b}_{z_2} z_2, \tag{4.206}$$

where $\tilde{b}_{z_1}$, and $\tilde{b}_{z_2}$ are control design parameters that determine the desired time response for the actuator dynamics of the stretched time-scale $\tau_2 = t/\varepsilon_1\varepsilon_2$ and selected as

$$\tilde{b}_{z_1} = \varepsilon_1 \varepsilon_2 b_{z_1} \tag{4.207}$$

$$\tilde{b}_{z_2} = \varepsilon_1 \varepsilon_2 b_{z_2}, \tag{4.208}$$

with

$$b_{z_1} = \omega_{n_{z^*}}^2, \tag{4.209}$$

$$b_{z_2} = 2\omega_{n_{z^*}} \zeta_{z^*}, \tag{4.210}$$

where $\omega_{n_{z^*}}$ represents the selected natural frequency, and ζ_{z^*} the selected damping ratio of the desired transient response of the boundary layer Σ_U-subsystem. By selecting the desired target dynamics for the boundary layer on the form above described in Eqns. (4.205–4.206), the requirement that the feedback control $u_{2_f} = \Gamma_f(x, \boldsymbol{y}, \boldsymbol{z})$ not to shift the equilibrium $\boldsymbol{z} = \mathbf{h}(x, \boldsymbol{y}, \Gamma_s(x, \boldsymbol{y}))$ of the boundary layer system is satisfied.

The design of u_{2_f} must also guarantee that $\boldsymbol{z} = \mathbf{h}(x, \boldsymbol{y}, \Gamma_s(x, \boldsymbol{y}))$ is an asymptotically stable equilibrium of Eqns. (4.203–4.204) uniformly in x and $\boldsymbol{y}$. The control problem can be solved if a control signal u_{2_f} is chosen such that Eqns. (4.203–4.204) behave like the target system defined in Eqns. (4.205–4.206). The control signal u_{2_f} is therefore chosen to be of the form

$$u_{2_f} = -\frac{1}{c_{11}}\left(a_9 z_1 + c_8 x^2 \sin z_1 + c_9 z_2 + c_{10} + c_{11} u_{2_s} + \tilde{b}_{z_1}(z_1 - \mathrm{h}_{1_c}(x, \boldsymbol{y})) + \tilde{b}_{z_2} z_2\right), \tag{4.211}$$

where u_{2_s} is defined in Eq. (4.196). The fast u_{2_f} control law can be rewritten by expanding the slow control signal u_{2_s}, and recalling the definition of $z_1 = \mathrm{h}_{1_c}(x, \boldsymbol{y}, u_{2_s})$ in Eq. (4.101), thus resulting in

$$\begin{aligned} u_{2_f} &= -\frac{1}{c_{11}}\left(a_9 z_1 + c_8 x^2 \sin z_1 + c_9 z_2 + c_{10} + c_{11} u_{2_s}\right) - \frac{1}{c_{11}}\left(\tilde{b}_{z_1}(z_1 - \mathrm{h}_{1_c}(x, \boldsymbol{y})) + \tilde{b}_{z_2} z_2\right) \\ &= -\frac{1}{c_{11}}\left(\tilde{b}_{z_1}(z_1 - \mathrm{h}_{1_c}(x, \boldsymbol{y})) + \tilde{b}_{z_2} z_2\right) - \frac{1}{c_{11}}\left(a_9\left(z_1 - \mathrm{h}_{1_c}(x, \boldsymbol{y})\right) + c_9 z_2\right) \\ &= -\frac{1}{c_{11}}\left[\left(\tilde{b}_{z_1} + a_9\right)\left(z_1 - \mathrm{h}_{1_c}(x, \boldsymbol{y})\right) + \left(\tilde{b}_{z_2} + c_9\right) z_2\right], \end{aligned} \tag{4.212}$$

where it can be observed that the fast control law u_{2_f} satisfies both requirements. The $\mathcal{CF}$-*TD* control signal u_{2_c} is therefore defined as the sum of the slow and the fast control signals, resulting in

$$\begin{aligned} u_{2_c}(x, y, z_1, y^*) = u_{2_s} + u_{2_f} &= K_b\left(1 + \sqrt{s_3 v(x, \boldsymbol{y})}\right)^2 + K_c + K_d x^2 \sin z_1 \\ &- \frac{1}{c_{11}}\left[\left(\tilde{b}_{z_1} + a_9\right)\left(z_1 - \mathrm{h}_{1_c}(x, \boldsymbol{y})\right) + \left(\tilde{b}_{z_2} + c_9\right) z_2\right]. \end{aligned} \tag{4.213}$$

The following section continues with the $\mathcal{CF}$-*TD* control methodology for the helicopter model by conducting the $\mathcal{CF}$-*BU* methodology that stabilizes the Σ_S-subsystem.

4.7.2 Control Design for u_1: 2^{nd} Stage of the *Composite Feedback Top-Down* Control Design for the Helicopter Model

The second stage of the $\mathcal{CF}$-*TD* control design focuses on the selection of u_1 such that stabilizes the Σ_S-subsystem. For that purpose, recall first that, after selecting the control signal $u_{2_c}(x, y, z_1, y^*)$, Eq. (4.213), the Σ_{FU}-subsystem, Eqns. (4.188–4.190) can be rewritten as

$$\frac{\mathrm{d}y_1}{\mathrm{d}\tau_1} = c_1 y_2, \tag{4.214}$$

$$\frac{\mathrm{d}y_2}{\mathrm{d}\tau_1} = x^2(c_2 + c_3 z_1 - \sqrt{c_4 + c_5 z_1}) + a_9 y_2 + a_9 y_2^2 + c_6, \tag{4.215}$$

$$\varepsilon_2 \frac{\mathrm{d}z_1}{\mathrm{d}\tau_1} = c_7 z_2, \tag{4.216}$$

$$\begin{aligned} \varepsilon_2 \frac{\mathrm{d}z_2}{\mathrm{d}\tau_1} &= a_9 z_1 + c_9 z_2 + J_2\left[\left(1 + \sqrt{s_3 v(x, \boldsymbol{y})}\right)^2 - 1\right] \\ &- \left(\tilde{b}_{z_1} + a_9\right)\left(z_1 - \mathrm{h}_{1_c}(x, \boldsymbol{y})\right) + \left(\tilde{b}_{z_2} + c_9\right) z_2, \end{aligned} \tag{4.217}$$

where Eq. (4.217) can be rewritten by considering the definition of $z_1 = \mathrm{h}_{1_c}(x, \boldsymbol{y}, u_{2_s})$, Eq. (4.199), resulting in

$$\begin{aligned} \varepsilon_2 \frac{\mathrm{d}z_2}{\mathrm{d}\tau_1} &= a_9 z_1 + c_9 z_2 + J_2\left[\left(1 + \sqrt{s_3 v(x, \boldsymbol{y})}\right)^2 - 1\right] \\ &- \left(\tilde{b}_{z_1} + a_9\right)\left(z_1 - \mathrm{h}_{1_c}(x, \boldsymbol{y})\right) + \left(\tilde{b}_{z_2} + c_9\right) z_2 \\ &= a_9\left(z_1 - s_2\left[\left(1 + \sqrt{s_3 v(x, \boldsymbol{y})}\right)^2 - 1\right]\right) + c_9 z_2 \\ &- \left(\tilde{b}_{z_1} + a_9\right)\left(z_1 - \mathrm{h}_{1_c}(x, \boldsymbol{y})\right) + \left(\tilde{b}_{z_2} + c_9\right) z_2 \\ &= a_9\left(z_1 - \mathrm{h}_{1_c}(x, \boldsymbol{y})\right) + c_9 z_2 - \left(\tilde{b}_{z_1} + a_9\right)\left(z_1 - \mathrm{h}_{1_c}(x, \boldsymbol{y})\right) + \left(\tilde{b}_{z_2} + c_9\right) z_2 \\ &= -\tilde{b}_{z_1}\left(z_1 - \mathrm{h}_{1_c}(x, \boldsymbol{y})\right) - \tilde{b}_{z_2} z_2, \end{aligned} \tag{4.218}$$

therefore rewritting the Σ_{FU}-subsystem as

$$\frac{\mathrm{d}y_1}{\mathrm{d}\tau_1} = c_1 y_2, \tag{4.219}$$

$$\frac{\mathrm{d}y_2}{\mathrm{d}\tau_1} = x^2(c_2 + c_3 z_1 - \sqrt{c_4 + c_5 z_1}) + a_9 y_2 + a_9 y_2^2 + c_6, \tag{4.220}$$
$$\varepsilon_2 \frac{\mathrm{d}z_1}{\mathrm{d}\tau_1} = c_7 z_2, \tag{4.221}$$
$$\varepsilon_2 \frac{\mathrm{d}z_2}{\mathrm{d}\tau_1} = -\tilde{b}_{z_1}\left(z_1 - \mathrm{h}_{1_c}(x, \boldsymbol{y})\right) - \tilde{b}_{z_2} z_2. \tag{4.222}$$

In order to determine the equilibria that will define the Σ_S-subsystem, Eq. (4.187), the Σ_{FU}-subsystem, Eqns. (4.214–4.217), can be decomposed into a two.time-scale system by applying the stretched time scale τ_2 resulting in the Σ_F-subsystem given by

$$\frac{\mathrm{d}y_1}{\mathrm{d}\tau_1} = c_1 y_2, \tag{4.223}$$
$$\frac{\mathrm{d}y_2}{\mathrm{d}\tau_1} = x^2(c_2 + c_3 \mathrm{h}_{1_c}(x, \boldsymbol{y}) - \sqrt{c_4 + c_5 \mathrm{h}_{1_c}(x, \boldsymbol{y})} + a_9 y_2 + a_9 y_2^2 + c_6, \tag{4.224}$$

and where the new boundary layer (fast) Σ_U-subsystem is defined by

$$\frac{\mathrm{d}z_1}{\mathrm{d}\tau_2} = c_7 z_2, \tag{4.225}$$
$$\frac{\mathrm{d}z_2}{\mathrm{d}\tau_2} = -\tilde{b}_{z_1}\left(z_1 - \mathrm{h}_{1_c}(x, \boldsymbol{y})\right) - \tilde{b}_{z_2} z_2. \tag{4.226}$$

where the quasi-steady-state equilibrium of the Σ_U-subsystem is given when $\varepsilon_2 = 0$, that is

$$0 = \hat{\boldsymbol{h}}(x, \boldsymbol{y}, \boldsymbol{z}) \rightarrow \boldsymbol{z} = \mathbf{h_c}(x, \boldsymbol{y}), \tag{4.227}$$

where

$$\boldsymbol{z} = \mathbf{h_c}(x, \boldsymbol{y}) = \begin{bmatrix} h_{1_c}(x, \boldsymbol{y}) \\ h_{2_c}(x, \boldsymbol{y}) \end{bmatrix}, \tag{4.228}$$

with

$$h_{1_c} = z_1 = \mathrm{h}_1(x, \boldsymbol{y}) = s_2\left[\left(1 + \sqrt{s_3 v_s(x, \boldsymbol{y})}\right)^2 - 1\right], \tag{4.229}$$
$$h_{2_c} = z_2 = \mathrm{h}_{2_c}(x, \boldsymbol{y}) = 0, \tag{4.230}$$

where recall that satisfies the requirement for the design of the fast control law u_{2_f} that the closed-loop system should remain a standard singularly perturbed system with a unique equilibrium given by $\boldsymbol{z} = \mathbf{h}(x, \boldsymbol{y})$, that is $\mathbf{h}(x, \boldsymbol{y}) \equiv \mathbf{h_c}(x, \boldsymbol{y})$, therefore being equivalent to the quasi-steady-state resulting from the first stage of the $\mathcal{CF}$-*TD* control strategy, Eqns. (4.199–4.200).

Recall that when substituting the quasi-steady-state equilibria of the Σ_U-subsystem, Eqns. (4.229–4.230) into Eqns. (4.225–4.226), they degenerate into the selected Σ_F target dynamics, Eqns. (4.73–4.74). Therefore, setting the perturbation parameter $\varepsilon_1 = 0$, degenerate into the equation that determine the roots of the fast manifold, defined as

$$0 = \hat{\boldsymbol{g}}(x, \boldsymbol{y}, \mathbf{h}(x, \boldsymbol{y})) \rightarrow \boldsymbol{y} = \mathbf{g}(x) = \begin{bmatrix} g_1(x) \\ g_2(x) \end{bmatrix}, \tag{4.231}$$

that is

$$0 = c_1 y_2 \rightarrow y_2 = \mathrm{g}_2(x), \tag{4.232}$$
$$0 = -\tilde{b}_{y_1}(y_1 - y_1^*) - \tilde{b}_{y_2} x_2 \rightarrow y_1 = \mathrm{g}_1(x), \tag{4.233}$$

therefore yielding the equilibria for the vertical motion of the helicopter given by

$$g_1(x) = y_1 = y^*, \tag{4.234}$$
$$g_2(x) = y_2 = 0, \tag{4.235}$$

where Eq. (4.234) represents that the equilibrium altitude position is the desired altitude, while Eq. (4.235), provides that, as expected, the equilibrium vertical position must be zero in order to achieve a vertical equilibrium point. Similarly as in the *TD* control design, the control law u_1 that stabilizes the slow Σ_S-subsystem is obtained by substituting the Σ_F and Σ_U-subsystem equilibria, Eqns. (4.234–4.235), and (4.229–4.230), respectively, into Eq. (4.187), yielding the reduced order Σ_S-subsystem given by

$$\dot{x} = a_8 x + a_{10} x^2 \sin \mathrm{h}_{1_{\mathrm{SS}}}(x, \mathbf{g}(x)) + a_9 x^2 + a_{11} + u_1, \tag{4.236}$$

where $\mathrm{h}_{1_{\mathrm{SS}}}(x, \mathbf{g}(x))$ represents the quasi-steady-state equilibrium of the collective pitch angle, Eq. (4.229), when substituting the quasi-steady-state equilibria for the vertical displacement dynamics, Eqns (4.234–4.235), resulting in

$$\mathrm{h}_{1_{\mathrm{SS}}}(x, \mathbf{g}(x)) = \mathrm{h}_1(x, \boldsymbol{y})|_{\boldsymbol{y}=\mathbf{g}(x)} = s_2 \left[\left(1 + \sqrt{s_3 v_{SS}(x, \mathbf{g}(x))} \right)^2 - 1 \right], \tag{4.237}$$

with $v_{SS}(x, \mathbf{g}(x))$ being the result of substituting the Σ_F equilibria, Eqns. (4.234) and (4.235), into Eq. (4.83), yielding

$$v_{SS}(x, \mathbf{g}(x)) = v(x, \boldsymbol{y})|_{\boldsymbol{y}=\mathbf{g}(x)} = -\frac{c_6}{x^2}. \tag{4.238}$$

Similarly as in the *TD* control design, the control law is selected by defining a target system of the form

$$\dot{x} = -b_x (x - x^*), \tag{4.239}$$

where b_x is a control design parameter that defines the desired transient response of the collective pitch angular velocity of the blades. The associated control law that stabilizes the Σ_S-subsystem is therefore selected as

$$\begin{aligned} u_1(x, x^*) &= -a_8 x - a_{10} x^2 \sin\left(\mathrm{h}_{1_{\mathrm{SS}}}(x, \mathbf{g}(x))\right) - a_9 x^2 - a_{11} - b_x (x - x^*) \\ &= -a_8 x - a_{10} x^2 \sin\left(\mathrm{h}_{1_{\mathrm{SS}}}(x)\right) - a_9 x^2 - a_{11} - b_x (x - x^*). \end{aligned} \tag{4.240}$$

This concludes the $\mathcal{CF}$-*TD* control design.

4.7.3 Closed-Loop *Composite Feedback* Dynamics

After substituting the selected control laws, Eqns. (4.213) and (4.240), into the original nonlinear equations of motion, Eqns. (2.339–2.343), the closed loop system is given by

$$\dot{x} = a_{10} x^2 \left(\sin z_1 - \sin \mathrm{h}_{1_{\mathrm{SS}}}(x) \right) - b_x \left(x - x^* \right), \tag{4.241}$$

$$\dot{y}_1 = y_2, \tag{4.242}$$

$$\dot{y}_2 = x^2 \left(a_1 + a_2 z_1 - \sqrt{a_3 + a_4 z_1} \right) + a_5 y_2 + a_6 y_2^2 + a_7, \tag{4.243}$$

$$\dot{z}_1 = z_2, \tag{4.244}$$

$$\dot{z}_2 = -\tilde{b}_{z_1} \left(z_1 - \mathrm{h}_{1_c}(x, \boldsymbol{y}) \right) - \tilde{b}_{z_2} z_2, \tag{4.245}$$

where

$$\mathrm{h}_{1_c}(x, \boldsymbol{y}) = s_2 \left[\left(1 + \sqrt{s_3 v_s(x, \boldsymbol{y})} \right)^2 - 1 \right], \tag{4.246}$$

$$v_s(x,\boldsymbol{y}) = -\frac{a_9 y_2^2 + (a_9 + \tilde{b}_{y_2}) y_2 + \tilde{b}_{y_1}(y_1 - y_1^*) + c_6}{x^2}, \tag{4.247}$$

$$\mathrm{h}_{1_{SS}}(x,\mathbf{g}(x)) = s_2 \left[\left(1 + \sqrt{s_3 v_{SS}(x,\mathbf{g}(x))}\right)^2 - 1 \right], \tag{4.248}$$

$$v_{SS}(\tilde{x}, G(\tilde{x})) = -\frac{c_6}{(\tilde{x} + x^*)^2}. \tag{4.249}$$

The transient response of the ultra-fast dynamics is given by a second order time response of the form

$$\ddot{z}_1 = -\omega_{n_{z^*}}^2 (z_1 - \mathrm{h}_{1_c}(x,\boldsymbol{y})) - 2\omega_{n_{z^*}} \zeta_{z^*} \dot{z}_1, \tag{4.250}$$

with $\omega_{n_{z^*}}$ being the desired natural frequency of the closed-loop ultra-fast system, and ζ_{z^*} being the desired damping ratio of the ultra-fast dynamics, which can be defined as

$$\omega_{n_{z^*}} = \sqrt{b_{z_1}}, \tag{4.251}$$

$$\zeta_z = \frac{b_{z_2}}{2\omega n_{z^*}} = \frac{b_{z_2}}{2\sqrt{b_{z_1}}}, \tag{4.252}$$

which differ from those obtained in the *TD* control strategy, Eqns. (4.129–4.130), since the $\mathcal{CF}$-*TD* allows to select the desired transient response. The equilibria of the closed-loop system for $\mathcal{CF}$-*TD* is equivalent to those obtained with the *TD* control strategy, Eqns. (4.124–4.125) for the ultra-fast collective pitch dynamics, Eqns. (4.133–4.134) for the fast vertical displacement dynamics, and Eq. (4.140) for the slow angular velocity of the blades dynamics, with the only difference between both control strategies, being the transient response of the ultra-fast-dynamics, Eqns (4.251–4.252) vs. Eqns (4.129–4.130). The asymptotic stability analysis of the resulting closed-loop system will be conducted in future sections. Simulations are conducted to test the proposed control laws on the helicopter model, and significate results are presented in the following section.

4.8 Numerical Results

This section describes the sensitivity analysis conducted for the proposed control laws. The simulations are conducted using a fourth order Runge-Kutta fixed step integration method with an integration step of 0.01 seconds, and written in the *MATLAB* interface ®. The study is performed for the helicopter model, by conducting a sensitivity study for different conditions. For completeness, the conducted analysis of the closed-loop systems is only presented for the helicopter problem and organized as

- Results for the *TD* control design.
- Results for the *Composite Feedback TD* control design.

Similar as the performance analysis of the thrust coefficient models conducted in Appendix A, in order to evaluate the performance of the *TD* control laws, and the $\mathcal{CF}$ *TD* control design for the helicopter model, a sensibility analysis is conducted by performing the same four distinctive maneuvers that include all possible helicopter maneuvers

1. Ascent flight with increasing engine *RPM*.
2. Ascent flight with decreasing engine *RPM*.
3. Descent flight with increasing engine *RPM*.
4. Descent flight with decreasing engine *RPM*.

where once again, for completeness of the thesis, despite the extensive sensitivity analysis conducted, only four significate cases are presented, which correspond to a simulation that includes all four distinctive maneuvers in one simulation, and that are defined by the bellow conditions

1. $y_1(0) = 1.85\ m$, $y_1^* = 0.5\ m$, $x(0) = 120\ rad/sec$, and $x^* = 140\ rad/sec$.
2. $y_1(0) = 0.5\ m$, $y_1^* = 1\ m$, $x(0) = 140\ rad/sec$, and $x^* = 120\ rad/sec$.
3. $y_1(0) = 1\ m$, $y_1^* = 1.5\ m$, $x(0) = 120\ rad/sec$, and $x^* = 170\ rad/sec$.
4. $y_1(0) = 1.5\ m$, $y_1^* = 0.75\ m$, $x(0) = 170\ rad/sec$, and $x^* = 140\ rad/sec$.

Needs to be noted that starting with the second maneuver, it is assumed that the helicopter has reached the desired target altitude and angular rotation of the blades, implying that the initial conditions for the second, third, and fourth maneuver, are the selected as desired target conditions of the previous maneuvers respectively. For the case in which the helicopter has not reached the assigned target condition, the new maneuver will start at whenever condition the helicopter is at the moment of the change in set point. Each maneuver is lapsed with an interval of twenty seconds, and after that time, it is assigned the new set points independently if the helicopter has reached or not the desired set point.

Figures 4.7 and 4.11 show the time evolution of the vertical position (y_1), axial velocity (y_2), and vertical acceleration (a_y) of the helicopter, for both the *TD* and the $\mathcal{CF}$-*TD* control strategies respectively. Figures 4.8 and 4.12 show the time evolution of the remainder states, the angular velocity of the blades (x), the collective pitch angle (z_1), and the collective pitch rate of the blades (z_2) for both the *TD* and the $\mathcal{CF}$-*TD* control strategies respectively. Figures 4.9 and 4.13 show the time evolution of the control signals u_1 and u_2 for both the *TD* and the $\mathcal{CF}$-*TD* control strategies respectively. And finally, Figures 4.10 and 4.14 show the time evolution of significate aerodynamic parameters, the trust coefficient (C_T), the normalized vertical speed (V/V_{i_9}), and the climb inflow (λ_c), for both the *TD* and the $\mathcal{CF}$-*TD* control strategies respectively. All simulations demonstrate that both control strategies are able to drive the helicopter model to de desired set points with reasonable time response.

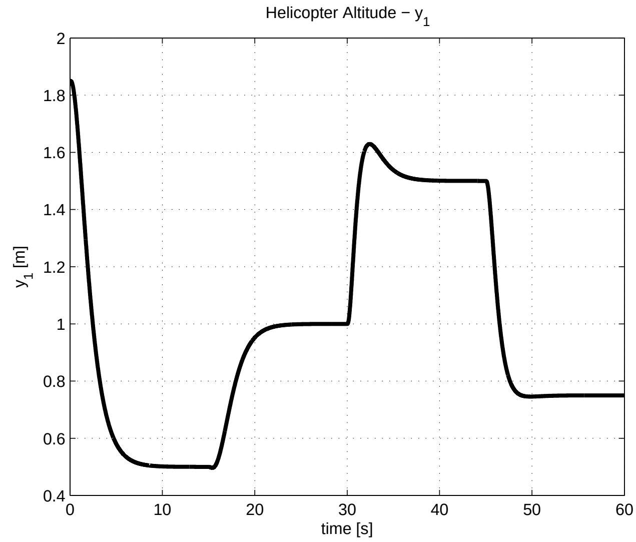

(a) y_1

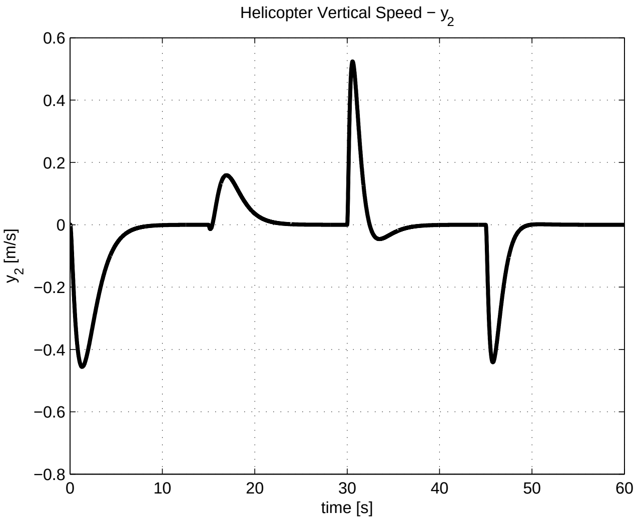

(b) y_2

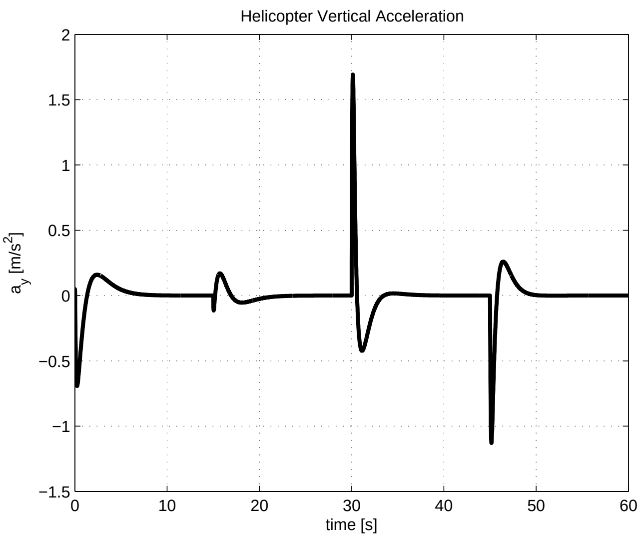

(c) a_y

Figure 4.7: States history for the *TD* control strategy.

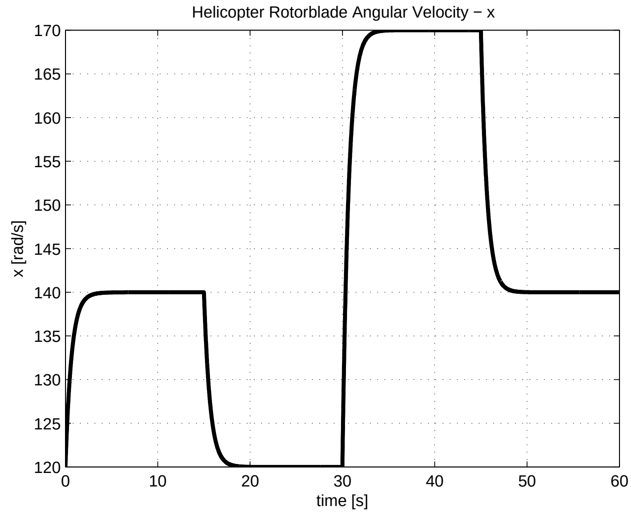

(a) x

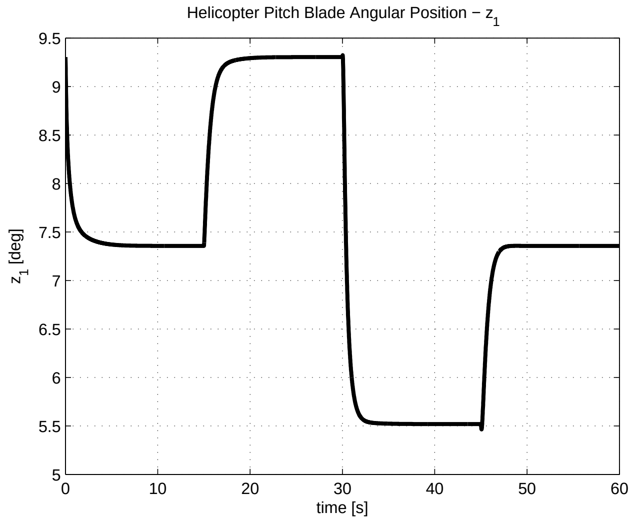

(b) z_1

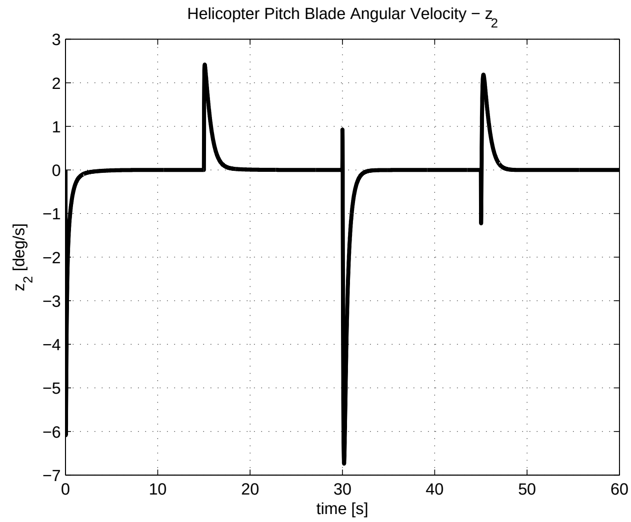

(c) z_2

Figure 4.8: States history for the *TD* control strategy.

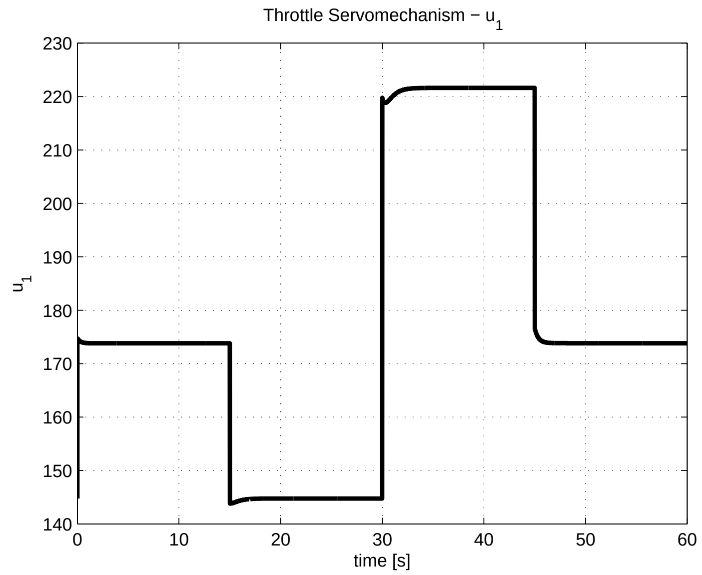

(a) u_1

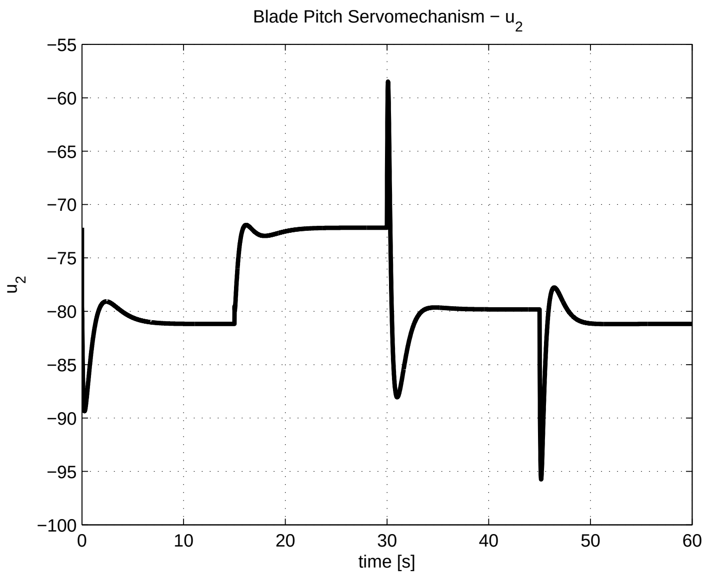

(b) u_2

Figure 4.9: Control signals history for the *TD* control strategy.

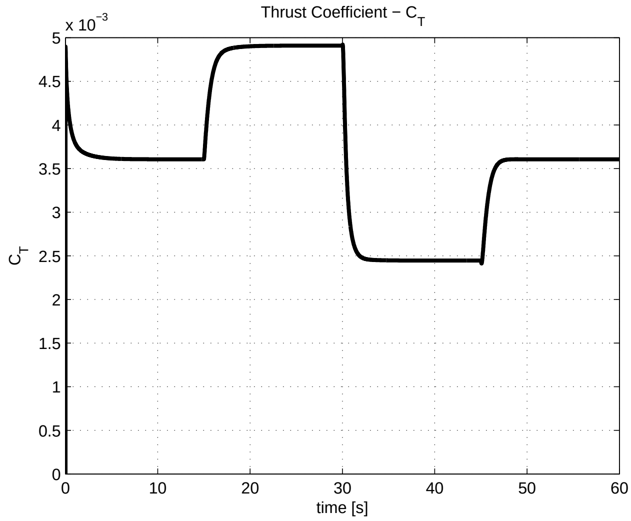

(a) C_T

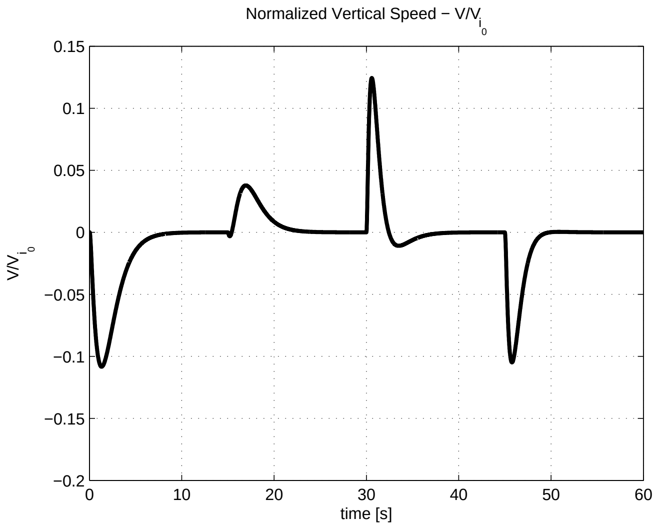

(b) y_2/v_i

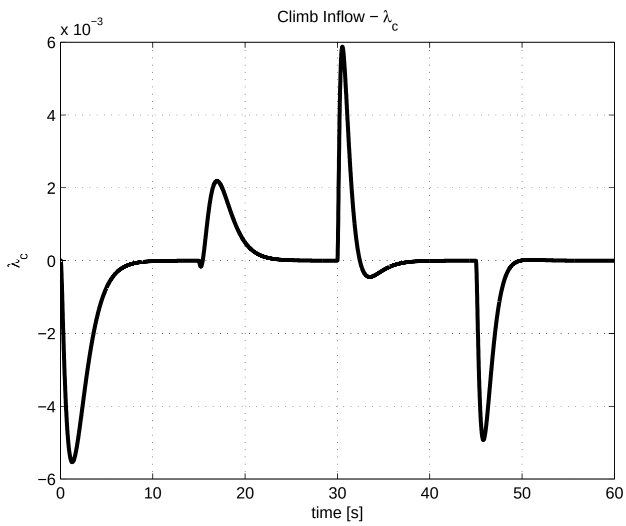

(c) λ_c

Figure 4.10: Significate aerodynamic parameters history for the *TD* control strategy.

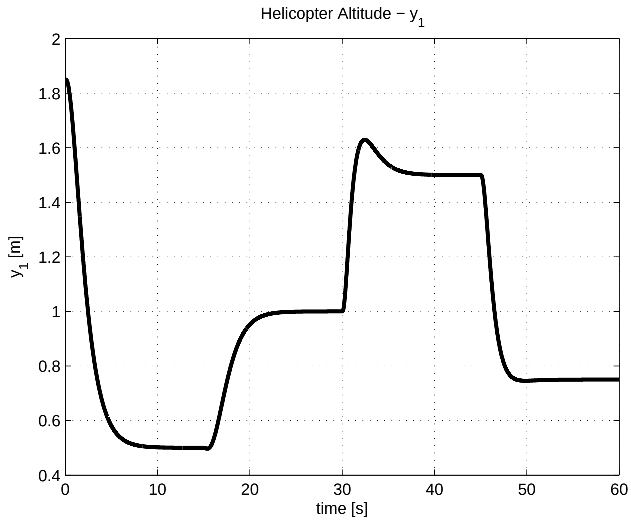

(a) y_1

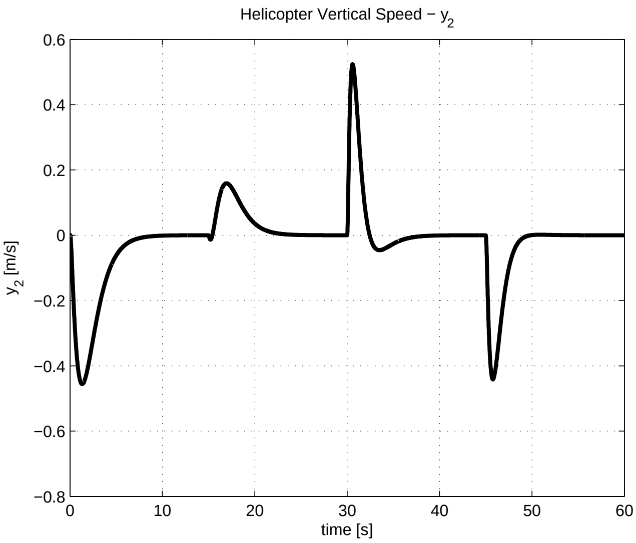

(b) y_2

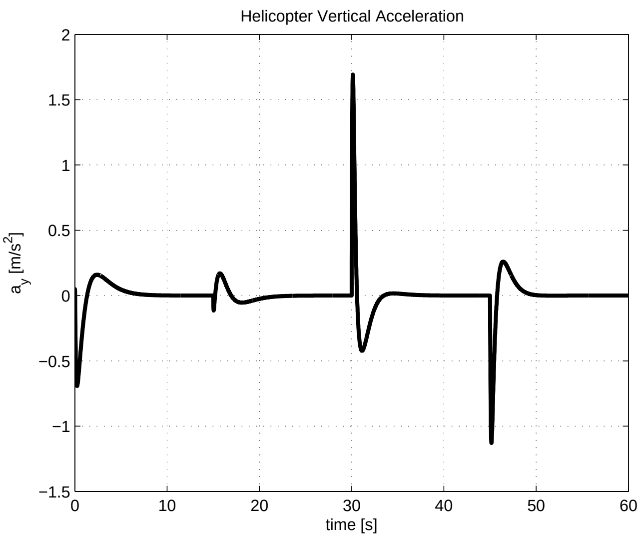

(c) a_y

Figure 4.11: States history for the $\mathcal{CF}$-TD control strategy.

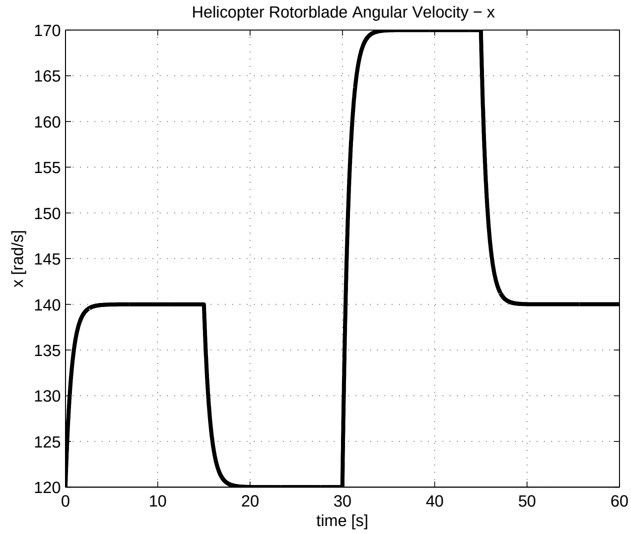

(a) x

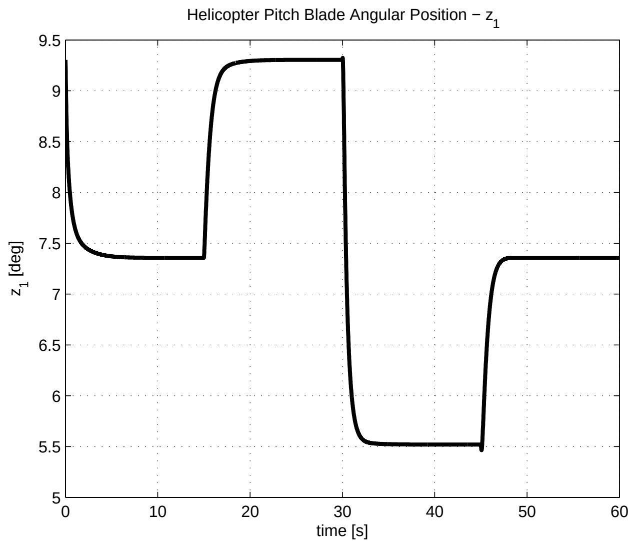

(b) z_1

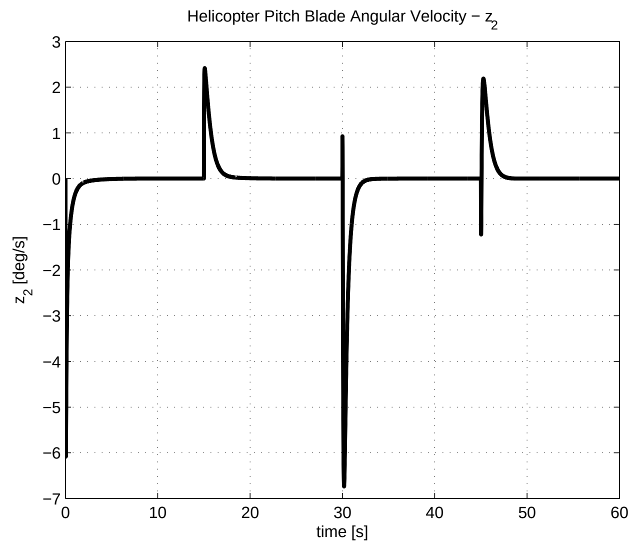

(c) z_2

Figure 4.12: States history for the $\mathcal{CF}$-TD control strategy.

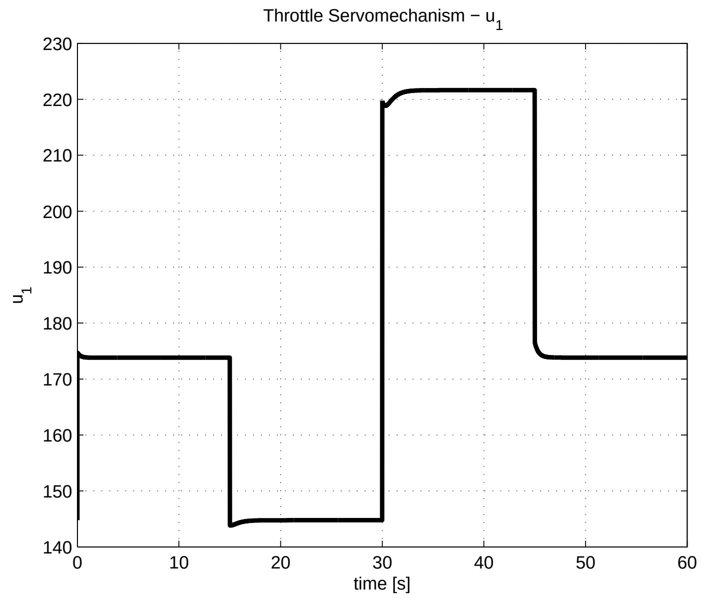

(a) u_1

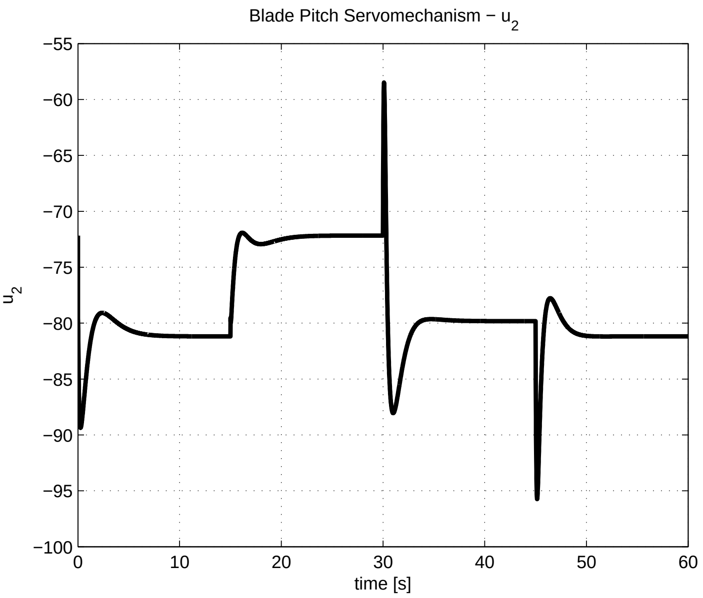

(b) u_2

Figure 4.13: Control signals history for the $\mathcal{CF}$-TD control strategy.

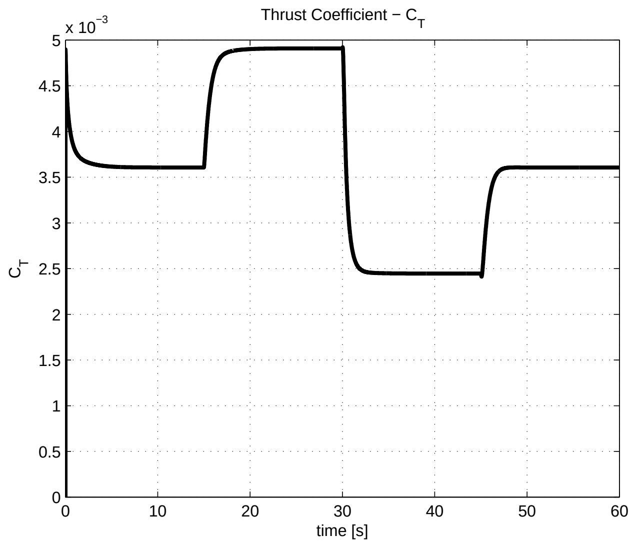

(a) C_T

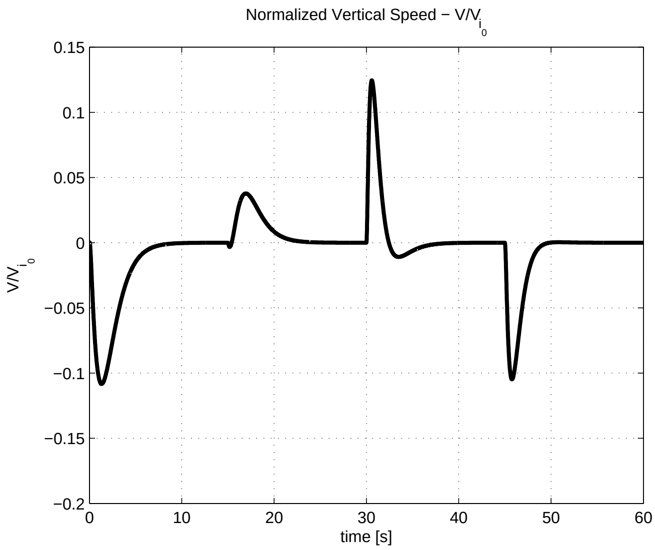

(b) y_2/v_i

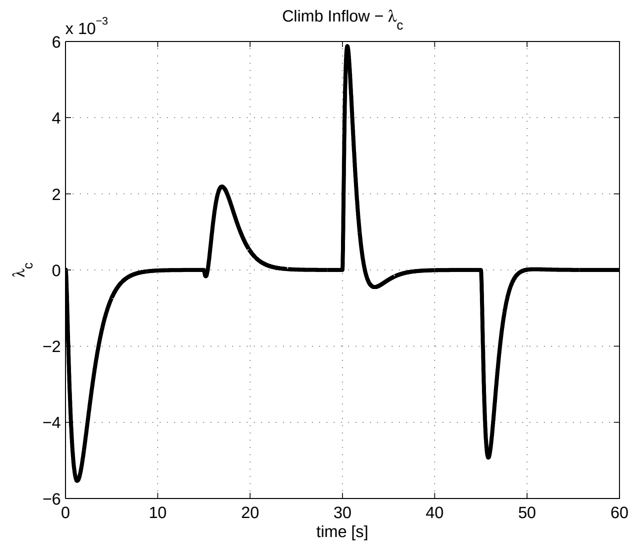

(c) λ_c

Figure 4.14: Significate aerodynamic parameters history for the $\mathcal{CF}$-TD control strategy.

4.9 Conclusions

The two presented control strategies, the *Top-Down* Control Design (TD), and the *Composite Feedback Top-Down* Control Design ($\mathcal{CF}$-TD), take advantage of the TD time-scale methodologies presented in chapter 3.

Both control strategies tackle the underactuated problem here studied by using a two-stage sequential strategy of the TD methodology, which results in two distinctive degenerated two-time-scale subproblems considerably simplified, that permits to easily obtain the appropriate control laws that stabilize each of the subsystems, the Σ_{FU} first, and the Σ_S secondly.

The first stage in the TD control strategy uses a sequential analysis to stabilize first the intermediate Σ_F-subsystem with the desired degree of stability, through the means of the control signal from the Σ_U-subsystem, and once has been stabilized, and assuming the ultra-fast Σ_U-subsystem becomes inherently stable with the control signal selected to stabilize the Σ_F-subsystem, then proceeds to stabilize the slowest Σ_S-subsystem with also a desired degree of stability by using the TD philosophy.

The $\mathcal{CF}$-TD control strategy uses a similar sequential application of the TD time-scale analysis, with the particularity that this methodology allows the user to define a prescribed degree of desired stability for the ultra-fast Σ_U-subsystem, therefore not being necessary to assume that the closed-loop ultra-fast subsystem has inherent stable properties. Following chapter will address the stability properties of the resulting closed-loop systems.

This page intentionally left blank

Chapter 5

Stability Analysis for the General Three-Time-Scale Singularly Perturbed System

5.1 Introduction

The three-time-scale helicopter problem here discussed, was previously identified as a three time-scale singular perturbation problem, chapter 3, and the appropriate control laws were designed using a sequential combination of two different time-scale problems using the proposed *TD* methodology, as seen in chapter 4. This chapter analyzes the properties that guarantee the asymptotic stability of the resulting autonomous systems for sufficiently small singular perturbation parameters, ε_1 and ε_2.

This is obtained by considering composite stability methods of large scale dynamical systems (Michel and Miller, 1977; Araki, 1978; Kokotović et al., 1986; Kokotović et al., 1987), which consider that the associated three-time-scale subsystems Σ_S, Σ_F, and Σ_U are each asymptotically stable, which is satisfied by the control design strategy described in chapter 4. This chapter derives the additional requirements that prove the asymptotic stability properties for the three-time-scale systems here studied by extending the well-known standard asymptotic stability requirements for the two-time-scale singular perturbation problems (Kokotović et al., 1987; Kokotović et al., 1986) to the three-time-scale problems here discussed.

The selected strategy, using a similar step-by-step process to the control strategy, obtains the associated Lyapunov functions for each of the subsystems based on the natural desired closed loop response of each of the resulting subsystem. This methodology, much simpler that the one employed in the existing multiparameter time-scale analysis (Abed, 1985d; Abed, 1985e; Abed, 1985b; Kokotović et al., 1987; Kokotović et al., 1986), permits to have Lyapunov function candidates for each of the defined subsystems a priori of starting the stability analysis, and with a simple structure, which differs from the alternative procedures, which derive the Lyapunov functions for the reduced order and boundary layer subsystems according to the fulfillment of the growth requirements that guarantee the asymptotic stability properties of the full system.

This translates to the fact that depending in the complexity of the growth requirements that need to satisfy the reduced order and boundary layer subsystems, the designer has to find appropriate Lyapunov functions for each of the subsystems, task that when encountering highly nonlinear problems like the one treated in this thesis, becomes an arduous task, which adds to the complexity of selecting proper comparison functions. The asymptotic stability analysis here presented does not relay on obtaining complex Lyapunov functions, since the Lyapunov structure is fixed a priori, reducing the fulfillment of the growth requirements among the different time-scale subsystems to obtain the appropriate comparison functions and demonstrating the growth requirements among the different subsystems.

The contents of this chapter include the general formulation for the asymptotic stability analysis of the two-time-scale singular perturbation problem, which is described in section 5.2; a description of the different three-time scale autonomous systems to be analyzed, is presented in section 5.3; the method proposed to derive the associated Lyapunov function is presented in section 5.4; and finally, the extension of the stability analysis to the general three-time-scale singular perturbation problem is presented in section 5.5, which is also extended to a more general N^{th}-order singular perturbed time-scale system in section 5.6.

For conciseness, this chapter only focusses on the asymptotic stability analysis of the general three-time-scale singularly perturbed autonomous system, and is left for Chapter 6, the asymptotic stability analysis for the three-time-scale helicopter model, while the stability analysis for the three-time-scale simplified model is left as a reference in Appendix C.

Also, for simplicity, and completeness of the thesis, the notation that indicates the different time-scale closed-loop subsystems is defined similarly as in the control design sections, that is, as a function of the form $\Sigma_{(\cdot)}$, where the subindex denotes the different subsystems. Note also that the state variables are now defined with the symbol $\tilde{\square}$, which denotes that the stability analysis will be conducted using their error dynamics formulation, as it will be defined in section 5.3.

5.2 Asymptotic Stability Analysis of a Two-Time-Scale Singularly Perturbed Autonomous System

The asymptotic stability analysis formulation for the general two-time-scale singular perturbation system outlined in this section, follows the well know theory of asymptotic stability analysis for two-time-scale singular perturbation problems (Kokotović et al., 1987; Kokotović et al., 1986). The general two-time-scale asymptotic stability analysis formulation serves as the basis for the proposed stability analysis for three-time-scale models. Although the two-time-scale formulation is a well established formulation, the author believes that by dedicating a section to recall the main important points of such theory, it will be easier for the reader to understand the extension to the three-time-scale asymptotic analysis that is conducted in the following sections. In order to start the general two-time-scale asymptotic formulation, let first recall the nonlinear autonomous two-time-scale singular perturbed system defined previously in Eqns. (3.1–3.2) and given by

$$\dot{x} = f(x,z), \; x \in \mathcal{R}^n, \tag{5.1}$$

$$\varepsilon \dot{z} = g(x,z), \; z \in \mathcal{R}^m, \tag{5.2}$$

which has an isolated equilibrium at the origin ($x = 0$, $z = 0$). Let also $B_x \subset \mathcal{R}^n$ and $B_z \subset \mathcal{R}^m$ denote closed sets. It is assumed throughout the formulation that f and g are smooth to ensure that for specified initial conditions, system (5.1-5.2) has a unique solution. The stability of the equilibrium is investigated by examining the reduced (slow) system given by

$$\dot{x} = f(x, \mathrm{h}(x)), \tag{5.3}$$

where $z = \mathrm{h}(x)$ is an associated root of $0 = g(x, z)$, and the boundary-layer (fast) system, which is given by

$$\frac{\mathrm{d}z}{\mathrm{d}\tau} = g(x, z(\tau)), \ \tau = \frac{t}{\varepsilon}, \tag{5.4}$$

where x is treated as a fixed parameter, and ε is the parasitic constant that defines the stretched time scale of the fast subsystem. The asymptotic stability properties of the singularly perturbed system can be defined by considering that if $x = 0$ is an asymptotically stable equilibrium of the reduced system, Eq. (5.3), $z = \mathrm{h}(x)$ is an asymptotically stable equilibrium of the boundary layer system, Eq. (5.4), uniformly in x, that is, the $\varepsilon - \delta$ definition of Lyapunov stability and convergence such that $z \to \mathrm{h}(x)$ are uniform in x (Vidyasagar, 2002), and if $f(\cdot,\cdot)$ and $g(\cdot,\cdot)$ satisfy certain growth conditions, then the origin is an asymptotically stable equilibrium of the singularly perturbed system defined by Eqns. (5.1–5.2).

These asymptotic stability requisites on the reduced and boundary-layer systems are expressed by requiring the existence of Lyapunov functions for both, the slow subsystem, and the fast subsystem, Eqns. (5.3) and (5.4), respectively, that satisfy certain growth conditions. The growth requirements of f and g take the form of inequalities that must be satisfied by the proposed Lyapunov functions. The following section describes in detail these growth requirement for the general two-time-scale singularly perturbed system.

5.2.1 Growth Requirements for the General Two-Time-Scale Singular Perturbation System

Prior to start defining the growth requirements, it is imperative to prove that the origin is a unique isolated equilibrium, which is presented in Assumption 5.2.1. The growth requirements of both the reduced and boundary layer system, separately, are addressed in Assumptions 5.2.2 and 5.2.3 respectively, while the growth requirements that combine both reduced and boundary layer system, called interconnection conditions, are defined in Assumptions 5.2.4 and 5.2.5, respectively. These assumptions are all described in detail bellow in their general two-time-scale formulation, which will be the basis for the extension to the three-time-scale formulation addressed in section 5.5.

Assumption 5.2.1 Isolated Equilibrium at the Origin
The origin ($x = 0$, $z = 0$) is a unique and isolated equilibrium of Eqns. (5.1-5.2), i.e.

$$0 = f(0, 0), \ \textit{and } 0 = g(0, 0), \tag{5.5}$$

moreover, $z = \mathrm{h}(x)$ is the unique root of the form given by

$$0 = g(x, z, 0), \tag{5.6}$$

in $B_x \times B_z$, i.e.

$$0 = g(x, \mathrm{h}(x)), \tag{5.7}$$

and there exists a class κ function $p(\cdot)$ such that

$$\| \mathrm{h}(x) \| \leq p\left(\| x \|\right). \tag{5.8}$$

To construct a Lyapunov function candidate for the singular perturbed system, Eqns. (5.1-5.2), let consider first each of the two systems separately. Let first consider the system in Eq. (5.1) by adding and subtracting $f(x, \mathrm{h}(x))$ to the right-hand side of Eq. (5.1) yielding

$$\dot{x} = f(x, \mathrm{h}(x)) + f(x, z) - f(x, \mathrm{h}(x)), \tag{5.9}$$

where the term $f(x,z) - f(x, \mathrm{h}(x))$ can be viewed as a perturbation of the reduced order system is given by

$$\dot{x} = f(x, \mathrm{h}(x)). \tag{5.10}$$

It is therefore natural to first satisfy the growth requirements for (5.10) and then consider the effect of the perturbation term $f(x,z) - f(x, \mathrm{h}(x))$. Therefore let proceed to define the reduced order growth condition.

Assumption 5.2.2 Reduced Order System Condition
There exists a positive-definite an decreasing Lyapunov function candidate $V(x)$ such that for all $x \in B_x$, satisfying that

$$0 < q_1 (\| x \|) \leq V(x) \leq q_2 (\| x \|), \tag{5.11}$$

for some class κ function $q_1(\cdot)$ and $q_2(\cdot)$ that satisfies the following inequality

$$\frac{\partial V}{\partial x} f(x, \mathrm{h}(x)) \leq -\alpha_1 \psi^2(x), \tag{5.12}$$

where $\psi(\cdot)$ is a scalar function of vector arguments which vanishes only when its argument are zero, and satisfying that $x = 0$ is a stable equilibrium of the reduced order system. Condition (5.12) guarantees that $x = 0$ is an asymptotically stable equilibrium of reduced order system (5.10).

Assumption 5.2.3 Boundary-Layer System Condition
There exists a positive-definite an decreasing Lyapunov function candidate $W(x,z)$ such that for all $(x,z) \in B_x \times B_z$, satisfying

$$0 < q_3 (\| z - \mathrm{h}(x) \|) \leq W(x,z) \leq q_4 (\| z - \mathrm{h}(x) \|), \tag{5.13}$$

for some class κ function $q_3(\cdot)$ and $q_4(\cdot)$, that satisfies

$$W(x,z) > 0, \ \forall z \neq \mathrm{h}(x) \text{ and } W(x, \mathrm{h}(x)) = 0, \tag{5.14}$$

and results in the following inequality

$$\frac{\partial W}{\partial z} g(x,z) \leq -\alpha_2 \phi^2(z - \mathrm{h}(x)), \ \alpha_2 > 0 \tag{5.15}$$

where $W(x,z)$ is a Lyapunov function of the boundary layer system (5.4), in which x is treated as a fixed parameter, and $\phi(\cdot)$ is a scalar function of vector arguments which vanishes only when its argument are zero, and satisfying that $z - \mathrm{h}(x)$ is a stable equilibrium of the boundary layer system.

Both $\psi(\cdot)$ and $\phi(\cdot)$ are scalar functions of vector arguments that vanish only when their arguments are zero, i.e., $\psi(x) = 0$ if and only if $x = 0$. Both $\psi(\cdot)$ and $\phi(\cdot)$, will be referred as comparison functions.

Assumption 5.2.4 First Interconnection Condition
$V(x)$ and $W(x,z)$ must satisfy the so called interconnection conditions. The first interconnection condition is obtained by computing the time derivative of $V(x)$ along the solution of Eq. (5.9), resulting in

$$\begin{aligned} \dot{V} &= \frac{\partial V}{\partial x} f(x, \mathrm{h}(x)) + \frac{\partial V}{\partial x} \left[f(x,z) - f(x, \mathrm{h}(x)) \right] \\ &\leq -\alpha_1 \phi^2(x) + \frac{\partial V}{\partial x} \left[f(x,z) - f(x, \mathrm{h}(x)) \right], \end{aligned} \tag{5.16}$$

where assuming that

$$\frac{\partial V}{\partial x} \left[f(x,z) - f(x, \mathrm{h}(x)) \right] \leq \beta_1 \phi(x) \phi(z - \mathrm{h}(x)). \tag{5.17}$$

so that

$$\dot{V} \leq -\alpha_1 \phi^2(x) + \beta_1 \phi(x)\phi(z - \mathrm{h}(x)). \tag{5.18}$$

Inequality (5.17) determines the allowed growth of f in z, and, in typical problems, verifying Assumption 5.2.4 reduces to verifying the following inequality

$$\|f(x,z) - f(x, \mathrm{h}(x))\| \leq \phi(x)\phi(z - \mathrm{h}(x)), \tag{5.19}$$

which implies that the rate of growth of f cannot be faster than the rate of growth of the comparison function $\phi(\cdot)$.

Assumption 5.2.5 Second Interconnection Condition
The second interconnection condition is defined by

$$\frac{\partial W}{\partial x} f(x,z) \leq \gamma \phi^2(z - \mathrm{h}(x)) + \beta_2 \phi(x)\phi(z - \mathrm{h}(x)), \tag{5.20}$$

where $\psi(\cdot)$ and $\phi(\cdot)$ are both scalar functions previously derived when satisfying Assumptions 5.2.2 and 5.2.3.

If assumptions 5.2.1, 5.2.2, 5.2.3, 5.2.4, and 5.2.5 are all satisfied, then the growth requirements of f and g are satisfied, and with the Lyapunov functions $V(x)$ and $W(x,z)$ obtained, a new Lyapunov function candidate $\nu(x,z)$ is considered and defined by the weighted sum of $V(x)$ and $W(x,z)$, and given by

$$\nu(x,z) = (1-d)V(x) + dW(x,z), \tag{5.21}$$

for $0 < d < 1$. The newly defined function $\nu(x,z)$ becomes the Lyapunov function candidate for the singular perturbed system (5.1-5.2). To explore the freedom when choosing the weights, let take d as an unspecified parameter $(0,1)$. From the properties of $V(x)$ and $W(x,z)$ and inequality (5.8) it follows that $\nu(x,z)$ is positive-definite and decreasing. Computing the derivative of $\nu(x,z)$ along the trajectories of Eqns. (5.1) and (5.2), results in

$$\begin{aligned} \dot{\nu} &= (1-d)\frac{\partial V}{\partial x} f(x,z) + \frac{d}{\varepsilon}\frac{\partial W}{\partial z} g(x,z) + d\frac{\partial W}{\partial x} f(x,z) \\ &= (1-d)\frac{\partial V}{\partial x} f(x,\mathrm{h}(x)) + (1-d)\frac{\partial V}{\partial x}\left[f(x,z) - f(x,\mathrm{h}(x))\right] \\ &+ \frac{d}{\varepsilon}\frac{\partial W}{\partial z} g(x,z) + d\frac{\partial W}{\partial x} f(x,z). \end{aligned} \tag{5.22}$$

Using inequalities (5.12), (5.15), (5.17), and (5.20), permits to express Eq. (5.22) as

$$\begin{aligned} \dot{\nu} &\leq -(1-d)\alpha_1\psi^2(x) + (1-d)\beta_1\psi(x)\phi(z-\mathrm{h}(x)) \\ &- \frac{d}{\varepsilon}\alpha_2\phi^2(z-\mathrm{h}(x)) + d\gamma\boldsymbol{\phi}^2(z-\mathrm{h}(x)) + d\beta_2\psi(x)\boldsymbol{\phi}(z-\mathrm{h}(x)) \\ &= -\begin{bmatrix} \psi(x) \\ \phi(z-\mathrm{h}(x)) \end{bmatrix}^T \begin{bmatrix} (1-d)\alpha_1 & -\frac{1}{2}(1-d)\beta_1 - \frac{1}{2}d\beta_2 \\ -\frac{1}{2}(1-d)\beta_1 - \frac{1}{2}d\beta_2 & d\left(\frac{\alpha_2}{\varepsilon} - \gamma\right) \end{bmatrix} \\ &\times \begin{bmatrix} \psi(x) \\ \phi(z-\mathrm{h}(x)) \end{bmatrix}. \end{aligned} \tag{5.23}$$

The right-hand side of inequality Eq. (5.23) is a quadratic form in the comparison functions $\psi(x)$ and $\phi(z - \mathrm{h}(x))$, where the quadratic form is negative-definite when

$$d(1-d)\alpha_1\left(\frac{\alpha_2}{\varepsilon} - \gamma\right) > \frac{1}{4}\left[(1-d)\beta_1 + d\beta_2\right]^2, \tag{5.24}$$

which is equivalent to

$$\frac{1}{\varepsilon} > \frac{1}{\alpha_1\alpha_2}\left[\alpha_1\gamma + \frac{1}{4(1-d)d}\left[(1-d)\beta_1 + d\beta_2\right]^2\right]. \tag{5.25}$$

Inequality (5.25) shows that for any choice of d, the corresponding $\nu(x,z)$ is a Lyapunov function for the singularly perturbed system (5.1–5.2) for all ε satisfying Eq. (5.25). Inequality (5.25) can be rewritten as

$$\varepsilon < \frac{\alpha_1\alpha_2}{\alpha_1\gamma + \frac{1}{4(1-d)d}\left[(1-d)\beta_1 + d\beta_2\right]^2} \equiv \varepsilon_d. \tag{5.26}$$

The dependance on the right-hand side of Eq. (5.26) on the unspecified parameter d is sketched in Figure 5.1. It can be easily checked that the maximum value of ε_d occurs at

$$d^* = \frac{\beta_1}{\beta_1 + \beta_2}, \tag{5.27}$$

being therefore

$$\varepsilon^* = \frac{\alpha_1\alpha_2}{\alpha_1\gamma + \beta_1\beta_2}. \tag{5.28}$$

Therefore it can be inferred that the equilibrium point of the singularly perturbed original system (5.1–5.2) is asymptotically stable for all $\varepsilon < \varepsilon^*$. The number ε^* is the best upper bound on ε that can be provided by the above presented stability analysis. The asymptotic stability analysis presented (Kokotović et al., 1986; Kokotović et al., 1987) can be summarizes in Theorem 5.2.1.

Theorem 5.2.1 *: Let inequalities (5.12), (5.15), (5.17), and (5.20) be satisfied. Then the origin is an asymptotically stable equilibrium of the singularly perturbed system (5.1–5.2) for all $\varepsilon \in (0, \varepsilon^*)$, where ε^* is given by (5.28). Moreover, for every number $d \in (0,1)$*

$$\nu(x,z) = (1-d_1)V(x) + d_1 W(x,y), \tag{5.29}$$

is a Lyapunov function for all $\varepsilon(0, \varepsilon_d)$, where $\varepsilon_d \leq \varepsilon^*$ is given by (5.26).

Theorem 5.2.1 can be summarized by understanding that if $x = 0$ is an asymptotically stable equilibrium of the reduced system, Eq. (5.3), $z = \mathrm{h}(x)$ is an asymptotically stable equilibrium of the boundary-layer system, Eq. (5.4), uniformly in x, that is, the $\varepsilon - \delta$ definition of *Lyapunov* stability and the convergence $z \to \mathrm{h}(x)$ are uniform in x (Vidyasagar, 2002), and if $f(\cdot,\cdot)$ and $g(\cdot,\cdot)$ satisfy the growth conditions on the reduced and boundary-layer systems, then the origin is an asymptotically stable equilibrium of the singularly perturbed system, Eqns. (5.1-5.2), for sufficiently small ε (Kokotović et al., 1986; Kokotović et al., 1987).

This concludes the asymptotic stability analysis for the general two-time-scale system. The extension to the three-time-scale systems is conducted in the following sections, and it is based in a double application of the two-time-scale asymptotic stability analysis employing either the *Top-Down* or the *Bottom-Up* time-scale analysis previously defined, although for the three-time-scale stability analysis conducted in this thesis is selected the *Bottom-Up* time-scale analysis.

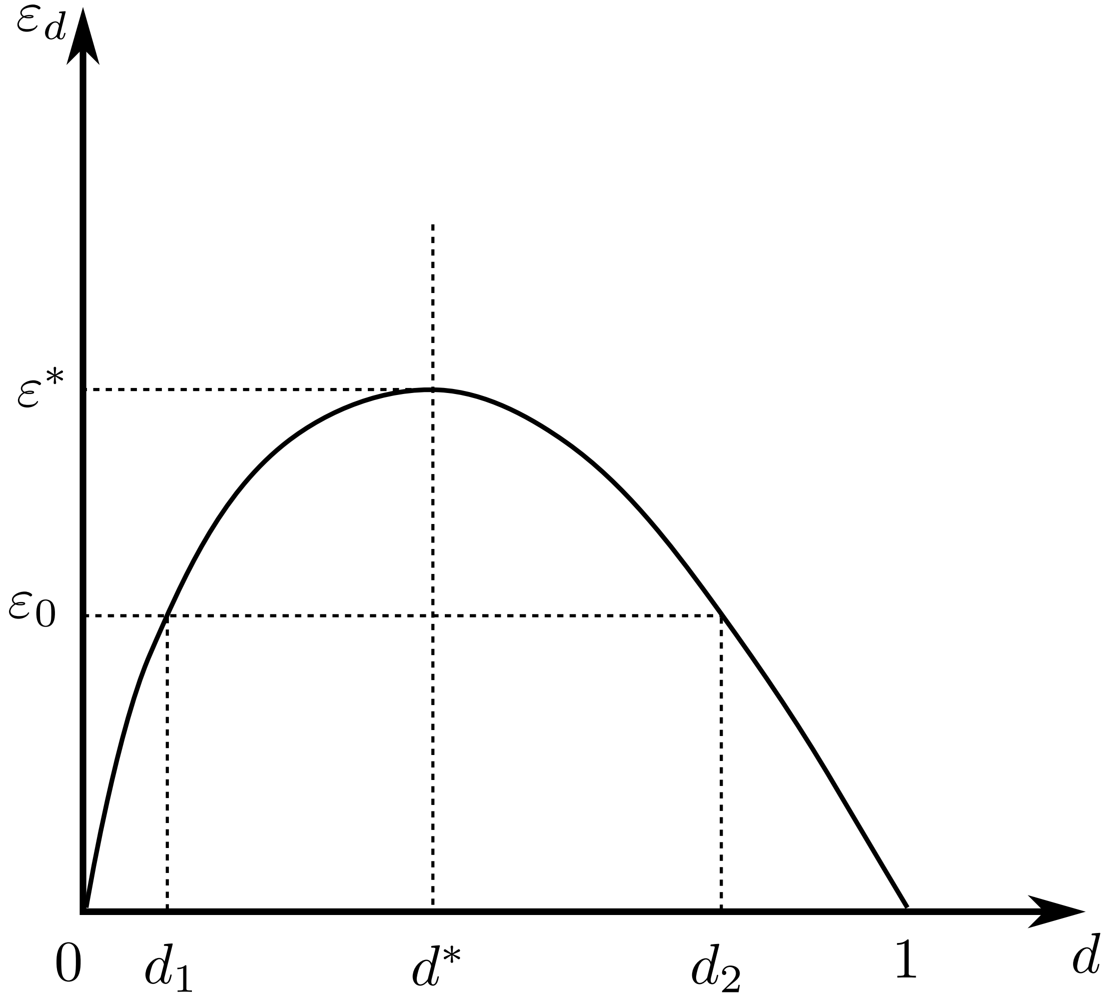

Figure 5.1: Stability upper bounds on ε (Kokotović et al., 1986).

5.3 Closed-Loop Error-Dynamics Model

As introduced in section 5.2.1, one of the requirements for the asymptotic stability analysis, is to guarantee that there exist asymptotic stability of the origin, which is expressed in Assumption 5.2.1. This translates to ensure that the boundary layer does not shift from its original equilibrium. Since the systems here studied present equilibria different from zero, in order to satisfy this requirement, a change of variables is introduced such that defines the new system in terms of its error-dynamics. For the three-time-scale helicopter model, the error dynamics are defined by introducing:

$$\tilde{x} = x - x^*, \tag{5.30}$$

$$\tilde{\boldsymbol{y}} = \boldsymbol{y} - \boldsymbol{y}^* = \begin{bmatrix} \tilde{y}_1 \\ \tilde{y}_2 \end{bmatrix} = \begin{bmatrix} x_1 - x_1^* \\ x_2 - x_2^* \end{bmatrix}, \tag{5.31}$$

$$\tilde{\boldsymbol{z}} = \boldsymbol{z} - \boldsymbol{z}^* = \begin{bmatrix} z_1 \\ z_2 \end{bmatrix} = \begin{bmatrix} z_1 - z_1^* \\ z_2 - z_2^* \end{bmatrix}, \tag{5.32}$$

where constants x^*, y_1^*, y_2^*, z_1^*, z_2^* represent the desired values of the states variables. Recall that, as discussed previously in the equilibrium analysis section, in order to have the helicopter at a given equilibrium position, that is, maintaining a stationery hover position, it is required that the vertical speed of the helicopter, y_2^*, and the collective pitch angular velocity of the blades, z_2^*, to be defined by $y_2^* = z_2^* = 0$. The desired collective pitch angle, z_1^*, can be obtained as a function of the selected angular velocity of the blades, x^* by using the equilibrium equation of the summation of the vertical forces, Eq. (2.356), therefore $z_1^* = z_1^*(x^*, y_1^*)$. It is proven in later sections that, both z_1^* and z_2^*, correspond with the solutions of quasi-steady-state equilibria of the ultra-fast dynamics, that is:

$$z_1^* = \mathrm{h}_1(x^*, \boldsymbol{y}^*), \tag{5.33}$$

$$z_2^* = \mathrm{h}_2(x^*, \boldsymbol{y}^*) = 0. \tag{5.34}$$

5.3.1 Singularly Perturbed Closed-Loop for the Helicopter Model

Recalling the three-time-scale helicopter model given by:

$$\dot{x} = a_8 x + a_{10} x^2 \sin z_1 + a_9 x^2 + a_{11} + u_1, \tag{5.35}$$

$$\varepsilon_1 \dot{y}_1 = c_1 y_2, \tag{5.36}$$

$$\varepsilon_1 \dot{y}_2 = x^2 (c_2 + c_3 z_1 - \sqrt{c_4 + c_5 z_1}) + a_9 y_2 + a_9 y_2^2 + c_6, \tag{5.37}$$

$$\varepsilon_1 \varepsilon_2 \dot{z}_1 = c_7 z_2, \tag{5.38}$$

$$\varepsilon_1 \varepsilon_2 \dot{z}_2 = a_9 z_1 + c_8 x^2 \sin z_1 + c_9 z_2 + c_{10} + c_{11} u_2, \tag{5.39}$$

the closed-loop dynamics are obtained substituting the control laws obtained in the *TD* control design section 4.4. Recall that the selected control laws for the *TD* control design, that is u_1 and u_2, are defined by

$$u_1 = -\left(a_8 x + a_{10} x^2 \sin \mathrm{h}_{1_{\mathrm{SS}}}(x, \mathbf{g}(x)) + a_9 x^2 + a_{11} + b_x (x - x^*)\right), \tag{5.40}$$

and

$$u_2 = K_b \left(1 + \sqrt{s_3 v(x, \boldsymbol{y})}\right)^2 + K_c + K_d x^2 \sin z_1, \tag{5.41}$$

with

$$v(x, \boldsymbol{y}) = -\frac{a_9 y_2^2 + \left(a_9 + \tilde{b}_{y_2}\right) y_2 + \tilde{b}_{y_1} (y_1 - y_1^*) + c_6}{x^2}, \tag{5.42}$$

and the coefficients of the control law are given by Eqns. (4.84–4.88). Therefore, after substituting the selected control laws, Eqs. (5.40) and (5.41), into the original nonlinear equations of motion, Eqs. (5.35 – 5.39), the closed loop system is given by:

$$\begin{aligned}
\dot{x} &= a_{10}x^2\left[\sin(z_1) - \sin \mathrm{h}_{1_{\mathrm{SS}}}(x)\right] - b_x(x - x^*), && (5.43)\\
\varepsilon_1\dot{y}_1 &= c_1 y_2, && (5.44)\\
\varepsilon_1\dot{y}_2 &= x^2(c_2 + c_3 z_1 - \sqrt{c_4 + c_5 z_1}) + a_9 y_2 + a_9 y_2^2 + c_6, && (5.45)\\
\varepsilon_1\varepsilon_2\dot{z}_1 &= c_7 z_2, && (5.46)\\
\varepsilon_1\varepsilon_2\dot{z}_2 &= a_9 z_1 + c_9 z_2 + J_2\left[\left(1 + \sqrt{s_3 v(x, \boldsymbol{y})}\right)^2 - 1\right]. && (5.47)
\end{aligned}$$

These closed-loop equations can be rewritten into its error dynamics formulation recalling the introduced error dynamics state vector (5.30–5.32) thus defining the closed-loop error dynamics as:

$$\begin{aligned}
\dot{\tilde{x}} &= a_{10}(\tilde{x} + x^*)^2\left[\sin(\tilde{z}_1 + z_1^*) - \sin \tilde{\mathrm{h}}_{1_{\mathrm{SS}}}(\tilde{x})\right] - b_x\tilde{x}, && (5.48)\\
\varepsilon_1\dot{\tilde{y}}_1 &= c_1\tilde{y}_2, && (5.49)\\
\varepsilon_1\dot{\tilde{y}}_2 &= (\tilde{x} + x^*)^2\left(c_2 + c_3(\tilde{z}_1 + z_1^*) - \sqrt{c_4 + c_5(\tilde{z}_1 + z_1^*)}\right) + a_9\tilde{y}_2 + a_9\tilde{y}_2^2 + c_6, && (5.50)\\
\varepsilon_1\varepsilon_2\dot{\tilde{z}}_1 &= c_7\tilde{z}_2, && (5.51)\\
\varepsilon_1\varepsilon_2\dot{\tilde{z}}_2 &= a_9(\tilde{z}_1 + z_1^*) + c_9\tilde{z}_2 + J_2\left[\left(1 + \sqrt{s_3\tilde{v}(x, \boldsymbol{y})}\right)^2 - 1\right], && (5.52)
\end{aligned}$$

where

$$K_e = K_c - a_{12} = -\frac{c_4}{c_5 c_{11} c_{13}}, \tag{5.53}$$

and

$$\begin{aligned}
\tilde{\mathrm{h}}_{1_{\mathrm{SS}}}(\tilde{x}, \mathbf{g}(\tilde{x})) &= s_2\left[\left(1 + \sqrt{s_3 v(x, \boldsymbol{y})}\right)^2 - 1\right], && (5.54)\\
\tilde{v}_{SS}(\tilde{x}, \mathbf{g}(\tilde{x})) &= -\frac{c_6}{(\tilde{x} + x^*)^2}, && (5.55)\\
\tilde{v}(\tilde{x}, \tilde{\boldsymbol{y}}) &= -\frac{a_9\tilde{y}_2^2 + (a_9 + \tilde{b}_{y_2})\tilde{y}_2 + \tilde{b}_{y_1}\tilde{y}_1 + c_6}{(\tilde{x} + x^*)^2}. && (5.56)
\end{aligned}$$

5.4 Lyapunov Function Candidates

The selection of proper Lyapunov functions to study the asymptotic stability properties of an autonomous system is one of the most challenging issues that a control engineer has to be faced with. The asymptotic stability analysis of the different time-scales requires the existence of Lyapunov functions for each one of the singularly perturbed subsystems, that is the Σ_S, Σ_F, and Σ_U-subsystems. The fulfillment of certain growth requirements between each of the Lyapunov functions, and the use of composite stability methods (Kokotović et al., 1999; Kokotović et al., 1987; Michel and Miller, 1977) ensures the existence of a composite Lyapunov function for the entire Σ_{SFU} system.

This sections describes the methods proposed in this thesis to determine the associated composite Lyapunov function that proves the asymptotic stability properties of the full Σ_{SFU} system. The philosophy employed to determine the Lyapunov functions for the associated time-scale subsystems uses the *TD* and *BU* time-scale decomposition philosophy, derived in chapter 3.

The strategy to determine the Lyapunov function candidates for each one of the singularly perturbed Σ_S, Σ_F, and Σ_U subsystems, consists on treating the three different time scales as two-distinct two-time-scale singular perturbed problems. The proposed methodology obtains the associated Lyapunov functions for each of the subsystems by taking advantage of the same properties that were exploited in the time-scale analysis, that is, the sequential application of both the *TD* and *BU* methodologies, which in return translates to a considerably simplification of the Lyapunov function selection.

The following sections describe in more detail the procedure to obtain the associated Lyapunov function candidates for a generic three-time-scale singularly perturbed system, and later extending the methodology to obtain the associated Lyapunov functions for the simplified example, and the helicopter model.

5.4.1 General *TD-BU* Lyapunov Function Candidate Selection

This section describes the general Lyapunov *TD* and *BU*, ($\mathcal{L}$-*TD-BU*), function candidate selection for the three-time-scale singularly perturbed closed-loop systems.

The strategy to determine the Lyapunov candidates for each one of the singularly perturbed Σ_S, Σ_F, and Σ_U subsystems, consists on treating the three different time-scales as two distinct two-time-scale singular perturbed problems. The following subsections describe in detail the two-distinct two-time-scale singularly perturbed subproblems, the $\mathcal{L}$-*TD* and $\mathcal{L}$-*BU*, that help in the selection of the Lyapunov function candidates for each of the singularly perturbed subsystems Σ_S, Σ_F, and Σ_U.

5.4.1.1 General Lyapunov Function Candidate for the Σ_S-Subsystem

The Lyapunov function candidate for the Σ_S-subsystem is obtained by applying the Lyapunov-*BU* ($\mathcal{L}$-*BU*) methodology, which, in a similar manner as the *BU* time-scale analysis, section 3.4.2, analyzes the subsystem resulting when considering the time-scale obtained when applying the stretched time-scale $\tau_2 = t/\varepsilon_1\varepsilon_2$, which in return results in the reduced (slow) Σ_{SF}-subsystem, Eqns. (3.69–3.70), and the associated boundary layer (fast) Σ_U-subsystem, Eq. (3.71), with the boundary layer Σ_U-subsystem's associated quasi-steady-state given by Eq. (3.72).

The associated Lyapunov function for the Σ_S-subsystem is obtained by recognizing that the boundary layer Σ_{SF}-subsystem, Eqns. (3.69–3.70), can be treated again like a two-time-scale singular perturbation problem by applying the stretched time-scale $\tau_1 = t/\varepsilon_1$, resulting in the new reduced (slow) Σ_S-subsystem, Eq. (3.73), and the associated new boundary layer (fast) Σ_F-subsystem, Eq. (3.74), and with the Σ_F-subsystem quasi-steady-state equilibrium given by Eq. (3.75).

Recall that following the control design strategy, the control signal u_1 was selected such that stabilizes the Σ_S-subsystem with a prescribed desired target dynamics, therefore being easy to define the Lyapunov function for the slow Σ_S-subsystem as the natural Lyapunov function of the selected target dynamics, denoted as $\mathcal{V}_S(\tilde{x})$.

5.4.1.2 General Lyapunov Function Candidate for the Σ_F-Subsystem

To obtain the Lyapunov function candidate for the Σ_F-subsystem let use the Lyapunov-*TD* ($\mathcal{L}$-*TD*) methodology, which, in a similar manner as in the *TD* time-scale analysis, section 3.4.1, analyzes the subsystem resulting when considering the time-scale defined by applying the stretched time-scale given by $\tau_1 = t/\varepsilon_1$, yielding the reduced order (slow) Σ_S-subsystem, Eq. (3.61), and the boundary layer (fast) Σ_{FU}-subsystem, Eqns. (3.62–3.63), with the associated quasi-steady-state equilibria of the boundary layer Σ_{FU}-subsystem being given by Eqns. (3.65–3.65).

The associated Lyapunov function for the Σ_F-subsystem is obtained by exploiting the fact that the boundary layer Σ_{FU}-subsystem, Eqns. (3.65–3.65), can be treated again like a two-time-scale singular perturbation problem, by applying the stretched time-scale given by $\tau_2 = \tau_1/\varepsilon_2 = t/\varepsilon_1\varepsilon_2$, resulting in a new reduced (slow) Σ_F-subsystem, Eq. (3.66), and a new boundary layer (fast) Σ_U-subsystem, Eq. (3.67), with its associated quasi-steady-state equilibrium defined by Eq. (3.68).

Recalling that following the control strategy methodology, the control signal u_2 is selected such that stabilizes the Σ_F-subsystem with a prescribed desired target dynamics, therefore, when substituting the equilibrium of the Σ_U-subsystems into Eq. (3.66), that is, substituting $\tilde{\mathrm{h}}(\tilde{x}, \tilde{y})$, yields the Σ_F-subsystem defined by the selected desired target dynamics, therefore being easy to define the Lyapunov function for the intermediate Σ_F-subsystem as the natural Lyapunov of the selected target dynamics, $\mathcal{V}_F(\tilde{y})$. The Σ_F-subsystem serves as both the boundary layer of the Σ_{SF}-subsystem, and the reduced order of the Σ_{FU}-subsystem, becoming the interconnection subsystem between the Σ_{SF} and Σ_{FU}-subsystems.

5.4.1.3 General Lyapunov Function Candidate for the Σ_U-Subsystem

The natural Lyapunov function candidate for the Σ_U-subsystem is obtained by recalling and analyzing the boundary layer of the Σ_U-subsystem resulting from the *Down* sequence of the $\mathcal{L}$-*TD* and given by Eq. (3.67). Recall that it is necessary to ensure that the boundary layer Σ_U-subsystem does not to shift from the equilibrium $\tilde{z} = \tilde{\mathrm{h}}(\tilde{x}, \tilde{y})$, since it is the equilibrium that defines the nature of the different reduced order subsystems, Σ_S and Σ_F-subsystems. It is therefore necessary to introduce a change of variables so that the equilibrium of this boundary-layer system is centered at zero, and thus permitting to select a natural Lyapunov function candidate that maintains the equilibrium $\tilde{z} = \tilde{\mathrm{h}}(\tilde{x}, \tilde{y})$. This is obtained by introducing a change of variables defined by the error dynamics between the fast variable, and its quasi-steady-state equilibrium that is

$$\hat{z} = \tilde{z} - \tilde{\mathrm{h}}(\tilde{x}, \tilde{y}). \tag{5.57}$$

The change of variables permits to express the boundary layer subsystem, Eq. (3.67), as a linear function of $\hat{z}$, thus being quite easy to select its natural associated Lyapunov function $\mathcal{V}_U(\tilde{z} - \tilde{\mathrm{h}}(\tilde{x}, \tilde{y}))$. The following sections extend this general formulation of the appropriate Lyapunov function candidates for all three subsystem for the three-time-scale singularly perturbed helicopter model.

5.4.2 Lyapunov *Top-Dow* and *BU* Function Candidate Selection for the Helicopter Model

This section determines the associated Lyapunov functions for the closed-loop three-time-scale singular perturbed helicopter model which is defined by Eqns. (5.48–5.52), where, similarly as for the general case, it is assumed that the system is an autonomous stable system with a prescribed stability properties given by the selection of appropriate control laws. The strategy to determine the Lyapunov candidates for each one of the singularly perturbed Σ_S, Σ_F, and Σ_U subsystems, consists on treating the three different time scales as two distinct two-time-scale singular perturbed problems. The following sections describe the selection of the Lyapunov function candidates for each of the singularly perturbed subsystems Σ_S, Σ_F, and Σ_U.

5.4.2.1 Lyapunov Function Candidate for the Helicopter Model Σ_S-Subsystem

The Lyapunov function candidate for the Σ_S-subsystem, uses the Lyapunov-*BU* ($\mathcal{L}$-*BU*) methodology previously presented, where by applying the stretched time-scale given by $\tau_2 = t/\varepsilon_1\varepsilon_2$, yields the reduced (slow) Σ_{SF}-subsystem defined by

$$\begin{aligned}
\dot{\tilde{x}} &= a_{10}(\tilde{x}+x^*)^2(\sin(\tilde{\mathrm{h}}_1(\tilde{x},\tilde{\boldsymbol{y}})+z_1^*)-\sin\tilde{\mathrm{h}}_{1_{\mathrm{SS}}})-b_x\tilde{x}, && (5.58)\\
\varepsilon_1\dot{\tilde{y}}_1 &= c_1\tilde{y}_2, && (5.59)\\
\varepsilon_1\dot{\tilde{y}}_2 &= (\tilde{x}+x^*)^2\left(c_2+c_3(\tilde{\mathrm{h}}_1(\tilde{x},\tilde{\boldsymbol{y}})+z_1^*)-\sqrt{c_4+c_5(\tilde{\mathrm{h}}_1(\tilde{x},\tilde{\boldsymbol{y}})+z_1^*)}\right)+a_9\tilde{y}_2\\
&+ a_9\tilde{y}_2^2+c_6, && (5.60)
\end{aligned}$$

and the boundary layer (fast) subsystem for the BU subproblem is defined by the Σ_U-subsystem

$$\begin{aligned}
\frac{d\tilde{z}_1}{d\tau_2} &= c_7\tilde{z}_2, && (5.61)\\
\frac{d\tilde{z}_2}{d\tau_2} &= a_9(\tilde{z}_1+z_1^*)+c_9\tilde{z}_2+J_2\left[\left(1+\sqrt{s_3\tilde{v}(\tilde{x},\tilde{\boldsymbol{y}})}\right)^2-1\right], && (5.62)
\end{aligned}$$

with the quasi-steady-state equilibria being given by

$$0=\hat{\boldsymbol{h}}(\tilde{x},\tilde{\boldsymbol{y}},\tilde{\boldsymbol{z}})\rightarrow\tilde{\boldsymbol{z}}=\tilde{\mathbf{h}}(\tilde{x},\tilde{\boldsymbol{y}})=\begin{bmatrix}\tilde{\mathrm{h}}_1(\tilde{x},\tilde{\boldsymbol{y}})\\ \tilde{\mathrm{h}}_2(\tilde{x},\tilde{\boldsymbol{y}})\end{bmatrix}, \tag{5.63}$$

with

$$\begin{aligned}
\tilde{\mathrm{h}}_1(\tilde{x},\tilde{\boldsymbol{y}}) &= \tilde{z}_1=s_2\left[\left(1+\sqrt{s_3\tilde{v}(\tilde{x},\tilde{\boldsymbol{y}})}\right)^2-1\right]-z_1^* && (5.64)\\
h_2(\tilde{x},\tilde{\boldsymbol{y}}) &= \tilde{z}_2=0, && (5.65)
\end{aligned}$$

and with s_2 defined in Eq. (4.103). The associated Lyapunov function for the Σ_S-subsystem is obtained by recognizing that the boundary layer Σ_{SF}-subsystem, Eqns. (5.58–5.60) can be treated again like a two-time-scale singular perturbation problem by applying the stretched-time-scale given by $\tau_1=t/\varepsilon_1$, resulting in the new reduced (slow) Σ_S-subsystem, which is now defined by

$$\dot{\tilde{x}} = \tilde{f}(\tilde{x},\tilde{\mathbf{g}}(\tilde{x}),\tilde{\mathbf{h}}(\tilde{x},\tilde{\boldsymbol{y}}))=a_{10}(\tilde{x}+x^*)^2\left[\sin(\tilde{\mathrm{h}}_1(\tilde{x},\tilde{\boldsymbol{y}})+z_1^*)-\sin\tilde{\mathrm{h}}_{1_{\mathrm{SS}}}\right]-b_x\tilde{x}, \tag{5.66}$$

and where the new boundary layer (fast) Σ_F-subsystem is defined as

$$\begin{aligned}
\frac{d\tilde{y}_1}{d\tau_1} &= c_1\tilde{y}_2, && (5.67)\\
\frac{d\tilde{y}_2}{d\tau_1} &= (\tilde{x}+x^*)^2\left[c_2+c_3(\tilde{\mathrm{h}}_1(\tilde{x},\tilde{\boldsymbol{y}})+z_1^*)-\sqrt{c_4+c_5(\tilde{\mathrm{h}}_1(\tilde{x},\tilde{\boldsymbol{y}})+z_1^*)}\right]\\
&+ a_9\tilde{y}_2+a_9\tilde{y}_2^2+c_6. && (5.68)
\end{aligned}$$

After substituting the Σ_U-subsystem equilibria, Eqns. (5.64–5.65), into the Σ_F-subsystem, Eqns. (5.67–5.68), reduces to

$$\begin{aligned}
\frac{d\tilde{y}_1}{d\tau_1} &= c_1\tilde{y}_2, && (5.69)\\
\frac{d\tilde{y}_2}{d\tau_1} &= -\tilde{b}_1\tilde{y}_1-\tilde{b}_2\tilde{y}_2, && (5.70)
\end{aligned}$$

where it can be identified that the resulting Σ_F-subsystem can be expressed in state space form as

$$\frac{d\tilde{y}}{d\tau_1}=\boldsymbol{A_F}\tilde{y}, \tag{5.71}$$

being

$$\boldsymbol{A_F}=\begin{pmatrix}0 & c_1\\ -\tilde{b}_{y_1} & -\tilde{b}_{y_2}\end{pmatrix}, \tag{5.72}$$

therefore being the quasi-steady-state equilibria for the Σ_F-subsystem, $\tilde{G}(\tilde{x})$, being given by

$$0 = \hat{\boldsymbol{g}}(\tilde{x}, \tilde{\boldsymbol{y}}, \tilde{\boldsymbol{z}}) \rightarrow \tilde{\boldsymbol{y}} = \tilde{\mathbf{g}}(\tilde{x}) = \begin{bmatrix} \tilde{g}_1(\tilde{x}) \\ \tilde{g}_2(\tilde{x}) \end{bmatrix}, \tag{5.73}$$

with the equilibria defined by

$$\tilde{g}_1(\tilde{x}) = y_1^*, \tag{5.74}$$

$$\tilde{g}_2(\tilde{x}) = 0, \tag{5.75}$$

therefore reducing the Σ_S-subsystem, Eq. (5.66), as

$$\dot{\tilde{x}} = \tilde{f}(\tilde{x}, \tilde{\mathbf{g}}(\tilde{x}), \tilde{\mathbf{h}}(\tilde{x}, \tilde{\mathbf{g}}(x))) = -b_x \tilde{x}. \tag{5.76}$$

With this in mind, it is easy to define the associated Lyapunov function for the slow Σ_S-subsystem as the natural quadratic Lyapunov function of the selected target dynamics, that is

$$V_S(\tilde{x}) = \frac{1}{2} P_S \tilde{x}^2, \tag{5.77}$$

where P_S is the solution of the associated Lyapunov function for the selected target dynamics and given by

$$P_S A_S + A_S P_S + Q_S = 0, \tag{5.78}$$

where Q_S is also a positive constant, $A_S = -b_x$, and P_S is given by

$$P_S = \frac{Q_S}{2b_x}, \tag{5.79}$$

where Q_S is a positive constant. Note that for completeness, and to avoid confusion due to the use of similar parameters that defined the Lyapunov functions, $V_{(\cdot)}$, the elements of the associated Lyapunov function, $P_{(\cdot)}$ and $Q_{(\cdot)}$, the closed-loop state-space systems, $A_{(\cdot)}$, and other parameters throughout the rest of the thesis, the subindexes of these parameters will identify to which model is referring, that is, the parameters that deal with the simplified model, will be denoted with lower case, i.e. V_s, while for the helicopter model will be denoted with capital letters, i.e. V_S.

5.4.2.2 Lyapunov Function Candidate for the Helicopter Model Σ_F-Subsystem

The Lyapunov function candidate for the Σ_F-subsystem is obtained using the Lyapunov-*TD* ($\mathcal{L}$-*TD*) methodology, by applying the *Top*-condition, which results in the reduced order (slow) Σ_S-subsystem defined by Eq. (5.66), and the boundary layer (fast) Σ_{FU}-subsystem given by

$$\frac{d\tilde{y}_1}{d\tau_1} = c_1 \tilde{y}_2, \tag{5.80}$$

$$\frac{d\tilde{y}_2}{d\tau_1} = (\tilde{x} + x^*)^2 \left(c_2 + c_3(\tilde{z}_1 + z_1^*) - \sqrt{c_4 + c_5(\tilde{z}_1 + z_1^*)} \right) + a_9 \tilde{y}_2 + a_9 \tilde{y}_2^2 + c_6, \tag{5.81}$$

$$\varepsilon_2 \frac{d\tilde{z}_1}{d\tau_1} = c_7 \tilde{z}_2, \tag{5.82}$$

$$\varepsilon_2 \frac{d\tilde{z}_2}{d\tau_1} = a_9(\tilde{z}_1 + z_1^*) + c_9 \tilde{z}_2 + J_2 \left[\left(1 + \sqrt{s_3 \tilde{v}(\tilde{x}, \tilde{\boldsymbol{y}})} \right)^2 - 1 \right]. \tag{5.83}$$

The associated Lyapunov functions for the Σ_F-subsystem is obtained by recognizing that the boundary layer Σ_{FU}-subsystem, Eqns. (5.80-5.83), can be decoupled into a two-time-scale singular perturbation problem by applying the stretched time-scale given by $\tau_2 = \tau_1/\varepsilon_2 = t/\varepsilon_1\varepsilon_2$, where the new reduced (slow) Σ_F-subsystem for the helicopter model is defined by Eqns. (5.69–5.70), which reduces to the selected target fast-dynamics

$$\begin{aligned}\frac{d\tilde{y}_1}{d\tau_1} &= c_1\tilde{y}_2 \\ \frac{d\tilde{y}_2}{d\tau_1} &= -\tilde{b}_{y_1}\tilde{y}_1 - \tilde{b}_{y_2}\tilde{y}_2,\end{aligned} \tag{5.84}$$

which can be rewritten in state-space as seen in Eq. (5.71). and where the new boundary layer Σ_U-subsystem of the Σ_{FU}-subsystem is given by Eqns. (5.61–5.62). It is therefore easy to select a natural Lyapunov function $V_F(\tilde{y})$ of the form

$$V_F(\tilde{y}) = \frac{1}{2}\tilde{\boldsymbol{y}}^T\boldsymbol{P_F}\tilde{\boldsymbol{y}}, \tag{5.85}$$

with $\boldsymbol{P_F}$ is a positive definite matrix that solves the associated Lyapunov equation

$$\boldsymbol{P_F}\boldsymbol{A_F} + \boldsymbol{A_F}^T\boldsymbol{P_F} + \boldsymbol{Q_F} = 0, \tag{5.86}$$

where $\boldsymbol{Q_F}$ and $\boldsymbol{P_F}$ are a positive definite matrices of the form

$$\boldsymbol{Q_F} = \begin{pmatrix} q_{f_1} & 0 \\ 0 & q_{f_2}\end{pmatrix}, \tag{5.87}$$

$$\boldsymbol{P_F} = \begin{pmatrix} p_{f_1} & p_{f_3} \\ p_{f_3} & p_{f_2}\end{pmatrix}, \tag{5.88}$$

where $\boldsymbol{P_F} = \boldsymbol{P_F}^T$. Solving Eq. (5.86) yields the Lyapunov function for the Σ_F-subsystem

$$V_F(\tilde{y}) = \frac{1}{2}\tilde{\boldsymbol{y}}^T\boldsymbol{P_F}\tilde{\boldsymbol{y}} = \frac{1}{2}p_{f_1}\tilde{y}_1^2 + \frac{1}{2}p_{f_3}\tilde{y}_2^2 + p_{f_2}\tilde{y}_1\tilde{y}_2, \tag{5.89}$$

with the solutions to the associated Lyapunov Eq. (5.86) given as

$$p_{f_1} = \frac{q_{f_1}(\tilde{b}_{y_1}c_1 + \tilde{b}_{y_2}^2) + \tilde{b}_{y_1}^2 q_{f_2}}{2\tilde{b}_{y_1}\tilde{b}_{y_2}c_1} = C_{f_1}q_{f_1} + C_{f_2}q_{f_2}, \tag{5.90}$$

$$p_{f_2} = \frac{q_{f_1}}{2\tilde{b}_{y_1}} = C_{f_3}q_{f_1}, \tag{5.91}$$

$$p_{f_3} = \frac{q_{f_1}c_1 + q_{f_2}\tilde{b}_{y_1}}{2\tilde{b}_{y_1}\tilde{b}_{y_2}} = C_{f_4}q_{f_1} + C_{f_5}q_{f_2}. \tag{5.92}$$

with

$$C_{f_1} = \frac{\tilde{b}_{y_1}c_1 + \tilde{b}_{y_2}^2}{2\tilde{b}_{y_1}\tilde{b}_{y_2}c_1}, \tag{5.93}$$

$$C_{f_2} = \frac{\tilde{b}_{y_1}^2}{2\tilde{b}_{y_1}\tilde{b}_{y_2}c_1}, \tag{5.94}$$

$$C_{f_3} = \frac{1}{2\tilde{b}_{y_1}}, \tag{5.95}$$

$$C_{f_4} = \frac{c_1}{2\tilde{b}_{y_1}\tilde{b}_{y_2}}, \tag{5.96}$$

$$C_{f_5} = \frac{\tilde{b}_{y_1}}{2\tilde{b}_{y_1}\tilde{b}_{y_2}}. \tag{5.97}$$

The Σ_F-subsystem, as seen previously, serves as both the boundary layer of the Σ_{SF}-subsystem, and the reduced order of the Σ_{FU}-subsystem, becoming the interconnection subsystem between both the Σ_{SF} and Σ_{FU}-subsystems.

5.4.2.3 Lyapunov Function Candidate for the Helicopter Model Σ_U Subsystem

The associated Lyapunov functions for the Σ_U-subsystem is obtained by recognizing that the Σ_{FU}-subsystem, Eqns. (5.80–5.83), can be treated again like a two-time-scale singular perturbation problem by applying the stretched time-scale given by $\tau_2 = \tau_1/\varepsilon_2 = t/\varepsilon_1\varepsilon_2$, where the new reduced (slow) Σ_F-subsystem reduces to the target fast dynamics, Eqns. (5.69–5.70), and and where the boundary layer Σ_U-subsystem is given by Eqns. (5.61–5.62).

Recall that it is necessary to ensure that the boundary layer Σ_U-subsystem does not to shift from the equilibrium $\tilde{\boldsymbol{z}} = \tilde{\mathbf{h}}(\tilde{x}, \tilde{\boldsymbol{y}})$, since it is the equilibrium that defines the nature of the different reduced order subsystems, Σ_S and Σ_F-subsystems. It is therefore necessary to introduce a change of variables so that the equilibrium of this boundary-layer system is centered at zero, and thus permitting to select a natural Lyapunov function candidate to maintain the given equilibrium $\tilde{\boldsymbol{z}} = \tilde{\mathbf{h}}(\tilde{x}, \tilde{\boldsymbol{y}})$. This is obtained by introducing a change of variables defined by

$$\hat{\boldsymbol{z}} = \tilde{\boldsymbol{z}} - \tilde{\mathbf{h}}(\tilde{x}, \tilde{\boldsymbol{y}}), \tag{5.98}$$

$$= \begin{bmatrix} \hat{z}_1 \\ \hat{z}_2 \end{bmatrix} = \begin{bmatrix} \tilde{z}_1 - \tilde{\mathrm{h}}_1(\tilde{x}, \tilde{\boldsymbol{y}}) \\ \tilde{z}_2 - \tilde{\mathrm{h}}_2(\tilde{x}, \tilde{\boldsymbol{y}}) \end{bmatrix}, \tag{5.99}$$

with $\tilde{\mathrm{h}}_1(\tilde{x}, \tilde{\boldsymbol{y}})$, and $\tilde{\mathrm{h}}_2(\tilde{x}, \tilde{\boldsymbol{y}})$ being defined in Eqns. (5.64) and (5.65) respectively. This change of variables permits to express the boundary layer subsystem, Eqns. (5.61–5.62), as a linear function of $\hat{z}$, which can be viewed as the true error dynamics vector for the ultra-fast dynamics, therefore rewriting the Σ_U-subsystem as

$$\frac{d\tilde{z}_1}{d\tau_2} = c_7 \tilde{z}_2, \tag{5.100}$$

$$\begin{aligned} \frac{d\tilde{z}_2}{d\tau_2} &= a_9(\tilde{z}_1 + z_1^*) + c_9\tilde{z}_2 + J_2\left[\left(1 + \sqrt{s_3\tilde{v}(\tilde{x}, \tilde{\boldsymbol{y}})}\right)^2 - 1\right] \\ &= a_9\left(\tilde{z}_1 - \tilde{\mathrm{h}}_1(\tilde{x}, \tilde{\boldsymbol{y}})\right) + c_9\left(\tilde{z}_2 - \tilde{\mathrm{h}}_2(\tilde{x}, \tilde{\boldsymbol{y}})\right) \\ &= a_9\hat{z}_1 + c_9\hat{z}_2. \end{aligned} \tag{5.101}$$

It can be recognized that the Σ_U can be rewritten in state space form as

$$\frac{d\tilde{\boldsymbol{z}}}{d\tau_2} = \boldsymbol{A_U}\hat{\boldsymbol{z}}, \tag{5.102}$$

where

$$\boldsymbol{A_U} = \begin{pmatrix} 0 & c_7 \\ a_9 & c_9 \end{pmatrix}. \tag{5.103}$$

With this in mind, it is easy to define the associated Lyapunov function for the ultra-fast dynamics Σ_U-subsystem as the natural quadratic Lyapunov function of the error-dynamics, that is

$$V_U(\tilde{x}, \tilde{\boldsymbol{y}}, \tilde{\boldsymbol{z}}) = V_U(\hat{\boldsymbol{z}}) = \frac{1}{2}\hat{\boldsymbol{z}}^T\boldsymbol{P_U}\hat{\boldsymbol{z}}, \tag{5.104}$$

where $\boldsymbol{P_U}$ is a positive definite matrix that solves the associated Lyapunov equation

$$\boldsymbol{P_U}\boldsymbol{A_U} + \boldsymbol{A}_{\boldsymbol{U}}^T\boldsymbol{P_U} + \boldsymbol{Q_U} = 0, \tag{5.105}$$

where $\boldsymbol{Q_U}$ and $\boldsymbol{P_U}$ are positive definite matrices of similar structure as $\boldsymbol{P_F}$ and $\boldsymbol{Q_F}$, that is

$$\boldsymbol{Q_U} = \begin{pmatrix} q_{u_1} & 0 \\ 0 & q_{u_2} \end{pmatrix}, \tag{5.106}$$

$$\boldsymbol{P_U} = \begin{pmatrix} p_{u_1} & p_{u_3} \\ p_{u_3} & p_{u_2} \end{pmatrix}, \tag{5.107}$$

with $\boldsymbol{P_U} = \boldsymbol{P_U^T}$ being the solution of Eq. (5.105). This yields an associated Lyapunov function of the form

$$V_U(\hat{z}) = \frac{1}{2}\hat{\boldsymbol{z}}^T \boldsymbol{P_U} \hat{\boldsymbol{z}} = \frac{1}{2}p_{u_1}\hat{z}_1^2 + \frac{1}{2}p_{u_3}\hat{z}_2^2 + p_{u_2}\hat{z}_1\hat{z}_2, \tag{5.108}$$

with the solutions to the associated Lyapunov Eq. (5.105) given as

$$p_{u_1} = \frac{q_{u_2}a_9^2 + c_9^2 q_{u_1} - a_9 c_7 q_{u_1}}{2a_9 c_7 c_9} = C_{u_1}q_{u_1} + C_{u_2}q_{u_2}, \tag{5.109}$$

$$p_{u_2} = -\frac{q_{u_1}}{2a_9} = C_{u_3}q_{u_1}, \tag{5.110}$$

$$p_{u_3} = \frac{c_7 q_{u_1} - q_{u_2}a_9}{2a_9 c_9} = C_{f_4}q_{u_1} + C_{u_5}q_{u_2}. \tag{5.111}$$

with

$$C_{u_1} = \frac{c_9^2 - a_9 c_7}{2a_9 c_7 c_9}, \tag{5.112}$$

$$C_{u_2} = \frac{a_9^2}{2a_9 c_7 c_9}, \tag{5.113}$$

$$C_{u_3} = -\frac{1}{2a_9}, \tag{5.114}$$

$$C_{u_4} = \frac{c_7}{2a_9 c_9}, \tag{5.115}$$

$$C_{u_5} = -\frac{a_9}{2a_9 c_9}. \tag{5.116}$$

5.5 Stability Analysis for General Three-Time-Scale Systems

Following with the philosophy of the proposed three-time-scale analysis methodologies employed up to this point, the proposed three-time-scale asymptotic stability analysis takes advantage of this same philosophy by employing a sequential time-scale analysis in order to prove the asymptotic stability properties of the resulting autonomous three-time-scale system. This stability analysis is based on a double application of the standard two-time-scale stability analysis (Kokotović et al., 1999; Kokotović et al., 1986; Kokotović et al., 1987) on the Σ_{SFU} full system, which is given by

$$\dot{\tilde{x}} = \tilde{f}(\tilde{x}, \tilde{y}, \tilde{z}),\ \tilde{x} \in \mathcal{R}^{\tilde{x}}, \tag{5.117}$$

$$\varepsilon_1\dot{\tilde{y}} = \hat{g}(\tilde{x}, \tilde{y}, \tilde{z}),\ \tilde{y} \in \mathcal{R}^{\tilde{y}}, \tag{5.118}$$

$$\varepsilon_1\varepsilon_2\dot{\tilde{z}} = \hat{h}(\tilde{x}, \tilde{y}, \tilde{z}),\ \tilde{z} \in \mathcal{R}^{\tilde{z}}, \tag{5.119}$$

with $B_{\tilde{x}} \subset \mathcal{R}^{\tilde{x}}, B_{\tilde{y}} \subset \mathcal{R}^{\tilde{y}}, B_{\tilde{z}} \subset \mathcal{R}^{\tilde{z}}$ denoting closed sets of the variables $\tilde{x}$, $\tilde{y}$ and $\tilde{z}$, respectively. It is assumed that Lyapunov function candidates are available for all three subsystems, which were derived and proposed in section 5.4. Up to this point, the obtention of the control laws, and the associated Lyapunov function candidates required the use of a combination of both the TD and BU methodologies in order to create the necessary interconnection properties among the TD and the BU subproblems. These interconnection properties between the Σ_{SF}-subsystem from the BU methodology and the Σ_{FU}-subsystem from the TD methodology, are signified through the interconnectivity playing role of the intermediate Σ_F-subsystem which serves, as indicated previously, as both the reduced order subsystem of the Σ_{FU}-subsystem, and also as the boundary layer for the Σ_{SF}-subsystem. These interconnection properties are better depicted in Figure 3.9.

In the control design, the pursued strategy is to select the appropriate control law that first stabilize the Σ_{FU}-subsystem, by applying the TD time-scale analysis, which ultimately provide the control signal that stabilizes the Σ_F-subsystem, and once stable, and using the Σ_F-subsystem as the interconnection subsystem, proceed with the design of the control law that stabilizes the Σ_S-subsystem. This control design philosophy is required in order to satisfy the natural flow required to design a stable three-time-scale system, in which the stable ultra-fast variable z evolves through the configuration space of the boundary layer Σ_U-subsystem, as seen in Figure 3.9(a), towards the surface that defines the quasi-steady-state equilibrium of the Σ_U-subsystem, that is $\tilde{z} = \tilde{\mathrm{h}}(\tilde{x}, \tilde{y})$, while $\tilde{x}$ and $\tilde{y}$ behave as fixed parameters.

This evolution of the ultra-fast variable is denoted by the BU time-scale analysis decomposition of the full Σ_{SFU} full system in section 3.4.2, which is obtained by applying first the stretched time-scale given by $\tau_2 = t/\varepsilon_1\varepsilon_2$, thus becoming the reduced (slow) Σ_{SF}-subsystem defined by Eqns. (3.69–3.70), while the boundary layer Σ_U-subsystem for the BU subproblem is given by Eq. (3.71), where the boundary layer Σ_U-subsystem represents the movement of the ultra-fast variable z through its configuration space, given by $\hat{h}(\tilde{x}, \tilde{y}, \tilde{z}) = 0$, which also provides its quasi-steady-state equilibrium, that is $\tilde{z} = \tilde{\mathrm{h}}(\tilde{x}, \tilde{y})$.

As seen in Figure 3.9(a), during these first instants, the variables of the reduced order Σ_{SF}-subsystem, $\tilde{x}$ and $\tilde{y}$, in Eqns. (3.69–3.70), remain almost unchanged. This movement is defined as the ultra-fast movement. To understand what happens after the ultra-fast variable reaches its configuration space, $\hat{h}(\tilde{x}, \tilde{y}, \tilde{z}) = 0$, it can be recognized that the reduced order Σ_{SF}-subsystem can be treated again like a two-time-scale singular perturbation problem by applying the second stretched time scale of the BU analysis, and given by $\tau_1 = t/\varepsilon_1$, which results in a new reduced (slow) Σ_S-subsystem defined by Eq. (3.73), and a new boundary layer Σ_F-subsystem given by Eq. (3.74) where the new boundary layer Σ_F-subsystem, Eq. (3.74), represents the movement of the fast variable $\tilde{y}$ as it moves on the configuration space of the boundary layer Σ_U-subsystem towards the surface that defines the quasi-steady-state equilibrium of the Σ_F-subsystem, and given by $\hat{g}(\tilde{x}, \tilde{y}, \tilde{\mathrm{h}}(\tilde{x}, \tilde{y})) = 0$, that is $\tilde{y} = \tilde{\mathrm{g}}(\tilde{x})$, as it can be seen in Figure 3.9(b).

It can also be observed that the slow variable x behaves as a fixed parameter, and z evolves on its manifold. This movement is defined as the fast movement. Finally, the slowest movement is defined by the evolution of the slow variable x as it moves in the manifold of the Σ_S-subsystem, which is given by the intersection between the planes $\hat{g}(\tilde{x}, \tilde{y}, \tilde{\mathrm{h}}(\tilde{x}, \tilde{y})) = 0$ and $\hat{h}(\tilde{x}, \tilde{y}, \tilde{z}) = 0$. The slowest movement is continued through $\hat{g}(\tilde{x}, \tilde{y}, \tilde{\mathrm{h}}(\tilde{x}, \tilde{y})) \cap \hat{h}(\tilde{x}, \tilde{y}, \tilde{z})$ until it reaches the equilibrium, which in Figure 3.9(c) is depicted at the origin. This natural flow of the variables for a stable three-time-scale system, are best described in the BU analysis, section 3.4.2, and is this analysis the one that serves as the basis to prove the asymptotic stability properties of the resulting closed-loop system.

The presented asymptotic stability analysis for the general three-time-scale autonomous system, similarly to the intuitively description of the three-time-scale decomposition above described, only the BU methodology is employed through a double application of the standard two-time-scale asymptotic stability analysis (Kokotović et al., 1986; Kokotović et al., 1987) similar as described in Figure 3.7. The stability analysis focusses its attention on proving the evolution of the different time-scale subsystems of the autonomous Σ_{SFU} full system.

The stability analysis is divided in two stages. In the first stage the stability analysis focusses on proving the stability properties of the degenerated Σ_{SF}-subsystem, while in the second stage, and using the results obtained, focuses on proving the stability properties for the full Σ_{SFU} system. Thus the first stage will be denoted as Σ_{SF} *Stability Analysis*, while the second stage will be denoted as Σ_{SFU} *Stability Analysis*.

The first stage of the asymptotic stability analysis for the general three-time-scale system is applied, by decomposing the Σ_{SFU} full system into a two-time-scale subsystem by applying first the *Bottom*-condition, that is, applying first the stretched time-scale given by $\tau_2 = t/\varepsilon_1\varepsilon_2$, and assuming that the ultra-fast variable $\tilde{z}$ evolves on its quasi-steady-state equilibrium, that is, $\tilde{z} = \tilde{\mathrm{h}}(\tilde{x}, \tilde{y})$. The resulting reduced order (slow) Σ_{SF}-subsystem is given by Eqns. (3.69–3.70), while the boundary layer Σ_U-subsystem for the BU subproblem is given by Eq. (3.71), the quasi-steady-state of the boundary layer Σ_U-subsystem is given by $\tilde{\mathrm{h}}(\tilde{x}, \tilde{y})$, with $\tilde{\mathrm{h}}(\tilde{x}, \tilde{y})$ evolving on its own configuration space, and both $\tilde{x}$ and $\tilde{y}$ are considered like fixed parameters. Figure 5.2 describes the *Bottom*-sequence of the BU time-scale decomposition, where, the solid-line box represents the full Σ_{SFU} system, while the Σ_{SF}-subsystem is encapsulated with the dotted-line box.

The asymptotic stability analysis of this first stage is continued by recognizing that the resulting Σ_{SF}-subsystem, Eqns. (3.69–3.70), can be treated again like a two-time-scale singular perturbation problem by dealing with the subsystem that results after applying the stretched time-scale given by $\tau_1 = t/\varepsilon_1$, where the new reduced (slow) Σ_S-subsystem is now defined by Eq. (3.73), and the new boundary layer (fast) Σ_F-subsystem is now given by Eq. (3.74), with $\tilde{y} = \tilde{\mathrm{g}}(\tilde{x})$ being an isolated root of $0 = \hat{g}(\tilde{x}, \tilde{y}, \tilde{\mathrm{h}}(\tilde{x}, \tilde{y}))$, and with $\tilde{x}$ being treated like a constant. Figure 5.3 describes the *Up*-sequence of the BU time-scale decomposition where, again, the solid line box represents the full Σ_{SFU} system, the Σ_{SF}-subsystem is encapsulated with the dotted line box, and the Σ_S-subsystem is depicted with the dash-dotted line box.

The stability analysis of the Σ_{SF}-subsystem, Eqns. (3.69–3.70), is performed assuming that the Σ_U-subsystem variables evolve in their own configuration space. The analysis of this first stage is performed using the standard method for two-time-scale systems (Kokotović et al., 1986; Kokotović et al., 1987; Kokotović et al., 1999), in which the associated Lyapunov functions for the Σ_S and Σ_F subsystems, must satisfy certain growth requirements on $\tilde{f}(\tilde{x}, \tilde{y}, \tilde{\mathrm{h}}(\tilde{x}, \tilde{y}))$ and $\hat{g}(\tilde{x}, \tilde{y}, \tilde{\mathrm{h}}(\tilde{x}, \tilde{y}))$ by satisfying certain inequalities. These growth requirements are described in detail in Section 5.5.1 for the general three-time-scale problem, and extended to the helicopter model in Chapter 6. As a result of the fulfillment of these growth requirements, a new Lyapunov function, $\mathcal{V}_1(\tilde{x}, \tilde{y})$, is obtained for the singularly perturbed Σ_{SF}-subsystem as a weighted sum of the associated Lyapunov functions $\mathcal{V}_S(\tilde{x})$ and $\mathcal{V}_F(\tilde{x}, \tilde{y})$, resulting in

$$\mathcal{V}_1(\tilde{x}, \tilde{y}) = (1 - d_1)\mathcal{V}_S(\tilde{x}) + d_1\mathcal{V}_F(\tilde{y}), \tag{5.120}$$

where $0 < d_1 < 1$. This concludes the Σ_{SF} *Stability Analysis*. Figure 5.4 resumes this first stage of the Σ_{SF} *Stability Analysis*, including the growth requirements on $\tilde{f}\left(\tilde{x}, \tilde{y}, \tilde{\mathrm{h}}(\tilde{x}, \tilde{y})\right)$ and $\hat{g}\left(\tilde{x}, \tilde{y}, \tilde{\mathrm{h}}(\tilde{x}, \tilde{y})\right)$ which are described in detail in Section 5.5.1. In the second stage of the stability analysis, denoted as the Σ_{SFU} *Stability Analysis*, the standard two-time-scale stability analysis method is applied again taking advantage of the results obtained in the previous stage.

The Σ_{SF} *Stability Analysis* analyzed and proved the asymptotic stability properties of the resulting reduced order Σ_{SF}-subsystem, Eqns (3.69–3.70), which is treated like a two-time-scale system in which the boundary layer Σ_U-subsystem is assumed to be moving through it configuration space. The Σ_{SF} *Stability Analysis* yielded a Lyapunov function for the Σ_{SF}-subsystem, $\mathcal{V}_1(\tilde{x}, \tilde{y})$, that can now be used to conduct the stability analysis for the complete Σ_{SFU} system, which, for convenience, is rewritten as

$$\dot{\tilde{\chi}} = \tilde{F}(\tilde{\chi}, \tilde{z}),\ \tilde{\chi} \in \mathcal{R}^{\tilde{\chi}}, \tag{5.121}$$

$$\varepsilon_1\varepsilon_2\dot{\tilde{z}} = \hat{h}(\tilde{\chi}, \tilde{z}),\ \tilde{z} \in \mathcal{R}^{\tilde{z}}, \tag{5.122}$$

with $B_{\tilde{\chi}} \subset \mathcal{R}^{\tilde{\chi}}, B_{\tilde{z}} \subset \mathcal{R}^{\tilde{z}}$ denoting closed sets, and with $\tilde{F}(\tilde{\chi}, \tilde{z})$ being given by Eqs. (5.117) and (5.118), that is given by

$$\tilde{F}(\tilde{\chi}, \tilde{z}) \triangleq \begin{bmatrix} \tilde{f}(\tilde{\chi}, \tilde{z}) \\ \hat{g}(\tilde{\chi}, \tilde{z}) \end{bmatrix} = \begin{bmatrix} \tilde{f}(\tilde{x}, \tilde{y}, \tilde{z}) \\ \hat{g}(\tilde{x}, \tilde{y}, \tilde{z}) \end{bmatrix}, \tag{5.123}$$

where $\tilde{\chi}$ represents the augmented state vector given by

$$\tilde{\chi} \triangleq \begin{bmatrix} \tilde{x} & \tilde{y} \end{bmatrix}^T. \tag{5.124}$$

The Lyapunov function obtained in the first stage of the stability analysis, $\mathcal{V}_1(\tilde{x}, \tilde{y}) = \mathcal{V}_1(\tilde{\chi})$, becomes the Lyapunov function for the $\tilde{F}(\tilde{\chi}, \tilde{z})$ system. The newly augmented singularly perturbed Σ_{SFU} system, Eqns. (5.121–5.122), can be treated like a two-time-scale singular perturbed system by applying again the *Bottom*-condition, that is making $\varepsilon_2 = 0$, yielding the reduced order Σ_{SF}-subsystem, given by

$$\dot{\tilde{\chi}} \quad = \quad \tilde{F}(\tilde{\chi}, \tilde{\mathrm{h}}(\tilde{\chi})) = \begin{bmatrix} \tilde{f}(\tilde{\chi}, \tilde{\mathrm{h}}(\tilde{\chi})) \\ \hat{g}(\tilde{\chi}, \tilde{\mathrm{h}}(\tilde{\chi})) \end{bmatrix}, \tag{5.125}$$

which is equivalent to the Σ_{SF}-subsystem defined previously in the first stage of the stability analysis, Eqns. (3.69–3.70), while the boundary layer Σ_U-subsystem is defined by

$$\frac{d\tilde{z}}{d\tau_2} \quad = \quad \hat{h}(\tilde{\chi}, \tilde{z}), \;\; \tau_2 = \frac{t}{\varepsilon_1 \varepsilon_2}, \tag{5.126}$$

with the associated Lyapunov function for the Σ_U-subsystem given by $\mathcal{V}_U(\tilde{\chi}, \tilde{z}) = \mathcal{V}_U(\tilde{z} - \tilde{\mathrm{h}}(\tilde{\chi})) = \mathcal{V}_U(\hat{z})$, where $\tilde{\mathrm{h}}(\tilde{\chi})$ represents the equilibria of the boundary layer Σ_U-subsystem, Eq. (5.126), which is given by

$$0 = \hat{h}(\tilde{\chi}, \tilde{z}) \rightarrow \tilde{z} = \tilde{\mathrm{h}}(\tilde{\chi}) = \tilde{\mathrm{h}}(\tilde{x}, \tilde{y}). \tag{5.127}$$

Figure 5.5 describes Σ_{SFU} stability analysis where again, the solid-line box represents the full Σ_{SFU} system, while the Σ_{SF}-subsystem is encapsulated with the dotted-line box. In a similar analysis to the one conducted in the first stage, the new Lyapunov functions must satisfy certain growth requirements for $\tilde{F}(\tilde{\chi}, \tilde{z})$ and $\hat{h}(\tilde{\chi}, \tilde{z})$ by satisfying certain inequalities. These growth requirements are described in detail in Section 5.5.3, and as a result of the fulfillment of these growth requirements, a new Lyapunov function, $\mathcal{V}_2(\tilde{\chi}, \tilde{z})$, is obtained for the full Σ_{SFU} system as a weighted sum of both $\mathcal{V}_1(\tilde{\chi})$ and $\mathcal{V}_U(\hat{z})$, resulting in

$$\mathcal{V}_2(\tilde{\chi}, \tilde{z}) = (1 - d_2)\mathcal{V}_1(\tilde{\chi}) + d_2 \mathcal{V}_U(\tilde{\chi}, \tilde{z}), \tag{5.128}$$

where $0 < d_2 < 1$. Figure 5.5 describes the complete Σ_{SFU} asymptotic stability analysis, including the growth requirements on $\tilde{F}(\tilde{\chi}, \tilde{z})$ and $\hat{h}(\tilde{\chi}, \tilde{z})$ which are described in detail in Section 5.5.3, while Figure 5.6 depicts both the Σ_{SF} and the Σ_{SFU} asymptotic stability analysis for the generic three-time-scale singularly perturbed system, where it can be observed the existing interconnection properties between both stages, such that the composite Lyapunov function $\mathcal{V}_1(\tilde{\chi})$ for the reduced order Σ_{SF}-subsystem in the Σ_{SFU} *Stability Analysis* is the composite Lyapunov function that was obtained during the Σ_{SF} *Stability Analysis*. Recall that the Lyapunov function candidate for the entire singular perturbation problem, $\mathcal{V}_2(\mathcal{V}_S, \mathcal{V}_F, \mathcal{V}_U)$, is defined as a weighted sum of the three Lyapunov functions of each of the three singularly perturbed subsystems, $\mathcal{V}_S$, $\mathcal{V}_F$, and $\mathcal{V}_U$, respectively, and therefore can be rewritten as

$$\mathcal{V}_2(\tilde{x}, \tilde{y}, \tilde{z}) = \alpha_1 \mathcal{V}_S(\tilde{x}) + \alpha_2 \mathcal{V}_F(\tilde{y}) + \alpha_3 \mathcal{V}_U(\tilde{x}, \tilde{y}, \tilde{z}), \tag{5.129}$$

with

$$\begin{aligned} \alpha_1 &= (1 - d_1)(1 - d_2) = 1 - d_1 - d_2 + d_1 d_2, \\ \alpha_2 &= (1 - d_2), \\ \alpha_3 &= d_2. \end{aligned}$$

The resulting Σ_S, Σ_F and Σ_U-subsystems, defined by Eqns. (3.73), (3.74), and (5.126), respectively, approximate the Σ_{SFU} system according to the theory of singular perturbed systems (Kokotović et al., 1999; Kokotović et al., 1986; Kokotović et al., 1987). Following sections describe the proposed three-time-scale asymptotic stability analysis for a generic model. For completeness purposes only the asymptotic stability analysis for the generic model is described in this chapter. The asymptotic stability analysis for the helicopter model is left for chapter 6, while the asymptotic stability analysis for the simplified example, is left, for completeness, to Appendix C.

5.5.1 General Σ_{SF} *Stability Analysis*

This section describes in detail the general asymptotic stability requirements for the Σ_{SF}-subsystem by applying the BU-methodology. The stability analysis of the Σ_{SF}-subsystem is performed assuming that the Σ_U-subsystem variables evolve in their own configuration space. The analysis of this first stage is performed using the standard method for two-time-scale systems (Kokotović et al., 1986; Kokotović et al., 1987; Kokotović et al., 1999), in which the previously derived Lyapunov functions for the Σ_S and Σ_F subsystems, that is $\mathcal{V}_S$ and $\mathcal{V}_F$, respectively, must satisfy certain growth requirements on $\tilde{f}(\tilde{x}, \tilde{y}, \tilde{\mathrm{h}}(\tilde{x}, \tilde{y}))$ and $\hat{g}(\tilde{x}, \tilde{y}, \tilde{\mathrm{h}}(\tilde{x}, \tilde{y}))$ by fulfilling certain inequalities. These growth requirements for the Σ_{SF}-subsystem take the form of inequalities that must be satisfied by the Lyapunov functions, and can be divided in three main groups:

- Reduced order growth requirements, if they refer to the properties that must posses the reduced order subsystem, $\tilde{f}(\tilde{x}, \tilde{\mathrm{g}}(\tilde{x}), \tilde{\mathrm{h}}(\tilde{x}, \tilde{y}))$ in Eq. (3.73).
- Boundary layer growth requirements, if they refer to the properties that must posses the boundary layer subsystem, $\hat{g}(\tilde{x}, \tilde{y}, \tilde{\mathrm{h}}(\tilde{x}, \tilde{y}))$ in Eq. (3.74).
- Interconnection growth requirements, if they refer to the properties that must posses both subsystems in conjunction to prove the continuity between both the reduced order and the boundary layer subsystems.

The properties for the isolated equilibrium at the origin are discussed in Assumption 5.5.1. The growth requirements of both, the reduced, and boundary layer subsystem are addressed in Assumptions 5.5.2 and 5.5.3, respectively, while the growth requirements that combine both reduced and boundary layer system requirements, called interconnection conditions, are defined in Assumptions 5.5.4 and 5.5.5. These Assumptions are all described in detail bellow.

Assumption 5.5.1 Isolated Equilibrium of the Origin
The origin ($\tilde{x} = 0$, $\tilde{y} = 0$) is a unique and isolated equilibrium of the Σ_{SF}-subsystem, Eqns. (3.69–3.70), i.e.

$$0 = \tilde{f}(0, 0, \tilde{\mathrm{h}}(\tilde{x}, \tilde{y})), \tag{5.130}$$

$$0 = \hat{g}(0, 0, \tilde{\mathrm{h}}(\tilde{x}, \tilde{y})), \tag{5.131}$$

moreover, $\tilde{y} = \tilde{\mathrm{g}}(\tilde{x})$ is the unique root of

$$0 = \hat{g}\left(\tilde{x}, \tilde{y}, \tilde{\mathrm{h}}(\tilde{x}, \tilde{y})\right), \tag{5.132}$$

in $B_{\tilde{x}} \times B_{\tilde{y}}$, i.e.

$$0 = \hat{g}(\tilde{x}, \tilde{\mathrm{g}}(\tilde{x}), \tilde{\mathrm{h}}(\tilde{x}, \tilde{y})), \tag{5.133}$$

and there exists a class κ function $p_1(\cdot)$ such that

$$\parallel \tilde{\mathrm{g}}(\tilde{x}) \parallel \leq p_1 (\parallel \tilde{x} \parallel) . \tag{5.134}$$

The reduced order growth requirements are obtained by first considering the system given by Eq. (3.69), and adding and subtracting $\tilde{f}(\tilde{x}, \tilde{\mathrm{g}}(\tilde{x}), \tilde{\mathrm{h}}(\tilde{x}, \tilde{y}))$ to the right-hand side of Eq. (3.69), resulting in the expression given by

$$\dot{\tilde{x}} = \tilde{f}\left(\tilde{x}, \tilde{\mathrm{g}}(\tilde{x}), \tilde{\mathrm{h}}(\tilde{x}, \tilde{y})\right) + \tilde{f}\left(\tilde{x}, \tilde{y}, \tilde{\mathrm{h}}(\tilde{x}, \tilde{y})\right) - \tilde{f}\left(\tilde{x}, \tilde{\mathrm{g}}(\tilde{x}), \tilde{\mathrm{h}}(\tilde{x}, \tilde{y})\right), \tag{5.135}$$

where the term $\tilde{f}(\tilde{x}, \tilde{x}, \tilde{\mathrm{h}}(\tilde{x}, \tilde{y})) - \tilde{f}(\tilde{x}, \tilde{\mathrm{g}}(\tilde{x}), \tilde{\mathrm{h}}(\tilde{x}, \tilde{y}))$ can be viewed as a perturbation of the reduced order Σ_S-subsystem, Eq. (3.73). Being therefore natural to first satisfy the growth requirements for Eq. (3.69) and then consider the effect of the perturbation term $\tilde{f}(\tilde{x}, \tilde{y}, \tilde{\mathrm{h}}(\tilde{x}, \tilde{y})) - \tilde{f}(\tilde{x}, \tilde{\mathrm{g}}(\tilde{x}), \tilde{\mathrm{h}}(\tilde{x}, \tilde{y}))$. Therefore let proceed to define first the reduced order growth condition.

Assumption 5.5.2 Reduced System Conditions
There exists a positive-definite and decreasing Lyapunov function candidate $\mathcal{V}_S(\tilde{x})$ that satisfies the following inequality

$$\left(\frac{\partial \mathcal{V}_S(\tilde{x})}{\partial \tilde{x}}\right)^T \tilde{f}\left(\tilde{x}, \tilde{\mathrm{g}}(\tilde{x}), \tilde{\mathrm{h}}(\tilde{x}, \tilde{y})\right) \leq -\alpha_1 \psi_1^2(\tilde{x}), \tag{5.136}$$

where $\psi_1(\cdot)$ is a scalar function of vector arguments which vanishes only when its argument are zero, and satisfying that $\tilde{x} = 0$ is a stable equilibrium of the reduced order system.

Assumption 5.5.3 Boundary-Layer System Conditions
There exists a positive-definite and decreasing Lyapunov function candidate $\mathcal{V}_F(\tilde{x}, \tilde{y})$ such that for all $(\tilde{x}, \tilde{y}) \in B_{\tilde{x}} \times B_{\tilde{y}}$ satisfies

$$\mathcal{V}_F(\tilde{x}, \tilde{y}) > 0, \ \forall \tilde{y} \neq \tilde{\mathrm{g}}(\tilde{x}) \text{ and } \mathcal{V}_F(\tilde{x}, \tilde{\mathrm{g}}(\tilde{x})) = 0, \tag{5.137}$$

and

$$\left(\frac{\partial \mathcal{V}_F}{\partial \tilde{y}}\right)^T \hat{g}\left(\tilde{x}, \tilde{y}, \tilde{\mathrm{h}}(\tilde{x}, \tilde{y})\right) \leq -\alpha_2 \phi_1^2(\tilde{y} - \tilde{\mathrm{g}}(\tilde{x})), \tag{5.138}$$

where $\mathcal{V}_F(\tilde{x}, \tilde{y})$ is the Lyapunov function candidate of the boundary layer Σ_F-subsystem, Eq. (3.74), in which $\tilde{x}$ is treated as a fixed parameter, and $\phi_1(\cdot)$ is a scalar function of vector arguments which vanishes only when its arguments are zero, and satisfying that $\tilde{y} - \tilde{\mathrm{g}}(\tilde{x})$ is a stable equilibrium of the boundary layer system.

Both $\psi_1(\cdot)$ and $\phi_1(\cdot)$ are scalar functions of vector arguments that vanish only when their arguments are zero, i.e., $\psi_1(\tilde{x}) = 0$ if and only if $\tilde{x} = 0$, and will both be referred as comparison functions.

Assumption 5.5.4 First Interconnection Condition
The Lyapunov functions $\mathcal{V}_S(\tilde{x})$ and $\mathcal{V}_F(\tilde{x}, \tilde{y})$ must satisfy the so called interconnection conditions. The first interconnection condition is obtained by computing the derivative of $\mathcal{V}_S(\tilde{x})$ along the solution of Eq. (5.135), yielding

$$\begin{aligned}
\dot{\mathcal{V}}_S(\tilde{x}) &= \frac{\partial \mathcal{V}_S}{\partial \tilde{x}} \tilde{f}\left(\tilde{x}, \tilde{\mathrm{g}}(\tilde{x}), \tilde{\mathrm{h}}(\tilde{x}, \tilde{y})\right) + \frac{\partial \mathcal{V}_S}{\partial \tilde{x}} \left[\tilde{f}\left(\tilde{x}, \tilde{y}, \tilde{\mathrm{h}}(\tilde{x}, \tilde{y})\right) - \tilde{f}\left(\tilde{x}, \tilde{\mathrm{g}}(\tilde{x}), \tilde{\mathrm{h}}(\tilde{x}, \tilde{y})\right)\right] \\
&\leq -\alpha_1 \psi_1^2(\tilde{x}) + \frac{\partial \mathcal{V}_S}{\partial \tilde{x}} \left[\tilde{f}\left(\tilde{x}, \tilde{y}, \tilde{\mathrm{h}}(\tilde{x}, \tilde{y})\right) - \tilde{f}\left(\tilde{x}, \tilde{\mathrm{g}}(\tilde{x}), \tilde{\mathrm{h}}(\tilde{x}, \tilde{y})\right)\right],
\end{aligned} \tag{5.139}$$

thus assuming that

$$\left(\frac{\partial \mathcal{V}_S(\tilde{x})}{\partial \tilde{x}}\right)^T \left[\tilde{f}\left(\tilde{x}, \tilde{y}, \tilde{\mathrm{h}}(\tilde{x}, \tilde{y})\right) - \tilde{f}\left(\tilde{x}, \tilde{\mathrm{g}}(\tilde{x}), \tilde{\mathrm{h}}(\tilde{x}, \tilde{y})\right)\right] \leq \beta_1 \psi_1(\tilde{x}) \phi_1(\tilde{y}). \tag{5.140}$$

so that

$$\dot{\mathcal{V}}_S \leq -\alpha_1 \psi_1^2(\tilde{x}) + \beta_1 \psi_1(\tilde{x}) \phi_1(\tilde{y} - \tilde{\mathrm{g}}(\tilde{x})). \tag{5.141}$$

Inequality (5.140) determines the allowed growth of $\tilde{f}\left(\tilde{x}, \tilde{y}, \tilde{\mathrm{h}}(\tilde{x}, \tilde{y})\right)$ in $\tilde{y}$, and in typical problems, verifying Assumption 5.5.4 reduces to verifying the inequality

$$\left\| \tilde{f}\left(\tilde{x}, \tilde{y}, \tilde{\mathrm{h}}(\tilde{x}, \tilde{y})\right) - \tilde{f}\left(\tilde{x}, \tilde{\mathrm{g}}(\tilde{x}), \tilde{\mathrm{h}}(\tilde{x}, \tilde{y})\right) \right\| \leq \psi_1(\tilde{x}) \phi_1(\tilde{y} - \tilde{\mathrm{g}}(\tilde{x})), \tag{5.142}$$

which implies that the rate of growth of $\tilde{f}\left(\tilde{x}, \tilde{y}, \tilde{\mathrm{h}}(\tilde{x}, \tilde{y})\right)$ cannot be faster than the rate of growth of the comparison function $\phi_1(\cdot)$.

Assumption 5.5.5 Second Interconnection Conditions
The second interconnection condition is defined by the inequality

$$\left(\frac{\partial \mathcal{V}_F(\tilde{y})}{\partial \tilde{x}}\right)^T \tilde{f}\left(\tilde{x}, \tilde{y}, \tilde{\mathrm{h}}(\tilde{x}, \tilde{y})\right) \leq \gamma_1 \phi_1^2(\tilde{y}) + \beta_2 \psi_1(\tilde{x}) \phi_1(\tilde{y}), \tag{5.143}$$

where $\psi_1(\cdot)$ and $\phi_1(\cdot)$ have been both previously defined by satisfying Assumptions 5.5.2 and 5.5.2.

5.5.2 Fulfillment of the General Σ_{SF} *Stability Analysis*

If assumptions 5.5.1, 5.5.2, 5.5.3, 5.5.4, and 5.5.5 are all satisfied, then the growth requirements of $\tilde{f}(\tilde{x}, \tilde{y}, \tilde{\mathrm{h}}(\tilde{x}, \tilde{y}))$ and $\hat{g}(\tilde{x}, \tilde{y}, \tilde{\mathrm{h}}(\tilde{x}, \tilde{x}))$ are satisfied, and with the Lyapunov functions $\mathcal{V}_S(\tilde{x})$ and $\mathcal{V}_F(\tilde{x}, \tilde{x})$ defined, a new Lyapunov function candidate $\mathcal{V}_1(\tilde{x}, \tilde{y})$ is considered and defined by the weighted sum of $\mathcal{V}_S(\tilde{x})$ and $\mathcal{V}_F(\tilde{x}, \tilde{y})$, results in

$$\mathcal{V}_1(\tilde{x}, \tilde{y}) = (1 - d_1)\mathcal{V}_S(\tilde{x}) + d_1 \mathcal{V}_F(\tilde{y}),\ d_1 \in (0, 1), \tag{5.144}$$

for $0 < d_1 < 1$. The newly defined function $\mathcal{V}_1(\tilde{x}, \tilde{y})$ becomes the Lyapunov function candidate for the singular perturbed Σ_{SF}-subsystem, Eqns. (3.69–3.70). To explore the freedom in choosing the weights, lets take d_1 as an unspecified parameter in the interval $(0, 1)$. From the properties of $\mathcal{V}_S(\tilde{x})$ and $\mathcal{V}_F(\tilde{x}, \tilde{y})$ and inequality (5.134), that is $\| \tilde{\mathrm{g}}(\tilde{x}) \| \leq p_1 (\| \tilde{x} \|)$, where $p_1(\cdot)$ is a κ function, it follows that $\mathcal{V}_1(\tilde{x}, \tilde{y})$ is positive-definite. Computing the time derivative of $\mathcal{V}_1(\tilde{x}, \tilde{y})$ along the trajectories of $\tilde{f}\left(\tilde{x}, \tilde{y}, \tilde{\mathrm{h}}(\tilde{x}, \tilde{y})\right)$ and $\hat{g}\left(\tilde{x}, \tilde{y}, \tilde{\mathrm{h}}(\tilde{x}, \tilde{y})\right)$, resulting in

$$\begin{aligned}
\dot{\mathcal{V}}_1 &= (1 - d_1)\frac{\partial \mathcal{V}_S}{\partial \tilde{x}} \tilde{f}\left(\tilde{x}, \tilde{y}, \tilde{\mathrm{h}}(\tilde{x}, \tilde{y})\right) + \frac{d_1}{\varepsilon_1}\frac{\partial \mathcal{V}_F}{\partial \tilde{y}} \hat{g}\left(\tilde{x}, \tilde{y}, \tilde{\mathrm{h}}(\tilde{x}, \tilde{y})\right) + d_1 \frac{\partial \mathcal{V}_F}{\partial \tilde{x}} \tilde{f}\left(\tilde{x}, \tilde{y}, \tilde{\mathrm{h}}(\tilde{x}, \tilde{y})\right) \\
&= (1 - d_1)\frac{\partial \mathcal{V}_S}{\partial \tilde{x}} \tilde{f}\left(\tilde{x}, \tilde{\mathrm{g}}(\tilde{x}), \tilde{\mathrm{h}}(\tilde{x}, \tilde{y})\right) \\
&+ (1 - d_1)\frac{\partial \mathcal{V}_S}{\partial \tilde{x}} \left[\tilde{f}\left(\tilde{x}, \tilde{y}, \tilde{\mathrm{h}}(\tilde{x}, \tilde{y})\right) - \tilde{f}\left(\tilde{x}, \tilde{\mathrm{g}}(\tilde{x}), \tilde{\mathrm{h}}(\tilde{x}, \tilde{y})\right)\right] \\
&+ \frac{d_1}{\varepsilon_1}\frac{\partial \mathcal{V}_F}{\partial \tilde{y}} \hat{g}\left(\tilde{x}, \tilde{y}, \tilde{\mathrm{h}}(\tilde{x}, \tilde{y})\right) + d_1 \frac{\partial \mathcal{V}_F}{\partial \tilde{x}} \tilde{f}\left(\tilde{x}, \tilde{y}, \tilde{\mathrm{h}}(\tilde{x}, \tilde{y})\right).
\end{aligned} \tag{5.145}$$

The fulfillment of inequalities defined in Assumptions 5.5.2, 5.5.3, 5.5.4 and 5.5.5, implies that Eq. (5.145) can be expressed as

$$\begin{aligned}
\dot{\mathcal{V}}_1 &\leq -(1 - d_1)\alpha_1 \psi_1^2(\tilde{x}) + (1 - d_1)\beta_1 \psi_1(\tilde{x}) \phi_1(\tilde{y} - \tilde{\mathrm{g}}(\tilde{x})) \\
&- \frac{d_1}{\varepsilon_1}\alpha_2 \phi_1^2(\tilde{y} - \tilde{\mathrm{g}}(\tilde{x})) + d_1 \gamma_1 \phi_1^2(\tilde{y} - \tilde{\mathrm{g}}(\tilde{x})) + d_1 \beta_2 \psi_1(\tilde{x}) \phi_1(\tilde{y} - \tilde{\mathrm{g}}(\tilde{x}))
\end{aligned}$$

$$= \quad -\begin{bmatrix} \psi_1(\tilde{x}) \\ \phi_1(\tilde{y}) \end{bmatrix}^T \begin{bmatrix} (1-d_1)\alpha_1 & -\frac{1}{2}(1-d_1)\beta_1 - \frac{1}{2}d_1\beta_2 \\ -\frac{1}{2}(1-d_1)\beta_1 - \frac{1}{2}d_1\beta_2 & d_1\left(\dfrac{\alpha_2}{\varepsilon_1} - \gamma_1\right) \end{bmatrix}$$
$$\times \quad \begin{bmatrix} \psi_1(\tilde{x}) \\ \phi_1(\tilde{y}) \end{bmatrix}. \tag{5.146}$$

This translates into that the right hand side of Eq. (5.146) is a quadratic form in $\psi_1(\tilde{x})$ and $\phi_1(\tilde{y}-\tilde{g}(\tilde{x}))$, where the quadratic form is negative-definite when

$$d_1(1-d_1)\alpha_1\left(\frac{\alpha_2}{\varepsilon_1} - \gamma_1\right) > \frac{1}{4}\left[(1-d_1)\beta_1 + d_1\beta_2\right]^2, \tag{5.147}$$

which is equivalent to

$$\frac{1}{\varepsilon_1} > \frac{1}{\alpha_1\alpha_2}\left[\alpha_1\gamma + \frac{1}{4(1-d)d}\left[(1-d)\beta_1 + d\beta_2\right]^2\right]. \tag{5.148}$$

It is important to note that in the above development only α_1 and α_2 are required by definition to be positive. The other three parameters, β_1, β_2, and γ could, in general, be positive, negative or zero. In most problems, however, when trying to satisfy the interconnection inequalities defined by Eqns. (5.140) and (5.143), it is common to do so using norm inequalities, leading automatically to nonnegative values of β_1, β_2, and γ_1. Therefore, as suggested in the literature (Kokotović et al., 1986; Kokotović et al., 1987; Kokotović et al., 1999) throughout the reminder of this thesis it is assumed that $\beta_1 \geq 0$, $\beta_2 \geq 0$, and $\gamma_1 \geq 0$. Inequality (5.148) can be rewritten as

$$\varepsilon_1 < \frac{\alpha_1\alpha_2}{\alpha_1\gamma_1 + \dfrac{1}{4(1-d_1)d_1}\left[(1-d_1)\beta_1 + d_1\beta_2\right]^2} \equiv \varepsilon_{1_d}. \tag{5.149}$$

Inequality (5.149) shows that for any choice of d_1, the corresponding $\mathcal{V}_1$ is a Lyapunov function for the singular perturbed Σ_{SF}-subsystem, Eqns. (3.69–3.70), for all ε_1 satisfying Eq. (5.149). The dependance on the right-hand side of Eq. (5.149) on the unspecified parameter d_1 is sketched in Figure 5.7. It can be easily seen that the maximum value of ε_{1_d} occurs at

$$d_1^* = \frac{\beta_1}{\beta_1 + \beta_2}, \tag{5.150}$$

yielding also the upper bounds on ε_1 such

$$\varepsilon_1^* = \frac{\alpha_1\alpha_2}{\alpha_1\gamma_1 + \beta_1\beta_2}. \tag{5.151}$$

Therefore, it can be inferred that the equilibrium point of the singularly perturbed Σ_{SF}-subsystem, Eqns. (3.69–3.70), is asymptotically stable for all $\varepsilon_1 < \varepsilon_1^*$. The number ε_1^* is the best upper bound on ε_1 that can be provided by the above presented stability analysis. Assumptions 5.5.2, 5.5.3, 5.5.4 and 5.5.5 are summarized in Table 5.1, where it can be seen the similarities between the two-time-scale growth requirements described in Section 5.2.1, and the three-time-scale growth requirements for the Σ_{SF}-subsystem. The asymptotic stability analysis presented can be summarizes in Theorem 5.5.1.

Theorem 5.5.1 *: Let inequalities (5.136), (5.138), (5.140), and (5.143) be satisfied. Then the origin is an asymptotically stable equilibrium of the singularly perturbed Σ_{SF}-subsystem, Eqns. (3.69–3.70) for all $\varepsilon_1 \in (0, \varepsilon_1^*)$, where ε_1^* is given by Eq. (5.151). Moreover, for every number $d_1 \in (0,1)$*

$$\mathcal{V}_1(\tilde{x},\tilde{y}) = (1-d_1)\mathcal{V}_S(\tilde{x}) + d_1\mathcal{V}_F(\tilde{x},\tilde{y}), \tag{5.152}$$

is a Lyapunov function for all $\varepsilon_1 \in (0, \varepsilon_{1_d})$, where $\varepsilon_{1_d} \leq \varepsilon_1^*$ is given by Eq. (5.149).

Theorem 5.5.1 can be summarized by understanding that $\tilde{x} = 0$ is an asymptotically stable equilibrium of the reduced Σ_S-subsystem, Eq. (3.73), and $\tilde{y} = \tilde{\mathrm{g}}(\tilde{x})$ is an asymptotically stable equilibrium of the boundary-layer Σ_F-subsystem, Eq. (3.74), uniformly in $\tilde{x}$, that is, the $\varepsilon - \delta$ definition of *Lyapunov* stability and the convergence $\tilde{y} \to \tilde{\mathrm{g}}(\tilde{x})$ are uniform in $\tilde{x}$ (Vidyasagar, 2002), and if $\tilde{f}\left(\tilde{x}, \tilde{y}, \tilde{\mathrm{h}}(\tilde{x}, \tilde{y})\right)$ and $\hat{g}\left(\tilde{x}, \tilde{y}, \tilde{\mathrm{h}}(\tilde{x}, \tilde{y})\right)$ satisfy certain growth conditions on the reduced and boundary-layer systems, Assumptions 5.5.2, 5.5.3, 5.5.4, and 5.5.5, then the origin is an asymptotically stable equilibrium of the singularly perturbed Σ_{SF}-subsystem, Eqns. (3.69–3.70), for sufficiently small ε_1. (Kokotović et al., 1986; Kokotović et al., 1987; Kokotović et al., 1999).

Corollary 5.5.2 *: Let assumptions of Theorem 5.5.1 hold for all $\tilde{x}$, $\tilde{y} \in R^n \times R^m$ and let $\mathcal{V}_S(\tilde{x})$ and $\mathcal{V}_F(\tilde{x}, \tilde{y})$ be radially unbounded (i.e $\mathcal{V}_S(\tilde{x}) \to \infty$ as $\|\tilde{x}\| \to \infty$ and $\mathcal{V}_F(\tilde{x}, \tilde{y}) \to \infty$ as $\|\tilde{y} - \tilde{\mathrm{g}}(\tilde{x})\| \to \infty$). Then, the equilibrium ($\tilde{x} = 0$, $\tilde{y} = 0$) is globally asymptotically stable for all $\varepsilon_1 < \varepsilon_1^*$.*

Corollary 5.5.3 *: Let all the assumptions of Theorem 5.5.1 hold with $\psi_1(\tilde{x}) = \|\tilde{x}\|$ and $\phi_1(\tilde{y} - \tilde{\mathrm{g}}(\tilde{x})) = \|\tilde{y} - \tilde{\mathrm{g}}(\tilde{x})\|$ and suppose, in addition, that $\mathcal{V}_S(\tilde{x})$ and $\mathcal{V}_F(\tilde{x}, \tilde{y})$ satisfy the inequalities*

$$
\begin{aligned}
e_1\psi_1^2(\tilde{x}) &\leq \mathcal{V}_{\mathcal{S}}(\tilde{x}) \leq e_2\psi_1^2(\tilde{x}),\ \forall \tilde{x} \in B_{\tilde{x}}, && (5.153)\\
e_3\phi_2^2(\tilde{y} - \tilde{\mathrm{g}}(\tilde{x})) &\leq \mathcal{V}_F(\tilde{x}, \tilde{y}) \leq e_4\phi_1^2(\tilde{y} - \tilde{\mathrm{g}}(\tilde{x})),\ \forall (\tilde{x}, \tilde{y}) \in B_{\tilde{x}} \times B_{\tilde{y}}, && (5.154)
\end{aligned}
$$

where e_1, ..., e_4 denote positive constants. Then, the conclusions of Theorem 5.5.1 hold, with exponential stability replacing asymptotic stability.

Corollary 5.5.4 *: Let $\tilde{f}\left(\tilde{x}, \tilde{y}, \tilde{\mathrm{h}}(\tilde{x}, \tilde{y})\right)$, $\hat{g}\left(\tilde{x}, \tilde{y}, \tilde{\mathrm{h}}(\tilde{x}, \tilde{y})\right)$, and $\tilde{\mathrm{h}}(\tilde{x}, \tilde{y})$ be continuously differentiable. Suppose that $\tilde{x} = 0$ is an exponentially stable equilibrium of the reduced Σ_S-subsystem, Eq. (3.73), and $\tilde{y} = \tilde{\mathrm{g}}(\tilde{x})$ is an exponentially stable equilibrium of the boundary layer ΣF-subsystem, Eq. (3.74), uniformly in $\tilde{x}$, i.e.*

$$
\|\tilde{y}(\tau_1) - \tilde{\mathrm{g}}(\tilde{x})\| \leq K_1 e^{-\alpha\tau_1}\|\tilde{y}(0) - \tilde{\mathrm{g}}(\tilde{x})\|, \tag{5.155}
$$

where α and K_1 are independent of $\tilde{x}$. Then, the origin is an exponentially stable equilibrium of the singularly perturbed Σ_{SF}-subsystem, Eqns. (3.69–3.70), for sufficiently small ε_1.

This concludes the first step of the asymptotic stability analysis, the Σ_{SF} *Stability Analysis*. The results obtained in this first step, the composite Lyapunov function for the Σ_{SF}-subsystem, $\mathcal{V}_1$, and the upper bounds, d_1^* and ε_1^*, along with the demonstration that the singularly perturbed Σ_{SF}-subsystem is asymptotically stable for $\varepsilon_1 \in (0, \varepsilon_{d_1})$, will be employed in the Σ_{SFU} *Stability Analysis* that is conducted in the following section.

5.5.3 General Σ_{SFU} *Stability Analysis*

Once proven the asymptotic stability of the Σ_{SF}-subsystem, Eqns. (3.69–3.70), the Σ_{SFU} *Stability Analysis* is conducted recalling that the Σ_{SF} *Stability Analysis* provides with a composite Lyapunov function, $\mathcal{V}_1(\tilde{x}, \tilde{y})$, Eq. (5.144), that satisfies the growth requirements between both $\tilde{f}(\tilde{x}, \tilde{y}, \tilde{\mathrm{h}}(\tilde{x}, \tilde{y}))$ and $\hat{g}(\tilde{x}, \tilde{y}, \tilde{\mathrm{h}}(\tilde{x}, \tilde{y}))$, therefore, and using these results, it can be continued to prove the asymptotic stability properties of the full Σ_{SFU} system, which for convenience is rewritten , as noted in Eqns. (5.121–5.122). The asymptotic stability of the newly defined, but equivalent Σ_{SFU} full system, is studied by treating the system like a two-time-scale problem, whose reduced (slow) Σ_{SF}-subsystem is given in Eq. (5.125), and the boundary layer Σ_U-subsystem given in Eq. (5.126).

The Lyapunov function obtained during the Σ_{SF} *Stability Analysis*, $\mathcal{V}_1$, Eq. (5.144) becomes the Lyapunov function for the $\tilde{F}(\tilde{\chi}, \tilde{z})$ system, while $\mathcal{V}_U$ becomes the Lyapunov function for the Σ_U-subsystem. In a similar analysis to the one conducted in the first stage, the new Lyapunov functions must define the growth requirements for $\tilde{F}(\tilde{\chi}, \tilde{z})$ and $\hat{h}(\tilde{\chi}, \tilde{z})$ by satisfying certain inequalities. These growth requirements can be divided in three main groups:

- Reduced order growth requirements, if they refer to the properties that must posses the reduced order subsystem, $\tilde{F}(\tilde{\chi}, \tilde{\mathrm{h}}(\tilde{\chi}))$ in Eq. (5.125).
- Boundary layer growth requirements, if they refer to the properties that must posses the boundary layer subsystem, $\hat{g}(\tilde{\chi}, \tilde{\mathrm{h}}(\tilde{\chi}))$ in Eq. (5.126).
- Interconnection growth requirements, if they refer to the properties that must posses both subsystems in conjunction to prove the continuity between both the reduced order and the boundary layer subsystems.

The properties for the isolated equilibrium at the origin are assumed in Assumption 5.5.6. The growth requirements of both the reduced and boundary layer system separately are addressed in Assumptions 5.5.7 and 5.5.8 respectively, while the growth requirements that combine both reduced Σ_{SF} and boundary layer Σ_U-subsystem requirements, called interconnection conditions, are defined in Assumptions 5.5.9 and 5.5.10. These Assumptions are all described in detail bellow.

Assumption 5.5.6 Asymptotic Stability of the Origin
The origin ($\tilde{\chi} = 0$, $\tilde{z} = 0$) is a unique and isolated equilibrium of Eqns. (5.121–5.122), i.e.

$$0 = \tilde{F}(0, 0), \tag{5.156}$$
$$0 = \hat{h}(0, 0), \tag{5.157}$$

moreover, $\tilde{z} = \tilde{\mathrm{h}}(\tilde{\chi})$ is the unique root of

$$0 = \hat{h}(\tilde{\chi}, \tilde{z}), \tag{5.158}$$

in $B_{\tilde{\chi}} \times B_{\tilde{z}}$, i.e.

$$0 = \hat{h}(\tilde{\chi}, \tilde{\mathrm{h}}(\tilde{\chi})), \tag{5.159}$$

and there exists a class κ function $p_2(\cdot)$ such that

$$\| \tilde{\mathrm{h}}(\tilde{\chi}) \| \leq p_2 \left(\| \tilde{\chi} \| \right). \tag{5.160}$$

The reduced order growth requirements are obtained by first considering the system given by Eq. (5.121), and adding and subtracting $\tilde{F}(\tilde{\chi}, \tilde{\mathrm{h}}(\tilde{\chi}))$ to the right-hand side of Eq. (5.121) resulting in the expression given by

$$\dot{\tilde{x}} = \tilde{F}(\tilde{\chi}, \tilde{\mathrm{h}}(\chi)) + \tilde{F}(\tilde{\chi}, \tilde{z}) - \tilde{F}(\tilde{\chi}, \tilde{\mathrm{h}}(\tilde{\chi})), \tag{5.161}$$

where the term $\tilde{F}(\tilde{\chi}, \tilde{z}) - \tilde{F}(\tilde{\chi}, \tilde{\mathrm{h}}(\tilde{\chi}))$ can be viewed as a perturbation of the reduced order Σ_{SF}-subsystem, Eq. (5.125). Similarly, as in the Σ_{SF} *Stability Analysis*, it is natural to first satisfy the growth requirements for Eq. (5.125), and then consider the effect of the perturbation term $\tilde{F}(\tilde{\chi}, \tilde{z}) - \tilde{F}(\tilde{\chi}, \tilde{\mathrm{h}}(\tilde{\chi}))$. Therefore let proceed to define first the reduced order growth condition.

Assumption 5.5.7 Reduced System Conditions
There exists a positive-definite and decreasing Lyapunov function candidate $\mathcal{V}_1(\tilde{\chi})$ that satisfies the following inequality

$$\left(\frac{\partial \mathcal{V}_1(\tilde{\chi})}{\partial \tilde{\chi}} \right)^T \tilde{F}\left(\tilde{\chi}, \tilde{\mathrm{h}}(\tilde{\chi})\right) \leq -\alpha_3 \psi_2^2(\tilde{\chi}), \tag{5.162}$$

where $\psi_2(\cdot)$ is a scalar function of vector arguments which vanishes only when its argument are zero, and satisfying that $\tilde{\chi} = 0$ is a stable equilibrium of the reduced order system.

Assumption 5.5.8 Boundary-Layer System Conditions
There exists a positive-definite and decreasing Lyapunov function candidate $\mathcal{V}_U(\tilde{\chi}, \tilde{z})$ such that for all $(\tilde{\chi}, \tilde{z}) \in B_{\tilde{\chi}} \times B_{\tilde{z}}$ satisfies

$$\mathcal{V}_U(\tilde{\chi}, \tilde{z}) > 0,\ \forall \tilde{z} \neq \tilde{\mathrm{h}}(\tilde{\chi}) \text{ and } \mathcal{V}_U(\tilde{\chi}, \tilde{\mathrm{h}}(\tilde{\chi})) = 0, \tag{5.163}$$

and

$$\left(\frac{\partial \mathcal{V}_U}{\partial \tilde{z}}\right)^T \hat{h}(\tilde{\chi}, \tilde{z}) \leq -\alpha_4 \phi_2^2(\tilde{z} - \tilde{\mathrm{h}}(\tilde{\chi})),\ \alpha_4 > 0, \tag{5.164}$$

where $\mathcal{V}_U(\tilde{\chi}, \tilde{z})$ is the Lyapunov function candidate of the boundary layer Σ_U-subsystem, Eq. (5.126), in which $\tilde{\chi}$ is treated as a fixed parameter, and $\phi_2(\cdot)$ is a scalar function of vector arguments which vanishes only when its arguments are zero, and satisfying that $\tilde{z} - \tilde{\mathrm{h}}(\tilde{\chi})$ is a stable equilibrium of the boundary layer Σ_U-subsystem.

Both $\psi_2(\cdot)$ and $\phi_2(\cdot)$ are scalar functions of vector arguments that vanish only when their arguments are zero, i.e., $\psi_2(\tilde{\chi}) = 0$ if and only if $\tilde{\chi} = 0$, and both will be referred as comparison functions.

Assumption 5.5.9 *: First Interconnection Condition*
The Lyapunov functions $\mathcal{V}_1(\tilde{\chi})$ and $\mathcal{V}_U(\tilde{\chi}, \tilde{z})$ must satisfy the so called interconnection conditions. The first interconnection condition is obtained by computing the derivative of $\mathcal{V}_S(\tilde{x})$ along the solution of Eq. (5.161), yielding

$$\begin{aligned} \dot{\mathcal{V}}_1(\tilde{\chi}) &= \frac{\partial \mathcal{V}_1}{\partial \tilde{\chi}} \tilde{F}\left(\tilde{\chi}, \tilde{\mathrm{h}}(\tilde{\chi})\right) + \frac{\partial \mathcal{V}_1}{\partial \tilde{\chi}}\left[\tilde{F}(\tilde{\chi}, \tilde{z}) - \tilde{F}(\tilde{\chi}, \tilde{\mathrm{h}}(\tilde{\chi}))\right] && (5.165)\\ &\leq -\alpha_3 \psi_2^2 \tilde{\chi} + \frac{\partial \mathcal{V}_1}{\partial \tilde{\chi}}\left[\tilde{F}(\tilde{\chi}, \tilde{z}) - \tilde{F}\left(\tilde{\chi}, \tilde{\mathrm{h}}(\tilde{\chi})\right)\right], && (5.166)\end{aligned}$$

thus assuming that

$$\left(\frac{\partial \mathcal{V}_1(\tilde{\chi})}{\partial \tilde{\chi}}\right)^T \left[\tilde{F}(\tilde{\chi}, \tilde{z}) - \tilde{F}\left(\tilde{\chi}, \tilde{\mathrm{h}}(\tilde{\chi})\right)\right] \leq \beta_3 \psi_2(\tilde{\chi}) \phi_2(\tilde{z} - \tilde{\mathrm{h}}(\tilde{\chi})). \tag{5.167}$$

so that

$$\dot{\mathcal{V}}_1 \leq -\alpha_3 \psi_2^2(\tilde{\chi}) + \beta_3 \psi_2(\tilde{\chi}) \phi_2(\tilde{\chi} - \tilde{\mathrm{h}}(\tilde{\chi})). \tag{5.168}$$

Inequality (5.167) determines the allowed growth of $\tilde{F}(\tilde{\chi}, \tilde{z})$ in $\tilde{z}$, and , similarly as in the Σ_{SF} *Stability Analysis*, in typical problems, verifying Assumption 5.5.9 reduces to verifying the inequality

$$\left\|\tilde{F}(\tilde{\chi}, \tilde{z}) - \tilde{F}\left(\tilde{\chi}, \tilde{\mathrm{h}}(\tilde{\chi})\right)\right\| \leq \psi_2(\tilde{\chi}) \phi_2(\tilde{z} - \tilde{\mathrm{h}}(\tilde{\chi})), \tag{5.169}$$

which implies that the rate of growth of $\tilde{F}(\tilde{\chi}, \tilde{z})$ cannot be faster than the rate of growth of the comparison function $\phi_2(\cdot)$.

Assumption 5.5.10 *: Second Interconnection Conditions*
The second interconnection condition is defined by the inequality

$$\left(\frac{\partial \mathcal{V}_U(\hat{z})}{\partial \tilde{\chi}}\right)^T \tilde{F}(\tilde{\chi}, \tilde{z}) \leq \gamma_2 \phi_2^2(\hat{z}) + \beta_4 \psi_2(\tilde{\chi}) \phi_2(\hat{z}), \tag{5.170}$$

where $\psi_2(\cdot)$ and $\phi_2(\cdot)$ have been previously defined by satisfying assumptions 5.5.7, and 5.5.8.

5.5.4 Fulfillment of the General Σ_{SFU} *Stability Analysis*

If assumptions 5.5.6, 5.5.7, 5.5.8, 5.5.9, and 5.5.10 are all satisfied, then the growth requirements of $\tilde{F}(\tilde{\chi},\tilde{z})$ and $\hat{g}(\tilde{\chi},\tilde{z})$ are satisfied, and with the Lyapunov functions $\mathcal{V}_1(\tilde{\chi})$ and $\mathcal{V}_U(\tilde{\chi},\tilde{z})$ defined, a new Lyapunov function candidate $\mathcal{V}_2(\tilde{\chi},\tilde{z})$ is considered and defined by the weighted sum of $\mathcal{V}_1(\tilde{\chi})$ and $\mathcal{V}_U(\tilde{\chi},\tilde{z})$, resulting in

$$\mathcal{V}_2(\tilde{\chi},\tilde{z}) = (1-d_2)\mathcal{V}_1(\tilde{\chi}) + d_2\mathcal{V}_U(\tilde{z}),\; d_2 \in (0,1), \tag{5.171}$$

for $0 < d_2 < 1$. The newly defined function $\mathcal{V}_2(\tilde{\chi},\tilde{z})$ becomes the Lyapunov function candidate for the singular perturbed Σ_{SFU} system, Eqns. (5.121–5.122). To explore the freedom in choosing the weights, lets take d_2 as an unspecified parameter in the interval $(0,1)$. From the properties of $\mathcal{V}_1(\tilde{\chi})$ and $\mathcal{V}_U(\tilde{\chi},\tilde{z})$ and inequality (5.160), that is $\parallel \tilde{\mathrm{h}}(\tilde{\chi}) \parallel \leq p_2(\parallel \tilde{\chi} \parallel)$, where $p_2(\cdot)$ is a κ function, it follows that $\mathcal{V}_2(\tilde{\chi},\tilde{z})$ is positive-definite. Computing the time derivative of $\mathcal{V}_2(\tilde{\chi},\tilde{z})$ along the trajectories of $\tilde{F}(\tilde{\chi},\tilde{z})$ and $\hat{g}(\tilde{\chi},\tilde{z})$ results in

$$\begin{aligned}
\dot{\mathcal{V}}_2 \;&=\; (1-d_2)\frac{\partial \mathcal{V}_1}{\partial \tilde{x}}\tilde{F}(\tilde{\chi},\tilde{z}) + \frac{d_2}{\varepsilon_1\varepsilon_2}\frac{\partial \mathcal{V}_U}{\partial \tilde{z}}\hat{g}(\tilde{\chi},\tilde{z}) + d_2\frac{\partial \mathcal{V}_U}{\partial \tilde{\chi}}\tilde{F}(\tilde{\chi},\tilde{z}) \\
&=\; (1-d_2)\frac{\partial \mathcal{V}_1}{\partial \tilde{\chi}}\tilde{F}\left(\tilde{\chi},\tilde{\mathrm{h}}(\tilde{\chi})\right) \\
&+\; (1-d_2)\frac{\partial \mathcal{V}_1}{\partial \tilde{\chi}}\left[\tilde{F}(\tilde{\chi},\tilde{z}) - \tilde{F}\left(\tilde{\chi},\tilde{\mathrm{h}}(\tilde{\chi})\right)\right] \\
&+\; \frac{d_2}{\varepsilon_1\varepsilon_2}\frac{\partial \mathcal{V}_U}{\partial \tilde{z}}\hat{g}(\tilde{\chi},\tilde{z}) + d_2\frac{\partial \mathcal{V}_U}{\partial \tilde{\chi}}\tilde{F}(\tilde{\chi},\tilde{z}).
\end{aligned} \tag{5.172}$$

The fulfillment of inequalities in Assumptions 5.5.7, 5.5.8, 5.5.9 and 5.5.10, implies that Eq. (5.172) can be expressed as

$$\begin{aligned}
\dot{\mathcal{V}}_2 \;&\leq\; -(1-d_2)\alpha_3\psi_1^2(\tilde{x}) + (1-d_2)\beta_3\psi_2(\tilde{\chi})\phi_2(\tilde{\chi}-\tilde{\mathrm{h}}(\tilde{\chi})) \\
&-\; \frac{d_2}{\varepsilon_1\varepsilon_2}\alpha_4\phi_2^2(\tilde{\chi}-\tilde{\mathrm{h}}(\tilde{\chi})) + d_2\gamma_2\phi_2^2(\tilde{\chi}-\tilde{\mathrm{h}}(\tilde{\chi})) + d_2\beta_4\psi_2(\tilde{\chi})\phi_2(\tilde{\chi}-\tilde{\mathrm{h}}(\tilde{\chi})) \\
&=\; -\begin{bmatrix} \psi_2(\tilde{\chi}) \\ \phi_2(\tilde{z}-\tilde{\mathrm{h}}(\tilde{\chi})) \end{bmatrix}^T \begin{bmatrix} (1-d_2)\alpha_3 & -\frac{1}{2}(1-d_2)\beta_3 - \frac{1}{2}d_2\beta_4 \\ -\frac{1}{2}(1-d_2)\beta_3 - \frac{1}{2}d_2\beta_4 & d_2\left(\dfrac{\alpha_4}{\varepsilon_1\varepsilon_2} - \gamma_2\right) \end{bmatrix} \\
&\times\; \begin{bmatrix} \psi_2(\tilde{\chi}) \\ \phi_2(\tilde{z}-\tilde{\mathrm{h}}(\tilde{\chi})) \end{bmatrix}.
\end{aligned} \tag{5.173}$$

The right hand side of Eq. (5.173) is a quadratic form in $\psi_2(\tilde{\chi})$ and $\phi_2(\tilde{\chi}-\tilde{\mathrm{h}}(\tilde{\chi}))$, where the quadratic form is negative-definite when

$$d_2(1-d_2)\alpha_3\left(\frac{\alpha_4}{\varepsilon_1\varepsilon_2} - \gamma_2\right) > \frac{1}{4}\left[(1-d_2)\beta_3 + d_2\beta_4\right]^2, \tag{5.174}$$

which is equivalent to

$$\frac{1}{\varepsilon_1\varepsilon_2} > \frac{1}{\alpha_3\alpha_4}\left[\alpha_3\gamma + \frac{1}{4(1-d)d}\left[(1-d)\beta_3 + d\beta_4\right]^2\right]. \tag{5.175}$$

It is important to note that in the above development only α_3 and α_4 are required by definition to be positive. The other three parameters, β_3, β_4, and γ could, in general, be positive, negative or zero, and similarly as in the Σ_{SF} *Stability Analysis*, and throughout the reminder of this thesis, it is assumed that $\beta_3 \geq 0$, $\beta_4 \geq 0$, and $\gamma_2 \geq 0$. Inequality (5.175) can be rewritten as

$$\varepsilon_1\varepsilon_2 < \frac{\alpha_3\alpha_4}{\alpha_3\gamma_2 + \dfrac{1}{4(1-d_2)d_2}\left[(1-d_2)\beta_3 + d_2\beta_4\right]^2} \equiv \varepsilon_{1_d}\varepsilon_{2_d}. \tag{5.176}$$

Recalling that in the Σ_{SF} *Stability Analysis*, ε_1 was selected as $\varepsilon_1 \leq \varepsilon_1^*$, therefore allowing to rewrite inequality (5.176) as

$$\varepsilon_2 < \frac{\alpha_3\alpha_4}{\varepsilon_1\left(\alpha_3\gamma_2 + \dfrac{1}{4(1-d_2)d_2}\left[(1-d_2)\beta_3 + d_2\beta_4\right]^2\right)} \equiv \varepsilon_{2_d}. \tag{5.177}$$

Recall also that from the Σ_{SF} *Stability Analysis*, the maximum value of ε_1 was given by Eq. (5.151) therefore, by selecting $\varepsilon_1 \equiv \varepsilon_1^*$, the smallest possible upper bound on ε_2, and thus the most conservative upper bound, becomes

$$\varepsilon_2 < \frac{\alpha_1\gamma_1 + \beta_1\beta_2}{\alpha_1\alpha_2}\frac{\alpha_3\alpha_4}{\alpha_3\gamma_2 + \dfrac{1}{4(1-d_2)d_2}\left[(1-d_2)\beta_3 + d_2\beta_4\right]^2} \equiv \varepsilon_{2_d}. \tag{5.178}$$

Inequality (5.178) shows that for any choice of d_2, the corresponding $\mathcal{V}_2$ is a Lyapunov function for the singular perturbed Σ_{SFU} system, Eqns. (5.121–5.122), for all ε_2 satisfying (5.178). The dependance on the right-hand side of Eq. (5.178) on the unspecified parameter d_2 is sketched in Figure 5.8. Therefore, it can be easily seen that maximum value of ε_{2_d} occurs at

$$d_2^* = \frac{\beta_3}{\beta_3 + \beta_4}, \tag{5.179}$$

yielding a conservative upper bound on ε_2

$$\varepsilon_2^* = \frac{\alpha_1\gamma_1 + \beta_1\beta_2}{\alpha_1\alpha_2}\frac{\alpha_3\alpha_4}{\alpha_3\gamma_2 + \beta_3\beta_4}. \tag{5.180}$$

Therefore, it can be inferred that the equilibrium point of the singularly perturbed Σ_{SFU} full system, Eqns. (5.121–5.122), is asymptotically stable for all $\varepsilon_2 < \varepsilon_2^*$. The number ε_2^* is the best upper bound on ε_2 that can be provided by the above presented stability analysis. Assumptions 5.5.7, 5.5.8, 5.5.9 and 5.5.10, are summarized in Table 5.2, where it can be seen the similarities between the two-time-scale growth requirements described in Section 5.2.1, and the three-time-scale growth requirements for the full Σ_{SFU} system. The asymptotic stability analysis presented can be summarizes in Theorem 5.5.5.

Theorem 5.5.5 *: Let inequalities (5.162), (5.164), (5.167), and (5.170) be satisfied. Then the origin is an asymptotically stable equilibrium of the singularly perturbed Σ_{SFU} full system, Eqns. (5.121–5.122) for all $\varepsilon_2 \in (0, \varepsilon_2^*)$, where ε_2^* is given by Eq. (5.180). Moreover, for every number $d_2 \in (0,1)$*

$$\mathcal{V}_2(\tilde{\chi},\tilde{z}) = (1-d_2)\mathcal{V}_1(\tilde{\chi}) + d_2\mathcal{V}_U(\tilde{\chi},\tilde{z}), \tag{5.181}$$

is a Lyapunov function for all $\varepsilon_2 \in (0, \varepsilon_{2_d})$, where $\varepsilon_{2_d} \leq \varepsilon_2^*$ is given by (5.176).

Theorem 5.5.5 can be summarized by understanding that $\tilde{\chi} = 0$ is an asymptotically stable equilibrium of the reduced Σ_{SF}-subsystem, Eq. (5.125), $\tilde{z} = \tilde{\mathrm{h}}(\tilde{\chi})$ is an asymptotically stable equilibrium of the boundary-layer Σ_U-subsystem, Eq. (5.126) uniformly in $\tilde{\chi}$, that is, the $\varepsilon - \delta$ definition of *Lyapunov* stability and the convergence $\tilde{z} \to \tilde{\mathrm{h}}(\tilde{\chi})$ are uniform in $\tilde{\chi}$ (Vidyasagar, 2002), and if $\tilde{F}(\tilde{\chi},\tilde{z})$ and $\hat{g}(\tilde{\chi},\tilde{z})$ satisfy certain growth conditions on the reduced and boundary-layer systems, assumptions 5.5.7, 5.5.8, 5.5.9 and 5.5.10, then the origin is an asymptotically stable equilibrium of the singularly perturbed Σ_{SFU} full system (5.121–5.122), for sufficiently small ε_2. (Kokotović et al., 1986; Kokotović et al., 1987; Kokotović et al., 1999).

Corollary 5.5.6 *: Let assumptions of Theorem 5.5.5 hold for all $\tilde{\chi}$, $\tilde{z} \in R^n \times R^m$ and let $\mathcal{V}_1(\tilde{\chi})$ and $\mathcal{V}_U(\tilde{\chi},\tilde{z})$ be radially unbounded (i.e $\mathcal{V}_1(\tilde{\chi}) \to \infty$ as $\|\tilde{\chi}\| \to \infty$ and $\mathcal{V}_U(\tilde{\chi},\tilde{z}) \to \infty$ as $\|\hat{z} - \tilde{\mathrm{h}}(\tilde{\chi})\| \to \infty$). Then, the equilibrium ($\tilde{\chi} = 0$, $\tilde{z} = 0$) is globally asymptotically stable for all $\varepsilon_2 < \varepsilon_2^*$.*

Corollary 5.5.7 *: Let all the assumptions of Theorem 5.5.5 hold with* $\psi_2(\tilde{\chi}) = \|\tilde{\chi}\|$ *and* $\phi_2(\tilde{\chi} - \tilde{\mathrm{h}}(\tilde{\chi})) = \|\tilde{z} - \tilde{\mathrm{h}}(\tilde{\chi})\|$ *and suppose, in addition, that* $\mathcal{V}_1(\tilde{\chi})$ *and* $\mathcal{V}_U(\tilde{\chi}, \tilde{z})$ *satisfy the inequalities*

$$e_5\psi_1^2(\tilde{\chi}) \leq \mathcal{V}_1(\tilde{\chi}) \leq e_6\psi_1^2(\tilde{\chi}), \forall\tilde{\chi} \in B_{\tilde{\chi}}, \tag{5.182}$$

$$e_7\phi_2^2(\tilde{\chi} - \tilde{\mathrm{h}}(\tilde{\chi})) \leq \mathcal{V}_U(\tilde{\chi}, \tilde{z}) \leq e_8\phi_2^2(\tilde{\chi} - \tilde{\mathrm{h}}(\tilde{\chi})), \forall(\tilde{\chi}, \hat{z}) \in B_{\tilde{\chi}} \times B_{\hat{z}}, \tag{5.183}$$

where e_5, ..., e_8 *denote positive constants. Then, the conclusions of Theorem 5.5.5 hold, with exponential stability replacing asymptotic stability.*

Corollary 5.5.8 *: Let* $\tilde{F}(\tilde{\chi}, \tilde{z})$, $\hat{g}(\tilde{\chi}, \tilde{z})$, *and* $\tilde{\mathrm{h}}(\tilde{\chi})$ *be continuously differentiable. Suppose that* $\tilde{\chi} = 0$ *is an exponentially stable equilibrium of the reduced* Σ_{SF}*-subsystem, Eq. (5.125), and* $\tilde{z} = \tilde{\mathrm{h}}(\tilde{\chi})$ *is an exponentially stable equilibrium of the boundary layer* Σ_U*-subsystem, Eq. (5.126), uniformly in* $\tilde{\chi}$*, i.e.*

$$\|\tilde{z}(\tau_2) - \tilde{\mathrm{h}}(\tilde{\chi})\| \leq K_2 e^{-\alpha\tau_2}\|\tilde{z}(0) - \tilde{\mathrm{h}}(\tilde{\chi})\|, \tag{5.184}$$

where α *and* K_2 *are independent of* $\tilde{\chi}$*. Then, the origin is an exponentially stable equilibrium of the singularly perturbed system (5.121–5.122), for sufficiently small* ε_2*.*

This concludes the second and final step of the Σ_{SFU} asymptotic stability analysis. The methodology here presented is applied to the three-time-scale helicopter problem in chapter 6, and for completeness and to help understanding the methodology, it is also applied to the simplified example and presented in Appendix C. The following section extends the singularly perturbed stability analysis to a more general N^{th}-time scale system by proposing a 4^{th}-order time-scale singularly perturbed system as an example, as conducted in chapter 3, to describe the *TD* and *BU* time scale analysis for the general N^{th}-time-scale analysis.

Assumption 5.5.2				
Section 5.2	$\frac{\partial V}{\partial x}$	$f(x, h(x))$	α_1	$\psi(x)$
Σ_{SF}	$\frac{\partial \mathcal{V}_S(\tilde{x})}{\partial \tilde{x}}$	$\tilde{f}(\tilde{x}, \tilde{\mathrm{g}}(\tilde{x}), \tilde{\mathrm{h}}(\tilde{x}, \tilde{y}))$	$\alpha_1 \geq 0$	$\psi_1(\tilde{x})$
Assumption 5.5.3				
Section 5.2	$\frac{\partial W}{\partial z}$	$g(x, z)$	α_2	$\phi(z - h(x))$
Σ_{SF}	$\left(\frac{\partial \mathcal{V}_F(\tilde{y})}{\partial \tilde{y}}\right)^T$	$\hat{g}(\tilde{x}, \tilde{y}, \tilde{\mathrm{h}}(\tilde{x}, \tilde{y}))$	$\alpha_2 \geq 0$	$\phi_1(\tilde{y} - \tilde{\mathrm{g}}(\tilde{x}))$
Assumption 5.5.4				
Section 5.2	$\frac{\partial V}{\partial x}$	$f(x, z)$	$f(x, h(x))$	β_1
Σ_{SF}	$\left(\frac{\partial \mathcal{V}_S(\tilde{x})}{\partial \tilde{x}}\right)^T$	$\tilde{f}(\tilde{x}, \tilde{y}, \tilde{\mathrm{h}}(\tilde{x}, \tilde{y}))$	$\tilde{f}(\tilde{x}, \tilde{\mathrm{g}}(\tilde{x}), \tilde{\mathrm{h}}(\tilde{x}, \tilde{y}))$	$\beta_1 \geq 0$
Assumption 5.5.5				
Section 5.2	$\frac{\partial W}{\partial x}$	$f(x, z)$	γ_1	β_2
Σ_{SF}	$\left(\frac{\partial \mathcal{V}_F(\tilde{y})}{\partial \tilde{x}}\right)^T$	$\tilde{f}(\tilde{x}, \tilde{y}, \tilde{\mathrm{h}}(\tilde{x}, \tilde{y}))$	$\gamma_1 \geq 0$	$\beta_2 \geq 0$

Table 5.1: Parameters for the Comparison Functions and Inequalities that Guarantee the Asymptotic Stability Requirements for the Σ_{SF} Subsystem.

Assumption 5.5.7				
Section 5.2	$\frac{\partial V}{\partial x}$	$f(x, h(x))$	α_3	$\psi(x)$
Σ_{SF}	$\frac{\partial \mathcal{V}_1(\tilde{\chi})}{\partial \tilde{\chi}}$	$\tilde{F}(\tilde{\chi}, \tilde{\mathrm{h}}(\tilde{\chi})$	$\alpha_3 \geq 0$	$\psi_2(\tilde{\chi})$
Assumption 5.5.8				
Section 5.2	$\frac{\partial W}{\partial z}$	$g(x, z)$	α_4	$\phi(z - h(x))$
Σ_{SF}	$\left(\frac{\partial \mathcal{V}_F(\hat{z})}{\partial \hat{z}}\right)^T$	$\hat{g}(\tilde{\chi}, \tilde{z})$	$\alpha_4 \geq 0$	$\phi_2(\tilde{\chi} - \tilde{\mathrm{h}}(\tilde{\chi}))$
Assumption 5.5.9				
Section 5.2	$\frac{\partial V}{\partial x}$	$f(x, z)$	$f(x, h(x))$	β_3
Σ_{SF}	$\left(\frac{\partial \mathcal{V}_1(\tilde{\chi})}{\partial \tilde{\chi}}\right)^T$	$\tilde{F}(\tilde{\chi}, \tilde{z})$	$\tilde{F}(\tilde{\chi}, \tilde{\mathrm{h}}(\tilde{\chi}))$	$\beta_3 \geq 0$
Assumption 5.5.10				
Section 5.2	$\frac{\partial W}{\partial x}$	$f(x, z)$	γ_2	β_4
Σ_{SF}	$\left(\frac{\partial \mathcal{V}_U(\hat{z})}{\partial \tilde{\chi}}\right)^T$	$\tilde{F}(\tilde{\chi}, \hat{z})$	$\gamma_2 \geq 0$	$\beta_4 \geq 0$

Table 5.2: Parameters for the Comparison Functions and Inequalities that Guarantee the Asymptotic Stability Requirements for the Σ_{SF} Subsystem.

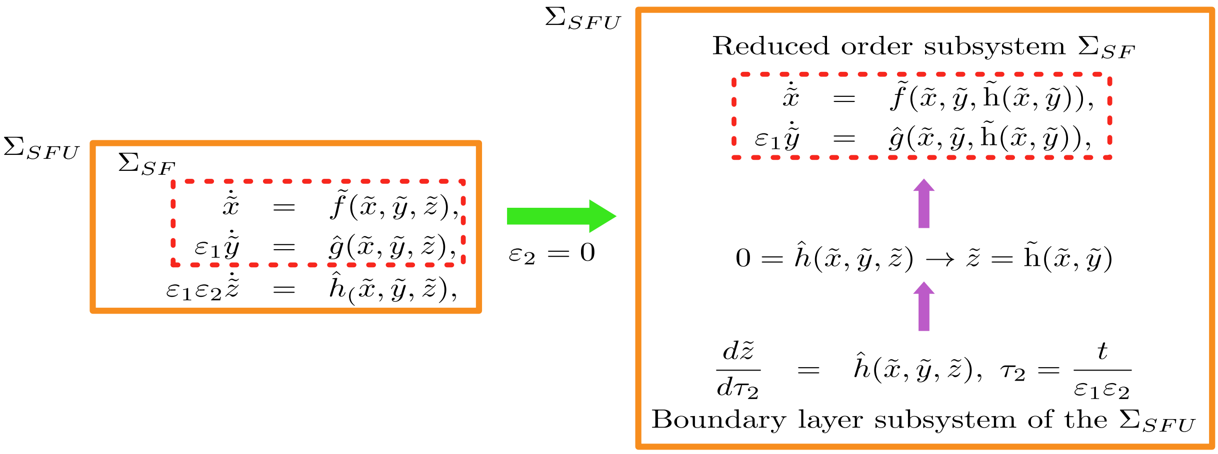

Figure 5.2: *Bottom*-sequence of the Σ_{SF} *Stability Analysis.*

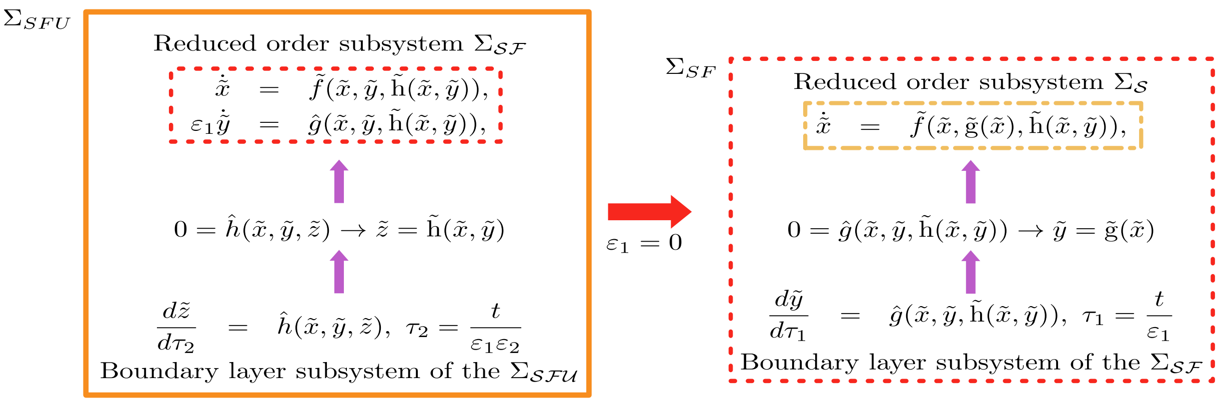

Figure 5.3: *Up*-sequence of the Σ_{SF} *Stability Analysis.*

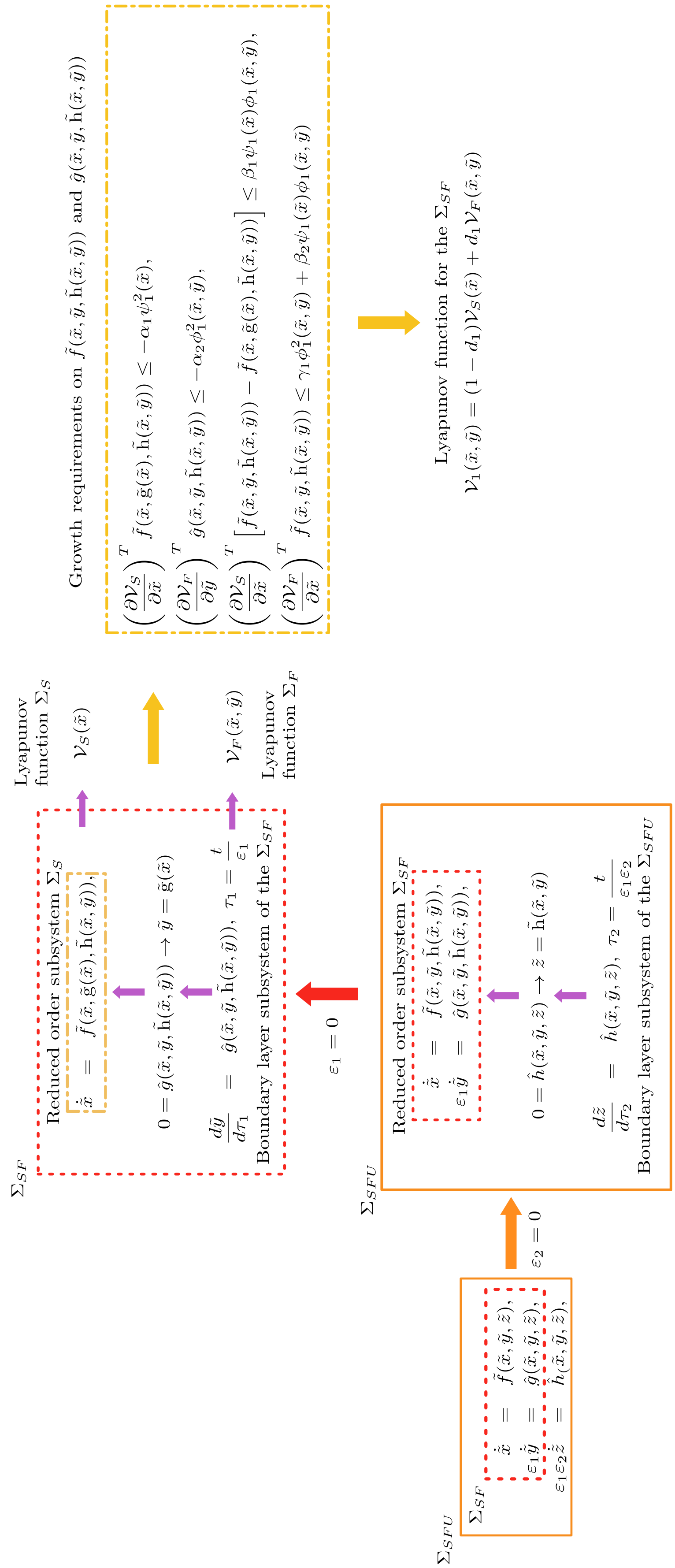

Figure 5.4: Σ_{SF} *Stability Analysis.*

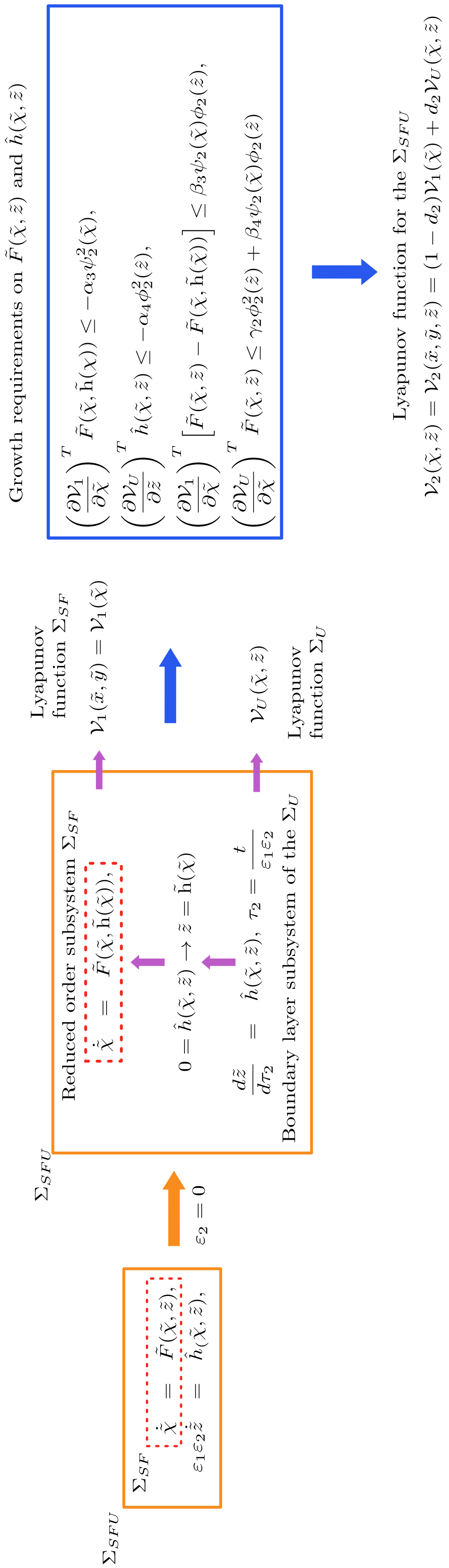

Figure 5.5: Σ_{SFU} *Stability Analysis.*

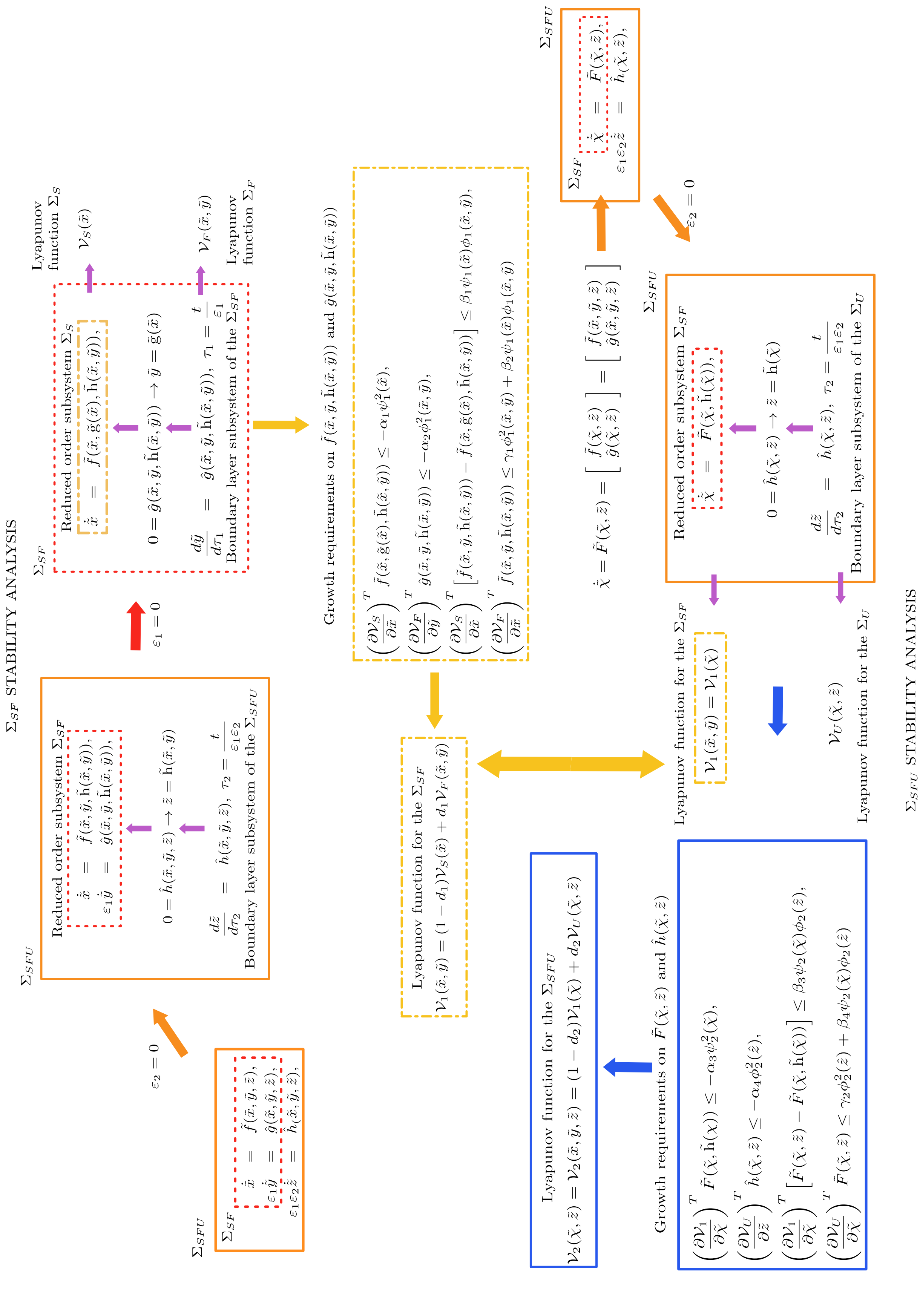

Figure 5.6: Σ_{SF} and Σ_{SFU} *Stability Analysis.*

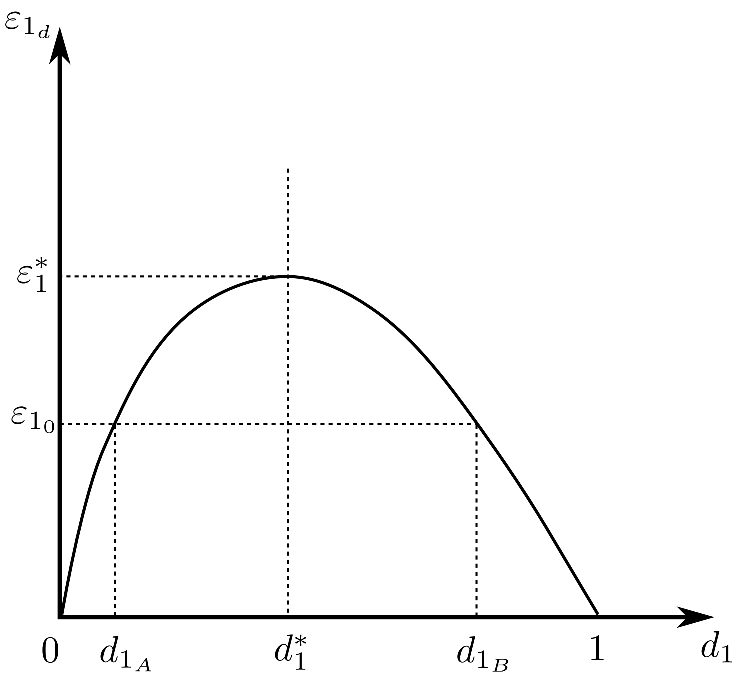

Figure 5.7: Stability upper bounds on ε_1 (Kokotović et al., 1986).

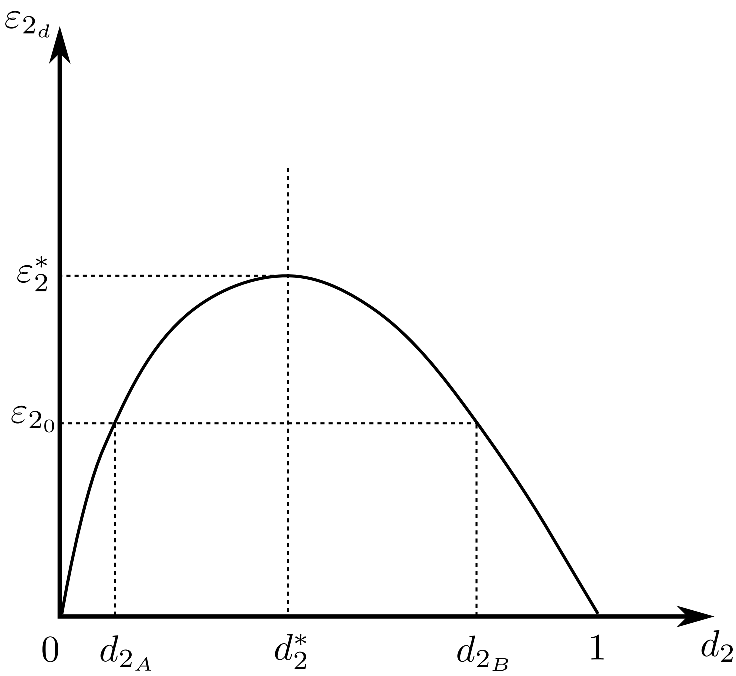

Figure 5.8: Stability upper bounds on ε_2 (Kokotović et al., 1986).

5.6 *Top-Down* and *Bottom-Up* Stability Analysis Extension for N^{th}-Time-Scale System

Similarly as conducted in section 3.6, in which the three-time-scale analysis was extended to a more general N^{th}-time-scale system, the Σ_{SFU} *Stability Analysis* can be extended to a more general N^{th}-time-scale system, thus becoming a valuable tool that can be used to analyze the asymptotic stability properties for any general singularly perturbed closed loop system. The major difference between the three-time-scale Σ_{SFU} *Stability Analysis* previously presented, and the N^{th}-time-scale general stability analysis, here resented, lies in the fact that after each subsystem reduction that results when applying the selected stretched time scale, the designer can continue with the selected time-scale decomposition using either the *TD* or the *BU* methodologies, depending on the system structure of the resulting reduced order and boundary layer subsystems, and what suits better in order to proceed with the time-scale decomposition. The methodology is divided in two steps

- In the first step the methodology defines the $N-1$ decomposed two-time-scale subsystems that will be used in the asymptotic stability analysis.
- In the second step, a stability analysis of the resulting $N-1$ reduced order two-time-scale singularly perturbed subsystem is conducted.

In the second step, the stability of each of resulting $N-1$ reduced order two-time-scale singularly perturbed subsystem is analyzed by starting with the smaller order reduced two-time-scale system, and continues by using the obtained stability results to demonstrate the stability properties of the higher order two-time-scale systems. Similarly as in section 3.6, to help in understanding the extension of the N^{th}-time-scale *Stability Analysis*, the author has chosen a general 4^{th}-time-scale system similar to the one previously defined in chapter 3, Eqns. (3.76–3.79), but expressed in error dynamics, that will allow to simplify the proposed asymptotic stability methodology. The proposed 4^{th}-time-scale system is rewritten in its error dynamics form given by

$$\dot{\tilde{x}} = \tilde{f}(\tilde{x},\tilde{y},\tilde{z},\tilde{w}),\ \tilde{x} \in \mathcal{R}^{\tilde{x}}, \tag{5.185}$$

$$\varepsilon_1\dot{\tilde{y}} = \hat{g}(\tilde{x},\tilde{y},\tilde{z},\tilde{w}),\ \tilde{y} \in \mathcal{R}^{\tilde{y}}, \tag{5.186}$$

$$\varepsilon_1\varepsilon_2\dot{\tilde{z}} = \hat{h}(\tilde{x},\tilde{y},\tilde{z},\tilde{w}),\ \tilde{z} \in \mathcal{R}^{\tilde{z}}, \tag{5.187}$$

$$\varepsilon_1\varepsilon_2\varepsilon_3\dot{\tilde{w}} = \hat{i}(\tilde{x},\tilde{y},\tilde{z},\tilde{w}),\ \tilde{x} \in \mathcal{R}^{\tilde{w}}. \tag{5.188}$$

with $B_{\tilde{x}} \subset \mathcal{R}^{\tilde{x}}$, $B_{\tilde{y}} \subset \mathcal{R}^{\tilde{y}}$, $B_{\tilde{z}} \subset \mathcal{R}^{\tilde{z}}$, and $B_{\tilde{w}} \subset \mathcal{R}^{\tilde{w}}$, denoting closed sets, and where for simplicity, Eqns. (5.185–5.188) will be denoted as the Σ_{SFU_2} full system. Recall also that, the error dynamics are defined by

$$\tilde{x} = x - x^*, \tag{5.189}$$

$$\tilde{y} = y - y^*, \tag{5.190}$$

$$\tilde{z} = z - z^*, \tag{5.191}$$

$$\tilde{w} = w - w^*, \tag{5.192}$$

with x^*, y^*, z^*, and w^* being the desired values of the state vectors x, y, z, and w, respectively. Figure 5.9 presents a schematic of the four possible solutions for the 4^{th}-time-scale, similarly to Figure 3.10, where the columns defined by A, B and C defined the three two-time-scale reduced order subsystems. For conciseness, only the third of the combinations, *Case* 3, will be briefly described in this section since uses a similar philosophy employed for the three-time-scale Σ_{SFU} *Stability Analysis* presented in this chapter.

5.6.1 1^{st}-Sequential Two-Time-Scale Decomposition for a 4^{th}-Time-Scale System

The first step, the sequential decomposition into the $N-1$ two-time-scale system, is a simple algebraic substitution in which the sequential order reduction is obtained after applying each of the three associated stretched time scales. That is, for *Case* 3 that will be described in this section, the sequential decomposition starts by first applying the stretched time scale given by

$$\tau_3 = \frac{t}{\varepsilon_1\varepsilon_2\varepsilon_3}, \tag{5.193}$$

resulting in the reduced order Σ_{SFU_1}-subsystem given by

$$\dot{\tilde{x}} = \tilde{f}\left(\tilde{x}, \tilde{y}, \tilde{z}, \tilde{\mathrm{i}}(\tilde{x}, \tilde{y}, \tilde{z})\right), \tag{5.194}$$

$$\varepsilon_1\dot{\tilde{y}} = \hat{g}\left(\tilde{x}, \tilde{y}, \tilde{z}, \tilde{\mathrm{i}}(\tilde{x}, \tilde{y}, \tilde{z})\right), \tag{5.195}$$

$$\varepsilon_1\varepsilon_2\dot{\tilde{z}} = \hat{h}\left(\tilde{x}, \tilde{y}, \tilde{z}, \tilde{\mathrm{i}}(\tilde{x}, \tilde{y}, \tilde{z})\right), \tag{5.196}$$

depicted with the short-dashed line box in *Case A*, Figure 5.9. The associated boundary layer system, denoted as $\Sigma_{U_{\tau_3}}$ for simplicity, is given by

$$\frac{d\tilde{w}}{d\tau_3} = \hat{i}\left(\tilde{x}, \tilde{y}, \tilde{z}, \tilde{w}\right), \tag{5.197}$$

with $\tilde{\mathrm{i}}\left(\tilde{x}, \tilde{y}, \tilde{z}\right)$ representing the quasi-steady-equilibrium of the $\Sigma_{U_{\tau_3}}$-subsystem when setting $\varepsilon_3 = 0$, that is

$$0 = \hat{i}\left(\tilde{x}, \tilde{y}, \tilde{z}, \tilde{w}\right) \rightarrow \tilde{w} = \tilde{\mathrm{i}}(\tilde{x}, \tilde{y}, \tilde{z}). \tag{5.198}$$

The second sequential decomposition continues by applying the second stretched time scale given by

$$\tau_2 = \frac{t}{\varepsilon_1\varepsilon_2}, \tag{5.199}$$

to the Σ_{SFU_1}-subsystem, Eqns. (5.194–5.196), resulting in the reduced order Σ_{SF}-subsystem given by

$$\dot{\tilde{x}} = \tilde{f}\left(\tilde{x}, \tilde{y}, \tilde{\mathrm{h}}(\tilde{x}, \tilde{y}), \tilde{\mathrm{i}}(\tilde{x}, \tilde{y})\right), \tag{5.200}$$

$$\varepsilon_1\dot{\tilde{y}} = \hat{g}\left(\tilde{x}, \tilde{y}, \tilde{\mathrm{h}}(\tilde{x}, \tilde{y}), \tilde{\mathrm{i}}(\tilde{x}, \tilde{y})\right), \tag{5.201}$$

depicted with the dashed-dot line box in *Case B*, Figure 5.9. The associated boundary layer system, denoted as $\Sigma_{U_{\tau_2}}$ for simplicity, is given by

$$\frac{d\tilde{z}}{d\tau_2} = \hat{h}\left(\tilde{x}, \tilde{y}, \tilde{z}, \tilde{\mathrm{i}}(\tilde{x}, \tilde{y}, \tilde{z})\right), \tag{5.202}$$

with $\tilde{\mathrm{h}}\left(\tilde{x}, \tilde{y}\right)$ representing the quasi-steady-equilibrium of the $\Sigma_{U_{\tau_2}}$-subsystem when setting $\varepsilon_2 = 0$, that is

$$0 = \hat{h}\left(\tilde{x}, \tilde{y}, \tilde{z}, \tilde{\mathrm{i}}(\tilde{x}, \tilde{y}, \tilde{z})\right) \rightarrow \tilde{z} = \tilde{\mathrm{h}}(\tilde{x}, \tilde{y}). \tag{5.203}$$

Finally, the third and last sequential decomposition is obtained by applying the last stretched time scale given by

$$\tau_1 = \frac{t}{\varepsilon_1}, \tag{5.204}$$

to the Σ_{SF}-subsystem, Eqns. (5.200–5.201), resulting in the reduced order Σ_S-subsystem given by

$$\dot{\tilde{x}} = \tilde{f}\left(\tilde{x}, \tilde{\mathrm{g}}(\tilde{x}), \tilde{\mathrm{h}}(\tilde{x}), \tilde{\mathrm{i}}(\tilde{x})\right), \tag{5.205}$$

and with the boundary layer system, denoted as $\Sigma_{U_{\tau_1}}$ for simplicity, is given by

$$\frac{d\tilde{y}}{d\tau_1} = \hat{g}\left(\tilde{x}, \tilde{y}, \tilde{\mathrm{h}}(\tilde{x}, \tilde{y}), \tilde{\mathrm{i}}(\tilde{x}, \tilde{y})\right), \tag{5.206}$$

with $\tilde{\mathrm{g}}(\tilde{x})$ representing the quasi-steady-equilibrium of the $\Sigma_{U_{\tau_1}}$-subsystem when setting $\varepsilon_1 = 0$, that is

$$0 = \hat{g}\left(\tilde{x}, \tilde{y}, \tilde{\mathrm{h}}(\tilde{x}, \tilde{y}), \tilde{\mathrm{i}}(\tilde{x}, \tilde{y}, \tilde{\mathrm{h}})\right) \to \tilde{y} = \tilde{\mathrm{g}}(\tilde{x}), \tag{5.207}$$

where both subsystems can be seen in *Case C* in Figure 5.9. The second step of the stability analysis starts by analyzing the stability of the smallest two-time-scale subsystem which, for *Case C*, corresponds to the Σ_{SF}-subsystem, Eqns. (5.200–5.201), which is decomposed into the reduced order Σ_S-subsystem, Eq. (5.205), and the boundary layer Σ_F-subsystem, Eq. (5.206). It is also assumed that the Lyapunov function candidates are chosen following the same guidelines as in Section 5.4, in which they are derived considering the natural Lyapunov functions for the associated equilibrium equations, resulting in Lyapunov functions of the form

$$\mathcal{V}_S = \mathcal{V}_S(\tilde{x}), \tag{5.208}$$
$$\mathcal{V}_F = \mathcal{V}_F\left(\tilde{y} - \tilde{\mathrm{g}}(\tilde{x})\right) = \mathcal{V}_F\left(\hat{y}\right), \tag{5.209}$$
$$\mathcal{V}_{U_1} = \mathcal{V}_{U_1}\left(\tilde{z} - \tilde{\mathrm{h}}(\tilde{x}, \tilde{y})\right) = \mathcal{V}_{U_1}\left(\hat{z}\right), \tag{5.210}$$
$$\mathcal{V}_{U_2} = \mathcal{V}_{U_2}\left(\tilde{w} - \tilde{\mathrm{i}}(\tilde{x}, \tilde{y}, \tilde{z})\right) = \mathcal{V}_{U_2}\left(\hat{w}\right), \tag{5.211}$$

with

$$\hat{y} = \tilde{y} - \tilde{\mathrm{g}}(\tilde{x}), \tag{5.212}$$
$$\hat{z} = \tilde{z} - \tilde{\mathrm{h}}(\tilde{x}, \tilde{y}), \tag{5.213}$$
$$\hat{w} = \tilde{w} - \tilde{\mathrm{i}}(\tilde{x}, \tilde{y}, \tilde{z}), \tag{5.214}$$

where $\hat{y}$, $\hat{z}$, and $\hat{w}$ represent the error between the state vectors and the quasi-steady-state equilibria of the associated boundary layer subsystem which they form part. In following sections, the stability analysis of the resulting decomposed two-time-scale subsystems, the second step, is briefly described.

5.6.2 2^{nd}-Sequential Two-Time-Scale Decomposition for a 4^{th}-Time-Scale System

The sequential stability analysis for the 3^{rd}-order two-time-scale system, which for the *Case C* corresponds to the Σ_{SF} subsystem, is performed, similarly as in the generic three-time-scale asymptotic stability analysis, using the standard method for two-time-scale systems (Kokotović et al., 1986; Kokotović et al., 1987; Kokotović et al., 1999), in which the Lyapunov functions for the Σ_S and Σ_F subsystems, that is $\mathcal{V}_S(\tilde{x})$ and $\mathcal{V}_F(\tilde{y})$, Eqns. (5.208) and (5.208), respectively, must satisfy the growth requirements on $\tilde{f}(\tilde{x}, \tilde{y}, \tilde{\mathrm{h}}, \tilde{\mathrm{i}})$ and $\hat{g}(\tilde{x}, \tilde{y}, \tilde{\mathrm{h}}, \tilde{\mathrm{i}})$ by satisfying similar inequalities to the one described in section 5.2.1, which are described bellow:

- *Reduced System Conditions* 5.2.2.
- *Boundary-Layer System Conditions* 5.2.3.
- *First Interconnection Condition* 5.2.4.
- *Second Interconnection Conditions* 5.2.5.

Assumption 5.2.2, applied to the Σ_{SF}-subsystem, Eqns. (5.200–5.201), is satisfied by recognizing that there exists a positive-definite and decreasing Lyapunov function candidate $\mathcal{V}_S(\tilde{x})$ that satisfies the following inequality

$$\left(\frac{\partial \mathcal{V}_S(\tilde{x})}{\partial \tilde{x}}\right)^T \tilde{f}(\tilde{x}, \tilde{\mathrm{g}}(\tilde{x}), \tilde{\mathrm{h}}(\tilde{x}), \tilde{\mathrm{i}}(\tilde{x})) \leq -\alpha_1 \psi_1^2(\tilde{x}), \tag{5.215}$$

where $\psi_1(\cdot)$ is a scalar function of vector arguments which vanishes only when its argument are zero, and satisfying that $\tilde{x} = 0$ is a stable equilibrium of the reduced order system. Assumption 5.2.3 applied to the Σ_{SF}-subsystem, is satisfied by recognizing that there exists a positive-definite and decreasing Lyapunov function candidate $\mathcal{V}_F(\tilde{x}, \tilde{y})$ such that for all $(\tilde{x}, \tilde{y}) \in B_{\tilde{x}} \times B_{\tilde{y}}$ satisfies the inequality given by

$$\left(\frac{\partial \mathcal{V}_F}{\partial \tilde{y}}\right)^T \hat{g}(\tilde{x}, \tilde{y}, \tilde{\mathrm{h}}(\tilde{x}, \tilde{y}), \tilde{\mathrm{i}}(\tilde{x}, \tilde{y})) \leq -\alpha_2 \phi_1^2(\tilde{y} - \tilde{\mathrm{g}}(\tilde{x})), \tag{5.216}$$

where $\phi_1(\cdot)$ is a scalar function of vector arguments which vanishes only when its arguments are zero, and satisfying that $\tilde{y} - \tilde{\mathrm{g}}(\tilde{x})$ is a stable equilibrium of the boundary layer system. The first interconnection condition for the Σ_{SF}-subsystem, Assumption 5.2.4, consist in satisfying the inequality given by

$$\left(\frac{\partial \mathcal{V}_S(\tilde{x})}{\partial \tilde{x}}\right)^T \left[\tilde{f}(\tilde{x}, \tilde{y}, \tilde{\mathrm{h}}(\tilde{x}, \tilde{y}), \tilde{\mathrm{i}}(\tilde{x}, \tilde{y})) - \tilde{f}\left(\tilde{x}, \tilde{\mathrm{g}}(\tilde{x}), \tilde{\mathrm{h}}(\tilde{x}), \tilde{\mathrm{i}}(\tilde{x})\right)\right] \leq \beta_1 \psi_1(\tilde{x}) \phi_1(\tilde{y}), \tag{5.217}$$

while the second interconnection condition for the Σ_{SF}-subsystem, Assumption 5.2.5, consist in satisfying the inequality given by

$$\left(\frac{\partial \mathcal{V}_F(\tilde{y})}{\partial \tilde{x}}\right)^T \tilde{f}\left(\tilde{x}, \tilde{y}, \tilde{\mathrm{h}}(\tilde{x}, \tilde{y}), \tilde{\mathrm{i}}(\tilde{x}, \tilde{y})\right) \leq \gamma_1 \phi_1^2(\tilde{y}) + \beta_2 \psi_1(\tilde{x}) \phi_1(\tilde{y}). \tag{5.218}$$

The fulfillment of assumptions 5.5.1, 5.5.2, 5.5.3, 5.5.4, and 5.5.5, applied to the helicopter Σ_{SF}-subsystem by the fulfillment of inequalities 5.215, 5.216, 5.217, and 5.218, proves that the growth requirements of $\tilde{f}(\tilde{x}, \tilde{y}, \tilde{\mathrm{h}}(\tilde{x}, \tilde{y}), \tilde{\mathrm{i}}(\tilde{x}, \tilde{y}))$ and $\hat{g}(\tilde{x}, \tilde{y}, \tilde{\mathrm{h}}(\tilde{x}, \tilde{x}), \tilde{\mathrm{i}}(\tilde{x}, \tilde{y}))$ are satisfied, and with the Lyapunov functions $\mathcal{V}_S(\tilde{x})$ and $\mathcal{V}_F(\tilde{x}, \tilde{y})$, a new Lyapunov function candidate $\mathcal{V}_1(\tilde{x}, \tilde{y})$ is considered and defined by the weighted sum of $\mathcal{V}_S(\tilde{x})$ and $\mathcal{V}_F(\tilde{x}, \tilde{y})$, given by

$$\mathcal{V}_1(\tilde{x}, \tilde{y}) = (1 - d_1)\mathcal{V}_S(\tilde{x}) + d_1 \mathcal{V}_F(\tilde{y}),\ d_1 \in (0, 1), \tag{5.219}$$

for $0 < d_1 < 1$. The newly defined function $\mathcal{V}_1(\tilde{x}, \tilde{y})$ becomes the Lyapunov function candidate for the singular perturbed system Σ_{SF}-subsystem, Eqns. (5.200–5.201). Similarly, as conducted for the general two-time-scale methodology, computing the derivative $\mathcal{V}_1(\tilde{x}, \tilde{y})$ along the trajectories of $\tilde{f}(\tilde{x}, \tilde{y}, \tilde{\mathrm{h}}(\tilde{x}, \tilde{y}), \tilde{\mathrm{i}}(\tilde{x}, \tilde{y}))$ and $\hat{g}(\tilde{x}, \tilde{y}, \tilde{\mathrm{h}}(\tilde{x}, \tilde{y}), \tilde{\mathrm{i}}(\tilde{x}, \tilde{y}))$ results in the upper bounds for both d_1^* and ε_1^* given by

$$d_1^* = \frac{\beta_1}{\beta_1 + \beta_2}, \tag{5.220}$$

and

$$\varepsilon_1^* = \frac{\alpha_1 \alpha_2}{\alpha_1 \gamma_1 + \beta_1 \beta_2}. \tag{5.221}$$

Therefore, it can be inferred that the equilibrium point of the singularly perturbed Σ_{SF}-subsystem, Eqns. (5.200–5.201), is asymptotically stable for all $\varepsilon_1 < \varepsilon_1^*$. The number ε_1^* is the best upper bound on ε_1 that can be provided by the above presented stability analysis. The asymptotic stability analysis presented can be summarizes in Theorem 5.6.1.

Theorem 5.6.1 *: Let inequalities (5.215), (5.216), (5.217), and (5.218) be satisfied. Then the origin is an asymptotically stable equilibrium of the singularly perturbed system Σ_{SF}-subsystem, Eqns (5.200–5.201) for all $\varepsilon_1 \in (0, \varepsilon_1^*)$, where ε_1^* is given by Eq. (5.221). Moreover, for every number $d_1 \in (0, 1)$, the resulting Lyapunov function $\mathcal{V}_1(\tilde{x}, \tilde{y})$, Eq. (5.219), is a Lyapunov function for all $\varepsilon_1(0, \varepsilon_{d_1})$, where $\varepsilon_1 \leq \varepsilon_1^*$ is given by Eq. (5.221).*

Theorem 5.6.1 can be summarized by understanding that $\tilde{x} = 0$ is an asymptotically stable equilibrium of the reduced Σ_S-subsystem, Eq. (5.205), and $\tilde{y} = \tilde{\text{g}}(\tilde{x})$ is an asymptotically stable equilibrium of the boundary-layer Σ_F-subsystem, Eq.(5.206) uniformly in $\tilde{x}$, that is, the $\varepsilon - \delta$ definition of *Lyapunov* stability and the convergence $\tilde{y} \to \tilde{\text{g}}(\tilde{x})$ are uniform in $\tilde{x}$ (Vidyasagar, 2002), and if $\tilde{f}(\tilde{x}, \tilde{y}, \tilde{\text{h}}(\tilde{x}, \tilde{y}))$ and $\hat{g}(\tilde{x}, \tilde{y}, \tilde{\text{h}}(\tilde{x}, \tilde{y}))$ satisfy certain growth conditions on the reduced and boundary-layer systems, assumptions 5.5.1, 5.5.2, 5.5.3, 5.5.4, and 5.5.5, then the origin is an asymptotically stable equilibrium of the singularly perturbed Σ_{SF}-subsystem, Eqns. (5.200–5.201), for sufficiently small ε_1. (Kokotović et al., 1986; Kokotović et al., 1987; Kokotović et al., 1999).

5.6.3 3^{rd}-Sequential Two-Time-Scale Decomposition for a 4^{th}-Time-Scale System

Once demonstrated the asymptotic stability properties for the Σ_{SF}-subsystem, Eqns. (5.200–5.201), resulting in a valid Lyapunov function, Eq. (5.219), and with the upper bounds d_1^* and ε_1^* being given by Eqns. (5.220) and (5.221), respectively, the strategy shifts towards, demonstrating the asymptotic stability properties for the next higher order two-time-scale subsystem, which is given by *Case B*, that is the Σ_{SFU_1}, Eqns. (5.194–5.196).

Recall that as discussed previously, the Σ_{SFU_1}-subsystem can be decomposed into a two-time-scale subsystem by applying the stretched time scale given by τ_2, Eq. (5.199), resulting in the reduced order (slow) model given by the Σ_{SF}-subsystem, Eq. (5.200–5.201), while the boundary (fast) layer is given by the $\Sigma_{U_{\tau_2}}$-subsystem, Eq. (5.202). Recall also that employing a methodology similar to the one used in the Σ_{SFU} *Stability Analysis* presented for the three-time-scale model in section 5.5.3, the stability analysis for the Σ_{SFU_1}-subsystem, Eq. (5.194–5.196), is conducted by considering the results obtained in the previous step. These results provide the associated Lyapunov function for the reduced order Σ_{SF}-subsystem, $\mathcal{V}_1(\tilde{x}, \tilde{y})$, and recalling that $\mathcal{V}_{U_1}(\hat{z})$, Eq. (5.210), is the associated Lyapunov function for the $\Sigma_{U_{\tau_2}}$-subsystem, Eq. (5.202), this permits to analyze the stability of the Σ_{SFU_1}-subsystem. Prior to start with the asymptotic stability analysis of the Σ_{SFU_1}-subsystem, let first introduced a change of variables that allows to rewrite the Σ_{SFU_1}-subsystem, Eqns. (5.194–5.196) as

$$\dot{\tilde{\chi}}_1 = \tilde{F}_1(\tilde{\chi}_1, \tilde{z}, \tilde{\text{i}}(\tilde{\chi}_1, \tilde{z})),\ \tilde{\chi}_1 \in \mathcal{R}^{\tilde{\chi}_1}, \tag{5.222}$$
$$\varepsilon_1\varepsilon_2\dot{\tilde{z}} = \hat{h}(\tilde{\chi}_1, \tilde{z}, \tilde{\text{i}}(\tilde{\chi}_1, \tilde{z})),\ \tilde{z} \in \mathcal{R}^{\tilde{z}}, \tag{5.223}$$

with $B_{\tilde{\chi}_1} \subset \mathcal{R}^{\tilde{\chi}_1}$ and $B_{\tilde{z}} \subset \mathcal{R}^{\tilde{z}}$ denoting closed sets, and where $\tilde{F}_1(\tilde{\chi}_1, \tilde{z}, \tilde{\text{i}}(\tilde{\chi}_1, \tilde{z}))$ represent the slow dynamics of the Σ_{SFU_1}-subsystem, when applying the stretched time scale $\tau_2 = t/(\varepsilon_1\varepsilon_2)$, which is also equivalent to the Σ_{SF}-subsystem defined in Eqns. (5.200–5.201), therefore, resulting in

$$\tilde{F}_1(\tilde{\chi}_1, \tilde{z}, \tilde{\text{i}}(\tilde{\chi}_1, \tilde{z})) \triangleq \begin{bmatrix} \tilde{f}(\tilde{\chi}_1, \tilde{z}, \tilde{\text{i}}(\tilde{\chi}_1, \tilde{z})) \\ \hat{g}(\tilde{\chi}_1, \tilde{z}, \tilde{\text{i}}(\tilde{\chi}_1, \tilde{z})) \end{bmatrix} = \begin{bmatrix} \tilde{f}(\tilde{x}, \tilde{y}, \tilde{z}, \tilde{\text{i}}(\tilde{\chi}_1, \tilde{z}) \\ \hat{g}(\tilde{x}, \tilde{y}, \tilde{z}, \tilde{\text{i}}(\tilde{\chi}_1, \tilde{z}) \end{bmatrix}, \tag{5.224}$$

where $\tilde{\chi}_1$ represents the augmented state vector given by

$$\tilde{\chi}_1 \triangleq \begin{bmatrix} \tilde{x} & \tilde{y} \end{bmatrix}^T. \tag{5.225}$$

Therefore, the Lyapunov function $\mathcal{V}_1(\tilde{\chi})$, Eq. (5.219), that was obtained in the previous stage of the stability analysis, becomes the Lyapunov function for the $\tilde{F}_1(\tilde{\chi}_1, \tilde{z}, \tilde{\text{i}}(\tilde{\chi}_1, \tilde{z}))$ subsystem. Both Lyapunov functions, $\mathcal{V}_1(\tilde{\chi}_1)$ and $\mathcal{V}_{U_1}(\tilde{\chi}_1, \tilde{z})$, must fulfill certain growth requirements for $\tilde{F}_1(\tilde{\chi}_1, \tilde{z}, \tilde{\text{i}}(\tilde{\chi}_1, \tilde{z}))$, and $\hat{h}(\tilde{\chi}_1, \tilde{z}, \tilde{\text{i}}(\tilde{\chi}_1, \tilde{z}))$, by satisfying similar inequalities to the one described in section 5.2.1. Assumption 5.2.2 applied to the Σ_{SFU_1}-subsystem, Eqns. (5.194–5.196) is satisfied by recognizing that there exists a positive-definite and decreasing Lyapunov function candidate $\mathcal{V}_1(\tilde{\chi})$ that satisfies inequality given by

$$\left(\frac{\partial \mathcal{V}_1(\tilde{\chi}_1)}{\partial \tilde{\chi}_1}\right)^T \tilde{F}_1(\tilde{\chi}_1, \tilde{\mathrm{h}}(\tilde{\chi}_1), \tilde{\mathrm{i}}(\tilde{\chi}_1)) \leq -\alpha_3 \psi_2^2(\tilde{\chi}_1), \tag{5.226}$$

where $\psi_2(\cdot)$ is a scalar function of vector arguments which vanishes only when its argument are zero, and satisfying that $\tilde{\chi}_1 = 0$ is a stable equilibrium of the reduced order system. Assumption 5.2.3 applied to the Σ_{SFU_1}-subsystem, is satisfied by recognizing that there exists a positive-definite and decreasing Lyapunov function candidate $\mathcal{V}_{U_1}(\tilde{\chi}_1, \tilde{z})$ such that for all $(\tilde{\chi}_1, \tilde{z}) \in B_{\tilde{\chi}_1} \times B_{\tilde{z}}$ satisfies inequality given by

$$\left(\frac{\partial \mathcal{V}_{U_1}}{\partial \tilde{z}}\right)^T \hat{h}(\tilde{\chi}_1, \tilde{z}, \tilde{\mathrm{i}}(\tilde{\chi}_1, \tilde{z}) \leq -\alpha_4 \phi_2^2(\tilde{z} - \tilde{\mathrm{h}}(\tilde{\chi}_1)), \tag{5.227}$$

where $\phi_2(\cdot)$ is a scalar function of vector arguments which vanishes only when its arguments are zero, and satisfying that $\tilde{z} - \tilde{\mathrm{h}}(\tilde{\chi}_1)$ is a stable equilibrium of the boundary layer system. The first interconnection condition for the Σ_{SFU_1}-subsystem, Assumption 5.2.4, consist in satisfying the inequality given by

$$\left(\frac{\partial \mathcal{V}_1(\tilde{\chi}_1)}{\partial \tilde{\chi}_1}\right)^T \left[\tilde{F}_1(\tilde{\chi}_1, \tilde{z}, \tilde{\mathrm{i}}(\tilde{\chi}_1, \tilde{z})) - \tilde{F}_1\left(\tilde{\chi}_1, \tilde{\mathrm{h}}(\tilde{\chi}_1), \tilde{\mathrm{i}}(\tilde{\chi}_1)\right)\right] \leq \beta_3 \psi_2(\tilde{\chi}_1)\phi_2(\tilde{z} - \tilde{\mathrm{h}}(\tilde{\chi}_1)), \tag{5.228}$$

while the second interconnection condition for the Σ_{SFU_1}-subsystem, Assumption 5.2.5, consist in satisfying the inequality given by

$$\left(\frac{\partial \mathcal{V}_{U_1}(\tilde{\chi}_1, \tilde{z})}{\partial \tilde{\chi}_1}\right)^T \tilde{F}_1\left(\tilde{\chi}_1, \tilde{z}, \tilde{\mathrm{i}}(\tilde{\chi}_1, \tilde{z})\right) \leq \gamma_2 \phi_2^2(\tilde{z} - \tilde{\mathrm{h}}(\tilde{\chi}_1)) + \beta_4 \psi_2(\tilde{\chi}_1)\phi_2(\tilde{z} - \tilde{\mathrm{h}}(\tilde{\chi}_1)). \tag{5.229}$$

The fulfillment of assumptions 5.5.1, 5.5.2, 5.5.3, 5.5.4, and 5.5.5, applied to the Σ_{SFU_1}-subsystem by the fulfillment of inequalities 5.226, 5.227, 5.228, and 5.229, proves that the growth requirements of $\tilde{F}_1\left(\tilde{\chi}_1, \tilde{z}, \tilde{\mathrm{i}}(\tilde{\chi}_1, \tilde{z})\right)$ and $\hat{h}\left(\tilde{\chi}_1, \tilde{z}, \tilde{\mathrm{i}}(\tilde{\chi}_1, \tilde{z})\right)$ are satisfied, and with the Lyapunov functions $\mathcal{V}_1(\tilde{\chi}_1)$ and $\mathcal{V}_{U_1}(\tilde{\chi}_1, \tilde{z})$, a new Lyapunov function candidate $\mathcal{V}_2(\tilde{\chi}_1, \tilde{z})$ is considered and given by

$$\mathcal{V}_2(\tilde{\chi}_1, \tilde{z}) = (1 - d_2)\mathcal{V}_1(\tilde{\chi}_1) + d_2 \mathcal{V}_{U_1}(\tilde{\chi}_1, \tilde{z}),\ d_2 \in (0, 1), \tag{5.230}$$

for $0 < d_2 < 1$. The newly defined function $\mathcal{V}_2(\tilde{\chi}_1, \tilde{z}_1)$ becomes the Lyapunov function candidate for the singular perturbed Σ_{SFU_1}-subsystem, Eqns. (5.194–5.196). Similarly as conducted for the general two-time-scale methodology, by computing the derivative $\mathcal{V}_2(\tilde{\chi}_1, \tilde{z})$ along the trajectories of $\tilde{F}_1\left(\tilde{\chi}_1, \tilde{z}, \tilde{\mathrm{i}}(\tilde{\chi}_1, \tilde{z})\right)$ and $\hat{h}\left(\tilde{\chi}_1, \tilde{z}, \tilde{\mathrm{i}}(\tilde{\chi}_1, \tilde{z})\right)$ results in the upper bounds for both d_2^* and ε_2^* given by

$$d_2^* = \frac{\beta_3}{\beta_3 + \beta_4}, \tag{5.231}$$

and

$$\varepsilon_2^* = \frac{1}{\varepsilon_1} \frac{\alpha_3 \alpha_4}{\alpha_3 \gamma_2 + \beta_3 \beta_4}, \tag{5.232}$$

where recalling that the upper bound on ε_1 was defined in Eq. (5.221), therefore, by selecting $\varepsilon_1 \equiv \varepsilon_1^*$, the smallest possible upper bound on ε_2, and thus the most conservative upper bound, becomes

$$\varepsilon_2^* = \frac{\alpha_1 \gamma_1 + \beta_1 \beta_2}{\alpha_1 \alpha_2} \frac{\alpha_3 \alpha_4}{\alpha_3 \gamma_2 + \beta_3 \beta_4}, \tag{5.233}$$

where it can also be observed that the upper bound on the Σ_{SFU_1}-subsystem is a function of the previously derived lower order stability analysis upperbounds. Therefore, it can be inferred that the equilibrium point of the singularly perturbed Σ_{SFU_1}-subsystem, Eqns. (5.194–5.196), is asymptotically stable for all $\varepsilon_2 < \varepsilon_2^*$. The number ε_2^* is the best upper bound on ε_2 that can be provided by the above presented stability analysis. The asymptotic stability analysis presented can be summarizes in Theorem 5.6.2.

Theorem 5.6.2 *: Let inequalities (5.226), (5.227), (5.228), and (5.229) be satisfied. Then the origin is* *an asymptotically stable equilibrium of the singularly perturbed system Σ_{SFU_1}-subsystem, Eqns. (5.194–5.196) for all $\varepsilon_2 \in (0, \varepsilon_2^*)$, where ε_2^* is given by Eq. (5.232). Moreover, for every number $d_2 \in (0,1)$, the resulting Lyapunov function $\mathcal{V}_2(\tilde{\chi}_1, \tilde{z})$, Eq. (5.243), is a Lyapunov function for all $\varepsilon_2(0, \varepsilon_{d_2})$, where $\varepsilon_2 \leq \varepsilon_2^*$ is given by Eq. (5.233).*

Theorem 5.6.2 can be summarized by understanding that $\tilde{\chi}_1 = 0$ is an asymptotically stable equilibrium of the reduced Σ_{SF}-subsystem, Eqns. (5.200–5.201), and $\tilde{z} = \tilde{\mathrm{h}}(\tilde{\chi}_1)$ is an asymptotically stable equilibrium of the boundary-layer $\Sigma_{U_{\tau_2}}$-subsystem, Eq. (5.202), uniformly in $\tilde{\chi}_1$, that is, the $\varepsilon - \delta$ definition of *Lyapunov* stability and the convergence $\tilde{z} \to \tilde{\mathrm{h}}(\tilde{\chi}_1)$ are uniform in $\tilde{\chi}_1$ (Vidyasagar, 2002), and if $\tilde{F}_1\left(\tilde{\chi}_1, \tilde{z}, \tilde{\mathrm{i}}(\tilde{\chi}_1, \tilde{z})\right)$ and $\hat{h}\left(\tilde{\chi}_1, \tilde{z}, \tilde{\mathrm{i}}(\tilde{\chi}_1, \tilde{z})\right)$ satisfy certain growth conditions on the reduced and boundary-layer systems, assumptions 5.5.1, 5.5.2, 5.5.3, 5.5.4, and 5.5.5, then the origin is an asymptotically stable equilibrium of the singularly perturbed Σ_{SFU_1}-subsystem, Eqns. (5.194–5.196), for sufficiently small ε_2. (Kokotović et al., 1986; Kokotović et al., 1987; Kokotović et al., 1999).

5.6.4 4^{th}-Sequential Two-Time-Scale Decomposition for a 4^{th}-Time-Scale System

Finally, once demonstrated the asymptotic stability properties for the Σ_{SFU_1}-subsystem, Eqns. (5.194–5.196), resulting in a valid Lyapunov function, Eq. (5.230), and with the upper bounds being given by Eqns. (5.231) and (5.233), the strategy shifts towards, demonstrating the asymptotic stability properties for the original higher order two-time-scale subsystem, which is given by *Case A*, that is the original Σ_{SFU_2} system, Eqns. (5.185–5.188).

As seen in *Case A*, Figure 5.9, the Σ_{SFU_2} original system is decomposed into a two-time-scale subsystem by applying the stretched time scale given by τ_3, Eq. (5.193), resulting in the reduced order (slow) model given by the Σ_{SFU_1}-subsystem, Eqns. (5.194–5.196), while the boundary (fast) layer is given by the $\Sigma_{U_{\tau_3}}$-subsystem, Eq. (5.197).

The stability analysis for the Σ_{SFU_2} system, Eqns. (5.194–5.196), is conducted by considering the results obtained in the previous step. These results provide the associated Lyapunov function for the reduced order subsystem, Σ_{SFU_1}-subsystem, resulting when applying the stretched time scale given by τ_3, given by $\mathcal{V}_2(\tilde{\chi}, \tilde{z})$, and recalling that $\mathcal{V}_{U_3}(\hat{w})$, Eq. (5.210), is the associated Lyapunov function for the $\Sigma_{U_{\tau_3}}$-subsystem, Eq. (5.197), which permits to analyze the stability of the full Σ_{SFU_2} system. Prior to start with the asymptotic stability analysis of the Σ_{SFU_2}-subsystem, and similarly as previously conducted, let extend the change of variables that allows to rewrite the Σ_{SFU_2}-subsystem (5.185–5.188) as

$$\dot{\tilde{\chi}}_2 = \tilde{F}_2(\tilde{\chi}_2, \tilde{w},),\ \tilde{\chi}_2 \in \mathcal{R}^{\tilde{\chi}_2}, \tag{5.234}$$

$$\varepsilon_1\varepsilon_2\varepsilon_3\dot{\tilde{w}} = \hat{i}(\tilde{\chi}_2, \tilde{w}),\ \tilde{w} \in \mathcal{R}^{\tilde{w}}, \tag{5.235}$$

with $B_{\tilde{\chi}_2} \subset \mathcal{R}^{\tilde{\chi}_2}$ and $B_{\tilde{w}} \subset \mathcal{R}^{\tilde{w}}$ denoting closed sets, and where $\tilde{F}_2(\tilde{\chi}_2, \tilde{w})$ represents the slow dynamics of the Σ_{SFU_2} system, when applying the stretched time scale $\tau_3 = t/(\varepsilon_1\varepsilon_2\varepsilon_3)$, which is given by Eqns. (5.194–5.196), that is

$$\tilde{F}_2(\tilde{\chi}_2, \tilde{w}) \triangleq \begin{bmatrix} \tilde{F}_1(\tilde{\chi}_2, \tilde{w}) \\ \hat{h}(\tilde{\chi}_2, \tilde{w}) \end{bmatrix}, \tag{5.236}$$

where $\tilde{F}_1$ was previously defined in Eq. (5.224) as

$$\tilde{F}_1(\tilde{\chi}_2, \tilde{w}) \triangleq \begin{bmatrix} \tilde{f}(\tilde{\chi}_2, \tilde{w}) \\ \hat{g}(\tilde{\chi}_2, \tilde{w}) \end{bmatrix}, \tag{5.237}$$

with $\tilde{\chi}_2$ being the augmented state vector given by

$$\tilde{\chi}_2 = \begin{bmatrix} \tilde{\chi}_1 & \tilde{z} \end{bmatrix}^T = \begin{bmatrix} \tilde{x} & \tilde{y} & \tilde{z} \end{bmatrix}^T, \tag{5.238}$$

Therefore, the Lyapunov function $\mathcal{V}_2(\tilde{\chi}_2)$ that was obtained in the previous stage of the stability analysis, Eq. (5.230), becomes the Lyapunov function for the $\tilde{F}_2(\tilde{\chi}_2, \tilde{w})$ subsystem. Both Lyapunov functions, $\mathcal{V}_2(\tilde{\chi}_2)$ and $\mathcal{V}_{U_2}(\tilde{\chi}_2, \tilde{z}_2)$, must fulfill the growth requirements for $\tilde{F}_2(\tilde{\chi}_2, \tilde{w})$ and $\hat{\imath}(\tilde{\chi}_2, \tilde{w})$ by satisfying certain inequalities. These growth requirements for the Σ_{SFU_2} system take the form of inequalities which are described bellow. Assumption 5.2.2 applied to the Σ_{SFU_2}-subsystem, Eqns. (5.185–5.188), is satisfied by recognizing that there exists a positive-definite and decreasing Lyapunov function candidate $\mathcal{V}_2(\tilde{\chi})$ that satisfies inequality given by

$$\left(\frac{\partial \mathcal{V}_2(\tilde{\chi}_2)}{\partial \tilde{\chi}_2}\right)^T \tilde{F}_2(\tilde{\chi}_2, \tilde{\mathrm{i}}(\tilde{\chi}_2)) \leq -\alpha_5 {\psi_3}^2(\tilde{\chi}_2), \tag{5.239}$$

where $\psi_3(\cdot)$ is a scalar function of vector arguments which vanishes only when its argument are zero, and satisfying that $\tilde{\chi}_2 = 0$ is a stable equilibrium of the reduced order system. Assumption 5.2.3 applied to the Σ_{SFU_2}-subsystem, is satisfied by recognizing that there exists a positive-definite and decreasing Lyapunov function candidate $\mathcal{V}_{U_2}(\tilde{\chi}, \tilde{z})$ such that for all $(\tilde{\chi}_2, \tilde{w}) \in \mathrm{B}_{\tilde{\chi}_2} \times B_{\tilde{w}}$ satisfies

$$\left(\frac{\partial \mathcal{V}_{U_2}}{\partial \tilde{w}}\right)^T \hat{\imath}(\tilde{\chi}_2, \tilde{w}) \leq -\alpha_6 {\phi_3}^2(\tilde{w} - \tilde{\mathrm{i}}(\tilde{\chi}_2)), \tag{5.240}$$

where $\phi_3(\cdot)$ is a scalar function of vector arguments which vanishes only when its arguments are zero, and satisfying that $\tilde{w} - \tilde{\mathrm{i}}(\tilde{\chi}_2)$ is a stable equilibrium of the boundary layer system. The first interconnection condition for the Σ_{SFU_2}-subsystem, Assumption 5.2.4, consist in satisfying the inequality given by

$$\left(\frac{\partial \mathcal{V}_2(\tilde{\chi}_2)}{\partial \tilde{\chi}_2}\right)^T \left[\tilde{F}_2(\tilde{\chi}_2, \tilde{w}) - \tilde{F}_2\left(\tilde{\chi}_2, \tilde{\mathrm{i}}(\tilde{\chi}_2)\right)\right] \leq \beta_5 \psi_3(\tilde{\chi}_2)\phi_3(\tilde{w} - \tilde{\mathrm{i}}(\tilde{\chi}_2)), \tag{5.241}$$

while the second interconnection condition for the Σ_{SFU_2}-subsystem, Assumption 5.2.5, consist in satisfying the inequality given by

$$\left(\frac{\partial \mathcal{V}_{U_2}(\tilde{\chi}_2, \tilde{w})}{\partial \tilde{\chi}_2}\right)^T \tilde{F}_2\left(\tilde{\chi}_2, \tilde{w}\right) \leq \gamma_3 {\phi_3}^2(\tilde{w} - \tilde{\mathrm{i}}(\tilde{\chi}_2)) + \beta_6 \psi_3(\tilde{\chi}_2)\phi_3(\tilde{w} - \tilde{\mathrm{i}}(\tilde{\chi}_2)). \tag{5.242}$$

The fulfillment of assumptions 5.5.1, 5.5.2, 5.5.3, 5.5.4, and 5.5.5, applied to the helicopter Σ_{SF}-subsystem by the fulfillment of inequalities 5.239, 5.240, 5.241, and 5.242, proves that the growth requirements of $\tilde{F}_2\left(\tilde{\chi}_2, \tilde{w}\right))$ and $\hat{\imath}\left(\tilde{\chi}_2, \tilde{w}\right)$ are satisfied, and with the Lyapunov functions $\mathcal{V}_2(\tilde{\chi}_2)$ and $\mathcal{V}_{U_2}(\tilde{\chi}_2, \tilde{w})$, a new Lyapunov function candidate $\mathcal{V}_3(\tilde{\chi}_2, \tilde{w})$ is considered and given by

$$\mathcal{V}_3(\tilde{\chi}_2, \tilde{z}) = (1 - d_3)\mathcal{V}_2(\tilde{\chi}_2) + d_3 \mathcal{V}_{U_2}(\tilde{\chi}_2, \tilde{z}),\ d_3 \in (0, 1), \tag{5.243}$$

for $0 < d_3 < 1$. The newly defined function $\mathcal{V}_3(\tilde{\chi}_2, \tilde{z}_2)$ becomes the Lyapunov function candidate for the singular perturbed Σ_{SFU_2}-subsystem, Eqns. (5.185–5.188). Similarly as conducted for the general two-time-scale methodology, by computing the derivative $\mathcal{V}_3(\tilde{\chi}_2, \tilde{w})$ along the trajectories of $\tilde{F}_2\left(\tilde{\chi}_2, \tilde{w}\right)$ and $\hat{\imath}\left(\tilde{\chi}_2, \tilde{w}\right)$ results in the upper bounds for both d_3^* and ε_3^* given by

$$d_3^* = \frac{\beta_5}{\beta_5 + \beta_6}, \tag{5.244}$$

and

$$\varepsilon_3^* = \frac{1}{\varepsilon_1 \varepsilon_2} \frac{\alpha_5 \alpha_6}{\alpha_5 \gamma_3 + \beta_5 \beta_6}. \tag{5.245}$$

Recalling that the selected upper bounds on ε_1 and ε_2 were defined in Eqns. (5.221), and (5.232), respectively, therefore, by selecting $\varepsilon_1 \equiv \varepsilon_1^*$, and $\varepsilon_2 \equiv \varepsilon_2^*$, the smallest possible upper bound on ε_2, and thus the most conservative upper bound, becomes

$$\begin{aligned}\varepsilon_3^* &= \frac{\alpha_1\gamma_1+\beta_1\beta_2}{\alpha_1\alpha_2}\frac{\alpha_1\alpha_2}{\alpha_1\gamma_1+\beta_1\beta_2}\frac{\alpha_3\gamma_2+\beta_3\beta_4}{\alpha_3\alpha_4}\frac{\alpha_5\alpha_6}{\alpha_5\gamma_3+\beta_5\beta_6}\\ &= \frac{\alpha_3\gamma_2+\beta_3\beta_4}{\alpha_3\alpha_4}\frac{\alpha_5\alpha_6}{\alpha_5\gamma_3+\beta_5\beta_6},\end{aligned} \tag{5.246}$$

where, again, it can be observed that the upper bound on the Σ_{SFU_2} system is a function of the previously derived lower order stability analysis upperbounds. Therefore, it can be inferred that the equilibrium point of the singularly perturbed Σ_{SFU_2} full system, Eqns. (5.185–5.188), is asymptotically stable for all $\varepsilon_3 < \varepsilon_3^*$. The number ε_3^* is the best upper bound on ε_3 that can be provided by the above presented stability analysis. The asymptotic stability analysis presented can be summarizes in Theorem 5.6.3.

Theorem 5.6.3 *: Let inequalities (5.239), (5.240), (5.241), and (5.242) be satisfied. Then the origin is an asymptotically stable equilibrium of the singularly perturbed system Σ_{SFU_2}-subsystem, Eqns. (5.185–5.188) for all $\varepsilon_3 \in (0, \varepsilon_3^*)$, where ε_3^* is given by Eq. (5.246). Moreover, for every number $d_3 \in (0,1)$, the resulting Lyapunov function $\mathcal{V}_3(\tilde{\chi}_2, \tilde{w})$, Eq. (5.243), is a Lyapunov function for all $\varepsilon_3(0, \varepsilon_{d_3})$, where $\varepsilon_d \leq \varepsilon_3^*$ is given by Eq. (5.246).*

Theorem 5.6.3 can be summarized by understanding that $\tilde{\chi}_2 = 0$ is an asymptotically stable equilibrium of the reduced Σ_{SFU_1}-subsystem, Eqns. (5.194–5.196), and $\tilde{w} = \tilde{\mathrm{i}}(\tilde{\chi}_2)$ is an asymptotically stable equilibrium of the boundary-layer $\Sigma_{U_{\tau_3}}$-subsystem, Eq. (5.197), uniformly in $\tilde{\chi}_2$, that is, the $\varepsilon - \delta$ definition of *Lyapunov* stability and the convergence $\tilde{w} \to \tilde{\mathrm{i}}(\tilde{\chi}_2)$ are uniform in $\tilde{\chi}_2$ (Vidyasagar, 2002), and if $\tilde{F}_2(\tilde{\chi}_2, \tilde{w})$ and $\hat{\imath}(\tilde{\chi}_2, \tilde{w})$ satisfy certain growth conditions on the reduced and boundary-layer systems, assumptions 5.5.1, 5.5.2, 5.5.3, 5.5.4, and 5.5.5, then the origin is an asymptotically stable equilibrium of the singularly perturbed Σ_{SFU_2} full system, Eqns. (5.185–5.188), for sufficiently small ε_3. (Kokotović et al., 1986; Kokotović et al., 1987; Kokotović et al., 1999).

This concludes the *Case* 3 of the four possible combinations that appear in Figure 5.9. Despite all four combinations should provide equivalent results, from the author's experience point view, *Case* 3 represents the more natural and simpler methods out of the possible *TD* and *BU* time-scale decompositions. The selection of *Case* 3 represents the simpler out of the possible combinations for the 3^{rd}-time-scale reduction, since follows the natural flow of time scales, starting with the stability analysis of the slowest, and simpler model, the Σ_{SF}-subsystem, Eqns. (5.200–5.201), which has been considerably simplified due to the fact that the quasi-steady-state equilibria of the associated boundary layer subsystems, $\tilde{\mathrm{h}}(\tilde{x})$, and $\tilde{\mathrm{i}}(\tilde{x})$, have been assumed to reach their space of configuration.

The extension to the N^{th}-time scale can easily be identified from the analysis of the 4^{th}-time-scale example above described. The sequential strategy of decomposing the 4^{th}-time-scale system, into simpler two-time-scale subsystems provides a valuable tool that permits determining the stability properties of any resulting singularly perturbed N^{th}-time-scale systems.

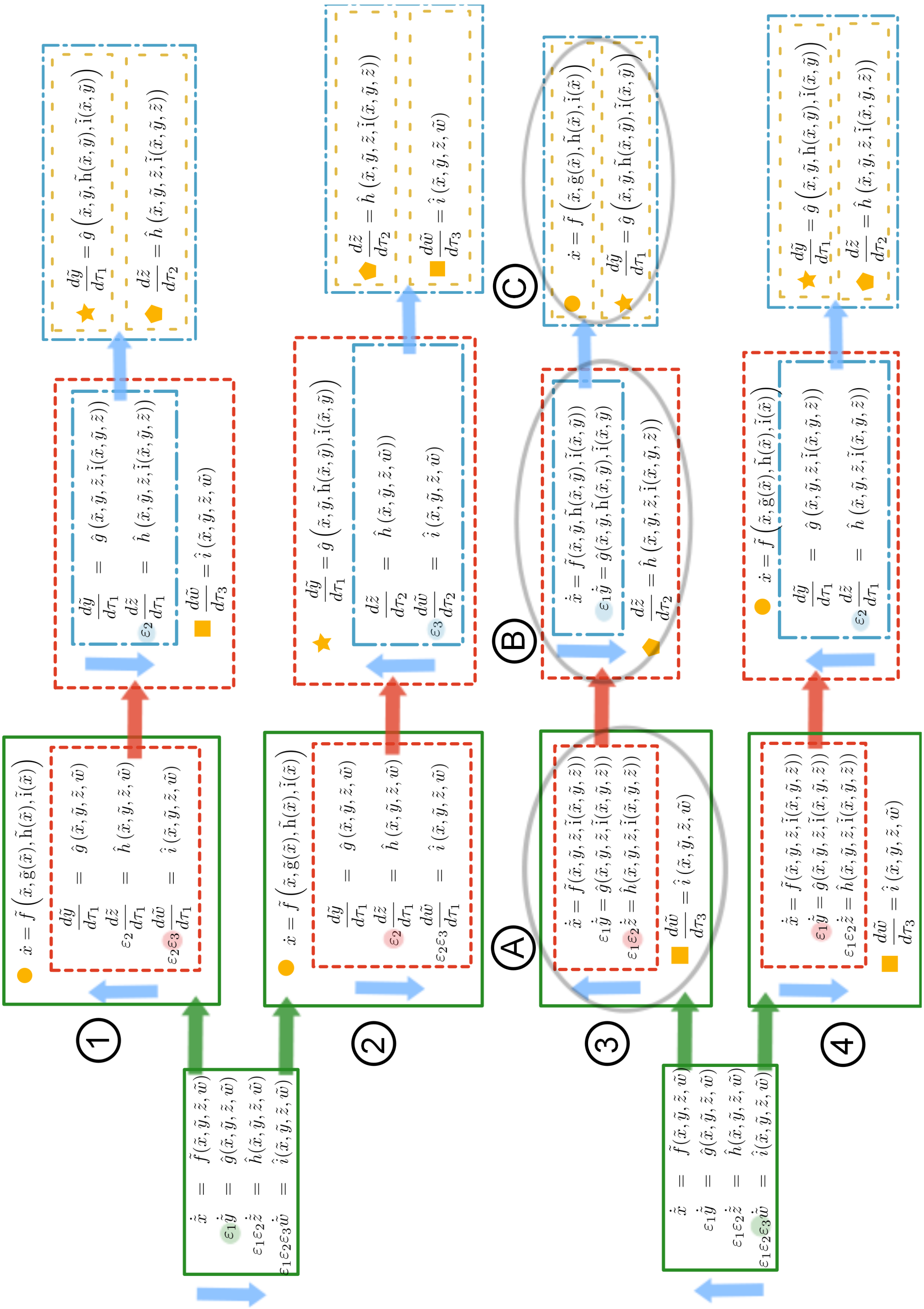

Figure 5.9: 4^{th}-time-scale *Top-Down* and *Bottom-Up* analysis strategy

5.7 Conclusions

A methodology that guarantee the asymptotic stability of the proposed control laws has been presented. In order to do so, and after analyzing the complexity of the existing methods to demonstrate the asymptotic stability properties of multiple time-scale singularly perturbed system, understanding for multiple time-scale systems those having at least three time-scales, a step-by-step sequential stability analysis methodology for three-time-scale systems has been derived and presented.

The asymptotic stability analysis methodology is based on the *TD* and/or *BU* time-scales analysis here presented, although for the system here analyze, and for completeness, only the *BU* asymptotic stability analysis is considered. The asymptotic stability analysis provides the necessary tools to guarantee the stability properties for any three-time-scale singularly perturbed autonomous systems, which permits to simplify the burden associated with the analysis multiple time-scale systems employing the existing stability methods.

The same philosophy that permits to analyze the asymptotical stability of an autonomous singular perturbed subsystem, provides, in a step-by-step process similar to the control strategy methodology, with the associated Lyapunov functions for each of the subsystems based on the natural desired closed loop response of each of the resulting subsystem. This methodology, much simpler that the one employed in the existing multiparameter time-scale analysis (Abed, 1985d; Abed, 1985e; Abed, 1985b; Kokotović et al., 1987; Kokotović et al., 1986), permits to have Lyapunov function candidates for each of the defined subsystems a priori of starting the stability analysis, and with a simple structure. The Lyapunov structure is fixed a priori, reducing the fulfillment of the growth requirements among the different time-scale subsystems to obtain the appropriate comparison functions and demonstrating the growth requirements among the different subsystems.

The proposed stability analysis methodology permits to simplify the burden associated with the analysis of non-autonomous singular perturbed systems by providing, in the same methodology, all the ingredients needed to infer asymptotical stability to an autonomous singular perturbed subsystem. The proposed sequential step-by-step two-step process allows to study the asymptotic stability properties of the closed loop system, and also proposes a methodology to obtain Lyapunov function candidate for each of the singularly perturbed subsystems. The validity of the methodology has been proved by obtaining the stability upper bound limits on the boundary layers, ε_1 and ε_2, and ensuring that the selected parasitic constants for the proposed three-time-scale model satisfy $\varepsilon_1 \leq \varepsilon_1^*$ and $\varepsilon_2 \leq \varepsilon_2^*$ for the three-time-scale model.

The *TD* and *BU* time scale analysis is also extended to the more general N^{th}-time scale analysis using a 4^{th}-time-scale general example. The sequential strategy of decomposing the 4^{th}-time-scale system, into simpler two-time-scale subsystems provides a valuable tool that will help in analyzing the stability properties of any general N^{th}-singularly perturbed time-scale system, and provide additional tools for the time-scale analysis for singularly perturbed systems.

Chapter 6

Stability Analysis for the Helicopter Model

6.1 Introduction

As noted in chapter 5, only the asymptotic stability analysis for helicopter problem is conducted in this chapter, while, for completeness and conciseness of the thesis, the complete stability analysis for the three-time-scale simplified model is left for Appendix C. The simplified example stability analysis can be used by the reader for better understanding the scope of the presented three-time-scale asymptotic stability analysis, following the same philosophy intended by the author throughout this thesis, which is to serve as an instrument that will ease the comprehension of the presented stability analysis methodology.

It is important to note that the simplified example has been an active part to the development of the selected strategies in both, the control and the asymptotic stability analysis, to the point that, in the final stages of this thesis, the simplified example has been the tool employed by the author for both, generate mathematical proofs, and validate the generality of the proposed strategies that have been later applied to the helicopter model. Furthermore, in order to reduce the readers's task, the simplified example stability analysis, presented in Appendix C, can be used as the solely source for understanding the asymptotic stability methodology here presented, and leave the asymptotic stability analysis for the helicopter model, for later reading, once the methodology have been fully understood.

Also for simplicity and conciseness of the thesis, the asymptotic stability analysis is only conducted on the TD control design for both the helicopter model in this chapter, and the simplified example in Appendix C, while the stability analysis for the $\mathcal{CF} - TD$ control design, although it has also been conducted with similar results to those obtained for the TD control design, are omitted to reduce the length of the thesis.

Similarly as in the general three-time-scale asymptotic stability analysis, section 5.5, the asymptotic stability analysis for the helicopter Σ_{SFU} full system is based on a double application of the standard two-time-scale stability analysis (Kokotović et al., 1999; Kokotović et al., 1986; Kokotović et al., 1987). Following sections describe in detail the asymptotic stability analysis for the helicopter model, although first, and for completeness of the chapter, a resumed description of the closed-loop helicopter model, with the different reduced and boundary layer subsystems is presented.

6.2 Helicopter Model for the Asymptotic Stability Analysis

This section describes the closed-loop error-dynamics for the helicopter model, which for conciseness, as previously mentioned, is only analyzed for the closed-loop error dynamics of the *TD* control design. Recall the original three-time-scale helicopter model given by Eqns. (3.56–3.60), and recall also that the closed-loop dynamics are obtained using the laws derived in *TD* control design, Eqns. (4.82) and (4.115),

Resulting in the three-time-scale closed-loop helicopter model given by

$$\begin{aligned}
\dot{x} &= a_{10}x^2\left[\sin(z_1) - \sin \mathrm{h}_{1_{\mathrm{SS}}}(x)\right] - b_x(x - x^*), && (6.1)\\
\varepsilon_1\dot{y}_1 &= c_1 y_2, && (6.2)\\
\varepsilon_1\dot{y}_2 &= x^2(c_2 + c_3 z_1 - \sqrt{c_4 + c_5 z_1}) + a_9 y_2 + a_9 y_2^2 + c_6, && (6.3)\\
\varepsilon_1\varepsilon_2\dot{z}_1 &= c_7 z_2, && (6.4)\\
\varepsilon_1\varepsilon_2\dot{z}_2 &= a_9 z_1 + c_9 z_2 + J_2\left[\left(1 + \sqrt{s_3 v(x,y)}\right)^2 - 1\right]. && (6.5)
\end{aligned}$$

These closed-loop equations can be rewritten into its error dynamics formulation recalling the introduced error dynamics state vector, Eqns. (5.30–5.32), thus defining the closed-loop error dynamics as

$$\begin{aligned}
\dot{\tilde{x}} &= a_{10}(\tilde{x} + x^*)^2\left[\sin(\tilde{z}_1 + z_1^*) - \sin \tilde{\mathrm{h}}_{1_{\mathrm{SS}}}(\tilde{x})\right] - b_x\tilde{x}, && (6.6)\\
\varepsilon_1\dot{\tilde{y}}_1 &= c_1\tilde{y}_2, && (6.7)\\
\varepsilon_1\dot{\tilde{y}}_2 &= (\tilde{x} + x^*)^2\left(c_2 + c_3(\tilde{z}_1 + z_1^*) - \sqrt{c_4 + c_5(\tilde{z}_1 + z_1^*)}\right) + a_9\tilde{y}_2 + a_9\tilde{y}_2^2 + c_6, && (6.8)\\
\varepsilon_1\varepsilon_2\dot{\tilde{z}}_1 &= \tilde{z}_2, && (6.9)\\
\varepsilon_1\varepsilon_2\dot{\tilde{z}}_2 &= a_9(\tilde{z}_1 + z_1^*) + c_9\tilde{z}_2 + J_2\left[\left(1 + \sqrt{s_3\tilde{v}(\tilde{x},\tilde{\boldsymbol{y}})}\right)^2 - 1\right], && (6.10)
\end{aligned}$$

where

$$K_e = K_c - a_{12} = -\frac{c_4}{c_5 c_{11} c_{13}}, \qquad (6.11)$$

and

$$\begin{aligned}
\tilde{v}(\tilde{x},\tilde{\boldsymbol{y}}) &= -\frac{a_9\tilde{y}_2^2 + (a_9 + \tilde{b}_{\tilde{y}_2})\tilde{y}_2 + \tilde{b}_{\tilde{y}_1}\tilde{y}_1 + c_6}{(\tilde{x} + x^*)^2}, && (6.12)\\
\tilde{v}_{SS}(\tilde{x},\tilde{\mathbf{g}}(\tilde{x})) &= -\frac{c_6}{(\tilde{x} + x^*)^2}, && (6.13)\\
\tilde{\mathrm{h}}_{1_{\mathrm{SS}}}(\tilde{x},\tilde{\mathbf{g}}(\tilde{x})) &= s_2\left[\left(1 + \sqrt{s_3\tilde{v}(\tilde{x},\tilde{\boldsymbol{y}})}\right)^2 - 1\right]. && (6.14)
\end{aligned}$$

See section 4.4 for further details in the control design. To help with the proof of the growth requirements that will be conducted in following sections, the following sections recap on the degenerated subsystems for the helicopter model, that is the Σ_S, Σ_F, Σ_U, Σ_{SF}, and Σ_{UF}-subsystems. It also describes the quasi-steady-state equilibria for the Σ_F and Σ_U-subsystems, that is $\tilde{\boldsymbol{y}} = \tilde{\mathbf{g}}(\tilde{x})$ and $\tilde{\boldsymbol{z}} = \tilde{\mathbf{h}}(\tilde{x},\tilde{\boldsymbol{y}})$, respectively, and also, the associated Lyapunov functions for the three degenerated subsystems, V_S, V_F and V_U. Recall that both $\tilde{\boldsymbol{y}} = \tilde{\mathbf{g}}(\tilde{x})$ and $\tilde{\boldsymbol{z}} = \tilde{\mathbf{h}}(\tilde{x},\tilde{\boldsymbol{y}})$ are expressed as in vector form to account for the equilibria of both the vertical displacement and collective pitch dynamics, Eqns. (6.35) and (6.23) respectively.

6.2.1 Degenerated Subsystems for the Helicopter Model

For completeness, and to help while reading the asymptotic stability analysis, this section collects the different degenerated subsystems employed throughout the rest of the asymptotic stability analysis for the helicopter model, that is the associated Σ_S, Σ_F, Σ_U, Σ_{SF}, and Σ_{UF}-subsystems. The associated quasi-steady-state equilibria for the Σ_F and Σ_U-subsystems are also collected. These subsystems were previously derived to determine the appropriate Lyapunov functions, thus the complete derivations will not be conducted again, and only a brief description is presented in this section. Further detains can be found in section 5.4.2.

Recalling from section 5.4.2, the reduced order Σ_{SF}-subsystem is given by

$$\begin{aligned}
\dot{\tilde{x}} &= a_{10}(\tilde{x}+x^*)^2(\sin(\tilde{\mathrm{h}}_1(\tilde{x},\tilde{\boldsymbol{y}})+z_1^*)-\sin\tilde{\mathrm{h}}_{1_{\mathrm{SS}}})-b_x\tilde{x}, && (6.15)\\
\varepsilon_1\dot{\tilde{y}}_1 &= c_1\tilde{y}_2, && (6.16)\\
\varepsilon_1\dot{\tilde{y}}_2 &= (\tilde{x}+x^*)^2\left(c_2+c_3(\tilde{\mathrm{h}}_1(\tilde{x},\tilde{\boldsymbol{y}})+z_1^*)-\sqrt{c_4+c_5(\tilde{\mathrm{h}}_1(\tilde{x},\tilde{\boldsymbol{y}})+z_1^*)}\right)\\
&+ a_9\tilde{y}_2+a_9\tilde{y}_2^2+c_6, && (6.17)
\end{aligned}$$

therefore being $\tilde{f}(\tilde{x},\tilde{\boldsymbol{y}},\tilde{\mathbf{h}}(\tilde{x},\tilde{\boldsymbol{y}}))$ given by

$$\dot{\tilde{x}} = a_{10}(\tilde{x}+x^*)^2(\sin(\tilde{\mathrm{h}}_1(\tilde{x},\tilde{\boldsymbol{y}})+z_1^*)-\sin\tilde{\mathrm{h}}_{1_{\mathrm{SS}}})-b_x\tilde{x}, \quad (6.18)$$

and $\hat{\boldsymbol{g}}(\tilde{x},\tilde{\boldsymbol{y}},\tilde{\mathbf{h}}(\tilde{x},\tilde{\boldsymbol{y}}))$ being defined by

$$\begin{aligned}
\varepsilon_1\dot{\tilde{y}}_1 &= c_1\tilde{y}_2, && (6.19)\\
\varepsilon_1\dot{\tilde{y}}_2 &= (\tilde{x}+x^*)^2\left(c_2+c_3(\tilde{\mathrm{h}}_1(\tilde{x},\tilde{\boldsymbol{y}})+z_1^*)-\sqrt{c_4+c_5(\tilde{\mathrm{h}}_1(\tilde{x},\tilde{\boldsymbol{y}})+z_1^*)}\right)\\
&+ a_9\tilde{y}_2+a_9\tilde{y}_2^2+c_6. && (6.20)
\end{aligned}$$

The boundary layer for the Σ_{SFU} system is given after applying the stretched time-scale Σ_U-subsystem

$$\begin{aligned}
\frac{d\tilde{z}_1}{d\tau_2} &= c_7\tilde{z}_2, && (6.21)\\
\frac{d\tilde{z}_2}{d\tau_2} &= a_9(\tilde{z}_1+z_1^*)+c_9\tilde{z}_2+J_2\left[\left(1+\sqrt{s_3\tilde{v}(\tilde{x},\tilde{\boldsymbol{y}})}\right)^2-1\right], && (6.22)
\end{aligned}$$

with $\tilde{\mathbf{h}}(\tilde{x},\tilde{\boldsymbol{y}})$ being the quasi-steady-state equilibria of the boundary layer Σ_U-subsystem, Eq. (6.21–6.22),

$$\tilde{\mathbf{h}}(\tilde{x},\tilde{\boldsymbol{y}}) = \begin{bmatrix} \tilde{\mathrm{h}}_1(\tilde{x},\tilde{\boldsymbol{y}}) \\ \tilde{\mathrm{h}}_2(\tilde{x},\tilde{\boldsymbol{y}}) \end{bmatrix}, \quad (6.23)$$

with the quasi-steady-state equilibria given by

$$\begin{aligned}
\tilde{\mathrm{h}}_1(\tilde{x},\tilde{\boldsymbol{y}}) &= \tilde{z}_1 = s_2\left[\left(1+\sqrt{s_3\tilde{v}(\tilde{x},\tilde{\boldsymbol{y}})}\right)^2-1\right]-z_1^* && (6.24)\\
\tilde{\mathrm{h}}_2(\tilde{x},\tilde{\boldsymbol{y}}) &= \tilde{z}_2 = 0. && (6.25)
\end{aligned}$$

The Σ_U-subsystem can be reorganized resulting in

$$\begin{aligned}
\frac{d\tilde{z}_1}{d\tau_2} &= c_7\tilde{z}_2, && (6.26)\\
\frac{d\tilde{z}_2}{d\tau_2} &= a_9(\tilde{z}_1+z_1^*)+c_9\tilde{z}_2+J_2\left[\left(1+\sqrt{s_3\tilde{v}(\tilde{x},\tilde{\boldsymbol{y}})}\right)^2-1\right]\\
&= a_9\left(\tilde{z}_1-\tilde{\mathrm{h}}_1(\tilde{x},\tilde{\boldsymbol{y}})\right)+c_9\left(\tilde{z}_2-\tilde{\mathrm{h}}_2(\tilde{x},\tilde{\boldsymbol{y}})\right). && (6.27)
\end{aligned}$$

The Σ_U-subsystem is rewritten in state space form by considering the change of variables given by $\hat{\boldsymbol{z}} = \tilde{\boldsymbol{z}} - \tilde{\mathbf{h}}(\tilde{x}, \tilde{\boldsymbol{y}})$, reducing to

$$\frac{d\tilde{z}}{d\tau_2} = \boldsymbol{A_U}\,\hat{\boldsymbol{z}}, \tag{6.28}$$

where

$$\boldsymbol{A_U} = \begin{pmatrix} 0 & c_7 \\ a_9 & c_9 \end{pmatrix}. \tag{6.29}$$

The $\tilde{f}(\tilde{x}, \tilde{\boldsymbol{y}}, \tilde{\mathbf{h}}(\tilde{x}, \tilde{\boldsymbol{y}}))$ subsystem reduces to

$$\dot{\tilde{x}} \;=\; a_{10}(\tilde{x}+x^*)^2\left[\sin\left(s_2\left[\left(1+\sqrt{s_3\tilde{v}(\tilde{x},\tilde{\boldsymbol{y}})}\right)^2-1\right]\right)-\sin\tilde{\mathrm{h}}_{1_{\mathrm{SS}}}\right]-b_x\tilde{x}, \tag{6.30}$$

and the Σ_{SF}-subsystem, $\hat{\boldsymbol{g}}(\tilde{x}, \tilde{\boldsymbol{y}}, \tilde{\mathbf{h}}(\tilde{x}, \tilde{\boldsymbol{y}}))$, reduces to

$$\frac{d\tilde{y}_1}{d\tau_1} \;=\; c_1\tilde{y}_2, \tag{6.31}$$

$$\frac{d\tilde{y}_2}{d\tau_1} \;=\; -\tilde{b}_{\tilde{y}_1}\tilde{y}_1-\tilde{b}_{\tilde{y}_2}\tilde{y}_2, \tag{6.32}$$

The Σ_F-subsystem can also be expressed in state space form as

$$\frac{d\tilde{y}}{d\tau_1} = \hat{\boldsymbol{g}}(\tilde{x}, \tilde{\boldsymbol{y}}, \tilde{\mathbf{h}}(\tilde{x}, \tilde{\boldsymbol{y}})) = \boldsymbol{A_F}\tilde{\boldsymbol{y}}, \tag{6.33}$$

being

$$\boldsymbol{A_F} = \begin{pmatrix} 0 & c_1 \\ -\tilde{b}_{y_1} & -\tilde{b}_{y_2} \end{pmatrix}. \tag{6.34}$$

The quasi-steady-state equilibrium of the Σ_F-subsystem, $\tilde{\mathbf{g}}(\tilde{x})$, is given by

$$\tilde{\mathbf{g}}(\tilde{x}) = \begin{bmatrix} \tilde{\mathrm{g}}_1(\tilde{x}) \\ \tilde{\mathrm{g}}_2(\tilde{x}) \end{bmatrix}, \tag{6.35}$$

with

$$\tilde{\mathrm{g}}_1(\tilde{x}) \;=\; y_1^*, \tag{6.36}$$

$$\tilde{\mathrm{g}}_2(\tilde{x}) \;=\; 0. \tag{6.37}$$

The Σ_S-subsystem, $\tilde{f}(\tilde{x}, \tilde{\mathbf{g}}(\tilde{x}), \tilde{\mathbf{h}}(\tilde{x}, \tilde{\boldsymbol{y}}))$, is given by

$$\begin{aligned} \dot{\tilde{x}} &= \tilde{f}(\tilde{x}, \tilde{\mathbf{g}}(\tilde{x}), \tilde{\mathbf{h}}(\tilde{x}, \tilde{\boldsymbol{y}})) = \tilde{f}(\tilde{x}, \tilde{\mathbf{g}}(\tilde{x}), \tilde{\mathbf{h}}(\tilde{x}, \tilde{\mathbf{g}}(\tilde{x}))) \\ &= a_{10}(\tilde{x}+x^*)^2\left[\sin(\tilde{\mathrm{h}}_1(\tilde{x}, \tilde{\mathbf{g}}(\tilde{x}))+z_1^*)-\sin\tilde{\mathrm{h}}_{1_{\mathrm{SS}}}\right]-b_x\tilde{x} \\ &= -b_x\tilde{x} = A_S\tilde{x}. \end{aligned} \tag{6.38}$$

6.2.2 Lyapunov Function Candidates for the Helicopter Problem

This section recaps on the associated Lyapunov functions for the different degenerated subsystems obtained in section 5.4, being the selected associated Lyapunov function for the slow Σ_S-subsystem given as

$$V_S(\tilde{x}) = \frac{1}{2}P_S\tilde{x}^2, \tag{6.39}$$

with

$$P_S = \frac{Q_S}{2b_x}, \tag{6.40}$$

therefore resulting in

$$V_S(\tilde{x}) = \frac{1}{2} P_S \tilde{x}^2 = \frac{Q_S}{4b_x}\tilde{x}^2. \tag{6.41}$$

The selected associated Lyapunov function candidate for the fast Σ_F-subsystem is given by

$$V_F(\tilde{\boldsymbol{y}}) = \frac{1}{2}\tilde{\boldsymbol{y}}^T \boldsymbol{P_F}\tilde{\boldsymbol{y}} = \frac{1}{2}p_{f_1}\tilde{y}_1^2 + \frac{1}{2}p_{f_3}\tilde{y}_2^2 + p_{f_2}\tilde{y}_1\tilde{y}_2, \tag{6.42}$$

with

$$\begin{aligned}
p_{f_1} &= \frac{q_{f_1}(\tilde{b}_{y_1}c_1 + \tilde{b}_{y_2}^2) + \tilde{b}_{y_1}^2 q_{f_2}}{2\tilde{b}_{y_1}\tilde{b}_{y_2}c_1} = C_{f_1}q_{f_1} + C_{f_2}q_{f_2}, && (6.43)\\
p_{f_2} &= \frac{q_{f_1}}{2\tilde{b}_{y_1}} = C_{f_3}q_{f_1}, && (6.44)\\
p_{f_3} &= \frac{q_{f_1}c_1 + q_{f_2}\tilde{b}_{y_1}}{2\tilde{b}_{y_1}\tilde{b}_{y_2}} = C_{f_4}q_{f_1} + C_{f_5}q_{f_2}, && (6.45)
\end{aligned}$$

with

$$\begin{aligned}
C_{f_1} &= \frac{\tilde{b}_{y_1}c_1 + \tilde{b}_{y_2}^2}{\tilde{b}_{y_1}\tilde{b}_{y_2}c_1}, && (6.46)\\
C_{f_2} &= \frac{\tilde{b}_{y_1}^2}{\tilde{b}_{y_1}\tilde{b}_{y_2}c_1}, && (6.47)\\
C_{f_3} &= \frac{1}{2\tilde{b}_{y_1}}, && (6.48)\\
C_{f_4} &= \frac{c_1}{2\tilde{b}_{y_1}\tilde{b}_{y_2}}, && (6.49)\\
C_{f_5} &= \frac{\tilde{b}_{y_1}}{2\tilde{b}_{y_1}\tilde{b}_{y_2}}. && (6.50)
\end{aligned}$$

Finally, the selected associated Lyapunov function candidate for the ultra-fast Σ_U-subsystem is given by

$$V_U(\hat{\boldsymbol{z}}) = \frac{1}{2}\hat{\boldsymbol{z}}^T \boldsymbol{P_U}\hat{\boldsymbol{z}} = \frac{1}{2}p_{u_1}\hat{z}_1^2 + \frac{1}{2}p_{u_3}\hat{z}_2^2 + p_{u_2}\hat{z}_1\hat{z}_2, \tag{6.51}$$

with

$$\hat{\boldsymbol{z}} = \tilde{\boldsymbol{z}} - \tilde{\mathbf{h}}(\tilde{x}, \tilde{\boldsymbol{y}}), \tag{6.52}$$

and with

$$\begin{aligned}
p_{u_1} &= -\frac{a_9c_7q_{u_1} - q_{u_2}a_9^2 - c_9^2q_{u_1}}{2a_9c_7c_9} = C_{u_1}q_{u_1} + C_{u_2}q_{u_2}, && (6.53)\\
p_{u_2} &= -\frac{q_{u_1}}{2a_9} = C_{u_3}q_{u_1}, && (6.54)\\
p_{u_3} &= \frac{c_7q_{u_1} - q_{u_2}a_9}{2a_9c_9} = C_{u_4}q_{u_1} + C_{u_5}q_{u_2}, && (6.55)
\end{aligned}$$

with

$$\begin{aligned}
C_{u_1} &= \frac{c_9^2 - a_9c_7}{2a_9c_7c_9}, && (6.56)\\
C_{u_2} &= -\frac{a_9}{2c_7c_9}, && (6.57)\\
C_{u_3} &= -\frac{1}{2a_9}, && (6.58)\\
C_{u_4} &= \frac{c_7}{2a_9c_9}, && (6.59)\\
C_{u_5} &= -\frac{a_9}{2a_9c_9}. && (6.60)
\end{aligned}$$

6.3 Σ_{SF} *Stability Analysis* for the Helicopter Model

This section provides the proof for the asymptotic stability requirements for the helicopter model Σ_{SF}-subsystem by applying the *Bottom-Up*-methodology using the same methodology as the one described previously for the general three-time-scale model in chapter 5. These requirements are defined by applying Assumptions, 5.5.1, 5.5.2, 5.5.3, 5.5.4, and 5.5.5, to the helicopter resulting autonomous system, Eqns. (6.6–6.10).

Similarly as in the Σ_{SF} general asymptotic stability analysis presented in section 5.5.1, the stability analysis for the helicopter Σ_{SF} *Stability Analysis* is performed assuming that the Σ_U-subsystem variables evolve in their own configuration space. The analysis of this first stage is performed using the standard method for two-time-scale systems (Kokotović et al., 1986; Kokotović et al., 1987; Kokotović et al., 1999), in which the previously derived Lyapunov functions for the Σ_S and Σ_F-subsystems, that is V_S, and V_F, Eqns. (6.41) and (6.42), respectively, must fulfill certain growth requirements on $\tilde{f}(\tilde{x}, \tilde{\boldsymbol{y}}, \tilde{\mathbf{h}}(\tilde{x}, \tilde{\boldsymbol{y}}))$ and $\hat{g}(\tilde{x}, \tilde{\boldsymbol{y}}, \tilde{\mathbf{h}}(\tilde{x}, \tilde{\boldsymbol{y}}))$, Eqns. (6.30) and (6.31–6.32), respectively, satisfying certain inequalities. The fulfillment of these inequalities for the Σ_{SF} helicopter subsystem are described bellow.

6.3.1 Isolated Equilibrium of the Origin for the Helicopter Σ_{SF}-Subsystem: Assumption 5.5.1

The origin ($\tilde{x} = 0$, $\tilde{\boldsymbol{y}} = 0$) is a unique and isolated equilibrium of the Σ_{SF}-subsystem, Eqns. (6.15–6.17), i.e.

$$0 = \tilde{f}(0, 0, \tilde{\mathbf{h}}(\tilde{x}, \tilde{\boldsymbol{y}})), \tag{6.61}$$

$$0 = \hat{\boldsymbol{g}}(0, 0, \tilde{\mathbf{h}}(\tilde{x}, \tilde{\boldsymbol{y}})), \tag{6.62}$$

moreover, $\tilde{\boldsymbol{y}} = \tilde{\mathbf{g}}(\tilde{x})$ is the unique root of

$$0 = \hat{\boldsymbol{g}}(\tilde{x}, \tilde{\boldsymbol{y}}, \tilde{\mathbf{h}}(\tilde{x}, \tilde{\boldsymbol{y}})), \tag{6.63}$$

in $B_{\tilde{x}} \times B_{\tilde{y}}$, i.e.

$$0 = \hat{\boldsymbol{g}}(\tilde{x}, \tilde{\mathbf{g}}(\tilde{x}), \tilde{\mathbf{h}}(\tilde{x}, \tilde{\boldsymbol{y}})), \tag{6.64}$$

and there exists a class κ function $p_1(\cdot)$ such that

$$\| \tilde{\mathbf{g}}(\tilde{x}) \| \leq p_1 (\| \tilde{x} \|) \,. \tag{6.65}$$

The reduced order growth requirements are obtained by first considering the system given by Eq. (6.30), and adding and subtracting $\tilde{f}(\tilde{x}, \tilde{\mathbf{g}}(\tilde{x}), \tilde{\mathbf{h}}(\tilde{x}, \tilde{\boldsymbol{y}}))$, Eq. (6.38), to the right-hand side of Eq. (6.30) yielding

$$\dot{\tilde{x}} = \tilde{f}\left(\tilde{x}, \tilde{\mathbf{g}}(\tilde{x}), \tilde{\mathbf{h}}(\tilde{x}, \tilde{\boldsymbol{y}})\right) + \tilde{f}(\tilde{x}, \tilde{\boldsymbol{y}}, \tilde{\mathbf{h}}(\tilde{x}, \tilde{\boldsymbol{y}})) - \tilde{f}\left(\tilde{x}, \tilde{\mathbf{g}}(\tilde{x}), \tilde{\mathbf{h}}(\tilde{x}, \tilde{\boldsymbol{y}})\right), \tag{6.66}$$

where the term $\tilde{f}(\tilde{x}, \tilde{\boldsymbol{y}}, \tilde{\mathbf{h}}(\tilde{x}, \tilde{\boldsymbol{y}})) - \tilde{f}(\tilde{x}, \tilde{\mathbf{g}}(\tilde{x}), \tilde{\mathbf{h}}(\tilde{x}, \tilde{\boldsymbol{y}}))$ can be viewed as a perturbation of the reduced order Σ_S-subsystem, $\tilde{f}(\tilde{x}, \tilde{\mathbf{g}}(\tilde{x}), \tilde{\mathbf{h}}(\tilde{x}, \tilde{\boldsymbol{y}}))$. It is therefore natural to first satisfy the growth requirements for Eq. (6.38) and then consider the effect of the perturbation term $\tilde{f}(\tilde{x}, \tilde{\boldsymbol{y}}, \tilde{\mathbf{h}}(\tilde{x}, \tilde{\boldsymbol{y}})) - \tilde{f}\left(\tilde{x}, \tilde{\mathbf{g}}(\tilde{x}), \tilde{\mathbf{h}}(\tilde{x}, \tilde{\boldsymbol{y}})\right)$. Therefore let proceed to define first the reduced order growth condition.

6.3.2 Proof of Assumption 5.5.2: Reduced System Conditions for the Helicopter Σ_{SF}-Subsystem

Recalling from Assumption 5.5.2, the Σ_S-subsystem Lyapunov function candidate, $V_S(\tilde{x})$, must be positive-definite and decreasing, and must also satisfy the following inequality

$$\left(\frac{\partial V_S(\tilde{x})}{\partial \tilde{x}}\right)^T \tilde{f}\left(\tilde{x}, \tilde{\mathbf{g}}(\tilde{x}), \tilde{\mathbf{h}}(\tilde{x}, \tilde{\boldsymbol{y}})\right) \leq -\alpha_1 \psi_1^2(\tilde{x}), \tag{6.67}$$

where $\psi_1(\cdot)$ is a scalar function of vector arguments which vanishes only when its argument are zero, and satisfying that $\tilde{x} = 0$ is a stable equilibrium of the reduced order system. The left-hand side of inequality (6.67) is given by recalling that

$$V_S\left(\tilde{x}\right) = \frac{1}{2} P_S \tilde{x}^2, \tag{6.68}$$

being therefore easy to see that

$$\left(\frac{\partial V_S(\tilde{x})}{\partial \tilde{x}}\right)^T \quad = \quad P_S \tilde{x}, \tag{6.69}$$

therefore substituting $\tilde{f}(\tilde{x}, \tilde{\mathbf{g}}(\tilde{x}), \tilde{\mathbf{h}}(\tilde{x}, \tilde{\boldsymbol{y}}))$, Eqns. (6.38), and Eq. (6.69) (6.67), and recalling that $P_S = \dfrac{Q_S}{2b_x}$ yields

$$\left(\frac{\partial V_S(\tilde{x})}{\partial \tilde{x}}\right)^T \tilde{f}(\tilde{x}, \tilde{\mathbf{g}}(\tilde{x}), \tilde{\mathbf{h}}(\tilde{x}, \tilde{\boldsymbol{y}})) = -P_S b_x \tilde{x}^2 = -\frac{1}{2} Q_S \tilde{x}^2, \tag{6.70}$$

therefore assumption (6.67) can be satisfied by selecting α_1 and $\psi_1(\tilde{x})$ such

$$\alpha_1 \quad \leq \quad 1, \tag{6.71}$$

$$\psi_1(\tilde{x}) \quad = \quad \sqrt{\tilde{Q}_S \tilde{x}^2}, \tag{6.72}$$

with

$$\tilde{Q}_S = \frac{1}{2} Q_S. \tag{6.73}$$

6.3.3 Proof of Assumption 5.5.3: Boundary-Layer System Conditions for the Helicopter Σ_{SF}-Subsystem

Recalling from Assumption 5.5.3, the Σ_F Lyapunov function candidate $V_F(\tilde{x}, \tilde{\boldsymbol{y}})$ must be positive-definite and decreasing, such that for all $(\tilde{x}, \tilde{\boldsymbol{y}}) \in B_{\tilde{x}} \times B_{\tilde{y}}$ satisfies inequality

$$V_F(\tilde{x}, \tilde{\boldsymbol{y}}) > 0, \ \forall \ \tilde{\boldsymbol{y}} \neq \tilde{\mathbf{g}}(\tilde{x}) \ \textit{and} \ V_F(\tilde{x}, \tilde{\mathbf{g}}(\tilde{x})) = 0, \tag{6.74}$$

and

$$\left(\frac{\partial V_F}{\partial \tilde{y}}\right)^T \hat{\boldsymbol{g}}(\tilde{x}, \tilde{\boldsymbol{y}}, \tilde{\mathbf{h}}(\tilde{x}, \tilde{\boldsymbol{y}})) \leq -\alpha_2 \phi_1^2(\tilde{\boldsymbol{y}} - \tilde{\mathbf{g}}(\tilde{x})), \tag{6.75}$$

where $\phi_1(\cdot)$ is a scalar function of vector arguments which vanishes only when its arguments are zero, and satisfying that $\tilde{\boldsymbol{y}} - \tilde{\mathbf{g}}(\tilde{x})$ is a stable equilibrium of the boundary layer Σ_F-subsystem. The left-hand side of inequality (6.75) is defined after recalling that

$$V_F(\tilde{\boldsymbol{y}}) = \frac{1}{2} \tilde{\boldsymbol{y}}^T \boldsymbol{P_F} \tilde{\boldsymbol{y}}, \tag{6.76}$$

where $\boldsymbol{P_F}$ represents the solution to the associated Lyapunov function given by

$$\boldsymbol{P_F} = \begin{pmatrix} p_{f_1} & p_{f_2} \\ p_{f_2} & p_{f_3} \end{pmatrix}, \tag{6.77}$$

with p_{f_1}, p_{f_2}, and p_{f_3} defined in Eqns. (6.43), (6.44), and (6.45) respectively, being therefore easy to see that

$$\left(\frac{\partial V_F}{\partial \tilde{\boldsymbol{y}}}\right)^T = (\boldsymbol{P_F}\tilde{\boldsymbol{y}})^T, \tag{6.78}$$

and also recalling Eq. (6.33), results in

$$\tilde{g}(\tilde{x}, \tilde{\boldsymbol{y}}, \tilde{\mathbf{h}}(\tilde{x}, \tilde{\boldsymbol{y}})) = \boldsymbol{A_F}\tilde{\boldsymbol{y}}, \tag{6.79}$$

and therefore, substituting Eqns. (6.78) and (6.79), into Eq. (6.75) results in

$$\left(\frac{\partial V_F}{\partial \tilde{\boldsymbol{y}}}\right)^T \hat{\boldsymbol{g}}(\tilde{x}, \tilde{\boldsymbol{y}}, \tilde{\mathbf{h}}(\tilde{x}, \tilde{\boldsymbol{y}})) = (\boldsymbol{P_F}\tilde{\boldsymbol{y}})^T \boldsymbol{A_F}\tilde{\boldsymbol{y}} = \tilde{\boldsymbol{y}}^T\boldsymbol{P_F}\boldsymbol{A_F}\tilde{\boldsymbol{y}} = \tilde{\boldsymbol{y}}^T\boldsymbol{M_F}\tilde{\boldsymbol{y}}, \tag{6.80}$$

with $\boldsymbol{M_F}$ defined by

$$\boldsymbol{M_F} = \boldsymbol{P_F}\boldsymbol{A_F} = \begin{pmatrix} m_{F_{11}} & m_{F_{12}} \\ m_{F_{21}} & m_{F_{22}} \end{pmatrix}, \tag{6.81}$$

being

$$m_{F_{11}} = -p_{f_2}\tilde{b}_{y_1}, \tag{6.82}$$
$$m_{F_{21}} = p_{f_1}c_1 - p_{f_2}\tilde{b}_{y_2}, \tag{6.83}$$
$$m_{F_{12}} = -p_{f_3}\tilde{b}_{y_1}, \tag{6.84}$$
$$m_{F_{22}} = p_{f_2}c_1 - p_{f_3}\tilde{b}_{y_2}, \tag{6.85}$$

where by substituting the solutions to the associated Lyapunov equation p_{f_1}, p_{f_2}, and p_{f_3}, Eqns. (6.43), (6.44), and (6.45), respectively, into Eq. (6.80) results in

$$\left(\frac{\partial V_F}{\partial \tilde{\boldsymbol{y}}}\right)^T \hat{\boldsymbol{g}}(\tilde{x}, \tilde{\boldsymbol{y}}, \tilde{\mathbf{h}}(\tilde{x}, \tilde{\boldsymbol{y}})) = \tilde{\boldsymbol{y}}^T\boldsymbol{M_F}\tilde{\boldsymbol{y}} = -\frac{1}{2}\left(\tilde{\boldsymbol{y}}^T\boldsymbol{Q_F}\tilde{\boldsymbol{y}}\right) = -\frac{1}{2}\left(\tilde{y}_1^2 q_{f_1} + \tilde{y}_2^2 q_{f_2}\right), \tag{6.86}$$

with $\boldsymbol{Q_F}$ being defined in Eq. (5.87), and let $\tilde{\boldsymbol{Q}}_{\boldsymbol{F}} = \frac{\boldsymbol{Q_F}}{2}$ and where

$$\tilde{q}_{f_1} = \frac{q_{f_1}}{2}, \tag{6.87}$$
$$\tilde{q}_{f_2} = \frac{q_{f_2}}{2}, \tag{6.88}$$

and therefore rewriting Eq. (6.80) as

$$\left(\frac{\partial V_F}{\partial \tilde{\boldsymbol{y}}}\right)^T \hat{\boldsymbol{g}}(\tilde{x}, \tilde{\boldsymbol{y}}, \tilde{\mathbf{h}}(\tilde{x}, \tilde{\boldsymbol{y}})) = -\left(\tilde{\boldsymbol{y}}^T\tilde{\boldsymbol{Q}}_{\boldsymbol{F}}\tilde{\boldsymbol{y}}\right) = -\left(\tilde{y}_1^2\tilde{q}_{f_1} + \tilde{y}_2^2\tilde{q}_{f_2}\right), \tag{6.89}$$

therefore, inequality (6.89) can be satisfied by selecting α_2 and $\phi(\hat{\boldsymbol{y}} - \tilde{\mathbf{g}}(\tilde{x}))$ such

$$\alpha_2 \leq 1, \tag{6.90}$$
$$\phi_1(\tilde{\boldsymbol{y}} - \tilde{\mathbf{g}}(\tilde{x})) = \left(\tilde{\boldsymbol{y}}^T\tilde{\boldsymbol{Q}}_{\boldsymbol{F}}\tilde{\boldsymbol{y}}\right)^{\frac{1}{2}} = \left(\tilde{q}_{f_1}\tilde{y}_1^2 + \tilde{q}_{f_2}\tilde{y}_2^2\right)^{\frac{1}{2}}. \tag{6.91}$$

For simplicity, from now on the comparison function $\phi_1(\tilde{\boldsymbol{y}} - \tilde{\mathbf{g}}(\tilde{x}))$ it is refereed as $\phi_1(\hat{\boldsymbol{y}})$.

6.3.4 Proof of Assumption 5.5.4: First Interconnection Condition for the Helicopter Σ_{SF}-Subsystem

The Lyapunov functions $V_S(\tilde{x})$ and $V_F(\hat{\boldsymbol{y}})$, Eqns. (6.41), and (6.42) respectively, must satisfy the so called interconnection conditions. The first interconnection condition is obtained by computing the derivative of $V_S(\tilde{x})$ along the solution of Eq. (6.66), resulting in a expression similar to Eq. (5.139), which provides the first interconnection inequality

$$\left(\frac{\partial V_S(\tilde{x})}{\partial \tilde{x}}\right)^T \left[\tilde{f}(\tilde{x}, \tilde{\boldsymbol{y}}, \tilde{\mathbf{h}}(\tilde{x}, \tilde{\boldsymbol{y}})) - \tilde{f}(\tilde{x}, \tilde{\mathbf{g}}(\tilde{x}), \tilde{\mathbf{h}}(\tilde{x}, \tilde{\boldsymbol{y}}))\right] \leq \beta_1 \psi_1(\tilde{x}) \phi_1(\hat{\boldsymbol{y}}), \tag{6.92}$$

with the comparison function $\psi_1(\tilde{x})$ and $\phi_1(\hat{\boldsymbol{y}})$, being defined in Eqns. (6.72) and (6.91) respectively. Inequality (6.92) determines the allowed growth of $\tilde{f}(\tilde{x}, \tilde{\boldsymbol{y}}, \tilde{\mathbf{h}}(\tilde{x}, \tilde{\boldsymbol{y}}))$ in $\tilde{y}$, and in typical problems, verifying inequality (6.92) reduces to verifying the inequality

$$\left\|\tilde{f}(\tilde{x}, \tilde{\boldsymbol{y}}, \tilde{\mathbf{h}}(\tilde{x}, \tilde{\boldsymbol{y}})) - \tilde{f}(\tilde{x}, \tilde{\mathbf{g}}(\tilde{x}), \tilde{\mathbf{h}}(\tilde{x}, \tilde{\boldsymbol{y}}))\right\| \leq \psi_1(\tilde{x}) \phi_1(\hat{\boldsymbol{y}}), \tag{6.93}$$

which implies that the rate of growth of $\tilde{f}(\tilde{x}, \tilde{\boldsymbol{y}}, \tilde{\mathbf{h}}(\tilde{x}, \tilde{\boldsymbol{y}}))$ cannot be faster than the rate of growth of the comparison function $\phi_1(\cdot)$. The left-hand side of inequality (6.92) is given by recalling the results of Eq. (6.78), and recalling both $\tilde{f}(\tilde{x}, \tilde{\mathbf{g}}(\tilde{x}), \tilde{\mathbf{h}}(\tilde{x}, \tilde{\boldsymbol{y}}))$ and $\tilde{f}(\tilde{x}, \tilde{\boldsymbol{y}}, \tilde{\mathbf{h}}(\tilde{x}, \tilde{\boldsymbol{y}}))$, Eqns. (6.38), and (6.30), respectively, yielding

$$\tilde{f}(\tilde{x}, \tilde{\boldsymbol{y}}, \tilde{\mathbf{h}}(\tilde{x}, \tilde{\boldsymbol{y}})) - \tilde{f}(\tilde{x}, \tilde{\mathbf{g}}(\tilde{x}), \tilde{\mathbf{h}}(\tilde{x}, \tilde{\boldsymbol{y}})) = a_{10}(\tilde{x} + x^*)^2 (\sin(\tilde{\mathrm{h}}_1(\tilde{x}, \tilde{\boldsymbol{y}}) + z_1^*) - \sin \tilde{\mathrm{h}}_{1_{\mathrm{SS}}}). \tag{6.94}$$

Substituting Eqns. (6.78) and (6.94) into inequality (6.92) results in

$$\begin{aligned} & \left(\frac{\partial V_S(\tilde{x})}{\partial \tilde{x}}\right)^T \left[\tilde{f}(\tilde{x}, \tilde{\boldsymbol{y}}, \tilde{\mathbf{h}}(\tilde{x}, \tilde{\boldsymbol{y}})) - \tilde{f}(\tilde{x}, \tilde{\mathbf{g}}(\tilde{x}), \tilde{\mathbf{h}}(\tilde{x}, \tilde{\boldsymbol{y}}))\right] \\ = & \frac{1}{2} \frac{Q_S}{b_x} \tilde{x} \left\{a_{10} (\tilde{x} + x^*)^2 \left[\sin\left(\tilde{\mathrm{h}}_1(\tilde{x}, \tilde{\boldsymbol{y}}) + z_1^*\right) - \sin \tilde{\mathrm{h}}_{1_{\mathrm{SS}}}\right]\right\} \leq \beta_1 \psi_1(\tilde{x}) \phi_1(\hat{\boldsymbol{y}}). \end{aligned} \tag{6.95}$$

In order to obtain the comparison function $\psi_1(\tilde{x})$ that satisfies inequality (6.95), a series of algebraic and trigonometric manipulations are conducted. Let first introduce the expressions

$$\mathcal{A}_1 = \tilde{\mathrm{h}}_1(\tilde{x}, \tilde{\boldsymbol{y}}) + z_1^* = s_2 \left[\left(1 + \sqrt{s_3 \tilde{v}(\tilde{x}, \tilde{\boldsymbol{y}})}\right)^2 - 1\right], \tag{6.96}$$

$$\mathcal{B}_1 = \tilde{\mathrm{h}}_{1_{\mathrm{SS}}} = s_2 \left[\left(1 + \sqrt{s_3 \tilde{v}_{SS}}\right)^2 - 1\right], \tag{6.97}$$

where $\tilde{v}$ and $\tilde{v}_{SS}$ are give in Eqns. (6.12–6.13), permitting therefore to rewrite Eq. (6.95) such

$$\begin{aligned} & \left(\frac{\partial V_S(\tilde{x})}{\partial \tilde{x}}\right)^T \left[\tilde{f}\left(\tilde{x}, \tilde{\boldsymbol{y}}, \tilde{\mathbf{h}}(\tilde{x}, \tilde{\boldsymbol{y}})\right) - \tilde{f}\left(\tilde{x}, \tilde{\mathbf{g}}(\tilde{x}), \tilde{\mathbf{h}}(\tilde{x}, \tilde{\boldsymbol{y}})\right)\right] \\ = & \frac{1}{2} \frac{Q_S}{b_x} \tilde{x} \left[a_{10} (\tilde{x} + x^*)^2 (\sin \mathcal{A}_1 - \sin \mathcal{B}_1)\right] \leq \beta_1 \psi_1(\tilde{x}) \phi_1(\hat{\boldsymbol{y}}). \end{aligned} \tag{6.98}$$

Recall the sum-to-product prosthaphaeresis trigonometric identity (Steele, 2004)

$$\sin(a) - \sin(b) = 2 \sin\left(\frac{a-b}{2}\right) \cos\left(\frac{a+b}{2}\right), \tag{6.99}$$

which can be used to rewrite the left-hand side of inequality (6.98) as

$$\begin{aligned} & \left(\frac{\partial V_S(\tilde{x})}{\partial \tilde{x}}\right)^T \left[\tilde{f}\left(\tilde{x}, \tilde{\boldsymbol{y}}, \tilde{\mathbf{h}}(\tilde{x}, \tilde{\boldsymbol{y}})\right) - \tilde{f}\left(\tilde{x}, \tilde{\mathbf{g}}(\tilde{x}), \tilde{\mathbf{h}}(\tilde{x}, \tilde{\boldsymbol{y}})\right)\right] \\ = & \frac{1}{2} \frac{Q_S}{b_x} \tilde{x} \left[a_{10} (\tilde{x} + x^*)^2 (\sin \mathcal{A}_1 - \sin \mathcal{B}_1)\right] \end{aligned}$$

$$= \frac{1}{2}\frac{Q_S}{b_x}\tilde{x}\left[a_{10}\left(\tilde{x}+x^*\right)^2 2\sin\left(\frac{\mathcal{A}_1-\mathcal{B}_1}{2}\right)\cos\left(\frac{\mathcal{A}_1+\mathcal{B}_1}{2}\right)\right]. \tag{6.100}$$

Due to the sign nature of the coefficients in $\tilde{v}$ and $\tilde{v}_{SS}$, Eqns. (6.12–6.13), and for the easiness while the reading and understanding process of the trigonometric and inequality operations that will be conducted to prove the different growth requirements, let introduce the following change in the variables to avoid having constants with negative values, such

$$\bar{a}_9 = -a_9, \tag{6.101}$$

$$\bar{c}_6 = -c_6 = \frac{a_7 a_9}{a_5}, \tag{6.102}$$

where recalling that $\bar{a}_9 > 0$, $\bar{c}_6 > 0$, see sections 2.8.5 and 3.3.2.2 for further details. Using Eqns. (6.101) and (6.102) into Eqns. (6.12–6.13), results in

$$\tilde{v}(\tilde{x},\tilde{\boldsymbol{y}}) = \frac{\bar{a}_9\tilde{y}_2^2+\left(\bar{a}_9-\tilde{b}_{y_2}\right)\tilde{y}_2-\tilde{b}_{y_1}\tilde{y}_1+\bar{c}_6}{(\tilde{x}+x^*)^2}, \tag{6.103}$$

$$\tilde{v}_{SS}(\tilde{x},\tilde{\mathbf{g}}(\tilde{x})) = \frac{\bar{c}_6}{(\tilde{x}+x^*)^2}. \tag{6.104}$$

Recalling that both $\tilde{b}_{y_1} > 0$, $\tilde{b}_{y_2} > 0$, it can be seen that with the proper selection of $\tilde{b}_{y_1}$ and $\tilde{b}_{y_2}$, results in $\tilde{v} > 0$ and $\tilde{v}_{SS} > 0$. In order to simplify the analysis let rewrite $\tilde{v}$, Eq. (6.103), such

$$\tilde{v}(\tilde{x},\tilde{\boldsymbol{y}}) = \frac{\bar{a}_9\tilde{y}_2^2+\left(\bar{a}_9-\tilde{b}_{y_2}\right)\tilde{y}_2-\tilde{b}_{y_1}\tilde{y}_1+\bar{c}_6}{(\tilde{x}+x^*)^2} = s_3\left(\nu_1\tilde{y}_2^2+\nu_2\tilde{y}_2+\nu_3\tilde{y}_1+\nu_4\right), \tag{6.105}$$

with ν_1 ,ν_2 ,ν_3, and ν_4 being defined by

$$\nu_1(\tilde{x}) = \frac{\bar{a}_9}{(\tilde{x}+x^*)^2}, \tag{6.106}$$

$$\nu_2(\tilde{x}) = \frac{\left(\bar{a}_9-\tilde{b}_{y_2}\right)}{(\tilde{x}+x^*)^2}, \tag{6.107}$$

$$\nu_3(\tilde{x}) = -\frac{\tilde{b}_{y_1}}{(\tilde{x}+x^*)^2}, \tag{6.108}$$

$$\nu_4(\tilde{x}) = \tilde{v}_{SS} = \frac{\bar{c}_6}{(\tilde{x}+x^*)^2}, \tag{6.109}$$

and recalling that s_3 was previously defined in Eq. (4.88) as

$$s_3 = 4c_{12} = 4\frac{c_3}{c_5} = 4\frac{a_2c_1}{a_4c_1^2} = \frac{a_2a_5}{a_4a_9}. \tag{6.110}$$

Recalling that

$$\tilde{x}+x^* \equiv x, \tag{6.111}$$

where x represents the angular velocity of the blades, and since $x > 0$, and $s_3 > 0$, thus

$$\nu_1 > 0, \tag{6.112}$$

$$\nu_2 < 0, \tag{6.113}$$

$$\nu_3 < 0, \tag{6.114}$$

$$\nu_4 > 0. \tag{6.115}$$

Let also introduce the functions

$$\mathcal{F}(\tilde{x},\tilde{\boldsymbol{y}}) = \left(\nu_1(\tilde{x})\tilde{y}_2^2+\nu_2(\tilde{x})\tilde{y}_2+\nu_3(\tilde{x})\tilde{y}_1\right), \tag{6.116}$$

$$\mathcal{C}(\tilde{x}) = \nu_4 = \tilde{v}_{SS} = \frac{\bar{c}_6}{(\tilde{x}+x^*)^2}, \tag{6.117}$$

where $0 \le \mathcal{F} \le 0$ depending on the sign of $\tilde{y}_1$, $\tilde{y}_2$, which translates to different error in the altitude and vertical speed of the helicopter, and also with $\mathcal{C} > 0$. Recalling the definitions of both $\tilde{y}_1$ and $\tilde{y}_2$ given as

$$\tilde{y}_1 = y_1 - y_1^*, \tag{6.118}$$

$$\tilde{y}_2 = y_2 - y_2^*. \tag{6.119}$$

In order to provide an insight view of the helicopter physical meaning of the mathematic expression here used, from a position of the helicopter perspective, a negative value of $\tilde{y}_1$, can be interpreted such that the helicopter, at the instant where $\tilde{y}_1$ is evaluated, has an altitude lower than the desired set point altitude, while a positive value of $\tilde{y}_1$, implies that the helicopter has an altitude higher than the desired set point altitude.

From the axial flight regime perspective, and recalling that a given desired altitude is achieved when the vertical speed it is zero, i.e. $y_2^* = 0$, a negative value of $\tilde{y}_2$ implies that the helicopter is descending trying to reach a lower desired set point altitude, while a positive $\tilde{y}_2$, implies that the helicopter is ascending trying to reach a higher desired set point altitude. With this in mind, and recalling that the helicopter can conduct any of the two maneuvers, ascent and descent flight, let continue the analysis by rewriting $\mathcal{A}_1$, Eq. (6.96), using the expressions derived in Eqns. (6.106–6.110), and Eqns. (6.116–6.117), resulting in

$$\begin{aligned}
\mathcal{A}_1 &= \tilde{\mathrm{h}}_1(\tilde{x}, \tilde{\boldsymbol{y}}) + z_1^* = s_2 \left[\left(1 + \sqrt{s_3 \tilde{v}(\tilde{x}, \tilde{\boldsymbol{y}})} \right)^2 - 1 \right] \\
&= s_2 \left[\left(1 + \sqrt{s_3 \left(\nu_1 \tilde{y}_2^2 + \nu_2 \tilde{y}_2 + \nu_3 \tilde{y}_1 + \nu_4 \right)} \right)^2 - 1 \right] \\
&= s_2 \left(2\sqrt{s_3 \left(\nu_1 \tilde{y}_2^2 + \nu_2 \tilde{y}_2 + \nu_3 \tilde{y}_1 + \nu_4 \right)} + s_3 \left(\nu_1 \tilde{y}_2^2 + \nu_2 \tilde{y}_2 + \nu_3 \tilde{y}_1 + \nu_4 \right) \right) \\
&= s_2 \left(2\sqrt{s_3 \left(\mathcal{F} + \mathcal{C} \right)} + s_3 \left(\mathcal{F} + \mathcal{C} \right) \right),
\end{aligned} \tag{6.120}$$

and rewriting $\mathcal{B}_1$, Eq. (6.97), as

$$\begin{aligned}
\mathcal{B}_1 &= \tilde{\mathrm{h}}_{1_{\mathrm{SS}}} = s_2 \left[\left(1 + \sqrt{s_3 \tilde{v}_{SS}} \right)^2 - 1 \right] \\
&= s_2 \left[(1 + \sqrt{s_3 \nu_4})^2 - 1 \right] = s_2 \left(2\sqrt{s_3 \nu_4} + s_3 \nu_4 \right) \\
&= s_2 \left[\left(1 + \sqrt{s_3 \mathcal{C}} \right)^2 - 1 \right] = s_2 \left(2\sqrt{s_3 \mathcal{C}} + s_3 \mathcal{C} \right),
\end{aligned} \tag{6.121}$$

where recalling that as previously defined

$$s_2 = -\frac{J_2}{a_9}, \tag{6.122}$$

$$J_2 = -\frac{a_3 a_9}{a_4}, \tag{6.123}$$

where it can be shown that $s_2 > 0$ and $J_2 > 0$. Recalling Eq. (6.100), let focuss only in the portion of Eq. (6.100) inside of the brackets and recalling the inequality identity $a \le |a|$, thus rewriting and simplifying Eq. (6.100)

$$\begin{aligned}
& 2a_{10}(\tilde{x} + x^*)^2 \sin\left(\frac{\mathcal{A}_1 - \mathcal{B}_1}{2} \right) \cos\left(\frac{\mathcal{A}_1 + \mathcal{B}_1}{2} \right) \\
\le\ & 2(\tilde{x} + x^*)^2 \cos\left(\frac{\mathcal{A}_1 + \mathcal{B}_1}{2} \right) \left| a_{10} \sin\left(\frac{\mathcal{A}_1 - \mathcal{B}_1}{2} \right) \right|.
\end{aligned} \tag{6.124}$$

Recalling also that due to the positive nature of the $\cos(a)$ function, that is $1 \ge \cos(a) \ge 0 \ \forall \ a \in \mathcal{R}$, it can therefore also be shown that

$$0 \le \cos\left(\frac{\mathcal{A}_1 + \mathcal{B}_1}{2} \right) \le 1, \tag{6.125}$$

further more, it can be shown that

$$0 \leq \cos\left(\frac{\mathcal{A}_1 + \mathcal{B}_1}{2}\right) \leq \mathcal{K}_1 \leq 1, \tag{6.126}$$

where it can be proven that the maximum value of Eq. (6.125) is achieved for

$$\mathcal{K}_1 = \cos\left(\frac{\mathcal{A}_{1_{MIN}} + \mathcal{B}_{1_{MIN}}}{2}\right) \leq 1, \tag{6.127}$$

being $\mathcal{A}_{1_{MIN}}$ and $\mathcal{B}_{1_{MIN}}$ the minimum possible value of Eqns. (6.96) and (6.97), respectively, and being defined by

$$\begin{aligned} \mathcal{A}_{1_{MIN}} &= [h_1(\tilde{x}, \tilde{\boldsymbol{y}}) + z_1^*]_{MIN} \\ &= s_2\left[\left(1 + \sqrt{s_3 \tilde{v}(\tilde{x}, \tilde{\boldsymbol{y}})}\right)^2 - 1\right]_{MIN} \\ &= s_2\left[\left(1 + \sqrt{s_3 \tilde{v}_{MIN}(\tilde{x}, \tilde{\boldsymbol{y}})}\right)^2 - 1\right], \end{aligned} \tag{6.128}$$

$$\begin{aligned} \mathcal{B}_{1_{MIN}} &= [\mathrm{h}_{1\mathrm{ss}}]_{MIN} \\ &= s_2\left[\left(1 + \sqrt{s_3 \tilde{v}_{SS}(\tilde{x})}\right)^2 - 1\right]_{MIN} \\ &= s_2\left[\left(1 + \sqrt{s_3 \tilde{v}_{SS_{MIN}}}\right)^2 - 1\right], \end{aligned} \tag{6.129}$$

where $\tilde{v}_{MIN}$ and $\tilde{v}_{SS_{MIN}}$ represents the minimum values for both $\tilde{v}$ and $\tilde{v}_{SS}$, Eqns. (6.12–6.13), respectively, which are obtained when the variables attain their maximum values which are defined in section 2.8.5.2 such

$$\tilde{x} = \tilde{x}_{MAX}, \tag{6.130}$$

$$\tilde{y}_1 = \tilde{y}_{1_{MAX}}, \tag{6.131}$$

$$\tilde{y}_2 = \tilde{y}_{2_{MAX}}, \tag{6.132}$$

where $\tilde{x}_{MAX}$ implies that the helicopter is flying at the maximum allowable angular rotation of the blades, $\tilde{y}_{1_{MAX}}$ implies that the helicopter is at its higher possible altitude, which is limited by the platform setup, and it is commanded instantaneously to descent to the lowest possible altitude, and $\tilde{y}_{2_{MAX}}$ implies that the helicopter has its maximum allowable ascending velocity. From a physical point of view, this translate to a very extreme situation in which the helicopter reaches the maximum altitude at the highest possible velocity, and instantaneously it is commanded to descent to the lowest possible altitude. This seems to be a highly improbable flight condition, thus making this solution a very conservative analysis, since any of the situations that will encounter the helicopter during both, the simulations and in the real setup, will be much more less demanding and restrictive. With the above analysis, expressions $\tilde{v}_{MIN}$ and $\tilde{v}_{SS_{MIN}}$ reduce to

$$\tilde{v}_{MIN} = \frac{\bar{a}_9 \tilde{y}_{2_{MAX}}^2 + \left(\bar{a}_9 - \tilde{b}_{y_2}\right) \tilde{y}_{2_{MAX}} - \tilde{b}_{y_1} \tilde{y}_{1_{MAX}} + \bar{c}_6}{x_{MAX}^2}, \tag{6.133}$$

$$\tilde{v}_{SS_{MIN}} = \frac{\bar{c}_6}{x_{MAX}^2}. \tag{6.134}$$

Recalling also that Eq. (6.124) can be rewritten by using Eq. (6.127), and also considering the sin inequality identity (Steele, 2004) given by

$$|\sin a| \leq |a|, \tag{6.135}$$

therefore, allowing to rewrite Eq. (6.124) by using Eqns. (6.127), and (6.135), resulting in

$$\begin{aligned}
& 2a_{10}(\tilde{x}+x^*)^2 \sin\left(\frac{\mathcal{A}_1-\mathcal{B}_1}{2}\right)\cos\left(\frac{\mathcal{A}_1+\mathcal{B}_1}{2}\right) \\
\leq\ & 2(\tilde{x}+x^*)^2 \cos\left(\frac{\mathcal{A}_1+\mathcal{B}_1}{2}\right)\left|a_{10}\sin\left(\frac{\mathcal{A}_1-\mathcal{B}_1}{2}\right)\right| \\
\leq\ & 2(\tilde{x}+x^*)^2\mathcal{K}_1\left|a_{10}\sin\left(\frac{\mathcal{A}_1-\mathcal{B}_1}{2}\right)\right| \\
\leq\ & (\tilde{x}+x^*)^2\mathcal{K}_1\left|a_{10}\left(\mathcal{A}_1-\mathcal{B}_1\right)\right|, \qquad (6.136)
\end{aligned}$$

where from the physical properties of the helicopter model $a_{10}<0$. Eq. (6.136) can be rewritten using the functions $\mathcal{F}(\tilde{x},\tilde{\boldsymbol{y}})$, and $\mathcal{C}(\tilde{x})$, Eqns. (6.116) and (6.117), respectively, resulting in

$$\begin{aligned}
& 2a_{10}(\tilde{x}+x^*)^2 \sin\left(\frac{\mathcal{A}_1-\mathcal{B}_1}{2}\right)\cos\left(\frac{\mathcal{A}_1+\mathcal{B}_1}{2}\right) \\
\leq\ & (\tilde{x}+x^*)^2\mathcal{K}_1\left|a_{10}\left(\mathcal{A}_1-\mathcal{B}_1\right)\right| \\
\leq\ & s_2\mathcal{K}_1(\tilde{x}+x^*)^2\left|a_{10}\left[2\left(\sqrt{s_3\left(\mathcal{F}(\tilde{x},\tilde{\boldsymbol{y}})+\mathcal{C}(\tilde{x})\right)}-\sqrt{s_3\mathcal{C}(\tilde{x})}\right)+s_3\mathcal{F}(\tilde{x},\tilde{\boldsymbol{y}})\right]\right|. \qquad (6.137)
\end{aligned}$$

Let redefine

$$\tilde{\mathcal{F}}(\tilde{x},\tilde{\boldsymbol{y}}) = s_3\mathcal{F}(\tilde{x},\tilde{\boldsymbol{y}}), \qquad (6.138)$$
$$\tilde{\mathcal{C}}(\tilde{x}) = s_3\mathcal{C}(\tilde{x}), \qquad (6.139)$$

and recalling that, as noted previously, due to the nature of the helicopter model here presented

$$s_3 > 0, \qquad (6.140)$$
$$\tilde{\mathcal{C}}(\tilde{x}) > 0, \qquad (6.141)$$
$$0 \geq \tilde{\mathcal{F}} \geq 0, \qquad (6.142)$$

and also recalling that it can also be shown that

$$\tilde{\mathcal{F}}+\tilde{\mathcal{C}} > 0, \qquad (6.143)$$

therefore, Eq. (6.137) can be further simplified by identifying that

$$\left|\tilde{\mathcal{F}}\right| \geq \tilde{\mathcal{F}}, \qquad (6.144)$$
$$\frac{\tilde{\mathcal{F}}^2}{4\tilde{\mathcal{C}}} \geq 0. \qquad (6.145)$$

Equation (6.145) can be rewritten by using Eq. (6.144), resulting in

$$\left|\tilde{\mathcal{F}}\right| - \tilde{\mathcal{F}} + \frac{\tilde{\mathcal{F}}^2}{4\tilde{\mathcal{C}}} \geq 0, \qquad (6.146)$$

and also recall that

$$\tilde{\mathcal{F}} \leq \left|\tilde{\mathcal{F}}\right| + \frac{\tilde{\mathcal{F}}^2}{4\tilde{\mathcal{C}}}, \qquad (6.147)$$

where adding $\tilde{\mathcal{C}}$ to both sides of inequality (6.147) results in

$$\tilde{\mathcal{F}}+\tilde{\mathcal{C}} \leq \left|\tilde{\mathcal{F}}\right| + \tilde{\mathcal{C}} + \frac{\tilde{\mathcal{F}}^2}{2\tilde{\mathcal{C}}} = \left(\sqrt{\tilde{\mathcal{C}}}+\frac{\left|\tilde{\mathcal{F}}\right|}{2\sqrt{\tilde{\mathcal{C}}}}\right)^2. \qquad (6.148)$$

Taking the square root of both sides of inequality (6.148) yields

$$\sqrt{\tilde{\mathcal{F}}+\tilde{\mathcal{C}}} \leq \sqrt{\tilde{\mathcal{C}}}+\frac{\left|\tilde{\mathcal{F}}\right|}{2\sqrt{\tilde{\mathcal{C}}}}. \tag{6.149}$$

Using the results obtained with inequalities (6.138), (6.139), and (6.149), into inequality (6.137) yields

$$\begin{aligned}
& 2a_{10}(\tilde{x}+x^*)^2 \sin\left(\frac{\mathcal{A}_1-\mathcal{B}_1}{2}\right)\cos\left(\frac{\mathcal{A}_1+\mathcal{B}_1}{2}\right) \\
\leq\ & s_2\mathcal{K}_1(\tilde{x}+x^*)^2\left|a_{10}\left[2\left(\sqrt{s_3\left(F+\mathcal{C}\right)}-\sqrt{s_3\mathcal{C}}\right)+s_3F\right]\right| \\
=\ & s_2\mathcal{K}_1(\tilde{x}+x^*)^2\left|a_{10}\left[2\left(\sqrt{\tilde{\mathcal{F}}+\tilde{\mathcal{C}}}-\sqrt{\tilde{\mathcal{C}}}\right)+\tilde{\mathcal{F}}\right]\right| \\
\leq\ & s_2\mathcal{K}_1(\tilde{x}+x^*)^2\left|a_{10}\left[2\left(\sqrt{\tilde{\mathcal{C}}}+\frac{\left|\tilde{\mathcal{F}}\right|}{2\sqrt{\tilde{\mathcal{C}}}}-\sqrt{\tilde{\mathcal{C}}}\right)+\tilde{\mathcal{F}}\right]\right| \\
=\ & s_2\mathcal{K}_1(\tilde{x}+x^*)^2\left|a_{10}\left(\frac{\left|\tilde{\mathcal{F}}\right|}{\sqrt{\tilde{\mathcal{C}}}}+\tilde{\mathcal{F}}\right)\right| \\
=\ & s_2\mathcal{K}_1(\tilde{x}+x^*)^2\left(\frac{1}{\sqrt{\tilde{\mathcal{C}}}}+1\right)\left|a_{10}\tilde{\mathcal{F}}\right|.
\end{aligned} \tag{6.150}$$

Recalling the definition of $\tilde{\mathcal{C}}(\tilde{x})$, Eq. (6.139), which can be expanded such that

$$\tilde{\mathcal{C}}(\tilde{x}) = s_3\tilde{v}_{SS}(\tilde{x}) = \frac{s_3\bar{c}_6}{(\tilde{x}+x^*)^2}, \tag{6.151}$$

and as noted previously, $\tilde{x}+x^* \equiv x$, and with the ranges defined by in section 2.8.5.2, it was defined $x_{MIN} \leq x \leq x_{MAX}$, therefore it can be shown that

$$1+\frac{1}{\sqrt{\tilde{\mathcal{C}}}} = 1+\frac{\tilde{x}+x^*}{\sqrt{s_3\bar{c}_6}} \leq 1+\frac{x_{MAX}}{\sqrt{s_3\bar{c}_6}} = 1+\sqrt{-\frac{a_4}{a_2a_7}}x_{MAX},$$

where $-\frac{a_4}{a_2a_7}>0$. Recalling also that function $\tilde{\mathcal{F}}(\tilde{x},\tilde{\boldsymbol{y}})$, Eq. (6.138), was defined as

$$\tilde{\mathcal{F}}(\tilde{x},\tilde{\boldsymbol{y}}) \quad = \quad s_3\frac{\bar{\nu}_1\tilde{y}_2^2+\bar{\nu}_2\tilde{y}_2+\bar{\nu}_3\tilde{y}_1}{(\tilde{x}+x^*)^2}, \tag{6.152}$$

with the new parameters being given by

$$\bar{\nu}_1 \quad = \quad \bar{a}_9, \tag{6.153}$$

$$\bar{\nu}_2 \quad = \quad \left(\bar{a}_9-\tilde{b}_{y_2}\right), \tag{6.154}$$

$$\bar{\nu}_3 \quad = \quad -\tilde{b}_{y_1}, \tag{6.155}$$

and recalling that s_3 was previously defined in Eq. (4.88) as

$$s_3 = \frac{a_2a_5}{a_4a_9}, \tag{6.156}$$

thus permitting to rewrite inequality (6.150) as

$$\begin{aligned}
& 2a_{10}(\tilde{x}+x^*)^2 \sin\left(\frac{\mathcal{A}_1-\mathcal{B}_1}{2}\right)\cos\left(\frac{\mathcal{A}_1+\mathcal{B}_1}{2}\right) \\
\leq\ & s_2\mathcal{K}_1(\tilde{x}+x^*)^2\left(\frac{1}{\sqrt{\tilde{\mathcal{C}}}}+1\right)\left|a_{10}\tilde{\mathcal{F}}\right| \\
=\ & s_2\mathcal{K}_1(\tilde{x}+x^*)^2\left(\frac{1}{\sqrt{\tilde{\mathcal{C}}}}+1\right)\left|a_{10}s_3\frac{\bar{\nu}_1\tilde{y}_2^2+\bar{\nu}_2\tilde{y}_2+\bar{\nu}_3\tilde{y}_1}{(\tilde{x}+x^*)^2}\right|
\end{aligned}$$

$$\leq \quad s_2\mathcal{K}_1(\tilde{x}+x^*)^2\left(1+\sqrt{-\frac{a_4}{a_2a_7}}x_{MAX}\right)\left|a_{10}s_3\frac{\bar{\nu}_1\tilde{y}_2^2+\bar{\nu}_2\tilde{y}_2+\bar{\nu}_3\tilde{y}_1}{(\tilde{x}+x^*)^2}\right|. \tag{6.157}$$

For conciseness introduce

$$\begin{aligned} s_4 &= s_2s_3\,|a_{10}|\left(1+\sqrt{-\frac{a_4}{a_2a_7}}x_{MAX}\right)\mathcal{K}_1 \\ &= \frac{4a_2a_3\,|a_{10}|\,\mathcal{K}_1}{a_4^2\varepsilon_1}\left(1+\sqrt{-\frac{a_4}{a_2a_7}}x_{MAX}\right), \end{aligned} \tag{6.158}$$

thus simplifying inequality (6.150) as

$$\begin{aligned} & 2a_{10}(\tilde{x}+x^*)^2\sin\left(\frac{\mathcal{A}_1-\mathcal{B}_1}{2}\right)\cos\left(\frac{\mathcal{A}_1+\mathcal{B}_1}{2}\right) \\ \leq \quad & s_2\mathcal{K}_1(\tilde{x}+x^*)^2\left(1+\sqrt{-\frac{a_4}{a_2a_7}}x_{MAX}\right)\left|a_{10}s_3\frac{\bar{\nu}_1\tilde{y}_2^2+\bar{\nu}_2\tilde{y}_2+\bar{\nu}_3\tilde{y}_1}{(\tilde{x}+x^*)^2}\right| \\ = \quad & s_4\left|\bar{\nu}_1\tilde{y}_2^2+\bar{\nu}_2\tilde{y}_2+\bar{\nu}_3\tilde{y}_1\right|. \end{aligned} \tag{6.159}$$

In order to simplify even further inequality (6.159), let also recall that, as defined in section 2.8.5.2 that

$$\tilde{y}_{2_{MIN}} < \tilde{y}_2 < \tilde{y}_{2_{MAX}}, \tag{6.160}$$

therefore, it can be proven that

$$|\tilde{y}_2| \leq \tilde{Y}_{2_{MAX}}, \tag{6.161}$$

with $\tilde{Y}_{2_{MAX}}$ being the absolute value of the maximum vertical velocity of the helicopter, and given by

$$\tilde{Y}_{2_{MAX}} = max\left(|\tilde{y}_{2_{MIN}}|, |\tilde{y}_{2_{MAX}}|\right), \tag{6.162}$$

thus allowing to rewrite

$$|\tilde{y}_2| \quad \leq \quad \tilde{Y}_{2_{MAX}}, \tag{6.163}$$

$$\tilde{y}_2^2 \quad \leq \quad \tilde{Y}_{2_{MAX}}\,|\tilde{y}_2|, \tag{6.164}$$

therefore using Eqns. (6.163), and (6.164), into inequality (6.159), yields

$$\begin{aligned} & 2a_{10}(\tilde{x}+x^*)^2\sin\left(\frac{\mathcal{A}_1-\mathcal{B}_1}{2}\right)\cos\left(\frac{\mathcal{A}_1+\mathcal{B}_1}{2}\right) \\ \leq \quad & s_4\left|\bar{\nu}_1\tilde{y}_2^2+\bar{\nu}_2\tilde{y}_2+\bar{\nu}_3\tilde{y}_1\right| \\ \leq \quad & s_4\left(\left|\bar{\nu}_1\tilde{y}_2^2\right|+|\bar{\nu}_2\tilde{y}_2|+|\bar{\nu}_3\tilde{y}_1|\right) \\ \leq \quad & s_4\left(\left|\bar{\nu}_1\tilde{Y}_{2_{MAX}}\tilde{y}_2\right|+|\bar{\nu}_2\tilde{y}_2|+|\bar{\nu}_3\tilde{y}_1|\right). \end{aligned} \tag{6.165}$$

Let also introduce

$$\mathcal{C}_1(\tilde{b}_{y_1}) \quad = \quad s_4\,|\bar{\nu}_3| = \frac{4a_2a_3\,|a_{10}|\,\tilde{b}_{y_1}\mathcal{K}_1}{a_4^2\varepsilon_1}\left(1+\sqrt{-\frac{a_4}{a_2a_7}}x_{MAX}\right) \tag{6.166}$$

$$\begin{aligned} \mathcal{C}_2(\tilde{b}_{y_2}) &= s_4\left(\left|\bar{\nu}_1\tilde{Y}_{2_{MAX}}\right|+|\bar{\nu}_2|\right) \\ &= \frac{4a_2a_3\,|a_{10}|\,\mathcal{K}_1}{a_4^2\varepsilon_1}\left(1+\sqrt{-\frac{a_4}{a_2a_7}}x_{MAX}\right)\left(\tilde{Y}_{2_{MAX}}\,|a_9|+\left|a_9+\tilde{b}_{y_2}\right|\right), \end{aligned} \tag{6.167}$$

with x_{MAX} being the maxim angular velocity of the blades. Using Eqns. (6.166), and (6.167), into inequality (6.165) yields

$$2a_{10}(\tilde{x}+x^*)^2\sin\left(\frac{\mathcal{A}_1-\mathcal{B}_1}{2}\right)\cos\left(\frac{\mathcal{A}_1+\mathcal{B}_1}{2}\right)$$

$$\begin{aligned}
&\leq s_4 \left(\left| \bar{\nu}_1 \tilde{Y}_{2_{MAX}} \tilde{y}_2 \right| + \left| \bar{\nu}_2 \tilde{y}_2 \right| + \left| \bar{\nu}_3 \tilde{y}_1 \right| \right) \\
&\leq \mathcal{C}_1 \left| \tilde{y}_1 \right| + \mathcal{C}_2 \left| \tilde{y}_2 \right|. \qquad (6.168)
\end{aligned}$$

Using the results obtained in inequality (6.168) into inequality (6.98), results in

$$\begin{aligned}
&\left(\frac{\partial V_S(\tilde{x})}{\partial \tilde{x}} \right)^T \left[\tilde{f}(\tilde{x}, \tilde{\boldsymbol{y}}, \tilde{\mathbf{h}}(\tilde{x}, \tilde{\boldsymbol{y}})) - \tilde{f}(\tilde{x}, \tilde{\mathbf{g}}(\tilde{x}), \tilde{\mathbf{h}}(\tilde{x}, \tilde{\boldsymbol{y}})) \right] \\
&= \frac{1}{2} \frac{Q_S}{b_x} \tilde{x} \left[2a_{10} (\tilde{x} + x^*)^2 \sin \left(\frac{\mathcal{A}_1 - \mathcal{B}_1}{2} \right) \cos \left(\frac{\mathcal{A}_1 + \mathcal{B}_1}{2} \right) \right] \\
&\leq \left| \frac{1}{2} \frac{Q_S}{b_x} \tilde{x} \left[2a_{10} (\tilde{x} + x^*)^2 \sin \left(\frac{\mathcal{A}_1 - \mathcal{B}_1}{2} \right) \cos \left(\frac{\mathcal{A}_1 + \mathcal{B}_1}{2} \right) \right] \right| \\
&\leq \left| \frac{1}{2} \frac{Q_S}{b_x} \tilde{x} \left(\mathcal{C}_1 \left| \tilde{y}_1 \right| + \mathcal{C}_2 \left| \tilde{y}_2 \right| \right) \right|, \qquad (6.169)
\end{aligned}$$

which can be further simplified by defining

$$\hat{\mathcal{C}}_1(b_x, \tilde{b}_{y_1}) = \frac{1}{2} \frac{Q_S}{b_x} \mathcal{C}_1(\tilde{b}_{y_1}), \qquad (6.170)$$

$$\hat{\mathcal{C}}_2(b_x \tilde{b}_{y_1}) = \frac{1}{2} \frac{Q_S}{b_x} \mathcal{C}_2(\tilde{b}_{y_1}). \qquad (6.171)$$

Substituting Eqns. (6.170) and (6.171) into inequality (6.169), results in

$$\begin{aligned}
&\left(\frac{\partial V_S(\tilde{x})}{\partial \tilde{x}} \right)^T \left[\tilde{f}(\tilde{x}, \tilde{\boldsymbol{y}}, \tilde{\mathbf{h}}(\tilde{x}, \tilde{\boldsymbol{y}})) - \tilde{f}(\tilde{x}, \tilde{\mathbf{g}}(\tilde{x}), \tilde{\mathbf{h}}(\tilde{x}, \tilde{\boldsymbol{y}})) \right] \\
&\leq \left| \frac{1}{2} \frac{Q_S}{b_x} \tilde{x} \left(\mathcal{C}_1 \left| \tilde{y}_1 \right| + \mathcal{C}_2 \left| \tilde{y}_2 \right| \right) \right| \\
&\leq \left(\hat{\mathcal{C}}_1 \left| \tilde{x} \tilde{y}_1 \right| + \hat{\mathcal{C}}_2 \left| \tilde{x} \tilde{y}_2 \right| \right), \qquad (6.172)
\end{aligned}$$

thus the original inequality , Eq. (6.92), becomes

$$\begin{aligned}
&\left(\frac{\partial V_S(\tilde{x})}{\partial \tilde{x}} \right)^T \left[\tilde{f}(\tilde{x}, \tilde{\boldsymbol{y}}, \tilde{\mathbf{h}}(\tilde{x}, \tilde{\boldsymbol{y}})) - \tilde{f}(\tilde{x}, \tilde{\mathbf{g}}(\tilde{x}), \tilde{\mathbf{h}}(\tilde{x}, \tilde{\boldsymbol{y}})) \right] \\
&\leq \left(\hat{\mathcal{C}}_1 \left| \tilde{x} \tilde{y}_1 \right| + \hat{\mathcal{C}}_2 \left| \tilde{x} \tilde{y}_2 \right| \right) \leq \beta_1 \psi_1(\tilde{x}) \phi(\hat{\boldsymbol{y}}), \qquad (6.173)
\end{aligned}$$

where recalling the selected comparison functions $\psi_1(\tilde{x})$ and $\phi_1(\hat{\boldsymbol{y}})$, Eqns. (6.72), and (6.91), respectively, it can be observed that satisfying inequality (6.173) is reduced to prove that

$$\left(\hat{\mathcal{C}}_1 \left| \tilde{x} \tilde{y}_1 \right| + \hat{\mathcal{C}}_2 \left| \tilde{x} \tilde{y}_2 \right| \right) \leq \beta_1 \psi_1(\tilde{x}) \phi(\hat{\boldsymbol{y}}) = \beta_1 \left(\frac{Q_S}{2} \tilde{x}^2 \right)^{\frac{1}{2}} \left(\frac{q_{f_1}}{2} \tilde{y}_1^2 + \frac{q_{f_2}}{2} \tilde{y}_2^2 \right)^{\frac{1}{2}}. \qquad (6.174)$$

In order to obtain the constant β_1 that guarantees the fulfillment of inequality (6.92), let square both sides of inequality (6.174), resulting in

$$\left(\hat{\mathcal{C}}_1 \left| \tilde{x} \tilde{y}_1 \right| + \hat{\mathcal{C}}_2 \left| \tilde{x} \tilde{y}_2 \right| \right)^2 \leq \beta_1^2 \tilde{Q}_s \tilde{x}^2 \left(\tilde{q}_{f_1} \tilde{y}_1^2 + \tilde{q}_{f_2} \tilde{y}_2^2 \right), \qquad (6.175)$$

where the left-hand side of inequality (6.175) can be expanded as

$$\left(\hat{\mathcal{C}}_1 \left| \tilde{x} \tilde{y}_1 \right| + \hat{\mathcal{C}}_2 \left| \tilde{x} \tilde{y}_2 \right| \right)^2 = \tilde{x}^2 \left(\hat{\mathcal{C}}_1^2 \tilde{y}_1^2 + \hat{\mathcal{C}}_2^2 \tilde{y}_2^2 + 2 \hat{\mathcal{C}}_1 \hat{\mathcal{C}}_2 \left| \tilde{y}_1 \tilde{y}_2 \right| \right), \qquad (6.176)$$

which can be further reduced by using the absolute value version of Young's inequality (Steele, 2004)

$$|ab| \leq \left| \frac{a^2 + b^2}{2} \right|, \qquad (6.177)$$

which permits to rewrite Eq. (6.176) as

$$\begin{aligned}
\tilde{x}^2\left(\hat{\mathcal{C}}_1^2\tilde{y}_1^2+\hat{\mathcal{C}}_2^2\tilde{y}_2^2+2\hat{\mathcal{C}}_1\hat{\mathcal{C}}_2\left|\tilde{y}_1\tilde{y}_2\right|\right) &\leq \tilde{x}^2\left[\hat{\mathcal{C}}_1^2\tilde{y}_1^2+\hat{\mathcal{C}}_2^2\tilde{y}_2^2+2\hat{\mathcal{C}}_1\hat{\mathcal{C}}_2\left(\frac{\tilde{y}_1^2+\tilde{y}_2^2}{2}\right)\right] \\
&= \tilde{x}^2\left(\hat{\mathcal{C}}_1^2\tilde{y}_1^2+\hat{\mathcal{C}}_2^2\tilde{y}_2^2+\hat{\mathcal{C}}_1\hat{\mathcal{C}}_2\tilde{y}_1^2+\hat{\mathcal{C}}_1\hat{\mathcal{C}}_2\tilde{y}_2^2\right) \\
&= \tilde{x}^2\left[\left(\hat{\mathcal{C}}_1^2+\hat{\mathcal{C}}_1\hat{\mathcal{C}}_2\right)\tilde{y}_1^2+\left(\hat{\mathcal{C}}_2^2+\hat{\mathcal{C}}_1\hat{\mathcal{C}}_2\right)\tilde{y}_2^2\right]. \qquad (6.178)
\end{aligned}$$

Using Eq. (6.178) permits to rewrite inequality (6.175) as

$$\begin{aligned}
\left(\hat{\mathcal{C}}_1\left|\tilde{x}\tilde{y}_1\right|+\hat{\mathcal{C}}_2\left|\tilde{x}\tilde{y}_2\right|\right)^2 &\leq \tilde{x}^2\left[\left(\hat{\mathcal{C}}_1^2+\hat{\mathcal{C}}_1\hat{\mathcal{C}}_2\right)\tilde{y}_1^2+\left(\hat{\mathcal{C}}_2^2+\hat{\mathcal{C}}_1\hat{\mathcal{C}}_2\right)\tilde{y}_2^2\right] \\
&\leq \beta_1^2\left(\tilde{q}_s\tilde{x}^2\right)^{\frac{1}{2}}\left(\tilde{q}_{f_1}\tilde{y}_1^2+\tilde{q}_{f_2}\tilde{y}_2^2\right), \qquad (6.179)
\end{aligned}$$

therefore, satisfying the original inequality (6.92) reduces to find β_1 that satisfies the following inequality

$$\tilde{x}^2\left[\left(\hat{\mathcal{C}}_1^2+\hat{\mathcal{C}}_1\hat{\mathcal{C}}_2\right)\tilde{y}_1^2+\left(\hat{\mathcal{C}}_2^2+\hat{\mathcal{C}}_1\hat{\mathcal{C}}_2\right)\tilde{y}_2^2\right]\leq\beta_1^2\left(\tilde{Q}_S\tilde{x}^2\right)\left(\tilde{q}_{f_1}\tilde{y}_1^2+\tilde{q}_{f_2}\tilde{y}_2^2\right), \qquad (6.180)$$

therefore inequality (6.92) can be satisfied by selecting β_1 such

$$\beta_1=\max\left(\beta_{1_a},\beta_{1_b}\right), \qquad (6.181)$$

where

$$\begin{aligned}
\beta_{1_a} &\geq \sqrt{\frac{\left(\hat{\mathcal{C}}_1^2+\hat{\mathcal{C}}_1\hat{\mathcal{C}}_2\right)}{\tilde{Q}_S\tilde{q}_{f_1}}}=\sqrt{\frac{4\left(\hat{\mathcal{C}}_1^2+\hat{\mathcal{C}}_1\hat{\mathcal{C}}_2\right)}{Q_Sq_{f_1}}}, \qquad (6.182) \\
\beta_{1_b} &\geq \sqrt{\frac{\left(\hat{\mathcal{C}}_2^2+\hat{\mathcal{C}}_1\hat{\mathcal{C}}_2\right)}{\tilde{Q}_S\tilde{q}_{f_2}}}=\sqrt{\frac{4\left(\hat{\mathcal{C}}_2^2+\hat{\mathcal{C}}_1\hat{\mathcal{C}}_2\right)}{Q_Sq_{f_2}}}, \qquad (6.183)
\end{aligned}$$

with $\hat{\mathcal{C}}_1$ and $\hat{\mathcal{C}}_2$, given by Eqns. (6.170) and (6.171), respectively, and where Q_S, is the Lyapunov matrix for the Σ_S-subsystem, and q_{f_1}, and q_{f_2} are the coefficients of the Lyapunov Matrix $\boldsymbol{Q_F}$ of the Σ_F-subsystem, see section 5.4.2 for further details. With this in mind, Eqns. (6.182) and (6.183) can be simplified to

$$\begin{aligned}
\beta_{1_a} &\geq \sqrt{Q_S\frac{\left(\mathcal{C}_1+\mathcal{C}_2\right)}{b_x^2}\frac{\mathcal{C}_1}{q_{f_1}}}, \qquad (6.184) \\
\beta_{1_b} &\geq \sqrt{Q_S\frac{\left(\mathcal{C}_1+\mathcal{C}_2\right)}{b_x^2}\frac{\mathcal{C}_2}{q_{f_2}}}, \qquad (6.185)
\end{aligned}$$

where recalling that for the problem here discussed $\mathcal{C}_2>\mathcal{C}_1$, therefore the selection of β_{1_a} or β_{1_b} depends on the ratio between the *stability parameters* q_{f_2} and q_{f_1}, such that if

$$\begin{aligned}
&\frac{\mathcal{C}_2}{\mathcal{C}_1}\geq q_{f_2}/q_{f_1}\rightarrow\beta_1=\max\left(\beta_{1_a},\beta_{1_b}\right)=\beta_{1_b}, \qquad (6.186) \\
&\frac{\mathcal{C}_2}{\mathcal{C}_1}\leq q_{f_2}/q_{f_1}\rightarrow\beta_1=\max\left(\beta_{1_a},\beta_{1_b}\right)=\beta_{1_a}. \qquad (6.187)
\end{aligned}$$

This translates into that by selecting the ration between both q_{f_2} and q_{f_1}, the analysis can be simplified, therefore, for simplicity, as it will be seen in future sections, a relation between q_{f_1} and q_{f_2} can be defined by equating Eqns. (6.184) and (6.185) resulting in

$$\sqrt{Q_S\frac{\left(\mathcal{C}_1+\mathcal{C}_2\right)}{b_x^2}\frac{\mathcal{C}_1}{q_{f_1}}}=\sqrt{Q_S\frac{\left(\mathcal{C}_1+\mathcal{C}_2\right)}{b_x^2}\frac{\mathcal{C}_2}{q_{f_2}}}, \qquad (6.188)$$

which reduces to

$$\frac{\mathcal{C}_2}{\mathcal{C}_1} = \frac{q_{f_2}}{q_{f_1}} = Q_{F_{21}}, \tag{6.189}$$

this implies that if the ratio between q_{f_2} and q_{f_1} is given by expression (6.189) which implies that

$$\beta_1 > \beta_{1_a} = \beta_{1_b} = \sqrt{Q_S \frac{(\mathcal{C}_1 + \mathcal{C}_2)}{b_x^2} \frac{\mathcal{C}_1}{q_{f_1}}} = \sqrt{Q_S \frac{(\mathcal{C}_1 + \mathcal{C}_2)}{b_x^2} \frac{\mathcal{C}_2}{q_{f_2}}}, \tag{6.190}$$

therefore reducing Eq. (6.181)

$$\beta_1 = \sqrt{Q_S \frac{(\mathcal{C}_1 + \mathcal{C}_2)}{b_x^2} \frac{\mathcal{C}_1}{q_{f_1}}}, \tag{6.191}$$

where

$$\frac{q_{f_2}}{q_{f_1}} = \tilde{Q}_{F_{21}}, \tag{6.192}$$

and satisfying that

$$\tilde{Q}_{F_{21}} \geq Q_{F_{21}} = \frac{\mathcal{C}_2}{\mathcal{C}_1}, \tag{6.193}$$

which can be obtained by defining

$$\tilde{Q}_{F_{21}} = \delta_1 Q_{F_{21}}, \tag{6.194}$$

with $\delta_1 > 1$. It can be proven that the value of δ_1 determines the range of permissible d_1 that fulfill the asymptotic stability properties for the Σ_{SF}-subsystem as it will be shown in future analysis.

6.3.5 Proof of Assumption 5.5.5: Second Interconnection Condition for the Helicopter Σ_{SF}-Subsystem

The second interconnection condition is defined by the inequality

$$\left(\frac{\partial V_F(\tilde{\boldsymbol{y}})}{\partial \tilde{x}}\right)^T \tilde{f}(\tilde{x}, \tilde{\boldsymbol{y}}, \tilde{\mathbf{h}}(\tilde{x}, \tilde{\boldsymbol{y}})) \leq \gamma_1 \phi_1^2(\hat{\boldsymbol{y}}) + \beta_2 \psi_1(\tilde{x}) \phi_1(\hat{\boldsymbol{y}}). \tag{6.195}$$

Inequality (6.195) can be rewritten by adding and subtracting $\tilde{f}(\tilde{x}, \tilde{\mathbf{g}}(\tilde{x}), \tilde{\mathbf{h}}(\tilde{x}, \tilde{\boldsymbol{y}}))$ to the $\tilde{f}(\tilde{x}, \tilde{\boldsymbol{y}}, \tilde{\mathbf{h}}(\tilde{x}, \tilde{\boldsymbol{y}}))$ in the left-hand side of (6.195) resulting in

$$\begin{aligned} \frac{\partial V_F}{\partial \tilde{x}} \tilde{f}(\tilde{x}, \tilde{\boldsymbol{y}}, \tilde{\mathbf{h}}(\tilde{x}, \tilde{\boldsymbol{y}})) \quad &\leq \quad \frac{\partial V_F}{\partial \tilde{x}} \tilde{f}(\tilde{x}, \tilde{\boldsymbol{y}}, \tilde{\mathbf{h}}(\tilde{x}, \tilde{\boldsymbol{y}})) \\ &+ \quad \frac{\partial V_F}{\partial \tilde{x}} \left[f(\tilde{x}, \tilde{\boldsymbol{y}}, \tilde{\mathbf{h}}(\tilde{x}, \tilde{\boldsymbol{y}})) - f(\tilde{x}, \tilde{\boldsymbol{y}}, \tilde{\mathbf{h}}(\tilde{x}, \tilde{\boldsymbol{y}})) \right] \\ &\leq \quad \beta_2 \psi_1(\tilde{x}) \phi_1(\hat{\boldsymbol{y}}) + \gamma_1 \phi_1^2(\hat{\boldsymbol{y}}). \end{aligned} \tag{6.196}$$

The resulting inequality Eq. (6.196), can be satisfied by first splitting into two simpler inequalities given by

$$\frac{\partial V_F}{\partial \tilde{x}} \tilde{f}(\tilde{x}, \tilde{\boldsymbol{y}}, \tilde{\mathbf{h}}(\tilde{x}, \tilde{\boldsymbol{y}})) \leq \beta_2 \psi_1(\tilde{x}) \phi_1(\hat{\boldsymbol{y}}) \tag{6.197}$$

$$\frac{\partial V_F}{\partial \tilde{x}} \left[\tilde{f}(\tilde{x}, \tilde{\boldsymbol{y}}, \tilde{\mathbf{h}}(\tilde{x}, \tilde{\boldsymbol{y}})) - \tilde{f}(\tilde{x}, \tilde{\mathbf{g}}(\tilde{x}), \tilde{\mathbf{h}}(\tilde{x}, \tilde{\boldsymbol{y}})) \right] \leq \gamma \phi_1^2(\hat{\boldsymbol{y}}), \tag{6.198}$$

therefore, assumption (6.195) will be proven, if both inequalities (6.197) and (6.198) are fulfilled. From the definition of $V_F(\hat{\boldsymbol{y}})$, it can be seen that

$$\frac{\partial V_F}{\partial \tilde{x}} = 0. \tag{6.199}$$

Due to the fact that the associated Lyapunov function, $V_F(\hat{\boldsymbol{y}})$, does not depend on the variable $\tilde{x}$, implies that the fulfillment of inequality (6.195) is trivial and is achieved by selecting $\beta_1 \geq 0$, and $\gamma_1 \geq 0$, thus, concluding that the sub-conditions (6.197) and (6.198) are satisfied by selecting

$$\beta_2 \;\geq\; 0, \tag{6.200}$$

$$\gamma_1 \;\geq\; 0. \tag{6.201}$$

These results provide an additional degree of freedom that will be exploited in later sections in order to determine desired upperbounds of the Σ_{SF} *Stability Analysis*.

6.4 Fulfillment of the Helicopter Σ_{SF} *Stability Analysis*

The fulfillment of assumptions 5.5.1, 5.5.2, 5.5.3, 5.5.4, and 5.5.5, applied to the helicopter Σ_{SF}-subsystem by the fulfillment of inequalities 6.67, 6.75, 6.92, and 6.195, proves that the growth requirements of $\tilde{f}(\tilde{x}, \tilde{\boldsymbol{y}}, \tilde{\mathbf{h}}(\tilde{x}, \tilde{\boldsymbol{y}}))$ and $\hat{\boldsymbol{g}}(\tilde{x}, \tilde{\boldsymbol{y}}, \tilde{\mathbf{h}}(\tilde{\mathbf{x}}, \tilde{\boldsymbol{y}}))$ are satisfied, and with the Lyapunov functions $V_S(\tilde{x})$ and $V_F(\hat{\boldsymbol{y}})$, Eqns. (6.41) and (6.42) respectively, satisfying the respective growth requirements, a new Lyapunov function candidate $V_1(\tilde{x}, \tilde{\boldsymbol{y}})$ is considered and defined by the weighted sum of $V_S(\tilde{x})$ and $V_F(\tilde{x}, \tilde{\boldsymbol{y}})$, given by

$$\begin{aligned} V_1(\tilde{x}, \tilde{\boldsymbol{y}}) &= (1-d_1)V_S(\tilde{x}) + d_1 V_F(\hat{\boldsymbol{y}}),\ d_1 \in (0,1) \\ &= (1-d_1)\frac{Q_S}{4b_x}\tilde{x}^2 + \frac{d_1}{2}p_{f_1}\tilde{y}_1^2 + \frac{d_1}{2}p_{f_3}\tilde{y}_2^2 + d_1 p_{f_2}\tilde{y}_1\tilde{y}_2, \end{aligned} \tag{6.202}$$

for $0 < d_1 < 1$. The newly defined function $V_1(\tilde{x}, \tilde{\boldsymbol{y}})$ becomes the Lyapunov function candidate for the singular perturbed Σ_{SF}-subsystem, Eqns. (6.15–6.17). Similarly as in the general case, to explore the freedom in choosing the weights, lets take d_1 as an unspecified parameter in the interval $(0, 1)$. From the properties of $V_S(\tilde{x})$ and $V_F(\hat{\boldsymbol{y}})$ and inequality (6.65), that is $\parallel \tilde{\mathbf{g}}(\tilde{x}) \parallel \leq p_1(\parallel \tilde{x} \parallel)$, where $p_1(\cdot)$ is a κ class function, it follows that $V_1(\tilde{x}, \tilde{\boldsymbol{y}})$ is positive-definite. Computing the time derivative of $V_1(\tilde{x}, \tilde{\boldsymbol{y}})$ along the trajectories of $\tilde{f}(\tilde{x}, \tilde{\boldsymbol{y}}, \tilde{\mathbf{h}}(\tilde{x}, \tilde{\boldsymbol{y}}))$ and $\hat{\boldsymbol{g}}(\tilde{x}, \tilde{\boldsymbol{y}}, \tilde{\mathbf{h}}(\tilde{x}, \tilde{\boldsymbol{y}}))$ yields an equation of similar structure as in Eq. (5.145), which can express as a function of the comparison functions $\psi_1(\tilde{x})$, and $\phi_1(\hat{\boldsymbol{y}})$ by employing the derived inequalities 6.67, 6.75, 6.92, and 6.195, resulting in

$$\begin{aligned} \dot{V}_1 &\leq -(1-d_1)\alpha_1\psi_1^2(\tilde{x}) + (1-d_1)\beta_1\psi_1(\tilde{x})\phi_1(\hat{\boldsymbol{y}}) \\ &- \frac{d_1}{\varepsilon_1}\alpha_2\phi_1^2(\hat{\boldsymbol{y}}) + d_1\gamma_1\phi_1^2(\hat{\boldsymbol{y}}) + d_1\beta_2\psi_1(\tilde{x})\phi_1(\hat{\boldsymbol{y}}) \\ &= -\begin{bmatrix} \psi_1(\tilde{x}) \\ \phi_1(\hat{\boldsymbol{y}}) \end{bmatrix}^T \begin{bmatrix} (1-d_1)\alpha_1 & -\frac{1}{2}(1-d_1)\beta_1 - \frac{1}{2}d_1\beta_2 \\ -\frac{1}{2}(1-d_1)\beta_1 - \frac{1}{2}d_1\beta_2 & d_1\left(\dfrac{\alpha_2}{\varepsilon_1} - \gamma_1\right) \end{bmatrix} \\ &\times \begin{bmatrix} \psi_1(\tilde{x}) \\ \phi_1(\hat{\boldsymbol{y}}) \end{bmatrix} \\ &= -\begin{bmatrix} \sqrt{\tilde{Q}_S\tilde{x}^2} \\ \sqrt{\tilde{\boldsymbol{y}}^T\tilde{\mathbf{Q}}_{\mathbf{F}}\tilde{\boldsymbol{y}}} \end{bmatrix}^T \begin{bmatrix} (1-d_1)\alpha_1 & -\frac{1}{2}(1-d_1)\beta_1 - \frac{1}{2}d_1\beta_2 \\ -\frac{1}{2}(1-d_1)\beta_1 - \frac{1}{2}d_1\beta_2 & d_1\left(\dfrac{\alpha_2}{\varepsilon_1} - \gamma_1\right) \end{bmatrix} \\ &\times \begin{bmatrix} \sqrt{\tilde{Q}_S\tilde{x}^2} \\ \sqrt{\tilde{\boldsymbol{y}}^T\tilde{\mathbf{Q}}_{\mathbf{F}}\tilde{\boldsymbol{y}}} \end{bmatrix}. \end{aligned} \tag{6.203}$$

In order to guarantee the negative-definiteness property of Eq. (6.203), and conducting the same algebraic transformations as in section 5.5.1, it can be obtained the following expression that defines the requirement to be satisfied by the parasitic constant ε_1 such that

$$\varepsilon_1 < \frac{\alpha_1\alpha_2}{\alpha_1\gamma_1 + \dfrac{1}{4(1-d_1)d_1}\left[(1-d_1)\beta_1 + d_1\beta_2\right]^2} \equiv \varepsilon_{1_d}. \tag{6.204}$$

Recalling from the general formulation, chapter 5, that although only α_1 and α_2 are required by definition to be positive, β_1, β_2, and γ_1 are also considered to be positive. Inequality (6.204) shows that for any choice of d_1, the corresponding $V_1(\tilde{x}, \tilde{\boldsymbol{y}})$, Eq. (6.202), is a Lyapunov function for the singular perturbed Σ_{SF}-subsystem, Eqns. (6.15–6.17), for all ε_1 satisfying Eq. (6.204). It can be easily seen that the maximum value of ε_{1_d} occurs at

$$d_1^* = \frac{\beta_1}{\beta_1 + \beta_2}, \tag{6.205}$$

yielding the upper bound on ε_1 given by

$$\varepsilon_1^* = \frac{\alpha_1\alpha_2}{\alpha_1\gamma_1 + \beta_1\beta_2}. \tag{6.206}$$

Therefore, it can be inferred that the equilibrium point of the singularly perturbed Σ_{SF}-subsystem, Eqns. (6.15–6.17), is asymptotically stable for all $\varepsilon_1 < \varepsilon_1^*$. The number ε_1^* is the best upper bound on ε_1 that can be provided by the above presented stability analysis. The results obtained from the fulfillment of inequalities (6.67), (6.75), (6.92) and (6.195) are summarized in Table 6.1, where it can be seen the similarities between the two-time-scale growth requirements described in Section 5.2.1, and the three-time-scale growth requirements for the Σ_{SF}-subsystem.

The asymptotic stability analysis presented proves that by fulfilling inequalities (6.67), (6.75), (6.92), and (6.195), then the origin is an asymptotically stable equilibrium of the singularly perturbed helicopter Σ_{SF}-subsystem (6.15–6.17) for all $\varepsilon_1 \in (0, \varepsilon_1^*)$, where ε_1^* is given by Eq. (6.206), thus, for every number $d_1 \in (0,1)$, $V_1(\tilde{x}, \tilde{\boldsymbol{y}})$, Eq. (6.202), is a Lyapunov function for all $\varepsilon_1(0, \varepsilon_d)$, where $\varepsilon_{1_d} \leq \varepsilon_1^*$ is given by Eq. (6.204), hence satisfying Theorem 5.5.1. As mentioned previously in section 6.3.4, it can be proven that the value of δ_1 determines the range of permissible d_1 that fulfill the asymptotic stability properties for the Σ_{SF}-subsystem, therefore, such that in order to satisfy that for every number $d_1 \in (0,1)$, $V_1(\tilde{x}, \tilde{\boldsymbol{y}})$, is a Lyapunov function for all $\varepsilon_1(0, \varepsilon_d)$, it is required that $\delta_1 \geq 10.66$. Nevertheless, as it will be proven in the Σ_{SFU} *Stability Analysis* in section 6.5, in order to satisfy the stability analysis it is required that $\delta_1 \in (1.02, 1.264)$.

The fulfillment of Theorem 5.5.1 for the helicopter Σ_{SF}-subsystem can be summarized by understanding that $\tilde{x} = 0$ is an asymptotically stable equilibrium of the reduced Σ_S-subsystem, Eq. (6.30), and $\tilde{\boldsymbol{y}} = \tilde{\mathbf{g}}(\tilde{x})$ is an asymptotically stable equilibrium of the boundary-layer Σ_F-subsystem, Eq. (6.19–6.20), uniformly in $\tilde{x}$, that is, the $\varepsilon - \delta$ definition of *Lyapunov* stability and the convergence $\tilde{\boldsymbol{y}} \to \tilde{\mathbf{g}}(\tilde{x})$ are uniform in $\tilde{x}$ (Vidyasagar, 2002), and since it has been proven that $\tilde{f}(\tilde{x}, \tilde{\boldsymbol{y}}, \tilde{\mathbf{h}}(\tilde{x}, \tilde{\boldsymbol{y}}))$ and $\hat{\boldsymbol{g}}(\tilde{x}, \tilde{\boldsymbol{y}}, \tilde{\mathbf{h}}(\tilde{x}, \tilde{\boldsymbol{y}}))$ satisfy certain growth conditions on the reduced and boundary-layer systems, assumptions 5.5.1, 5.5.2, 5.5.3, 5.5.4, and 5.5.5 applied to the helicopter Σ_{SF}-subsystem, then the origin is an asymptotically stable equilibrium of the singularly perturbed system (6.15–6.17), for sufficiently small ε_1 (Kokotović et al., 1986; Kokotović et al., 1987; Kokotović et al., 1999).

Due to the fact that the system is expressed in its error dynamics form, and that the use of the full range of reachable state variables has been required in order to satisfy the inequalities that guarantee the asymptotic stability properties at the origin of the Σ_{SF}-subsystem, these asymptotic stability properties are also extended to semiglobal stability, by the definition in (Kokotović, 1992; Sussmann and Kokotović, 1991; Braslavsky and Miidleton, 1996), by providing upper bounds on the parasitic singularly perturbed parameters for the entire range of admissible state values, thus extending the domain of attraction to that same rage of admissible states.

Assumption 5.5.2 for the Helicopter Σ_{SF}-Subsystem				
Section 5.2	$\frac{\partial V}{\partial x}$	$f(x, \mathrm{h}(x))$	α_1	$\psi(x)$
Σ_{SF}	$\frac{\partial V_S(\tilde{x})}{\partial \tilde{x}}$	$\tilde{f}(\tilde{x}, \tilde{\mathbf{g}}(\tilde{x}), \tilde{\mathbf{h}}(\tilde{x}, \tilde{\boldsymbol{y}}))$	$\alpha_1 \leq 1$	$\psi_1(\tilde{x}) = \sqrt{\tilde{Q}_s \tilde{x}^2}$
Assumption 5.5.3 for the Helicopter Σ_{SF}-Subsystem				
Section 5.2	$\frac{\partial W}{\partial z}$	$g(x, z)$	α_2	$\phi(z - \mathrm{h}(x))$
Σ_{SF}	$\left(\frac{\partial V_F(\tilde{y})}{\partial \tilde{y}}\right)^T$	$\hat{\boldsymbol{g}}(\tilde{x}, \tilde{\boldsymbol{y}}, \tilde{\mathbf{h}}(\tilde{x}, \tilde{\boldsymbol{y}}))$	$\alpha_2 \leq 1$	$\phi_1(\hat{\boldsymbol{y}}) = \sqrt{\tilde{\boldsymbol{y}}^T \tilde{\mathbf{Q}}_{\mathbf{F}} \tilde{\boldsymbol{y}}}$
Assumption 5.5.4 for the Helicopter Σ_{SF}-Subsystem				
Section 5.2	$\frac{\partial V}{\partial x}$	$f(x, z)$	$f(x, \mathrm{h}(x))$	β_1
Σ_{SF}	$\left(\frac{\partial V_S(\tilde{x})}{\partial \tilde{x}}\right)^T$	$\tilde{f}(\tilde{x}, \tilde{\boldsymbol{y}}, \tilde{\mathbf{h}}(\tilde{x}, \tilde{\boldsymbol{y}}))$	$\tilde{f}(\tilde{x}, \tilde{\mathbf{g}}(\tilde{x}), \tilde{\mathbf{h}}(\tilde{x}, \tilde{\boldsymbol{y}}))$	$\beta_1 \geq \max(\beta_{1_a}, \beta_{1_b})$
Assumption 5.5.5 for the Helicopter Σ_{SF}-Subsystem				
Section 5.2	$\frac{\partial W}{\partial x}$	$f(x, z)$	γ_1	β_2
Σ_{SF}	$\left(\frac{\partial V_F(\tilde{y})}{\partial \tilde{x}}\right)^T$	$\tilde{f}(\tilde{x}, \tilde{\boldsymbol{y}}, \tilde{\mathbf{h}}(\tilde{x}, \tilde{\boldsymbol{y}}))$	$\gamma_1 \geq 0$	$\beta_2 \geq 0$

Table 6.1: Parameters for the Comparison Functions and Inequalities that Guarantee the Asymptotic Stability Requirements for the Helicopter Σ_{SF} Subsystem.

6.4.1 Bounds for the *Stability Parameter* of the Σ_{SF} *Stability Analysis*

Needs to be noted that, due to the existent freedom on selecting β_2 and γ_1, the upper-bound ε_1^*, Eq. (6.206), and its d_1^* parameter, Eq. (6.205), can be precisely obtained to match the required parameters that guarantee the asymptotic stability for the full Σ_{SFU} system by selecting the combination of γ_1 and β_2 that generates the appropriate combination of both d_1^* and ε_1^*. This is obtained by solving Eqns. (6.205) and (6.206) such that yields

$$\varepsilon_1^* = \frac{\alpha_1 \alpha_2}{\alpha_1 \gamma_1 + \beta_1 \beta_2} \rightarrow \gamma_1(\varepsilon_1^\bigstar) = \frac{1}{\alpha_1}\left(\frac{\alpha_1 \alpha_2}{\varepsilon_1^\bigstar} - \beta_1 \beta_2\right) \tag{6.207}$$

and where β_2 is defined by

$$d_1^* = \frac{\beta_1}{\beta_1 + \beta_2} \rightarrow \beta_2(d_1^\bigstar) = \frac{\beta_1}{d_1^\bigstar} - \beta_1, \tag{6.208}$$

where recall that $d_1^\bigstar$ and $\varepsilon_1^\bigstar$ are the selected values by the author that satisfy the asymptotic stability properties of the full system, not to confuse with d_1^* and ε_1^*, that are given by Eqns. (6.205) and (6.206), respectively. The major difference between both, $d_1^\bigstar$, $\varepsilon_1^\bigstar$ and d_1^*, ε_1^*, is that the first appear only for the special type of problems in which the degrees of freedom that appear during the stability analysis allow to select $\beta_2(d_1^\bigstar)$ and $\gamma_1(\varepsilon_1^\bigstar)$, thus permitting to select the desired values for both ε_1 and d_1 by selecting $\varepsilon_1^\bigstar$ and $d_1^\bigstar$ from Eqns. (6.207) and (6.208), respectively. This reduces Eqns. (6.205) and (6.206) to

$$d_1^* = \frac{\beta_1}{\beta_1 + \beta_2(d_1^\bigstar)}, \tag{6.209}$$

yielding the upper bound on ε_1 given by

$$\varepsilon_1^* = \frac{\alpha_1 \alpha_2}{\alpha_1 \gamma_1(\varepsilon_1^\bigstar) + \beta_1 \beta_2(d_1^\bigstar)}. \tag{6.210}$$

The power to select ε_1^*, can be better understood since the fulfillment of the Σ_{SF} *Stability Analysis* depends on the fulfillment that the chosen ε_1 in the time-scale selection (see selection 3.5) satisfies $\varepsilon_1 < \varepsilon_1^*$. The power to select d_1^* will be fully understood when completing the satisfy the Σ_{SFU} *Stability Analysis*, but initially can be thought as a requirement to calculate the upper bound on ε_1^*, Eq. (6.210), which requires the calculation of both $\beta_2(d_1^\bigstar)$, and $\gamma_1(\varepsilon_1^\bigstar)$, Eqns. (6.208) and (6.207), respectively.

As it will be shown in section 6.6, in order to satisfy the Σ_{SFU} *Stability Analysis*, it is required that $d_1 \in (0.0543, 0.5243)$. Therefore, by selecting $d_1^* = 0.5$, the Σ_{SFU} *Stability Analysis* will be satisfied, and in addition, the percentage contribution on the Lyapunov function $V_1(\tilde{x}, \hat{\boldsymbol{y}})$, Eq. (6.202), is equally distributed for both Lyapunov functions $V_S(\tilde{x})$ and $V_F(\hat{\boldsymbol{y}})$. The selection of $\varepsilon_1^\bigstar$ is more straight forward, recalling the time-scale of the helicopter problem here analyzed, which was selected as $\varepsilon_1 = 0.028$. Therefore, recalling Eq. (6.207), and identifying that for margin let $\varepsilon_1^\bigstar = \delta_{\varepsilon_1}\varepsilon_1 = 0.02940$, where it is selected as $\delta_{\varepsilon_1} = 1.05$.

Recall also that need to select the *stability parameters* Q_S, q_{f_1}, and q_{f_2}, and where although arbitrary values can be selected in order to satisfy the asymptotic stability properties of the Σ_{SF}-subsystem, as it will be proven in the stability analysis for the full Σ_{SFU} system, a specific ratio between all three parameters is required in order to guarantee the stability properties of the Σ_{SFU} system, such that

$$q_{f_1} = \tilde{Q}_{SF} Q_S, \tag{6.211}$$

$$q_{f_2} = \tilde{Q}_{F_{21}} \tilde{Q}_{SF} Q_S, \tag{6.212}$$

where both $\tilde{Q}_{SF} = \delta_1 Q_{SF}$ and $\tilde{Q}_{F_{21}} = \delta_1 Q_{F_{21}}$, represent the required ratios to prove the asymptotic stability analysis for the full Σ_{SFU} helicopter system, and will be derived in the Σ_{SFU} *Stability Analysis* in section 6.5. These ratios, for the physical parameters of the helicopter here discussed, and recalling that in order to satisfy that the range of permissible unspecified parameter d_1 is $d_1 \in (0.0543, 0.5243)$, and with $\delta_1 = 1.05$ results in

$$Q_{SF} = 0.259974, \tag{6.213}$$

$$Q_{F_{21}} = 2.567205, \tag{6.214}$$

therefore, by selecting $Q_S = 0.5$, results in

$$q_{f_1} = 0.129987, \tag{6.215}$$

$$q_{f_2} = 0.333703, \tag{6.216}$$

which results, according to Eqns. (6.207) and (6.208), results in $\gamma_1 = 31.7007576$, and $\beta_2 = 0.76260$, respectively, which results in the new coefficients that fulfill the growth requirements

$$\begin{aligned} \alpha_1 &= 0.95, \\ \alpha_2 &= 0.95, \\ \beta_1 &= 0.76260 \\ \beta_2 &= 0.76260, \\ \gamma_1 &= 31.7007576. \end{aligned}$$

Figure 6.1 shows the dependance on the right-hand side of Eq. (6.204) on the unspecified parameter d_1, being able to identify that the maximum value is achieved at the selected $d_1^\bigstar = 0.5$, and with the value of the also selected $\varepsilon_1^\bigstar = \varepsilon_1^* = 0.02940$, which satisfies the requirements $\varepsilon_1 < \varepsilon_1^*$, and $d_1^\bigstar = 0.5$. This concludes the first step of the asymptotic stability analysis, the Σ_{SF} *Stability Analysis*. The following section describes the second step of the asymptotic stability analysis, the Σ_{SFU} *Stability Analysis* for the helicopter problem.

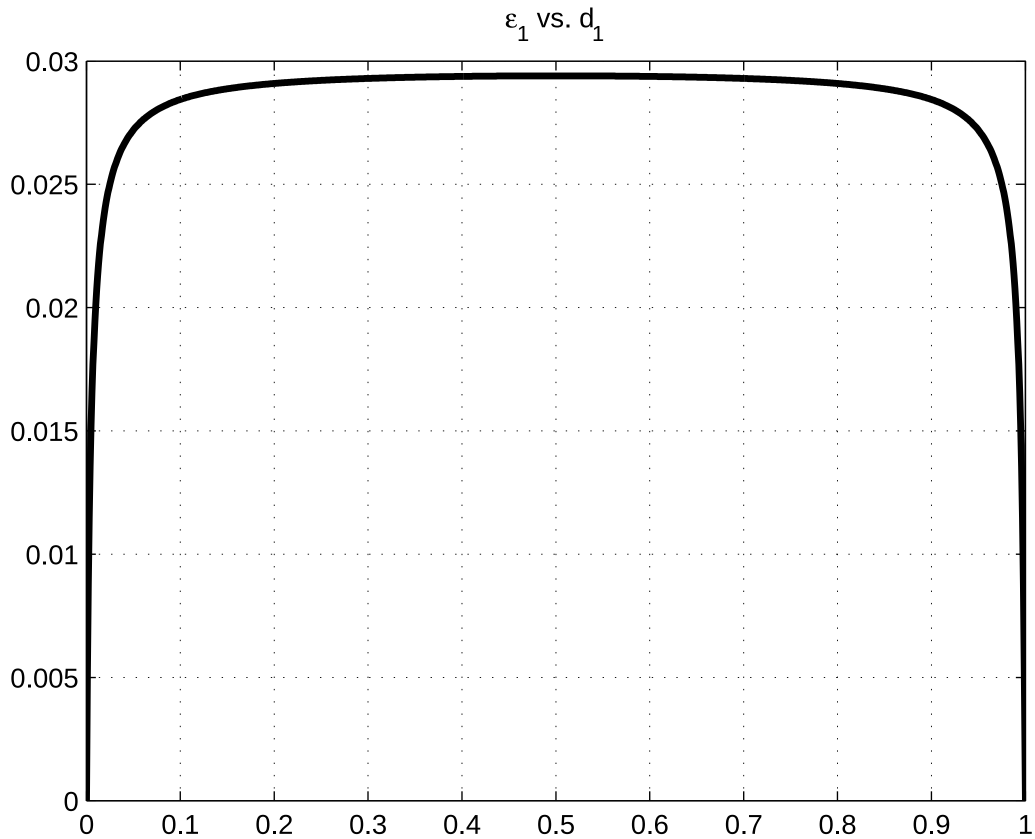

Figure 6.1: Adjusted Stability Upper Bounds on ε_1 for the Stability Analysis of the Σ_{SF} Subsystem

6.5 Σ_{SFU} *Stability Analysis* for the Helicopter Model

Once proven the asymptotic stability of the Σ_{SF}-subsystem, Eqns. (6.15–6.17), the Σ_{SFU} *Stability Analysis* is conducted recalling that the Σ_{SF} *Stability Analysis* provides a composite Lyapunov function, $V_1(\tilde{x}, \tilde{\boldsymbol{y}})$, Eq. (6.202), that satisfies the growth requirements between both $\tilde{f}(\tilde{x}, \tilde{\boldsymbol{y}}, \tilde{\mathbf{h}}(\tilde{x}, \tilde{\boldsymbol{y}}))$ and $\hat{\boldsymbol{g}}(\tilde{x}, \tilde{\boldsymbol{y}}, \tilde{\mathbf{h}}(\tilde{x}, \tilde{\boldsymbol{y}}))$, therefore, and using these results, it can be continued to prove the asymptotic stability properties of the full Σ_{SFU} system, which, for convenience, is first rewritten as

$$\dot{\tilde{\boldsymbol{\chi}}} = \tilde{\boldsymbol{F}}(\tilde{\boldsymbol{\chi}}, \tilde{\boldsymbol{z}}),\ \tilde{\boldsymbol{\chi}} \in \mathcal{R}^{\tilde{\chi}}, \tag{6.217}$$

$$\varepsilon_1 \varepsilon_2 \dot{\tilde{\mathbf{z}}} = \hat{\boldsymbol{h}}(\tilde{\boldsymbol{\chi}}, \tilde{\boldsymbol{z}}),\ \tilde{\boldsymbol{z}} \in \mathcal{R}^{\tilde{z}}, \tag{6.218}$$

with $B_{\tilde{\chi}} \subset \mathcal{R}^{\tilde{\chi}}, B_{\tilde{z}} \subset \mathcal{R}^{\tilde{z}}$ denoting closed sets, and where $\tilde{\boldsymbol{F}}(\tilde{\boldsymbol{\chi}}, \tilde{\boldsymbol{z}})$ represents the augmented system given by

$$\tilde{\boldsymbol{F}}(\tilde{\boldsymbol{\chi}}, \tilde{\boldsymbol{z}}) \triangleq \begin{bmatrix} \tilde{f}(\tilde{\boldsymbol{\chi}}, \tilde{\boldsymbol{z}}) \\ \hat{g}(\tilde{\boldsymbol{\chi}}, \tilde{\boldsymbol{z}}) \end{bmatrix} = \begin{bmatrix} \tilde{f}\,(\tilde{x}, \tilde{\boldsymbol{y}}, \tilde{\boldsymbol{z}}) \\ \hat{g}\,(\tilde{x}, \tilde{\boldsymbol{y}}, \tilde{\boldsymbol{z}}) \end{bmatrix}, \tag{6.219}$$

where $\tilde{\boldsymbol{\chi}}$ represents the augmented state vector given by

$$\tilde{\boldsymbol{\chi}} \triangleq \begin{bmatrix} \tilde{x} & \tilde{\boldsymbol{y}} \end{bmatrix}^T = \begin{bmatrix} \tilde{x} & \tilde{y}_1 & \tilde{y}_2 \end{bmatrix}^T. \tag{6.220}$$

The Σ_{SFU} *Stability Analysis* is continued by applying again the *Bottom* time-scale to the Σ_{SFU} full system, Eqns. (6.217–6.218), resulting in the new (slow) augmented reduced order Σ_{SF}-subsystem, given by

$$\dot{\tilde{\boldsymbol{\chi}}} = \tilde{\boldsymbol{F}}\left(\tilde{\boldsymbol{\chi}}, \tilde{\mathbf{h}}(\tilde{\boldsymbol{\chi}})\right) = \begin{bmatrix} \tilde{f}(\tilde{\boldsymbol{\chi}}, \tilde{\mathbf{h}}(\tilde{\boldsymbol{\chi}})) \\ \hat{\boldsymbol{g}}(\tilde{\boldsymbol{\chi}}, \tilde{\mathbf{h}}(\tilde{\boldsymbol{\chi}})) \end{bmatrix} = \begin{bmatrix} \tilde{f}\left(\tilde{x}, \tilde{\boldsymbol{y}}, \tilde{\mathbf{h}}(\tilde{x}, \tilde{\boldsymbol{y}})\right) \\ \hat{\boldsymbol{g}}\left(\tilde{x}, \tilde{\boldsymbol{y}}, \tilde{\mathbf{h}}(\tilde{x}, \tilde{\boldsymbol{y}})\right) \end{bmatrix}, \tag{6.221}$$

which is equivalent to the subsystem analyzed in the Σ_{SF} *Stability Analysis*, Eqns. (6.15–6.17), and therefore, whose associated Lyapunov function is the one obtained as a result of Σ_{SF} *Stability Analysis*, $V_1(\tilde{\boldsymbol{\chi}}) \equiv V_1(\tilde{x}, \tilde{\boldsymbol{y}})$, while the boundary layer Σ_U-subsystem is defined by

$$\frac{d\tilde{\mathbf{z}}}{d\tau_2} = \hat{\boldsymbol{h}}(\tilde{\boldsymbol{\chi}}, \tilde{\boldsymbol{z}}), \tag{6.222}$$

which is also equivalent to the boundary layer Σ_U-subsystem, Eq. (6.21–6.22), and whose quasi-steady-state equilibrium, $\tilde{\boldsymbol{z}} = \tilde{\mathbf{h}}(\tilde{\boldsymbol{\chi}})$ is equivalent to the one obtained in the Σ_{SF} *Stability Analysis*, that is $\tilde{\mathbf{h}}(\tilde{\boldsymbol{\chi}}) \equiv \tilde{\mathbf{h}}(\tilde{x}, \tilde{\boldsymbol{y}})$, and with $V_U(\hat{\mathbf{z}})$ being its associated Lyapunov function, Eq. (6.51).

Similarly as in the Σ_{SFU} general asymptotic stability analysis presented in section 5.5.3, the helicopter Σ_{SFU} *Stability Analysis* is performed using the standard method for two-time-scale systems (Kokotović et al., 1986; Kokotović et al., 1987; Kokotović et al., 1999), in which the previously derived Lyapunov functions for the Σ_{SF} and Σ_U-subsystems, that is $V_1(\tilde{\boldsymbol{\chi}})$ and $V_U(\hat{\mathbf{z}})$, Eqns. (6.202) and (6.51), respectively, must fulfill certain growth requirements on $\tilde{\boldsymbol{F}}\,(\tilde{\boldsymbol{\chi}}, \tilde{\boldsymbol{z}})$, Eqns. (6.6–6.8), and $\hat{\boldsymbol{h}}\,(\tilde{\boldsymbol{\chi}}, \tilde{\boldsymbol{z}})$, Eqns. (6.21–6.22) by satisfying certain inequalities. The fulfillment of these inequalities for the full Σ_{SFU} helicopter subsystem are described bellow.

6.5.1 Isolated Equilibrium of the Origin for the Helicopter Σ_{SFU} System: Assumption 5.5.1

The origin ($\tilde{\boldsymbol{\chi}} = 0,\ \tilde{\boldsymbol{z}} = 0$) is a unique and isolated equilibrium for the Σ_{SFU} system, Eqns. (6.6–6.10), i.e.

$$0 = \tilde{\boldsymbol{F}}(0, 0), \tag{6.223}$$

$$0 = \hat{\boldsymbol{h}}(0, 0), \tag{6.224}$$

moreover, $\tilde{\boldsymbol{z}} = \tilde{\mathbf{h}}(\tilde{\boldsymbol{\chi}})$ is the unique root of

$$0 = \hat{\boldsymbol{h}}(\tilde{\boldsymbol{\chi}}, \tilde{\boldsymbol{z}}), \tag{6.225}$$

in $B_{\tilde{\boldsymbol{\chi}}} \times B_{\tilde{z}}$, i.e.

$$0 = \hat{\boldsymbol{h}}(\tilde{\boldsymbol{\chi}}, \tilde{\mathbf{h}}(\tilde{\boldsymbol{\chi}})), \tag{6.226}$$

and there exists a class κ function $p_2(\cdot)$ such that

$$\| \tilde{\mathbf{h}}(\tilde{\boldsymbol{\chi}}) \| \leq p_2 \left(\| \tilde{\boldsymbol{\chi}} \|\right). \tag{6.227}$$

The reduced order growth requirements are obtained by first considering the system given by Eq. (6.217), and adding and subtracting $\tilde{\boldsymbol{F}}(\tilde{\boldsymbol{\chi}}, \tilde{\mathbf{h}}(\tilde{\boldsymbol{\chi}}))$ to the right-hand side of Eq. (6.217) yielding

$$\dot{\tilde{x}} = \tilde{\boldsymbol{F}}\left(\tilde{\boldsymbol{\chi}}, \tilde{\mathbf{h}}(\chi)\right) + \tilde{\boldsymbol{F}}\left(\tilde{\boldsymbol{\chi}}, \tilde{\boldsymbol{z}}\right) - \tilde{\boldsymbol{F}}\left(\tilde{\boldsymbol{\chi}}, \tilde{\mathbf{h}}(\tilde{\boldsymbol{\chi}})\right), \tag{6.228}$$

where the term $\tilde{\boldsymbol{F}}\left(\tilde{\boldsymbol{\chi}}, \tilde{\boldsymbol{z}}\right) - \tilde{\boldsymbol{F}}(\tilde{\boldsymbol{\chi}}, \tilde{\mathbf{h}}(\tilde{\boldsymbol{\chi}}))$ can be viewed as a perturbation of the reduced order Σ_{SF}-subsystem given by

$$\dot{\tilde{\boldsymbol{\chi}}} = \tilde{\boldsymbol{F}}\left(\tilde{\boldsymbol{\chi}}, \tilde{\mathbf{h}}(\tilde{\boldsymbol{\chi}})\right), \tag{6.229}$$

with $\tilde{\boldsymbol{F}}\left(\tilde{\boldsymbol{\chi}}, \tilde{\boldsymbol{z}}\right)$ being given by

$$\tilde{\boldsymbol{F}}\left(\tilde{\boldsymbol{\chi}}, \tilde{\boldsymbol{z}}\right) = \begin{bmatrix} \tilde{F}_1\left(\tilde{\boldsymbol{\chi}}, \tilde{\boldsymbol{z}}\right) \\ \tilde{F}_2\left(\tilde{\boldsymbol{\chi}}, \tilde{\boldsymbol{z}}\right) \\ \tilde{F}_3\left(\tilde{\boldsymbol{\chi}}, \tilde{\boldsymbol{z}}\right) \end{bmatrix} = \begin{bmatrix} \tilde{f}(\tilde{\boldsymbol{\chi}}, \tilde{\boldsymbol{z}}) \\ \hat{\boldsymbol{g}}(\tilde{\boldsymbol{\chi}}, \tilde{\boldsymbol{z}}) \end{bmatrix} = \begin{bmatrix} \tilde{f}\left(\tilde{x}, \tilde{\boldsymbol{y}}, \tilde{\boldsymbol{z}}\right) \\ \hat{\boldsymbol{g}}\left(\tilde{x}, \tilde{\boldsymbol{y}}, \tilde{\boldsymbol{z}}\right) \end{bmatrix}, \tag{6.230}$$

with

$$\tilde{F}_1\left(\tilde{\boldsymbol{\chi}}, \tilde{\boldsymbol{z}}\right) = a_{10}(\tilde{x} + x^*)^2 \left[\sin\left(\tilde{z}_1 + z_1^*\right) - \sin \tilde{\mathrm{h}}_{1_{\mathrm{SS}}}\right] - b_x \tilde{x}, \tag{6.231}$$

$$\tilde{F}_2\left(\tilde{\boldsymbol{\chi}}, \tilde{\boldsymbol{z}}\right) = c_1 \tilde{y}_2, \tag{6.232}$$

$$\begin{aligned} \tilde{F}_3\left(\tilde{\boldsymbol{\chi}}, \tilde{\boldsymbol{z}}\right) &= (\tilde{x} + x^*)^2 \left(c_2 + c_3(\tilde{z}_1 + z_1^*) - \sqrt{c_4 + c_5(\tilde{z}_1 + z_1^*)}\right) \\ &+ a_9 \tilde{y}_2 + a_9 \tilde{y}_2^2 + c_6, \end{aligned} \tag{6.233}$$

and with $\tilde{\boldsymbol{F}}(\tilde{\boldsymbol{\chi}}, \tilde{\mathbf{h}}(\tilde{\boldsymbol{\chi}}))$ given after substituting the ultra-fast quasi-steady-state equilibrium, $\tilde{z} = \tilde{\mathbf{h}}(\tilde{\boldsymbol{\chi}})$, into Eq. (6.233), resulting in

$$\tilde{F}(\tilde{\boldsymbol{\chi}}, \tilde{\mathbf{h}}(\tilde{\boldsymbol{\chi}})) = \begin{bmatrix} \tilde{F}_1\left(\tilde{\boldsymbol{\chi}}, \tilde{\boldsymbol{z}}\right)\Big|_{\tilde{z}=\tilde{\mathbf{h}}(\boldsymbol{\chi})} = \tilde{F}_{H_1}\left(\tilde{\boldsymbol{\chi}}, \tilde{\mathbf{h}}(\tilde{\boldsymbol{\chi}})\right) \\ \tilde{F}_2\left(\tilde{\boldsymbol{\chi}}, \tilde{\boldsymbol{z}}\right)\Big|_{\tilde{z}=\tilde{\mathbf{h}}(\boldsymbol{\chi})} = \tilde{F}_{H_2}\left(\tilde{\boldsymbol{\chi}}, \tilde{\mathbf{h}}(\tilde{\boldsymbol{\chi}})\right) \\ \tilde{F}_3\left(\tilde{\boldsymbol{\chi}}, \tilde{\boldsymbol{z}}\right)\Big|_{\tilde{z}=\tilde{\mathbf{h}}(\boldsymbol{\chi})} = \tilde{F}_{H_3}\left(\tilde{\boldsymbol{\chi}}, \tilde{\mathbf{h}}(\tilde{\boldsymbol{\chi}})\right) \end{bmatrix}, \tag{6.234}$$

with

$$\tilde{F}_{H_1}\left(\tilde{\boldsymbol{\chi}}, \tilde{\mathbf{h}}(\tilde{\boldsymbol{\chi}})\right) = a_{10}(\tilde{x} + x^*)^2 \left[\sin\left(\tilde{\mathrm{h}}_1\left(\tilde{\boldsymbol{\chi}}\right) + z_1^*\right) - \sin \tilde{\mathrm{h}}_{1_{\mathrm{SS}}}\right] - b_x \tilde{x}, \tag{6.235}$$

$$\tilde{F}_{H_2}\left(\tilde{\boldsymbol{\chi}}, \tilde{\mathbf{h}}(\tilde{\boldsymbol{\chi}})\right) = c_1 \tilde{y}_2, \tag{6.236}$$

$$\tilde{F}_{H_3}\left(\tilde{\boldsymbol{\chi}}, \tilde{\mathbf{h}}(\tilde{\boldsymbol{\chi}})\right) = -\tilde{b}_{y_1} \tilde{y}_1 - \tilde{b}_{y_2} \tilde{y}_2, \tag{6.237}$$

where

$$\tilde{\mathrm{h}}_1\left(\tilde{\boldsymbol{\chi}}\right) = \left[s_2 \left(\left(1 + \sqrt{s_3 \tilde{v}(\tilde{\boldsymbol{\chi}})}\right)^2 - 1\right)\right] - z_1^*, \tag{6.238}$$

where recall that $\tilde{\mathrm{h}}_1(\tilde{\boldsymbol{\chi}}) \equiv \tilde{\mathrm{h}}_1(\tilde{x}, \tilde{\boldsymbol{y}})$. Similarly as in the Σ_{SF} *Stability Analysis*, it is therefore natural to first satisfy the growth requirements for Eq. (6.229) and then consider the effect of the perturbation term $\tilde{\boldsymbol{F}}(\tilde{\boldsymbol{\chi}}, \tilde{\boldsymbol{z}}) - \tilde{\boldsymbol{F}}(\tilde{\boldsymbol{\chi}}, \tilde{\mathbf{h}}(\tilde{\boldsymbol{\chi}}))$. Therefore let proceed to define first the reduced order growth condition.

6.5.2 Proof of Assumption 5.5.7: Reduced System Conditions for the Helicopter Σ_{SFU} System

Recalling from Assumption 5.5.7, the Σ_{SF} Lyapunov function candidate $V_1(\tilde{\boldsymbol{\chi}})$ must be positive-definite and decreasing, and must also satisfy the following inequality given by

$$\left(\frac{\partial V_1(\tilde{\boldsymbol{\chi}})}{\partial \tilde{\boldsymbol{\chi}}}\right)^T \tilde{\boldsymbol{F}}\left(\tilde{\boldsymbol{\chi}}, \tilde{\mathbf{h}}(\tilde{\boldsymbol{\chi}})\right) \leq -\alpha_3 \psi_2^2(\tilde{\boldsymbol{\chi}}), \tag{6.239}$$

where $\psi_2(\cdot)$ is a scalar function of vector arguments which vanishes only when its argument are zero, and satisfying that $\tilde{\boldsymbol{\chi}} = 0$ is a stable equilibrium of the reduced order system. The left-hand side of inequality (6.239) is given by recalling that $V_1(\tilde{\boldsymbol{\chi}})$, Eq. (6.202) is defined as

$$V_1(\tilde{\boldsymbol{\chi}}) = (1-d_1)\, V_S(\tilde{x}) + d_1 V_F(\hat{\boldsymbol{y}}) = (1-d_1)\left(\frac{1}{2}P_S\tilde{x}^2\right) + d_1\left(\frac{1}{2}\tilde{\boldsymbol{y}}^T \boldsymbol{P_F}\tilde{\boldsymbol{y}}\right), \tag{6.240}$$

being therefore easy to see that

$$\left(\frac{\partial V_1(\tilde{\boldsymbol{\chi}})}{\partial \tilde{\boldsymbol{\chi}}}\right)^T = \begin{bmatrix} \frac{\partial V_1(\tilde{\boldsymbol{\chi}})}{\partial \tilde{x}} \\ \frac{\partial V_1(\tilde{\boldsymbol{\chi}})}{\partial \tilde{\boldsymbol{y}}} \end{bmatrix} = \begin{bmatrix} \frac{\partial V_1(\tilde{\boldsymbol{\chi}})}{\partial \tilde{x}} \\ \frac{\partial V_1(\tilde{\boldsymbol{\chi}})}{\partial \tilde{y}_1} \\ \frac{\partial V_1(\tilde{\boldsymbol{\chi}})}{\partial \tilde{y}_2} \end{bmatrix} = \begin{bmatrix} \mathcal{V}_1\tilde{x} \\ \mathcal{V}_2\tilde{y}_1 + \mathcal{V}_3\tilde{y}_2 \\ \mathcal{V}_3\tilde{y}_1 + \mathcal{V}_4\tilde{y}_2 \end{bmatrix}, \tag{6.241}$$

with

$$\mathcal{V}_1 = (1-d_1)P_S = (1-d_1)\frac{Q_S}{2b_x}, \tag{6.242}$$
$$\mathcal{V}_2 = d_1 p_{f_1} = d_1\left(C_{f_1}q_{f_1} + C_{f_2}q_{f_2}\right), \tag{6.243}$$
$$\mathcal{V}_3 = d_1 p_{f_2} = d_1 C_{f_3}q_{f_1}, \tag{6.244}$$
$$\mathcal{V}_4 = d_1 p_{f_3} = d_1\left(C_{f_4}q_{f_1} + C_{f_5}q_{f_2}\right), \tag{6.245}$$

and also recalling that $\tilde{\boldsymbol{F}}(\tilde{\boldsymbol{\chi}}, \tilde{\mathbf{h}}(\tilde{\boldsymbol{\chi}}))$ is given by Eq. (6.234). For completeness recall that the variables $\mathcal{A}_1$ and $\mathcal{B}_1$ were defined in Eqns. (6.96) and (6.97), respectively, thus rewriting Eqns. (6.235–6.237) as

$$\tilde{F}_{H_1}\left(\tilde{\boldsymbol{\chi}}, \tilde{\mathbf{h}}(\tilde{\boldsymbol{\chi}})\right) = a_{10}(\tilde{x}+x^*)^2(\sin\mathcal{A}_1 - \sin\mathcal{B}_1) - b_x\tilde{x}, \tag{6.246}$$
$$\tilde{F}_{H_2}\left(\tilde{\boldsymbol{\chi}}, \tilde{\mathbf{h}}(\tilde{\boldsymbol{\chi}})\right) = c_1\tilde{y}_2, \tag{6.247}$$
$$\tilde{F}_{H_3}\left(\tilde{\boldsymbol{\chi}}, \tilde{\mathbf{h}}(\tilde{\boldsymbol{\chi}})\right) = -\tilde{b}_{y_1}\tilde{y}_1 - \tilde{b}_{y_2}\tilde{y}_2, \tag{6.248}$$

where for simplicity, Eqns. (6.246–6.248), $\tilde{F}_{(\cdot)}\left(\tilde{\boldsymbol{\chi}}, \tilde{\mathbf{h}}(\tilde{\boldsymbol{\chi}})\right)$ will fe referred as $\tilde{F}_{(\cdot)}$. Recalling the sum-to-product prosthaphaeresis trigonometric identity, Eq. (6.99), the left hand-side of inequality (6.239) can be expressed as

$$\begin{aligned}
&\left(\frac{\partial V_1(\tilde{\boldsymbol{\chi}})}{\partial \tilde{\boldsymbol{\chi}}}\right)^T \tilde{\boldsymbol{F}}(\tilde{\boldsymbol{\chi}}, \tilde{\mathbf{h}}(\tilde{\boldsymbol{\chi}})) = \frac{\partial V_1(\tilde{\boldsymbol{\chi}})}{\partial \tilde{x}}\tilde{F}_{H_1} + \frac{\partial V_1(\tilde{\boldsymbol{\chi}})}{\partial \tilde{y}_1}\tilde{F}_{H_2} + \frac{\partial V_1(\tilde{\boldsymbol{\chi}})}{\partial \tilde{y}_2}\tilde{F}_{H_3} \\
=\; & \mathcal{V}_1\tilde{x}\left[a_{10}(\tilde{x}+x^*)^2(\sin\mathcal{A}_1 - \sin\mathcal{B}_1) - b_x\tilde{x}\right] + c_1\tilde{y}_2\left(\mathcal{V}_2\tilde{y}_1 + \mathcal{V}_3\tilde{y}_2\right) \\
+\; & \left(\mathcal{V}_3\tilde{y}_1 + \mathcal{V}_4\tilde{y}_2\right)\left(-\tilde{b}_{y_1}\tilde{y}_1 - \tilde{b}_{y_2}\tilde{y}_2\right) \\
=\; & \mathcal{V}_1\tilde{x}a_{10}(\tilde{x}+x^*)^2\left(\sin\mathcal{A}_1 - \sin\mathcal{B}_1\right) - b_x\mathcal{V}_1\tilde{x}^2 - \tilde{b}_{y_1}\mathcal{V}_3\tilde{y}_1^2 \\
-\; & \left(\tilde{b}_{y_2}\mathcal{V}_4 - c_1\mathcal{V}_3\right)\tilde{y}_2^2 - \left(\tilde{b}_{y_1}\mathcal{V}_4 + \tilde{b}_{y_2}\mathcal{V}_3 - c_1\mathcal{V}_2\right)\tilde{y}_1\tilde{y}_2 \\
=\; & \mathcal{V}_1 a_{10}\tilde{x}(\tilde{x}+x^*)^2 2\sin\left(\frac{\mathcal{A}_1 - \mathcal{B}_1}{2}\right)\cos\left(\frac{\mathcal{A}_1 + \mathcal{B}_1}{2}\right) - t_1\tilde{x}^2 - t_2\tilde{y}_1^2 - t_3\tilde{y}_2^2 - t_4\tilde{y}_1\tilde{y}_2,
\end{aligned} \tag{6.249}$$

with

$$
\begin{aligned}
t_1 &= b_x \mathcal{V}_1, && (6.250)\\
t_2 &= \tilde{b}_{y_1} \mathcal{V}_3, && (6.251)\\
t_3 &= \tilde{b}_{y_2} \mathcal{V}_4 - c_1 \mathcal{V}_3, && (6.252)\\
t_4 &= \tilde{b}_{y_1} \mathcal{V}_4 + \tilde{b}_{y_2} \mathcal{V}_3 - c_1 \mathcal{V}_2. && (6.253)
\end{aligned}
$$

Recalling that P_S, p_{f_1}, p_{f_2} and p_{f_3} are given in Eqns. (6.40), (6.43), (6.44), and (6.45), respectively, which after being substituted into Eqns. (6.242–6.245), results in

$$
\begin{aligned}
t_1 &= \frac{1}{2}(1 - d_1) Q_S, && (6.254)\\
t_2 &= \frac{1}{2} d_1 q_{f_1}, && (6.255)\\
t_3 &= \frac{1}{2} d_1 q_{f_2}, && (6.256)\\
t_4 &= \tilde{b}_{y_1} \mathcal{V}_4 + \tilde{b}_{y_2} \mathcal{V}_3 - c_1 \mathcal{V}_2 = 0. && (6.257)
\end{aligned}
$$

Recalling that for the helicopter Σ_{SF} *Stability Analysis*, section 6.3, it was proven that

$$
2a_{10}(\tilde{x} + x^*)^2 \sin\left(\frac{\mathcal{A}_1 - \mathcal{B}_1}{2}\right) \cos\left(\frac{\mathcal{A}_1 + \mathcal{B}_1}{2}\right) \le \mathcal{C}_1 |\tilde{y}_1| + \mathcal{C}_2 |\tilde{y}_2|, \tag{6.258}
$$

therefore, inequality (6.249) can be rewritten using the results in Eq. (6.258), resulting in

$$
\begin{aligned}
&\left(\frac{\partial V_1(\tilde{\boldsymbol{\chi}})}{\partial \tilde{\boldsymbol{\chi}}}\right)^T \tilde{\boldsymbol{F}}(\tilde{\boldsymbol{\chi}}, \tilde{\mathbf{h}}(\tilde{\boldsymbol{\chi}}))\\
&= \mathcal{V}_1 a_{10} \tilde{x} (\tilde{x} + x^*)^2 2 \sin\left(\frac{\mathcal{A}_1 - \mathcal{B}_1}{2}\right) \cos\left(\frac{\mathcal{A}_1 + \mathcal{B}_1}{2}\right) - t_1 \tilde{x}^2 - t_2 \tilde{y}_1^2 - t_3 \tilde{y}_2^2\\
&\le \left| \mathcal{V}_1 a_{10} \tilde{x} (\tilde{x} + x^*)^2 2 \sin\left(\frac{\mathcal{A}_1 - \mathcal{B}_1}{2}\right) \cos\left(\frac{\mathcal{A}_1 + \mathcal{B}_1}{2}\right) \right| - t_1 \tilde{x}^2 - t_2 \tilde{y}_1^2 - t_3 \tilde{y}_2^2\\
&\le |\mathcal{V}_1 \tilde{x} (\mathcal{C}_1 |\tilde{y}_1| + \mathcal{C}_2 |\tilde{y}_2|)| - t_1 \tilde{x}^2 - t_2 \tilde{y}_1^2 - t_3 \tilde{y}_2^2, \qquad (6.259)
\end{aligned}
$$

which can be simplified by introducing

$$
\begin{aligned}
\tilde{\mathcal{C}}_1 = \mathcal{V}_1 \mathcal{C}_1 &= (1 - d_1) \frac{Q_S}{2b_x} \frac{4a_2 a_3 |a_{10}| \tilde{b}_{y_1} \mathcal{K}_1}{a_4^2 \varepsilon_1} \left(1 + \sqrt{-\frac{a_4}{a_2 a_7}} x_{MAX}\right), && (6.260)\\
\tilde{\mathcal{C}}_2 = \mathcal{V}_1 \mathcal{C}_2 &= (1 - d_1) \frac{Q_S}{2b_x} \frac{4a_2 a_3 |a_{10}| \mathcal{K}_1}{a_4^2 \varepsilon_1} \left(1 + \sqrt{-\frac{a_4}{a_2 a_7}} x_{MAX}\right)\\
&\times \left(\tilde{Y}_{2_{MAX}} |a_9| + \left|a_9 + \tilde{b}_{y_2}\right|\right), && (6.261)
\end{aligned}
$$

where recall that $\mathcal{K}_1$ was previously defined in Eq. (6.127), x_{MAX} is the maxim angular velocity of the blades, and $\tilde{Y}_{2_{MAX}}$ is the absolute value of the maxim vertical velocity of the helicopter, previously defined in Eq. (6.162). Using Eqns. (6.260) and (6.261) into inequality (6.259) results in

$$
\begin{aligned}
&\left(\frac{\partial V_1(\tilde{\boldsymbol{\chi}})}{\partial \tilde{\boldsymbol{\chi}}}\right)^T \tilde{\boldsymbol{F}}(\tilde{\boldsymbol{\chi}}, \tilde{\mathbf{h}}(\tilde{\boldsymbol{\chi}}))\\
&= \mathcal{V}_1 a_{10} \tilde{x} (\tilde{x} + x^*)^2 2 \sin\left(\frac{\mathcal{A}_1 - \mathcal{B}_1}{2}\right) \cos\left(\frac{\mathcal{A}_1 + \mathcal{B}_1}{2}\right) - t_1 \tilde{x}^2 - t_2 \tilde{y}_1^2 - t_3 \tilde{y}_2^2\\
&\le |\mathcal{V}_1 \tilde{x} (\mathcal{C}_1 |\tilde{y}_1| + \mathcal{C}_2 |\tilde{y}_2|)| - t_1 \tilde{x}^2 - t_2 \tilde{y}_1^2 - t_3 \tilde{y}_2^2\\
&\le \tilde{\mathcal{C}}_1 |\tilde{x} \tilde{y}_1| + \tilde{\mathcal{C}}_2 |\tilde{x} \tilde{y}_2| - t_1 \tilde{x}^2 - t_2 \tilde{y}_1^2 - t_3 \tilde{y}_2^2, \qquad (6.262)
\end{aligned}
$$

Inequality (6.262) can be further simplified employing Young's inequality, Eq. (6.177, thus permitting to rewrite Eq. (6.262) as

$$\begin{aligned}
&\left(\frac{\partial V_1(\tilde{\boldsymbol{\chi}})}{\partial \tilde{\boldsymbol{\chi}}}\right)^T \tilde{\boldsymbol{F}}(\tilde{\boldsymbol{\chi}}, \tilde{\mathbf{h}}(\tilde{\boldsymbol{\chi}})) \\
&= \mathcal{V}_1 a_{10}\tilde{x}(\tilde{x}+x^*)^2 2\sin\left(\frac{\mathcal{A}_1-\mathcal{B}_1}{2}\right)\cos\left(\frac{\mathcal{A}_1+\mathcal{B}_1}{2}\right) - t_1\tilde{x}^2 - t_2\tilde{y}_1^2 - t_3\tilde{y}_2^2 \\
&\leq \tilde{\mathcal{C}}_1\left|\tilde{x}\tilde{y}_1\right| + \tilde{\mathcal{C}}_2\left|\tilde{x}\tilde{y}_2\right| - t_1\tilde{x}^2 - t_2\tilde{y}_1^2 - t_3\tilde{y}_2^2 \\
&\leq \tilde{\mathcal{C}}_1\left(\frac{\tilde{x}^2+\tilde{y}_1^2}{2}\right) + \tilde{\mathcal{C}}_2\left(\frac{\tilde{x}^2+\tilde{y}_2^2}{2}\right) - t_1\tilde{x}^2 - t_2\tilde{y}_1^2 - t_3\tilde{y}_2^2 \\
&\leq -\mathcal{R}_1\tilde{x}^2 - \mathcal{R}_1\tilde{y}_1^2 - \mathcal{R}_1\tilde{y}_2^2 = \left(\tilde{\boldsymbol{\chi}}^T\boldsymbol{\mathcal{R}}\tilde{\boldsymbol{\chi}}\right), \qquad (6.263)
\end{aligned}$$

where $\boldsymbol{\mathcal{R}}$ is a 3×3 positive definite matrix given by

$$\boldsymbol{\mathcal{R}} = \begin{pmatrix} \mathcal{R}_1 & 0 & 0 \\ 0 & \mathcal{R}_2 & 0 \\ 0 & 0 & \mathcal{R}_3 \end{pmatrix}, \qquad (6.264)$$

with

$$\begin{aligned}
\mathcal{R}_1 &= t_1 - \frac{\tilde{\mathcal{C}}_1+\tilde{\mathcal{C}}_2}{2} = \frac{(1-d_1)\,Q_S}{2}\left[1 - s_4\frac{\tilde{b}_{y_1} + \tilde{Y}_{2_{MAX}}\left|a_9\right| + \left|a_9+\tilde{b}_{y_2}\right|}{2b_x}\right], && (6.265)\\
\mathcal{R}_2 &= t_2 - \frac{\tilde{\mathcal{C}}_1}{2} = \frac{1}{2}d_1 q_{f_1} - \frac{(1-d_1)\,Q_S s_4}{4b_x}\tilde{b}_{y_1}, && (6.266)\\
\mathcal{R}_3 &= t_3 - \frac{\tilde{\mathcal{C}}_2}{2} = \frac{1}{2}d_1 q_{f_2} - \frac{(1-d_1)\,Q_S s_4}{4b_x}\left[\tilde{Y}_{2_{MAX}}\left|a_9\right| + \left|a_9+\tilde{b}_{y_2}\right|\right], && (6.267)
\end{aligned}$$

with s_4 being previously defined in Eq. (6.158). Equations. (6.265), (6.266) and (6.267) can be simplified by introducing

$$\begin{aligned}
\tilde{r}_1 &= \frac{1-d_1}{2}\left(1 - \frac{\mathcal{C}_1+\mathcal{C}_2}{2b_x}\right), && (6.268)\\
\tilde{r}_2 &= \frac{d_1}{2}, && (6.269)\\
\tilde{r}_3 &= (1-d_1)\,\frac{\mathcal{C}_1}{4b_x}, && (6.270)\\
\tilde{r}_4 &= (1-d_1)\,\frac{\mathcal{C}_2}{4b_x}, && (6.271)
\end{aligned}$$

therefore rewriting

$$\begin{aligned}
\mathcal{R}_1 &= \tilde{r}_1 Q_S, && (6.272)\\
\mathcal{R}_2 &= \tilde{r}_2 q_{f_1} - \tilde{r}_3 Q_S, && (6.273)\\
\mathcal{R}_3 &= \tilde{r}_2 q_{f_2} - \tilde{r}_4 Q_S, && (6.274)
\end{aligned}$$

thus the original inequality (6.239) becomes

$$\begin{aligned}
&\left(\frac{\partial V_1(\tilde{\boldsymbol{\chi}})}{\partial \tilde{\boldsymbol{\chi}}}\right)^T \tilde{\boldsymbol{F}}(\tilde{\boldsymbol{\chi}}, \tilde{\mathbf{h}}(\tilde{\boldsymbol{\chi}})) \\
&= \mathcal{V}_1 a_{10}\tilde{x}(\tilde{x}+x^*)^2 2\sin\left(\frac{\mathcal{A}_1-\mathcal{B}_1}{2}\right)\cos\left(\frac{\mathcal{A}_1+\mathcal{B}_1}{2}\right) - t_1\tilde{x}^2 - t_2\tilde{y}_1^2 - t_3\tilde{y}_2^2 \\
&\leq -\left(\tilde{\boldsymbol{\chi}}^T\boldsymbol{\mathcal{R}}\tilde{\boldsymbol{\chi}}\right) \leq -\alpha_3\psi_2^2(\tilde{\boldsymbol{\chi}}), \qquad (6.275)
\end{aligned}$$

where needs to ensure that $\boldsymbol{\mathcal{R}} > 0$ is a positive definite matrix, that is $\mathcal{R}_1 > 0$, $\mathcal{R}_2 > 0$, and $\mathcal{R}_3 > 0$, which can be done by ensuring the appropriate coefficients selection. This is achieved such that for $\mathcal{R}_1 > 0$ it is required that

$$
\begin{aligned}
b_x &> \frac{\mathcal{C}_1+\mathcal{C}_2}{2} \\
&> \frac{4a_2a_3\,|a_{10}|\,\mathcal{K}_1}{2a_4^2\varepsilon_1}\left(1+\sqrt{-\frac{a_4}{a_2a_7}}x_{MAX}\right)(\tilde{b}_{y_1}+\tilde{Y}_{2_{MAX}}\,|a_9|+\left|a_9+\tilde{b}_{y_2}\right|), \qquad (6.276)
\end{aligned}
$$

for $\mathcal{R}_2 > 0$ it is required that

$$
\begin{aligned}
q_{f_1} &> \frac{(1-d_1)Q_S}{2d_1b_x}\mathcal{C}_1 \\
&> \frac{(1-d_1)Q_S}{2d_1b_x}\frac{4a_2a_3\,|a_{10}|\,\tilde{b}_{y_1}\mathcal{K}_1}{a_4^2\varepsilon_1}\left(1+\sqrt{-\frac{a_4}{a_2a_7}}x_{MAX}\right), \qquad (6.277)
\end{aligned}
$$

and finally for $\mathcal{R}_3 > 0$ it is required that

$$
\begin{aligned}
q_{f_2} &> \frac{(1-d_1)Q_S}{2d_1b_x}\mathcal{C}_2 \\
&> \frac{(1-d_1)Q_S}{2d_1b_x}\frac{4a_2a_3\,|a_{10}|\,\mathcal{K}_1}{a_4^2\varepsilon_1}\left(1+\sqrt{-\frac{a_4}{a_2a_7}}x_{MAX}\right) \\
&\times \left(\tilde{Y}_{2_{MAX}}\,|a_9|+\left|a_9+\tilde{b}_{y_2}\right|\right), \qquad (6.278)
\end{aligned}
$$

therefore it can be seen that with the proper selection of parameters it is ensured that $\boldsymbol{\mathcal{R}}$ is positive definite, that is $\boldsymbol{\mathcal{R}} > 0$, for

$$
\begin{aligned}
b_x &> \frac{\mathcal{C}_1+\mathcal{C}_2}{2}, \qquad (6.279)\\
q_{f_1} &> \frac{(1-d_1)Q_S}{2d_1b_x}\mathcal{C}_1, \qquad (6.280)\\
q_{f_2} &> \frac{(1-d_1)Q_S}{2d_1b_x}\mathcal{C}_2, \qquad (6.281)
\end{aligned}
$$

and therefore Assumption (5.5.7) and inequality (6.239) are satisfied by selecting α_3 and $\psi_2(\tilde{\boldsymbol{\chi}})$ such

$$
\begin{aligned}
\alpha_3 &\leq 1, \qquad (6.282)\\
\psi_2(\tilde{\boldsymbol{\chi}}) &= \left(\tilde{\boldsymbol{\chi}}^T\boldsymbol{\mathcal{R}}\tilde{\boldsymbol{\chi}}\right)^{\frac{1}{2}} = \sqrt{\mathcal{R}_1\tilde{x}^2+\mathcal{R}_2\tilde{y}_1^2+\mathcal{R}_3\tilde{y}_2^2}. \qquad (6.283)
\end{aligned}
$$

From Eqns. (6.280) and (6.281) it can be inferred a series of important relations between the *stability parameters* that will help in the remainder of stability analysis. First, from Eq. (6.280) it can be defined a relation between q_{f_1} and Q_S by identifying that, in order to guarantee the positive definiteness of $\boldsymbol{\mathcal{R}}$, needs to be selected such

$$
q_{f_1} > Q_{SF}Q_S, \qquad (6.284)
$$

with

$$
Q_{SF} = \frac{(1-d_1)}{2d_1b_x}\mathcal{C}_1. \qquad (6.285)
$$

For simplicity of the analysis that will be conducted in future derivations, inequality (6.284) can be converted into expressions by defining

$$
\tilde{Q}_{SF} > Q_{SF}, \qquad (6.286)
$$

therefore rewriting Eqns. (6.284) as

$$
q_{f_1} = \tilde{Q}_{SF}Q_S, \qquad (6.287)
$$

where

$$
\tilde{Q}_{SF} = \delta_2 Q_{SF}, \qquad (6.288)
$$

with $\delta_2 > 1$, therefore permitting to delimit the range of the *stability parameter* q_{f_1} such

$$q_{f_1} \quad = \quad \tilde{Q}_{SF} Q_S. \tag{6.289}$$

The second relation is equivalent with the relation obtained in the Σ_{SF} *Stability Analysis* conducted previously in section 6.3, which provides an expression for the desired ratio between the *stability parameters* q_{f_1} and q_{f_2}. This same second relation is also obtained by dividing (6.281) by (6.280) resulting in the expression given by

$$\frac{q_{f_2}}{q_{f_1}} > Q_{F_{21}}, \tag{6.290}$$

where

$$Q_{F_{21}} = \frac{\mathcal{C}_2}{\mathcal{C}_1}, \tag{6.291}$$

which similarly as in the Σ_{SF} *Stability Analysis* in section 6.3

$$\frac{q_{f_2}}{q_{f_1}} = \tilde{Q}_{F_{21}}, \tag{6.292}$$

with

$$\tilde{Q}_{F_{21}} = \delta_1 Q_{F_{21}}, \tag{6.293}$$

with $\delta_1 > 1$, therefore permitting to delimit the range of the *stability parameter* q_{f_2} such

$$q_{f_2} \quad = \quad \tilde{Q}_{F_{21}} q_{f_1}. \tag{6.294}$$

Both relations (6.289) and (6.294) will be of great importance when defining the upper-bounds on ε_2 that will be conducted at the end of this section.

6.5.3 Proof of Assumption 5.5.8: Boundary-Layer System Conditions for the Helicopter Σ_{SFU} System

Recalling from Assumption 5.5.8, the Σ_U Lyapunov function candidate $V_U(\tilde{\boldsymbol{\chi}}, \tilde{\boldsymbol{z}})$ must be positive-definite and decreasing, such that for all $(\tilde{\boldsymbol{\chi}}, \tilde{\boldsymbol{z}}) \in B_{\tilde{\chi}} \times B_{\tilde{z}}$ satisfies the following inequality

$$V_U(\tilde{\boldsymbol{\chi}}, \tilde{\boldsymbol{z}}) > 0, \ \forall \tilde{\boldsymbol{z}} \neq \tilde{\mathbf{h}}(\tilde{\boldsymbol{\chi}}) \ and \ V_U(\tilde{\boldsymbol{\chi}}, \tilde{\mathbf{h}}(\tilde{\boldsymbol{\chi}})) = 0, \tag{6.295}$$

and where

$$\left(\frac{\partial V_U}{\partial \tilde{\boldsymbol{z}}}\right)^T \hat{\boldsymbol{h}}(\tilde{\boldsymbol{\chi}}, \tilde{\boldsymbol{z}}) \leq -\alpha_4 \phi_2^2(\tilde{z} - \tilde{\mathbf{h}}(\tilde{\boldsymbol{\chi}})), \ \alpha_4 > 0, \tag{6.296}$$

where $\phi_2(\cdot)$ is a scalar function of vector arguments which vanishes only when its arguments are zero, and satisfying that $\tilde{\boldsymbol{z}} - \tilde{\mathbf{h}}(\tilde{\boldsymbol{\chi}})$ is a stable equilibrium of the boundary layer Σ_U-subsystem, where $\hat{\boldsymbol{h}}\,(\tilde{\boldsymbol{\chi}}, \tilde{\boldsymbol{z}})$ is the boundary layer Σ_U-subsystem, Eqns. (6.21–6.22), and $V_U(\tilde{\boldsymbol{\chi}}, \tilde{\boldsymbol{z}})$, Eq. (6.51), is the Lyapunov function candidate of the Σ_U-subsystem. The left-hand side of inequality (6.296) is defined after recalling that, as previously defined

$$V_U(\hat{\mathbf{z}}) = \frac{1}{2}\hat{\mathbf{z}}^T \boldsymbol{P}_U \hat{\mathbf{z}} = \frac{1}{2} p_{u_1} \hat{z}_1^2 + \frac{1}{2} p_{u_3} \hat{z}_2^2 + p_{u_2} \hat{z}_1 \hat{z}_2, \tag{6.297}$$

where recall that

$$\hat{\mathbf{z}} = \tilde{\boldsymbol{z}} - \tilde{\mathbf{h}}(\tilde{x}, \tilde{\boldsymbol{y}}), \tag{6.298}$$

and with

$$\boldsymbol{P_U} = \begin{pmatrix} p_{u_1} & p_{u_2} \\ p_{u_2} & p_{u_3} \end{pmatrix}. \tag{6.299}$$

Recalling that p_{u_1}, p_{u_2}, and p_{u_3} are defined in Eqns. (6.53), (6.54), and (6.55), respectively, being therefore easy to see that

$$\left(\frac{\partial V_U}{\partial \tilde{\boldsymbol{z}}}\right)^T = \left(\boldsymbol{P_U}\hat{\mathbf{z}}\right)^T, \tag{6.300}$$

and also recalling, from section 6.2.1, that the $\hat{\boldsymbol{h}}(\tilde{\boldsymbol{\chi}}, \tilde{\boldsymbol{z}})$ subsystem can be rewritten in terms of its quasi-steady-state equilibrium error as

$$\hat{\boldsymbol{h}}(\tilde{\boldsymbol{\chi}}, \tilde{\boldsymbol{z}}) = \boldsymbol{A_U}\hat{\mathbf{z}}, \tag{6.301}$$

with $\boldsymbol{A_U}$ given by Eq. (6.29). Substituting both Eqns. (6.300) and (6.301) into the left-hand side of inequality (6.296) yields

$$\left(\frac{\partial V_U}{\partial \tilde{\boldsymbol{z}}}\right)^T \hat{\boldsymbol{h}}(\tilde{\boldsymbol{\chi}}, \tilde{\boldsymbol{z}}) = \left(\boldsymbol{P_U}\hat{\mathbf{z}}\right)^T \boldsymbol{A_U}\hat{\mathbf{z}} = \hat{\mathbf{z}}^T\boldsymbol{P_U}\boldsymbol{A_U}\hat{\mathbf{z}} = \hat{\mathbf{z}}^T\boldsymbol{\mathcal{A}_U}\hat{\mathbf{z}}, \tag{6.302}$$

being $\boldsymbol{\mathcal{A}_U}$ defined in

$$\boldsymbol{\mathcal{A}_U} = \boldsymbol{P_U}\boldsymbol{A_U} = \begin{pmatrix} \alpha_{11} & \alpha_{12} \\ \alpha_{21} & \alpha_{22} \end{pmatrix}, \tag{6.303}$$

with

$$\alpha_{11} = a_9 p_{u_2}, \tag{6.304}$$

$$\alpha_{12} = c_7 p_{u_1} + c_9 p_{u_2}, \tag{6.305}$$

$$\alpha_{21} = a_9 p_{u_3}, \tag{6.306}$$

$$\alpha_{22} = c_7 p_{u_2} + c_9 p_{u_3}. \tag{6.307}$$

Substituting the solutions to the associated Lyapunov equation, p_{u_1}, p_{u_2}, and p_{u_3}, Eqns. (6.53), (6.53) and (6.53), respectively into inequality (6.311) reduces to

$$\left(\frac{\partial V_U}{\partial \tilde{\boldsymbol{z}}}\right)^T \hat{\boldsymbol{h}}(\tilde{\boldsymbol{\chi}}, \tilde{\boldsymbol{z}}) = -\frac{1}{2}\left(q_{u_1}\hat{z}_1^2 + q_{u_2}\hat{z}_2^2\right) = -\frac{1}{2}\left(\hat{\mathbf{z}}^T\boldsymbol{Q_U}\hat{\mathbf{z}}\right), \tag{6.308}$$

where $\boldsymbol{Q_U}$ is the matrix of the associated Lyapunov equation defined in Eq. (5.106). For simplicity, let introduce the variables

$$\tilde{q}_{u_1} = \frac{q_{u_1}}{2}, \tag{6.309}$$

$$\tilde{q}_{u_2} = \frac{q_{u_2}}{2}, \tag{6.310}$$

and let also $\tilde{\boldsymbol{Q}}_{\boldsymbol{U}} = \boldsymbol{Q_U}/2$, thus inequality (6.296) can be rewritten such

$$\left(\frac{\partial V_U}{\partial \tilde{\boldsymbol{z}}}\right)^T \hat{\boldsymbol{h}}(\tilde{\boldsymbol{\chi}}, \tilde{\boldsymbol{z}}) = -\left(\hat{\mathbf{z}}^T\tilde{\boldsymbol{Q}}_{\boldsymbol{U}}\hat{\mathbf{z}}\right) \leq -\alpha_4\phi_2^2(\tilde{\boldsymbol{z}} - \tilde{\mathbf{h}}(\tilde{\boldsymbol{\chi}})), \tag{6.311}$$

thus Assumption 5.5.8 and inequality (6.296) can be satisfied by selecting α_4 and $\phi_2(\tilde{\boldsymbol{z}} - \tilde{\mathbf{h}}(\tilde{\boldsymbol{\chi}}))$ such

$$\alpha_4 \leq 1, \tag{6.312}$$

$$\phi_2(\tilde{\boldsymbol{z}} - \tilde{\mathbf{h}}(\tilde{\boldsymbol{\chi}})) = \left(\hat{\mathbf{z}}^T\tilde{\boldsymbol{Q}}_{\boldsymbol{U}}\hat{\mathbf{z}}\right)^{\frac{1}{2}} = \sqrt{\tilde{q}_{u_1}\hat{z}_1^2 + \tilde{q}_{u_2}\hat{z}_2^2}. \tag{6.313}$$

For simplicity, and noting that $\hat{\boldsymbol{z}} = \tilde{\boldsymbol{z}} - \tilde{\mathbf{h}}(\tilde{\boldsymbol{\chi}}, \tilde{\boldsymbol{z}})$, $\phi_2(\hat{\boldsymbol{z}})$ is used instead of $\phi_2(\tilde{\boldsymbol{z}} - \tilde{\mathbf{h}}(\tilde{\boldsymbol{\chi}}, \tilde{\boldsymbol{z}}))$ throughout the remainder of the document.

6.5.4 Proof of Assumption 5.5.9: First Interconnection Condition for the Helicopter Σ_{SFU} System

The Lyapunov functions $V_1(\tilde{\boldsymbol{\chi}})$ and $V_U(\tilde{\boldsymbol{\chi}}, \tilde{\boldsymbol{z}})$, Eqns. (6.202) and (6.51), respectively, must satisfy the so called interconnection conditions. The first interconnection condition is obtained by computing the derivative of $V_1(\tilde{\boldsymbol{\chi}})$ along the solution of Eq. (6.228), resulting in a expression similar to Eq. (5.166), which provides the first interconnection inequality

$$\left(\frac{\partial V_1(\tilde{\boldsymbol{\chi}})}{\partial \tilde{\boldsymbol{\chi}}}\right)^T \left[\tilde{\boldsymbol{F}}\left(\tilde{\boldsymbol{\chi}}, \tilde{\boldsymbol{z}}\right) - \tilde{\boldsymbol{F}}\left(\tilde{\boldsymbol{\chi}}, \tilde{\mathbf{h}}(\tilde{\boldsymbol{\chi}})\right)\right] \le \beta_3 \psi_2(\tilde{\boldsymbol{\chi}}) \phi_2(\tilde{\boldsymbol{z}} - \tilde{\mathbf{h}}(\tilde{\boldsymbol{\chi}})), \tag{6.314}$$

where the comparison functions $\psi_2(\tilde{\boldsymbol{\chi}})$ and $\phi_2(\tilde{\boldsymbol{\chi}}, \tilde{\boldsymbol{z}})$, are defined in Eqns. (6.313) and (6.283), respectively. Inequality (6.314) determines the allowed growth of $\tilde{\boldsymbol{F}}\left(\tilde{\boldsymbol{\chi}}, \tilde{\boldsymbol{z}}\right)$ in $\tilde{z}$, and in typical problems, verifying Assumption 6.5.4 reduces to verifying the inequality

$$\left\|\tilde{\boldsymbol{F}}\left(\tilde{\boldsymbol{\chi}}, \tilde{\boldsymbol{z}}\right) - \tilde{\boldsymbol{F}}\left(\tilde{\boldsymbol{\chi}}, \tilde{\mathbf{h}}(\tilde{\boldsymbol{\chi}})\right)\right\| \le \psi_2(\tilde{\boldsymbol{\chi}}) \phi_2(\tilde{\boldsymbol{z}} - \tilde{\mathbf{h}}(\tilde{\boldsymbol{\chi}})), \tag{6.315}$$

which implies that the rate of growth of $\tilde{\boldsymbol{F}}\left(\tilde{\boldsymbol{\chi}}, \tilde{\boldsymbol{z}}\right)$ cannot be faster than the rate of growth of the comparison function $\phi_2(\cdot)$. The left-hand side of inequality (6.314) is given by recalling Eq. (6.241), and defining

$$\tilde{\boldsymbol{F}}(\tilde{\boldsymbol{\chi}}, \tilde{\boldsymbol{z}}) - \tilde{\boldsymbol{F}}(\tilde{\boldsymbol{\chi}}, \tilde{\mathbf{h}}(\tilde{\boldsymbol{\chi}})) = \begin{bmatrix} \tilde{F}_1 - \tilde{F}_{H_1} \\ \tilde{F}_2 - \tilde{F}_{H_2} \\ \tilde{F}_3 - \tilde{F}_{H_3} \end{bmatrix} = \begin{bmatrix} \hat{F}_1 \\ \hat{F}_2 \\ \hat{F}_3 \end{bmatrix}, \tag{6.316}$$

recalling that $\tilde{F}_1$, $\tilde{F}_2$, and $\tilde{F}_3$ are defined in Eqns. (6.231), (6.232), and (6.233), respectively, and that $\tilde{F}_{H_1}$, $\tilde{F}_{H_2}$, and $\tilde{F}_{H_3}$, are defined in Eqns. (6.235), (6.236), and (6.237), respectively, yielding

$$\hat{F}_1 = a_{10} \left(\tilde{x} + x^*\right)^2 \left(\sin\left(\tilde{z}_1 + z_1^*\right) - \sin\left(\tilde{\mathrm{h}}_1(\tilde{\boldsymbol{\chi}}) + z_1^*\right)\right), \tag{6.317}$$

$$\hat{F}_2 = 0, \tag{6.318}$$

$$\hat{F}_3 = \left(\tilde{x} + x^*\right)^2 \left[c_3 \left(\tilde{z}_1 - \tilde{\mathrm{h}}_1(\tilde{\boldsymbol{\chi}})\right) - \left(\sqrt{c_4 + c_5\left(\tilde{z}_1 + z_1^*\right)} - \sqrt{c_4 + c_5\left(\tilde{\mathrm{h}}_1(\tilde{\boldsymbol{\chi}}) + z_1^*\right)}\right)\right], \tag{6.319}$$

where Eqns. (6.317–6.318) can be simplified by introducing

$$\mathcal{A}_2 = \tilde{z}_1 + z_1^*, \tag{6.320}$$

$$\mathcal{B}_2 = \tilde{\mathrm{h}}_1(\tilde{\boldsymbol{\chi}}) + z_1^*, \tag{6.321}$$

thus rewriting Eqns. (6.317–6.318) as

$$\hat{F}_1 = a_{10}(\tilde{x} + x^*)^2 2 \sin\left(\frac{\mathcal{A}_2 - \mathcal{B}_2}{2}\right) \cos\left(\frac{\mathcal{A}_2 + \mathcal{B}_2}{2}\right), \tag{6.322}$$

$$\hat{F}_2 = 0, \tag{6.323}$$

$$\hat{F}_3 = \left(\tilde{x} + x^*\right)^2 \left[c_3 \hat{z}_1 - \left(\sqrt{c_4 + c_5 \mathcal{A}_2} - \sqrt{c_4 + c_5 \mathcal{B}_2}\right)\right], \tag{6.324}$$

Substituting Eqns. (6.241) and (6.316) into the left-hand side of inequality (6.314), and using Eqns. (6.320) and (6.321) yields

$$\begin{aligned} & \left(\frac{\partial V_1(\tilde{\boldsymbol{\chi}})}{\partial \tilde{\boldsymbol{\chi}}}\right)^T \left[\tilde{\boldsymbol{F}}(\tilde{\boldsymbol{\chi}}, \tilde{\boldsymbol{z}}) - \tilde{\boldsymbol{F}}(\tilde{\boldsymbol{\chi}}, \tilde{\mathbf{h}}(\tilde{\boldsymbol{\chi}}))\right] \\ = & \frac{\partial V_1(\tilde{\boldsymbol{\chi}})}{\partial \tilde{x}} \hat{F}_1 + \frac{\partial V_1(\tilde{\boldsymbol{\chi}})}{\partial \tilde{y}_1} \hat{F}_2 + \frac{\partial V_1(\tilde{\boldsymbol{\chi}})}{\partial \tilde{y}_2} \hat{F}_3 \end{aligned}$$

$$\begin{aligned} &= \mathcal{V}_1\tilde{x}\left[a_{10}(\tilde{x}+x^*)^2\sin\left(\frac{\mathcal{A}_2-\mathcal{B}_2}{2}\right)\cos\left(\frac{\mathcal{A}_2+\mathcal{B}_2}{2}\right)\right] \\ &+ (\mathcal{V}_3\tilde{y}_1+\mathcal{V}_4\tilde{y}_2)\left\{(\tilde{x}+x^*)^2\left[c_3\hat{z}_1-\left(\sqrt{c_4+c_5\mathcal{A}_2}-\sqrt{c_4+c_5\mathcal{B}_2}\right)\right]\right\}. \end{aligned} \tag{6.325}$$

Focussing in the first term in Eq. (6.325) it can be rewritten as

$$\begin{aligned} & 2a_{10}(\tilde{x}+x^*)^2\sin\left(\frac{\mathcal{A}_2-\mathcal{B}_2}{2}\right)\cos\left(\frac{\mathcal{A}_2+\mathcal{B}_2}{2}\right) \\ \leq\ & 2(\tilde{x}+x^*)^2\cos\left(\frac{\mathcal{A}_2+\mathcal{B}_2}{2}\right)\left|a_{10}\sin\left(\frac{\mathcal{A}_2-\mathcal{B}_2}{2}\right)\right|, \end{aligned} \tag{6.326}$$

and recalling that due to the positive nature of the function $\cos(a)$, that is $1 \geq \cos(a) \geq 0\ \forall a \in \mathcal{R}$, it can also be shown that

$$0 \leq \cos\left(\frac{\mathcal{A}_2+\mathcal{B}_2}{2}\right) \leq 1, \tag{6.327}$$

further more it can be shown that

$$0 \leq \cos\left(\frac{\mathcal{A}_2+\mathcal{B}_2}{2}\right) \leq \mathcal{K}_2 \leq 1, \tag{6.328}$$

where it can be proven that the maximum value of Eq. (6.327) is achieved for

$$\mathcal{K}_2 = \cos\left(\frac{\mathcal{A}_{2_{MIN}}+\mathcal{B}_{2_{MIN}}}{2}\right) \leq 1, \tag{6.329}$$

being $\mathcal{A}_{2_{MIN}}$ and $\mathcal{B}_{2_{MIN}}$ the minimum possible value of Eqns. (6.320) and (6.321) respectively, and being defined by

$$\mathcal{A}_{2_{MIN}} = (\tilde{z}_1+z_1^*)_{MIN} = z_{1_{MIN}}, \tag{6.330}$$

$$\begin{aligned} \mathcal{B}_{2_{MIN}} &= h_{1_{MIN}}(\tilde{\boldsymbol{\chi}}) + z_1^* = s_2\left[\left(1+\sqrt{s_3\tilde{v}(\tilde{\boldsymbol{\chi}})}\right)^2-1\right]_{MIN} \\ &= s_2\left[\left(1+\sqrt{s_3\tilde{v}_{MIN}(\tilde{\boldsymbol{\chi}})}\right)^2-1\right], \end{aligned} \tag{6.331}$$

where $z_{1_{MIN}}$ represents the minimum collective pitch angle, which is defined in Table 2.3, and where $\tilde{v}_{MIN}$ was defined in Eq. (6.133). Equation (6.326) can be rewritten using Eq. (6.329), and the sine inequality identity given by $|\sin a| \leq |a|$, yielding

$$\begin{aligned} & 2a_{10}(\tilde{x}+x^*)^2\sin\left(\frac{\mathcal{A}_2-\mathcal{B}_2}{2}\right)\cos\left(\frac{\mathcal{A}_2+\mathcal{B}_2}{2}\right) \\ \leq\ & 2(\tilde{x}+x^*)^2\cos\left(\frac{\mathcal{A}_2+\mathcal{B}_2}{2}\right)\left|a_{10}\sin\left(\frac{\mathcal{A}_2-\mathcal{B}_2}{2}\right)\right| \\ \leq\ & 2(\tilde{x}+x^*)^2\mathcal{K}_2\left|a_{10}\sin\left(\frac{\mathcal{A}_2-\mathcal{B}_2}{2}\right)\right| \\ \leq\ & (\tilde{x}+x^*)^2\mathcal{K}_2\left|a_{10}\left(\mathcal{A}_2-\mathcal{B}_2\right)\right|. \end{aligned} \tag{6.332}$$

Inequality (6.332) can be further simplified by recalling the definition introduced in the error dynamics formulation, section 2.8.5.2, such

$$(\tilde{x}+x^*) \triangleq x, \tag{6.333}$$

and identifying that as seen in Table 2.3, resulting in

$$x_{MAX} \geq x \geq x_{MIN}, \tag{6.334}$$

therefore allowing to rewrite (6.332) as

$$2a_{10}(\tilde{x}+x^*)^2\sin\left(\frac{\mathcal{A}_2-\mathcal{B}_2}{2}\right)\cos\left(\frac{\mathcal{A}_2+\mathcal{B}_2}{2}\right)$$

$$
\begin{aligned}
&\leq \quad (\tilde{x}+x^*)^2\mathcal{K}_2\left|a_{10}\left(\mathcal{A}_2-\mathcal{B}_2\right)\right| \\
&\leq \quad x_{MAX}^2\mathcal{K}_2\left|a_{10}\left(\mathcal{A}_2-\mathcal{B}_2\right)\right|, \qquad (6.335)
\end{aligned}
$$

which can be further simplified by introducing

$$
s_6 = x_{MAX}^2\mathcal{K}_2\left|a_{10}\right|, \qquad (6.336)
$$

therefore rewriting inequality (6.335) as

$$
\begin{aligned}
& \quad 2a_{10}(\tilde{x}+x^*)^2\sin\left(\frac{\mathcal{A}_2-\mathcal{B}_2}{2}\right)\cos\left(\frac{\mathcal{A}_2+\mathcal{B}_2}{2}\right) \\
&\leq \quad x_{MAX}^2\mathcal{K}_2\left|a_{10}\left(\mathcal{A}_2-\mathcal{B}_2\right)\right| \\
&\leq \quad s_6\left|\left(\mathcal{A}_2-\mathcal{B}_2\right)\right|. \qquad (6.337)
\end{aligned}
$$

Substituting back $\mathcal{A}_2$ and $\mathcal{B}_2$, Eqns. (6.320) and (6.321), respectively, into inequality (6.337) results in

$$
\begin{aligned}
& \quad 2a_{10}(\tilde{x}+x^*)^2\sin\left(\frac{\mathcal{A}_2-\mathcal{B}_2}{2}\right)\cos\left(\frac{\mathcal{A}_2+\mathcal{B}_2}{2}\right) \\
&\leq \quad s_6\left|\left(\mathcal{A}_2-\mathcal{B}_2\right)\right| \\
&= \quad s_6\left|(\tilde{z}_1+z_1^*)-(h_1(\tilde{x},\tilde{\boldsymbol{y}})+z_1^*)\right| = s_6\left|\tilde{z}_1-h_1(\tilde{x},\tilde{\boldsymbol{y}})\right| = s_6\left|\hat{z}_1\right|. \qquad (6.338)
\end{aligned}
$$

Let recall that $\hat{z}_1$ represents the quasi-steady-state equilibrium error of the ultra fast dynamics given by $\hat{z}_1 = \tilde{z}_1 - \tilde{\mathrm{h}}_1(\tilde{\boldsymbol{\chi}})$, therefore using the results obtained in Eq. (6.338) into inequality (6.389) results in

$$
\begin{aligned}
& \quad \left(\frac{\partial V_1(\tilde{\boldsymbol{\chi}})}{\partial\tilde{\boldsymbol{\chi}}}\right)^T\left[\tilde{\boldsymbol{F}}(\tilde{\boldsymbol{\chi}},\tilde{\boldsymbol{z}})-\tilde{\boldsymbol{F}}(\tilde{\boldsymbol{\chi}},\tilde{\mathrm{h}}(\tilde{\boldsymbol{\chi}}))\right] \\
&= \quad \mathcal{V}_1\tilde{x}\left[a_{10}(\tilde{x}+x^*)^2\sin\left(\frac{\mathcal{A}_2-\mathcal{B}_2}{2}\right)\cos\left(\frac{\mathcal{A}_2+\mathcal{B}_2}{2}\right)\right] \\
&+ \quad (\mathcal{V}_3\tilde{y}_1+\mathcal{V}_4\tilde{y}_2)\left\{(\tilde{x}+x^*)^2\left[c_3\hat{z}_1-\left(\sqrt{c_4+c_5\mathcal{A}_2}-\sqrt{c_4+c_5\mathcal{B}_2}\right)\right]\right\} \\
&\leq \quad \left|\mathcal{V}_1\tilde{x}\left[a_{10}(\tilde{x}+x^*)^2\sin\left(\frac{\mathcal{A}_2-\mathcal{B}_2}{2}\right)\cos\left(\frac{\mathcal{A}_2+\mathcal{B}_2}{2}\right)\right]\right| \\
&+ \quad \left|(\mathcal{V}_3\tilde{y}_1+\mathcal{V}_4\tilde{y}_2)\left\{(\tilde{x}+x^*)^2\left[c_3\hat{z}_1-\left(\sqrt{c_4+c_5\mathcal{A}_2}-\sqrt{c_4+c_5\mathcal{B}_2}\right)\right]\right\}\right| \\
&\leq \quad \left|s_6\mathcal{V}_1\tilde{x}\left|\hat{z}_1\right|\right| + \left|(\mathcal{V}_3\tilde{y}_1+\mathcal{V}_4\tilde{y}_2)\left\{(\tilde{x}+x^*)^2\left[c_3\hat{z}_1-\left(\sqrt{c_4+c_5\mathcal{A}_2}-\sqrt{c_4+c_5\mathcal{B}_2}\right)\right]\right\}\right| \\
&\leq \quad \left|s_6\mathcal{V}_1\tilde{x}\left|\hat{z}_1\right|\right| + (\tilde{x}+x^*)^2\left|(\mathcal{V}_3\tilde{y}_1+\mathcal{V}_4\tilde{y}_2)\left[c_3\hat{z}_1-\left(\sqrt{c_4+c_5\mathcal{A}_2}-\sqrt{c_4+c_5\mathcal{B}_2}\right)\right]\right|. \qquad (6.339)
\end{aligned}
$$

In order to further simplify inequality (6.339) let introduce the following inequality property. Assume that for $a > 0$ and $a + bx > 0$ it holds that

$$
\sqrt{a+bx} \leq \sqrt{a} + \frac{bx}{2\sqrt{a}}, \qquad (6.340)
$$

where the proof is given by multiplying both sides of Eq. (6.340) by $\sqrt{a}$ resulting in

$$
\sqrt{a}\sqrt{a+bx} \leq a + \frac{bx}{2}, \qquad (6.341)
$$

let square both sides of Eq. (6.342) such

$$
a\left(a+bx\right) \leq a^2 + abx + \frac{b^2x^2}{4}, \qquad (6.342)
$$

which can be simplified by canceling terms reducing to

$$
0 \leq \frac{b^2x^2}{4}, \qquad (6.343)
$$

which holds inequality (6.340). Let apply the results of Eq. (6.340), to the second term of inequality (6.339), that is

$$(\tilde{x}+x^*)^2 \left|(\mathcal{V}_3\tilde{y}_1+\mathcal{V}_4\tilde{y}_2)\left[c_3\hat{z}_1-\left(\sqrt{c_4+c_5\mathcal{A}_2}-\sqrt{c_4+c_5\mathcal{B}_2}\right)\right]\right|, \tag{6.344}$$

where it can be shown that, by using the derived inequality (6.340), that

$$\left|c_3\hat{z}_1-\left(\sqrt{c_4+c_5\mathcal{A}_2}-\sqrt{c_4+c_5\mathcal{B}_2}\right)\right| \leq \mathcal{D}\left|\hat{z}_1\right|, \tag{6.345}$$

where $\mathcal{D}$ is defined as

$$\mathcal{D}=\max_{\xi\in\{\tilde{z}_1,\tilde{\mathrm{h}}_1\}}\left(\left|\frac{c_5}{2\sqrt{c_4+c_5\left(\xi+z_1^*\right)}}-c_3\right|\right). \tag{6.346}$$

Inequality (6.345) can be expanded by recalling the definitions of both $\mathcal{A}_2$ and $\mathcal{B}_2$, Eqns. (6.320) and (6.321), respectively, and the definition of $\hat{z}_1=\tilde{z}_1-\tilde{\mathrm{h}}_1(\tilde{\boldsymbol{\chi}})$, such

$$\left|c_3\left(\tilde{z}_1-\tilde{\mathrm{h}}_1(\tilde{\boldsymbol{\chi}})\right)-\left(\sqrt{c_4+c_5\left(\tilde{z}_1+z_1^*\right)}-\sqrt{c_4+c_5\left(\tilde{\mathrm{h}}_1(\tilde{\boldsymbol{\chi}})+z_1^*\right)}\right)\right| \leq \mathcal{D}\left|\hat{z}_1\right|. \tag{6.347}$$

Fulfilment of inequality (6.347) implies that needs to be proven that

$$\begin{aligned}&\left|c_3\left(\tilde{z}_1-\tilde{\mathrm{h}}_1(\tilde{\boldsymbol{\chi}})\right)-\left(\sqrt{c_4+c_5\left(\tilde{z}_1+z_1^*\right)}-\sqrt{c_4+c_5\left(\tilde{\mathrm{h}}_1(\tilde{\boldsymbol{\chi}})+z_1^*\right)}\right)\right|\\ \leq\ &\max_{\xi\in\{\tilde{z}_1,\tilde{\mathrm{h}}_1\}}\left(\left|\frac{c_5}{2\sqrt{c_4+c_5\left(\xi+z_1^*\right)}}-c_3\right|\right).\end{aligned} \tag{6.348}$$

For completeness let define

$$\mathcal{A}_3 = c_3\left(\tilde{z}_1-\tilde{\mathrm{h}}_1(\tilde{\boldsymbol{\chi}})\right), \tag{6.349}$$

$$\mathcal{B}_3 = \left(\sqrt{c_4+c_5\left(\tilde{z}_1+z_1^*\right)}-\sqrt{c_4+c_5\left(\tilde{\mathrm{h}}_1(\tilde{\boldsymbol{\chi}})+z_1^*\right)}\right), \tag{6.350}$$

thus reducing Eq. (6.348) such

$$\left|\mathcal{A}_3-\mathcal{B}_3\right| \leq \max_{\xi\in\{\tilde{z}_1,\tilde{\mathrm{h}}_1\}}\left(\left|\frac{c_5}{2\sqrt{c_4+c_5\left(\xi+z_1^*\right)}}-c_3\right|\right), \tag{6.351}$$

where it can be noted that two different cases can be encountered and given by

$$\mathcal{A}_3 > \mathcal{B}_3, \tag{6.352}$$

$$\mathcal{A}_3 < \mathcal{B}_3. \tag{6.353}$$

For case 1, Eq. (6.352) it can be shown that the left hand side of inequality (6.351) reduces to

$$\left|\mathcal{A}_3-\mathcal{B}_3\right|=\mathcal{A}_3-\mathcal{B}_3=c_3\left(\tilde{z}_1-\tilde{\mathrm{h}}_1(\tilde{\boldsymbol{\chi}})\right)+\sqrt{c_4+c_5\left(\tilde{\mathrm{h}}_1(\tilde{\boldsymbol{\chi}})+z_1^*\right)}-\sqrt{c_4+c_5\left(\tilde{z}_1+z_1^*\right)}, \tag{6.354}$$

the second term of the right hand side of Eq. (6.354) can be rewritten by adding and subtracting $\tilde{z}_1$ and reorganizing such

$$\begin{aligned}\sqrt{c_4+c_5\left(\tilde{\mathrm{h}}_1(\tilde{\boldsymbol{\chi}})+z_1^*\right)} &= \sqrt{c_4+c_5\left(\tilde{\mathrm{h}}_1(\tilde{\boldsymbol{\chi}})+z_1^*+\tilde{z}_1-\tilde{z}_1\right)}\\ &= \sqrt{\left[c_4+c_5\left(\tilde{z}_1+z_1^*\right)\right]+c_5\left[\tilde{\mathrm{h}}_1(\tilde{\boldsymbol{\chi}})-\tilde{z}_1\right]}.\end{aligned} \tag{6.355}$$

By recognizing that by definition

$$c_4 + c_5\left(\tilde{z}_1 + z_1^*\right) = c_4 + c_5 z_1 > 0 \;\forall\; z_1, \tag{6.356}$$

therefore Eq. (6.355) can be rewritten by recalling inequality (6.340) such that

$$\sqrt{\left[c_4 + c_5\left(\tilde{z}_1 + z_1^*\right)\right] + c_5\left[\tilde{\mathrm{h}}_1(\tilde{\boldsymbol{\chi}}) - \tilde{z}_1\right]} \leq \sqrt{c_4 + c_5\left(\tilde{z}_1 + z_1^*\right)} + \frac{c_5\left[\tilde{\mathrm{h}}_1(\tilde{\boldsymbol{\chi}}) - \tilde{z}_1\right]}{2\sqrt{c_4 + c_5\left(\tilde{z}_1 + z_1^*\right)}}, \tag{6.357}$$

Therefore, substituting Eq. (6.357) into Eq. (6.354) results in

$$\begin{aligned}
|\mathcal{A}_3 - \mathcal{B}_3| &= c_3\left(\tilde{z}_1 - \tilde{\mathrm{h}}_1(\tilde{\boldsymbol{\chi}})\right) + \sqrt{c_4 + c_5\left(\tilde{\mathrm{h}}_1(\tilde{\boldsymbol{\chi}}) + z_1^*\right)} - \sqrt{c_4 + c_5\left(\tilde{z}_1 + z_1^*\right)} \\
&\leq c_3\left(\tilde{z}_1 - \tilde{\mathrm{h}}_1(\tilde{\boldsymbol{\chi}})\right) + \sqrt{c_4 + c_5\left(\tilde{z}_1 + z_1^*\right)} + \frac{c_5\left(\tilde{\mathrm{h}}_1(\tilde{\boldsymbol{\chi}}) - \tilde{z}_1\right)}{2\sqrt{c_4 + c_5\left(\tilde{z}_1 + z_1^*\right)}} \\
&- \sqrt{c_4 + c_5\left(\tilde{z}_1 + z_1^*\right)},
\end{aligned} \tag{6.358}$$

which after simplifying reduces to

$$\begin{aligned}
|\mathcal{A}_3 - \mathcal{B}_3| &\leq c_3\left(\tilde{z}_1 - \tilde{\mathrm{h}}_1(\tilde{\boldsymbol{\chi}})\right) + \frac{c_5\left(\tilde{\mathrm{h}}_1(\tilde{\boldsymbol{\chi}}) - \tilde{z}_1\right)}{2\sqrt{c_4 + c_5\left(\tilde{z}_1 + z_1^*\right)}} \\
&= \left(c_3 - \frac{c_5}{2\sqrt{c_4 + c_5\left(\tilde{z}_1 + z_1^*\right)}}\right)\left(\tilde{z}_1 - \tilde{\mathrm{h}}_1(\tilde{\boldsymbol{\chi}})\right) \\
&\leq \left|c_3 - \frac{c_5}{2\sqrt{c_4 + c_5\left(\tilde{z}_1 + z_1^*\right)}}\right|\left|\tilde{z}_1 - \tilde{\mathrm{h}}_1(\tilde{\boldsymbol{\chi}})\right|.
\end{aligned} \tag{6.359}$$

For case 2, Eq. (6.353), it can be shown that the left hand side of inequality (6.351) reduces to

$$|\mathcal{A}_3 - \mathcal{B}_3| = \mathcal{B}_3 - \mathcal{A}_3 = \sqrt{c_4 + c_5\left(\tilde{z}_1 + z_1^*\right)} - \sqrt{c_4 + c_5\left(\tilde{\mathrm{h}}_1(\tilde{\boldsymbol{\chi}}) + z_1^*\right)} - c_3\left(\tilde{z}_1 - \tilde{\mathrm{h}}_1(\tilde{\boldsymbol{\chi}})\right), \tag{6.360}$$

the second term of the right hand side of Eq. (6.360) can be rewritten by adding and subtracting $\tilde{\mathrm{h}}_1(\tilde{\boldsymbol{\chi}})$ and reorganizing such

$$\begin{aligned}
\sqrt{c_4 + c_5\left(\tilde{z}_1 + z_1^*\right)} &= \sqrt{c_4 + c_5\left(\tilde{z}_1 - \tilde{\mathrm{h}}_1(\tilde{\boldsymbol{\chi}}) + \tilde{\mathrm{h}}_1(\tilde{\boldsymbol{\chi}}) + z_1^*\right)} \\
&= \sqrt{\left[c_4 + c_5\left(\tilde{\mathrm{h}}_1(\tilde{\boldsymbol{\chi}}) + z_1^*\right)\right] + c_5\left[\tilde{z}_1 - \tilde{\mathrm{h}}_1(\tilde{\boldsymbol{\chi}})\right]}.
\end{aligned} \tag{6.361}$$

By recognizing that by definition

$$c_4 + c_5\left(\tilde{\mathrm{h}}_1(\tilde{\boldsymbol{\chi}}) + z_1^*\right) = c_4 + c_5 z_1 > 0 \;\forall\; z_1, \tag{6.362}$$

therefore Eq. (6.361) can be rewritten by recalling inequality (6.340) such

$$\begin{aligned}
\sqrt{\left[c_4 + c_5\left(\tilde{\mathrm{h}}_1(\tilde{\boldsymbol{\chi}}) + z_1^*\right)\right] + c_5\left[\tilde{z}_1 - \tilde{\mathrm{h}}_1(\tilde{\boldsymbol{\chi}})\right]} &\leq \sqrt{c_4 + c_5\left(\tilde{\mathrm{h}}_1(\tilde{\boldsymbol{\chi}}) + z_1^*\right)} \\
&+ \frac{c_5\left[\tilde{z}_1 - \tilde{\mathrm{h}}_1(\tilde{\boldsymbol{\chi}})\right]}{2\sqrt{c_4 + c_5\left(\tilde{\mathrm{h}}_1(\tilde{\boldsymbol{\chi}}) + z_1^*\right)}},
\end{aligned} \tag{6.363}$$

Therefore, substituting Eq. (6.363) into Eq. (6.360) results in

$$|\mathcal{A}_3 - \mathcal{B}_3| = \sqrt{c_4 + c_5\left(\tilde{z}_1 + z_1^*\right)} - \sqrt{c_4 + c_5\left(\tilde{\mathrm{h}}_1(\tilde{\boldsymbol{\chi}}) + z_1^*\right)} - c_3\left(\tilde{z}_1 - \tilde{\mathrm{h}}_1(\tilde{\boldsymbol{\chi}})\right)$$

$$\begin{aligned}
&\leq \sqrt{c_4 + c_5\left(\tilde{\mathrm{h}}_1(\tilde{\chi}) + z_1^*\right)} + \frac{c_5\tilde{z}_1 - \tilde{\mathrm{h}}_1(\tilde{\chi})}{2\sqrt{c_4 + c_5\left(\tilde{\mathrm{h}}_1(\tilde{\chi}) + z_1^*\right)}} - \sqrt{c_4 + c_5\left(\tilde{\mathrm{h}}_1(\tilde{\chi}) + z_1^*\right)} \\
&- c_3\left(\tilde{z}_1 - \tilde{\mathrm{h}}_1(\tilde{\chi})\right), \qquad (6.364)
\end{aligned}$$

which after simplifying reduces to

$$\begin{aligned}
|\mathcal{A}_3 - \mathcal{B}_3| &\leq \frac{c_5\left[\tilde{z}_1 - \tilde{\mathrm{h}}_1(\tilde{\chi})\right]}{2\sqrt{c_4 + c_5\left(\tilde{\mathrm{h}}_1(\tilde{\chi}) + z_1^*\right)}} - c_3\left(\tilde{z}_1 - \tilde{\mathrm{h}}_1(\tilde{\chi})\right) \\
&= \left(\frac{c_5}{2\sqrt{c_4 + c_5\left(\tilde{\mathrm{h}}_1(\tilde{\chi}) + z_1^*\right)}} - c_3\right)\left(\tilde{z}_1 - \tilde{\mathrm{h}}_1(\tilde{\chi})\right) \\
&\leq \left|\frac{c_5}{2\sqrt{c_4 + c_5\left(\tilde{\mathrm{h}}_1(\tilde{\chi}) + z_1^*\right)}} - c_3\right|\left|\tilde{z}_1 - \tilde{\mathrm{h}}_1(\tilde{\chi})\right|, \qquad (6.365)
\end{aligned}$$

thus, both case 1, Eq. (6.365), and case 2, Eq. (6.365) hold inequality (6.348). Let recall that $\mathcal{D}$ in Eq. (6.346) can be defined as

$$\mathcal{D} = \max_{\xi\in\{\tilde{z}_1,\tilde{\mathrm{h}}_1\}}\left(\left|\frac{c_5}{2\sqrt{c_4 + c_5\left(\xi + z_1^*\right)}} - c_3\right|\right) = \max\left(\mathcal{D}_1, \mathcal{D}_2\right), \qquad (6.366)$$

where $\mathcal{D}_1$ is the solution of Eq. (6.366) when $\xi = \tilde{z}_1$, that is

$$\mathcal{D}_1 = \left(\left|\frac{c_5}{2\sqrt{c_4 + c_5\left(\tilde{z}_1 + z_1^*\right)}} - c_3\right|\right) = \left(\left|\frac{c_5}{2\sqrt{c_4 + c_5\mathcal{A}_2}} - c_3\right|\right), \qquad (6.367)$$

and where $\mathcal{D}_2$ is the solution of Eq. (6.366) when $\xi = \tilde{\mathrm{h}}_1(\tilde{\chi})$, that is

$$\mathcal{D}_2 = \left(\left|\frac{c_5}{2\sqrt{c_4 + c_5\left(\tilde{\mathrm{h}}_1 + z_1^*\right)}} - c_3\right|\right) = \left(\left|\frac{c_5}{2\sqrt{c_4 + c_5\mathcal{B}_2}} - c_3\right|\right). \qquad (6.368)$$

With these results, inequality (6.345) can be further simplified by defining

$$\left|c_3\hat{z}_1 - \left(\sqrt{c_4 + c_5\mathcal{A}_2} - \sqrt{c_4 + c_5\mathcal{B}_2}\right)\right| \leq \mathcal{D}\,|\hat{z}_1| \leq \mathcal{D}_{MAX}\,|\hat{z}_1|, \qquad (6.369)$$

and recalling that it can be shown that

$$\mathcal{D} \leq \mathcal{D}_{MAX}, \qquad (6.370)$$

with

$$\mathcal{D}_{MAX} = \max\left(\mathcal{D}_{1_{MAX}}, \mathcal{D}_{2_{MAX}}\right), \qquad (6.371)$$

where $\mathcal{D}_{1_{MAX}}$ is given by

$$\mathcal{D}_{1_{MAX}} = \left|\frac{c_5}{2\sqrt{c_4 + c_5\left(\tilde{z}_1 + z_1^*\right)}} - c_3\right|_{MAX} = \left|\frac{c_5}{2\sqrt{c_4 + c_5\mathcal{A}_{2_{MIN}}}} - c_3\right|, \qquad (6.372)$$

and where $\mathcal{D}_{2_{MAX}}$ is given by

$$\mathcal{D}_{2_{MAX}} = \left|\frac{c_5}{2\sqrt{c_4 + c_5\left(\tilde{\mathrm{h}}_1 + z_1^*\right)}} - c_3\right|_{MAX} = \left|\frac{c_5}{2\sqrt{c_4 + c_5\mathcal{B}_{2_{MIN}}}} - c_3\right|. \qquad (6.373)$$

Recalling that $\mathcal{A}_{2_{MIN}}$ and $\mathcal{B}_{2_{MIN}}$ were previously defined in Eqns. (6.330) and (6.331), respectively, therefore, reducing Eqns. (6.372) and (6.373), such

$$\mathcal{D}_{1_{MAX}} = \left|\frac{c_5}{2\sqrt{c_4 + c_5\left(\tilde{z}_1 + z_1^*\right)}} - c_3\right|_{MAX} = \left|\frac{c_5}{2\sqrt{c_4 + c_5 z_{1_{MIN}}}} - c_3\right|, \tag{6.374}$$

where $z_{1_{MIN}}$ represents the minimum collective pitch angle, which is defined in Table 2.3, and $\mathcal{D}_{2_{MAX}}$ is given by

$$\mathcal{D}_{2_{MAX}} = \left|\frac{c_5}{2\sqrt{c_4 + c_5\left(\tilde{\mathrm{h}}_1 + z_1^*\right)}} - c_3\right|_{MAX} = \left|\frac{c_5}{2\sqrt{c_4 + c_5\left(\tilde{\mathrm{h}}_1 + z_1^*\right)_{MIN}}} - c_3\right|, \tag{6.375}$$

where as seen previously

$$\left(\tilde{\mathrm{h}}_1 + z_1^*\right)_{MIN} = s_2\left[\left(1 + \sqrt{s_3\tilde{v}(\tilde{\boldsymbol{\chi}})}\right)^2 - 1\right]_{MIN} = s_2\left[\left(1 + \sqrt{s_3\tilde{v}_{MIN}(\tilde{\boldsymbol{\chi}})}\right)^2 - 1\right], \tag{6.376}$$

with $\tilde{v}_{MIN}$ given by Eq. (6.133). Therefore, using Eq. (6.369) reduces inequality (6.314) as

$$\begin{aligned}
&\left(\frac{\partial V_1(\tilde{\boldsymbol{\chi}})}{\partial\tilde{\boldsymbol{\chi}}}\right)^T\left[\tilde{\boldsymbol{F}}(\tilde{\boldsymbol{\chi}},\tilde{\boldsymbol{z}}) - \tilde{\boldsymbol{F}}(\tilde{\boldsymbol{\chi}},\tilde{\mathbf{h}}(\tilde{\boldsymbol{\chi}}))\right] \\
=\;& \mathcal{V}_1\tilde{x}\left[a_{10}(\tilde{x}+x^*)^2\sin\left(\frac{\mathcal{A}_2-\mathcal{B}_2}{2}\right)\cos\left(\frac{\mathcal{A}_2+\mathcal{B}_2}{2}\right)\right] \\
+\;& (\tilde{x}+x^*)^2\left|(\mathcal{V}_3\tilde{y}_1+\mathcal{V}_4\tilde{y}_2)\left[c_3\hat{z}_1 - \left(\sqrt{c_4+c_5\mathcal{A}_2} - \sqrt{c_4+c_5\mathcal{B}_2}\right)\right]\right| \\
\leq\;& |s_6\mathcal{V}_1\tilde{x}\,|\hat{z}_1|| + \mathcal{D}_{MAX}\left(\tilde{x}+x^*\right)^2|(\mathcal{V}_3\tilde{y}_1+\mathcal{V}_4\tilde{y}_2)\,|\hat{z}_1||\,,
\end{aligned} \tag{6.377}$$

where similarly as seen previously, inequality (6.377) can be further simplified by identifying that $(\tilde{x} + x^*) \triangleq x$, and identifying that, as seen in Table 2.3, $x_{MAX} \geq x \geq x_{MIN}$, therefore allowing to rewrite inequality (6.377) as

$$\begin{aligned}
&\left(\frac{\partial V_1(\tilde{\boldsymbol{\chi}})}{\partial\tilde{\boldsymbol{\chi}}}\right)^T\left[\tilde{\boldsymbol{F}}(\tilde{\boldsymbol{\chi}},\tilde{\boldsymbol{z}}) - \tilde{\boldsymbol{F}}(\tilde{\boldsymbol{\chi}},\tilde{\mathbf{h}}(\tilde{\boldsymbol{\chi}}))\right] \\
=\;& \mathcal{V}_1\tilde{x}\left[a_{10}(\tilde{x}+x^*)^2\sin\left(\frac{\mathcal{A}_2-\mathcal{B}_2}{2}\right)\cos\left(\frac{\mathcal{A}_2+\mathcal{B}_2}{2}\right)\right] \\
+\;& (\tilde{x}+x^*)^2\left|(\mathcal{V}_3\tilde{y}_1+\mathcal{V}_4\tilde{y}_2)\left[c_3\hat{z}_1 - \left(\sqrt{c_4+c_5\mathcal{A}_2} - \sqrt{c_4+c_5\mathcal{B}_2}\right)\right]\right| \\
\leq\;& |s_6\mathcal{V}_1\tilde{x}\,|\hat{z}_1|| + \mathcal{D}_{MAX}\left(\tilde{x}+x^*\right)^2|(\mathcal{V}_3\tilde{y}_1+\mathcal{V}_4\tilde{y}_2)\,|\hat{z}_1|| \\
\leq\;& s_7\,|\tilde{x}\hat{z}_1| + \mathcal{D}_{MAX}x_{MAX}^2\,|(\mathcal{V}_3\tilde{y}_1+\mathcal{V}_4\tilde{y}_2)\,|\hat{z}_1|| \\
\leq\;& s_7\,|\tilde{x}\hat{z}_1| + s_8\,|\tilde{y}_1\hat{z}_1| + s_9\,|\tilde{y}_2\hat{z}_1|\,,
\end{aligned} \tag{6.378}$$

with

$$s_7 = s_6\mathcal{V}_1 = x_{MAX}^2\mathcal{K}_2\,|a_{10}|\,(1-d_1)P_S, \tag{6.379}$$
$$s_8 = \mathcal{V}_3\mathcal{D}_{MAX}x_{MAX}^2 = d_1 p_{f_2}\mathcal{D}_{MAX}x_{MAX}^2, \tag{6.380}$$
$$s_9 = \mathcal{V}_4\mathcal{D}_{MAX}x_{MAX}^2 = d_1 p_{f_3}\mathcal{D}_{MAX}x_{MAX}^2, \tag{6.381}$$

where $\mathcal{V}_1$, $\mathcal{V}_2$, $\mathcal{V}_3$ and $\mathcal{V}_4$ are defined in Eqns. (6.242), (6.243), (6.244) and (6.245) respectively, and s_6 is defined in Eq. (6.336). Recalling the definition of P_S, Eq. (6.40), and the definitions of p_{f_1}, and p_{f_2}, Eqns. (6.43) and (6.44), respectively, allows to rewrite Eqns. (6.379), (6.380) and (6.381) as

$$s_7 = \tilde{s}_7 Q_S, \tag{6.382}$$
$$s_8 = \tilde{s}_8 q_{f_1}, \tag{6.383}$$
$$s_9 = \tilde{s}_9 q_{f_1} + \tilde{s}_{10} q_{f_2}, \tag{6.384}$$

where

$$\begin{aligned}
\tilde{s}_7 &= x_{MAX}^2\mathcal{K}_2\,|a_{10}|\,(1-d_1)\frac{1}{2b_x}, && (6.385)\\
\tilde{s}_8 &= d_1\mathcal{D}_{MAX}x_{MAX}^2C_{f_3} = d_1\mathcal{D}_{MAX}x_{MAX}^2\frac{1}{2\tilde{b}_{y_1}}, && (6.386)\\
\tilde{s}_9 &= d_1\mathcal{D}_{MAX}x_{MAX}^2C_{f_4} = d_1\mathcal{D}_{MAX}x_{MAX}^2\frac{c_1}{2\tilde{b}_{y_1}\tilde{b}_{y_2}}, && (6.387)\\
\tilde{s}_{10} &= d_1\mathcal{D}_{MAX}x_{MAX}^2C_{f_5} = d_1\mathcal{D}_{MAX}x_{MAX}^2\frac{\tilde{b}_{y_1}}{2\tilde{b}_{y_1}\tilde{b}_{y_2}}. && (6.388)
\end{aligned}$$

Using Eqns. (6.382), (6.383) and (6.384) reduces the original inequality (6.314) to

$$\begin{aligned}
&\left(\frac{\partial V_1(\tilde{\boldsymbol{\chi}})}{\partial\tilde{\boldsymbol{\chi}}}\right)^T\left[\tilde{\boldsymbol{F}}(\tilde{\boldsymbol{\chi}},\tilde{\boldsymbol{z}})-\tilde{\boldsymbol{F}}(\tilde{\boldsymbol{\chi}},\tilde{\mathbf{h}}(\tilde{\boldsymbol{\chi}}))\right]\\
\leq\;& s_7\,|\tilde{x}\hat{z}_1| + s_8\,|\tilde{y}_1\hat{z}_1| + s_9\,|\tilde{y}_2\hat{z}_1| \leq \beta_3\psi_2(\tilde{\boldsymbol{\chi}})\phi_2(\hat{\boldsymbol{z}}), && (6.389)
\end{aligned}$$

where recalling the selected comparison functions $\psi_2(\tilde{\boldsymbol{\chi}})$ and $\phi_2(\hat{\boldsymbol{z}})$, Eqns. (6.283) and (6.313), it can be observed that satisfying inequality (6.389) is reduced to prove that

$$s_7\,|\tilde{x}\hat{z}_1| + s_8\,|\tilde{y}_1\hat{z}_1| + s_9\,|\tilde{y}_2\hat{z}_1| \leq \beta_3\left(\tilde{\boldsymbol{\chi}}^T\boldsymbol{\mathcal{R}}\tilde{\boldsymbol{\chi}}\right)^{\frac{1}{2}}\left(\hat{\boldsymbol{z}}^T\tilde{\boldsymbol{Q}}_{\boldsymbol{U}}\hat{\boldsymbol{z}}\right)^{\frac{1}{2}}. \qquad (6.390)$$

In order to obtain the constant β_3 that guarantees the fulfillment of inequality (6.314), that is, fulfilling Assumption 5.5.9 for helicopter Σ_{SFU} system, let square both sides of inequality (6.390), resulting in

$$\left(s_7\,|\tilde{x}\hat{z}_1| + s_8\,|\tilde{y}_1\hat{z}_1| + s_9\,|\tilde{y}_2\hat{z}_1|\right)^2 \leq \beta_3^2\left(\tilde{\boldsymbol{\chi}}^T\boldsymbol{\mathcal{R}}\tilde{\boldsymbol{\chi}}\right)\left(\hat{\boldsymbol{z}}^T\tilde{\boldsymbol{Q}}_{\boldsymbol{U}}\hat{\boldsymbol{z}}\right), \qquad (6.391)$$

expanding the left hand-side of inequality (6.391) results in

$$\begin{aligned}
&\left(s_7\,|\tilde{x}\hat{z}_1| + s_8\,|\tilde{y}_1\hat{z}_1| + s_9\,|\tilde{y}_2\hat{z}_1|\right)^2\\
=\;& s_7^2\tilde{x}^2\hat{z}_1^2 + s_8^2\tilde{y}_1^2\hat{z}_1^2 + s_9^2\tilde{y}_2^2\hat{z}_1^2 + 2s_7s_8\,|\tilde{x}\hat{y}_1|\,\hat{z}_1^2 + 2s_7s_9\,|\tilde{x}\hat{y}_2|\,\hat{z}_1^2 + 2s_8s_9\,|\tilde{y}_1\hat{y}_2|\,\hat{z}_1^2. && (6.392)
\end{aligned}$$

Inequality (6.392) can be further simplified employing Young's inequality, Eq. (6.177), permitting to rewrite Eq. (6.416) as

$$\begin{aligned}
& s_7^2\tilde{x}^2\hat{z}_1^2 + s_8^2\tilde{y}_1^2\hat{z}_1^2 + s_9^2\tilde{y}_2^2\hat{z}_1^2 + 2s_7s_8\,|\tilde{x}\hat{y}_1|\,\hat{z}_1^2 + 2s_7s_9\,|\tilde{x}\hat{y}_2|\,\hat{z}_1^2 + 2s_8s_9\,|\tilde{y}_1\hat{y}_2|\,\hat{z}_1^2 && (6.393)\\
\leq\;& s_7^2\tilde{x}^2\hat{z}_1^2 + s_8^2\tilde{y}_1^2\hat{z}_1^2 + s_9^2\tilde{y}_2^2\hat{z}_1^2 + 2s_7s_8\left(\frac{\tilde{x}^2+\tilde{y}_1^2}{2}\right)\hat{z}_1^2 + 2s_7s_9\left(\frac{\tilde{x}^2+\tilde{y}_2^2}{2}\right)\hat{z}_1^2 && (6.394)\\
+\;& 2s_8s_9\left(\frac{\tilde{y}_1^2+\tilde{y}_2^2}{2}\right)\hat{z}_1^2 && (6.395)\\
=\;& \hat{z}_1^2\left(\mathcal{L}_1\tilde{x}^2 + \mathcal{L}_2\tilde{y}_1^2 + \mathcal{L}_3\tilde{y}_2^2\right) = \hat{z}_1^2\left(\tilde{\boldsymbol{\chi}}^T\boldsymbol{\mathcal{L}}\tilde{\boldsymbol{\chi}}\right), && (6.396)
\end{aligned}$$

where $\mathcal{L}$ is a symmetric positive definite matrix, defined by

$$\boldsymbol{\mathcal{L}} = \begin{pmatrix} \mathcal{L}_1 & 0 & 0\\ 0 & \mathcal{L}_2 & 0\\ 0 & 0 & \mathcal{L}_3 \end{pmatrix}, \qquad (6.397)$$

with

$$\begin{aligned}
\mathcal{L}_1 &= s_7^2 + s_7s_8 + s_7s_9, && (6.398)\\
\mathcal{L}_2 &= s_8^2 + s_7s_8 + s_8s_9, && (6.399)\\
\mathcal{L}_3 &= s_9^2 + s_7s_9 + s_8s_9, && (6.400)
\end{aligned}$$

where recalling Eqns. (6.382), (6.383) and (6.384), for the definitions of s_7, s_8, and s_9 respectively, thus allowing to rewrite Eqns. (6.398), (6.399), and (6.400) as a function of the *stability parameters* such

$$\mathcal{L}_1 = \mathcal{L}_{1_a} Q_S^2 + \mathcal{L}_{1_b} Q_S q_{f_1} + \mathcal{L}_{1_c} Q_S q_{f_2}, \quad (6.401)$$
$$\mathcal{L}_2 = \mathcal{L}_{2_a} q_{f_1}^2 + \mathcal{L}_{2_b} Q_S q_{f_1} + \mathcal{L}_{2_c} q_{f_1} q_{f_2}, \quad (6.402)$$
$$\mathcal{L}_3 = \mathcal{L}_{3_a} q_{f_1}^2 + \mathcal{L}_{3_b} q_{f_2}^2 + \mathcal{L}_{3_c} Q_S q_{f_1} + \mathcal{L}_{3_d} Q_S q_{f_2} + \mathcal{L}_{3_e} q_{f_1} q_{f_2}, \quad (6.403)$$

where

$$\mathcal{L}_{1_a} = \tilde{s}_7^2, \quad (6.404)$$
$$\mathcal{L}_{1_b} = \tilde{s}_7\tilde{s}_8 + \tilde{s}_7\tilde{s}_9, \quad (6.405)$$
$$\mathcal{L}_{1_b} = \tilde{s}_7\tilde{s}_{10}, \quad (6.406)$$
$$\mathcal{L}_{2_a} = \tilde{s}_8^2 + \tilde{s}_8\tilde{s}_9, \quad (6.407)$$
$$\mathcal{L}_{2_b} = \tilde{s}_7\tilde{s}_8, \quad (6.408)$$
$$\mathcal{L}_{2_c} = \tilde{s}_8\tilde{s}_{10}, \quad (6.409)$$
$$\mathcal{L}_{3_a} = \tilde{s}_9^2 + \tilde{s}_8\tilde{s}_9, \quad (6.410)$$
$$\mathcal{L}_{3_b} = \tilde{s}_{10}^2, \quad (6.411)$$
$$\mathcal{L}_{3_c} = \tilde{s}_7\tilde{s}_9, \quad (6.412)$$
$$\mathcal{L}_{3_d} = \tilde{s}_7\tilde{s}_{10}, \quad (6.413)$$
$$\mathcal{L}_{3_e} = 2\tilde{s}_9\tilde{s}_{10} + \tilde{s}_8\tilde{s}_{10}, \quad (6.414)$$

with $\tilde{s}_7$, $\tilde{s}_8$, $\tilde{s}_9$, and $\tilde{s}_{10}$, defined in Eqns. (6.385), (6.386), (6.387), and (6.388), respectively. With this in mind, let proceed to expand the right-hand side of inequality (6.391) resulting in

$$\beta_3^2 \left(\tilde{\boldsymbol{\chi}}^T \boldsymbol{\mathcal{R}} \tilde{\boldsymbol{\chi}}\right) \left(\hat{\boldsymbol{z}}^T \tilde{\boldsymbol{Q}}_{\boldsymbol{U}} \hat{\boldsymbol{z}}\right) = \beta_3^2 \left(\tilde{q}_{u_1}\hat{z}_1^2 + \tilde{q}_{u_2}\hat{z}_2^2\right) \left(\mathcal{R}_1\tilde{x}^2 + \mathcal{R}_2\tilde{y}_1^2 + \mathcal{R}_3\tilde{y}_2^2\right), \quad (6.415)$$

therefore using both Eqns. (6.396) and (6.415), into inequality (6.390) results in

$$\hat{z}_1^2 \left(\mathcal{L}_1\tilde{x}^2 + \mathcal{L}_2\tilde{y}_1^2 + \mathcal{L}_3\tilde{y}_2^2\right) \leq \beta_3^2 \left(\tilde{q}_{u_1}\hat{z}_1^2 + \tilde{q}_{u_2}\hat{z}_2^2\right) \left(\mathcal{R}_1\tilde{x}^2 + \mathcal{R}_2\tilde{y}_1^2 + \mathcal{R}_3\tilde{y}_2^2\right). \quad (6.416)$$

It can be shown that the right-hand side of inequality (6.416) can be rewritten as

$$\beta_3^2\tilde{q}_{u_1}\hat{z}_1^2 \left(\mathcal{R}_1\tilde{x}^2 + \mathcal{R}_2\tilde{y}_1^2 + \mathcal{R}_3\tilde{y}_2^2\right) \leq \beta_3^2 \left(\tilde{q}_{u_1}\hat{z}_1^2 + \tilde{q}_{u_2}\hat{z}_2^2\right) \left(\mathcal{R}_1\tilde{x}^2 + \mathcal{R}_2\tilde{y}_1^2 + \mathcal{R}_3\tilde{y}_2^2\right), \quad (6.417)$$

therefore reducing the fulfillment of the original inequality (6.314) to find the β_3 constant that satisfies the inequality given by

$$\hat{z}_1^2 \left(\mathcal{L}_1\tilde{x}^2 + \mathcal{L}_2\tilde{y}_1^2 + \mathcal{L}_3\tilde{y}_2^2\right) \leq \beta_3^2\tilde{q}_{u_1}\hat{z}_1^2 \left(\mathcal{R}_1\tilde{x}^2 + \mathcal{R}_2\tilde{y}_1^2 + \mathcal{R}_3\tilde{y}_2^2\right), \quad (6.418)$$

with β_3 given by

$$\beta_3 = \max\left(\beta_{3_a}, \beta_{3_b}, \beta_{3_c}\right), \quad (6.419)$$

where $\tilde{q}_{u_1} = q_{u_1}/2$, and $\tilde{q}_{u_2} = q_{u_2}/2$, thus resulting in

$$\beta_{3_a} \geq \sqrt{\frac{2\mathcal{L}_1}{q_{u_1}\mathcal{R}_1}}, \quad (6.420)$$
$$\beta_{3_b} \geq \sqrt{\frac{2\mathcal{L}_2}{q_{u_1}\mathcal{R}_2}}, \quad (6.421)$$
$$\beta_{3_c} \geq \sqrt{\frac{2\mathcal{L}_3}{q_{u_1}\mathcal{R}_3}}, \quad (6.422)$$

with $\mathcal{R}_1$, $\mathcal{R}_2$, and $\mathcal{R}_3$ given in Eqns. (6.272), (6.273), and (6.274) respectively, and $\mathcal{L}_1$, $\mathcal{L}_2$, and $\mathcal{L}_3$ are given in (6.401), 6.402), and (6.403), thus resulting in

$$\beta_{3_a} \geq \sqrt{\frac{2\left(\mathcal{L}_{1_a}Q_S^2 + \mathcal{L}_{1_b}Q_S q_{f_1} + \mathcal{L}_{1_c}Q_S q_{f_2}\right)}{\tilde{r}_1 Q_S q_{u_1}}}, \tag{6.423}$$

$$\beta_{3_b} \geq \sqrt{\frac{2\left(\mathcal{L}_{2_a}q_{f_1}^2 + \mathcal{L}_{2_b}Q_S q_{f_1} + \mathcal{L}_{2_c}q_{f_1}q_{f_2}\right)}{\left(\tilde{r}_2 q_{f_1} - \tilde{r}_3 Q_S\right) q_{u_1}}}, \tag{6.424}$$

$$\beta_{3_c} \geq \sqrt{\frac{2\left(\mathcal{L}_{3_a}q_{f_1}^2 + \mathcal{L}_{3_b}q_{f_2}^2 + \mathcal{L}_{3_c}Q_S q_{f_1} + \mathcal{L}_{3_d}Q_S q_{f_2} + \mathcal{L}_{3_e}q_{f_1}q_{f_2}\right)}{\left(\tilde{r}_2 q_{f_2} - \tilde{r}_4 Q_S\right) q_{u_1}}}. \tag{6.425}$$

In order to obtain a single relation for β_3, let recall the relation Eq. (6.294) that defines the relation between the *stability parameters* q_{f_1} and q_{f_2}, by defining $q_{f_2} = \tilde{Q}_{F21}q_{f_1}$, allowing to rewrite Eqns. (6.420), (6.421), and (6.422) as

$$\beta_{3_a} \geq \sqrt{\frac{2\left(\mathcal{L}_{1_a}Q_S^2 + \left(\mathcal{L}_{1_b} + \tilde{Q}_{F21}\mathcal{L}_{1_c}\right) Q_S q_{f_1}\right)}{\tilde{r}_1 Q_S q_{u_1}}}, \tag{6.426}$$

$$\beta_{3_b} \geq \sqrt{\frac{2\left(\mathcal{L}_{2_a}q_{f_1}^2 + \left(\mathcal{L}_{2_b} + \tilde{Q}_{F21}\mathcal{L}_{2_c}\right) Q_S q_{f_1}\right)}{\left(\tilde{r}_2 q_{f_1} - \tilde{r}_3 Q_S\right) q_{u_1}}}, \tag{6.427}$$

$$\beta_{3_c} \geq \sqrt{\frac{2\left[\left(\mathcal{L}_{3_a} + \tilde{Q}_{F_{21}}^2\mathcal{L}_{3_b} + \tilde{Q}_{F21}\mathcal{L}_{3_e}\right) q_{f_1}^2 + \left(\mathcal{L}_{3_c} + \mathcal{L}_{3_d}\right) Q_S q_{f_1}\right]}{\left(\tilde{r}_2 \tilde{Q}_{F21} q_{f_1} - \tilde{r}_4 Q_S\right) q_{u_1}}}. \tag{6.428}$$

Recalling also the expression in Eq. (6.289), $q_{f_1} = \tilde{Q}_{SF}Q_S$, permits to rewrite Eqns. (6.429), (6.430), and (6.431) such

$$\beta_{3_a} \geq \mathcal{B}_{3_a}\sqrt{\frac{Q_S}{q_{u_1}}}, \tag{6.429}$$

$$\beta_{3_b} \geq \mathcal{B}_{3_b}\sqrt{\frac{Q_S}{q_{u_1}}}, \tag{6.430}$$

$$\beta_{3_c} \geq \mathcal{B}_{3_c}\sqrt{\frac{Q_S}{q_{u_1}}}, \tag{6.431}$$

where

$$\mathcal{B}_{3_a} = \sqrt{\frac{2\left[\mathcal{L}_{1_a} + \left(\mathcal{L}_{1_b} + \tilde{Q}_{F_{21}}\mathcal{L}_{1_c}\right)\tilde{Q}_{SF}\right]}{\tilde{r}_1}}, \tag{6.432}$$

$$\mathcal{B}_{3_b} = \sqrt{\frac{2\left(\mathcal{L}_{2_a}\tilde{Q}_{SF}^2 + \left(\mathcal{L}_{2_b} + \tilde{Q}_{F21}\mathcal{L}_{2_c}\right)\tilde{Q}_{SF}\right)}{\tilde{r}_2\tilde{Q}_{SF} - \tilde{r}_3}}, \tag{6.433}$$

$$\mathcal{B}_{3_c} = \sqrt{\frac{2\left[\left(\mathcal{L}_{3_a} + \tilde{Q}_{F_{21}}^2\mathcal{L}_{3_b} + \tilde{Q}_{F21}\mathcal{L}_{3_e}\right)\tilde{Q}_{SF}^2 + \left(\mathcal{L}_{3_c} + \mathcal{L}_{3_d}\right)\tilde{Q}_{SF}\right]}{\tilde{r}_2\tilde{Q}_{F21}\tilde{Q}_{SF} - \tilde{r}_4}}, \tag{6.434}$$

therefore permitting easily to prove that for the physical parameters here used, and the selected target dynamic parameters, $\mathcal{B}_{3_b} > \mathcal{B}_{3_c} > \mathcal{B}_{3_a}$. This is true as long as d_1 is selected such $d_1 \in (0.0543, 0.6788)$ as it can be seen in Figure 6.2, where it is analyzed the variation of the parameters $\mathcal{B}_{3_a}$, $\mathcal{B}_{3_b}$, and $\mathcal{B}_{3_c}$, Eqns. (6.432), (6.433), and (6.434), respectively, as the unspecified parameter $d_1^\bigstar$ is varied in the interval of interest $d_1 \in (0, 1)$, with $\mathcal{B}_{3_b}$ denoted by the solid line.

Similarly, and recalling the definition of $\tilde{Q}_{SF}$, Eq. (6.288), Figure 6.3 shows the variation of $\mathcal{B}_{3_a}$, $\mathcal{B}_{3_b}$, and $\mathcal{B}_{3_c}$ as a function of δ_1, and where it can be seen that for the range of interest $\delta_1 \in (1, 1.5)$, $\mathcal{B}_{3_b}$, Eq. (6.433), is the largest of the three parameters. Figure 6.4 also shows the variation of $\mathcal{B}_{3_a}$, $\mathcal{B}_{3_b}$, and $\mathcal{B}_{3_c}$ as a function of $d_1^\bigstar$ and δ_1. Therefore, by selecting $d_1^\bigstar \in (0.0543, 0.6788)$, Eq. (6.419) reduces by selecting $\mathcal{B}_{3_b}$, such

$$\beta_3 \geq \beta_{3_b} = \sqrt{\frac{2\left(\mathcal{L}_{2_a}\tilde{Q}_{SF}^2 + \left(\mathcal{L}_{2_b} + \tilde{Q}_{F_{21}}\mathcal{L}_{2_c}\right)\tilde{Q}_{SF}\right)}{\tilde{r}_2\tilde{Q}_{SF} - \tilde{r}_3}}\sqrt{\frac{Q_S}{q_{u_1}}}. \tag{6.435}$$

6.5.5 Proof of Assumption 5.5.10: Second Interconnection Condition for the Helicopter Σ_{SFU} System

The second interconnection condition is defined by the inequality

$$\left(\frac{\partial V_U(\hat{\boldsymbol{z}})}{\partial \tilde{\boldsymbol{\chi}}}\right)^T \tilde{\boldsymbol{F}}\left(\tilde{\boldsymbol{\chi}}, \tilde{\boldsymbol{z}}\right) \leq \gamma_2\phi_2^2(\hat{\boldsymbol{z}}) + \beta_4\psi_2(\tilde{\boldsymbol{\chi}})\phi_2(\hat{\boldsymbol{z}}), \tag{6.436}$$

Inequality (6.436) can be rewritten by adding and subtracting $\tilde{\boldsymbol{F}}(\tilde{\boldsymbol{\chi}}, \tilde{\mathrm{h}}(\tilde{\boldsymbol{\chi}}))$ to the $\tilde{\boldsymbol{F}}(\tilde{\boldsymbol{\chi}}, \tilde{\boldsymbol{z}})$ in the left-hand side of (6.436) resulting in

$$\begin{aligned}\frac{\partial V_U}{\partial \tilde{\boldsymbol{\chi}}}\tilde{\boldsymbol{F}}(\tilde{\boldsymbol{\chi}}, \tilde{\boldsymbol{z}}) &\leq \frac{\partial V_U}{\partial \tilde{\boldsymbol{\chi}}}\tilde{\boldsymbol{F}}(\tilde{\boldsymbol{\chi}}, \tilde{\mathrm{h}}(\tilde{\boldsymbol{\chi}})) + \frac{\partial V_U}{\partial \tilde{\boldsymbol{\chi}}}\left[\tilde{\boldsymbol{F}}(\tilde{\boldsymbol{\chi}}, \tilde{\boldsymbol{z}}) - \tilde{\boldsymbol{F}}(\tilde{\boldsymbol{\chi}}, \tilde{\mathrm{h}}(\tilde{\boldsymbol{\chi}}))\right] \\ &\leq \beta_4\psi_2(\tilde{\boldsymbol{\chi}})\phi_2(\hat{\boldsymbol{z}}) + \gamma_2\phi_2^2(\hat{\boldsymbol{z}}),\end{aligned} \tag{6.437}$$

therefore, inequality (6.437) can be fulfilled by splitting in two inequalities given by

$$\frac{\partial V_U}{\partial \tilde{\boldsymbol{\chi}}}\left[\tilde{\boldsymbol{F}}(\tilde{\boldsymbol{\chi}}, \tilde{\boldsymbol{z}}) - \tilde{\boldsymbol{F}}(\tilde{\boldsymbol{\chi}}, \tilde{\mathrm{h}}(\tilde{\boldsymbol{\chi}}))\right] \leq \gamma_2\phi_2^2(\hat{\boldsymbol{z}}) \tag{6.438}$$

$$\frac{\partial V_U}{\partial \tilde{\boldsymbol{\chi}}}\tilde{\boldsymbol{F}}(\tilde{\boldsymbol{\chi}}, \tilde{\mathrm{h}}(\tilde{\boldsymbol{\chi}})) \leq \beta_4\psi_2(\tilde{\boldsymbol{\chi}})\phi_2(\hat{\boldsymbol{z}}), \tag{6.439}$$

therefore, inequality (6.436) can be proved, if both new resulting inequalities, Eqns. (6.438) and (6.439), are fulfilled. Considering the first inequality, Eq. (6.438), it can be seen that the left-hand side of inequality (6.438) is defined by

$$\left[\frac{\partial V_U}{\partial \tilde{\boldsymbol{\chi}}}\right] = \begin{bmatrix}\dfrac{\partial V_U}{\partial x} \\[2ex] \dfrac{\partial V_U}{\partial \tilde{y}}\end{bmatrix} = \begin{bmatrix}\dfrac{\partial V_U}{\partial \tilde{x}} \\[2ex] \dfrac{\partial V_U}{\partial \tilde{y}_1} \\[2ex] \dfrac{\partial V_U}{\partial \tilde{y}_2}\end{bmatrix}, \tag{6.440}$$

where

$$\frac{\partial V_U}{\partial \tilde{x}} = -\left(p_{u_1}\hat{z}_1 + p_{u_2}\hat{z}_2\right)\frac{\partial \tilde{\mathrm{h}}_1(\tilde{\boldsymbol{\chi}})}{\partial \tilde{x}}, \tag{6.441}$$

$$\frac{\partial V_U}{\partial \tilde{y}_1} = -\left(p_{u_1}\hat{z}_1 + p_{u_2}\hat{z}_2\right)\frac{\partial \tilde{\mathrm{h}}_1(\tilde{\boldsymbol{\chi}})}{\partial \tilde{y}_1}, \tag{6.442}$$

$$\frac{\partial V_U}{\partial \tilde{y}_2} = -\left(p_{u_1}\hat{z}_1 + p_{u_2}\hat{z}_2\right)\frac{\partial \tilde{\mathrm{h}}_1(\tilde{\boldsymbol{\chi}})}{\partial \tilde{y}_2}, \tag{6.443}$$

with

$$\begin{aligned}\hat{z}_1 &= \tilde{z}_1 - \tilde{\mathrm{h}}_1\left(\boldsymbol{\chi}\right) \\ &= \tilde{z}_1 - \left\{s_2\left[\left(1 + \sqrt{s_3\tilde{v}}\right)^2 - 1\right] - z_1^*\right\},\end{aligned} \tag{6.444}$$

$$\hat{z}_2 = \tilde{z}_2 - \tilde{\mathrm{h}}_2\left(\boldsymbol{\chi}\right) = \tilde{z}_2, \tag{6.445}$$

and where Eqns. (6.441), (6.442), and (6.443) can be simplified by introducing

$$\hat{\mathcal{P}} = \left(p_{u_1}\hat{z}_1 + p_{u_2}\hat{z}_2\right), \tag{6.446}$$

resulting in

$$\begin{aligned}
\frac{\partial V_U}{\partial \tilde{x}} &= -\hat{\mathcal{P}}\frac{\partial \tilde{\mathrm{h}}_1(\tilde{\boldsymbol{\chi}})}{\partial \tilde{x}}, && (6.447)\\
\frac{\partial V_U}{\partial \tilde{y}_1} &= -\hat{\mathcal{P}}\frac{\partial \tilde{\mathrm{h}}_1(\tilde{\boldsymbol{\chi}})}{\partial \tilde{y}_1}, && (6.448)\\
\frac{\partial V_U}{\partial \tilde{y}_2} &= -\hat{\mathcal{P}}\frac{\partial \tilde{\mathrm{h}}_1(\tilde{\boldsymbol{\chi}})}{\partial \tilde{y}_2}, && (6.449)
\end{aligned}$$

where

$$\begin{aligned}
\frac{\partial \tilde{\mathrm{h}}_1(\tilde{\boldsymbol{\chi}})}{\partial \tilde{x}} &= s_2 s_3 \frac{1+R}{R}\frac{\partial \tilde{v}(\tilde{\boldsymbol{\chi}})}{\partial \tilde{x}}, && (6.450)\\
\frac{\partial \tilde{\mathrm{h}}_1(\tilde{\boldsymbol{\chi}})}{\partial \tilde{x}} &= s_2 s_3 \frac{1+R}{R}\frac{\partial \tilde{v}(\tilde{\boldsymbol{\chi}})}{\partial \tilde{y}_1}, && (6.451)\\
\frac{\partial \tilde{\mathrm{h}}_1(\tilde{\boldsymbol{\chi}})}{\partial \tilde{x}} &= s_2 s_3 \frac{1+R}{R}\frac{\partial \tilde{v}(\tilde{\boldsymbol{\chi}})}{\partial \tilde{y}_2}, && (6.452)
\end{aligned}$$

with

$$s_2 s_3 = \frac{4a_2 a_3}{a_4^2 \varepsilon_1}, \tag{6.453}$$

and

$$R = \sqrt{s_3 \tilde{v}(\tilde{\boldsymbol{\chi}})}, \tag{6.454}$$

where

$$\tilde{v}(\tilde{\boldsymbol{\chi}}) = -\frac{a_9\tilde{y}_2^2 + (a_9 + \tilde{b}_{y_2})\tilde{y}_2 + \tilde{b}_{y_1}\tilde{y}_1 + c_6}{(\tilde{x}+x^*)^2}, \tag{6.455}$$

therefore defining

$$\begin{aligned}
\frac{\partial \tilde{v}(\tilde{\boldsymbol{\chi}})}{\partial \tilde{x}} &= -2\frac{\tilde{v}(\tilde{\boldsymbol{\chi}})}{\tilde{x}+x^*} = \frac{2\left(a_9\tilde{y}_2^2 + (a_9 + \tilde{b}_{y_2})\tilde{y}_2 + \tilde{b}_{y_1}\tilde{y}_1 + c_6\right)}{(\tilde{x}+x^*)^3}, && (6.456)\\
\frac{\partial \tilde{v}(\tilde{\boldsymbol{\chi}})}{\partial \tilde{y}_1} &= -\frac{\tilde{b}_{y_1}}{(\tilde{x}+x^*)^2}, && (6.457)\\
\frac{\partial \tilde{v}(\tilde{\boldsymbol{\chi}})}{\partial \tilde{y}_2} &= -\frac{2a_9\tilde{y}_2 + a_9 + \tilde{b}_{y_2}}{(\tilde{x}+x^*)^2}. && (6.458)
\end{aligned}$$

For completeness let also define

$$\begin{aligned}
\tilde{v}_{\tilde{x}} &= -\frac{\partial \tilde{\mathrm{h}}_1(\tilde{\boldsymbol{\chi}})}{\partial \tilde{x}} = s_2 s_3 \frac{1+R}{R}\left(2\frac{\tilde{v}(\tilde{\boldsymbol{\chi}})}{\tilde{x}+x^*}\right), && (6.459)\\
\tilde{v}_{\tilde{y}_1} &= -\frac{\partial \tilde{\mathrm{h}}_1(\tilde{\boldsymbol{\chi}})}{\partial \tilde{y}_1} = s_2 s_3 \frac{1+R}{R}\left(\frac{\tilde{b}_{y_1}}{(\tilde{x}+x^*)^2}\right), && (6.460)\\
\tilde{v}_{\tilde{y}_2} &= -\frac{\partial \tilde{\mathrm{h}}_1(\tilde{\boldsymbol{\chi}})}{\partial \tilde{y}_2} = s_2 s_3 \frac{1+R}{R}\left(\frac{2a_9\tilde{y}_2 + a_9 + \tilde{b}_{y_2}}{(\tilde{x}+x^*)^2}\right), && (6.461)
\end{aligned}$$

therefore rewriting Eqns. (6.462), (6.463), and (6.464) as

$$\begin{aligned}
\frac{\partial V_U}{\partial \tilde{x}} &= \hat{\mathcal{P}}\tilde{v}_{\tilde{x}}, && (6.462)\\
\frac{\partial V_U}{\partial \tilde{y}_1} &= \hat{\mathcal{P}}\tilde{v}_{\tilde{y}_1}, && (6.463)
\end{aligned}$$

$$\frac{\partial V_U}{\partial \tilde{y}_2} = \hat{\mathcal{P}}\tilde{v}_{\tilde{y}_2}. \tag{6.464}$$

Recalling that in the left-hand side of inequality (6.438), $\tilde{\boldsymbol{F}}(\tilde{\boldsymbol{\chi}}, \tilde{\boldsymbol{z}}) - \tilde{\boldsymbol{F}}(\tilde{\boldsymbol{\chi}}, \tilde{\mathbf{h}}(\tilde{\boldsymbol{\chi}}))$ was previously defined in Eq. (6.316) as

$$\tilde{\boldsymbol{F}}(\tilde{\boldsymbol{\chi}}, \tilde{\boldsymbol{z}}) - \tilde{\boldsymbol{F}}(\tilde{\boldsymbol{\chi}}, \tilde{\mathbf{h}}(\tilde{\boldsymbol{\chi}})) = \begin{bmatrix} \hat{F}_1 \\ \hat{F}_2 \\ \hat{F}_3 \end{bmatrix} \tag{6.465}$$

with $\hat{F}_1$, $\hat{F}_2$, and $\hat{F}_3$, being defined in Eqns. (6.317), (6.318), and (6.319), respectively, and recalling $\mathcal{A}_2$ and $\mathcal{B}_2$, Eqns. (6.320) and (6.321), respectively, permitting therefore to rewrite the left-hand side of inequality (6.438) as

$$\begin{aligned}
& \frac{\partial V_U}{\partial \tilde{\boldsymbol{\chi}}} \left[\tilde{\boldsymbol{F}}(\tilde{\boldsymbol{\chi}}, \tilde{\boldsymbol{z}}) - \tilde{\boldsymbol{F}}(\tilde{\boldsymbol{\chi}}, \tilde{\mathbf{h}}(\tilde{\boldsymbol{\chi}}))\right] \\
= & \frac{\partial V_U}{\partial \tilde{x}}\hat{F}_1 + \frac{\partial V_U}{\partial \tilde{y}_1}\hat{F}_2 + \frac{\partial V_U}{\partial \tilde{y}_2}\hat{F}_2 \\
= & \hat{\mathcal{P}}\tilde{v}_{\tilde{x}} \left[2a_{10}(\tilde{x} + x^*)^2 \sin\left(\frac{\mathcal{A}_2 - \mathcal{B}_2}{2}\right) \cos\left(\frac{\mathcal{A}_2 + \mathcal{B}_2}{2}\right)\right] \\
+ & \hat{\mathcal{P}}\tilde{v}_{\tilde{y}_2} \left\{(\tilde{x} + x^*)^2 \left[c_3\hat{z}_1 - \left(\sqrt{c_4 + c_5\mathcal{A}_2} - \sqrt{c_4 + c_5\mathcal{B}_2}\right)\right]\right\}. \qquad (6.466)
\end{aligned}$$

Inequality (6.466) can be simplified by recalling that, as proved in Eq. (6.338), the left-hand side of the expanded inequality can be rewritten as

$$2a_{10}(\tilde{x} + x^*)^2 \sin\left(\frac{\mathcal{A}_2 - \mathcal{B}_2}{2}\right) \cos\left(\frac{\mathcal{A}_2 + \mathcal{B}_2}{2}\right) \leq s_6 \left|\hat{z}_1\right|, \tag{6.467}$$

with s_6 being given by Eq. (6.336). Similarly, inequality (6.466) can be further simplified by recalling that as proved in (6.369), the right-hand side of the expanded inequality can be rewritten as

$$c_3\hat{z}_1 - \left(\sqrt{c_4 + c_5\mathcal{A}_2} - \sqrt{c_4 + c_5\mathcal{B}_2}\right) \leq \mathcal{D}_{MAX} \left|\hat{z}_1\right|, \tag{6.468}$$

therefore, using Eqns. (6.467) and (6.468) into inequality (6.466) can be rewritten as

$$\begin{aligned}
& \frac{\partial V_U}{\partial \tilde{\boldsymbol{\chi}}} \left[\tilde{\boldsymbol{F}}(\tilde{\boldsymbol{\chi}}, \tilde{\boldsymbol{z}}) - \tilde{\boldsymbol{F}}(\tilde{\boldsymbol{\chi}}, \tilde{\mathbf{h}}(\tilde{\boldsymbol{\chi}}))\right] = \frac{\partial V_U}{\partial \tilde{x}}\hat{F}_1 + \frac{\partial V_U}{\partial \tilde{y}_1}\hat{F}_2 + \frac{\partial V_U}{\partial \tilde{y}_2}\hat{F}_2 \qquad (6.469) \\
= & \hat{\mathcal{P}}\tilde{v}_{\tilde{x}} \left[2a_{10}(\tilde{x} + x^*)^2 \sin\left(\frac{\mathcal{A}_2 - \mathcal{B}_2}{2}\right) \cos\left(\frac{\mathcal{A}_2 + \mathcal{B}_2}{2}\right)\right] \\
+ & \hat{\mathcal{P}}\tilde{v}_{\tilde{y}_2} \left\{(\tilde{x} + x^*)^2 \left[c_3\hat{z}_1 - \left(\sqrt{c_4 + c_5\mathcal{A}_2} - \sqrt{c_4 + c_5\mathcal{B}_2}\right)\right]\right\} \qquad (6.470) \\
\leq & \left|\hat{\mathcal{P}}\tilde{v}_{\tilde{x}} \left\{2a_{10}(\tilde{x} + x^*)^2 \sin\left(\frac{\mathcal{A}_2 - \mathcal{B}_2}{2}\right) \cos\left(\frac{\mathcal{A}_2 + \mathcal{B}_2}{2}\right)\right\}\right| \\
+ & \left|\hat{\mathcal{P}}\tilde{v}_{\tilde{y}_2} \left\{(\tilde{x} + x^*)^2 \left[c_3\hat{z}_1 - \left(\sqrt{c_4 + c_5\mathcal{A}_2} - \sqrt{c_4 + c_5\mathcal{B}_2}\right)\right]\right\}\right| \qquad (6.471) \\
\leq & \left|\hat{\mathcal{P}}\tilde{v}_{\tilde{x}} s_6 \left|\hat{z}_1\right|\right| + \left|\hat{\mathcal{P}}\tilde{v}_{\tilde{y}_2} \mathcal{D}_{MAX} \left|\hat{z}_1\right|\right| \qquad (6.472) \\
\leq & \left|\hat{\mathcal{P}}\hat{z}_1\right| \left(s_6\tilde{v}_{\tilde{x}} + \mathcal{D}_{MAX}\tilde{v}_{\tilde{y}_2}\right). \qquad (6.473)
\end{aligned}$$

Recalling that $\tilde{x} + x^* \triangleq x$, and from previous analysis of the states as seen in Table 2.3, that the ranges of the state variables is given by

$$\begin{aligned}
& x_{MAX} \geq x \geq x_{MIN}, && (6.474) \\
& \tilde{y}_{1_{MAX}} \geq \tilde{y}_1 \geq \tilde{y}_{1_{MIN}}, && (6.475) \\
& \tilde{y}_{2_{MAX}} \geq \tilde{y}_2 \geq \tilde{y}_{2_{MIN}}, && (6.476)
\end{aligned}$$

with $\tilde{y}_{1_{MIN}} = -\tilde{y}_{1_{MAX}}$, $\tilde{y}_{2_{MIN}} = -\tilde{y}_{2_{MAX}}$. With this in mind, and recalling the definitions of $\tilde{v}_{\tilde{x}}$, $\tilde{v}_{\tilde{y}_1}$, $\tilde{v}_{\tilde{y}_2}$, Eqns. (6.459), (6.460), and (6.461), respectively, it can be proved that inequality (6.473) can be further reduced by trying to maximize the function $s_6\tilde{v}_{\tilde{x}}s_6 + \mathcal{D}_{MAX}\tilde{v}_{\tilde{y}_2}$ such as

$$s_6\tilde{v}_{\tilde{x}}s_6 + \mathcal{D}_{MAX}\tilde{v}_{\tilde{y}_2} \leq s_6\tilde{v}_{\tilde{x}_{MAX}}s_6 + \mathcal{D}_{MAX}\tilde{v}_{\tilde{y}_{2_{MAX}}}, \tag{6.477}$$

with $\tilde{v}_{\tilde{x}_{MAX}}$ and $\tilde{v}_{\tilde{y}_{2_{MAX}}}$ being given as the maximum values of Eqns. (6.459) and (6.461), respectively, that is

$$\tilde{v}_{\tilde{x}_{MAX}} = \left[s_2 s_3 \frac{1+R}{R}\left(2\frac{\tilde{v}(\tilde{\boldsymbol{\chi}})}{\tilde{x}+x^*}\right)\right]_{MAX}, \tag{6.478}$$

$$\tilde{v}_{\tilde{y}_{2_{MAX}}} = \left[s_2 s_3 \frac{1+R}{R}\left(\frac{2a_9\tilde{y}_2 + a_9 + \tilde{b}_{y_2}}{(\tilde{x}+x^*)^2}\right)\right]_{MAX}, \tag{6.479}$$

where it can be proven that both Eqns. (6.478) and (6.479), are maximized by selecting

$$(\tilde{x}+x^*) \triangleq x \rightarrow x_{MIN}, \tag{6.480}$$

$$\tilde{y}_1 \rightarrow \tilde{y}_{1_{MIN}}, \tag{6.481}$$

$$\tilde{y}_2 \rightarrow \tilde{y}_{2_{MIN}}, \tag{6.482}$$

where $\tilde{x}_{MIN}$ implies that the helicopter is flying at the minimum allowable angular rotation of the blades, $\tilde{y}_{1_{MIN}}$, implies that the helicopter is at its lower possible altitude, and it is instantaneously commanded to ascent to the highest possible altitude, and $\tilde{y}_{2_{MIN}}$ implies that the helicopter has its maximum allowable descent velocity .

Similarly as for the Σ_{SF} *Stability Analysis*, this translate to a very extreme situation in which the helicopter reaches the minimum altitude at the highest possible descent velocity, and instantaneously it is commanded to ascent to the highest possible altitude. Again, this represents a highly improbable flight condition, thus making this solution a very conservative analysis, since any of the situations that will encounter the helicopter will be much more less restrictive. Using the above expression allows to rewrite Eqns. (6.478) and (6.479) as

$$\tilde{v}_{\tilde{x}_{MAX}} = \frac{4a_2a_3}{a_4^2\varepsilon_1}\frac{1+R_{MAX}}{R_{MAX}}\left(2\frac{\tilde{v}_{MAX}(\tilde{\boldsymbol{\chi}})}{x_{MIN}}\right), \tag{6.483}$$

$$\tilde{v}_{\tilde{x}_{MAX}} = \frac{4a_2a_3}{a_4^2\varepsilon_1}\frac{1+R_{MAX}}{R_{MAX}}\left(\frac{2a_9\tilde{y}_{2_{MIN}} + a_9 + \tilde{b}_{y_2}}{(x_{MIN})^2}\right), \tag{6.484}$$

where

$$R_{MAX} = \sqrt{s_3\tilde{v}_{MAX}(\tilde{\boldsymbol{\chi}})}, \tag{6.485}$$

and

$$\tilde{v}_{MAX}(\tilde{\boldsymbol{\chi}}) = -\frac{a_9\tilde{y}_{2_{MIN}}^2 + \left(a_9 + \tilde{b}_{y_2}\right)\tilde{y}_{2_{MIN}} + \tilde{b}_{y_1}\tilde{y}_{1_{MIN}} + c_6}{(x_{MIN})^2}. \tag{6.486}$$

Let also define

$$\mathcal{N} = \frac{4a_2a_3}{a_4^2\varepsilon_1}\frac{1+R_{MAX}}{R_{MAX}}\left(2s_6\frac{\tilde{v}_{MAX}(\tilde{\boldsymbol{\chi}})}{x_{MIN}} + \mathcal{D}_{MAX}\frac{2a_9\tilde{y}_{2_{MIN}} + a_9 + \tilde{b}_{y_2}}{(x_{MIN})^2}\right), \tag{6.487}$$

therefore allowing to rewrite inequality (6.473) as

$$\frac{\partial V_U}{\partial \tilde{\boldsymbol{\chi}}}\left[\tilde{\boldsymbol{F}}(\tilde{\boldsymbol{\chi}}, \tilde{\boldsymbol{z}}) - \tilde{\boldsymbol{F}}(\tilde{\boldsymbol{\chi}}, \tilde{\mathbf{h}}(\tilde{\boldsymbol{\chi}}))\right] = \frac{\partial V_U}{\partial \tilde{x}}\hat{F}_1 + \frac{\partial V_U}{\partial \tilde{y}_1}\hat{F}_2 + \frac{\partial V_U}{\partial \tilde{y}_2}\hat{F}_2 \tag{6.488}$$

$$\begin{aligned} &= \hat{\mathcal{P}}\tilde{v}_{\tilde{x}}\left[2a_{10}(\tilde{x}+x^*)^2\sin\left(\frac{\mathcal{A}_2 - \mathcal{B}_2}{2}\right)\cos\left(\frac{\mathcal{A}_2 + \mathcal{B}_2}{2}\right)\right] \\ &+ \hat{\mathcal{P}}\tilde{v}_{\tilde{y}_2}\left((\tilde{x}+x^*)^2\left[c_3\hat{z}_1 - \left(\sqrt{c_4 + c_5\mathcal{A}_2} - \sqrt{c_4 + c_5\mathcal{B}_2}\right)\right]\right) \end{aligned} \tag{6.489}$$

$$
\begin{aligned}
&\leq \left|\hat{\mathcal{P}}\hat{z}_1\right| \left(s_6\tilde{v}_{\tilde{x}} + \mathcal{D}_{MAX}\tilde{v}_{\tilde{y}_2}\right) \\
&\leq \left|\hat{\mathcal{P}}\hat{z}_1\right| \mathcal{N},
\end{aligned} \tag{6.490}
$$

where recalling the definition of $\hat{\mathcal{P}}$, Eq. (6.446), permits to rewrite inequality (6.491) as

$$
\begin{aligned}
&\frac{\partial V_U}{\partial \tilde{\boldsymbol{\chi}}} \left[\tilde{\boldsymbol{F}}(\tilde{\boldsymbol{\chi}}, \tilde{\boldsymbol{z}}) - \tilde{\boldsymbol{F}}(\tilde{\boldsymbol{\chi}}, \tilde{\mathbf{h}}(\tilde{\boldsymbol{\chi}}))\right] = \frac{\partial V_U}{\partial \tilde{x}}\hat{F}_1 + \frac{\partial V_U}{\partial \tilde{y}_1}\hat{F}_2 + \frac{\partial V_U}{\partial \tilde{y}_2}\hat{F}_2 \\
&= \hat{\mathcal{P}}\tilde{v}_{\tilde{x}}\left[2a_{10}(\tilde{x}+x^*)^2 \sin\left(\frac{\mathcal{A}_2-\mathcal{B}_2}{2}\right)\cos\left(\frac{\mathcal{A}_2+\mathcal{B}_2}{2}\right)\right] \\
&+ \hat{\mathcal{P}}\tilde{v}_{\tilde{y}_2}\left\{(\tilde{x}+x^*)^2\left[c_3\hat{z}_1 - \left(\sqrt{c_4+c_5\mathcal{A}_2} - \sqrt{c_4+c_5\mathcal{B}_2}\right)\right]\right\} \\
&\leq \left|\hat{\mathcal{P}}\hat{z}_1\right|\mathcal{N} \\
&= \left|\left(p_{u_1}\hat{z}_1 + p_{u_2}\hat{z}_2\right)\hat{z}_1\right|\mathcal{N} \\
&\leq \left(p_{u_1}\hat{z}_1^2 + p_{u_2}\left|\hat{z}_1\hat{z}_2\right|\right)\mathcal{N}.
\end{aligned} \tag{6.491}
$$

The right-hand side of inequality (6.491) can be further simplified employing Young's inequality, Eq. (6.177), which permits to rewrite the right-hand side of Eq. (6.491) as

$$
\begin{aligned}
\mathcal{N}\left(p_{u_1}\hat{z}_1^2 + p_{u_2}\left|\hat{z}_1\hat{z}_2\right|\right) &\leq \mathcal{N}\left[p_{u_1}\hat{z}_1^2 + p_{u_2}\left(\frac{\hat{z}_1^2+\hat{z}_2^2}{2}\right)\right] \\
&= \mathcal{N}\left[p_{u_1}\hat{z}_1^2 + p_{u_2}\left(\frac{\hat{z}_1^2+\hat{z}_2^2}{2}\right)\right] \\
&= \mathcal{P}_{u_1}\hat{z}_1^2 + \mathcal{P}_{u_2}\hat{z}_2^2,
\end{aligned} \tag{6.492}
$$

with $\mathcal{P}_{u_1}$ and $\mathcal{P}_{u_2}$ defined as

$$
\mathcal{P}_{u_1} = \mathcal{N}\left(p_{u_1} + \frac{p_{u_2}}{2}\right), \tag{6.493}
$$

$$
\mathcal{P}_{u_2} = \mathcal{N}\frac{p_{u_2}}{2}, \tag{6.494}
$$

therefore the fulfillment of inequality (6.436) reduces to satisfy

$$
\mathcal{P}_{u_1}\hat{z}_1^2 + \mathcal{P}_{u_2}\hat{z}_2^2 \leq \gamma_2\left(\tilde{q}_{u_1}\hat{z}_1^2 + \tilde{q}_{u_2}\hat{z}_2^2\right), \tag{6.495}
$$

therefore reducing the fulfillment of the original inequality (6.436), to find the γ_2 constant that satisfies the above inequality, Eq. (6.495), with is fulfilled with γ_2 given by;

$$
\gamma_2 = \max\left(\gamma_{2_a}, \gamma_{2_b}\right), \tag{6.496}
$$

where

$$
\gamma_{2_a} \geq \frac{\mathcal{P}_{u_1}}{\tilde{q}_{u_1}}, \tag{6.497}
$$

$$
\gamma_{2_b} \geq \frac{\mathcal{P}_{u_2}}{\tilde{q}_{u_2}}, \tag{6.498}
$$

with $\mathcal{P}_{u_1}$, and $\mathcal{P}_{u_2}$, defined in Eqns. (6.493) and (6.494), respectively. In order to obtain a single relation for γ_2, let recall the definitions for the variables p_{u_1}, and p_{u_2}, Eqns. (6.53), and (6.53) respectively, allowing to rewrite Eqns (6.497) and (6.498) such

$$
\gamma_{2_a} \geq \frac{\mathcal{P}_{u_1}}{\tilde{q}_{u_1}} = 2\mathcal{N}\left(C_{u_1} + \frac{C_{u_3}}{2} + C_{u_2}\frac{q_{u_2}}{q_{u_1}}\right), \tag{6.499}
$$

$$
\gamma_{2_b} \geq \frac{\mathcal{P}_{u_2}}{\tilde{q}_{u_2}} = \mathcal{N}C_{u_3}\frac{q_{u_1}}{q_{u_2}}, \tag{6.500}
$$

with C_{u_1}, C_{u_2}, and C_{u_3}, defined in Eqns. (6.56), (6.57), and (6.58), respectively, and $\mathcal{N}$ being defined in Eq. (6.487). Analyzing both Eqns. (6.499) and (6.500), and recalling that both only depend on the physic parameters of the problem, and the *stability parameters* q_{u_1}, and q_{u_2}, it can be obtained a relation between these last two, by equating both equations resulting in

$$2\mathcal{N}\left(C_{u_1}+\frac{C_{u_3}}{2}+C_{u_2}\frac{q_{u_2}}{q_{u_1}}\right)=2\mathcal{N}C_{u_3}\frac{q_{u_1}}{q_{u_2}}, \tag{6.501}$$

which results in a quadratic expression in q_{u_2}/q_{u_1} given as

$$2C_{u_2}\left(\frac{q_{u_2}}{q_{u_1}}\right)^2+(2C_{u_1}+C_{u_3})\frac{q_{u_2}}{q_{u_1}}-C_{u_3}=0, \tag{6.502}$$

which can be solved for $\frac{q_{u_2}}{q_{u_1}}$, resulting

$$\frac{q_{u_2}}{q_{u_1}}=\frac{-(2C_{u_1}+C_{u_3})\pm\sqrt{(2C_{u_1}+C_{u_3})^2+8C_{u_2}C_{u_3}}}{4C_{u_2}}, \tag{6.503}$$

where since both, q_{u_1}, and q_{u_2}, are by definition positive, only the positive solution is valid therefore resulting in

$$\frac{q_{u_2}}{q_{u_1}}=\frac{-(2C_{u_1}+C_{u_3})+\sqrt{(2C_{u_1}+C_{u_3})^2+8C_{u_2}C_{u_3}}}{4C_{u_2}}. \tag{6.504}$$

Expression (6.504) represents the ratio of q_{u_2} and q_{u_1} where γ_2 is smallest, such that both Eqns. (6.497) and (6.498) coincides such reducing

$$\gamma_{2_a}\equiv\gamma_{2_b}=\frac{\mathcal{P}_{u_2}}{\tilde{q}_{u_2}}=\mathcal{N}C_{u_3}\frac{q_{u_1}}{q_{u_2}}. \tag{6.505}$$

This is a really important relation, since provides the ratio that minimizes γ_2, and in addition provides a relation between both q_{u_1} and q_{u_2} that will help to obtain the upper-bounds on ε_2 and given by

$$q_{u_2}=Q_{U_{21}}q_{u_1}, \tag{6.506}$$

with $Q_{U_{21}}$ given by Eq. (6.504)

$$Q_{U_{21}}=\frac{-(2C_{u_1}+C_{u_3})+\sqrt{(2C_{u_1}+C_{u_3})^2+8C_{u_2}C_{u_3}}}{4C_{u_2}}, \tag{6.507}$$

therefore allowing to reduce Rq. (6.496) to

$$\gamma_2\geq 2\mathcal{N}\left(C_{u_1}+\frac{C_{u_3}}{2}+C_{u_2}Q_{U_{21}}\right). \tag{6.508}$$

Once the first interconnection inequality, Eq. (6.438), is satisfied, let shift towards the second interconnection inequality, Eq. (6.439), where

$$\tilde{\boldsymbol{F}}(\tilde{\boldsymbol{\chi}},\tilde{\mathbf{h}}(\tilde{\boldsymbol{\chi}}))=\begin{bmatrix}\tilde{F}_{H_1}\\ \tilde{F}_{H_2}\\ \tilde{F}_{H_3}\end{bmatrix}, \tag{6.509}$$

with $\tilde{F}_{H_1}$, $\tilde{F}_{H_2}$ and $\tilde{F}_{H_3}$ being defined by Eqns. (6.235), (6.236), and (6.237), respectively, and where recalling the definitions of $\mathcal{A}_1$ and $\mathcal{B}_1$, (6.96) and (6.97) respectively, thus $\tilde{F}_{H_1}$ can be rewritten as

$$\tilde{F}_{H_1} = a_{10}(\tilde{x}+x^*)^2\left[\sin\mathcal{A}_1-\sin\mathcal{B}_1\right]-b_x\tilde{x}, \tag{6.510}$$

which can be rewritten by using the sum-to-product prosthaphaeresis trigonometric identity, Eq. (6.99), thus allowing to rewrite (6.510) as

$$\tilde{F}_{H_1} = a_{10}(\tilde{x}+x^*)^2\left[\sin\mathcal{A}_1-\sin\mathcal{B}_1\right]-b_x\tilde{x}$$

$$= \quad a_{10}(\tilde{x}+x^*)^2 2\sin\left(\frac{\mathcal{A}_1-\mathcal{B}_1}{2}\right)\cos\left(\frac{\mathcal{A}_1+\mathcal{B}_1}{2}\right) - b_x\tilde{x}. \tag{6.511}$$

The left-hand side of inequality (6.512) can be expanded using Eqns. (6.446), (6.459), (6.460), (6.461), (6.96) and (6.97), such

$$\begin{aligned}
& \frac{\partial V_U}{\partial \tilde{\boldsymbol{\chi}}}\tilde{\boldsymbol{F}}(\tilde{\boldsymbol{\chi}},\tilde{\mathbf{h}}(\tilde{\boldsymbol{\chi}})) \\
= \quad & \frac{\partial V_U}{\partial \tilde{x}}\tilde{F}_{H_1} + \frac{\partial V_U}{\partial \tilde{y}_1}\tilde{F}_{H_2} + \frac{\partial V_U}{\partial \tilde{y}_2}\tilde{F}_{H_3} \\
= \quad & \hat{\mathcal{P}}\tilde{v}_{\tilde{x}}\left[2a_{10}(\tilde{x}+x^*)^2\sin\left(\frac{\mathcal{A}_1-\mathcal{B}_1}{2}\right)\cos\left(\frac{\mathcal{A}_1+\mathcal{B}_1}{2}\right) - b_x\tilde{x}\right] \\
+ \quad & \hat{\mathcal{P}}\tilde{v}_{\tilde{y}_1}c_1\tilde{y}_2 + \hat{\mathcal{P}}\tilde{v}_{\tilde{y}_2}\left(-\tilde{b}_{y_1}\tilde{y}_1 - \tilde{b}_{y_2}\tilde{y}_2\right) \\
= \quad & \hat{\mathcal{P}}\tilde{v}_{\tilde{x}}\left[2a_{10}(\tilde{x}+x^*)^2\sin\left(\frac{\mathcal{A}_1-\mathcal{B}_1}{2}\right)\cos\left(\frac{\mathcal{A}_1+\mathcal{B}_1}{2}\right)\right] \\
- \quad & \hat{\mathcal{P}}\tilde{v}_{\tilde{x}}b_x\tilde{x} + \hat{\mathcal{P}}\tilde{v}_{\tilde{y}_1}c_1\tilde{y}_2 + \hat{\mathcal{P}}\tilde{v}_{\tilde{y}_2}\left(-\tilde{b}_{y_1}\tilde{y}_1 - \tilde{b}_{y_2}\tilde{y}_2\right).
\end{aligned} \tag{6.512}$$

Inequality (6.512) can be simplified by recalling Eq. (6.168) in section 6.3, where it was proved that

$$2a_{10}(\tilde{x}+x^*)^2\sin\left(\frac{\mathcal{A}_1-\mathcal{B}_1}{2}\right)\cos\left(\frac{\mathcal{A}_1+\mathcal{B}_1}{2}\right) \le \mathcal{C}_1|\tilde{y}_1| + \mathcal{C}_2|\tilde{y}_2|, \tag{6.513}$$

therefore permitting to rewrite inequality (6.512) as

$$\begin{aligned}
& \frac{\partial V_U}{\partial \tilde{\boldsymbol{\chi}}}\tilde{\boldsymbol{F}}(\tilde{\boldsymbol{\chi}},\tilde{\mathbf{h}}(\tilde{\boldsymbol{\chi}})) \\
= \quad & \hat{\mathcal{P}}\tilde{v}_{\tilde{x}}\left[2a_{10}(\tilde{x}+x^*)^2\sin\left(\frac{\mathcal{A}_1-\mathcal{B}_1}{2}\right)\cos\left(\frac{\mathcal{A}_1+\mathcal{B}_1}{2}\right)\right] \\
- \quad & \hat{\mathcal{P}}\tilde{v}_{\tilde{x}}b_x\tilde{x} + \hat{\mathcal{P}}\tilde{v}_{\tilde{y}_1}c_1\tilde{y}_2 + \hat{\mathcal{P}}\tilde{v}_{\tilde{y}_2}\left(-\tilde{b}_{y_1}\tilde{y}_1 - \tilde{b}_{y_2}\tilde{y}_2\right) \\
\le \quad & \left|\hat{\mathcal{P}}\tilde{v}_{\tilde{x}}\left[2a_{10}(\tilde{x}+x^*)^2\sin\left(\frac{\mathcal{A}_1-\mathcal{B}_1}{2}\right)\cos\left(\frac{\mathcal{A}_1+\mathcal{B}_1}{2}\right)\right]\right| \\
+ \quad & \left|\hat{\mathcal{P}}\tilde{v}_{\tilde{x}}b_x\tilde{x}\right| + \left|\hat{\mathcal{P}}\tilde{v}_{\tilde{y}_1}c_1\tilde{y}_2\right| + \left|\hat{\mathcal{P}}\tilde{v}_{\tilde{y}_2}\left(-\tilde{b}_{y_1}\tilde{y}_1 - \tilde{b}_{y_2}\tilde{y}_2\right)\right| \\
\le \quad & \left|\hat{\mathcal{P}}\tilde{v}_{\tilde{x}}\left(\mathcal{C}_1|\tilde{y}_1| + \mathcal{C}_2|\tilde{y}_2|\right)\right| + \left|\hat{\mathcal{P}}\tilde{v}_{\tilde{x}}b_x\tilde{x}\right| + \left|\hat{\mathcal{P}}\tilde{v}_{\tilde{y}_1}c_1\tilde{y}_2\right| + \left|\hat{\mathcal{P}}\tilde{v}_{\tilde{y}_2}\left(\tilde{b}_{y_1}\tilde{y}_1 + \tilde{b}_{y_2}\tilde{y}_2\right)\right|.
\end{aligned} \tag{6.514}$$

Inequality (6.514) can be further simplified by recalling that $\tilde{v}_{\tilde{x}}$, $\tilde{v}_{\tilde{y}_1}$, and $\tilde{v}_{\tilde{y}_2}$, Eqns. (6.459), (6.460), and (6.461), respectively, can be maximized by selecting

$$(\tilde{x}+x^*) \triangleq x \quad \rightarrow \quad x_{MIN}, \tag{6.515}$$

$$\tilde{y}_1 \quad \rightarrow \quad \tilde{y}_{1_{MIN}}, \tag{6.516}$$

$$\tilde{y}_2 \quad \rightarrow \quad \tilde{y}_{2_{MIN}}, \tag{6.517}$$

where similarly as in Eqns. (6.478) and (6.479), $\tilde{v}_{\tilde{x}_{MAX}}$, $\tilde{v}_{\tilde{y}_{1_{MAX}}}$ and $\tilde{v}_{\tilde{x}_{2_{MAX}}}$ are given by

$$\tilde{v}_{\tilde{x}_{MAX}} \quad = \quad \left[s_2 s_3\frac{1+R}{R}\left(2\frac{\tilde{v}(\tilde{\boldsymbol{\chi}})}{\tilde{x}+x^*}\right)\right]_{MAX}, \tag{6.518}$$

$$\tilde{v}_{\tilde{y}_{1_{MAX}}} \quad = \quad \left[s_2 s_3\frac{1+R}{R}\left(\frac{\tilde{b}_{y_1}}{(\tilde{x}+x^*)^2}\right)\right]_{MAX}, \tag{6.519}$$

$$\tilde{v}_{\tilde{y}_{2_{MAX}}} \quad = \quad \left[s_2 s_3\frac{1+R}{R}\left(\frac{2a_9\tilde{y}_2 + a_9 + \tilde{b}_{y_2}}{(\tilde{x}+x^*)^2}\right)\right]_{MAX}, \tag{6.520}$$

which after substituting Eqns. (6.515), (6.516), and (6.517), reduces to

$$\tilde{v}_{\tilde{x}_{MAX}} = \frac{4a_2a_3}{a_4^2\varepsilon_1}\frac{1+R_{MAX}}{R_{MAX}}\left(2\frac{\tilde{v}_{MAX}(\tilde{\boldsymbol{\chi}})}{x_{MIN}}\right), \tag{6.521}$$

$$\tilde{v}_{\tilde{y}_{1_{MAX}}} = \frac{4a_2a_3}{a_4^2\varepsilon_1}\frac{1+R_{MAX}}{R_{MAX}}\left(\frac{\tilde{b}_{y_1}}{x_{MIN}^2}\right), \tag{6.522}$$

$$\tilde{v}_{\tilde{y}_{2_{MAX}}} = \frac{4a_2a_3}{a_4^2\varepsilon_1}\frac{1+R_{MAX}}{R_{MAX}}\left(\frac{2a_9\tilde{y}_{2_{MIN}}+a_9+\tilde{b}_{y_2}}{x_{MIN}^2}\right), \tag{6.523}$$

with R_{MAX} and $\tilde{v}_{MAX}(\tilde{\boldsymbol{\chi}})$ defined in Eqns. (6.485) and (6.486) respectively. Substituting Eqns. (6.521), (6.522), and (6.523) into Eq. (6.514) results in

$$\begin{aligned}
&\frac{\partial V_U}{\partial \tilde{\boldsymbol{\chi}}}\tilde{\boldsymbol{F}}(\tilde{\boldsymbol{\chi}},\tilde{\mathbf{h}}(\tilde{\boldsymbol{\chi}}))\\
= \;& \hat{\mathcal{P}}\tilde{v}_{\tilde{x}}\left[2a_{10}(\tilde{x}+x^*)^2\sin\left(\frac{\mathcal{A}_1-\mathcal{B}_1}{2}\right)\cos\left(\frac{\mathcal{A}_1+\mathcal{B}_1}{2}\right)\right]\\
- \;& \hat{\mathcal{P}}\tilde{v}_{\tilde{x}}b_x\tilde{x}+\hat{\mathcal{P}}\tilde{v}_{\tilde{y}_1}c_1\tilde{y}_2+\hat{\mathcal{P}}\tilde{v}_{\tilde{y}_2}\left(-\tilde{b}_{y_1}\tilde{y}_1-\tilde{b}_{y_2}\tilde{y}_2\right)\\
\leq \;& \left|\hat{\mathcal{P}}\tilde{v}_{\tilde{x}}\left(\mathcal{C}_1\left|\tilde{y}_1\right|+\mathcal{C}_2\left|\tilde{y}_2\right|\right)\right|+\left|\hat{\mathcal{P}}\tilde{v}_{\tilde{x}}b_x\tilde{x}\right|+\left|\hat{\mathcal{P}}\tilde{v}_{\tilde{y}_1}c_1\tilde{y}_2\right|+\left|\hat{\mathcal{P}}\tilde{v}_{\tilde{y}_2}\left(\tilde{b}_{y_1}\tilde{y}_1+\tilde{b}_{y_2}\tilde{y}_2\right)\right|\\
\leq \;& \left|\hat{\mathcal{P}}\tilde{v}_{\tilde{x}_{MAX}}\left(\mathcal{C}_1\left|\tilde{y}_1\right|+\mathcal{C}_2\left|\tilde{y}_2\right|\right)\right|+\left|\hat{\mathcal{P}}\tilde{v}_{x_{MAX}}b_x\tilde{x}\right|+\left|\hat{\mathcal{P}}\tilde{v}_{\tilde{y}_{1_{MAX}}}c_1\tilde{y}_2\right|\\
+ \;& \left|\hat{\mathcal{P}}\tilde{v}_{\tilde{y}_{2_{MAX}}}\left(\tilde{b}_{y_1}\tilde{y}_1+\tilde{b}_{y_2}\tilde{y}_2\right)\right|.
\end{aligned} \tag{6.524}$$

For completeness, inequality (6.524) can be further simplified by introducing

$$\mathcal{M}_1 = \left|\tilde{v}_{x_{MAX}}b_x\right|, \tag{6.525}$$

$$\mathcal{M}_2 = \left|\tilde{v}_{x_{MAX}}\mathcal{C}_1\right|+\left|\tilde{v}_{\tilde{y}_{2_{MAX}}}\tilde{b}_{y_1}\right|, \tag{6.526}$$

$$\mathcal{M}_3 = \left|\tilde{v}_{x_{MAX}}\mathcal{C}_2\right|+\left|\tilde{v}_{\tilde{y}_{1_{MAX}}}c_1\right|+\left|\tilde{v}_{\tilde{y}_{1_{MAX}}}\tilde{b}_{y_2}\right|, \tag{6.527}$$

therefore rewriting Eq. (6.524) as

$$\begin{aligned}
&\frac{\partial V_U}{\partial \tilde{\boldsymbol{\chi}}}\tilde{\boldsymbol{F}}(\tilde{\boldsymbol{\chi}},\tilde{\mathbf{h}}(\tilde{\boldsymbol{\chi}}))\\
= \;& \hat{\mathcal{P}}\tilde{v}_{\tilde{x}}\left[2a_{10}(\tilde{x}+x^*)^2\sin\left(\frac{\mathcal{A}_1-\mathcal{B}_1}{2}\right)\cos\left(\frac{\mathcal{A}_1+\mathcal{B}_1}{2}\right)\right]\\
- \;& \hat{\mathcal{P}}\tilde{v}_{\tilde{x}}b_x\tilde{x}+\hat{\mathcal{P}}\tilde{v}_{\tilde{y}_1}c_1\tilde{y}_2+\hat{\mathcal{P}}\tilde{v}_{\tilde{y}_2}\left(-\tilde{b}_{y_1}\tilde{y}_1-\tilde{b}_{y_2}\tilde{y}_2\right)\\
\leq \;& \left|\hat{\mathcal{P}}\tilde{v}_{\tilde{x}_{MAX}}\left(\mathcal{C}_1\left|\tilde{y}_1\right|+\mathcal{C}_2\left|\tilde{y}_2\right|\right)\right|+\left|\hat{\mathcal{P}}\tilde{v}_{\tilde{x}_{MAX}}b_x\tilde{x}\right|+\left|\hat{\mathcal{P}}\tilde{v}_{\tilde{y}_{1_{MAX}}}c_1\tilde{y}_2\right|+\left|\hat{\mathcal{P}}\tilde{v}_{\tilde{y}_{2_{MAX}}}\left(\tilde{b}_{y_1}\tilde{y}_1+\tilde{b}_{y_2}\tilde{y}_2\right)\right|\\
\leq \;& \mathcal{M}_1\left|\hat{\mathcal{P}}\tilde{x}\right|+\mathcal{M}_2\left|\hat{\mathcal{P}}\tilde{y}_1\right|+\mathcal{M}_3\left|\hat{\mathcal{P}}\tilde{y}_2\right|\\
= \;& \left|\hat{\mathcal{P}}\right|\left(\mathcal{M}_1\left|\tilde{x}\right|+\mathcal{M}_2\left|\tilde{y}_1\right|+\mathcal{M}_3\left|\tilde{y}_2\right|\right).
\end{aligned} \tag{6.528}$$

This reduces the original inequality (6.436) to

$$\frac{\partial V_U}{\partial \tilde{\boldsymbol{\chi}}}\tilde{\boldsymbol{F}}(\tilde{\boldsymbol{\chi}},\tilde{\mathbf{h}}(\tilde{\boldsymbol{\chi}})) \leq \left|\hat{\mathcal{P}}\right|\left(\mathcal{M}_1\left|\tilde{x}\right|+\mathcal{M}_2\left|\tilde{y}_1\right|+\mathcal{M}_3\left|\tilde{y}_2\right|\right) \leq \beta_4\psi_2(\tilde{\boldsymbol{\chi}})\phi_2(\hat{\boldsymbol{z}}), \tag{6.529}$$

where recalling the selected comparison functions $\psi_2(\tilde{\boldsymbol{\chi}})$ and $\phi_2(\hat{\boldsymbol{z}})$, Eqns. (6.283) and (6.313), respectively, it can be observed that satisfying inequality (6.529) is reduced to prove that

$$\left|\hat{\mathcal{P}}\right|\left(\mathcal{M}_1\left|\tilde{x}\right|+\mathcal{M}_2\left|\tilde{y}_1\right|+\mathcal{M}_3\left|\tilde{y}_2\right|\right) \leq \beta_4\left(\mathcal{R}_1\tilde{x}^2+\mathcal{R}_2\tilde{y}_1^2+\mathcal{R}_3\tilde{y}_2^2\right)^{\frac{1}{2}}\left(\tilde{q}_{u_1}\hat{z}_1^2+\tilde{q}_{u_2}\hat{z}_2^2\right)^{\frac{1}{2}}. \tag{6.530}$$

In order to obtain the constant β_4 that guarantees the fulfillment of inequality (6.436), let square both sides of inequality (6.530), resulting in

$$\hat{\mathcal{P}}^2\left(\mathcal{M}_1\left|\tilde{x}\right|+\mathcal{M}_2\left|\tilde{y}_1\right|+\mathcal{M}_3\left|\tilde{y}_2\right|\right)^2 \leq \beta_4^2\left(\mathcal{R}_1\tilde{x}^2+\mathcal{R}_2\tilde{y}_1^2+\mathcal{R}_3\tilde{y}_2^2\right)\left(\tilde{q}_{u_1}\hat{z}_1^2+\tilde{q}_{u_2}\hat{z}_2^2\right). \tag{6.531}$$

Expanding the left hand-side of inequality (6.531) results in

$$\begin{aligned}
& \hat{\mathcal{P}}^2\left[\left(\mathcal{M}_1\left|\tilde{x}\right|+\mathcal{M}_2\left|\tilde{y}_1\right|+\mathcal{M}_3\left|\tilde{y}_2\right|\right)\right]^2 \\
= & \hat{\mathcal{P}}^2\left(\mathcal{M}_1^2\tilde{x}^2+\mathcal{M}_2^2\tilde{y}_1^2+\mathcal{M}_3^2\tilde{y}_2^2+2\mathcal{M}_1\mathcal{M}_2\left|\tilde{x}\tilde{y}_1\right|\right. \\
+ & \left.2\mathcal{M}_1\mathcal{M}_3\left|\tilde{x}\tilde{y}_2\right|+2\mathcal{M}_2\mathcal{M}_3\left|\tilde{y}_1\tilde{y}_2\right|\right),
\end{aligned} \tag{6.532}$$

which can be simplified by using Young's inequality, Eq. (6.177), permits to rewrite Eq. (6.532) as

$$\begin{aligned}
& \hat{\mathcal{P}}^2\left(\mathcal{M}_1^2\tilde{x}^2+\mathcal{M}_2^2\tilde{y}_1^2+\mathcal{M}_3^2\tilde{y}_2^2+2\mathcal{M}_1\mathcal{M}_2\left|\tilde{x}\tilde{y}_1\right|+2\mathcal{M}_1\mathcal{M}_3\left|\tilde{x}\tilde{y}_2\right|+2\mathcal{M}_2\mathcal{M}_3\left|\tilde{y}_1\tilde{y}_2\right|\right) \\
\leq & \hat{\mathcal{P}}^2\left[\mathcal{M}_1^2\tilde{x}^2+\mathcal{M}_2^2\tilde{y}_1^2+\mathcal{M}_3^2\tilde{y}_2^2+2\mathcal{M}_1\mathcal{M}_2\left(\frac{\tilde{x}^2+\tilde{y}_1^2}{2}\right)\right. \\
+ & \left.2\mathcal{M}_1\mathcal{M}_3\left(\frac{\tilde{x}^2+\tilde{y}_2^2}{2}\right)+2\mathcal{M}_2\mathcal{M}_3\left(\frac{\tilde{y}_1^2+\tilde{y}_2^2}{2}\right)\right] \\
= & \hat{\mathcal{P}}^2\left(\tilde{\mathcal{M}}_1^2\tilde{x}^2+\tilde{\mathcal{M}}_2^2\tilde{y}_1^2+\tilde{\mathcal{M}}_3^2\tilde{y}_2^2\right),
\end{aligned} \tag{6.533}$$

where

$$\tilde{\mathcal{M}}_1 = \mathcal{M}_1^2+\mathcal{M}_1\mathcal{M}_2+\mathcal{M}_1\mathcal{M}_3, \tag{6.534}$$

$$\tilde{\mathcal{M}}_2 = \mathcal{M}_2^2+\mathcal{M}_1\mathcal{M}_2+\mathcal{M}_2\mathcal{M}_3, \tag{6.535}$$

$$\tilde{\mathcal{M}}_3 = \mathcal{M}_3^2+\mathcal{M}_1\mathcal{M}_3+\mathcal{M}_2\mathcal{M}_3. \tag{6.536}$$

Recall the definition of $\hat{\mathcal{P}}$, Eq. (6.446), then $\hat{\mathcal{P}}^2$ can be expanded such

$$\begin{aligned}
\hat{\mathcal{P}}^2 &= \left(p_{u_1}\hat{z}_1+p_{u_1}\hat{z}_2\right)^2 \\
&= p_{u_1}^2\hat{z}_1^2+p_{u_2}^2\hat{z}_2^2+2p_{u_1}p_{u_2}\hat{z}_1\hat{z}_2 \\
&\leq p_{u_1}^2\hat{z}_1^2+p_{u_2}^2\hat{z}_2^2+p_{u_1}p_{u_2}\left(\hat{z}_1^2+\hat{z}_2^2\right) \\
&= \tilde{p}_{u_1}\hat{z}_1^2+\tilde{p}_{u_2}\hat{z}_2^2,
\end{aligned} \tag{6.537}$$

where with the definitions of p_{u_1}, and p_{u_2}, Eqns. (6.53) and (6.54), respectively, results in

$$\tilde{p}_{u_1} = p_{u_1}^2+p_{u_1}p_{u_2} = \left(C_{u_1}q_{u_1}+C_{u_2}q_{u_2}\right)^2+\left(C_{u_1}q_{u_1}+C_{u_2}q_{u_2}\right)C_{u_3}q_{u_1}, \tag{6.538}$$

$$\tilde{p}_{u_2} = \left(C_{u_3}q_{u_1}\right)^2+\left(C_{u_1}q_{u_1}+C_{u_2}q_{u_2}\right)C_{u_3}q_{u_1}, \tag{6.539}$$

therefore permitting to rewrite inequality (6.531) such

$$\begin{aligned}
& \left(\tilde{p}_{u_1}\hat{z}_1^2+\tilde{p}_{u_2}\hat{z}_2^2\right)\left(\tilde{\mathcal{M}}_1\tilde{x}^2+\tilde{\mathcal{M}}_2\tilde{y}_1^2+\tilde{\mathcal{M}}_3\tilde{y}_2^2\right) \\
\leq & \beta_4^2\left(\frac{q_{u_1}}{2}\hat{z}_1^2+\frac{q_{u_2}}{2}\hat{z}_2^2\right)\left(\mathcal{R}_1\tilde{x}^2+\mathcal{R}_2\tilde{y}_1^2+\mathcal{R}_3\tilde{y}_2^2\right).
\end{aligned} \tag{6.540}$$

The fulfillment of the original inequality (6.436) reduces to find the β_4 constant that satisfies inequality (6.540), where β_4 is given by

$$\beta_4 = \max\left(\beta_{4_A}\beta_{4_B}\right), \tag{6.541}$$

with

$$\beta_{4_A} = \max\left(\beta_{4_a},\beta_{4_b},\beta_{4_c}\right), \tag{6.542}$$

$$\beta_{4_B} = \max\left(\beta_{4_d},\beta_{4_e},\beta_{4_f}\right), \tag{6.543}$$

and where

$$\beta_{4_a} \geq \sqrt{2\frac{\tilde{p}_{u_1}\tilde{\mathcal{M}}_1}{q_{u_1}\mathcal{R}_1}}, \tag{6.544}$$

$$\beta_{4_b} \geq \sqrt{2\frac{\tilde{p}_{u_1}\tilde{\mathcal{M}}_2}{q_{u_1}\mathcal{R}_2}}, \tag{6.545}$$

$$\beta_{4_c} \geq \sqrt{2\frac{\tilde{p}_{u_1}\tilde{\mathcal{M}}_3}{q_{u_1}\mathcal{R}_3}}, \tag{6.546}$$

$$\beta_{4_d} \geq \sqrt{2\frac{\tilde{p}_{u_2}\tilde{\mathcal{M}}_1}{q_{u_2}\mathcal{R}_1}}, \tag{6.547}$$

$$\beta_{4_e} \geq \sqrt{2\frac{\tilde{p}_{u_2}\tilde{\mathcal{M}}_2}{q_{u_2}\mathcal{R}_2}}, \tag{6.548}$$

$$\beta_{4_f} \geq \sqrt{2\frac{\tilde{p}_{u_2}\tilde{\mathcal{M}}_3}{q_{u_2}\mathcal{R}_3}}, \tag{6.549}$$

with $\mathcal{R}_1$, $\mathcal{R}_2$, and $\mathcal{R}_3$ given in Eqns. (6.272), (6.273), (6.274) respectively, $\mathcal{M}_1$, $\mathcal{M}_2$, and $\mathcal{M}_3$, given in Eqns. (6.534), (6.535), and (6.535) respectively, and $\tilde{p}_{u_1}$ and $\tilde{p}_{u_2}$ given by Eqns. (6.538) and (6.539) respectively, resulting in

$$\beta_{4_a} \geq \sqrt{2\frac{\tilde{\mathcal{M}}_1\left[\left(C_{u_1}^2+C_{u_1}C_{u_3}\right)q_{u_1}^2+C_{u_2}^2q_{u_2}^2+\left(2C_{u_1}C_{u_2}+C_{u_2}C_{u_3}\right)q_{u_1}q_{u_2}\right]}{q_{u_1}\left(\tilde{r}_1Q_S\right)}}, \tag{6.550}$$

$$\beta_{4_b} \geq \sqrt{2\frac{\tilde{\mathcal{M}}_2\left[\left(C_{u_1}^2+C_{u_1}C_{u_3}\right)q_{u_1}^2+C_{u_2}^2q_{u_2}^2+\left(2C_{u_1}C_{u_2}+C_{u_2}C_{u_3}\right)q_{u_1}q_{u_2}\right]}{q_{u_1}\left(\tilde{r}_2q_{f_1}-\tilde{r}_3Q_S\right)}}, \tag{6.551}$$

$$\beta_{4_c} \geq \sqrt{2\frac{\tilde{\mathcal{M}}_3\left[\left(C_{u_1}^2+C_{u_1}C_{u_3}\right)q_{u_1}^2+C_{u_2}^2q_{u_2}^2+\left(2C_{u_1}C_{u_2}+C_{u_2}C_{u_3}\right)q_{u_1}q_{u_2}\right]}{q_{u_1}\left(\tilde{r}_2q_{f_2}-\tilde{r}_4Q_S\right)}}, \tag{6.552}$$

$$\beta_{4_d} \geq \sqrt{2\frac{\tilde{\mathcal{M}}_1\left[\left(C_{u_3}^2+C_{u_1}C_{u_3}\right)q_{u_1}^2+C_{u_2}C_{u_3}q_{u_1}q_{u_2}\right]}{q_{u_2}\left(\tilde{r}_1Q_S\right)}}, \tag{6.553}$$

$$\beta_{4_e} \geq \sqrt{2\frac{\tilde{\mathcal{M}}_2\left[\left(C_{u_3}^2+C_{u_1}C_{u_3}\right)q_{u_1}^2+C_{u_2}C_{u_3}q_{u_1}q_{u_2}\right]}{q_{u_2}\left(\tilde{r}_2q_{f_1}-\tilde{r}_3Q_S\right)}}, \tag{6.554}$$

$$\beta_{4_f} \geq \sqrt{2\frac{\tilde{\mathcal{M}}_3\left[\left(C_{u_3}^2+C_{u_1}C_{u_3}\right)q_{u_1}^2+C_{u_2}C_{u_3}q_{u_1}q_{u_2}\right]}{q_{u_2}\left(\tilde{r}_2q_{f_2}-\tilde{r}_4Q_S\right)}}. \tag{6.555}$$

In order to obtain a single relation for β_4, let recall that the above expressions can be further reduced by employing the relations previously derived $q_{f_2} = \tilde{Q}_{F_{21}}q_{f_1}$, and $q_{u_2} = Q_{U_{21}}q_{u_1}$, reducing to

$$\beta_{4_a} \geq \sqrt{2\frac{\tilde{\mathcal{M}}_1\left[C_{u_1}^2+C_{u_1}C_{u_3}+Q_{U_{21}}^2C_{u_2}^2+Q_{U_{21}}\left(2C_{u_1}C_{u_2}+C_{u_2}C_{u_3}\right)\right]q_{u_1}^2}{q_{u_1}\left(\tilde{r}_1Q_S\right)}}, \tag{6.556}$$

$$\beta_{4_b} \geq \sqrt{2\frac{\tilde{\mathcal{M}}_2\left[C_{u_1}^2+C_{u_1}C_{u_3}+Q_{U_{21}}^2C_{u_2}^2+Q_{U_{21}}\left(2C_{u_1}C_{u_2}+C_{u_2}C_{u_3}\right)\right]q_{u_1}^2}{q_{u_1}\left(\tilde{r}_2q_{f_1}-\tilde{r}_3Q_S\right)}}, \tag{6.557}$$

$$\beta_{4_c} \geq \sqrt{2\frac{\tilde{\mathcal{M}}_3\left[C_{u_1}^2+C_{u_1}C_{u_3}+Q_{U_{21}}^2C_{u_2}^2+Q_{U_{21}}\left(2C_{u_1}C_{u_2}+C_{u_2}C_{u_3}\right)\right]q_{u_1}^2}{q_{u_1}\left(\tilde{r}_2\tilde{Q}_{F_{21}}q_{f_1}-\tilde{r}_4Q_S\right)}}, \tag{6.558}$$

$$\beta_{4_d} \geq \sqrt{2\frac{\tilde{\mathcal{M}}_1\left[C_{u_3}^2+C_{u_1}C_{u_3}+Q_{U_{21}}C_{u_2}C_{u_3}\right]q_{u_1}^2}{Q_{U_{21}}q_{u_1}\left(\tilde{r}_1Q_S\right)}}, \tag{6.559}$$

$$\beta_{4_e} \geq \sqrt{2\frac{\tilde{\mathcal{M}}_1\left[C_{u_3}^2+C_{u_1}C_{u_3}+Q_{U_{21}}C_{u_2}C_{u_3}\right]q_{u_1}^2}{Q_{U_{21}}q_{u_1}\left(\tilde{r}_2q_{f_1}-\tilde{r}_3Q_S\right)}}, \tag{6.560}$$

$$\beta_{4_f} \geq \sqrt{2\frac{\tilde{\mathcal{M}}_1 \left[C_{u_3}^2 + C_{u_1}C_{u_3} + Q_{U21}C_{u_2}C_{u_3}\right] q_{u_1}^2}{Q_{U_{21}} q_{u_1} \left(\tilde{r}_2 \tilde{Q}_{F_{21}} q_{f_1} - \tilde{r}_4 Q_S\right)}}, \tag{6.561}$$

which simplifies to

$$\beta_{4_a} \geq \sqrt{\frac{\tilde{\mathcal{P}}_1 q_{u_1}}{\tilde{r}_1 Q_S}}, \tag{6.562}$$

$$\beta_{4_b} \geq \sqrt{\frac{\tilde{\mathcal{P}}_2 q_{u_1}}{\tilde{r}_2 q_{f_1} - \tilde{r}_3 Q_S}}, \tag{6.563}$$

$$\beta_{4_c} \geq \sqrt{\frac{\tilde{\mathcal{P}}_3 q_{u_1}}{\tilde{r}_2 \tilde{Q}_{F_{21}} q_{f_1} - \tilde{r}_4 Q_S}}, \tag{6.564}$$

$$\beta_{4_d} \geq \sqrt{\frac{\tilde{\mathcal{P}}_4 q_{u_1}}{Q_{U_{21}} \left(\tilde{r}_1 Q_S\right)}}, \tag{6.565}$$

$$\beta_{4_e} \geq \sqrt{\frac{\tilde{\mathcal{P}}_5 q_{u_1}}{Q_{U_{21}} \left(\tilde{r}_2 q_{f_1} - \tilde{r}_3 Q_S\right)}}, \tag{6.566}$$

$$\beta_{4_f} \geq \sqrt{\frac{\tilde{\mathcal{P}}_6 q_{u_1}}{Q_{U_{21}} \left(\tilde{r}_2 \tilde{Q}_{F_{21}} q_{f_1} - \tilde{r}_4 Q_S\right)}}, \tag{6.567}$$

where

$$\tilde{\mathcal{P}}_1 = 2\tilde{\mathcal{M}}_1 \left[C_{u_1}^2 + C_{u_1}C_{u_3} + Q_{U_{21}}^2 C_{u_2}^2 + Q_{U_{21}} \left(2C_{u_1}C_{u_2} + C_{u_2}C_{u_3}\right)\right], \tag{6.568}$$

$$\tilde{\mathcal{P}}_2 = 2\tilde{\mathcal{M}}_2 \left[C_{u_1}^2 + C_{u_1}C_{u_3} + Q_{U_{21}}^2 C_{u_2}^2 + Q_{U_{21}} \left(2C_{u_1}C_{u_2} + C_{u_2}C_{u_3}\right)\right], \tag{6.569}$$

$$\tilde{\mathcal{P}}_3 = 2\tilde{\mathcal{M}}_3 \left[C_{u_1}^2 + C_{u_1}C_{u_3} + Q_{U_{21}}^2 C_{u_2}^2 + Q_{U_{21}} \left(2C_{u_1}C_{u_2} + C_{u_2}C_{u_3}\right)\right], \tag{6.570}$$

$$\tilde{\mathcal{P}}_4 = 2\tilde{\mathcal{M}}_1 \left[C_{u_3}^2 + C_{u_1}C_{u_3} + Q_{U_{21}} C_{u_2}C_{u_3}\right], \tag{6.571}$$

$$\tilde{\mathcal{P}}_5 = 2\tilde{\mathcal{M}}_2 \left[C_{u_3}^2 + C_{u_1}C_{u_3} + Q_{U_{21}} C_{u_2}C_{u_3}\right], \tag{6.572}$$

$$\tilde{\mathcal{P}}_6 = 2\tilde{\mathcal{M}}_3 \left[C_{u_3}^2 + C_{u_1}C_{u_3} + Q_{U_{21}} C_{u_2}C_{u_3}\right], \tag{6.573}$$

where expression $\tilde{\mathcal{P}}_1$, $\tilde{\mathcal{P}}_2$, $\tilde{\mathcal{P}}_3$, $\tilde{\mathcal{P}}_4$, $\tilde{\mathcal{P}}_5$, and $\tilde{\mathcal{P}}_6$ only depend on the physical parameters of the helicopter, the selected target dynamics parameters, that is b_x, $\tilde{b}_{y_1}$, and $\tilde{b}_{y_2}$, and the ratio $Q_{U_{21}}$. Recalling expression in Eq. (6.289), $q_{f_1} = \tilde{Q}_{SF} Q_S$, permits to rewrite Eqns. (6.562), (6.563), (6.564), (6.565), (6.566), and (6.567) such

$$\beta_{4_a} \geq \mathcal{B}_{4_a} \sqrt{\frac{q_{u_1}}{Q_S}}, \tag{6.574}$$

$$\beta_{4_b} \geq \mathcal{B}_{4_b} \sqrt{\frac{q_{u_1}}{Q_S}}, \tag{6.575}$$

$$\beta_{4_c} \geq \mathcal{B}_{4_c} \sqrt{\frac{q_{u_1}}{Q_S}}, \tag{6.576}$$

$$\beta_{4_d} \geq \mathcal{B}_{4_d} \sqrt{\frac{q_{u_1}}{Q_S}}, \tag{6.577}$$

$$\beta_{4_e} \geq \mathcal{B}_{4_e} \sqrt{\frac{q_{u_1}}{Q_S}}, \tag{6.578}$$

$$\beta_{4_f} \geq \mathcal{B}_{4_f} \sqrt{\frac{q_{u_1}}{Q_S}}, \tag{6.579}$$

where

$$\mathcal{B}_{4_a} = \sqrt{\frac{\tilde{\mathcal{P}}_1}{\tilde{r}_1}}, \tag{6.580}$$

$$\mathcal{B}_{4_b} = \sqrt{\frac{\tilde{\mathcal{P}}_2}{\tilde{r}_2\tilde{Q}_{SF} - \tilde{r}_3}}, \tag{6.581}$$

$$\mathcal{B}_{4_c} = \sqrt{\frac{\tilde{\mathcal{P}}_3}{\tilde{r}_2\tilde{Q}_{F_{21}}\tilde{Q}_{SF} - \tilde{r}_4}}, \tag{6.582}$$

$$\mathcal{B}_{4_d} = \sqrt{\frac{\tilde{\mathcal{P}}_4}{Q_{U_{21}}\tilde{r}_1}}, \tag{6.583}$$

$$\mathcal{B}_{4_e} = \sqrt{\frac{\tilde{\mathcal{P}}_5}{Q_{U_{21}}\left(\tilde{r}_2\tilde{Q}_{SF} - \tilde{r}_3\right)}}, \tag{6.584}$$

$$\mathcal{B}_{4_f} = \sqrt{\frac{\tilde{\mathcal{P}}_6}{Q_{U_{21}}\left(\tilde{r}_2\tilde{Q}_{F_{21}}\tilde{Q}_{SF} - \tilde{r}_4\right)}}, \tag{6.585}$$

where expression $\mathcal{B}_{4_a}$, $\mathcal{B}_{4_b}$, $\mathcal{B}_{4_c}$, $\mathcal{B}_{4_d}$, $\mathcal{B}_{4_e}$, and $\mathcal{B}_{4_f}$ only depend on the physical parameters of the helicopter, the selected target dynamics parameters, that is b_x, $\tilde{b}_{y_1}$, and $\tilde{b}_{y_2}$, and the ratios $Q_{U_{21}}$, $\tilde{Q}_{F_{21}}$ and $\tilde{Q}_{SF}$. It can be also proven that, for the physical parameter here used, and the selected target dynamics behavior, $\mathcal{B}_{4_e} > \mathcal{B}_{4_f} > \mathcal{B}_{4_b} > \mathcal{B}_{4_c} > \mathcal{B}_{4_d} > \mathcal{B}_{4_a}$. This is true as long as d_1 is selected such $d_1 \in (0, 0.5243)$ as it can be seen in Figure 6.5, where it is analyzed the variation of the parameters $\mathcal{B}_{4_a}$, $\mathcal{B}_{4_b}$, and $\mathcal{B}_{4_c}$, $\mathcal{B}_{4_d}$, $\mathcal{B}_{4_e}$, and $\mathcal{B}_{4_f}$, Eqns. (6.580), (6.581), (6.582), (6.583), (6.584) and (6.585), respectively, as the unspecified parameter $d_1^\star$ is varied in the interval of interest $d_1 \in (0, 1)$, with $\mathcal{B}_{4_e}$ denoted by the solid line.

Similarly, and recalling the definition of $\tilde{Q}_{SF}$, Eq. (6.288), Figure 6.6 shows the variation of $\mathcal{B}_{4_a}$, $\mathcal{B}_{4_b}$, $\mathcal{B}_{4_c}$, $\mathcal{B}_{4_d}$, $\mathcal{B}_{4_e}$ and $\mathcal{B}_{4_f}$ as a function of δ_1, and where it can be seen that for the range of interest $\delta_1 \in (1, 1.5)$ $\mathcal{B}_{4_e}$, Eq. (6.584), is the largest of the six parameters for $\delta_1 \in (1.02, 1.264)$. Figure 6.7 also shows the variation of $\mathcal{B}_{4_a}$, $\mathcal{B}_{4_b}$, and $\mathcal{B}_{4_c}$, $\mathcal{B}_{4_d}$, $\mathcal{B}_{4_e}$, and $\mathcal{B}_{4_f}$ as a function of both $d_1^\star$ and δ_1. Therefore, by selecting $d_1^\star \in (0, 0.5243)$, and $\delta_1 \in (1.02, 1.264)$., Eq. (6.541) reduces by using $\mathcal{B}_{4_e}$ such

$$\beta_4 \geq \beta_{4_e} = \mathcal{B}_{4_e}\sqrt{\frac{q_{u_1}}{Q_S}}. \tag{6.586}$$

The proper selection of γ_2 and β_4, Eqns. (6.496) and (6.541), respectively, satisfies both inequalities (6.438) and (6.439), therefore satisfying the original inequality (6.436), and concluding the asymptotic stability analysis of the full Σ_{SFU} system.

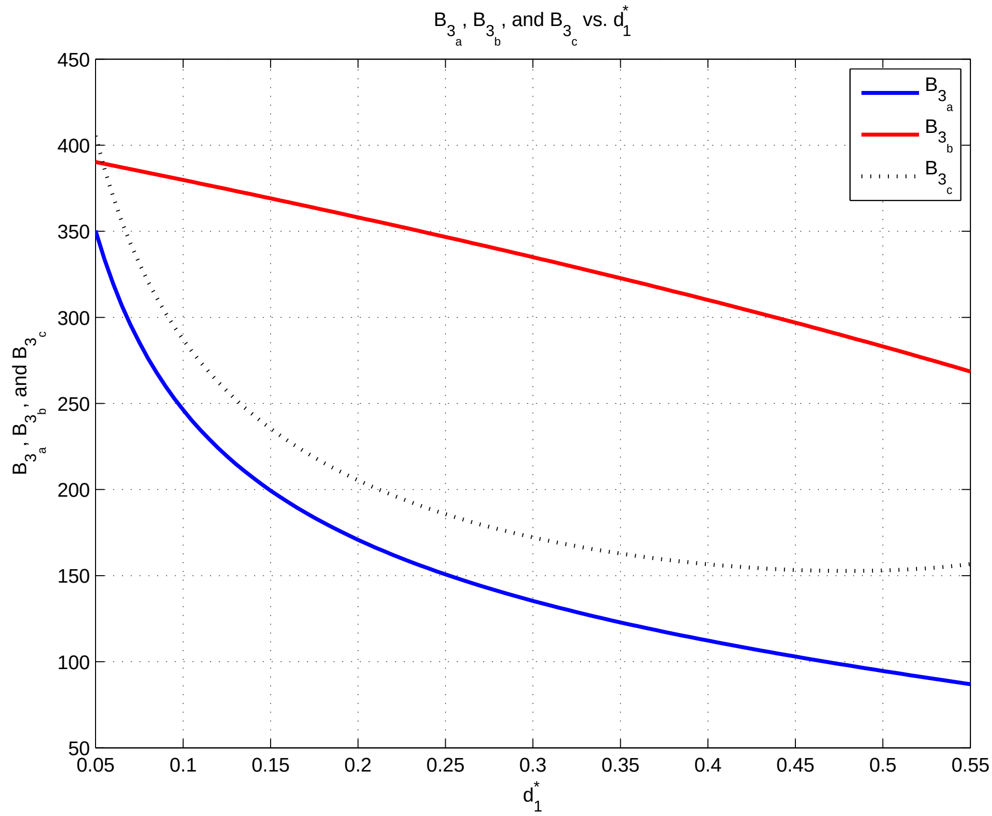

Figure 6.2: Variation of $\mathcal{B}_{3_a}$, $\mathcal{B}_{3_b}$, and $\mathcal{B}_{3_c}$ vs. $d_1^{\star}$ - helicopter Σ_{SFU} system.

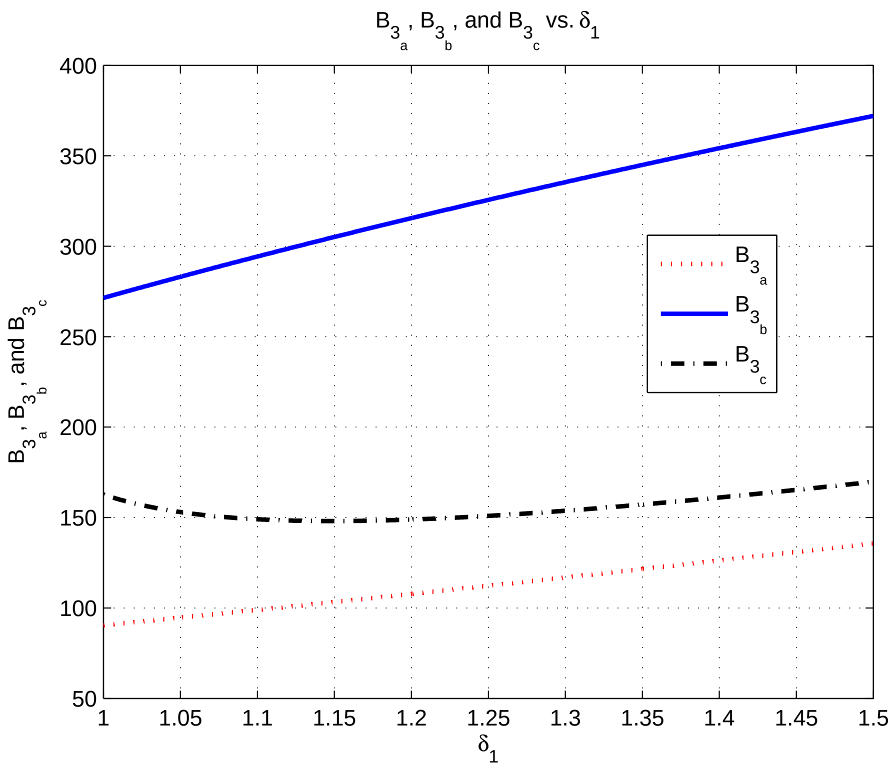

Figure 6.3: Variation of $\mathcal{B}_{3_a}$, $\mathcal{B}_{3_b}$, and $\mathcal{B}_{3_c}$ vs. δ_1 - helicopter Σ_{SFU} system.

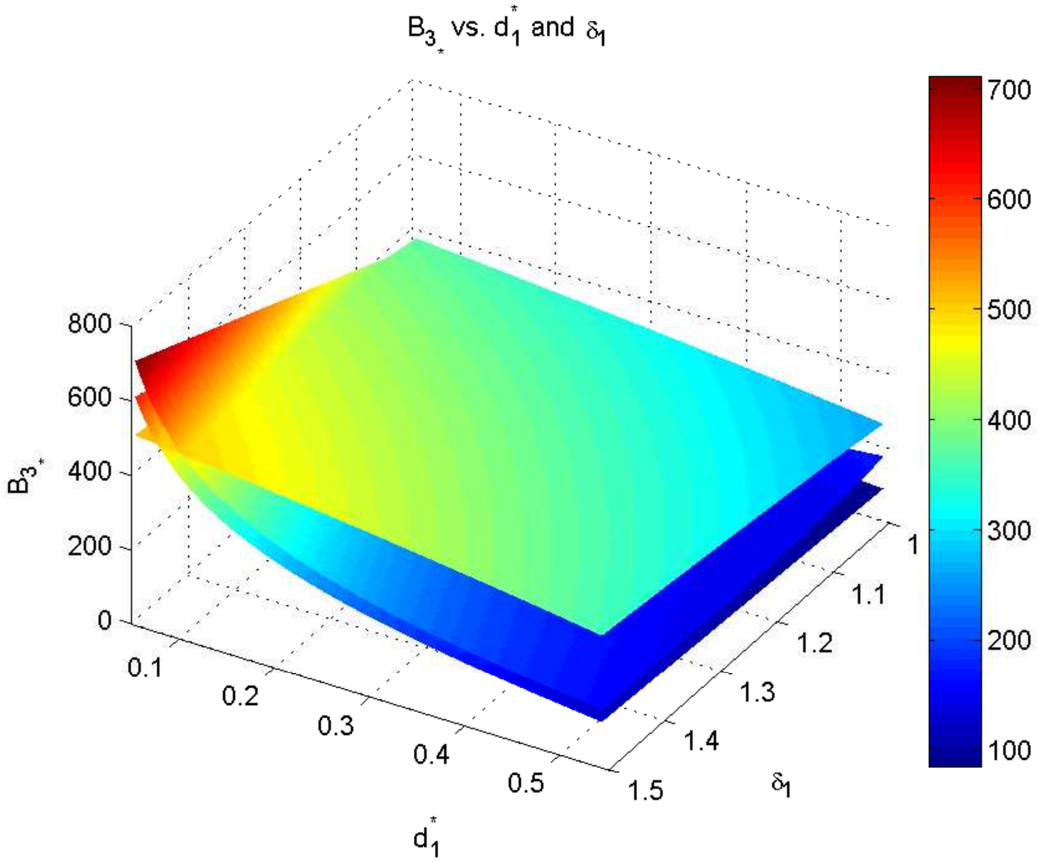

Figure 6.4: Variation of $\mathcal{B}_{3_a}$, $\mathcal{B}_{3_b}$, and $\mathcal{B}_{3_c}$ vs. $d_1^\bigstar$ and δ_1 - helicopter Σ_{SFU} system.

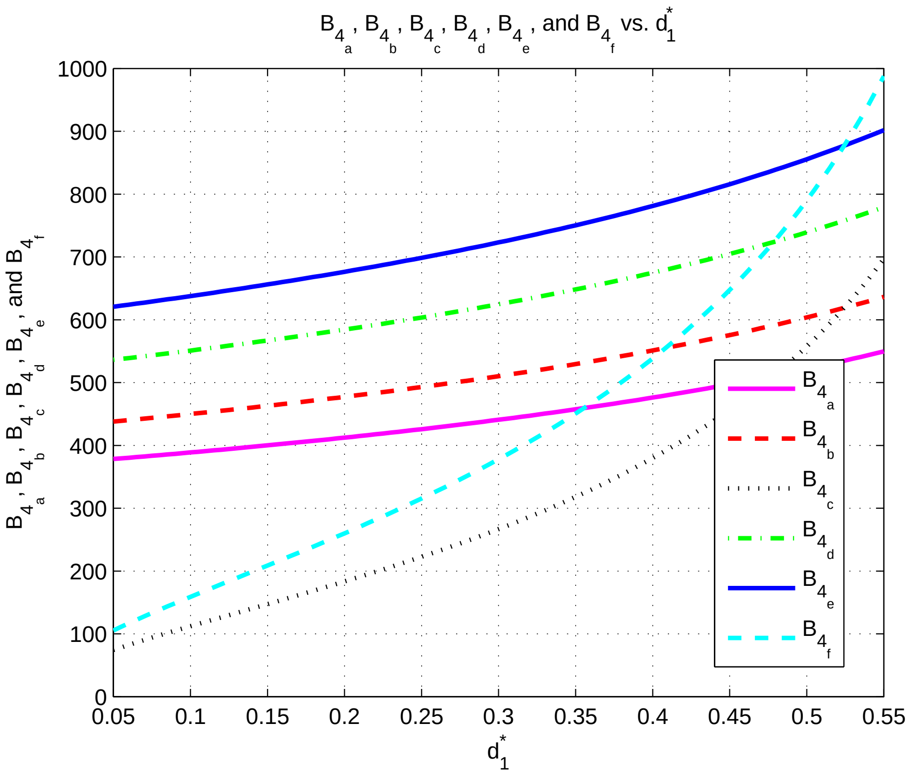

Figure 6.5: Variation of $\mathcal{B}_{4_a}$, $\mathcal{B}_{4_b}$, $\mathcal{B}_{4_c}$, $\mathcal{B}_{4_d}$, $\mathcal{B}_{4_e}$, and $\mathcal{B}_{4_f}$ vs. $d_1^\bigstar$ - helicopter Σ_{SFU} system.

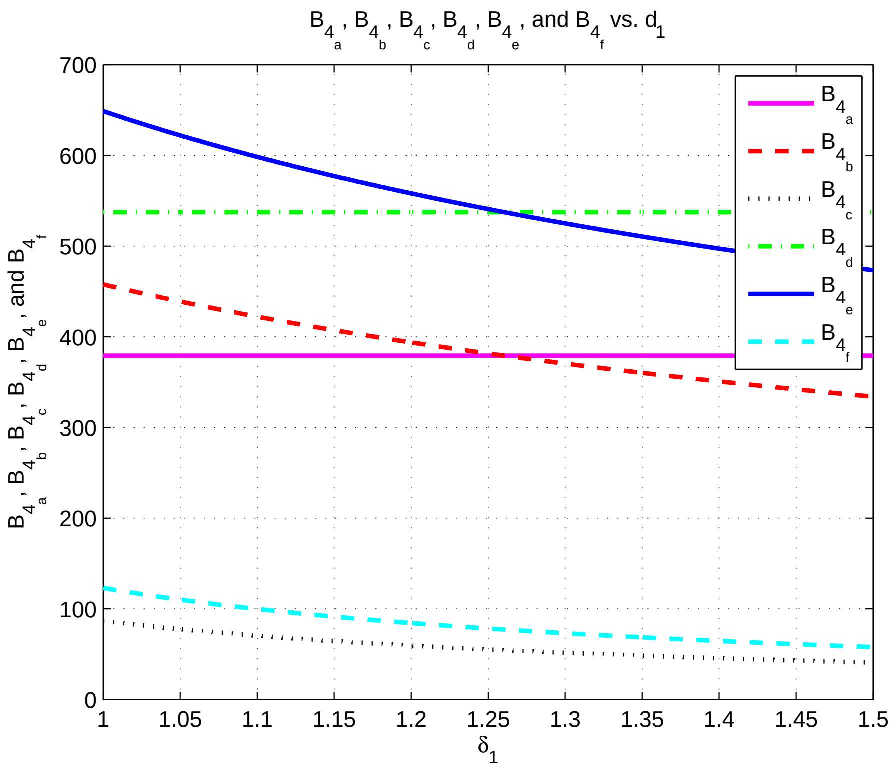

Figure 6.6: Variation of $\mathcal{B}_{4_a}$, $\mathcal{B}_{4_b}$, $\mathcal{B}_{4_c}$, $\mathcal{B}_{4_d}$, $\mathcal{B}_{4_e}$, and $\mathcal{B}_{4_f}$ vs. δ_1 - helicopter Σ_{SFU} system.

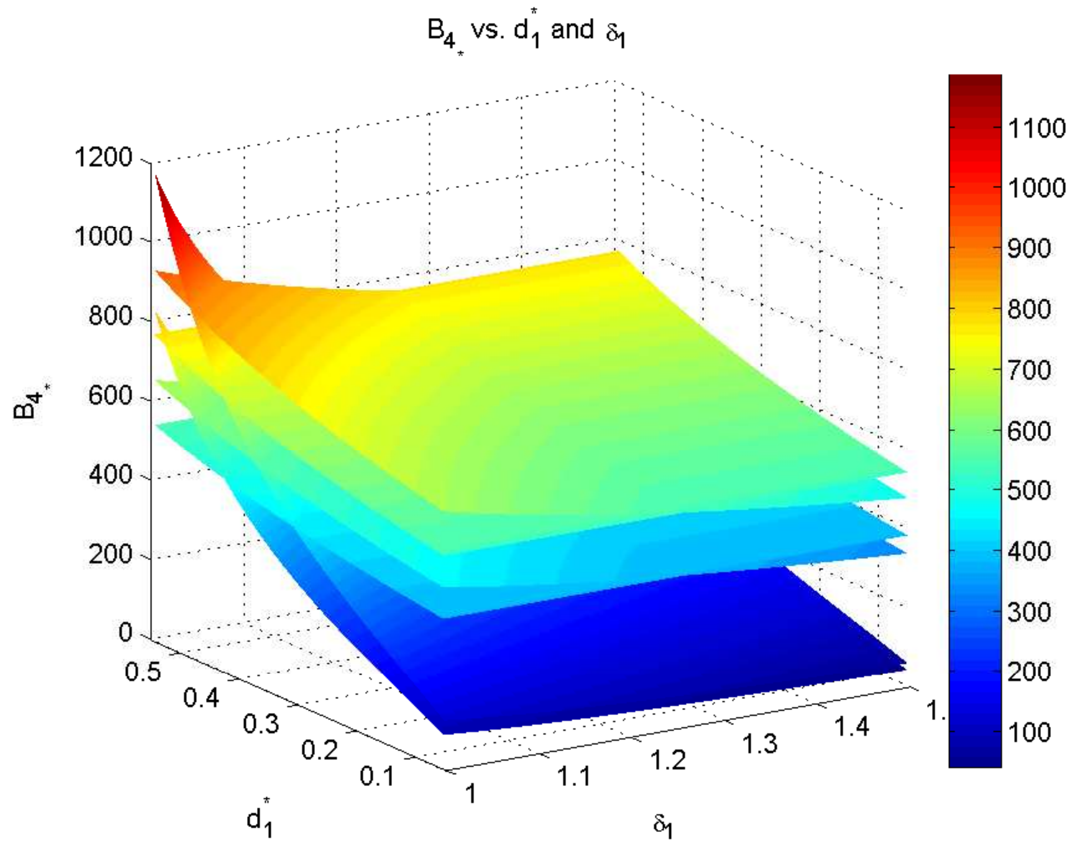

Figure 6.7: Variation of $\mathcal{B}_{4_a}$, $\mathcal{B}_{4_b}$, $\mathcal{B}_{4_c}$, $\mathcal{B}_{4_d}$, $\mathcal{B}_{4_e}$, and $\mathcal{B}_{4_f}$ vs. $d_1^{\star}$ and δ_1 - helicopter Σ_{SFU} system.

6.6 Fulfillment of the Helicopter Σ_{SFU} *Stability Analysis*

The fulfillment of assumptions 5.5.6, 5.5.7, 5.5.8, 5.5.9, and 5.5.10, applied to the helicopter Σ_{SFU} full system by the fulfillment of inequalities 6.239, 6.296, 6.314, and 6.436, proves that the growth requirements of $\tilde{\boldsymbol{F}}(\tilde{\boldsymbol{\chi}}, \tilde{\boldsymbol{z}})$ and $\hat{\boldsymbol{g}}(\tilde{\boldsymbol{\chi}}, \tilde{\boldsymbol{z}})$ are satisfied, and with the Lyapunov functions $V_1(\tilde{\boldsymbol{\chi}})$ and $V_U(\tilde{\boldsymbol{\chi}}, \tilde{\boldsymbol{z}})$, Eqns. (6.202) and (6.51), respectively, a new Lyapunov function candidate $V_2(\tilde{\boldsymbol{\chi}}, \tilde{\boldsymbol{z}})$ is considered and defined by the weighted sum of $V_1(\tilde{\boldsymbol{\chi}})$ and $V_U(\tilde{\boldsymbol{\chi}}, \tilde{\boldsymbol{z}})$, given by

$$V_2(\tilde{\boldsymbol{\chi}}, \tilde{\boldsymbol{z}}) = (1 - d_2)V_1(\tilde{\boldsymbol{\chi}}) + d_2 V_U(\hat{\boldsymbol{z}}),\ d_2 \in (0, 1), \tag{6.587}$$

for $0 < d_2 < 1$. The newly defined function $V_2(\tilde{\boldsymbol{\chi}}, \tilde{\boldsymbol{z}})$ becomes the Lyapunov function candidate for the singular perturbed system (6.6–6.10). Similarly as in the general Σ_{SFU} *Stability Analysis*, to explore the freedom in choosing the weights, lets take d_2 as an unspecified parameter in the interval $(0, 1)$. From the properties of $V_1(\tilde{\boldsymbol{\chi}})$ and $V_U(\tilde{\boldsymbol{\chi}}, \tilde{\boldsymbol{z}})$ and inequality (6.227), that is $\| \tilde{\mathbf{h}}(\tilde{\boldsymbol{\chi}}) \| \leq p_2(\| \tilde{\boldsymbol{\chi}} \|)$, where $p_2(\cdot)$ is a κ function, it follows that $V_2(\tilde{\boldsymbol{\chi}}, \tilde{\boldsymbol{z}})$ is positive-definite.

Computing the time derivative of $V_2(\tilde{\boldsymbol{\chi}}, \tilde{\boldsymbol{z}})$ along the trajectories of along the trajectories of $\tilde{\boldsymbol{F}}(\tilde{\boldsymbol{\chi}}, \tilde{\boldsymbol{z}})$ and $\hat{\boldsymbol{g}}(\tilde{\boldsymbol{\chi}}, \tilde{\boldsymbol{z}})$ yields an equation of similar structure as in Eq. (5.172), which can express as a function of the comparison functions $\psi_2(\tilde{\boldsymbol{\chi}})$, and $\phi_2(\hat{\boldsymbol{z}})$ by employing the derived inequalities 6.239, 6.296, 6.314, and 6.436, resulting in

$$\begin{aligned}
\dot{V}_2 \ &\leq\ -(1-d_2)\alpha_3\psi_1^2(\tilde{\boldsymbol{\chi}}) + (1-d_2)\beta_3\psi_2(\tilde{\boldsymbol{\chi}})\phi_2(\hat{\boldsymbol{z}}) \\
&-\ \frac{d_2}{\varepsilon_1\varepsilon_2}\alpha_4\phi_2^2(\hat{\boldsymbol{z}}) + d_2\gamma_2\phi_2^2(\hat{\boldsymbol{z}}) + d_2\beta_4\psi_2(\tilde{\boldsymbol{\chi}})\phi_2(\hat{\boldsymbol{z}}) \\
&=\ -\begin{bmatrix} \psi_2(\tilde{\boldsymbol{\chi}}) \\ \phi_2(\hat{\boldsymbol{z}}) \end{bmatrix}^T \begin{bmatrix} (1-d_2)\alpha_3 & -\frac{1}{2}(1-d_2)\beta_3 - \frac{1}{2}d_2\beta_4 \\ -\frac{1}{2}(1-d_2)\beta_3 - \frac{1}{2}d_2\beta_4 & d_2\left(\dfrac{\alpha_4}{\varepsilon_1\varepsilon_2} - \gamma_2\right) \end{bmatrix} \\
&\times\ \begin{bmatrix} \psi_2(\tilde{\boldsymbol{\chi}}) \\ \phi_2(\hat{\boldsymbol{z}}) \end{bmatrix} \\
&=\ -\begin{bmatrix} \sqrt{\tilde{\boldsymbol{\chi}}^T\boldsymbol{\mathcal{R}}\tilde{\boldsymbol{\chi}}} \\ \sqrt{\hat{z}^T\tilde{Q}_U\hat{z}} \end{bmatrix}^T \begin{bmatrix} (1-d_2)\alpha_3 & -\frac{1}{2}(1-d_2)\beta_3 - \frac{1}{2}d_2\beta_4 \\ -\frac{1}{2}(1-d_2)\beta_3 - \frac{1}{2}d_2\beta_4 & d_2\left(\dfrac{\alpha_4}{\varepsilon_1\varepsilon_2} - \gamma_2\right) \end{bmatrix} \\
&\times\ \begin{bmatrix} \sqrt{\tilde{\boldsymbol{\chi}}^T\boldsymbol{\mathcal{R}}\tilde{\boldsymbol{\chi}}} \\ \sqrt{\hat{\boldsymbol{z}}^T\tilde{\boldsymbol{Q}}_U\hat{\boldsymbol{z}}} \end{bmatrix}.
\end{aligned} \tag{6.588}$$

In order to guarantee the negative-definiteness property of Eq. (6.588), and conducting the same algebraic transformations as in section 5.5.3, it can be obtained the following expression that defines the requirement to be satisfied by the parasitic constant ε_2 such

$$\varepsilon_1\varepsilon_2 < \frac{\alpha_3\alpha_4}{\alpha_3\gamma_2 + \dfrac{1}{4(1-d_2)d_2}\left[(1-d_2)\beta_3 + d_2\beta_4\right]^2} \equiv \varepsilon_{1_d}\varepsilon_{2_d}, \tag{6.589}$$

where from (6.590) it can be obtained an expression for ε_2 as

$$\varepsilon_2 < \frac{\alpha_3\alpha_4}{\varepsilon_1\left[\alpha_3\gamma_2 + \dfrac{1}{4(1-d_2)d_2}\left[(1-d_2)\beta_3 + d_2\beta_4\right]^2\right]} \equiv \varepsilon_{2_d}. \tag{6.590}$$

Recalling from the general formulation, chapter 5, that although only α_3 and α_4 are required by definition to be positive, β_3, β_4, and γ_2 are also considered to be positive. Analyzing equation (6.590) it can be observed that ε_2 depends on the selected ε_1, but not solely on it, since recalling the definitions of the selected β_3, β_4 and γ_2, Eqns. (6.419), (6.541), and (6.496), respectively, it can be observed that they are influenced by many more design parameters, which are resumed as

$$\beta_3 \quad \rightarrow \quad \beta_3(d_1, Q_S, Q_F, Q_U, b_x, \tilde{b}_{y_1}, \tilde{b}_{y_2}, \varepsilon_1, x_{MAX}, \tilde{y}_{1_{MAX}}, \tilde{y}_{2_{MAX}}, z_{1_{MIN}}, \tilde{Y}_{2_{MAX}}), \tag{6.591}$$

$$\beta_4 \quad \rightarrow \quad \beta_4(d_1, Q_S, Q_F, Q_U, b_x, \tilde{b}_{y_1}, \tilde{b}_{y_2}, \varepsilon_1, \varepsilon_2, x_{MIN}, \tilde{y}_{1_{MIN}}, \tilde{y}_{2_{MIN}}, \tilde{Y}_{2_{MAX}}), \tag{6.592}$$

$$\gamma_2 \quad \rightarrow \quad \gamma_2(Q_U, \tilde{b}_{y_1}, \tilde{b}_{y_2}, \varepsilon_1, \varepsilon_2, x_{MIN}, z_{1_{MIN}}, x_{MAX}, \tilde{y}_{1_{MIN}}, \tilde{y}_{2_{MIN}}), \tag{6.593}$$

therefore being quite difficult to optimize all parameters such that the upper-bound of ε_2 is maximized. Rather than trying to find the optimum combination, these parameters are divided in two groups *Fixed Parameters* and *Stability Parameters*, where

- *Fixed Parameters* denote the parameters that are determined by the physics of the problem and the control design strategy.
- *Stability Parameters* denote that parameters that are introduced solely in the stability analysis.

The first group, the *Fixed Parameters*, are defined by the constant coefficients that take part on the definition of β_3, β_4 and γ_2, being the lower and upper bounds for both the state variables (x_{MIN},x_{MAX},$z_{1_{MIN}}$), and its error dynamics ($\tilde{y}_{1_{MIN}}$, $\tilde{y}_{2_{MIN}}$, $\tilde{y}_{1_{MIN}}$, $\tilde{y}_{2_{MIN}}$, $\tilde{Y}_{2_{MIN}}$), which are all defined by the physics of the problem. This group also includes the control design parameters (b_x, $\tilde{b}_{y_1}$, $\tilde{b}_{y_2}$), which are defined by the selected desired dynamics of the different time-scale subsystems, and the parasitic time constants (ε_1,ε_2), which are given by the selection for the time-scales which depend also on the physics of the problem.

The second group, the *Stability Parameters*, denote the variables that are introduced in the stability analysis in order to satisfy the growth requirements of the different time-scale subsystems, that is Q_S, q_{f_1}, q_{f_2}, q_{u_1}, q_{u_2}, and d_1. Although in the first group, there are some parameters that are subject to modification in order to satisfy the stability requirements, such the desired dynamics coefficients (b_x, $\tilde{b}_{y_1}$, $\tilde{b}_{y_2}$), in this study are maintained fixed, and only the *Stability Parameters* are *tuned* in order to satisfy the growth requirements.

From inequality (6.590), it can be seen that, depending on the nature of the selected ε_1, it will translate into different upper-bounds on ε_{2_d}. This implies that for the conservative upper bound on ε_1, that is larger upper-bounds in ε_1 that required, i.e. $\varepsilon_1^\bigstar > \varepsilon_1$, this translate into a less conservative upper-bound on ε_2. Ultimately, the goal of the stability analysis here conducted, is to prove that the equilibrium point of the singularly perturbed Σ_{SFU}-subsystem is asymptotically stable for all $\varepsilon_2 < \varepsilon_2^*$, therefore it is desired to have ε_1^* strictly larger than the selected ε_1.

This implies that the largest possible ε_{2_d}, that in return will satisfy $\varepsilon_2 < \varepsilon_2^*$, it is given by the minimum allowable value of ε_1 that guarantees the asymptotic stability properties of the Σ_{SF}-subsystem. This is achieved by selecting the $\varepsilon_1^\bigstar$ that was chosen in the Σ_{SF} stability analysis, that is $\varepsilon_1^\bigstar = d_{\varepsilon_1}\varepsilon_1$, where d_{ε_1} represents the percentage of margin that is applied to the upper-bound, where for the problem here studied, it is selected as $d_{\varepsilon_1} = 1.05$, that is, for safety, the ε_1^* is assumed to be 5% higher than the selected ε_1. Recalling from the Σ_{SF} asymptotic stability analysis conducted in section 6.3, is given in Eq. (6.210) as

$$\varepsilon_1^* = \varepsilon_1^\bigstar = \frac{\alpha_1\alpha_2}{\alpha_1(d_1^\bigstar)\gamma_1(\varepsilon_1^\bigstar) + \beta_1\beta_2}, \tag{6.594}$$

therefore, substituting Eq. (6.594) into Eq. (6.590) results in

$$\varepsilon_2 < \frac{\alpha_1\gamma_1(\varepsilon_1^\bigstar) + \beta_1(d_1^\bigstar)\beta_2}{\alpha_1\alpha_2} \frac{\alpha_3\alpha_4}{\varepsilon_1\left[\alpha_3\gamma_2 + \dfrac{1}{4(1-d_2)d_2}\left[(1-d_2)\beta_3 + d_2\beta_4\right]^2\right]} \equiv \varepsilon_{2_d}. \tag{6.595}$$

Therefore inequality (6.595) shows that for any choice of d_2, the corresponding $V_2(\tilde{\boldsymbol{\chi}}, \tilde{\boldsymbol{z}})$ is a Lyapunov function for the singular perturbed Σ_{SFU} system for all ε_2 satisfying inequality (6.595). Analyzing (6.595), it can be easily seen that the maximum value of ε_{2_d} occurs at

$$d_2^* = \frac{\beta_3}{\beta_3 + \beta_4}, \tag{6.596}$$

yielding for the upper-bound on ε_2

$$\varepsilon_2^* = \frac{\alpha_3\alpha_4}{\varepsilon_1^\bigstar\,(\alpha_3\gamma_2 + \beta_3\beta_4)}. \tag{6.597}$$

Therefore it can be inferred that the equilibrium point of the singularly perturbed Σ_{SFU}-subsystem (6.6–6.10) is asymptotically stable for all $\varepsilon_2 < \varepsilon_2^*$. The number ε_2^* is the best upper bound on ε_2 that can be provided by the above presented stability analysis. The results obtained from the fulfillment inequalities (6.239), (6.296), (6.314) and (6.436) are summarized in Table 6.2, where it can be seen the similarities between the two-time-scale growth requirements described in Section 5.2.1, and the three-time-scale growth requirements for the full Σ_{SFU} system.

The asymptotic stability analysis presented proves that by fulfilling inequalities (6.239), (6.296), (6.314), and (6.436), then the origin is an asymptotically stable equilibrium of the singularly perturbed helicopter Σ_{SFU} system, Eqns. (6.6–6.10) for all $\varepsilon_2 \in (0, \varepsilon_2^*)$, where ε_2^* is given by Eq. (6.597), thus, for every number $d_2 \in (0,1)$, $V_2(\tilde{\boldsymbol{\chi}}, \tilde{\boldsymbol{z}})$, Eq. (6.587), is a Lyapunov function for all $\varepsilon_2(0, \varepsilon_d)$, where $\varepsilon_{2_d} \leq \varepsilon_2^*$ is given by Eq. (6.597), hence satisfying Theorem 5.5.5.

The fulfillment of Theorem 5.5.5 for the helicopter Σ_{SFU} full system can be summarized by understanding that $\tilde{\boldsymbol{\chi}} = 0$ is an asymptotically stable equilibrium of the reduced system (6.221), $\tilde{z} = \tilde{\mathbf{h}}(\tilde{\boldsymbol{\chi}})$ is an asymptotically stable equilibrium of the boundary-layer system (6.222) uniformly in $\tilde{\boldsymbol{\chi}}$, that is, the $\varepsilon - \delta$ definition of *Lyapunov* stability and the convergence $\tilde{\boldsymbol{z}} \to \tilde{\mathbf{h}}(\tilde{\boldsymbol{\chi}})$ are uniform in $\tilde{\boldsymbol{\chi}}$ (Vidyasagar, 2002), and if $\tilde{\boldsymbol{F}}(\tilde{\boldsymbol{\chi}}, \tilde{\boldsymbol{z}})$ and $\hat{\boldsymbol{g}}(\tilde{\boldsymbol{\chi}}, \tilde{\boldsymbol{z}})$ satisfy certain growth conditions on the reduced and boundary-layer systems, assumptions 5.5.6, 5.5.7, 5.5.8, 5.5.9, and 5.5.10 applied to the helicopter Σ_{SFU} full system, then the origin is an asymptotically stable equilibrium of the singularly perturbed system (6.6–6.10), for sufficiently small ε_2. (Kokotović et al., 1986; Kokotović et al., 1987; Kokotović et al., 1999).

Similarly as in Σ_{SF} *Stability Analysis*, due to the fact that the system is expressed in its error dynamics form, and that the use of the full range of reachable state variables has been required in order to satisfy the inequalities that guarantee the asymptotic stability properties at the origin of the Σ_{SFU}-subsystem, these asymptotic stability properties are also extended to semiglobal stability, by the definition in (Kokotović, 1992; Sussmann and Kokotović, 1991; Braslavsky and Miidleton, 1996), by providing upper bounds on the parasitic singularly perturbed parameters for the entire range of admissible state values, thus extending the domain of attraction to that same rage of admissible states.

6.6.1 Bounds for the *Stability Parameter* of the Σ_{SFU} *Stability Analysis*

Recalling from the Σ_{SF} stability analysis, that due to the existent freedom on selecting β_2 and γ_1, the upper-bound ε_1^*, Eq. (6.206), and its d_1^* parameter, Eq. (6.205), can be precisely obtained to match the required parameters that guarantee the asymptotic stability for the full Σ_{SFU} system. This is achieved by selecting the appropriate combination of γ_1 and β_2, which in return generates the desired combination of both $\varepsilon_1^\bigstar$ and $d_1^\bigstar$, which are both obtained using Eqns. (6.206) and (6.205) such

$$\gamma_1(\varepsilon_1^\bigstar) \quad = \quad \frac{1}{\alpha_1}\left(\frac{\alpha_1\alpha_2}{\varepsilon_1^\bigstar} - \beta_1\beta_2\right), \tag{6.598}$$

Assumption 5.5.7 for the Helicopter Σ_{SFU} System				
Section 5.2	$\frac{\partial V}{\partial x}$	$f(x, \mathrm{h}(x))$	α_1	$\psi(x)$
Σ_{SFU}	$\left(\frac{\partial V_1(\tilde{\chi})}{\partial \tilde{\chi}}\right)^T$	$\tilde{F}(\tilde{\chi}, \tilde{\mathrm{h}}(\tilde{\chi}))$	$\alpha_3 \leq 1$	$\psi_2(\tilde{\chi}) = \sqrt{\tilde{\chi}^T \mathcal{R} \tilde{\chi}}$
Assumption 5.5.8 for the Helicopter Σ_{SFU} System				
Section 5.2	$\frac{\partial W}{\partial z}$	$g(x, z)$	α_2	$\phi(z - \mathrm{h}(x))$
Σ_{SFU}	$\left(\frac{\partial V_U(\hat{z})}{\partial \hat{z}}\right)^T$	$\hat{h}(\tilde{\chi}, \tilde{z})$	$\alpha_4 \leq 1$	$\phi_2(\hat{z}) = \sqrt{\hat{z}^T \tilde{Q}_U \hat{z}}$
Assumption 5.5.9 for the Helicopter Σ_{SFU} System				
Section 5.2	$\frac{\partial V}{\partial x}$	$f(x, z)$	$f(x, \mathrm{h}(x))$	β_1
Σ_{SFU}	$\left(\frac{\partial V_1(\tilde{\chi})}{\partial \tilde{\chi}}\right)^T$	$\tilde{F}(\tilde{\chi}, \tilde{z})$	$\tilde{F}(\tilde{\chi}, \tilde{\mathrm{h}}(\tilde{\chi}))$	$\beta_3 \geq \max(\beta_{3_a} \beta_{3_b})$
Assumption 5.5.10 for the Helicopter Σ_{SFU} System				
Section 5.2	$\frac{\partial W}{\partial x}$	$f(x, z)$	γ_1	β_2
Σ_{SFU}	$\left(\frac{\partial V_U(\hat{z})}{\partial \hat{z}}\right)^T$	$\tilde{F}(\tilde{\chi}, \tilde{z})$	$\gamma_2 \geq \max(\gamma_{2_a} \gamma_{2_b})$	$\beta_4 \geq \max(\beta_{4_A} \beta_{4_B})$

Table 6.2: Parameters for the Comparison Functions and Inequalities that Guarantee the Asymptotic Stability Requirements for the Helicopter Σ_{SFU} System.

$$\beta_2(d_1^\star) = \frac{\beta_1}{d_1^\star} - \beta_1, \tag{6.599}$$

where $\varepsilon_1^\star = d_{\varepsilon_1}\varepsilon_1$, with $d_{\varepsilon_1} = 1.05$, and $d_1^\star = 0.5$, therefore resulting in the expression

$$\varepsilon_2 < \frac{\alpha_1\gamma_1(\varepsilon_1^\star) + \beta_1\beta_2(d_1^\star)}{\alpha_1\alpha_2} \frac{\alpha_3\alpha_4}{\varepsilon_1\left(\alpha_3\gamma_2 + \frac{1}{4(1-d_2)d_2}\left[(1-d_2)\beta_3 + d_2\beta_4\right]^2\right)}\varepsilon_{2_d}, \tag{6.600}$$

which has also a maximum for d_2^*

$$d_2^* = \frac{\beta_3}{\beta_3 + \beta_4}, \tag{6.601}$$

thus resulting in the upper bound for ε_2 as

$$\varepsilon_2^* = \frac{\alpha_1\gamma_1(\varepsilon_1^\star) + \beta_1\beta_2(d_1^\star)}{\alpha_1\alpha_2} \frac{\alpha_3\alpha_4}{\alpha_3\gamma_2 + \beta_3\beta_4}. \tag{6.602}$$

Recalling the definitions of β_3, β_4 and γ_2, given in Eqns. (6.435), (6.505), and (6.586), respectively, such

$$\beta_3 \geq \sqrt{\frac{2\left(\mathcal{L}_{2_a}\tilde{Q}_{SF}^2 + \left(\mathcal{L}_{2_b} + \tilde{Q}_{F_{21}}\mathcal{L}_{2_c}\right)\tilde{Q}_{SF}\right)}{\tilde{r}_2\tilde{Q}_{SF} - \tilde{r}_3}}\sqrt{\frac{Q_S}{q_{u_1}}}, \tag{6.603}$$

$$\gamma_2 \geq 2\mathcal{N}\left(C_{u_1} + \frac{C_{u_3}}{2} + C_{u_2}Q_{U_{21}}\right), \tag{6.604}$$

$$\beta_4 \geq \beta_{4_e} = \sqrt{\frac{2\tilde{\mathcal{M}}_2\left[C_{u_3}^2 + C_{u_1}C_{u_3} + Q_{U_{21}}C_{u_2}C_{u_3}\right]}{Q_{U_{21}}\left(\tilde{r}_2\tilde{Q}_{SF} - \tilde{r}_3\right)}}\sqrt{\frac{q_{u_1}}{Q_S}}, \tag{6.605}$$

where, as previously derived, the different ratio between the *stability parameters* are given by

$$\tilde{Q}_{SF} = \delta_1\frac{(1-d_1)}{2d_1b_x}\mathcal{C}_1, \tag{6.606}$$

$$Q_{U_{21}} = \frac{-\left(2C_{u_1} + C_{u_3}\right) + \sqrt{\left(2C_{u_1} + C_{u_3}\right)^2 + 8C_{u_2}C_{u_3}}}{4C_{u_2}}, \tag{6.607}$$

where recalling from the results obtained in sections 6.5.4 and 6.5.5, it is required that $d_1^{\bigstar} \in (0, 0.5243)$, and $\delta_1 \in (1.02, 1.264)$, therefore selecting $d_1^{\bigstar} = 0.5$, and $\delta_1 = 1.05$. In addition to the ratios defined in Eqns. (6.606) and (6.607), an additional ratio was previously derived

$$\tilde{Q}_{F_{21}} > \frac{\mathcal{C}_2}{\mathcal{C}_1}, \tag{6.608}$$

therefore resulting in

$$q_{f_1} = \tilde{Q}_{SF} Q_S, \tag{6.609}$$

$$q_{f_2} = \tilde{Q}_{F_{21}} \tilde{Q}_{SF} Q_S, \tag{6.610}$$

$$q_{u_2} = Q_{U_{21}} q_{u_1}. \tag{6.611}$$

In order to completely define the upper bounds on ε_2, all the *stability parameters*, Q_S, q_{f_1} or q_{f_2}, q_{u_1} and q_{u_2}, need to be selected, where needs to be noted that only the ratios $\tilde{Q}_{SF}$, and $Q_{U_{21}}$, Eqns. (6.609) and (6.611), respectively, are completely bounded, and $\tilde{Q}_{F_{21}}$ it is defined by the above expression, but needs to be bounded. This implies that, by initially selecting a reference value for the *stability parameter* Q_S, only q_{f_1} is completely defined and bounded by using Eq. (6.609). The rest of the stability parameters can be determined by analyzing the extended version for the upper-bounds ε_2^* and d_2^*, Eqns. (6.602) and (6.613), respectively. The expression that determines the upper-bound in ε_2, Eq. (6.435), can be rewritten by substituting in β_3, γ_2, and β_4, Eqns. (6.603), (6.604), and (6.605), respectively, resulting in

$$\varepsilon_2^* = \frac{\alpha_3\alpha_4\left(\alpha_1\gamma_1(\varepsilon_1^{\bigstar}) + \beta_1\beta_2(d_1^{\bigstar})\right)}{\alpha_1\alpha_2\left(\alpha_3\gamma_2 + \sqrt{\frac{4\tilde{\mathcal{M}}_2\left(\mathcal{L}_{2_a}\tilde{Q}_{SF}^2 + \left(\mathcal{L}_{2_b} + \tilde{Q}_{F_{21}}\mathcal{L}_{2_c}\right)\tilde{Q}_{SF}\right)\left[C_{u_3}^2 + C_{u_1}C_{u_3} + Q_{U_{21}}C_{u_2}C_{u_3}\right]}{Q_{U_{21}}\left(\tilde{r}_2\tilde{Q}_{SF} - \tilde{r}_3\right)^2}}\right)}, \tag{6.612}$$

with γ_2 being given in Eq. (6.604), and similarly with d_2^* resulting in

$$d_2^* = \frac{\sqrt{\frac{2\left(\mathcal{L}_{2_a}\tilde{Q}_{SF}^2 + \left(\mathcal{L}_{2_b} + \tilde{Q}_{F_{21}}\mathcal{L}_{2_c}\right)\tilde{Q}_{SF}\right)\frac{Q_S}{q_{u_1}}}{\tilde{r}_2\tilde{Q}_{SF} - \tilde{r}_3}}}{\sqrt{\frac{2\left(\mathcal{L}_{2_a}\tilde{Q}_{SF}^2 + \left(\mathcal{L}_{2_b} + \tilde{Q}_{F_{21}}\mathcal{L}_{2_c}\right)\tilde{Q}_{SF}\right)}{\tilde{r}_2\tilde{Q}_{SF} - \tilde{r}_3}\frac{Q_S}{q_{u_1}}} + \sqrt{\frac{2\tilde{\mathcal{M}}_2\left[C_{u_3}^2 + C_{u_1}C_{u_3} + Q_{U_{21}}C_{u_2}C_{u_3}\right]}{Q_{U_{21}}\left(\tilde{r}_2\tilde{Q}_{SF} - \tilde{r}_3\right)}\frac{q_{u_1}}{Q_S}}}. \tag{6.613}$$

It can be recognized that the fulfillment of the asymptotic stability properties for the Σ_{SFU} full system can be achieved by the proper selection of *stability parameters* Q_S, q_{f_1}, q_{f_2}, q_{u_1}, q_{u_2}, $d_1^{\bigstar}$, and $\varepsilon_1^{\bigstar}$, with $d_1^{\bigstar} = 0.5$, and $\varepsilon_1^{\bigstar} = 1.05\varepsilon_1$, as seen previously. Observing Eq. (6.612), it can be recognized that the upper-bound on ε_2^* only depends on the physical parameters of the problem, the control design parameters b_x, $\tilde{b}_{y_1}$, and $\tilde{b}_{y_2}$ that determine the selected target dynamics response, and the *stability parameter* ratios $\tilde{Q}_{SF}$, $\tilde{Q}_{F_{21}}$, $Q_{U_{21}}$. Observing the denominator in Eq. (6.612) it can be also recognized that it is required to satisfy that $\tilde{Q}_{SF} > \frac{\tilde{r}_3}{\tilde{r}_2}$, which after substituting the expressions for both $\tilde{r}_2$ and $\tilde{r}_3$, Eqns. (6.269) and (6.271), respectively, it can be recognized that it is equivalent to the expression derived in the Σ_{SF} *Stability Analysis*, that resulted in the expression defined in Eq. (6.606), thus being consistent with the analysis previously derived.

Recalling that one of the principal results of the Σ_{SFU} Stability Analysis is the obtention of the upper bounds on the parasitic constant ε_2^*, to identify if the selected $\varepsilon_2 < \varepsilon_2^*$ which is one of the requirements to guarantee the asymptotic stability properties for the system being analyzed, the three-time-scale helicopter model. This can be achieved by designing the ratios that define the values of the *Stability Parameters* such that both ε_2^* and d_2^* are bounded. This can be done by starting first to select the desired value of ε_2 as $\varepsilon_2^\star = d_{\varepsilon_2}\varepsilon_2$ in Eq. (6.612), where d_{ε_2} is the selected safety margin for the parasitic constant ε_2, and selected as $d_{\varepsilon_2} = 1.05$. This implies that the upper bound of ε_2^* is selected to be a 5% increment with respect to the selected ε_2 for the helicopter problem here discussed. With this in mind, Eq. (6.612) can be solved to obtain the ratio Q_{F21} resulting in

$$\tilde{Q}_{F_{21}} = \frac{Q_{U_{21}}\left(r_2\tilde{Q}_{SF} - r_3\right)^2\left(\frac{\alpha_3\alpha_4}{\varepsilon_1^\star\varepsilon_2^\star} - \alpha_3\gamma_2\right)^2}{4\mathcal{L}_{2_c}\tilde{\mathcal{M}}_2\left(C_{u_3}^2 + C_{u_1}C_{u_3} + Q_{U_{21}}C_{u_2}C_{u_3}\right)\tilde{Q}_{SF}} - \frac{\mathcal{L}_{2_a}\tilde{Q}_{SF}^2 + \mathcal{L}_{2_b}\tilde{Q}_{SF}}{\mathcal{L}_{2_c}\tilde{Q}_{SF}}, \tag{6.614}$$

were it can be seen that $\tilde{Q}_{F_{21}}$ is a function of $\tilde{Q}_{F_{21}}\left(Q_S, \tilde{Q}_{SF}, Q_{U_{21}}\right)$, with $\tilde{Q}_{SF}$ and $Q_{U_{21}}$ being defined in Eqns. (6.606) and (6.607), respectively. Recalling that for the helicopter model here described the control design parameters are selected as

$$b_x = 1.5 \tag{6.615}$$

$$\tilde{b}_{y_1} = \varepsilon_1\omega_{n_y}^2 \tag{6.616}$$

$$\tilde{b}_{y_2} = 2\varepsilon_1\zeta_{n_y}\omega_{n_y}, \tag{6.617}$$

where recall that ω_{n_y} is desired natural frequency of the vertical displacement target dynamics, and selected as $\omega_{n_y} = 1$ and ζ_{n_y} is the desired damping ratio for the vertical displacement target dynamics, and selected as $\zeta_{n_y} = 0.9$, therefore resulting in

$$\tilde{Q}_{SF} = 0.259974, \tag{6.618}$$

$$Q_{F_{21}} = 2.567205, \tag{6.619}$$

$$Q_{U_{21}} = 0.0041970. \tag{6.620}$$

Therefore, by selecting an arbitrary value for Q_S, ie. $Q_S = 0.5$, and recalling Eqns. (6.609), and (6.610), results in

$$q_{f_1} = 0.129987, \tag{6.621}$$

$$q_{f_2} = 0.333703. \tag{6.622}$$

This translate to having bounded values for three out of the five *stability parameters*, where still missing a relation to provide bounded values for both q_{u_1} and q_{u_2}, although it can be reduced to obtain a relation for only one of the two, since the proper ratio between both q_{u_1} and q_{u_2} is given by Eq. (6.607). This can be achieved by analyzing Eq. (6.613), and recognizing that, by selecting the value of $d_2^* = d_2^\star$, it can be obtained an expression that determines the missing relation that allows to obtain both q_{u_1} and q_{u_2}, with the use of Eq. (6.611). Rewriting Eq. (6.613) results in

$$d_2^* = \frac{\beta_3}{\beta_3 + \beta_4}, \rightarrow \frac{1 - d_2^\star}{d_2^\star} = \frac{\beta_4}{\beta_3}, \tag{6.623}$$

therefore, after substituting both β_3 and β_4, Eqns. (6.603) and (6.605), respectively, results in

$$\frac{1 - d_2^\star}{d_2^\star} = \frac{q_{u_1}}{Q_S}\sqrt{\frac{4\tilde{\mathcal{M}}_2\left(C_{u_3}^2 + C_{u_1}C_{u_3} + Q_{U_{21}}C_{u_2}C_{u_3}\right)\left(\mathcal{L}_{2_a}\tilde{Q}_{SF}^2 + \left(\mathcal{L}_{2_b} + \tilde{Q}_{F_{21}}\mathcal{L}_{2_c}\right)\tilde{Q}_{SF}\right)}{Q_{U_{21}}}}, \tag{6.624}$$

therefore identifying that a expression that relates q_{u_1} and Q_S can be obtained from Eq. (6.624) resulting in

$$\frac{q_{u_1}}{Q_S} = \frac{1 - d_2^\star}{d_2^\star\sqrt{\frac{4\tilde{\mathcal{M}}_2\left(C_{u_3}^2 + C_{u_1}C_{u_3} + Q_{U_{21}}C_{u_2}C_{u_3}\right)\left(\mathcal{L}_{2a}\tilde{Q}_{SF}^2 + \left(\mathcal{L}_{2_b} + \tilde{Q}_{F_{21}}\mathcal{L}_{2c}\right)\tilde{Q}_{SF}\right)}{Q_{U_{21}}}}} = Q_{US}, \tag{6.625}$$

where Q_{US} defines the ratio between Q_S and q_{u_1} such $q_{u_1} = Q_{US}Q_S$, with Q_S being the arbitrary *stability parameter*, selected as $Q_S = 0.5$. This result, along with the rest stability ratio parameters, yields $Q_{US} = 0.330899$. This completes the stability ratio parameters such that all *stability parameters* that satisfy the asymptotic stability analysis are bounded, and that can be defined as a function of the arbitrary parameter Q_S such

$$q_{f_1} = \tilde{Q}_{SF} Q_S, \tag{6.626}$$

$$q_{f_2} = \tilde{Q}_{F_{21}} \tilde{Q}_{SF} Q_S, \tag{6.627}$$

$$q_{u_1} = Q_{US} Q_S, \tag{6.628}$$

$$q_{u_2} = Q_{U_{21}} q_{u_1} = Q_{U_{21}} Q_{US} Q_S. \tag{6.629}$$

Using the definitions of the ratios, $\tilde{Q}_{SF}$, $\tilde{Q}_{F_{21}}$, Q_{US}, and $Q_{U_{21}}$, Eqns. (6.606), (6.614), (6.624), and (6.607), respectively, results in

$$Q_S = 0.5, \tag{6.630}$$

$$q_{f_1} = 1.05 \frac{(1-d_1)}{2 d_1 b_x} \mathcal{C}_1 Q_S, \tag{6.631}$$

$$\begin{aligned} q_{f_2} = {} & 1.05 \frac{(1-d_1)}{2 d_1 b_x} \mathcal{C}_1 Q_S \left[\frac{Q_{U_{21}} \left(r_2 \tilde{Q}_{SF} - r_3 \right)^2 \left(\frac{\alpha_3 \alpha_4}{\varepsilon_1^\star \varepsilon_2^\star} - \alpha_3 \gamma_2 \right)^2}{4 \mathcal{L}_{2_c} \tilde{\mathcal{M}}_2 \left(C_{u_3}^2 + C_{u_1} C_{u_3} + Q_{U_{21}} C_{u_2} C_{u_3} \right) \tilde{Q}_{SF}} \right. \\ & \left. - \frac{\mathcal{L}_{2_a} \tilde{Q}_{SF}^2 + \mathcal{L}_{2_b} \tilde{Q}_{SF}}{\mathcal{L}_{2_c} \tilde{Q}_{SF}} \right], \end{aligned} \tag{6.632}$$

$$q_{u_1} = \frac{Q_S \left(1 - d_2^\star \right)}{d_2^\star \sqrt{\frac{4 \tilde{\mathcal{M}}_2 \left(C_{u_3}^2 + C_{u_1} C_{u_3} + Q_{U_{21}} C_{u_2} C_{u_3} \right) \left(\mathcal{L}_{2_a} \tilde{Q}_{SF}^2 + \left(\mathcal{L}_{2_b} + \tilde{Q}_{F_{21}} \mathcal{L}_{2_c} \right) \tilde{Q}_{SF} \right)}{Q_{U_{21}}}}}, \tag{6.633}$$

$$q_{u_2} = \frac{Q_S \left(1 - d_2^\star \right) \left(-\left(2 C_{u_1} + C_{u_3} \right) + \sqrt{\left(2 C_{u_1} + C_{u_3} \right)^2 + 8 C_{u_2} C_{u_3}} \right)}{4 C_{u_2} d_2^\star \sqrt{\frac{4 \tilde{\mathcal{M}}_2 \left(C_{u_3}^2 + C_{u_1} C_{u_3} + Q_{U_{21}} C_{u_2} C_{u_3} \right) \left(\mathcal{L}_{2_a} \tilde{Q}_{SF}^2 + \left(\mathcal{L}_{2_b} + \tilde{Q}_{F_{21}} \mathcal{L}_{2_c} \right) \tilde{Q}_{SF} \right)}{Q_{U_{21}}}}}, \tag{6.634}$$

where for the physical parameters here employed, the parameters become

$$Q_S = 0.5, \tag{6.635}$$

$$q_{f_1} = 0.129986, \tag{6.636}$$

$$q_{f_2} = 0.333703, \tag{6.637}$$

$$q_{u_1} = 0.165449, \tag{6.638}$$

$$q_{u_2} = 5.455576 \times 10^{-4}. \tag{6.639}$$

Recall that the *stability parameters* depend on the selected upper-bounds, $d_1^\star$, $d_2^\star$, $\varepsilon_1^\star$, and $\varepsilon_2^\star$, the selected target dynamics coefficients, b_x, $\tilde{b}_{y_1}$, and $\tilde{b}_{y_2}$, and the physical parameters of the helicopter, including the selected parasitic constants, ε_1 and ε_2. Recall that $d_1^\star$ and $d_2^\star$ represent the desired values for the upper-bound constants d_1^* and d_2^*, where ε_1 and ε_2 are maximum, Eqns. (6.204) and (6.600), respectively.

The unspecified parameters $d_1^\star$ and $d_2^\star$, differ from d_1^* and d_2^*, Eqns. (6.205) and (6.596), respectively, in the fact that $d_1^\star$ and $d_2^\star$ are selected rather than obtained by using their respective definitions. In addition, the selection of these parameters is done satisfying the different growth requirements for the asymptotic stability analysis, which bounds these values such that the asymptotic stability properties are guaranteed.

As seen in previous derivations, it was chosen $d_1^\star = 0.5$, and for completeness, although it is not required, and it is also selected $d_2^\star = 0.5$, such that the distribution for both ε_1 and ε_2 are centered as it can be seen in Figure 6.8. This is a really powerful result, since implies the existence of a closed form solution for the proper selection of the *stability parameters* q_{f_1}, q_{f_2}, q_{u_1}, and q_{u_2} as a function of the arbitrary Q_S, which are given in Eqns. (6.631), (6.632), (6.633), and (6.634). This translates to the fact that, thanks to the proposed three-time-scale methodology employed to fulfill assumptions 5.5.6, 5.5.7, 5.5.8, 5.5.9, and 5.5.10, which in return implies that the origin is an asymptotically stable equilibrium of the singularly perturbed helicopter Σ_{SFU} system (6.6–6.10) for all $\varepsilon_2 \in (0, \varepsilon_2^*)$, the results obtained through the fulfillment of inequalities (6.239), (6.296), (6.314), and (6.436), it also provides the tools to determine the selection of the *stability parameters* that guarantee the asymptotic stability properties for the helicopter Σ_{SFU} full system. Expanding $V_2(\tilde{\boldsymbol{\chi}}, \tilde{\boldsymbol{z}})$ it can be seen that the resulting Lyapunov function is also a function of the *stability parameters* such

$$
\begin{aligned}
V_2(\tilde{\boldsymbol{\chi}}, \tilde{\boldsymbol{z}}) &= (1-d_2)V_1(\tilde{\boldsymbol{\chi}}) + d_2 V_U(\hat{\boldsymbol{z}}) \\
&= \lambda_1 \frac{Q_S}{4b_x}\tilde{x}^2 + \frac{\lambda_2}{2}\left[\left(C_{f_1}q_{f_1} + C_{f_2}q_{f_2}\right)\tilde{y}_1^2 + \frac{d_1}{2}\left(C_{f_4}q_{f_1} + C_{f_5}q_{f_2}\right)\tilde{y}_2^2 + d_1 C_{f_3}q_{f_1}\tilde{y}_1\tilde{y}_2\right] \\
&+ \lambda_3\left[\frac{1}{2}\left(C_{u_1}q_{u_1} + C_{u_2}q_{u_2}\right)\hat{z}_1^2 + \frac{1}{2}\left(C_{u_4}q_{u_1} + C_{u_5}q_{u_2}\right)\hat{z}_2^2 + C_{u_3}q_{u_1}\hat{z}_1\hat{z}_2\right],
\end{aligned}
\tag{6.640}
$$

where

$$\lambda_1 = (1-d_1^\bigstar)(1-d_2^\bigstar) = 1 - d_1^\bigstar - d_2^\bigstar + d_1 d_2^\bigstar, \tag{6.641}$$

$$\lambda_2 = (1-d_2^\bigstar), \tag{6.642}$$

$$\lambda_3 = d_2^\bigstar, \tag{6.643}$$

therefore, the definition of the *stability parameters*, also provide a valid Lyapunov function for the complete helicopter Σ_{SFU} singularly perturbed system. Figure 6.8 shows the dependance on the right-hand side of Eq. (6.595) on the unspecified parameter d_2, and as it can be seen, the maximum value of the ε_2 parameter is given a $\varepsilon_2^\bigstar = 1.26250 \times 10^{-4}$. Recall that for the problem here stated it was selected $\varepsilon_2 = 1.25 \times 10^{-4}$, thus satisfying that $\varepsilon_2 < \varepsilon_2^\bigstar$. Figure 6.9 shows the linear dependance of the *stability parameters* q_{f_1}, q_{f_2}, q_{u_1}, and q_{u_2} for varying Q_S.

The described stability process can be better understood by describing the dependance on both the *Stability Parameters*, Eqns. (6.630), (6.631), (6.632), (6.633) and (6.634), and their ratios, Eqns. (6.606), (6.608), and (6.607), as a function of varying the desired $d_1^\bigstar$, and $d_2^\bigstar$ while still maintaining constant the desired upper-bound $\varepsilon_2^\bigstar$. Some of these *Stability Parameters*, like the ratio $\tilde{Q}_{SF}$, and $Q_{F_{21}}$, and the parameters q_{f_1} and q_{f_2} have no dependance on the desired $d_2^\bigstar$. Figures 6.10, 6.11, show the variation of the *Stability Parameter* ratios Q_{SF}, and $Q_{F_{21}}$, respectively, as the desired parameter $d_1^\bigstar$ is varied from $(0, 1)$.

Figure 6.12 shows also the variation of the *Stability Parameters* q_{f_1}, and q_{f_2} as the desired parameter $d_1^\bigstar$ is varied in the feasible range that satisfies asymptotic stability, $d_1^\bigstar \in (0.0543, 0.5243)$. On the other side, since the *Stability Parameter* ratio Q_{US} does depend on both the desired $d_1^\bigstar$ and $d_2^\bigstar$, the *Stability Parameters* q_{u_1} and q_{u_2}, also vary as both $d_1^\bigstar$ and $d_2^\bigstar$ are also varied. Figures 6.13, and 6.14 show the variation of ratio Q_{US}, and the *Stability Parameters* q_{u_1} and q_{u_2}, respectively as both $d_1^\bigstar$ and $d_2^\bigstar$ are varied, but, still maintaining constant the desired upper-bound $\varepsilon_2^\bigstar = d_{\varepsilon_2}\varepsilon_2$. The rest of the *Stability Parameters*, q_{f_1}, q_{u_1}, q_{u_2}, remain constant since only depend on the *Stability Parameters* Q_S.

These figures show the power of the final results here described, where, thanks to the proposed Σ_{SFU} *Stability Analysis* approach, the designer has total control over the *Stability Parameters*, as long as they satisfy the bounds and the ratios that have been obtained through the fulfillment of the proposed asymptotic stability methodology, thus allowing to select them in order to satisfy the asymptotic stability properties of the closed loop resulting system.

Furthermore, since the same philosophy was used to design the proper control laws, the asymptotic stability analysis is performed in a fluent and straight forward manner, which once completed, even might seem trivial, but this is thanks to the proposed methodology. The difficulties encountered when trying to stabilize a multiparameter time-scale nonlinear system are well known (Abed, 1985d; Abed, 1985e; Abed, 1985b; Desoer and Shahruz, 1986; Kokotović et al., 1987; Naidu, 2002; Grammel, 2004), and most of the time, they become just theoretical applications due to the complexity of the proposed methods. In addition, the determination of the stability properties require the obtention of complicated Lyapunov function candidates for each of the studied subsystems, which are obtained at the same time than the fulfillment of the associated growth requirements that fulfill the asymptotic properties (Kokotović et al., 1986; Kokotović et al., 1987), which complicates even further the entire analysis process, and not even mention the fact that the studied systems, are autonomous problems in which the design of the control strategy is not considered. The proposed methodology in this thesis provides an all-in-one tool that provide the control strategy, a Lyapunov time scale derivation, and a time-scale asymptotic stability analysis of the singularly perturbed system, becoming a really powerful tool for the analysis of nonlinear singularly perturbed systems.

Therefore, recalling from the previous stability analysis, the coefficients that fulfill the growth requirements are therefore given by

$$\begin{aligned}
\alpha_3 &= 0.95, \\
\alpha_4 &= 0.95, \\
\beta_3 &= 492.14288, \\
\beta_4 &= 492.14288, \\
\gamma_2 &= 11128.12913.
\end{aligned}$$

The upper-bound (6.612) is given by $\varepsilon_2^* = 1.26250 \times 10^{-4}$. Recall that for the problem here stated it was selected $\varepsilon_2 = 1.25 \times 10^{-4}$, thus satisfying that $\varepsilon_2 < \varepsilon_2^*$. Recall that (6.595) depends on the selection of the variable d_1, and the maximum value of ε_2 is achieved with $d_1^* = d_1^\bigstar = 0.5$, and $d_2^* = d_2^\bigstar = 0.5$. It has been proven that with proper selection of the *Stability Parameters*, Q_S, q_{f_1}, q_{f_2}, q_{u_1}, and q_{u_2}, the value of ε_1^* in the Σ_{SF}-subsystem and ε_2^* in the Σ_{SFU} full system have been obtained such that $\varepsilon_1 < \varepsilon_1^*$, and $\varepsilon_2 < \varepsilon_2^*$, therefore, since all the growth requirements are satisfied, then the origin $\tilde{\boldsymbol{\chi}} = 0$, $\tilde{\boldsymbol{z}} = 0$, is an asymptotically stable equilibrium of the singularly perturbed Σ_{SFU} system for all $\varepsilon_2 \in (0, \varepsilon_2^*)$. Due to the methodology here presented, in which in order to demonstrate the fulfillment of all growth requirements, the full range of helicopter attainable states was considered to prove all inequalities, this defines the domain of attraction of the proposed stability analysis as the full range of helicopter attainable states. A sensitivity analysis for the results for the asymptotic stability analysis for the helicopter model is presented in Appendix D.

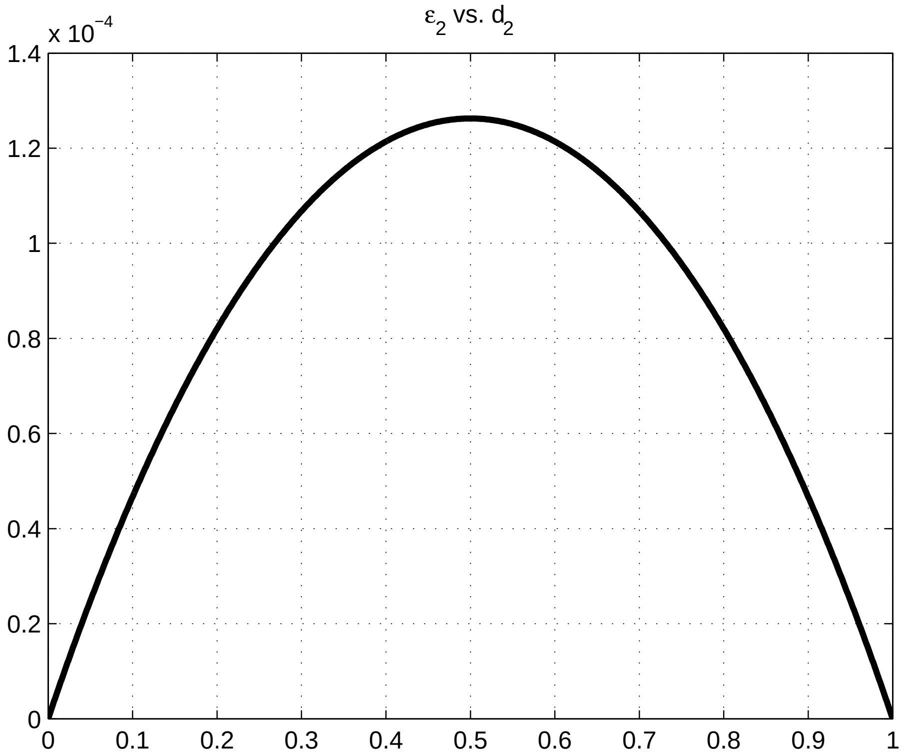

Figure 6.8: Stability upper bounds on ε_2 for the *Stability Analysis* of the Σ_{SFU} system.

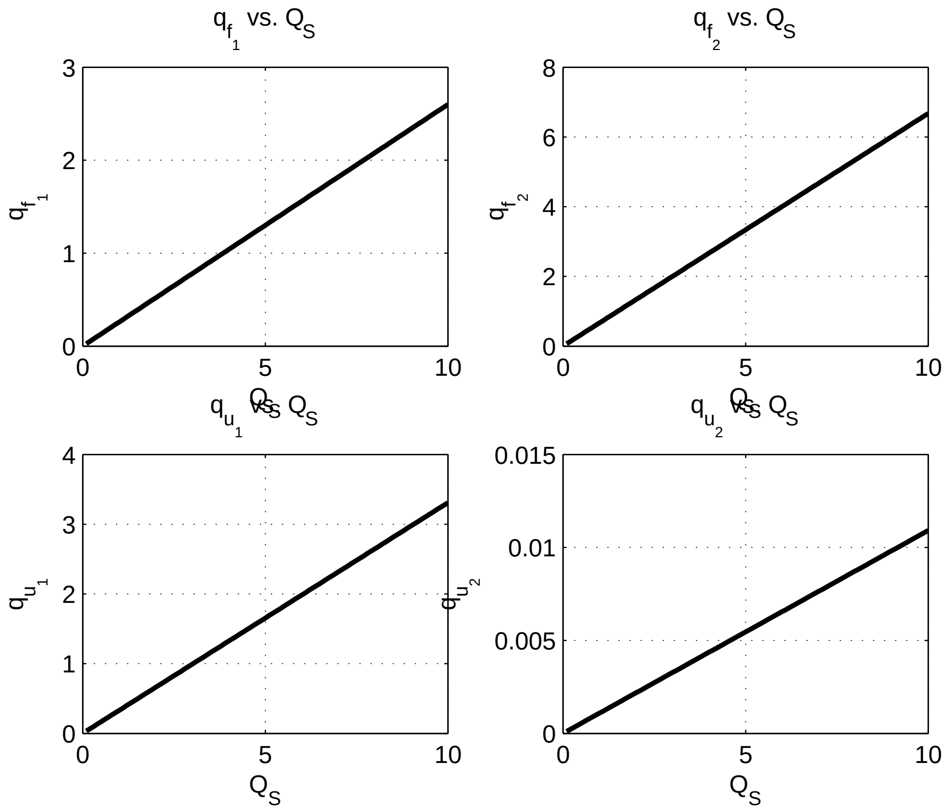

Figure 6.9: *Stability Parameters* q_{f_1}, q_{f_2}, q_{u_1}, and q_{u_2} vs. Q_S.

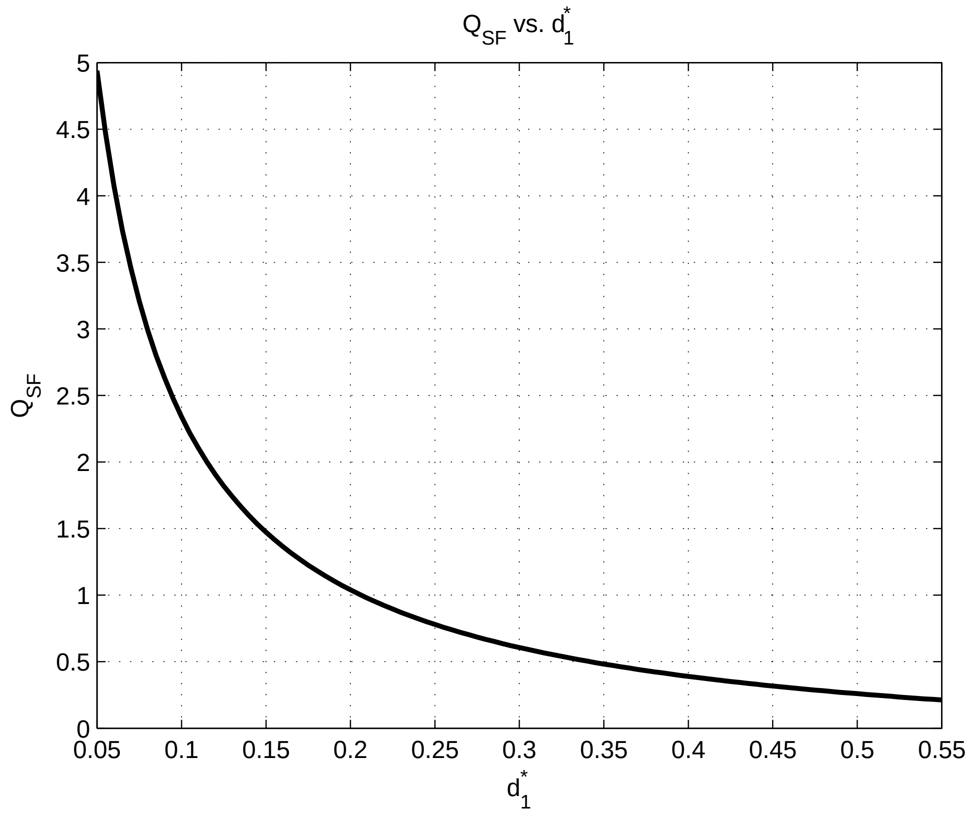

Figure 6.10: Variation of *Stability Parameter* Q_{SF} vs. $d_1^\bigstar$ - helicopter Σ_{SFU} system.

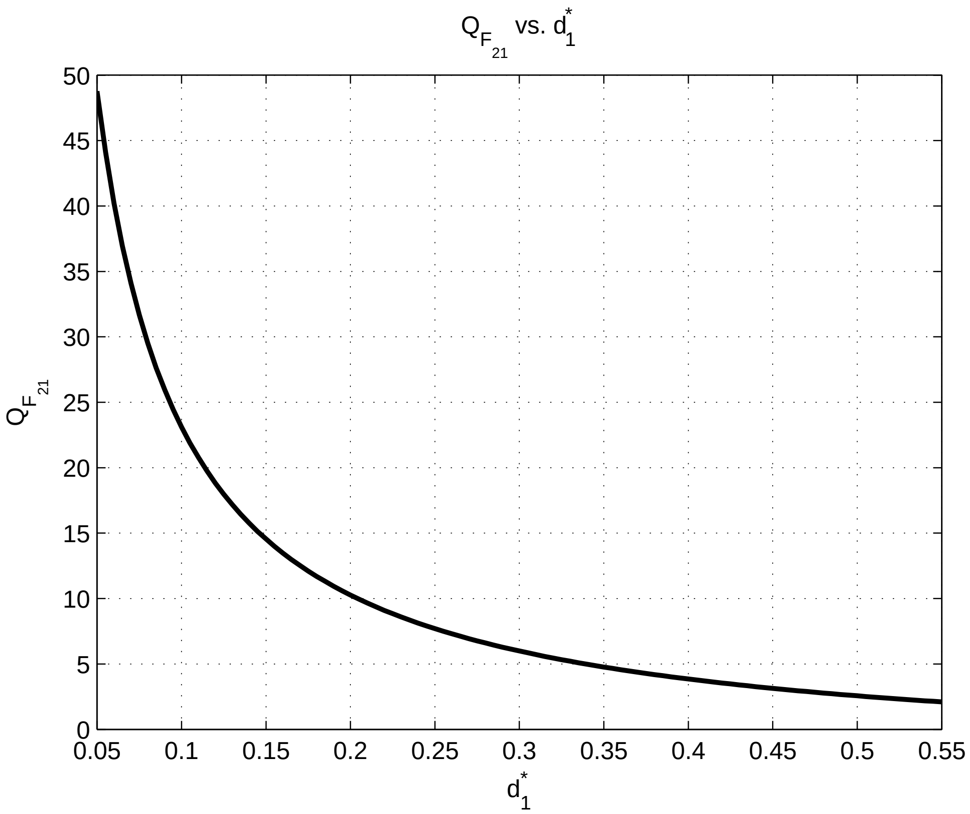

Figure 6.11: Variation of *Stability Parameter* $Q_{F_{21}}$ vs. $d_1^\bigstar$ - helicopter Σ_{SFU} system.

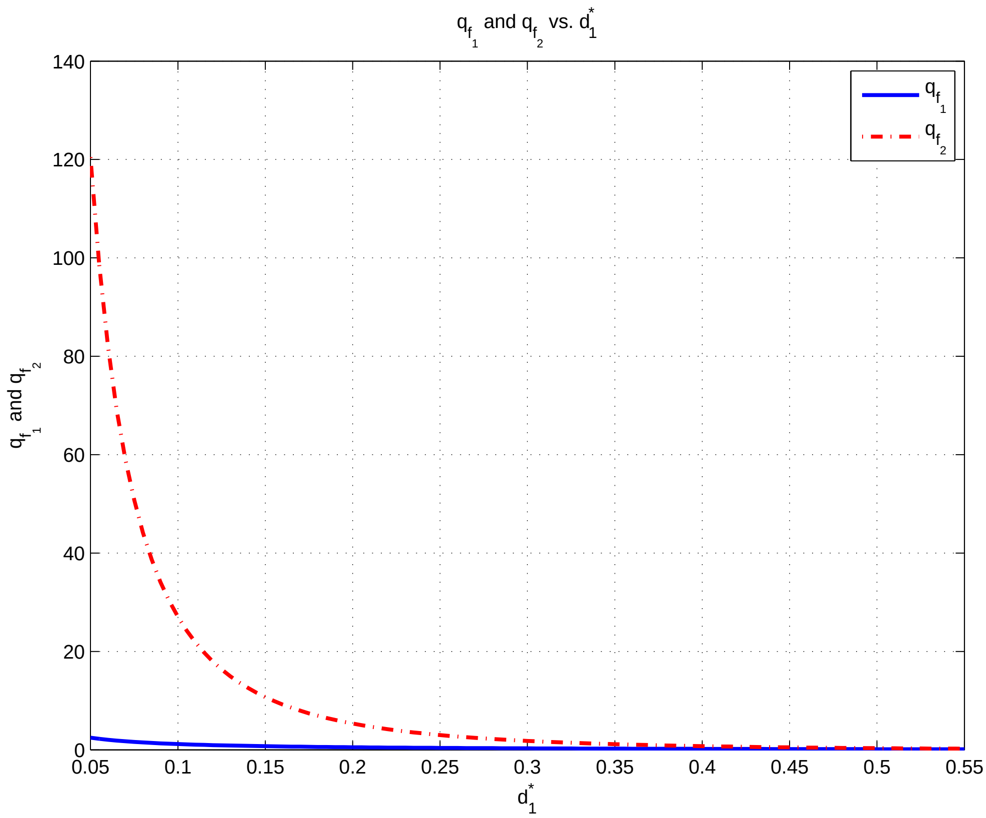

Figure 6.12: Variation of *Stability Parameter* q_{f_1} and q_{f_2} vs. $d_1^\bigstar$ - helicopter Σ_{SFU} system.

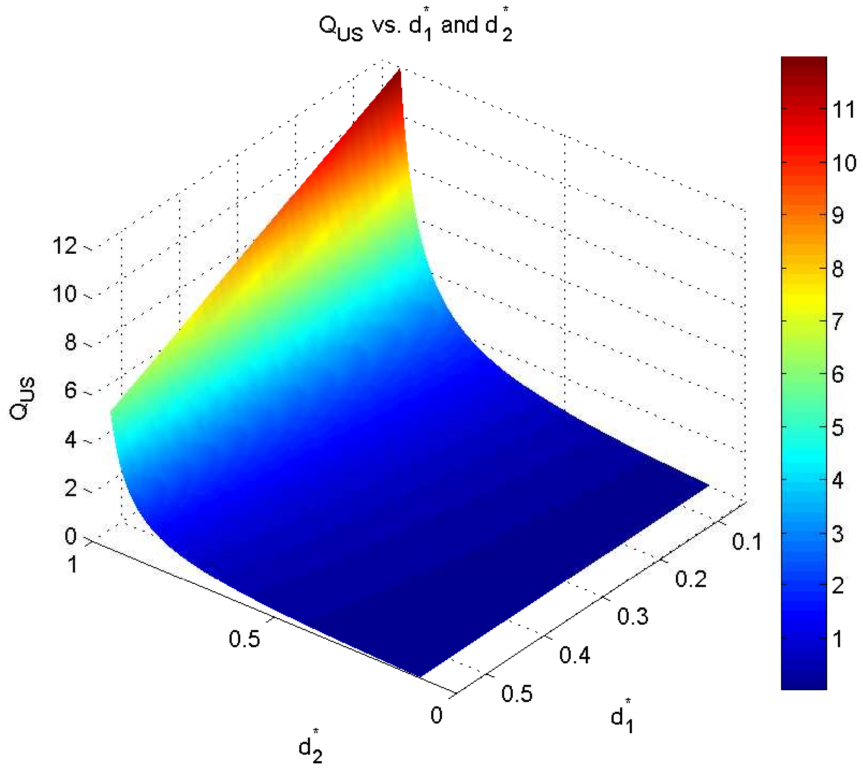

Figure 6.13: Variation of *Stability Parameter* Q_{US} vs. $d_1^\bigstar$ and $d_2^\bigstar$ - helicopter Σ_{SFU} system

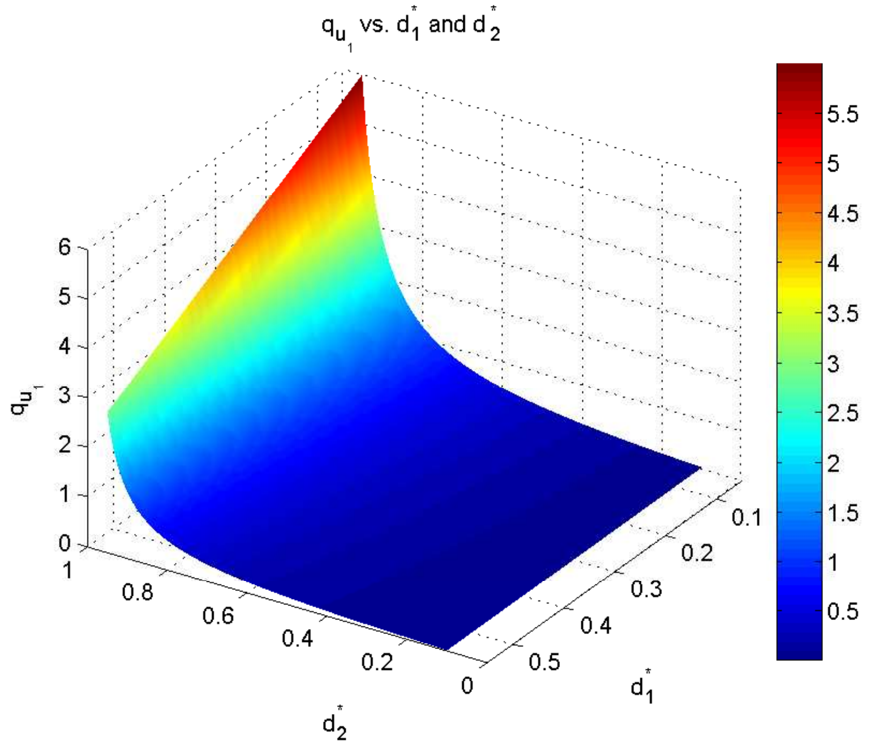

Figure 6.14: Variation of *Stability Parameter* q_{u_1} vs. $d_1^{\bigstar}$ and $d_2^{\bigstar}$ - helicopter Σ_{SFU} system.

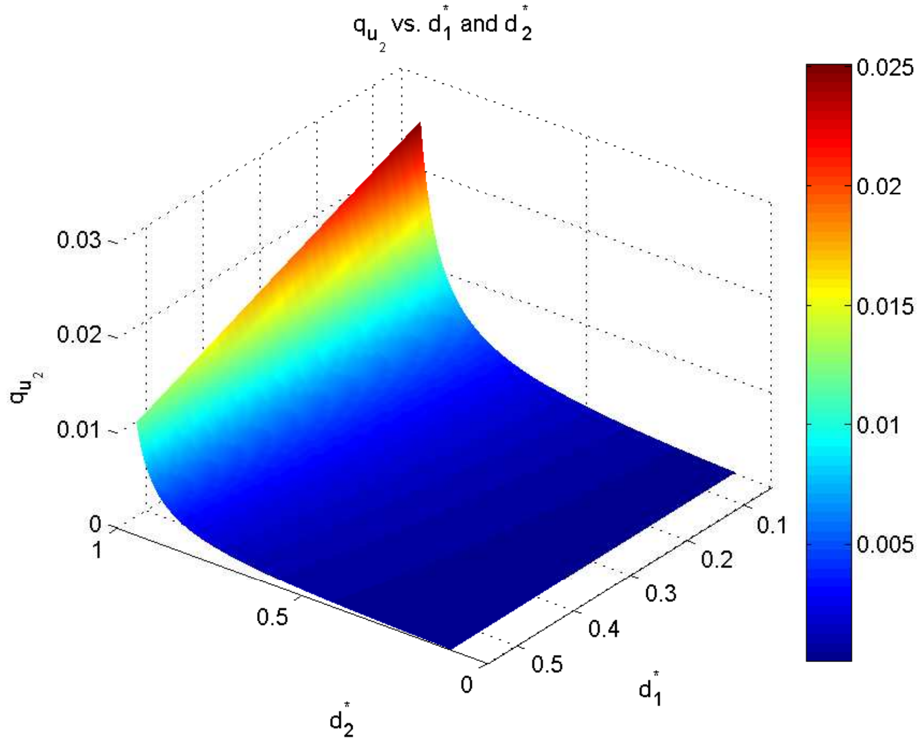

Figure 6.15: Variation of *Stability Parameter* q_{u_2} vs. $d_1^{\bigstar}$ and $d_2^{\bigstar}$ - helicopter Σ_{SFU} system.

6.7 Conclusions

The Asymptotic Stability Analysis presented in chapter 5 has been applied to the three-time-scale autonomous helicopter model obtained in chapter 4. The proposed two-step process defined in chapter 3 allows to study the asymptotic stability properties of the closed loop system, and also proposes a methodology to obtain a Lyapunov function candidate for the entire system, $V_2(\tilde{x}, \tilde{\boldsymbol{y}}, \tilde{\boldsymbol{z}})$, by using a weighted sum of the proposed Lyapunov function candidates of the three time-scale subsystems.

The validity of the methodology has been proved by obtaining the stability upper bound limits on the boundary layers, ε_1 and ε_2, and ensuring that the selected parasitic constants for the proposed control law satisfy $\varepsilon_1 \leq \varepsilon_1^*$ and $\varepsilon_2 \leq \varepsilon_2^*$ for the helicopter model here employed. The use of the full range of reachable state variables has been required in order to satisfy the inequalities that guarantee the asymptotic stability properties at the origin of the Σ_{SFU}-subsystem, which results in extending the asymptotic stability properties to semiglobal stability, by the definition in (Kokotović, 1992; Sussmann and Kokotović, 1991; Braslavsky and Miidleton, 1996), by providing upper bounds on the parasitic singularly perturbed parameters for the entire range of admissible state values, thus extending the domain of attraction to that same rage of admissible states.

The stability results have also presented a closed form solution for the proper selection of the *stability parameters* q_{f_1}, q_{f_2}, q_{u_1}, and q_{u_2} as a function of the arbitrary *stability parameter* Q_S, such that fulfill assumptions 5.5.6, 5.5.7, 5.5.8, 5.5.9, and 5.5.10, providing asymptotic stability for the helicopter Σ_{SFU} full system with prescribed upperbounds on the parasitic parameters.

Chapter 7

Considerations of Unmodeled Dynamics

7.1 Introduction

Having in mind that the derived control strategies here presented are intended to be implemented in the future in the *GCNL* autonomous helicopter platform, Fig. 2.24, this chapter analyzes the behaviour of the mentioned control laws, under some of the possible unmodeled dynamics encountered when applied in the real platform.

Although many forms of unmodeled dynamics can be analyzed, and the study of all of them would be a difficult tasks, and what it is most important, out of the scope of the work here presented, only one type of unmodeled dynamics will be considered, and that is the unmodeled dynamics introduced by the modeling of the thrust coefficient of the main rotor. As discussed in chapter 2, and in Appendix A in more detail, the momentum theory provided some good insight into how the helicopter hovers by providing definitions for the inflow ratio depending on the flight condition, while blade element theory provide physical explanations at how the collective pitch and rotational speed affect the developed thrust, but lack to provided closed-form solutions, since the integral form described in Eq. (2.239) depends on the inflow angle. Therefore being necessary to combine both theories in order to obtain closed-form solutions of the thrust coefficient (C_T).

There are many proposed closed-form solutions in the literature (Leishman, 2006) for the thrust coefficient C_T which depends on the flight condition that it is assumed, the type of blade, and the assumed flow distribution along the blade of the rotor. Some of these models, in special the ones chosen by the author to test the behavior under unmodeled dynamics of the proposed control laws, are denoted bellow, following the standard literature nomenclature:

- Moment theory for uniform inflow in hover flight condition - MT_H
- Moment theory for uniform inflow in axial flight condition - MT_C
- Combined blade element theory and momentum theory - $BEMT$.
- Combined blade element theory and momentum theory with Prandtl's Tip-Loss Model - $BEMT_{TL}$.

The first proposed model, the MT_H model, has been previously presented in chapter 2, and is the selected C_T model to be implemented in the helicopter dynamics presented in this thesis. As previously mentioned, although the model implies a series of hypothesis, it can be proven (Johnson, 1994;

Leishman, 2006) that for maneuvers in which the climb and descent velocities are low enough, the MT_H is a really good approximation without any loss of generality, as it will be proven in the simulations. Also, and most important, the first model is the only closed-form continuous model of the four proposed models, therefore, becoming a good candidate, if not the only candidate, that can be used for a control strategy of the continuous type.

Although the selected MT_H model is the only continuous implementable model, one of the objectives of this thesis is to provide a series of control laws that will be able to be implemented into the *GCNL* autonomous helicopter platform, thus, although the MT_H model is a good approximation for low axial flight conditions, it is desired to see how the proposed control laws perform under a more realistic helicopter environment. Although there are much more precise, and also much more complex thrust coefficient models in the literature (Cuerva et al., 2006a; Cuerva et al., 2006b; Theodore, 2000), the author has chosen these three models, the MT_C, $BEMT$ and the $BEMT_{TL}$ models as significate models that are both, much more complex than the selected thrust model, MT_H, but are also easily implemented in the numerical simulation platform defined by the author. See Appendix A for more detail on the above mentioned models.

These *alternative* models will serve as great bench problems where to test the behavior of the proposed control strategies under unmodeled uncertainties. This chapter will conduct a sensitivity analysis on the proposed derived control laws to see how they perform on the three alternative different C_T models, and investigate if it is necessary to include some additional control regulation in order to take into account for the introduced unmodeled dynamics having in mind the scenario that will take place when trying to implement the presented control laws into the real *GCNL* autonomous helicopter platform.

7.2 Proposed Thrust Coefficient Models

Prior to conduct the sensitivity analysis let recall the proposed thrust model coefficients that will be used as test bench problems, by recalling the most important equations that define the four proposed models. For the first defined model, the MT_H, the thrust coefficient is given in Eq. (2.251) by

$$C_T = \left[\frac{\sigma C_{l_\alpha}}{12}\left(-\frac{3}{2\sqrt{2}} + \sqrt{\frac{9}{8} + \frac{24\theta_c}{\sigma C_{l_\alpha}}}\right)\right]^2, \tag{7.1}$$

which it also has a closed-form solution for the thrust force due to the employed simplifications resulting in

$$T = \rho N_b c(\Omega R)^2 R \frac{\sigma C_{l_\alpha}^2}{144}\left(\frac{3}{2\sqrt{2}} + \sqrt{\frac{9}{8} + \frac{24\theta_c}{\sigma C_{l_\alpha}}}\right)^2, \tag{7.2}$$

where recall both virtual control signals, the collective pitch angle, θ_c and the angular velocity of the blades, Ω, contribute to the generation of thrust as seen in Eq. (7.2). For the second model, the MT_C, the thrust coefficient for the three flight axial conditions is divided in three terms given by

$$C_{T_{MT_C}} = -\frac{\rho A\sigma C_{L_\alpha} R\Omega\left(-3\sigma C_{L_\alpha} R\Omega + \mathcal{T}_1 - 32R\theta_c\Omega + 24V_c\right)}{192\rho A\Omega^2 R^2}, \tag{7.3}$$

$$C_{T_{MT_D}} = \frac{T_{MT_D}}{\rho A\Omega^2 R^2}, \tag{7.4}$$

$$C_{T_{MT_{WM}}} = -\frac{\rho A\sigma C_{L_\alpha} R\Omega\left(3\sigma C_{L_\alpha} R\Omega - \mathcal{T}_2 - 32R\theta_c\Omega + 24V_c\right)}{192\rho A\Omega^2 R^2}, \tag{7.5}$$

where each of the three thrust coefficients, $C_{T_{MT_C}}$, $C_{T_{MT_D}}$, or $C_{T_{MT_{WM}}}$, are selected depending on the magnitude and the nature of the axial flight regime, and given by

$$V_c/v_h \geq 0 \quad \rightarrow \quad C_{T_{MT_C}}, \tag{7.6}$$

$$-2 \leq V_c/v_h \leq 0 \quad \rightarrow \quad C_{T_{MT_D}}, \tag{7.7}$$

$$-2 \geq V_c/v_h \quad \rightarrow \quad C_{T_{MT_{WM}}}, \tag{7.8}$$

where the reader can refer to Appendix A for further details on the derivation of the proposed models. For the third model, the $BEMT$, the thrust coefficient in axial ascent is given by integrating along the entire blade of the integral dC_T given by

$$dC_T = \frac{\sigma C_{l_\alpha}}{2}\left(\theta_c r^2 - \lambda r\right) dr, \tag{7.9}$$

with the inflow ratio given in (A.71) as

$$\lambda(r, \lambda_c) = \sqrt{\left(\frac{\sigma C_{l_\alpha}}{16} - \frac{\lambda_c}{2}\right)^2 + \frac{\sigma C_{l_\alpha}}{8}\theta r} - \left(\frac{\sigma C_{l_\alpha}}{16} - \frac{\lambda_c}{2}\right), \tag{7.10}$$

and where for the particular case in which the hover flight condition is considered, thus $\lambda_c = 0$, Eq. (7.10) simplifies to

$$\lambda(r) \equiv \lambda_i(r) = \frac{\sigma C_{l_\alpha}}{16}\left(\sqrt{1 + \frac{32}{\sigma C_{l_\alpha}}\theta r} - 1\right), \tag{7.11}$$

while for the axial descent is given by

$$C_{T_{MT_D}} = \frac{T_{MT_D}}{\rho A \Omega^2 R^2}, \tag{7.12}$$

$$C_{T_{MT_{WM}}} = -\frac{\rho A \sigma C_{L_\alpha} R\Omega \left(3\sigma C_{L_\alpha} R\Omega - \mathcal{T}_2 - 32R\theta_c\Omega + 24V_c\right)}{192\rho A \Omega^2 R^2}, \tag{7.13}$$

where similarly, as for the M_{T_C} model, the thrust coefficient for the $BEMT$ model in axial descent regime is given depending on the magnitude of the helicopter's descent velocity as

$$-2 \leq V_c/v_h \leq 0 \quad \rightarrow \quad C_{T_{MT_D}}, \tag{7.14}$$

$$-2 \geq V_c/v_h \quad \rightarrow \quad C_{T_{MT_{WM}}}. \tag{7.15}$$

And finally, for the fourth model, the $BEMT_{TL}$, the thrust coefficient is also given by integrating along the entire blade of the integral dC_T given as

$$dC_T = \frac{\sigma C_{l_\alpha}}{2}\left(\theta_c r^2 - \lambda r\right) dr, \tag{7.16}$$

with the inflow ratio given in (7.10) as

$$\lambda(r) = \sqrt{\left(\frac{\sigma C_{l_\alpha}}{16F(r,\lambda(r))} - \frac{\lambda_c}{2}\right)^2 + \frac{\sigma C_{l_\alpha}}{8F(r,\lambda(r))}\theta r} - \left(\frac{\sigma C_{l_\alpha}}{16F(r,\lambda(r))} - \frac{\lambda_c}{2}\right), \tag{7.17}$$

and where for the particular case in which the hover flight condition is considered, thus $\lambda_c = 0$, Eq. (7.17) simplifies to

$$\lambda(r) \equiv \lambda_i(r) = \frac{\sigma C_{l_\alpha}}{16F(r,\lambda(r))}\left(\sqrt{1 + \frac{32F(r,\lambda(r))}{\sigma C_{l_\alpha}}\theta r} - 1\right), \tag{7.18}$$

while again, for the axial descent, the C_T is given by the different flight regimes given by Eq. (7.13). Recall that both MT_H and MT_C produce close-form solutions for the thrust coefficient C_T (2.248) which are both explicit functions of the collective pitch angle θ_c and the inflow angle. Recall also that while for the MT_H model the inflow angle is a function of C_T, this resulting in a continuous closed-form solution for the thrust coefficient, while the MT_C model, presents nonlinearities depending on the nature of the climb flight region, and therefore being unfeasible to integrate into a set of continuous differential equations if the goal is to design continuous and differentiable control laws.

On the other side, for both blade element theory models, $BEMT$ and $BEMT_{TL}$, it is required numerical integration at each instant in order to obtain the thrust coefficient, therefore making impossible to obtain a closed-form solution to which be able to design a proper control law to regulate the amount of thrust generated, but they will serve as a great bench problems where to test the validity of the selected model, and to test the performance of the proposed control laws under model uncertainties. It is important to note the great mathematical differences between the selected MT_H model, and the selected MT_C, $BEMT$ and $BEMT_{TL}$ thrust coefficient models, in special the discontinuities present in the proposed C_T models when the helicopter is in axial descends flight regime, as it will be seen in the sensitivity analysis that will be conducted in the following sections.

7.3 Sensitivity Analysis under Unmodeled Thrust Coefficient Model

In order to evaluate the performance of the derived control laws under unmodeled dynamics, a sensibility analysis is conducted by performing four distinctive maneuvers that include all possible helicopter maneuvers:

1. Ascent flight with increasing engine RPM.
2. Ascent flight with decreasing engine RPM.
3. Descent flight with increasing engine RPM.
4. Descent flight with decreasing engine RPM.

Despite the extensive sensitivity analysis conducted, only four significate cases are presented, which correspond to a sequential simulation that includes all four distinctive maneuvers, and that are defined by the bellow conditions:

1. $y_1(0) = 1.85\ m$, $y_1^* = 0.5\ m$, $x(0) = 120\ rad/sec$, and $x^* = 140\ rad/sec$.
2. $y_1(0) = 0.5\ m$, $y_1^* = 1\ m$, $x(0) = 140\ rad/sec$, and $x^* = 120\ rad/sec$.
3. $y_1(0) = 1\ m$, $y_1^* = 1.5\ m$, $x(0) = 120\ rad/sec$, and $x^* = 145\ rad/sec$.
4. $y_1(0) = 1.5\ m$, $y_1^* = 0.75\ m$, $x(0) = 145\ rad/sec$, and $x^* = 120\ rad/sec$.

Needs to be noted that starting with the second maneuver, it is assumed that the helicopter has reached the desired target altitude and angular rotation of the blades, thus the initial conditions for the second, third and fourth maneuver are the selected as desired target conditions of the previous maneuvers respectively. For the case in which the helicopter has not reached the assigned target condition, the new maneuver will start at whenever condition the helicopter is at the moment of the change in set point. Each maneuver is lapsed with an interval of twenty seconds, and after that time it is assigned the new set points independently if the helicopter has reached or not the desired set point.

Due the continuous/discontinuous nature of the C_T models the sensitivity analysis is conducted considering first continuous C_T simplified models, as discussed in section 7.4.1, and later, the simulations are extended analyzing the discontinuous models as it will be seen in section 7.4.2. These results are described in following sections.

7.3.1 Sensitivity Analysis for Continuous Unmodeled Thrust Coefficient Models

The first sensibility analysis will be conducted assuming that the model formulation for the MT_C, $BEMT$, and $BEMT_{TL}$, are continuous by assuming that, for both ascent and descent axial flight, the model can be defined by that of the ascent flight for all three models. This approximation can be taken since as noted by (Johnson, 1994; Leishman, 2006), for small V_c/v_i, the use of the axial flight models are reasonable approximations to the axial flight dynamics without loss of generality, and this will be observed in the simulations where $V_c/v_i > -0.15$ as it can be seen in the middle sub-figure in Figure 7.4.

The conducted sensitivity analysis with this approximation will prove that the proposed selected control laws are able to stabilize the helicopter in approximately the same amount of time for all three proposed *alternative* propulsive models, see the trends in the vertical velocity and acceleration of the helicopter in the middle and bottom subfigures, respectivelty, in Figure 7.1. It needs to be noted that for the $BEMT$ and $BEMT_{TL}$ models it does so to different altitudes than the selected target altitude, see top subfigure in Figure 7.1, and therefore will be necessary to include an simple extra-robustness law to compensate for this steady-state error in the final altitude of the helicopter.

Figures 7.1 to 7.4 show some representative simulations of the sensitivity analysis conducted. As expected the different commanded angular rotation of the blades are properly tracked, since no uncertainties are introduced into the propulsive model. The collective pitch angle history in the middle subfigure in Figure 7.2, shows that different collective pitch angles are demanded by the different control signal u_2 in order to achieve equilibrium flight, despite the different amount of C_T generated by of the four presented test bench C_T models, as it can be seen in the zoomed portion of the top sub-figure in Figure 7.4. The different control signals for all four maneuvers can be seen in Figure 7.3.

The difference in altitude is almost imperceptible for the MT_C model, while it is most noticeable for both $BEMT$, and $BEMT_{TL}$, producing a positive steady-state error in the altitude for the $BEMT$, and a negative steady-state error for the $BEMT_{TL}$ model, which is consistent with the literature (Johnson, 1994; Leishman, 2006) where the for a given collective pitch angle and angular rotational speed of the blades, the $BEMT$ model produces a higher thrust coefficient that the MT_H, while the $BEMT_{TL}$ model produces a lower thrust coefficient that the MT_H.

Although strictly speaking, this trend cannot be exactly appreciated in the sensitivity analysis here conducted since the control signals are different for each of the analyzed C_T models, this trend can be seen in the sensitivity analysis conducted in Appendix A.5, in which in order to conduct a comparable performance analysis between the selected MT_H model, against the more precise models, the MT_C, the $BEMT$ and the $BEMT_{TL}$, the same control signal, resulting from analyzing the equilibrium points of the original helicopter model, is applied to all four C_T. See A.5.1 for more details. The important conclusion that can be drawn are that despite the clear unmodeled dynamics, the control strategy presents robust behavior on stabilizing the helicopter, although doing so at a different altitude.

7.3.2 Sensitivity Analysis for Discontinuous Unmodeled Thrust Coefficient Models

Additional sensitivity studies are conducted considering now that all three test bench models, MT_C, $BEMT$, and $BEMT_{TL}$ respectively, have discontinuities when transition from ascent to descent flight condition according to their original formulations. These discontinuities will introduce higher complexity to the unmodeled dynamics study, since not only the control laws will have to account for different magnitudes of C_T, but also for the discontinuities of all three models when transition to the descent flight regime.

Similarly as in the continuous case, in order to evaluate the performance of the derived control laws under unmodeled dynamics, the sensibility analysis is conducted by performing the same four distinctive maneuvers described above, and where again despite the extensive sensitivity analysis conducted, only four significate cases are presented, which correspond to a simulation that includes all four distinctive maneuvers in one simulation with the same properties as described in section 7.3

The same trends are observed for the discontinuous models simulations, Figures 7.5-7.8. The proposed selected control laws are able to stabilize the helicopter for all three proposed *alternative* propulsive models, see the trends in the vertical velocity and acceleration of the helicopter in the middle and bottom subfigures, respectivelty, in Figure 7.5, although for the $BEMT$ and $BEMT_{TL}$ models to different altitudes than the selected target altitude, see top subfigure in Figure 7.5, with some chattering behavior when reaching the equilibrium condition, that is reaching a zero vertical velocity $y = 2 \to 0$, where the discontinuity creates oscillatory behaviour in the vertical movement as it can be seen in the evident chattering in the vertical acceleration.

This is specially amplified for the $BEMT_{TL}$ model as seen in the bottom subfigure of Figure 7.5, which is due to the erratic C_T behaviour near the region that serves as the switching point between the discontinuous C_T models as it can be seen in the top subfigure in Figure 7.8. The collective pitch angle history in the middle subfigure in Figure 7.6, shows that different collective pitch angles are demanded by the control signal u_2 in order to achieve equilibrium flight, according to the amount of generated thrust for each of the four presented test bench C_T models, and the different control signals for all four maneuvers can be seen in Figure 7.7.

The discontinuities can be better observed in the nature of the thrust coefficient (C_T) when either transition from either an initial stationary flight to a descending flight, or an ascending flight to a descending flight. The discontinuities can also observed when the helicopter is in the vicinity of reaching the desired final altitude in which, due to the typical damped oscillation, the C_T model shows the discontinuous behavior when oscillating around zero vertical velocity, and appearing the discontinuous structure for all three proposed alternative C_T models. This is much more distinct for the $BEMT_{TL}$ discontinuous model.

Again, and similarly as for the continuous sensitivity analysis previously conducted, the discontinuous sensitivity analysis shows that the proposed selected control laws are able to stabilize the helicopter for all three proposed *alternative* propulsive models, despite the great differences in the models, that can be thought as of large unmodeled dynamics, but it does so to a different altitude than the selected target altitude, and therefore will be necessary to include an simple extra-robust law to compensate for this steady-state error in the final altitude of the helicopter. Despite the discontinuous C_T models, the derived control laws are able to stabilize the helicopter. These results infer the derived control laws with some degree of robustness against the most than probable unmodeled C_T dynamics that will be encounter when applying the obtained control laws to the actual *ESI* autonomous helicopter platform, but still not enough to guarantee the precise regulation to the desired altitude which will require of some type of simple extra-robust law to compensate for the existing steady-state error in the final altitude of the helicopter. This extra-control law will be presented in the following section.

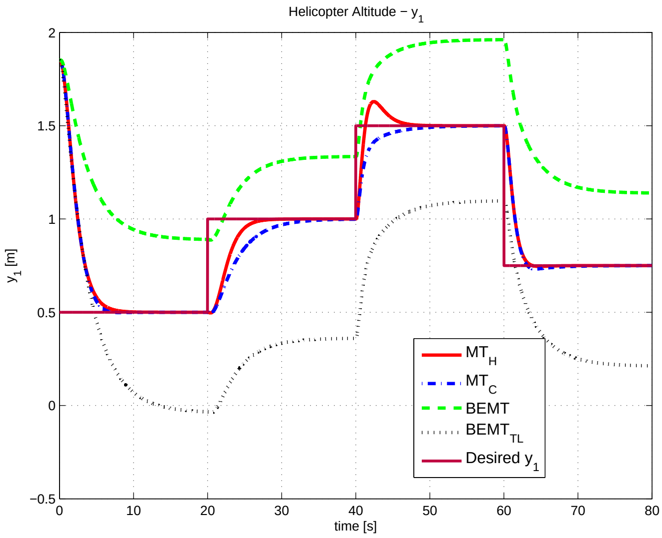

(a) y_1

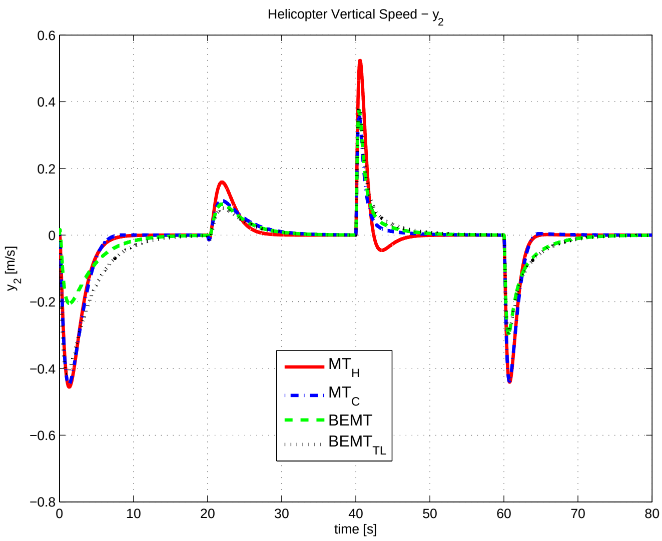

(b) y_2

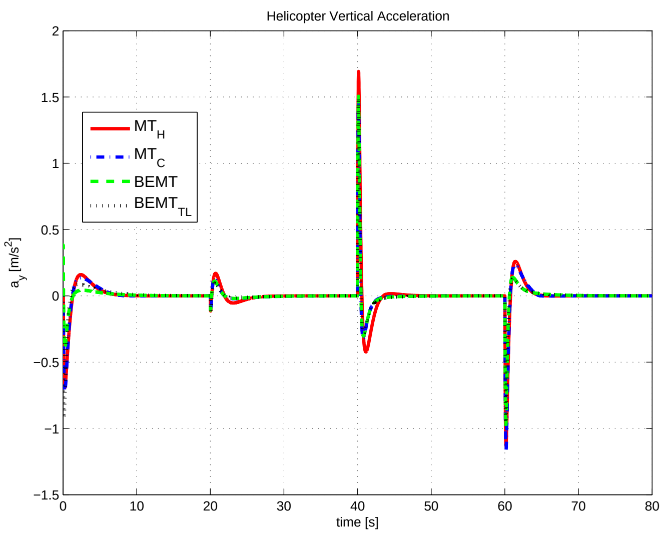

(c) a_y

Figure 7.1: States History for the Continuous Unmodeled C_T and the *BU-TD* Control Design

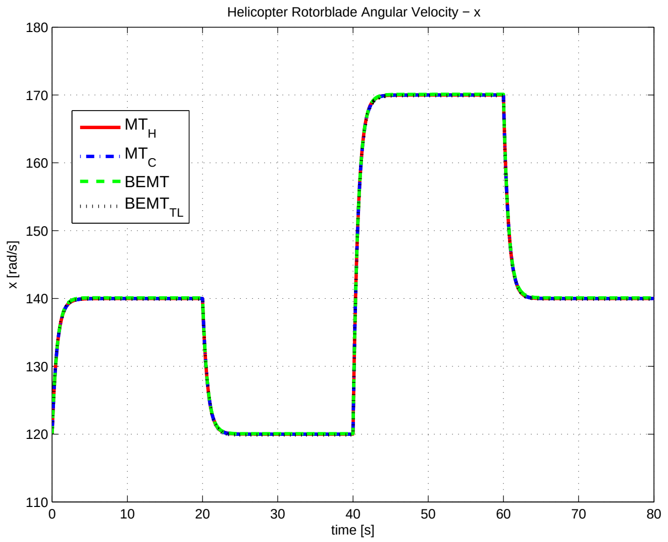

(a) x

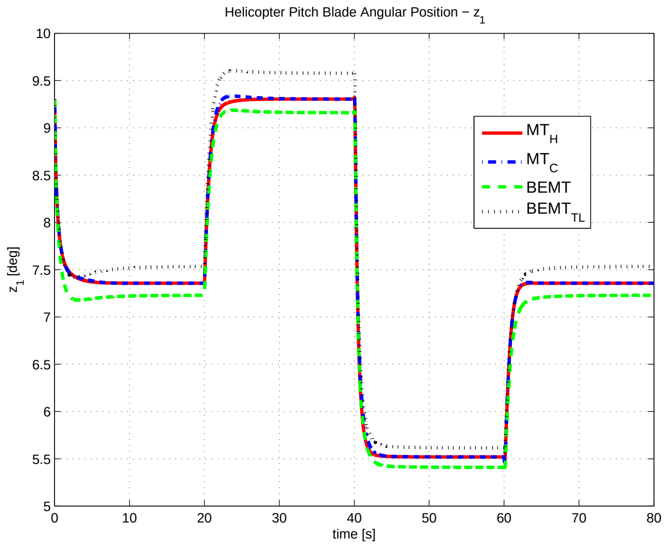

(b) z_1

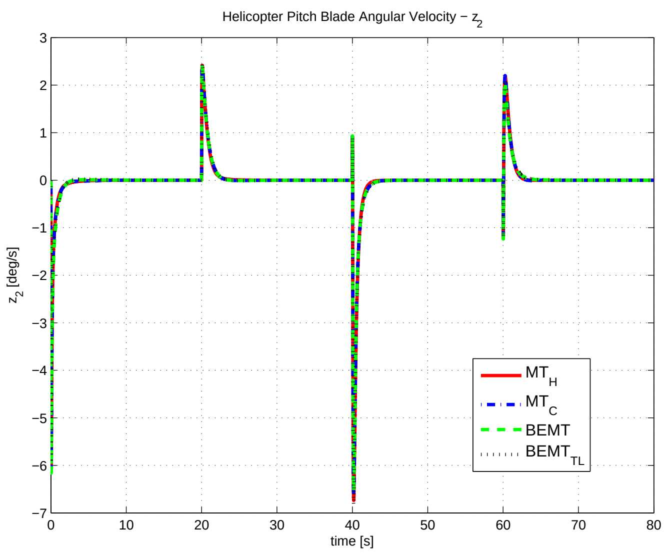

(c) z_2

Figure 7.2: States History for the Continuous Unmodeled C_T and the *BU-TD* Control Design

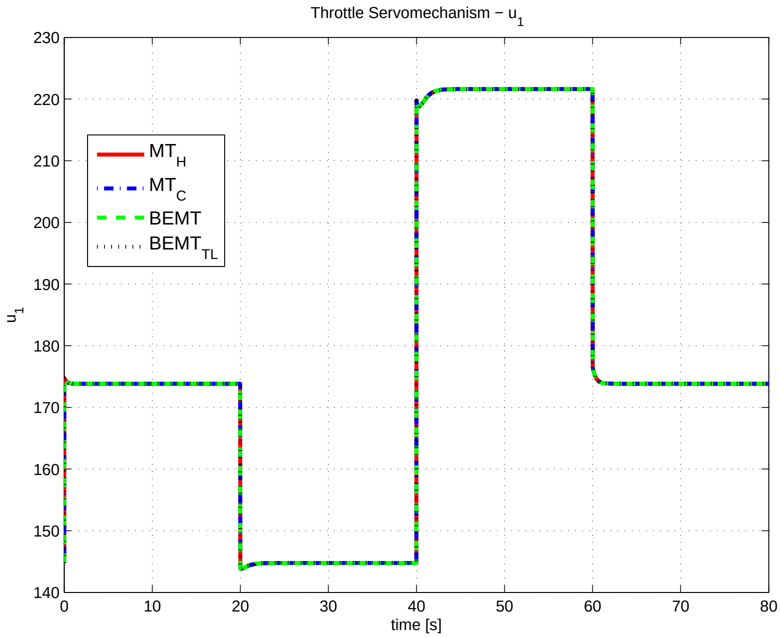

(a) u_1

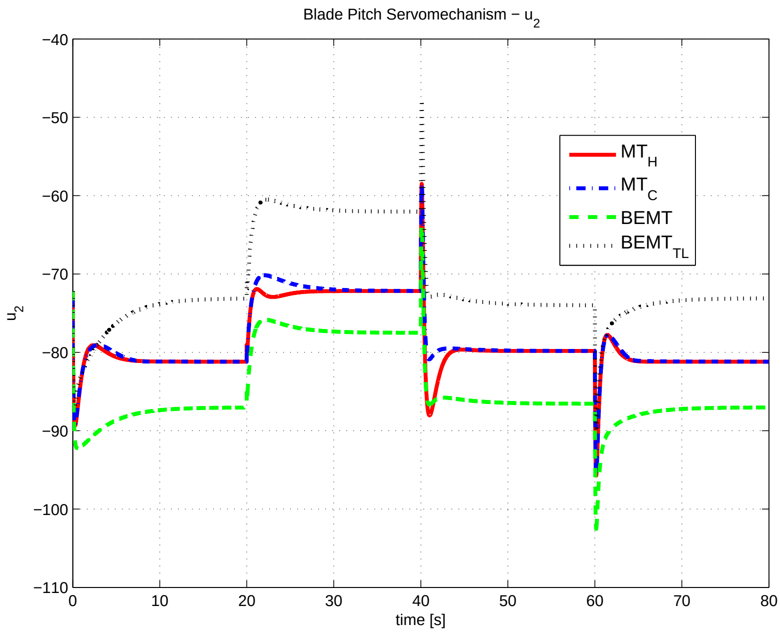

(b) u_2

Figure 7.3: Control History for the Continuous Unmodeled C_T and the *BU-TD* Control Design.

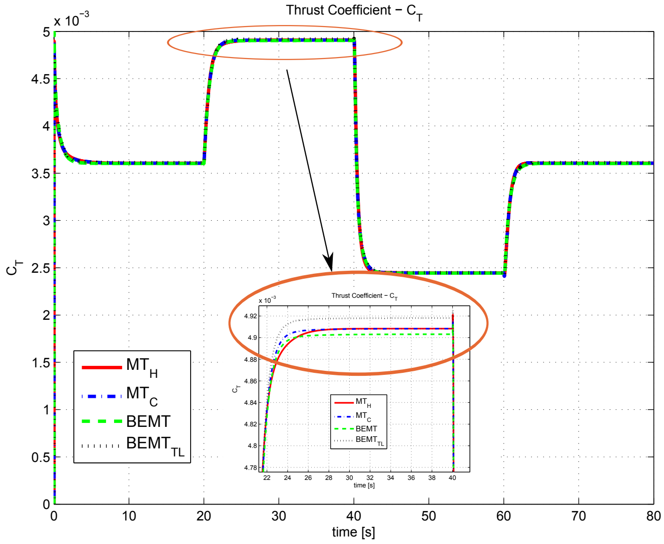

(a) C_T

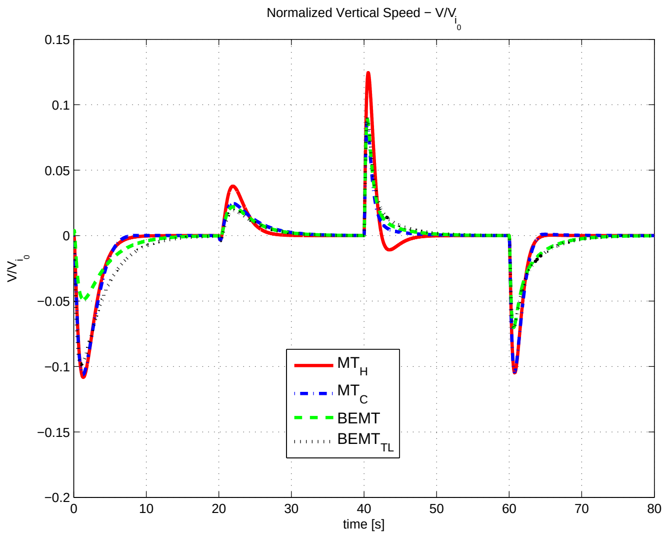

(b) y_2/v_i

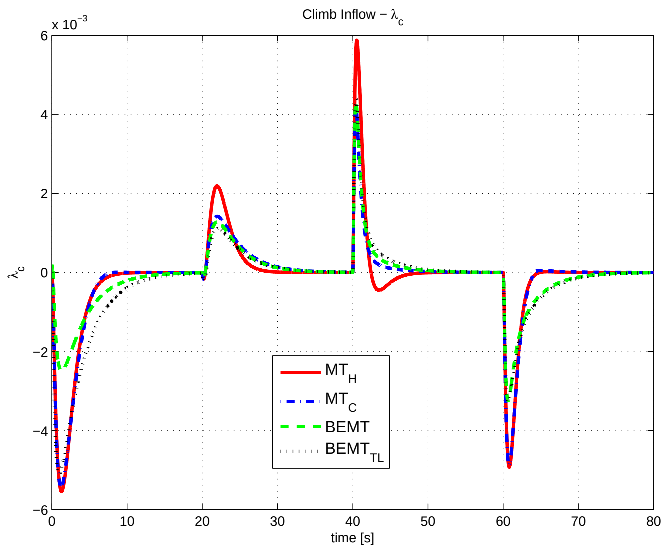

(c) λ_c

Figure 7.4: States and Significate Aerodynamic Parameters History for the Continuous Unmodeled C_T and the *BU-TD* Control Design.

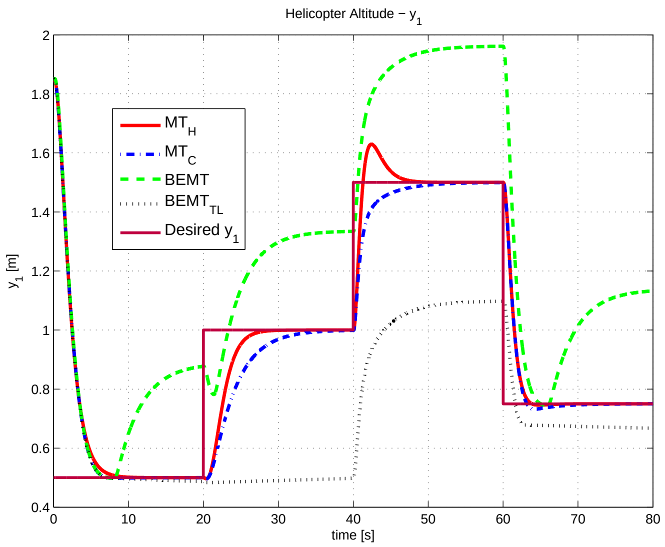

(a) y_1

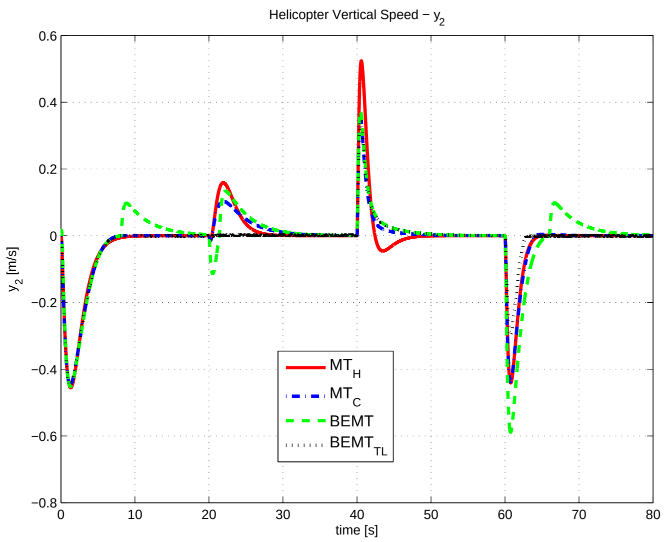

(b) y_2

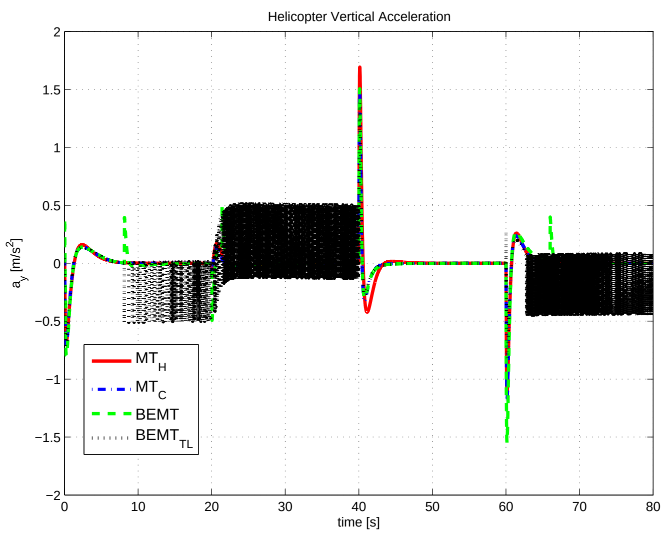

(c) a_y

Figure 7.5: States History for the Discontinuous Unmodeled C_T and the *BU-TD* Control Design

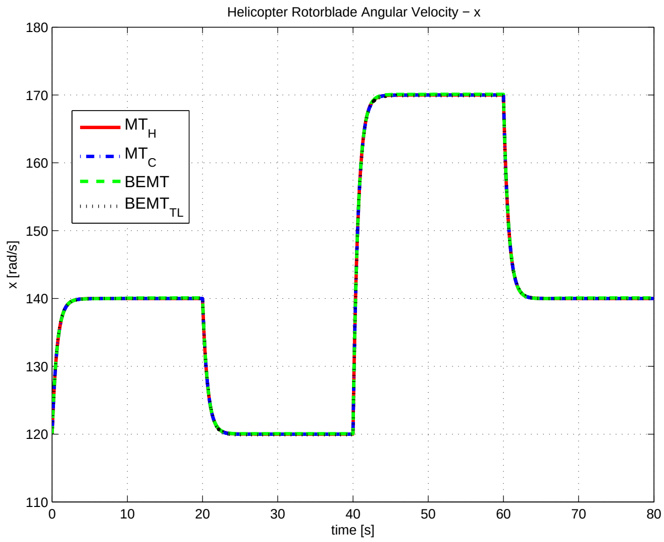

(a) x

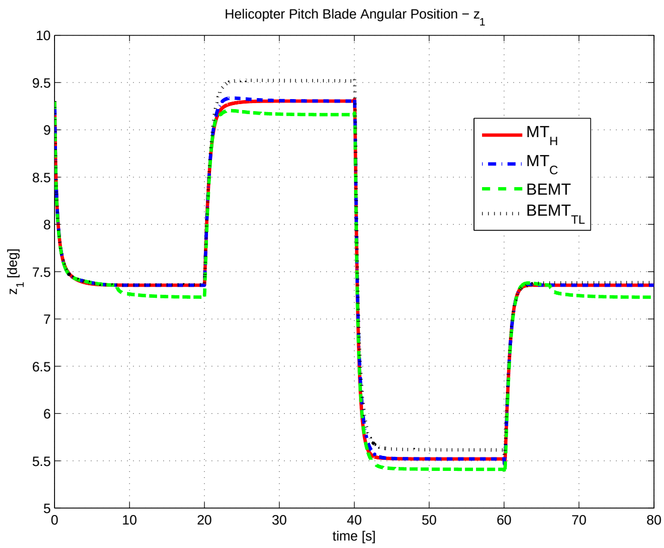

(b) z_1

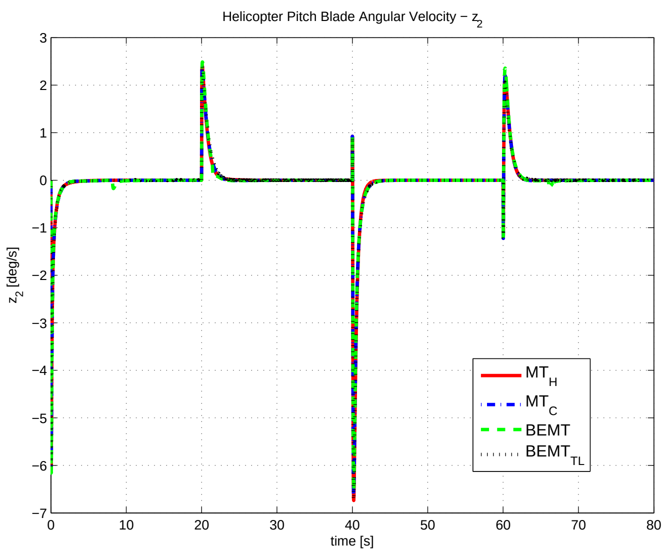

(c) z_2

Figure 7.6: States History for the Discontinuous Unmodeled C_T and the *BU-TD* Control Design

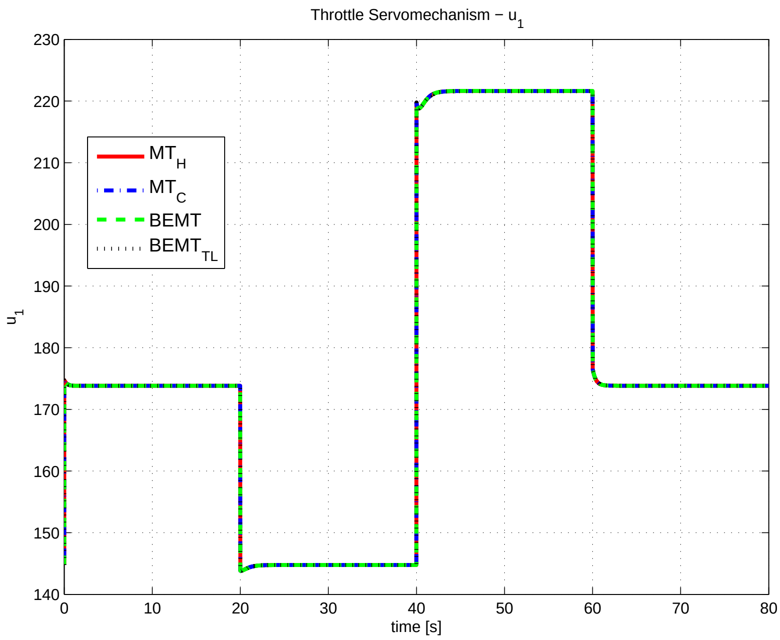

(a) u_1

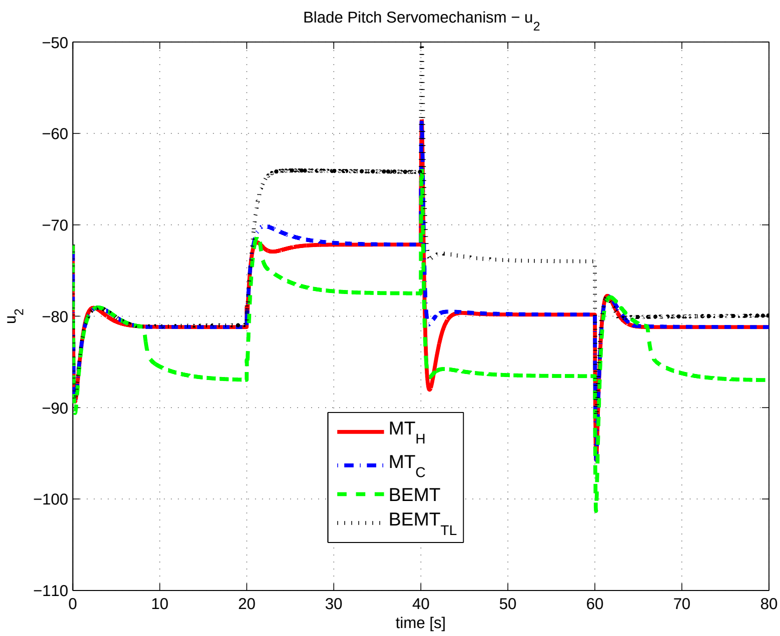

(b) u_2

Figure 7.7: Control History for the Discontinuous Unmodeled C_T and the *BU-TD* Control Design.

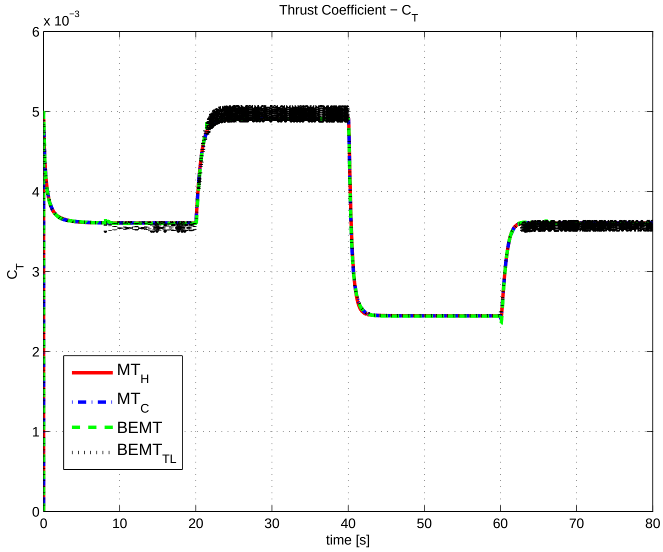

(a) C_T

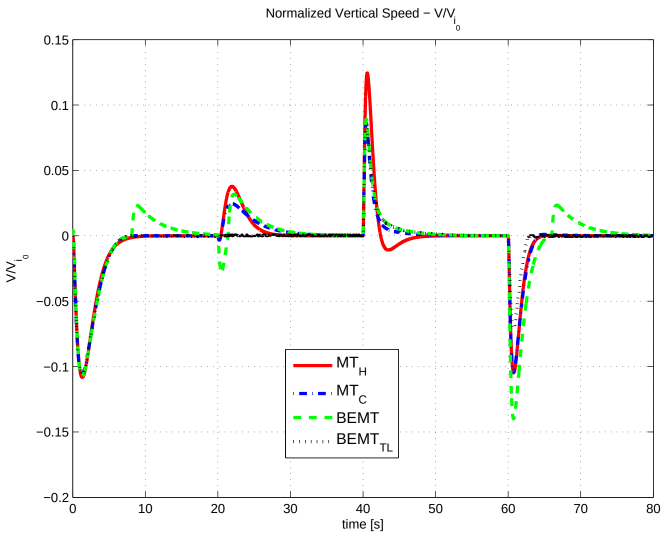

(b) y_2/v_i

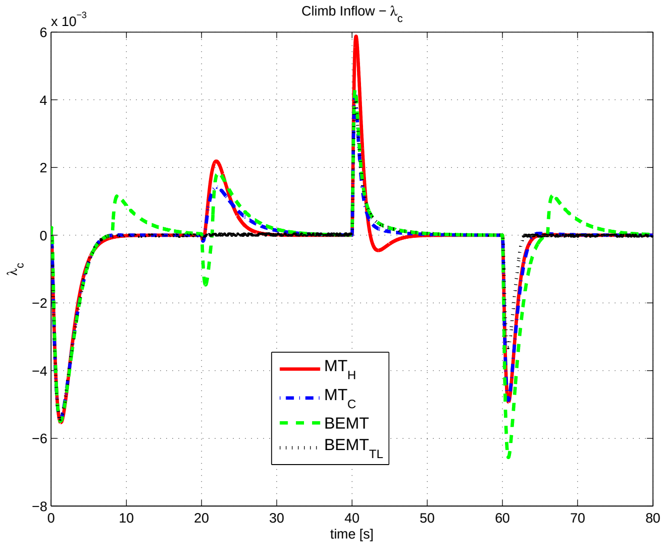

(c) λ_c

Figure 7.8: States and Significate Aerodynamic Parameters History for the Discontinuous Unmodeled C_T and the *BU-TD* Control Design.

7.4 Control Strategy for Unmodeled Dynamics

In order to account for the unmodeled thrust coefficients of the MT_C, $BEMT$, and $BEMT_{TL}$ models, a simple solution is selected which consists on adding an additional *PID* based control signal to the collective pitch angle control signal u_2. The extra control signal is added linearly to the existing control signal as seen in Figure (7.9). For the *TD-BU* control strategy, the new closed loop system would become

$$\begin{aligned}
\dot{x} &= a_{10}x^2\left[\sin(z_1 - \sin h_{1_{SS}}(x))\right] - b_x(x - x^*) && (7.19)\\
\dot{y}_1 &= y_2 && (7.20)\\
\dot{y}_2 &= x^2\left(a_1 + a_2 z_1 - \sqrt{a_3 + a_4 z_1}\right) + a_5 y_2 + a_6 y_2^2 + a_7 && (7.21)\\
\dot{z}_1 &= z_2 && (7.22)\\
\dot{z}_2 &= a_{13}z_1 + a_{15}z_2 + K_b\left[\left(1 + \sqrt{s_3 v(x, \mathbf{y})}\right)^2 - 1\right] + u_{2_{PID}}, && (7.23)
\end{aligned}$$

while for the $\mathcal{CF}$-*TD-BU* control design would become

$$\begin{aligned}
\dot{x} &= a_{10}x^2\left(\sin z_1 - \sin h_{1_{SS}}(x)\right) - b_x\left(x - x^*\right), && (7.24)\\
\dot{y}_1 &= y_2, && (7.25)\\
\dot{y}_2 &= x^2\left(a_1 + a_2 z_1 - \sqrt{a_3 + a_4 z_1}\right) + a_5 y_2 + a_6 y_2^2 + a_7, && (7.26)\\
\dot{z}_1 &= z_2, && (7.27)\\
\dot{z}_2 &= -\tilde{b}_{z_1}\left(z_1 - h_{1_c}(x, y)\right) - \tilde{b}_{z_2}z_2 + u_{2_{PID}}, && (7.28)
\end{aligned}$$

with the extra control signal $u_{2_{PID}}$ given by

$$u_{2_{PID}}(t) = K_p\left(e(t) + \frac{1}{T_i}\int_0^t e(\tau)d\tau + T_d\frac{de(t)}{dt}\right), \qquad (7.29)$$

with K_p, T_i, and T_d being the standard tuning parameters for the three-term *PID* control signal. Refer to the literature for more detail (Visioli, 2006; Åström and Hägglund, 1995; Åström and Hägglund, 2006). The chosen structure can be seen in Figure 7.9. Simulations are conducted for both the continuous and discontinuous test cases described in previous sections, and the results for the conducted sensitivity analysis, are limited to the same four distinctive maneuvers that include all possible helicopter maneuvers flight regimes:

1. Ascent flight with increasing engine *RPM*.
2. Ascent flight with decreasing engine *RPM*.
3. Descent flight with increasing engine *RPM*.
4. Descent flight with decreasing engine *RPM*.

with the same set point conditions used in previous sections. For conciseness also, only the simulations for the *TD-BU* control design are presented since the simulations on the $\mathcal{CF}$-*TD-BU* control design do not change significantly.

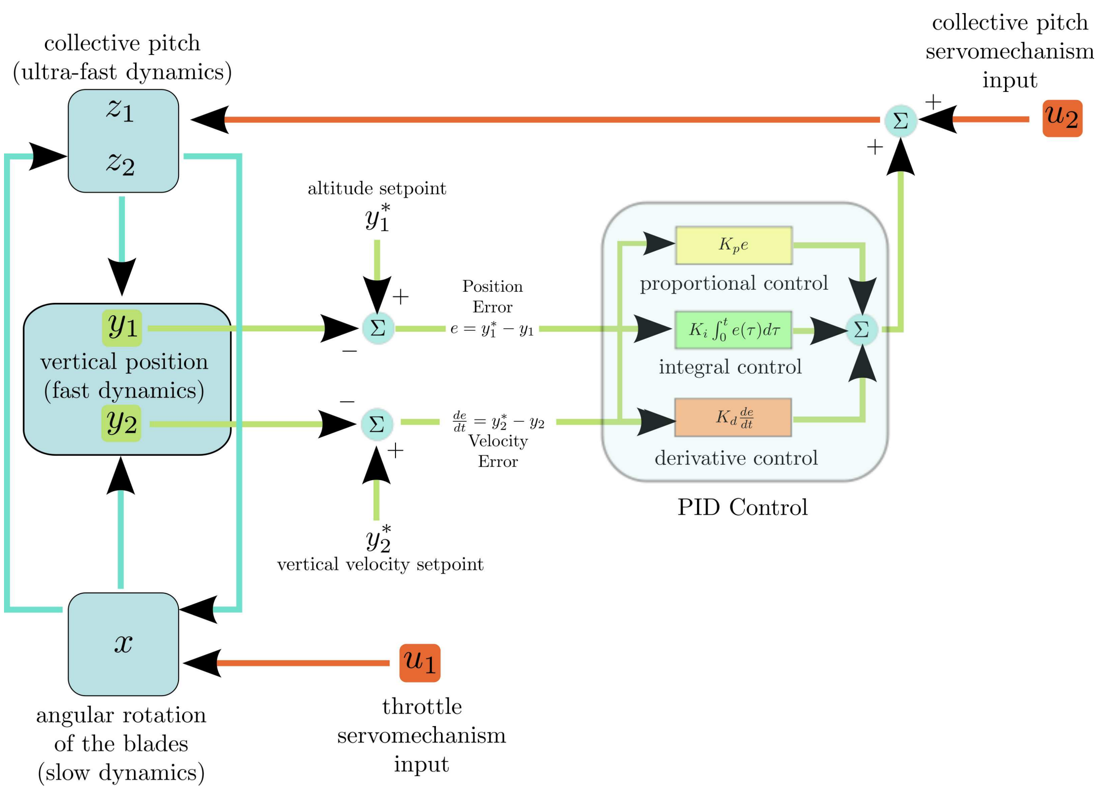

Figure 7.9: PID control.

7.4.1 Sensitivity Analysis for Continuous Unmodeled Thrust Coefficient Models with Added extra Control Signal ($u_{2_{PID}}$)

Similarly as for the sensibility analysis conducted previously for the continuous model, the analysis is first conducted assuming that the model formulation for the MT_C, $BEMT$, and $BEMT_{TL}$, are continuous. A sensitivity analysis is conducted following standard tuning rules to adjust the different *PID* parameters to obtain approximate desired time responses. The simulations that will be shown for both the continuous and discontinuous models use $K_p = 50$, $T_d = 0.5$, and $T_i = 4$.

The simulations with the *PID* extra control signal show not only that that the new proposed selected control law is able to stabilize the helicopter in approximately the same amount of time for all three proposed *alternative* propulsive models, but also doing so to the different desired set point altitudes as seen in Figure 7.10. Figure 7.11 shows the tracking of the commanded angular rotation of the blades, and the collective pitch angle and velocity. The different control signals for all four maneuvers can be seen in Figure 7.12, while Figure 7.13 shows the time history for the C_T, the normalized vertical velocity, and the inflow angle.

7.4.2 Sensitivity Analysis for Discontinuous Unmodeled Thrust Coefficient Models with Added extra Control Signal ($u_{2_{PID}}$)

Similarly as for the sensibility continuous case, the sensitivity analysis is extended to the discontinuous models for the MT_C, $BEMT$, and $BEMT_{TL}$. The sensitivity analysis is conducted using the same tuning rules to adjust the different *PID* parameters that is $K_p = 50$, $T_d = 0.5$, and $T_i = 4$. The simulations with the *PID* extra control signal show again not only that that the new proposed selected control law is able to stabilize the helicopter in approximately the same amount of time for all three proposed *alternative* propulsive models, but also doing so to the different desired set point altitudes as seen in Figure 7.14.

Figure 7.15 shows the tracking of the commanded angular rotation of the blades, and the collective pitch angle and velocity. The different control signals for all four maneuvers can be seen in Figure 7.16, while Figure 7.13 shows the time history for the C_T, the normalized vertical velocity, and the inflow angle. These results infer the derived control laws with some degree of robustness against the most than probable unmodeled C_T that will be encounter when applying the obtained control laws to the actual *ESI* autonomous helicopter platform.

7.5 Conclusions

A performance sensitivity analysis is conducted for both the continuous and discontinuous presented test bench models, the MT_C, $BEMT$, and $BEMT_{TL}$, and, after identifying that for $BEMT$, and $BEMT_{TL}$ models, the selected control strategy presented a steady state error in the helicopter altitude, a simple extra control signal is presented and tested again with the test bench problems, providing a certain type of robustness under thrust coefficient modeling.

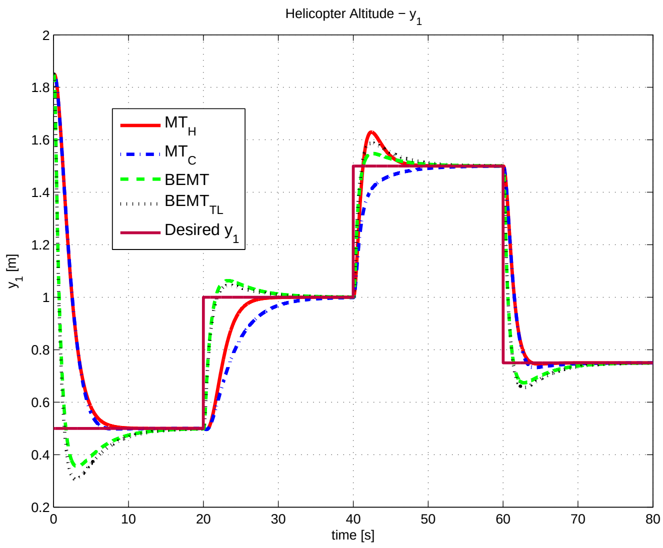

(a) y_1

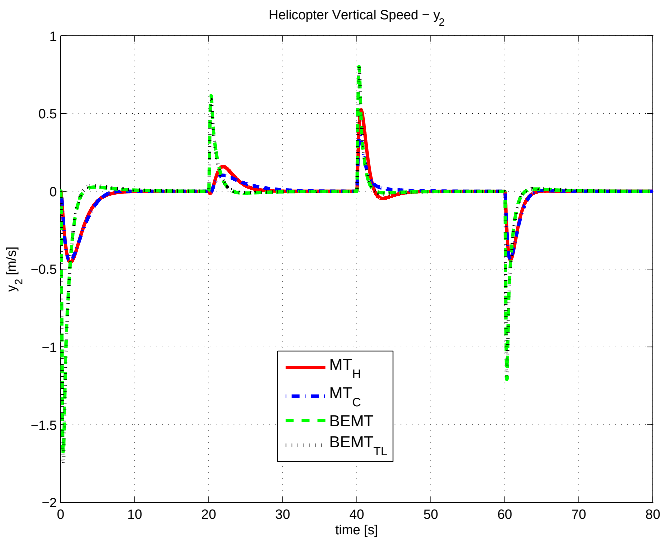

(b) y_2

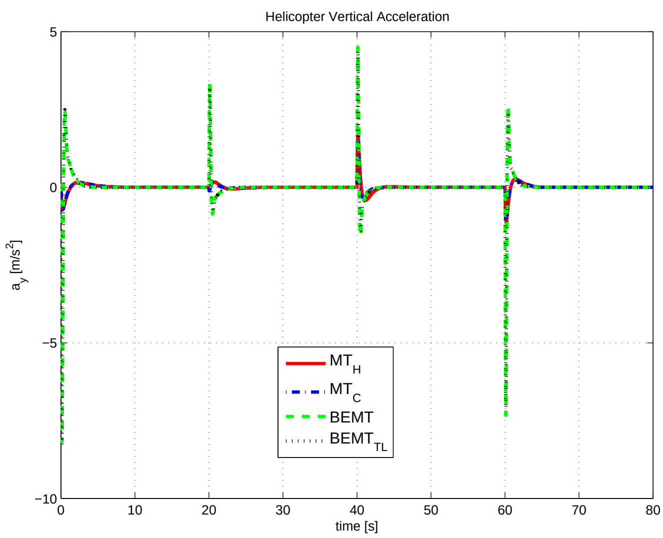

(c) a_y

Figure 7.10: States History for the Continuous Unmodeled C_T and the *BU-TD-PID* Control Design

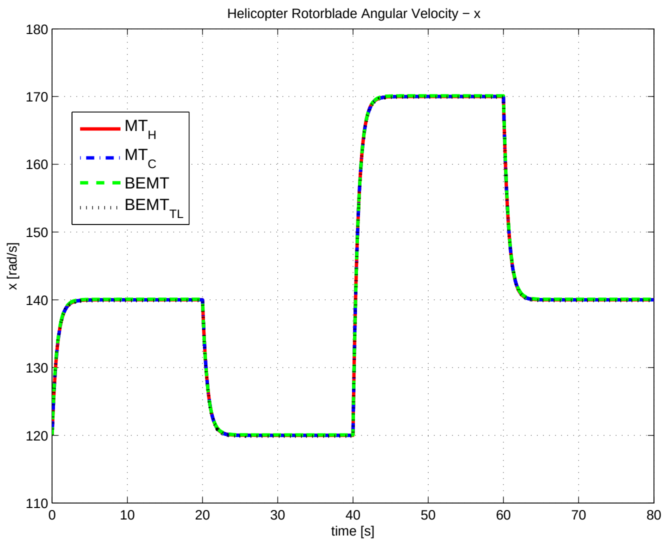

(a) x

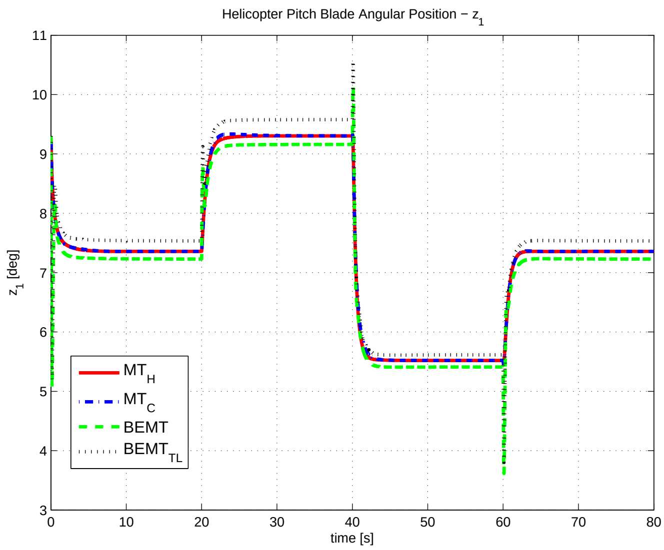

(b) z_1

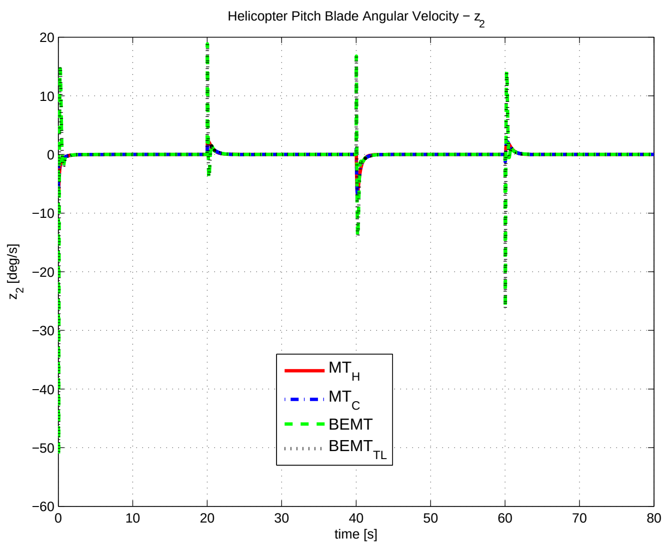

(c) z_2

Figure 7.11: States History for the Continuous Unmodeled C_T and the *BU-TD-PID* Control Design

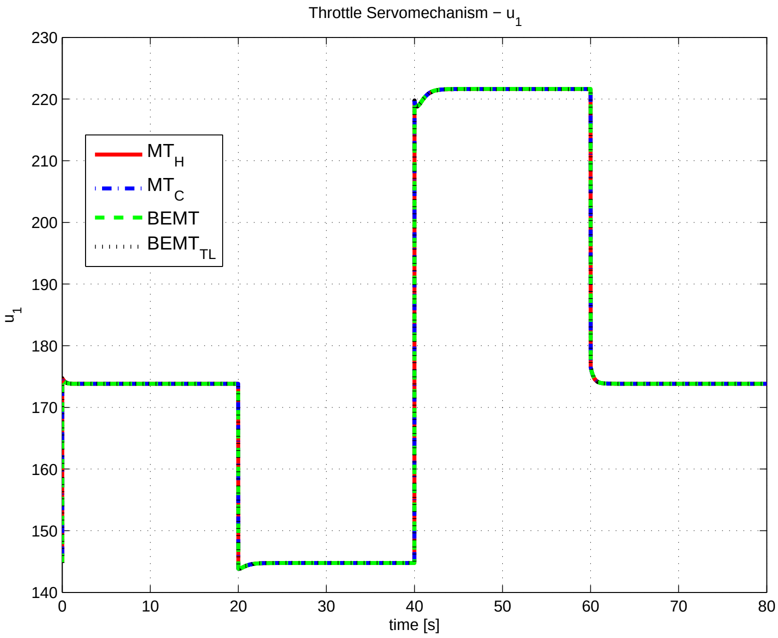

(a) u_1

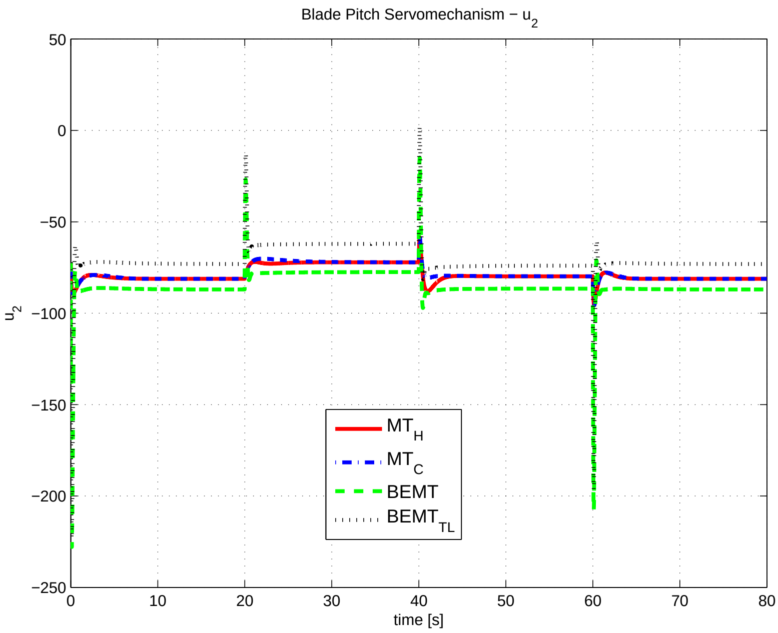

(b) u_2

Figure 7.12: Control History for the Continuous Unmodeled C_T and the *BU-TD-PID* Control Design.

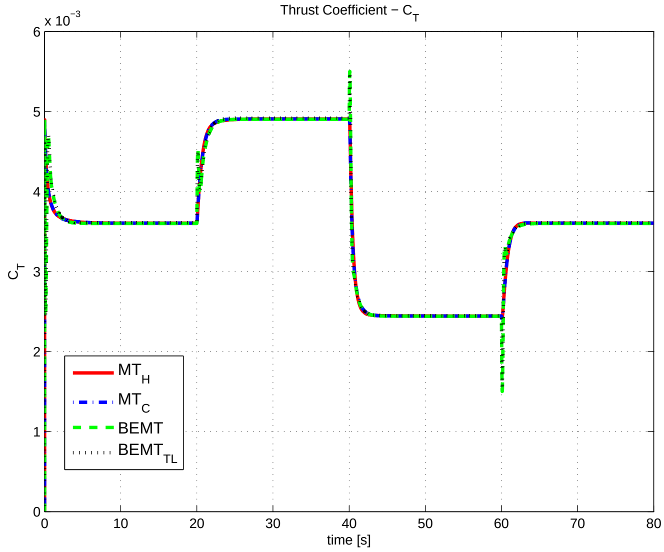

(a) C_T

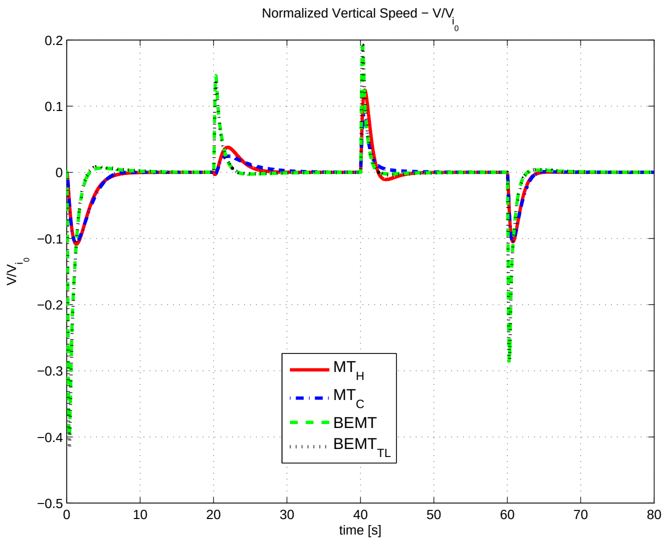

(b) y_2/v_i

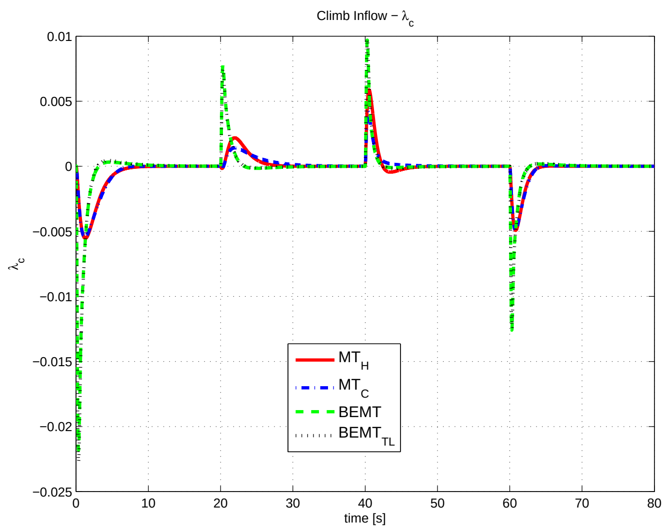

(c) λ_c

Figure 7.13: Significate Aerodynamic Parameters History for the Continuous Unmodeled C_T and the *BU-TD-PID* Control Design.

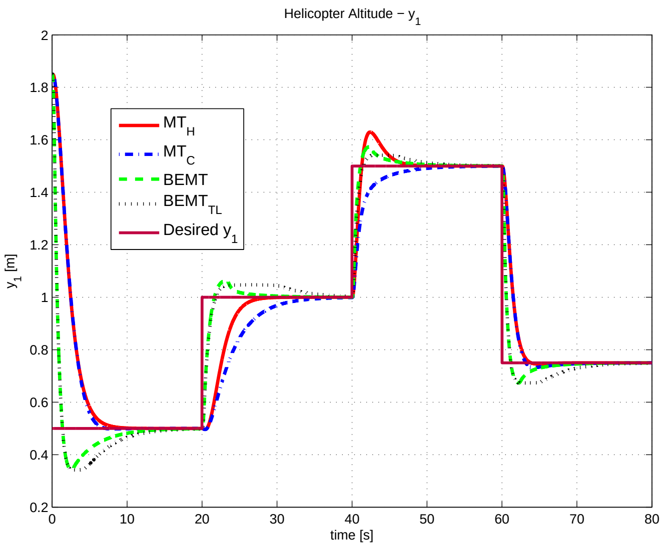

(a) y_1

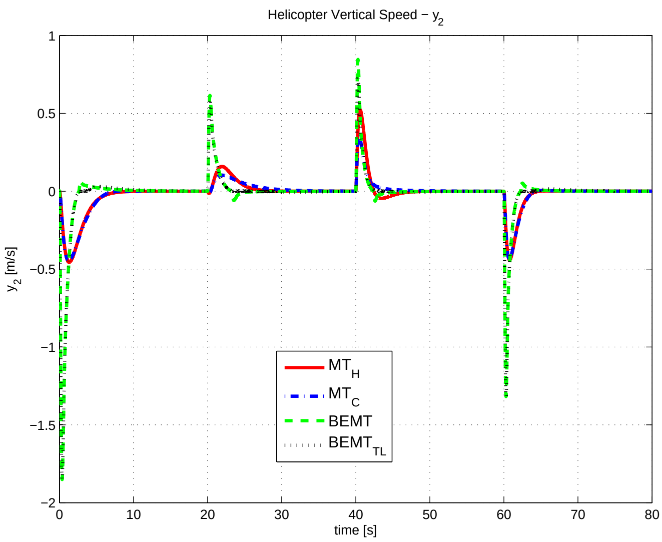

(b) y_2

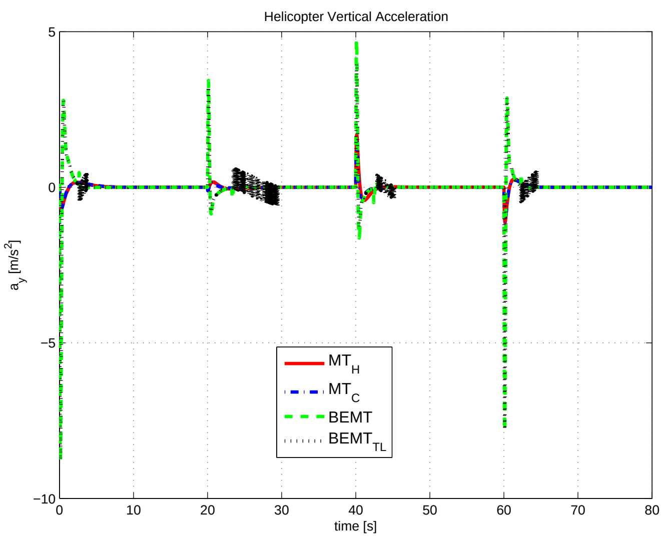

(c) a_y

Figure 7.14: States History for the Discontinuous Unmodeled C_T and the *BU-TD-PID* Control Design

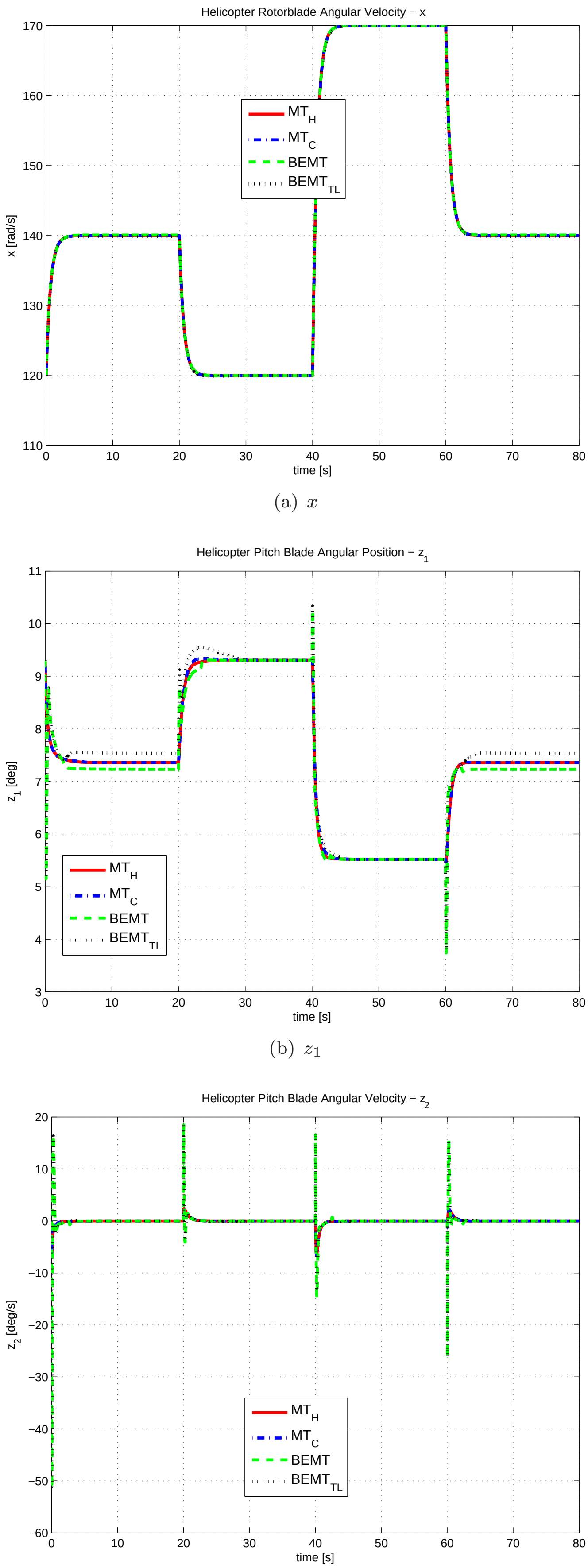

(a) x

(b) z_1

(c) z_2

Figure 7.15: States History for the Discontinuous Unmodeled C_T and the *BU-TD-PID* Control Design

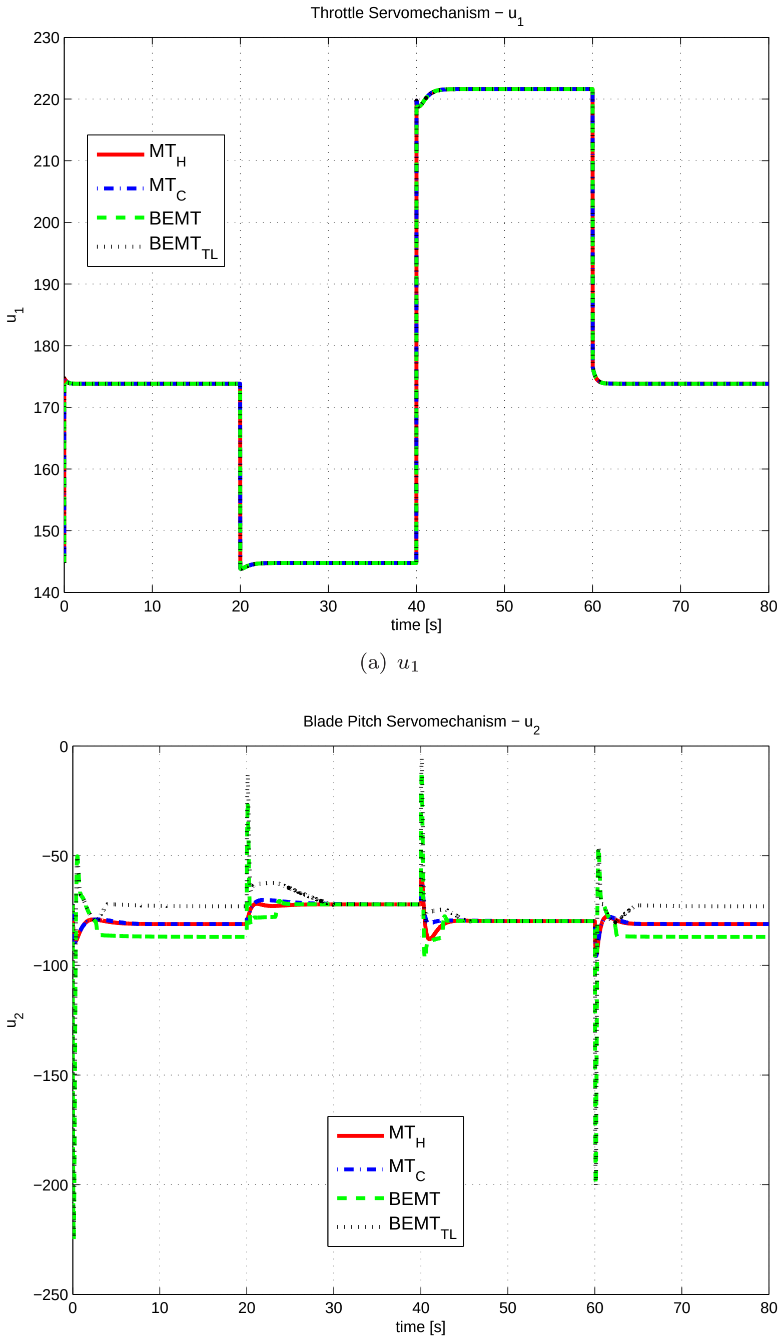

(a) u_1

(b) u_2

Figure 7.16: Control History for the Discontinuous Unmodeled C_T and the *BU-TD-PID* Control Design.

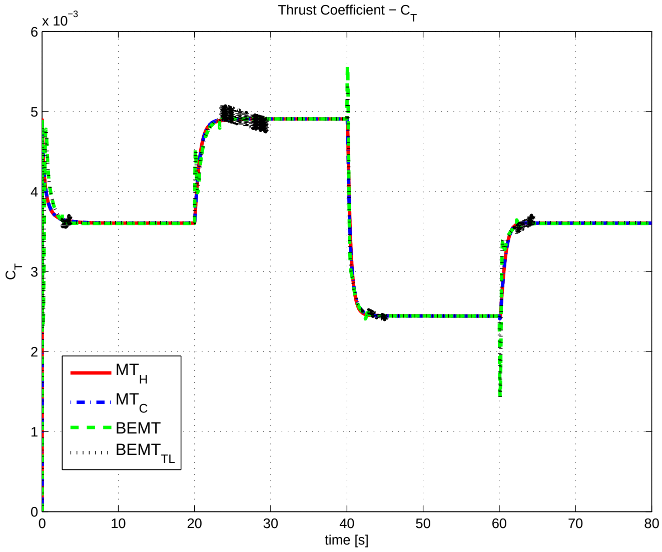

(a) C_T

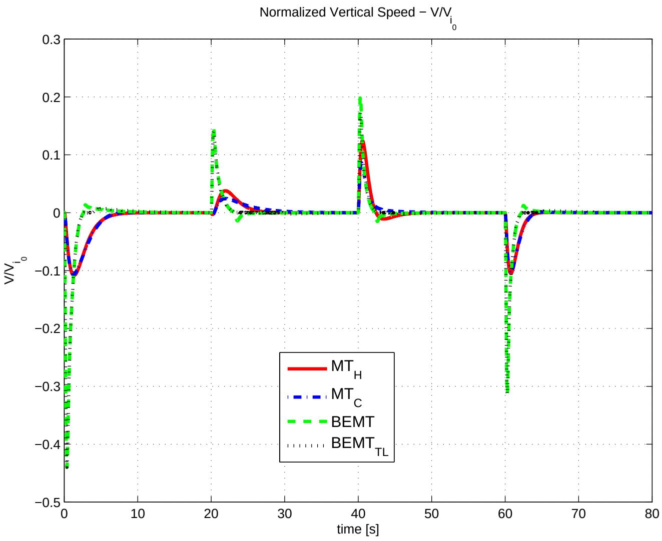

(b) y_2/v_i

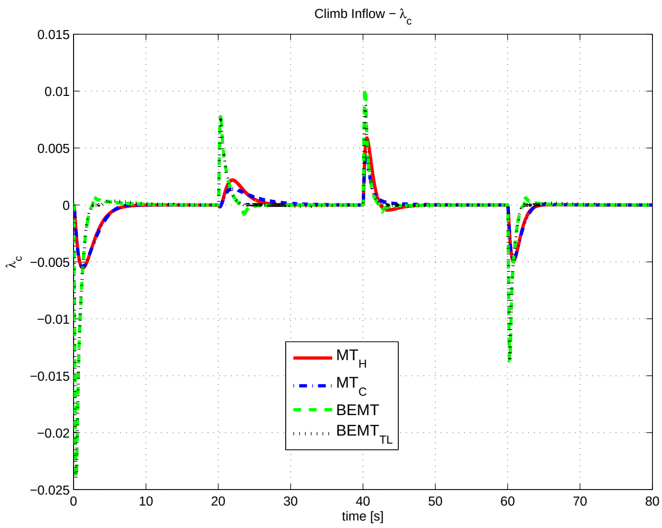

(c) λ_c

Figure 7.17: Significate Aerodynamic Parameters History for the Discontinuous Unmodeled C_T and the *BU-TD-PID* Control Design.

This page intentionally left blank

Chapter 8

Summary and Main Conclusions

Two singularly perturbation approaches that permit to analyze three-time-scale systems have been presented. These two methodologies are based in a sequential application of the general two-time-scale singular perturbation formulation, which allows to decouple the three-time-scale problem into two simpler two-time-scale models depending on the direction in which the methodology is applied. The direction, the *Top-Down* (TD) or the *Bottom-Up* (BU), refers to the order in which the stretched time-scales are applied to the full singularly perturbed system in order to reduce the order of the original system. These methodologies become a valuable tool that simplify the burden of both, designing appropriate control laws, and demonstrate the asymptotic stability of singularly perturbed systems.

The TD and BU methodologies provide a step-by-step procedure that allows to design the proper control laws that guarantee a desired degree of stability, and in addition, select an appropriate composite Lyapunov function for the complete singularly perturbed system, and demonstrate the asymptotic stability for the resulting closed-loop nonlinear singularly perturbed system for sufficiently small singular perturbation parameters, and everything in an all-in-one step-by-step methodology. The equivalency between both the TD and BU methodologies, permits the designer to choose which *direction* is to be used, depending in which combination of both methodologies is the most appropriate according to the natural flow of the variables.

The TD and BU time scale analysis is also extended to the more general N^{th}-time scale analysis using a 4^{th}-time-scale general example. The sequential strategy of decomposing the 4^{th}-time-scale system, into simpler two-time-scale subsystems provides a valuable tool that will help in analyzing any general singularly perturbed N^{th}-time-scale system, and provide additional tools for the time-scale analysis of singularly perturbed systems.

The presented control strategy takes advantage of the TD and BU time-scale analysis methodologies, resulting in two singular-perturbation-based control strategies: the TD and BU control design strategies. For the special underactuated system here studied, a three-time-scale system with two control signals, a modified version of the TD control strategy is presented, along with the *Composite Feedback* TD control design, where both control strategies take advantage of the philosophy of the TD time scale analysis, in which the control laws that stabilize the full problem are obtained by sequentially applying the TD strategy, that results in two distinctive degenerated two-time-scale subproblems considerably simplified, thus permitting to easily obtain the appropriate control laws that stabilize each of the subsystems, and ultimately, stabilizing the full Σ_{SFU} system.

The selected based TD control strategies, are divided in two stages, being each stage dedicated to design each of the two control signals. The first stage of the TD based control strategies, apply sequentially the *Top* and *Down* time constant conditions, to select the control law that stabilizes the Σ_{FU}-subsystem using singular perturbation time-scale analysis to obtain the appropriate control law (u_2) that stabilizes the Σ_F-subsystem, assuming that the closed-loop ultra-fast subsystem has inherent stable properties. The second stage of the *TD* control strategy focuses on the *Top* sequence by using the first time-scale decomposition, along with the obtained results in the second time-scale decomposition of the first stage, and proceeds to stabilize the Σ_S-subsystem with the proper u_1.

The $\mathcal{CF}$-*TD* control strategy uses a similar sequential application of the *TD* time-scale analysis as conducted in the *TD* control design, with the particularity that this methodology allows the user to define a prescribed degree of desired stability for the ultra-fast subsystem, Σ_U, therefore permiting to stabilize the boundary layer Σ_U-subsystem if becomes unstable after substituting the control law that stabilizes the Σ_F-subsystems, which occurs at the end of the first stage of the *TD* control design. It could also happen that the resulting closed-loop boundary layer Σ_U-subsystem does not have the desired degree of prescribed stability, therefore, would require a different control strategy in order to provide that same desired degree of stability to the Σ_U-subsystem. In any of the two possible scenarios in which the *TD* control design lacks to provide the sufficient stability properties to the Σ_U-subsystem, the $\mathcal{CF}$-*TD* control design, adapted to the three-time-scale singularly perturbed problem, will satisfy these stability requirements on the ultra-fast Σ_U-subsystem.

Once the control strategy has provided with autonomous stable systems, the attention is shifted to guarantee the asymptotic stability of the proposed control laws, and to identify the domain of attraction for the resulting closed loop system. The asymptotic stability analysis methodology is also based on the *TD* and/or *BU* time-scales analysis here presented, although for the system here analyze, and for completeness, only the *BU* asymptotic stability analysis is considered. The asymptotic stability analysis provides the necessary tools to guarantee the stability properties for any three-time-scale singularly perturbed autonomous systems, which permits to simplify the burden associated with the analysis multiple time-scale systems employing the existing stability methods.

The same philosophy that permits to analyze the asymptotical stability of an autonomous singular perturbed subsystem, provides, in a step-by-step process similar to the control strategy methodology, with the associated Lyapunov functions for each of the subsystems based on the natural desired closed loop response of each of the resulting subsystem. This methodology, much simpler that the one employed in the existing multiparameter time-scale analysis (Abed, 1985d; Abed, 1985e; Abed, 1985b; Kokotović et al., 1987; Kokotović et al., 1986), permits to have Lyapunov function candidates for each of the defined subsystems a priori of starting the stability analysis, and with a simple structure. The Lyapunov structure is fixed a priori, reducing the fulfillment of the growth requirements among the different time-scale subsystems to obtain the appropriate comparison functions and demonstrating the growth requirements among the different subsystems.

The validity of the methodology has been proved by obtaining the stability upper bound limits for the three-time-scale boundary layers, ε_1 and ε_2, and ensuring that the selected parasitic constants for the proposed control law satisfy $\varepsilon_1 \leq \varepsilon_1^*$ and $\varepsilon_2 \leq \varepsilon_2^*$ for both the helicopter and the simplified model here employed. The use of the full range of reachable state variables has been required in order to satisfy the inequalities that guarantee the asymptotic stability properties at the origin of the Σ_{SFU}-subsystem, which results in extending the asymptotic stability properties to semiglobal stability, by the definition in (Kokotović, 1992; Sussmann and Kokotović, 1991; Braslavsky and Miidleton, 1996), by providing upper bounds on the parasitic singularly perturbed parameters for the entire range of admissible state values, thus extending the domain of attraction to that same rage of admissible states.

The stability results have also presented a closed form solution for the proper selection of the *stability parameters* such that fulfill the required growth requirements among different singularly perturbed subsystem, providing asymptotic stability for the helicopter Σ_{SFU} full system with prescribed upperbounds on the parasitic parameters.

The work conducted in this thesis differs from the studies of multiparameter time-scale singularly perturbed systems that have been conducted extensively in the literature (Saberi and Khalil, 1984; Saberi and Khalil, 1985; Khalil, 1987), in that they do not provide mathematical expressions on the upper bounds for the parasitic constants that define the stretched time scales. These works generally state that the asymptotic stability properties of the system being studied will be satisfied for sufficiently small singularly perturbed parameters, but do not provide precise mathematic expressions on the bounds.

Although for two-time-scale systems, general expression for the upper bounds are provided in the literature (Kokotović et al., 1999; Kokotović et al., 1987), but the expressions are subject to the satisfaction of the growth requirements inequalities for the time-scale subsystems with the selection arbitrary constants, but no precise mathematical expressions are provided. This is even more evident when dealing with multiparameter time-scale systems, systems with more than two-time-scales. Again, several works that appear in the literature approach the multi-parameter asymptotic stability analysis (Abed, 1985c; Abed, 1986; Desoer and Shahruz, 1986; Kokotović et al., 1987) using all similar methods based on composite stability methods of large scale dynamical systems (Michel and Miller, 1977; Araki, 1978), but again without defining mathematical upper bounds on the singularly perturbed parameters. The main contribution of the study conducted in this thesis is providing a methodology that permits to obtain the mathematical expressions that define the upper bounds for the parasitic constants that guaranteed the time-scale selection.

The TD and BU time scale analysis is also extended to the more general N^{th}-time-scale analysis using a 4^{th}-time-scale general example. The sequential strategy of decomposing the 4^{th}-time-scale system, into simpler two-time-scale subsystems provides a valuable tool that will help in analyzing the stability properties of any general singularly perturbed N^{th}-time-scale system, and provide additional tools for the time-scale analysis for singularly perturbed systems.

A performance sensitivity analysis has been also conducted for both the continuous and discontinuous presented test bench models, the MT_C, $BEMT$, and $BEMT_{TL}$, and, after identifying that for $BEMT$, and $BEMT_{TL}$ models, the selected control strategies, despite the discontinuities that present such systems comparing with the selected C_T model, and the quantitative differences on the amount of thrust coefficient generated for a given control signal, both above and bellow the nominal value of the selected C_T, both control strategies are still able to stabilize the helicopter, although they presented a steady state error in the helicopter altitude, which is eliminated by including a simple extra control signal, which is also tested again with the test bench problems, providing a certain type of robustness under thrust coefficient modeling.

The TD and BU singularly perturbed strategy here presented has shown the ability to solve the main problems treated on this thesis:

1. Define a control design strategy that permits to select the desired degree of stability of each of the time-scale subsystems.
2. Define a methodology that permits to demonstrate the asymptotic stability properties of the resulting closed loop full system, by selecting the Lyapunov functions for each of the singularly perturbed subsystems, and construct the associated composite Lyapunov function for the full system.

This page intentionally left blank

Chapter 9

Future Work

The work conducted in this thesis only tries to provide the initial guidelines that will help in extending the work here conducted to a more realistic helicopter model and to other aerospace systems. Possible future works conceived at the time of witting this chapter diverge into two principal lines which are both clearly independent but also intrinsically linked:

- Open problems related to the helicopter model.
- Open problems regarding the multiparameter singular perturbation methodology here presented.

Regarding the first line, the problems related to the helicopter modeling can be divided again into two lines of investigation:

- A more theoretical line and focused on the asymptotic stability analysis conducted on the helicopter problem.
- A more practical regarding the helicopter model.

The first line will address some of the open lines of investigation, that for completeness were left out of this thesis, like a comprehensive study of how the upper bounds on the parasitic parameters are affected by the variation of the *Fixed Parameters*, that is, the variation of the physics of the problem and the control design strategy. For conciseness, these parameters were assumed to be fixed, that is, the helicopter model are not varied $(a_1, a_2, \dots a_{15})$, neither the control design parameters $(b_x, \tilde{b}_{y_1}, \tilde{b}_{y_2})$, which are defined by the selected desired dynamics of the different time-scale subsystems, or the parasitic time constants $(\varepsilon_1,\varepsilon_2)$, which are given by the selection for the time-scales which depend also on the physics of the problem. This study will be of great interest in order to allow to use the same control strategy to a wide range of helicopter systems, since each helicopter will have its own dynamics, and the different missions will also require different time responses.

In addition to study the dependance of the upper bounds on the *Fixed Parameters*, it will also carried the following lines of investigation:

- Extension of the asymptotic stability properties at the origin and the semiglobal stability to exponential stability.
- The study of the implications of actuator saturations.
- A more extensive study of unmodeled dynamics and perturbations for:
  - Further investigate the unmodeled Thrust Coefficient.
  - Extend to the unmodeled engine characterization as introduced in chapter 2.

- Disturbance rejection for the real platform.
- Control design for robustness under external disturbances with the associated asymptotic stability analysis.

As a second line of investigation related to the helicopter model, short term goals imply the implementation of the control laws into the real helicopter platform developed by the *Grupo de Control No Lineal* (*GCNL*). On a more long term goal, and having in mind that it is desirable to control the helicopter in all three axis, will be desirable to extend the 2-DOF helicopter model creating full longitudinal and lateral directional models for helicopters, in which suitable control strategies can be derived in order to provide the helicopter with full autonomous capability.

Regarding the open problems for the multiparameter singular perturbation methodology here presented, some of the future work, that the author has already started, imply extending the three-time-scale TD and BU methodology to a more general N^{th}-time-scale singular perturbation system, although the work has already been started for both time-scale and stability analysis. Also, specifically, for a three-time-scale model, will be investigated a combined one-step TD and BU asymptotic stability methodology which has been applied to a simplified model with interesting and encouraging results when compared with the Σ_{SFU} *Stability Analysis*.

In addition, due to the natural singular perturbation behavior of aerospace systems, and aerospace background of the author, the TD and BU will be extended to different classes of nonlinear aerospace systems, which in general, use systematically singular perturbation and time-scale theory to reduce the order of the system, but do not conduct asymptotic stability analysis to demonstrate the bounds of the parasitic parameters due to the inherent complexities encountered using the existing methods.

Bibliography

Abed, E. (1985a). A new parameter estimate in singular perturbations. *Systems & Control Letters*, 6(3):193–198.

Abed, E. (1985b). Decomposition and stability of multiparameter singular perturbation problems. Technical Report TR-85-50, Department of Electrical Engineering and Systems Research Center, University of Maryland, College Park.

Abed, E. (1985c). Multiparameter singular perturbation problems: Iterative expansions and asymptotic stability. *Systems & Control Letters*, 5(4):279–282.

Abed, E. (1985d). Stability of multiparameter singular perturbation problems with parameters bounds, i. time varying systems with cone-restricted perturbations. Technical Report TR-85-5, Department of Electrical Engineering and Systems Research Center, University of Maryland, College Park.

Abed, E. (1985e). Stability of multiparameter singular perturbation problems with parameters bounds, ii. time-invariant systems with arbitrary perturbations. Technical Report TR-85-6, Department of Electrical Engineering and Systems Research Center, University of Maryland, College Park.

Abed, E. (1986). Strong D-stability. *Systems & Control Letters*, 7(3):207–212.

Abed, E. and Silva-Madriz, R. (1988). Controlability of multiparameter singularly perturbed systems. Technical Report TR-88-73, Department of Electrical Engineering and Systems Research Center, University of Maryland, College Park.

Active Distribution LTD (2004). Active flying stand: Assembly instructions. Technical report, 16 Woodfields, Christleton, Chester CH3 7AX, UK.

Ahmed, A., Schwartz, H., and Aitken, V. (2005). Sliding mode control for singularly perturbed system. In *Control Conference, 2004. 5th Asian*, volume 3, pages 1946–1950. IEEE.

Alvarez-Gallegos, J. and Silva-Navarro, G. (1997). Two-time scale sliding-mode control for a class of nonlinear systems. *International Journal of Robust and Nonlinear Control*, 7(9):865–879.

Anderson Jr., J. (1989). *Introduction to Flight*. McGraw-Hill Inc., New York.

Anderson Jr., J. (1991). *Fundamentals of Aerodynamics*. McGraw-Hill Inc., New York.

Araki, M. (1978). Stability of large-scale nonlinear systems–Quadratic-order theory of composite-system method using M-matrices. *IEEE Transactions on Automatic Control*, 23(2):129–142.

Ardema, M. (1976). Solution of the minimum time-to-climb problem by matched asymptotic expansions. *AIAA Journal*, 14:843–850.

Ardema, M. (1977). Singular perturbations in flight mechanics. Report No:A-5706, NASA-TM-X-62380.

Ardema, M. (1980). Nonlinear singularly perturbed optimal control problems with singular arcs. *Automatica*, 16(1):99–104.

Ardema, M. (1983). Solution algorithms for non-linear singularly perturbed optimal control problems. *Optimal Control Applications and Methods*, 4(4):283–302.

Ardema, M. and Rajan, N. (1985a). Separation of Time-Scales in Aircraft Trajectory Optimization. *Journal of Guidance, Control, and Dynamics*, 8(2):275–278.

Ardema, M. and Rajan, N. (1985b). Slow and fast state variables for three-dimensional flight dynamics. *Journal of Guidance, Control, and Dynamics*, 8(4):532–535.

Ardema, M. and Yang, L. (1988). Interior transition layers in flight-path optimization. *Journal of Guidance, Control, and Dynamics*, 11(1):13–18.

Ashley, H. (1967). Multiple scaling in flight vehicle dynamic analysis—a preliminary look. In *Proceedings of the AIAA Guidance, Control and Dynamics Conference, New York, USA*, pages 1–9. AIAA.

Åström, K. and Hägglund, T. (1995). *PID Controllers:[theory, Design, and Tuning]*. The International Society for Measurement and Control.

Åström, K. and Hägglund, T. (2006). Advanced PID control.

Avanzini, G. and de Matteis, G. (2001). Two-timescale inverse simulation of a helicopter model. *Journal of Guidance, Control, and Dynamics*, 24(2):330–339.

Avanzini, G., de Matteis, G., and de Socio, L. (1999). Two timescale integration method for inverse simulation. *Journal of Guidance, Control, and Dynamics*, 22(3):395–401.

Balakrishnan, S. and Biega, V. (1996). Adaptive-critic-based neural networks for aircraft optimal control. *Journal of Guidance, Control, and Dynamics*, 19(4):893–898.

Balakrishnan, S. and Esteban, S. (2001). Nonlinear flight control systems with neural networks. In *Proceedings of the AIAA Guidance, Navigation and Control Conference and Exhibit, Montreal*. AIAA.

Balakrishnan, S. and Han, D. (2002). Adaptive critic based neural networks for agile missile control. volume 25, pages 404–407.

Bertin, J. and Smith, M. (2002). *Aerodynamics for Engineers*. Prentice Hall.

Bertrand, S., Hamel, T., and Piet-Lahanier, H. (2008). Stability analysis of an uav controller using singular perturbation theory. In *Proceedings of the* 17^{th} *IFAC World Congress, Seoul, Korea*. IFAC.

Betz, A. (1919). Schraubenpropeller mit geringstem Energieverlust Dissertation.

Boverie, S., Jamshidi, M., Titli, A., and Zadeh, L. (1997). *Applications of Fuzzy Logic: Towards High Machine Intelligence Quotient Systems*. Prentice Hall.

Bramwell, A., Done, G., and Balmford, D. (2001). *Bramwell's helicopter dynamics*. Butterworth-Heinemann.

Braslavsky, J. and Miidleton, R. (1996). Global and semi-global stabilizability in certain cascade non-linear systems. *Automatic Control, IEEE Transactions on*, 41(6):876–881.

Breakwell, J. (1977). Optimal flight-path-angle transitions in minimum-time airplane climbs. *Journal of Aircraft*, 14(8):782–786.

Breakwell, J. (1978). More about flight-path-angle transitions in optimal airplane climbs. *Journal of Guidance, Control, and Dynamics*, 1(3):205–208.

Brockett, R. (1978). Feedback invariants for nonlinear systems. In *A link between science and applications of automatic control: proceedings of the seventh Triennial World Congress of the IFAC, Helsinki, Finland*, pages 1115–1120. IFAC.

Bryson, A. (1968). Energy-state approximation in performance optimization of supersonic aircraft. *Journal of Aircraft*, 6:481–488.

Bryson, A. (1971). Minimum time turns for a supersonic airplane at constant altitude. *Journal of Aircraft*, 8:182–187.

Bryson, A. and Ho, Y. (1975). *Applied Optimal Control*. Hemisphere Publishing Co.

Bryson Jr, A. and Lele, M. (1969). Minimum fuel lateral turns at constant altitude. *AIAA Journal*, 7:559–560.

Budiyono, A., Sudiyanto, T., and Lesmana, H. (2008). First principle approach to modeling of small scale helicopter. *Arxiv preprint arXiv:0804.3895*.

Buffington, J., Sparks, A., and Banda, S. (1993). Full conventional envelope longitudinal axis flight control with thrust vectoring. In *American Control Conference*, pages 415–419. IEEE.

Bugajski, D., Enns, D., and Elgersma, M. (1990). A dynamic inversion based control law with application to the high angle-of- attack research vehicle. In *Proceedings of the AIAA Guidance, Navigation and Control Conference and Exhibit, Portland, USA*, pages 826–839. AIAA.

Calise, A. (1976). Singular perturbation methods for variational problems in aircraft flight. *IEEE Transactions on Automatic Control*, 21(3):345–353.

Calise, A. (1977a). A singular perturbation analysis of optimal thrust control with proportional navigation guidance. In *IEEE Conference on Decision and Control*, pages 1167–1176. IEEE.

Calise, A. (1977b). Extended energy management methods for flight performance optimization. *AIAA Journal*, 15:314–321.

Calise, A. (1978). A new boundary layer matching procedure for singularly perturbed systems. *IEEE Transactions on Automatic Control*, 23(3):434–438.

Calise, A. (1979). A singular perturbation analysis of optimal aerodynamic and thrust magnitude control. volume 24, pages 720–730. IEEE.

Calise, A. and Johnson, E. (2001). Reusable lauch vehicle adaptive guidance and control using neural networks. In *Proceedings of the AIAA Guidance, Navigation and Control Conference and Exhibit, Montreal, Canada*, volume 4381. AIAA.

Calise, A., Lee, S., and Sharma, M. (1998). Direct adaptive reconfigurable control of a tailless fighter aircraft. In *Proceedings of the AIAA Guidance, Navigation and Control Conference and Exhibit, Boston, USA*, volume 4108. AIAA.

Calise, A., Lee, S., and Sharma, M. (2000). Development of a reconfigurable flight control law for the X-36 tailles fighter aircraft. In *Proceedings of the AIAA Guidance, Navigation and Control Conference and Exhibit, Denver, USA*. AIAA.

Calise, A., Markopoulos, N., and Corban, J. (1994). Nondimensional forms for singular perturbation analyses of aircraft energy climbs. *Journal of Guidance, Control, and Dynamics*, 17(3):584–590.

Calise, A. and Rysdyk, R. (1998). Fault tolerant flight control via adaptive neural network augmentation. In *Proceedings of the AIAA Guidance, Navigation and Control Conference and Exhibit, Boston, USA*, volume 4483. AIAA.

Chakrabortty, A. and Arcak, M. (2007). A two-time-scale redesign for robust stabilization and performance recovery of uncertain nonlinear systems. In *American Control Conference*, pages 4643–4648. IEEE.

Chakrabortty, A. and Arcak, M. (2008). A Three-time-scale redesign for robust stabilization and performance recovery of nonlinear systems with input uncertainties. In *2007* 46^{th} *IEEE Conference on Decision and Control*, pages 3484–3489. IEEE.

Chakrabortty, A. and Arcak, M. (2009). Time-scale separation redesigns for stabilization and performance recovery of uncertain nonlinear systems. *Automatica*, 45(1):34–44.

Cheeseman, I. and Bennett, W. (1957). The effect of the ground on a helicopter rotor in forward flight. *Aeronautical Research Council R&M*, 3021.

Chen, C. (1998). *Linear system theory and design*. Oxford University Press, Inc.

Chen, C. (2002). Global exponential stabilisation for nonlinear singularly perturbed systems. In *IEE Proceedings Control Theory and Applications*, volume 145, pages 377–382. IET.

Chen, F. and Khalil, H. (1990). Two-time-scale longitudinal control of airplanes using singular perturbation. *Journal of Guidance, Control, and Dynamics*, 13(6):952–960.

Christofides, P. (2000). Robust output feedback control of nonlinear singularly perturbed systems. *Automatica*, 36(1):45–52.

Çimen, T. (2008). State-Dependent Riccati equation (SDRE) control: a survey. In *Proceedings of the* 17^{th} *IFAC World Congress, Seoul, Korea*, pages 3761–3775.

Cliff, E., Kelley, H., and Lefton, L. (1982). Thrust-vectored energy turns. *Automatica*, 18(5):559–564.

Cliff, E., Well, K., and Schnepper, K. (1992). Flight-test guidance for airbreathing hypersonic vehicles. In *Proceedings of the AIAA Guidance, Navigation and Control Conference and Exhibit, SC, USA*, volume A92-55151 23-63. AIAA.

Cloutier, J., D'Souza, C., and Mracek, C. (1996a). Nonlinear regulation and nonlinear h_∞ control via the state-dependent riccati equation technique: Part I, theory. volume 13, pages 117–130.

Cloutier, J., D'Souza, C., and Mracek, C. (1996b). Nonlinear regulation and nonlinear h_∞ control via the state-dependent riccati equation technique: Part II, examples. volume 13, pages 131–141.

Connor, M. (1967). Optimization of a lateral turn at constant height. *AIAA Journal*, 5:335–338.

Cooke, A., Fitzpatrick, E., (Firm), Q., and Corporation, E. (2002). *Helicopter test and evaluation*. AIAA.

Cuerva, A., Espino, J., López, O., Messeguer, J., and Sanz, A. (2009). *Teoría de los Helicópteros*. IDR/UPM.

Cuerva, A., Sanz-Andrés, A., Meseguer, J., and Espino, J. (2006a). An engineering modification of the blade element momentum equation for vertical descent: an autorotation case study. *Journal of the American Helicopter Society*, 51(4):349–354.

Cuerva, A., Sanz-Andrés, A., Meseguer, J., and Espino, J. (2006b). An Engineering Modification of the Blade Element Momentum Equation for Vertical Descent: Fundamentals and Validation. *Journal of the American Helicopter Society*, 51(4):341–348.

Curtiss Jr., H. (2003). Rotorcraft stability and control: Past, present, and future the 20th annual alexander a. nikolsky lecture. *Journal of the American Helicopter Society*, 48(1):3–11.

Deng, B. (2001). Food chain chaos due to junction-fold point. *Chaos: An Interdisciplinary Journal of Nonlinear Science*, 11:514.

Deng, B. and Hines, G. (2002). Food chain chaos due to Shilnikov's orbit. *Chaos: An Interdisciplinary Journal of Nonlinear Science*, 12:533.

Deng, B. and Hines, G. (2003). Food chain chaos due to transcritical point. *Chaos: An Interdisciplinary Journal of Nonlinear Science*, 13:578.

Department of the Army (2007). Field manual - fundamentals of flight. Fm 3-04.203.

Desoer, C. and Shahruz, S. (1986). Stability of nonlinear systems with three time scales. *Circuits, Systems, and Signal Processing*, 5(4):449–464.

Dosanjh, D., Gasparek, E., and Eskinazi, S. (1962). Decay of a viscous trailing vortex. *The Aeronautical Quarterly*, 3(3):167–188.

Dragan, V. and Halanay, A. (1987). High-gain feedback stabilization of linear systems. *International Journal of Control*, 45(2):549–577.

Dreier, M. (2007). *Introduction to helicopter and tiltrotor simulation*. AIAA.

Dzul, A., Lozano, R., and Castillo, P. (2004). Adaptive control for a radio-controlled helicopter in a vertical flying stand. *International journal of adaptive control and signal processing*, 18(5):473–485.

Esteban, S., Aracil, J., and Gordillo, F. (2005a). Three-time scale singular perturbation control for a radio-control helicopter on a platform. In *Proceedings of the AIAA Guidance, Navigation and Control Conference and Exhibit, San Francisco, USA*, volume 6236, pages 1–19. AIAA.

Esteban, S., Aracil, J., and Gordillo, F. (2008a). Lyapunov based asymptotic stability analysis of a three-time scale radio/control helicopter model. In *Proceedings of the AIAA Guidance, Navigation and Control Conference and Exhibit, Hawaii, USA*, volume 6566, pages 1–32. AIAA.

Esteban, S., Balakrishnan, S., Gordillo, F., and Aracil, J. (2008b). Nonlinear control techniques for regulating the altitude of a radio/control helicopter. In *Proceedings of the AIAA Guidance, Navigation and Control Conference and Exhibit, Hawaii, USA*, volume 6564, pages 1–33. AIAA.

Esteban, S., Gordillo, F., and Aracil, J. (2005b). Stability analysis of a three-time scale singular perturbation control for a radio-control helicopter on a platform. In *Proceedings of the* 2^{nd} *Int. Conference on Informatics in Control, Automation and Robotics, Barcelona*. ICINCO.

Esteban, S., Gordillo, F., and Aracil, J. (2007). Lyapunov based stability analisis of a three-time scale model for a helicopter on a platform. In *Proceedings of the* 17^{th} *IFAC Symposium on Automatic Control in Aerospace, Toulouse, France*. IFAC.

Esteban-Roncero, S. (2002). Nonlinear flight control using adaptive critic based neural networks. Aerospace Engineering M.S., University of Missouri - Rolla, Rolla, MO.

Etkin, B. and Reid, L. Dynamics of flight: stability and control.

Federal Aviation Administration (2000). Rotorcraft flying handbook.

Ferrari, S. and Stengel, R. (2002). Classical/neural synthesis of nonlinear control systems. volume 25, pages 442–448.

Frazzoli, E., Dahleh, M., and Feron, E. (2000). Trajectory tracking control design for autonomous helicopters using a backstepping algorithm. In *Proceedings of the 2000 American Control Conference*, volume 6, pages 4102–4107. IEEE.

Friedrichs, K. and Wasow, W. Singular perturbations of non-linear oscillations. *Duke Mathematical Journal*, 13(3):367–381.

Futaba®(2006). Futaba digital FET servos. Technical report.

Gablehouse, C. (1967). *Helicopters and autogiros: a chronicle of rotating-wing aircraft*. Lippincott.

Gablehouse, C. (1969). *Helicopters and autogiros: a history of rotating-wing and V/STOL aviation.* Lippincott.

Garratt, M. (2007). *Biologically inspired vision and control for an autonomous flying vehicle.* PhD thesis, The Australian National University, Canberra, Australia.

Gavrilets, V. (2003). *Autonomous Aerobatic Maneuvering of Miniature Helicopters: Modeling and Control.* PhD thesis, PhD thesis, Massachusetts Institute of Technology, Cambridge, MA.

Gavrilets, V., Martinos, I., Mettler, B., and Feron, E. (2002a). Control logic for automated acrobatic flight of a miniature helicopter. In *Proceedings of the AIAA Guidance, Navigation and Control Conference and Exhibit, Monterrey, CA, USA.*

Gavrilets, V., Mettler, B., and Feron, E. (2001). Dynamic model for a miniature aerobatic helicopter. In *Proceedings of the AIAA Guidance, Navigation and Control Conference and Exhibit, Montreal, Canada.* AIAA.

Gavrilets, V., Mettler, B., and Feron, E. (2002b). Dynamic model for X-cell 60 helicopter in low advance ratio flight. Technical Report P-2543, MIT Laboratory for Information and Decision Systems.

Gessow, A. and Center, N.-L. R. (1948). *Effect of Rotor-Blade Twist and Plan-Form Taper on Helicopter Hovering Performance.* National Advisory Committee for Aeronautics.

Gessow, A. and Gustafson, F. (1945). Flight Tests of the Sikorsky HNS-1 (Army YR-4B) Helicopter. 2-Hovering and Vertical-Flight Performance with the Original and an Alternative Set of Main-Rotor Blades, Including a Comparison with Hovering Performance Theory. Technical report.

Gessow, A. and Myers, G. (1985). *Aerodynamics of the Helicopter.* College Park Press.

Gilmore, D. and Gartshore, I. The development of an efficient hovering propeller/rotor performance prediction method. *AGARD Aerodyn. of Rotary Wings*, 42.

Glauert, H. (1935). Airplane propellers. *Aerodynamic theory*, 4:169–360.

Goldstein, S. (1929). On the vortex theory of screw propellers. *Proceedings of the Royal Society of London. Series A*, 123(792):440.

Grammel, G. (2004). On nonlinear control systems with multiple time scales. *Journal of Dynamical and Control Systems*, 10(1):11–28.

Green, J. A. and Sasiadek, J. Z. (2002). Inverse dynamics and fuzzy repetitive learning flexible robot control. In *Proceedings of the* 15^{th} *Triennial World Congress of the IFAC, Barcelona, Spain.*

Gruss Guido Büscher, RC-Discount (2006). Swashplate on a radio-controlled helicopter.

Hamidi, E. and Ohta, H. (1995). Helicopter flight controller design using nonlinear transformation. In *Proceedings of the* 34^{th} *SICE Annual Conference*, pages 1481–1486. IEEE.

Hartana, P. and Sasiadek, J. (2002). Adaptive fuzzy logic system for sensor fusion in dead-reckoning mobile robot navigation. In *Proceedings of the* 15^{th} *Triennial World Congress of the IFAC, Barcelona, Spain.*

Heck, B. (1991). Sliding-mode control for singularly perturbed systems. *International Journal of Control*, 53(4):985–1001.

Hedrick, J. and Bryson, A. (1971). Minimum Time Turns for a Supersonic Airplane at Constant Altitude. *AIAA Journal of Aircraft*, 8:182–187.

Hedrick, J. and Bryson Jr, A. (1972). Three-dimensional, minimum-time turns for a supersonic aircraft. *Journal of Aircraft*, 9(2):115–121.

Heiges, M., Menon, P., and Schrager, D. (1992). Synthesis of a helicopter full-authority controller. *Journal of Guidance, Control, and Dynamics*, 15(1):222–227.

Hitec (2007). Hitec HSR-8498HB digital servo operation and interface.

Holland, J. (1975). *Adaptation in Natural and Artificial Systems*. Cambridge, MIT Press.

Huang, Z. and Balakrishnan, S. (2005). Robust neurocontrollers for systems with model uncertainties: a helicopter application. *Journal of guidance, control, and dynamics*, 28(3):516–523.

Hunt, L., Su, R., and Meyer, G. (1983). Global transformations of nonlinear systems. *IEEE Transactions on Automatic Control*, 28(1):24–31.

Idan, M., Johnson, M., Calise, A., and Kaneshige, J. (2002). Intelligent aerodynamic/propulsion flight control for flight safety: A nonlinear adaptive approach. In *Proceedings of the 2001 American Control Conference*, volume 4, pages 2918–2923. IEEE.

Ioannou, P. and Tsakalis, K. (2002). A robust direct adaptive controller. *IEEE Transactions on Automatic Control*, 31(11):1033–1043.

Isidori, A., Marconi, L., and Serrani, A. (2003). Robust nonlinear motion control of a helicopter. *IEEE Transactions on Automatic Control*, 48(3):413–426.

Jagannathan, S. and Lewis, F. (1996). Multilayer discrete-time neural-net controller with guaranteed performance. *IEEE Transactions on Neural Networks*, 7(1):107–130.

Jalics, J., Krupa, M., and Rotstein, H. (2010). Mixed-mode oscillations in a three time-scale system of ODEs motivated by a neuronal model. *Dynamical Systems*, 99999(1):1–38.

Jiménez-González, A. (2007). Implementación de sensores de altitud en plataforma de pruebas para helicópteros rc. Technical Report Proyecto Fin de Carrera PT. 1377, Department of Systems Engineering,University of Seville. Tutors: Francisco Durán Sánchez and Manuel Gil Ortega Linares.

Johnson, E., Calise, A., El-Shirbiny, H., and Rysdyk, R.

Johnson, W. (1994). *Helicopter Theory*. Dover Pubns.

Kaiser, F. (1944). Der Steifflug mit Strahflugzeugen teilbericht. Technical report, Messerschmitt, A.G., Lechfeld, Germany.

Kaloust, J., Ham, C., and Qu, Z. (2002). Nonlinear autopilot control design for a 2-DOF helicopter model. In *IEE Proceedings Control Theory and Applications*, volume 144, pages 612–616. IET.

Kaneshige, J., Bull, J., and Totah, J. (2000). Generic neural flight control and autopilot system. In *Proceedings of the AIAA Guidance, Navigation and Control Conference and Exhibit, Denver, USA*, volume 4281, pages 14–17. AIAA.

Kaplun, S., Lagerstrom, P., Howard, L., and Liu, C. (1967). *Fluid mechanics and singular perturbations*. Academic Press New York.

Kelley, H. (1959). An investigation of optimal zoom climb techniques. *Journal of the Aerospace Sciences*, 26(12):794–802.

Kelley, H. (1970a). Boundary-layer approximation to powered-flight attitude transients. *Journal of Spacecraft and Rockets*, 7(7):879.

Kelley, H. (1970b). Singular perturbations for a Mayer variational problem. *AIAA Journal*, 8(6):1177–1178.

Kelley, H. (1971a). Flight path optimization with multiple time scales. *Journal of Aircraft*, 8(4):238–240.

Kelley, H. (1971b). Flight path optimization with multiple time scales. *Journal of Aircraft*, 8:238–240.

Kelley, H. (1973). Aircraft maneuver optimization of reduced-order approximation. *Control and dynamic systems*, pages 131–178.

Kelley, H., Cliff, E., and Weston, A. (1986). Energy state revisited. *Optimal Control Applications and Methods*, 7(2):195–200.

Kelley, H. and Lefton, L. (1972). Supersonic aircraft energy turns. *Automatica*, 8(5):575–580.

Kelly, H. and Edelbaum, T. (1986). Energy Climbs, Energy Turns and Asymptotic Expansions. *Singular perturbations in systems and control*, 4:290.

Khalil, H. (1981). Asymptotic stability of non-linear multiparameter singularly perturbed systems. *Automatica*, 17(6):797–804.

Khalil, H. (1987). Stability analysis of nonlinear multiparameter singularly perturbed systems. *IEEE Transactions on Automatic Control*, (3):260–263.

Khalil, H. (1996). *Nonlinear Systems*. Prentice Hall.

Khalil, H. (2002). *Nonlinear Systems*. Prentice-Hall, 3rd edition.

Khalil, H. and Kokotović, P. (1979a). Control of linear systems with multiparamter singular perturbations. *Automatica*, 15(2):197–207.

Khalil, H. and Kokotović, P. (1979b). *D*-Stability and Multi-Parameter Singular Perturbation. *SIAM Journal on Control and Optimization*, 17:56.

Khorasani, K. (1989). Robust stabilization of non-linear systems with unmodelled dynamics. *International Journal of Control*, 50(3):827–844.

Khorasani, K. and Pai, M. (1984). Asymptotic stability improvements of multiparameter nonlinear singularly perturbed systems. *IEEE Transactions on Automatic Control*, (8):802–804.

Khorasani, K. and Pai, M. (1985). Asymptotic stability of nonlinear singularly perturbed systems using higher order corrections. *Automatica*, (6):717–727.

Kim, B. and Calise, A. (1997). Nonlinear Flight Control Using Neural Networks. *Journal of Guidance, Control, and Dynamics*, 20(1):26–33.

Kim, H. and Shim, D. (2003). A flight control system for aerial robots: algorithms and experiments. *Control engineering practice*, 11(12):1389–1400.

Kocurek, J., Tangler, J., et al. (1977). A prescribed wake lifting surface hover performance analysis. *Journal of the American Helicopter Society*, 22:24–35.

Kokotović, P. (1981). Subsystems, time scales and multimodeling. *Automatica*, 17(6):789–795.

Kokotović, P. (1984). Applications of singular perturbation techniques to control problems. *Siam Review*, 26(4):501–550.

Kokotović, P. (1985). Recent trends in feedback design- An overview. *Automatica*, 21:225–236.

Kokotović, P. (1992). The joy of feedback: nonlinear and adaptive. *Control Systems Magazine, IEEE*, 12(3):7–17.

Kokotović, P., Bensoussan, A., and Blankenship, G. (1987). *Singular perturbations and asymptotic analysis in control systems*. Number 90. Springer-Verlag Berlin.

Kokotović, P., Khalil, H., and O'reilly, J. (1999). *Singular perturbation methods in control: analysis and design*. Society for Industrial Mathematics.

Kokotović, P., O'Malley, J., and Sannuti, P. (1976). Singular perturbations and order reduction in control theory–an overview. *Automatica*, 12(2):123–132.

Kokotović, P., O'Reilly, J., and Khalil, H. (1986). *Singular Perturbation Methods in Control: Analysis and Design*. Academic Press, Inc., Orlando, FL, USA.

Koo, T. and Sastry, S. (2002). Output tracking control design of a helicopter model based on approximate linearization. In *Proceedings of the* 37^{th} *IEEE Conference on Decision and Control*, volume 4, pages 3635–3640. IEEE.

Krupa, M., Popović, N., Kopell, N., and Rotstein, H. (2008). Mixed-mode oscillations in a three time-scale model for the dopaminergic neuron. *Chaos: An Interdisciplinary Journal of Nonlinear Science*, 18:015106.

Ladde, G. and Siljak, D. (1983). Multiparameter singular perturbations of linear systems with multiple time scales. *Automatica*, 19(4):385–394.

Landgrebe, A. (1969). An analytical method for predicting rotor wake geometry. *Journal of the American Helicopter Society*, 14:20–32.

Lara-González, M. (2008). Simulación e integración en el tiempo real con el modelo de un mini-helicóptero. Technical Report Proyecto Fin de Carrera PT. 1534, Department of Systems Engineering,University of Seville. Tutors: Sergio Esteban Roncero and Manolo López Martínez.

Layton, D. (1984). *Helicopter Performance*. Matrix Publisher, Inc.

Lee, T. and Kim, Y. (2001). Nonlinear adaptive flight control using backstepping and neural networks controller. *Journal of Guidance, Control, and Dynamics*, 24(4):675–682.

Leishman, J. (2006). *Principles of helicopter aerodynamics*. Cambridge University Press.

Levinson, N. (1950). Perturbations of discontinuous solutions of non-linear systems of differential equations. *Acta Mathematica*, 82(1):71–106.

Lewis, F. and Stevens, B. (2003). *Aircraft Control and Simulation*. John Wiley & Sons, Inc.

Lewis, M. and Aiken, E. (1985). Piloted Simulation of One-on-One Helicopter Air Combat at NOE (Nap-of-the-Earth) Flight Levels. Technical report.

Lock, C. *The Application of Goldstein's Theory to the Practical Design of Airscrews*. British Aeronautical Research Council.

López-Martínez, M., Ortega, M., Vivas, C., and Rubio, F. (2007). Nonlinear L_2 control of a laboratory helicopter with variable speed rotors. *Automatica*, 43(4):655–661.

López Ruiz, J. (1993). *Helicópteros: Teoría y Diseño Conceptual*. Universidad Politécnica de Madrid.

López, O. and Valenzuela, A. (2010). *Temario Helicópteros*, volume Astronáutica y Aeronaves Diversas of *Asignaturas en la Red 2009-2010*. Universidad de Sevilla - Enseñanza Virtual.

Mahony, R. and Hamel, T. (2004). Robust trajectory tracking for a scale model autonomous helicopter. *International Journal of Robust and Nonlinear Control*, 14(12):1035–1059.

Marconi, L. and Naldi, R. (2007). Robust full degree-of-freedom tracking control of a helicopter. *Automatica*, 43(11):1909–1920.

McLean, D. (1990). *Automatic Flight Control Systems*. Prentice Hall.

Mehra, R., Washburn, R., Sajan, S., and Carrol, J. (1979). A study of the application of singular perturbation theory. NASA CR-3167.

Menon, P., Badgett, M., Walker, R., and Duke, E. (1987). Nonlinear flight test trajectory controllers for aircraft. *Journal of Guidance, Control, and Dynamics*, 10(1):67–72.

Merritt, S., Cliff, E., and Kelley, H. (1985). Energy-modelled climb and climb-dash–the Kaiser technique. *Automatica*, 21(3):319–321.

Meyer, G., Su, R., and Hunt, L. (1984). Application of nonlinear transformations to automatic flight control. In *IFAC Congress*, volume 20, pages 103–107. IFAC.

Michel, A. and Miller, R. (1977). *Qualitative analysis of large scale dynamical systems.* Academic Press.

Miele, A. (1950). Problemi di Minimo Tempo nel Volo Non-Stazionario degli Aeroplani. *Atti della Accademia delle Scienze di Torino, Classe di Scienze Matematiche, Fisiche e Naturali*, 85:41–52.

Miniature Aircraft USA (1999). X-cell 50 technical manual. Technical report, Orlando, Fla.

Moerder, D. and Calise, A. (1984). Near-optimal output feedback regulation of ill-conditioned linear systems. In *The* 23^{rd} *IEEE Conference on Decision and Control*, volume 23, pages 919–925. IEEE.

Moerder, D. and Calise, A. (1985a). Convergence of a numerical algorithm for calculating optimal output feedback gains. *IEEE Transactions on Automatic Control*, 30(9):900–903.

Moerder, D. and Calise, A. (1985b). Two-time scale stabilization of systems with output feedback. *Journal of Guidance, Control, and Dynamics*, 8:731–736.

Mukaidani, H., Xu, H., and Mizukami, K. (2003). New results for near-optimal control of linear multi-parameter singularly perturbed systems. *Automatica*, 39(12):2157–2167.

Naidu, D. (2002). Singular perturbations and time scales in control theory and applications: an overview. *Dynamics of Continuous Discrete and Impulsive Systems Series B*, 9:233–278.

Naidu, D. and Calise, A. (2001). Singular perturbations and time scales in guidance and control of aerospace systems: A survey. *Journal of Guidance, Control and Dynamics*, 24(6):1057–1078.

Naidu, D. and Price, D. (1988). Singular perturbations and time scales in the design of digital flight control systems. TP 2844.

Navarro-Collado, J. (2010). Diseño e implementación de sensores de las variables de estado de un helicóptero. Technical Report Proyecto Fin de Carrera PT. 1534, Department of Systems Engineering,University of Seville. Tutors: Sergio Esteban Roncero and Francisco Gordillo.

Ng, A., Coates, A., Diel, M., Ganapathi, V., Schulte, J., Tse, B., Berger, E., and Liang, E. (2006). Autonomous inverted helicopter flight via reinforcement learning. *Experimental Robotics IX*, pages 363–372.

Nise, N. (1995). *Control Systems Engineering.* Addison-Wesley Publishing Company.

Njaka, C., Menon, P., and Cheng, V. (1994). Towards an advanced nonlinear rotorcraft flight control system design. In 13^{th} *DASC. AIAA/IEEE Digital Avionics Systems Conference*, pages 190–197.

of Robots, S. (2008). What is the difference between an analog and digital servo?

Oh, S. and Khalil, H. (1997). Nonlinear Output-Feedback Tracking Using High-gain Observer and Variable Structure Control. *Automatica*, 33(10):1845–1856.

O'Malley Jr, R. (1971). Boundary layer methods for nonlinear initial value problems. *SIAM Review*, 13(4):425–434.

O'Malley Jr, R. (1991). *Singular perturbation methods for ordinary differential equations.* Springer-Verlag New York, Inc.

OS Engines (2010). 50SX-H ringed hyper heli engine. Technical report.

Padfield, G. (2007). *Helicopter flight dynamics: the theory and application of flying qualities and simulation modelling*. Wiley-Blackwell.

Pallet, T. and Ahmad, S. (1991). Real-time helicopter flight control: Modelling and control. Technical Report TR-EE 91-35.

Pallet, T., Wolfert, B., and Ahmad, S. (1991). Real Time Helicopter Flight Control Test Bed. Technical Report TR-EE 91-28.

Pallett, T. and Ahmad, S. (1993). Adaptive neural network control of a helicopter in vertical flight. In *The First IEEE Regional Conference on Aerospace Control Systems*, pages 264–268. IEEE.

Pan, Z. and Başar, T. (1995). Multi-time scale zero-sum differential games with perfect state measurements. *Dynamics and Control*, 5(1):7–29.

Payne, P. (1959). *Helicopter dynamics and aerodynamics*. Macmillan.

Plumer, E. (1996). Optimal control of terminal processes using neural networks. *IEEE Transactions on Neural Networks*, (2):408–418.

Prandtl, L. (1904). Uber Flussigkeits bewegung bei sehr kleiner Reibung, Verhaldlg III Int. *Math. Kong.(Heidelberg: Teubner)*, pages 484–491.

Prasad, J., Calise, A., Pei, Y., and Corban, J. (1999). Adaptive nonlinear controller synthesis and flight test evaluation on an unmanned helicopter. In *Proceedings of the IEEE International Conference on Control Applications*, volume 1, pages 137–142. IEEE.

Prasad, J. and Lipp, A. (1993). Synthesis of a helicopter nonlinear flight controller using approximate model inversion. *Mathematical and Computer Modelling*, 18(3-4):89–100.

Prouty, R. (1986). *Helicopter Performance, Stability and Control*. PWS Engineering, Boston Mass.

Pujol-Pérez, P. (2007). Aplicación de tiempo real para sistemas de control de vuelo de un helicóptero de aeromodelismo. Technical Report Proyecto Fin de Carrera PT. 0029, Department of Systems Engineering,University of Seville. Tutored by Fabio Gómez-Estern Aguilar.

Rajan, N. and Ardema, M. Interception in three dimensions - An energy formulation. In *Proceedings of the AIAA Atmospheric Flight Mechanics Conference, Gatlinburg, TN*, volume 1983-2121.

Ramnath, R. (2010). *Multiple Scales Theory and Aerospace Applications*. AIAA.

Raymer, D. (2006). *Aircraft design: a conceptual approach*. AIAA.

Rechenberg, I. (1973). *Evolutionsstrategie*. Frommann-Holzboog, Stuttgart, Germany.

Reiner, J., Balas, G., and Garrard, W. (1995). Robust dynamic inversion for control of highly maneuverable aircraft. *Journal of Guidance, Control, and Dynamics*, 18(1):18–24.

Reiner, J., Balas, G., and Garrard, W. (1996). Flight control design using robust dynamic inversion and time-scale separation. *Automatica*, 32(11):1493–1504.

Ridgely, D., Banda, S., and Dazzo, J. (1984). Decoupling of high-gain multivariable tracking systems. *Journal of Guidance, Control, and Dynamics*, 8(1):44–49.

Roskam, J. (2001). *Airplane flight dynamics and automatic flight controls*. DARcorporation.

Roskam, J. and Lan, C. (1997). *Airplane aerodynamics and performance*. DARcorporation.

Rutowski, E. (1954). Energy approach to the general aircraft performance problem. *Journal of the Aeronautical Sciences*, 21(3):187–195.

Saberi, A. (1987). Output-feedback control with almost-disturbance-decoupling property—a singular perturbation approach. *International Journal of Control*, 45(5):1705–1722.

Saberi, A. and Khalil, H. (1984). Quadratic-type Lyapunov functions for singularly perturbed systems. *IEEE Transactions on Transactions on Automatic Control*, 29(6):542–550.

Saberi, A. and Khalil, H. (1985). Stabilization and regulation of nonlinear singularly perturbed systems–Composite control. *IEEE Transactions on Automatic Control*, 30(8):739–747.

Saini, G., Balakrishnan, S., and Person, C. (1997). Adaptive critic based neurocontroller for autolanding of aircraft with varying glideslopes. In *International Conference on Neural Networks, 1997.*, volume 4, pages 2288–2293.

Saksena, V., O'reilly, J., and Kokotović, P. (1984). Singular perturbations and time-scale methods in control theory: Survey 1976-1983. *Automatica*, 20(3):273–293.

Santos-García, J. (2007). Caja aviónica para teleoperación y control desde estación base terrestre adaptable al helicóptero comercial de radio control x-cell-spectra-g-3d. Technical Report Proyecto Fin de Carrera PT, Department of Systems Engineering,University of Seville. Tutors: José Ángel Acosta Rodríguez.

ServoCity (2008). How servos work?

Shi, P., Shue, S., and Agrawal, R. (1998). Robust disturbance attenuation with stability for a class of uncertain singularly perturbed systems. *International Journal of Control*, 70(6):873–891.

Shim, H., Koo, T., Hoffmann, F., and Sastry, S. (1998). A comprehensive study of control design for an autonomous helicopter. In *Proceedings of the* 37^{th} *IEEE Conference on Decision and Control*, volume 4, pages 3653–3658. IEEE.

Shinar, J. and Farber, N. (1984). Horizontal variable-speed interception game solved by forced singular perturbation technique. *Journal of Optimization Theory and Applications*, 42(4):603–636.

Sira-Ramírez, H., Zribi, M., and Ahmad, S. (1994). Dynamical Sliding Mode Control Approach for Vertical Flight Regulation in Helicopters. *IEE Proceedings-Control Theory & Applications*, 141(1):19–24.

Sissingh, G. (1939). Contribution to the Aerodynamics of Rotating-wing Aircraft. TM No. 921.

Sissingh, G. (1941). Contribution to the Aerodynamics of Rotating-wing Aircraft: Part II. TM No. 990.

Snell, S., Enns, D., and Garrard, W. (1992). Nonlinear inversion flight control for a supermaneuverable aircraft. *Journal of Guidance, Control, and Dynamics*, 15(4):976–984.

Soloway, D. and Haley, P. (2001). Aircraft reconfiguration using neural generalized predictivecontrol. In *Proceedings of the 2001 American Control Conference*, volume 4, pages 2294–2929. IEEE, ACC.

Steele, M. (2004). *The Cauchy-Schwarz Master Class*. Cambridge University Press.

Sussmann, H. and Kokotović, P. (1991). The peaking phenomenon and the global stabilization of nonlinear systems. *IEEE Transactions on Automatic Control*, 36(4):424–440.

Tee, K., Ge, S., and Tay, F. (2008). Adaptive neural network control for helicopters in vertical flight. *IEEE Transactions on Control Systems Technology*, 16(4):753–762.

The International Civil Aviation Organization (2009). ICAO Annex 7. Technical report.

Theodore, C. (2000). *Helicopter flight dynamics simulation with refined aerodynamic modeling*. PhD thesis, University of Maryland.

Tikhonov, A. (1948). On the dependence of the solutions of differential equations on a small parameter. *Matematicheskii Sbornik*, 22(64)(2):193–204.

Tikhonov, A. (1952). Systems of differential equations containing small parameters in the derivatives. *Matematicheskii Sbornik*, 31(73)(3):575–586.

Tischler, M. (1987). Digital control of highly augmented combat rotorcraft. TM 88346.

Tischler, M. (1989). Assessment of digital flight-control technology for advanced combat rotorcraft. *Journal of the American Helicopter Society*, (4):66–76.

US DoT - FAA (2006a). Description of helicopter torque effect.

US DoT - FAA (2006b). Diagram of forces effecting an anti-torque tail rotor system. faa - h808321.

van Dyke, M. (1975). Perturbation methods in fluid mechanics/Annotated edition. NASA STI/Recon Technical Report A.

Vasil'eva, A. (1963). Asymptotic behaviour of solutions to certain problems involving non-linear differential equations containing a small parameter multiplying the highest derivatives. *Russian Mathematical Surveys*, 18:13.

Vasil'Eva, A. (1976). The development of the theory of ordinary differential equations with a small parameter multiplying the highest derivative during the period 1966-1976. *Russian Mathematical Surveys*, 31:109.

Vasil'Eva, A. (1994). On the development of singular perturbation theory at Moscow State University and elsewhere. *SIAM review*, 36(3):440–452.

Vasil'eva, A., Butuzov, V., and Kalachev, L. (1995). The boundary function method for singular perturbation problems.

Vian, J. and Moore, J. (1989). Trajectory optimization with risk minimization for military aircraft. *Journal of Guidance, Control and Dynamics*, 12(3):311–317.

Vidyasagar, M. (2002). *Nonlinear systems analysis*. Society for Industrial Mathematics.

Visioli, A. (2006). *Practical PID control*. Springer Verlag.

Walker, D. (2003). Multivariable control of the longitudinal and lateral dynamics of a fly-by-wire helicopter. *Control Engineering Practice*, 11(7):781–795.

Walker, D., Turner, M., Smerlas, A., Strange, M., and Gubbeis, A. (1999). Robust control of the longitudinal and lateral dynamics of the Bell 205 helicopter. In *Proceedings of the American Control Conference*, volume 4, pages 2742–2746. IEEE.

Wang, Y., Frank, P., and Wu, N. (1994). Near-optimal control of nonstandard singularly perturbed systems. *Automatica*, 30(2):277–292.

Weston, A., Cliff, E., and Kelley, H. (1983). Altitude transitions in energy climbs. *Automatica*, 19(2):199–202.

Wikipedia, the free encyclopedia (2010a). Servo control.

Wikipedia, the free encyclopedia (2010b). Servomechanism.

Winkelman, J., Chow, J., Allemong, J., and Kokotović, P. (1980). Multi-time-scale analysis of a power system. *Automatica*, 16(1):35–43.

Xin, M. and Balakrishnan, S. (2002). A new method for suboptimal control of a class of nonlinear systems. In *Decision and Control, 2002, Proceedings of the 41st IEEE Conference on*, volume 3, pages 2756–2761. IEEE.

Xin, M., Balakrishnan, S., Stansbery, D., and Ohlmeyer, E. (2004). Nonlinear missile autopilot design with $\theta - d$ technique. *Journal of guidance, control, and dynamics*, 27(3):406–417.

Xin, M. and S.N., B. (2008). Nonlinear H_∞ missile longitudinal autopilot design with $\theta - D$ method. volume 44, pages 41–56. IEEE.

Yeo, H., Bousman, W., and Johnson, W. (2004). Performance Analysis of a Utility Helicopter with Standard and Advanced Rotors. Technical report.

Young, C. (1978). A Note of the Velocity Induced by a Helicopter Rotor in the Vortex Ring State. Technical report, RAE Technical Report - 78125.

Zadeh, L. (1965). Fuzzy sets. *Information and control*, 8(3):338–353.

(Zephyris), R. W. (2005). Basic anatomy of a helicopter.

Appendix A

Proposed Test Bench Helicopter Axial Flight Models

A.1 Introduction

This Appendix is dedicated to described in detail the proposed test bench helicopter axial flight models that will be used to test the robustness of the proposed control laws. These models, similarly to the selected model, the moment theory with uniform inflow and hover flight condition model (MT_H), described in section A.3, are based on the combination of both the momentum theory (MT) and blade element theory (BE), with the peculiarity, that while the MT_H model is based in the hover condition, all three proposed models in this appendix, take into account the axial flight conditions of the helicopter, therefore being able to capture much more of the highly nonlinear dynamics that affects the generation of thrust/lift during the course of these maneuvers. Although the selected model imply a series of hypothesis, such that the inflow ratio along the blades is constant and equal to that of a hovering helicopter, therefore not taking into account the axial movement of the helicopter, it can be proven (Johnson, 1994) that for small enough axial velocities the simplification is valid and permits to have quite precise predictions of the rotor performance, as it will be seen in the robustness section. Both the momentum theory (MT), simplified to hovering flight, and the blade element theory (BE), for the general case, are described in detail in sections 2.6.1.1 and 2.6.2, respectively, and will not be rewritten again, but will be refereed throughout the rest of this Appendix. Prior to described the three proposed test bench helicopter axial flight models, it is necessary to extend the momentum theory analysis to the more general axial flight condition which is described in the following section

A.2 Momentum Theory Analysis in Axial Flight

Similarly as in the hover case, it is assumed that the flow through the rotor is one-dimensional, quasi-steady, incompressible and inviscid, with the only difference that in the axial flight regime, with a climb velocity different from zero, the relative velocity far upstream relative to the rotor is now given by V_c (Leishman, 2006). Therefore resulting this that in the plane of the rotor, the velocity is now defined by $V_c + v_i$, and the velocity far downstream, at station 2, is given by $V_c + w$ as seen in Figure A.1. By the conservation of mass, Eq. (2.174), the mass flow rate is constant within the boundaries of the wake, therefore

$$\dot{m} = \int_{\infty} \rho \mathbf{V} \cdot \mathrm{d}\mathbf{S} = \int_{2} \rho \mathbf{V} \cdot \mathrm{d}\mathbf{S}, \tag{A.1}$$

where d$\mathbf{S}$ is again the outward pointing normal from the control volume, and therefore resulting in

$$\dot{m} = \rho A_{\infty} (V_c + w) = \rho A (V_c + v_i), \tag{A.2}$$

and the application of the conservation of momentum (2.175) results in

$$T = \int_{\infty} \rho (\mathbf{V} \cdot \mathrm{d}\mathbf{S}) \mathbf{V} - \int_{0} \rho (\mathbf{V} \cdot \mathrm{d}\mathbf{S}) \mathbf{V}. \tag{A.3}$$

Assuming a steady climb flight condition, the velocity far upstream of the rotor is finite, so that both terms on the right-hand side of Eq. (A.3) are nonzero, while compared with the hover problem, in which the right hand side was zero. This results that for the climb case

$$T = \dot{m} (V_c + w) - \dot{m} V_c = \dot{m} w, \tag{A.4}$$

which is equivalent to the rotor thrust obtained in the hover flight condition (2.180). Since the work done by the climbing rotor in now given by $T(V_c + v_i)$ then

$$\begin{aligned} T (V_c + v_i) &= \int_{\infty} \rho (\mathbf{V} \cdot \mathrm{d}\mathbf{S}) \mathbf{V}^2 - \int_{0} \rho (\mathbf{V} \cdot \mathrm{d}\mathbf{S}) \mathbf{V}^2 \\ &= \frac{1}{2} \dot{m} (V_c + w)^2 - \frac{1}{2} \dot{m} V_c^2 = \frac{1}{2} \dot{m} w (2V_c + w). \end{aligned} \tag{A.5}$$

Using equations (A.4) and (A.5) it can be seen that, similarly as the hover case, $w = 2v_i$. Recalling that the relationship between the rotor thrust and the induced velocity at the rotor disk in hover was given in Eq. (2.186), and that can be used in (A.4) to prove that

$$T = \dot{m} w = \rho A (V_c + v_i) w = 2\rho A (V_c + v_i) v_i, \tag{A.6}$$

such that

$$\frac{T}{2\rho A} = v_h^2 = (V_c + v_i) v_i = V_c v_i + v_i^2, \tag{A.7}$$

where dividing (A.7) by v_h^2 results in

$$\left(\frac{v_i}{v_h}\right)^2 + \frac{V_c}{v_h}\frac{v_i}{v_h} - 1 = 0, \tag{A.8}$$

which is a quadratic form in (v_i/v_h) with the solution given by

$$\frac{v_i}{v_h} = -\frac{1}{2}\left(\frac{V_c}{v_h}\right) \pm \sqrt{\frac{1}{4}\left(\frac{V_c}{v_h}\right)^2 + 1}, \tag{A.9}$$

where the only valid solution in climb is the positive solution, therefore yielding

$$\frac{v_i}{v_h} = -\frac{1}{2}\left(\frac{V_c}{v_h}\right) + \sqrt{\frac{1}{4}\left(\frac{V_c}{v_h}\right)^2 + 1}, \tag{A.10}$$

which can be rewritten in terms off the induced velocity v_i by solving in (A.10) resulting

$$v_i = -\frac{V_c}{2} + \sqrt{\frac{V_c^2}{4} + v_h}, \tag{A.11}$$

where recall as seen in (A.7)

$$v_h = \sqrt{\frac{T}{2\rho A}}, \tag{A.12}$$

therefore rewriting Eq. (A.34) as

$$v_i = -\frac{V_c}{2} + \sqrt{\frac{V_c^2}{4} + \sqrt{\frac{T}{2\rho A}}}. \tag{A.13}$$

This implies that the induce velocity in climb flight decreases as the climb velocity increases, which is called the normal working state of the rotor, with the hover flight condition being the lower limit. However, taking a look at (A.9), as the rotor begins to descend there can be two possible flow directions, which violates the assumed flow model, so this solution is physically invalid, so the momentum theory can only be assumed valid for low rates of descent (Leishman, 2006). This implies that the climb flow model cannot be used in a descent with the descend velocity being more than twice the average induced velocity V_c, which corresponds with a flight condition in which the slipstream will be above the rotor. This implies that for cases where the descend velocity is in the range $-2v_h \leq V_c \leq 0$, the velocity at any plane through the rotor slipstream can be either upward or downward, which creates complicated recirculating flow patterns at the rotor and momentum theory cannot be used in this situation since no definitive control volume surrounding the rotor and its wake can be established (Glauert, 1935; Leishman, 2006). For the descending flight case, the control volume surrounding the descending rotor is given in Figure (A.2)

Therefore, with this in mind, in order to determine the proper relationships for the descend flight, let assume that $|V_c| > 2v_h$ so that a well-defined slipstream will always exists above the rotor and encompassing the rotor disk. Far upstream (well bellow) the rotor, the magnitude of the velocity is the descend velocity, which is equal to $|V_c|$, therefore at the plane of the rotor, the velocity is $|V_c| - v_i$, and in the far wake (above the rotor), the velocity is $|V_c| - w$. Recalling the conservation of mass (2.174), the fluid mass flow rate through the rotor disk for the descend flight conditions given by

$$\dot{m} = \int_\infty \rho \mathbf{V} \cdot \mathrm{d}\mathbf{S} = \int_2 \rho \mathbf{V} \cdot \mathrm{d}\mathbf{S}, \tag{A.14}$$

and where similarly as for the climb case

$$\dot{m} = \rho A_\infty \left(V_c + w\right) = \rho A \left(V_c + v_i\right), \tag{A.15}$$

and similarly, the application of the conservation of momentum (2.175) results in

$$T = -\left[\int_\infty \rho \left(\mathbf{V} \cdot \mathrm{d}\mathbf{S}\right) \mathbf{V} - \int_0 \left(\rho \mathbf{V} \cdot \mathrm{d}\mathbf{S}\right) \mathbf{V}\right], \tag{A.16}$$

where it can be see that the difference with the climb case (A.3) is just the sign, which arises since the flow direction is now reversed. Assuming a steady descent, the velocity far upstream of the rotor must be finite so both terms on the right hand-side of (A.16) are non-zero and given by

$$T = \left(-\dot{m}\right)\left(V_c + w\right) - (-\dot{m})V_c = -\dot{m}w, \tag{A.17}$$

and since the work done by the rotor in the descent flight condition is now given by $T(V_c + v_i)$ then

$$\begin{aligned} T\left(V_c + v_i\right) &= \int_\infty \rho \left(\mathbf{V} \cdot \mathrm{d}\mathbf{S}\right) \mathbf{V}^2 - \int_0 \rho \left(\mathbf{V} \cdot \mathrm{d}\mathbf{S}\right) \mathbf{V}^2 \\ &= \frac{1}{2}\dot{m}V_c^2 - \frac{1}{2}\dot{m}\left(V_c + w\right)^2 = -\frac{1}{2}\dot{m}w\left(2V_c + w\right), \end{aligned} \tag{A.18}$$

which is a negative quantity, which implies that the rotor is extracting power from the airstream. Using equations (A.16) and (A.17) it can be seen again that similarly as in the hover case, and the climb case, $w = 2v_i$, with the difference that the net velocity in the slipstream is less than $|V_c|$, and from continuity considerations the wake boundary expands above the descending rotor disk. Recalling that the relationship between the rotor thrust and the induced velocity at the rotor disk in hover was derived in Eq. (2.186), and using (A.17) it can be shown that

$$T = -\dot{m}w = -\rho A \left(V_c + v_i\right) w = -2\rho A \left(V_c + v_i\right) v_i, \tag{A.19}$$

such that

$$\frac{T}{2\rho A} = v_h^2 = -\left(V_c + v_i\right) v_i = -V_c v_i - v_i^2, \tag{A.20}$$

where dividing (A.7) by v_h^2 results in

$$\left(\frac{v_i}{v_h}\right)^2 + \frac{V_c}{v_h}\frac{v_i}{v_h} + 1 = 0, \tag{A.21}$$

which is a quadratic form in (v_i/v_h) with the solution given by

$$\frac{v_i}{v_h} = -\frac{1}{2}\left(\frac{V_c}{v_h}\right) \pm \sqrt{\frac{1}{4}\left(\frac{V_c}{v_h}\right)^2 - 1}, \tag{A.22}$$

similarly as in the climb case (A.9) there are two solutions, and it can be seen that one of the solution produces values of $v_i/v_h > 1$ which violates the assumed flow in this case, therefore the only valid solution is given by

$$\frac{v_i}{v_h} = -\frac{1}{2}\left(\frac{V_c}{v_h}\right) - \sqrt{\frac{1}{4}\left(\frac{V_c}{v_h}\right)^2 - 1}, \tag{A.23}$$

which is valid only for the region $V_c/v_h \leq -2$. Similarly as in the ascend flight condition, Eq. (A.23) can be rewritten in terms off the induced velocity v_i resulting in

$$v_i = -\frac{V_c}{2} - \sqrt{\frac{V_c^2}{4} - v_h}, \tag{A.24}$$

where recall as seen in (A.7)

$$v_h = \sqrt{\frac{T}{2\rho A}}, \tag{A.25}$$

therefore rewriting Eq. (A.36) as

$$v_i = -\frac{V_c}{2} - \sqrt{\frac{V_c^2}{4} - \sqrt{\frac{T}{2\rho A}}}. \tag{A.26}$$

Expression (A.47) corresponds to the so called wind-mill region (Leishman, 2006). In the region $-2 \leq V_c/v_h \leq 0$ momentum theory is strictly speaking invalid because the flow can take two possible directions and a well-defined slipstream ceases to exist, which implies that a control volume cannot be defined that encompasses only the physical limits of the rotor disk. However, the velocity curve can still be defined empirically on the basis of flight test or other experiments with rotors, that can be used to find the best-fit approximation for v_i at any given descent rate. Following Young (Young, 1978) one approximation is given by

$$\frac{v_i}{v_h} = \kappa + k_1\left(\frac{V_c}{v_h}\right) + k_2\left(\frac{V_c}{v_h}\right)^2 + k_3\left(\frac{V_c}{v_h}\right)^3 + k_4\left(\frac{V_c}{v_h}\right)^4, \tag{A.27}$$

with κ being the measured induced power factor in hover, which is a coefficient derived from rotor measurements or flight test and includes a number of noideal, but physical effects that are out of the scope of this thesis. Also let

$$k_1 = -1.125, \tag{A.28}$$

$$k_2 = -1.372, \tag{A.29}$$

$$k_3 = -1.718, \tag{A.30}$$

$$k_4 = -0.655, \tag{A.31}$$

which is valid of the full range $-2 \leq V_c/v_h \leq 0$. This last model completes the full range of axial flight. Although as a control design, and due to the nature of the predesign maneuvers for the *RC* helicopter used in this thesis, the velocities in axial descend flight will never reach the values of $V_c/v_h \leq -2$, it is important to introduce this distinction for future considerations. This concludes the momentum theory for the axial flight, and although the momentum theory provides some good insights into how the helicopter hovers, it does not provide a physical explanation at how the collective pitch and rotational speed affect the developed thrust. This insight view, will be provided in the blade-element-theory formulation.

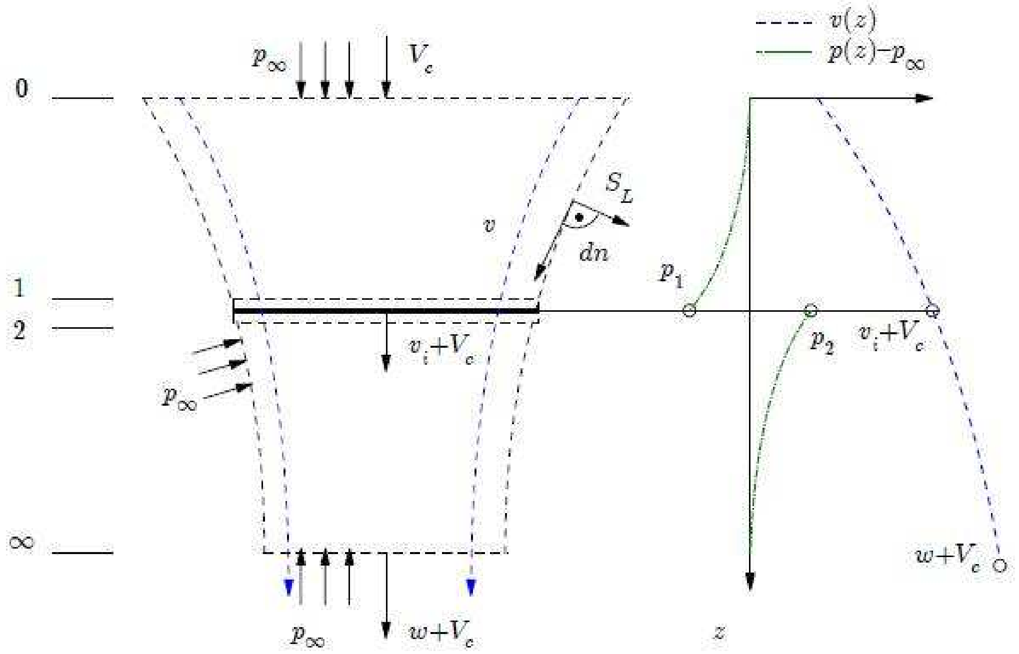

Figure A.1: Flow model for momentum theory analysis of a rotor in axial climbing flight (Leishman, 2006; Cuerva et al., 2009).

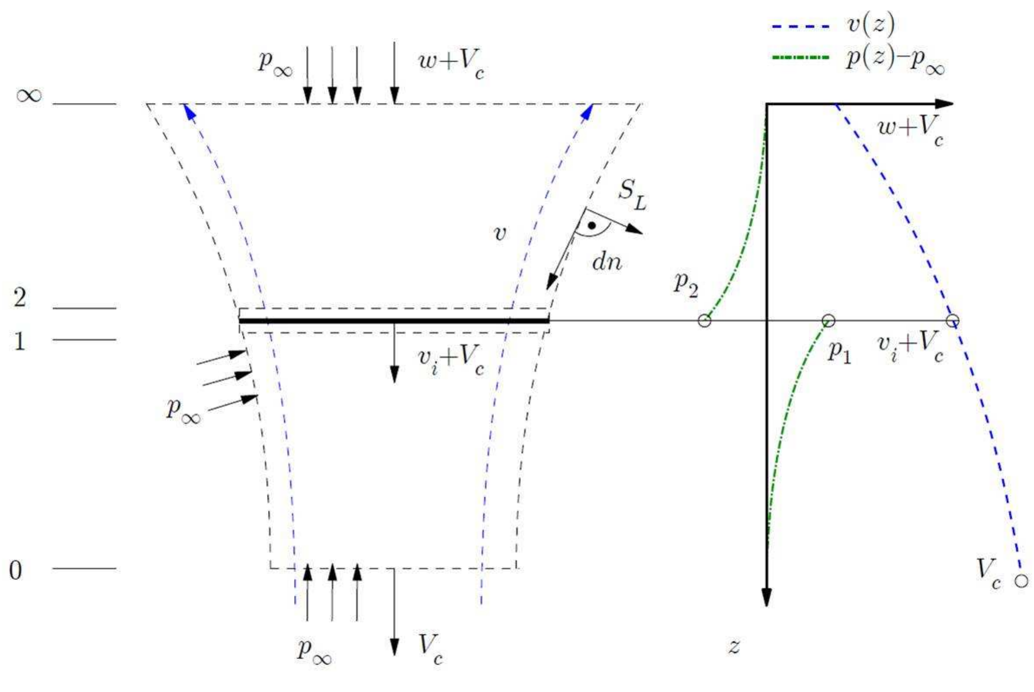

Figure A.2: Flow model for momentum theory analysis of a rotor in axial descend flight (Leishman, 2006; Cuerva et al., 2009).

A.3 Proposed Closed-Form Solutions for the Thrust Coefficient Model C_T

As seen previously in chapter 2, the momentum theory provided some good insight into how the helicopter hovers by providing definitions for the inflow ratio depending on the flight condition, while blade element theory provide physical explanations at how the collective pitch and rotational speed affect the developed thrust, but lack to provided closed-form solutions since the integral form (2.239) depends on the inflow angle. Therefore being necessary to combine both theories in order to obtain closed-form solutions of the thrust coefficient which could be used in the proposed axial flight dynamic model for this thesis. This appendix collects some of the proposed closed-form solutions in the literature (Leishman, 2006) for the thrust coefficient C_T which depends on the flight condition that it is assumed, the type of blade, and the assumed flow distribution along the blade of the rotor. These models will be denoted, following the standard literature nomenclature, and are given by:

- Moment theory for uniform inflow in hover flight condition - MT_H
- Moment theory for uniform inflow in axial flight condition - MT_C
- Combined blade element theory and momentum theory - $BEMT$.
- Combined blade element theory and momentum theory with Prandtl's Tip-Loss Model - $BEMT_{TL}$.

The first proposed model, the MT_H model, has been previously presented in chapter 2, and is the selected C_T model to be implemented in the helicopter dynamics presented in this thesis. As previously mentioned, although the model implies a series of hypothesis, it can be proven (Johnson, 1994; Leishman, 2006) that for maneuvers in which the climb and descent velocities are low enough, the MT_H is a really good approximation without any loss of generality, as it will be proven in the simulations. Also, and most important, the first model is the only closed-form continuous model of the four proposed models, therefore, becoming a good candidate, if not the only candidate, that can be used for a control strategy of the continuous type.

Although there are much more precise, and also much more complex thrust coefficient models in the literature (Cuerva et al., 2006a; Cuerva et al., 2006b; Theodore, 2000), the author has chosen the MT_C, $BEMT$ and the $BEMT_{TL}$ models as significate models that are both, much more complex than the selected thrust model MT_H, but are also easily implemented in the simulation platform defined by the author. These "alternative" models will serve as great test-bench problems where to test the robustness of the proposed control strategies under model uncertainties. The first of the proposed models, the MT_H, has been previously defined in detail in section 2.8, therefore, only the following three models, MT_C, $BEMT$, and $BEMT_{TL}$, respectively, will be described in detail in the following sections.

A.3.1 Moment Theory with Uniform Inflow in Axial Flight Model - MT_C

In order to obtain the closed-form blade element and moment theory for uniform inflow let recall the integral form of the thrust coefficient obtained in the BET analysis, and given by Eq. (2.239) as

$$C_T = \frac{1}{2}\sigma C_{l_\alpha} \int_0^1 (\theta_c r^2 - \lambda r)\mathrm{d}r. \tag{A.32}$$

Let also recall that in the MT_H proposed model, it was assumed that the helicopter was at the hover flight condition, thus reducing the inflow ratio, $\lambda = \sqrt{C_T}/2$. This assumption, although valid for small axial velocities near the hover condition (Johnson, 1994; Leishman, 2006) only uses the momentum theory derived in the hover flight condition, and it is necessary to include the derivations obtained in section

A.2 for the axial flight conditions. Recall that similarly as in the MT_H, to obtain the MT_C model, it is assumed that inflow ratio is uniform, and thus the thrust coefficient Eq. (2.239) can be rewritten as

$$\begin{aligned} C_T &= \frac{1}{2}\sigma C_{l_\alpha}\int_0^1 (\theta_c r^2 - \lambda r)\mathrm{dr} = \frac{1}{2}\sigma C_{l_\alpha}\left[\frac{\theta_0 r^3}{3} - \frac{\lambda r^2}{2}\right]_0^1 \\ &= \frac{1}{2}\sigma C_{l_\alpha}\left[\frac{\theta_0}{3} - \frac{\lambda}{2}\right]. \end{aligned} \tag{A.33}$$

The main difference between the MT_H and the MT_C models is the model of inflow ratio which is given depending on the flight condition for the MT_C, (i.e. $\lambda_{climb} \neq \lambda_{descent}$ for climb or descent flight). Following the results obtained in section A.2, for axial climb it was defined by Eq. (A.10) as

$$\frac{v_i}{v_h} = -\frac{1}{2}\left(\frac{V_c}{v_h}\right) + \sqrt{\frac{1}{4}\left(\frac{V_c}{v_h}\right)^2 + 1}, \tag{A.34}$$

while for the axial flight descent region given by $-2 \leq V_c/v_h \leq 0$, the inflow ratio was given by Eq. (A.27) as

$$\frac{v_i}{v_h} = \kappa + k_1\left(\frac{V_c}{v_h}\right) + k_2\left(\frac{V_c}{v_h}\right)^2 + k_3\left(\frac{V_c}{v_h}\right)^3 + k_4\left(\frac{V_c}{v_h}\right)^4, \tag{A.35}$$

and finally, for the wind mill axial descent region given by $|V_c| > 2v_h$ is given by Eq. (A.23) as

$$\frac{v_i}{v_h} = -\frac{1}{2}\left(\frac{V_c}{v_h}\right) - \sqrt{\frac{1}{4}\left(\frac{V_c}{v_h}\right)^2 - 1}. \tag{A.36}$$

From the definitions for the inflow velocities for the three different axial flight regimes, the thrust coefficient C_T can be defined by recalling that the inflow ratio is given by

$$\lambda = \frac{V_c + v_i}{\Omega R}, \tag{A.37}$$

then Eq. (2.248) can be rewritten as

$$C_T = \frac{1}{2}\sigma C_{l_\alpha}\left[\frac{\theta_0}{3} - \frac{\lambda}{2}\right] = \frac{1}{2}\sigma C_{l_\alpha}\left[\frac{\theta_0}{3} - \frac{V_c}{2\Omega R} - \frac{v_i}{2\Omega R}\right], \tag{A.38}$$

with the induced velocity given by the expression for the different axial flight regimes. For the axial flight climb condition, recall that the induced velocity is given by (A.13) as

$$v_i = -\frac{V_c}{2} + \sqrt{\frac{V_c^2}{4} + \sqrt{\frac{T}{2\rho A}}}, \tag{A.39}$$

therefore substituting (A.39) into (A.38) results in

$$C_T = \frac{1}{2}\sigma C_{l_\alpha}\left[\frac{\theta_0}{3} - \frac{V_c}{2\Omega R} - \frac{1}{2\Omega R}\left(-\frac{V_c}{2} + \sqrt{\frac{V_c^2}{4} + \sqrt{\frac{T}{2\rho A}}}\right)\right], \tag{A.40}$$

where recall that the derived thrust coefficient in (A.40) is a function of the thrust force T, and this in due to the fact that it is necessary to ensure that induced velocity of the helicopter, v_h, equals to the amount of thrust at each instant, which is given by (2.189) as

$$C_T = \frac{T}{\rho A \Omega^2 R^2}. \tag{A.41}$$

Equating both (A.38) and (A.41) results in

$$\frac{T}{\rho A \Omega^2 R^2} = \frac{1}{2}\sigma C_{l_\alpha}\left[\frac{\theta_0}{3} - \frac{V_c}{2\Omega R} - \frac{1}{2\Omega R}\left(-\frac{V_c}{2} + \sqrt{\frac{V_c^2}{4} + \sqrt{\frac{T}{2\rho A}}}\right)\right], \tag{A.42}$$

which results in a function of T, that can be solved for an empirical function in T, and given as

$$T_{MT_C} = -\frac{\rho A \sigma C_{L_\alpha} R\Omega\left(-3\sigma C_{L_\alpha} R\Omega \pm \mathcal{T}_1 - 32R\theta_c\Omega + 24V_c\right)}{192}, \tag{A.43}$$

with $\mathcal{T}_1$ given by

$$\mathcal{T}_1 = \sqrt{\left(3\sigma C_{L_\alpha}\Omega R\right)^2 + \left(24V_c\right)^2 + \sigma C_{L_\alpha}\Omega R\left(192\Omega R\theta_c - 144V_c\right)}, \tag{A.44}$$

where it can be seen that (A.43) has two possible solutions and the solution for positive T is the selected, which corresponds to

$$T_{MT_C} = -\frac{\rho A \sigma C_{L_\alpha} R\Omega\left(-3\sigma C_{L_\alpha} R\Omega + \mathcal{T}_1 - 32R\theta_c\Omega + 24V_c\right)}{192}. \tag{A.45}$$

Since for implementation purposes it is desirable to have an expression for the thrust coefficient C_T, it can be obtained by using the formal definition of C_T, Eq. (A.41) such

$$C_{T_{MT_C}} = -\frac{\rho A \sigma C_{L_\alpha} R\Omega\left(-3\sigma C_{L_\alpha} R\Omega + \mathcal{T}_1 - 32R\theta_c\Omega + 24V_c\right)}{192\rho A\Omega^2 R^2}. \tag{A.46}$$

For the axial flight descent regimes recall that two distinct flight regimes were defined: the region given by $-2 \leq V_c/v_h \leq 0$, and the wind mill state in which the descent flight condition is given by $|V_c| > 2v_h$. Let first obtain the thrust coefficient for the second descent region, the wind mill state region with $|V_c| > 2v_h$. In a similar manner as for the case of the ascend velocity, but replacing (A.47) with

$$v_i = -\frac{V_c}{2} - \sqrt{\frac{V_c^2}{4} - \sqrt{\frac{T}{2\rho A}}}, \tag{A.47}$$

and conducting the same analysis results in that the thrust coefficient in the wind-mill state is given by

$$T_{MT_{WM}} = -\frac{\rho A \sigma C_{L_\alpha} R\Omega\left(3\sigma C_{L_\alpha} R\Omega - \mathcal{T}_2 - 32R\theta_c\Omega + 24V_c\right)}{192}, \tag{A.48}$$

with $\mathcal{T}_2$ given by

$$\mathcal{T}_2 = \sqrt{\left(3\sigma C_{L_\alpha}\Omega R\right)^2 + \left(24V_c\right)^2 - \sigma C_{L_\alpha}\Omega R\left(192\Omega R\theta_c + 144V_c\right)}, \tag{A.49}$$

where it can be seen that (A.49) has two possible solutions, and the solution selected is the solution that satisfies the wind mill state conditions. Again, since for implementation purposes it is desirable to have an expression for the thrust coefficient C_T, it can be obtained by using the formal definition of C_T, Eq. (A.41) such

$$C_{T_{MT_{WM}}} = -\frac{\rho A \sigma C_{L_\alpha} R\Omega\left(3\sigma C_{L_\alpha} R\Omega - \mathcal{T}_2 - 32R\theta_c\Omega + 24V_c\right)}{192\rho A\Omega^2 R^2}. \tag{A.50}$$

Finally, to obtain the thrust coefficient for the descent region $-2 \leq V_c/v_h \leq 0$ let recall that the induced velocity as given in Eq. (A.27) is defined as

$$\begin{aligned} v_i &= v_h\left[\kappa + k_1\left(\frac{V_c}{v_h}\right) + k_2\left(\frac{V_c}{v_h}\right)^2 + k_3\left(\frac{V_c}{v_h}\right)^3 + k_4\left(\frac{V_c}{v_h}\right)^4\right] \\ &= v_h\kappa + k_1 V_c + k_2\frac{V_c^2}{v_h} + k_3\frac{V_c^3}{v_h^2} + k_4\frac{V_c^4}{v_h^3}, \end{aligned} \tag{A.51}$$

where recall that from Eq. (A.7) that

$$v_h = \sqrt{\frac{T}{2\rho A}}. \tag{A.52}$$

In a similar manner as the two previous flight conditions, Eq. (A.51) is substituted into Eq. (A.38) resulting in

$$C_T = \frac{1}{2}\sigma C_{l_\alpha}\left[\frac{\theta_0}{3} - \frac{V_c + \left(v_h\kappa + k_1 V_c + k_2\frac{V_c^2}{v_h} + k_3\frac{V_c^3}{v_h^2} + k_4\frac{V_c^4}{v_h^3}\right)}{2\Omega R}\right], \tag{A.53}$$

therefore, and similar as for the previous axial flight conditions, equating both Eqns. (2.189) and (A.53), results in

$$\frac{T}{\rho A\Omega^2 R^2} = \frac{1}{2}\sigma C_{l_\alpha}\left[\frac{\theta_0}{3} - \frac{V_c + \left(v_h\kappa + k_1 V_c + k_2\frac{V_c^2}{v_h} + k_3\frac{V_c^3}{v_h^2} + k_4\frac{V_c^4}{v_h^3}\right)}{2\Omega R}\right], \tag{A.54}$$

this resulting in an implicit function in T which has to be solved using numerical methods, and once obtained the thrust force, it can be expressed in the normalized form of the C_T using

$$C_{T_{MT_D}} = \frac{T_{MT_D}}{\rho A\Omega^2 R^2}, \tag{A.55}$$

with T_{MT_D} being the thrust force obtained from solving numerically (A.54). This results in the three thrust coefficients for the three axial flight conditions and resumed as

$$C_{T_{MT_C}} = -\frac{\rho A\sigma C_{L_\alpha} R\Omega\left(-3\sigma C_{L_\alpha} R\Omega + \mathcal{T}_1 - 32R\theta_c\Omega + 24V_c\right)}{192\rho A\Omega^2 R^2}, \tag{A.56}$$

$$C_{T_{MT_D}} = \frac{T_{MT_D}}{\rho A\Omega^2 R^2}, \tag{A.57}$$

$$C_{T_{MT_{WM}}} = -\frac{\rho A\sigma C_{L_\alpha} R\Omega\left(3\sigma C_{L_\alpha} R\Omega - \mathcal{T}_2 - 32R\theta_c\Omega + 24V_c\right)}{192\rho A\Omega^2 R^2}, \tag{A.58}$$

where

$$V_c/v_h \geq 0 \rightarrow C_{T_{MT_C}}, \tag{A.59}$$

$$-2 \leq V_c/v_h \leq 0 \rightarrow C_{T_{MT_D}}, \tag{A.60}$$

$$-2 \geq V_c/v_h \rightarrow C_{T_{MT_{WM}}}. \tag{A.61}$$

Recall that both MT_H and MT_C are required to integrate (2.239) along the entire blade to obtain a relationship of C_T as a function of the collective pitch angle θ_c, and the only difference is the selected inflow ratio. Due to the non-dependance of the integral form in the inflow ratio (i.e. the inflow ratio is uniform, λ = constant), the integral dC_T can be solved resulting in (2.248) which is a explicit function of the collective pitch angle θ_c and the inflow angle. While for the hover flight condition the inflow angle is a function of C_T (2.198), resulting in a continuous closed-form solution for the thrust coefficient, in the axial flight condition, the proposed model for MT_C has nonlinearities depending on the nature of the climb flight region, and therefore making impossible to integrate into a set of continuous differential equations. Since for the proposed methodology in this thesis it is desired that the control laws have to be continuous and differentiable throughout all the range, this model will be only used as a test bench model to test the validity of the selected model, and to test the robustness of the proposed control laws under model uncertainties.

A.3.2 Combined Blade Element Theory and Momentum Theory ($BEMT$)

The blade element momentum theory ($BEMT$) presented in this section is a hybrid method for hovering rotors (Gessow and Gustafson, 1945; Gessow and Center, 1948) that combines the basic principles from both the blade element and momentum theory approaches. The principles involve the invocation of the equivalence between the circulation and momentum theories of lift. With certain assumptions, the $BEMT$ allows the inflow distribution along the blade to be estimated. See (Leishman, 2006) for more references.

Consider first the application of the conservation laws to an annulus of the rotor disk, as shown in Figure (A.3) which is the essence essence of Froude's original differential theory for propellers in axial motion. This annulus is at a distance y from the rotational axis, and has a width dy. The area of this annulus is, therefore, $dA = 2\pi y dy$. The incremental thrust, dT , on this annulus may be calculated on the basis of simple momentum theory and with the 2-D assumption that successive rotor annuli have no mutual effects on each other, although this has good validity except near the blade tips.

Using the same one-dimensional momentum theory developed in section 2.6.1.1,the incremental thrust on the rotor annulus, is obtained as the product of the mass flow rate through the annulus and twice the induced velocity at that section, thus becoming the mass flow rate over the annulus of the disk given by

$$d\dot{m} = \rho dA\left(V_c + v_i\right) = 2\pi\rho\left(V_c + v_i\right) y dy, \tag{A.62}$$

such that the incremental thrust on the annulus is given by

$$dT = 2\rho\left(V_c + v_i\right) v_i dA = 4\pi\rho\left(V_c + v_i\right) v_i y dy. \tag{A.63}$$

which is also known as the Froude-Finsterwalder equation. Since it is more convenient to work with the nondimensional form Eq. (A.63) let rewrite

$$\begin{aligned} \mathrm{dC_T} &= \frac{dT}{\rho(\pi R^2)(\Omega R)^2} = \frac{2\rho\left(V_c + v_i\right) v_i dA}{\rho(\pi R^2)(\Omega R)^2} \\ &= \frac{2\rho\left(V_c + v_i\right) v_i (2\pi y dy)}{\rho\pi R^2(\Omega R)^2} = 4\frac{\left(V_c + v_i\right)}{\Omega R}\left(\frac{v_i}{\Omega R}\right)\left(\frac{y}{R}\right) d\left(\frac{y}{R}\right), \end{aligned} \tag{A.64}$$

which can be simplified to

$$\mathrm{dC_T} = 4\lambda\lambda_i r \mathrm{dr}, \tag{A.65}$$

Therefore, the incremental thrust coefficient on the annulus can be written as

$$\mathrm{dC_T} = 4\lambda\lambda_i r\mathrm{dr} = 4\lambda(\lambda - \lambda_c) r\mathrm{dr}, \tag{A.66}$$

since it can be shown that $\lambda_i = \lambda - \lambda_c$. With the integral thrust coefficient obtained for the blade element theory (A.66), the challenge is to devise an approach that can solve for the inflow directly, without making any assumptions as to its magnitude and form. It is clear that if the inflow can be determined, considerably information about the rotor performance can be obtained. One solution can be obtained using a hybrid blade element and momentum approach using the principles of the equivalence between the circulation theory of lift and the momentum theory of lift, which provides the so called radial inflow equation (Gessow and Gustafson, 1945; Gessow and Center, 1948; Leishman, 2006). Recall that from BET analysis it was proven that the incremental thrust produced on an annulus of the disk is given by

$$\mathrm{dC_T} = \frac{1}{2}\sigma C_l r^2 \mathrm{dr} = \frac{\sigma C_{l_\alpha}}{2}\left(\theta_c r^2 - \lambda r\right), \mathrm{dr} \tag{A.67}$$

where equating the incremental thrust coefficients from the momentum and blade element theories, that is using Eqns. (A.66) and (A.67), respectively, it can be shown that

$$\frac{\sigma C_{l_\alpha}}{2}\left(\theta_c r^2 - \lambda r\right) = 4\lambda(\lambda - \lambda_c) r \mathrm{d}r, \tag{A.68}$$

which gives

$$\frac{\sigma C_{l_\alpha}}{8}\theta_c r - \frac{\sigma C_{l_\alpha}}{8}\lambda = \lambda^2 - \lambda_c \lambda, \tag{A.69}$$

which can also be rewritten as

$$\lambda^2 + \left(\frac{\sigma C_{l_\alpha}}{8} - \lambda_c\right)\lambda - \frac{\sigma C_{l_\alpha}}{8}\theta_c r = 0, \tag{A.70}$$

which is a quadratic equation in λ and can be solved as

$$\lambda(r, \lambda_c) = \sqrt{\left(\frac{\sigma C_{l_\alpha}}{16} - \frac{\lambda_c}{2}\right)^2 + \frac{\sigma C_{l_\alpha}}{8}\theta_c r} - \left(\frac{\sigma C_{l_\alpha}}{16} - \frac{\lambda_c}{2}\right). \tag{A.71}$$

For the particular case in which the hover flight condition is considered, ($\lambda_c = 0$), Eq. (A.71) simplifies to

$$\lambda(r) \equiv \lambda_i(r) = \frac{\sigma C_{l_\alpha}}{16}\left(\sqrt{1 + \frac{32}{\sigma C_{l_\alpha}}\theta_c r} - 1\right). \tag{A.72}$$

Equations (A.71) and (A.72) allow for a solution of the inflow as a function of radius for any given blade pitch, blade twist distribution, planform (chord distribution), and airfoil section (through the effect of lift-curve-slope C_{l_α} and zero-lift angle α_0 via θ_c). Once the inflow is obtained, the rotor thrust can be found by integrating across the rotor disk using Eq. (A.67). This model requires of numerical integration at each instant in order to obtain the thrust coefficient, and again, it will be only used as a test bench model to test the validity of the selected model, and to test the robustness of the proposed control laws under model uncertainties. It is important to note that the validity of this model only applies the axial ascent flight condition, although it has been proven (Johnson, 1994; Leishman, 2006), that it is also valid for moderate small descent velocities, while for higher descent velocities, the only available model is the one presented for the MT_C. Therefore, while for the flight condition given by the region $V_c/v_h \geq 0$ it will used the numerical integration method that uses Eq. (A.71) and (A.67), for the descent flight conditions it will be used the descent flight condition model presented on the MT_C model, in which the thrust coefficient is given in the two defined descent given by regions

$$-2 \leq V_c/v_h \leq 0 \quad \rightarrow \quad C_{T_{MT_D}}, \tag{A.73}$$

$$-2 \geq V_c/v_h \quad \rightarrow \quad C_{T_{MT_{WM}}}. \tag{A.74}$$

with

$$C_{T_{MT_D}} = \frac{T_{MT_D}}{\rho A \Omega^2 R^2}, \tag{A.75}$$

$$C_{T_{MT_{WM}}} = -\frac{\rho A \sigma C_{L_\alpha} R\Omega\left(3\sigma C_{L_\alpha} R\Omega - \mathcal{T}_2 - 32 R\theta_c \Omega + 24 V_c\right)}{192 \rho A \Omega^2 R^2}. \tag{A.76}$$

This will introduce a discontinuity when changing from the ascent to the descent flight condition, or viceversa, creating instantaneous changes in the thrust coefficient when reaching the discontinuity. As it will be seen in the simulations this will create an inconsistency in the behaviour of the helicopter, and it will be address both in the comparison of the proposed models, and in the simulations to test the robustness of the proposed control laws. In the first one, the comparison of the proposed models, it will be shown that as predicted (Johnson, 1994; Leishman, 2006), due to the slow descent velocities encountered by the helicopter's maneuvers, the use of the $BEMT$ model for both the ascent and the descent flight conditions gives good results. In the second one, the testing for the robustness of the derived control laws in the different proposed models, the discontinuity of the model will cause the helicopter to react in a inconsistent manner when reaching the hover flight condition. This behaviour can be eliminated by using the $BEMT$ model in ascent flight for the descent flight conditions also. This will represent a challenge when testing the robustness of the proposed control laws, since not only there will be unmodeled dynamics, but discontinuous models that the selected control laws and the proposed extra control laws will have to deal with. As it will be seen in the robustness analysis in section 7, the extra control signal will perform great even with the non-continuous $BEMT$ model for different flight conditions.

A.3.3 Combined Blade Element Theory and Momentum Theory with Prandtl's Tip-Loss Model ($BEMT_{TL}$)

The last proposed mode, is a modification of the combined blade element and momentum theory ($BEMT$) with the addition of the Prandtl's Tip-Loss function. See (Leishman, 2006; López and Valenzuela, 2010) for more references. Instead of assuming a value for the tip-loss factor as selected in section A.2, using a method proposed by Prandtl (Betz, 1919), the tip-loss effects can be computed by taking into account the induced effects associated with finite number of blades.

Without getting into details, see (Betz, 1919; Goldstein, 1929; Lock,) for more detail, Prandtl's final result can be expressed in terms of a correction factor given by

$$F(r) = \left(\frac{2}{\pi}\right) \cos^{-1}\left(exp(-f)\right), \tag{A.77}$$

where f is given in terms of the number of blades and the radial position of the blade element, r by

$$f = \frac{N_b}{2}\left(\frac{1-r}{r\phi_i}\right), \tag{A.78}$$

and where ϕ_i is the inflow angle, where recall that it is defined as

$$\phi_i = \frac{\lambda r}{r}, \tag{A.79}$$

therefore resulting in

$$f(r, \lambda(r)) = \frac{N_b}{2}\left[\frac{1-r}{\lambda(r)}\right], \tag{A.80}$$

thus rewriting Eq. (A.77) as

$$F(r, \lambda(r)) = \left(\frac{2}{\pi}\right) \cos^{-1}\left[exp\left(-\frac{N_b}{2}\left(\frac{1-r}{\lambda(r)}\right)\right)\right]. \tag{A.81}$$

The basic effect of the $F(r, \lambda(r))$ function is to increase the induced velocity over the tip region and reduce the amount of lift generated at the tip. The application of the Prandtl's tip-loss method can be incorporated into the $BEMT$ proposed model by in a similar methodology as the presented for the $BEMT$, let consider the integral thrust coefficient for the blade element and the momentum theory (A.67) and (A.66) respectively, and given by

$$\mathrm{dC_T} = \frac{1}{2}\sigma C_l r^2 \mathrm{dr} = \frac{\sigma C_{l_\alpha}}{2}\left(\theta_c r^2 - \lambda r\right) \mathrm{dr}, \tag{A.82}$$

and let

$$\mathrm{dC_T} = 4\lambda\lambda_i r \mathrm{dr} = 4F(r, \lambda(r))\lambda(\lambda - \lambda_c) r \mathrm{dr}, \tag{A.83}$$

where it can be seen that the main difference is that the incremental thrust coefficients for the momentum theory includes Prandt's Tip-Loss function $F(r, \lambda(r))$, therefore by equating both (A.83) and (A.82) results in

$$\frac{\sigma C_{l_\alpha}}{2}\left(\theta_c r^2 - \lambda r\right) = 4F(r,\lambda(r))\lambda(\lambda-\lambda_c)r\mathrm{d}r, \tag{A.84}$$

which gives

$$\lambda^2 + \left(\frac{\sigma C_{l_\alpha}}{8F(r,\lambda(r))} - \lambda_c\right)\lambda - \frac{\sigma C_{l_\alpha}}{8F(r,\lambda(r))}\theta_c r = 0, \tag{A.85}$$

which is a quadratic equation in $\lambda(r)$ and can be solved as

$$\lambda(r) = \sqrt{\left(\frac{\sigma C_{l_\alpha}}{16F(r,\lambda(r))} - \frac{\lambda_c}{2}\right)^2 + \frac{\sigma C_{l_\alpha}}{8F(r,\lambda(r))}\theta_c r} - \left(\frac{\sigma C_{l_\alpha}}{16F(r,\lambda(r))} - \frac{\lambda_c}{2}\right), \tag{A.86}$$

and where for the particular case in which the hover flight condition is considered, thus $\lambda_c = 0$, Eq. (A.86) simplifies to

$$\lambda(r) \equiv \lambda_i(r) = \frac{\sigma C_{l_\alpha}}{16F(r,\lambda(r))}\left(\sqrt{1+\frac{32F(r,\lambda(r))}{\sigma C_{l_\alpha}}\theta_c r} - 1\right), \tag{A.87}$$

where it can be seen that since (A.87) is an implicit function, that is $\lambda(r) = f(F(r,\lambda(r)), r)$, is required to be solved by using an iterative method. The net result of the application of Prandtl's Tip-Loss function on the blade thrust distribution is a reduction of the thrust generated over the immediate tip region. Once the corrected inflow is obtained, the rotor thrust can be found by integrating across the rotor disk using Eq. (A.82). This model requires also of numerical integration at each instant in order to obtain the thrust coefficient, and again, it will be only used as a test bench model to test the validity of the selected model, and to test the robustness of the proposed control laws under model uncertainties.

In a similar manner as for the $BEMT$ model, the validity of this model only applies the axial ascent flight condition, although it has also been proven that it is also valid for moderate descent velocities (Johnson, 1994; Leishman, 2006). Therefore, while for the flight condition given by the region $V_c/v_h \geq 0$ it will used the numerical integration method that uses Eq. (A.86) and (A.82), for the descent flight conditions it will be used the descent flight condition model presented on the MT_C model, in which the thrust coefficient is given in the two defined descent regions given by

$$-2 \leq V_c/v_h \leq 0 \quad \rightarrow \quad C_{T_{MT_D}}, \tag{A.88}$$

$$-2 \geq V_c/v_h \quad \rightarrow \quad C_{T_{MT_{WM}}}, \tag{A.89}$$

that is

$$C_{T_{MT_D}} = \frac{T_{MT_D}}{\rho A \Omega^2 R^2}, \tag{A.90}$$

$$C_{T_{MT_{WM}}} = -\frac{\rho A \sigma C_{L_\alpha} R\Omega \left(3\sigma C_{L_\alpha} R\Omega - \mathcal{T}_2 - 32R\theta_c\Omega + 24V_c\right)}{192\rho A \Omega^2 R^2}. \tag{A.91}$$

This will introduce a discontinuity when changing from the ascent to the descent flight condition, or viceversa, creating instantaneous changes in the thrust coefficient when reaching the discontinuity. As it will be seen in the simulations this will create an inconsistency in the behaviour of the helicopter, and it will be address both in the comparison of the proposed models, and in the simulations to test the robustness of the proposed control laws. In the first one, the comparison of the proposed models, it will be shown that as predicted (Johnson, 1994; Leishman, 2006), due to the slow descent velocities encountered by the helicopter's maneuvers, the use of the $BEMT$ model for both the ascent and the descent flight conditions gives good results.

In the second one, the testing for the robustness of the derived control laws in the different proposed models, the discontinuity of the model will cause the helicopter to react in a inconsistent manner when reaching the hover flight condition. Again, similarly as for the $BEMT$ model, this behaviour can be eliminated by using the $BEMT$ model in ascent flight for the descent flight conditions also. This will represent a challenge when testing the robustness of the proposed control laws, since not only there will be unmodeled dynamics, but discontinuous models that the selected control laws and the proposed extra control laws will have to deal with. As it will be seen in the robustness analysis in section 7, the extra control signal will perform great even with the non-continuous $BEMT$ model for different flight conditions.

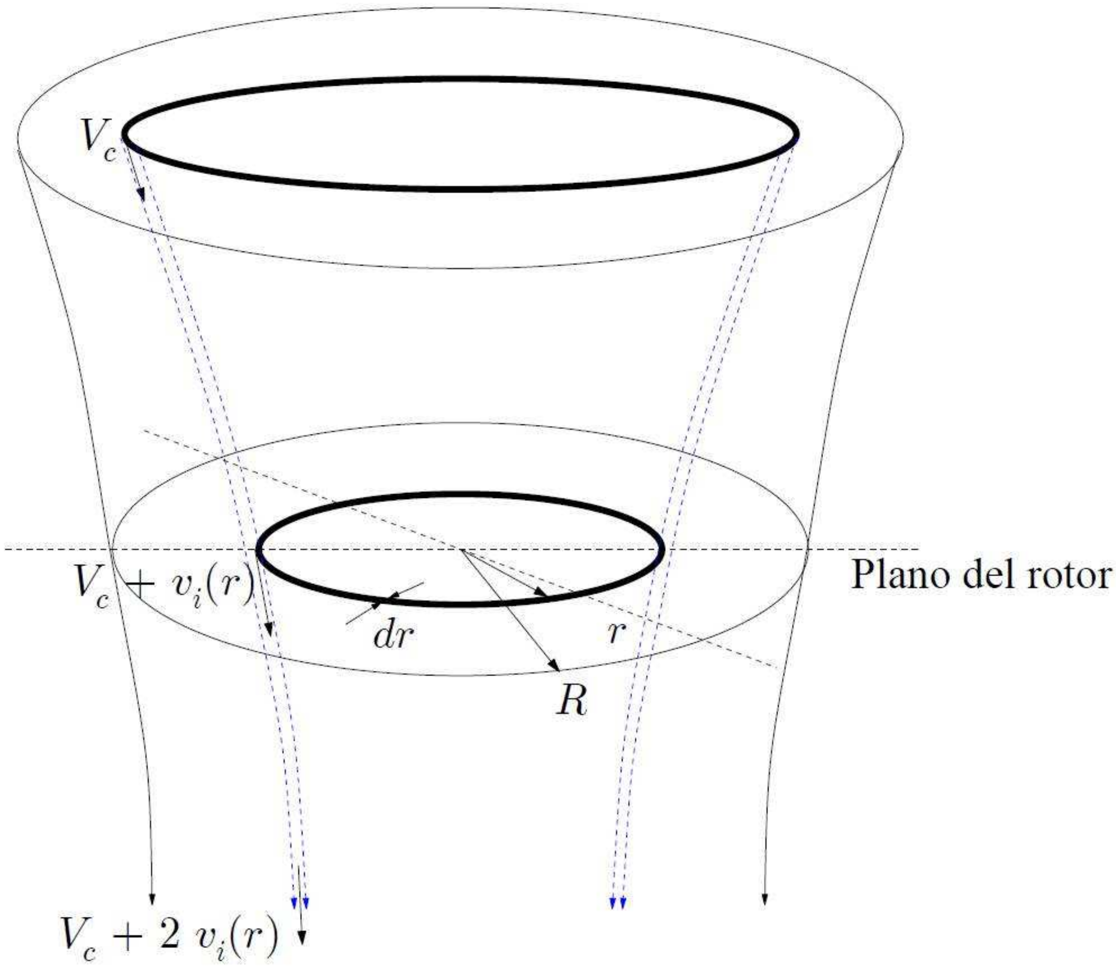

Figure A.3: Annulus of rotor disk for a local momentum analysis of the hovering rotor (Leishman, 2006; Cuerva et al., 2009).

A.4 Proposed Thrust Coefficient Model

This concludes the section dedicated to define the proposed models thrust coefficients, and this section serves to collect the most important equations that define the four proposed models. For the first defined model, the MT_H, the thrust coefficient is given in(2.251) by

$$C_T = \left[\frac{\sigma C_{l_\alpha}}{12}\left(-\frac{3}{2\sqrt{2}}+\sqrt{\frac{9}{8}+\frac{24\theta_c}{\sigma C_{l_\alpha}}}\right)\right]^2, \tag{A.92}$$

which it also has a closed-form solution for the thrust force due to the employed simplifications resulting in

$$T = \rho N_b c(\Omega R)^2 R\frac{\sigma C_{l_\alpha}^2}{144}\left(\frac{3}{2\sqrt{2}}+\sqrt{\frac{9}{8}+\frac{24\theta_c}{\sigma C_{l_\alpha}}}\right)^2. \tag{A.93}$$

For the second model, the MT_C, the thrust coefficient for the three flight axial conditions is as

$$C_{T_{MT_C}} = -\frac{\rho A\sigma C_{L_\alpha} R\Omega\left(-3\sigma C_{L_\alpha} R\Omega+\mathcal{T}_1-32R\theta_c\Omega+24V_c\right)}{192\rho A\Omega^2 R^2}, \tag{A.94}$$

$$C_{T_{MT_D}} = \frac{T_{MT_D}}{\rho A\Omega^2 R^2}, \tag{A.95}$$

$$C_{T_{MT_{WM}}} = -\frac{\rho A\sigma C_{L_\alpha} R\Omega\left(3\sigma C_{L_\alpha} R\Omega-\mathcal{T}_2-32R\theta_c\Omega+24V_c\right)}{192\rho A\Omega^2 R^2}, \tag{A.96}$$

where

$$V_c/v_h \geq 0 \quad \rightarrow \quad C_{T_{MT_C}}, \tag{A.97}$$

$$-2 \leq V_c/v_h \leq 0 \quad \rightarrow \quad C_{T_{MT_D}}, \tag{A.98}$$

$$-2 \geq V_c/v_h \quad \rightarrow \quad C_{T_{MT_{WM}}}. \tag{A.99}$$

For the third model, the $BEMT$, the thrust coefficient in axial ascent is given by integrating along the entire blade of the integral dC_T given by

$$\mathrm{dC_T} = \frac{\sigma C_{l_\alpha}}{2}\left(\theta_c r^2-\lambda r\right)\mathrm{dr}, \tag{A.100}$$

with the inflow ratio given in (A.71) as

$$\lambda(r,\lambda_c) = \sqrt{\left(\frac{\sigma C_{l_\alpha}}{16}-\frac{\lambda_c}{2}\right)^2+\frac{\sigma C_{l_\alpha}}{8}\theta_c r}-\left(\frac{\sigma C_{l_\alpha}}{16}-\frac{\lambda_c}{2}\right), \tag{A.101}$$

and where for the particular case in which the hover flight condition is considered, thus $\lambda_c = 0$, Eq. (A.101) simplifies to

$$\lambda(r) \equiv \lambda_i(r) = \frac{\sigma C_{l_\alpha}}{16}\left(\sqrt{1+\frac{32}{\sigma C_{l_\alpha}}\theta_c r}-1\right), \tag{A.102}$$

while for the axial descent is given by

$$C_{T_{MT_D}} = \frac{T_{MT_D}}{\rho A\Omega^2 R^2}, \tag{A.103}$$

$$C_{T_{MT_{WM}}} = -\frac{\rho A\sigma C_{L_\alpha} R\Omega\left(3\sigma C_{L_\alpha} R\Omega-\mathcal{T}_2-32R\theta_c\Omega+24V_c\right)}{192\rho A\Omega^2 R^2}, \tag{A.104}$$

where

$$-2 \leq V_c/v_h \leq 0 \quad \rightarrow \quad C_{T_{MT_D}}, \tag{A.105}$$

$$-2 \geq V_c/v_h \quad \rightarrow \quad C_{T_{MT_{WM}}}. \tag{A.106}$$

And finally, for the fourth model, the $BEMT_{TL}$, the thrust coefficient is also given by integrating along the entire blade of the integral dC_T given as

$$\mathrm{dC_T} = \frac{\sigma C_{l_\alpha}}{2}\left(\theta_c r^2 - \lambda r\right)\mathrm{dr}, \tag{A.107}$$

with the inflow ratio given in Eq. (A.86) as

$$\lambda r = \sqrt{\left(\frac{\sigma C_{l_\alpha}}{16F(r,\lambda(r))} - \frac{\lambda_c}{2}\right)^2 + \frac{\sigma C_{l_\alpha}}{8F(r,\lambda(r))}\theta_c r} - \left(\frac{\sigma C_{l_\alpha}}{16F(r,\lambda(r))} - \frac{\lambda_c}{2}\right), \tag{A.108}$$

and where for the particular case in which the hover flight condition is considered, thus $\lambda_c = 0$, Eq. (A.108) simplifies to

$$\lambda(r) \equiv \lambda_i(r) = \frac{\sigma C_{l_\alpha}}{16F(r,\lambda(r))}\left(\sqrt{1 + \frac{32F(r,\lambda(r))}{\sigma C_{l_\alpha}}\theta_c r} - 1\right), \tag{A.109}$$

while again, for the axial descent is given by

$$C_{T_{MT_D}} = \frac{T_{MT_D}}{\rho A \Omega^2 R^2}, \tag{A.110}$$

$$C_{T_{MT_{WM}}} = -\frac{\rho A \sigma C_{L_\alpha} R\Omega\left(3\sigma C_{L_\alpha} R\Omega - \mathcal{T}_2 - 32R\theta_c\Omega + 24V_c\right)}{192\rho A\Omega^2 R^2}, \tag{A.111}$$

where

$$-2 \le V_c/v_h \le 0 \quad \rightarrow \quad C_{T_{MT_D}}, \tag{A.112}$$

$$-2 \ge V_c/v_h \quad \rightarrow \quad C_{T_{MT_{WM}}}. \tag{A.113}$$

As previously mentioned in section A.4, let recall that both MT_H and MT_C produce close-form solutions for the thrust coefficient C_T (2.248) which are both explicit functions of the collective pitch angle θ_c and the inflow angle. Recall also that while for the MT_H model, the hover flight condition, the inflow angle is a function of C_T, resulting in a continuous closed-form solution for the thrust coefficient. The proposed MT_C model presents nonlinearities depending on the nature of the climb flight region, and therefore being unfeasible to integrate into a set of continuous differential equations if the goal is to design continuous and differentiable control laws.

On the other side, for both blade element theory models, $BEMT$ and $BEMT_{TL}$, it is required numerical integration at each instant in order to obtain the thrust coefficient, therefore making impossible to obtain a closed-form solution to which be able to design a proper control law to regulate the amount of thrust generated, but they will serve as a great test bench problems where to test the validity of the selected model, and to test the robustness of the proposed control laws under model uncertainties.

With this in mind, this makes MT_H the only implementable thrust coefficient model C_T, and will be the model employed for the helicopter dynamics proposed in section 2.8, which, once integrated into the proposed dynamics for axial flight, it will be tested against the rest of models, and it will be shown, via simulations, that the MT_H model, although much more simpler, it reproduces the dynamics of the more detailed and complex models (MT_C, $BEMT$ and $BEMT_{TL}$) without loss of generality for the low vertical speeds at which the RC helicopter is to be operated, thus corroborating the validity of its selection (Johnson, 1994; Leishman, 2006).

Nevertheless, the validity of the MT_H model is subject to the series of hypothesis that have been exposed throughout the previous derivations, and are exposed in the following sections to justify that the selected model can be implemented in the RC helicopter model. As previously mentioned in section A.4, these hypothesis are standard and well established hypothesis, which are necessary in order to be able to obtain reduced empirical models that are able to model, to a certain degree, the highly complex and non linear behavior of rotating blades (Leishman, 2006).

The most important of the hypothesis used throughout the model definition are justified or, corrections are introduced in the proposed model, to account for the various effects not accounted for in the original model. These hypothesis (Prouty, 1986; Pallet and Ahmad, 1991) are divided in two big groups: hypothesis on the flow characteristics (hypothesis 1 through 5), and the hypothesis on the physical geometry and characteristics of the RC helicopter's main rotor (hypothesis 6 through 12):

1. Uniform Induced Velocities over the Entire Disk.
2. Non Rotating Wake and Tip Vortices Not Affecting the Angle of Attack of the Blades.
3. No Effects Due to Radial Flow.
4. No Loss Due to Airflow Over Helicopter's Body.
5. The lifting portion of the blade extends from the hub to the tip of the blade.
6. Blades have a constant chord, no taper, and ideal twist.
7. The blades have ideal twist.
8. The blades are torsionally rigid and thus no structural twisting occurs.
9. Airfoil lift and drag characteristics are the same as the National Advisory Committee for Aeronautics (NACA) 0012.
10. Airfoil characteristics are not a function of local stall or compressibility effects.
11. The rotor is far above the ground, no ground effect.

These hypothesis are described in the following sections.

A.4.1 Hypothesis 1 - Uniform Induced Velocities over the Entire Disk

In the real RC helicopter, as expected, the induced velocities will not be uniform along the blade of the rotor, and as a result, the theoretic thrust coefficient will be somehow overestimated when comparing with the actual thrust coefficient, which will be observed when using the $BEMT$ and $BEMT_{TL}$ models to test the validity of the selected model, although that overestimation should be quite small for the reduced vertical axial velocities encountered by the RC helicopter.

The assumption that the air moves smoothly and uniformly through the rotor blades neglects the fact that the helicopter body sits below the rotor disk area and takes up area where it would desirable to push air through. This will result in measurable loss in thrust developed that will be referred as D_{const}. Other problems like the wind blowing across the wake, or the fact that the blade will have no ideal twist will also be affected by the actual nonuniform airflow. As seen in the $BEMT$ and $BEMT_{TL}$ models, sections A.3.2 and A.3.3, respectively, the use of nonuniform inflow models is quite restrictive if it is desired to have a simple enough thrust coefficient model that can be dealt with. Otherwise, if more realistic inflow distributions are employed, it is necessary the use of numerical integration tools to obtain the associated thrust coefficient. Therefore, and assuming that the constant drag due to the body of the helicopter is the major cause for losses assuming there is negligible wind present, the only possible modeling approach is to include all the losses due to the nonuniform inflow in the D_{const} term. This constant drag loss will be included in the axial flight dynamics of the helicopter, rather than in the main rotor dynamics. The D_{const} term will be used as a hodgepodge where to include most of the rotor losses, and it will be left to the parameter estimation for proper estimation.

A.4.2 Hypothesis 2 - Non Rotating Wake and Tip Vortices Not Affecting the Angle of Attack of the Blades

The understanding and prediction of the effects of the rotor wake is an important key to the successful prediction of the loads of a blade, and many other aerodynamics helicopter problems. A helicopter rotor wake is dominated by strong vortices that are trailed down from the tips of each blade. The nature of the rotor wake, in terms of geometry, strength, and the aerodynamic effects produced on the blades, depends principally on the operating state and flight condition of the helicopter. In the hover flight condition, the tip vortices follow nominally helical trajectories bellow the rotor as seen in Figure A.4. Although this is the simplest of the possible operating states comparing with the forward flight operating flight condition in which the vortex trajectories become interlocked, but nominally epicycloidal, but even so, in the hover condition the wake structure becomes relatively complicated to model (Leishman, 2006). Some complex models have been developed to enable predictions of the inflow through the disk considering generalized prescribed vortex wake models, but without the expense and uncertainties associated with explicit calculating the force-free positions of the wake. These models prescribe the locations of the rotor tip vortices (and sometimes also the inner vortex sheet) as functions of the wake age ψ_w on the basis of experimental observations (Leishman, 2006). Some of the works for hovering flight, generalized prescribed vortex wake models have been developed in (Landgrebe, 1969; Gilmore and Gartshore, ; Kocurek et al., 1977).

In a rotating wake model in the hover operating condition, as seen in Figure A.4, there exists a rotational speed of the rotors, Ω, and a induced wake rotation and ω. This wake rotation will result in some of the input power being lost to wake rotation instead of all of it going to producing lift. This effect can be thought of as a drag on the airfoil which is proportional to the angular velocity of the blade, that is, the faster the rotational speed, the more loss in terms of power, and as it will be shown in the modeling of the combustion engine and the rotational velocity equation, also proportional to the collective pitch angle, that is the higher the collective pitch angle the higher the total projection of the blade surface area sees the flow, and therefore higher the profile drag.

The assumption that the wake is non rotating neglects this loss of power, and although the proposed dynamic model is not concern with power loss, but on the generation of lift itself, this effect needs to be taken into account when modeling the combustion engine output, the rotation speed equation, and how throttle effects the resulting rotational speed, which will be dealt in more detail in section 2.8.

Similarly, as for the assumption for the non rotating wake, and directly associated to the rotation of the wake, is the fact that the proposed models assume that the tip vortices generated by the rotating wake do not affect in the effective angle of attack of the blades. Tip vortex formation is a complex problem involving high velocities with shear, flow separation, pressure equalization, and turbulence production. The tip region is enclosed in a region of high vorticity, which rolls up quickly into a dominant vortex (Leishman, 2006), as it can be seen in subfigure A.5(a), which describes the tip vortex locations with wake interference and subfigure A.5(b)that describes the tip vortex locations without wake interference, and Figure A.6 that shows the tip vortex interference, the tip vortices effect the angle of attack as each following blade goes through an area in which the air has been disturbed by the previous blade, and therefore the velocity component that sees the blade at the tip has been altered by the tip vortex. Although many tip vortex models have been hypothesized, some of them solely taking into account the velocity field models for helicopters (Leishman, 2006), and some other based on tip vortices for airplane fixed-wings (Dosanjh et al., 1962), it is difficult, if not impossible to account for any of these predicted behaviors in the differential proposed equations for axial flight, therefore the change of angle of attack in the blades due to tip vortices is left to be accounted in the parameter estimation for the proposed model.

A.4.3 Hypothesis 3 - No Effects Due to Radial Flow

Radial flow is the result of molecules in contact with the rotor blade flowing along the rotor blade due to centrifugal pumping, wake contraction, spanwise pressure gradient, and undeveloped tip vortices (Prouty, 1986). Studies have shown that this flow can be either inboard or outboard depending on these four effects. The conclusion (Prouty, 1986) which is based on what is known of the problem at this time, is that it is acceptable to neglect radial flow. Therefore, it will also be neglected.

A.4.4 Hypothesis 4 - No Loss Due to Airflow Over Helicopter's Body

The assumption that the airflow over the body of the helicopter while descending or climbing has no effect on the thrust produced is again conservative. There will be a drag produced called parasitic drag that will result in losses to the thrust when moving through the air. The loss in thrust that will be appreciated as the helicopter moves through the air will be of the form given by:

$$T_{loss} = \frac{1}{2}\rho V_c^2 f, \tag{A.114}$$

where f is the parasitic drag area and V_c is the climb velocity of the helicopter. This term will be taken into account in the position equation and as with some of the above hypothesis, the determination of the parasite drag area, f, will be left to the parameter estimation described in more detain in section 2.8.4.1.

A.4.5 Hypothesis 5 - The lifting portion of the blade extends from the hub to the tip of the blade

As seen in section 2.6.1.2, the formation of a trailed vortex at the tip of each blade produces a high local inflow over the tip region and effectively reduces the lifting capability there, this results in that the lifting-line theory is not strictly valid near wing tips. When the chord at the tip is finite, blade element theory gives a nonzero lift all the way out to the end of the blade. In reality the amount of lift produced will drop off near the hub and at the tip, as shown in Figure (2.19).

As suggested (Johnson, 1994; Leishman, 2006), one way to account for loss of lift at the at the tip is to integrate the incremental lift from some r_0 to BR where r_0 is radius of the root cut-out, and BR is the effective outer radius, $R_e < R$. These values are chosen such that the area under the theoretical curve out to BR is the same as the area under the actual lift curve out to R. Recall the empirical equation by Prandtl and Betz (Betz, 1919) gives good correlation to numerical method determinations (Glauert, 1935; Johnson, 1994; Prouty, 1986; Leishman, 2006) and results in an empirical correction factor derived in section 2.6.1.2 and given by (2.199) as

$$B = 1 - \frac{\sqrt{C_T}}{N_b}. \tag{A.115}$$

Therefore, by replacing the radius of the blade R by BR, then then root and tip cut-out losses are taken into account. As seen in the literature (Leishman, 2006) typical values for B range from 0.95 to 0.98. In order to choose an appropriate value for B let use the available collective pitch angles, which will be defined in section 2.8.5.2 and are given as $1° \leq \theta_c \leq 20°$, and substitute them into the thrust coefficient selected model (7.1) and study the allowed values for B. Figure A.7 shows the thrust coefficient value for the ranges of available collective pitch angles, and the solution to the Prandtl's B factor. From figure A.8 it can be seen that for the range of available collective pitch angles B is limited to $0.94349 \leq B \leq 0.99329$. Therefore a safe assumption is $B = 0.9684$. A more exact Prandtl's factor can be obtained by conducting experiments on the helicopter platform and recording the collective pitch angles θ_c associated to several thrust coefficients C_T which is described in more detain in section 2.8.4.1

A.4.6 Hypothesis 6 - Constant Chord No Taper Blades

Generally the blades that are used in RC helicopter, are straight and have no taper, which is the case for the RC model here employed, therefore the will not be a concern.

A.4.7 Hypothesis 7 - Blades Have Ideal Twist

Recalling the $BEMT$ model, in which the thrust coefficient was given by integrating along the entire blade of the integral dC_T given by

$$\mathrm{dC_T} = \frac{\sigma C_{l_\alpha}}{2}\left(\theta_c r^2 - \lambda r\right)\mathrm{d}r, \tag{A.116}$$

with the inflow ratio given in Eq. (A.86) as

$$\lambda(r,\lambda_c) = \sqrt{\left(\frac{\sigma C_{l_\alpha}}{16} - \frac{\lambda_c}{2}\right)^2 + \frac{\sigma C_{l_\alpha}}{8}\theta_c r} - \left(\frac{\sigma C_{l_\alpha}}{16} - \frac{\lambda_c}{2}\right), \tag{A.117}$$

and where for the particular case in which the hover flight condition is considered, thus $\lambda_c = 0$, Eq. (A.117) simplifies to

$$\lambda(r) \equiv \lambda_i(r) = \frac{\sigma C_{l_\alpha}}{16}\left(\sqrt{1 + \frac{32}{\sigma C_{l_\alpha}}\theta_c r} - 1\right), \tag{A.118}$$

it can be shown that (Gessow and Center, 1948) if

$$\theta_c r = constant = \theta_{tip}, \tag{A.119}$$

there is a special solution to the inflow equation in (A.118) that gives uniform inflow, that is,

$$\theta_c(r) = \frac{\theta_{tip}}{r}. \tag{A.120}$$

This twist distribution, called ideal twist, is depicted in Figure A.9. With ideal twist the performance of the rotor can now be recalculated, and using Eq. (A.119) results in

$$C_T = \frac{1}{2}\sigma C_{l_\alpha}\int_0^1 (\theta_{tip} r^2 - \lambda r)\mathrm{d}r = \frac{1}{2}\sigma C_{l_\alpha}\left(\frac{\theta_{tip}}{2} + \frac{\lambda}{2}\right). \tag{A.121}$$

Recalling that the inflow ratio can be written as

$$\lambda = \frac{V_c + v_i}{\Omega R} = \frac{V_c + v_i}{\Omega y}\left(\frac{\Omega y}{\Omega R}\right) = \frac{U_P}{U_T}\left(\frac{y}{R}\right) = \phi_i r = \phi_{tip}, \tag{A.122}$$

thus rewritten (A.121) by using (2.230) yields

$$C_T = \frac{1}{4}\sigma C_{l_\alpha}\left(\theta_{tip} - \phi_{tip}\right) = \frac{\sigma C_{l_\alpha}}{4}\alpha_{tip}, \tag{A.123}$$

and where using (A.117) and (A.120) gives

$$\lambda(r) = \frac{\sigma C_{l_\alpha}}{16}\left(\sqrt{1 + \frac{32}{\sigma C_{l_\alpha}}\theta_{tip} r} - 1\right) = \text{constant} = \sqrt{\frac{C_T}{2}}, \tag{A.124}$$

which is equivalent to the assumption considered for the MT_H proposed model. Therefore, if it is assumed that the blades have ideal twist, then the nonuniform flow of the $BEMT$ model, collapses into the MT_H model in hover. Although ideal twist blades have much more implications that the simplification of the inflow in the hover condition, like minimum induced power rotors (Johnson, 1994; Prouty, 1986; Leishman, 2006), ideally twisted blades are extremely difficulty of construction and thus not feasible in practice for large rotors, although it is raising great interest among the Micro UAV's.

A.4.8 Hypothesis 8 - Blades are Torsionally Rigid

The assumption that the rotor blades are rigid is not entirely true for full scale helicopters and thus dynamic twisting of the rotor blades should be taken into account. The main concern here is that as the blades begin to twist, the angle of attack will change and the resulting lift will vary. This will cause discrepancies in correlating measured thrust with measured collective pitch. But, since both power and thrust are effected by the same degree, small angular differences in the twist will have little or no effect on power to thrust relationships. For the case of small *RC* helicopters, the blades are much stronger in relation to the amount of torsion that they will see than their counterparts on large scale helicopters. Therefore, it would be expected that only a minimal amount of twisting of the blade will be seen and that this assumption should hold for this type of *RC* models.

A.4.9 Hypothesis 9 - The Helicopter's Blade are NACA 0012 Airfoils

It will be assumed that the airfoil that the main rotor of the helicopter model presented used a NACA 0012, which according to (Prouty, 1986), that is the case for most rotor blades, and for which there exists a great deal of results. As a result, it is assumed that the airfoil of the rotor blades of the *RC* helicopter exhibit similar characteristics to that of the NACA 0012 and assume that any differences can be made up in the parameter estimation experiments. Figure A.10 shows the main aerodynamic characteristics for the NACA 0012 airfoil

A.4.10 Hypothesis 10 - Airfoil Characteristics are not a Function of local Stall or Compressibility Effects

Since the helicopter will be operated only in hover flight, the assumption regarding the drag divergence which limit the maximum forward speed and maneuvering capability of the helicopter will be valid since the *RC* helicopter will not be flying hear the regions where stall and drag divergence can have a significant affect on hover performance.

A.4.11 Hypothesis 11 - No Ground Effects

Helicopter performance is affected by the presence of the ground or any other boundary that may alter or constrain the flow into the rotor or constrain the development of the rotor wake. When a rotor is in ground effect, the rotor slipstream tends to rapidly expand as it approaches the surface. This alters the slipstream velocity, the induced velocity in the plane of the rotor, and, therefore, the rotor thrust and power, resulting in that the rotor thrust is found to be increased for a given power (Leishman, 2006). Lots of works on ground effect have been conducted through experimental analysis and the data suggests that significant effects on hovering performance for heights less than one rotor diameter are encountered (Leishman, 2006) as seen in Figure A.11. Some methods have been proposed to simulate ground effect (Cheeseman and Bennett, 1957), in which the rotor thrust can be expressed by

$$\left[\frac{T}{T_\infty}\right]_{P=\text{const}} = \frac{1}{1-\frac{(R/4z)^2}{1+(\mu/\lambda_i)^2}}, \tag{A.125}$$

where z is the height off the ground and λ_i is the induced velocity at the rotor. This equation has a validity for $z/R > 0.5$, where R is the radius of the blade. Incorporating the effect of blade loading given by

$$\frac{C_T}{\sigma} = \frac{T}{\rho A(\Omega R^2)}\left(\frac{A}{A_b}\right) = \frac{T}{\rho A_b(\Omega R)^2}, \tag{A.126}$$

where A_b is the area of the blades, and μ is the rotor advance ratio, given by $\mu = V_\infty \cos\alpha/\Omega R$ and therefore rewriting Eq. (A.127) such

$$\left[\frac{T}{T_\infty}\right]_{P=\text{const}} = \frac{1}{1 - \frac{\sigma C_{l_\alpha}\lambda_i}{4C_T}\frac{(R/4z)^2}{1+(\mu/\lambda_i)^2}}, \tag{A.127}$$

For hovering effects, and neglecting any blade-loading effects (A.127) can be reduced to

$$\left[\frac{T}{T_\infty}\right]_{P=\text{const}} = \frac{1}{1-(\frac{R}{4z})^2}. \tag{A.128}$$

This relationship has to be taken into account when flying near the ground, but since the helicopter will be mounted in a stand that is already elevated from the ground a rotor diameter, as it will be seen in section 2.8, the ground effects can be neglected.

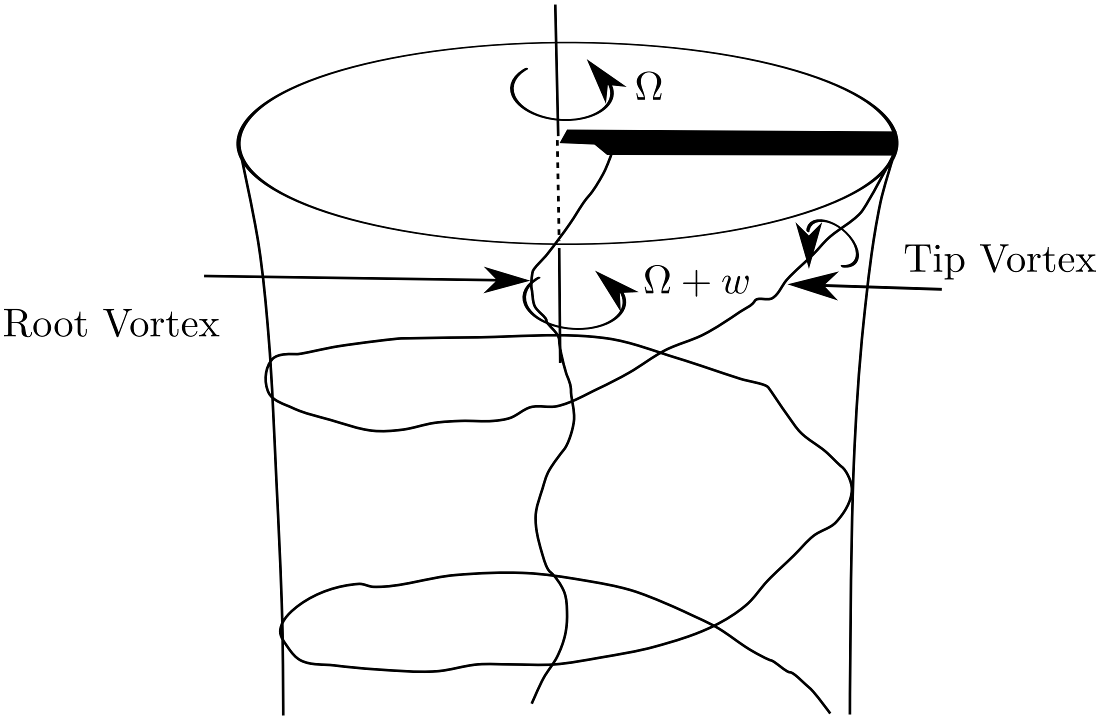

Figure A.4: Wake rotation (Prouty, 1986).

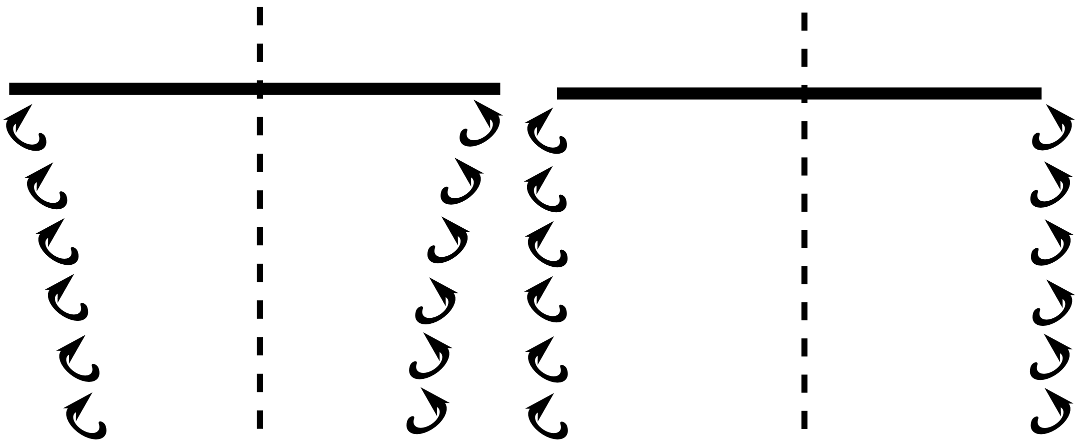

Figure A.5: Tip vortex locations with: (a) wake contraction and (b) without wake contraction (Prouty, 1986).

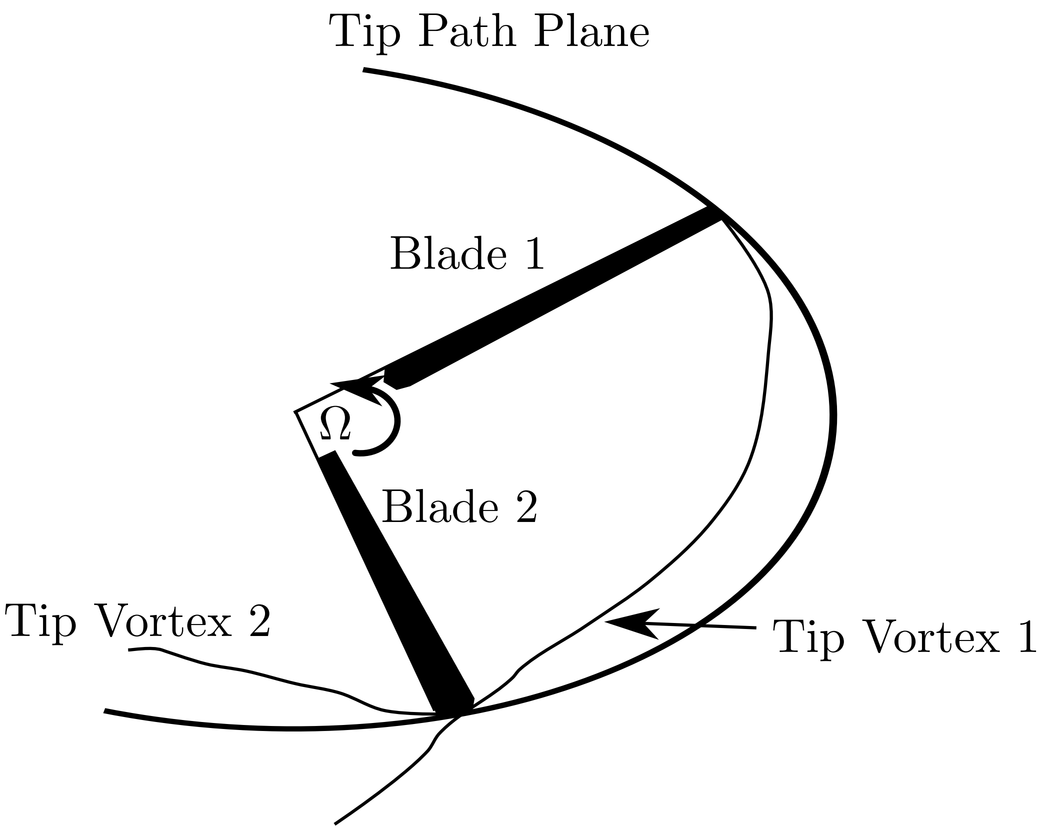

Figure A.6: Tip vortex interference (Prouty, 1986).

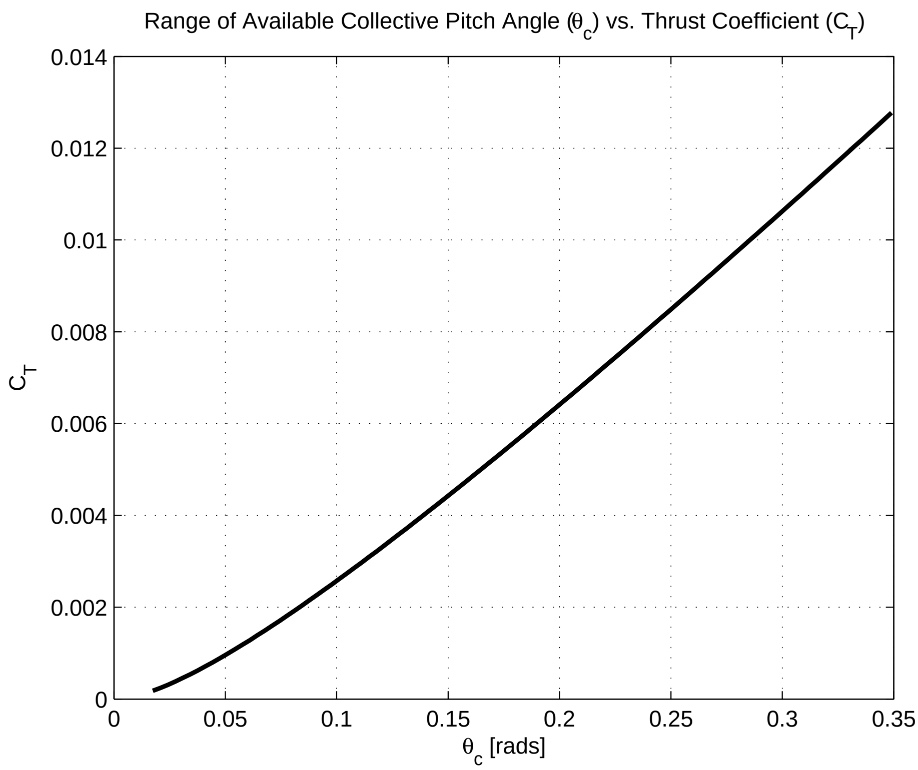

Figure A.7: Permissive collective pitch angle, θ_c, vs. thrust coefficient, C_T.

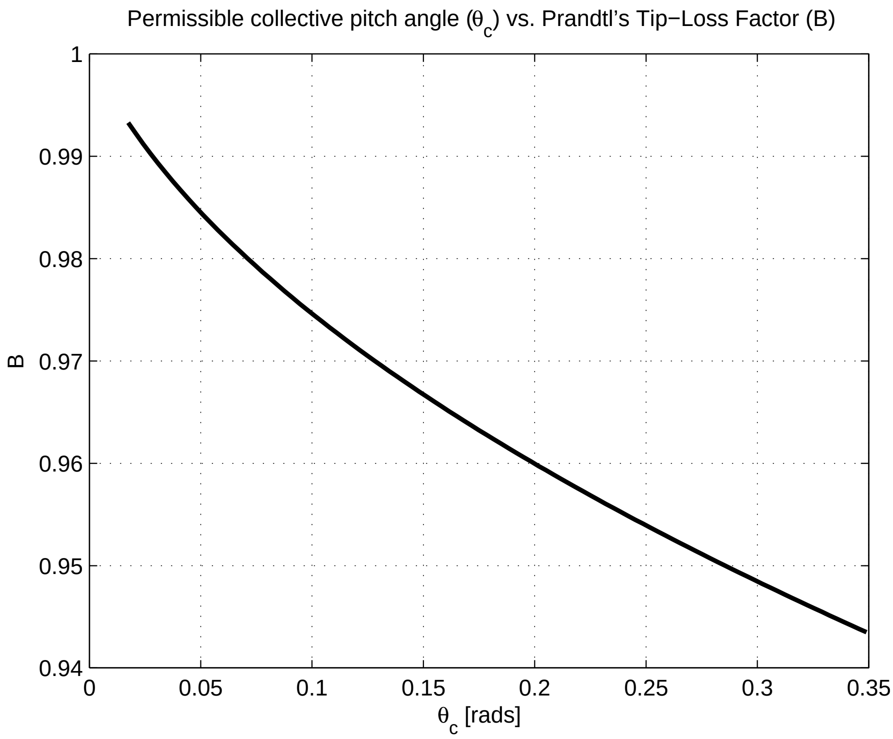

Figure A.8: Permissive collective pitch angle, θ_c, vs. Prandtl's tip-loss factor, B C_T.

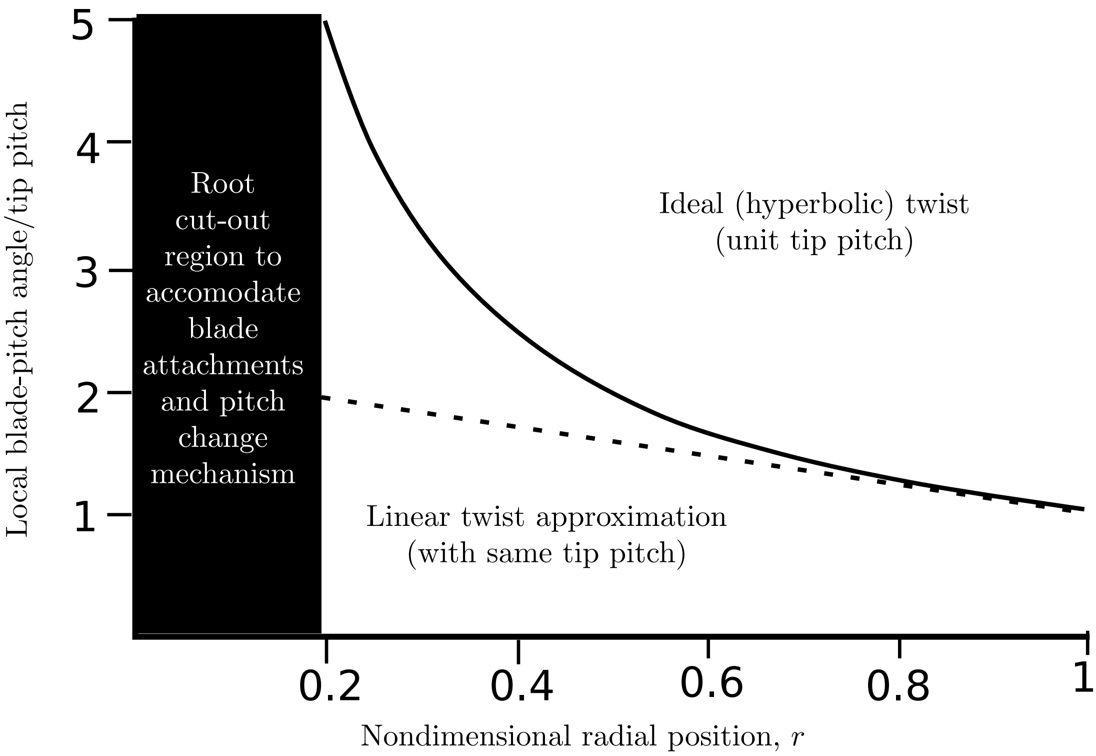

Figure A.9: Radial distribution of blade twist in ideal case (Leishman, 2006).

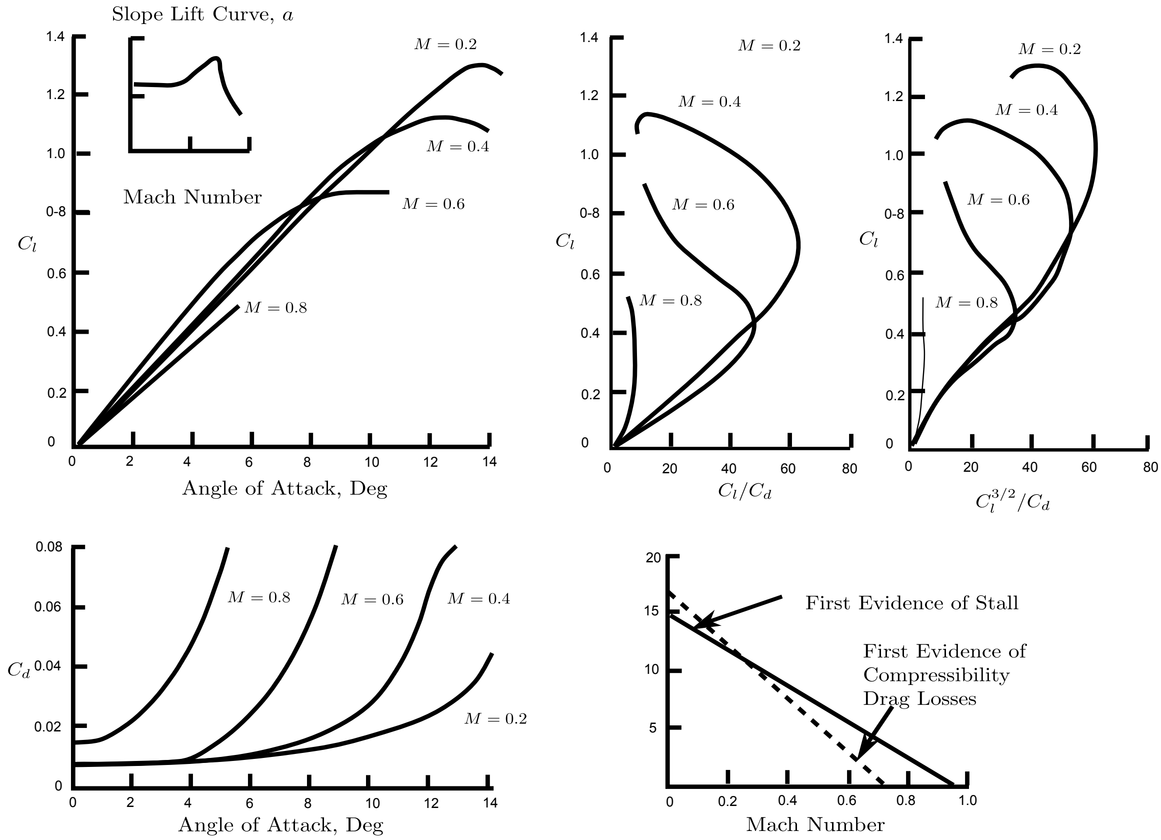

Figure A.10: Aerodynamic properties for a NACA 0012 blade (Prouty, 1986).

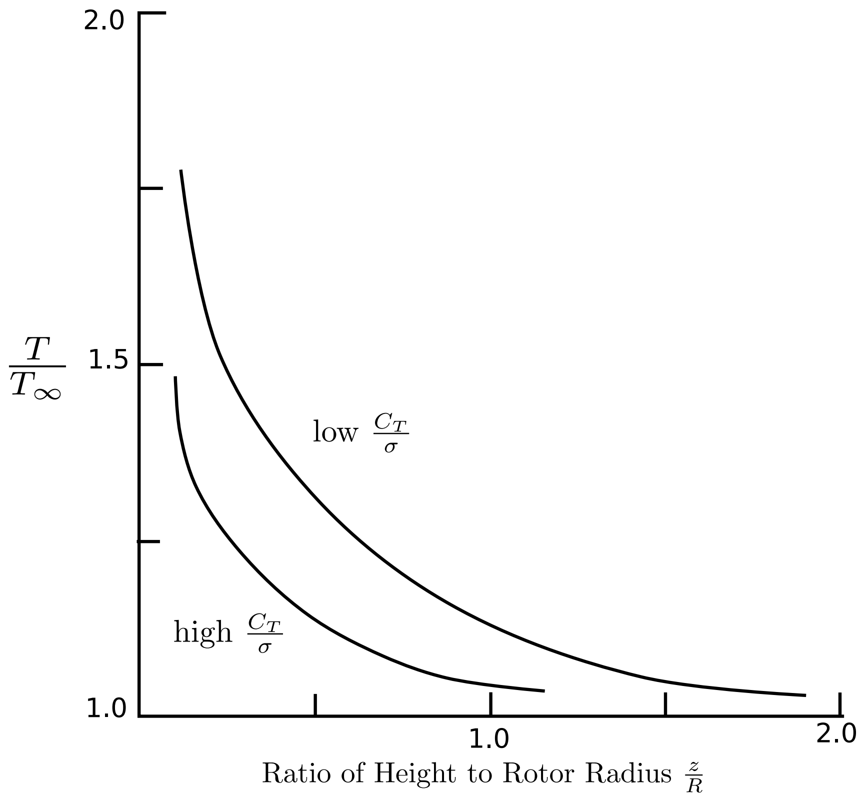

Figure A.11: Ground effect: thrust increase at constant power (Johnson, 1994).

A.5 Performance Analysis Comparisons for the Proposed Models

The validity of the proposed thrust coefficient model, MT_H defined in section 2.8 and applied in (2.339–2.343), is tested against the different thrust coefficient proposed models, the MT_C defined in section A.3.1, the $BEMT$ defined in section A.3.2, and the $BEMT_{TL}$ defined in A.3.3. Recalling the selected helicopter model defined in (2.339–2.343) and given by

$$\dot{x} = a_8 x + a_{10} x^2 \sin z_1 + a_9 x^2 + a_{11} + u_1, \tag{A.129}$$

$$\dot{y}_1 = y_2, \tag{A.130}$$

$$\dot{y}_2 = x^2(a_1 + a_2 z_1 - \sqrt{a_3 + a_4 z_1}) + a_5 y_2 + a_6 y_2^2 + a_7, \tag{A.131}$$

$$\dot{z}_1 = z_2, \tag{A.132}$$

$$\dot{z}_2 = a_{13} z_1 + a_{14} x^2 \sin z_1 + a_{15} z_2 + a_{12} + u_2, \tag{A.133}$$

which recall this model is unique for the selected thrust coefficient MT_H and given by

$$C_T = \left[\frac{\sigma C_{l_\alpha}}{12}\left(-\frac{3}{\sqrt{2}} + \sqrt{\frac{9}{8} + \frac{24\theta_c}{\sigma C_{l_\alpha}}}\right)\right]^2, \tag{A.134}$$

then Eq. (A.131) is rewritten as

$$\dot{y}_2 = K_1 C_T x^2 + a_5 y_2 + a_6 y_2^2 + a_7, \tag{A.135}$$

where recall that from section 2.8.4.1 that K_1 is given by (A.136) as

$$K_1 = \frac{\rho N_b c R^3}{\sigma m}. \tag{A.136}$$

In order to test the proposed methods it is necessary to define the values of the parameters in the proposed nonlinear RC axial flight dynamics (2.339–2.343). In section 2.8.4.1, methods are proposed to determine the characteristics of all the constants, K_1 through K_{12}, that define the complete set of five differential equations that has been selected as the dynamics in axial flight for the RC helicopter, equations (2.305), (2.294), and (2.332). As shown in the parameter determination section 2.8.4.1, some of these parameters could be obtained via analysis of the dynamics of the problem, i.e. K_1 in (A.136), but some others required of experiment setups to determine their nominal value.

The ultimate goal of the work proposed in this thesis is to be able to generate a series of control laws that will be able to test in the RC helicopter model that the investigation Non-Linear Group (NLG) of the Departamento de Ingeniería de Sistemas y Automática at the University of Seville is preparing as a test bench. The author, along with several other researchers from the group, have been working in the past years to get the platform ready by conducting several final degree projects with several students that have been in charge programming a PC-104 with a RTL OS as the core for all the controlled operations (Pujol-Pérez, 2007), design and construction of the avionics box to safely allocate the PC-104 and the rest of electronic sensors and provide the necessary power to all the electronic equipment (Santos-García, 2007), is allocated and all the control, the design, construction and integration of the different required sensors, i.e. altitude sensor (Jiménez-González, 2007), the collective pitch and the rotational speed of the rotor sensors (Navarro-Collado, 2010), the design and integration of a communications interface between the avionic box and the ground PC, and a RTL 6-DOF helicopter simulation software where to test the control laws prior to test them in the real RC helicopter (Lara-González, 2008).

At this stage, the experiments to identify the different parameters, following the tips defined in section 2.8, has not been conducted, therefore, the author has chosen to select the values of the constants appearing in the reference from which this model is inspired (Pallet and Ahmad, 1991). Pallet and Ahmad (Pallet and Ahmad, 1991) give these parameters for their helicopter platform after conducting the required identification process for all the parameters, and did that with a similar helicopter to the one the experiments will be conducted in the future. The identification process is conducted in a helicopter flying stand made by Whitman Industries, see figure 2.23, similar to the platform that was selected by the NLG which was acquired in Active Distribution Limited (Active Distribution LTD, 2004), and can be seen in figure 2.23 and in figure A.12 after being modified to elevate teh platform from the ground and therefore reducing, if not eliminating completely, the ground effect. Both flying stands allow the helicopter not only to move in axial flight, but also in pitch, yaw, and roll, but similarly as in (Pallet and Ahmad, 1991), the flying stand has been modified to limit the helicopter motion to the vertical plane.

The helicopter chassis in the report is an X-Cell model 50 RC aircraft manufactured by Miniature Aircraft, Florida, USA (Miniature Aircraft USA, 1999), which is powered by a 0.5 in^3 displacement two-cycle combustion engine made by Webra Model-Building Inc (Germany), while the selected RC helicopter is a Raptor 30 with an OS 0.5 in^3 displacement two-cycle combustion engine (OS Engines, 2010). Therefore, the nominal values of the constants of the model here employed (Pallet and Ahmad, 1991) are defined in Table A.1.

Some of the physical parameters of the associated helicopter are not identified in (Pallet and Ahmad, 1991), i.e. the mass of the helicopter, the radius, and the chord, but they can be calculated from the data given in the report and the formulation of the selected MT_H model. Recall that K_1 is given by an empirical equation defined as

$$K_1 \quad = \quad \frac{\rho N_b c R^3}{\sigma m}, \tag{A.137}$$

where

$$\sigma = \frac{c N_b}{\pi R}, \tag{A.138}$$

recalling that from experimentation in (Pallet and Ahmad, 1991), K_1 is obtained as $K_1 = 0.25$. Recalling that the X-Cell 50 kit uses a 620 mm blades, that after connected to the hub of the rotor results in a rotor span of 1405 mm, that is $R = 702.5$ m, and that the blades used ar the SAB 620 that have a chord of 58 mm, then the mass of the helicopter can be approximated by using (A.139), and recalling that the effective radius of the blade is corrected with Prandtl's Tip-Loss coefficient of $B = B = 0.9569$ (Pallet and Ahmad, 1991) then the mass, m can be obtained as

$$m \quad = \quad \frac{\rho N_b c R^3}{\sigma K_1} = \frac{\pi \rho (BR)^4}{K_1}, \tag{A.139}$$

resulting in that the mass of the helicopter in the experiments (Pallet and Ahmad, 1991) is approximately $m = 3.1487$ kg, which matches really close the RC helicopters of the same class (Miniature Aircraft USA, 1999). With this in mind, it can also be completed the C_T models which are given by

$$C_T \quad = \quad \left[\frac{\sigma C_{l_\alpha}}{12}\left(-\frac{3}{\sqrt{2}} + \sqrt{\frac{9}{8} + \frac{24\theta_c}{\sigma C_{l_\alpha}}}\right)\right]^2, \tag{A.140}$$

which recall that can also be written as

$$C_T \quad = \quad \left(-K_{C1} + \sqrt{K_{C1}^2 + K_{C2}\theta_c}\right)^2, \tag{A.141}$$

with

$$K_{C1} \quad = \quad \frac{\sigma C_{l_\alpha}}{8\sqrt{2}}, \tag{A.142}$$

$$K_{C2} = \frac{2\sigma C_{l_\alpha}}{12}, \tag{A.143}$$

where for

$$\sigma = \frac{cN_b}{\pi BR}, \tag{A.144}$$

with $c = 0.060$ m, $N_b = 2$, $B = 0.9569$ and $R = 702.5$ m, results that the calculated values for K_{C1} and K_{C2} are

$$K_{C1} = \frac{\sigma C_{l_\alpha}}{8\sqrt{2}} = 0.032242, \tag{A.145}$$

$$K_{C2} = \frac{2\sigma C_{l_\alpha}}{12} = 0.0607971, \tag{A.146}$$

where recalling that from (Pallet and Ahmad, 1991) $K_{C1} = 0.032592$ and $K_{C2} = 0.061456$ which represents only 1% error with respect to the employed coefficients. Therefore, and recalling the rest of the definitions of the equivalent parameters in (A.129-A.133) and defined in Table A.1 results in the constants defined in defined in Table 2.1, which will be the constant that will be used throughout the remainder of the thesis.

In order to conduct a comparable performance analysis between the selected MT_H model, against the more precise models, the MT_C, the $BEMT$ and the $BEMT_{TL}$, it is necessary to select a control signal that can be used to test the behavior of all four systems. The analysis of the equilibrium equations conducted in section 2.8.5.1 resulted in two sets of expressions that obtained the equilibrium space of configuration for the helicopter model depending if the collective pitch angle, z_1^*, or the angular velocity of the blades, x^*, were set at a desired condition, being the first set defined in (2.353–2.355), and the second set defined in (2.356–2.358). Selecting the second set, which implies selecting a nominal angular velocity of the blades, and using the collective pitch angle as the active control signal, which is what it is commonly use in helicopter axial flight control, both the small scale and the full scale counterpart results in

$$\bar{z}_1(x^*) = \frac{a_4 x^* + \sqrt{C_a {x^*}^2 + C_b}}{2a_2^2 x^*} + C_c + \frac{C_d}{{x^*}^2}, \tag{A.147}$$

$$\bar{u}_1(x^*) = -a_8 x^* - {x^*}^2 (a_{10} \sin \bar{z}_1 + a_9) - a_{11} \tag{A.148}$$

$$\bar{u}_2(x^*) = -a_{13}\bar{z}_1 - a_{14}{x^*}^2 \sin \bar{z}_1 - a_{12}, \tag{A.149}$$

being the constants defined by

$$\begin{aligned} C_a &= a_4^2 - 4a_2 a_1 a_4 + 4a_2^2 a_3, \\ C_b &= -4a_2 a_7 a_4, \\ C_c &= -\frac{a_1}{a_2}, \\ C_d &= -\frac{a_7}{a_2}, \end{aligned}$$

where Equation (A.148) and (A.149), define the control signals required to achieve the selected equilibrium points, and where (A.147) defines the space of configuration of the collective pitch angle, $\bar{z}_1(x^*)$, associated to a selected desired rotational speed of the blades, x^*.

$K_1 = 0.25$	$K_2 = 0.1$	$K_3 = 0.1$	$K_4 = 7.86$	$K_5 = 0.7$
$K_6 = 0.0028$	$K_7 = 0.005$	$K_8 = -0.1088$	$K_9 = -13.92$	$K_{10} = 800$
$K_{11} = 65$	$K_{12} = 0.1$	$K_{C_1} = 0.03259$	$K_{C_2} = 0.061456$	

Table A.1: Values for the helicopter estimated physical coefficients K_*.

A.5.1 Simulation Results for the Performance Analysis Comparisons for the Proposed Models

Simulations are conducted using the equilibrium control laws, (A.148) and (A.149) to test the validity of the different C_T models. The simulations are conducted using a fourth order Runge-Kutta fixed step integration method with an integration step of 0.01 seconds. The study is performed for the closed-loop error dynamics model (4.116–4.120) by conducting a sensitivity study for variable initial conditions in helicopter collective pitch angle, $z_1(0)$ and angular rotational speed of the blades, $x(0)$, while fixing the final rotational speed of the rotor at the desired operational value, x^*. Since there is no control in the vertical position of the helicopter with this law, the only possible way of conducting ascent and descent flight is by selecting increases in the angular rotation speed of the blades, that is $x(0) > x^*$, and descent flight conditions by decreasing the angular rotation speed of the blades, that is $x(0) < x^*$, which through (A.147) translates to a different equilibrium collective pitch angle. The simulations are started at an equilibrium condition, that is governed by no initial vertical velocity, $x_2(0) = 0$, nor collective pitch velocity of the blades, $z_2(0) =$ and the pair of initial angular rotation of the blades, and the collective pitch angle, $x(0)$ and $z_1(0)$ respectively, given by (A.147).

In order to evaluate the performance of the new derived control law under unmodeled dynamics, a sensibility analysis is conducted by performing the same four distinctive maneuvers that include all possible helicopter maneuvers:

1. Ascent flight with increasing engine *RPM*.
2. Ascent flight with decreasing engine *RPM*.
3. Descent flight with increasing engine *RPM*.
4. Descent flight with decreasing engine *RPM*.

where once again, despite the extensive sensitivity analysis conducted, only four significate cases are presented, which correspond to a maneuver that includes all four distinctive maneuvers in one simulation, and that are defined by the bellow conditions:

1. $y_1(0) = 1.85\ m$, $y_1^* = 0.5\ m$, $x(0) = 120\ rad/sec$, and $x^* = 140\ rad/sec$.
2. $y_1(0) = 0.5\ m$, $y_1^* = 1\ m$, $x(0) = 140\ rad/sec$, and $x^* = 120\ rad/sec$.
3. $y_1(0) = 1\ m$, $y_1^* = 1.5\ m$, $x(0) = 120\ rad/sec$, and $x^* = 145\ rad/sec$.
4. $y_1(0) = 1.5\ m$, $y_1^* = 0.75\ m$, $x(0) = 145\ rad/sec$, and $x^* = 120\ rad/sec$.

As a close note of this section, it is important to remember that although the selected model might not be completely accurate with the performance of a real *RC* helicopter in all the axial flight conditions, and although the presented MT_H, $BEMT$ and $BEMT_{TL}$ models reproduce with more detail the nonlinear dynamics of a helicopter in axial flight, the complexity added with these models makes quite difficult to approach the regulation of the *RC* helicopter's altitude. Therefore, the MT_H, and the rest of the selected dynamics, that is the collective pitch dynamics, and the rotational speed of the main rotor, presents a feasible solution that can tackle the nonlinear problem or controlling the vertical position of a helicopter by actuating in the collective pitch and the angular rotational speed of the blades. This selected dynamics of the helicopter becomes a highly nonlinear control problem that will require of advanced nonlinear control techniques, which are the main contribution of this thesis, and the perfection of a more detailed helicopter model that will model closely some of the nonlinear effects that are not contemplated, such the rotor model, the engine model or the collective pitch dynamics, will be left for later work since they are out of the scope of this thesis. This concludes the performance analysis comparisons for the proposed models, and following chapters will deal with the proposed control strategy to deal regulate this problem.

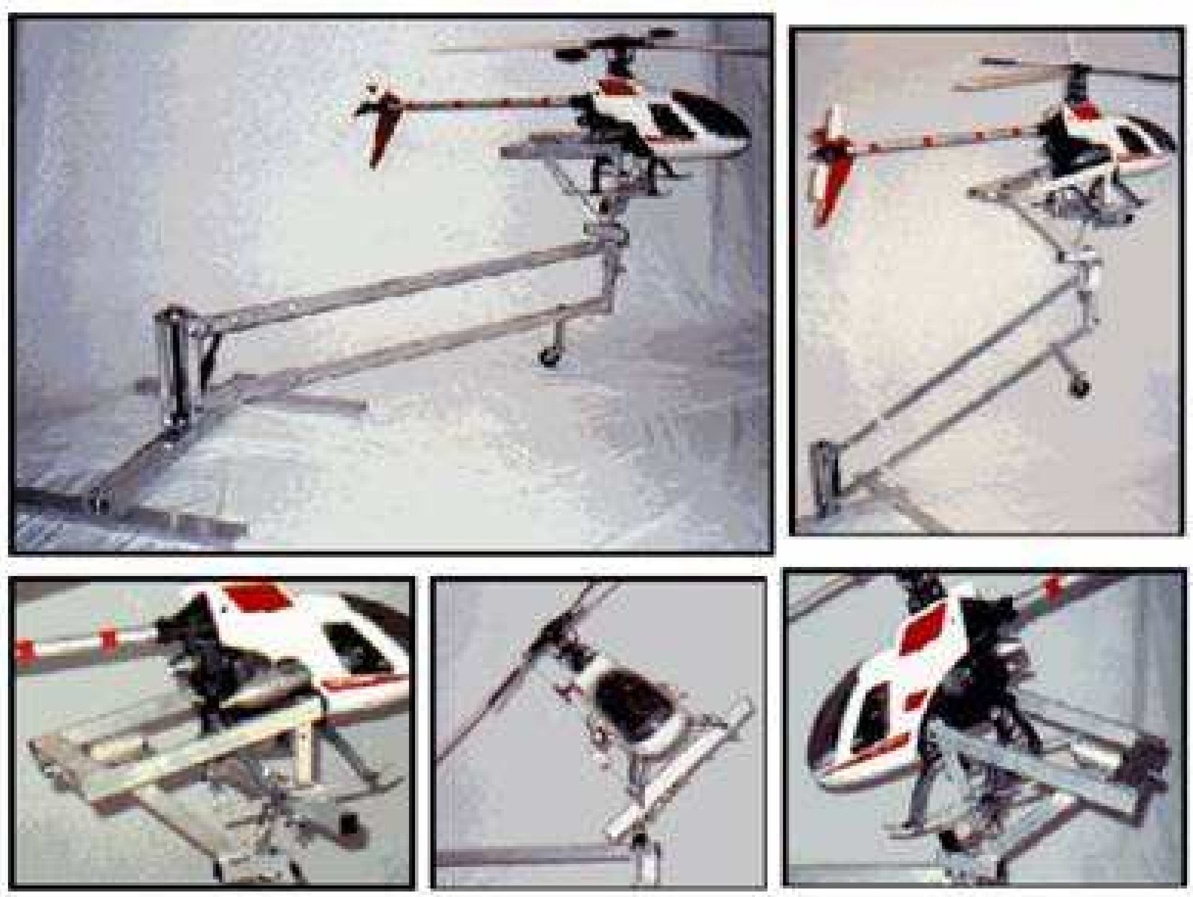

Figure A.12: Degrees of Freedom for the *Grupo de Control Nolineal* autonomous platform.

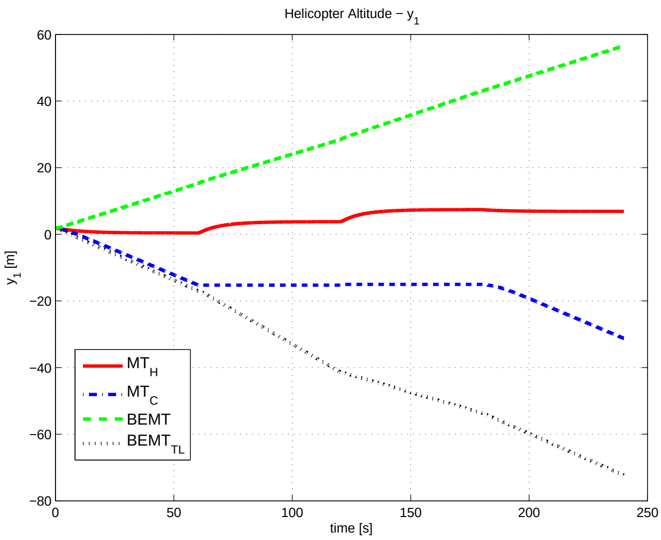

(a) y_1

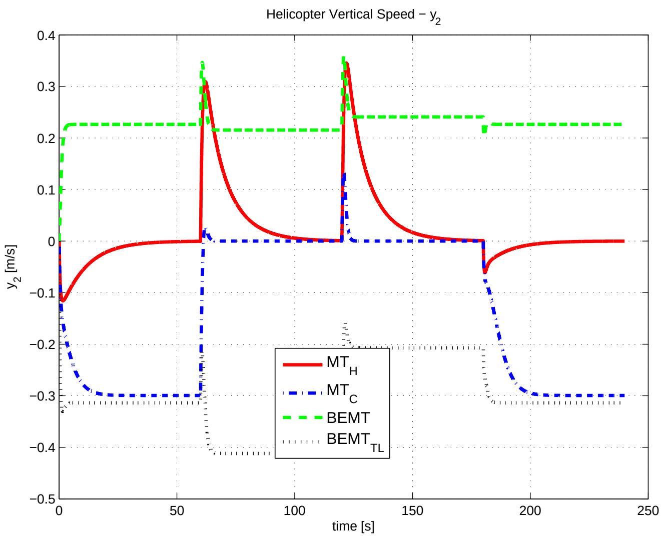

(b) y_2

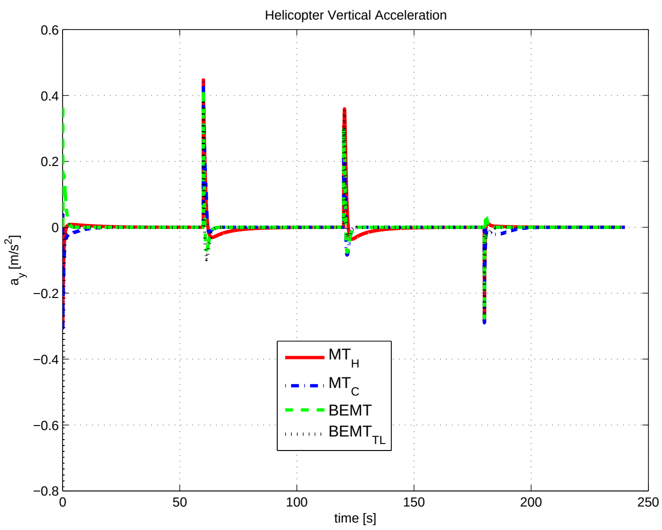

(c) a_y

Figure A.13: States History Comparing the Continuous MT_H, MT_C, $BEMT$ and $BEMT_{TL}$ Models for Constant Control

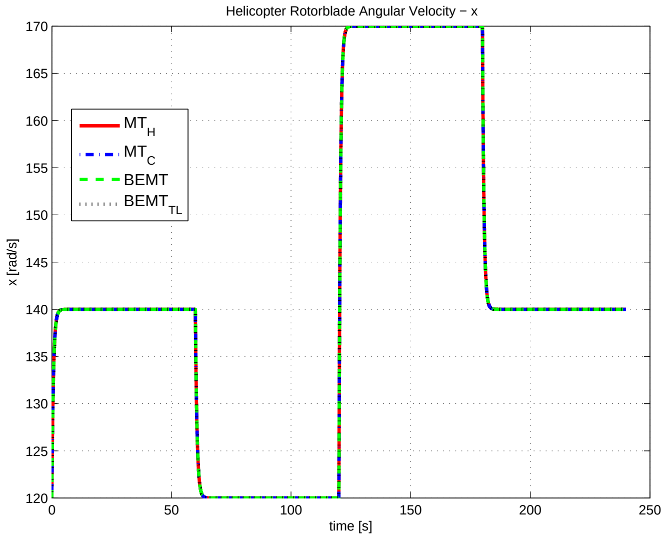

(a) x

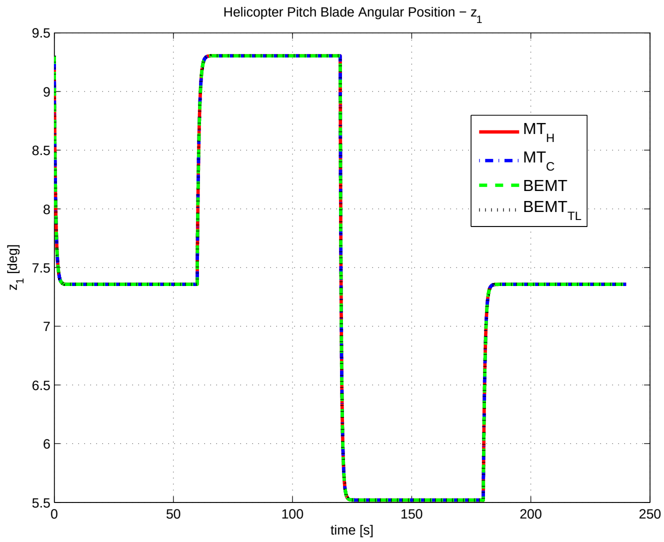

(b) z_1

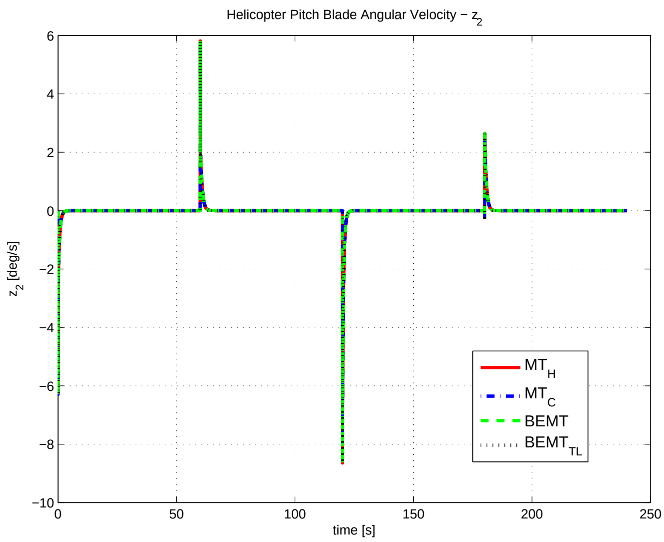

(c) z_2

Figure A.14: States History Comparing the Continuous MT_H, MT_C, $BEMT$ and $BEMT_{TL}$ Models for Constant Control

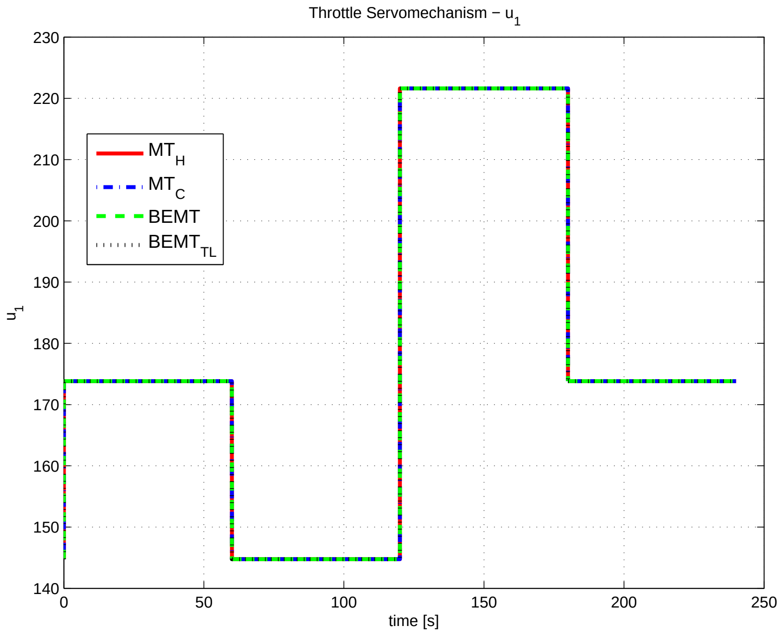

(a) u_1

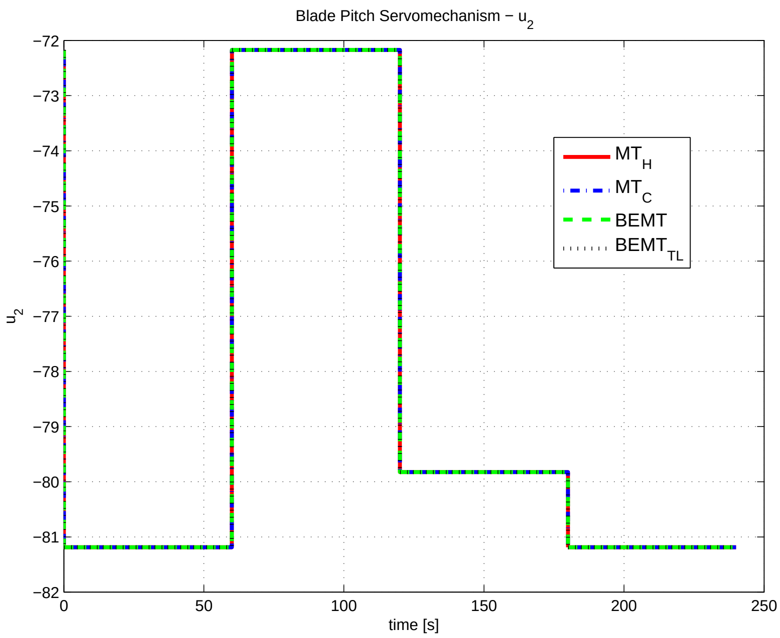

(b) u_2

Figure A.15: Control Signals History Comparing the Continuous MT_H, MT_C, $BEMT$ and $BEMT_{TL}$ Models for Constant Control

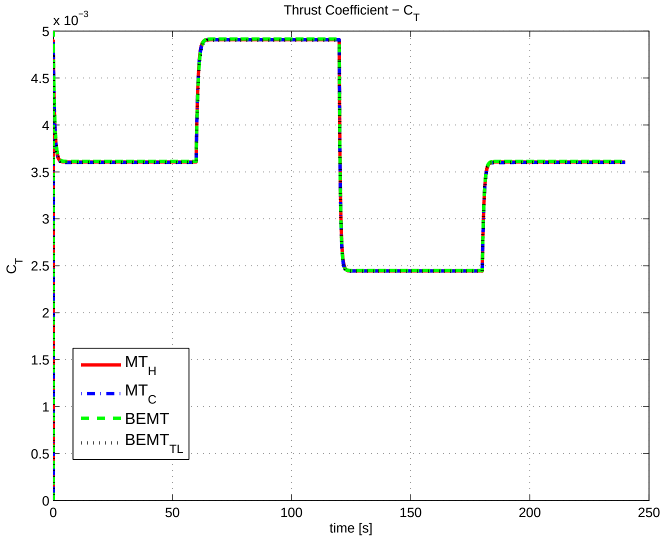

(a) C_T

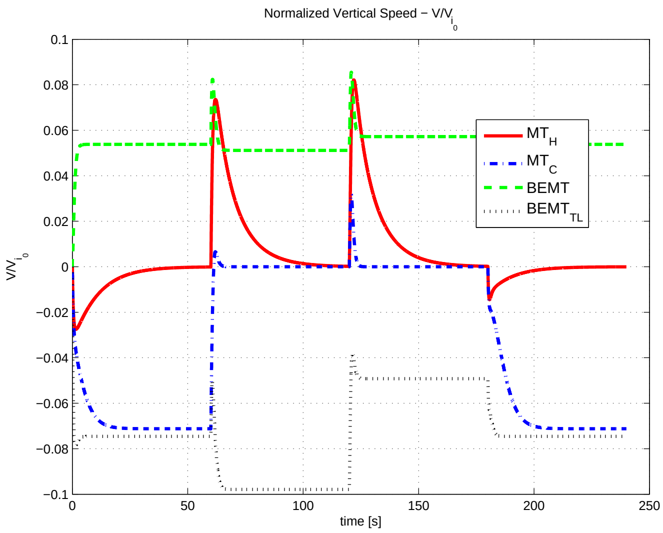

(b) y_2/v_i

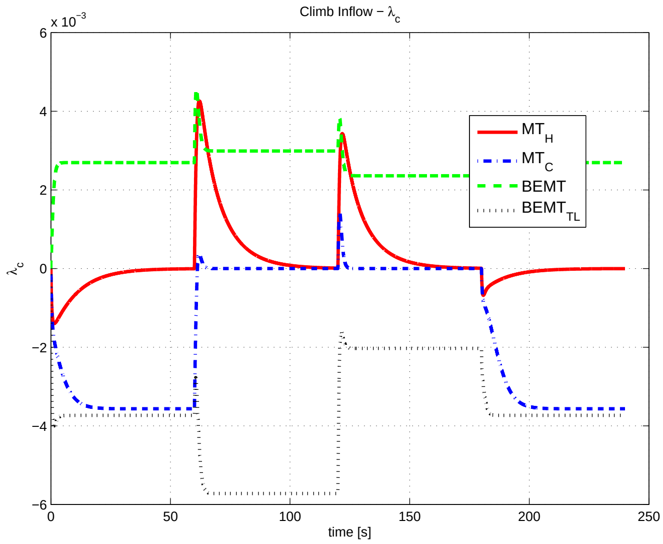

(c) λ_c

Figure A.16: Significate Aerodynamic Parameters History Comparing the Continuous MT_H, MT_C, $BEMT$ and $BEMT_{TL}$ Models for Constant Control

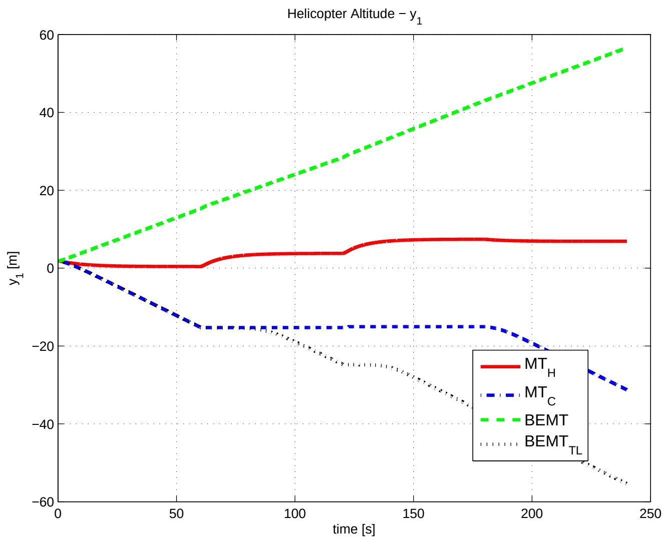

(a) y_1

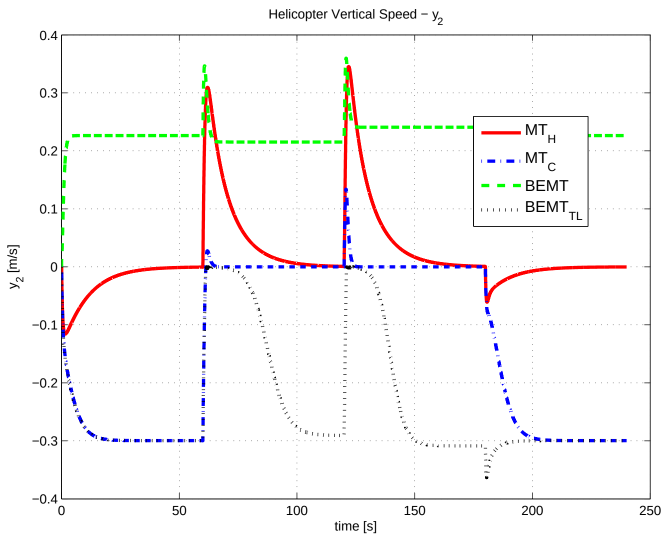

(b) y_2

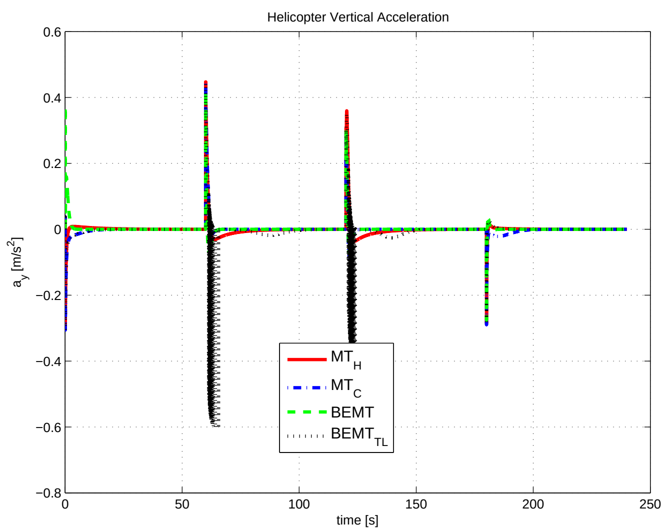

(c) a_y

Figure A.17: States History Comparing the Continuous MT_H, MT_C, $BEMT$ and $BEMT_{TL}$ Models for Constant Control

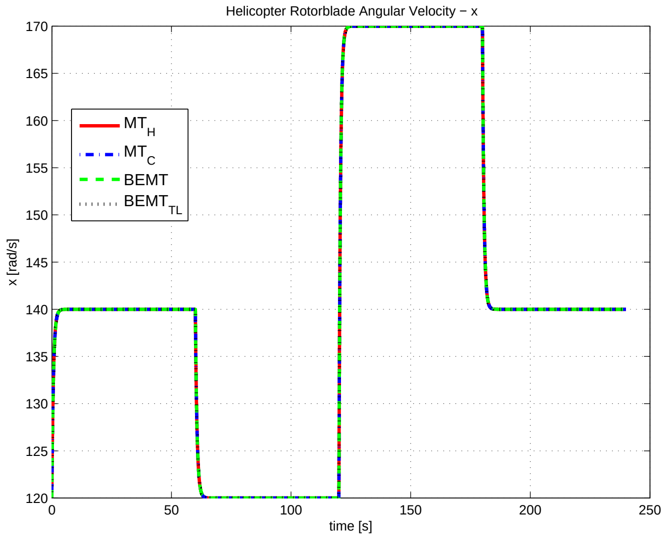

(a) x

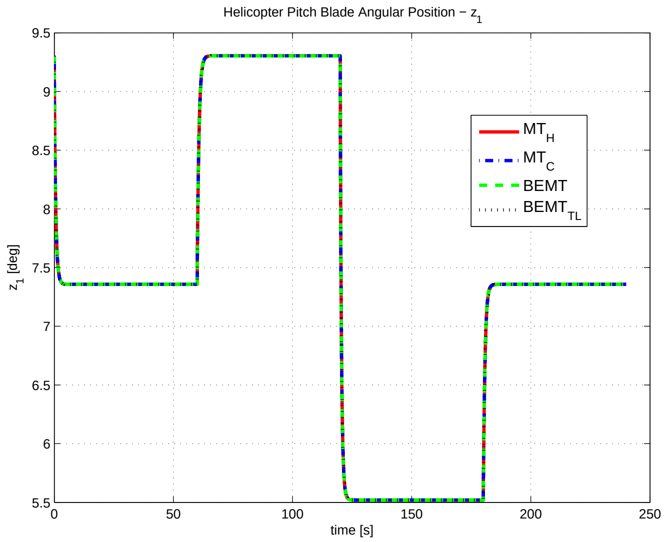

(b) z_1

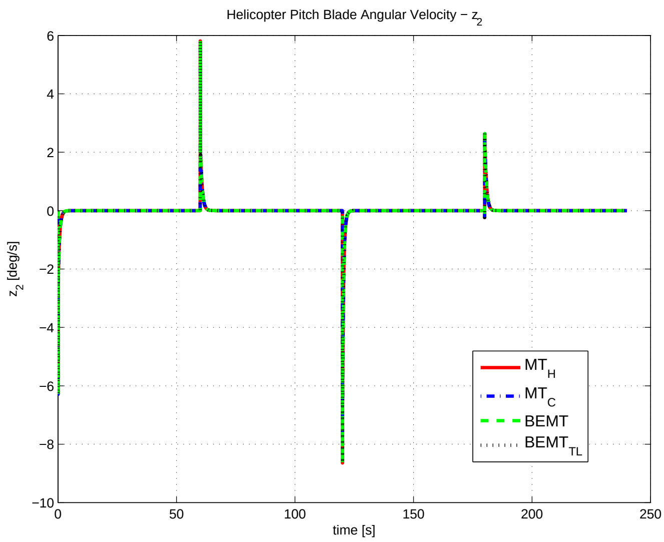

(c) z_2

Figure A.18: States History Comparing the Continuous MT_H, MT_C, $BEMT$ and $BEMT_{TL}$ Models for Constant Control

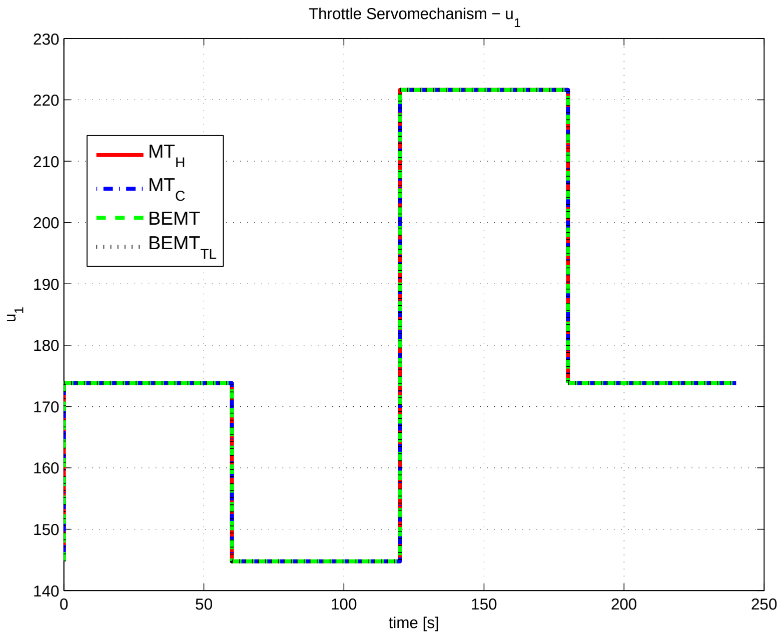

(a) u_1

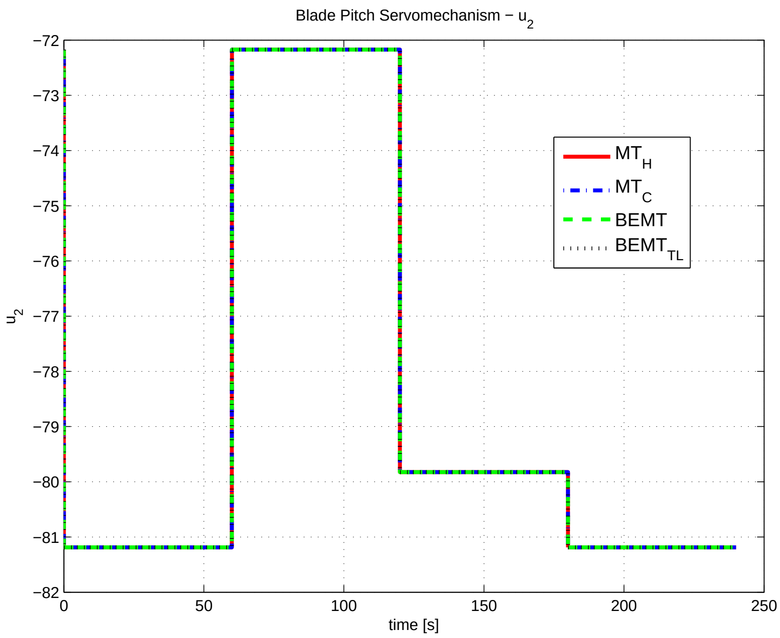

(b) u_2

Figure A.19: Control Signals History Comparing the Continuous MT_H, MT_C, $BEMT$ and $BEMT_{TL}$ Models for Constant Control

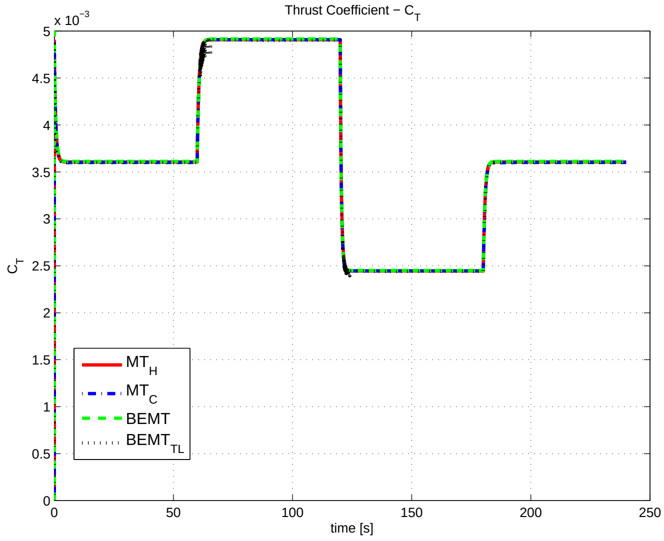

(a) C_T

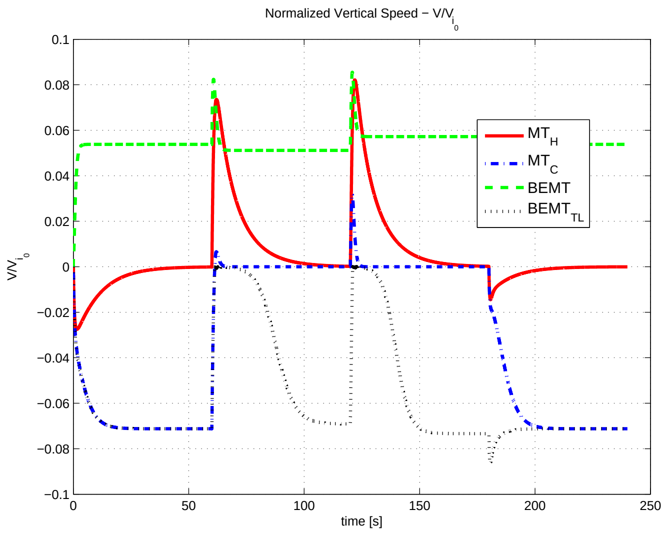

(b) y_2/v_i

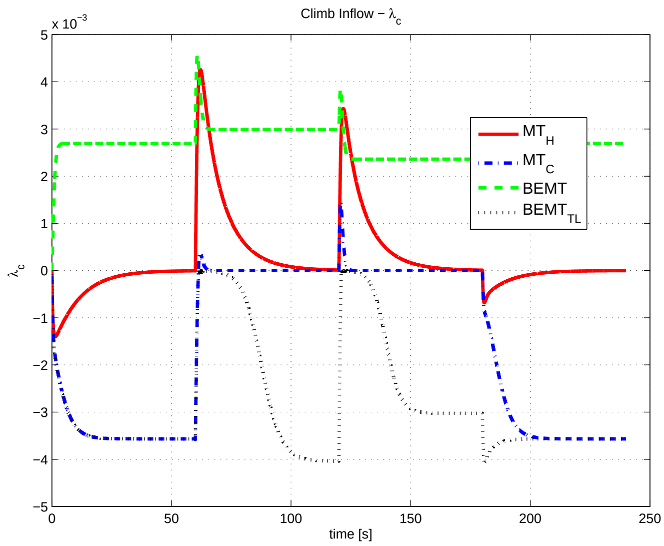

(c) λ_c

Figure A.20: Significate Aerodynamic Parameters History Comparing the Continuous MT_H, MT_C, $BEMT$ and $BEMT_{TL}$ Models for Constant Control

This page intentionally left blank

Appendix B

Control Strategies for the Simplified Example

B.1 Introduction

For completeness purposes, the proposed control strategies for both the *Top-Down* and *Bottom-Up* and the *Composite Feedback TD*, applied to the simplified model are presented in this appendix. The use of the simplified example will aid understanding these control strategies, and the reader can focus only on these example and only proceed to read in detail the helicopter's control strategy if wants to get into the details.

B.2 *Top-Down* Control Design for the Simplified Model

This section extends the *TD* control design for the simplified model by describing in detail both stages of the *TD* control design strategy for the simplified model, recalling that the simplified three-time-scale singularly perturbed model is given by

$$\dot{x} = -\rho_1\left(x + x^2 z + y\right) + u_1, \tag{B.1}$$

$$\varepsilon_1 \dot{y} = -\eta_1\left(y + xz + 1\right), \tag{B.2}$$

$$\varepsilon_1 \varepsilon_2 \dot{z} = -\eta_2\left(z + x^2 + y\right) + \eta_3 u_2. \tag{B.3}$$

Similarly as in the helicopter control design, the *TD* control strategy is divided in two stages, being each stage dedicated to design each of the two control signals. The first stage of the *TD* control strategy, applies sequentially the *Top* and *Down* time constant conditions, to select the control law that stabilizes the Σ_{FU}-subsystem using singular perturbation time-scale analysis to obtain the appropriate control law (u_2).

The second stage of the *TD* control strategy focuses on the *Top* sequence by using the first time-scale decomposition, along with the obtained results in the first time-scale decomposition, and proceeds to stabilize the Σ_S-subsystem with the proper u_1. The following sections describe in detail both stages of the *TD* control formulation applied to the simplified model.

B.2.1 Control Design for u_2: 1^{st} Stage of the *Top-Down* Control Design for the Simplified Model

The *TD* control strategy applies the *Top* stretched time constant, τ_1, to the Σ_{SFU} full system, Eqns. (B.1–B.3), resulting in the reduced order (slow) Σ_S-subsystem, given by

$$\dot{x} \quad = \quad \rho_1 \left[x + x^2 \mathrm{h}(x, u_2) + \mathrm{g}(x, u_2) \right] + u_1, \tag{B.4}$$

while the boundary layer (fast) Σ_{FU}-subsystem for the *TD* problem is defined by

$$\frac{\mathrm{d}y}{\mathrm{d}\tau_1} \quad = \quad -\eta_1 \left(y + xz + 1 \right), \tag{B.5}$$

$$\varepsilon_2 \frac{\mathrm{d}z}{\mathrm{d}\tau_1} \quad = \quad -\eta_2 \left(z + x^2 + y \right) + \eta_3 u_2, \tag{B.6}$$

where x is treated like a fix parameter, and $\tau_1 = t/\varepsilon_1$, and where functions $\mathrm{g}(x, u_2)$ and $\mathrm{h}(x, u_2)$ represent the quasi-steady-state equilibria of the boundary layer Σ_{FU}-subsystem, obtained by solving simultaneously when setting $\varepsilon_1 = 0$ in Eqns. (B.5–B.6), yielding

$$0 \quad = \quad \hat{h}(x, y, z, u_2) \to y = \mathrm{g}(x, u_2) = \frac{1}{1-x} \left(x^2 - \frac{\eta_3}{\eta_2} x u_2 \right) \tag{B.7}$$

$$0 \quad = \quad \hat{g}(x, y, z) \to z = \mathrm{h}(x, u_2) = -x^2 \left(1 + \frac{1}{1-x} \right) + \frac{\eta_3}{\eta_2} u_2 \left(1 + \frac{x}{1-x} \right), \tag{B.8}$$

where both $\mathrm{g}(x, u_2)$ and $\mathrm{h}(x, u_2)$ depend on the control law u_2, therefore being necessary to complete the *Down* sequence in order to completely determine both, the quasi-steady-state equilibria, and the control law u_2. The control law u_2 is selected by recognizing that the Σ_{FU}-subsystem can be decomposed again into a two-time-scale singular perturbation problem by applying the *Down* stretched time constant, $\tau_2 = \tau_1/\varepsilon_2 = t/(\varepsilon_1 \varepsilon_2)$, resulting in the new reduced (slow) Σ_F-subsystem given by

$$\frac{\mathrm{d}y}{\mathrm{d}\tau_1} \quad = \quad -\eta_1 \left(y + x\mathrm{h}(x, y, u_2) + 1 \right), \tag{B.9}$$

while the new boundary layer Σ_U-subsystem is given by

$$\frac{\mathrm{d}z}{\mathrm{d}\tau_2} \quad = \quad \hat{h}(x, y, z, u_2) = -\eta_2 \left(z + x^2 + y \right) + \eta_3 u_2, \tag{B.10}$$

with variables x and y being treated like fixed parameters. The quasi-steady-equilibrium $\mathrm{h}(x, y, u_2)$ of the new boundary layer Σ_U-subsystem, Eq. (B.10), is obtained by setting $\varepsilon_2 = 0$, resulting in

$$0 = \hat{h}(x, y, z, u_2) \to z = \mathrm{h}(x, y, u_2), \tag{B.11}$$

being

$$\mathrm{h}(x, y, u_2) = z = -x^2 - y + \frac{\eta_3}{\eta_2} u_2. \tag{B.12}$$

The control signal is embedded in the quasi-steady-state equilibrium $z = \mathrm{h}(x, y, u_2)$, Eq. (B.12), and it is substituted back into the reduced order Σ_F-subsystem, Eq. (B.9) resulting in

$$\begin{aligned} \frac{\mathrm{d}y}{\mathrm{d}\tau_1} \quad &= \quad -\eta_1 \left(y + x \left(-x^2 - y + \frac{\eta_3}{\eta_2} u_2 \right) + 1 \right) \\ &= \quad -\eta_1 \left(y - x^3 - x + 1 \right) - \frac{\eta_1 \eta_3}{\eta_2} x u_2. \end{aligned} \tag{B.13}$$

In order to stabilize the Σ_F-subsystem, let select the control signal such that the target dynamics behaves like

$$\frac{\mathrm{d}y}{\mathrm{d}\tau_1} \quad = \quad -\tilde{b}_y \left(y - y^* \right) = -\varepsilon_1 b_y \left(y - y^* \right), \tag{B.14}$$

where $\tilde{b}_y$ is the time constant that defines the desired dynamics of the stretched time-scale $\tau_1 = t/\varepsilon_1$, and selected as $\tilde{b}_y = \varepsilon_1 b_y$, where b_y is the time constant that defines the desired dynamics for the y variable, and y^* is the desired value of y, thus the control signal u_2 is selected such

$$u_2(x, y, y^*) = \frac{\eta_2}{\eta_1 \eta_3 x} \left(-\eta_1 \left(y - x^3 - yx + 1 \right) + \tilde{b}_y \left(y - y^* \right) \right). \tag{B.15}$$

As seen previously, it is assumed that the boundary layer is stable after selecting the control signal that stabilizes the Σ_F-subsystem, but does not provide a control strategy to stabilize the Σ_U-subsystem, which it is therefore, assumed to be inherently stable after substituting the derived control signal u_2. This can be proven by substituting u_2 in the Σ_U-subsystem, Eq. (B.10), which results in

$$\frac{\mathrm{d}z}{\mathrm{d}\tau_2} = -\eta_2 z - \frac{\eta_2}{x} \left(y + 1 - \frac{\tilde{b}_y}{\eta_1} \left(y - y^* \right) \right), \tag{B.16}$$

whose new quasi-steady-state equilibrium, $\mathrm{h}(x, y)$, is given by substituting Eq. (B.15) into (B.12) resulting in

$$z = \mathrm{h}(x, y) = -\frac{1}{x} \left(y + 1 - \frac{\tilde{b}_y}{\eta_1} \left(y - y^* \right) \right), \tag{B.17}$$

The stability of the Σ_U-subsystem can be analyzed by recognizing that the closed-loop Σ_U-subsystem, Eq. (B.16), posses inherent stability properties that can be identified by rewriting Eq. (B.16) using the definition of the quasi-steady-state equilibrium, Eq. (B.12) thus becoming

$$\begin{aligned} \frac{\mathrm{d}z}{\mathrm{d}\tau_2} &= -\eta_2 z - \frac{\eta_2}{x} \left(y + 1 - \frac{\tilde{b}_y}{\eta_1} \left(y - y^* \right) \right) \\ &= -\eta_2 \left[z + \frac{1}{x} \left(y + 1 - \frac{\tilde{b}_y}{\eta_1} \left(y - y^* \right) \right) \right] \\ &= -\eta_2 \left(z - \mathrm{h}(x, y) \right) = -\eta_2 \hat{z}, \end{aligned} \tag{B.18}$$

where $\hat{z}$ can be seen as the augmented state variable of the error between the ultra-fast state z and its quasi-steady-state equilibrium, $\mathrm{h}(x, y)$, which is stable, and with eigenvalue $\lambda = -\eta_2$, with $\eta_2 > 0$, therefore satisfying that the boundary layer Σ_U-subsystem is stable after selecting the control signal that stabilizes the Σ_F-subsystem.

This control strategy implies that the response of the Σ_U-subsystem can not be modified to include the desired stable behavior of the boundary layer, i.e. $\lambda = \lambda^*$ where λ^* is the desired eigenvalue of the closed-loop Σ_U-subsystem. An alternative control strategy for three-time-scale systems is derived in the Composite *Top-Down* and *Bottom-Up* ($\mathcal{CF}$-*TD*) control design section 4.6.1 that allows to select a desired behavior for the Σ_U-subsystem. For the *TD* control design described in this section, it is assumed that the prescribed degree of stability of the closed-loop Σ_U-subsystem, Eq. (B.18), satisfies the requirements of both stability and speed of the response. This concludes the first stage of the *TD* control design, and the following section describes the second stage of the *TD* control design.

B.2.2 Control Design for u_1: 2^{nd} Stage of the *Top-Down* Control Design for the Simplified Model

The second stage of the *TD* subproblem focuses on the control design for u_1 for the stabilization of the Σ_S-subsystem. For that purpose, recall first that after selecting the control signal $u_2(x, y, y^*)$, the Σ_{FU}-subsystem, Eqns. (B.5–B.6), can be rewritten as

$$\frac{\mathrm{d}y}{\mathrm{d}\tau_1} = -\eta_1 \left(y + xz + 1 \right), \tag{B.19}$$

$$\varepsilon_2 \frac{\mathrm{d}z}{\mathrm{d}\tau_1} = -\eta_2 \left(z - \mathrm{h}(x,y)\right) = -\eta_2 \hat{z}, \tag{B.20}$$

In order to determine the equilibria that will define the Σ_S-subsystem, Eq. (B.4), the Σ_{FU}-subsystem, Eqns. (B.19–B.20), can be decomposed by applying the stretched time scale τ_2 resulting in the Σ_F-subsystem given by

$$\frac{\mathrm{d}y}{\mathrm{d}\tau_1} = -\eta_1 \left(y + x\mathrm{h}(x,y) + 1\right), \tag{B.21}$$

and where the new boundary layer (fast) Σ_U-subsystem is defined by

$$\frac{\mathrm{d}z}{\mathrm{d}\tau_2} = -\eta_2 \left(z - \mathrm{h}(x,y)\right), \tag{B.22}$$

where the Σ_U-subsystem quasi-steady-state equilibria, $\mathrm{h}(x,y)$ is given in Eq. (B.17), which after being substituted into the Σ_F-subsystem, Eq. (B.21), reduces to

$$\frac{\mathrm{d}y}{\mathrm{d}\tau_1} = -\tilde{b}_y \left(y - y^*\right), \tag{B.23}$$

where the quasi-steady-state equilibrium of the boundary layer, Eq. (B.23), is obtained by setting $\varepsilon_1 = 0$, resulting in

$$0 = \hat{g}(x,y,\mathrm{h}(x,y)) = -\tilde{b}_y \left(y - y^*\right) \to y = \mathrm{g}(x) = y^*. \tag{B.24}$$

Recalling the quasi-steady-state equilibria for both the Σ_F and Σ_U-subsystems, that is $y = \mathrm{g}(x)$ and $z = \mathrm{h}(x,y)$, respectively, given by Eqns. (B.24) and (B.17), respectively, and also recall that substituting $\mathrm{g}(x)$ into Eq. (B.17), results in

$$z = \mathrm{h}(x,\mathrm{g}(x)) = -\frac{y^* + 1}{x}. \tag{B.25}$$

Therefore, substituting both quasi-steady-state equilibria, $y = \mathrm{g}(x)$ and $z = \mathrm{h}(x,\mathrm{g}(x))$, into the reduced order Σ_S-subsystem, Eq. (B.4), results in

$$\dot{x} = f(x,\mathrm{g}(x),\mathrm{h}(x,\mathrm{g}(x)),u_1) = -\rho_1 \left(x - xy^* + y^*\right) + u_1. \tag{B.26}$$

The control signal u_1 is selected such that stabilizes the Σ_S-subsystem by selecting a target dynamics of the form

$$\dot{x} = -b_x \left(x - x^*\right), \tag{B.27}$$

where b_x is the selected time constant for the target dynamics, and x^* is the desired value of x, thus the control signal u_1 is selected such

$$u_1(x,x^*,y^*) = \rho_1 y^* \left(1 - x\right) - b_x \left(x - x^*\right), \tag{B.28}$$

which concludes the *TD* control design.

B.2.3 Closed-Loop of the Simplified Model

After substituting the selected control laws, Eqns. (B.15) and (B.28), into the original nonlinear equations of motion, Eqns. (B.1–B.3), the closed loop system is given by

$$\dot{x} = -\rho_1 x \left(1 + xz + y^*\right) - \rho_1 \left(y - y^*\right) - b_x \left(x - x^*\right) \tag{B.29}$$

$$\dot{y} = -\rho_2 \left(y + xz + 1\right) \tag{B.30}$$

$$\dot{z} = -\rho_3 z - \frac{\rho_3}{x} \left(y + 1 - \frac{\tilde{b}_y}{\eta_1} \left(y - y^*\right)\right). \tag{B.31}$$

The equilibria of the closed-loop system are obtained by setting all derivatives of (B.29–B.33) to zero, resulting in the equilibrium of ultra-fast dynamics, Eq. (B.33) given by

$$z = h(x,y) = -\frac{1}{x}\left(y + 1 - \frac{\tilde{b}_y}{\eta_1}\left(y - y^*\right)\right), \tag{B.32}$$

Recall that observing the closed-loop ultra-fast dynamics, Eqns. (B.33), can be expressed as a function of a pseudo error dynamics by using the definition of the quasi-steady-state equilibrium $h_1(x,y)$, Eq. (B.32), resulting in

$$\begin{aligned}\dot{z} &= -\rho_3 z - \frac{\rho_3}{x}\left(y + 1 - \frac{\tilde{b}_y}{\eta_1}\left(y - y^*\right)\right) \\ &= -\rho_3\left(z - h(x,y)\right),\end{aligned} \tag{B.33}$$

where ρ_3 provides the transient response of the ultra-fast dynamics. The substitution of the equilibrium of the ultra-fast subsystem, Eq. (B.32) into the equilibrium equation for the fast dynamics, , Eq. (B.30), results in

$$\begin{aligned}0 &= -\rho_2\left(y + xh(x) + 1\right), \\ &= -\rho_2\left\{y + x\left[-\frac{1}{x}\left(y + 1 - \frac{\tilde{b}_y}{\eta_1}\left(y - y^*\right)\right)\right] + 1\right\} \\ &= -\frac{\rho_2}{\eta_1}b_y\left(y - y^*\right),\end{aligned} \tag{B.34}$$

yielding the fast equilibrium given by

$$y = y^*, \tag{B.35}$$

and finally, substituting the equilibria of both the ultra-fast subsystem, Eq. (B.32), and the fast subsystem, Eq. (B.35), into the equilibrium equation for the slow dynamics, Eq. (B.29), results in

$$\begin{aligned}0 &= -\rho_1 x\left\{1 + x\left[-\frac{1}{x}\left(y^* + 1 - \frac{\tilde{b}_y}{\eta_1}\left(y^* - y^*\right)\right)\right] + y^*\right\} - \rho_1\left(y^* - y^*\right) \\ &- b_x\left(x - x^*\right) \qquad (B.36) \\ &= -b_x\left(x - x^*\right), \qquad (B.37)\end{aligned}$$

yielding the equilibrium of the slow dynamics

$$x = x^*. \tag{B.38}$$

The asymptotic stability analysis of the resulting closed-loop system will be conducted in future chapters.

B.3 *Composite Feedback TD* Control Design for the Simplified Model

This section extends the $\mathcal{CF}$-*TD* control design for the nonlinear underactuated three-time-scale singularly perturbed simplified model given by

$$\begin{aligned}\dot{x} &= \rho_1\left(x + x^2 z + 1\right) + u_1, \qquad (B.39) \\ \varepsilon_1\dot{y} &= -\eta_1\left(y + xz + 1\right), \qquad (B.40) \\ \varepsilon_1\varepsilon_2\dot{z} &= -\eta_2\left(z + x^2 + y\right) + \eta_3 u_{2_c} = -\eta_2\left(z + x^2 + y\right) + \eta_3\left(u_{2_s} + u_{2_f}\right). \qquad (B.41)\end{aligned}$$

where the main difference with the Σ_{SFU} subsystem analyzed in the *TD* control design, Eqns. (B.1–B.3), is the fact that the control signal in the ultra-fast dynamics is divided into two components, $u_{2_c} = u_{2_s} + u_{2_f}$, which will allow to select the desired transient behavior for the Σ_U-subsystem.

The control strategy focuses first on defining a control signal, $u_{2_s} = \Gamma_s(x, \boldsymbol{y})$, that stabilizes the intermediate fast Σ_F-subsystem with the desired degree of stability, while $u_{2_f} = \Gamma_f(x, \boldsymbol{y}, \boldsymbol{z})$ is a feedback function of x, y, and z, that stabilizes the ultra-fast Σ_U-subsystem with the desired degree of stability. Once stabilized the Σ_{FU}-subsystem, the control strategy shifts towards obtaining the control signal u_1 that stabilizes the Σ_S-subsystem. The following subsections describe in detail each one of the $\mathcal{CF}$-*TD* control methods for the helicopter problem.

B.3.1 Control Design for u_2: 1^{st} Stage of the *Composite Feedback Top-Down* Control Design for the Simplified Model

Similarly as in the *TD* control methodology, the $\mathcal{CF}$-*TD* control design starts by considering the subsystem that results when applying the *Top* condition to the original Σ_{SFU} (B.39–B.41), resulting in the reduced order (slow) Σ_S-subsystem, given by

$$\dot{x} \quad = \quad \rho_1 \left(x + x^2 \mathrm{h_c}(x, u_{2_c}) + \mathrm{g_c}(x, u_{2_c})\right) + u_1, \tag{B.42}$$

while the boundary layer (fast) Σ_{FU}-subsystem for the *TD* problem is defined by

$$\frac{\mathrm{d}y}{\mathrm{d}\tau_1} \quad = \quad -\eta_1 \left(y + xz + 1\right), \tag{B.43}$$

$$\varepsilon_2 \frac{\mathrm{d}z}{\mathrm{d}\tau_1} \quad = \quad -\eta_2 \left(z + x^2 + y\right) + \eta_3 u_{2_c}, \tag{B.44}$$

where x is treated like a fix parameter, and $\tau_1 = t/\varepsilon_1$, and where functions $\mathrm{g_c}(x, u_{2_c})$ and $\mathrm{h_c}(x, u_{2_c})$ represent the quasi-steady-state equilibrium of the boundary layer Σ_{FU}-subsystem, obtained by solving simultaneously when setting $\varepsilon_1 = 0$ in Eq. (B.43–B.44), given by

$$0 \quad = \quad \hat{h}(x, y, z, u_{2_c}) \rightarrow y = \mathrm{g_c}(x, u_{2_c}), \tag{B.45}$$

$$0 \quad = \quad \hat{g}(x, y, z) \rightarrow z = \mathrm{h_c}(x, u_{2_c}), \tag{B.46}$$

where

$$y \quad = \quad \mathrm{g_c}(x, u_{2_c}) = \frac{1}{1-x}\left(x^2 - \frac{\eta_3}{\eta_2} x u_{2_c}\right), \tag{B.47}$$

$$z \quad = \quad \mathrm{h_c}(x, u_{2_c}) = -x^2\left(1 + \frac{1}{1-x}\right) + \frac{\eta_3}{\eta_2} u_{2_c}\left(1 + \frac{x}{1-x}\right). \tag{B.48}$$

where both $\mathrm{g_c}(x, u_{2_c})$ and $\mathrm{h_c}(x, u_{2_c})$ depend on the control law u_{2_c}, therefore being necessary to complete the *Down* sequence in order to completely determine both, the quasi-steady-state equilibria, and the control law u_{2_c}. The control strategy employed obtains the associated control law u_{2_c} that stabilizes the Σ_{FU}-subsystem by applying the *Down* condition, by recalling that the $\mathcal{CF}$ control method seeks the control signal of the Σ_U-subsystem as the sum of the slow and fast control signals, that is

$$u_{2_c} = u_{2_s} + u_{2_f}, \tag{B.49}$$

with

$$u_{2_s} = \Gamma_s(x, y), \tag{B.50}$$

and

$$u_{2_f} = \Gamma_f(x, y, z), \tag{B.51}$$

thus becoming the Σ_{FU}-subsystem defined by

$$\frac{\mathrm{d}y}{\mathrm{d}\tau_1} = -\eta_1 \left(y + xz + 1\right), \tag{B.52}$$

$$\varepsilon_2 \frac{\mathrm{d}z}{\mathrm{d}\tau_1} = -\eta_2 \left(z + x^2 + y\right) + \eta_3 \left(u_{2_s} + u_{2_f}\right). \tag{B.53}$$

The fast feedback function $\Gamma_f(x, y, z)$ is designed to satisfy two crucial requirements. First, when the feedback control, Eq. (B.49), is applied to Eqns. (B.52–B.53), the closed-loop system should remain a standard singularly perturbed system, that is, the equilibrium equation given by

$$0 = \hat{h}(x, y, z, \Gamma_s(x) + \Gamma_f(x, z)), \tag{B.54}$$

should have a unique root given by $z = \mathrm{h_c}(x, y)$ in $B_x \times B_z$. This requirement assures that the choice of Γ_f will not destroy this property of the function $\hat{h}$ in the open-loop system. The second requirement on $\Gamma_f(x, y, z)$ is that it be *inactive* for $z = \mathrm{h_c}(x, y, u_{2_s})$, which translates in that

$$\Gamma_f(x, y, \mathrm{h_c}(x, y, \Gamma_s(x, y))) = 0, \tag{B.55}$$

therefore, by Eqns. (B.54) and (B.55), the new reduced (slow) subsystem, is now defined by

$$\frac{\mathrm{d}y}{\mathrm{d}\tau_1} = \hat{g}(x, y, \mathrm{h_c}(x, y, u_{2_s})) = -\eta_1 \left(y + x\mathrm{h_c}(x, y, u_{2_s}) + 1\right), \tag{B.56}$$

while the boundary layer Σ_U-subsystem of the Σ_{FU}-subsystem, Eqns. (B.43–B.44), is defined by

$$\frac{\mathrm{d}z}{\mathrm{d}\tau_2} = \hat{h}(x, y, z, u_{2_s}) = -\eta_2 \left(z + x^2 + y\right) + \eta_3 u_{2_s}, \tag{B.57}$$

where x and y are treated like fixed parameters, and where the quasi-steady-state equilibrium is given by

$$\mathrm{h_c}(x, y, u_{2_s}) = z = -x^2 - y + \frac{\eta_3}{\eta_2} u_{2_s}. \tag{B.58}$$

Substituting the quasi-steady-state equilibrium, Eq. (B.58), back into the reduced order system results in

$$\frac{\mathrm{d}y}{\mathrm{d}\tau_1} = -\eta_1 \left[+x \left(-x^2 - y + \frac{\eta_3}{\eta_2} u_{2_s} \right) + 1 \right] \tag{B.59}$$

$$= -\eta_1 \left(y - x^3 - yx + 1\right) - \frac{\eta_1 \eta_3}{\eta_2} x u_{2_s}. \tag{B.60}$$

In order to stabilize the Σ_F-subsystem, similarly as in the *TD* control strategy, let select the control signal such that the target dynamics behaves like

$$\frac{\mathrm{d}y}{\mathrm{d}\tau_1} = -\tilde{b}_y \left(y - y^*\right) = -\varepsilon_1 b_y \left(y - y^*\right), \tag{B.61}$$

where $\tilde{b}_y$ is the time constant that defines the desired dynamics of the stretched time-scale $\tau_1 = t/\varepsilon_1$, and is selected as $\tilde{b}_y = \varepsilon_1 b_y$, where b_y is the time constant that defines the desired dynamics for the y variable, and y^* is the desired value of y. The control signal u_{2_s} is therefore selected as

$$u_{2_s} = \frac{\eta_2}{\eta_1 \eta_3 x} \left[-\eta_1 \left(y - x^3 - yx + 1\right) + \tilde{b}_y \left(y - y^*\right) \right]. \tag{B.62}$$

therefore, recalling the definition of $\mathrm{h_c}(x, y, u_{2_s})$ in Eq. (B.58), the quasi-steady-state equilibrium reduces to

$$\mathrm{h_c}(x, y, u_{2_s}) = \mathrm{h_c}(x, y) = -x^2 - y + \frac{\eta_3}{\eta_2} u_{2_s}$$

$$= \quad -\frac{1}{x}\left(y+1-\frac{\tilde{b}_y}{\eta_1}\left(y-y^*\right)\right). \tag{B.63}$$

Once the design of the slow control $u_{2_s} = \Gamma_s(x,y)$ has been conducted, the strategy shifts towards selecting the desired degree of stability of the boundary layer Σ_U-subsystem. Let first analyze the resulting boundary layer after substituting the slow control $u_{2_s} = \Gamma_s(x,y)$, Eq. (B.62), resulting in

$$\begin{aligned}\frac{\mathrm{d}z}{\mathrm{d}\tau_2} &= -\eta_2\left(z+x^2+y\right)+\eta_3\left(u_{2_s}+u_{2_f}\right)\\ &= -\eta_2\left(z-\mathrm{h_c}(x,y)\right)+\eta_3 u_{2_f}.\end{aligned} \tag{B.64}$$

The requirement in Eq. (B.55) is now interpreted as a requirement on the feedback control $u_{2_f} = \Gamma_f(x,y,z)$ not to shift the equilibrium $z = \mathrm{h_c}(x,y,\Gamma_s(x,y))$ of the boundary layer system, Eq. (B.64). The design of u_{2_f} must guarantee that $z = \mathrm{h_c}(x,y,\Gamma_s(x,y))$ is an asymptotically stable equilibrium of Eq. (B.64) uniformly in x and y. Let therefore select a desired target dynamics for the boundary layer of the form

$$\frac{\mathrm{d}z}{\mathrm{d}\tau_2} = -\tilde{b}_z\left(z-\mathrm{h_c}(x,y)\right), \tag{B.65}$$

where $\tilde{b}_z$ is the time constant that defines the desired dynamics of the stretched time-scale $\tau_2 = t/\varepsilon_1\varepsilon_2$ and selected as $\tilde{b}_z = \varepsilon_1\varepsilon_2 b_z$. By selecting the target dynamics in that form, it is guaranteed that the requirement in Eq. (B.55) is satisfied. Analyzing the new boundary layer, Eq. (B.64), the fast control law is selected as

$$\begin{aligned}u_{2_f} &= \frac{1}{\eta_3}\left[\eta_2\left(z+x^2+1\right)-\tilde{b}_z\left(z-\mathrm{h_c}(x,y)\right)\right]+u_{2_s} = \frac{\eta_2-\tilde{b}_z}{\eta_3}\left(z-\mathrm{h_c}(x,y)\right)\\ &= \frac{\eta_2-\tilde{b}_z}{\eta_3}\left[z+\frac{1}{x}\left(y+1-\frac{\tilde{b}_y}{\eta_1}\left(y-y^*\right)\right)\right],\end{aligned} \tag{B.66}$$

therefore becoming the $\mathcal{CF}$-TD control law defined by

$$\begin{aligned}u_{2_c}(x,y,z,y^*) &= u_{2_s}+u_{2_f} = \frac{\eta_2}{\eta_3}\left(x^2+1+\mathrm{h_c}(x,y)\right)+\frac{\eta_2-\tilde{b}_z}{\eta_3}\left(z-\mathrm{h_c}(x,y)\right)\\ &= \frac{1}{\eta_3}\left[\eta_2\left(z+x^2+y\right)-\tilde{b}_z\left(z-\mathrm{h_c}(x,y)\right)\right],\end{aligned} \tag{B.67}$$

therefore becoming the closed loop boundary layer Σ_U-subsystem

$$\frac{\mathrm{d}z}{\mathrm{d}\tau_2} = -\eta_2\left(z+x^2+y\right)+\eta_3\left(u_{2_s}+u_{2_f}\right) = -\tilde{b}_z\left(z-\mathrm{h_c}(x,y)\right). \tag{B.68}$$

The design of u_{2_f} guarantees that $z = \mathrm{h_c}(x,y,\Gamma_s(x,y))$ is an asymptotically stable equilibrium of (B.64) uniformly in x and y. This has been satisfied with the appropriate selection of both u_{2_s} and u_{2_f} as seen in Eq. (B.68). This concludes the fisrt stage of the $\mathcal{CF}$-TD control design, which has only stabilized the Σ_{FU}-subsystem, and the following section focuses on stabilizing the remainder Σ_S-subsystem, starting with the stabilized Σ_{FU}-subsystem.

B.3.2 Control Design for u_1: 2^{nd} Stage of the *Composite Feedback Top-Down* Control Design for the Simplified Model

The second stage of the $\mathcal{CF}$-TD control design focuses on the selection of u_1 such that stabilizes the Σ_S-subsystem. For that purpose, recall first that, after selecting the control signal $u_{2_c}(x,y,z_1,y^*)$, Eq. (B.67), the Σ_{FU}-subsystem, Eqns. (B.52–B.53) can be rewritten as

$$\frac{\mathrm{d}y}{\mathrm{d}\tau_1} = -\eta_1\left(y+xz+1\right), \tag{B.69}$$

$$\varepsilon_2 \frac{\mathrm{d}z}{\mathrm{d}\tau_1} = -\tilde{b}_z \left[z + \frac{1}{x} \left(y + 1 - \frac{\tilde{b}_y}{\eta_1} (y - y^*) \right) \right] = -\tilde{b}_z (z - \mathrm{h_c}(x,y)) \,. \tag{B.70}$$

In order to determine the equilibria that will define the Σ_S-subsystem, Eq. (B.42), the Σ_{FU}-subsystem, Eqns. (B.69–B.70), can be decomposed into a two-time-scale subsystem by applying the stretched time scale τ_2 resulting in the Σ_F-subsystem given by

$$\frac{\mathrm{d}y}{\mathrm{d}\tau_1} = \hat{g}(x, y, \mathrm{h_c}(x,y)) = -\eta_1 (y + x\mathrm{h_c}(x,y) + 1) \,, \tag{B.71}$$

and the new boundary layer (fast) Σ_U-subsystem being defined by

$$\frac{\mathrm{d}z}{\mathrm{d}\tau_2} = \hat{h}(x,y,z) = -\tilde{b}_z \left[z + \frac{1}{x} \left(y + 1 - \frac{\tilde{b}_y}{\eta_1} (y - y^*) \right) \right] = -\tilde{b}_z (z - \mathrm{h_c}(x,y)) \,, \tag{B.72}$$

where, as previously defined in Eq. (B.63), the quasi-steady-state equilibrium of the Σ_U-subsystem being defined by

$$z = \mathrm{h_c}(x,y) = -\frac{1}{x} \left(y + 1 - \frac{\tilde{b}_y}{\eta_1} (y - y^*) \right) . \tag{B.73}$$

Recall that when substituting the quasi-steady-state equilibria of the Σ_U-subsystem, Eq. (B.73) into Eq. (B.71), the Σ_F-subsystem degenerates into the selected Σ_F-subsystem target dynamics given by and in the equivalent boundary layer Σ_F-subsystem, such

$$\frac{\mathrm{d}y}{\mathrm{d}\tau_1} = \hat{g}(x, y, \mathrm{h_c}(x,y)) = -\tilde{b}_y (y - y^*) \,, \tag{B.74}$$

therefore, with the quasi-steady-state equilibria $\mathrm{g_c}(x)$ being given by

$$y = \mathrm{g_c}(x) = y^*. \tag{B.75}$$

Similarly as in the *TD* control design, the control law u_1 that stabilizes the slow Σ_S-subsystem is obtained by substituting the Σ_F and Σ_U-subsystem equilibria, Eqns. (B.75) and (B.73), respectively, into Eq. (B.42), yielding the reduced order Σ_S-subsystem given by

$$\dot{x} = f(x, \mathrm{g_c}(x), \mathrm{h_c}(x,y), u_1) = \rho_1 x y^* - \rho_1 + u_1, \tag{B.76}$$

the control signal (u_1) is selected such that stabilizes the Σ_S-subsystem by selecting a target dynamics of the form

$$\dot{x} = -b_x (x - x^*) \,, \tag{B.77}$$

resulting in

$$u_1 = -\rho_1 x y^* + \rho_1 - b_x (x - x^*) \,, \tag{B.78}$$

thus concluding with the $\mathcal{CF}$-*TD* control design.

B.3.3 Closed-Loop of the Simplified Model

After substituting the selected control laws, Eqns. (B.67) and (B.78), into the original nonlinear equations of motion, Eqns. (B.1–B.3), the closed loop system is given by

$$\dot{x} = -\rho_1 x (1 + xz + y^*) - b_x (x - x^*) \,, \tag{B.79}$$

$$\dot{y} = -\rho_2 (y + xz + 1) \,, \tag{B.80}$$

$$\dot{z} = -b_z (z - \mathrm{h_c}(x,y)) = -b_z \left[z + \frac{1}{x} \left(y + 1 - \frac{\tilde{b}_y}{\eta_1} (y - y^*) \right) \right] . \tag{B.81}$$

with the equilibria of the closed-loop system being equivalent to those obtained with the *TD* control strategy, Eqns. (B.38), (B.35) and (B.32), with the only difference between both control strategies, being the transient response of the ultra-fast-dynamics.

Appendix C

Asymptotic Stability Analysis for the Simplified Model

C.1 Introduction

C.2 Simplified Example Model for the Asymptotic Stability Analysis

This Appendix describes the stability analysis conducted for the simplified model, which for conciseness, only is analyzed the closed-loop error dynamics for the *TD-BU* control design, see section B.2 for further details. As noted in chapter 6, the use of the simplified example stability analysis can be used by the reader for better understanding the scope of the presented three-time-scale asymptotic stability analysis, following the same philosophy intended by the author throughout this thesis, which is to serve as an instrument that will ease in the understanding of the presented analysis complexity. As discussed in previous chapters, the use of the three-time-scale simplified example stability analysis can be used as the solely source for understanding the asymptotic stability methodology here presented, and leave the asymptotic stability analysis for the helicopter model, once the methodology have been fully understood. Therefore, proceeding with the asymptotic stability analysis for the simplified example let first recall the original three-time-scale simplified model given by

$$\begin{aligned} \dot{x} &= \rho_1 \left(x + x^2 z + 1\right) + u_1, && \text{(C.1)} \\ \varepsilon_1 \dot{y} &= -\eta_1 \left(y + xz + 1\right), && \text{(C.2)} \\ \varepsilon_1 \varepsilon_2 \dot{z} &= -\eta_2 \left(z + x^2 + 1\right) + \eta_3 u_2. && \text{(C.3)} \end{aligned}$$

The closed-loop dynamics are obtained by recalling the laws derived in *Top-Down* and *BU* control design, that is u_1 and u_2, respectively, and given by

$$u_1 = -\rho_1 x y^* + \rho_1 - b_x \left(x - x^*\right), \tag{C.4}$$

and

$$u_2 = \frac{\eta_2}{\eta_1 \eta_3 x} \left(-\eta_1 \left(y - x^3 - x + 1\right) + \tilde{b}_y \left(y - y^*\right)\right). \tag{C.5}$$

Therefore, after substituting the selected control laws, Eqns. (C.4) and (C.5), into the original nonlinear equations of motion, Eqns. (C.1 – C.3), the closed loop system is given by

$$\begin{aligned}
\dot{x} &= -\rho_1 x\left(1 + xz + y^*\right) - b_x\left(x - x^*\right), && \text{(C.6)}\\
\varepsilon_1 \dot{y} &= -\eta_1\left(y + xz + 1\right), && \text{(C.7)}\\
\varepsilon_1\varepsilon_2 \dot{z} &= -\eta_2 z - \frac{\eta_2}{x}\left(y + 1 - \frac{\tilde{b}_y}{\eta_1}\left(y - y^*\right)\right). && \text{(C.8)}
\end{aligned}$$

As introduced in section 5.2.1, one of the requirements for the asymptotic stability analysis, is to guarantee that there exist asymptotic stability of the origin, which is expressed in Assumption 5.2.1. This translates to ensure that the boundary layer does not shift from its original equilibrium, that is, that the fastest time-scale maintains its quasi-steady-state equilibrium, given by $z = h(x)$. Since the systems here studied present equilibria different from zero, in order to satisfy this requirement, a change of variables is introduced such that defines the new system in terms of its error-dynamics.For the simplified three-time-scale model the error dynamics are defined by introducing

$$\begin{aligned}
\tilde{x} &= x - x^*, && \text{(C.9)}\\
\tilde{y} &= y - y^*, && \text{(C.10)}\\
\tilde{z} &= z - z^*, && \text{(C.11)}
\end{aligned}$$

where x^*, y^*, and z^* represent the desired values of the state variables. Due to the nature of the singularly perturbed systems, and its property of maintaining the equilibrium of the boundary layer, only the desired values of the slow and fast subsystems, that is x^*, y^*, are defined by the designer, while z^* is left as a free variable in the error dynamics formulation since the true error dynamics of the ultra-fast subsystem is considered when being compared with its quasi-steady-state equilibrium, $z = h(x, y)$. As the selected control law drives the slow and fast variables towards their desired states, that is $x \to x^*$ and $y \to y^*$, the ultra-fast variable moves through its configuration space given by $z = h(x, y)$, therefore becoming the equilibrium $z^* = h(x^*, y^*)$. It can be proven that the quasi-steady-state equilibrium of the ultra-fast dynamics, $z^* = h(x^*, y^*)$, is defined by the equilibrium differential equation of the intermediate dynamics, that is, the fast dynamics, resulting in

$$0 = y + xz + 1 \to z^* = -\frac{y^* + 1}{x^*}, \tag{C.12}$$

implying that, for a pair of desired x^* and y^*, the desired value of z^* is defined by Eq. (C.12). Therefore, the closed-loop equations can be rewritten into its error dynamics as

$$\begin{aligned}
\dot{\tilde{x}} &= -\rho_1\left(\tilde{x} + x^*\right)\left(1 + \left(\tilde{x} + x^*\right)\left(\tilde{z} + z^*\right) + y^*\right) - b_x\tilde{x}, && \text{(C.13)}\\
\varepsilon_1\dot{\tilde{y}} &= -\eta_1\left(\left(\tilde{y} + y^*\right) + \left(\tilde{x} + x^*\right)\left(\tilde{z} + z^*\right) + 1\right), && \text{(C.14)}\\
\varepsilon_1\varepsilon_2\dot{\tilde{z}} &= -\eta_2\left(\tilde{z} + z^*\right) - \frac{\eta_2}{\tilde{x} + x^*}\left(\left(\tilde{y} + y^*\right) + 1 - \frac{\tilde{b}_y}{\eta_1}\tilde{y}\right). && \text{(C.15)}
\end{aligned}$$

To help with the demonstration of the growth requirements, the following sections recap on the degenerated subsystems for the simplified model, that is the Σ_S, Σ_F, Σ_U, Σ_{SF}, and Σ_{UF}-subsystems. It also describes the quasi-steady-state equilibria for the Σ_F and Σ_U-subsystems, that is $\tilde{y} = \tilde{\mathrm{g}}(\tilde{x})$ and $\tilde{z} = \tilde{\mathrm{h}}(\tilde{x}, \tilde{y})$, respectively, and also, the associated Lyapunov functions for the three degenerated subsystems, V_s, V_f and V_u.

C.3 Lyapunov *Top-Dow* and *Bottom-Up* Function Candidate Selection for the Simplified Example

This section determines the associated Lyapunov functions for the closed-loop simplified example three-time-scale singular perturbed system, Eqns. (C.13–C.15), where it is assumed that the system is an autonomous stable system, with prescribed stability properties given by the selection of appropriate control laws derived following the *TD* and *BU* methodologies. The strategy to determine the Lyapunov candidates for each one of the singularly perturbed subsystems, Σ_S, Σ_F, and Σ_U, respectively, consists on treating the three different time scales as two distinct two-time-scale singular perturbed problems, as described in the general $\mathcal{L}$-*TDBU* function selection, section 5.4.1. The following sections describe the selection of the Lyapunov function candidates for each of the singularly perturbed Σ_S, Σ_F, and Σ_U subsystems.

C.3.1 Lyapunov Function Candidate for the Simplified Example Σ_S-Subsystem

The Lyapunov function candidate for the Σ_S-subsystem is obtained by applying the stretched time-scale $\tau_2 = t/\varepsilon_1\varepsilon_2$, yielding the reduced (slow) Σ_{SF}-subsystem defined by

$$\begin{aligned} \dot{\tilde{x}} &= \tilde{f}(\tilde{x},\tilde{y},\tilde{\mathrm{h}}(\tilde{x},\tilde{y})) = \rho_1\left((\tilde{x}+x^*) + (\tilde{x}+x^*)^2\,\tilde{\mathrm{h}}(\tilde{x},\tilde{y}) + (\tilde{x}+x^*)\,y^*\right) - b_x\tilde{x}, && \text{(C.16)}\\ \varepsilon_1\dot{\tilde{y}} &= \tilde{g}(\tilde{x},\tilde{y},\tilde{\mathrm{h}}(\tilde{x},\tilde{y})) = -\eta_1\left((\tilde{y}+y^*) + (\tilde{x}+x^*)\,\tilde{\mathrm{h}}(\tilde{x},\tilde{y}) + 1\right), && \text{(C.17)} \end{aligned}$$

and where the boundary layer (fast) subsystem for the *BU* subproblem is defined by the Σ_U-subsystem

$$\frac{d\tilde{z}}{d\tau_2} = \tilde{h}(\tilde{x},\tilde{y},\tilde{z}) = -\eta_2\,(\tilde{z}+z^*) - \frac{\eta_2}{\tilde{x}+x^*}\left((\tilde{y}+y^*) + 1 - \frac{\tilde{b}_y}{\eta_1}\tilde{y}\right), \tag{C.18}$$

where the quasi-steady-state of the boundary layer $\tilde{\mathrm{h}}(\tilde{x},\tilde{y})$ is given by

$$\tilde{\mathrm{h}}(\tilde{x},\tilde{y}) = -\frac{1}{\tilde{x}+x^*}\left[(\tilde{y}+y^*) + 1 - \frac{\tilde{b}_y}{\eta_1}\tilde{y}\right] - z^*. \tag{C.19}$$

The boundary layer Σ_{SF}-subsystem is decomposed again into a two-time-scale singular perturbation problem by applying the stretched time-scale given by $\tau_1 = t/\varepsilon_1$, where the new reduced (slow) Σ_S-subsystem, is now defined by

$$\begin{aligned} \dot{\tilde{x}} &= \tilde{f}(\tilde{x},\tilde{\mathrm{g}}(\tilde{x}),\tilde{\mathrm{h}}(\tilde{x},\tilde{\mathrm{g}}(\tilde{x}))\\ &= \rho_1\left((\tilde{x}+x^*) + (\tilde{x}+x^*)^2\,\tilde{\mathrm{h}}(\tilde{x},\tilde{\mathrm{g}}(\tilde{x})) + (\tilde{x}+x^*)\,y^*\right) - b_x\tilde{x}\\ &= -b_x\tilde{x}, && \text{(C.20)} \end{aligned}$$

and the new boundary layer (fast) Σ_F-subsystem is defined as

$$\frac{d\tilde{y}}{d\tau_1} = \tilde{g}(\tilde{x},\tilde{y},\tilde{\mathrm{h}}(\tilde{x},\tilde{y})) = -\tilde{b}_y\tilde{y}, \tag{C.21}$$

with the quasi-steady-state equilibria of the boundary layer Σ_F-subsystem, Eq. (C.21), being given by

$$0 = \tilde{g}(\tilde{x},\tilde{y},\tilde{z}) = \tilde{g}(\tilde{x},\tilde{y},\tilde{\mathrm{h}}(\tilde{x},\tilde{y})) \rightarrow \tilde{y} = \tilde{\mathrm{g}}(\tilde{x}), \tag{C.22}$$

being the quasi-steady-state defined by

$$\tilde{y} = \tilde{\mathrm{g}}(\tilde{x}) = y^*. \tag{C.23}$$

Recall that following the control design strategy described in section B.2.2, the Σ_S-subsystem is stabilized with a prescribed desired target dynamics, therefore the new reduced order Σ_S-subsystem, Eq. (C.45) it is defined by the same target dynamics, making it easy to define the associated Lyapunov function for the slow Σ_S-subsystem as the natural quadratic Lyapunov function of the selected target dynamics, that is

$$V_s\left(\tilde{x}\right) = \frac{1}{2} P_s \tilde{x}^2, \tag{C.24}$$

where P_s is the solution of the associated Lyapunov function for the selected target dynamics of the Σ_S-subsystem, and given by

$$P_s A_s + A_s P_s + Q_s = 0, \tag{C.25}$$

where Q_s is also a positive constant, $A_s = -b_x$, therefore P_s is given by

$$P_s = \frac{Q_s}{2b_x}, \tag{C.26}$$

where Q_s is a positive constant. Thus yielding the associated Lyapunov function

$$V_s\left(\tilde{x}\right) = \frac{1}{2} P_s \tilde{x}^2 = \frac{Q_s}{4\tilde{b}_x}\tilde{x}^2. \tag{C.27}$$

C.3.2 Lyapunov Function Candidate for the Simplified Example Σ_F-Subsystem

To obtaining the Lyapunov function candidate for the Σ_F-subsystem, let use the Lyapunov-*Top-Down* ($\mathcal{L}$-*TD*) methodology, which studies the system resulting by applying the stretched time-scale given by $\tau_1 = t/\varepsilon_1$, yielding the reduced order (slow) Σ_S-subsystem defined by Eq. (C.45), and where the boundary layer (fast) Σ_{FU}-subsystem is given by

$$\frac{d\tilde{y}}{d\tau_1} = \tilde{g}(\tilde{x},\tilde{y},\tilde{z}) = -\eta_1\left[(\tilde{y}+y^*) + (\tilde{x}+x^*)\left(\tilde{z}+z^*\right)+1\right], \tag{C.28}$$

$$\varepsilon_2\frac{dz}{d\tau_1} = \tilde{h}(\tilde{x},\tilde{y},\tilde{z}) = -\eta_2\tilde{z} - \frac{\eta_2}{\tilde{x}+x^*}\left[(\tilde{y}+y^*)+1-\frac{\tilde{b}_y}{\eta_1}\tilde{y}\right]. \tag{C.29}$$

The associated Lyapunov function for the Σ_F-subsystem is obtained by recognizing that the boundary layer Σ_{FU}-subsystem, Eqns. (C.28-C.29), can be treated again like a two-time-scale singular perturbation problem by dealing with the subsystem that results by applying the stretched time-scale given by $\tau_2 = \tau_1/\varepsilon_2 = t/\varepsilon_1\varepsilon_2$, where the new reduced (slow) Σ_F-subsystem for the simplified model is defined by Eq. (C.18), the boundary layer Σ_U-subsystem of the Σ_{FU}-subsystem is given by Eq. (C.18) and, with the quasi-steady-state equilibrium of the boundary layer Σ_U-subsystem, $\tilde{\mathrm{h}}(\tilde{x},\tilde{y})$, is given by Eq. (C.19). With this in mind, it is easy to define the associated Lyapunov function candidate for the Σ_F-subsystem as the natural quadratic Lyapunov function of the selected target dynamics, Eq. (C.21), that is

$$V_f\left(\tilde{y}\right) = \frac{1}{2} P_f \tilde{y}^2, \tag{C.30}$$

where P_f is the solution of the associated Lyapunov function for the selected target dynamics and given by

$$P_f A_f + A_f P_f + Q_f = 0, \tag{C.31}$$

where Q_f is also a positive constant, $A_f = -\tilde{b}_y$, and P_f is given by

$$P_f = \frac{Q_f}{2\tilde{b}_y}, \tag{C.32}$$

where Q_f is a positive constant. Thus yielding the associated Lyapunov function given by

$$V_f\left(\tilde{y}\right) = \frac{1}{2}P_f\tilde{y}^2 = \frac{Q_f}{4\tilde{b}_y}\tilde{y}^2. \tag{C.33}$$

The Σ_F-subsystem, as seen previously, serves as both the boundary layer of the Σ_{SF}-subsystem, and the reduced order of the Σ_{FU}-subsystem, becoming the interconnection subsystem between both the Σ_{SF} and Σ_{FU}-subsystems.

C.3.3 Lyapunov Function Candidate for the Simplified Example Σ_U-Subsystem

The associated Lyapunov functions for the Σ_U-subsystem is obtained by recognizing that the Σ_{FU}-subsystem, Eqns. (C.28–C.29), can be treated again like a two-time-scale singular perturbation problem by applying the stretched time-scale given by $\tau_2 = \tau_1/\varepsilon_2 = t/\varepsilon_1\varepsilon_2$, where the new reduced (slow) Σ_F-subsystem for the simplified model is now defined by Eq. (C.18), and the new boundary layer Σ_U-subsystem is given by Eq. (C.18).

Recall that it is necessary to ensure that the boundary layer Σ_U-subsystem does not to shift from the equilibrium $\tilde{z} = \tilde{\mathrm{h}}(\tilde{x},\tilde{y})$, since it is the equilibrium that defines the nature of the different reduced order subsystems, Σ_S and Σ_F-subsystems, respectively. It is therefore necessary to introduce a change of variables so that the equilibrium of this boundary-layer system is centered at zero, and thus permitting to select a natural Lyapunov function candidate to maintain the equilibrium $\tilde{z} = \tilde{\mathrm{h}}(\tilde{x},\tilde{y})$. This is obtained by introducing a change of variables defined by

$$\hat{z} = \tilde{z} - \tilde{\mathrm{h}}(\tilde{x},\tilde{y}), \tag{C.34}$$

with $\tilde{\mathrm{h}}(\tilde{x},\tilde{y})$ being the quasi-steady-state equilibrium for the Σ_U-subsystem and being defined by Eq. (C.19). This change of variable permits to express the boundary layer Σ_U-subsystem, Eq. (C.18), as a linear function of $\hat{z}$, which can be viewed as the true error dynamics vector for the ultra-fast dynamics,therefore rewriting the Σ_U-subsystem as

$$\begin{aligned}\frac{d\tilde{z}}{d\tau_2} &= -\eta_2\left(\tilde{z}+z^*\right) - \frac{\eta_2}{\tilde{x}+x^*}\left(\left(\tilde{y}+y^*\right)+1-\frac{\tilde{b}_y}{\eta_1}\tilde{y}\right)\\ &= -\eta_2\left[\tilde{z}-\left[-\frac{1}{\tilde{x}+x^*}\left(\left(\tilde{y}+y^*\right)+1-\frac{\tilde{b}_y}{\eta_1}\tilde{y}\right)-z^*\right]\right]\\ &= -\eta_2\left(\tilde{z}-\tilde{\mathrm{h}}\left(\tilde{x},\tilde{y}\right)\right) = -\eta_2\hat{z},\end{aligned} \tag{C.35}$$

thus being quite simple to select its natural associated Lyapunov function V_u of the form given by

$$V_u(\tilde{x},\tilde{y},\tilde{z}) = V_u(\hat{z}) = \frac{1}{2}P_u\hat{z}^2, \tag{C.36}$$

where P_u is a positive constant that solves the associated Lyapunov equation

$$P_uA_u + A_u^TP_u + Q_u = 0, \tag{C.37}$$

where Q_u is also a positive constant, $A_u = -\eta_2$, and with $\eta_2 > 0$, and P_u is given by

$$P_u = \frac{Q_u}{2\eta_2}, \tag{C.38}$$

therefore yielding the associated Lyapunov function

$$V_u(\hat{z}) = \frac{1}{2}P_u\hat{z}^2 = \frac{Q_u}{4\eta_2}\hat{z}^2. \tag{C.39}$$

C.3.4 Degenerated Subsystems for the Simplified Model

For completeness, and to help while reading the asymptotic stability analysis, this section collects the different degenerated subsystems employed throughout the rest of the asymptotic stability analysis for the simplified model, that is the associated Σ_S, Σ_F, Σ_U, Σ_{SF}, and Σ_{UF}-subsystems. The associated quasi-steady-state equilibria for the Σ_F and Σ_U-subsystems are also collected. These subsystems were previously derived to determine the appropriate Lyapunov functions, therefore the complete derivations will not be conducted again, and only a brief description will be presented. Recalling from section C.3, the Σ_{SF}-subsystem is given by

$$\begin{aligned}
\dot{x} &= -\rho_1\left(\tilde{x}+x^*\right)\left(1+\left(\tilde{x}+x^*\right)\left(\tilde{\mathrm{h}}(\tilde{x},\tilde{y})+z^*\right)+y^*\right)-b_x\tilde{x}, &\text{(C.40)}\\
\varepsilon_1\dot{y} &= -\eta_1\left(\left(\tilde{y}+y^*\right)+\left(\tilde{x}+x^*\right)\left(\tilde{\mathrm{h}}(\tilde{x},\tilde{y})+z^*\right)+1\right), &\text{(C.41)}
\end{aligned}$$

therefore being $\tilde{f}(\tilde{x},\tilde{y},\tilde{\mathrm{h}}(\tilde{x},\tilde{y}))$ given by

$$\dot{x} = -\rho_1\left(\tilde{x}+x^*\right)\left(1+\left(\tilde{x}+x^*\right)\left(\tilde{\mathrm{h}}(\tilde{x},\tilde{y})+z^*\right)+y^*\right)-b_x\tilde{x}, \tag{C.42}$$

and $\tilde{g}(\tilde{x},\tilde{y},\tilde{\mathrm{h}}(\tilde{x},\tilde{y}))$ being defined by

$$\varepsilon_1\dot{y} = -\eta_1\left(\left(\tilde{y}+y^*\right)+\left(\tilde{x}+x^*\right)\left(\tilde{\mathrm{h}}(\tilde{x},\tilde{y})+z^*\right)+1\right). \tag{C.43}$$

The associated boundary layer for the Σ_U-subsystem is given by

$$\frac{d\tilde{z}}{d\tau_2} = -\eta_2\left(\tilde{z}+z^*\right)-\frac{\eta_2}{\tilde{x}+x^*}\left(\left(\tilde{y}+y^*\right)+1-\frac{\tilde{b}_y}{\eta_1}\tilde{y}\right), \tag{C.44}$$

with the quasi-steady-state equilibria of the boundary layer Σ_U-subsystem, Eq. (C.44), being given by

$$\tilde{\mathrm{h}}(\tilde{x},\tilde{y}) = \tilde{z} = -\frac{1}{\tilde{x}+x^*}\left[\left(\tilde{y}+y^*\right)+1-\frac{\tilde{b}_y}{\eta_1}\tilde{y}\right]-z^*. \tag{C.45}$$

The Σ_U-subsystem can be reorganized resulting in

$$\begin{aligned}
\frac{d\tilde{z}}{d\tau_2} &= -\eta_2\left(\tilde{z}+z^*\right)-\frac{\eta_2}{\tilde{x}+x^*}\left(\left(\tilde{y}+y^*\right)+1-\frac{\tilde{b}_y}{\eta_1}\tilde{y}\right)\\
&= -\eta_2\left[\tilde{z}-\left[-\frac{1}{\tilde{x}+x^*}\left(\left(\tilde{y}+y^*\right)+1-\frac{b_y}{\eta_1}\tilde{y}\right)-z^*\right]\right]\\
&= -\eta_2\left(\tilde{z}-\tilde{\mathrm{h}}\left(\tilde{x},\tilde{y}\right)\right), &\text{(C.46)}
\end{aligned}$$

where it can be recognized that the Σ_U-subsystem can be rewritten in state space form by considering the change of variables

$$\hat{z} = \tilde{z}-\tilde{\mathrm{h}}(\tilde{x},\tilde{y}), \tag{C.47}$$

reducing to

$$\frac{d\tilde{z}}{d\tau_2} = A_u\hat{z}, \tag{C.48}$$

where

$$A_u = -\eta_2. \tag{C.49}$$

The $\tilde{f}(\tilde{x}, \tilde{y}, \tilde{\mathrm{h}}(\tilde{x}, \tilde{y}))$ can be rewritten by substituting Eq. (C.45) into Eq. (C.42), resulting in

$$\begin{aligned} \dot{x} &= -\rho_1 (\tilde{x} + x^*) \left\{ 1 + (\tilde{x} + x^*) \left(-\frac{\eta_2}{\tilde{x} + x^*} \left((\tilde{y} + y^*) + 1 - \frac{\tilde{b}_y}{\eta_1} \tilde{y} \right) \right) + y^* \right\} - b_x \tilde{x} \\ &= (\tilde{x} + x^*)\, \tilde{y} \left(\rho_1 - \frac{\rho_1}{\eta_1} b_x \right) - b_x \tilde{x}, \end{aligned} \tag{C.50}$$

where recalling that from the time-scale selection

$$\varepsilon_1 = \frac{\rho_1}{\rho_2}, \tag{C.51}$$

and recalling that

$$\eta_1 = \rho_2 \varepsilon_1, \tag{C.52}$$

thus, using Eq. (C.51) into Eq. (C.52) results in

$$\eta_1 = \rho_2 \varepsilon_1 = \rho_2 \frac{\rho_1}{\rho_2} = \rho_1, \tag{C.53}$$

therefore using Eq. (C.53) into Eq. (C.50) reduces to

$$\tilde{f}(\tilde{x}, \tilde{y}, \tilde{\mathrm{h}}(\tilde{x}, \tilde{y})) \quad = \quad (\tilde{x} + x^*)\, \tilde{y}\, (\rho_1 - b_y) - b_x \tilde{x}. \tag{C.54}$$

Similarly, rewriting $\tilde{g}(\tilde{x}, \tilde{y}, \tilde{\mathrm{h}}(\tilde{x}, \tilde{y}))$, by substituting Eq. (C.45) into Eq. (C.43) results in

$$\frac{d\tilde{y}}{d\tau_1} = \tilde{g}(\tilde{x}, \tilde{y}, \tilde{\mathrm{h}}(\tilde{x}, \tilde{y})) = -\tilde{b}_y \tilde{y} = A_f \tilde{y}. \tag{C.55}$$

The quasi-steady-state equilibrium of the Σ_F-subsystem, $\tilde{\mathrm{g}}(\tilde{x})$, is given by

$$\tilde{\mathrm{g}}(\tilde{x}) \quad = \quad 0. \tag{C.56}$$

The Σ_S-subsystem $\tilde{f}(\tilde{x}, \tilde{\mathrm{g}}(\tilde{x}), \tilde{\mathrm{h}}(\tilde{x}, \tilde{y}))$, is given by

$$\dot{\tilde{x}} \quad = \quad \tilde{f}(\tilde{x}, \tilde{\mathrm{g}}(\tilde{x}), \tilde{\mathrm{h}}(\tilde{x}, \tilde{y})) = \tilde{f}(\tilde{x}, \tilde{\mathrm{g}}(\tilde{x}), \tilde{\mathrm{h}}(\tilde{x}, \tilde{\mathrm{g}}(\tilde{x}))) = -b_x \tilde{x} = A_s \tilde{x}, \tag{C.57}$$

C.4 Σ_{SF} *Stability Analysis* for the Simplified Model

This section provides the proof for the asymptotic stability requirements for the Σ_{SF}-subsystem simplified example, by applying the *Bottom-Up*-methodology using the same methodology as the one described previously for the general model in chapter 5. These requirements are defined by applying the assumptions defined in section 5.5.1, that is, Assumptions, 5.5.1, 5.5.2, 5.5.3, 5.5.4, and 5.5.5, to the simplified example resulting autonomous system, Eqns. (C.13–C.15.).

The Σ_{SF} *Stability Analysis* is performed assuming that the Σ_U-subsystem variables evolve in their own configuration space. The analysis of this first stage is performed using the standard method for two-time-scale systems (Kokotović et al., 1986; Kokotović et al., 1987; Kokotović et al., 1999), in which the previously derived Lyapunov functions for the Σ_S and Σ_F-subsystems, $V_s(\tilde{x})$ and $V_f \tilde{y}$, Eqns. (C.27)and (C.30), respectively, must fulfill certain growth requirements on $\tilde{f}(\tilde{x}, \tilde{y}, \tilde{\mathrm{h}}(\tilde{x}, \tilde{y}))$, and $\hat{g}(\tilde{x}, \tilde{y}, \tilde{\mathrm{h}}(\tilde{x}, \tilde{y}))$, Eqns. (C.42) and (C.43), respectively, by satisfying certain inequalities. The fulfillment of these inequalities for the Σ_{SF} simplified example is described bellow.

C.4.1 Isolated Equilibrium of the Origin for the Simplified Example Σ_{SF}-Subsystem: Assumption 5.5.1

The origin ($\tilde{x}=0$, $\tilde{y}=0$) is a unique and isolated equilibrium of the Σ_{SF}-subsystem, Eqns. (C.40–C.41), i.e.:

$$0 = \tilde{f}(0,0,\tilde{\mathrm{h}}(\tilde{x},\tilde{y})), \tag{C.58}$$

$$0 = \hat{g}(0,0,\tilde{\mathrm{h}}(\tilde{x},\tilde{y})), \tag{C.59}$$

moreover, $\tilde{y}=\tilde{\mathrm{g}}(\tilde{x})$ is the unique root of:

$$0 = \hat{g}\left(\tilde{x},\tilde{y},\tilde{\mathrm{h}}(\tilde{x},\tilde{y})\right), \tag{C.60}$$

in $B_{\tilde{x}} \times B_{\tilde{y}}$, i.e.:

$$0 = \hat{g}(\tilde{x},\tilde{\mathrm{g}}(\tilde{x}),\tilde{\mathrm{h}}(\tilde{x},\tilde{y})), \tag{C.61}$$

and there exists a class κ function $p_1(\cdot)$ such that:

$$\parallel \tilde{\mathrm{g}}(\tilde{x}) \parallel \leq p_1\left(\parallel \tilde{x} \parallel\right). \tag{C.62}$$

The reduced order growth requirements are obtained by first considering the system given by Eq. (C.40), and adding and subtracting $\tilde{f}(\tilde{x},\tilde{\mathrm{g}}(\tilde{x}),\tilde{\mathrm{h}}(\tilde{x},\tilde{y}))$, Eq. (C.57), to the right-hand side of Eq. (C.40) yielding:

$$\dot{\tilde{x}} = \tilde{f}\left(\tilde{x},\tilde{\mathrm{g}}(\tilde{x}),\tilde{\mathrm{h}}(\tilde{x},\tilde{y})\right) + \tilde{f}\left(\tilde{x},\tilde{y},\tilde{\mathrm{h}}(\tilde{x},\tilde{y})\right) - \tilde{f}\left(\tilde{x},\tilde{\mathrm{g}}(\tilde{x}),\tilde{\mathrm{h}}(\tilde{x},\tilde{y})\right), \tag{C.63}$$

where the term $\tilde{f}(\tilde{x},\tilde{y},\tilde{\mathrm{h}}(\tilde{x},\tilde{y})) - \tilde{f}(\tilde{x},\tilde{\mathrm{g}}(\tilde{x}),\tilde{\mathrm{h}}(\tilde{x},\tilde{y}))$ can be viewed as a perturbation of the reduced order Σ_S-subsystem, that is, $\tilde{f}(\tilde{x},\tilde{\mathrm{g}}(\tilde{x}),\tilde{\mathrm{h}}(\tilde{x},\tilde{y}))$, Eq. (C.57), and with $\tilde{f}(\tilde{x},\tilde{y},\tilde{\mathrm{h}}(\tilde{x},\tilde{y}))$ defined in Eq. (C.40). It is therefore natural to first satisfy the growth requirements for Eq. (C.57) and then consider the effect of the perturbation term $\tilde{f}(\tilde{x},\tilde{y},\tilde{\mathrm{h}}(\tilde{x},\tilde{y})) - \tilde{f}(\tilde{x},\tilde{\mathrm{g}}(\tilde{x}),\tilde{\mathrm{h}}(\tilde{x},\tilde{y}))$. Therefore let proceed to define first the reduced order growth condition.

C.4.2 Proof of Assumption 5.5.2: Reduced System Conditions for the Simplified Example

Recalling from Assumption 5.5.2, the Σ_S Lyapunov function candidate $V_s(\tilde{x})$ must be positive-definite and decreasing, and must also satisfy the following inequality:

$$\left(\frac{\partial V_s(\tilde{x})}{\partial \tilde{x}}\right)^T \tilde{f}\left(\tilde{x},\tilde{\mathrm{g}}(\tilde{x}),\tilde{\mathrm{h}}(\tilde{x},\tilde{y})\right) \leq -\alpha_1 \psi_1^2(\tilde{x}), \tag{C.64}$$

where $\psi_1(\cdot)$ is a scalar function of vector arguments which vanishes only when its argument are zero, and satisfying that $\tilde{x}=0$ is a stable equilibrium of the reduced order system. The left-hand side of inequality (C.64) is given by recalling that $V_s\left(\tilde{x}\right)$ is given by Eq. (C.24), being therefore easy to see that:

$$\left(\frac{\partial V_s(\tilde{x})}{\partial \tilde{x}}\right)^T = P_s\tilde{x}, \tag{C.65}$$

therefore substituting $\tilde{f}(\tilde{x}, \tilde{\mathrm{g}}(\tilde{x}), \tilde{\mathrm{h}}(\tilde{x}, \tilde{\mathrm{g}}(x)))$, Eq. (C.57), and Eq. (C.65) into Eq. (C.64), and recalling that $P_s = \dfrac{Q_s}{2b_x}$ yields:

$$\left(\frac{\partial V_s(\tilde{x})}{\partial \tilde{x}}\right)^T \tilde{f}(\tilde{x}, \tilde{\mathrm{g}}(\tilde{x}), \tilde{\mathrm{h}}(\tilde{x}, \tilde{y})) = -P_s b_x \tilde{x}^2 = -\frac{1}{2} Q_s \tilde{x}^2, \tag{C.66}$$

therefore Assumption (C.64) can be satisfied by selecting α_1 and $\psi_1(\tilde{x})$ such:

$$\alpha_1 \leq 1, \tag{C.67}$$

$$\psi_1(\tilde{x}) = \sqrt{\tilde{Q}_s \tilde{x}^2}, \tag{C.68}$$

with:

$$\tilde{Q}_s = \frac{1}{2} Q_s. \tag{C.69}$$

C.4.3 Proof of Assumption 5.5.3: Boundary-Layer System Conditions for the Simplified Example

Recalling from Assumption 5.5.3, the Σ_F Lyapunov function candidate $V_f(\tilde{x}, \tilde{y})$ must be positive-definite and decreasing, such that for all $(\tilde{x}, \tilde{y}) \in B_{\tilde{x}} \times B_{\tilde{y}}$ satisfies the following inequality:

$$V_f(\tilde{x}, \tilde{y}) > 0, \ \forall \ \tilde{y} \neq \tilde{\mathrm{g}}(\tilde{x}) \ \textit{and} \ V_f(\tilde{x}, \tilde{\mathrm{g}}(\tilde{x})) = 0, \tag{C.70}$$

and:

$$\left(\frac{\partial V_f}{\partial \tilde{y}}\right)^T \hat{g}\left(\tilde{x}, \tilde{y}, \tilde{\mathrm{h}}(\tilde{x}, \tilde{y})\right) \leq -\alpha_2 \phi_1^2(\tilde{y} - \tilde{\mathrm{g}}(\tilde{x})), \tag{C.71}$$

where $\phi_1(\cdot)$ is a scalar function of vector arguments which vanishes only when its arguments are zero, and satisfying that $\tilde{y} - \tilde{\mathrm{g}}(\tilde{x})$ is a stable equilibrium of the boundary layer Σ_F-subsystem, where $\hat{g}\left(\tilde{x}, \tilde{y}, \tilde{\mathrm{h}}(\tilde{x}, \tilde{y})\right)$ is the boundary layer Σ_F-subsystem, Eq. (C.43), and $V_f(\tilde{x}, \tilde{y})$, Eq. (C.33), is the Lyapunov function candidate of the Σ_F-subsystem. The left-hand side of inequality (C.71) is defined after recalling that $V_f(\tilde{y})$ is given by Eq. (C.30), being therefore easy to see that:

$$\left(\frac{\partial V_f}{\partial \tilde{y}}\right)^T = (P_f \tilde{y})^T, \tag{C.72}$$

and also recalling from section C.3.4 that:

$$\tilde{g}(\tilde{x}, \tilde{y}, \tilde{\mathrm{h}}(\tilde{x}, \tilde{y})) = A_f \tilde{y}, \tag{C.73}$$

being:

$$A_f = -\tilde{b}_y, \tag{C.74}$$

and therefore substituting, Eqns. (C.72), and (C.73) into Eq. (C.71) resulting in:

$$\left(\frac{\partial V_f}{\partial \tilde{y}}\right)^T \hat{g}(\tilde{x}, \tilde{y}, \tilde{\mathrm{h}}(\tilde{x}, \tilde{y})) = (P_f \tilde{y})^T A_f \tilde{y} = \tilde{y}^T P_f A_f \tilde{y} = \tilde{y}^T M_f \tilde{y}, \tag{C.75}$$

with M_f defined by:

$$M_f = -P_f \tilde{b}_y = -\frac{Q_f}{2}, \tag{C.76}$$

therefore rewriting the left-hand side of inequality (C.75) as:

$$\left(\frac{\partial V_f}{\partial \tilde{y}}\right)^T \hat{g}(\tilde{x}, \tilde{y}, \tilde{\mathrm{h}}(\tilde{x}, \tilde{y})) = \tilde{y}^T M_f \tilde{y} = -\frac{1}{2}\left(\tilde{y}^T Q_f \tilde{y}\right) = -\frac{1}{2} Q_f \tilde{y}^2, \tag{C.77}$$

with Q_F being the associated Lyapunov matrix. For simplicity let also introduce:

$$\tilde{Q}_f = \frac{1}{2} Q_f, \tag{C.78}$$

and rewriting (C.75) as:

$$\left(\frac{\partial V_f}{\partial \tilde{y}}\right)^T \hat{g}(\tilde{x}, \tilde{y}, \tilde{\mathrm{h}}(\tilde{x}, \tilde{y})) = -\left(\tilde{y}^T \tilde{Q}_f \tilde{y}\right) = -\tilde{Q}_f \tilde{y}^2, \tag{C.79}$$

therefore the fulfillment of inequality (C.79) is achieved by selecting α_2 and $\phi(\hat{y} - \tilde{\mathrm{g}}(\tilde{x}))$ such:

$$\alpha_2 \leq 1, \tag{C.80}$$

$$\phi_1(\tilde{y} - \tilde{\mathrm{g}}(\tilde{x})) = \left(\tilde{y}^T \tilde{Q}_f \tilde{y}\right)^{\frac{1}{2}} = \left(\tilde{Q}_f \tilde{y}^2\right)^{\frac{1}{2}}. \tag{C.81}$$

For simplicity, from now on the comparison function $\phi_1(\tilde{y} - \tilde{\mathrm{g}}(\tilde{x}))$ it is refereed as $\phi_1(\hat{y})$.

C.4.4 Proof of Assumption 5.5.4: First Interconnection Condition for the Simplified Example

The Lyapunov functions $V_s(\tilde{x})$ and $V_f(\tilde{x}, \tilde{y})$, Eqns. (C.27), and (C.33) respectively, must satisfy the so called interconnection conditions. The first interconnection condition is obtained by computing the derivative of $V_s(\tilde{x})$ along the solution of Eq. (C.63), resulting in a expression similar to Eq. (5.139), which provides the first interconnection inequality:

$$\left(\frac{\partial V_s(\tilde{x})}{\partial \tilde{x}}\right)^T \left[\tilde{f}\left(\tilde{x}, \tilde{y}, \tilde{\mathrm{h}}(\tilde{x}, \tilde{y})\right) - \tilde{f}\left(\tilde{x}, \tilde{\mathrm{g}}(\tilde{x}), \tilde{\mathrm{h}}(\tilde{x}, \tilde{y})\right)\right] \leq \beta_1 \psi_1(\tilde{x}) \phi_1(\tilde{y}), \tag{C.82}$$

where the comparison function $\psi_1(\tilde{x})$ and $\phi_1(\hat{y})$, are defined in Eqns. (C.68) and (C.81) respectively. Inequality (C.82) determines the allowed growth of $\tilde{f}(\tilde{x}, \tilde{y}, \tilde{\mathrm{h}}(\tilde{x}, \tilde{y}))$ in $\tilde{y}$, and in typical problems, verifying inequality (C.82) reduces to verifying the inequality:

$$\left\|\tilde{f}\left(\tilde{x}, \tilde{y}, \tilde{\mathrm{h}}(\tilde{x}, \tilde{y})\right) - \tilde{f}\left(\tilde{x}, \tilde{\mathrm{g}}(\tilde{x}), \tilde{\mathrm{h}}(\tilde{x}, \tilde{y})\right)\right\| \leq \psi_1(\tilde{x}) \phi_1(\hat{y}), \tag{C.83}$$

which implies that the rate of growth of $\tilde{f}(\tilde{x}, \tilde{y}, \tilde{\mathrm{h}}(\tilde{x}, \tilde{y}))$ cannot be faster than the rate of growth of the comparison function $\phi_1(\cdot)$. The left-hand side of inequality (C.82) is given by recalling the results of Eq. (C.72), and recalling both $\tilde{f}(\tilde{x}, \tilde{\mathrm{g}}(\tilde{x}), \tilde{\mathrm{h}}(\tilde{x}, \tilde{y}))$ and $\tilde{f}(\tilde{x}, \tilde{y}, \tilde{\mathrm{h}}(\tilde{x}, \tilde{y}))$, Eqns. (C.57), and (C.54), respectively, yielding:

$$\tilde{f}(\tilde{x}, \tilde{y}, \tilde{\mathrm{h}}(\tilde{x}, \tilde{y})) - \tilde{f}(\tilde{x}, \tilde{\mathrm{g}}(\tilde{x}), \tilde{\mathrm{h}}(\tilde{x}, \tilde{y})) = (\tilde{x} + x^*)\, \tilde{y}\, (\rho_1 - b_y). \tag{C.84}$$

Substituting Eqns. (C.65) and (C.84) into inequality (C.82) results in:

$$\begin{aligned} & \left(\frac{\partial V_s(\tilde{x})}{\partial \tilde{x}}\right)^T \left[\tilde{f}\left(\tilde{x}, \tilde{y}, \tilde{\mathrm{h}}(\tilde{x}, \tilde{y})\right) - \tilde{f}\left(\tilde{x}, \tilde{\mathrm{g}}(\tilde{x}), \tilde{\mathrm{h}}(\tilde{x}, \tilde{y})\right)\right] \\ = \; & \frac{1}{2} \frac{Q_s}{b_x} (\tilde{x} + x^*)(\rho_1 - b_y)\, \tilde{x} \tilde{y} \leq \beta_1 \psi_1(\tilde{x}) \phi_1(\hat{y}), \end{aligned} \tag{C.85}$$

where recalling the selected comparison functions $\psi_1(\tilde{x})$ and $\phi_1(\hat{y})$, Eqns. (C.68) and (C.81), respectively, it can be observed that fulfillment of inequality (C.82) is reduced to prove that:

$$\frac{1}{2} \frac{Q_s}{b_x} (\rho_1 - b_y)(\tilde{x} + x^*)\, \tilde{x} \tilde{y} \leq \beta_1 \left(\tilde{Q}_s \tilde{x}^2\right)^{\frac{1}{2}} \left(\tilde{Q}_f \tilde{y}^2\right)^{\frac{1}{2}}. \tag{C.86}$$

The left-hand side of inequality (C.86) can be simplified by recalling from the error state vector definition that $\tilde{x} + x^* \triangleq x$, and from the results presented in Table 2.3, where it was defined that:

$$x_{MAX} \geq x \geq x_{MIN}, \tag{C.87}$$

where x_{MIN} is the minimum allowable value of the slow variable x, and x_{MAX} is the maximum allowable value of the slow variable x. With this in mind, the left hand side of inequality (C.88) can be bounded and given by:

$$\frac{1}{2}\frac{Q_s}{b_x}(\rho_1 - b_y)(\tilde{x}+x^*)\,\tilde{x}\tilde{y} \leq \mathcal{C}\tilde{x}\tilde{y}, \tag{C.88}$$

with:

$$\mathcal{C} = \frac{1}{2}\frac{Q_s}{b_x}(\rho_1 - b_y)\,x_{MAX}, \tag{C.89}$$

therefore inequality (C.85) can be rewritten as:

$$\begin{aligned}
&\left(\frac{\partial V_s(\tilde{x})}{\partial \tilde{x}}\right)^T \left[\tilde{f}\left(\tilde{x},\tilde{y},\tilde{\mathrm{h}}(\tilde{x},\tilde{y})\right) - \tilde{f}\left(\tilde{x},\tilde{\mathrm{g}}(\tilde{x}),\tilde{\mathrm{h}}(\tilde{x},\tilde{y})\right)\right] \\
= \;& \frac{1}{2}\frac{Q_s}{b_x}(\tilde{x}+x^*)(\rho_1 - b_y)\,\tilde{x}\tilde{y} \\
\leq \;& \mathcal{C}\tilde{x}\tilde{y} \\
\leq \;& \beta_1\left(\tilde{Q}_s\tilde{x}^2\right)^{\frac{1}{2}}\left(\tilde{Q}_f\tilde{y}^2\right)^{\frac{1}{2}},
\end{aligned} \tag{C.90}$$

therefore the fulfillment of the original inequality (C.82), reduces to prove:

$$\mathcal{C}\tilde{x}\tilde{y} \leq \beta_1\left(\tilde{Q}_s\tilde{x}^2\right)^{\frac{1}{2}}\left(\tilde{Q}_f\tilde{y}^2\right)^{\frac{1}{2}}. \tag{C.91}$$

In order to obtain the constant β_1 that guarantees the fulfillment of inequality (C.91), let square both sides of inequality (C.91), resulting in:

$$\mathcal{C}^2\tilde{x}^2\tilde{y}^2 \leq \beta_1^2\tilde{Q}_s\tilde{Q}_f\tilde{x}^2\tilde{y}^2, \tag{C.92}$$

thus inequality (C.82) can be satisfied by selecting β_1 such:

$$\beta_1 \geq \sqrt{\frac{\mathcal{C}^2}{\tilde{Q}_s\tilde{Q}_f}}, \tag{C.93}$$

where $\mathcal{C}$ is defined in Eq. (C.89), $\tilde{Q}_s$ defined in Eq. (C.69), and $\tilde{Q}_f$, given in Eq. (C.78).

C.4.5 Proof of Assumption 5.5.5: Second Interconnection Condition for the Simplified Example

The second interconnection condition is defined by the inequality:

$$\left(\frac{\partial V_f(\tilde{y})}{\partial \tilde{x}}\right)^T \tilde{f}\left(\tilde{x},\tilde{y},\tilde{\mathrm{h}}(\tilde{x},\tilde{y})\right) \leq \gamma_1\phi_1^2(\tilde{y}) + \beta_2\psi_1(\tilde{x})\phi_1(\hat{y}). \tag{C.94}$$

Inequality (C.94) can be rewritten by adding and subtracting $\tilde{f}(\tilde{x},\tilde{\mathrm{g}}(\tilde{x}),\tilde{\mathrm{h}}(\tilde{x},\tilde{y}))$ to the $\tilde{f}(\tilde{x},\tilde{y},\tilde{\mathrm{h}}(\tilde{x},\tilde{y}))$ in the left-hand side of Eq. (C.94) resulting in:

$$\begin{aligned}
\frac{\partial V_f}{\partial \tilde{x}}\tilde{f}(\tilde{x},\tilde{y},\tilde{\mathrm{h}}(\tilde{x},\tilde{y})) \;\leq\; & \frac{\partial V_f}{\partial \tilde{x}}\tilde{f}(\tilde{x},\tilde{y},\tilde{\mathrm{h}}(\tilde{x},\tilde{y})) \\
+\; & \frac{\partial V_f}{\partial \tilde{x}}\left[f(\tilde{x},\tilde{y},\tilde{\mathrm{h}}(\tilde{x},\tilde{y})) - f(\tilde{x},\tilde{y},\tilde{\mathrm{h}}(\tilde{x},\tilde{y}))\right] \\
\leq\; & \beta_2\psi_1(\tilde{x})\phi_1(\hat{y}) + \gamma_1\phi_1^2(\tilde{x}),
\end{aligned} \tag{C.95}$$

where the resulting inequality (C.95) can be satisfied by first splitting into two simpler inequalities given by:

$$\frac{\partial V_f}{\partial \tilde{x}}\tilde{f}(\tilde{x},\tilde{y},\tilde{\mathrm{h}}(\tilde{x},\tilde{y})) \leq \beta_2\psi_1(\tilde{x})\phi_1(\hat{y}) \tag{C.96}$$

$$\frac{\partial V_f}{\partial \tilde{x}} \left[\tilde{f}(\tilde{x}, \tilde{y}, \tilde{\mathrm{h}}(\tilde{x}, \tilde{y})) - \tilde{f}(\tilde{x}, \tilde{\mathrm{g}}(\tilde{x}), \tilde{\mathrm{h}}(\tilde{x}, \tilde{y})) \right] \le \gamma \phi_1^2(\tilde{y}), \tag{C.97}$$

therefore, assumption (6.195) can be proven, if both inequalities (C.96) and (C.97) are fulfilled. From the structure of $V_f(\tilde{x})$ it can be seen that:

$$\frac{\partial V_f}{\partial \tilde{x}} = 0. \tag{C.98}$$

Due to the fact that the associated Lyapunov function $V_f(\hat{y})$ does not depend on the variable $\tilde{x}$, implies that the fulfillment of inequality (C.94) is trivial and is achieved by selecting $\beta_1 \ge 0$, and $\gamma_1 \ge 0$, thus, concluding that thesub-conditions (C.96) and (C.97) are satisfied by selecting:

$$\beta_2 \quad \ge \quad 0, \tag{C.99}$$

$$\gamma_1 \quad \ge \quad 0. \tag{C.100}$$

These results provide an additional degree of freedom that will be exploited in later sections in order to determine desired upperbounds of the Σ_{SF} *Stability Analysis*.

C.5 Fulfillment of the Simplified Example Σ_{SF} *Stability Analysis*

The fulfillment of assumptions 5.5.1, 5.5.2, 5.5.3, 5.5.4, and 5.5.5, applied to the simplified example Σ_{SF}-subsystem by the fulfillment of inequalities C.64, C.71, C.82, and C.94, proves that the growth requirements of $\tilde{f}(\tilde{x}, \tilde{y}, \tilde{\mathrm{h}}(\tilde{x}, \tilde{y}))$ and $\hat{g}(\tilde{x}, \tilde{y}, \tilde{\mathrm{h}}(\tilde{x}, \tilde{x}))$ are satisfied, and with the Lyapunov functions $V_s(\tilde{x})$ and $V_f(\tilde{x}, \tilde{x})$, Eqns. (C.27) and (C.46), respectively, a new Lyapunov function candidate $V_1(\tilde{x}, \tilde{y})$ is considered and defined by the weighted sum of $V_S(\tilde{x})$ and $V_F(\tilde{x}, \tilde{y})$, given by:

$$V_1(\tilde{x}, \tilde{y}) = (1 - d_1)V_s(\tilde{x}) + d_1 V_f(\tilde{y}),\ d_1 \in (0, 1), \tag{C.101}$$

for $0 < d_1 < 1$. The newly defined function $V_1(\tilde{x}, \tilde{y})$ becomes the Lyapunov function candidate for the singular perturbed Σ_{SF}-subsystem, Eqns. (C.40–C.41). Similarly as in the general case, and the helicopter problem, to explore the freedom in choosing the weights, lets take d_1 as an unspecified parameter in the interval $(0, 1)$. From the properties of $V_s(\tilde{x})$ and $V_f(\tilde{x}, \tilde{y})$, and inequality (C.62), that is $\| \tilde{\mathrm{g}}(\tilde{x}) \| \le p_1(\| \tilde{x} \|)$, where $p_1(\cdot)$ is a κ class function, it follows that $V_1(\tilde{x}, \tilde{y})$ is positive-definite. Computing the time derivative of $V_1(\tilde{x}, \tilde{y})$ along the trajectories of $\tilde{f}\left(\tilde{x}, \tilde{y}, \tilde{\mathrm{h}}(\tilde{x}, \tilde{y})\right)$ and $\hat{g}\left(\tilde{x}, \tilde{y}, \tilde{\mathrm{h}}(\tilde{x}, \tilde{y})\right)$ yields an equation of similar structure as in Eq. (5.145), which can express as a function of the comparison functions $\psi_1(\tilde{x})$, and $\phi_1(\hat{y})$ by employing the derived inequalities C.64, C.71, C.82, and C.94, resulting in:

$$\begin{aligned}
\dot{V}_1 \quad &\le \quad -(1 - d_1)\alpha_1 \psi_1^2(\tilde{x}) + (1 - d_1)\beta_1 \psi_1(\tilde{x})\phi_1(\hat{y}) \\
&- \quad \frac{d_1}{\varepsilon_1}\alpha_2 \phi_1^2(\hat{y}) + d_1 \gamma_1 \phi_1^2(\hat{y}) + d_1 \beta_2 \psi_1(\tilde{x})\phi_1(\hat{y}) \\
&= \quad - \begin{bmatrix} \psi_1(\tilde{x}) \\ \phi_1(\hat{y}) \end{bmatrix}^T \begin{bmatrix} (1 - d_1)\alpha_1 & -\frac{1}{2}(1 - d_1)\beta_1 - \frac{1}{2}d_1\beta_2 \\ -\frac{1}{2}(1 - d_1)\beta_1 - \frac{1}{2}d_1\beta_2 & d_1 \left(\dfrac{\alpha_2}{\varepsilon_1} - \gamma_1 \right) \end{bmatrix} \\
&\times \quad \begin{bmatrix} \psi_1(\tilde{x}) \\ \phi_1(\hat{y}) \end{bmatrix} \\
&= \quad - \begin{bmatrix} \sqrt{\tilde{Q}_s \tilde{x}^2} \\ \sqrt{\tilde{Q}_f \tilde{y}^2} \end{bmatrix}^T \begin{bmatrix} (1 - d_1)\alpha_1 & -\frac{1}{2}(1 - d_1)\beta_1 - \frac{1}{2}d_1\beta_2 \\ -\frac{1}{2}(1 - d_1)\beta_1 - \frac{1}{2}d_1\beta_2 & d_1 \left(\dfrac{\alpha_2}{\varepsilon_1} - \gamma_1 \right) \end{bmatrix}
\end{aligned}$$

$$\times \quad \begin{bmatrix} \sqrt{\tilde{Q}_s \tilde{x}^2} \\ \sqrt{\tilde{Q}_f \tilde{y}^2} \end{bmatrix}. \tag{C.102}$$

In order to guarantee the negative-definiteness property of Eq. (C.102), and conducting the same algebraic transformations as in section 5.5.1, it can be obtained the following expression that defines the requirement to be satisfied by the parasitic constant ε_1 such:

$$\varepsilon_1 < \frac{\alpha_1 \alpha_2}{\alpha_1 \gamma_1 + \dfrac{1}{4(1-d_1)d_1} \left[(1-d_1)\beta_1 + d_1 \beta_2\right]^2} \equiv \varepsilon_{1_d}. \tag{C.103}$$

Recalling from the general formulation, chapter 5, that although only α_1 and α_2 are required by definition to be positive, β_1, β_2, and γ_1 are also considered to be positive. Inequality (C.103) shows that for any choice of d_1, the corresponding $V_1(\tilde{x}, \tilde{y})$, Eq. (C.101), is a Lyapunov function for the singular perturbed Σ_{SF}-subsystem, Eqns. (C.40–C.41), for all ε_1 satisfying Eq. (C.103). It can be easily seen that the maximum value of ε_{1_d} occurs at:

$$d_1^* = \frac{\beta_1}{\beta_1 + \beta_2}, \tag{C.104}$$

yielding the upper bound on ε_1:

$$\varepsilon_1^* = \frac{\alpha_1 \alpha_2}{\alpha_1 \gamma_1 + \beta_1 \beta_2}. \tag{C.105}$$

Therefore, it can be inferred that the equilibrium point of the singularly perturbed Σ_{SF}-subsystem, Eqns. (C.40–C.41), is asymptotically stable for all $\varepsilon_1 < \varepsilon_1^*$. The number ε_1^* is the best upper bound on ε_1 that can be provided by the above presented stability analysis. The results obtained from the fulfillment of inequalities (C.64), (C.71), (C.82) and (C.94) are summarized in Table C.1, where it can be seen the similarities between the two-time-scale growth requirements described in Section 5.2.1, and the three-time-scale growth requirements for the Σ_{SF}-subsystem.

The asymptotic stability analysis presented proves that by fulfilling inequalities (C.64), (C.71), (C.82), and (C.94), then the origin is an asymptotically stable equilibrium of the singularly perturbed helicopter Σ_{SF}-subsystem (C.40–C.41) for all $\varepsilon_1 \in (0, \varepsilon_1^*)$, where ε_1^* is given by Eq. (C.105), thus, for every number $d_1 \in (0,1)$, $V_1(\tilde{x}, \tilde{y})$, Eq. (C.101), is a Lyapunov function for all $\varepsilon_1(0, \varepsilon_d)$, where $\varepsilon_{1_d} \leq \varepsilon_1^*$ is given by Eq. (C.103), hence satisfying Theorem 5.5.1.

The fulfillment of Theorem 5.5.1 for the simplified example Σ_{SF}-subsystem can be summarized by understanding that $\tilde{x} = 0$ is an asymptotically stable equilibrium of the reduced Σ_S-subsystem, Eq. (C.57), $\tilde{y} = \tilde{\mathrm{g}}(\tilde{x})$ is an asymptotically stable equilibrium of the boundary-layer Σ_F-subsystem, Eq. (C.43), uniformly in $\tilde{x}$, that is, the $\varepsilon - \delta$ definition of *Lyapunov* stability and the convergence $\tilde{y} \to \tilde{\mathrm{g}}(\tilde{x})$ are uniform in $\tilde{x}$ (Vidyasagar, 2002), and if $\tilde{f}\left(\tilde{x}, \tilde{y}, \tilde{\mathrm{h}}(\tilde{x}, \tilde{y})\right)$ and $\hat{g}\left(\tilde{x}, \tilde{y}, \tilde{\mathrm{h}}(\tilde{x}, \tilde{y})\right)$ satisfy certain growth conditions on the reduced and boundary-layer systems, then the origin is an asymptotically stable equilibrium of the singularly perturbed Σ_{SF}-subsystem, Eqns. (C.40–C.41), for sufficiently small ε_1 (Kokotović et al., 1986; Kokotović et al., 1987; Kokotović et al., 1999).

Due to the fact that the system is expressed in its error dynamics form, and that the use of the full range of reachable state variables has been required in order to satisfy the inequalities that guarantee the asymptotic stability properties at the origin of the Σ_{SF}-subsystem, these asymptotic stability properties are also extended to semiglobal stability, by the definition in (Kokotović, 1992; Sussmann and Kokotović, 1991; Braslavsky and Miidleton, 1996), by providing upper bounds on the parasitic singularly perturbed parameters for the entire range of admissible state values, thus extending the domain of attraction to that same rage of admissible states.

Assumption 5.5.7				
Section 5.2	$\frac{\partial V}{\partial x}$	$f(x, \mathrm{h}(x))$	α_1	$\psi(x)$
Σ_{SF}	$\frac{\partial V_s(\tilde{x})}{\partial \tilde{x}}$	$\tilde{f}(\tilde{x}, \tilde{\mathrm{g}}(\tilde{x}), \tilde{\mathrm{h}}(\tilde{x}, \tilde{y}))$	$\alpha_1 \leq 1$	$\psi_1(\tilde{x}) = \sqrt{\tilde{Q}_s \tilde{x}^2}$
Assumption 5.5.8				
Section 5.2	$\frac{\partial W}{\partial z}$	$g(x, z)$	α_2	$\phi(z - \mathrm{h}(x))$
Σ_{SF}	$\left(\frac{\partial V_f(\tilde{y})}{\partial \tilde{y}}\right)^T$	$\hat{g}(\tilde{x}, \tilde{y}, \tilde{\mathrm{h}}(\tilde{x}, \tilde{y}))$	$\alpha_2 \leq 1$	$\phi_1(\tilde{y}) = \sqrt{\tilde{Q}_f \tilde{y}^2}$
Assumption 5.5.9				
Section 5.2	$\frac{\partial V}{\partial x}$	$f(x, z)$	$f(x, \mathrm{h}(x))$	β_1
Σ_{SF}	$\left(\frac{\partial V_s(\tilde{x})}{\partial \tilde{x}}\right)^T$	$\tilde{f}(\tilde{x}, \tilde{y}, \tilde{\mathrm{h}}(\tilde{x}, \tilde{y}))$	$\tilde{f}(\tilde{x}, \tilde{\mathrm{g}}(\tilde{x}), \tilde{\mathrm{h}}(\tilde{x}, \tilde{y}))$	$\beta_1 \geq \sqrt{\frac{\mathcal{C}^2}{\tilde{Q}_s \tilde{Q}_f}}$
Assumption 5.5.10				
Section 5.2	$\frac{\partial W}{\partial x}$	$f(x, z)$	γ_1	β_2
Σ_{SF}	$\left(\frac{\partial V_f(\tilde{y})}{\partial \tilde{x}}\right)^T$	$\tilde{f}(\tilde{x}, \tilde{y}, \tilde{\mathrm{h}}(\tilde{x}, \tilde{y}))$	$\gamma_1 \geq 0$	$\beta_2 \geq 0$

Table C.1: Parameters for the Comparison Functions and Inequalities that Guarantee the Asymptotic Stability Requirements for the Simplified Example Σ_{SF} Subsystem.

C.5.1 Bounds for the *Stability Parameter* of the Σ_{SF} *Stability Analysis*

Needs to be noted that, due to the existent freedom on selecting β_2 and γ_1, the upper-bound ε_1^*, Eq. (C.105), and its d_1^* parameter, Eq. (C.104), can be precisely obtained to match the required parameters that guarantee the asymptotic stability for the full Σ_{SFU} system by selecting the combination of γ_1 and β_2 that generates the appropriate combination of both ε_1^* and d_1^*. This is obtained by solving Eqns. (C.105) and (C.104) such:

$$\varepsilon_1^* = \frac{\alpha_1 \alpha_2}{\alpha_1 \gamma_1 + \beta_1 \beta_2} \rightarrow \gamma_1(\varepsilon_1^{\bigstar}) = \frac{1}{\alpha_1}\left(\frac{\alpha_1 \alpha_2}{\varepsilon_1^{\bigstar}} - \beta_1 \beta_2\right), \tag{C.106}$$

and where β_2 is defined by:

$$d_1^* = \frac{\beta_1}{\beta_1 + \beta_2} \rightarrow \beta_2(d_1^{\bigstar}) = \frac{\beta_1}{d_1^{\bigstar}} - \beta_1, \tag{C.107}$$

where recall that $\varepsilon_1^{\bigstar}$ and $d_1^{\bigstar}$ are the selected values by the author that satisfy the asymptotic stability properties of the full system, not to confuse with ε_1^* and d_1^*, that are given by Eqns. (C.105) and (C.104). The major difference between both, $\varepsilon_1^{\bigstar}$, $d_1^{\bigstar}$ and ε_1^* and d_1^*, is that the first appear only for the special type of problems in which the degrees of freedom that appear during the stability analysis allow to select $\beta_2(d_1^{\bigstar})$ and $\gamma_1(\varepsilon_1^{\bigstar})$, thus permitting to select the desired values of both ε_1 and d_1 by selecting $\varepsilon_1^{\bigstar}$ and $d_1^{\bigstar}$ from Eqns (C.106) and (C.107), respectively. This reduces Eqns. (C.104) and (C.105) to:

$$d_1^* = \frac{\beta_1}{\beta_1 + \beta_2(d_1^{\bigstar})}, \tag{C.108}$$

yielding the upper bound on ε_1

$$\varepsilon_1^* = \frac{\alpha_1 \alpha_2}{\gamma_1(\varepsilon_1^{\bigstar})\gamma_1 + \beta_1 \beta_2(d_1^{\bigstar})}. \tag{C.109}$$

The power to select ε_1^*, can be better understood since the fulfillment of the Σ_{SF} *Stability Analysis* depends on the fulfillment that the chosen ε_1 in the time-scale selection (see selection 3.5) satisfies $\varepsilon_1 < \varepsilon_1^*$.

The power to select d_1^* will be fully understood when completing the satisfy the Σ_{SFU} *Stability Analysis*, but initially can be thought as a requirement to calculate the upper bound on ε_1^*, Eq. (C.109), which requires the calculation of both $\beta_2(d_1^\bigstar)$, and $\gamma_1(\varepsilon_1^\bigstar)$, Eqns. (C.107) and (C.106), respectively, into Eq. (C.109). By selecting $d_1^* = 0.5$, the Σ_{SFU} *Stability Analysis*, the percentage contribution on the Lyapunov function $V_1(\tilde{x}, \tilde{y})$, Eq. (C.101), is equally distributed for both Lyapunov functions $V_s(\tilde{x})$ and $V_f(\tilde{y})$. The selection of $\varepsilon_1^\bigstar$ is more straight forward, recalling the time-scale of the simplified example problem here analyzed, which was selected as $\varepsilon_1 = 0.01$. Therefore, recalling Eq. (C.106), and identifying that for margin let $\varepsilon_1^\bigstar = \delta_{\varepsilon_1}\varepsilon_1 = 0.0105$, where $\delta_{\varepsilon_1} = 1.05$.

Recall also that need to select the *stability parameters* Q_s, and Q_f. Although arbitrary values can be selected in order to satisfy the asymptotic stability properties of the Σ_{SF}-subsystem, as it will be proven in the stability analysis for the full Σ_{SFU} system, a specific ratio between both Q_s, and Q_f needs to be chosen in order to guarantee the stability properties of the Σ_{SFU} system, that is:

$$Q_f = Q_{sf} Q_s, \tag{C.110}$$

where Q_{sf} is the ratio between both *stability parameters*. Also, as it will be proven in section C.6, this ratio, for the physical parameters of the problem here discussed is given by:

$$Q_{sf} = 146.0304329, \tag{C.111}$$

therefore, by selecting $Q_s = 15$, results in $Q_f = 2190.45649$, which results in:

$$\gamma_1 = 90.476068, \tag{C.112}$$
$$\beta_2 = 0.010757, \tag{C.113}$$

which also results in $\beta_1 = 0.010757$, which, along with the selection for the rest of the coefficients:

$$\alpha_1 = 0.95,$$
$$\alpha_2 = 0.95,$$

which results in $\varepsilon_1^* = \varepsilon_1^\bigstar = 0.0105$, which satisfies the requirements $\varepsilon_1 < \varepsilon_1^*$, and $d_1^\bigstar = 0.5$, and with the dependance on the right-hand side of Eq. (C.103) on the unspecified parameter d_1 sketched in Figure C.1, which as it can be see it is adjusted to the selected $d_1^\bigstar = 0.5$ and $\varepsilon_1^* = 0.0105$.

This concludes the first step of the asymptotic stability analysis. The Σ_{SF} *Stability Analysis* asymptotic stability analysis. The following section describes the second step of the generic asymptotic stability analysis, the Σ_{SFU} *Stability Analysis* for the simplified problem.

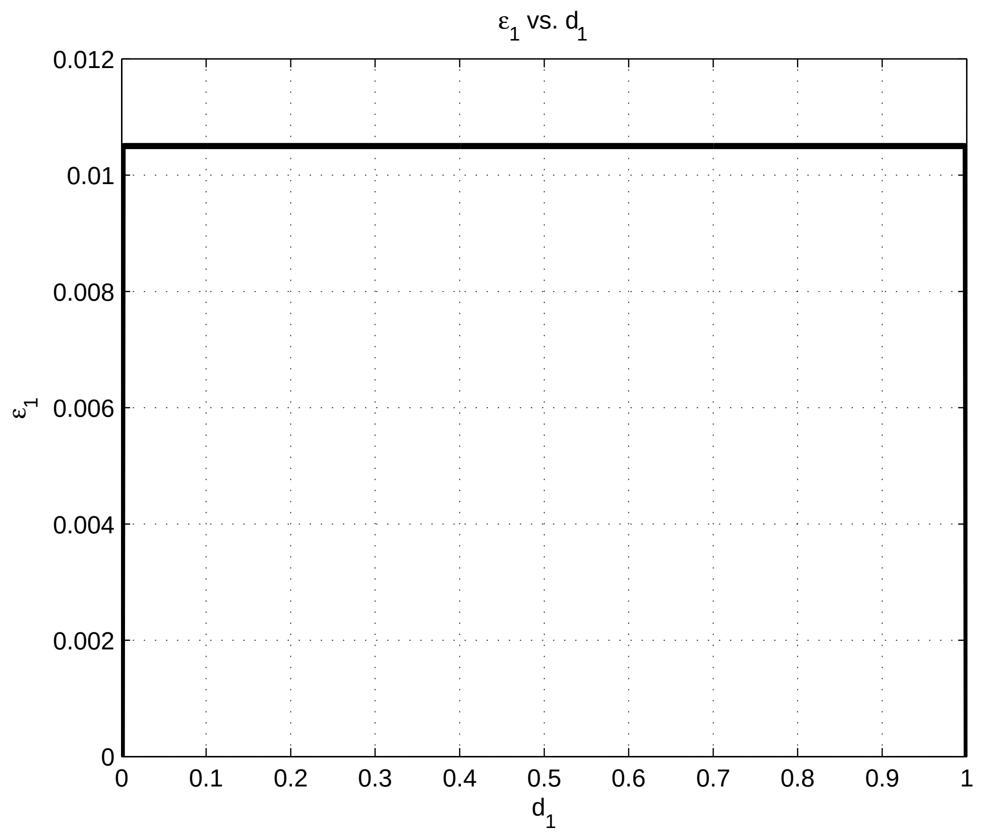

Figure C.1: Adjusted Stability Upper Bounds on ε_1 for the Stability Analysis of the Σ_{SF} Subsystem

C.6 Σ_{SFU} *Stability Analysis* for the Simplified Model

Once proven the asymptotic stability of the Σ_{SF}-subsystem, Eqns. (C.40–C.41), and a valid Lyapunov function candidate has been obtained, Eq. (C.101). The Σ_{SFU} *Stability Analysis* is conducted recalling that the Σ_{SF} *Stability Analysis* provides a composite Lyapunov function, $\mathcal{V}_1$, that satisfies the growth requirements between both $\tilde{f}\left(\tilde{x}, \tilde{y}, \tilde{\mathrm{h}}(\tilde{x}, \tilde{y})\right)$ and $\hat{g}\left(\tilde{x}, \tilde{y}, \tilde{\mathrm{h}}(\tilde{x}, \tilde{y})\right)$, therefore, and using these results, it can be continued to prove the asymptotic stability properties of the full Σ_{SFU} system, which, for convenience, is rewritten as:

$$\dot{\tilde{\boldsymbol{\chi}}} = \tilde{\boldsymbol{F}}(\tilde{\boldsymbol{\chi}}, \tilde{z}), \tag{C.114}$$

$$\varepsilon_1 \varepsilon_2 \dot{\tilde{z}} = \hat{h}(\tilde{\boldsymbol{\chi}}, \tilde{z}), \tag{C.115}$$

where $\tilde{\boldsymbol{F}}(\tilde{\boldsymbol{\chi}}, \tilde{z})$ represents the slow dynamics of the Σ_{SFU} full system, when applying the stretched time constant τ_2, and is given by Eqs. (C.13) and (C.14), that is

$$\tilde{\boldsymbol{F}}(\tilde{\boldsymbol{\chi}}, \tilde{z}) \triangleq \left[\begin{array}{c} \tilde{f}(\tilde{\boldsymbol{\chi}}, \tilde{z}) \\ \hat{g}(\tilde{\boldsymbol{\chi}}, \tilde{z}) \end{array} \right] = \left[\begin{array}{c} \tilde{f}\,(\tilde{x}, \tilde{y}, \tilde{z}) \\ \hat{g}\,(\tilde{x}, \tilde{y}, \tilde{z}) \end{array} \right], \tag{C.116}$$

where $\tilde{\boldsymbol{\chi}}$ represents the augmented state vector given by

$$\tilde{\boldsymbol{\chi}} \triangleq \left[\begin{array}{cc} \tilde{x} & \tilde{y} \end{array} \right]^T. \tag{C.117}$$

The Lyapunov function obtained during the Σ_{SF} *Stability Analysis*, $V_1(\tilde{\boldsymbol{\chi}})$, becomes the Lyapunov function for the $\tilde{\boldsymbol{F}}(\tilde{\boldsymbol{\chi}}, \tilde{z})$ system, where

$$V_1(\tilde{\boldsymbol{\chi}}) = (1 - d_1)\, V_s + d_1 V_f. \tag{C.118}$$

Identifying that the new singularly perturbed Σ_{SFU} full system defined in Eqns. (C.114–C.115) can be decomposed into a two-time-scale by applying the stretched time scale τ_2, yielding the reduced order Σ_{SF}-subsystem

$$\dot{\tilde{\boldsymbol{\chi}}} = \tilde{\boldsymbol{F}}(\tilde{\boldsymbol{\chi}}, \tilde{\mathrm{h}}(\tilde{\boldsymbol{\chi}})) = \left[\begin{array}{c} \tilde{f}\left(\tilde{x}, \tilde{y}, \tilde{\mathrm{h}}(\tilde{x}, \tilde{y})\right) \\ \hat{g}\left(\tilde{x}, \tilde{y}, \tilde{\mathrm{h}}(\tilde{x}, \tilde{y})\right) \end{array} \right] = \left[\begin{array}{c} \tilde{f}(\tilde{\boldsymbol{\chi}}, \tilde{\mathrm{h}}(\tilde{\boldsymbol{\chi}})) \\ \hat{g}(\tilde{\boldsymbol{\chi}}, \tilde{\mathrm{h}}(\tilde{\boldsymbol{\chi}})) \end{array} \right], \tag{C.119}$$

which is equivalent to the subsystem analyzed in the Σ_{SF} *Stability Analysis*, while the boundary layer Σ_U-subsystem is defined by

$$\frac{d\tilde{z}}{d\tau_2} = \hat{h}(\tilde{\boldsymbol{\chi}}, \tilde{z}), \tag{C.120}$$

and with $V_U(\hat{z})$ being its associated Lyapunov function. The quasi-steady-state equilibria $\tilde{z} = \tilde{\mathrm{h}}(\tilde{\boldsymbol{\chi}})$ that defines the Σ_{SF}-subsystem, Eq. (C.119) is given by

$$0 = \hat{h}(\tilde{\boldsymbol{\chi}}, \tilde{z}) \rightarrow \tilde{z} = \tilde{\mathrm{h}}(\tilde{\boldsymbol{\chi}}). \tag{C.121}$$

In a similar analysis to the one conducted in the first stage, the new Lyapunov functions must define the growth requirements for $\tilde{\boldsymbol{F}}(\tilde{\boldsymbol{\chi}}, \tilde{z})$ and $\hat{h}(\tilde{\boldsymbol{\chi}}, \tilde{z})$ by satisfying certain inequalities. These growth requirements can be divided in three main groups:

- Reduced order growth requirements, if they refer to the properties that must posses the reduced order subsystem, $\tilde{\boldsymbol{F}}(\tilde{\boldsymbol{\chi}}, \tilde{\mathrm{h}}(\tilde{\boldsymbol{\chi}}))$.
- Boundary layer growth requirements, if they refer to the properties that must posses the boundary layer subsystem, $\hat{g}(\tilde{\boldsymbol{\chi}}, \tilde{\mathrm{h}}(\tilde{\boldsymbol{\chi}}))$.
- Interconnection growth requirements, if they refer to the properties that must posses both subsys-

tems in conjunction to prove the continuity between both the reduced order and the boundary layer subsystems.

The properties for the isolated equilibrium at the origin are discussed in Assumption C.6.1. The growth requirements of both the reduced and boundary layer system separately are addressed in Assumptions C.6.2 and C.6.3 respectively, while the growth requirements that combine both reduced Σ_{SF} and boundary layer Σ_U-subsystem requirements, called interconnection conditions, are defined in Assumptions C.6.4 and C.6.5. These Assumptions are all described in detail bellow.

C.6.1 Isolated Equilibrium of the Origin for the Simplified Example Σ_{SFU} System: Assumption 5.5.1

The origin ($\tilde{\boldsymbol{\chi}} = 0$, $\tilde{z} = 0$) is a unique and isolated equilibrium of Eqns. (C.114–C.115), i.e.

$$0 = \tilde{\boldsymbol{F}}(0,0), \tag{C.122}$$

$$0 = \hat{h}(0,0), \tag{C.123}$$

moreover, $\tilde{z} = \tilde{\mathrm{h}}(\tilde{\boldsymbol{\chi}})$ is the unique root of

$$0 = \hat{h}(\tilde{\boldsymbol{\chi}}, \tilde{z}), \tag{C.124}$$

in $B_{\tilde{\boldsymbol{\chi}}} \times B_{\tilde{z}}$, i.e.

$$0 = \hat{h}(\tilde{\boldsymbol{\chi}}, \tilde{\mathrm{h}}(\tilde{\boldsymbol{\chi}})), \tag{C.125}$$

and there exists a class κ function $p_2(\cdot)$ such that

$$\| \tilde{\mathrm{h}}(\tilde{\boldsymbol{\chi}}) \| \leq p_2 (\| \tilde{\boldsymbol{\chi}} \|)\,. \tag{C.126}$$

The reduced order growth requirements are obtained by first considering the subsystem given by Eq. (C.114), and adding and subtracting $\tilde{\boldsymbol{F}}(\tilde{\boldsymbol{\chi}}, \tilde{\mathrm{h}}(\tilde{\boldsymbol{\chi}}))$ to the right-hand side of Eq. (C.114) yielding

$$\dot{\tilde{x}} = \tilde{\boldsymbol{F}}\left(\tilde{\boldsymbol{\chi}}, \tilde{\mathrm{h}}(\chi)\right) + \tilde{\boldsymbol{F}}\left(\tilde{\boldsymbol{\chi}}, \tilde{z}\right) - \tilde{\boldsymbol{F}}\left(\tilde{\boldsymbol{\chi}}, \tilde{\mathrm{h}}(\tilde{\boldsymbol{\chi}})\right), \tag{C.127}$$

where the term $\tilde{\boldsymbol{F}}(\tilde{\boldsymbol{\chi}}, \tilde{z}) - \tilde{\boldsymbol{F}}(\tilde{\boldsymbol{\chi}}, \tilde{\mathrm{h}}(\tilde{\boldsymbol{\chi}}))$ can be viewed as a perturbation of the reduced order Σ_{SF}-subsystem given by

$$\dot{\tilde{\boldsymbol{\chi}}} = \tilde{\boldsymbol{F}}\left(\tilde{\boldsymbol{\chi}}, \tilde{\mathrm{h}}(\tilde{\boldsymbol{\chi}})\right), \tag{C.128}$$

with $\tilde{\boldsymbol{F}}\left(\tilde{\boldsymbol{\chi}}, \tilde{z}\right)$ given by

$$\tilde{\boldsymbol{F}}\left(\tilde{\boldsymbol{\chi}}, \tilde{z}\right) = \begin{bmatrix} \tilde{F}_1\left(\tilde{\boldsymbol{\chi}}, \tilde{z}\right) \\ \tilde{F}_2\left(\tilde{\boldsymbol{\chi}}, \tilde{z}\right) \end{bmatrix} = \begin{bmatrix} \tilde{f}(\tilde{\boldsymbol{\chi}}, \tilde{z}) \\ \hat{g}(\tilde{\boldsymbol{\chi}}, \tilde{z}) \end{bmatrix} = \begin{bmatrix} \tilde{f}\left(\tilde{x}, \tilde{y}, \tilde{z}\right) \\ \hat{g}\left(\tilde{x}, \tilde{y}, \tilde{z}\right) \end{bmatrix}, \tag{C.129}$$

and where

$$\tilde{F}_1\left(\tilde{\boldsymbol{\chi}}, \tilde{z}\right) = -\rho_1\left(\tilde{x} + x^*\right)\left(1 + \left(\tilde{x} + x^*\right)\left(\tilde{z} + z^*\right) + y^*\right) - b_x \tilde{x}, \tag{C.130}$$

$$\tilde{F}_2\left(\tilde{\boldsymbol{\chi}}, \tilde{z}\right) = -\eta_1\left(\left(\tilde{y} + y^*\right) + \left(\tilde{x} + x^*\right)\left(\tilde{z} + z^*\right) + 1\right), \tag{C.131}$$

and with $\tilde{\boldsymbol{F}}(\tilde{\boldsymbol{\chi}}, \tilde{\mathrm{h}}(\tilde{\boldsymbol{\chi}}))$ given by

$$\tilde{\boldsymbol{F}}(\tilde{\boldsymbol{\chi}}, \tilde{\mathrm{h}}(\tilde{\boldsymbol{\chi}})) = \begin{bmatrix} \tilde{F}_{H_1}\left(\tilde{\boldsymbol{\chi}}, \tilde{\mathrm{h}}(\tilde{\boldsymbol{\chi}})\right) = \tilde{F}_1\left(\tilde{\boldsymbol{\chi}}, \tilde{z}\right)\Big|_{\tilde{z}=\tilde{\mathrm{h}}(\chi)} \\ \tilde{F}_{H_2}\left(\tilde{\boldsymbol{\chi}}, \tilde{\mathrm{h}}(\tilde{\boldsymbol{\chi}})\right) = \tilde{F}_2\left(\tilde{\boldsymbol{\chi}}, \tilde{z}\right)\Big|_{\tilde{z}=\tilde{\mathrm{h}}(\chi)} \end{bmatrix}, \tag{C.132}$$

therefore

$$\tilde{F}_1\left(\tilde{\boldsymbol{\chi}}, \tilde{\mathrm{h}}(\tilde{\boldsymbol{\chi}})\right) = (\tilde{x}+x^*)\,\tilde{y}\,(\rho_1 - b_y) - b_x\tilde{x}, \tag{C.133}$$

$$\tilde{F}_2\left(\tilde{\boldsymbol{\chi}}, \tilde{\mathrm{h}}(\tilde{\boldsymbol{\chi}})\right) = -\tilde{b}_y\tilde{y}. \tag{C.134}$$

Similarly as in the Σ_{SF} *Stability Analysis*, it is therefore natural to first satisfy the growth requirements for (C.128), and then consider the effect of the perturbation term $\tilde{\boldsymbol{F}}(\tilde{\boldsymbol{\chi}}, \tilde{z}) - \tilde{\boldsymbol{F}}(\tilde{\boldsymbol{\chi}}, \tilde{\mathrm{h}}(\tilde{\boldsymbol{\chi}}))$. Therefore let proceed to define first the reduced order growth condition.

C.6.2 Proof of Assumption 5.5.7: Reduced System Conditions for the Simplified Example

There exists a positive-definite and decreasing Lyapunov function candidate $V_1(\tilde{\boldsymbol{\chi}})$ that satisfies the following inequality

$$\left(\frac{\partial V_1(\tilde{\boldsymbol{\chi}})}{\partial \tilde{\boldsymbol{\chi}}}\right)^T \tilde{\boldsymbol{F}}\left(\tilde{\boldsymbol{\chi}}, \tilde{\mathrm{h}}(\tilde{\boldsymbol{\chi}})\right) \leq -\alpha_3\psi_2^2(\tilde{\boldsymbol{\chi}}), \tag{C.135}$$

where $\psi_2(\cdot)$ is a scalar function of vector arguments which vanishes only when its argument are zero, and satisfying that $\tilde{\boldsymbol{\chi}} = 0$ is a stable equilibrium of the reduced order system. The left-hand side of inequality (C.135) is given by recalling that $V_1(\tilde{\boldsymbol{\chi}})$ is the associated Lyapunov function previously derived in the Σ_{SF}-subsystem *Stability Analysis*, Eq. (6.202), and defined as

$$V_1(\tilde{\boldsymbol{\chi}}) = (1-d_1)\,V_s(\tilde{x}) + d_1 V_f(\hat{y}) = \frac{1-d_1}{2}P_s\tilde{x}^2 + \frac{d_1}{2}P_f\tilde{y}^2, \tag{C.136}$$

being therefore easy to see that

$$\left(\frac{\partial V_1(\chi)}{\partial \tilde{\boldsymbol{\chi}}}\right)^T = \begin{bmatrix} \frac{\partial V_1(\tilde{\boldsymbol{\chi}})}{\partial \tilde{x}} \\ \frac{\partial V_1(\tilde{\boldsymbol{\chi}})}{\partial \tilde{y}} \end{bmatrix} = \begin{bmatrix} \nu_1\tilde{x} \\ \nu_2\tilde{y} \end{bmatrix}, \tag{C.137}$$

with

$$\nu_1 = (1-d_1)P_s, \tag{C.138}$$

$$\nu_2 = d_1 P_f, \tag{C.139}$$

and also recalling that $\tilde{\boldsymbol{F}}(\tilde{\boldsymbol{\chi}}, \tilde{\mathrm{h}}(\tilde{\boldsymbol{\chi}}))$ is given by

$$\tilde{\boldsymbol{F}}(\tilde{\boldsymbol{\chi}}, \tilde{\mathrm{h}}(\tilde{\boldsymbol{\chi}})) = \begin{bmatrix} \tilde{F}_{H_1}\left(\tilde{\boldsymbol{\chi}}, \tilde{\mathrm{h}}(\tilde{\boldsymbol{\chi}})\right) = \tilde{F}_1\left(\tilde{\boldsymbol{\chi}}, \tilde{z}\right)\Big|_{\tilde{z}=\tilde{\mathrm{h}}(\chi)} \\ \tilde{F}_{H_2}\left(\tilde{\boldsymbol{\chi}}, \tilde{\mathrm{h}}(\tilde{\boldsymbol{\chi}})\right) = \tilde{F}_2\left(\tilde{\boldsymbol{\chi}}, \tilde{z}\right)\Big|_{\tilde{z}=\tilde{\mathrm{h}}(\chi)} \end{bmatrix}, \tag{C.140}$$

with

$$\tilde{F}_1\left(\tilde{\boldsymbol{\chi}}, \tilde{\mathrm{h}}(\tilde{\boldsymbol{\chi}})\right) = (\tilde{x}+x^*)\,\tilde{y}\,(\rho_1 - b_y) - b_x\tilde{x}, \tag{C.141}$$

$$\tilde{F}_2\left(\tilde{\boldsymbol{\chi}}, \tilde{\mathrm{h}}(\tilde{\boldsymbol{\chi}})\right) = -\tilde{b}_y\tilde{y}. \tag{C.142}$$

Expanding the left hand side of inequality (C.135) by using Eqns. (C.137) and (C.140), and noting that from a control design point point of view it is desired that $b_x > \rho_1$, therefore resulting in

$$\begin{aligned}\left(\frac{\partial V_1(\tilde{\boldsymbol{\chi}})}{\partial \tilde{\boldsymbol{\chi}}}\right)^T \tilde{\boldsymbol{F}}\left(\tilde{\boldsymbol{\chi}}, \tilde{\mathrm{h}}(\tilde{\boldsymbol{\chi}})\right) &= \nu_1\tilde{x}\left[(\tilde{x}+x^*)\,\tilde{y}\,(\rho_1-b_y) - b_x\tilde{x}\right] - \nu_2\tilde{b}_y\tilde{y}^2 \\ &= -\nu_1\tilde{x}\left[(\tilde{x}+x^*)\,\tilde{y}\,(b_y-\rho_1) - b_x\tilde{x}\right] - \nu_2\tilde{b}_y\tilde{y}^2 \\ &= -\nu_1\,(\tilde{x}+x^*)\,(b_y-\rho_1)\,\tilde{x}\tilde{y} - \nu_1 b_x\tilde{x}^2 - \nu_2\tilde{b}_y\tilde{y}^2.\end{aligned} \tag{C.143}$$

Equation (C.143) can be simplified by recalling that $\tilde{x} + x^* \triangleq x$, and also considering that $x_{MAX} \geq x \geq x_{MIN}$. With this in mind, inequality (C.143) is rewritten as

$$\begin{aligned}\left(\frac{\partial V_1(\tilde{\boldsymbol{\chi}})}{\partial \tilde{\boldsymbol{\chi}}}\right)^T \tilde{\boldsymbol{F}}\left(\tilde{\boldsymbol{\chi}}, \tilde{\mathrm{h}}(\tilde{\boldsymbol{\chi}})\right) &= -\nu_1 (\tilde{x} + x^*)(b_y - \rho_1)\tilde{x}\tilde{y} - \nu_1 b_x \tilde{x}^2 - \nu_2 \tilde{b}_y \tilde{y}^2, \\ &\leq -\nu_1 x_{MAX}(b_y - \rho_1)\tilde{x}\tilde{y} - \nu_1 b_x \tilde{x}^2 - \nu_2 \tilde{b}_y \tilde{y}^2 \\ &= -\mathcal{R}_1 \tilde{x}^2 - \mathcal{R}_2 \tilde{y}^2 - \mathcal{R}_3 \tilde{x}\tilde{y} = -(\tilde{\boldsymbol{\chi}}^T \boldsymbol{\mathcal{R}}_{\tilde{\boldsymbol{\chi}}} \tilde{\boldsymbol{\chi}}),\end{aligned} \tag{C.144}$$

with $\boldsymbol{\mathcal{R}}_{\tilde{\boldsymbol{\chi}}}$ being given by

$$\boldsymbol{\mathcal{R}}_{\tilde{\boldsymbol{\chi}}} = \begin{pmatrix} \mathcal{R}_1 & \mathcal{R}_3 \\ \mathcal{R}_3 & \mathcal{R}_2 \end{pmatrix}, \tag{C.145}$$

where

$$\mathcal{R}_1 = \nu_1 b_x, \tag{C.146}$$

$$\mathcal{R}_2 = \nu_2 \tilde{b}_y, \tag{C.147}$$

$$\mathcal{R}_3 = \frac{1}{2}\nu_1 x_{MAX}(b_y - \rho_1), \tag{C.148}$$

where it is required that $\mathcal{R}$ to be positive definite, that is, $\boldsymbol{\mathcal{R}}_{\tilde{\boldsymbol{\chi}}} > 0$, which is satisfied by observing that $\mathcal{R}_1 > 0$, $\mathcal{R}_2 > 0$ and $\mathcal{R}_3 > 0$, being this last one due to the selection of $b_x > \rho_1$. Therefore, the fulfilment of Assumption (C.6.2) reduces to prove that

$$-(\tilde{\boldsymbol{\chi}}^T \boldsymbol{\mathcal{R}}_{\tilde{\boldsymbol{\chi}}} \tilde{\boldsymbol{\chi}}) \leq -\alpha_3 \psi_2^2(\tilde{\boldsymbol{\chi}}), \tag{C.149}$$

thus, the fulfillment of inequality (C.149), and, therefore, the original inequality (C.135), is done by selecting α_3 and $\psi_2(\tilde{\boldsymbol{\chi}})$ such

$$\alpha_3 \leq 1, \tag{C.150}$$

$$\psi_2(\tilde{\boldsymbol{\chi}}) = \left(\tilde{\boldsymbol{\chi}}^T \boldsymbol{\mathcal{R}}_{\tilde{\boldsymbol{\chi}}} \tilde{\boldsymbol{\chi}}\right)^{\frac{1}{2}}. \tag{C.151}$$

C.6.3 Proof of Assumption 5.5.8: Boundary-Layer System Conditions for the Simplified Example

There exists a positive-definite and decreasing Lyapunov function candidate $V_u(\tilde{\boldsymbol{\chi}}, \tilde{z})$ such that for all $(\tilde{\boldsymbol{\chi}}, \tilde{z}) \in B_{\tilde{\boldsymbol{\chi}}} \times B_{\tilde{z}}$ satisfies

$$V_u(\tilde{\boldsymbol{\chi}}, \tilde{z}) > 0,\ \forall \tilde{z} \neq \tilde{\mathrm{h}}(\tilde{\boldsymbol{\chi}}) \ \textit{and}\ V_u(\tilde{\boldsymbol{\chi}}, \tilde{\mathrm{h}}(\tilde{\boldsymbol{\chi}})) = 0, \tag{C.152}$$

and also satisfies

$$\left(\frac{\partial V_u}{\partial \tilde{z}}\right)^T \hat{h}(\tilde{\boldsymbol{\chi}}, \tilde{z}) \leq -\alpha_4 \phi_2^2(\tilde{z} - \tilde{\mathrm{h}}(\tilde{\boldsymbol{\chi}})),\ \alpha_4 > 0, \tag{C.153}$$

where $V_u(\tilde{\boldsymbol{\chi}}, \tilde{z})$ is the Lyapunov function candidate of the boundary layer Σ_U-subsystem, Eq. (C.120) in which $\tilde{\boldsymbol{\chi}}$ is treated as a fixed parameter, and $\phi_2(\cdot)$ is a scalar function of vector arguments which vanishes only when its arguments are zero, and satisfying that $\tilde{z} - \tilde{\mathrm{h}}(\tilde{\boldsymbol{\chi}})$ is a stable equilibrium of the boundary layer system. Both $\psi_2(\cdot)$ and $\phi_2(\cdot)$ will be referred as comparison functions. The left-hand side of inequality (C.153) is given by recalling that V_u is the Lyapunov function for the Σ_U-subsystem, Eq. (C.120), and is given by

$$V_u(\hat{z}) = \frac{1}{2}\hat{z}^T P_u \hat{z} = \frac{Q_u}{4\eta_2}\hat{z}^2, \tag{C.154}$$

with

$$\hat{z} = \tilde{z} - \tilde{\mathrm{h}}(\tilde{\boldsymbol{\chi}}), \tag{C.155}$$

being therefore easy to see that

$$\left(\frac{\partial V_u}{\partial \tilde{z}}\right)^T = (P_u \hat{z})^T = \frac{Q_u}{2\eta_2}\hat{z}, \tag{C.156}$$

and also recalling from section C.3.4, that the Σ_U-subsystem, Eq. (C.120), can be rewritten in terms of Eq. (C.155), yielding

$$\hat{h}(\tilde{\boldsymbol{\chi}}, \tilde{z}) = A_u \hat{z}, \tag{C.157}$$

where

$$A_u = -\eta_2. \tag{C.158}$$

Substituting both Eqns. (C.156) and (C.157), into the left-hand side of inequality (C.153) yields

$$\left(\frac{\partial V_u}{\partial \tilde{z}}\right)^T \hat{h}(\tilde{\boldsymbol{\chi}}, \tilde{z}) = (P_u \hat{z})^T A_u \hat{z} = \hat{z}^T P_u A_u \hat{z} = -\hat{z}^T \mathcal{A}_u \hat{z}, \tag{C.159}$$

being $\mathcal{A}_u$ defined as

$$\mathcal{A}_u = P_u A_u = \frac{Q_u}{2}. \tag{C.160}$$

Therefore the left-hand side of inequality (C.6.3) reduces to

$$\left(\frac{\partial V_U}{\partial \tilde{z}}\right)^T \hat{h}(\tilde{\boldsymbol{\chi}}, \tilde{z}) = -\frac{1}{2}\left(\hat{z}^T Q_u \hat{z}\right), \tag{C.161}$$

where Q_u is given by Eq. (C.37). Let introduce $\tilde{Q}_u = \frac{Q_u}{2}$, thus inequality (C.153) can be rewritten as

$$\left(\frac{\partial V_u}{\partial \tilde{z}}\right)^T \hat{h}(\tilde{\boldsymbol{\chi}}, \tilde{z}) = -\left(\hat{z}^T \tilde{Q}_U \hat{z}\right) \leq -\alpha_4 \phi_2^2(\tilde{z} - \tilde{\mathrm{h}}(\tilde{\boldsymbol{\chi}})). \tag{C.162}$$

Therefore inequality (C.153) can be satisfied by selecting α_4 and $\phi_2(\hat{z})$ such

$$\alpha_4 \leq 1, \tag{C.163}$$

$$\phi_2(\hat{z}) = \left(\hat{z}^T \tilde{Q}_u \hat{z}\right)^{\frac{1}{2}} = \left(\tilde{Q}_u \hat{z}^2\right)^{\frac{1}{2}}. \tag{C.164}$$

For simplicity $\phi_2(\hat{z})$ will be used instead of $\phi_2(\tilde{z} - \tilde{\mathrm{h}}(\tilde{\boldsymbol{\chi}}))$ throughout the reminder of the document, recalling that $\hat{z} = \tilde{z} - \tilde{\mathrm{h}}(\tilde{\boldsymbol{\chi}}, \tilde{z})$.

C.6.4 Proof of Assumption 5.5.9: First Interconnection Condition for the Simplified Example

The Lyapunov functions $V_1(\tilde{\boldsymbol{\chi}})$ and $V_u(\tilde{\boldsymbol{\chi}}, \tilde{z})$ must satisfy the so called interconnection conditions. The first interconnection condition is obtained by computing the derivative of $V_{\mathcal{S}}(\tilde{x})$ along the solution of Eq. (C.127), resulting in

$$\dot{V}_1(\tilde{\boldsymbol{\chi}}) = \frac{\partial V_1}{\partial \tilde{\boldsymbol{\chi}}} \tilde{\boldsymbol{F}}\left(\tilde{\boldsymbol{\chi}}, \tilde{\mathrm{h}}(\tilde{\boldsymbol{\chi}})\right) + \frac{\partial V_1}{\partial \tilde{\boldsymbol{\chi}}}\left[\tilde{\boldsymbol{F}}(\tilde{\boldsymbol{\chi}}, \tilde{z}) - \tilde{\boldsymbol{F}}(\tilde{\boldsymbol{\chi}}, \tilde{\mathrm{h}}(\tilde{\boldsymbol{\chi}}))\right] \tag{C.165}$$

$$\leq -\alpha_3 \psi_2^2 \tilde{\boldsymbol{\chi}} + \frac{\partial V_1}{\partial \tilde{\boldsymbol{\chi}}}\left[\tilde{\boldsymbol{F}}(\tilde{\boldsymbol{\chi}}, \tilde{z}) - \tilde{\boldsymbol{F}}\left(\tilde{\boldsymbol{\chi}}, \tilde{\mathrm{h}}(\tilde{\boldsymbol{\chi}})\right)\right], \tag{C.166}$$

thus assuming that

$$\left(\frac{\partial V_1(\tilde{\boldsymbol{\chi}})}{\partial \tilde{\boldsymbol{\chi}}}\right)^T \left[\tilde{\boldsymbol{F}}\left(\tilde{\boldsymbol{\chi}}, \tilde{z}\right) - \tilde{\boldsymbol{F}}\left(\tilde{\boldsymbol{\chi}}, \tilde{\mathrm{h}}(\tilde{\boldsymbol{\chi}})\right)\right] \leq \beta_3 \psi_2(\tilde{\boldsymbol{\chi}})\phi_2(\tilde{z} - \tilde{\mathrm{h}}(\tilde{\boldsymbol{\chi}})), \tag{C.167}$$

so that

$$\dot{V}_1 \leq -\alpha_3 \psi_2^2(\tilde{\boldsymbol{\chi}}) + \beta_3 \psi_2(\tilde{\boldsymbol{\chi}})\phi_2(\tilde{\boldsymbol{\chi}} - \tilde{\mathrm{h}}(\tilde{\boldsymbol{\chi}})). \tag{C.168}$$

Inequality (C.167) determines the allowed growth of $\tilde{\boldsymbol{F}}\left(\tilde{\boldsymbol{\chi}}, \tilde{z}\right)$ in $\tilde{z}$, and in typical problems, verifying Assumption C.6.4 reduces to verifying the inequality

$$\left\| \tilde{\boldsymbol{F}}\left(\tilde{\boldsymbol{\chi}}, \tilde{z}\right) - \tilde{\boldsymbol{F}}\left(\tilde{\boldsymbol{\chi}}, \tilde{\mathrm{h}}(\tilde{\boldsymbol{\chi}})\right)\right\| \leq \psi_2(\tilde{\boldsymbol{\chi}})\phi_2(\tilde{z} - \tilde{\mathrm{h}}(\tilde{\boldsymbol{\chi}})), \tag{C.169}$$

which implies that the rate of growth of $\tilde{\boldsymbol{F}}\left(\tilde{\boldsymbol{\chi}}, \tilde{z}\right)$ cannot be faster than the rate of growth of the comparison function $\phi_2(\cdot)$. The left-hand side of inequality (C.167) is given by recalling that, as previously derived

$$\left(\frac{\partial V_1(\chi)}{\partial \tilde{\boldsymbol{\chi}}}\right)^T = \begin{bmatrix} \frac{\partial V_1(\tilde{\boldsymbol{\chi}})}{\partial \tilde{x}} \\ \frac{\partial V_1(\tilde{\boldsymbol{\chi}})}{\partial \tilde{y}} \end{bmatrix} = \begin{bmatrix} \nu_1 \tilde{x} \\ \nu_2 \tilde{y} \end{bmatrix}, \tag{C.170}$$

with

$$\nu_1 = (1 - d_1) P_s, \tag{C.171}$$

$$\nu_2 = d_1 P_f, \tag{C.172}$$

and recalling that as seen previously, $\tilde{\boldsymbol{F}}\left(\tilde{\boldsymbol{\chi}}, \tilde{z}\right)$ is given by

$$\tilde{\boldsymbol{F}}\left(\tilde{\boldsymbol{\chi}}, \tilde{z}\right) = \begin{bmatrix} \tilde{F}_1\left(\tilde{\boldsymbol{\chi}}, \tilde{z}\right) \\ \tilde{F}_2\left(\tilde{\boldsymbol{\chi}}, \tilde{z}\right) \end{bmatrix} = \begin{bmatrix} \tilde{f}(\tilde{\boldsymbol{\chi}}, \tilde{z}) \\ \tilde{g}(\tilde{\boldsymbol{\chi}}, \tilde{z}) \end{bmatrix} = \begin{bmatrix} \tilde{f}\left(\tilde{x}, \tilde{y}, \tilde{z}\right) \\ \tilde{g}\left(\tilde{x}, \tilde{y}, \tilde{z}\right) \end{bmatrix}, \tag{C.173}$$

with

$$\tilde{F}_1\left(\tilde{\boldsymbol{\chi}}, \tilde{z}\right) = -\rho_1\left(\tilde{x} + x^*\right)\left[1 + \left(\tilde{x} + x^*\right)\left(\tilde{z} + z^*\right) + y^*\right] - b_x \tilde{x}, \tag{C.174}$$

$$\tilde{F}_2\left(\tilde{\boldsymbol{\chi}}, \tilde{z}\right) = -\eta_1\left[\left(\tilde{y} + y^*\right) + \left(\tilde{x} + x^*\right)\left(\tilde{z} + z^*\right) + 1\right], \tag{C.175}$$

and with $\tilde{\boldsymbol{F}}\left(\tilde{\boldsymbol{\chi}}, \tilde{\mathrm{h}}(\tilde{\boldsymbol{\chi}})\right)$ given by

$$\tilde{\boldsymbol{F}}(\tilde{\boldsymbol{\chi}}, \tilde{\mathrm{h}}(\tilde{\boldsymbol{\chi}})) = \begin{bmatrix} \tilde{F}_{H_1}\left(\tilde{\boldsymbol{\chi}}, \tilde{\mathrm{h}}(\tilde{\boldsymbol{\chi}})\right) = \tilde{F}_1\left(\tilde{\boldsymbol{\chi}}, \tilde{z}\right)\Big|_{\tilde{z}=\tilde{\mathrm{h}}(\chi)} \\ \tilde{F}_{H_2}\left(\tilde{\boldsymbol{\chi}}, \tilde{\mathrm{h}}(\tilde{\boldsymbol{\chi}})\right) = \tilde{F}_2\left(\tilde{\boldsymbol{\chi}}, \tilde{z}\right)\Big|_{\tilde{z}=\tilde{\mathrm{h}}(\chi)} \end{bmatrix}, \tag{C.176}$$

with

$$\tilde{F}_1\left(\tilde{\boldsymbol{\chi}}, \tilde{\mathrm{h}}(\tilde{\boldsymbol{\chi}})\right) = \left(\tilde{x} + x^*\right)\tilde{y}\left(\rho_1 - b_y\right) - b_x \tilde{x}, \tag{C.177}$$

$$\tilde{F}_2\left(\tilde{\boldsymbol{\chi}}, \tilde{\mathrm{h}}(\tilde{\boldsymbol{\chi}})\right) = -\tilde{b}_y \tilde{y}, \tag{C.178}$$

therefore having that

$$\tilde{\boldsymbol{F}}(\tilde{\boldsymbol{\chi}}, \tilde{z}) - \tilde{\boldsymbol{F}}(\tilde{\boldsymbol{\chi}}, \tilde{\mathrm{h}}(\tilde{\boldsymbol{\chi}})) = \begin{bmatrix} \tilde{F}_1 - \tilde{F}_{H_1} \\ \tilde{F}_2 - \tilde{F}_{H_2} \end{bmatrix} = \begin{bmatrix} \hat{F}_1 \\ \hat{F}_2 \end{bmatrix}, \tag{C.179}$$

being

$$\hat{F}_1 = -\rho_1\left(\tilde{x} + x^*\right)\left[1 + \left(\tilde{x} + x^*\right)\left(\tilde{z} + z^*\right) + y^*\right] - \left(\tilde{x} + x^*\right)\tilde{y}\left(\rho_1 - b_y\right), \tag{C.180}$$

$$\hat{F}_2 = -\eta_1\left[\left(\tilde{y} + y^*\right) + \left(\tilde{x} + x^*\right)\left(\tilde{z} + z^*\right) + 1\right] + \tilde{b}_y \tilde{y}. \tag{C.181}$$

It can be proven that both, $\hat{F}_1$ and $\hat{F}_2$, Eqns. (C.180) and (C.181), respectively, can be expressed in terms of the quasi-steady-state equilibrium (6.23) where

$$\tilde{\mathrm{h}}(\tilde{\boldsymbol{\chi}}) = \tilde{\mathrm{h}}(\tilde{x},\tilde{y}) \quad = \quad \tilde{z} = -\frac{1}{\tilde{x}+x^*}\left[(\tilde{y}+y^*)+1-\frac{\tilde{b}_y}{\eta_1}\tilde{y}\right]-z^*, \tag{C.182}$$

resulting in

$$\begin{aligned} \hat{F}_1 &= -\rho_1\left(\tilde{x}+x^*\right)\left[1+\left(\tilde{x}+x^*\right)\left(\tilde{z}+z^*\right)+y^*\right]-\left(\tilde{x}+x^*\right)\tilde{y}\left(\rho_1-b_y\right) \\ &= -\rho_1\left(\tilde{x}+x^*\right)^2\left(\tilde{z}-\tilde{\mathrm{h}}(\tilde{x},\tilde{y})\right) \\ &= -\rho_1\left(\tilde{x}+x^*\right)^2\hat{z}, \end{aligned} \tag{C.183}$$

$$\begin{aligned} \hat{F}_2 &= -\eta_1\left[(\tilde{y}+y^*)+\left(\tilde{x}+x^*\right)\left(\tilde{z}+z^*\right)+1\right]+\tilde{b}_y\tilde{y} \\ &= -\eta_1\left(\tilde{x}+x^*\right)^2\left(\tilde{z}-\tilde{\mathrm{h}}(\tilde{x},\tilde{y})\right) \\ &= -\eta_1\left(\tilde{x}+x^*\right)^2\hat{z}, \end{aligned} \tag{C.184}$$

therefore using (C.170), (C.183), and (C.184) into inequality (C.169) results in

$$\begin{aligned} \left(\frac{\partial V_1(\tilde{\boldsymbol{\chi}})}{\partial\tilde{\boldsymbol{\chi}}}\right)^T\left[\tilde{\boldsymbol{F}}\left(\tilde{\boldsymbol{\chi}},\tilde{z}\right)-\tilde{\boldsymbol{F}}\left(\tilde{\boldsymbol{\chi}},\tilde{\mathrm{h}}(\tilde{\boldsymbol{\chi}})\right)\right] &= -\nu_1\tilde{x}\rho_1\left(\tilde{x}+x^*\right)^2\hat{z}-\nu_2\tilde{y}\eta_1\left(\tilde{x}+x^*\right)^2\hat{z} \\ &\le \beta_3\psi_2(\tilde{\boldsymbol{\chi}})\phi_2(\tilde{z}-\tilde{\mathrm{h}}(\tilde{\boldsymbol{\chi}})). \end{aligned} \tag{C.185}$$

Recalling the definition of the comparison functions $\psi_2(\tilde{\boldsymbol{\chi}})$ and $\phi_2(\hat{z})$, Eqns. (C.151) and (C.164), respectively, permits to rewrite inequality (C.185) as

$$\begin{aligned} \left(\frac{\partial V_1(\tilde{\boldsymbol{\chi}})}{\partial\tilde{\boldsymbol{\chi}}}\right)^T\left[\tilde{\boldsymbol{F}}\left(\tilde{\boldsymbol{\chi}},\tilde{z}\right)-\tilde{\boldsymbol{F}}\left(\tilde{\boldsymbol{\chi}},\tilde{\mathrm{h}}(\tilde{\boldsymbol{\chi}})\right)\right] &= -\nu_1\tilde{x}\rho_1\left(\tilde{x}+x^*\right)^2\hat{z}-\nu_2\tilde{y}\eta_1\left(\tilde{x}+x^*\right)^2\hat{z} \\ &\le \beta_3\left(\tilde{\boldsymbol{\chi}}^T\boldsymbol{\mathcal{R}}_{\tilde{\boldsymbol{\chi}}}\tilde{\boldsymbol{\chi}}\right)^{\frac{1}{2}}\left(\tilde{Q}_u\hat{z}^2\right)^{\frac{1}{2}}, \end{aligned} \tag{C.186}$$

therefore, the fulfillment of the original inequality (C.167) reduces to prove

$$-\nu_1\tilde{x}\rho_1\left(\tilde{x}+x^*\right)^2\hat{z}-\nu_2\tilde{y}\eta_1\left(\tilde{x}+x^*\right)^2\hat{z} \le \beta_3\left(\tilde{\boldsymbol{\chi}}^T\boldsymbol{\mathcal{R}}_{\tilde{\boldsymbol{\chi}}}\tilde{\boldsymbol{\chi}}\right)^{\frac{1}{2}}\left(\tilde{Q}_u\hat{z}^2\right)^{\frac{1}{2}}. \tag{C.187}$$

The left-hand side of inequality (C.187) can be simplified by recalling that $\tilde{x}+x^* \triangleq x$, and also $x_{MAX} \ge x \ge x_{MIN}$. With this in mind, let define

$$\mathcal{D}_1 = \nu_1\rho_1 x_{MAX}^2 = (1-d_1)P_s\rho_1 x_{MAX}^2, \tag{C.188}$$

$$\mathcal{D}_2 = \nu_2\eta_1 x_{MAX}^2 = d_1 P_f\eta_1 x_{MAX}^2, \tag{C.189}$$

therefore the left hand side of inequality (C.187) can be rewritten as

$$\begin{aligned} -\nu_1\tilde{x}\rho_1\left(\tilde{x}+x^*\right)^2\hat{z}-\nu_2\tilde{y}\eta_1\left(\tilde{x}+x^*\right)^2\hat{z} &\le -\hat{z}\left(\mathcal{D}_1\tilde{x}+\mathcal{D}_2\tilde{y}\right) \\ &\le \beta_3\left(\tilde{\boldsymbol{\chi}}^T\boldsymbol{\mathcal{R}}_{\tilde{\boldsymbol{\chi}}}\tilde{\boldsymbol{\chi}}\right)^{\frac{1}{2}}\left(\tilde{Q}_u\hat{z}^2\right)^{\frac{1}{2}}, \end{aligned} \tag{C.190}$$

therefore fulfillment of Assumption C.6.4 reduces to prove inequality

$$-\hat{z}\left(\mathcal{D}_1\tilde{x}+\mathcal{D}_2\tilde{y}\right) \le \beta_3\left(\tilde{\boldsymbol{\chi}}^T\boldsymbol{\mathcal{R}}_{\tilde{\boldsymbol{\chi}}}\tilde{\boldsymbol{\chi}}\right)^{\frac{1}{2}}\left(\tilde{Q}_u\hat{z}^2\right)^{\frac{1}{2}}. \tag{C.191}$$

In order to obtain the constant β_3 that guarantees the fulfillment of inequality (C.191), that is, fulfilling Assumption C.6.4 for the first interconnection growth requirement, let square both sides of inequality (C.191), resulting in

$$\hat{z}^2\left(\mathcal{D}_1\tilde{x}+\mathcal{D}_2\tilde{y}\right)^2 \le \beta_3^2\left(\tilde{\boldsymbol{\chi}}^T\boldsymbol{\mathcal{R}}_{\tilde{\boldsymbol{\chi}}}\tilde{\boldsymbol{\chi}}\right)\left(\tilde{Q}_u\hat{z}^2\right), \tag{C.192}$$

therefore reducing the fulfillment of the original inequality (C.167) to find the β_3 constant that satisfies the inequality given by

$$\hat{z}^2 \left(\mathcal{D}_1^2 \tilde{x}^2 + \mathcal{D}_2^2 \tilde{y}^2 + 2\mathcal{D}_1\mathcal{D}_2\tilde{x}\tilde{y}\right)^2 \leq \beta_3^2 \tilde{Q}_u \hat{z}^2 \left(\mathcal{R}_1\tilde{x}^2 + \mathcal{R}_2\tilde{y}_1^2 + 2\mathcal{R}_3\tilde{x}\tilde{y}\right), \tag{C.193}$$

with β_3 given by

$$\beta_3 = \max\left(\beta_{3_a}, \beta_{3_b}, \beta_{3_c}\right), \tag{C.194}$$

where

$$\beta_{3_a} \geq \sqrt{\frac{\mathcal{D}_1^2}{\tilde{Q}_u\mathcal{R}_1}}, \tag{C.195}$$

$$\beta_{3_b} \geq \sqrt{\frac{\mathcal{D}_2^2}{\tilde{Q}_u\mathcal{R}_2}}, \tag{C.196}$$

$$\beta_{3_c} \geq \sqrt{\frac{\mathcal{D}_1\mathcal{D}_2}{\tilde{Q}_u\mathcal{R}_3}}, \tag{C.197}$$

with $\mathcal{R}_1$, $\mathcal{R}_2$, and $\mathcal{R}_3$ given in Eqns. (C.146), (C.147), and (C.148), respectively, and $\mathcal{D}_1$, and $\mathcal{D}_2$ given in (C.188), (C.189). The expressions (C.195), (C.196) and (C.197) can be expanded resulting in

$$\beta_{3_a} \geq \sqrt{\frac{\mathcal{D}_1^2}{\tilde{Q}_u\mathcal{R}_1}} = \sqrt{\frac{(1-d_1)\rho_1^2 x_{MAX}^4}{b_x^2}\frac{Q_s}{Q_u}}, \tag{C.198}$$

$$\beta_{3_b} \geq \sqrt{\frac{\mathcal{D}_2^2}{\tilde{Q}_u\mathcal{R}_2}} = \sqrt{\frac{d_1\eta_1^2 x_{MAX}^4}{\tilde{b}_y^2}\frac{Q_f}{Q_u}}, \tag{C.199}$$

$$\beta_{3_c} \geq \sqrt{\frac{\mathcal{D}_1\mathcal{D}_2}{\tilde{Q}_u\mathcal{R}_3}} = \sqrt{\frac{2d_1\rho_1\eta_1 x_{MAX}^3}{\tilde{b}_y\left(\tilde{b}_y - \rho_1\right)}\frac{Q_f}{Q_u}}, \tag{C.200}$$

where observing Eqns. (C.198–C.200), the final selection of β_3 depends on physical parameters given by the problem, and the selection of Q_s and Q_f. From inspection it can be proven that, for $Q_s > 0$ and $Q_f > 0$, $\beta_{3_b} > \beta_{3_a}$ and $\beta_{3_b} > \beta_{3_c}$ therefore resulting in

$$\beta_3 = \max\left(\beta_{3_a}, \beta_{3_b}, \beta_{3_c}\right) = \beta_{3_b} = \sqrt{\frac{d_1\eta_1^2 x_{MAX}^4}{\tilde{b}_y^2}\frac{Q_f}{Q_u}}, \tag{C.201}$$

where as it will be shown in the stability results, see section C.6, the proper selection of both, Q_s and Q_f, will determine the final properties of the stability analysis for the full Σ_{SFU} system. Such selection will be described in detail in section C.7.

C.6.5 Proof of Assumption 5.5.10: Second Interconnection Condition for the Simplified Example

The second interconnection condition is defined by the inequality

$$\left(\frac{\partial V_u(\hat{z})}{\partial \tilde{\boldsymbol{\chi}}}\right)^T \tilde{\boldsymbol{F}}\left(\tilde{\boldsymbol{\chi}}, \tilde{z}\right) \leq \gamma_2\phi_2^2(\hat{z}) + \beta_4\psi_2(\tilde{\boldsymbol{\chi}})\phi_2(\hat{z}), \tag{C.202}$$

where $\psi_2(\cdot)$ and $\phi_2(\cdot)$ have been previously derived by satisfying the assumptions C.6.2 and C.6.3. The left-hand side of inequality (C.202) is defined after recalling $V_u(\hat{z})$, Eq. (C.36), and $\tilde{\boldsymbol{F}}\left(\tilde{\boldsymbol{\chi}}, \tilde{z}\right)$, Eq. (C.116), with

$$\tilde{\boldsymbol{F}}\left(\tilde{\boldsymbol{\chi}}, \tilde{z}\right) = \begin{bmatrix} \tilde{F}_1\left(\tilde{\boldsymbol{\chi}}, \tilde{z}\right) \\ \tilde{F}_2\left(\tilde{\boldsymbol{\chi}}, \tilde{z}\right) \end{bmatrix}, \tag{C.203}$$

with

$$\begin{aligned}\tilde{F}_1(\tilde{\boldsymbol{\chi}},\tilde{z}) &= -\rho_1(\tilde{x}+x^*)\left[1+(\tilde{x}+x^*)(\tilde{z}+z^*)+y^*\right]-b_x\tilde{x}, &\text{(C.204)}\\ \tilde{F}_2(\tilde{\boldsymbol{\chi}},\tilde{z}) &= -\eta_1\left[(\tilde{y}+y^*)+(\tilde{x}+x^*)(\tilde{z}+z^*)+1\right]. &\text{(C.205)}\end{aligned}$$

Inequality (C.202) can therefore be rewritten by adding and subtracting $\tilde{\boldsymbol{F}}\left(\tilde{\boldsymbol{\chi}},\tilde{\mathrm{h}}(\tilde{\boldsymbol{\chi}})\right)$ to $\tilde{\boldsymbol{F}}(\tilde{\boldsymbol{\chi}},\tilde{z})$ in the left-hand side of Eq. (C.202) resulting in

$$\begin{aligned}\frac{\partial V_u}{\partial\tilde{\boldsymbol{\chi}}}\tilde{\boldsymbol{F}}(\tilde{\boldsymbol{\chi}},\tilde{z}) &\leq \frac{\partial V_u}{\partial\tilde{\boldsymbol{\chi}}}\tilde{\boldsymbol{F}}(\tilde{\boldsymbol{\chi}},\tilde{\mathrm{h}}(\tilde{\boldsymbol{\chi}}))+\frac{\partial V_u}{\partial\tilde{\boldsymbol{\chi}}}\left[\tilde{\boldsymbol{F}}(\tilde{\boldsymbol{\chi}},\tilde{z})-\tilde{\boldsymbol{F}}(\tilde{\boldsymbol{\chi}},\tilde{\mathrm{h}}(\tilde{\boldsymbol{\chi}}))\right]\\ &\leq \beta_4\psi_2(\tilde{\boldsymbol{\chi}})\phi_2(\hat{z})+\gamma_2\phi_2^2(\hat{z}). &\text{(C.206)}\end{aligned}$$

Fulfillment of inequality (C.206) can be fulfilled by splitting it into two inequalities given by

$$\begin{aligned}\frac{\partial V_u}{\partial\tilde{\boldsymbol{\chi}}}\left[\tilde{\boldsymbol{F}}(\tilde{\boldsymbol{\chi}},\tilde{z})-\tilde{\boldsymbol{F}}(\tilde{\boldsymbol{\chi}},\tilde{\mathrm{h}}(\tilde{\boldsymbol{\chi}}))\right] &\leq \gamma_2\phi_2^2(\hat{z}), &\text{(C.207)}\\ \frac{\partial V_u}{\partial\tilde{\boldsymbol{\chi}}}\tilde{\boldsymbol{F}}(\tilde{\boldsymbol{\chi}},\tilde{\mathrm{h}}(\tilde{\boldsymbol{\chi}})) &\leq \beta_4\psi_2(\tilde{\boldsymbol{\chi}})\phi_2(\hat{z}), &\text{(C.208)}\end{aligned}$$

therefore, assumption (C.202) will be proven if both inequalities, Eqns. (C.207) and (C.208), respectively, are fulfilled. Considering the first inequality, Eq. (C.207), it can be seen that the left-hand side of assumption (C.207) is defined by

$$\left[\frac{\partial V_u}{\partial\tilde{\boldsymbol{\chi}}}\right]=\begin{bmatrix}\dfrac{\partial V_u}{\partial x}\\ \\ \dfrac{\partial V_u}{\partial\tilde{y}}\end{bmatrix}, \tag{C.209}$$

where

$$\begin{aligned}\frac{\partial V_u}{\partial\tilde{x}} &= -P_u\hat{z}\frac{\partial\tilde{\mathrm{h}}(\tilde{\boldsymbol{\chi}})}{\partial\tilde{x}}, &\text{(C.210)}\\ \frac{\partial V_u}{\partial\tilde{y}} &= -P_u\hat{z}\frac{\partial\tilde{\mathrm{h}}(\tilde{\boldsymbol{\chi}})}{\partial\tilde{y}}, &\text{(C.211)}\end{aligned}$$

where for conciseness let

$$\begin{aligned}\tilde{\mathrm{h}}_{\tilde{x}} &= \frac{\partial\tilde{\mathrm{h}}(\tilde{\boldsymbol{\chi}})}{\partial\tilde{x}}=-\frac{\tilde{\mathrm{h}}(\tilde{\boldsymbol{\chi}})}{\tilde{x}+x^*}=\frac{1}{(\tilde{x}+x^*)^2}\left[(\tilde{y}+y^*)+1-\frac{\tilde{b}_y}{\eta_1}\tilde{y}\right], &\text{(C.212)}\\ \tilde{\mathrm{h}}_{\tilde{y}} &= \frac{\partial\tilde{\mathrm{h}}(\tilde{\boldsymbol{\chi}})}{\partial\tilde{y}}=-\frac{1}{\tilde{x}+x^*}\left[1-\frac{\tilde{b}_y}{\eta_1}\right]. &\text{(C.213)}\end{aligned}$$

Recall that, from a control point of view, it is desired that $\tilde{b}_y>\eta_1$, and therefore, $\frac{\tilde{b}_y}{\eta_1}>1$, thus rewriting Eq. (C.213) as

$$\tilde{\mathrm{h}}_{\tilde{y}}=\frac{1}{\tilde{x}+x^*}\left[\frac{\tilde{b}_y}{\eta_1}-1\right]. \tag{C.214}$$

Therefore, using Eqns. (C.212) and (C.214), permits to rewrite Eq. (C.209) as

$$\left[\frac{\partial V_u}{\partial\tilde{\boldsymbol{\chi}}}\right]=\begin{bmatrix}\dfrac{\partial V_u}{\partial x}\\ \\ \dfrac{\partial V_u}{\partial\tilde{y}}\end{bmatrix}=\begin{bmatrix}-P_u\hat{z}\tilde{\mathrm{h}}_{\tilde{x}}\\ -P_u\hat{z}\tilde{\mathrm{h}}_{\tilde{y}}\end{bmatrix}, \tag{C.215}$$

with $\tilde{\mathrm{h}}_{\tilde{x}}$ and $\tilde{\mathrm{h}}_{\tilde{y}}$ being defined in Eqns. (C.212) and (C.213), respectively. Recalling that $\hat{F}_1$ and $\hat{F}_2$ are given in Eqns. (C.183) and (C.184). Expanding the left-hand side of inequality (C.207) results in

$$
\begin{aligned}
\frac{\partial V_u}{\partial \tilde{\boldsymbol{\chi}}}\left[\tilde{\boldsymbol{F}}(\tilde{\boldsymbol{\chi}},\tilde{z})-\tilde{\boldsymbol{F}}(\tilde{\boldsymbol{\chi}},\tilde{\mathrm{h}}(\tilde{\boldsymbol{\chi}}))\right] &= \frac{\partial V_u}{\partial \tilde{x}}\hat{F}_1+\frac{\partial V_u}{\partial \tilde{y}}\hat{F}_2 \\
&= P_u\left(\tilde{x}+x^*\right)^2\hat{z}^2\left(\rho_1\tilde{\mathrm{h}}_{\tilde{x}}+\eta_1\tilde{\mathrm{h}}_{\tilde{y}}\right) \\
&\leq \gamma_2\phi_2^2(\hat{z}).
\end{aligned}
\tag{C.216}
$$

The left-hand side of inequality (C.216) can be simplified by introducing

$$
\hat{H}_{\tilde{x}} = \left(\tilde{x}+x^*\right)^2\tilde{\mathrm{h}}_{\tilde{x}} = \left(\tilde{y}+y^*\right)+1-\frac{\tilde{b}_y}{\eta_1}\tilde{y}, \tag{C.217}
$$

$$
\hat{H}_{\tilde{y}} = \left(\tilde{x}+x^*\right)^2\tilde{\mathrm{h}}_{\tilde{y}} = -\left(\tilde{x}+x^*\right)\left[1-\frac{\tilde{b}_y}{\eta_1}\right], \tag{C.218}
$$

and recalling that $\tilde{x}+x^* \triangleq x$, and $x_{MAX} \geq x \geq x_{MIN}$, therefore permitting to rewrite inequality (C.216) as

$$
\begin{aligned}
\frac{\partial V_u}{\partial \tilde{\boldsymbol{\chi}}}\left[\tilde{\boldsymbol{F}}(\tilde{\boldsymbol{\chi}},\tilde{z})-\tilde{\boldsymbol{F}}(\tilde{\boldsymbol{\chi}},\tilde{\mathrm{h}}(\tilde{\boldsymbol{\chi}}))\right] &= \frac{\partial V_u}{\partial \tilde{x}}\hat{F}_1+\frac{\partial V_u}{\partial \tilde{y}}\hat{F}_2 \\
&= P_u\left(\tilde{x}+x^*\right)^2\hat{z}^2\left(\rho_1\tilde{\mathrm{h}}_{\tilde{x}}+\eta_1\tilde{\mathrm{h}}_{\tilde{y}}\right) \\
&\leq P_u\hat{z}^2\left(\rho_1\hat{H}_{\tilde{x}}+\eta_1\hat{H}_{\tilde{y}}\right) \\
&\leq \gamma_2\phi_2^2(\hat{z}),
\end{aligned}
\tag{C.219}
$$

therefore, the fulfillment of inequality (C.207) reduces to satisfy

$$
P_u\hat{z}^2\left(\rho_1\hat{H}_{\tilde{x}}+\eta_1\hat{H}_{\tilde{y}}\right) \leq \gamma_2\phi_2^2(\hat{z}), \tag{C.220}
$$

Recalling also that from previous analysis of the states as seen in Table 2.3 that

$$
\tilde{y}_{MAX} \geq \tilde{y} \geq \tilde{y}_{MIN}, \tag{C.221}
$$

with $\tilde{y}_{MIN} = -\tilde{y}_{MAX}$, therefore, and recalling the definitions of $\hat{H}_{\tilde{x}}$ and $\hat{H}_{\tilde{y}}$, Eqns. (C.217) and (C.218), respectively, it can be shown that inequality (C.220) can be further reduced by maximizing the left hand side resulting in

$$
\begin{aligned}
P_u x_{MAX}^2\hat{z}^2\left(\rho_1\tilde{\mathrm{h}}_{\tilde{x}}+\eta_1\tilde{\mathrm{h}}_{\tilde{y}}\right) &\leq P_u x_{MAX}^2\hat{z}^2\left(\rho_1\hat{H}_{\tilde{x}_{MAX}}(\tilde{b}_y)+\eta_1\hat{H}_{\tilde{y}_{MAX}}(\tilde{b}_y)\right) \\
&\leq \gamma_2\phi_2^2(\hat{z}),
\end{aligned}
\tag{C.222}
$$

with $\hat{H}_{\tilde{x}_{MAX}}(\tilde{b}_y)$ and $\hat{H}_{\tilde{y}_{MAX}}(\tilde{b}_y)$ being the maximum values of (C.217) and (C.218), respectively, and given by

$$
\hat{H}_{\tilde{x}_{MAX}}(\tilde{b}_y) = \left(\left(\tilde{y}+y^*\right)+1-\frac{\tilde{b}_y}{\eta_1}\tilde{y}\right)_{MAX}, \tag{C.223}
$$

$$
\hat{H}_{\tilde{y}_{MAX}}(\tilde{b}_y) = \left[\left(\tilde{x}+x^*\right)\left(\frac{\tilde{b}_y}{\eta_1}-1\right)\right]_{MAX}, \tag{C.224}
$$

where it can be proven that both, Eq. (C.223) and Eq. (C.224), are maximized by selecting

$$
\left(\tilde{x}+x^*\right) \triangleq x \quad \rightarrow \quad x_{MAX}, \tag{C.225}
$$

$$
\left(\tilde{y}+y^*\right) \triangleq y \quad \rightarrow \quad y_{MIN}, \tag{C.226}
$$

$$
\tilde{y} \quad \rightarrow \quad \tilde{y}_{MIN}, \tag{C.227}
$$

therefore allowing to rewrite Eqns. (C.223) and (C.224) as

$$
\hat{H}_{\tilde{x}_{MAX}}(\tilde{b}_y) = y_{MIN}+1-\frac{\tilde{b}_y}{\eta_1}\tilde{y}_{MIN}, \tag{C.228}
$$

$$\hat{H}_{\tilde{y}_{MAX}}(\tilde{b}_y) \quad = \quad x_{MAX}\left[\frac{\tilde{b}_y}{\eta_1} - 1\right]. \tag{C.229}$$

Inequality (C.222) can therefore be rewritten as

$$P_u\left(\rho_1\hat{H}_{\tilde{x}_{MAX}}(\tilde{b}_y) + \eta_1\hat{H}_{\tilde{y}_{MAX}}(\tilde{b}_y)\right)\hat{z}^2 = \tilde{\mathcal{N}}\hat{z}^2 \leq \gamma_2\tilde{Q}_u\hat{z}^2, \tag{C.230}$$

with

$$\tilde{\mathcal{N}} = P_u\left(\rho_1\hat{H}_{\tilde{x}_{MAX}}(\tilde{b}_y) + \eta_1\hat{H}_{\tilde{y}_{MAX}}(\tilde{b}_y)\right), \tag{C.231}$$

this allowing to rewrite the original inequality (C.202) as

$$\frac{\partial V_u}{\partial\tilde{\boldsymbol{\chi}}}\left[\tilde{\boldsymbol{F}}(\tilde{\boldsymbol{\chi}},\tilde{z}) - \tilde{\boldsymbol{F}}(\tilde{\boldsymbol{\chi}},\tilde{\mathrm{h}}(\tilde{\boldsymbol{\chi}}))\right] \leq \tilde{\mathcal{N}}\hat{z}^2 \leq \gamma_2\tilde{Q}_u\hat{z}^2, \tag{C.232}$$

therefore, reducing the fulfillment of the original inequality (C.202) to find the γ_2 constant that satisfies the inequality (C.232), which is achieved by selecting γ_2 as

$$\gamma_2 \geq \frac{\tilde{\mathcal{N}}}{\tilde{Q}_u}. \tag{C.233}$$

It can be shown by expanding the right-hand side of Eq (C.233), and using the definition of $P_u = \frac{Q_u}{2\eta_2}$ that

$$\frac{\tilde{\mathcal{N}}}{\tilde{Q}_u} = \frac{2P_u\left(\rho_1\hat{H}_{\tilde{x}_{MAX}}(\tilde{b}_y) + \eta_1\hat{H}_{\tilde{y}_{MAX}}(\tilde{b}_y)\right)}{Q_u} = \frac{\rho_1\hat{H}_{\tilde{x}_{MAX}}(\tilde{b}_y) + \eta_1\hat{H}_{\tilde{y}_{MAX}}(\tilde{b}_y)}{\eta_2}, \tag{C.234}$$

thus implying that γ_2 does only depend on the problem variables

$$\gamma_2 \geq \frac{\rho_1\hat{H}_{\tilde{x}_{MAX}}(\tilde{b}_y) + \eta_1\hat{H}_{\tilde{y}_{MAX}}(\tilde{b}_y)}{\eta_2}, \tag{C.235}$$

with $\hat{H}_{\tilde{x}_{MAX}}(\tilde{b}_y)$ and $\hat{H}_{\tilde{y}_{MAX}}(\tilde{b}_y)$ defined in Eqns. (C.228) and (C.229), respectively. Once proven the first inequality, let proceed to prove the second interconnection inequality , Eq. (C.208), which is given by

$$\frac{\partial V_u}{\partial\tilde{\boldsymbol{\chi}}}\tilde{\boldsymbol{F}}(\tilde{\boldsymbol{\chi}},\tilde{\mathrm{h}}(\tilde{\boldsymbol{\chi}})) \quad \leq \quad \beta_4\psi_2(\tilde{\boldsymbol{\chi}})\phi_2(\hat{z}), \tag{C.236}$$

where the left-hand side of assumption (C.236) is defined by

$$\left[\frac{\partial V_u}{\partial\tilde{\boldsymbol{\chi}}}\right] = \begin{bmatrix} \dfrac{\partial V_u}{\partial x} \\ \\ \dfrac{\partial V_u}{\partial\tilde{y}} \end{bmatrix} = \begin{bmatrix} -P_u\hat{z}\tilde{\mathrm{h}}_{\tilde{x}} \\ -P_u\hat{z}\tilde{\mathrm{h}}_{\tilde{y}} \end{bmatrix}, \tag{C.237}$$

and where

$$\tilde{\boldsymbol{F}}(\tilde{\boldsymbol{\chi}},\tilde{\mathrm{h}}(\tilde{\boldsymbol{\chi}})) = \begin{bmatrix} \tilde{F}_{H_1}\left(\tilde{\boldsymbol{\chi}},\tilde{\mathrm{h}}(\tilde{\boldsymbol{\chi}})\right) = \tilde{F}_1\left(\tilde{\boldsymbol{\chi}},\tilde{z}\right)\Big|_{\tilde{z}=\tilde{\mathrm{h}}(\chi)} \\ \tilde{F}_{H_2}\left(\tilde{\boldsymbol{\chi}},\tilde{\mathrm{h}}(\tilde{\boldsymbol{\chi}})\right) = \tilde{F}_2\left(\tilde{\boldsymbol{\chi}},\tilde{z}\right)\Big|_{\tilde{z}=\tilde{\mathrm{h}}(\chi)} \end{bmatrix}, \tag{C.238}$$

with

$$\begin{aligned} \tilde{F}_{H_1}\left(\tilde{\boldsymbol{\chi}},\tilde{\mathrm{h}}(\tilde{\boldsymbol{\chi}})\right) \quad &= \quad (\tilde{x}+x^*)\,\tilde{y}\,(\rho_1 - b_y) - b_x\tilde{x} \\ &= \quad -(\tilde{x}+x^*)\,\tilde{y}\,(b_y - \rho_1) - b_x\tilde{x}, \end{aligned} \tag{C.239}$$

$$\tilde{F}_{H_2}\left(\tilde{\boldsymbol{\chi}},\tilde{\mathrm{h}}(\tilde{\boldsymbol{\chi}})\right) \quad = \quad -\tilde{b}_y\tilde{y}. \tag{C.240}$$

The left-hand side of inequality (C.236) can be expanded using Eqns. (C.237), (C.239), and (C.240), thus becoming

$$\begin{aligned}
\frac{\partial V_u}{\partial \tilde{\boldsymbol{\chi}}} \tilde{\boldsymbol{F}}(\tilde{\boldsymbol{\chi}}, \tilde{\mathrm{h}}(\tilde{\boldsymbol{\chi}})) &= \frac{\partial V_u}{\partial \tilde{x}} \tilde{F}_{H_1} + \frac{\partial V_u}{\partial \tilde{y}} \tilde{F}_{H_2} \\
&= P_u \tilde{\mathrm{h}}_{\tilde{x}} \hat{z} \left[(\tilde{x} + x^*) (b_y - \rho_1) \tilde{y} + b_x \tilde{x} \right] + P_u \tilde{\mathrm{h}}_{\tilde{y}} \tilde{b}_y \tilde{y} \hat{z} \\
&= P_u \hat{z} \left[(\tilde{x} + x^*) b_x \tilde{\mathrm{h}}_{\tilde{x}} \tilde{x} + \left[(\tilde{x} + x^*) (b_y - \rho_1) \tilde{\mathrm{h}}_{\tilde{x}} + \tilde{\mathrm{h}}_{\tilde{y}} \tilde{b}_y \right] \tilde{y} \right] \\
&= \hat{z} \left(\tilde{\mathcal{L}}_1 \tilde{x} + \tilde{\mathcal{L}}_2 \tilde{y} \right),
\end{aligned} \tag{C.241}$$

with

$$\tilde{\mathcal{L}}_1 = P_u (\tilde{x} + x^*) b_x \tilde{\mathrm{h}}_{\tilde{x}}, \tag{C.242}$$

$$\tilde{\mathcal{L}}_2 = P_u \left[(\tilde{x} + x^*) (b_y - \rho_1) \tilde{\mathrm{h}}_{\tilde{x}} + \tilde{\mathrm{h}}_{\tilde{y}} \tilde{b}_y \right], \tag{C.243}$$

where $\tilde{\mathrm{h}}_{\tilde{x}}$ and $\tilde{\mathrm{h}}_{\tilde{y}}$ are given by using Eqns. (C.212) and (C.214), therefore the fulfillment of inequality (C.236) reduces to satisfy the inequality given by

$$\hat{z} \left(\tilde{\mathcal{L}}_1 \tilde{x} + \tilde{\mathcal{L}}_2 \tilde{y} \right) \leq \beta_4 \psi_2(\tilde{\boldsymbol{\chi}}) \phi_2(\hat{z}). \tag{C.244}$$

It can be shown that inequality (C.244) can be further reduced by maximizing the left hand side such that results in

$$\hat{z} \left(\tilde{\mathcal{L}}_1 \tilde{x} + \tilde{\mathcal{L}}_2 \tilde{y} \right) \leq \hat{z} P_u \left(\tilde{\mathcal{L}}_{1_{MAX}}(b_x, \tilde{b}_y) \tilde{x} + \tilde{\mathcal{L}}_{2_{MAX}}(\tilde{b}_y) \tilde{y} \right) \leq \beta_4 \psi_2(\tilde{\boldsymbol{\chi}}) \phi_2(\hat{z}), \tag{C.245}$$

with $\tilde{\mathcal{L}}_{1_{MAX}}(b_x, \tilde{b}_y)$ and $\tilde{\mathcal{L}}_{2_{MAX}}(\tilde{b}_y)$ being the maximum allowable values of Eqns. (C.242) and (C.243), respectively, where

$$\tilde{\mathcal{L}}_{1_{MAX}}(b_x, \tilde{b}_y) = \left[(\tilde{x} + x^*) b_x \tilde{\mathrm{h}}_{\tilde{x}} \right]_{MAX}, \tag{C.246}$$

$$\tilde{\mathcal{L}}_{2_{MAX}}(\tilde{b}_y) = \left[(\tilde{x} + x^*) (b_y - \rho_1) \tilde{\mathrm{h}}_{\tilde{x}} + \tilde{\mathrm{h}}_{\tilde{y}} \tilde{b}_y \right]_{MAX}, \tag{C.247}$$

where recalling the definitions of both $\tilde{\mathrm{h}}_{\tilde{x}}$ and $\tilde{\mathrm{h}}_{\tilde{y}}$, Eqns. (C.212) and (C.214), respectively, thus rewriting

$$\tilde{\mathcal{L}}_{1_{MAX}}(b_x, \tilde{b}_y) = b_x \left[\frac{1}{\tilde{x} + x^*} \left[(\tilde{y} + y^*) + 1 - \frac{\tilde{b}_y}{\eta_1} \tilde{y} \right] \right]_{MAX}, \tag{C.248}$$

$$\tilde{\mathcal{L}}_{2_{MAX}}(\tilde{b}_y) = \left\{ (b_y - \rho_1) \left[\frac{1}{\tilde{x} + x^*} \left((\tilde{y} + y^*) + 1 - \frac{\tilde{b}_y}{\eta_1} \tilde{y} \right) \right] + \tilde{b}_y \left(\frac{\tilde{b}_y}{\eta_1} - 1 \right) \right\}_{MAX}, \tag{C.249}$$

where it can be proven that both Eq. (C.248), and Eq. (C.249), are maximized by selecting

$$(\tilde{x} + x^*) \triangleq x \rightarrow x_{MIN}, \tag{C.250}$$

$$(\tilde{y} + y^*) \triangleq y \rightarrow y_{MAX}, \tag{C.251}$$

$$\tilde{y} \rightarrow \tilde{y}_{MIN}, \tag{C.252}$$

$$x^* \rightarrow x^*_{MAX}, \tag{C.253}$$

$$y^* \rightarrow y^*_{MIN}, \tag{C.254}$$

therefore, rewriting Eq. (C.248) and Eq. (C.249) as

$$\tilde{\mathcal{L}}_{1_{MAX}}(b_x, \tilde{b}_y) = b_x \left[\frac{1}{x_{MIN}} \left(y_{MAX} + 1 - \frac{\tilde{b}_y}{\eta_1} \tilde{y}_{MIN} \right) \right], \tag{C.255}$$

$$\tilde{\mathcal{L}}_{2_{MAX}}(\tilde{b}_y) = \left\{ (b_y - \rho_1) \left[\frac{1}{x_{MIN}} \left(y_{MAX} + 1 - \frac{\tilde{b}_y}{\eta_1} \tilde{y}_{MIN} \right) \right] + \tilde{b}_y \left(\frac{\tilde{b}_y}{\eta_1} - 1 \right) \right\}. \tag{C.256}$$

In order to obtain the constant β_4 that guarantees the fulfillment of inequality (C.245), that is, fulfilling

Assumption C.6.5 for the first interconnection growth requirement, let square both sides of inequality (C.245), resulting in

$$P_u^2\hat{z}^2\left(\tilde{\mathcal{L}}_{1_{MAX}}(b_x,\tilde{b}_y)\tilde{x}+\tilde{\mathcal{L}}_{2_{MAX}}(\tilde{b}_y)\tilde{y}\right)^2 \leq \beta_4^2\left(\tilde{\boldsymbol{\chi}}^T\boldsymbol{\mathcal{R}}_{\tilde{\boldsymbol{\chi}}}\tilde{\boldsymbol{\chi}}\right)\tilde{Q}_u\hat{z}^2, \tag{C.257}$$

where, after expanding, results in

$$\begin{aligned} & P_u^2\left(\left(\tilde{\mathcal{L}}_{1_{MAX}}(b_x,\tilde{b}_y)\right)^2\tilde{x}^2+\left(\tilde{\mathcal{L}}_{2_{MAX}}(\tilde{b}_y)\right)^2\tilde{y}^2+2\tilde{\mathcal{L}}_{1_{MAX}}(b_x,\tilde{b}_y)\tilde{\mathcal{L}}_{2_{MAX}}(\tilde{b}_y)\tilde{x}\tilde{y}\right)^2\hat{z}^2 \\ \leq\ & \beta_4^2\left(\mathcal{R}_1\tilde{x}^2+\mathcal{R}_2\tilde{y}_1^2+2\mathcal{R}_3\tilde{x}\tilde{y}\right)\tilde{Q}_u\hat{z}^2, \end{aligned} \tag{C.258}$$

therefore reducing the fulfillment of the original inequality (C.208) to find the β_4 constant that satisfies inequality (C.258) with β_4 given by

$$\beta_4 = \max\left(\beta_{4_a},\beta_{4_b},\beta_{4_c}\right), \tag{C.259}$$

where

$$\beta_{4_a} \geq \sqrt{\frac{P_u^2\left(\tilde{\mathcal{L}}_{1_{MAX}}(b_x,\tilde{b}_y)\right)^2}{\tilde{Q}_u\mathcal{R}_1}}, \tag{C.260}$$

$$\beta_{4_b} \geq \sqrt{\frac{P_u^2\left(\tilde{\mathcal{L}}_{2_{MAX}}(\tilde{b}_y)\right)^2}{\tilde{Q}_u\mathcal{R}_2}}, \tag{C.261}$$

$$\beta_{4_c} \geq \sqrt{\frac{P_u^2\tilde{\mathcal{L}}_{1_{MAX}}(b_x,\tilde{b}_y)\tilde{\mathcal{L}}_{2_{MAX}}(\tilde{b}_y)}{\tilde{Q}_u\mathcal{R}_3}}, \tag{C.262}$$

with $\mathcal{R}_1$, $\mathcal{R}_2$, and $\mathcal{R}_3$ given in Eqns. (C.146), (C.147), and (C.148), respectively, and $\tilde{\mathcal{L}}_{1_{MAX}}(b_x,\tilde{b}_y)$, and $\tilde{\mathcal{L}}_{2_{MAX}}(\tilde{b}_y)$ given in Eqns. (C.255), and (C.256), respectively. The expressions (C.260), (C.261) and (C.262) can be expanded resulting in

$$\beta_{4_a} \geq \sqrt{\frac{\left(\tilde{\mathcal{L}}_{1_{MAX}}(b_x,\tilde{b}_y)\right)^2}{\tilde{Q}_u\mathcal{R}_1}} = \sqrt{\frac{\left(\tilde{\mathcal{L}}_{1_{MAX}}(b_x,\tilde{b}_y)\right)^2}{\eta_2^2(1-d_1)}\frac{Q_u}{Q_s}}, \tag{C.263}$$

$$\beta_{4_b} \geq \sqrt{\frac{\left(\tilde{\mathcal{L}}_{2_{MAX}}(\tilde{b}_y)\right)^2}{\tilde{Q}_u\mathcal{R}_2}} = \sqrt{\frac{\left(\tilde{\mathcal{L}}_{2_{MAX}}(\tilde{b}_y)\right)^2}{\eta_2^2 d_1}\frac{Q_u}{Q_f}}, \tag{C.264}$$

$$\beta_{4_c} \geq \sqrt{\frac{\tilde{\mathcal{L}}_{1_{MAX}}(b_x,\tilde{b}_y)\tilde{\mathcal{L}}_{2_{MAX}}(\tilde{b}_y)}{\tilde{Q}_u\mathcal{R}_3}} = \sqrt{\frac{\tilde{\mathcal{L}}_{1_{MAX}}(b_x,\tilde{b}_y)\tilde{\mathcal{L}}_{2_{MAX}}(\tilde{b}_y)}{\eta_2^2(1-d_1)x_{MAX}\left(\tilde{b}_y-\rho_1\right)}\frac{Q_u}{Q_s}}, \tag{C.265}$$

where observing Eqns. (C.263–C.265), the final selection of β_4 depends on physical parameters given by the problem, and the selection of *stability parameters*, Q_s, Q_f, and Q_u. From inspection it can be proven that, for positive $Q_s > 0$, results in $Q_f > 0$ and $Q_u > 0$, $\beta_{4_a} > \beta_{4_b}$ and $\beta_{4_a} > \beta_{4_b}$ therefore resulting in

$$\beta_4 = \max\left(\beta_{4_a},\beta_{4_b},\beta_{4_c}\right) = \beta_{4_a} = \sqrt{\frac{\left(\tilde{\mathcal{L}}_{1_{MAX}}(b_x,\tilde{b}_y)\right)^2}{\eta_2^2(1-d_1)}\frac{Q_u}{Q_s}}, \tag{C.266}$$

where as it will be shown in the stability results, see section C.7, the proper selection of both, Q_s and Q_f, will determine the final properties of the stability analysis for the full Σ_{SFU} system. Such selection will be described in detail in section C.7. The proper selection of γ_2, Eq. (C.233), and β_4, Eq. (C.259), satisfies both inequalities (C.207) and (C.208), therefore, satisfying inequality (C.202) and concluding the asymptotic stability analysis of the full Σ_{SFU} system.

C.7 Fulfillment of the Simplified Example Σ_{SFU} *Stability Analysis*

If assumptions C.6.1, C.6.2, C.6.3, C.6.4, and C.6.5 are all satisfied, then the growth requirements of $\tilde{\boldsymbol{F}}(\tilde{\boldsymbol{\chi}}, \tilde{z})$ and $\hat{g}(\tilde{\boldsymbol{\chi}}, \tilde{z})$ are satisfied, and with the Lyapunov functions $V_1(\tilde{\boldsymbol{\chi}})$ and $V_u(\tilde{\boldsymbol{\chi}}, \tilde{z})$ defined, a new Lyapunov function candidate $V_2(\tilde{\boldsymbol{\chi}}, \tilde{z})$ is considered and defined by the weighted sum of $V_1(\tilde{\boldsymbol{\chi}})$ and $V_u(\tilde{\boldsymbol{\chi}}, \tilde{z})$, given by

$$V_2(\tilde{\boldsymbol{\chi}}, \tilde{z}) = (1 - d_2)V_1(\tilde{\boldsymbol{\chi}}) + d_2 V_u(\hat{z}),\ d_2 \in (0, 1), \tag{C.267}$$

for $0 < d_2 < 1$. The newly defined function $V_2(\tilde{\boldsymbol{\chi}}, \tilde{z})$ becomes the Lyapunov function candidate for the singular perturbed Σ_{SFU} full system (C.114–C.115). To explore the freedom in choosing the weights, lets take d_2 as an unspecified parameter in the interval $(0, 1)$. From the properties of $V_1(\tilde{\boldsymbol{\chi}})$ and $V_u(\tilde{\boldsymbol{\chi}}, \tilde{z})$ and inequality (C.126), that is $\| \tilde{\mathrm{h}}(\tilde{\boldsymbol{\chi}}) \| \leq p_2(\| \tilde{\boldsymbol{\chi}} \|)$, where $p_2(\cdot)$ is a κ function, it follows that $V_2(\tilde{\boldsymbol{\chi}}, \tilde{z})$ is positive-definite. Computing the time derivative of $V_2(\tilde{\boldsymbol{\chi}}, \tilde{z})$ along the trajectories of $\tilde{\boldsymbol{F}}(\tilde{\boldsymbol{\chi}}, \tilde{z})$ and $\hat{g}(\tilde{\boldsymbol{\chi}}, \tilde{z})$ results in

$$\begin{aligned}
\dot{V}_2 &= (1-d_2)\frac{\partial V_1}{\partial \tilde{\boldsymbol{\chi}}}\tilde{\boldsymbol{F}}(\tilde{\boldsymbol{\chi}}, \tilde{z}) + \frac{d_2}{\varepsilon_1\varepsilon_2}\frac{\partial V_u}{\partial \tilde{z}}\hat{g}(\tilde{\boldsymbol{\chi}}, \tilde{z}) + d_2\frac{\partial V_u}{\partial \tilde{\boldsymbol{\chi}}}\tilde{\boldsymbol{F}}(\tilde{\boldsymbol{\chi}}, \tilde{z}) \\
&= (1-d_2)\frac{\partial V_1}{\partial \tilde{\boldsymbol{\chi}}}\tilde{\boldsymbol{F}}\left(\tilde{\boldsymbol{\chi}}, \tilde{\mathrm{h}}(\tilde{\boldsymbol{\chi}})\right) \\
&+ (1-d_2)\frac{\partial V_1}{\partial \tilde{\boldsymbol{\chi}}}\left[\tilde{\boldsymbol{F}}(\tilde{\boldsymbol{\chi}}, \tilde{z}) - \tilde{\boldsymbol{F}}\left(\tilde{\boldsymbol{\chi}}, \tilde{\mathrm{h}}(\tilde{\boldsymbol{\chi}})\right)\right] \\
&+ \frac{d_2}{\varepsilon_1\varepsilon_2}\frac{\partial V_u}{\partial \tilde{z}}\hat{g}(\tilde{\boldsymbol{\chi}}, \tilde{z}) + d_2\frac{\partial V_u}{\partial \tilde{\boldsymbol{\chi}}}\tilde{\boldsymbol{F}}(\tilde{\boldsymbol{\chi}}, \tilde{z}).
\end{aligned} \tag{C.268}$$

Using the inequalities in Assumptions C.6.2, C.6.3, C.6.4 and C.6.5, allows to rewrite Eq. (C.268) as

$$\begin{aligned}
\dot{V}_2 &\leq -(1-d_2)\alpha_3\psi_1^2(\tilde{x}) + (1-d_2)\beta_3\psi_2(\tilde{\boldsymbol{\chi}})\phi_2(\tilde{\boldsymbol{\chi}} - \tilde{\mathrm{h}}(\tilde{\boldsymbol{\chi}})) \\
&- \frac{d_2}{\varepsilon_1\varepsilon_2}\alpha_4\phi_2^2(\tilde{\boldsymbol{\chi}} - \tilde{\mathrm{h}}(\tilde{\boldsymbol{\chi}})) + d_2\gamma_2\phi_2^2(\tilde{\boldsymbol{\chi}} - \tilde{\mathrm{h}}(\tilde{\boldsymbol{\chi}})) + d_2\beta_4\psi_2(\tilde{\boldsymbol{\chi}})\phi_2(\tilde{\boldsymbol{\chi}} - \tilde{\mathrm{h}}(\tilde{\boldsymbol{\chi}})) \\
&= -\begin{bmatrix} \psi_2(\tilde{\boldsymbol{\chi}}) \\ \phi_2(\tilde{z}) - \tilde{\mathrm{h}}(\tilde{\boldsymbol{\chi}}) \end{bmatrix}^T \begin{bmatrix} (1-d_2)\alpha_3 & -\frac{1}{2}(1-d_2)\beta_3 - \frac{1}{2}d_2\beta_4 \\ -\frac{1}{2}(1-d_2)\beta_3 - \frac{1}{2}d_2\beta_4 & d_2\left(\dfrac{\alpha_4}{\varepsilon_1\varepsilon_2} - \gamma_2\right) \end{bmatrix} \\
&\times \begin{bmatrix} \psi_2(\tilde{\boldsymbol{\chi}}) \\ \phi_2(\tilde{z} - \tilde{\mathrm{h}}(\tilde{\boldsymbol{\chi}})) \end{bmatrix}.
\end{aligned} \tag{C.269}$$

The right-hand side of Eq. (C.269) is a quadratic form in $\psi_2(\tilde{\boldsymbol{\chi}})$ and $\phi_2(\tilde{\boldsymbol{\chi}} - \tilde{\mathrm{h}}(\tilde{\boldsymbol{\chi}}))$, where the quadratic form is negative-definite when

$$d_2(1-d_2)\alpha_3\left(\frac{\alpha_4}{\varepsilon_1\varepsilon_2} - \gamma_2\right) > \frac{1}{4}\left[(1-d_2)\beta_3 + d_2\beta_4\right]^2, \tag{C.270}$$

which is equivalent to

$$\frac{1}{\varepsilon_1\varepsilon_2} > \frac{1}{\alpha_3\alpha_4}\left[\alpha_3\gamma + \frac{1}{4(1-d)d}\left[(1-d)\beta_3 + d\beta_4\right]^2\right], \tag{C.271}$$

where from (C.271) it can be obtained an expression for ε_2 as

$$\varepsilon_2 < \frac{\alpha_3\alpha_4}{\varepsilon_1\left[\alpha_3\gamma_2 + \dfrac{1}{4(1-d_2)d_2}\left[(1-d_2)\beta_3 + d_2\beta_4\right]^2\right]} \equiv \varepsilon_{2_d}. \tag{C.272}$$

From inequality (C.272), it can be seen that, depending on the nature of the selected ε_1, it will translate into different upper-bounds on ε_{2_d}, where the most conservative upper-bound, that is the smallest possible ε_{2_d}, is given by the maximum allowable value of ε_1 that guarantees the asymptotic stability properties of the Σ_{SF}-subsystem, which is obtained by selecting the $\varepsilon_1^{\bigstar}$ that was chosen in the Σ_{SF} *Stability Analysis*, resulting in a conservative upper-bound for the problem here studied.

Therefore, by defining $\varepsilon_1^{\bigstar} = d_{\varepsilon_1}\varepsilon_1$, where d_{ε_1} represents the percentage of margin that is applied to the upper-bound, where for the problem here studied, it is selected as $d_{\varepsilon_1} = 1.05$, translating that for safety, the ε_1^* is assumed to be 5% higher than the ε_1 selected for the three-time-scale model. For the simplified problem, the selected parasitic constant for the Σ_{SF}-subsystem and given by $\varepsilon_1 = 0.01$, thus $\varepsilon_1^{\bigstar} = 0.0105$. Recalling from the Σ_{SF} asymptotic stability analysis conducted in section C.4, is given in Eq. (C.109) as

$$\varepsilon_1^* = \varepsilon_1^{\bigstar} = \frac{\alpha_1\alpha_2}{\alpha_1(d_1^{\bigstar})\gamma_1(\varepsilon_1^{\bigstar}) + \beta_1\beta_2}, \tag{C.273}$$

therefore, substituting Eq. (C.273) into Eq. (C.272) results in

$$\varepsilon_2 < \frac{\alpha_1\gamma_1(\varepsilon_1^{\bigstar}) + \beta_1(d_1^{\bigstar})\beta_2}{\alpha_1\alpha_2} \frac{\alpha_3\alpha_4}{\varepsilon_1\left[\alpha_3\gamma_2 + \dfrac{1}{4(1-d_2)d_2}\left[(1-d_2)\beta_3 + d_2\beta_4\right]^2\right]} \equiv \varepsilon_{2_d}, \tag{C.274}$$

where ε_2 represents a more conservative upper-bound on ε_2. The choice of ε_2, Eq. (C.274), is a more suitable expression for the stability analysis conducted on the Σ_{SFU} full system, since considers a suitable upper-bound value with a safety margin given by selecting $\varepsilon_1^{\bigstar} = d_{\varepsilon_1}\varepsilon_1$, where $d_{\varepsilon_1} = 1.05$. Therefore, with this in mind, to satisfy the stability properties of the full Σ_{SFU} system, the results from Eq. (C.274) are sufficient since imply the maximum upper-bound on ε_2 for the selected $\varepsilon_1^{\bigstar}$. Therefore inequality (C.274) shows that for any choice of d_2, the corresponding $V_2(\tilde{\boldsymbol{\chi}}, \tilde{z})$ is a Lyapunov function for the singular perturbed Σ_{SFU} system for all ε_2 satisfying inequality (C.274). The dependance on the right-hand side of Eq. (C.274) on the unspecified parameter d_2 will be studied in section C.6. Analyzing (C.274), the maximum value of ε_2 occurs at

$$d_2^* = \frac{\beta_3}{\beta_3 + \beta_4}, \tag{C.275}$$

yielding for the upper-bound

$$\varepsilon_2^* = \frac{\alpha_3\alpha_4}{\varepsilon_1^{\bigstar}\left(\alpha_3\gamma_2 + \beta_3\beta_4\right)}. \tag{C.276}$$

Therefore it can be inferred that the equilibrium point of the singularly perturbed Σ_{SFU} full system (C.114–C.115) is asymptotically stable for all $\varepsilon_2 < \varepsilon_2^*$. The number ε_2^* is the best upper bound on ε_2 that can be provided by the above presented stability analysis. Assumptions C.6.2, C.6.3, C.6.4 and C.6.5 are summarized in Table C.7, where it can be seen the similarities between the two-time-scale growth requirements described in Section 5.2.1, and the three-time-scale growth requirements for the full Σ_{SFU} system here derived. The asymptotic stability analysis presented can be summarizes in Theorem C.7.1.

Theorem C.7.1 *: Let inequalities (C.135), (C.153), (C.167), and (C.202) be satisfied. Then the origin is an asymptotically stable equilibrium of the singularly perturbed Σ_{SFU} system, Eqns. (C.114–C.115), for all $\varepsilon_2 \in (0, \varepsilon_2^*)$, where ε_2^* is given by Eq. (C.276). Moreover, for every number $d_2 \in (0, 1)$*

$$V_2(\tilde{\boldsymbol{\chi}}, \tilde{z}) = (1-d_2)V_1(\tilde{\boldsymbol{\chi}}) + d_2 V_u(\tilde{\boldsymbol{\chi}}, \tilde{z}), \tag{C.277}$$

is a Lyapunov function for all $\varepsilon_2 \in (0, \varepsilon_{2_d})$, where $\varepsilon_{2_d} \le \varepsilon_2^*$ is given by Eq. (C.276).

Theorem C.7.1 can be summarized by understanding that $\tilde{\boldsymbol{\chi}} = 0$ is an asymptotically stable equilibrium of the reduced Σ_{SF}-subsystem, Eq. (C.119), and $\tilde{z} = \tilde{\mathrm{h}}(\tilde{\boldsymbol{\chi}})$ is an asymptotically stable equilibrium of the boundary-layer Σ_U-subsystem, Eq. (C.120), uniformly in $\tilde{\boldsymbol{\chi}}$, that is, the $\varepsilon - \delta$ definition of *Lyapunov* stability and the convergence $\tilde{z} \to \tilde{\mathrm{h}}(\tilde{\boldsymbol{\chi}})$ are uniform in $\tilde{\boldsymbol{\chi}}$ (Vidyasagar, 2002), and if $\tilde{\boldsymbol{F}}(\tilde{\boldsymbol{\chi}}, \tilde{z})$ and $\hat{g}(\tilde{\boldsymbol{\chi}}, \tilde{z})$ satisfy certain growth conditions on the reduced and boundary-layer systems, then the origin is an asymptotically stable equilibrium of the singularly perturbed Σ_{SFU} full system, Eqns. (C.114–C.115), for sufficiently small ε_2. (Kokotović et al., 1986; Kokotović et al., 1987; Kokotović et al., 1999).

Similarly as in Σ_{SF} *Stability Analysis*, due to the fact that the system is expressed in its error dynamics form, and that the use of the full range of reachable state variables has been required in order to satisfy the inequalities that guarantee the asymptotic stability properties at the origin of the Σ_{SFU}-subsystem, these asymptotic stability properties are also extended to semiglobal stability, by the definition in (Kokotović, 1992; Sussmann and Kokotović, 1991; Braslavsky and Miidleton, 1996), by providing upper bounds on the parasitic singularly perturbed parameters for the entire range of admissible state values, thus extending the domain of attraction to that same rage of admissible states.

Assumption 5.5.7				
Section 5.2	$\frac{\partial V}{\partial x}$	$f(x, \mathrm{h}(x))$	α_1	$\psi(x)$
Σ_{SFU}	$\left(\frac{\partial V_1(\tilde{\boldsymbol{\chi}})}{\partial \tilde{\boldsymbol{\chi}}}\right)^T$	$\tilde{\boldsymbol{F}}(\tilde{\boldsymbol{\chi}}, \tilde{\mathrm{h}}(\tilde{\boldsymbol{\chi}}))$	$\alpha_3 \leq 1$	$\psi_2(\tilde{\boldsymbol{\chi}}) = \left(\tilde{\boldsymbol{\chi}}^T \boldsymbol{\mathcal{R}}_{\tilde{\boldsymbol{\chi}}} \tilde{\boldsymbol{\chi}}\right)^{\frac{1}{2}}$
Assumption 5.5.8				
Section 5.2	$\frac{\partial W}{\partial z}$	$g(x, z)$	α_2	$\phi(z - \mathrm{h}(x))$
Σ_{SFU}	$\left(\frac{\partial V_u(\hat{z})}{\partial \tilde{z}}\right)^T$	$\hat{h}(\tilde{\boldsymbol{\chi}}, \tilde{z})$	$\alpha_4 \leq 1$	$\phi_2(\hat{z}) = \left(\tilde{Q}_u \hat{z}^2\right)^{\frac{1}{2}}$
Assumption 5.5.9				
Section 5.2	$\frac{\partial V}{\partial x}$	$f(x, z)$	$f(x, \mathrm{h}(x))$	β_1
Σ_{SFU}	$\left(\frac{\partial V_1(\tilde{\boldsymbol{\chi}})}{\partial \tilde{\boldsymbol{\chi}}}\right)^T$	$\tilde{\boldsymbol{F}}(\tilde{\boldsymbol{\chi}}, \tilde{z})$	$\tilde{\boldsymbol{F}}(\tilde{\boldsymbol{\chi}}, \tilde{\mathrm{h}}(\tilde{\boldsymbol{\chi}}))$	$\beta_3 \geq \max(\beta_{3_a}, \beta_{3_b}, \beta_{3_c})$
Assumption 5.5.10				
Section 5.2	$\frac{\partial W}{\partial x}$	$f(x, z)$	γ_1	β_2
Σ_{SFU}	$\left(\frac{\partial V_u(\hat{z})}{\partial \tilde{y}}\right)^T$	$\tilde{\boldsymbol{F}}(\tilde{\boldsymbol{\chi}}, \tilde{z})$	$\gamma_2 \geq \frac{\tilde{\mathcal{N}}}{\tilde{Q}_u}$	$\beta_4 \geq \max(\beta_{4_a}, \beta_{4_b}, \beta_{4_c})$

Table C.2: Parameters for the Comparison Functions and Inequalities that Guarantee the Asymptotic Stability Requirements for the Σ_{SFU} Subsystem.

C.7.1 Bounds for the *Stability Parameter* of the Σ_{SFU} *Stability Analysis*

Recalling from the Σ_{SF} stability analysis, that due to the existent freedom on selecting β_2 and γ_1, the upper-bound ε_1^*, Eq. (C.105), and its d_1^* parameter, Eq. (C.104), can be precisely obtained to match the required parameters that guarantee the asymptotic stability for the full Σ_{SFU} system. This is achieved by selecting the appropriate combination of γ_1 and β_2, which in return generates the desired combination of both ε_1^* and d_1^*, which are both obtained using Eqns. (C.105) and (C.104) such

$$\gamma_1(\varepsilon_1^\bigstar) = \frac{1}{\alpha_1}\left(\frac{\alpha_1\alpha_2}{\varepsilon_1^\bigstar} - \beta_1\beta_2\right), \tag{C.278}$$

$$\beta_2(d_1^\bigstar) = \frac{\beta_1}{d_1^\bigstar} - \beta_1, \tag{C.279}$$

where $\varepsilon_1^\star = d_{\varepsilon_1}\varepsilon_1$, with $d_{\varepsilon_1} = 1.05$, and $d_1^\star = 0.5$, therefore resulting in the expression

$$\varepsilon_2 < \frac{\alpha_1\gamma_1(\varepsilon_1^\star) + \beta_1\beta_2(d_1^\star)}{\alpha_1\alpha_2} \frac{\alpha_3\alpha_4}{\varepsilon_1\left(\alpha_3\gamma_2 + \dfrac{1}{4(1-d_2)d_2}\left[(1-d_2)\beta_3 + d_2\beta_4\right]^2\right)}\varepsilon_{2_d}, \tag{C.280}$$

which has also a maximum for d_2^*, given by

$$d_2^* = \frac{\beta_3}{\beta_3 + \beta_4}, \tag{C.281}$$

thus resulting in

$$\varepsilon_2^* = \frac{\alpha_1\gamma_1(\varepsilon_1^\star) + \beta_1\beta_2(d_1^\star)}{\alpha_1\alpha_2} \frac{\alpha_3\alpha_4}{\alpha_3\gamma_2 + \beta_3\beta_4}, \tag{C.282}$$

Recalling from the definitions of β_3, β_4 and γ_2, given in Eqns. (C.201), (C.235), and (C.266), respectively, resulting in

$$\beta_3 \geq \sqrt{\frac{d_1\eta_1^2 x_{MAX}^4}{\tilde{b}_y^2}\frac{Q_f}{Q_u}}, \tag{C.283}$$

$$\gamma_2 \geq \frac{\rho_1\hat{H}_{\tilde{x}_{MAX}}(\tilde{b}_y) + \eta_1\hat{H}_{\tilde{y}_{MAX}}(\tilde{b}_y)}{\eta_2}, \tag{C.284}$$

$$\beta_4 \geq \sqrt{\frac{\left(\tilde{\mathcal{L}}_{1_{MAX}}(b_x,\tilde{b}_y)\right)^2}{\eta_2^2(1-d_1)}\frac{Q_u}{Q_s}}, \tag{C.285}$$

therefore the expression that determines the upper-bound in ε_2, Eq. (C.282), can be rewritten by substituting in Eqns. (C.283–C.285), resulting in

$$\varepsilon_2^* = \frac{\alpha_3\alpha_4\left(\alpha_1\gamma_1(\varepsilon_1^\star) + \beta_1\beta_2(d_1^\star)\right)}{\alpha_1\alpha_2\left(\alpha_3\frac{\rho_1\hat{H}_{\tilde{x}_{MAX}}(\tilde{b}_y)+\eta_1\hat{H}_{\tilde{y}_{MAX}}(\tilde{b}_y)}{\eta_2} + \sqrt{\frac{d_1\eta_1^2x_{MAX}^4\left(\tilde{\mathcal{L}}_{1_{MAX}}(b_x,\tilde{b}_y)\right)^2}{(1-d_1)\tilde{b}_y^2\eta_2^2}\frac{Q_f}{Q_s}}\right)}, \tag{C.286}$$

and similarly with d_2^* resulting in

$$d_2^* = \frac{\sqrt{\frac{d_1\eta_1^2x_{MAX}^4}{\tilde{b}_y^2}\frac{Q_f}{Q_u}}}{\sqrt{\frac{d_1\eta_1^2x_{MAX}^4}{\tilde{b}_y^2}\frac{Q_f}{Q_u}} + \sqrt{\frac{\left(\tilde{\mathcal{L}}_{1_{MAX}}(b_x,\tilde{b}_y)\right)^2}{\eta_2^2(1-d_1)}\frac{Q_u}{Q_s}}}. \tag{C.287}$$

It can be recognized that the fulfillment of the asymptotic stability properties for the Σ_{SFU} full system can be achieved by the proper selection of *stability parameters* Q_s, Q_f, Q_u, $d_1^\star$, and $\varepsilon_1^\star$, with $d_1^\star = 0.5$, and $\varepsilon_1^\star = 1.05\varepsilon_1$. Observing Eq. (C.286), it can be seen that the upper-bound on ε_2^* only depends on the physical parameters of the problem, the control design parameters b_x, and $\tilde{b}_y$, that determine the selected target dynamics response, and the *stability parameters* Q_s, and Q_f, while not depending on Q_u. The *stability parameters* Q_u, as it can be seen in Eq. (C.287), only influences in the parameter d_2^*. Furthermore, it can be seen that the upper-bound ε_2^* can be expressed as a function of the ratio $\frac{Q_f}{Q_s}$, which is given by the expression

$$\frac{Q_f}{Q_s} = Q_{fs} = \frac{(1-d_1)\tilde{b}_y^2\eta_2^2}{d_1\eta_1^2x_{MAX}^4\left(\tilde{\mathcal{L}}_{1_{MAX}}(b_x,\tilde{b}_y)\right)^2} \times \left(\frac{\alpha_3\alpha_4\left(\alpha_1\gamma_1(\varepsilon_1^\star) + \beta_1\beta_2(d_1^\star)\right)}{\alpha_1\alpha_2\varepsilon_2^\star} - \alpha_3\frac{\rho_1\hat{H}_{\tilde{x}_{MAX}}(\tilde{b}_y) + \eta_1\hat{H}_{\tilde{y}_{MAX}}(\tilde{b}_y)}{\eta_2}\right)^2, \tag{C.288}$$

where recall that ε_2^* is substituted by $\varepsilon_2^\star$, implying that is selected such that $\varepsilon_2^\star = d_{\varepsilon_2}\varepsilon_2^*$, with $d_{\varepsilon_2} =$

1.05. Also recall that for the simplified model here described the control design parameters are selected as $b_x = 0.25$, and $\tilde{b}_y = 0.0075$, which results in $\hat{H}_{\tilde{x}_{MAX}}(\tilde{b}_y) = 8.12500$, $\hat{H}_{\tilde{y}_{MAX}}(\tilde{b}_y) = 32.500$, and $\tilde{\mathcal{L}}_{1_{MAX}}(b_x, \tilde{b}_y) = 2.0312500$, thus resulting in $Q_{fs} = 177.51647$. It can be observed in Eq. (C.287) that, by selecting the value of $d_2^* = d_2^{\bigstar}$, it can be obtained an expression that determines the necessary value of the *stability parameter* Q_u, resulting in the expression

$$Q_u = \frac{d_1^{\bigstar} Q_f \eta_1^2 x_{MAX}^2 \eta_2^4 Q_s^2 \tilde{b}_y^2 \left(d_1^{\bigstar} - 1 - 2d_1^{\bigstar} d_2^{\bigstar} + 2d_2^{\bigstar} + d_1^{\bigstar} d_2^{\bigstar} - d_2^{\bigstar}\right)^2}{\sqrt{-d_1^{\bigstar} Q_f \eta_1^2 b_x^2 \hat{H}_{\tilde{x}_{MAX}}^2 d_2^{\bigstar} \eta_2^6 Q_s^3 \tilde{b}_y^6 \left(d_1^{\bigstar} - 1 - 2d_1^{\bigstar} d_2^{\bigstar} + 2d_2^{\bigstar} + d_1^{\bigstar} d_2^{\bigstar} - d_2^{\bigstar}\right)^3}}, \tag{C.289}$$

where $d_1^{\bigstar}$ and $d_2^{\bigstar}$ represent the desired values for the upper-bound constants d_1^* and d_2^*, where ε_1 and ε_2 are maximum, Eqns. (C.103) and (C.280), respectively. The unspecified parameters $d_1^{\bigstar}$ and $d_2^{\bigstar}$, differ from d_1^* and d_2^*, Eqns. (C.104) and (C.275), respectively, in the fact that $d_1^{\bigstar}$ and $d_2^{\bigstar}$ are selected such that the distribution of both ε_1 and ε_2 are centered, that is, selecting $d_1^{\bigstar} = 0.5$ and $d_2^{\bigstar} = 0.5$.

This is a really powerful result, since implies the existence of a closed form solution for the proper selection of the stability parameters Q_s, Q_f and Q_u, which are given in Eqns. (C.288) and (C.289), recalling that Eq. (C.288) implies also that either Q_s or Q_f has to be fixed initially, since the expression only provides a relation for Q_f/Q_s. This implies that it can be selected the values at which the derived Lyapunov function for the singularly perturbed Σ_{SFU} full system, $V_2(\tilde{\chi}, \tilde{z})$, can guaranteed that the given system is asymptotically stable for all $\varepsilon_2 < \varepsilon_2^*$.

These conclusions can be better observed in Figures C.2, C.4, C.3, C.6, and C.7. Figure C.2 shows the variation of ε_2 vs. Q_s and Q_f, where the range of Q_s is given by $10 \leq Q_s \leq 20$ and the range of Q_f is given by Eq. (C.288), that is $10Q_{fs} \leq Q_f \leq 20Q_{fs}$, where for the problem here discuses $Q_{fs} = 177.51647$. It can be seen that as long as the ratio of the selected *stability parameters* Q_s^* and Q_f^*, are greater than the ratio in Eq. (C.288), that is $Q_f^*/Q_s^* \geq Q_f/Q_s$, the resulting upper-bound $\varepsilon_2^* \geq 1.1025 \times 10^{-3}$, thus satisfying $\varepsilon_2 < \varepsilon_2^*$.

Figure C.3 shows the variation of ε_2 and the unspecified parameters d_1 and d_2. It can be seen that as selected in the previous calculations, the required expression $\varepsilon_2 < \varepsilon_2^*$ it is satisfied for the combination of $d_1 = 0.5$ and $d_2 = 0.5$, and also, as seen by the color scheme in the same figure, but view from the azimuthal perspective as depicted in Figure C.4, where it can be observed that for $d_2 \neq 0.5$, there exist two combinations for $d_1 > 0.5$ and $d_1 < 0.5$, that satisfy $\varepsilon_2 < \varepsilon_2^*$.

This can also be also seen for the case in which expression Eq. (C.280) is analyzed for $d_1^{\bigstar} = 0.5$ and $\varepsilon_1^{\bigstar} = 1.05\varepsilon_1 = 0.0105$ as seen in Figure C.5. Figures C.6 and C.7 show the variation of the unspecified parameter d_2 as a function of Q_s and Q_f, in Figure C.6, and Q_f and Q_u, in Figure C.7. The range in both figures is determined by the expressions described in Eqns. (C.288) and (C.289), therefore, selecting $10 \leq Q_s \leq 20$, resulting in

$$1460.304329 \leq Q_f \leq 2920.60865, \tag{C.290}$$

$$0.099153 \leq Q_u \leq 0.1983065. \tag{C.291}$$

Figure C.6 shows that in order to maintain $d_2 = 0.5$, as Q_s is increased, Q_f needs to be reduced, and the opposite, as Q_s is decreased, Q_f needs to be increased, always maintaining the Q_{fs} ratio. The same trends are depicted in Figure C.7, thus concluding that by maintaining the ratio given by Eqns. (C.288) and (C.289), it can be obtained the desired $d_2^{\bigstar}$. Therefore, recalling from the previous stability analysis, the coefficients that fulfill the growth requirements are therefore given by

$$\alpha_3 = 0.95,$$

$$\alpha_4 = 0.95,$$

$$\begin{aligned}\beta_3 &= 286.04338,\\ \beta_4 &= 286.04338,\\ \gamma_2 &= 40.625,\end{aligned}$$

and the *stability parameters* that produce such parameters are selected as

$$\begin{aligned}Q_s &= 15,\\ Q_f &= 2190.45649,\\ Q_u &= 0.1487299.\end{aligned}$$

The upper-bound (C.286) is given by $\varepsilon_2^* = 1.1025 \times 10^{-3}$. Recall that for the problem here stated it was selected $\varepsilon_2 = 1 \times 10^{-3}$, thus satisfying that $\varepsilon_2 < \varepsilon_2^*$. Recall that (C.274) depends on the selection of the variable d_1, and the maximum value of ε_2 is achieved with $d_1^* = d_1^\bigstar = 0.5$, and $d_2^* = d_2^\bigstar = 0.5$. It has been proven that with proper selection of the *Stability Parameters*, Q_s, Q_f, and Q_u, the value of ε_1^* in the Σ_{SF}-subsystem and ε_2^* in the Σ_{SFU} full system have been obtained such that $\varepsilon_1 < \varepsilon_1^*$, and $\varepsilon_2 < \varepsilon_2^*$, therefore, since all the growth requirements are satisfied, then the origin $\tilde{\boldsymbol{\chi}} = 0$, $\tilde{z} = 0$, is an asymptotically stable equilibrium of the singularly perturbed Σ_{SFU} system for all $\varepsilon_2 \in (0, \varepsilon_2^*)$. This concludes Σ_{SFU} *Stability Analysis* for the simplified example.

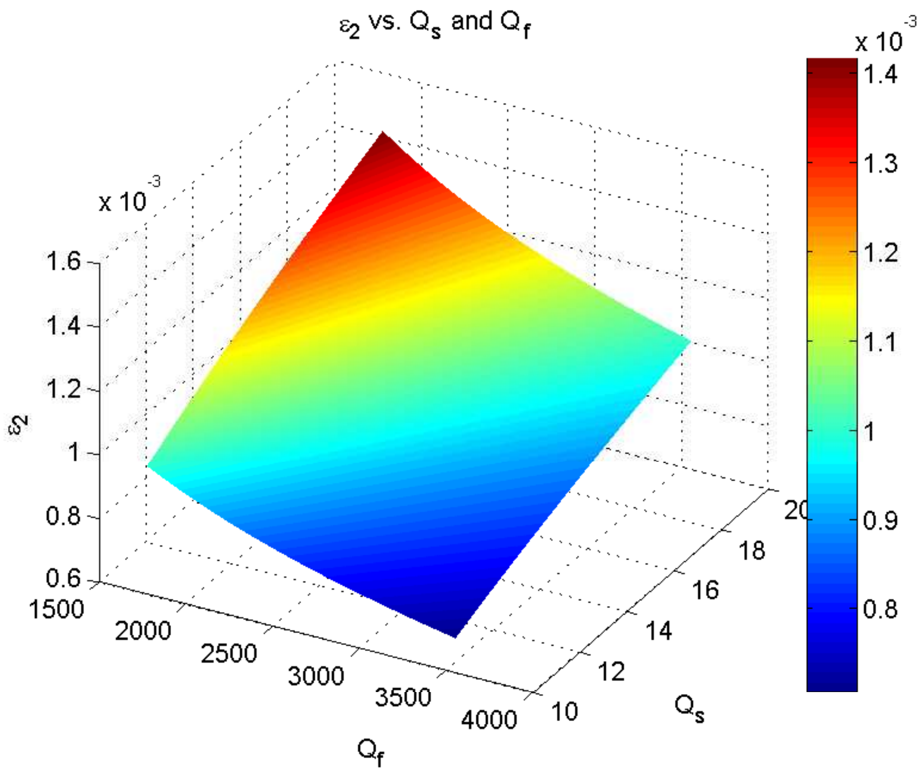

Figure C.2: ε_2 vs. Q_s and Q_f.

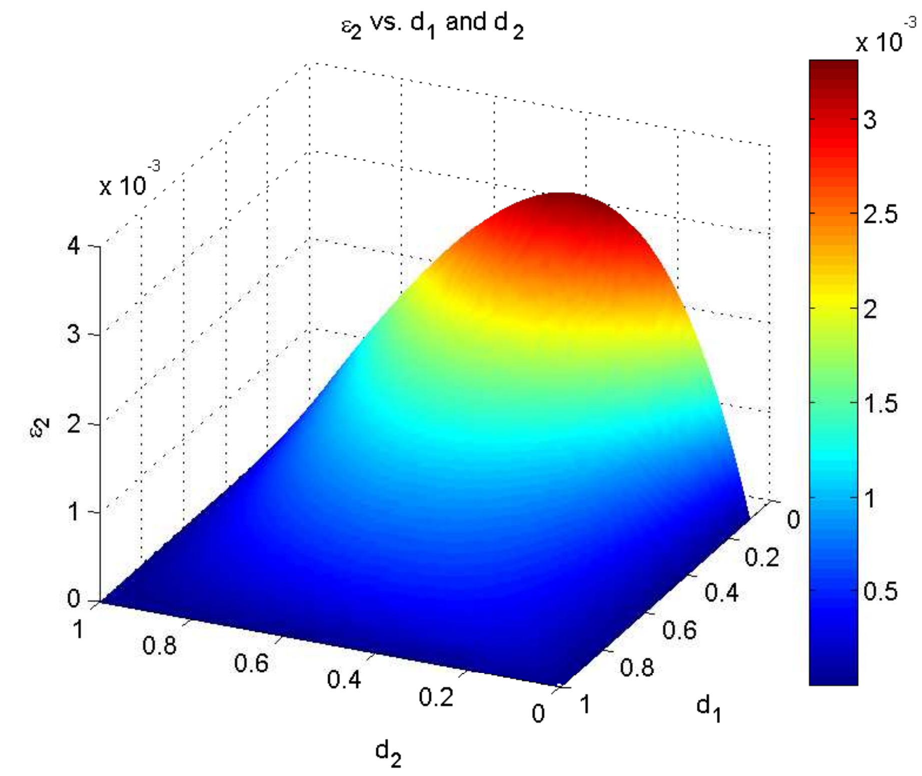

Figure C.3: ε_2 vs. d_1 and d_2.

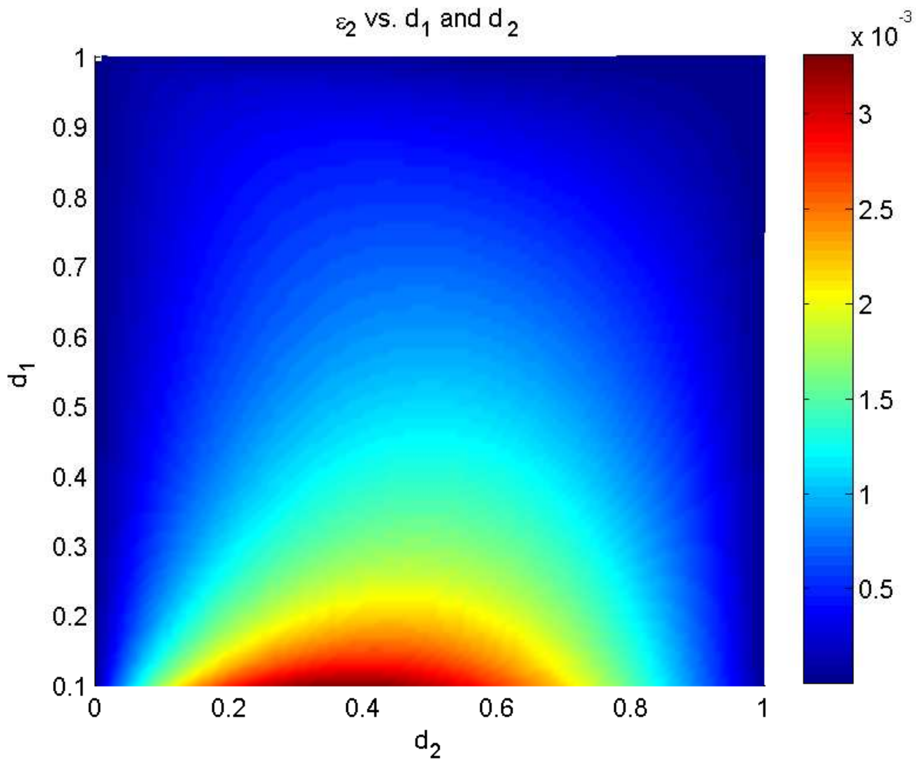

Figure C.4: ε_2 vs. d_1 and d_2.

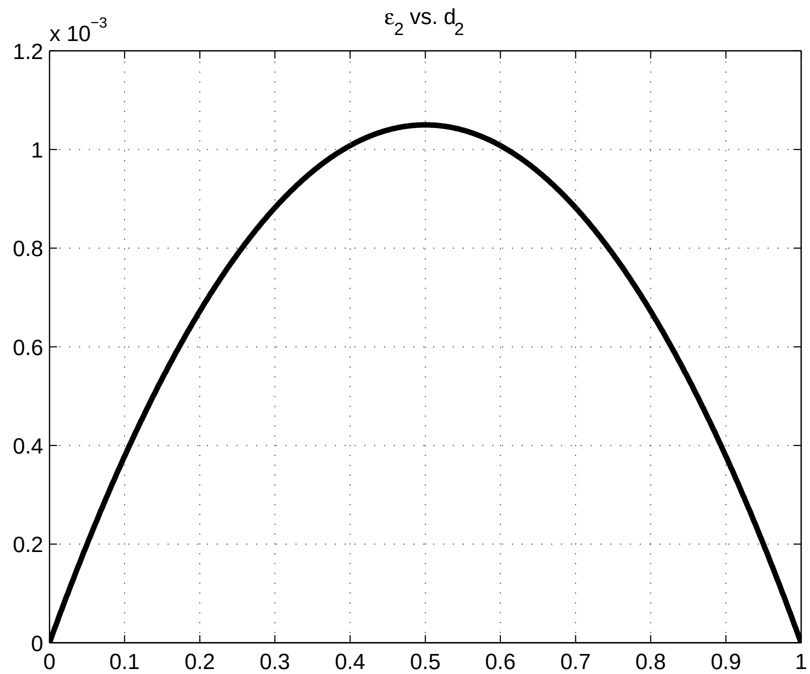

Figure C.5: Stability upper bounds on ε_2 for the *Stability Analysis* of the Σ_{SFU} simplified system.

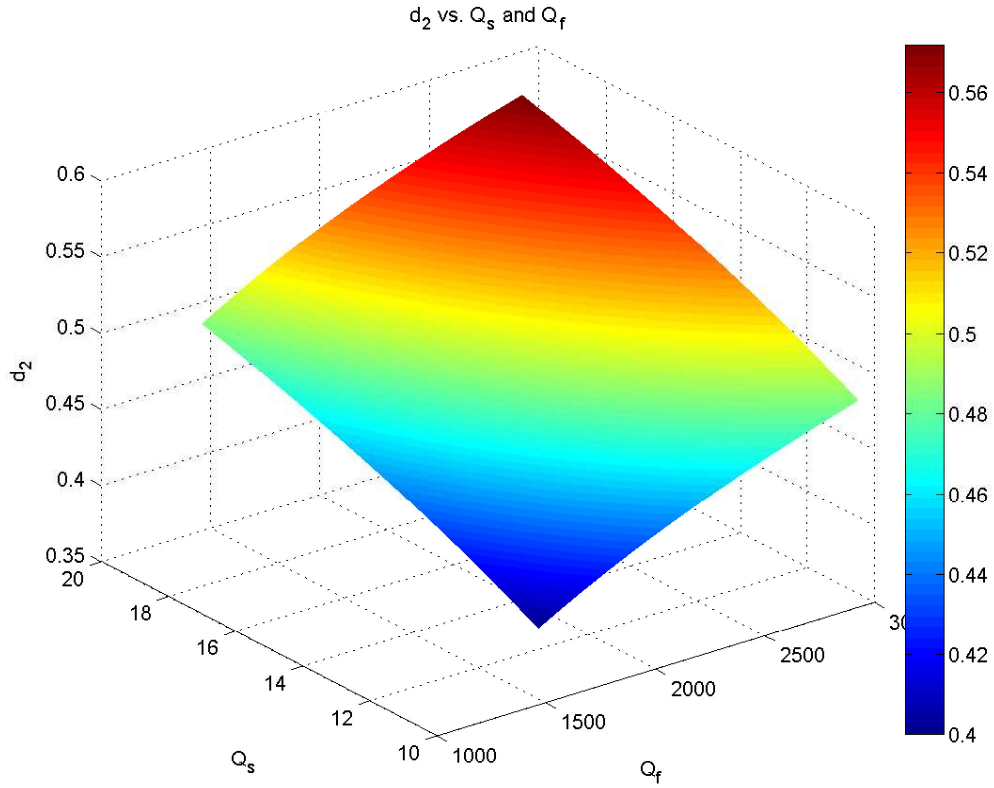

Figure C.6: d_2 vs. Q_s and Q_f.

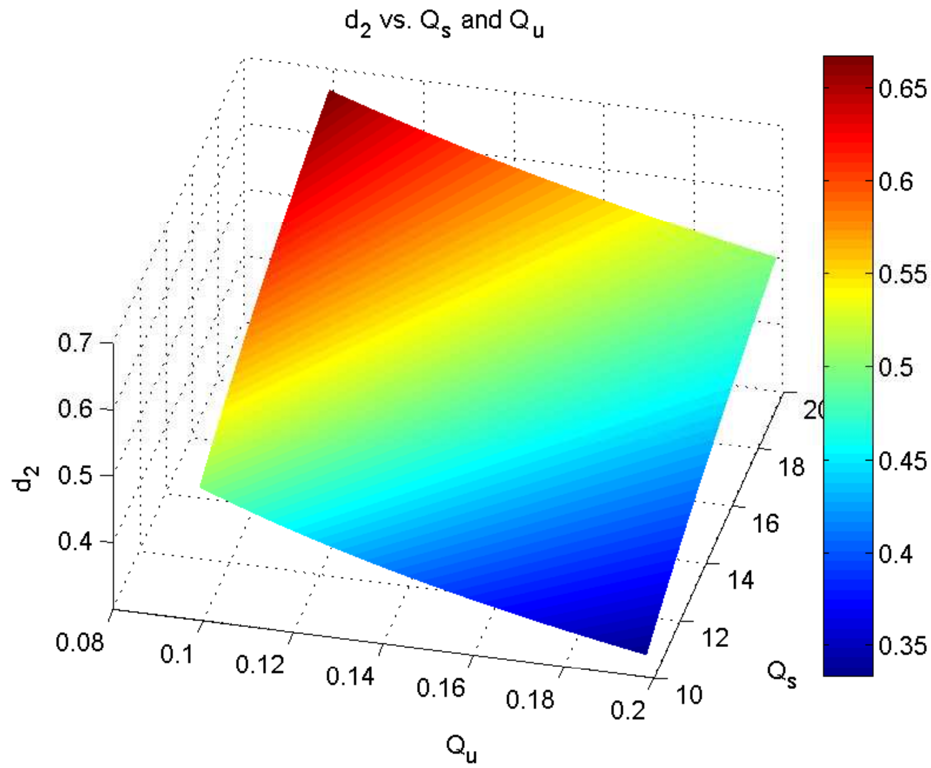

Figure C.7: d_2 vs. Q_s and Q_u.

C.8 Conclusions

The Asymptotic Stability Analysis presented in chapter 5 has been applied to the three-time-scale autonomous simplified example model obtained in chapter 4. The proposed two-step process defined in chapter 3 allows to study the asymptotic stability properties of the closed loop system, and also proposes a methodology to obtain a Lyapunov function candidate for the entire system, $V_2(\tilde{x}, \tilde{y}, \tilde{z})$, by using a weighted sum of the proposed Lyapunov function candidates of the three time-scale subsystems.

The validity of the methodology has been proved by obtaining the stability upper bound limits on the boundary layers, ε_1 and ε_2, and ensuring that the selected parasitic constants for the proposed control law satisfy $\varepsilon_1 \leq \varepsilon_1^*$ and $\varepsilon_2 \leq \varepsilon_2^*$ for the helicopter model here employed. The use of the full range of reachable state variables has been required in order to satisfy the inequalities that guarantee the asymptotic stability properties at the origin of the Σ_{SFU}-subsystem, which results in extending the asymptotic stability properties to semiglobal stability, by the definition in (Kokotović, 1992; Sussmann and Kokotović, 1991; Braslavsky and Miidleton, 1996), by providing upper bounds on the parasitic singularly perturbed parameters for the entire range of admissible state values, thus extending the domain of attraction to that same rage of admissible states.

The stability results have also presented a closed form solution for the proper selection of the *stability parameters* Q_f, and Q_u as a function of the arbitrary *stability parameter* Q_S, such that fulfill assumptions 5.5.6, 5.5.7, 5.5.8, 5.5.9, and 5.5.10, providing asymptotic stability for the helicopter Σ_{SFU} full system with prescribed upperbounds on the parasitic parameters.

This page intentionally left blank

Appendix D

Results for the Asymptotic Stability Analysis for the Helicopter Model

A sensitivity analysis for the results for the asymptotic stability analysis for the helicopter model is here presented by performing the same four distinctive maneuvers that include all possible helicopter maneuvers:

1. Ascent flight with increasing engine RPM.
2. Ascent flight with decreasing engine RPM.
3. Descent flight with increasing engine RPM.
4. Descent flight with decreasing engine RPM.

where once again, despite the extensive sensitivity analysis conducted, only four significate cases are presented, which correspond to a maneuver that includes all four distinctive maneuvers in one simulation, and that are defined by the bellow conditions:

1. $y_1(0) = 1.85\ m$, $y_1^* = 0.5\ m$, $x(0) = 120\ rad/sec$, and $x^* = 140\ rad/sec$.
2. $y_1(0) = 0.5\ m$, $y_1^* = 1\ m$, $x(0) = 140\ rad/sec$, and $x^* = 120\ rad/sec$.
3. $y_1(0) = 1\ m$, $y_1^* = 1.5\ m$, $x(0) = 120\ rad/sec$, and $x^* = 145\ rad/sec$.
4. $y_1(0) = 1.5\ m$, $y_1^* = 0.75\ m$, $x(0) = 145\ rad/sec$, and $x^* = 120\ rad/sec$.

Figures D.2 and D.3 show the fulfillment of the reduced order and boundary layer inequalities for the Σ_{SF}-subsystem, inequalities (6.67) and (6.75), respectively. The fulfillment of these inequalities are represented graphically by recalling that Eqns. (6.67) and (6.75) can be rewritten as

$$0 \quad < \quad -\alpha_1\psi_1^2(x) - \frac{dV_S}{d_x}\tilde{f}\left[\tilde{x}, \tilde{\mathbf{g}}\left(\tilde{x}\right), \tilde{\mathbf{h}}\left(\tilde{x}, \tilde{\mathbf{g}}\left(\tilde{x}\right)\right)\right], \tag{D.1}$$

$$0 \quad < \quad -\alpha_2\phi_1^2(\hat{\boldsymbol{y}}) - \frac{dV_F}{d\tilde{\boldsymbol{y}}}\hat{\boldsymbol{g}}\left[\tilde{x}, \tilde{\boldsymbol{y}}, \tilde{\mathbf{h}}(\tilde{x}, \tilde{\mathbf{g}}(\tilde{x}))\right], \tag{D.2}$$

where, the fulfillment of both, the reduced, and boundary layer inequalities, assumptions 6.3.2, 6.3.3, is achieved if Eqns. (D.1), and (D.2) are positive, or equal to zero, for the entire range of the conducted simulations for all eight distinctive helicopter maneuvers, as it can be seen in Figures D.2 and D.3. Figures D.4, D.5, shown the evolution of the comparison functions $\psi_1(\tilde{x})$, and $\phi_1(\hat{\boldsymbol{z}})$, for all eight helicopter maneuvers.

Similarly, Figures D.6, D.7, D.8, and D.9, show the fulfillment of the reduced order, boundary layer, and interconnection inequalities for the Σ_{SFU}-subsystem, inequalities (6.239), (6.296), (6.314), and (6.436) respectively. The fulfillment of these inequalities are represented graphically by recalling that Eqns. (6.239), (6.296), (6.314), and (6.436) can be rewritten as eq.

$$0 \;<\; -\alpha_3\psi_2^2(\tilde{\boldsymbol{\chi}}) - \left(\frac{dV_1}{d\tilde{\boldsymbol{\chi}}}\right)^T \tilde{\boldsymbol{F}}\left(\tilde{\boldsymbol{\chi}}, \tilde{\mathbf{h}}(\tilde{\boldsymbol{\chi}})\right), \tag{D.3}$$

$$0 \;<\; -\alpha_4\phi_2^2(\hat{\boldsymbol{z}}) - \left(\frac{dV_U}{d\tilde{\boldsymbol{z}}}\right)^T \hat{\boldsymbol{g}}\left[\tilde{\boldsymbol{\chi}}, \tilde{\mathbf{h}}(\tilde{\boldsymbol{\chi}})\right], \tag{D.4}$$

$$0 \;<\; \beta_3\psi_2(\tilde{\boldsymbol{\chi}})\phi_2(\hat{\boldsymbol{z}}) - \left(\frac{dV_1}{d\tilde{\boldsymbol{\chi}}}\right)^T \left[\tilde{\boldsymbol{F}}(\tilde{\boldsymbol{\chi}}, \tilde{\boldsymbol{z}}) - \tilde{\boldsymbol{F}}(\tilde{\boldsymbol{\chi}}, \tilde{\mathbf{h}}(\tilde{\boldsymbol{\chi}}))\right], \tag{D.5}$$

$$0 \;<\; \gamma_2\phi_2^2(\hat{\boldsymbol{z}}) + \beta_4\psi_2(\tilde{\boldsymbol{\chi}})\phi_2(\hat{\boldsymbol{z}}) - \left(\frac{dV_U}{d\tilde{\boldsymbol{\chi}}}\right)^T \tilde{\boldsymbol{F}}\left(\tilde{\boldsymbol{\chi}}, \tilde{\boldsymbol{z}}\right), \tag{D.6}$$

where, the fulfillment of these inequalities, assumptions 6.5.2, 6.5.3, 6.5.4, and 6.5.5, is achieved if Eqns. (D.3), (D.4), (D.5), and (D.6), are positive, or equal to zero, for the entire range of the conducted simulations for all eight distinctive helicopter maneuvers, as it can be seen in Figures D.6, D.7, D.8, and D.9. Figures D.10, D.11, shown the evolution of the comparison functions $\psi_2(\tilde{\boldsymbol{\chi}})$, and $\phi_2(\hat{\boldsymbol{z}})$. This concludes the Σ_{SFU} *Stability Analysis* asymptotic stability analysis for the simplified example.

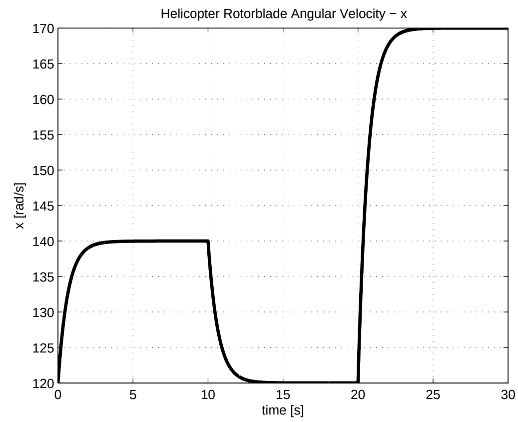

(a) x

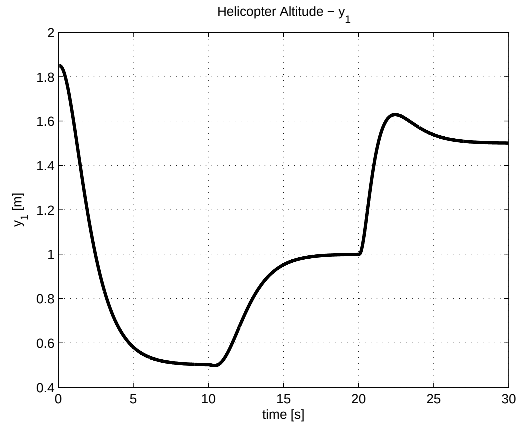

(b) y_1

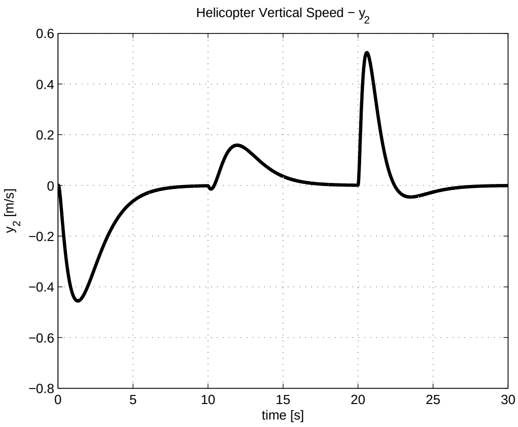

(c) y_2

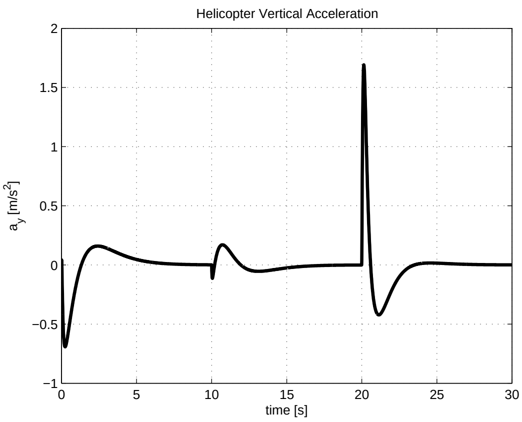

(d) a_y

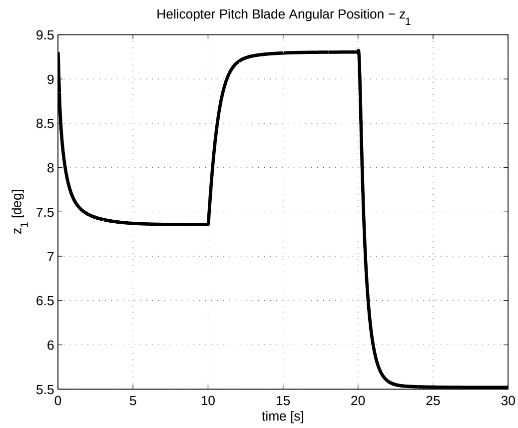

(e) z_1

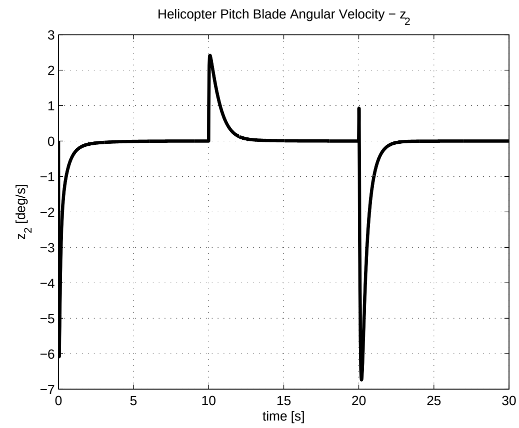

(f) z_2

Figure D.1: States History for the *TD* Control Strategy

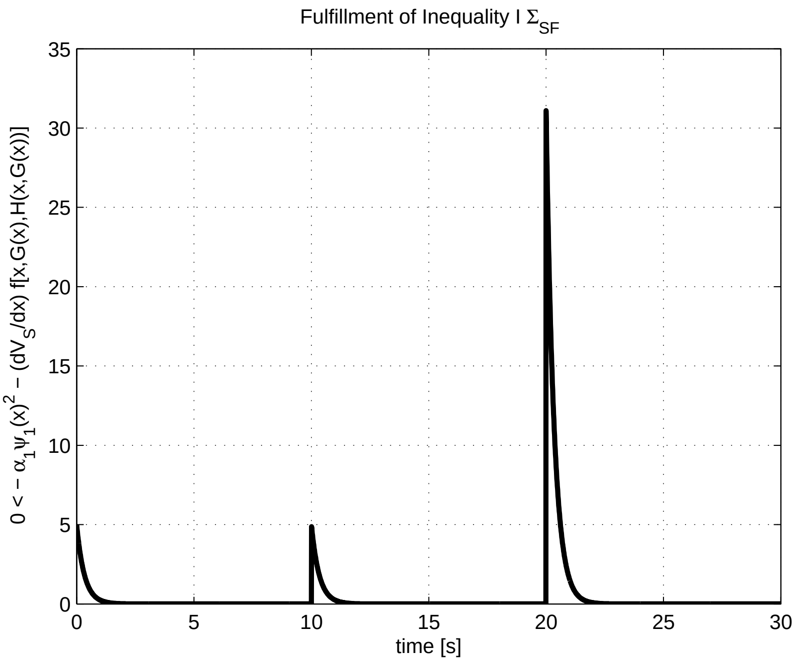

Figure D.2: Fulfillment of the reduced order inequality for the Σ_{SF}-subsystem: $0 < -\alpha_1\psi_1^2(x) - \frac{dV_S}{d_x}\tilde{f}\left[\tilde{x}, \tilde{\mathbf{g}}\left(\tilde{x}\right), \tilde{\mathbf{h}}\left(\tilde{x}, \tilde{\mathbf{g}}\left(\tilde{x}\right)\right)\right]$.

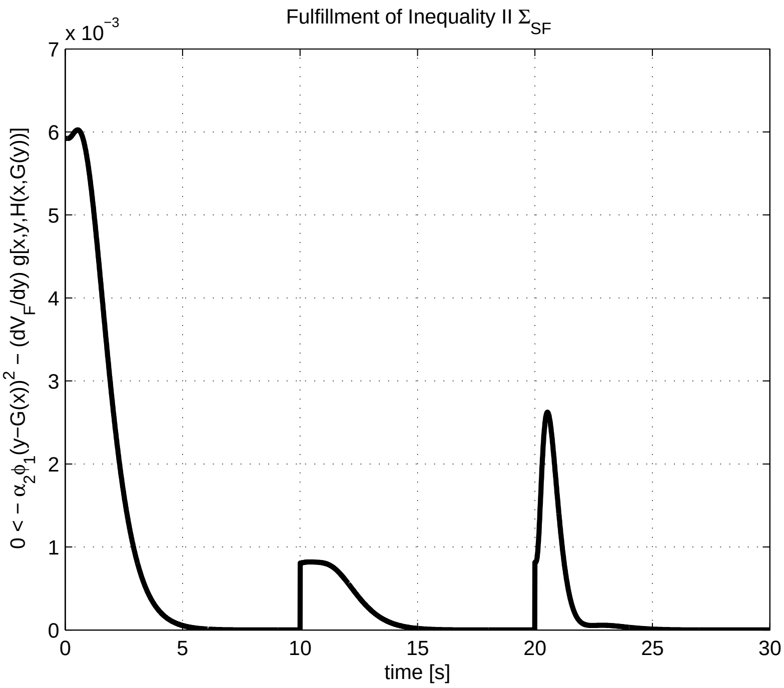

Figure D.3: Fulfillment of boundary layer inequality for the Σ_{SF}-subsystem: $0 < -\alpha_2\phi_1^2(\hat{\boldsymbol{y}}) - \frac{dV_F}{d\tilde{y}}\hat{\boldsymbol{g}}\left[\tilde{x}, \tilde{\boldsymbol{y}}, \tilde{\mathbf{h}}(\tilde{x}, \tilde{\mathbf{g}}(\tilde{\boldsymbol{y}}))\right]$.

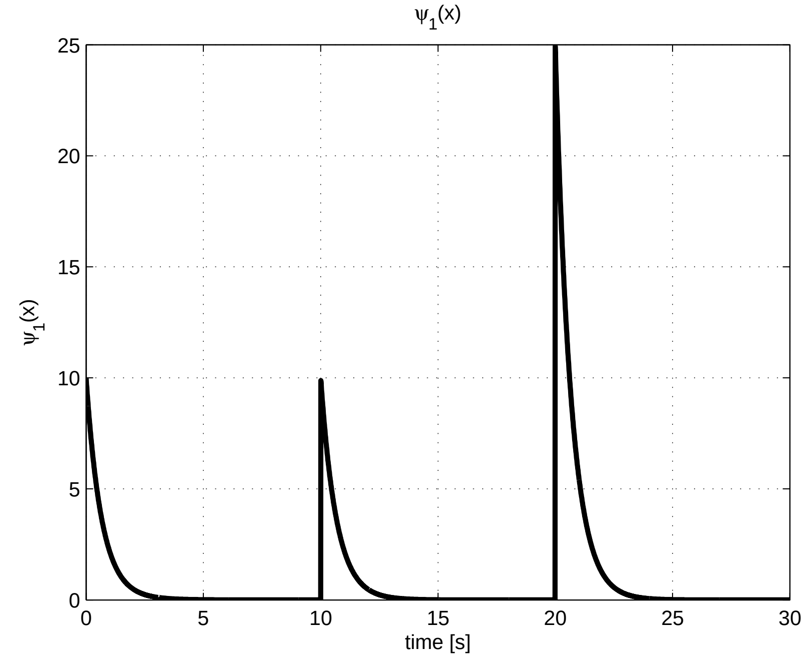

Figure D.4: Comparison function $\psi_1(\tilde{x})$ for the Σ_{SF}-subsystem.

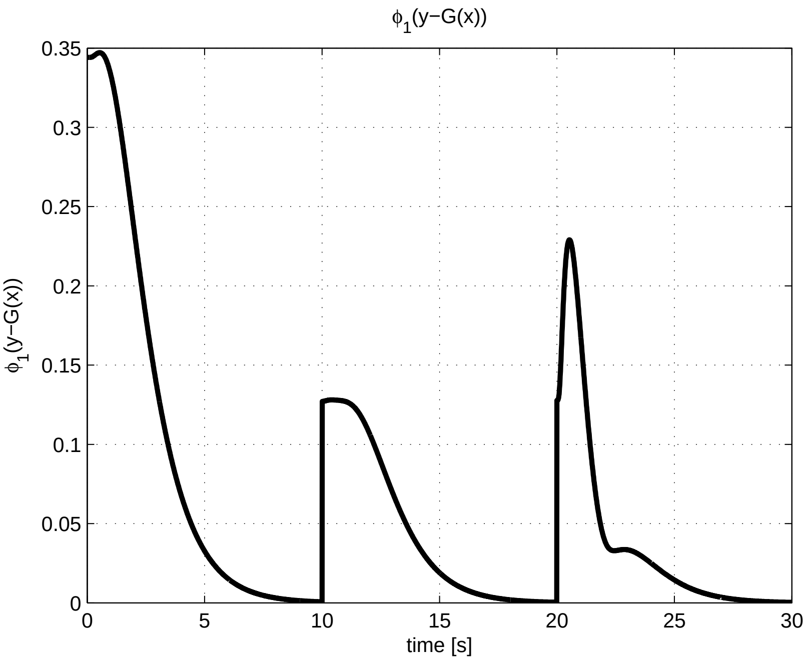

Figure D.5: Comparison function $\phi_1\left(\hat{\boldsymbol{y}}\right)$ for the Σ_{SF}-subsystem.

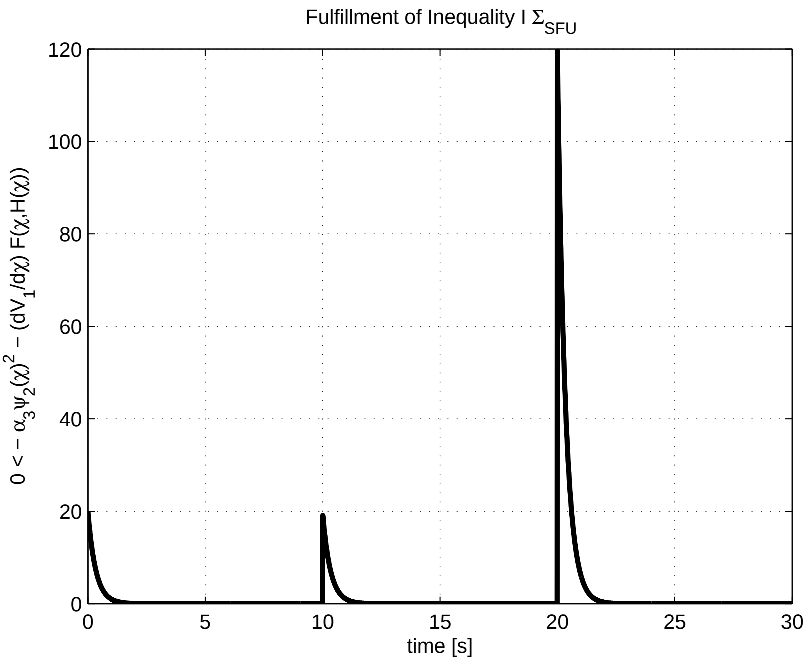

Figure D.6: Fulfillment of the reduced order inequality for the Σ_{SFU} system: $0 < -\alpha_3\psi_2^2(\tilde{\boldsymbol{\chi}}) - \left(\frac{dV_1}{d\tilde{\boldsymbol{\chi}}}\right)^T \tilde{\boldsymbol{F}}\left(\tilde{\chi}, \tilde{\mathbf{h}}(\tilde{\chi})\right)$.

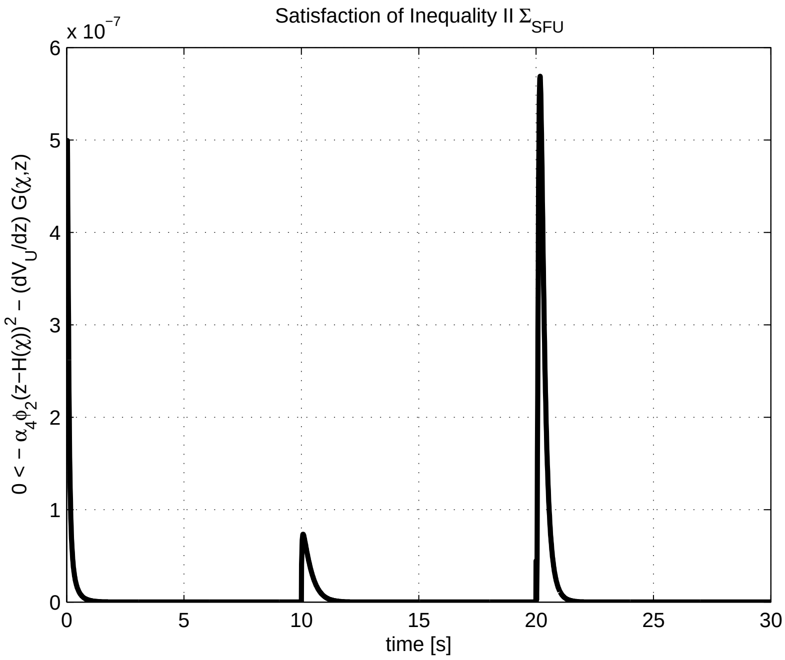

Figure D.7: Fulfillment of the boundary layer inequality for the Σ_{SFU} full system: $0 < -\alpha_4\phi_2^2(\hat{\boldsymbol{z}}) - \left(\frac{dV_U}{d\tilde{z}}\right)^T \hat{\boldsymbol{g}}\left[\tilde{\chi}, \tilde{\mathbf{h}}(\tilde{\chi})\right]$.

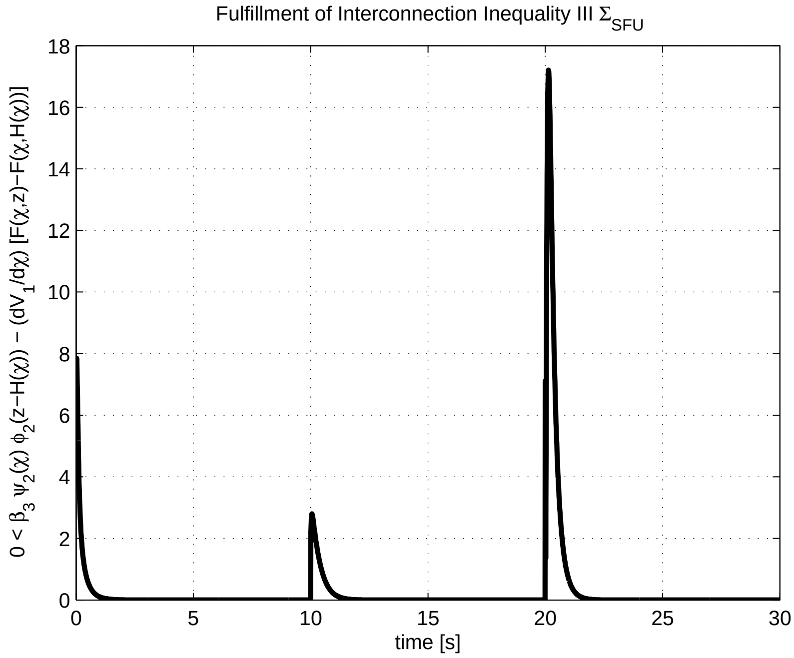

Figure D.8: Fulfillment of the first interconnection inequality for the Σ_{SFU} full system: $0 < \beta_3\psi_2(\tilde{\boldsymbol{\chi}})\phi_2(\hat{\boldsymbol{z}}) - \left(\frac{dV_1}{d\tilde{\boldsymbol{\chi}}}\right)^T \left[\tilde{\boldsymbol{F}}(\tilde{\boldsymbol{\chi}}, \tilde{\boldsymbol{z}}) - \tilde{\boldsymbol{F}}(\tilde{\boldsymbol{\chi}}, \tilde{\mathbf{h}}(\tilde{\boldsymbol{\chi}}))\right]$.

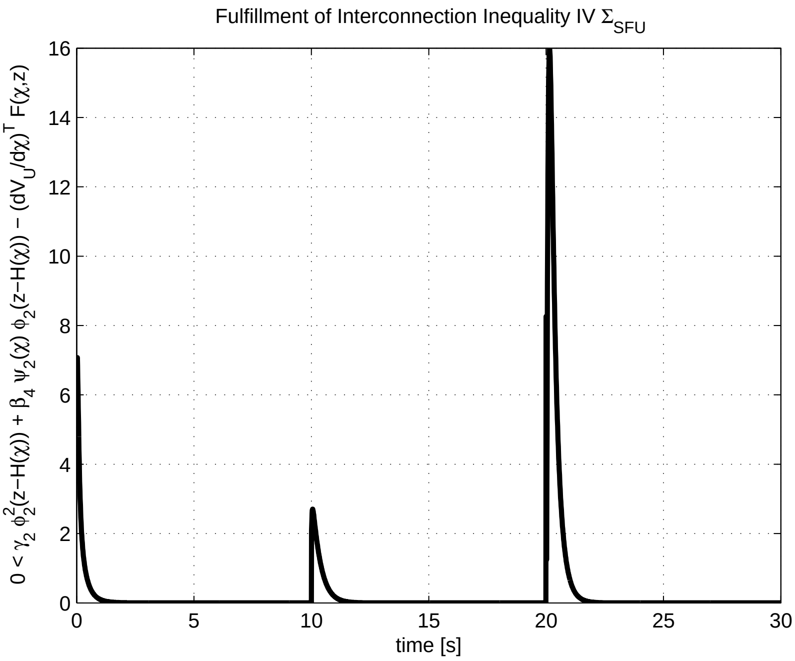

Figure D.9: Fulfillment of the second interconnection inequality for the Σ_{SFU} full system: $0 < \gamma_2\phi_2^2(\hat{\boldsymbol{z}}) + \beta_4\psi_2(\tilde{\boldsymbol{\chi}})\phi_2(\hat{\boldsymbol{z}}) - \left(\frac{dF_U}{d\tilde{\boldsymbol{\chi}}}\right)^T \tilde{\boldsymbol{F}}(\tilde{\boldsymbol{\chi}}, \tilde{\boldsymbol{z}})$.

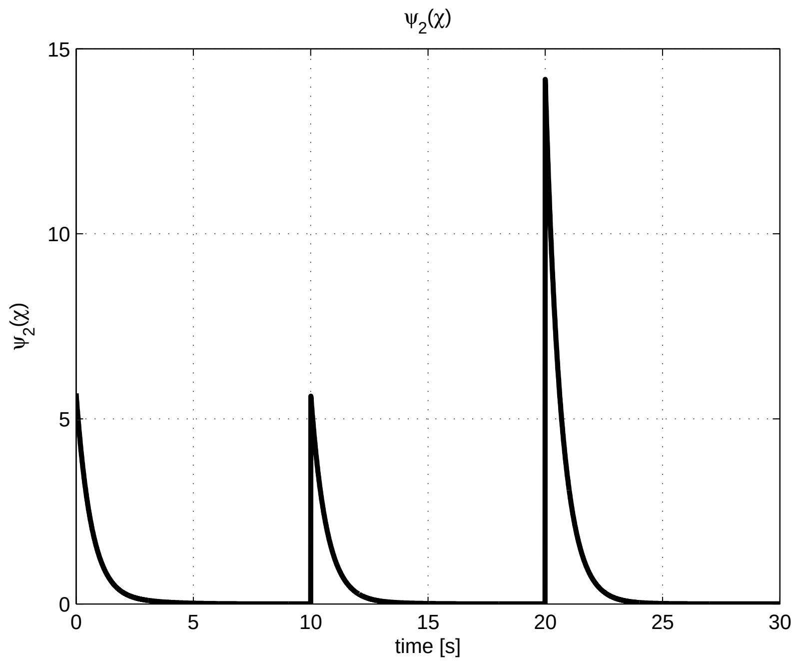

Figure D.10: Comparison function $\psi_2(\tilde{\chi})$ for the Σ_{SFU} full system.

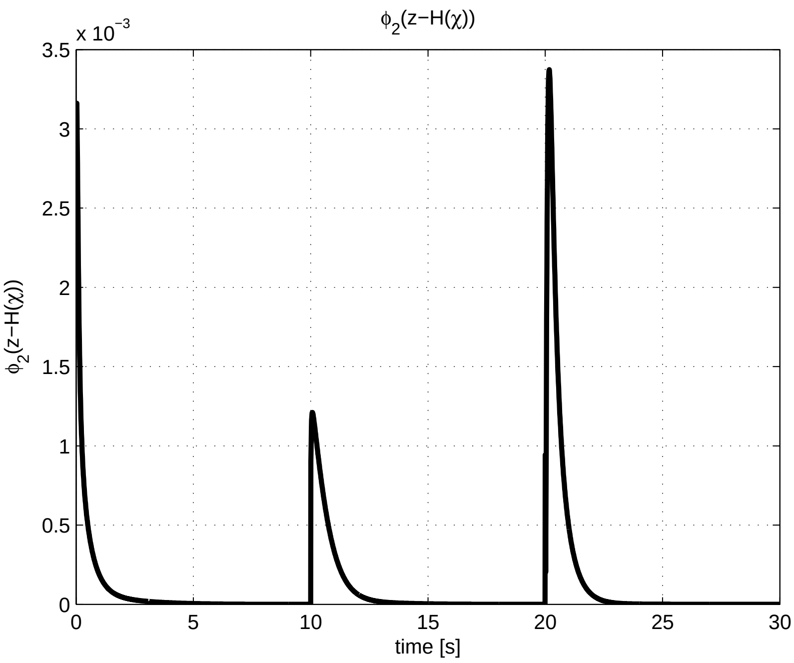

Figure D.11: Comparison function $\phi_2(\hat{z})$ for the Σ_{SFU} full system.